

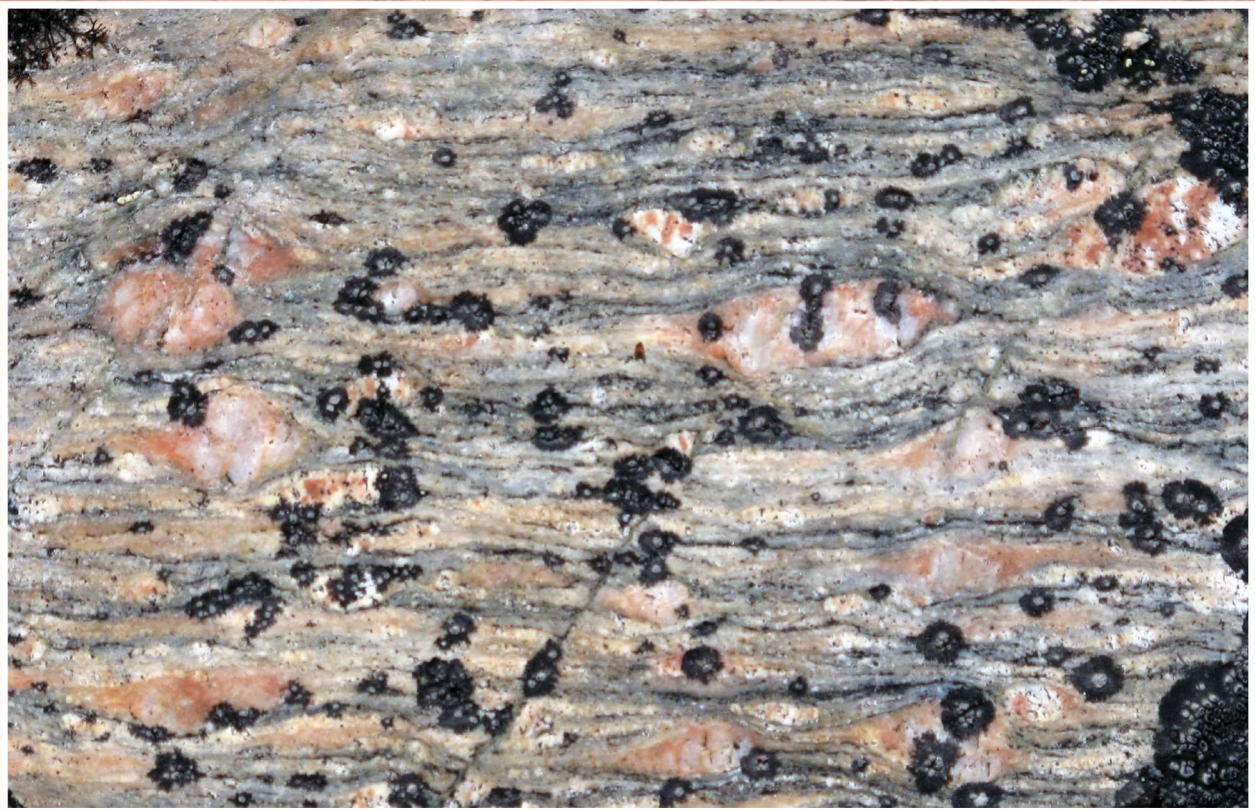


Natural Resources
Canada

Ressources naturelles
Canada



Geological Survey of Canada Bulletin 612



**Canada's northern shield: new perspectives from the
Geo-mapping for Energy and Minerals program**

**Edited by
S.J. Pehrsson, N. Wodicka, N. Rogers, and J.A. Percival**

2024

Canada

Geological Survey of Canada
Bulletin 612

**Canada's northern shield: new perspectives from
the Geo-mapping for Energy and
Minerals program**

Edited by
S.J. Pehrsson, N. Wodicka, N. Rogers, and J.A. Percival

2024

© His Majesty the King in Right of Canada, as represented by the Minister of Natural Resources, 2024

ISSN 2560-7219

ISBN 978-0-660-33966-5

Catalogue No. M42-612E-PDF

<https://doi.org/10.4095/332492>

A copy of this publication is also available for reference in depository libraries across Canada through access to the Depository Services Program's Web site at <http://dsp-psd.pwgsc.gc.ca>.

This publication is available for free download through GEOSCAN (<https://geoscan.nrcan.gc.ca>).

Recommended citation

Pehrsson, S.J., Wodicka, N., Rogers, N., and Percival, J.A. (ed.), 2024. Canada's northern shield: new perspectives from the Geo-mapping for Energy and Minerals program; Geological Survey of Canada, Bulletin 612, 419 p. <https://doi.org/10.4095/332492>

Cover illustration

Mylonite of the Snowbird tectonic zone exposed north of Kasba Lake, Northwest Territories. Approximate width of field of view: 20 cm. Photograph by S.J. Pehrsson. NRCan photo 2023-048

Editors

S.J. Pehrsson (sally.pehrsson@nrcan-rncan.gc.ca)

N. Wodicka (natasha.wodicka@nrcan-rncan.gc.ca)

N. Rogers (neil.rogers@nrcan-rncan.gc.ca)

J.A. Percival (john.percival@nrcan-rncan.gc.ca)

Geological Survey of Canada

601 Booth Street

Ottawa, Ontario

K1A 0E8

Information contained in this publication or product may be reproduced, in part or in whole, and by any means, for personal or public non-commercial purposes, without charge or further permission, unless otherwise specified.

You are asked to:

- exercise due diligence in ensuring the accuracy of the materials reproduced;
- indicate the complete title of the materials reproduced, and the name of the author organization; and
- indicate that the reproduction is a copy of an official work that is published by Natural Resources Canada (NRCan) and that the reproduction has not been produced in affiliation with, or with the endorsement of, NRCan.

Commercial reproduction and distribution is prohibited except with written permission from NRCan. For more information, contact NRCan at copyright-droitdauteur@nrcan-rncan.gc.ca.

CONTENTS

• Introduction and summary <i>S.J. Pehrsson, N. Wodicka, J.A. Percival, and N. Rogers</i>	1
• Introduction et sommaire <i>S.J. Pehrsson, N. Wodicka, J.A. Percival et N. Rogers</i>	27
• Advancing exploration for iron oxide–copper–gold and affiliated deposits in Canada: context, scientific overview, outcomes, and impacts <i>L. Corriveau and E.G. Potter</i>	55
• Record of Precambrian orogenic unroofing preserved in fluvial strata of western Nunavut <i>A. Ielpi, R.H. Rainbird, and W.J. Davis</i>	99
• Crustal architecture and evolution of the central Thelon tectonic zone, Nunavut: insights from Sm–Nd and O isotope analysis, U–Pb zircon geochronology, and targeted bedrock mapping <i>R.G. Berman, B.E. Taylor, W.J. Davis, M. Sanborn-Barrie, and J.B. Whalen</i>	115
• Overview of the geology of the Montresor belt, Nunavut (<i>short contribution</i>) <i>J.A. Percival, V. Tschirhart, and W.J. Davis</i>	159
• Geology and metallogeny of the northeast Thelon Basin region, Nunavut, and comparison with the Athabasca Basin, Saskatchewan <i>C.W. Jefferson, S.J. Pehrsson, V. Tschirhart, T.D. Peterson, L.B. Chorlton, K.M. Bethune, J.C. White, W.J. Davis, V.J. McNicoll, R.C. Paulen, and N. Rayner</i>	163
• New crustal subdivision and architecture of the south Rae Craton, Northwest Territories: a synthesis (<i>short contribution</i>) <i>S.J. Pehrsson</i>	283
• An overview of Archean and Proterozoic history of the Tehery Lake–Wager Bay area, central Rae Craton, Nunavut (<i>short contribution</i>) <i>N. Wodicka, H.M. Steenkamp, T.D. Peterson, I. Therriault, J.B. Whalen, V. Tschirhart, C.J.M. Lawley, C. Guilmette, D.A. Kellett, O.M. Weller, W. Garrison, J. Kendrick, and W.J. Davis</i>	289
• Geophysical contributions to a synthesis of western Churchill geology and metallogeny, Northwest Territories, Nunavut, and Saskatchewan <i>V. Tschirhart, S.J. Pehrsson, N. Wodicka, J.A. Percival, C.W. Jefferson, T.D. Peterson, and R.G. Berman</i>	295
• Summary of GEM results: Manitoba Far North Geomapping Initiative (<i>short contribution</i>) <i>C.O. Böhm and N.M. Rayner</i>	327
• Overview of the lithotectonic framework of the Core Zone, southeastern Churchill Province, Quebec and Newfoundland and Labrador (<i>short contribution</i>) <i>D. Corrigan</i>	335
• Rae Province at 2.6 Ga: a sanukitoid storm on the Canadian Shield, Nunavut <i>T.D. Peterson, N. Wodicka, S.J. Pehrsson, P. Acosta-Góngora, V. Tschirhart, C.W. Jefferson, H.M. Steenkamp, E. Martel, J.A. Percival, and D. Corrigan</i>	339
• Paleoproterozoic dyke swarms and large igneous provinces of northern Canada and their use in understanding extension, rifting, and paleocontinental reconstructions <i>K.L. Buchan and R.E. Ernst</i>	375
• Thermochronological history of the northern Canadian Shield: a synthesis (<i>short contribution</i>) <i>D.A. Kellett, S.J. Pehrsson, D.R. Skipton, D. Regis, A. Camacho, D.A. Schneider, and R.G. Berman</i>	411
• Summary of the Statherian–Calymmian paleogeography of northwestern Laurentia (<i>short contribution</i>) <i>R.H. Rainbird and W.J. Davis</i>	417

Introduction et sommaire

S.J. Pehrsson^{1*}, N. Wodicka¹, J.A. Percival¹ et N. Rogers¹

Pehrsson, S.J., Wodicka, N., Percival, J.A. et Rogers, N., 2024. Introduction et sommaire; in Canada's northern shield: new perspectives from the Geo-mapping for Energy and Minerals program, (éd.) S.J. Pehrsson, N. Wodicka, N. Rogers et J.A. Percival; Commission géologique du Canada, Bulletin 612, p. 27–54. <https://doi.org/10.4095/332494>

Résumé : Le programme Géocartographie de l'énergie et des minéraux (GEM) a fait l'objet d'un financement de 2008 à 2020 pour faire progresser les connaissances géologiques sur le Nord, dans le but de réduire les risques liés à l'exploration minérale et d'éclairer les décisions propres à l'utilisation des terres et à la gestion future du Nord. Vingt et une activités régionales ont été entreprises dans le nord du Bouclier canadien, qui comprend le nord des provinces des Prairies et du Québec, le Labrador ainsi qu'une grande partie du Nunavut et des Territoires du Nord-Ouest. Cinq autres activités étaient de nature thématique. Le Bulletin 612 présente les résultats de 12 de ces activités, notamment des études géoscientifiques intégrées sur le substratum rocheux à l'échelle régionale, des levés géophysiques et des analyses de bassin, ainsi que des synthèses thématiques sur la thermochronologie, la géochimie et les grandes provinces ignées. Les résultats montrent que le programme GEM a contribué à une nouvelle ère de connaissances sur le nord du Bouclier canadien, en élargissant considérablement son cadre et en élaborant un modèle de plus en plus complexe des cratons de l'Archéen, des microcontinents de l'Archéen/Protérozoïque et de la croûte juvénile du Paléoprotérozoïque qui met en évidence l'existence d'une douzaine de nouveaux microcontinents allant d'entités péricratoniques à des éléments exotiques en rubans au sein d'une mosaïque autrefois considérée comme formée de grandes masses cratoniques soudées par des orogènes paléoprotérozoïques. Ce portrait émergent soulève d'autres questions pour les futures études sur le Nord, particulièrement en ce qui concerne la granularité de la subdivision des plus grands blocs, l'incidence des énigmatiques orogènes du Paléoprotérozoïque initial et la dynamique de l'assemblage des terranes exotiques et peu connus.

Abstract: The Geo-mapping for Energy and Minerals (GEM) program was funded between 2008 and 2020 with the aim of advancing geological knowledge of the North to reduce risk for mineral exploration and inform land-use decisions and future management of the North. Twenty-one regional activities were undertaken across Canada's northern shield, spanning northern Prairie Provinces, northern Quebec, Labrador, along with much of Nunavut and Northwest Territories. A further five activities were thematic in nature. Bulletin 612 presents results from 12 of these endeavours, including integrated regional bedrock geoscience studies, geophysical surveys, and basin analyses, as well as thematic thermochronology, geochemistry and large igneous province syntheses. The results highlight that GEM has contributed to new era of understanding of the northern Canadian Shield, expanding its framework substantially and developing an increasingly complex model of Archean cratons, Archean/Proterozoic microcontinents, and juvenile Paleoproterozoic crust that highlights the existence of a dozen new pericratonic to exotic ribbon microcontinents within a mosaic once considered as mostly large cratonic masses welded by Paleoproterozoic orogens. This emerging picture brings additional questions for future northern studies — particularly in the granularity of subdivision of the largest blocks, the impact of enigmatic earliest Paleoproterozoic orogens, and dynamics of assembly of exotic and little-known terranes.

¹Commission géologique du Canada, 601, rue Booth, Ottawa (Ontario) K1A 0E8

*Auteur correspondant : S.J. Pehrsson (courriel : sally.pehrsson@nrcan-mcan.gc.ca)

INTRODUCTION

Le programme Géocartographie de l'énergie et des minéraux (GEM) de la Commission géologique du Canada (CGC) de 2008 à 2020 a été entrepris pour faire progresser les connaissances géologiques sur le Nord, dans le but de réduire les risques liés à l'exploration minérale, d'éclairer les décisions relatives à l'utilisation des terres et d'atteindre un équilibre entre la conservation et la mise en valeur responsable des ressources (Geological Survey of Canada, 2018). La recherche géoscientifique sur le substratum rocheux à l'appui de ces objectifs a été entreprise dans le nord du Bouclier canadien, qui constitue la zone de pergélisol discontinu dans le nord des provinces des Prairies et du Québec, au Labrador ainsi que dans une grande partie du Nunavut et des Territoires du Nord-Ouest. Le programme a été réalisé en partenariat avec le Bureau géoscientifique des Territoires du Nord-Ouest (la Commission géologique des Territoires du Nord-Ouest depuis 2015), la Commission géologique de la Saskatchewan, les Levés géologiques du Manitoba, le Bureau géoscientifique Canada-Nunavut, le ministère de l'Énergie et des Ressources naturelles du Québec et la Commission géologique de Terre-Neuve-et-Labrador, ainsi qu'avec les résidents du Nord, les établissements du Nord, le milieu universitaire et l'industrie. L'objectif sous-jacent des activités menées était de combler les importantes lacunes dans les connaissances géoscientifiques sur le nord du Bouclier canadien, lesquelles découlaient d'une combinaison de facteurs liés à l'échelle et à l'ancienneté de la cartographie antérieure, de la complexité géologique, de l'exposition et de l'accès. Au cours des deux phases du programme GEM (2008-2013 et 2013-2020), plus de 40 chercheurs universitaires et 9 boursiers postdoctoraux ont reçu du financement, et plus de 50 mémoires de premier cycle et d'études supérieures ont été réalisés, en lien avec des études couvrant près d'une douzaine de subdivisions lithotectoniques actuelles du nord du Bouclier canadien (fig. 1).

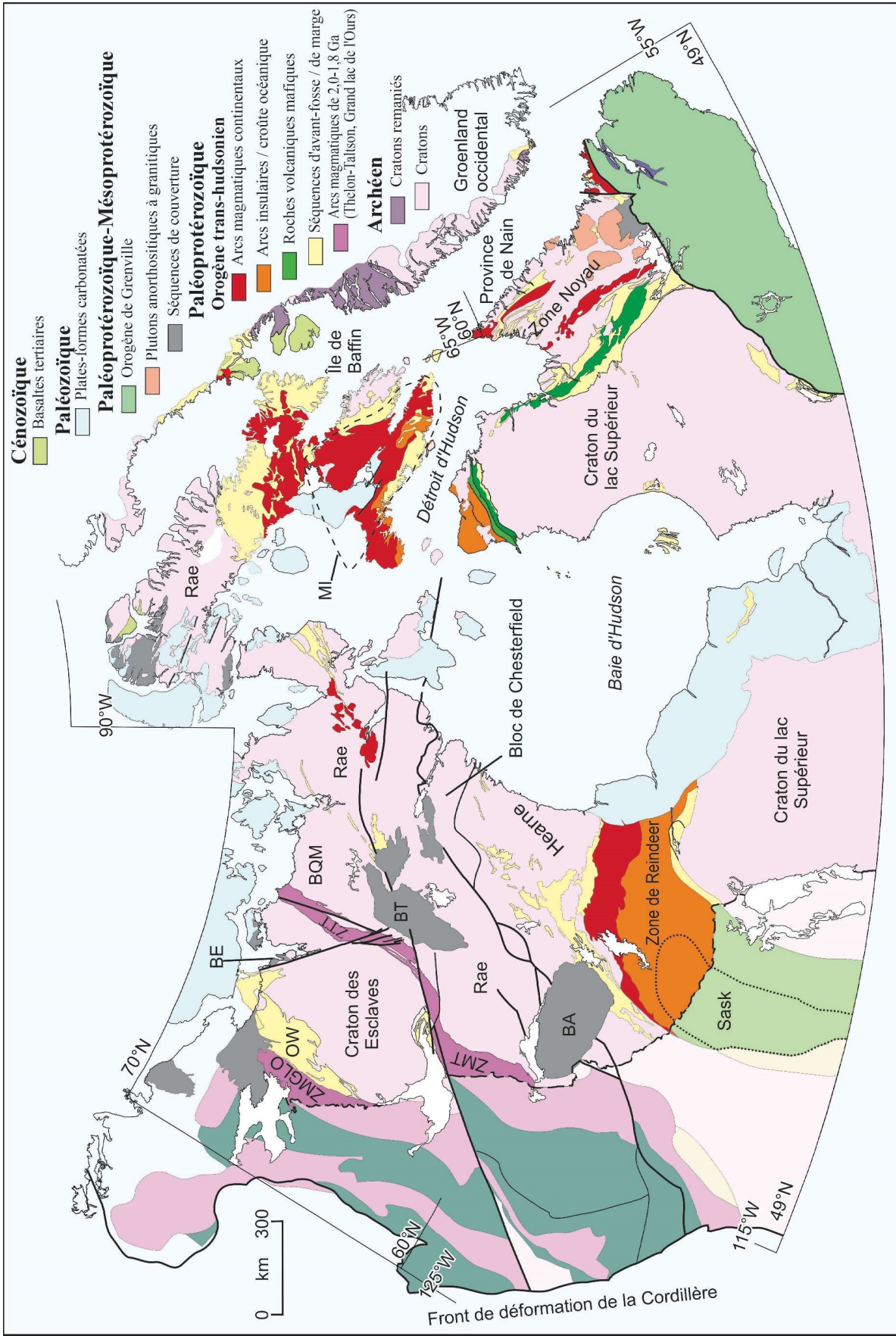
Le Bulletin 612 de la CGC résume les progrès réalisés dans la compréhension de la géologie du substratum rocheux dans bon nombre des parties les moins connues du nord du Bouclier canadien, grâce aux recherches sur le terrain ou en laboratoire menées dans le cadre du programme GEM. Il rassemble les conclusions de 14 études distinctes (ci-après appelées *activités*) afin de présenter un aperçu cohérent de l'évolution tectonique du nord du Bouclier canadien et de son potentiel métallogénique. Le bulletin comprend 10 synthèses régionales sur le substratum rocheux, suivies de 4 synthèses thématiques à l'échelle du bouclier. Elles sont fondées sur plus de 50 articles de revues scientifiques et documents de recherche, des rapports et des compilations de données diffusées sous forme de dossiers publics, notamment sur la lithogéochimie, la géochronologie et la géophysique.

Dans les sections suivantes, nous examinons brièvement : 1) l'état des connaissances sur le nord du Bouclier canadien avant les recherches du programme GEM; 2) les principales questions scientifiques abordées par le programme GEM sur le nord du Bouclier canadien; et 3) les principaux résultats régionaux et thématiques présentés dans ce volume. Le tableau 1 offre une vue synthétique des projets menés dans le cadre du programme GEM. Le tableau 2 présente les principales divisions lithotectoniques, nouvelles ou révisées, ainsi que la compréhension scientifique du nord du Bouclier canadien acquise grâce au programme GEM. Bien que ces documents ne constituent pas un aperçu exhaustif des résultats du programme GEM pour le nord du Bouclier canadien, ils présentent une synthèse préliminaire des résultats de recherche et mettent en évidence les questions en suspens pour les études futures.

LE NORD DU BOUCLIER CANADIEN ET LE PROGRAMME GEM

L'évolution, l'assemblage et l'architecture du Bouclier canadien (fig. 1), le cœur précambrien de la masse continentale du Canada, ont été étudiés pendant plus d'un siècle afin de comprendre sa richesse minérale et son histoire géologique diversifiée, qui s'étend sur plus de trois milliards d'années. La cartographie régionale de même que les études de la formation de la croûte terrestre et de l'évolution tectonothermique réalisées par nombre d'instituts de recherche et de services géologiques ont étayé cette

Figure 1. Carte lithotectonique du Bouclier canadien (*modifiée d'après* Corrigan et al., 2018) et des bassins du Précambrien adjacents au début du programme Géocartographie de l'énergie et des minéraux. Abréviations : BA = bassin d'Athabasca; BE = bassin d'Elu; BQM = bloc de Queen Maud; BT = bassin de Thelon; MI = terrane de Meta Ignognita; OW = orogène de Wopmay; ZMGLO = zone magmatique du Grand lac de l'Ours; ZMT = zone magmatique de Taltson; ZTT = zone tectonique de Thelon.



compréhension, tout comme la recherche géophysique axée sur la croûte et le manteau terrestres (Clowes et al., 1999). Cependant, les études sur le terrain ont été limitées sur le plan spatial par certains aspects pratiques en matière d'accès et d'exposition. Par conséquent, les connaissances sur les cratons et les orogènes constituants étaient beaucoup plus étendues et approfondies au sud de 60° N (p. ex., Province du lac Supérieur, orogène de Grenville et orogène trans-hudsonien; fig. 1) ou à proximité des grands corridors de transport du Nord (p. ex., Province des Esclaves, orogène de Wopmay, zone magmatique du Grand lac de l'Ours).

Le Bouclier canadien représente plus de 50 % de la masse continentale du Canada et forme le cœur du paléocontinent Laurentie, un collage en grande partie paléoprotérozoïque de cratons archéens, de microcontinents et de systèmes d'arcs plus jeunes qui se sont initialement réunis vers 1,8 Ga (Hoffman, 1988). Le Bouclier canadien joue un rôle important sur deux plans : 1) géologique, en raison des progrès fondamentaux réalisés dans la compréhension des processus tectoniques du Précambrien après des décennies de recherches financées sur le terrain; et 2) économique, en raison de son statut de principal contributeur à la production minérale du Canada.

Le nord du Bouclier canadien, principal centre d'intérêt du programme GEM, est composé de cratons archéens, de nombreux microcontinents et coeaux crustaux, et d'un volume moindre de croûte juvénile du Paléoprotérozoïque, tous recouverts par des séquences de couverture cratonique du Paléoprotérozoïque et du Mésoprotérozoïque (fig. 1). Les six principaux cratons – des Esclaves, de Rae, de Hearne, du lac Supérieur et de Nain, ainsi que celui de Mackenzie, qui est enfoui – présentent des marges passives ou des séquences de marge continentale âgées de 2,5 à 2,1 Ga, et ont été réunis et remaniés à divers degrés au cours des orogénèses de Taltson-Thelon, de Snowbird, trans-hudsonienne, de Wopmay et du Nouveau-Québec entre 2,0 et 1,8 Ga (Eglington et al., 2013). Ce cadre de base de cratons distincts délimités par des orogènes paléoprotérozoïques a d'abord été défini dans l'article *United Plates of America* d'Hoffman (1988) et dans un article connexe du même auteur (Hoffman, 1990) et enrichi par des progrès majeurs provenant des innovations en matière de datation isotopique et de géophysique. Des vagues successives de programmes de recherche par les gouvernements et le milieu universitaire entre 2000 et 2010, comme le Projet de la marge du Bouclier du CARTNAT, le Projet de la Province de Churchill occidentale du CARTNAT, le programme EXTECH et, sans doute le plus important, le projet LITHOPROBE (Percival et al., 2012), ont contribué à élargir considérablement ce cadre. Entre autres, la reconnaissance et l'incorporation de microcontinents, comme le bloc de Chesterfield et le craton de Sask (fig. 1, tableau 2), de même que le classement des orogènes en catégories, ont permis d'approfondir notre compréhension de cette mosaïque complexe d'orogènes de collision classiques (p. ex., orogène de Wopmay, orogène trans-hudsonien-zone de Reindeer) et d'orogènes d'accrétion (orogène de l'Alberta Est, orogène de Snowbird), qui présentent des structures s'étendant à la croûte terrestre et au manteau supérieur largement analogues à celles d'orogènes plus jeunes (Clowes et al., 1999). L'intégration de l'histoire de la croûte terrestre à la caractérisation sophistiquée de l'architecture sous-continentale a permis d'affiner davantage ce modèle (Snyder et Kjarsgaard, 2013).

Ces avancées ont été réalisées dans le contexte d'une décennie où notre compréhension de l'évolution de la Terre au cours de l'Archéen et du Paléoprotérozoïque a rapidement été transformée (Reddy et Evans, 2009). De nombreux chercheurs ont adhéré à une forme moderne de tectonique des plaques qui s'opérait déjà en grande partie vers 1,9 Ga (Condie et Kröner, 2008), mais une étude controversée a étendu son applicabilité à 2,5 Ga ou à des périodes plus anciennes (Stern, 2020). Le grand épisode d'oxygénation survenu au début du Paléoprotérozoïque marque la première augmentation importante de la concentration d'oxygène dans l'atmosphère, qui atteignait environ la moitié de la concentration actuelle vers 2,3 Ga (Lyons et al., 2014), après une baisse importante de la température du manteau (Korenaga, 2008). Elle chevauche dans le temps d'autres grands événements planétaires, comme le premier épisode de terre boule de neige (Kopp et al., 2005; Hoffman, 2013) et les déviations de la composition isotopique du carbone dans l'eau de mer (Eguchi et al., 2022). Une accalmie dans l'ajout de croûte juvénile constaté dans les roches conservées, ce qui est qualifié de « lacune magmatique » vers 2,3 Ga, témoignerait selon Condie et ses collaborateurs (Condie et al., 2009) d'un ralentissement ou d'un arrêt de la convection mantellique qui aurait pu déclencher une tectonique des plaques moderne après 2,2 Ga. Cette interprétation n'est toutefois pas universellement acceptée (p. ex., Pehrsson et al., 2014a). La reconstitution des supercratons et supercontinents de l'Archéen et du Paléoprotérozoïque commençaient à être effectuée avec un degré de confiance croissant (Bleeker, 2003; Salminen et al., 2021). D'autres progrès importants ont été réalisés grâce à l'étude de l'histoire précoce de la Terre (Reimink et al., 2016; Shimojo et al., 2016) et à la multiplication des études de la lithosphère du nord du Bouclier canadien (Canil, 2008; Pearson et Witting,

2014), par exemple, la constatation que des quilles cratoniques de l'Archéen étaient en partie refertilisées par l'assemblage du Paléoprotérozoïque, mais qu'elles enregistraient néanmoins certaines des premières indications d'un retour de l'eau de mer au manteau dans les signatures isotopiques de diamants archéens (Pearson et al., 2014).

Comme il en a été fait mention précédemment, une compréhension générale de certaines parties du nord du Bouclier canadien avait été établie avant la mise en œuvre du programme GEM, mais les connaissances essentielles à la définition des processus orogéniques et du potentiel métallogénique régional sont demeurées insuffisantes. De grandes parties du Bouclier canadien sont demeurées non subdivisées et mal encadrées, et même dépourvues d'une cartographie à une échelle de 1/250 000. L'architecture globale de l'orogène trans-hudsonien et de l'orogène de Taltson-Thelon, en particulier leurs arrières-pays, était incomplète, et le nombre, l'origine et la composition lithotectonique des microcontinents enchâssés dans les orogènes paléoprotérozoïques étaient mal compris, particulièrement à l'ouest du craton des Esclaves et à l'ouest de la baie d'Hudson. Des précisions concernant la topologie, les paramètres qui contrôlent le magmatisme et l'âge des principales zones de suture sont demeurées insuffisantes pour résoudre certaines controverses, comme la nature par accréation ou par collision interne des orogènes de Snowbird et de Taltson-Thelon, lesquels avaient par ailleurs été interprétés comme des zones de suture du Néoarchéen au Paléoprotérozoïque initial. Même les orogènes cartographiés plus en détail, comme celui de la zone du Grand lac de l'Ours-Wopmay, recelaient des énigmes, notamment pour ce qui concerne la genèse du terrane précoce de Hottah et l'étendue du craton des Esclaves sous l'orogène de Wopmay. À l'échelle du craton, la corrélation des domaines de part et d'autre de la baie d'Hudson demeure un obstacle à l'évolution des modèles.

Le programme GEM

Avec l'objectif ambitieux d'achever une carte à résolution grossière du substratum rocheux du Nord pour 2020, le programme GEM visait à combler les lacunes les plus urgentes en matière de connaissances sur la composition, l'évolution et l'assemblage du nord du Bouclier canadien. Un examen de l'ensemble des connaissances sur le Nord a révélé des lacunes persistantes et importantes dans les connaissances géoscientifiques relatives aux structures géologiques de surface et souterraines et aux systèmes terrestres au fil du temps, particulièrement dans le craton de Rae et la Zone noyau (fig. 1). Cette situation est attribuable à l'insuffisance de travaux antérieurs de cartographie du substratum rocheux ainsi qu'à la complexité géologique, à l'exposition limitée et à l'accès restreint. Souvent, la situation est exacerbée par le manque de données géochimiques, géochronologiques ou isotopiques modernes. Les cratons ayant fait l'objet d'études plus récentes ou les secteurs possédant un accès routier étendu (c.-à-d., les provinces des Esclaves et du lac Supérieur) ne faisaient pas partie des principales cibles du programme GEM, mais ils ont été inclus dans les évaluations thématiques générales du projet trans-GEM. La formation et l'évolution du craton des Esclaves sont résumées dans un livre soutenu par le programme GEM (Helmstaedt et al., 2021).

La première phase du programme GEM dans le nord du Bouclier canadien comprenait huit activités régionales centrées sur la partie continentale de la Province de Churchill et la zone du Grand lac de l'Ours-Wopmay, ainsi que des études thématiques approfondies portant sur les diamants et l'uranium (2008-2013; tableau 1; fig. 2, 3). L'objectif commun des activités régionales était d'améliorer la compréhension géoscientifique et les modèles géologiques des terranes de l'Archéen et du Paléoprotérozoïque qui ont le potentiel de contenir des métaux communs et précieux, des minéraux critiques et précieux, de la pierre à sculpter et des agrégats. Les recherches comprenaient la réalisation d'une cartographie géologique-cadre, d'une cartographie thématique, de levés géophysiques aéroportés, de levés géochimiques régionaux et d'une variété d'études géoscientifiques connexes, notamment lithogéochimiques, isotopiques et géochronologiques. Des recherches sur les diamants ont été menées dans le craton des Esclaves et dans les corridors baie Repulse-presqu'île Boothia et presqu'île Melville-nord-ouest de l'île de Baffin du craton de Rae. Les recherches sur l'uranium ont été concentrées dans le nord du bassin d'Athabasca et du craton de Rae ainsi que dans la région du lac Cinquante dans le bloc de Chesterfield (fig. 1).

L'exercice « Les frontières de la géocartographie », mené de 2010 à 2012, était une opération majeure de reconnaissance et de travail documentaire qui avait pour but d'accéder aux données non numériques des premiers grands projets de cartographie de reconnaissance menés dans le Nord au cours des années 1950 et 1960, à savoir les opérations Keewatin, Bathurst, Baker, Wager et Thelon (Harris et al., 2013). Par la suite, les régions de Rae, d'Hudson-Ungava et de Baffin ont été définies comme les principales zones

Tableau 1. Projets du programme GEM (2008-2020) exécutés dans le nord du Bouclier canadien et éléments lithotectoniques sur lesquels les recherches étaient concentrées.

Projet	Administration	Région géologique	Publications choisies : rapports d'activités ou synthèses	Levés de soutien
Phase 1 (2008–2013)				
Île Great-Grand Nord	Manitoba	Craton de Hearne	Rayner, 2010; Kremer et al., 2011	aéromagnétique
Presqu'île Melville	Nunavut-Kitikemeot	Craton de Rae	Corrigan et al., 2013	aéromagnétique, MT, géochimique
Péninsule Cumberland	Nunavut-Qikiqtani	Craton de Rae	Sanborn-Barrie et Young, 2011; Whalen et al., 2012	aéromagnétique
Péninsule Hall	Nunavut-Qikiqtani	Craton de Rae	Skipton et al., 2013; Rayner, 2014	aéromagnétique, MT
Bassin de Thelon Nord-Est	Nunavut-Kivalliq	Craton de Rae	Jefferson et al., 2011, 2015, 2022, le présent volume	aéromagnétique, gravimétrique
Régions pionnières de GEM	Nunavut/Territoires du Nord-Ouest	Province de Churchill	Pehrsson et al., 2014a	aéromagnétique, gravimétrique
Opération GEM	Nunavut/Territoires du Nord-Ouest	Province de Churchill	Pehrsson et al., 2014b	aéromagnétique, gravimétrique
Chesterfield	Nunavut-Kivalliq	Bloc de Chesterfield	Pehrsson et al., 2014b, c	aéromagnétique, gravimétrique
Zone du Grand lac de l'Ours-orogène de Wopmay	Territoires du Nord-Ouest	Zone du Grand lac de l'Ours-orogène de Wopmay	Craven et al., 2013; Corriveau et al., 2015	aéromagnétique, gravimétrique, MT
Île Victoria	Nunavut-Kitikemeot	Archipel Arctique	Rainbird et al., 2015; Bédard et al., 2016	
Île Southampton	Nunavut-Kivalliq	Craton de Rae	Sanborn-Barrie et al., 2009, 2018	
Phase 2 (2013–2020)				
Rae Sud	Territoires du Nord-Ouest	Craton de Rae Sud	Pehrsson et al., 2015a, b, c; Percival et al., 2016	aéromagnétique, géochimique
Chantrey-Thelon-Montresor	Nunavut-Kitikemeot	Orogène de Thelon et craton de Rae Nord-Central	Berman et al., 2015a, b; 2016, 2018	aéromagnétique, MT, gravimétrique, géochimique
Lac Tehery-baie Wager	Nunavut-Kivalliq	Craton de Rae Central	Wodicka et al., 2016, 2017	aéromagnétique, MT, gravimétrique, géochimique
Inlet Elu	Nunavut-Kitikemeot	Craton des Esclaves	Ielpi et al., le présent volume	
Zone Noyau	Québec, Labrador	Province de Churchill Sud-Est	McClenaghan et al., 2014; Corrigan et al., 2015, 2016	aéromagnétique, géochimique
Bassins mésoprotérozoïques	Territoires du Nord-Ouest	Province de l'Ours	Rainbird et Davis, le présent volume	
Circum-Ungava	Québec, Nunavut	Zone de Reindeer, ceinture de Cape Smith	Corrigan et al., 2021	
Baffin Nord	Nunavut-Qikiqtani	Craton de Rae Nord	Saumur et al., 2018; Skipton et al., 2017, 2019	aéromagnétique
Baffin Sud	Nunavut-Qikiqtani	Terrane de Meta Incognita	Rayner et al., 2014	aéromagnétique
Boothia-Somerset	Nunavut-Qikiqtani	Craton de Rae Nord	Sanborn Barrie et al., 2016, 2018, 2019	aéromagnétique
Études thématiques ou trans-GEM				
Les ressources en uranium du Nord canadien	Saskatchewan, Nunavut	Cartons de Rae et de Hearne	Jefferson et al., 2013; le présent volume	
Diamants	Territoires du Nord-Ouest, Nunavut	Cratons des Esclaves et de Rae		télésismique
Compilation des GPI	Diverse	Nord du Bouclier canadien	Buchau et Ernst, 2013	
Géochimie de la Suite de Snow Island	Territoires du Nord-Ouest, Nunavut	Craton de Rae/bloc de Chesterfield	Peterson et al., le présent volume	
Thermochronologie de basse température	Diverse	Tout le NBC et zone de Reindeer	Kellett et al., le présent volume	
Abréviations : GPI= grande province ignée; MT=magnétellurique; NBC=nord du Bouclier canadien				

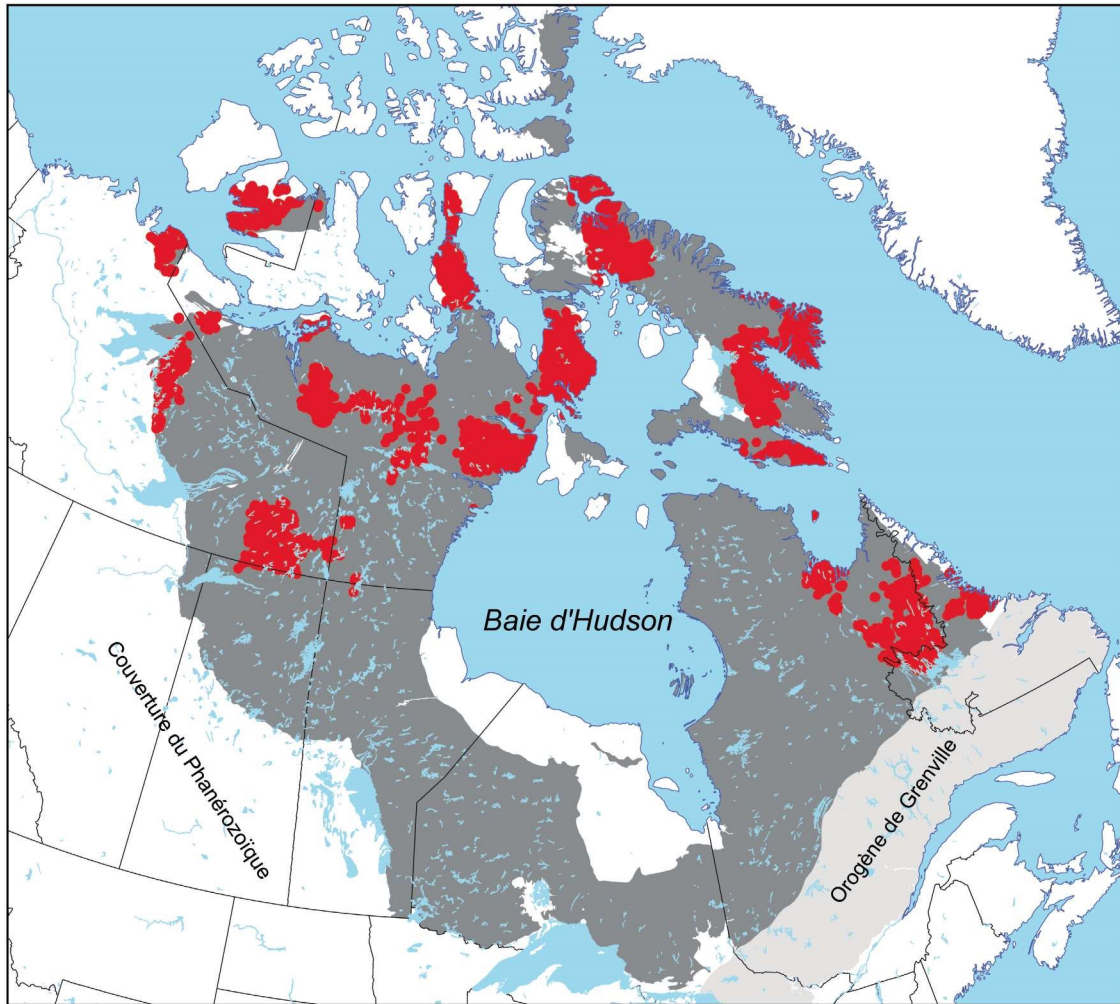


Figure 2. Répartition des projets du programme GEM dans le nord du Bouclier canadien illustrée par l'emplacement des stations (en rouge). La région en gris foncé représente la partie exposée du nord du Bouclier canadien.

d'intérêt pour la deuxième phase du programme GEM (2013-2020), ce qui a élargi la portée du programme à d'autres parties du nord du Bouclier canadien. Dix nouveaux projets ont été axés sur les parties les plus méconnues du Bouclier canadien, notamment le nord, le centre et le sud du craton de Rae, la Province de Churchill Sud-Est au Québec et au Labrador, l'orogène trans-hudsonien dans le sud de l'île de Baffin, l'orogène de Thelon dans les Territoires du Nord-Ouest, les terranes et bassins protérozoïques circum-Ungava, et les bassins du Paléoprotérozoïque et du Mésoprotérozoïque surmontant la zone magmatique du Grand lac de l'Ours et le craton des Esclaves (tableau 1; fig. 2, 3). Les projets à l'échelle des régions pionnières (c.-à-d. le craton de Rae Sud et la région du lac Tehery-baie Wager, généralement une cartographie à l'échelle de 1/250 000) avaient pour objectif de fournir des connaissances de base sur la répartition des principales unités lithologiques, de documenter leur histoire géologique et d'effectuer une évaluation préliminaire de leur potentiel économique. Des activités propres à un district ou à un orogène (p. ex., Chantrey-Thelon, Zone noyau) ont été menées à une échelle plus détaillée pour résoudre des questions précises, comme la genèse des architectures établies. Toutes les activités régionales portaient sur l'architecture orogénique et cratonique, les limites des domaines en trois dimensions et le potentiel minéral par rapport à celui de cratons mieux connus comme ceux du lac Supérieur ou de Yilgarn. Les recherches thématiques connexes comprenaient de nouvelles compilations et synthèses des grandes provinces ignées et de la thermochronologie de basse température dans le Nord, y compris le nord du Bouclier canadien, et de la Suite de Snow Island dans le craton de Rae et le bloc de Chesterfield.

Les résultats préliminaires du programme GEM ont été diffusés au moyen de multiples articles dans la série des Recherches en cours, de rapports d'activités dans la série des Dossiers publics, de rapports d'activités du Bureau géoscientifique Canada-Nunavut et de publications sommaires dans des revues scientifiques (tableau 1). De nouvelles études géophysiques (levés aéromagnétiques, gravimétriques, magnétotelluriques) ou géochimiques (sédiments et eau de lac et de ruisseau; voir McClenaghan et al., 2022) à l'échelle régionale faisaient partie intégrante de nombreuses activités (tableau 1). Toutes ces ressources se trouvent dans la base de données GEOSCAN et l'Entrepôt de données géophysiques de RNCAN. Les études des formations superficielles du programme GEM qui chevauchent le nord du Bouclier canadien sont incluses dans le Bulletin 611 (McMartin, 2023) et les résultats des études portant sur l'île de Baffin sont présentés dans le Bulletin 608 (Dafoe et Bingham-Koslowski, 2022).

ARTICLES DU BULLETIN 612

Synthèses régionales sur le substratum rocheux

Zone magmatique du Grand lac de l'Ours

Corriveau et Potter (le présent volume) présentent la minéralisation contenue dans la zone magmatique du Grand lac de l'Ours (d'env. 1,86 à 1,78 Ga) comme étude de cas afin de définir des empreintes géologiques et géophysiques propres aux systèmes à oxydes de fer-cuivre-or (IOCG), un important système de minéralisations associé au magmatisme d'arc calco-alcalin et shoshonitique. Pour ce faire, ils commencent par offrir une compilation des gisements canadiens et mondiaux d'IOCG, de leurs géométries, de leurs altérations et de leurs teneurs en métaux, puis ils se servent de l'approche des systèmes minéralisateurs comme cadre d'exploration. Ils mettent à l'essai et peaufinent des méthodes de recherche dans les zones éloignées du Bouclier canadien, démontrant comment les principaux critères de prospectivité des gisements d'IOCG de Skirrow (2010) peuvent être appliqués sur les plans de la géodynamique, des faciès, des unités et des voies structurales, afin de créer une représentation spatiale et temporelle de l'architecture des systèmes de fluides d'altération. Ils montrent que la zone magmatique du Grand lac de l'Ours abrite un spectre de systèmes métasomatiques, depuis les corridors d'albite précoces et stériles jusqu'à la minéralisation à oxydes de fer-apatite (\pm terres rares) entraînée par une altération de haute température et à des variantes d'IOCG riches en cobalt et autres métaux critiques (Potter et al., 2013). Ils intègrent de nouvelles connaissances stratigraphiques et structurales acquises à l'échelle du gisement NICO, le plus grand gisement canadien d'IOCG, ainsi que du district historique de Port Radium et de la mine d'uranium de Rayrock pour montrer qu'il existe un lien entre les chapeaux de fer et l'altération albitique dans le toit des intrusions subvolcaniques, une empreinte déterminante et largement applicable à l'exploration.

La synthèse des IOCG du programme GEM démontre que la cartographie de l'altération pétrologique et les levés géophysiques à l'échelle du district peuvent servir à l'élaboration de cibles pour les IOCG. Plus particulièrement, l'intégration de nouvelles techniques de modélisation gravimétrique, tout comme l'utilisation de levés aéromagnétiques pour calculer la pseudogravité, permet de tirer le maximum de connaissances des levés régionaux (Hayward et Oneschuk, 2011; Kiss et Coyle, 2011a-f; Hayward et al., 2013). Des recherches magnétotelluriques connexes dans la zone magmatique du Grand lac de l'Ours ont permis de repérer des conducteurs liés à des zones de préparation du terrain et à de cryptiques limites de lithosphère épaissie, ainsi que d'acquérir une nouvelle compréhension de l'architecture des bassins de recouvrement (Hoggard et al., 2019). Corriveau et Potter terminent par un résumé des recherches collaboratives menées avec d'autres services géologiques nationaux et institutions, et de l'application de leur méthode à la ceinture minérale centrale du Labrador.

Bassin d'Elu

Ielpi et ses collaborateurs (le présent volume) décrivent les systèmes fluviaux du bassin de Kilohigok (de 1,9 à 1,6 Ga) et du bassin d'Elu (de 1,6 à 1,2 Ga), dans l'ouest du Nunavut. Ces bassins ont été étudiés pour la dernière fois dans les années 1970. L'objectif de l'étude était d'examiner la stratigraphie, la sédimentologie et le potentiel économique de ces bassins sédimentaires du Paléoprotérozoïque-Mésoprotérozoïque, en mettant l'accent sur la prospectivité du bassin d'Elu à l'égard des minéralisations d'uranium, stratoïdes ou associées à des discordances. Trois saisons de cartographie sur le terrain ont

mené à la reconnaissance de deux formations de grès terrigènes, toutes deux présentant d'importants intervalles de dépôts éoliens (Rainbird et Ielpi, 2015). En intégrant l'analyse de bassin à l'échelle régionale, ils ont démontré l'existence d'un paléocéoulement dirigé vers l'ouest qui, combiné à la géochronologie des zircons détritiques, a montré que les matériaux sédimentaires provenaient directement de la partie centrale de l'orogène de Thelon (*voir* Berman et al., le présent volume) et que, vers 1,6 Ga, est survenu un important apport de matériaux provenant de l'orogène d'Arrowsmith (de 2,4 à 2,3 Ga), dans la partie orientale du bloc de Queen Maud. Leurs recherches appuient les modèles classiques proposés pour la partie sommitale du bassin de Kilohigok, qui témoignerait de l'existence d'une avant-fosse liée à la collision entre le craton des Esclaves et le craton de Rae. Ces recherches montrent en outre une dénudation par érosion d'une grande partie du relief des orogènes de Thelon et trans-hudsonien au cours d'une période de moins de 200 millions d'années puisque, au moment de la formation du bassin d'Elu, il n'y avait pas de barrière topographique au transport des sédiments au large de la partie ouest du craton de Rae. Ces critères régionaux permettent aux auteurs d'établir une corrélation entre la Formation d'Ellice (bassin d'Elu) et d'autres séquences de grès intracontinentales de même âge du nord du Bouclier canadien, soit les groupes de Barrenland et d'Athabasca surmontant le craton de Rae, ainsi que les groupes de Mountain Lake et de Dismal Lakes surmontant les roches du socle de la zone du Grand lac de l'Ours-orogène de Wopmay. Ielpi et ses collaborateurs sont d'accord avec les modèles précédents selon lesquels ces grès constituent les vestiges d'érosion d'une nappe de grès autrefois plus vaste qui recouvrait le Bouclier canadien. Ils montrent également de façon très pertinente comment ces dépocentres ont évolué pendant l'assemblage et l'existence du supercontinent Nuna, de 1,8 à 1,4 Ga, en reliant la morphologie inhabituelle des chenaux fluviaux aux paléolatitudes tropicales proposées et à une circulation d'alizés plus secs à l'intérieur d'un supercontinent précambrien non végétalisé.

Région de Chantrey-Thelon

Berman et ses collaborateurs (le présent volume) exposent les résultats pour la zone tectonique de Thelon (TTZ) centrale (fig. 1), une entité géologique majeure du nord du Bouclier canadien qui suscite une controverse importante depuis sa définition initiale. D'après des modèles contradictoires, cette zone serait apparue sous la forme d'un arc magmatique marquant la subduction et la suture entre les cratons des Esclaves et de Rae, de 2,0 à 1,95 Ga (Hoffman, 1988), ou elle représenterait plutôt une zone magmatique principalement intracontinentale qui se serait formée loin d'une bordure de plaque active, mais près d'une suture de collision antérieure (d'env. 2,4 à 2,3 Ga) (Chacko et al., 2000). Selon cette dernière interprétation, il s'agirait d'un prolongement direct de la zone magmatique de Taltson (de 1,97 à 1,90 Ga), entre le craton de Rae et le terrane de Buffalo Head (fig. 3). Cependant, d'autres modèles associent le magmatisme de la zone tectonique de Thelon à d'autres sutures enfouies du sud-ouest du Bouclier canadien (Card et al., 2014).

Les auteurs présentent un aperçu de six nouveaux sous-domaines de la zone tectonique de Thelon découlant d'une cartographie du substratum rocheux échelonnée sur deux ans, qui a été accompagnée d'études géochronologiques, pétrogénétiques et tectonothermiques. Les résultats montrent que la suite magmatique de Thelon précoce (de 2,03 à 1,96 Ga) présente des signatures géochimiques compatibles avec un cadre de marge de convergence et des compositions isotopiques de l'oxygène qui tendent vers des valeurs du manteau semblables à celles observées dans les arcs continentaux du Cénozoïque. De nouvelles données de datation Sm-Nd indiquent que la zone tectonique de Thelon s'est construite en partie sur la croûte ancienne du bloc de Queen Maud qui s'était détachée à la suite d'un rifting ayant mené à la formation d'un microcontinent péricratonique (domaine de Duggan Lake, 3,2-3,1 Ga). Un tel cadre géodynamique passant de la phase de rift à celle de la dérive explique la provenance et la composition d'une séquence volcanosédimentaire nouvellement reconnue, de faible degré métamorphique et contemporaine de la zone tectonique de Thelon, qui présente un potentiel quant à la présence de sulfures massifs volcanogènes de milieu d'arrière-arc (ceinture supracrustale d'Ellice River), séquence qui a été renversée et migmatisée au cours d'un important épisode de fort métamorphisme concomitant à un magmatisme leucogranitique de 1,93 à 1,90 Ga. Ces données laissent entendre qu'il n'y a pas de corrélation directe entre la zone tectonique de Thelon et la zone magmatique de Taltson, comme le prescrit le modèle de batholithe orogénique intracratonique, et appuient le modèle de Hoffman (1988) d'une origine liée à un arc paléopro-térozoïque, ce qui souligne l'importance de disposer de données pétrogénétiques et isotopiques détaillées pour comprendre l'assemblage du nord du Bouclier canadien dans toute sa complexité.

Ceinture de Montresor

Il est difficile de comprendre l'évolution tectonique au Paléoprotérozoïque de la Province de Churchill remaniée en raison de son histoire polyorogénique, mais l'une des voies les plus fructueuses pour élucider son architecture postérieure à 2,3 Ga consiste à étudier les ceintures sédimentaires du Paléoprotérozoïque qui délimitent la paléosurface du Néoarchéen terminal des accumulations subséquentes. Comme bon nombre des assemblages paléoprotérozoïques du nord du craton de Rae, la ceinture de Montresor, située dans le centre nord de ce même craton, a été cartographiée pour la dernière fois dans le cadre d'études de reconnaissance à la fin des années 1970 et dans les années 1980, après quoi elle a été relativement peu explorée (Rainbird et al., 2010). Percival et ses collaborateurs (le présent volume) résument les résultats de deux saisons de recherches sur le terrain et présentent un nouveau modèle pour l'évolution du bassin.

La ceinture de Montresor se compose de roches détritiques et de roches carbonatées conservées dans une structure synforme ouverte à l'histoire complexe, comme le démontrent de nouvelles données géologiques et géophysiques. Ce bassin de plate-forme initialement vaste se divise en un groupe inférieur fortement imbriqué et de degré de métamorphisme élevé, composé de grès, de mudstone et de roches carbonatées qui se sont déposés vers 2 194 à 2 045 Ma, et en un groupe supérieur de degré de métamorphisme plus faible, postérieur à environ 1 924 Ma, constitué d'un mélange de roches détritiques et de roches carbonatées exposées dans une structure synforme plus simple. Les modes de la provenance des sédiments dans le groupe supérieur correspondent à une source située dans le bloc de Queen Maud. Avec son dépôt juste avant la reprise de l'orogénèse de Thelon vers 1,92 à 1,89 Ga, ce groupe représente un dépôt de milieu s'étendant de l'avant-pays à l'avant-fosse, qui s'est formé au cours des phases de déclin du magmatisme de Thelon, à la suite de la collision entre le craton des Esclaves et le craton de Rae. La comparaison de la géométrie et de l'âge de la déformation et du métamorphisme de la séquence inférieure imbriquée avec la géométrie plus simple du mélange de roches carbonatées de rampe et de roches détritiques de la séquence supérieure laisse supposer une transition dans le temps à une déformation polyphasée de source éloignée liée à l'orogénèse trans-hudsonienne de 1,89 à 1,80 Ga. Cette ceinture fait partie d'une série de séquences de marge qui se sont déposées après l'orogénèse d'Arrowsmith échelonnée de 2,5 à 2,3 Ga (Berman et al., 2013). Elle illustre une géométrie régionale qui est essentielle pour comprendre le style structural de 1,9 à 1,8 Ga, notamment la formation déterminante de failles de décollement de 1 848 à 1 837 Ma liée à une minéralisation hydrothermale (Percival et Tschirhart, 2017). Percival et ses collaborateurs démontrent que la ceinture de Montresor se compare favorablement à d'autres ceintures semblables au nord de Baker Lake qui montrent un chevauchement important du socle granitique et du quartzite de la séquence basale. Cette géométrie, également caractéristique des régions de Woodburn et de Thelon Nord-Est, complique la reconnaissance de la séquence stratigraphique originale du Paléoprotérozoïque, mais met également en évidence l'étendue transversale du remaniement de l'orogène trans-hudsonien très loin dans son arrière-pays de la plaque supérieure constituée du craton de Rae.

Les travaux de recherche en cours visent à comprendre l'incidence de la géométrie structurale à l'échelle régionale sur les styles de minéralisation et à étudier les sphérules d'impact reconnues dans le mudstone d'un complexe de mur structural. Déterminer la nature et l'origine des sphérules sera probablement important pour résoudre les questions liées à l'évolution atmosphérique et biologique de la Terre, leur formation étant survenue juste après la transition à un environnement nouvellement oxygéné.

Région du bassin de Thelon Nord-Est

Le cadre géodynamique du bassin intracontinental de Thelon du Paléoprotérozoïque tardif est important en raison de sa relation avec le bassin d'Athabasca du même âge (de 1,7 à 1,4 Ga), qui est l'hôte de gisements d'uranium liés à une discordance de classe mondiale (fig. 1). Jefferson et ses collaborateurs (le présent volume) offrent un résumé complet de la géologie et de la métallogénie du bassin de Thelon Nord-Est, centrée sur le lac Aberdeen, au Nunavut, et de son socle environnant remontant au Néoarchéen et au Paléoprotérozoïque précoce. Cette région abrite des gîtes connus d'uranium dans le socle, mais le manque de connaissances à leur sujet ne permettait pas d'en contextualiser la formation. De la cartographie géologique, ainsi que des études de géochronologie U-Pb, de géophysique et de géologie structurale ont permis de parfaire et d'élargir les connaissances sur la répartition structurale et chronologique des séquences du socle du Néoarchéen présentant une prospectivité uranifère. De plus, elles définissent et permettent de mettre en corrélation les séquences de couverture du Paléoprotérozoïque qui flanquent le bassin de Thelon et s'étendent sous celui-ci, et élucident l'architecture du socle qui a influencé les structures minéralisatrices réactivées.

La cartographie détaillée des grès quartzeux, lithiques et arkosiques contenus dans le bassin ainsi que des groupes directement sous-jacents de Wharton et de Baker Lake âgés d'environ 1,83 à 1,75 Ga, de même que de l'architecture complexe du socle des orogènes de Snowbird et trans-hudsonien ont permis de reconnaître de multiples événements diagénétiques qui ont profondément altéré les grès, ainsi que des cassures majeures de la croûte qui étaient jusqu'alors inconnues et vers où convergent les voies de circulation des fluides (Jefferson et al., 2012). Les auteurs montrent que, bien que le bassin de Thelon Nord-Est et le bassin d'Athabasca présentent des histoires diagénétiques et métallogéniques relativement indépendantes sur les plans temporel et spatial, y compris une architecture stratigraphique et des roches hôtes du socle distinctes, le bassin de Thelon, moins exploré, abrite néanmoins des métallotectes uranifères semblables à ceux du bassin d'Athabasca. Une conclusion possible serait que les décalages le long des failles du bassin de Thelon étaient beaucoup plus importants et que la sédimentation était de caractère beaucoup plus proximal dans la région du lac Aberdeen que dans le bassin d'Athabasca, démontrant ainsi comment les strates conservées et les altérations du socle, de même que des horsts majeurs définis par des mesures structurales ou par la géophysique, pointent vers une étendue du bassin de Thelon initialement beaucoup plus grande. Les auteurs avancent que les suites magmatiques de 2,6 Ga, de 1,8 Ga et de 1,75 Ga étaient d'importantes sources d'uranium. Ils mettent l'accent sur la suite ignée de Kivalliq, une série post-tectonique de 1,75 Ga, à laquelle seraient associées une silicification envahissante et la formation initiale de failles avant le dépôt de la Formation de Thelon, et donc de la minéralisation qu'elle renferme. Leur examen a montré que les failles de 1,75 Ga et les failles plus anciennes, ainsi que d'autres failles, ont été réactivées à plusieurs reprises pour régir l'espace nécessaire ainsi que la paléotopographie et pour concentrer l'altération à chlorite+argiles+apatite+uraninite dans les roches du socle autour des gîtes d'uranium, alors que de telles données sont insuffisantes dans le cas de la Formation de Thelon. Dans l'ensemble, leurs travaux comparent les différents cadres géodynamiques de la formation des bassins, le bassin de Thelon étant entièrement situé dans le craton de Rae avec ses séquences de couverture faiblement métamorphisées, et celui d'Athabasca chevauchant la suture de Rae-Hearne où les séquences de couverture conductrices sont fortement métamorphisées sur toute la zone. Jefferson et ses collaborateurs s'écartent des modèles antérieurs qui suggéraient que ces grès étaient des vestiges de l'érosion d'un dépôt sédimentaire autrefois plus vaste qui recouvrait le Bouclier canadien, en ce sens que les bassins qui ont été conservés sont en grande partie des bassins de sédimentation, ce qui réduit au minimum la quantité de sédiments qui se seraient déposés à l'origine entre les grands bassins. Ils permettent d'élucider les différences subtiles, mais importantes, dans les processus diagénétiques et minéralisateurs ainsi que les cibles entre les bassins majeurs.

Craton de Rae Sud

Pehrsson (le présent volume) offre un bref résumé de la géologie du craton de Rae Sud, dans les Territoires du Nord-Ouest, fondé sur une nouvelle synthèse et une nouvelle subdivision élaborées à partir d'un transect cartographique de 400 km recoupant le craton de Hearne, du lac Kasba au lac Porter, au sud-est de la zone de cisaillement du Grand lac des Esclaves. Elle intègre quatre nouvelles cartes à l'échelle de 1/250 000 ainsi que des études géochronologiques U-Pb, isotopiques et tectonométamorphiques pour montrer que le craton de Rae Sud comprend neuf domaines crustaux distincts datés de l'Archéen au Paléoproterozoïque précoce, délimités par des zones de cisaillement à l'échelle de la croûte nouvellement reconnues, qui révèlent une longue histoire de déformation et de réactivation entre 2,5 Ga et environ 1,7 Ga.

Le craton de Rae Sud date principalement du Néoarchéen tardif et présente des preuves de contamination crustale du Paléoarchéen et du Mésoarchéen qui sont limitées aux domaines de l'ouest, lesquels comprennent des roches potentiellement corrélées avec le complexe de socle de Taltson. L'activité tectonométamorphique et magmatique vers 2,5 Ga (orogénèse de MacQuoid) est limitée aux domaines de l'est qui se trouvent à moins de 75 km de la zone tectonique de Snowbird. L'orogénèse d'Arrowsmith (d'env. 2,4 à 2,3 Ga) se manifeste à l'ouest de la zone de cisaillement de Black Bay, où les structures dominantes des grands domaines granulitiques d'échelle régionale rendent compte de la surimpression d'un métamorphisme statique de haute pression vers 1,9 Ga. Après l'orogénèse d'Arrowsmith, des sédiments se sont déposés vers 2,2 à 2,0 Ga en milieu littoral jusqu'en milieu marin franc dans la plupart des domaines, sauf le long de la zone tectonique de Snowbird, où un bassin à regard est s'est formé, dans lequel se sont déposées des roches détritiques et des roches volcaniques, en milieu marin de moyenne à grande profondeur. Un magmatisme étendu au Paléoproterozoïque, se manifestant notamment par des essaims de dykes

mafiques et des complexes stratifiés (d'env. 2,29 à 2,0 Ga) ainsi que par des plutons de type arc (env. 1,9 Ga), révèle une histoire géologique beaucoup plus complexe que celle établie précédemment, notamment en ce qui concerne l'existence d'un remaniement tectonométamorphique au Paléoprotérozoïque causé par les orogènes de Snowbird et trans-hudsonienne, et dont les effets s'observent jusqu'à 300 km à l'ouest de la zone tectonique de Snowbird. Pehrsson propose des corrélations vérifiables de domaines et de structures qui s'étendent au nord de la Saskatchewan et au Nunavut. Elle suggère en outre que la linéarité des domaines crustaux et leur architecture interne complexe sont le résultat des effets combinés de l'orogène de collision d'Arrowsmith à l'ouest et des cycles subséquents d'épaississement et d'effondrement crustal de 1,9 à 1,82 Ga engendrés par l'accrétion du microcontinent de Hearne et la fermeture de l'océan intérieur du supercontinent Nuna.

Région de lac Tehery-baie Wager

Wodicka et ses collaborateurs (le présent volume) donnent un aperçu concis de l'histoire archéenne et protérozoïque de la région de lac Tehery-baie Wager, au Nunavut, qui s'étend à la partie nord du bloc de Chesterfield et au bloc de Repulse Bay du craton de Rae. La cartographie ciblée du substratum rocheux (2012 et 2015-2017), accompagnée d'études de la géochronologie U-Pb, de la géochimie sur roche totale, de la géochimie isotopique Sm-Nd, de la pétrologie métamorphique ainsi que d'études géophysiques, a permis de reconnaître six domaines lithotectoniques, chacun présentant un âge protolithique et des caractéristiques lithologiques, métamorphiques, isotopiques et/ou géophysiques distincts, séparés par des structures à grande échelle. Le domaine de Gordon, du Mésoarchéen au Néoarchéen, est séparé du domaine de Lunan, du Néoarchéen, par une zone de transition comprenant une séquence supracrustale du Néoarchéen (ceinture de Lorillard), des zones d'intense déformation à mouvement inverse et un linéament magnéto-gravimétrique en profondeur. La ceinture de Lorillard de 2,7 Ga et les domaines de Gordon et de Lunan se sont probablement réunis au large du protocraton de Rae, avant que se manifeste le très volumineux magmatisme d'arc de la Suite de Snow Island, de 2,62 à 2,58 Ga (Peterson et al., le présent volume). Le domaine de Kummel Lake et le complexe de Daly Bay du faciès des granulites définissent tous deux des crêtes gravimétriques importantes dans la partie sud de la région de lac Tehery-baie Wager, mais diffèrent sur le plan de l'âge et de la géométrie du sous-sol. D'après la modélisation gravimétrique à l'échelle régionale et les données structurales, le domaine de Kummel Lake du Néoarchéen ressemble à un complexe à noyau métamorphique aux unités faiblement à modérément inclinées vers l'extérieur, tandis que le complexe de Daly Bay du Paléoprotérozoïque présente des marges fortement inclinées vers l'intérieur et a été juxtaposé à des gneiss du faciès des amphibolites du domaine de Gordon par un chevauchement dirigé vers le nord (Tschirhart et al., le présent volume). Entre les zones de cisaillement de Chesterfield et de Wager, deux structures proéminentes d'échelle régionale présentant une activité de longue durée qui s'échelonne de l'Archéen au Paléoprotérozoïque, se trouve le domaine de Douglas Harbour, lequel se caractérise par une zone de plissement et chevauchement de tectonique de socle qui a touché des roches supracrustales paléoprotérozoïques du faciès des amphibolites inférieur et intermédiaire (équivalent du Groupe de Ketyet inférieur de la ceinture de Pennington) et des gneiss du socle du Mésoarchéen et du Néoarchéen. Le domaine d'Ukkusiksalik, situé le plus au nord, est délimité au nord-ouest par un grand massif de monzogranite de la Suite de Snow Island de 2,61 Ga et au sud par la zone de cisaillement de Wager. Ce domaine représente l'étendue la plus au sud-ouest du bloc de Repulse Bay.

Bien que les preuves des événements tectonométamorphiques du Néoarchéen soient conservées localement dans les roches archéennes de la région de lac Tehery-baie Wager, toutes les roches, à l'exception des dykes de Mackenzie du Mésoprotérozoïque, ont été considérablement déformées et métamorphosées pendant l'orogène de Snowbird et/ou l'orogène trans-hudsonienne. Des études en cours visent à élucider le paléocadre tectonique du volcanisme et de la sédimentation de l'Archéen et les processus orogéniques actifs à des niveaux crustaux intermédiaires à profonds dans cette partie du craton de Rae pendant l'assemblage du supercontinent Nuna.

Géophysique régionale

Tschirhart et ses collaborateurs (le présent volume) offrent un aperçu des nouveaux ensembles de données géophysiques pour les régions de neuf projets du programme GEM dans la Province de Churchill occidentale, depuis les presqu'îles Melville et Boothia jusqu'au sud-ouest du craton de Rae et à la zone tectonique de Thelon. Les données acquises par le programme GEM comprennent des données

aéromagnétiques, des données de levés magnétotelluriques à longue période et à large bande, ainsi que des données de levés gravimétriques au sol. L'intégration de ces données aux contraintes quantitatives imposées par les propriétés des roches liées, à la géologie du substratum rocheux, à la géochronologie, à la pétrochronologie et aux données isotopiques a permis de délimiter de nombreux nouveaux domaines internes et terranes ainsi que leur architecture. On a constaté que les principales limites de la croûte terrestre se manifestent sous forme de discontinuités texturales transversales soulignées par des zones démagnétisées, d'anomalies de faible résistivité coïncidant avec des changements dans la structure du manteau, de crêtes magnétiques fortement atténuées associées à une mylonitisation ductile de forte intensité, ou d'une troncature abrupte avec déplacement latéral ou atténuation sur des anomalies curvilignes de plis d'interférence internes.

Des modèles d'inversion tridimensionnelle sont présentés, lesquels laissent supposer que le craton de Rae, qui constituait la plaque supérieure lors de l'orogénèse de Thelon (env. 2,0 Ga), a chevauché de nouveau le craton des Esclaves pendant la poussée continue exercée par la progression des orogènes extérieurs de Wopmay et de Racklan-Forward (d'env. 1,8 à 1,6 Ga). Un thème commun émergeant de plusieurs régions étudiées (ceinture de Montesor, lac Tehery-baie Wager, bloc de Chesterfield, Rae Sud) est que la déformation tardive par failles de détachement en régime extensif est beaucoup plus répandue et étendue dans le craton de Rae, lequel formait l'avant-pays fortement remanié et ramolli thermiquement de plaque supérieure lors de la collision éloignée avec le craton du lac Supérieur.

Il a été démontré que la combinaison des levés gravimétriques au sol et de la modélisation inverse des données de levés magnétotelluriques est particulièrement efficace pour résoudre la formation des principales crêtes gravimétriques d'échelle régionale le long de l'inlet Chesterfield, jadis considérées comme liées à la zone tectonique de Snowbird (1,9 Ga) sur les plans de leur genèse et de leur géométrie. Les crêtes gravimétriques dans la partie sud de la région de lac Tehery-baie Wager ne correspondent pas à une seule suite cohérente d'entités du faciès des granulites de pression modérée à élevée. Ils correspondent plutôt à des domaines distincts déplacés le long d'un chevauchement fortement incliné vers l'est (complexe de Daly Bay) ou d'un décollement faiblement incliné vers le nord (domaine de Kummel Lake) (*voir* Wodicka et al., le présent volume), ce qui illustre l'exhumation de la croûte profonde du craton de Rae par deux processus, à savoir un chevauchement précoce contemporain de la collision et la formation tardive d'un complexe à noyau métamorphique.

Enfin, les ensembles de données géophysiques tirés des activités individuelles ont été combinés aux données régionales existantes, et ont été filtrés par prolongement vers le haut et au moyen de divers autres procédés afin de créer deux grandes mosaïques composites pour la Province de Churchill occidentale, soit une carte de l'anomalie de Bouguer montrant la composante résiduelle du champ total de grande longueur d'onde et une carte du gradient gravimétrique horizontal de l'anomalie de Bouguer en transparence sur les anomalies isostatiques résiduelles de l'anomalie de Bouguer. Ces produits permettront de mieux comprendre l'évolution complexe de l'architecture du nord du Bouclier canadien et son incidence sur la minéralisation.

Grand Nord du Manitoba

Böhm et Rayner (le présent volume) résument les recherches financées par le programme GEM, menées par les Levés géologiques du Manitoba dans le cadre de son initiative de géocartographie du Grand Nord. Cette initiative visait à comprendre la nature, l'évolution et le potentiel minéral du craton de Hearne de l'Archéen, l'un des principaux composants géologiques du Bouclier canadien au Manitoba.

Quatre saisons de travaux sur le terrain, répartis sur plusieurs grandes secteurs compris entre le lac Nejanilini, près de la limite du Nunavut, et l'île Great, à l'ouest de Churchill, ont été menés pour mettre à l'épreuve les corrélations tectonostratigraphiques régionales dans le craton de Hearne, de la Saskatchewan au Nunavut. Les données de levés aéromagnétiques et de rayonnement gamma dans les régions de l'île Great et de la rivière Seal ont permis de définir de nouvelles entités de premier ordre, comme des bassins supracrustaux et des discordances régionales, la fabrique tectonique et des zones de cisaillement, ainsi que des domaines granitoïdes d'importance. Un vaste programme régional de géochronologie U-Pb a mené à la délimitation de deux nouveaux sous-domaines au sein du craton de Hearne ainsi qu'à la reconnaissance de séquences volcaniques et sédimentaires de milieu d'arc et d'arrière-arc du Paléoprotérozoïque non reconnues auparavant (Rayner, 2022). Ce cadre régional radicalement révisé illustre que le craton de Hearne, plutôt que d'être un noyau archéen intact, s'est probablement assemblé au Paléoprotérozoïque

par l'accrétion d'une série de microblocs et d'arcs qui occupaient des positions intermédiaires. La dérivéation d'une vaste suite magmatique du Néoarchéen tardif (de 2 570 à 2 550 Ma) à partir d'une croûte amincie plutôt qu'épaissie indique qu'une partie du collage pourrait s'être assemblée pendant la transition vers l'orogénèse de MacQuoid, autour de 2,55 Ga. Les implications importantes de cette nouvelle architecture stratigraphique et structurale pour la métallogénie régionale comprennent la reconnaissance de quatre séquences métasédimentaires de couverture distinctes, notamment une séquence de marge passive post-2,5 Ga, un ensemble deltaïque marin >2 050-1 984 Ma, et une séquence de flysch-molasse de bassin successeur <1 880-1 764 Ma, contemporaine de l'orogénèse trans-hudsonienne. D'après des comparaisons avec des séquences corrélatives à l'échelle régionale en Saskatchewan et au Nunavut, le potentiel économique de ces divers ensembles sédimentaires comprend des minéralisations d'uranium, d'or ou de métaux rares. Une ceinture de roches vertes du Néoarchéen récemment reconnue dans la région de l'île Great, laquelle renferme des occurrences connues d'or, souligne le potentiel minéral inexploité de la région, tout comme la découverte de vestiges de lithosphère cratonique de 3,5 Ga dans la région de la rivière Seal. Cette dernière découverte montre qu'il existe un potentiel diamantifère favorable dans certaines sections de ce micro-assemblage continental.

Zone noyau

Corrigan (le présent volume) offre une synthèse des recherches du programme GEM menées dans la Province de Churchill Sud-Est au Québec et au Labrador, une région appelée « Zone noyau ». Cette région était auparavant considérée comme un prolongement du craton de Rae de l'Archéen coincé entre les orogènes paléoproterozoïques de Torngat et du Nouveau-Québec, qui ont ultimement soudé les cratons du lac Supérieur et de l'Atlantique Nord (fig. 1). Les données géochronologiques, la cartographie ciblée et les études géoscientifiques de soutien menées dans le cadre du programme GEM, en collaboration avec le ministère de l'Énergie et des Ressources naturelles du Québec et la Commission géologique de Terre-Neuve-et-Labrador, laissent entendre que l'évolution de la Zone noyau à l'Archéen n'est pas liée à celles des principales plaques adjacentes. Une subdivision lithotectonique interne tripartite est proposée, en s'appuyant sur l'évolution distincte de la croûte terrestre au Néoarchéen et au Paléoproterozoïque précoce. Les nouvelles microplaques de George River (de 2,86 à 2,57 Ga), de Mistinibi-Raude (de 2,37 à 1,987 Ga) et de Falcoz River (de 2,89 à 1,9 Ga) sont délimitées par des zones de cisaillement ductile à pendage abrupt d'échelle crustale, interprétées comme des paléosutures. Une exception à ces blocs exotiques est le domaine de Kuujuaq, interprété comme un fragment du craton du lac Supérieur qui en a été séparé par un rifting puis est revenu, accompagné du bloc de George River, par charriage, avant la mise en place du batholite de De Pas. Une nouvelle constatation importante qui renverse les modèles précédents est que l'orogénèse des Torngat était principalement limitée à la Zone noyau et à la marge du craton de l'Atlantique Nord, tandis que le tectonométamorphisme et la déformation s'étendant à une plus vaste étendue régionale sont liés à l'orogénèse du Nouveau-Québec, plus récente, et qu'une tectonique de transpression complexe domine dans la Province de Churchill Sud-Est. La corrélation de la séquence de couverture du bloc de Falcoz River avec le Groupe de Lake Harbour de l'île de Baffin donne à penser qu'elle a été transportée latéralement le long de la marge. La reconnaissance des microplaques et des principales structures de transpression de la Zone noyau aidera à formuler des modèles métallogéniques propres aux différents domaines.

Synthèses thématiques

Suite de Snow Island du Néoarchéen

Peterson et ses collaborateurs (le présent volume) fournissent la première synthèse d'une importante province magmatique du Néoarchéen qui constitue une entité de premier ordre du craton de Rae. La Suite de Snow Island (de 2,62 à 2,58 Ga) s'étend de la région du lac Athabasca à la presqu'île de Melville et à l'île Southampton. Elle comporte des roches plutoniques mafiques à felsiques, avec de plus rares roches volcaniques et sédimentaires subaériennes, préférentiellement conservées sous la couverture paléoproterozoïque. En intégrant la lithogéochimie de près d'une centaine d'échantillons précisément datés de la Suite de Snow Island avec 50 analyses isotopiques Sm-Nd, les auteurs montrent que les différentes phases temporelles de la suite ont des attributs géochimiques distincts. La plus grande partie de la suite est composée de roches granitoïdes infracrustales à signatures très évoluées. La transformation du volcanisme

mafique précurseur et de la sédimentation d'arrière-arc à 2,62 Ga en un magmatisme sanukitoïde dominant vers 2,60 Ga semble refléter la collision d'une masse continentale contenant le bloc de Chesterfield actuel avec un arc océanique. Les variations des sous-ensembles géochimiques de la suite à la grandeur de la région d'étude sont interprétées de façon à tenir compte des différentes compositions des blocs crustaux constitutifs pré-2,62 Ga. Par exemple, un brusque changement de composition au sud du lac Dubawnt coïncide avec une limite précoce d'un socle plus tonalitique au sud, dans le protocraton de Rae Sud. L'existence de telles limites à des angles élevés par rapport au grain structural sud-ouest–nord-est actuellement dominant, qui remonte au Paléoprotérozoïque, reflète une configuration d'âges primaires et de variations de composition, laquelle témoignerait de l'existence d'un arc continental à vergence ouest ayant réuni les différents noyaux du craton de Rae. La conservation des composants extrusifs de la suite uniquement dans la partie centrale du craton de Rae souligne davantage les différences majeures dans la stratigraphie, le métamorphisme et la métallogénie du Néoarchéen et du Paléoprotérozoïque décrites par Jefferson et ses collaborateurs (le présent volume), lesquelles distinguent la partie centrale du craton de Rae de sa partie sud et du bloc de Committee Bay. Surtout, la Suite de Snow Island fournit un grand ensemble de données à l'échelle du craton qui éclairera plus largement les modèles d'évolution des régions sources de sanukitoïdes et leur influence sur la composition des liquides magmatiques subséquents.

Essaims de dykes et grandes provinces ignées du nord du Canada

Buchan et Ernst (le présent volume) offrent une synthèse des essaims de dykes géants du Paléoprotérozoïque (généralement de la diabase) et des grandes provinces ignées du nord du Canada en mettant l'accent sur l'âge, la répartition et le paléomagnétisme, ainsi que sur les liens possibles avec les reconstitutions paléoc Continentales et les événements magmatiques ou de rupture continentale du même âge. Ils couvrent près de 40 suites mafiques majeures et suites felsiques mineures, et présentent une carte synthèse à une échelle de 1/3 000 000 pour les régions du nord du Bouclier canadien qui comprennent les cratons des Esclaves, de Rae et du lac Supérieur ainsi que les séquences de recouvrement du Mésoprotérozoïque. Les unités sont classées par âge et par craton, en mettant l'accent sur les suites bien datées et les unités corrélatives possibles entre 2,50 et 1,59 Ga environ. Plusieurs éléments sont inclus afin de mettre en évidence les futures cibles de recherche, à savoir : des exemples mal datés qui ont néanmoins des implications significatives pour les reconstitutions métallogéniques et cratoniques régionales; des événements non datés et en partie nouveaux dans les cratons des Esclaves et de Rae ainsi que dans le terrane de Meta Incognita; et de nombreux ensembles volcaniques dans les bassins sédimentaires cratoniques ou de marge passive dans la Province de Churchill.

À partir des plus récentes données sur les paléopôles primaires et les âges, les auteurs résument l'importance potentielle des événements magmatiques majeurs par rapport au rifting, à la rupture continentale et aux reconstitutions paléogéographiques. Ils mettent à l'épreuve plusieurs modèles proposés pour la Laurentie et l'ensemble du Bouclier canadien, y compris des liens hypothétiques de longue date avec la Baltica, de l'assemblage du supercontinent Nuna jusqu'à celui du supercontinent Rodinia. Des révisions critiques de la trajectoire de la dérive apparente des pôles de l'Amérique du Nord au Paléoprotérozoïque sont présentées et l'on aborde l'accrétion du terrane d'arc exotique de Bonnetia (env. 1,71 Ga) à la protomarge occidentale de la Laurentie. Si l'on remonte plus loin dans le temps, les modèles des supercratons précédents, comme Superia, Sclavia et Nunavutia, sont mis à l'épreuve. Les auteurs soutiennent que les liens les plus pertinents sur le plan temporel pour les cratons de Hearne et du lac Supérieur se situent entre les dykes de diabase de Kaminak (env. 2,5 Ga) de la partie centrale du craton de Hearne et les dykes de Ptarmigan, du même âge, du craton du lac Supérieur. Ils proposent que cette configuration du Paléoprotérozoïque initial ne se soit rompue qu'après la sédimentation et le magmatisme mafique de rift enregistrés sur les deux cratons, vers 2,11 Ga. L'ajustement au Paléoprotérozoïque précoce entre les dykes de Dogrib (env. 2,19 Ga) du craton des Esclaves et l'essaim de Tulemalu du craton de Rae est évalué et jugé incompatible avec les cratons des Esclaves et de Rae dans leur configuration actuelle à environ 2,3 Ga, comme proposé auparavant (De et al., 1998). Les trajectoires détaillées de dérive apparente des pôles de 2,23 à 1,88 Ga pour les cratons des Esclaves et du lac Supérieur ne se chevauchent pas, ce qui laisse croire que les deux cratons ne dérivent pas au sein d'un seul et même supercontinent au cours de cet intervalle (Buchan et al., 2016), ce qui est compatible avec les modèles dominants préconisant l'existence de deux supercratons distincts au cours de cette période (Salminen et al., 2021). Les données sur les essaims de dykes plus jeunes (1,89 Ga) laissent entrevoir que la Siberia se trouvait au nord du craton de Rae dans le supercontinent Nuna, une configuration demeurée stable de 1,9 à 0,72 Ga et qui pousse à établir des comparaisons favorables entre des unités importantes sur le plan métallogénique telles que

les unités à Au et à ÉTR encaissées dans la suite ignée de Kivalliq (1,75 Ga) et celles de la suite ignée de Timpson de Sibérie. Le lien exotique proposé, à 1,59 Ga environ, entre l'ouest de la Laurentie et la partie sud du craton de Gawler, en Australie, est largement appuyé par les paléopôles des dykes de diabase de Cleaver, dans l'ouest de la partie nord du Bouclier canadien.

Refroidissement régional du Bouclier canadien

Kellett et ses collaborateurs (le présent volume) offrent un résumé de la synthèse qu'ils ont publiée sur le refroidissement postmétamorphique du nord du Bouclier canadien. Fondée sur un ensemble de données regroupant des données d'archives de plus de 2 000 âges K-Ar et de nouveaux âges de refroidissement $^{40}\text{Ar}/^{39}\text{Ar}$ recueillis dans le cadre du programme GEM, l'étude révèle un contraste frappant entre les histoires du métamorphisme et du refroidissement des divers cratons et terranes archéens impliqués dans les collisions au Paléoprotérozoïque lors de l'assemblage de la Laurentie. On constate que des configurations de refroidissement très différentes sont généralement liées à la position des plaques pendant la collision et l'accrétion. Les cratons de plus grande taille occupant la plaque inférieure, comme ceux du lac Supérieur et des Esclaves, se comportent comme des blocs stables et froids et présentent un certain remaniement thermique aux marges. En revanche, la Province de Churchill, un collage de microcontinents plus petits accrétés au craton de Rae avant sa collision avec le craton du lac Supérieur, a subi un remaniement thermique presque complet à la fin du Paléoprotérozoïque. On présume que la Province de Churchill occupait un cadre tectonique de plaque supérieure pendant une grande partie du Paléoprotérozoïque en raison de ses antécédents sur les plans du magmatisme, de la structure et du remaniement thermique, alors que ces caractéristiques ne se retrouvent pas dans les cratons limitrophes du lac Supérieur et des Esclaves. Les contrastes dans l'histoire thermique entre plaques ou microplaques sont présentés dans six coupes transversales à l'intérieur du nord du Bouclier canadien, qui s'étendent de l'île de Baffin au sud de la Saskatchewan.

Une tendance générale d'ouest en est du refroidissement est définie par deux profils thermochronologiques à l'échelle du Bouclier canadien : d'une part, un transect nord qui s'étend du craton des Esclaves jusqu'à l'intérieur de la Province du lac Supérieur, en passant par la zone tectonique de Thelon, la partie nord du craton de Rae (ceinture de Committee Bay, péninsule de Hall de l'île de Baffin et ceinture de Cape Smith) et, d'autre part, un transect sud à travers le craton des Esclaves, la zone magmatique de Taltson, la partie sud du craton de Rae, la zone tectonique de Snowbird, la zone de Reindeer du craton de Hearne et la Province du lac Supérieur. Les deux profils révèlent une configuration en creux asymétrique dans les roches de la Province de Churchill, les âges de refroidissement les plus récents (env. 1,7 Ga) étant centrés à l'intérieur de l'orogène trans-hudsonien, et les âges de refroidissement les plus anciens étant situés à l'extrémité ouest de la Province de Churchill. À l'ouest, plus particulièrement dans le craton de Rae Sud, les âges de refroidissement sont structuralement contrôlés par des failles bordières de domaine, tandis qu'à l'est, à l'intérieur de l'orogène trans-hudsonien, les âges de refroidissement sont plus uniformes. Les âges de refroidissement les plus récents dans le profil nord sont de 50 millions d'années plus jeunes (env. 1,650 Ga) que dans le sud (env. 1,700 Ga), ce qui indique un diachronisme dans l'équilibre thermique postérieur à la collision et l'exhumation des roches de l'orogène trans-hudsonien.

À la suite de la phase terminale de la collision trans-hudsonienne entre les provinces de Churchill et du lac Supérieur, la Province de Churchill a peut-être subi un délaminage lithosphérique, comme en témoignent les perturbations thermiques tardives, et s'est par la suite comportée comme une masse continentale stable. Bien qu'elle ait été impliquée dans des collisions subséquentes lorsqu'elle faisait partie du supercontinent Nuna (p. ex., orogène de Grenville), elle occupait une position de plaque inférieure au moment de ces collisions. Kellett et ses collaborateurs concluent que le contraste dans l'historique du refroidissement entre la plaque supérieure (Churchill) et les plaques inférieures (lac Supérieur, des Esclaves ou Churchill) laisse supposer que la plaque supérieure au cours d'un cycle de Wilson est fortement conditionnée thermiquement par la chaleur, les fluides et le magma produits lors des événements tectoniques de subduction et d'accrétion.

Paléogéographie du nord-ouest de la Laurentie au Stathérien-Calymmien

À la suite de l'assemblage principal du nord du Bouclier canadien au Paléoprotérozoïque, d'importants bassins intracontinentaux se sont formés dans un certain nombre de dépo-centres, notamment dans le nord-ouest de la Laurentie. Rainbird et Davis (le présent volume) offrent un résumé de la géochronologie U-Pb sur zircon détritique et une mise à jour de la stratigraphie de l'un de ces bassins, à savoir le bassin de Horny Bay du Mésoprotérozoïque, situé sur la marge ouest affleurante du nord du Bouclier canadien, au nord-est du Grand lac de l'Ours. Ce bassin, âgé de 1,75 à 1,27 Ga environ, renferme les groupes de Big Bear, de Mountain Lake et de Dismal Lakes. Le groupe de Big Bear comprend principalement des roches détritiques immatures à grain grossier déposées par des rivières à forte énergie dans des bassins confinés délimités par des failles, lesquels seraient semblables aux rifts renfermant les bassins de Thelon et d'Athabasca. En intégrant la provenance des zircons détritiques aux compositions isotopiques de Hf, Rainbird et Davis définissent les régions sources possibles des composants détritiques du bassin. Ils proposent que les matériaux des roches sédimentaires du groupe de Big Bear proviennent de sources occupant le sous-sol des orogènes et des terranes du Paléoprotérozoïque dans les environs du Grand lac de l'Ours, ainsi que de sources plus à l'est, comme la zone tectonique de Thelon. En revanche, le groupe de Mountain Lake nouvellement défini s'est formé à l'intérieur d'une dépression de bassin plus vaste, probablement liée à une subsidence thermique. Les trois formations constituantes, qui comprennent des grès fluviaux d'un réseau de rivières anastomosées à l'échelle continentale et des roches détritiques marines de faciès transgressifs à régressifs, se sont déposées de 1,7 à 1,63 Ga environ. L'analyse de leur provenance rend compte du recyclage intermédiaire du Supergroupe de Coronation et d'unités corrélatives, mais plus distales, du Supergroupe de Goulburn, dans le bassin de Kilohigok. Le groupe de Mountain Lake a par la suite été plissé et faillé pendant l'orogénèse de Racklan-Forward liée à la collision de l'Australie avec le nord-ouest de la Laurentie, vers 1 600 Ma. Après le soulèvement et l'érosion associés, le groupe de Dismal Lakes (de 1,59 à 1,27 Ga) à lithologies principalement marines s'est déposé.

Une comparaison détaillée des faciès avec le Supergroupe de Wernecke du Yukon, les signatures isotopiques de Nd et de C des unités respectives de shale et de roches carbonatées, et l'historique sédimentaire détaillée du bassin de Hornby Bay sont combinés pour élaborer un nouveau modèle paléogéographique pour le nord-ouest de la Laurentie à cette époque. Il est proposé qu'un prisme détritique de marge passive à regard ouest avec des composants à la fois terrestres (bassin de Hornby Bay) et marins (Supergroupe de Wernecke) ait évolué pour former une plate-forme carbonatée stable, dont les éléments corrélatifs ont été transférés au nord-est de l'Australie avant la rupture du supercontinent Nuna.

UN PORTRAIT ÉMERGENT

Comme il ressort de ce qui précède, la nouvelle ère du programme GEM en matière de cartographie du Nord a considérablement élargi le cadre du Bouclier canadien et a ajouté des détails à un modèle de plus en plus complexe de la mosaïque de cratons archéens, de microcontinents de l'Archéen/Protérozoïques et de croûte juvénile du Paléoprotérozoïque qui constitue le nord du Bouclier canadien (tableau 2, fig. 3). En plus des six grands cratons archéens (des Esclaves, de Rae, de Hearne, du lac Supérieur, de Nain [Atlantique Nord] et de Mackenzie enfoui), on sait maintenant que le Bouclier canadien comprend au moins une douzaine de microcontinents en rubans de natures et d'origines variées. Certains blocs constituaient des terranes péricratoniques à la suite d'un rifting du Paléoprotérozoïque (Hall Peninsula-Aasiaat, Duggan Lake, Kuujuaq; blocs de Chesterfield et de Repulse Bay sur le protocraton de Rae), tandis que d'autres s'étaient séparés par rifting de leurs supercratons parents proposés (p. ex., Superia, Nunavutia) et réassemblés (Sask-Partridge Breast, Buffalo Head). D'autres blocs semblent exotiques, par exemple le domaine de Chipman du Mésoarchéen-Néoarchéen coïncé entre les cratons de Rae et de Hearne, le bloc de Queen Maud sur le flanc ouest du craton de Rae, le terrane de Boothia du Néoarchéen terminal situé au nord de la baie Queen Maud (et qui s'étend possiblement jusqu'à l'île Devon; Regis et Sanborn-Barrie, 2023) et le terrane de Wabamun enfoui dans la partie centre sud du Canada. Les blocs de George River, de Falcoz River et de Sugluk près du craton du lac Supérieur ont également des origines incertaines. Un sous-ensemble important est formé de microcontinents qui ont considérablement été remaniés et se sont accrues par le magmatisme pendant l'assemblage au Paléoprotérozoïque et ne contiennent que des fragments de composants archéens (Meta Incognita, Hottah, Mistibini-Raude).

Tableau 2. Mise à jour des éléments tectoniques du nord du Bouclier canadien à la suite des recherches du programme GEM (2006-2020).

Craton ou bloc	Subdivisions nouvelles ou révisées	Formation de la croûte ¹	Séquences de marge continentale du Paléoprotérozoïque ²	Événements orogéniques du Paléoprotérozoïque	Références choisies
Cratons archéens					
Craton des Esclaves		4,0-2,58 Ga	Supergroupe de Coronation (2,014-1,88 Ga) Supergroupe de Goulbourn inférieur (2,02-1,9 Ga) Supergroupe d'East Arm (env. 2,045-1,94 Ga)	Talson-Thelon; Wopmay	Heimstaedt et Pehrsson, 2012; Jackson et al., 2013; Davis et al., 2014 Hoffman et al., 2011; Rainbird et Davis, 2022 Wright et al., 2013; Sheen et al., 2019
Craton de Rae					
<i>Nord³</i>	Blocs de Repulse Bay-Prince Albert (y compris le domaine d'Ukkusiksalik) Bloc de Prince Albert Bloc de Committee Bay	2,97-2,60 Ga 2,73-2,58 Ga	Groupes de Penrhyn-Piling-Ketyet River Groupes de Penrhyn-Piling-Ketyet River (env. 2,16-1,88 Ga) Groupe de Ketyet River (<2,19 Ga)	MacQuoid, trans-hudsonien MacQuoid, Ellesmere-Ingfield, trans-hudsonien Arrowsmith, Snowbird, trans-hudsonien	Peterson et al., le présent volume; Wodicka et al., 2017, le présent volume Wodicka et al., 2011; Corrigan et al., 2013; Berman et al., 2015a; Skipton et al., 2019 Pehrsson et al., 2013; Sanborn-Barrie et al., 2014; Skulski et al., 2018; Davis, 2021; Jefferson et al., le présent volume
<i>Central</i>	Bloc de Chesterfield (y compris les domaines de Gordon, de Luman et de Kummel Lake)	2,90-2,58 Ga	Ceinture de Pennington (équivalent du Groupe de Ketyet River inférieur)	Snowbird et/ou trans-hudsonien	Wodicka et al., 2017, le présent volume; Steenkamp et al., 2023a, b, c; Pehrsson, le présent volume; Peterson et al., le présent volume; Tschirhart et al., le présent volume
<i>Sud</i>	Domaine de Douglas Harbour Bloc de Committee Bay central Domaine de Porter	2,90-2,61 Ga 3,0-2,58 Ga 2,74-2,56 Ga	Groupes d'Amer-Ketyet River-Montresor Assemblage de Lamarre Lake (2,04 Ga)	trans-hudsonien Snowbird, trans-hudsonien MacQuoid, Arrowsmith	Steenkamp et al., 2023a, b, c; Wodicka et al., le présent volume; Peterson et al., le présent volume Jefferson et al., le présent volume MacLachlan et al., 2005; Davis et al., 2006; Lawley et al., 2016; Wodicka et al., 2017; Pehrsson, le présent volume Rainbird et al., 2010; Corrigan et al., 2013; Laflamme et al., 2014; Skipton et al., 2019; Pehrsson, le présent volume
Craton de Heame	Domaine de Penylan Domaines de McCann-Zemlack Domaine de Firdrake Domaines de Snowbird-Dodge Domaine de West Kasba	2,04-2,02 Ga 2,7-2,04 Ga 2,74-2,58 Ga 2,72-1,96 Ga 2,55-1,9 Ga	inconnue Roches métasédimentaires de McCann (2,54-2,35 Ga) Roches métasédimentaires d'Imikula (2,55-1,90 Ga) Roches métasédimentaires de Snowbird (2,07-1,95 Ga) Ceinture de Bourassa Lake (env. 2,55-1,9 Ga)	trans-hudsonien Arrowsmith, Snowbird, trans-hudsonien Snowbird, trans-hudsonien Tallson, Snowbird MacQuoid, Snowbird	Harfau et al., 2005; Pehrsson, le présent volume; Mantel et al., le présent volume Pehrsson, le présent volume Pehrsson, le présent volume Pehrsson, le présent volume Pehrsson, le présent volume Pehrsson, le présent volume Böhm et al., le présent volume Böhm et al., le présent volume
Craton de Heame	Domaine de Seal River Domaine de Nejanilini	3,5-2,55 Ga 2,7-2,48 Ga	Ceinture de Hatle Lake (env. 2,8-2,56 Ga) Roches métasédimentaires de Misty Lake (<1,97 Ga) Roches métasédimentaires de Kasmera-Nejanilini (<2,5 Ga)	MacQuoid, Snowbird trans-hudsonien trans-hudsonien	Pehrsson, le présent volume Böhm et al., le présent volume Eslève et al., 2020
Craton de Mackenzie		inconnue			
Craton du lac Supérieur		4,3-2,57 Ga	Groupes de Povungnituk, de Chukolait, nord-est (2,07-1,88 Ga)	trans-hudsonien, Nouveau-Québec	Bleeker et Kamo, 2020
Craton de Nain		3,8-3,0 Ga		Tongat	James et al., 2002; Corrigan et al., le présent volume
Microcontinents de l'Archéen/Protérozoïque					
Microcontinents péricratoniques		Formation de la croûte	Origine cratonique lorsqu'applicable	Événements orogéniques du Paléoprotérozoïque	Références choisies
	Domaine de Duggan Lake Domaines de Hall Peninsula-Aasiat Domaine de Kuujuaq	3,2-3,1 Ga 2,98-2,701 Ga 3,0-2,72 Ga	Bloc de Queen Maud Nain (Atlantique Nord) Craton du lac Supérieur	Arrowsmith, Thelon Nagssugtoqidian, Tongat, trans-hudsonien Nouveau-Québec	Berman et al., 2019b; le présent volume Skipton et al., 2016; From et al., 2016, 2018 Rayner et al., 2017; Corrigan et al., 2018, le présent volume
Microcontinents accrétés du Paléoprotérozoïque principalement					
	Bloc de Mistibini-Raude Terrane de Hoitah	<2,6-2,3 Ga 2,5-1,895 Ga	Groupe de Treasure Lake (1,885-1,873 Ga)	environ 2,1 Ga Wopmay	Corrigan et al., 2018, 2021; le présent volume Davis et al., 2015; Ootes et al., 2015
Microcontinents exotiques ou aux affinités incertaines					
	Domaine de Chipman Terrane de Boothia Bloc de Queen Maud Bloc de George River Bloc de Falcoz River Sask-Partridge Breast	3,2-2,56 Ga 2,56-2,48 Ga 3,26-2,35 Ga 2,86-2,57 Ga 2,89-2,57 Ga 3,3-2,55	Séquence de Boothia 1 (2,51-2,48 Ga) Assemblage d'Ellice River (2,1-2,02 Ga)	Snowbird Arrowsmith, Thelon Arrowsmith, Thelon Nouveau-Québec Tongat, Nouveau-Québec trans-hudsonien	Peterson et al., le présent volume Sanborn-Barrie et al., 2019 Davis et al., 2021; Berman et al., le présent volume Corrigan et al., 2018, 2021; le présent volume Corrigan et al., 2018, 2021; le présent volume Ashton et al., 1999; Czás et al., 2020
Arcs du Paléoprotérozoïque					
	Ceinture plutonique de la zone tectonique de Thelon Zone magmatique du Grand lac de l'Ours	2,07-1,95 Ga 1,88-1,86 Ga	Groupe de Treasure Lake (1,88 Ga)	Thelon, trans-hudsonien Grand lac de l'Ours-Wopmay	Berman et al., le présent volume Corriveau et al., le présent volume
¹ « Formation de la croûte » fait référence à l'intervalle d'âges global des domaines internes constituants du nord du Bouclier canadien durant l'assemblage de celui-ci à l'exception des épisodes magmatiques de rift, des grandes provinces ignées et du magmatisme de collision du Protérozoïque. ² ne comprend pas les séquences épicratoniques pour lesquelles une évolution menant à un rifting n'a pas été démontrée. ³ Les noms en italique indiquent qu'il s'agit de subdivisions existantes mises à jour ou de nouvelles subdivisions proposées dans le cadre du programme GEM. Pour les références concernant le craton de Mackenzie enroulé et les microcontinents de Sask-Partridge Breast voir Corrigan et al., 2021. Pour les références concernant les projets circum-Jungava de GEM voir Dafoe et Bingham-Koslowski, 2022.					

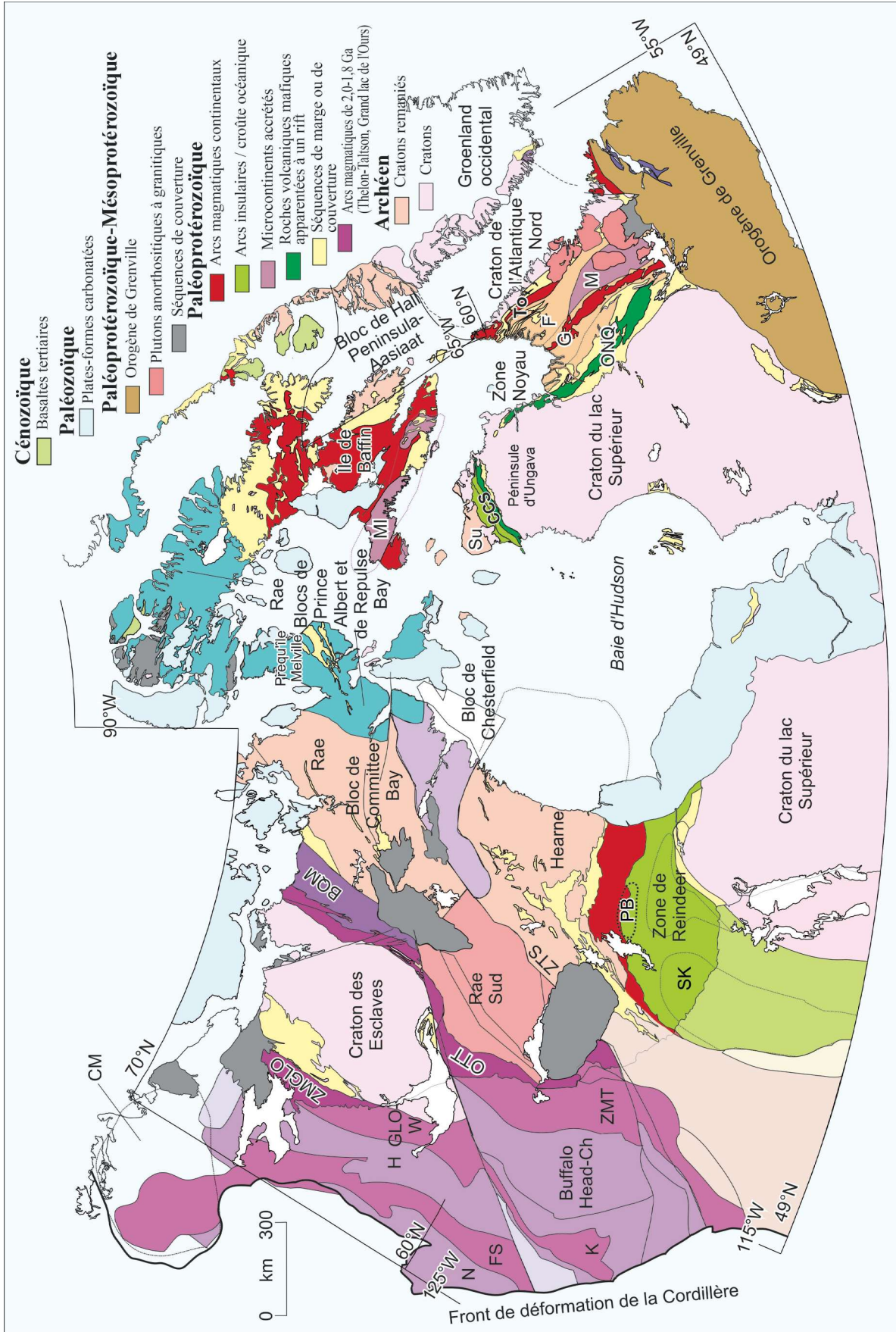


Figure 3. Mise à jour des subdivisions et des éléments du nord du Bouclier canadien à la suite des recherches de GEM-1 et de GEM-2. Les divisions de diverses couleurs du craton de Rae de l'Archéen mettent en évidence les subdivisions internes de celui-ci, mais toutes, à l'exclusion du bloc de Queen Maud, ont été intensément remaniées au Paléoproterozoïque. Abréviations : BQM = bloc de Queen Maud; CCS = ceinture de Cape Smith; Ch = Chinchaga; CM = craton de Mackenzie; F = bloc de Falcoz River; FS = terrane de Fort Simpson; G = bloc de George River; OTT = orogène de Taltson-Thelon H = terrane de Hottah; K = orogène de Kitsuan; M = bloc de Mistinibi-Raude; MI = terrane de Meta Incognita; N = terrane de Nahanni; ONQ = orogène du Nouveau-Québec; OTT = orogène de Taltson-Thelon PB = terrane de Partridge Breast; SK = craton de Sask; Su = Sugluk; To = orogène des Torngat; GLO-W = zone du Grand lac de l'Ours-orogène de Wopmay; ZMGLO = zone magmatique du Grand lac de l'Ours; ZMT = zone magmatique de Taltson; ZTS = zone tectonique de Snowbird.

Les plus grands cratons, comme ceux des Esclaves, de Rae, de Nain et du lac Supérieur, présentent des subdivisions internes distinctes avec des filiations du Paléoarchéen et du Mésoarchéen plutôt que du Néoarchéen, reflétant l'activité orogénique mésoarchéenne et néoarchéenne qui a assemblé ces composants dans leurs protocratons naissants. Avant 2,8 Ga, bon nombre des composants anciens ont connu un épisode de rifting et se sont séparés pour ensuite être assemblés de nouveau dans les importants supercratons Nunavutia et Superia du Néoarchéen. Le craton de Rae, en particulier, a été l'un des centres d'intérêt des recherches du programme GEM, et des progrès importants ont été réalisés dans les connaissances de son architecture et de son évolution. La présence de zircons détritiques du Paléoarchéen et du Mésoarchéen, et plus rarement de l'Hadéen dans les roches sédimentaires du Néoarchéen et du Paléoproterozoïque laisse croire que le craton de Rae possède une histoire archéenne complexe, possiblement aussi longue que celle des cratons des Esclaves et du lac Supérieur, mieux connus. L'établissement de l'architecture crustale du craton de Rae avant la mise en place des intrusions répandues de la Suite de Snow Island s'est avéré difficile et pourrait nécessiter des études régionales du système Lu-Hf dans les zircons ou par d'autres méthodes isotopiques pour tirer au clair le remaniement magmatique qui s'est produit vers 2,6 Ga.

L'orogénèse de MacQuoid (de 2,5 à 2,0 Ga) a amorcé l'assemblage progressif et le remaniement de la Province de Churchill occidentale et a été suivie de près par l'orogénèse d'Arrowsmith (de 2,5 à 2,3 Ga). Alors que les effets tectoniques de l'orogénèse d'Arrowsmith semblent être localisés le long de la limite entre le bloc de Queen Maud et la partie ouest du craton de Rae, son empreinte métamorphique s'étend sur des centaines de kilomètres dans le craton de Rae, sauf dans sa partie centrale (Jefferson et al., le présent volume). De l'érosion a été suivie par le dépôt de nombreuses séquences de marge continentale ou de couverture du Paléoproterozoïque précoce avant la rupture du supercraton (Wodicka et al., 2014). Les principaux cratons archéens et un grand nombre de microcontinents et de lambeaux crustaux de l'Archéen au Paléoproterozoïque initial qui se sont détachés de ces configurations, aujourd'hui conservés entre les cratons de Rae, du lac Supérieur et de Nain, étaient dispersés dans ce qui était autrefois le domaine océanique de Manikewan, qui s'est refermé entre 1,92 et 1,83 Ga environ avec l'assemblage du supercontinent Nuna. Du côté ouest du craton de Rae, une activité magmatique précoce dans la zone tectonique de Thelon (de 2,03 à 1,96 Ga) a accompagné la subduction, après quoi s'est produite une collision avec le craton des Esclaves de même qu'une déformation relativement localisée le long de la zone. La déformation le long de la zone tectonique de Snowbird au sud-est du craton de Rae est de caractère polyphasé résultant de la collision avec le craton de Hearne pendant l'orogénèse de Snowbird vers 1,9 Ga et du remaniement subséquent pendant l'orogénèse trans-hudsonienne et la fermeture définitive de l'Océan Manikewan, vers 1,85 Ga. Les deux événements ont entraîné une déformation et un métamorphisme généralisés du socle du craton de Rae et de ses séquences de marge continentale et de couverture. Cette surimpression progressive par des événements du Paléoproterozoïque (de 2,5 à 1,85 Ga) distingue le craton de Rae des autres régions archéennes stabilisées avant 2,5 Ga. Ce phénomène a été attribué à un cadre tectonique de plaque supérieure pour le craton de Rae pendant les collisions paléoproterozoïques et a probablement retardé l'établissement d'une lithosphère mantellique stable. L'activité mantellique continue est évidente en raison des intrusions alcalines répandues et du magmatisme associé (de 1,83 à 1,75 Ga) dans la partie centrale du craton de Rae.

Le cœur de la partie nord du Bouclier canadien et du supercontinent Nuna étant dorénavant assemblé, des mouvements de coulissage liés aux collisions périphériques (p. ex., Hottah, Nain) se sont poursuivis et l'accrétion a pris de l'ampleur en périphérie du supercontinent (le Yukon actuel), ce qui a mené à la formation de l'arc continental du Grand lac de l'Ours, à l'ajout d'un certain nombre de terranes enfouis

sous le Bassin sédimentaire de l'Ouest du Canada et, finalement, à la collision du craton d'Australie Nord avec le nord-ouest de la Laurentie, avant 1,59 Ga. À l'intérieur, des failles tardives ont formé des bassins de rift localisés dans la partie centrale du craton de Rae et dans le craton de Hearne de 1,75 à 1,27 Ga environ, lesquels semblent avoir joué un rôle clé dans la localisation des gisements d'uranium liés à une discordance. Les bassins sédimentaires susmentionnés du même âge dans le nord-ouest de la Laurentie témoignent d'un transport sédimentaire sur de longues distances par de grandes rivières. Cette période est associée à un refroidissement relativement lent à la suite des multiples événements de remaniement au Paléoprotérozoïque, d'un magmatisme tardif, de la formation de failles et de la sédimentation.

Ce portrait d'ensemble, bien que considérablement amélioré par le programme GEM, comporte néanmoins de nombreux aspects insuffisamment circonscrits qui constitueraient des cibles appropriées pour de futures recherches. Le type de subdivision interne détaillée qui a été établi pour la Province du lac Supérieur au fil de décennies de recherche dans des régions relativement accessibles, essentiel à la compréhension de sa métallogénie régionale, n'a pas encore été réalisé pour les cratons des Esclaves et de Rae. La reconnaissance de l'empreinte limitée de l'orogénèse de Taltson-Thelon dans le bloc de Queen Maud et le craton de Rae Sud a mis en évidence l'importance de comprendre les répercussions tectoniques de l'énigmatique orogénèse d'Arrowsmith (d'env. 2,4 à 2,3 Ga). La découverte d'un grand nombre de nouvelles séquences supracrustales et volcaniques du Paléoprotérozoïque dans des régions précédemment peu étudiées complique nécessairement les choses, mais permet également de délimiter l'architecture tectonique. Ce n'est qu'avec une plus grande densité de données, une couverture accrue par des levés géophysiques modernes et des ensembles enrichis de données géochimiques, isotopiques et géochronologiques *in situ* de haute précision que nous serons en mesure de répondre à des questions courantes ou plus précises concernant l'évolution crustale, l'architecture tectonique, les orogénèses et le potentiel métallogénique de nombreuses parties du nord du Bouclier canadien.

REMERCIEMENTS

Nous tenons à remercier tous les collègues dont les recherches dévouées au cours de la dernière décennie ont énormément contribué au programme GEM, ainsi que la direction du programme pour son soutien et ses encouragements continus. Nous remercions grandement Eric Potter, Sonya Banal et Natalie Morisset d'avoir piloté ce projet en cette période d'incertitude et d'avoir rendu la synthèse possible. Nous remercions les géoscientifiques suivants d'avoir accepté d'examiner de façon critique les manuscrits inclus dans ce volume de synthèse : Colin Card (Commission géologique de la Saskatchewan), Quentin Gall (consultant en géologie), Nathan Hayward (CGC), Rebecca Hunter (Forum Energy Metals Corp.), Dawn Kellett (CGC), Bruce Kjarsgaard (CGC), Tony LeCheminant (CGC), Robert MacNaughton (CGC), Ali Polat (Université de Windsor), Eric Potter (CGC), Rob Rainbird (CGC), Daniele Regis (CGC), Anthony Reid (Australian National University), Mary Sanborn-Barrie (CGC) et Richard Smith (Université Laurentienne). La révision technique complète et approfondie par Marie-France Dufour, Evelyn Inglis et Alison Weatherston, la révision de la traduction par Benoît Couture et la mise en page par Paul Champagne ont amélioré la clarté et l'uniformité du produit final. Cette recherche a été soutenue par le programme GEM, le Programme du plateau continental polaire et l'Initiative géoscientifique ciblée de la CGC.

RÉFÉRENCES

- Ashton, K., Heaman, L., Lewry, J., Hartlaub, R.P. et Shi, R., 1999. Age and origin of the Jan Lake complex: a glimpse at the buried Archean craton of the Trans-Hudson Orogen; *Canadian Journal of Earth Sciences*, v. 36, p. 185–208. <https://doi.org/10.1139/e98-038>
- Bédard, J.H., Hayes, B., Hryciuk, M., Beard, C., Williamson, N., Dell'Oro, T.A., Rainbird, R.H., Prince, J., Baragar, W.R.A., Nabelek, P.I., Weis, D., Wing, B., Scoates, J., Naslund, H.R., Cousens, B., Williamson, M.-C., Hulbert, L.J., Montjoie, R., Girard, É., Ernst, R. et Lissenberg, C.J., 2016. Geochemical database of Franklin sills, Natkusiak basalts and Shaler Supergroup rocks, Victoria Island, Northwest Territories, and correlatives from Nunavut and the mainland; Geological Survey of Canada, Open File 8009, 1 .zip file. <https://doi.org/10.4095/297842>
- Berman, R.G., Pehrsson, S.L., Davis, W.L., Ryan, J.J., Qui, H. et Ashton, K., 2013. The Arrowsmith orogeny: geochronological and thermobarometric constraints on its extent and tectonic setting in the Rae craton, with implications for pre-Nuna supercontinent reconstruction; *Precambrian Research*, v. 232, p. 44–69. <https://doi.org/10.1016/j.precamres.2012.10.015>

- Berman, R.G., Nadeau, L., McMartin, I., McCurdy, M.W., Craven, J.A., Girard, E., Sanborn-Barrie, M., Carr, S., Pehrsson, S.J., Whalen, J., Davis, W.J., Roberts, B.J., et Grenier, A., 2015a. Report of activities for the Geology and Mineral Potential of the Chantrey-Thelon Area: GEM-2 Thelon tectonic zone project; Geological Survey of Canada, Open File 7693, 14 p. <https://doi.org/10.4095/295644>
- Berman, R.G., Davis, W.J., Corrigan, D. et Nadeau, L., 2015b. Insights into the tectonothermal history of Melville Peninsula, Nunavut, provided by in situ SHRIMP geochronology and thermobarometry; Geological Survey of Canada, Current Research 2015-4, 18 p. <https://doi.org/10.4095/295852>
- Berman, R.G., Sanborn-Barrie, M., Nadeau, L., Brouillette, P., Camacho, A., Davis, W.J., McCurdy, M.W., McMartin, I., Weller, O.M., Chadwick, T., Liikane, D. et Ma, S., 2016. Report of activities for the geology and mineral potential of the Chantrey-Thelon area: GEM-2 Rae project; Geological Survey of Canada, Open File 8129, 15 p. <https://doi.org/10.4095/299386>
- Berman, R.G., Davis, W.J., Sanborn-Barrie, M., Whalen, J.B., Taylor, B.E., McMartin, I., McCurdy, M.W., Mitchell, R.K., Ma, S., Coyle, M., Roberts, B. et Craven, J.A., 2018. Report of activities for the GEM-2 Chantrey-Thelon activity: Thelon tectonic zone project, Nunavut; Geological Survey of Canada, Open File 8372, 22 p. <https://doi.org/10.4095/306622>
- Bleeker, W., 2003. The late Archean record: puzzle in ca. 35 pieces; *Lithos*, v. 71, p. 99–134. <https://doi.org/10.1016/j.lithos.2003.07.003>
- Bleeker, W. et Kamo, S.L., 2020. Structural-stratigraphic setting and U-Pb geochronology of Ni-Cu-Co-PGE ore environments in the central Cape Smith Belt, Circum-Superior Belt; *in* Targeted Geoscience Initiative 5: advances in the understanding of Canadian Ni-Cu-PGE and Cr ore systems — examples from the Midcontinent Rift, the Circum-Superior Belt, the Archean Superior Province, and Cordilleran Alaskan-type intrusions, (ed.) W. Bleeker and M.G. Houlé; Geological Survey of Canada, Open File 8722, p. 65–98. <https://doi.org/10.4095/326882>
- Buchan, K.L. et Ernst, R.E., 2013. Diabase dyke swarms of Nunavut, Northwest Territories and Yukon, Canada; Geological Survey of Canada, Open File 7464, 1 .zip file. <https://doi.org/10.4095/293149>
- Buchan, K.L., Mitchell, R.N., Bleeker, W., Hamilton, M.A. et LeCheminant, A.N., 2016. Paleomagnetism of ca. 2.13–2.11 Ga Indin and ca. 1.885 Ga Ghost dyke swarms of the Slave craton: implications for the Slave craton APW path and relative drift of Slave, Superior and Siberian cratons in the Paleoproterozoic; *Precambrian Research*, v. 275, p. 151–175. <https://doi.org/10.1016/j.precamres.2016.01.012>
- Canil, D., 2008. Canada's craton: a bottoms-up view; *GSA Today*, v. 18, no. 6, p. 4–10. <https://doi.org/10.1130/GSAT01806A.1>
- Card, C., Bethune, K., Davis, W.J., Rayner, N. et Ashton, K.E., 2014. The case for a distinct Taltson Orogeny: evidence from northwest Saskatchewan, Canada, *Precambrian Research*, v. 255, p. 245–265. <https://doi.org/10.1016/j.precamres.2014.09.022>
- Chacko, T., De, S.K., Creaser, R.A. et Muehlenbachs, K., 2000. Tectonic setting of the Taltson magmatic zone at 1.9–2.0 Ga: a granitoid-based perspective; *Canadian Journal of Earth Sciences*, v. 37, p. 1597–1609. <https://doi.org/10.1139/e00-029>
- Clowes, R., Cook, F., Hajnal, Z., Hall, J., Lewry, J., Lucas, S. et Wardle, R., 1999. Canada's Lithoprobe project: collaborative, multidisciplinary geoscience research leads to new understanding of continental evolution; *Episodes*, v. 22, p. 3–20. <https://doi.org/10.18814/epiugs/1999/v22i1/002>
- Condie, K.C. et Kröner, A., 2008. When did plate tectonics begin? Evidence from the geologic record; *in* When Did Plate Tectonics Begin on Planet Earth?, (ed.) K.C. Condie and V. Pease; Geological Society of America, Special Paper 440, p. 281–294. [https://doi.org/10.1130/2008.2440\(14\)](https://doi.org/10.1130/2008.2440(14))
- Condie, K.C., O'Neill, C. et Aster, R.C., 2009. Evidence and implications for a widespread magmatic shutdown for 250 My on Earth; *Earth and Planetary Science Letters*, v. 282, p. 294–298. <https://doi.org/10.1016/j.epsl.2009.03.033>
- Corrigan, D., Nadeau, L., Brouillette, P., Wodicka, N., Houlé, M.G., Tremblay, T., Machado, G. et Keating, P., 2013. Overview of the GEM Multiple Metals - Melville Peninsula project, central Melville Peninsula, Nunavut; Geological Survey of Canada, Current Research 2013-19, 17 p. <https://doi.org/10.4095/292862>
- Corrigan, D., Brouillette, P., Morin, A., Van Rooyen, D., Wodicka, N., Houlé, M.G., Douma, S.L. et Robillard, K., 2015. Report of activities for the Core Zone and bounding orogens: tectonic framework and mineral potential; Geological Survey of Canada, Open File 7706, 10 p. <https://doi.org/10.4095/296141>
- Corrigan, D., Van Rooyen, D., Morin, A., Houlé, M.G. et Bédard, M.-P., 2016. Report of activities for the Core Zone and Bounding Orogens: recent observations from the New Quebec Orogen in the Schefferville area, Quebec and Labrador, GEM-2 Hudson-Ungava project; Geological Survey of Canada, Open File 8127, 11 p. <https://doi.org/10.4095/299249>

- Corrigan, D., Wodicka, N., McFarlane, C., Lafrance, I., van Rooyen, D., Bandyayera, D. et Bilodeau, C., 2018. Lithotectonic framework of the Core Zone, southeastern Churchill Province, Canada; *Geoscience Canada*, v. 45, no. 1, p. 1–24. <https://doi.org/10.12789/geocanj.2018.45.128>
- Corrigan, D., van Rooyen, D. et Wodicka, N., 2021. Indenter tectonics in the Canadian Shield: a case study for Paleoproterozoic lower crust exhumation, orocline development, and lateral extrusion; *Precambrian Research*, v. 355, p. 106083. <https://doi.org/10.1016/j.precamres.2020.106083>
- Corriveau, L., Lauzière, K., Montreuil, J.-F., Potter, E.G., Hanes, R. et Prémont, S., 2015. Dataset of geochemical data from iron oxide alkali-altered mineralising systems of the Great Bear magmatic zone, Northwest Territories; Geological Survey of Canada, Open File 7643, 1 .zip file. <https://doi.org/10.4095/296301>
- Craven, J., Roberts, B., Hayward, N., Stefanescu, M. et Corriveau, L., 2013. A magnetotelluric survey and preliminary geophysical inversion and visualization of the NICO IOCG deposit, Northwest Territories; Geological Survey of Canada, Open File 7465, 26 p. <https://doi.org/10.4095/292869>
- Czas, J., Pearson, D.G., Stachel, T., Kjarsgaard, B. et Read, G., 2020. A Palaeoproterozoic diamond-bearing lithospheric mantle root beneath the Archean Sask Craton, Canada; *Lithos*, v. 356–357, no. 105301, 14 p. <https://doi.org/10.1016/j.lithos.2019.105301>
- Dafoe, L. et Bingham-Koslowski, N. (ed.), 2022. Geological synthesis of Baffin Island (Nunavut) and the Labrador–Baffin Seaway; Geological Survey of Canada, Bulletin 608, 432 p. <https://doi.org/10.4095/314542>
- Davis, W.J., 2021. U-Pb zircon age data for supracrustal samples from the White Hills Lake to Amer Lake area, Rae Province, Nunavut, Canada; Geological Survey of Canada, Open File 8807, 1 .zip file. <https://doi.org/10.4095/328453>
- Davis, W.J., Hanmer, S., Tella, S., Sandeman, H.A. et Ryan, J.J., 2006. U-Pb geochronology of the MacQuoid supracrustal belt and Cross Bay plutonic complex: key components of the northwestern Hearne subdomain, western Churchill Province, Nunavut, Canada; *Precambrian Research*, v. 145, p. 53–80. <https://doi.org/10.1016/j.precamres.2005.11.016>
- Davis, W.J., Berman, R.G., Nadeau, L. et Percival, J.A., 2014. U-Pb zircon geochronology of a transect across the Thelon tectonic zone, Queen Maud region, and adjacent Rae craton, Kitikmeot Region, Nunavut, Canada; Geological Survey of Canada, Open File 7652, 1. zip file. <https://doi.org/10.4095/295177>
- Davis, W.J., Ootes, L., Newton, L., Jackson, V. et Stern, R.A., 2015. Characterization of the Paleoproterozoic Hottah terrane, Wopmay Orogen using multi-isotopic (U-Pb, Hf and O) detrital zircon analyses: an evaluation of linkages to northwest Laurentian Paleoproterozoic domains; *Precambrian Research*, v. 269, p. 296–310. <https://doi.org/10.1016/j.precamres.2015.08.012>
- Davis, W.J., Sanborn-Barrie, M., Berman, R.G. et Pehrsson, S., 2021. Timing and provenance of Paleoproterozoic supracrustal rocks in the central Thelon tectonic zone, Canada: implications for the tectonic evolution of western Laurentia from ca. 2.1 to 1.9 Ga; *Canadian Journal of Earth Sciences*, v. 58, no. 4, p. 378–395. <https://doi.org/10.1139/cjes-2020-0046>
- De, S.K., Chacko, T., Creaser, R.A. et Muehlenbachs, K., 2000. Geochemical and Nd–Pb–O isotope systematics of granites from the Taltson magmatic zone, NE Alberta: implications for Early Proterozoic tectonics in western Laurentia; *Precambrian Research*, v. 102, p. 221–249. [https://doi.org/10.1016/S0301-9268\(00\)00068-1](https://doi.org/10.1016/S0301-9268(00)00068-1)
- Eglington, B.M., Pehrsson, S.J., Ansdell, K.M., Lescuyer, J.-L., Quirt, D., Milesi, J.-P. et Brown, P., 2013. A domain-based digital summary of the lithostratigraphy, geochronology and geodynamics of the Palaeoproterozoic of North America and Greenland and associated unconformity-type uranium mineralization; *Precambrian Research*, v. 232, p. 4–26. <https://doi.org/10.1016/j.precamres.2013.01.021>
- Eguchi, J., Diamond, C.W. et Lyons, T.W., 2022. Proterozoic supercontinent break-up as a driver for oxygenation events and subsequent carbon isotope excursions; *PNAS Nexus*, v. 1, no. 2, p. 1–10. <https://doi.org/10.1093/pnasnexus/pgac036>
- Estève, C., Audet, P., Schaeffer, A., Schutt, D., Aster, R.C. et Cubley, J.F., 2020. Seismic evidence for craton chiseling and displacement of lithospheric mantle by the Tintina fault in the northern Canadian Cordillera; *Geology*, v. 48, p. 1120–1125. <https://doi.org/10.1130/G47688.1>
- From, R.E., Rayner, N.M. et Camacho, A., 2016. Archean magmatism and metamorphism of eastern Hall Peninsula, southern Baffin Island, Nunavut; Canada-Nunavut Geoscience Office, Summary of Activities 2015, p. 73–88.
- From, R.E., Camacho, A., Pearson, D.G. et Luo, Y., 2018. U-Pb and Lu-Hf isotopes of the Archean orthogneiss complex on eastern Hall Peninsula, southern Baffin Island, Nunavut: identification of exotic Paleo- to Mesoproterozoic crust beneath eastern Hall Peninsula; *Precambrian Research*, v. 305, p. 341–357. <https://doi.org/10.1016/j.precamres.2017.12.024>

- Geological Survey of Canada, 2018. Geological Survey of Canada, strategic plan 2018–2023; Natural Resources Canada, 32 p. <https://doi.org/10.4095/313405> [Publication de la Commission géologique du Canada également disponible en français]
- Harris, J.R., Hillary, E.M., Percival, J.A., Buller, G., Buenviaje, R., Bazor, D., Baer, S., Kiessling, G.M., Pehrsson, S.J., Davis, W.J., Berman, R.G., Wodicka, N., Beauchemin, M., Coyne, M. et Therriault, A.M., 2013. Geo-mapping Frontiers: updated information on the regions covered by Operations Baker, Bathurst, Keewatin, Northern Keewatin, Thelon and Wager; Nunavut and Northwest Territories: GIS components; Geological Survey of Canada, Open File 7434, 1 .zip file. <https://doi.org/10.4095/292744>
- Hartlaub, R.P., Chacko, T., Heaman, L.M., Creaser, R.A., Ashton, K.E. et Simonetti, A., 2005. Ancient (Meso- to Paleoproterozoic) crust in the Rae Province, Canada: evidence from Sm–Nd and U–Pb constraints; Precambrian Research, v. 141, p. 137–153. <https://doi.org/10.1016/j.precamres.2005.09.001>
- Hayward, N. et Oneschuk, D., 2011. Geophysical series, regional geophysical compilation project, Great Bear Magmatic Zone, Northwest Territories and Nunavut, NTS 85-M and N, and 86-C, D, E, F, K, and L; Geological Survey of Canada, Open File 6835; Northwest Territories Geoscience Office, NWT Open File 2011-05, scale 1:500 000.
- Hayward, N., Enkin, R.J., Corriveau, L., Montreuil, J.-F. et Kerswill, J., 2013. The application of rapid potential field methods for the targeting of IOCG mineralisation based on physical property data, Great Bear magmatic zone, Canada; Journal of Applied Geophysics, v. 94, p. 42–58. <https://doi.org/10.1016/j.jappgeo.2013.03.017>
- Helmstaedt, H.H. et Pehrsson, S.J., 2012. Geology and tectonic evolution of the Slave Province — a post-Lithoprobe perspective; in Tectonic Styles in Canada: The LITHOPROBE Perspective, (ed.) J.A. Percival, F.A. Cook, and R.M. Clowes; Geological Association of Canada, Special Paper 49, p. 379–466.
- Helmstaedt, H., Pehrsson, S.J. et Stuble, M.P., 2021. The Slave Province, Canada — geological evolution of an Archean diamondiferous craton; Geological Association of Canada, Special Paper 51, 216 p.
- Hoffman, P.F., 1988. United plates of America, the birth of a craton; early Proterozoic assembly and growth of Laurentia; Annual Review of Earth and Planetary Sciences, v. 16, p. 543–603. <https://doi.org/10.1146/annurev.ea.16.050188.002551>
- Hoffman, P.F., 1990. Subdivision of the Churchill Province and extent of the Trans-Hudson Orogen; in The Early Proterozoic Trans-Hudson Orogen of North America, (ed.) J.F. Lewry and M.R. Stauffer; Geological Association of Canada, Special Paper 37, p. 15–40.
- Hoffman, P.F., 2013. The Great Oxidation and a Siderian snowball Earth: MIF-S based correlation of Paleoproterozoic glacial epochs; Chemical Geology, v. 362, p. 143–156. <https://doi.org/10.1016/j.chemgeo.2013.04.018>
- Hoffman, P.F., Bowring, S.A., Buchwaldt, R. et Hildebrand, R.S., 2011. Birthdate for the Coronation paleocean: age of initial rifting in Wopmay orogen, Canada; Canadian Journal of Earth Sciences, v. 48, p. 281–293. <https://doi.org/10.1139/E10-038>
- Hoggard, M.J., Czarnota, K., Richards, F.D., Huston, D. et Jaques, L., 2019. Treasure maps and the billion-year stability of cratonic lithosphere; in SGTSG and SGSEG 2019 abstracts: biennial meeting of the Specialist Group for Tectonics and Structural Geology and the Specialist Group in Solid Earth Geophysics, Convergence on the Coast, (ed.) S. Glorie, T. Wise, and R. Dutch; Department for Energy and Mining, South Australia, Report Book 2019/00019, p. 87.
- Jackson, V.A., van Breemen, O., Ootes, L., Bleeker, W., Bennett, V., Davis, W.J., Ketchum, J.W.F. et Smar, L., 2013. U–Pb zircon ages and field relationships of Archean basement and Proterozoic intrusions, south-central Wopmay Orogen, NWT: implications for tectonic assignments; Canadian Journal of Earth Sciences, v. 50, no. 10, p. 979–1006. <https://doi.org/10.1139/cjes-2013-0046>
- Jefferson, C.W., Chorlton, L.B., Pehrsson, S.J., Peterson, T., Wollenberg, P., Scott, J., Tschirhart, V., McEwan, B., Bethune, K., Calhoun, L., White, J.C., Leblon, B., LaRocque, A., Shelat, Y., Lentz, D., Patterson, J., Riegler, T., Skulski, T., Robinson, S., Paulen, R., McClenaghan, B., Layton-Matthews, D., MacIsaac, D., Riemer, W., Stieber, C. et Tschirhart, P., 2011. Northeast Thelon Region: Geomapping for Uranium in Nunavut; Geological Survey of Canada, Open File 6962, 1 .zip file. <https://doi.org/10.4095/289037>
- Jefferson, C.W., Chorlton, L.B., Pehrsson, S., Peterson, T., Potter, E., Davis, W., Gandhi, S., Bleeker, W., Keating, P., Quirt, D., Wollenberg, P., Tschirhart, V., Ramaekers, P., LeCheminant, A.N., Robinson, S., White, J. et Bethune, K., 2012. Uranium potential of northern Canada's Proterozoic basins; in Prospectors and Developers Association of Canada, Annual Meeting 2012 Abstracts, p. 1.
- Jefferson, C.W., Peterson, T., Tschirhart, V., Davis, W., Scott, J.M.J., Reid, K., Ramaekers, P., Gandhi, S.S., Bleeker, W., Pehrsson, S., Morris, W.A., Fayek, M., Potter, E., Bridge, N., Grunsky, E., Keating, P., Ansdell, K. et Banerjee, N., 2013. LIPS and Proterozoic uranium (U) deposits of the Canadian Shield; Geological Survey of Canada, Open File 7352, 1 .zip file. <https://doi.org/10.4095/292377>

- Jefferson, C.W., White, J.C., Young, G.M., Patterson, J., Tschirhart, V.L., Pehrsson, S.J., Calhoun, L., Rainbird, R.H., Peterson, T.D., Davis, W.J., Tella, S., Chorlton, L.B., Scott, J.M.J., Percival, J.A., Morris, W.A., Keating, P., Anand, A., Shelat, Y. et MacIsaac, D., 2015. Outcrop and remote predictive geology of the Amer Belt and basement beside and beneath the northeast Thelon Basin, in parts of NTS 66-A, B, C, F, G and H, Kivalliq Region, Nunavut; Geological Survey of Canada, Open File 7242, 1 poster. <https://doi.org/10.4095/296825>
- Jefferson, C.W., Rainbird, R.H., Young, G.M., White, J.C., Tschirhart, V. et Creaser, R.A., 2022. The Paleoproterozoic Amer supergroup, Amer Fold Belt, Nunavut: stratigraphy, structure, correlations, and uranium metallogeny; *in* Understanding the Precambrian: a collection of papers in celebration of Grant McAdam Young; Canadian Journal of Earth Sciences, posted Open Access 21 November 2022, 35 p. <https://doi.org/10.1139/cjes-2022-0077>
- Kiss, F. et Coyle, M., 2011a. Composante résiduelle du champ magnétique total, levé aéromagnétique de la région du lac Hottah, SNRC parties de 86 C/5, 12, 86 D/5, 6, 7, 8, 9, 10, 11, 12, Territoires du Nord-Ouest / Residual total magnetic field, Hottah Lake aeromagnetic survey, parts of NTS 86 C/5, 12, 86 D/5, 6, 7, 8, 9, 10, 11, 12, Northwest Territories; Commission géologique du Canada, Dossier public 6851, échelle 1/100 000. <https://doi.org/10.4095/288787>
- Kiss, F. et Coyle, M., 2011b. Dérivée première verticale du champ magnétique, levé aéromagnétique de la région du lac Hottah, SNRC parties de 86 C/5, 12, 86 D/5, 6, 7, 8, 9, 10, 11, 12, Territoires du Nord-Ouest / First vertical derivative of the magnetic field, Hottah Lake aeromagnetic survey, parts of NTS 86 C/5, 12, 86 D/5, 6, 7, 8, 9, 10, 11, 12, Northwest Territories; Commission géologique du Canada, Dossier public 6852, échelle 1/100 000. <https://doi.org/10.4095/288788>
- Kiss, F. et Coyle, M., 2011c. Composante résiduelle du champ magnétique total, levé aéromagnétique de la région du lac Hottah, SNRC parties de 86 C/13, 86 D/13, 14, 15, 16, 86 E/1, 2, 3, Territoires du Nord-Ouest / Residual total magnetic field, Hottah Lake aeromagnetic survey, parts of NTS 86 C/13, 86 D/13, 14, 15, 16, 86 E/1, 2, 3, Northwest Territories; Commission géologique du Canada, Dossier public 6853, échelle 1/100 000. <https://doi.org/10.4095/288789>
- Kiss, F. et Coyle, M., 2011d. Dérivée première verticale du champ magnétique, levé aéromagnétique de la région du lac Hottah, SNRC parties de 86 C/13, 86 D/13, 14, 15, 16, 86 E/1, 2, 3, Territoires du Nord-Ouest / First vertical derivative of the magnetic field, Hottah Lake aeromagnetic survey, parts of NTS 86 C/13, 86 D/13, 14, 15, 16, 86 E/1, 2, 3, Northwest Territories; Commission géologique du Canada, Dossier public 6854, échelle 1/100 000. <https://doi.org/10.4095/288790>
- Kiss, F. et Coyle, M., 2011e. Hottah Lake aeromagnetic survey, Northwest Territories, parts of NTS 86 C/5, 12, 86 D/5, 6, 7, 8, 9, 10, 11, 12, BLOCK A, Sheet 1 of 2, 1:100 000 scale; Northwest Territories Geoscience Office, NWT Open File 2011-03, 4 cartes et données numériques.
- Kiss, F. et Coyle, M., 2011f. Hottah Lake aeromagnetic survey, Northwest Territories, parts of NTS 86 C/13, 86 D/13, 14, 15, 16, 86 E/1, 2, 3, BLOCK B, Sheet 2 of 2, 1:100 000 scale; Northwest Territories Geoscience Office, NWT Open File 2011-03, 4 cartes et données numériques.
- Kopp, R.E., Kirschvink, J.L., Hilburn, I.A. et Nash, C.Z., 2005. The Paleoproterozoic snowball Earth: A climate disaster triggered by the evolution of oxygenic photosynthesis; Proceedings of the National Academy of Sciences of the United States of America, v. 102, p. 11131–11136. <https://doi.org/10.1073/pnas.0504878102>
- Korenaga, J., 2008. Urey ratio and the structure and evolution of Earth's mantle; Reviews of Geophysics, v. 46, no. 2, cit. no. RG2007. <https://doi.org/10.1029/2007RG000241>
- Kremer, P.D., Böhm, C.O. et Rayner, N., 2011. Far north geomapping initiative: bedrock geology of the Snyder Lake area, northwestern Manitoba (part of NTS 64N5); Manitoba Industry, Trade and Mines, Manitoba Geological Survey, Report of Activities 2011, 12 p.
- LaFlamme, C., McFarlane, C.R.M., Corrigan, D. et Wodicka, N., 2014. Origin and tectonometamorphic history of the Repulse Bay block, Melville Peninsula, Nunavut: exotic terrane or deeper level of the Rae craton?; Canadian Journal of Earth Sciences, v. 51, p. 1097–1122. <https://doi.org/10.1139/cjes-2014-0040>
- Lawley, C.J.M., McNicoll, V., Sandeman, H., Pehrsson, S., Simard, M., Castonguay, S., Mercier-Langevin, P. et Dubé, B., 2016. Age and geological setting of the Rankin Inlet greenstone belt and its relationship to the gold endowment of the Meliadine gold district, Nunavut, Canada; Precambrian Research, v. 275, p. 471–495. <https://doi.org/10.1016/j.precamres.2016.01.008>
- Lyons, T.W., Reinhard, C.T. et Planavsky, N.J., 2014. The rise of oxygen in Earth's early ocean and atmosphere; Nature, v. 506, p. 307–315. <https://doi.org/10.1038/nature13068>
- MacLachlan, K., Davis, W. et Relf, C., 2005. U/Pb geochronological constraints on Neoproterozoic tectonism: multiple compressional events in the Northwestern Hearne domain, Western Churchill Province, Canada; Canadian Journal of Earth Sciences, v. 42, p. 85–109. <https://doi.org/10.1139/e04-104>

- McClenaghan, M.B., Paulen, R.C., Rice, J.M., Sanborn-Barrie, M., McCurdy, M.W., Spirito, W.A., Adcock, S.W., Veillette, J.J., Garrett, R.G., Grunsky, E.C., Pickett, J., Layton-Matthews, D. et Corrigan, D., 2014. GEM 2 Hudson-Ungava Project: southern Core Zone surficial geology, geochemistry, and bedrock mapping activities in Northern Quebec and Labrador; Geological Survey of Canada, Open File 7705, 18 p. <https://doi.org/10.4095/295521>
- McClenaghan, M.B., Spirito, W.A., Day, S.J.A., McCurdy, M.W., McNeil, R.J. et Adcock, S.W., 2022. Overview of surficial geochemistry and indicator mineral surveys and case studies from the Geological Survey of Canada's GEM Program; *Geochemistry: Exploration, Environment, Analysis*, v. 22, no. 1, geochem2021-070, 21 p. <https://doi.org/10.1144/geochem2021-070>
- McMartin, I. (ed.), 2023. Surficial geology of northern Canada: a summary of Geo-mapping for Energy and Minerals contributions; Geological Survey of Canada, Bulletin 611, 265 p. <https://doi.org/10.4095/331418>
- Ootes, L., Davis, W.J., Jackson, V.A. et van Breemen, O., 2015. Chronostratigraphy of the Hottah terrane and Great Bear magmatic zone of Wopmay Orogen, Canada, and exploration of a terrane translation model; *Canadian Journal of Earth Sciences*, v. 52, no. 12, p. 1062–1092. <https://doi.org/10.1139/cjes-2015-0026>
- Pearson, D.G. et Wittig, N., 2008. Formation of Archaean continental lithosphere and its diamonds: the root of the problem; *Journal of the Geological Society*, v. 165, p. 895–914. <https://doi.org/10.1144/0016-76492008-003>
- Pearson, D., Brenker, F., Nestola, F., McNeill, J., Hutchison, M.T., Matveev, S., Mather, K., Silversmit, G., Schmitz, S., Vekemans, B. et Vincze, L., 2014. Hydrous mantle transition zone indicated by ringwoodite included within diamond; *Nature*, v. 507, p. 221–224. <https://doi.org/10.1038/nature13080>
- Pehrsson, S., Berman, R.G. et Davis, W.J., 2013. Paleoproterozoic orogenesis during Nuna aggregation: a case study of reworking of the Rae craton, Woodburn Lake, Nunavut; *Precambrian Research*, v. 232, p. 167–188. <https://doi.org/10.1016/j.precamres.2013.02.010>
- Pehrsson, S.J., Buchan, K.L., Eglington, B.M., Berman, R.M. et Rainbird, R.H., 2014a. Did plate tectonics shutdown in the Palaeoproterozoic? A view from the Siderian geologic record; *Gondwana Research*, v. 26, p. 803–815. <https://doi.org/10.1016/j.gr.2014.06.001>
- Pehrsson, S.J., Percival, J.A., Davis, W.J., McCurdy, M.W., Berman, R.G., Hillary, E.M., Kiss, F., MacKinnon, A. et Jefferson, C.W., 2014b. Operation GEM South Rae: reconnaissance geology of the most poorly known part of the Churchill Province, Northwest Territories and Nunavut; Geological Survey of Canada, Open File 7410, 25 p. <https://doi.org/10.4095/293762>
- Pehrsson, S.J., Coyle, M. et Berman, R., 2014c. The GEM Chesterfield gold project: understanding controls on western Churchill gold endowment from the bottom up; Geological Survey of Canada, Open File 7490, 31 p. <https://doi.org/10.4095/293763>
- Pehrsson, S.J., Campbell, J.E., Martel, E., McCurdy, M.W., Acosta-Góngora, P., Thiessen, E., Jamieson, D., Lauzon, G., Buller, G., Falck, H. et Dyke, A.S., 2015. Report of 2015 activities for the geologic and metallogenic framework of the south Rae Craton, southeast Northwest Territories: GEM 2 South Rae Quaternary and Bedrock project; Geological Survey of Canada, Open File 7958, 24 p. <https://doi.org/10.4095/297387>
- Percival, J.A., Cook, F.A. et Clowes, R.M. (ed.), 2012. Tectonic styles in Canada: the LITHOPROBE perspective; Geological Association of Canada, Special Paper 49, 498 p.
- Percival, J.A., Martel, E., Pehrsson, S.J., Acosta-Góngora, P., Regis, D., Thiessen, E., Jamieson, D., Neil, B. et Knox, B., 2016. Report of 2016 bedrock activities for the geologic and metallogenic framework of the south Rae Craton, southeast NWT: GEM 2 South Rae Quaternary and Bedrock project; Geological Survey of Canada, Open File 8142, 17 p. <https://doi.org/10.4095/299469>
- Potter, E.G., Montreuil, J.-F., Corriveau, L. et De Toni, A., 2013. Geology and hydrothermal alteration of the Fab Lake region, Northwest Territories; Geological Survey of Canada, Open File 7339, 1 .zip file. <https://doi.org/10.4095/292562>
- Rainbird, R.H. et Davis, W.J., 2022. On the Statherian-Callymian palaeogeography of northwestern Laurentia; *Journal of the Geological Society*, v. 179, art. no. jgs-2022-062, 20 p. <https://doi.org/10.1144/jgs2022-062>
- Rainbird, R.H. et Ielpi, A., 2015. Reconnaissance geological mapping and thematic studies of the Elu Basin, Nunavut; Geological Survey of Canada, Open File 7730, 10 p. <https://doi.org/10.4095/295696>
- Rainbird, R.H., Davis, W.J., Pehrsson, S.J., Wodicka, N., Rayner, N. et Skulski, T., 2010. Early Paleoproterozoic supracrustal assemblages of the Rae domain, Nunavut, Canada: Intracratonic basin development during supercontinent break-up and assembly; *Precambrian Research*, v. 181, p. 167–186. <https://doi.org/10.1016/j.precamres.2010.06.005>

- Rainbird, R.H., Harrison, J.C., Hillary, E.M., Ford, A., Hulbert, L.J., Christie, R.L. et Campbell, F.H.A., 2015. Geology, tectonic assemblage map of Hadley Bay, Victoria and Prince of Wales islands, Nunavut–Northwest Territories; Geological Survey of Canada, Canadian Geoscience Map 75 (2nd preliminary edition), scale 1:500 000. <https://doi.org/10.4095/295861>
- Rayner, N., 2010. Far north geomapping initiative: new U-Pb geochronological results from the Seal River region, northeastern Manitoba (parts of NTS 54L, M, 64I, P); Manitoba Department of Energy and Mines, Geological Services, Report of Activities 2010, p. 23–35.
- Rayner, N.M., 2014. New U-Pb geochronological results from Hall Peninsula, Baffin Island, Nunavut; Canada-Nunavut Geoscience Office, Summary of Activities 2013, p. 39–52.
- Rayner, N., 2022. U-Pb geochronology data from the 2008–2011 Manitoba Far North Geomapping Initiative; Geological Survey of Canada, Open File 8868, 1 .zip file. <https://doi.org/10.4095/329641>
- Rayner, N.M., St-Onge, M.R. et Miles, W.F., 2014. Report of activities for completing the regional bedrock mapping of the southern half of Baffin Island: GEM 2 Baffin Project; Geological Survey of Canada, Open File 7704, 9 p. <https://doi.org/10.4095/295525>
- Reddy, S.M. et Evans, D.A.D., 2009. Palaeoproterozoic supercontinents and global evolution; correlations from core to atmosphere; *in* Palaeoproterozoic Supercontinents and Global Evolution, (ed.) S. Reddy, R. Mazumder, D.A.D. Evans, and A.S. Collins; Geological Society of London, Special Publication 323, p. 1–26. <https://doi.org/10.1144/SP323.1>
- Regis, D.R. et Sanborn-Barrie, M., 2023. Detrital U-Pb detrital zircon geochronological constraints on Siderian and Orosirian rocks of Boothia Peninsula and Somerset Island (Nunavut, Canada); *Precambrian Research*, v. 387, art. no. 106991, 22 p. <https://doi.org/10.1016/j.precamres.2023.106991>
- Reimink, J.R., Chacko, T., Stern, R.A. et Heaman, L.M., 2016. The birth of a cratonic nucleus: litho-geochemical evolution of the 4.02–2.94 Ga Acasta Gneiss Complex; *Precambrian Research*, v. 281, p. 453–472. <https://doi.org/10.1016/j.precamres.2016.06.007>
- Salminen, J., Pehrsson, S., Evans, D.A.D. et Wang, C., 2021. Neoproterozoic-Paleoproterozoic supercycles; Chapter 15 *in* Ancient Supercontinents and the Paleogeography of Earth, (ed.) L.J. Pesonen, J. Salminen, S.-Å. Elming, D.A.D. Evans, and T. Veikkolainen; Elsevier, p. 465–498. <https://doi.org/10.1016/B978-0-12-818533-9.00014-X>
- Sanborn-Barrie, M. et Young, M., 2011. Bulk compositional data for sulfidic and gossanous rocks from Cumberland Peninsula, Baffin Island, Nunavut; Geological Survey of Canada, Open File 6916, 1 .zip file. <https://doi.org/10.4095/288710>
- Sanborn-Barrie, M., Chakungal, J. et Buller, G., 2009. Bedrock field data and photographic record of exposed Precambrian basement, Southampton Island, Nunavut; Geological Survey of Canada, Open File 6177, 1 .zip file. <https://doi.org/10.4095/247890>
- Sanborn-Barrie, M., Davis, W.J., Berman, R.G., Rayner, N., Skulski, T. et Sandeman, H., 2014. Neoproterozoic continental crust formation and Paleoproterozoic deformation of the central Rae craton, Committee Bay belt, Nunavut; *Canadian Journal of Earth Sciences*, v. 51, p. 635–667. <https://doi.org/10.1139/cjes-2014-0010>
- Sanborn-Barrie, M., Ford, A., Hillary, E.M., Tschirhart, V.L., Tremblay, T. et Maharaj, J., 2016. Report of activities for the GEM-2 Boothia Peninsula-Somerset Island project: integrated geoscience of the Northwest Passage; Geological Survey of Canada, Open File 8128, 11 p. <https://doi.org/10.4095/299381>
- Sanborn-Barrie, M., Regis, D., Ford, A., Osinchuk, A. et Drayson, D., 2018. Report of activities for the GEM-2 Boothia Peninsula-Somerset Island Project: integrated geoscience of the Northwest Passage, Nunavut; Geological Survey of Canada, Open File 8339, 16 p. <https://doi.org/10.4095/306597>
- Sanborn-Barrie, M., Regis, D. et Ford, A., 2019. Integrated geoscience of the Northwest Passage, Nunavut: GEM-2 Boothia Peninsula–Somerset Island project, report of activities 2018; Geological Survey of Canada, Open File 8557, 17 p. <https://doi.org/10.4095/314501>
- Saumur, B.M., Skipton, D.R., St-Onge, M.R., Bros, E.R., Acosta-Góngora, P., Kelly, C.J., Morin, A., O’Brien, M.E., Johnston, S.T. et Weller, O.M., 2018. Precambrian geology of the surroundings of Steensby Inlet and western Barnes Ice Cap (parts of NTS 37E, 37F, 37G), Baffin Island, Nunavut; Canada-Nunavut Geoscience Office, Summary of Activities 2018, p. 29–46.
- Sheen, A.I., Heaman, L.M., Kjarsgaard, B., Ootes, L., Pearson, D.G. et Creaser, R.A., 2019. Athapuscow aulacogen revisited: Geochronology and geochemistry of the 2046 Ma Union Island Group mafic magmatism, East Arm of Great Slave Lake, Northwest Territories, Canada; *Precambrian Research*, v. 321, p. 85–102. <https://doi.org/10.1016/j.precamres.2018.11.012>

- Shimojo, M., Yamamoto, S., Sakata, S., Yokoyama, T.D., Maki, K., Sawaki, Y., Ishikawa, A., Aoki, K., Aoki, S., Koshida, K., Tashiro, T., Hirata, T., Collerson, K.D. et Komiya, T., 2016. Occurrence and geochronology of the Eoarchean, ~3.9 Ga, Iqaluk Gneiss in the Saglek Block, northern Labrador, Canada: Evidence for the oldest supracrustal rocks in the world; *Precambrian Research*, v. 278, p. 218–243. <https://doi.org/10.1016/j.precamres.2016.03.018>
- Skipton, D.R., Schneider, D.A. et St-Onge, M.R., 2013. Preliminary observations on Archean and Paleoproterozoic metamorphism and deformation of the southern Hall Peninsula, Baffin Island, Nunavut; Canada-Nunavut Geoscience Office, Summary of Activities 2012, p. 29–42.
- Skipton, D.R., Saumur, B.M., St-Onge, M.R., Wodicka, N., Bros, E.R., Morin, A., Brouillette, P., Weller, O.M. et Johnston, S.T., 2017. Precambrian bedrock geology of the Pond Inlet–Mary River area, northern Baffin Island, Nunavut; Canada-Nunavut Geoscience Office, Summary of Activities 2017, p. 49–68.
- Skipton, D.R., Wodicka, N., McNicoll, V., Saumur, B.M., St-Onge, M.R. et Young, M.D., 2019. U-Pb zircon geochronology of Archean greenstone belts (Mary River Group) and surrounding Archean to Paleoproterozoic rocks, northern Baffin Island, Nunavut; Geological Survey of Canada, Open File 8585, 1. zip file. <https://doi.org/10.4095/314938>
- Skirrow, R.G., 2010. “Hematite-group” IOCG±U ore systems: tectonic settings, hydrothermal characteristics, and Cu–Au and U mineralizing processes; *in* Exploring for iron oxide copper-gold deposits: Canada and Global Analogues, (ed.) L. Corriveau and A.H. Mumin; Geological Association of Canada, Short Course Notes 20, p. 39–58.
- Skulski, T., Paul, D., Sandeman, H., Berman, R.G., Chorlton, L., Pehrsson, S.J., Rainbird, R.H., Davis, W.J. et Sanborn-Barrie, M., 2018. Bedrock geology, central Rae Craton and eastern Queen Maud Block, western Churchill Province, Nunavut; Geological Survey of Canada, Canadian Geoscience Map 307, scale 1:550 000. <https://doi.org/10.4095/308348>
- Snyder, D.B. et Kjarsgaard, B.A., 2013. Mantle roots of major Precambrian shear zones inferred from structure of the Great Slave Lake shear zone, northwest Canada; *Lithosphere*, v. 5, no. 6, p. 539–546. <https://doi.org/10.1130/L299.1>
- Steenkamp, H.M., Wodicka, N., Lawley, C.J.M., Peterson, T., Garrison, W., Therriault, I., Kendrick, J., Weller, O.M. et Tschirhart, V., 2023a. Bedrock geology, Daly Bay area, Kivalliq, Nunavut, NTS 56-A, 46-D west, 46-E southwest, and 56-H south; Geological Survey of Canada, Canadian Geoscience Map 458, scale 1:150 000. <https://doi.org/10.4095/331888>
- Steenkamp, H.M., Wodicka, N., Lawley, C.J.M., Peterson, T., Weller, O.M., Kendrick, J. et Tschirhart, V., 2023b. Bedrock geology, Armit Lake area, Kivalliq, Nunavut, NTS 56-B and 56-C east; Geological Survey of Canada, Canadian Geoscience Map 459, scale 1:150 000. <https://doi.org/10.4095/331889>
- Steenkamp, H.M., Wodicka, N., Weller, O.M., Kendrick, J., Therriault, I., Peterson, T., Lawley, C.J.M. et Tschirhart, V., 2023c. Bedrock geology, Wager Bay area, Kivalliq, Nunavut, parts of NTS 56-F and 56-G; Geological Survey of Canada, Canadian Geoscience Map 460, scale 1:150 000. <https://doi.org/10.4095/331890>
- Stern, R.J., 2020. The Mesoproterozoic single-lid tectonic episode: prelude to modern plate tectonics; *GSA Today*, v. 30, no. 12, p. 4–10. <https://doi.org/10.1130/GSATG480A.1>
- Whalen, J.B., Sanborn-Barrie, M. et Young, M., 2012. Geochemical data from Archean and Paleoproterozoic plutonic and volcanic rocks of Cumberland Peninsula, eastern Baffin Island, Nunavut; Geological Survey of Canada, Open File 6933, 1 .zip file. <https://doi.org/10.4095/291453>
- Wodicka, N., Corrigan, D., Nadeau, L. et Erdmann, S., 2011. New U-Pb geochronological results from Melville Peninsula: unravelling the Archean and early Paleoproterozoic magmatic history of the north-central Rae craton; Geological Association of Canada–Mineralogical Association of Canada, Abstracts, v. 34, p. 236.
- Wodicka, N., St-Onge, M.R., Corrigan, D., Scott, D.J. et Whalen, J.B., 2014. Did a proto-ocean basin form along the southeastern Rae cratonic margin? Evidence from U-Pb geochronology, geochemistry (Sm-Nd and whole-rock), and stratigraphy of the Paleoproterozoic Piling Group, northern Canada; *Geological Society of America Bulletin*, v. 126, p. 1625–1653. <https://doi.org/10.1130/B31028.1>
- Wodicka, N., Steenkamp, H.M., Weller, O.M., Kendrick, J., Tschirhart, V.L., Peterson, T.D. et Girard, É., 2016. Report of 2016 activities for the bedrock geology and economic potential of the Tehery-Wager area: GEM 2 Rae Project; Geological Survey of Canada, Open File 8149, 21 p. <https://doi.org/10.4095/299392>
- Wodicka, N., Steenkamp, H.M., Peterson, T.D., McMartin, I., Day, S.J.A. et Tschirhart, V.L., 2017. Report of 2017 activities for the geology and economic potential of the Tehery-Wager area, Nunavut: GEM-2 Rae Project; Geological Survey of Canada, Open File 8318, 20 p. <https://doi.org/10.4095/305979>
- Wright, D.F., Ambrose, E.J., Lemkow, D. et Bonham-Carter, G. (ed.), 2013. Mineral and energy resource assessment of the proposed Thaidene Nene National Park Reserve in the area of the east arm of Great Slave Lake, Northwest Territories. Geological Survey of Canada, Open File 7196, 1 .zip file. <https://doi.org/10.4095/292447>

Introduction and summary

S.J. Pehrsson^{1*}, N. Wodicka¹, J.A. Percival¹, and N. Rogers¹

Pehrsson, S.J., Wodicka, N., Percival, J.A., and Rogers, N., 2024. Introduction and summary; in Canada's northern shield: new perspectives from the Geo-mapping for Energy and Minerals program, (ed.) S.J. Pehrsson, N. Wodicka, N. Rogers, and J.A. Percival; Geological Survey of Canada, Bulletin 612, p. 1–26. <https://doi.org/10.4095/332493>

Abstract: The Geo-mapping for Energy and Minerals (GEM) program was funded between 2008 and 2020 with the aim of advancing geological knowledge of the North to reduce risk for mineral exploration and inform land-use decisions and future management of the North. Twenty-one regional activities were undertaken across Canada's northern shield, spanning northern Prairie Provinces, northern Quebec, Labrador, along with much of Nunavut and Northwest Territories. A further five activities were thematic in nature. Bulletin 612 presents results from 12 of these endeavours, including integrated regional bed-rock geoscience studies, geophysical surveys, and basin analyses, as well as thematic thermochronology, geochemistry and large igneous province syntheses. The results highlight that GEM has contributed to new era of understanding of the northern Canadian Shield, expanding its framework substantially and developing an increasingly complex model of Archean cratons, Archean/Proterozoic microcontinents, and juvenile Paleoproterozoic crust that highlights the existence of a dozen new pericratonic to exotic ribbon microcontinents within a mosaic once considered as mostly large cratonic masses welded by Paleoproterozoic orogens. This emerging picture brings additional questions for future northern studies — particularly in the granularity of subdivision of the largest blocks, the impact of enigmatic earliest Paleoproterozoic orogens, and dynamics of assembly of exotic and little-known terranes.

Résumé : Le programme Géocartographie de l'énergie et des minéraux (GEM) a fait l'objet d'un financement de 2008 à 2020 pour faire progresser les connaissances géologiques sur le Nord, dans le but de réduire les risques liés à l'exploration minérale et d'éclairer les décisions propres à l'utilisation des terres et à la gestion future du Nord. Vingt et une activités régionales ont été entreprises dans le nord du Bouclier canadien, qui comprend le nord des provinces des Prairies et du Québec, le Labrador ainsi qu'une grande partie du Nunavut et des Territoires du Nord-Ouest. Cinq autres activités étaient de nature thématique. Le Bulletin 612 présente les résultats de 12 de ces activités, notamment des études géoscientifiques intégrées sur le substratum rocheux à l'échelle régionale, des levés géophysiques et des analyses de bassin, ainsi que des synthèses thématiques sur la thermochronologie, la géochimie et les grandes provinces ignées. Les résultats montrent que le programme GEM a contribué à une nouvelle ère de connaissances sur le nord du Bouclier canadien, en élargissant considérablement son cadre et en élaborant un modèle de plus en plus complexe des cratons de l'Archéen, des microcontinents de l'Archéen/Protérozoïque et de la croûte juvénile du Paléoprotérozoïque qui met en évidence l'existence d'une douzaine de nouveaux microcontinents allant d'entités péricratoniques à des éléments exotiques en rubans au sein d'une mosaïque autrefois considérée comme formée de grandes masses cratoniques soudées par des orogènes paléoprotérozoïques. Ce portrait émergent soulève d'autres questions pour les futures études sur le Nord, particulièrement en ce qui concerne la granularité de la subdivision des plus grands blocs, l'incidence des énigmatiques orogènes du Paléoprotérozoïque initial et la dynamique de l'assemblage des terranes exotiques et peu connus.

¹Geological Survey of Canada, 601 Booth Street, Ottawa, Ontario K1A 0E8

*Corresponding author: S.J. Pehrsson (email: sally.pehrsson@nrcan-rncan.gc.ca)

INTRODUCTION

The 2008 to 2020 Geological Survey of Canada (GSC) led Geo-Mapping for Energy and Minerals (GEM) program was undertaken to advance geological knowledge of the North, with the intention of reducing risk for mineral exploration and to inform land-use decisions, balancing conservation and responsible resource development (Geological Survey of Canada, 2018). Bedrock geoscience research in support of these goals was undertaken in the northern Canadian Shield, which constitutes the area of discontinuous permafrost within the northern Prairie Provinces, Quebec, Labrador, along with much of Nunavut and Northwest Territories. The program was delivered in partnership with the Northwest Territories Geoscience Office (Northwest Territories Geological Survey since 2015), Saskatchewan Geological Survey, Manitoba Geological Survey, Canada-Nunavut Geoscience Office, Ministère de l'Énergie et des Ressources naturelles du Québec, and Geological Survey of Newfoundland and Labrador, as well as Northerners, Northern institutions, academia, and industry. The underlying objective of these activities was to fill major gaps in geoscience understanding of the northern Canadian Shield stemming from a combination of the scale and vintage of previous mapping, geological complexity, exposure, and access. Over the two GEM phases (2008–2013 and 2013–2020) more than 40 academic researchers and 9 postdoctoral fellows were supported, with over 50 graduate and undergraduate theses produced, encompassing nearly a dozen existing lithotectonic subdivisions of the northern Canadian Shield (Fig. 1).

GSC Bulletin 612 summarizes advances in understanding of bedrock geology in many of the least known parts of the shield generated through field- or lab-based research conducted by the GEM program. It draws together insights from 14 individual studies (referred to herein as *activities*) to present a coherent overview of the tectonic evolution and metallogenic potential of the northern Canadian Shield. The bulletin includes 10 regional bedrock syntheses, followed by 4 shield-scale thematic syntheses. These are based on over 50 journal and research papers, reports, and open file data compilations including lithogeochemistry, geochronology, and geophysics.

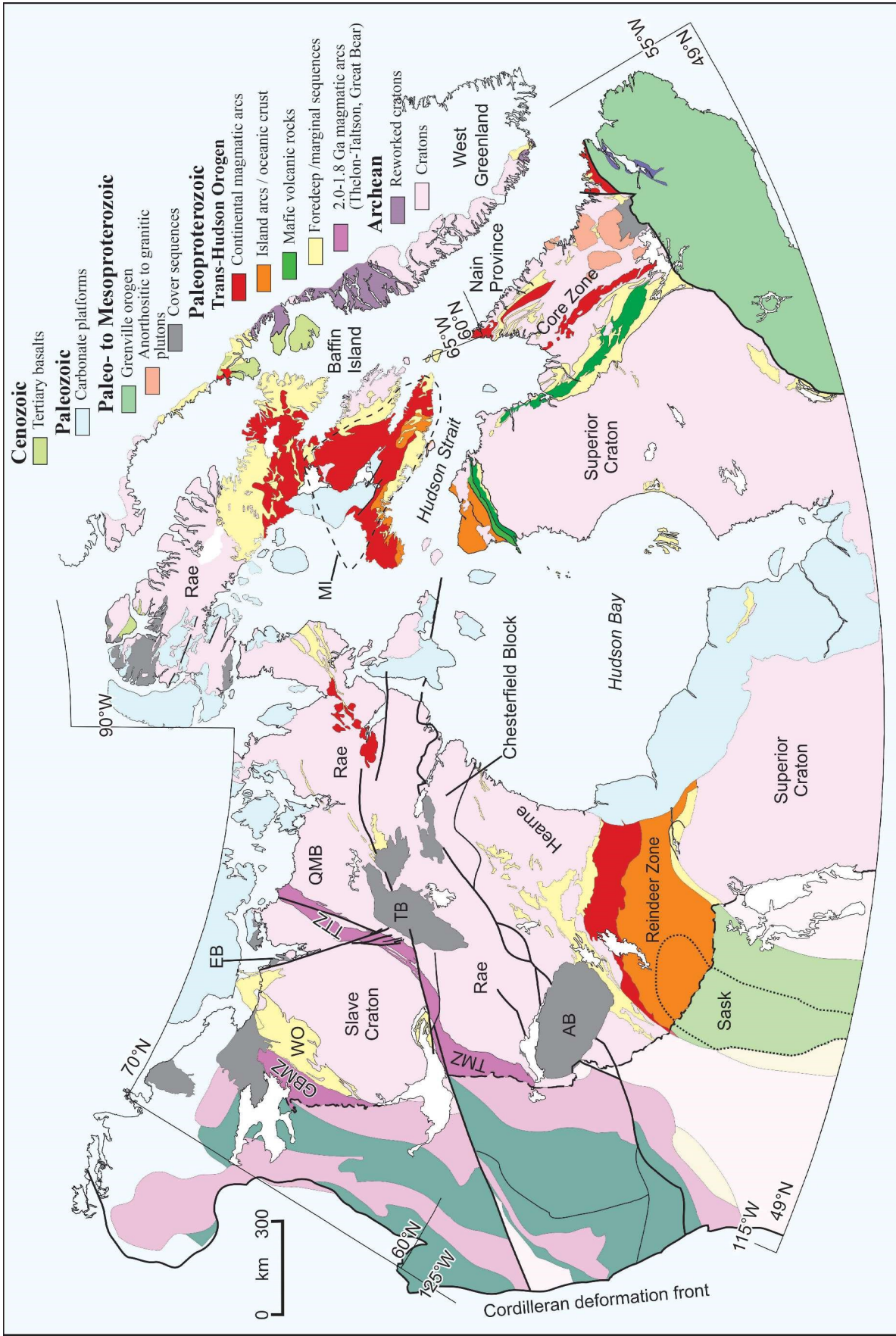
In the following sections we briefly discuss 1) the state of understanding of the northern Canadian Shield prior to GEM research; 2) the major science questions GEM addressed for the northern Canadian Shield; and 3) the major regional and thematic results presented in this volume. Table 1 summarizes projects conducted under GEM. Table 2 presents key new or revised lithotectonic divisions and scientific understanding of the shield generated by GEM. Although these papers are not an exhaustive overview of northern Canadian Shield GEM results, they do provide a preliminary synthesis of research results and highlight outstanding questions for future study.

CANADA'S NORTHERN SHIELD AND GEM

The evolution, assembly, and architecture of the Canadian Shield (Fig. 1), the Precambrian heart of the Canadian landmass, has been investigated for over a century in order to understand its mineral wealth and diverse geological history that spans more than 3 billion years. Regional mapping, crust-formation, and tectonothermal studies, as well as crust-mantle focused geophysical research by numerous research institutes and geological surveys have underpinned this (Clowes et al., 1999). However, the field-based studies have been spatially constrained by practicalities of access and exposure, with the result that the broadest and deepest understanding of its constituent cratons and orogens was focused either south of 60°N (e.g. Superior Province, Grenville and Trans-Hudson orogens; Fig. 1) or near major northern transportation corridors (e.g. Slave Province, Wopmay Orogen, Great Bear magmatic zone).

The shield represents over 50% of Canada's landmass and forms the core of the paleocontinent Laurentia, a largely Paleoproterozoic collage of Archean cratons, microcontinents, and younger arc systems that were first assembled by 1.8 Ga (Hoffman, 1988). The Canadian Shield is important both geologically

Figure 1. Lithotectonic map of the Canadian Shield (*modified after* Corrigan et al., 2018) and adjacent Precambrian basins at the outset of the Geo-mapping for Energy and Minerals program. Abbreviations: AB = Athabasca Basin; EB = Elu Basin; GBMZ = Great Bear magmatic zone; MI = Meta Incognita terrane; QMB = Queen Maud Block; TB = Thelon Basin; TMZ = Taltson Magmatic Zone; TTZ = Thelon Tectonic Zone; WO = Wopmay Orogen.



and economically: geologically for the fundamental advances in understanding of Precambrian tectonic processes following decades of field-based and supported research; and economically for its stature as a major contributor to Canada's mineral production.

The northern Canadian Shield, the main focus of GEM, is composed of Archean cratons, numerous microcontinents and crustal slivers, and a smaller volume of juvenile Paleoproterozoic crust, all overlain by Paleo- to Mesoproterozoic cratonic cover sequences (Fig. 1). The six major cratons — Slave, Rae, Hearne, Superior and Nain, along with the buried Mackenzie — have ca. 2.5 to 2.1 Ga passive margins or marginal sequences and were amalgamated and reworked to varying degrees during the 2.0 to 1.8 Ga Taltson-Thelon, Snowbird, Trans-Hudson, Wopmay, and New Quebec orogenies (Eglington et al., 2013). This basic framework of distinct cratons bounded by Paleoproterozoic orogens was first defined in Hoffman's United Plates of America and related papers (Hoffman 1988, 1990), with major advances coming from innovations in isotopic dating and geophysics. Successive waves of research programs by government and academia between 2000 and 2010, such as the Shield Margin NATMAP, Western Churchill NATMAP, EXTECH, and, arguably most importantly, LITHOPROBE (Percival et al., 2012), expanded this framework substantially, including the recognition/incorporation of microcontinents, such as Chesterfield Block and Sask Craton (Fig. 1, Table 2), and the categorization of orogens that refined our comprehension of an intricate mosaic of classic collisional (e.g. Wopmay Orogen, Trans-Hudson Orogen-Reindeer zone) and accretionary (East Alberta Orogen, Snowbird Orogen) orogens that display crustal to upper mantle structures largely analogous to younger orogens (Clowes et al., 1999). Integration of crustal history with sophisticated characterization of subcontinental architecture further focused this model (Snyder and Kjarsgaard, 2013).

These advances took place against a backdrop of a decade of rapid evolution in understanding the development of the Archean and Paleoproterozoic Earth (Reddy and Evans, 2009). Many researchers accepted a form of modern-style plate tectonics that was largely operative by 1.9 Ga (Condie and Kröner, 2008), but controversy extended its applicability to 2.5 Ga or older periods (Stern, 2020). The Great Oxygenation Event (GOE) at the onset of the Paleoproterozoic saw the first major rise of atmospheric oxygen, reaching roughly half of the present-day amount by 2.3 Ga (Lyons et al., 2014), following a substantial decline in mantle temperature (Korenaga, 2008) and overlapping in time with major global events like the first Snowball Earth (Kopp et al., 2005; Hoffman, 2013) and C isotope excursions in seawater (Eguchi et al., 2022). A noted lull in preserved juvenile crustal addition, the so-called ca 2.3 Ga 'magmatic gap', was proposed by Condie et al., (2009) to represent a slowdown or cessation of mantle convection that may have triggered modern-style plate tectonics post 2.2 Ga, although this interpretation is not universally accepted (e.g. Pehrsson et al., 2014a). Archean to Paleoproterozoic supercratons and supercontinents were beginning to be reconstructed with increasing confidence (Bleeker, 2003; Salminen et al., 2021). Important additional advances came from the study of early Earth history (Reimink et al., 2016; Shimojo et al., 2016) and burgeoning studies of northern Canadian Shield lithosphere (Canil, 2008; Pearson and Wittig, 2014), for example, that Archean cratonic keels were in part refertilized by Paleoproterozoic assembly, but nevertheless record, through the isotopic signatures of Archean diamonds, some of the earliest indications of the return of seawater to the mantle (Pearson et al., 2014).

As indicated above, a general understanding for parts of the northern Canadian Shield had been established prior to GEM; however, knowledge crucial to defining orogenic processes and regional metallogenic potential remained inadequate. Large parts of the Shield remained unsubdivided and poorly constrained, even lacking 1:250 000 scale mapping. The overall architecture of Trans-Hudson and Taltson-Thelon orogens, particularly their hinterlands, was incomplete, and the number, origin, and lithotectonic makeup of microcontinents caught in the Paleoproterozoic orogens were poorly understood, particularly west of Slave Craton and west of Hudson Bay. Details such as the topology, controls on magmatism, and age of major suture zones remained insufficient to resolve controversies such as the accretionary or internal collisional nature of the Snowbird and Taltson-Thelon orogens, both of which were alternatively proposed as Neoproterozoic to earliest Paleoproterozoic sutures. Even orogens mapped in more detail, such as the Great Bear-Wopmay, contained enigmas — for example the genesis of early Hottah terrane and extent of Slave Craton below Wopmay Orogen. At the craton scale, correlation of domains across Hudson Bay remained a barrier to evolving models.

GEM program

With an ambitious goal of completing a coarse-scale bedrock map of the North by 2020, the focus for GEM was to address the most pressing knowledge gaps in composition, evolution, and assembly of the northern Canadian Shield. A review across the North revealed persistent and significant geoscience knowledge gaps in surface and subsurface geological structures and earth systems through time, particularly in the Rae Craton and Core Zone (Fig. 1). This was due to insufficient previous bedrock mapping combined with geological complexity, limited exposure, and restricted access. Frequently, the situation is exacerbated by scant modern geochemical geochronological or isotopic data. More recently studied cratons or areas with extensive road access (i.e. Slave and Superior) were not primary targets of GEM but were included in broad thematic assessments for the Trans-GEM project. The Slave Craton's formation and evolution are summarized in a GEM-supported book (Helmstaedt et al., 2021).

The first phase of GEM in the northern Canadian Shield encompassed eight regional activities centred in mainland Churchill and Great Bear-Wopmay provinces and broad thematic studies covering diamonds and uranium (2008–2013; Table 1; Fig. 2, 3). The common goal of the regional activities was to upgrade geoscience understanding and geological models for Archean to Paleoproterozoic terranes with potential for base and precious metals, critical and precious minerals, carving stone, and aggregate. Research included framework geological mapping, thematic mapping, airborne geophysics, regional geochemical surveys, and a variety of supporting geoscience including lithochemical, isotopic, and geochronological studies. Diamond-related research occurred in the Slave Craton and the Repulse Bay–Boothia Peninsula and Melville Peninsula–northwest Baffin Island corridors of the Rae Craton. Uranium-related research was focused on the northern Athabasca Basin/Rae Craton and the Lac Cinquante area of the Chesterfield Block (Fig. 1).

The 2010 to 2012 'Geo-mapping Frontiers' exercise was a major desktop and reconnaissance operation to access non-digital data from the first major northern reconnaissance mapping projects of the 1950s and 60s: Operations Keewatin, Bathurst, Baker, Wager, and Thelon (Harris et al., 2013). Following on from this, the Rae, Hudson-Ungava, and Baffin were defined as the main areas of interest for the second phase of GEM (2013–2020), thereby expanding the reach of the program to other parts of the northern Canadian Shield. Ten new projects were focused on the most poorly known parts of the shield, including north, central, and south Rae Craton, southeast Churchill Province of Quebec and Labrador, Trans-Hudson Orogen of south Baffin Island, Thelon Orogen of Northwest Territories, Proterozoic terranes and basins of Circum-Ungava, and Paleo- to Mesoproterozoic basins overlying Great Bear magmatic zone and Slave Craton (Table 1; Fig. 2, 3). Frontier-scale projects (typically 1:250 000 scale mapping; i.e. south Rae and Tehery Lake-Wager Bay area) had the goal of providing basic knowledge on the distribution of major rock units, documenting their geological histories, and a preliminary evaluation of their economic potential. Orogen- or district-specific activities (e.g. Chantrey-Thelon, Core Zone) were conducted at a more detailed scale to resolve specific questions like the genesis of established architectures. All the regional activities addressed orogenic and cratonic architecture, domain boundaries in three dimensions, and mineral potential by comparison to better known cratons such as Superior or Yilgarn. Related thematic research included new compilations and syntheses of large igneous provinces and low-temperature thermochronology across the North, including the northern Canadian Shield, and of the Snow Island Suite in Rae Craton and Chesterfield Block.

Preliminary GEM results have been disseminated through multiple Current Research papers, Open File Reports of Activities, Canada-Nunavut Geoscience Office Report of Activities and/or summary journal publications (Table 1). New regional geophysical (aeromagnetic, gravity, magnetotelluric) or geochemical (lake, stream sediment, water; *see* McClenaghan et al., 2022) surveys were integral parts of many activities (Table 1). All of these resources can be found in NRCan's GEOSCAN and Geophysical Data Repository. GEM surficial studies that overlap the northern Canadian Shield are included in Bulletin 611 (McMartin, 2023) and results from Baffin Island are presented in Bulletin 608 (Dafoe and Bingham-Koslowski, 2022).

Table 1. GEM projects (2008–2020) based in the northern Canadian Shield and lithotectonic elements in which they were focused.

Project	Jurisdiction	Geological region	Selected Report of Activities or Summary publications	Supporting surveys
Phase 1 (2008–2013)				
Great Island-Far North	Manitoba	Hearne Craton	Rayner, 2010; Kremer et al., 2011	Aeromagnetic
Melville Peninsula	Nunavut-Kitikemeot	Rae Craton	Corrigan et al., 2013	Aeromagnetic, MT, Geochemical
Cumberland Peninsula	Nunavut-Qikiqtani	Rae Craton	Sanborn-Barrie and Young, 2011; Whalen et al., 2012	Aeromagnetic
Hall Peninsula	Nunavut-Qikiqtani	Rae Craton	Skipton et al., 2013; Rayner, 2014	Aeromagnetic, MT
Northeast Thelon Basin	Nunavut-Kivalliq	Rae Craton	Jefferson et al., 2011, 2015, 2022, this volume	Aeromagnetic, Gravity
GEM Frontiers	Nunavut/Northwest Territories	Churchill Province	Pehrsson et al., 2014a	Aeromagnetic, Gravity
Operation GEM	Nunavut/Northwest Territories	Churchill Province	Pehrsson et al., 2014b	Aeromagnetic, Gravity
Chesterfield	Nunavut-Kivalliq	Chesterfield Block	Pehrsson et al., 2014b, c	Aeromagnetic, Gravity
Great Bear-Wopmay	Northwest Territories	Great Bear/Wopmay Orogen	Craven et al., 2013; Corriveau et al., 2015	Aeromagnetic, Gravity, MT
Victoria Island	Nunavut-Kitikemeot	Arctic islands	Rainbird et al., 2015; Bédard et al., 2016	
Southampton Island	Nunavut-Kivalliq	Rae Craton	Sanborn-Barrie et al., 2009, 2018	
Phase 2 (2013–2020)				
South Rae	Northwest Territories	South Rae Craton	Pehrsson et al., 2015a, b, c; Percival et al., 2016	Aeromagnetic, Geochemical
Chantrey-Thelon-Montresor	Nunavut-Kitikemeot	Thelon Orogen and north-central Rae Craton	Berman et al., 2015a, b; 2016, 2018	Aeromagnetic, MT, Gravity, Geochemical
Tehery Lake-Wager Bay	Nunavut-Kivalliq	Central Rae Craton	Wodicka et al., 2016, 2017	Aeromagnetic, MT, Gravity, Geochemical
Elu Inlet	Nunavut-Kitikemeot	Slave Craton	Ielpi et al., this volume	
Core Zone	Quebec, Labrador	SE Churchill Province	McClenaghan et al., 2014; Corrigan et al., 2015, 2016	Aeromagnetic, Geochemical
Mesoproterozoic basins	Northwest Territories	Bear Province	Rainbird and Davis, this volume	
Circum-Ungava	Quebec, Nunavut	Reindeer zone, Cape Smith	Corrigan et al., 2021	
North Baffin	Nunavut-Qikiqtani	North Rae Craton	Saumur et al., 2018; Skipton et al., 2017, 2019	Aeromagnetic
South Baffin	Nunavut-Qikiqtani	Meta Incogita terrane	Rayner et al., 2014	Aeromagnetic
Boothia-Somerset	Nunavut-Qikiqtani	North Rae Craton	Sanborn Barrie et al., 2016, 2018, 2019	Aeromagnetic
Thematic or Trans-GEM				
Northern uranium for Canada	Saskatchewan, Nunavut	Rae, Hearne cratons	Jefferson et al., 2013; this volume	
Diamonds	Northwest Territories, Nunavut	Slave, Rae cratons		Teleseismic
LIP compilation	various	northern Canadian Shield	Buchau and Ernst, 2013	
Snow Island Suite geochemistry	Nunavut, Northwest Territories	Rae Craton/Chesterfield Block	Peterson et al., this volume	
Low-temperature thermochronology	various	Shield-wide and Reindeer zone	Kellett et al., this volume	
Abbreviations: LIP=large igneous provinces; MT=Magnetotelluric; SE=Southeast				

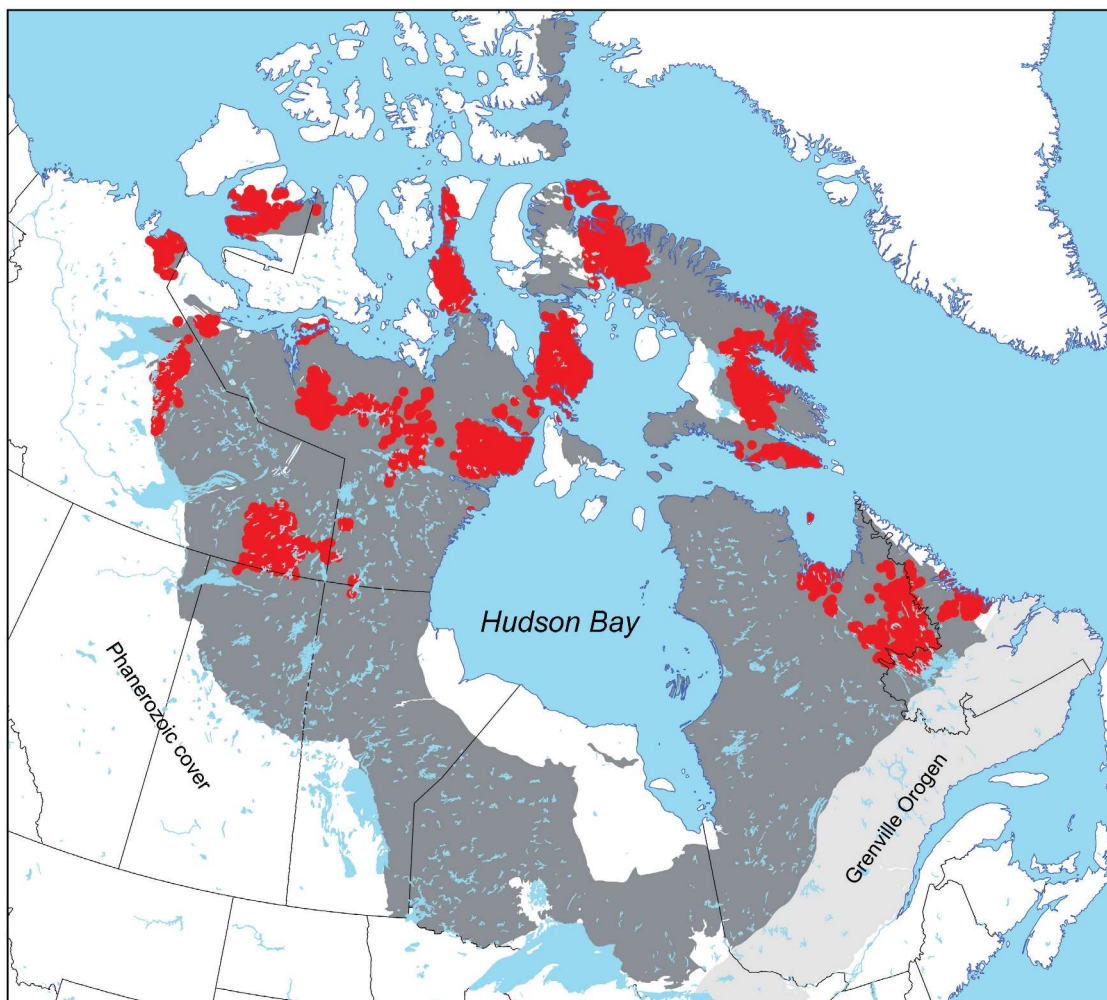


Figure 2. GEM projects of the northern Canadian Shield illustrated by station locations (red). Dark grey region represents the exposed northern Canadian Shield.

PAPERS OF BULLETIN 612

Regional bedrock syntheses

Great Bear magmatic zone

Corriveau and Potter (this volume) present mineralization within the ca. 1.86 to 1.78 Ga Great Bear magmatic zone as a case study to develop geological and geophysical fingerprints for iron oxide-copper-gold (IOCG) systems, an important ore system associated with calc-alkaline arc and shoshonitic magmatism. To facilitate this, they begin with a compilation of Canadian and global IOCG deposits, their geometry, alteration, and metal tenor; then use ore systems as the framework for exploration. They test and refine research approaches in remote shield areas, demonstrating how the major IOCG prospectivity criteria of Skirrow (2010) can be applied in terms of geodynamics, facies, units, and structural pathways, to build a spatial and temporal picture of the architecture of fluid alteration systems. They show that the Great Bear magmatic zone hosts a spectrum of metasomatic systems from early and barren albitite corridors to high-temperature alteration-driven iron oxide-apatite (\pm rare-earth) mineralization and IOCG variants rich in cobalt and other critical metals (Potter et al., 2013). They integrate new stratigraphic, structural, and deposit-scale knowledge of NICO, the largest Canadian IOCG deposit, the historic Port Radium district, and Rayrock uranium mine to show that there is an association between gossan and albitite alteration in the roof of subvolcanic intrusions, a key, widely applicable exploration footprint.

The GEM IOCG synthesis demonstrates that petrological alteration mapping and geophysical surveying at the district scale can be used to develop IOCG targets. In particular, integrating new gravity-modelling techniques, as well as using aeromagnetic surveys to calculate pseudogravity, maximizes knowledge from regional surveys (Hayward and Oneschuk, 2011; Kiss and Coyle, 2011a–f; Hayward et al., 2013). Related magnetotelluric research in the Great Bear magmatic zone identified conductors linked to zones of ground preparation and cryptic, thickened lithospheric boundaries, as well as new understanding of the architecture of overlapping basins (Hoggard et al., 2019). Corriveau and Potter finish with a brief summary of collaborative research with other national geological surveys and institutions, and the application of their approach to the central mineral belt in Labrador.

Elu Basin

Ielpi et al. (this volume) describe fluvial systems in the 1.9 to 1.6 Ga Kilohigok and 1.6 to 1.2 Ga Elu Basins, western Nunavut, that were last studied in the 1970s. The aim therein is to examine the stratigraphy, sedimentology, and economic potential of these Paleo- to Mesoproterozoic sedimentary basins, with emphasis on the prospectivity of the Elu Basin to host stratabound and/or unconformity-associated uranium mineralization. Three field seasons of mapping led to the recognition of two terrigenous sandstone formations, both with important aeolian intervals (Rainbird and Ielpi, 2015). By integrating regional basin analysis, they demonstrated westward paleoflow, which, combined with detrital-zircon geochronology, showed sedimentary materials derived directly from the central Thelon Orogen (*see* Berman et al., this volume), and, by ca. 1.6 Ga, important input from 2.4 to 2.3 Ga Arrowsmith Orogen materials associated with the eastern Queen Maud Block. Their research supports conventional models of the uppermost Kilohigok Basin as a foredeep related to Slave and Rae craton collision. Furthermore, it demonstrates erosional unroofing of much of the Thelon and Trans-Hudson orographic relief in under 200 Ma, as by Elu Basin formation there was no topographic barrier to sediment transport off the western Rae Craton. The authors use regional criteria to correlate Ellice Formation (Elu Basin) with other contemporaneous intracontinental northern Canadian Shield sandstone sequences: Barrenland and Athabasca groups on the Rae Craton; and Mountain Lake and Dismal Lakes groups on Great Bear-Wopmay Orogen basement rocks. Ielpi et al. concur with previous models that suggested these sandstones are erosional remnants of a once wider deposit that blanketed the Canadian Shield, and importantly demonstrate how these depocentres evolved during amalgamation and tenure of the 1.8 to 1.4 Ga supercontinent Nuna, linking unusual fluvial channel morphology to proposed tropical paleolatitudes and a drier trade-wind circulation in a non-vegetated Precambrian supercontinental interior.

Chantrey-Thelon area

Berman et al. (this volume) present results for the central Thelon tectonic zone (Fig. 1), a major geological feature of the northern Canadian Shield about which there has been significant controversy since its original definition. Contrasting models propose that it formed as a magmatic arc marking subduction and suturing between Slave and Rae cratons at 2.0 to 1.95 Ga (Hoffman, 1988), or that it represents a dominantly intracontinental magmatic zone formed far from an active plate boundary, but near an earlier (ca. 2.4–2.3 Ga) collisional suture (Chacko et al., 2000). In the latter interpretation, it is considered a direct extension of the 1.97 to 1.90 Ga Taltson magmatic zone between the Rae Craton and Buffalo Head terrane (Fig. 3). However, alternate models link Thelon tectonic zone magmatism to other buried sutures of the southwestern Canadian Shield (Card et al., 2014).

The authors present an overview of six new Thelon tectonic zone subdomains stemming from two years of bedrock mapping accompanied by geochronological, petrogenetic, and tectonothermal studies. Results show that the early (2.03–1.96 Ga) Thelon magmatic suite has geochemical signatures consistent with a convergent margin setting and oxygen isotope compositions skewed toward mantle values similar to those observed in Cenozoic continental arcs. New Sm-Nd data indicate that Thelon tectonic zone was built in part on ancient Queen Maud Block crust that had rifted to form a pericratonic microcontinent (3.2–3.1 Ga Duggan Lake Domain). Such a rift-to-drift setting explains provenance and compositions of a newly recognized syn-Thelon tectonic zone, low-grade volcano-sedimentary sequence with back-arc VMS potential (Ellice River supracrustal belt) that was inverted and migmatized during major high-grade metamorphism concurrent with 1.93 to 1.90 Ga leucogranite magmatism. These data suggest no direct correlation between Thelon tectonic zone and Taltson magmatic zone as required by the intracratonic,

orogenic batholith model and support the Paleoproterozoic arc origin model of Hoffman (1988), highlighting how important detailed petrogenetic and isotopic data are for unravelling the complexity of northern Canadian Shield assembly.

Montresor belt

Understanding the Paleoproterozoic tectonic evolution of the reworked Churchill Province is challenging owing to its polyorogenic history, but one of the most fruitful avenues to elucidating its post-2.3 Ga architecture involves investigating the Paleoproterozoic sedimentary belts that demarcate the original latest Neoproterozoic paleosurface and subsequent loading. Like many of the northern Rae Paleoproterozoic assemblages, the Montresor belt, north-central Rae Craton, was last mapped by late 1970s to 80s reconnaissance studies and has received relatively little exploration attention (Rainbird et al., 2010). Percival et al. (this volume) summarize the results of two field seasons and present a new model for the basin's evolution.

The Montresor belt is underlain by clastic and carbonate rocks preserved in a broadly synformal structure with a complex history as demonstrated by new geological and geophysical information. This originally broad platformal basin is divided into a lower, highly imbricated, high-grade group comprising sandstone, mudstone, and carbonate deposited between ca. 2194 and 2045 Ma, and a ca. <1924 Ma upper group at lower metamorphic grade consisting of mixed clastic and carbonate rocks exposed in a simpler synformal structure. Provenance modes in the upper group are consistent with a Queen Maud block derivation that, along with its deposition just prior to renewed ca. 1.92 to 1.89 Ga Thelon orogenesis, allows it to represent a foreland to foredeep deposit formed during the waning phases of Thelon magmatism following Slave and Rae collision. Comparison of the geometry and ages of deformation/metamorphism of the imbricated lower sequence to the simpler geometry of the upper carbonate-mixed ramp suggests a transition through time to more far-field polyphase deformation related to the 1.89 to 1.80 Ga Trans-Hudson Orogen. This belt is part of a series of marginal sequences deposited after the 2.5 to 2.3 Ga Arrowsmith Orogeny (Berman et al., 2013). It exemplifies a regional geometry that is key to understanding the 1.9 to 1.8 Ga structural style, including crucial 1848 to 1837 Ma detachment faulting linked to hydrothermal mineralization. Percival et al. demonstrate that Montresor belt compares favourably with other similar belts north of Baker Lake that show significant thrusting of granitic basement and quartzite of the basal sequence. This geometry, also characteristic of the Woodburn and northeast Thelon regions, complicates recognition of the original Paleoproterozoic stratigraphic sequence but also highlights the across-strike extent of Trans-Hudson reworking well into its far-field hinterland of the Rae upper plate.

Ongoing research includes working to understand the implication of the regional structural geometry for styles of mineralization and investigating impact spherules recognized in mudstone of the footwall complex. Determining the nature and origin of the spherules will likely be significant for resolving the Earth's atmospheric and biological evolution, forming as they did just after the transition to an early oxygenated environment.

Northeast Thelon Basin region

The geodynamic setting of the late Paleoproterozoic intracontinental Thelon Basin has significance due to its relation to the contemporaneous 1.7 to 1.4 Ga Athabasca Basin that hosts world-class unconformity-uranium deposits (Fig. 1). Jefferson et al. (this volume) present a comprehensive summary of the geology and metallogeny of the northeast Thelon Basin, centred on Aberdeen Lake, Nunavut, and its surrounding Neoproterozoic to early Paleoproterozoic basement. This area contains known basement-hosted U deposits, but they lacked sufficient knowledge to contextualize their formation. Geological mapping, U-Pb geochronological, geophysical and structural studies have refined and expanded knowledge of the structural and age distribution of U-prospective Neoproterozoic basement sequences. Furthermore, they define and correlate Paleoproterozoic cover sequences that flank and extend beneath the Thelon Basin, and they elucidate basement architecture that influenced reactivated mineralizing structures.

Detailed mapping of the arkosic-lithic quartzose sandstone basin fill, subjacent ca. 1.83 to 1.75 Ga Wharton and Baker Lake groups, and complex Snowbird and Trans-Hudson orogenic basement architecture has enabled recognition of multiple diagenetic events that pervasively altered the sandstone, along with hitherto unknown major crustal breaks that focus fluid paths (Jefferson et al., 2012). The authors show

that although northeast Thelon and Athabasca basins have somewhat temporally and spatially independent diagenetic and metallogenic histories, including distinct stratigraphic architecture and basement host rocks, the less-explored Thelon Basin nevertheless hosts similar U metallotects to those of the Athabasca Basin. A conclusion is that Thelon Basin fault offsets were much greater, and sedimentation was much more proximal in the Aberdeen Lake area than in the Athabasca Basin, demonstrating how preserved strata and basement alteration, and structurally/geophysically defined major horsts point to an originally much greater extent for the Thelon Basin. They propose that 2.6, 1.8, and 1.75 Ga magmatic suites were important uranium sources. They highlight the post-tectonic 1.75 Ga Kivalliq igneous suite as associated with pervasive silicification and initial faulting prior to deposition and mineralization of the Thelon Formation. Their review showed that the 1.75 Ga and older faults, plus additional faults, were multiply reactivated to control accommodation space and paleotopography, and to focus chlorite+clay+apatite+uraninite alteration of basement rocks around uranium deposits, with insufficient such data in the Thelon Formation. Overall, their work compares differing geodynamic settings of basin formation, the Thelon, wholly within Rae Craton, with its weakly metamorphosed cover sequences, and the Athabasca, straddling the Rae-Hearne suture where the conductive cover sequences are highly metamorphosed throughout. Jefferson et al. depart from previous models that suggested these sandstones are erosional remnants of a once wider deposit that blanketed the Canadian Shield, in that the preservational basins are largely depositional basins, minimizing the amount of sediment originally deposited between major basins. They further elucidate subtle but important differences in diagenetic and mineralizing processes and targets between major basin regions.

South Rae Craton

Pehrsson (this volume) presents a short summary of the geology of the south Rae Craton, Northwest Territories, based on a new synthesis and subdivision that was developed from a two-year, 400 km long, mapping transect from the Hearne Craton at Kasba Lake to Porter Lake, southeast of the Great Slave Lake shear zone. She integrates four new 1:250 000 maps, U-Pb geochronological, isotopic, and tectonometamorphic studies to show that the south Rae Craton comprises nine distinct Archean to early Paleoproterozoic crustal domains bounded by newly recognized crustal-scale shear zones with a protracted history of deformation and reactivation between 2.5 Ga and ca. 1.7 Ga.

The south Rae Craton is predominantly late Neoproterozoic in age, with evidence for Paleo- to Mesoproterozoic crustal contamination restricted to western domains that include rocks potentially correlative with the Taltson basement complex. Tectonometamorphism and magmatism at ca. 2.5 Ga (MacQuoid Orogeny) are restricted to eastern domains that lie within 75 km of the Snowbird tectonic zone. The ca. 2.4 to 2.3 Ga Arrowsmith Orogeny manifests west of the Black Bay shear zone, where the dominant structures of large regional granulite domains are statically overprinted by high pressure ca. 1.9 Ga metamorphism. Following the Arrowsmith Orogeny, ca. 2.2 to 2.0 Ga nearshore to marine sediments were deposited in most domains, except along the Snowbird tectonic zone where an east-facing basin formed with moderate to deep-water marine clastic and volcanic rocks. Widespread Paleoproterozoic magmatism, including ca. 2.29 to 2.0 Ga mafic dyke swarms and layered complexes, as well as ca. 1.9 Ga arc-like plutons, highlight a significantly more complex geological history than previously established, including Paleoproterozoic tectonometamorphic reworking up to 300 km west of the Snowbird tectonic zone, by both the Snowbird and Trans-Hudson orogenies. Pehrsson proposes testable correlations of domains and structures into northern Saskatchewan and Nunavut. Furthermore, she suggests that the linearity of crustal domains and their complex internal architecture resulted from the combined effects of the Arrowsmith collisional orogeny to the west and subsequent cycles of 1.9 to 1.82 Ga thickening and collapse imposed during accretion of the Hearne microcontinent and closure of the Nuna supercontinent's interior ocean.

Tehery Lake–Wager Bay area

Wodicka et al. (this volume) provide a concise overview of the Archean and Proterozoic history of the Tehery Lake–Wager Bay area, Nunavut, spanning the northern Chesterfield Block and the Repulse Bay Block of the Rae Craton. Targeted bedrock mapping (2012 and 2015–2017) accompanied by U-Pb geochronology, whole-rock and Sm-Nd isotope geochemistry, metamorphic petrology, and geophysical studies enabled recognition of six lithotectonic domains, each with distinct lithological, protolith age, metamorphic, isotopic, and/or geophysical characteristics, separated by large-scale structures. The Meso- to Neoproterozoic

Gordon Domain is separated from the Neoproterozoic Lunan Domain by a transition zone comprising a Neoproterozoic supracrustal sequence (Lorillard belt), reverse-sense high strain zones, and a magnetic-gravity lineament at depth. The 2.7 Ga Lorillard belt along with the Gordon and Lunan domains were likely amalgamated outboard of the proto-Rae Craton, prior to voluminous 2.62 to 2.58 Ga Snow Island suite arc magmatism (Peterson et al., this volume). The granulite-facies Kummel Lake Domain and Daly Bay Complex both define prominent gravity highs in the southern part of the Tehery Lake–Wager Bay area but differ in age and subsurface geometry. Based on regional gravity modelling and structural data, the Neoproterozoic Kummel Lake Domain resembles a metamorphic core complex with a shallow to moderately outward-dipping geometry, whereas the dominantly Paleoproterozoic Daly Bay Complex has steep inward-dipping margins and was juxtaposed against amphibolite-facies gneiss of the Gordon Domain by northward thrusting (Tschirhart et al., this volume). Between the Chesterfield and Wager shear zones, two prominent regional-scale structures with potentially long-lived, Archean to Paleoproterozoic histories, lies the Douglas Harbour Domain, which is characterized by a thick-skinned fold-thrust belt involving low to middle amphibolite-facies Paleoproterozoic supracrustal rocks (lower Ketyet Group-equivalent Pennington belt) and Meso- to Neoproterozoic gneiss basement. The northernmost Ukkusiksalik Domain, bounded to the northwest by a large 2.61 Ga Snow Island suite monzogranite body and to the south by the Wager shear zone, may represent the southwestern-most extent of the Repulse Bay Block.

Although evidence for Neoproterozoic tectonometamorphic events is locally preserved in Tehery Lake–Wager Bay area Archean rocks, all rocks, except for the Mesoproterozoic Mackenzie dykes, were extensively deformed and metamorphosed during the Snowbird and/or Trans-Hudson orogenies. Ongoing studies aim to elucidate the paleotectonic setting of Archean volcanism/sedimentation and the orogenic processes operating at mid- to deep-crustal levels in this part of the Rae Craton during Nuna supercontinent amalgamation.

Regional geophysics

Tschirhart et al. (this volume) present an overview of new geophysical data sets for nine GEM project areas in the western Churchill Province spanning from Melville and Boothia peninsulas to southwestern Rae Craton and the Thelon tectonic zone. The GEM-acquired data include aeromagnetic, long period and broadband magnetotelluric, and ground gravity data. Integration of these data with quantitative constraints of linked rock properties, bedrock geology, geochronology, petrochronology, and isotopic data has enabled delineation of numerous new internal domains and terranes and their architecture. Major crustal boundaries are shown to vary from demagnetized zones cross-cutting textural discontinuities, low-resistivity anomalies coincident with changes in mantle structure, highly attenuated magnetic highs associated with high-grade ductile mylonitization, or abrupt truncation and lateral displacement/attenuation on curvilinear anomalies of internal interference folds.

Three-dimensional inversion models are presented that suggest that Rae Craton, the upper plate during ca. 2.0 Ga Thelon orogenesis, was thrust over the Slave Craton again during continued indentation related to outboard Wopmay and Racklan-Forward orogens (ca. 1.8–1.6 Ga). A common theme emerging from several study areas (Montesor belt, Tehery Lake–Wager Bay, Chesterfield Block, south Rae) is significantly more extensive and widespread late extensional detachment faulting in the Rae Craton, which formed the heavily reworked foreland and thermally softened, far-field upper plate to Superior Craton collision.

Combining ground gravity and inverse modelling with magnetotelluric surveys is shown to be particularly powerful for resolving the genesis of major regional high-gravity features along Chesterfield Inlet that were once thought to be genetically and geometrically linked to the 1.9 Ga Snowbird tectonic zone. Gravity highs in the southern portion of the Tehery Lake–Wager Bay area do not correspond to a single coherent suite of moderate- to high-pressure granulite-facies features, but distinct domains carried on a steeply eastward dipping thrust (Daly Bay Complex) or a gently north-dipping detachment (Kummel Lake domain) (*see* Wodicka et al., this volume) illustrating exhumation of Rae's deep crust via two processes: early syn-collisional thrusting and late metamorphic core complex formation.

Lastly, the geophysical data sets of individual activities were combined with existing regional data and filtered through upward continuation and a range of other processing to create two major mosaic composites for the western Churchill Province: Bouguer gravity with long wavelength residual total field, and Bouguer gravity data transparent on isostatic residual Bouguer gravity data. These products will facilitate further unravelling of the complex evolution of northern Canadian Shield architecture and its bearing on mineralization.

Manitoba's far north

Böhm and Rayner (this volume) summarize GEM-supported research by the Manitoba Geological Survey through their Far North Geomapping initiative. This initiative aimed to understand the nature, evolution, and mineral potential of the Archean Hearne Craton, one of the principal geological building blocks of the shield in Manitoba.

Four field seasons dispersed over several major field areas between Nejanilini Lake, near the Nunavut border, and Great Island, west of Churchill, were conducted to test regional tectono-stratigraphic correlations across the Hearne Craton from Saskatchewan into Nunavut. Aeromagnetic and gamma-ray surveys of the Great Island and Seal River areas enabled new definitions of first order features, such as supracrustal basins and regional unconformities, tectonic fabrics and shear zones, and major granitoid domains. An extensive program of regional U-Pb geochronology led to delineation of two new subdomains within Hearne Craton and previously unrecognized Paleoproterozoic arc and back-arc volcanic and sedimentary sequences (Rayner, 2022). This radically revised regional framework illustrates that the Hearne Craton, rather than being an intact Archean nucleus, was likely assembled via accretion from a series of micro-blocks and intervening Paleoproterozoic arcs. Derivation of an extensive late Neoproterozoic magmatic suite (2570–2550 Ma) from thinned rather than thickened crust hints that some part of the collage may have assembled during the transition to the ca. 2.55 Ga MacQuoid Orogeny. Important implications of this new stratigraphic and structural architecture for regional metallogeny include recognition of four distinct metasedimentary cover sequences, including: a passive margin formed post-2.5 Ga; a pre-2050 to 1984 Ma marine deltaic package; and a syn-Trans-Hudson, ca. <1880 to 1764 Ma flysch-molasse successor basin. The economic potential of these diverse packages includes uranium, gold, and/or rare metal mineralization based on comparisons with regionally correlative sequences in Saskatchewan and Nunavut. A recently recognized Neoproterozoic greenstone belt in the Great Island area that hosts known gold occurrences emphasizes the untapped mineral potential of the area, as does the discovery of remnants of ancient, 3.5 Ga cratonic lithosphere in the Seal River area. The latter discovery illustrates that a favourable diamond potential exists in some sections of this microcontinental assemblage.

Core Zone

Corrigan (this volume) presents a synthesis of GEM research in the southeastern Churchill Province of Quebec and Labrador, a region termed therein as the 'Core Zone'. This region was previously considered an extension of the Archean Rae Craton caught between Paleoproterozoic Torngat and New Quebec orogens that ultimately welded the Superior and North Atlantic cratons (Fig. 1). Geochronological data, targeted mapping, and supporting geoscience conducted by GEM in collaboration with the Ministère de l'Énergie et des Ressources naturelles du Québec and Newfoundland and Labrador Geological Survey suggest that the Core Zone's Archean evolution does not link to the adjacent major plates. A tripartite, internal lithotectonic subdivision is proposed based on distinct Neoproterozoic to early Paleoproterozoic crustal evolution. The new 2.86 to 2.57 Ga George River, 2.37 to 1.987 Ga Mistinibi-Raude, and 2.89 to 1.9 Ga Falcoz River microplates are bounded by steeply-dipping, crustal-scale ductile shear zones interpreted as paleo-sutures. An exception to these exotic blocks is the Kuujuaq Domain, interpreted as a sliver of Superior Craton that rifted away and was thrust back with George River Block prior to emplacement of the De Pas batholith. An important new finding overturning previous models is that the Torngat Orogeny was principally restricted to the Core Zone/North Atlantic Craton margin, whereas broader regional tectonometamorphism and deformation is related to the younger New Quebec Orogeny, and complex transpression tectonics dominate in the southeastern Churchill Province. Correlation of Falcoz River Block cover with the Lake Harbour Group of Baffin Island suggests it was laterally transported along the margin. Recognition of the Core zone's microplates and major transpressional structures will help formulate domain-specific metallogenic models.

Thematic syntheses

Neoproterozoic Snow Island Suite

Peterson et al. (this volume) provide the first synthesis of a major Neoproterozoic magmatic province that is a first-order feature of the Rae Craton. The 2.62 to 2.58 Ga Snow Island Suite spans the region from Lake Athabasca to Melville Peninsula and Southampton Island, comprising mafic to felsic plutonic rocks,

with rarer subaerial volcanic and sedimentary rocks preferentially preserved beneath Paleoproterozoic cover. Integrating litho-geochemistry from nearly a hundred precisely dated Snow Island Suite samples with 50 Sm-Nd isotopic analyses, the authors show that different temporal phases of the suite have distinct geochemical attributes. Most of the suite comprises infracrustal granitoid rocks with highly evolved signatures. A shift from precursor mafic volcanism and back-arc sedimentation at 2.62 Ga to dominant sanukitoid magmatism by 2.60 Ga, is thought to reflect collision of a continental mass containing the current Chesterfield Block with an oceanic arc. Variations in geochemical sub-suites across the study area are interpreted to reflect compositional differences in the original pre-2.62 Ga constituent crustal blocks. For example, an abrupt compositional shift south of Dubawnt Lake coincides with an early boundary with more tonalitic basement to the south in proto-south Rae Craton. The existence of such boundaries at high angles to the current dominant southwest-northeast Paleoproterozoic structural grain reflects a pattern of primary age and compositional variation, interpreted to represent an originally west-verging continental arc that assembled the various Rae nuclei. Preservation of extrusive components of the suite only in the central Rae Craton reinforces major differences in Neoproterozoic and Paleoproterozoic stratigraphy, metamorphism, and metallogeny outlined by Jefferson et al. (this volume) that distinguish the central Rae from the south Rae Craton and Committee Bay block. Importantly, the Snow Island Suite provides a craton-wide major data set that will more broadly inform models of development of sanukitoid source regions and their influence on composition of subsequent melts.

Dyke swarms and large igneous provinces of northern Canada

Buchan and Ernst (this volume) present a synthesis of Paleoproterozoic giant (typically diabase) dyke swarms and large igneous provinces of northern Canada, with an emphasis on age, distribution, and paleomagnetism, along with potential linkages to paleocontinental reconstructions and coeval magmatic or continental breakup events. They cover nearly 40 major mafic and minor felsic suites and present a 1:3 000 000 scale synthesis map for areas of the northern Canadian Shield including Slave, Rae, and Superior cratons and Mesoproterozoic overlap sequences. Units are categorized by age and craton, emphasizing well dated suites and possible correlatives ranging from ca. 2.50 to 1.59 Ga. Poorly dated examples that nevertheless have significant implications for regional metallogeny and cratonic reconstructions; undated, in part new, events on Slave and Rae cratons and Meta Incognita terrane; and numerous volcanic packages in cratonic or passive margin sedimentary basins across the Churchill Province are included to highlight future research targets.

Utilizing the latest primary paleopoles and age data, the authors summarize the potential significance of major magmatic events in relation to rifting, continental breakup, and paleogeographic reconstruction. They test several proposed models for Laurentia and the broader Canadian Shield, including long postulated links with Baltica from Nuna to Rodinia supercontinent assembly. Critical revisions to the Paleoproterozoic North American apparent-polar-wander path (APWP) are presented and the accretion of the exotic ca. 1.71 Ga Bonnetia arc terrane to the ancestral western margin of Laurentia is discussed. Moving further back in time, models for preceding supercratons, such as Superia, Sclavia, and Nunavutia, are tested. The authors argue that the most temporally relevant links for the Hearne and Superior cratons are between the ca. 2.5 Ga Kaminak diabase dykes of the central Hearne Craton and coeval Ptarmigan dykes of the Superior Craton. They propose that this earliest Paleoproterozoic configuration did not break up until after ca. 2.11 Ga rift sedimentation and mafic magmatism recorded on both cratons. The early Paleoproterozoic fit between the ca. 2.19 Ga Dogrib dykes of the Slave Craton and Tulemalu swarm of the Rae Craton is assessed and found to be inconsistent with Slave and Rae cratons in their current configuration by ca. 2.3 Ga as has been previously proposed (De et al., 2000). Detailed 2.23 to 1.88 Ga APWPs for Slave and Superior cratons do not overlap, suggesting that the two cratons were not drifting as part of a single supercontinent over that time interval (Buchan et al., 2016), consistent with prevailing models for two separate supercratons in that period (Salminen et al., 2021). The record of younger 1.89 Ga dyke swarms allows for Siberia lying to the north of the Rae Craton within the Nuna supercontinent, a stable 1.9 to 0.72 Ga configuration that prompts favourable comparisons between metallogenetically important units such as the Au- and REE-hosting 1.75 Ga Kivalliq igneous suite and the Timpton igneous suite of Siberia. The proposed exotic ca. 1.59 Ga link between west Laurentia and south Australia's Gawler Craton is broadly permitted by paleopoles of the Cleaver diabase dykes of the western northern Canadian Shield.

Regional cooling of the shield

Kellett et al. (this volume) present a summary of their published synthesis on post-metamorphic cooling of the northern Canadian Shield. Founded on a data set of over 2000 archival K-Ar ages and new $^{40}\text{Ar}/^{39}\text{Ar}$ cooling ages collected during GEM, the data reveals a stark contrast between metamorphic and cooling histories of the various Archean cratons and terranes involved in Paleoproterozoic collisions during assembly of Laurentia. Markedly different cooling patterns are seen to be generally linked to plate position during collision and accretion. Lower plate-positioned larger cratons, such as the Superior and Slave, behave as cold, stable blocks with some marginal thermal reworking. In contrast, the Churchill Province, a collage of smaller microcontinents accreted to the Rae Craton before Superior collision, was almost entirely thermally reworked during the late Paleoproterozoic. The Churchill Province is inferred to have occupied an upper plate setting during much of the Paleoproterozoic based on its record of magmatism, structural, and thermal reworking in contrast to the lack of these features in the bounding Superior and Slave cratons. Contrasts in inter-plate or microplate thermal history are presented in six cross-sections across the interior of the northern Canadian Shield from Baffin Island to southern Saskatchewan.

A general west-to-east cooling pattern is defined by two shield-scale thermochronological profiles: a northern transect extending from the Slave Craton through the Thelon tectonic zone, northern Rae Craton (Committee Bay belt, Hall Peninsula of Baffin Island, and Cape Smith belt), and into the Superior; and a southern traverse through the Slave Craton, Taltson magmatic zone, south Rae Craton, Snowbird Tectonic Zone, Reindeer zone of the Hearne Craton, and into the Superior Province. Both profiles reveal an asymmetric trough pattern within Churchill Province rocks, with the youngest (ca. 1.7 Ga) cooling ages centred within the Trans-Hudson Orogen proper, and oldest cooling ages located at the westernmost edges of the Churchill Province. In the west, particularly in the south Rae Craton, cooling ages are structurally controlled by domain-bounding faults, whereas in the east, within the Trans-Hudson Orogen, cooling ages are more uniform. The youngest cooling ages in the northern profile are 50 Ma younger (ca. 1.650 Ga) than in the south (ca. 1.700 Ga), indicating diachroneity in the post-collisional thermal equilibration and exhumation of Trans-Hudson Orogen rocks.

Following the terminal Trans-Hudson collision between the Churchill and Superior provinces, the Churchill Province may have undergone lithospheric delamination, as evidenced by late thermal perturbations, and subsequently behaved as a stable continental mass. Although it has been involved in subsequent collisions as part of Nuna (e.g. Grenville Orogen), it occupied a lower plate position for these. Kellett et al. conclude that the contrast in cooling history between the upper plate (Churchill) and lower plates (Superior, Slave, or Churchill) suggests that the upper plate during a Wilson cycle is intensely thermally conditioned via heat, fluids, and magma generated during subduction tectonics and accretion events.

Statherian-Calymmian paleogeography of northwestern Laurentia

Following principal Paleoproterozoic northern Canadian Shield assembly, major intracontinental basins formed in a number of depocentres, including northwestern Laurentia. Rainbird and Davis (this volume) present a summary of new U-Pb detrital zircon geochronology and updated stratigraphy of one of these basins: the Mesoproterozoic Hornby Bay Basin situated on the western margin of the exposed northern Canadian Shield, northeast of Great Bear Lake. The ca. 1.75 to 1.27 Ga basin includes the Big Bear, Mountain Lake, and Dismal Lakes groups. The Big Bear group comprises mainly immature, coarse-grained, clastic rocks deposited by high-energy rivers in restricted fault-bounded basins and is proposed to be similar to rifts underlying the Thelon and Athabasca basins. Integrating detrital zircon provenance with Hf isotopic compositions, Rainbird and Davis define possible source areas of the basin's clastic detritus. They propose derivation of Big Bear group sedimentary rocks from sources underlying the Paleoproterozoic orogens and terranes in the environs of Great Bear Lake, along with more easterly sources such as Thelon tectonic zone. In contrast, the newly defined Mountain Lake group formed within a broader basinal depression possibly due to thermal subsidence. Its three formations, including fluvial sandstone of a continental-scale braided river system and marine transgressive to regressive clastic rocks, were deposited between ca. 1.7 to 1.63 Ga, with provenance reflecting intermediate recycling of the Coronation Supergroup and the correlative but more distal Goulburn Supergroup of Kilohigok Basin. The Mountain Lake group was subsequently folded and faulted during Racklan-Forward Orogeny related to ca. 1600 Ma collision of Australia with northwest Laurentia. After associated uplift and erosion, the dominantly marine 1.59 to 1.27 Ga Dismal Lakes group was deposited.

Detailed facies comparison with the Yukon's Wernecke Supergroup, Nd and C isotopic signatures of respective shale and carbonate units, along with Hornby Bay Basin's detailed depositional history, are combined to build a new paleogeographic model for northwest Laurentia at that time. A west-facing, passive-margin clastic wedge with both terrestrial (Hornby Bay Basin) and marine components (Wernecke Supergroup) is proposed to have evolved to a stable carbonate platform, correlative elements of which were transferred to northeastern Australia prior to the break-up of supercontinent Nuna.

AN EMERGING PICTURE

As is evident from the foregoing, GEM's new era of northern mapping has expanded the Canadian Shield's framework substantially and has added detail to an increasingly complex model of the mosaic of Archean cratons, Archean/Proterozoic microcontinents, and juvenile Paleoproterozoic crust that makes up the northern Canadian Shield (Table 2; Fig. 3). In addition to the six major Archean cratons — Slave, Rae, Hearne, Superior, Nain (North Atlantic), and buried Mackenzie — the shield is now known to comprise at least a dozen ribbon microcontinents of varied nature and/or origin. Some blocks originated as pericratonic terranes following Paleoproterozoic rifting (Hall Peninsula–Asiaat, Duggan Lake, Kuujjuaq; Chesterfield and Repulse Bay blocks on the proto-Rae Craton) while others were rifted from proposed parent supercratons (e.g. Superia, Nunavutia) and reassembled (Sask-Partridge Breast, Buffalo Head) Other blocks appear exotic, for example the Meso- to Neoproterozoic Chipman Domain caught between Rae and Hearne cratons, the Queen Maud Block on the Rae Craton's western flank, the latest Neoproterozoic Boothia terrane situated north of Queen Maud Gulf (possibly extending onto Devon Island; Regis and Sanborn-Barrie, 2023), and the buried Wabamun terrane in south-central Canada. George River, Falcoz River and Sugluk blocks about Superior also have uncertain origins. A significant subset of the microcontinents were heavily reworked and augmented magmatically during Paleoproterozoic assembly and include only fragmentary Archean records (Meta Incognita, Hottah, Mistibini-Raude).

The larger cratons such as Slave, Rae, Nain, and Superior have distinct internal subdivisions with varying Paleo- to Mesoproterozoic versus Neoproterozoic parentage reflecting Mesoproterozoic to Neoproterozoic orogenic activity that assembled these components into their nascent proto-cratons. By 2.8 Ga many of the ancient pieces underwent rifting and separation and were subsequently assembled into the major Neoproterozoic supercratons Nunavutia and Superia. Rae, in particular, has been a focus of GEM research and substantial progress has been made on its architecture and evolution. The presence of Paleo- and Mesoproterozoic, and rare Hadean, detrital zircons in Neoproterozoic and Paleoproterozoic sediments suggests that the Rae Craton has a complex Archean history, perhaps as extended as that of better-known Slave and Superior cratons. Establishing the crustal architecture of the Rae Craton prior to emplacement of the widespread Snow Island Suite has proved challenging and may require regional studies of zircon Lu-Hf or other isotopic methods to see through ca. 2.6 Ga magmatic reworking.

The MacQuoid Orogeny (2.5–2.0 Ga) began the progressive assembly and reworking of the western Churchill Province, followed closely by the Arrowsmith Orogeny (2.5–2.3 Ga). Whereas the tectonic effects of the Arrowsmith Orogeny appear to be localized along the western Rae–Queen Maud block boundary, its metamorphic imprint extends hundreds of kilometres into the Rae Craton, except for the central Rae (Jefferson et al., this volume). Erosion was followed by deposition of many early Paleoproterozoic marginal or cover sequences before and leading up to supercraton breakup (Wodicka et al., 2014). The principal Archean cratons and host of Archean to earliest Paleoproterozoic microcontinents and crustal slices that broke out of these configurations, now preserved between Rae, Superior, and Nain cratons, were scattered in what was once the Manikewan Oceanic realm, which closed between ca. 1.92 and 1.83 Ga with the assembly of supercontinent Nuna. On the west side of Rae Craton, early magmatic activity on the Thelon tectonic zone (2.03–1.96 Ga) accompanied subduction, followed by collision with Slave Craton and relatively localized deformation along the zone. Deformation along the Snowbird tectonic zone to the southeast of Rae is polyphase, resulting from collision with the Hearne Craton during the Snowbird Orogeny ca. 1.9 Ga and subsequent reworking during the Trans-Hudson Orogeny and final closure of Manikewan Ocean ca. 1.85 Ga. Both events resulted in widespread deformation and metamorphism of Rae basement and its marginal and cover sequences. This progressive overprinting by Paleoproterozoic events (2.5–1.85 Ga) distinguishes Rae Craton from other Archean regions stabilized by 2.5 Ga. This phenomenon has been attributed to an upper plate tectonic setting for the Rae Craton during Paleoproterozoic collisions and likely delayed establishment of stable mantle lithosphere. Continued mantle activity is evident from widespread alkaline and associated magmatism (1.83–1.75 Ga) in central Rae.

Table 2. Revised lithotectonic elements of the northern Canadian Shield following GEM research (2008–2020).

Craton or block	New or revised subdivisions	Crust formation ¹	Paleoproterozoic marginal sequences ²	Paleoproterozoic orogenic events	Selected references
Archean cratons					
Slave		4.0–2.58 Ga	2.014–1.88 Ga Coronation Supergroup 2.02–1.9 Ga Lower Goulbourn Supergroup ca. 2.045–1.94 Ga East-Arm Supergroup	Talson-Thelon; Wopmay	Heimstaedt and Pehrsson, 2012; Jackson et al., 2013; Davis et al., 2014 Hoffman et al., 2011; Rainbird and Davis, 2022 Wright et al., 2013; Sheen et al., 2019
Rae					
<i>North³</i>	Repulse Bay-Prince Albert blocks (incl. Ukkuksalik Domain)		ca. 2.16–1.88 Ga Penrhyn-Pilling-Ketyet River groups	MacQuoid, Trans-Hudson	Peterson et al., this volume; Wodicka et al., 2017, this volume
	Prince Albert Block	2.97–2.60 Ga	ca. 2.16–1.88 Ga Penrhyn-Pilling-Ketyet River groups	MacQuoid, Ellesmere-Ingletfield, Trans-Hudson	Wodicka et al., 2011; Corrigan et al., 2013; Berman et al., 2015a; Skipton et al., 2019
	Committee Bay Block	2.73–2.58 Ga	< 2.19 Ga Ketyet River Group	Arrowsmith, Snowbird, Trans-Hudson	Pehrsson et al., 2013; Santborn-Barrie et al., 2014; Skulski et al., 2018; Davis, 2021; Jefferson et al., this volume
<i>Central</i>	Chesterfield Block (incl. Gordon, Lunan, and Kummel Lake domains)	2.90–2.58 Ga	Pennington belt (lower Ketyet River Group equivalent)	Snowbird and/or Trans-Hudson	Wodicka et al., 2017, this volume; Steenkamp et al., 2023a, b, c; Pehrsson, this volume; Pehrsson et al., this volume; Tschirhart et al., this volume
	Douglas Harbour Domain	2.90–2.61 Ga	Amer-Ketyet River-Montresor groups	Trans-Hudson	Steenkamp et al., 2023 a, b, c; Wodicka et al., this volume; Peterson et al., this volume
	Central Committee Bay Block	3.0–2.58 Ga	2.04 Ga Lamarre Lake assemblage	Snowbird, Trans-Hudson	Jefferson et al., this volume
	Porter Domain	2.74–2.56 Ga	unknown	MacQuoid, Arrowsmith	MacLachlan et al., 2005; Davis et al., 2006; Lawley et al., 2016; Wodicka et al., 2017; Pehrsson, this volume
<i>South</i>	Penylan Domain	2.04–2.02 Ga	unknown	Trans-Hudson	Rainbird et al., 2010; Corrigan et al., 2013; Laflamme et al., 2014; Skipton et al., 2019; Pehrsson, this volume
	McCann-Zemlack domains	2.7–2.04 Ga	2.54–2.35 Ga McCann metasedimentary rocks	Arrowsmith, Snowbird, Trans-Hudson	Hartlaub et al., 2005; Pehrsson, this volume; Martel et al., this volume
	Friedlake Domain	2.74–2.58 Ga	2.55–1.90 Ga Imikula metasedimentary rocks	Snowbird, Trans-Hudson	Pehrsson, this volume
	Snowbird-Dodge domains	2.72–1.96 Ga	2.07–1.95 Ga Snowbird metasedimentary rocks	Talson, Snowbird	Pehrsson, this volume
	West Kasba Domain	2.55–1.9 Ga	ca. 2.55–1.9 Ga Bourassa Lake belt	MacQuoid, Snowbird	Pehrsson, this volume
	Seal River Domain	2.8–2.56 Ga	ca. 2.6–2.56 Ga Helle Lake belt	MacQuoid, Snowbird	Pehrsson, this volume
	Nejanlini Domain	3.5–2.55 Ga	< 1.97 Ga Misty Lake metasedimentary rocks	Trans-Hudson	Böhm et al., this volume
		2.7–2.48 Ga	< 2.5 Ga Kasner-Nejanlini metasedimentary rocks	Trans-Hudson	Böhm et al., this volume
Mackenzie Superior		unknown			Estève et al., 2020
Nain		4.3–2.57 Ga 3.8–3.0 Ga	2.07–1.88 Ga Povungnituk, Chukotat gp. northeast Torngat	Trans-Hudson, New Quebec	Bleeker and Kamo, 2020 James et al., 2002; Corrigan et al., this volume
Archean/Proterozoic microcontinents					
Pericratonic					
	Duggan Lake Domain	3.2–3.1 Ga	Queen Maud Block	Arrowsmith, Thelon	Berman et al., 2019b; this volume
	Hall Peninsula-Aasiaat domains	2.98–2.70 Ga	Nain (North Atlantic)	Nagsugtoqidian, Torngat, Trans-Hudson	Skipton et al., 2016; From et al., 2016, 2018
	Kuujuuaq Domain	3.0–2.72 Ga	Superior Craton	New Quebec	Rayner et al., 2017; Corrigan et al., 2018, this volume
Dominantly Paleoproterozoic accreted microcontinents					
	Misibini-Raude Block	<2.6–2.3 Ga	1.885–1.873 Ga Treasure Lake Group	ca. 2.1 Ga	Corrigan et al., 2018, 2021; this volume
	Hottan terrane	2.5–1.895 Ga		Wopmay	Davis et al., 2015; Ooles et al., 2015
Exotic or uncertain affinity					
	Chipman Domain	3.2–2.56 Ga		Snowbird	Peterson et al., this volume
	Boothia terrane	2.56–2.48 Ga	Boothia Sequence 1: 2.51–2.48 Ga	Arrowsmith, Thelon	Santborn-Barrie et al., 2019
	Queen Maud Block	3.26–2.35 Ga	2.1–2.02 Ga Ellice River assemblage	Arrowsmith, Thelon	Davis et al., 2021; Berman et al., this volume
	George River Block	2.86–2.57 Ga		New Quebec	Corrigan et al., 2018, 2021; this volume
	Falcoz River Block	2.89–2.57 Ga		Torngat, New Quebec	Corrigan et al., 2018, 2021; this volume
	Sask-Partridge Breast	3.3–2.55 Ga		Trans-Hudson	Ashton et al., 1999; Czás et al., 2020
Paleoproterozoic arcs					
	Thelon tectonic zone plutonic belt	2.07–1.95 Ga		Thelon, Trans-Hudson	Berman et al., this volume
	Great Bear magmatic zone	1.88–1.86 Ga	Treasure Lake Group, 1.88 Ga	Great Bear-Wopmay	Corriveau et al., this volume

¹"Crust formation" refers to overall age range of constituent internal domains excluding Proterozoic rift magmatic events, large igneous provinces, and collisional magmatism during northern Canadian Shield assembly.

²Excludes epicratonic sequences not demonstrated to have progressed to rifting.

³Words in italic indicate where GEM has revised existing subdivisions or proposed new ones.

For references regarding the buried Mackenzie Craton and Sask-Partridge Breast microcontinents see Corrigan et al., 2021. For references to Circum-Ungava GEM projects see Daboe and Bingham-Kosowski, 2022.

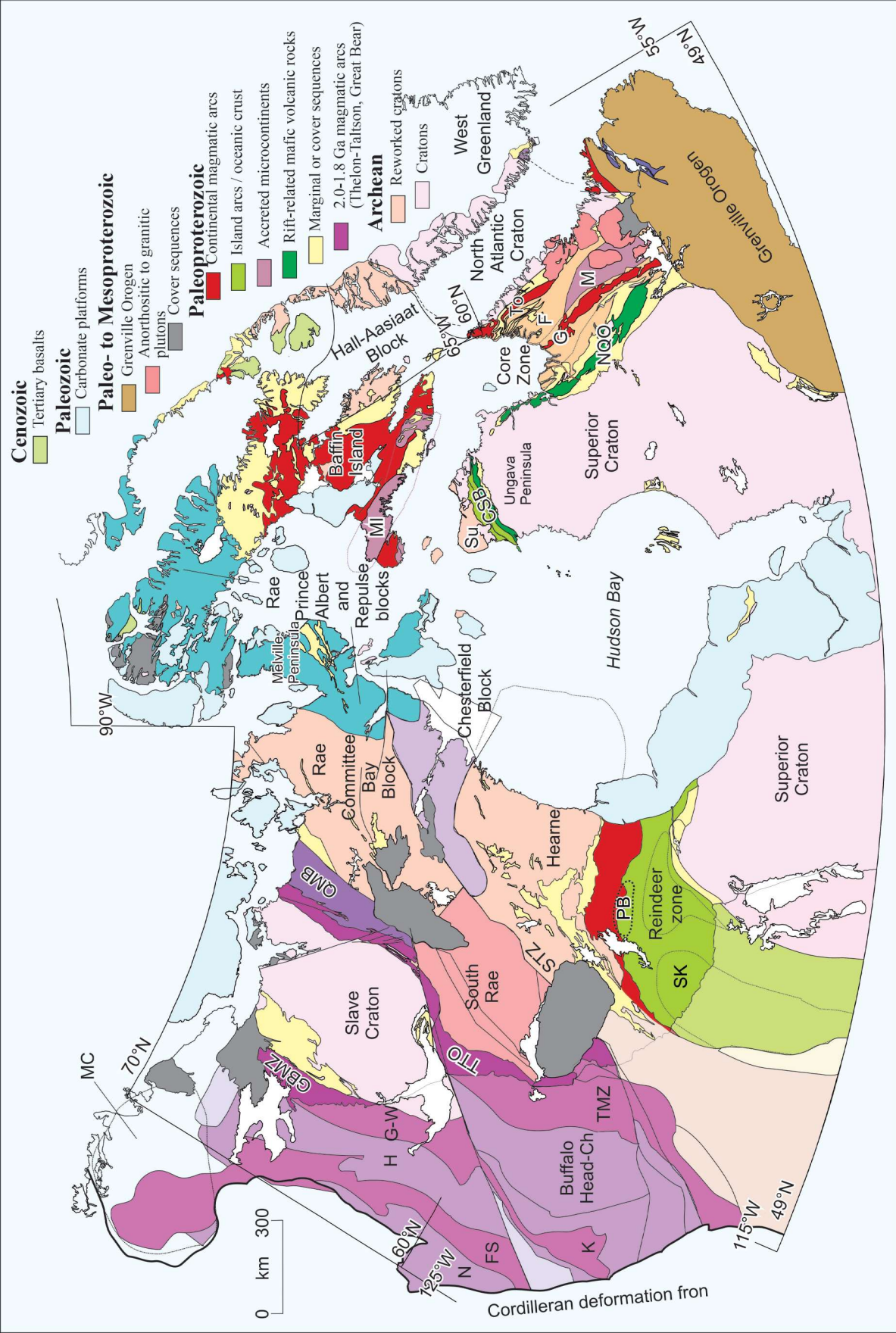


Figure 3. Updated subdivisions and elements of the northern Canadian Shield following GEM-1 and -2 research. Coloured subdivisions of the Archean Rae Craton are shown to highlight internal subdivision, but all, excluding Queen Maud Block, were thoroughly reworked in the Paleoproterozoic. Abbreviations: Ch = Chinchaga; CSB = Cape Smith belt; F = Falcoz River Block; FS = Fort Simpson terrane; G = George River Block; GBMZ = Great Bear magmatic zone; G-W = Great Bear–Wopmay Orogen; H = Hottah terrane; K = Kitsuan Orogen; M = Mistinibi-Raude Block; MC = Mackenzie Craton; MI = Meta Incognita terrane; N = Nahanni terrane; NQO = New Quebec Orogen; PB = Partridge Breast terrane; QMB = Queen Maud Block; SK = Sask Craton; STZ = Snowbird Tectonic Zone; Su = Sugluk; TMZ = Taltson magmatic zone; To = Torngat Orogen; TTO = Taltson–Thelon Orogen.

With the core of the northern Canadian Shield and Nuna assembled, strike-slip motions related to peripheral collision (e.g. Hottah, Nain) continued and accretion stepped out into the supercontinent's periphery (present day Yukon), leading to formation of the Great Bear continental arc, addition of a number of buried terranes below the western Canada sedimentary basin and, ultimately, collision of the North Australia Craton with northwest Laurentia by 1.59 Ga. Inboard, late faults formed localized rift basins in the central Rae and Hearne cratons ca. 1.75–1.27 Ga and appear to have been key for localizing unconformity-related uranium. The aforementioned sedimentary basins of similar age in northwest Laurentia reflect long-distance transport by large rivers. This period is associated with relatively slow cooling following the multiple Paleoproterozoic reworking events, late magmatism, faulting and sedimentation.

This overall picture, although substantially enhanced by GEM, nevertheless contains many aspects that are incompletely constrained and would be suitable targets for future research. The kind of detailed internal subdivision that has been established for the Superior Province through decades of research across relatively accessible regions, which is crucial for understanding its regional metallogeny, has yet to be achieved for the Slave and Rae cratons. Recognition of the restricted imprint of Taltson-Thelon Orogeny within the Queen Maud Block and south Rae Craton has highlighted the importance of understanding the tectonic impacts of the enigmatic ca. 2.4 to 2.3 Ga Arrowsmith Orogeny. Discovery of many new Paleoproterozoic supracrustal and volcanic sequences in previously little studied regions necessarily complicates matters, but also enables delineation of tectonic architecture. Only with greater data density, increased coverage of modern geophysical surveys, and enhanced geochemical, isotopic, and in situ and high-precision geochronological data sets will we be able to tackle ongoing or more specific questions pertaining to the crustal evolution, tectonic architecture, orogenesis, and metallogenic potential of many parts of the northern Canadian Shield.

ACKNOWLEDGMENTS

Thanks are extended to all the colleagues whose dedicated research over the past decade has contributed so much to GEM; and to GEM management for continued support and encouragement. Eric Potter, Sonya Banal, and Natalie Morisset are greatly thanked for shepherding this through uncertain times and making the synthesis possible. The following geoscientists are gratefully thanked for kindly agreeing to critically review the manuscripts included in this synthesis volume: Colin Card (Saskatchewan Geological Survey), Quentin Gall (Geological Consultant), Nathan Hayward (GSC), Rebecca Hunter (Forum Energy Metals Corp.), Dawn Kellett (GSC), Bruce Kjarsgaard (GSC), Tony LeCheminant (GSC), Robert MacNaughton (GSC), Ali Polat (University of Windsor), Eric Potter (GSC), Rob Rainbird (GSC), Daniele Regis (GSC), Anthony Reid (Australian National University), Mary Sanborn-Barrie (GSC), and Richard Smith (Laurentian University). Comprehensive and thorough technical editing by Marie-France Dufour, Evelyn Inglis, and Alison Weatherston, translation editing by Benoît Couture, and layout by Paul Champagne enhanced clarity and consistency of the final product. This research was supported by the GEM program, the Polar Continental Shelf Project, and the GSC's Targeted Geoscience Initiative.

REFERENCES

- Ashton, K., Heaman, L., Lewry, J., Hartlaub, R.P., and Shi, R., 1999. Age and origin of the Jan Lake complex: a glimpse at the buried Archean craton of the Trans-Hudson Orogen; *Canadian Journal of Earth Sciences*, v. 36, p. 185–208. <https://doi.org/10.1139/e98-038>
- Bédard, J.H., Hayes, B., Hryciuk, M., Beard, C., Williamson, N., Dell’Oro, T.A., Rainbird, R.H., Prince, J., Baragar, W.R.A., Nabelek, P.I., Weis, D., Wing, B., Scoates, J., Naslund, H.R., Cousens, B., Williamson, M.-C., Hulbert, L.J., Montjoie, R., Girard, É., Ernst, R., and Lissenberg, C.J., 2016. Geochemical database of Franklin sills, Natkusiak basalts and Shaler Supergroup rocks, Victoria Island, Northwest Territories, and correlatives from Nunavut and the mainland; Geological Survey of Canada, Open File 8009, 1 .zip file. <https://doi.org/10.4095/297842>
- Berman, R.G., Pehrsson, S.L., Davis, W.L., Ryan, J.J., Qui, H., and Ashton, K., 2013. The Arrowsmith orogeny: geochronological and thermobarometric constraints on its extent and tectonic setting in the Rae craton, with implications for pre-Nuna supercontinent reconstruction; *Precambrian Research*, v. 232, p. 44–69. <https://doi.org/10.1016/j.precamres.2012.10.015>
- Berman, R.G., Nadeau, L., McMartin, I., McCurdy, M.W., Craven, J.A., Girard, E., Sanborn-Barrie, M., Carr, S., Pehrsson, S.J., Whalen, J., Davis, W.J., Roberts, B.J., and Grenier, A., 2015a. Report of activities for the Geology and Mineral Potential of the Chantrey-Thelon Area: GEM-2 Thelon tectonic zone project; Geological Survey of Canada, Open File 7693, 14 p. <https://doi.org/10.4095/295644>
- Berman, R.G., Davis, W.J., Corrigan, D., and Nadeau, L., 2015b. Insights into the tectonothermal history of Melville Peninsula, Nunavut, provided by in situ SHRIMP geochronology and thermobarometry; Geological Survey of Canada, Current Research 2015-4, 18 p. <https://doi.org/10.4095/295852>
- Berman, R.G., Sanborn-Barrie, M., Nadeau, L., Brouillette, P., Camacho, A., Davis, W.J., McCurdy, M.W., McMartin, I., Weller, O.M., Chadwick, T., Liikane, D., and Ma, S., 2016. Report of activities for the geology and mineral potential of the Chantrey-Thelon area: GEM-2 Rae project; Geological Survey of Canada, Open File 8129, 15 p. <https://doi.org/10.4095/299386>
- Berman, R.G., Davis, W.J., Sanborn-Barrie, M., Whalen, J.B., Taylor, B.E., McMartin, I., McCurdy, M.W., Mitchell, R.K., Ma, S., Coyle, M., Roberts, B., and Craven, J.A., 2018. Report of activities for the GEM-2 Chantrey-Thelon activity: Thelon tectonic zone project, Nunavut; Geological Survey of Canada, Open File 8372, 22 p. <https://doi.org/10.4095/306622>
- Bleeker, W., 2003. The late Archean record: puzzle in ca. 35 pieces; *Lithos*, v. 71, p. 99–134. <https://doi.org/10.1016/j.lithos.2003.07.003>
- Bleeker, W. and Kamo, S.L., 2020. Structural-stratigraphic setting and U-Pb geochronology of Ni-Cu-Co-PGE ore environments in the central Cape Smith Belt, Circum-Superior Belt; *in Targeted Geoscience Initiative 5: advances in the understanding of Canadian Ni-Cu-PGE and Cr ore systems — examples from the Midcontinent Rift, the Circum-Superior Belt, the Archean Superior Province, and Cordilleran Alaskan-type intrusions*, (ed.) W. Bleeker and M.G. Houlé; Geological Survey of Canada, Open File 8722, p. 65–98. <https://doi.org/10.4095/326882>
- Buchan, K.L. and Ernst, R.E., 2013. Diabase dyke swarms of Nunavut, Northwest Territories and Yukon, Canada; Geological Survey of Canada, Open File 7464, 1 .zip file. <https://doi.org/10.4095/293149>
- Buchan, K.L., Mitchell, R.N., Bleeker, W., Hamilton, M.A., and LeCheminant, A.N., 2016. Paleomagnetism of ca. 2.13–2.11 Ga Indin and ca. 1.885 Ga Ghost dyke swarms of the Slave craton: implications for the Slave craton APW path and relative drift of Slave, Superior and Siberian cratons in the Paleoproterozoic; *Precambrian Research*, v. 275, p. 151–175. <https://doi.org/10.1016/j.precamres.2016.01.012>
- Canil, D., 2008. Canada’s craton: a bottoms-up view; *GSA Today*, v. 18, no. 6, p. 4–10. <https://doi.org/10.1130/GSAT01806A.1>
- Card, C., Bethune, K., Davis, W.J., Rayner, N., and Ashton, K.E., 2014. The case for a distinct Taltson Orogeny: evidence from northwest Saskatchewan, Canada, *Precambrian Research*, v. 255, p. 245–265. <https://doi.org/10.1016/j.precamres.2014.09.022>
- Chacko, T., De, S.K., Creaser, R.A., and Muehlenbachs, K., 2000. Tectonic setting of the Taltson magmatic zone at 1.9–2.0 Ga: a granitoid-based perspective; *Canadian Journal of Earth Sciences*, v. 37, p. 1597–1609. <https://doi.org/10.1139/e00-029>
- Clowes, R., Cook, F., Hajnal, Z., Hall, J., Lewry, J., Lucas, S., and Wardle, R., 1999. Canada’s Lithoprobe project: collaborative, multidisciplinary geoscience research leads to new understanding of continental evolution; *Episodes*, v. 22, p. 3–20. <https://doi.org/10.18814/epiugs/1999/v22i1/002>

- Condie, K.C. and Kröner, A., 2008. When did plate tectonics begin? Evidence from the geologic record; *in* When Did Plate Tectonics Begin on Planet Earth?, (ed.) K.C. Condie and V. Pease; Geological Society of America, Special Paper 440, p. 281–294. [https://doi.org/10.1130/2008.2440\(14\)](https://doi.org/10.1130/2008.2440(14))
- Condie, K.C., O'Neill, C., and Aster, R.C., 2009. Evidence and implications for a widespread magmatic shutdown for 250 My on Earth; *Earth and Planetary Science Letters*, v. 282, p. 294–298. <https://doi.org/10.1016/j.epsl.2009.03.033>
- Corrigan, D., Nadeau, L., Brouillette, P., Wodicka, N., Houlé, M.G., Tremblay, T., Machado, G., and Keating, P., 2013. Overview of the GEM Multiple Metals–Melville Peninsula project, central Melville Peninsula, Nunavut; Geological Survey of Canada, Current Research 2013-19, 17 p. <https://doi.org/10.4095/292862>
- Corrigan, D., Brouillette, P., Morin, A., Van Rooyen, D., Wodicka, N., Houlé, M.G., Douma, S.L., and Robillard, K., 2015. Report of activities for the Core Zone and bounding orogens: tectonic framework and mineral potential; Geological Survey of Canada, Open File 7706, 10 p. <https://doi.org/10.4095/296141>
- Corrigan, D., Van Rooyen, D., Morin, A., Houlé, M.G., and Bédard, M.-P., 2016. Report of activities for the Core Zone and Bounding Orogens: recent observations from the New Quebec Orogen in the Schefferville area, Quebec and Labrador, GEM-2 Hudson-Ungava project; Geological Survey of Canada, Open File 8127, 11 p. <https://doi.org/10.4095/299249>
- Corrigan, D., Wodicka, N., McFarlane, C., Lafrance, I., van Rooyen, D., Bandyayera, D., and Bilodeau, C., 2018. Lithotectonic framework of the Core Zone, southeastern Churchill Province, Canada; *Geoscience Canada*, v. 45, no. 1, p. 1–24. <https://doi.org/10.12789/geocanj.2018.45.128>
- Corrigan, D., van Rooyen, D., and Wodicka, N., 2021. Indenter tectonics in the Canadian Shield: a case study for Paleoproterozoic lower crust exhumation, orocline development, and lateral extrusion; *Precambrian Research*, v. 355, p. 106083. <https://doi.org/10.1016/j.precamres.2020.106083>
- Corriveau, L., Lauzière, K., Montreuil, J.-F., Potter, E.G., Hanes, R., and Prémont, S., 2015. Dataset of geochemical data from iron oxide alkali-altered mineralising systems of the Great Bear magmatic zone, Northwest Territories; Geological Survey of Canada, Open File 7643, 1 .zip file. <https://doi.org/10.4095/296301>
- Craven, J., Roberts, B., Hayward, N., Stefanescu, M., and Corriveau, L., 2013. A magnetotelluric survey and preliminary geophysical inversion and visualization of the NICO IOCG deposit, Northwest Territories; Geological Survey of Canada, Open File 7465, 26 p. <https://doi.org/10.4095/292869>
- Czas, J., Pearson, D.G., Stachel, T., Kjarsgaard, B., and Read, G., 2020. A Palaeoproterozoic diamond-bearing lithospheric mantle root beneath the Archean Sask Craton, Canada; *Lithos*, v. 356–357, no. 105301, 14 p. <https://doi.org/10.1016/j.lithos.2019.105301>
- Dafoe, L. and Bingham-Kosłowski, N. (ed.), 2022. Geological synthesis of Baffin Island (Nunavut) and the Labrador–Baffin Seaway; Geological Survey of Canada, Bulletin 608, 432 p. <https://doi.org/10.4095/314542>
- Davis, W.J., 2021. U-Pb zircon age data for supracrustal samples from the White Hills Lake to Amer Lake area, Rae Province, Nunavut, Canada; Geological Survey of Canada, Open File 8807, 1 .zip file. <https://doi.org/10.4095/328453>
- Davis, W.J., Hanmer, S., Tella, S., Sandeman, H.A., and Ryan, J.J., 2006. U-Pb geochronology of the MacQuoid supracrustal belt and Cross Bay plutonic complex: key components of the northwestern Hearne subdomain, western Churchill Province, Nunavut, Canada; *Precambrian Research*, v. 145, p. 53–80. <https://doi.org/10.1016/j.precamres.2005.11.016>
- Davis, W.J., Berman, R.G., Nadeau, L., and Percival, J.A., 2014. U-Pb zircon geochronology of a transect across the Thelon tectonic zone, Queen Maud region, and adjacent Rae craton, Kitikmeot Region, Nunavut, Canada; Geological Survey of Canada, Open File 7652, 1. zip file. <https://doi.org/10.4095/295177>
- Davis, W.J., Ootes, L., Newton, L., Jackson, V., and Stern, R.A., 2015. Characterization of the Paleoproterozoic Hottah terrane, Wopmay Orogen using multi-isotopic (U-Pb, Hf and O) detrital zircon analyses: an evaluation of linkages to northwest Laurentian Paleoproterozoic domains; *Precambrian Research*, v. 269, p. 296–310. <https://doi.org/10.1016/j.precamres.2015.08.012>
- Davis, W.J., Sanborn-Barrie, M., Berman, R.G., and Pehrsson, S., 2021. Timing and provenance of Paleoproterozoic supracrustal rocks in the central Thelon tectonic zone, Canada: implications for the tectonic evolution of western Laurentia from ca. 2.1 to 1.9 Ga; *Canadian Journal of Earth Sciences*, v. 58, no. 4, p. 378–395. <https://doi.org/10.1139/cjes-2020-0046>
- De, S.K., Chacko, T., Creaser, R.A., and Muehlenbachs, K., 2000. Geochemical and Nd–Pb–O isotope systematics of granites from the Taltson magmatic zone, NE Alberta: implications for Early Proterozoic tectonics in western Laurentia; *Precambrian Research*, v. 102, p. 221–249. [https://doi.org/10.1016/S0301-9268\(00\)00068-1](https://doi.org/10.1016/S0301-9268(00)00068-1)

- Eglington, B.M., Pehrsson, S.J., Ansdell, K.M., Lescuyer, J.-L., Quirt, D., Milesi, J.-P., and Brown, P., 2013. A domain-based digital summary of the lithostratigraphy, geochronology and geodynamics of the Palaeoproterozoic of North America and Greenland and associated unconformity-type uranium mineralization; *Precambrian Research*, v. 232, p. 4–26. <https://doi.org/10.1016/j.precamres.2013.01.021>
- Eguchi, J., Diamond, C.W., and Lyons, T.W., 2022. Proterozoic supercontinent break-up as a driver for oxygenation events and subsequent carbon isotope excursions; *PNAS Nexus*, v. 1, no. 2, p. 1–10. <https://doi.org/10.1093/pnasnexus/pgac036>
- Estève, C., Audet, P., Schaeffer, A., Schutt, D., Aster, R.C., and Cubley, J.F., 2020. Seismic evidence for craton chiseling and displacement of lithospheric mantle by the Tintina fault in the northern Canadian Cordillera; *Geology*, v. 48, p. 1120–1125. <https://doi.org/10.1130/G47688.1>
- From, R.E., Rayner, N.M., and Camacho, A., 2016. Archean magmatism and metamorphism of eastern Hall Peninsula, southern Baffin Island, Nunavut; Canada-Nunavut Geoscience Office, Summary of Activities 2015, p. 73–88.
- From, R.E., Camacho, A., Pearson, D.G., and Luo, Y., 2018. U-Pb and Lu-Hf isotopes of the Archean orthogneiss complex on eastern Hall Peninsula, southern Baffin Island, Nunavut: identification of exotic Paleo- to Mesoproterozoic crust beneath eastern Hall Peninsula; *Precambrian Research*, v. 305, p. 341–357. <https://doi.org/10.1016/j.precamres.2017.12.024>
- Geological Survey of Canada, 2018. Geological Survey of Canada, strategic plan 2018–2023; Natural Resources Canada, 32 p. <https://doi.org/10.4095/313405>
- Harris, J.R., Hillary, E.M., Percival, J.A., Buller, G., Buenviaje, R., Bazor, D., Baer, S., Kiessling, G.M., Pehrsson, S.J., Davis, W.J., Berman, R.G., Wodicka, N., Beauchemin, M., Coyne, M., and Therriault, A.M., 2013. Geo-mapping Frontiers: updated information on the regions covered by Operations Baker, Bathurst, Keewatin, Northern Keewatin, Thelon and Wager; Nunavut and Northwest Territories: GIS components; Geological Survey of Canada, Open File 7434, 1 .zip file. <https://doi.org/10.4095/292744>
- Hartlaub, R.P., Chacko, T., Heaman, L.M., Creaser, R.A., Ashton, K.E., and Simonetti, A., 2005. Ancient (Meso- to Paleoproterozoic) crust in the Rae Province, Canada: evidence from Sm–Nd and U–Pb constraints; *Precambrian Research*, v. 141, p. 137–153. <https://doi.org/10.1016/j.precamres.2005.09.001>
- Hayward, N. and Oneschuk, D., 2011. Geophysical series, regional geophysical compilation project, Great Bear Magmatic Zone, Northwest Territories and Nunavut, NTS 85-M and N, and 86-C, D, E, F, K, and L; Geological Survey of Canada, Open File 6835; Northwest Territories Geoscience Office, NWT Open File 2011-05, scale 1:500 000.
- Hayward, N., Enkin, R.J., Corriveau, L., Montreuil, J.-F., and Kerswill, J., 2013. The application of rapid potential field methods for the targeting of IOCG mineralisation based on physical property data, Great Bear magmatic zone, Canada; *Journal of Applied Geophysics*, v. 94, p. 42–58. <https://doi.org/10.1016/j.jappgeo.2013.03.017>
- Helmstaedt, H.H. and Pehrsson, S.J., 2012. Geology and tectonic evolution of the Slave Province — a post-Lithoprobe perspective; *in* *Tectonic Styles in Canada: The LITHOPROBE Perspective*, (ed.) J.A. Percival, F.A. Cook, and R.M. Clowes; Geological Association of Canada, Special Paper 49, p. 379–466.
- Helmstaedt, H., Pehrsson, S.J., and Stubley, M.P., 2021. The Slave Province, Canada — geological evolution of an Archean diamondiferous craton; Geological Association of Canada, Special Paper 51, 216 p.
- Hoffman, P.F., 1988. United plates of America, the birth of a craton; early Proterozoic assembly and growth of Laurentia; *Annual Review of Earth and Planetary Sciences*, v. 16, p. 543–603. <https://doi.org/10.1146/annurev.ea.16.050188.002551>
- Hoffman, P.F., 1990. Subdivision of the Churchill Province and extent of the Trans-Hudson Orogen; *in* *The Early Proterozoic Trans-Hudson Orogen of North America*, (ed.) J.F. Lewry and M.R. Stauffer; Geological Association of Canada, Special Paper 37, p. 15–40.
- Hoffman, P.F., 2013. The Great Oxidation and a Siderian snowball Earth: MIF-S based correlation of Paleoproterozoic glacial epochs; *Chemical Geology*, v. 362, p. 143–156. <https://doi.org/10.1016/j.chemgeo.2013.04.018>
- Hoffman, P.F., Bowring, S.A., Buchwaldt, R., and Hildebrand, R.S., 2011. Birthdate for the Coronation paleocean: age of initial rifting in Wopmay orogen, Canada; *Canadian Journal of Earth Sciences*, v. 48, p. 281–293. <https://doi.org/10.1139/E10-038>
- Hoggard, M.J., Czarnota, K., Richards, F.D., Huston, D., and Jaques, L., 2019. Treasure maps and the billion-year stability of cratonic lithosphere; *in* *SGTSG and SGSEG 2019 abstracts: biennial meeting of the Specialist Group for Tectonics and Structural Geology and the Specialist Group in Solid Earth Geophysics, Convergence on the Coast*, (ed.) S. Glorie, T. Wise, and R. Dutch; Department for Energy and Mining, South Australia, Report Book 2019/00019, p. 87.

- Jackson, V.A., van Breemen, O., Ootes, L., Bleeker, W., Bennett, V., Davis, W.J., Ketchum, J.W.F., and Smar, L., 2013. U-Pb zircon ages and field relationships of Archean basement and Proterozoic intrusions, south-central Wopmay Orogen, NWT: implications for tectonic assignments; *Canadian Journal of Earth Sciences*, v. 50, no. 10, p. 979–1006. <https://doi.org/10.1139/cjes-2013-0046>
- Jefferson, C.W., Chorlton, L.B., Pehrsson, S.J., Peterson, T., Wollenberg, P., Scott, J., Tschirhart, V., McEwan, B., Bethune, K., Calhoun, L., White, J.C., Leblon, B., LaRocque, A., Shelat, Y., Lentz, D., Patterson, J., Riegler, T., Skulski, T., Robinson, S., Paulen, R., McClenaghan, B., Layton-Matthews, D., MacIsaac, D., Riemer, W., Stieber, C., and Tschirhart, P., 2011. Northeast Thelon Region: Geomapping for Uranium in Nunavut; Geological Survey of Canada, Open File 6962, 1 .zip file. <https://doi.org/10.4095/289037>
- Jefferson, C.W., Chorlton, L.B., Pehrsson, S., Peterson, T., Potter, E., Davis, W., Gandhi, S., Bleeker, W., Keating, P., Quirt, D., Wollenberg, P., Tschirhart, V., Ramaekers, P., LeCheminant, A.N., Robinson, S., White, J., and Bethune, K., 2012. Uranium potential of northern Canada's Proterozoic basins; *in* Prospectors and Developers Association of Canada, Annual Meeting 2012 Abstracts, p. 1.
- Jefferson, C.W., Peterson, T., Tschirhart, V., Davis, W., Scott, J.M.J., Reid, K., Raemaekers, P., Gandhi, S.S., Bleeker, W., Pehrsson, S., Morris, W.A., Fayek, M., Potter, E., Bridge, N., Grunsky, E., Keating, P., Ansdell, K., and Banerjee, N., 2013. LIPS and Proterozoic uranium (U) deposits of the Canadian Shield; Geological Survey of Canada, Open File 7352, 1 .zip file. <https://doi.org/10.4095/292377>
- Jefferson, C.W., White, J.C., Young, G.M., Patterson, J., Tschirhart, V.L., Pehrsson, S.J., Calhoun, L., Rainbird, R.H., Peterson, T.D., Davis, W.J., Tella, S., Chorlton, L.B., Scott, J.M.J., Percival, J.A., Morris, W.A., Keating, P., Anand, A., Shelat, Y., and MacIsaac, D., 2015. Outcrop and remote predictive geology of the Amer Belt and basement beside and beneath the northeast Thelon Basin, in parts of NTS 66-A, B, C, F, G and H, Kivalliq Region, Nunavut; Geological Survey of Canada, Open File 7242, 1 poster. <https://doi.org/10.4095/296825>
- Jefferson, C.W., Rainbird, R.H., Young, G.M., White, J.C., Tschirhart, V., and Creaser, R.A., 2022. The Paleoproterozoic Amer supergroup, Amer Fold Belt, Nunavut: stratigraphy, structure, correlations, and uranium metallogeny; *in* Understanding the Precambrian: a collection of papers in celebration of Grant McAdam Young; *Canadian Journal of Earth Sciences*, posted Open Access 21 November 2022, 35 p. <https://doi.org/10.1139/cjes-2022-0077>
- Kiss, F. and Coyle, M., 2011a. Residual total magnetic field, Hottah Lake aeromagnetic survey, parts of NTS 86 C/5, 12, 86 D/5, 6, 7, 8, 9, 10, 11, 12, Northwest Territories / Composante résiduelle du champ magnétique total, levé aéromagnétique de la région du lac Hottah, SNRC parties de 86 C/5, 12, 86 D/5, 6, 7, 8, 9, 10, 11, 12, Territoires du Nord-Ouest; Geological Survey of Canada, Open File 6851, scale 1:100 000. <https://doi.org/10.4095/288787>
- Kiss, F. and Coyle, M., 2011b. First vertical derivative of the magnetic field, Hottah Lake aeromagnetic survey, parts of NTS 86 C/5, 12, 86 D/5, 6, 7, 8, 9, 10, 11, 12, Northwest Territories / Dérivée première verticale du champ magnétique, levé aéromagnétique de la région du lac Hottah, SNRC parties de 86 C/5, 12, 86 D/5, 6, 7, 8, 9, 10, 11, 12, Territoires du Nord-Ouest; Geological Survey of Canada, Open File 6852, scale 1:100 000. <https://doi.org/10.4095/288788>
- Kiss, F. and Coyle, M., 2011c. Residual total magnetic field, Hottah Lake aeromagnetic survey, parts of NTS 86 C/13, 86 D/13, 14, 15, 16, 86 E/1, 2, 3, Northwest Territories / Composante résiduelle du champ magnétique total, levé aéromagnétique de la région du lac Hottah, SNRC parties de 86 C/13, 86 D/13, 14, 15, 16, 86 E/1, 2, 3, Territoires du Nord-Ouest; Geological Survey of Canada, Open File 6853, scale 1:100 000. <https://doi.org/10.4095/288789>
- Kiss, F. and Coyle, M., 2011d. First vertical derivative of the magnetic field, Hottah Lake aeromagnetic survey, parts of NTS 86 C/13, 86 D/13, 14, 15, 16, 86 E/1, 2, 3, Northwest Territories / Dérivée première verticale du champ magnétique, levé aéromagnétique de la région du lac Hottah, SNRC parties de 86 C/13, 86 D/13, 14, 15, 16, 86 E/1, 2, 3, Territoires du Nord-Ouest; Geological Survey of Canada, Open File 6854, scale 1:100 000. <https://doi.org/10.4095/288790>
- Kiss, F. and Coyle, M., 2011e. Hottah Lake aeromagnetic survey, Northwest Territories, parts of NTS 86 C/5, 12, 86 D/5, 6, 7, 8, 9, 10, 11, 12, BLOCK A, Sheet 1 of 2, 1:100 000 scale; Northwest Territories Geoscience Office, NWT Open File 2011-03, 4 maps and digital data.
- Kiss, F. and Coyle, M., 2011f. Hottah Lake aeromagnetic survey, Northwest Territories, parts of NTS 86 C/13, 86 D/13, 14, 15, 16, 86 E/1, 2, 3, BLOCK B, Sheet 2 of 2, 1:100 000 scale; Northwest Territories Geoscience Office, NWT Open File 2011-03, 4 maps and digital data.
- Kopp, R.E., Kirschvink, J.L., Hilburn, I.A., and Nash, C.Z., 2005. The Paleoproterozoic snowball Earth: A climate disaster triggered by the evolution of oxygenic photosynthesis; *Proceedings of the National Academy of Sciences of the United States of America*, v. 102, p. 11131–11136. <https://doi.org/10.1073/pnas.0504878102>
- Korenaga, J., 2008. Urey ratio and the structure and evolution of Earth's mantle; *Reviews of Geophysics*, v. 46, no. 2, cit. no. RG2007. <https://doi.org/10.1029/2007RG000241>

- Kremer, P.D., Böhm, C.O., and Rayner, N., 2011. Far north geomapping initiative: bedrock geology of the Snyder Lake area, northwestern Manitoba (part of NTS 64N5); Manitoba Industry, Trade and Mines, Manitoba Geological Survey, Report of Activities 2011, 12 p.
- LaFlamme, C., McFarlane, C.R.M., Corrigan, D., and Wodicka, N., 2014. Origin and tectonometamorphic history of the Repulse Bay block, Melville Peninsula, Nunavut: exotic terrane or deeper level of the Rae craton?; *Canadian Journal of Earth Sciences*, v. 51, p. 1097–1122. <https://doi.org/10.1139/cjes-2014-0040>
- Lawley, C.J.M., McNicoll, V., Sandeman, H., Pehrsson, S., Simard, M., Castonguay, S., Mercier-Langevin, P., and Dubé, B., 2016. Age and geological setting of the Rankin Inlet greenstone belt and its relationship to the gold endowment of the Meliadine gold district, Nunavut, Canada; *Precambrian Research*, v. 275, p. 471–495. <https://doi.org/10.1016/j.precamres.2016.01.008>
- Lyons, T.W., Reinhard, C.T., and Planavsky, N.J., 2014. The rise of oxygen in Earth's early ocean and atmosphere; *Nature*, v. 506, p. 307–315. <https://doi.org/10.1038/nature13068>
- MacLachlan, K., Davis, W., and Relf, C., 2005. U/Pb geochronological constraints on Neoproterozoic tectonism: multiple compressional events in the Northwestern Hearne domain, Western Churchill Province, Canada; *Canadian Journal of Earth Sciences*, v. 42, p. 85–109. <https://doi.org/10.1139/e04-104>
- McClenaghan, M.B., Paulen, R.C., Rice, J.M., Sanborn-Barrie, M., McCurdy, M.W., Spirito, W.A., Adcock, S.W., Veillette, J.J., Garrett, R.G., Grunsky, E.C., Pickett, J., Layton-Matthews, D., and Corrigan, D., 2014. GEM 2 Hudson-Ungava Project: southern Core Zone surficial geology, geochemistry, and bedrock mapping activities in Northern Quebec and Labrador; Geological Survey of Canada, Open File 7705, 18 p. <https://doi.org/10.4095/295521>
- McClenaghan, M.B., Spirito, W.A., Day, S.J.A., McCurdy, M.W., McNeil, R.J., and Adcock, S.W., 2022. Overview of surficial geochemistry and indicator mineral surveys and case studies from the Geological Survey of Canada's GEM Program; *Geochemistry: Exploration, Environment, Analysis*, v. 22, no. 1, geochem2021–070, 21 p. <https://doi.org/10.1144/geochem2021-070>
- McMartin, I. (ed.), 2023. Surficial geology of northern Canada: a summary of Geo-mapping for Energy and Minerals contributions; Geological Survey of Canada, Bulletin 611, 265 p. <https://doi.org/10.4095/331418>
- Ootes, L., Davis, W.J., Jackson, V.A., and van Breemen, O., 2015. Chronostratigraphy of the Hottah terrane and Great Bear magmatic zone of Wopmay Orogen, Canada, and exploration of a terrane translation model; *Canadian Journal of Earth Sciences*, v. 52, no. 12, p. 1062–1092. <https://doi.org/10.1139/cjes-2015-0026>
- Pearson, D.G. and Wittig, N., 2008. Formation of Archaean continental lithosphere and its diamonds: the root of the problem; *Journal of the Geological Society*, v. 165, p. 895–914. <https://doi.org/10.1144/0016-76492008-003>
- Pearson, D., Brenker, F., Nestola, F., McNeill, J., Hutchison, M.T., Matveev, S., Mather, K., Silversmit, G., Schmitz, S., Vekemans, B., and Vincze, L., 2014. Hydrous mantle transition zone indicated by ringwoodite included within diamond; *Nature*, v. 507, p. 221–224. <https://doi.org/10.1038/nature13080>
- Pehrsson, S., Berman, R.G., and Davis, W.J., 2013. Paleoproterozoic orogenesis during Nuna aggregation: a case study of reworking of the Rae craton, Woodburn Lake, Nunavut; *Precambrian Research*, v. 232, p. 167–188. <https://doi.org/10.1016/j.precamres.2013.02.010>
- Pehrsson, S.J., Buchan, K.L., Eglington, B.M., Berman, R.M., and Rainbird, R.H., 2014a. Did plate tectonics shutdown in the Palaeoproterozoic? A view from the Siderian geologic record; *Gondwana Research*, v. 26, p. 803–815. <https://doi.org/10.1016/j.gr.2014.06.001>
- Pehrsson, S.J., Percival, J.A., Davis, W.J., McCurdy, M.W., Berman, R.G., Hillary, E.M., Kiss, F., MacKinnon, A., and Jefferson, C.W., 2014b. Operation GEM South Rae: reconnaissance geology of the most poorly known part of the Churchill Province, Northwest Territories and Nunavut; Geological Survey of Canada, Open File 7410, 25 p. <https://doi.org/10.4095/293762>
- Pehrsson, S.J., Coyle, M., and Berman, R., 2014c. The GEM Chesterfield gold project: understanding controls on western Churchill gold endowment from the bottom up; Geological Survey of Canada, Open File 7490, 31 p. <https://doi.org/10.4095/293763>
- Pehrsson, S.J., Campbell, J.E., Martel, E., McCurdy, M.W., Acosta-Góngora, P., Thiessen, E., Jamieson, D., Lauzon, G., Buller, G., Falck, H., and Dyke, A.S., 2015. Report of 2015 activities for the geologic and metallogenic framework of the south Rae Craton, southeast Northwest Territories: GEM 2 South Rae Quaternary and Bedrock project; Geological Survey of Canada, Open File 7958, 24 p. <https://doi.org/10.4095/297387>
- Percival, J.A., Cook, F.A., and Clowes, R.M. (ed.), 2012. Tectonic styles in Canada: the LITHOPROBE perspective; Geological Association of Canada, Special Paper 49, 498 p.

- Percival, J.A., Martel, E., Pehrsson, S.J., Acosta-Góngora, P., Regis, D., Thiessen, E., Jamison, D., Neil, B., and Knox, B., 2016. Report of 2016 bedrock activities for the geologic and metallogenic framework of the south Rae Craton, southeast NWT: GEM 2 South Rae Quaternary and Bedrock project; Geological Survey of Canada, Open File 8142, 17 p. <https://doi.org/10.4095/299469>
- Potter, E.G., Montreuil, J.-F., Corriveau, L., and De Toni, A., 2013. Geology and hydrothermal alteration of the Fab Lake region, Northwest Territories; Geological Survey of Canada, Open File 7339, 1 .zip file. <https://doi.org/10.4095/292562>
- Rainbird, R.H. and Davis, W.J., 2022. On the Statherian-Callymian palaeogeography of northwestern Laurentia; *Journal of the Geological Society*, v. 179, art. no. jgs-2022-062, 20 p. <https://doi.org/10.1144/jgs2022-062>
- Rainbird, R.H. and Ielpi, A., 2015. Reconnaissance geological mapping and thematic studies of the Elu Basin, Nunavut; Geological Survey of Canada, Open File 7730, 10 p. <https://doi.org/10.4095/295696>
- Rainbird, R.H., Davis, W.J., Pehrsson, S.J., Wodicka, N., Rayner, N., and Skulski, T., 2010. Early Paleoproterozoic supracrustal assemblages of the Rae domain, Nunavut, Canada: Intracratonic basin development during supercontinent break-up and assembly; *Precambrian Research*, v. 181, p. 167–186. <https://doi.org/10.1016/j.precamres.2010.06.005>
- Rainbird, R.H., Harrison, J.C., Hillary, E.M., Ford, A., Hulbert, L.J., Christie, R.L., and Campbell, F.H.A., 2015. Geology, tectonic assemblage map of Hadley Bay, Victoria and Prince of Wales islands, Nunavut–Northwest Territories; Geological Survey of Canada, Canadian Geoscience Map 75 (2nd preliminary edition), scale 1:500 000. <https://doi.org/10.4095/295861>
- Rayner, N., 2010. Far north geomapping initiative: new U-Pb geochronological results from the Seal River region, northeastern Manitoba (parts of NTS 54L, M, 64I, P); Manitoba Department of Energy and Mines, Geological Services, Report of Activities 2010, p. 23–35.
- Rayner, N.M., 2014. New U-Pb geochronological results from Hall Peninsula, Baffin Island, Nunavut; Canada-Nunavut Geoscience Office, Summary of Activities 2013, p. 39–52.
- Rayner, N., 2022. U-Pb geochronology data from the 2008–2011 Manitoba Far North Geomapping Initiative; Geological Survey of Canada, Open File 8868, 1 .zip file. <https://doi.org/10.4095/329641>
- Rayner, N.M., St-Onge, M.R., and Miles, W.F., 2014. Report of activities for completing the regional bedrock mapping of the southern half of Baffin Island: GEM 2 Baffin Project; Geological Survey of Canada, Open File 7704, 9 p. <https://doi.org/10.4095/295525>
- Reddy, S.M. and Evans, D.A.D., 2009. Palaeoproterozoic supercontinents and global evolution; correlations from core to atmosphere; *in* *Palaeoproterozoic Supercontinents and Global Evolution*, (ed.) S. Reddy, R. Mazumder, D.A.D. Evans, and A.S. Collins; Geological Society of London, Special Publication 323, p. 1–26. <https://doi.org/10.1144/SP323.1>
- Regis, D.R. and Sanborn-Barrie, M., 2023. Detrital U-Pb detrital zircon geochronological constraints on Siderian and Orosirian rocks of Boothia Peninsula and Somerset Island (Nunavut, Canada); *Precambrian Research*, v. 387, art. no. 106991, 22 p. <https://doi.org/10.1016/j.precamres.2023.106991>
- Reimink, J.R., Chacko, T., Stern, R.A., and Heaman, L.M., 2016. The birth of a cratonic nucleus: lithochemical evolution of the 4.02–2.94 Ga Acasta Gneiss Complex; *Precambrian Research*, v. 281, p. 453–472. <https://doi.org/10.1016/j.precamres.2016.06.007>
- Salminen, J., Pehrsson, S., Evans, D.A.D., and Wang, C., 2021. Neoproterozoic supercycles; Chapter 15 *in* *Ancient Supercontinents and the Paleogeography of Earth*, (ed.) L.J. Pesonen, J. Salminen, S.-Å. Elming, D.A.D. Evans, and T. Veikkolainen; Elsevier, p. 465–498. <https://doi.org/10.1016/B978-0-12-818533-9.00014-X>
- Sanborn-Barrie, M. and Young, M., 2011. Bulk compositional data for sulfidic and gossanous rocks from Cumberland Peninsula, Baffin Island, Nunavut; Geological Survey of Canada, Open File 6916, 1 .zip file. <https://doi.org/10.4095/288710>
- Sanborn-Barrie, M., Chakungal, J., and Buller, G., 2009. Bedrock field data and photographic record of exposed Precambrian basement, Southampton Island, Nunavut; Geological Survey of Canada, Open File 6177, 1 .zip file. <https://doi.org/10.4095/247890>
- Sanborn-Barrie, M., Davis, W.J., Berman, R.G., Rayner, N., Skulski, T., and Sandeman, H., 2014. Neoproterozoic continental crust formation and Paleoproterozoic deformation of the central Rae craton, Committee Bay belt, Nunavut; *Canadian Journal of Earth Sciences*, v. 51, p. 635–667. <https://doi.org/10.1139/cjes-2014-0010>
- Sanborn-Barrie, M., Ford, A., Hillary, E.M., Tschirhart, V.L., Tremblay, T., and Maharaj, J., 2016. Report of activities for the GEM-2 Boothia Peninsula-Somerset Island project: integrated geoscience of the Northwest Passage; Geological Survey of Canada, Open File 8128, 11 p. <https://doi.org/10.4095/299381>

- Sanborn-Barrie, M., Regis, D., Ford, A., Osinchuk, A., and Drayson, D., 2018. Report of activities for the GEM-2 Boothia Peninsula-Somerset Island Project: integrated geoscience of the Northwest Passage, Nunavut; Geological Survey of Canada, Open File 8339, 16 p. <https://doi.org/10.4095/306597>
- Sanborn-Barrie, M., Regis, D., and Ford, A., 2019. Integrated geoscience of the Northwest Passage, Nunavut: GEM-2 Boothia Peninsula-Somerset Island project, report of activities 2018; Geological Survey of Canada, Open File 8557, 17 p. <https://doi.org/10.4095/314501>
- Saumur, B.M., Skipton, D.R., St-Onge, M.R., Bros, E.R., Acosta-Góngora, P., Kelly, C.J., Morin, A., O'Brien, M.E., Johnston, S.T., and Weller, O.M., 2018. Precambrian geology of the surroundings of Steensby Inlet and western Barnes Ice Cap (parts of NTS 37E, 37F, 37G), Baffin Island, Nunavut; Canada-Nunavut Geoscience Office, Summary of Activities 2018, p. 29–46.
- Sheen, A.I., Heaman, L.M., Kjarsgaard, B., Ootes, L., Pearson, D.G., and Creaser, R.A., 2019. Athapuscow aulacogen revisited: Geochronology and geochemistry of the 2046 Ma Union Island Group mafic magmatism, East Arm of Great Slave Lake, Northwest Territories, Canada; *Precambrian Research*, v. 321, p. 85–102. <https://doi.org/10.1016/j.precamres.2018.11.012>
- Shimojo, M., Yamamoto, S., Sakata, S., Yokoyama, T.D., Maki, K., Sawaki, Y., Ishikawa, A., Aoki, K., Aoki, S., Koshida, K., Tashiro, T., Hirata, T., Collerson, K.D., and Komiya, T., 2016. Occurrence and geochronology of the Eoarchean, ~3.9 Ga, Iqaluk Gneiss in the Saglek Block, northern Labrador, Canada: Evidence for the oldest supracrustal rocks in the world; *Precambrian Research*, v. 278, p. 218–243. <https://doi.org/10.1016/j.precamres.2016.03.018>
- Skipton, D.R., Schneider, D.A., and St-Onge, M.R., 2013. Preliminary observations on Archean and Paleoproterozoic metamorphism and deformation of the southern Hall Peninsula, Baffin Island, Nunavut; Canada-Nunavut Geoscience Office, Summary of Activities 2012, p. 29–42.
- Skipton, D.R., Saumur, B.M., St-Onge, M.R., Wodicka, N., Bros, E.R., Morin, A., Brouillette, P., Weller, O.M., and Johnston, S.T., 2017. Precambrian bedrock geology of the Pond Inlet–Mary River area, northern Baffin Island, Nunavut; Canada-Nunavut Geoscience Office, Summary of Activities 2017, p. 49–68.
- Skipton, D.R., Wodicka, N., McNicoll, V., Saumur, B.M., St-Onge, M.R., and Young, M.D., 2019. U-Pb zircon geochronology of Archean greenstone belts (Mary River Group) and surrounding Archean to Paleoproterozoic rocks, northern Baffin Island, Nunavut; Geological Survey of Canada, Open File 8585, 1. zip file. <https://doi.org/10.4095/314938>
- Skirrow, R.G., 2010. “Hematite-group” IOCG±U ore systems: tectonic settings, hydrothermal characteristics, and Cu–Au and U mineralizing processes; *in Exploring for iron oxide copper-gold deposits: Canada and Global Analogues*, (ed.) L. Corriveau and A.H. Mumin; Geological Association of Canada, Short Course Notes 20, p. 39–58.
- Skulski, T., Paul, D., Sandeman, H., Berman, R.G., Chorlton, L., Pehrsson, S.J., Rainbird, R.H., Davis, W.J., and Sanborn-Barrie, M., 2018. Bedrock geology, central Rae Craton and eastern Queen Maud Block, western Churchill Province, Nunavut; Geological Survey of Canada, Canadian Geoscience Map 307, scale 1:550 000. <https://doi.org/10.4095/308348>
- Snyder, D.B. and Kjarsgaard, B.A., 2013. Mantle roots of major Precambrian shear zones inferred from structure of the Great Slave Lake shear zone, northwest Canada; *Lithosphere*, v. 5, no. 6, p. 539–546. <https://doi.org/10.1130/L299.1>
- Steenkamp, H.M., Wodicka, N., Lawley, C.J.M., Peterson, T., Garrison, W., Therriault, I., Kendrick, J., Weller, O.M., and Tschirhart, V., 2023a. Bedrock geology, Daly Bay area, Kivalliq, Nunavut, NTS 56-A, 46-D west, 46-E southwest, and 56-H south; Geological Survey of Canada, Canadian Geoscience Map 458, scale 1:150 000. <https://doi.org/10.4095/331888>
- Steenkamp, H.M., Wodicka, N., Lawley, C.J.M., Peterson, T., Weller, O.M., Kendrick, J., and Tschirhart, V., 2023b. Bedrock geology, Armit Lake area, Kivalliq, Nunavut, NTS 56-B and 56-C east; Geological Survey of Canada, Canadian Geoscience Map 459, scale 1:150 000. <https://doi.org/10.4095/331889>
- Steenkamp, H.M., Wodicka, N., Weller, O.M., Kendrick, J., Therriault, I., Peterson, T., Lawley, C.J.M., and Tschirhart, V., 2023c. Bedrock geology, Wager Bay area, Kivalliq, Nunavut, parts of NTS 56-F and 56-G; Geological Survey of Canada, Canadian Geoscience Map 460, scale 1:150 000. <https://doi.org/10.4095/331890>
- Stern, R.J., 2020. The Mesoproterozoic single-lid tectonic episode: prelude to modern plate tectonics; *GSA Today*, v. 30, no. 12, p. 4–10. <https://doi.org/10.1130/GSATG480A.1>
- Whalen, J.B., Sanborn-Barrie, M., and Young, M., 2012. Geochemical data from Archean and Paleoproterozoic plutonic and volcanic rocks of Cumberland Peninsula, eastern Baffin Island, Nunavut; Geological Survey of Canada, Open File 6933, 1. zip file. <https://doi.org/10.4095/291453>

GSC Bulletin 612

- Wodicka, N., Corrigan, D., Nadeau, L., and Erdmann, S., 2011. New U-Pb geochronological results from Melville Peninsula: unravelling the Archean and early Paleoproterozoic magmatic history of the north-central Rae craton; Geological Association of Canada–Mineralogical Association of Canada, Abstracts, v. 34, p. 236.
- Wodicka, N., St-Onge, M.R., Corrigan, D., Scott, D.J., and Whalen, J.B., 2014. Did a proto-ocean basin form along the southeastern Rae cratonic margin? Evidence from U-Pb geochronology, geochemistry (Sm-Nd and whole-rock), and stratigraphy of the Paleoproterozoic Piling Group, northern Canada; Geological Society of America Bulletin, v. 126, p. 1625–1653. <https://doi.org/10.1130/B31028.1>
- Wodicka, N., Steenkamp, H.M., Weller, O.M., Kendrick, J., Tschirhart, V.L., Peterson, T.D., and Girard, É., 2016. Report of 2016 activities for the bedrock geology and economic potential of the Tehery-Wager area: GEM 2 Rae Project; Geological Survey of Canada, Open File 8149, 21 p. <https://doi.org/10.4095/299392>
- Wodicka, N., Steenkamp, H.M., Peterson, T.D., McMartin, I., Day, S.J.A., and Tschirhart, V.L., 2017. Report of 2017 activities for the geology and economic potential of the Tehery-Wager area, Nunavut: GEM-2 Rae Project; Geological Survey of Canada, Open File 8318, 20 p. <https://doi.org/10.4095/305979>
- Wright, D.F., Ambrose, E.J., Lemkow, D., and Bonham-Carter, G. (ed.), 2013. Mineral and energy resource assessment of the proposed Thaidene Nene National Park Reserve in the area of the east arm of Great Slave Lake, Northwest Territories. Geological Survey of Canada, Open File 7196, 1 .zip file. <https://doi.org/10.4095/292447>

Advancing exploration for iron oxide–copper–gold and affiliated deposits in Canada: context, scientific overview, outcomes, and impacts

L. Corriveau^{1*} and E.G. Potter²

Corriveau, L. and Potter, E.G., 2024. Advancing exploration for iron oxide–copper–gold and affiliated deposits in Canada: context, scientific overview, outcomes, and impacts; in Canada's northern shield: new perspectives from the Geo-mapping for Energy and Minerals program; (ed.) S.J. Pehrsson, N. Wodicka, N. Rogers, and J.A. Percival; Geological Survey of Canada, Bulletin 612, p. 55–98. <https://doi.org/10.4095/332495>

Abstract: The Geo-mapping for Energy and Minerals (GEM) and Targeted Geoscience Initiative (TGI) programs conducted extensive collaborative research on mineral systems with iron oxide–copper–gold (IOCG) and affiliated deposits in prospective settings of Canada. Regional alteration mapping as well as geochemical and geophysical modelling undertaken under the GEM program documented the evolution of polymetallic metasomatic systems with iron-oxide and alkali-calcic alteration and led to an increased recognition of the mineral potential of poorly explored areas and historic deposits of the Great Bear magmatic zone in the Northwest Territories, thus providing a solid framework for exploration. Early and barren albitite corridors form across the mineral systems and locally host uranium mineralization associated with telescoping of alteration facies by tectonic activity during the metasomatic growth of the systems. Subsequent to albitization, high-temperature Ca-Fe and Ca-K-Fe alteration form iron oxide–apatite (\pm rare-earth element) mineralization and IOCG variants rich in cobalt and other critical metals, respectively. Systems that further mature to K-Fe alteration form IOCG mineralization and can evolve to mineralized near-surface phyllic alteration and epithermal caps. Transitional facies also host polymetallic skarn mineralization. Rare-earth element enrichments within iron oxide–apatite zones are strongest where remobilization has occurred, particularly along deformation zones.

The TGI projects documented the pertinence for a GEM activity in the Great Bear magmatic zone and subsequently synthesized GEM geoscientific data into a system-scale, ore-deposit model, and outlined criteria for mineral resource assessment. This model, and newly developed field-mapping and lithogeochemical tools were shown to be efficient mineral exploration and regional mapping methods in Canada and were also applied to the archetype IOCG deposit, Olympic Dam, and other deposits in the Olympic Cu–Au metallogenic province of Australia. Case examples also include the Romanet Horst in the Trans-Hudson Orogen (second phase of GEM), the Central Mineral Belt in Labrador (TGI), the Wanapitei Lake district in Ontario (private sector exploration results used by TGI), and the Bondy gneiss complex in Quebec (TGI).

Résumé : Les programmes Géocartographie de l'énergie et des minéraux (GEM) et de l'Initiative géoscientifique ciblée (IGC) ont permis la réalisation de recherches collaboratives poussées sur les systèmes minéralisateurs à gîtes d'oxydes de fer-cuivre-or (IOCG) et à gîtes affiliés au sein de contextes prometteurs au Canada. La cartographie de l'altération à l'échelle régionale, de même que la modélisation géochimique et géophysique menées dans le cadre du programme GEM ont permis de documenter l'évolution de systèmes métasomatiques à minéralisation polymétallique présentant une altération alcalino-calcique et à oxydes de fer, et ont mené à une reconnaissance accrue du potentiel minéral de zones sous-explorées et de gisements historiques de la zone magmatique de Grand lac de l'Ours, dans les Territoires du Nord-Ouest, fournissant ainsi un cadre solide pour l'exploration. Ces systèmes métasomatiques forment des couloirs d'albitite précoces et stériles qui peuvent par la suite servir localement d'hôtes à une minéralisation uranifère associée au télescopage des faciès d'altération en contexte de tectonique active synmétasomatique. À la suite de l'albitisation, l'altération à Ca-Fe et l'altération à Ca-K-Fe de haute température forment respectivement de la minéralisation d'oxydes de fer-apatite (\pm éléments de terres rares) et des variantes de gîtes d'IOCG riches en cobalt et autres métaux critiques. Les systèmes qui connaissent une évolution plus poussée, caractérisée par l'altération à K-Fe, forment de la minéralisation d'IOCG et peuvent ultimement aboutir à la formation, près de la surface, d'une altération phyllique et de chapeaux épithermaux minéralisés. Les faciès de transition peuvent aussi renfermer une minéralisation de skarn polymétallique. Les enrichissements en éléments de terres rares au sein des zones à oxydes de fer-apatite sont les plus forts là où il y a eu remobilisation, en particulier le long des zones de déformation.

Les projets de l'IGC ont d'abord démontré la pertinence de mener une activité de GEM dans la zone magmatique du Grand lac de l'Ours, puis ont permis de synthétiser les données géoscientifiques de GEM de façon à produire un modèle pour les gîtes minéraux à l'échelle du système minéralisateur et de définir des critères d'évaluation des ressources minérales. Ce modèle et les nouveaux outils de cartographie de terrain et de lithogéochimie développés se sont révélés être des méthodes efficaces d'exploration minérale et de cartographie géologique régionale au Canada, puis ont été appliqués à l'archétype des gîtes d'IOCG, le gisement d'Olympic Dam, et à d'autres gîtes de la province métallogénique à Cu–Au d'Olympic, en Australie. Les exemples de cas comprennent également le horst de Romanet dans l'orogène trans-hudsonien (deuxième phase de GEM), la ceinture minérale centrale du Labrador (IGC), la région du lac Wanapitei en Ontario (résultats d'exploration du secteur privé utilisés par l'IGC) et le complexe gneissique de Bondy au Québec (IGC).

¹Geological Survey of Canada, 490, rue de la Couronne, Québec, Québec G1K 9A9

²Geological Survey of Canada, 601 Booth Street, Ottawa, Ontario K1A 0E8

*Corresponding author: L. Corriveau (email: louise.corriveau@nrcan-rncan.gc.ca)

INTRODUCTION

Iron oxide–copper–gold (IOCG) deposits, first recognized in the early nineteen nineties (Hitzman et al., 1992), have iron oxide– rather than sulphide-dominant polymetallic ore zones with economic copper concentrations. The metasomatic iron oxide and alkali-calcic alteration (IOAA) systems that host this deposit type are now known to host affiliated deposit types, including many with critical metals as primary commodities. These deposit types display a wide range of mineralization styles and ore assemblages, and form within the regular sequence of alteration ‘facies’ that defines the mineral system. Deposits include iron oxide–apatite (IOA), locally with rare-earth element (REE) or nickel mineralization (REE in the deposits of the Missouri district, U.S.A., and Josette deposit, Quebec; Day et al., 2016; Gagnon et al., 2018; nickel in the Carajás district, Brazil; Ferreira Filho et al., 2021); iron and polymetallic skarn (Punt Hill, Australia; Fabris et al., 2018a, b; Middle-lower Yangtze River metallogenic belt, China; Hu et al., 2020); cobalt deposits with variable amounts of Au, Bi, and Cu as well as abundant iron oxides or iron silicates (NICO deposit, Northwest Territories, and deposits of the Idaho Cobalt Belt, U.S.A.; Slack, 2013; Acosta-Góngora et al., 2015a; Montreuil et al., 2016b); gold-rich mineralization with variable amounts of Cu, Bi, and iron oxides or iron silicates (Scadding deposit, Ontario, and Tennant Creek district, Australia; Skirrow and Walshe, 2002; Schandl and Gorton, 2007); molybdenum-rhenium mineralization with low contents of iron oxides (Merlin deposit, Australia; Babo et al., 2017); uranium-REE mineralization with low iron-oxide contents (Mount Kathleen deposit, Australia); albitite-hosted Au-Co-(U) deposits with variable amounts of iron-oxides (Rajapalot deposit, Finland; Rantala et al., 2021); albitite-hosted uranium mineralization with variable iron-oxide contents (Valhalla deposit, Australia, and Michelin deposit and Southern Breccia prospect, Canada; Wilde, 2013; Wilde et al., 2013; Montreuil et al., 2015; Potter et al., 2019), and base- and precious-metal mineralization with low contents of iron oxides (Romanet Horst, Quebec; Corriveau et al., 2014). Such mineral systems remain identifiable even when metamorphosed to high grades (Corriveau et al., 2007, 2018a; Corriveau and Spry, 2014). Collectively, these deposits can be endowed in precious and base metals such as Au, Cu, Ag, Ni, Pb, Zn, and Fe (Williams et al., 2005), and can include a large spectrum of critical metals such as Bi, Co, F, Mo, Nb, REE (both heavy and light REE), U, V, W, and, locally, platinum-group elements (Pd, Pt, Re) (cf. Corriveau et al., 2018b, 2022c).

In Canada, IOCG and affiliated deposits remain significantly under-represented in terms of defined mineral resources (Corriveau, 2007; Corriveau et al., 2010a). No IOCG or iron oxide–apatite (IOA) deposits are currently being mined, but the NICO deposit in the Great Bear magmatic zone

(Northwest Territories; Fig. 1) is fully permitted for mining and is an example of a gold- and critical metal-bearing (cobalt and bismuth) variant of IOCG deposits (Fortune Minerals Limited, 2019). The Josette REE deposit in the Grenville Province of Quebec is an IOA deposit formed within a larger system that evolved to IOCG mineralization (Fig. 1; Perreault and Lafrance, 2015; Corriveau et al., 2022a). The Michelin deposit in the Central Mineral Belt of Labrador is one of many albitite-hosted uranium deposits known globally to occur within mineral provinces that also host IOCG mineralization (Fig. 1; Sparkes, 2017; Sparkes et al., 2017; Acosta-Góngora et al., 2018a). The Bondy gneiss complex in Quebec was subjected to granulite-facies metamorphism yet has all the depth to near-surface alteration facies of IOAA systems and hosts IOCG and IOA mineralization (Fig. 1; Corriveau, 2013; Dufréchoy et al., 2015; Corriveau et al., 2018a; Trapy, 2018).

Canada is endowed with several prospective settings with extensive, glacially polished field exposures that provide windows into mineral system processes. To provide industry with the knowledge and tools to explore for IOCG and affiliated exploration targets in Canada, the Geomapping for Energy and Minerals program (GEM) launched the multidisciplinary and collaborative IOCG/Great Bear project in 2008 to study the mineral systems of the Great Bear magmatic zone. The Great Bear magmatic zone was used by Hitzman et al. (1992) to define the IOCG deposit type and is an excellent location in which to demonstrate the relationships between IOA, IOCG, and affiliated deposits within the broader mineral system.

This synthesis addresses the relevance and context of the GEM IOCG/Great Bear project and Targeted Geoscience Initiative (TGI) IOCG-related activities, the multiple streams of research undertaken, project results, and impacts. Overall, the GEM and TGI projects have shown that the Great Bear magmatic zone is a key exploration target for base, precious, and critical metals as well as for uranium and, potentially, thorium. New ore-deposit models, field-based mapping protocols and broad-based exploration methodologies were integrated with the well documented regional case studies of IOAA mineral systems. The Great Bear magmatic zone mineral systems were shown to be comparable to global mining districts hosting IOCG and affiliated deposits in terms of the geological attributes, geodynamic settings, and metal associations. By combining the GEM and TGI mandates, the Geological Survey of Canada (GSC) and its partners have positioned the Great Bear magmatic zone as a global reference for IOAA systems containing IOA, IOCG, albitite-hosted uranium, and affiliated critical metal mineralization types with exceptional field exposures of the preserved systems, even though the belt remains significantly underexplored.

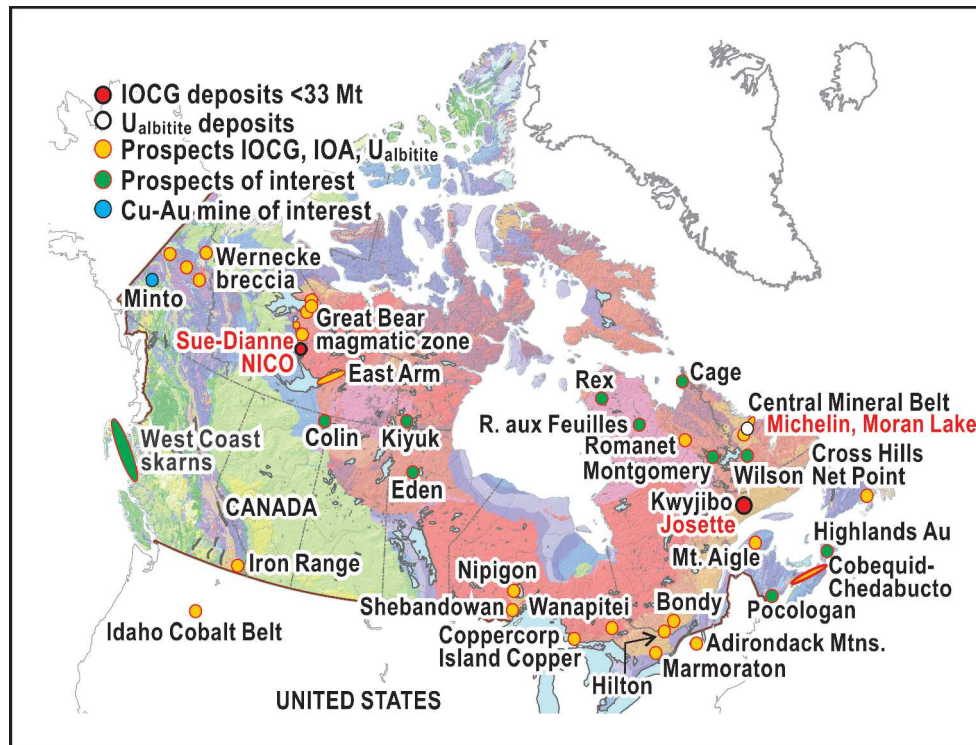


Figure 1. Location of Canadian iron oxide–alkali-calcic-altered districts and their iron oxide–apatite (IOA), iron oxide–copper–gold (IOCG), albitite-hosted U (Au–Co–Cu), and affiliated deposits and prospects. Currently prospective settings occur within the Precambrian Shield (in varieties of pink), in Precambrian inliers within the Cordillera, and in the Appalachian orogens. Geology from Wheeler et al. (1996).

CANADIAN PERSPECTIVE ON IOCG AND AFFILIATED DEPOSITS

Characterized by extensive felsic magmatism, most prospective settings for IOCG and affiliated deposits differ geologically from the traditional Archean greenstone belts and sedimentary basins usually associated with Canadian exploration districts (Gandhi et al., 2001; Wade et al., 2012; de Melo et al., 2019; Reid, 2019). As a result, these prospective settings remain undermapped, undervalued, and underexplored (Corriveau, 2007; Corriveau and Mumin, 2010). In the last few decades, defined resources and discovery rates in mining districts with IOCG, IOA, and affiliated deposits have significantly increased worldwide, with deposits being found within continental settings (Fig. 2) ranging in age from Archean to Quaternary (Porter, 2010; Corriveau et al., 2018b). The Neoproterozoic to Paleoproterozoic Carajás mineral province of Brazil, which hosts widespread granitic intrusions, also has several large-tonnage IOCG deposits such as the giant Salobo deposit with reserves of 1.19 Bt at 0.61% Cu, 0.32 g/t Au, and additional measured and indicated resources of 204 Mt grading 0.64% Cu and 0.33 g/t Au (Burns et al., 2017; Xavier et al., 2017; de Melo et al., 2019; *see* resources listed in Corriveau et al., 2018b). In Australia, the Mesoproterozoic Olympic Copper–Gold Province hosts

the supergiant Olympic Dam deposit within a granitic intrusion with total resources of 10 070 Mt at 0.62% Cu, 0.21 kg/t U_3O_8 , 0.27 g/t Au, and 1 g/t Ag mineable by open-pit methods and approximately 1041 Mt at 1.68% Cu, 0.47 kg/t U_3O_8 , 0.63 g/t Au, and 3 g/t Ag of underground ore (Ehrig et al., 2012, 2017a, b, 2021; BHP, 2020). The deposit also has about 0.3% light REE and 0.01% heavy REE (Corriveau et al., 2018b). The Olympic Dam deposit contains the largest uranium resource, fifth largest copper resource (being superseded by porphyry deposits), and third largest gold resource (superseded by the Witwatersrand and Grasberg deposits) in a single deposit (BHP, 2015, 2017; Corriveau et al., 2018b).

The Olympic Dam deposit also remains open at depth; the deepest diamond drilling intersected mineralization at a depth of 2.3 km, where it is rich in magnetite (Apukhtina et al., 2017; Ehrig et al., 2017b). At the largest metasomatic iron and alkali-calcic (MIAC)-related deposit in Canada, diamond drilling has reached a depth of 250 m to 300 m (Burgess et al., 2014) with a few deeper holes reaching 612 m (R. Goad, pers. comm., 2021), nearly an order of magnitude less than many settings worldwide. In addition to Olympic Dam, the Olympic Copper–Gold Province also includes six other IOCG deposits with resources ranging from 100 to 400 Mt (*see* resources listed in Corriveau et al., 2018b), as well as many additional prospects (Fabris, 2022;

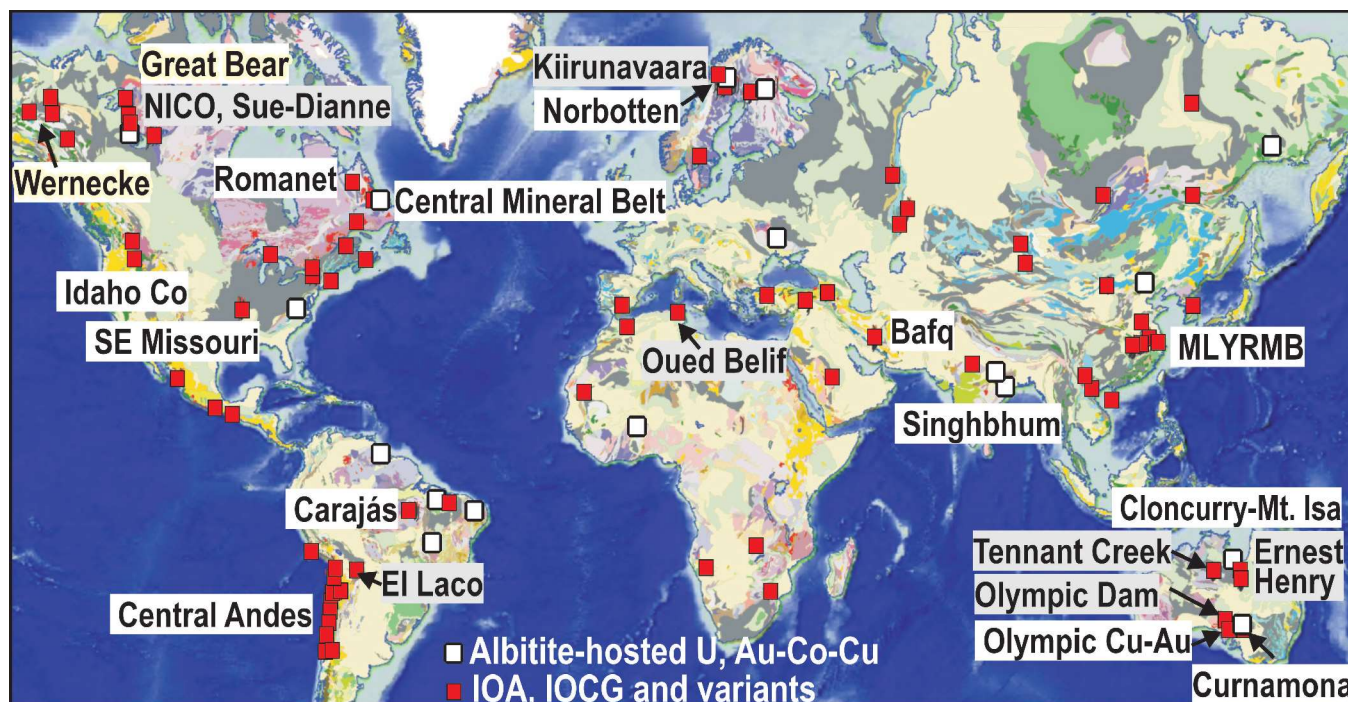


Figure 2. Distribution of iron oxide–copper–gold (IOCG), iron oxide–apatite (IOA) and affiliated deposits (red squares), and albitite-hosted U deposits (white squares) on a geological map of the world *after* Chorlton (2007). *Updated from* Williams et al. (2005), Barton (2014), and Corriveau et al. (2018b). MLYRMB = Middle-lower Yangtze River metallogenic belt

Skirrow, 2022). Other Australian IOCG districts include the Cloncurry district, Curnamona Province, and Tennant Creek district (*see* resources listed in Corriveau et al., 2018b; Skirrow et al., 2019). Mesozoic districts include those of the central Andes in Chile and Peru, and the youngest known deposits and prospects include the 2 Ma El Laco IOA deposit in Chile and the 9 Ma Oued Belif IOCG prospect in Tunisia (Corriveau et al., 2018b).

The genesis of IOCG, IOA, and affiliated deposits requires: 1) formation of IOAA systems through crustal-scale element mobility driven by significant thermal anomalies and ascent of large hypersaline fluid plume(s), to which additional ingress of fluids can add metals and disrupt the physicochemical conditions of the plume; and 2) consecutive, repeated and focused precipitation of metals within key structural and lithological traps at certain alteration facies as the main fluid plume ascends through the upper crust along and above fault zones (Table 1; Oliver et al., 2004; Williams et al., 2005; Porter, 2010; Skirrow, 2010, 2022; Corriveau et al., 2016, 2022a, b, c, d; Heinson et al., 2018; Reid, 2019). The fluid-rock reactions and associated fluid recharges-discharges in elements significantly change the composition of the fluid plume during ascent, as does ingress of a significant volume of external fluids where they occur (Corriveau et al., 2022a, b, c, d). Lateral extents of IOAA systems are comparable to the thickness of the crust (Porter, 2010; Mumin, 2015). Variations in commodities and mineralization styles result from consecutive alteration facies that, ultimately, lead to an extraordinary

range of IOCG and affiliated deposits (Corriveau et al., 2016, 2022c) that includes a continuum to porphyry and epithermal systems (Mumin et al., 2010; Richards and Mumin, 2013a, b).

Metasomatic IOAA systems form across hundreds of cubic kilometres of the upper crust and are commonly spatially associated and coeval with pre- and postmineralization calc-alkaline to shoshonitic volcanoplutonic magmatism, caldera-related explosive volcanic systems, and A-type granite intrusions from the Archean to recent Phanerozoic (Table 1; Hildebrand et al., 1987; Hauck, 1990; Williams et al., 2005; Porter, 2010; Decrée et al., 2013; Montreuil et al., 2016a; Ootes et al., 2017; Corriveau et al., 2018b, in 2022a, d; Ovalle et al., 2018; Pollard et al., 2019; Reid, 2019; Sillitoe et al., 2020). Earlier sedimentary basins are common and can be sources of metals and fluids (Table 1; Gandhi and van Breemen, 2005; Skirrow, 2010; Bennett et al., 2012; Reid and Fabris, 2015). No other deposit type supplies both energy and mineral resources to society and globally, large tonnage IOCG and affiliated critical metal deposits can significantly enhance mineral resources of a nation, as illustrated in Australia, Brazil, China, and South America (e.g. Huston et al., 2012; *also see* resources listed in Corriveau et al., 2018b, 2022c).

In Canada, NICO is the largest IOCG-related deposit, with National Instrument 43-101 compliant reserves of 33 Mt at 1.02 g/t Au, 0.12% Co, 0.14% Bi, and 0.04% Cu (Burgess et al., 2014). The NICO deposit is an Au-Co-Bi-Cu±W variant of the magnetite-group IOCG deposit

Table 1. Great Bear magmatic zone attributes that satisfy the criteria for settings prospective for iron oxide–copper–gold (IOCG) deposits (*adapted from* criteria in Skirrow, 2010).

Criteria	Great Bear magmatic zone
Uranium-rich felsic subaerial volcanic rocks and high-level intrusions (A-type)	Great Bear calc-alkaline to shoshonitic intermediate to felsic magmatism evolved to A-type granitic intrusions, rich in uranium (Ootes et al., 2013; Montreuil et al., 2016a, c).
Dynamic tectonic activity involving change from compression to extension during magmatism	Best examples of synmetasomatic ductile deformation in a compressive setting are found at DeVries Lake and at the NICO deposit, where the rocks are folded after 1.88 Ga and at the onset of the 1.87 Ga magmatism, whereas extension is widespread during and subsequent to iron-oxide and alkali-calcic alteration (IOAA) metasomatism (Bennett et al., 2012; Montreuil et al., 2016a, b). The ductile deformation that also takes place at the high-temperature Ca-Fe alteration facies due to the high temperature of the fluid should be noted (Somarin and Mumin, 2014; Corriveau et al., 2022b).
Continental arc, back-arc, and intracontinental arc	Continental margin setting, postcollisional (Hildebrand et al., 2010a, b; Montreuil et al., 2016a; Ootes et al., 2017)
Subvolcanic to epithermal settings (preserved)	The best vertical profile exposed across IOAA systems from subvolcanic intrusions through an overlying volcanic sequence and up to a preserved epithermal cap is across the Contact Lake Belt in the Port Radium–Echo Bay district (Mumin et al., 2007, 2010).
Sedimentary basin predating IOAA metasomatism	Treasure Lake Group 1.88 Ga metasedimentary rocks (Bennett et al., 2012)
Crustal-scale structural pathways for magmas and/or fluid	Major discontinuities lie west of the Slave Craton, with lithospheric magnetotelluric patterns similar to those of the Olympic Dam deposit area (Spratt et al., 2009; Jones et al., 2014). A major transcrustal discontinuity has also been imaged by Craven et al. (2013). Additionally, the distribution of the post-IOAA system A-type granite transects the Great Bear magmatic zone at an angle and the front is spatially associated with the largest IOAA systems, suggesting a fundamental role of the geodynamic architecture in generating fluid and magmas and their pathways (cf. Hayward and Corriveau, 2014).
Mafic magmas → crustal-scale thermal anomalies	Minor basalt and late flows of tholeiitic affinities (Hildebrand et al., 2010b) and mafic sources for some mineralization
Syn- to postcompressional magnetite alteration	Port Radium–Echo Bay; DeVries, Fab, NICO, Peanut Lake, LP's and LJLVS
Magnetite-rich alteration telescoped against oxidized caldera fluids and evidence of fluid mixing	Southern Breccia vs. NICO vs. Chalco and Summit Peak prospects, and K2 all display magnetite-rich evolving to hematite-rich alteration. Caldera lakes are likely preserved at Mile Lake prospect in the Port Radium–Echo Bay district (Mumin et al., 2007) and possibly in the Grouard Lake region (Corriveau et al., 2022d).
Leaching of uranium-rich hosts to sites of fluid upflow	1.87 Ga volcanic and intrusive rocks of the southern Great Bear magmatic zone contain elevated uranium contents (Ootes et al., 2013), uranium mineralization occurs in multiple phases as albitite-hosted uranium mineralization at 1.87 Ga (Montreuil et al., 2015; Potter et al., 2019) as well as along unconformities (Ootes et al., 2015), in 1.85 Ga intrusions (Somarin and Mumin, 2012) and in late-stage veins (Gandhi et al., 2018).
Hematite-rich alteration lateral to and/or above magnetite alteration	K2, Mag Hill iron oxide–apatite prospect is overlain by an extensive hematite-rich alteration zone (Mumin et al., 2010; Somarin and Mumin, 2014).

class (Goad et al., 2000a, b; Acosta-Góngora et al., 2015b; Corriveau et al., 2016, 2022a, c, d). The Sue-Dianne Cu-U-Ag-Au±Bi deposit is a typical magnetite-to-hematite-group IOCG deposit (Fig. 1; Gandhi, 1994; Goad et al., 2000a, b) with total resources of 8.4 Mt at 0.80% Cu, 0.07 g/t Au, and 3.2 g/t Ag (Hennessey and Puritch, 2008). Other deposits include the Josette REE deposit in the Grenville Province (Clark et al., 2010; Gagnon et al., 2018; Sappin and Perreault, 2021; Corriveau et al., 2022a) and the Michelin and Moran Lake (upper C zone) uranium deposits in the Central Mineral Belt (Fig. 1; e.g. Hitzman and Valenta, 2005; Froude, 2006; Sparkes and Kerr, 2008; Sparkes et al., 2016). The Josette deposit has resources of 6.92 Mt at 2.72 weight per cent REE₂O₃, 53 weight per cent Fe₂O₃

(measured plus indicated) and 1.33 Mt at 3.64 weight per cent REE₂O₃, 48 weight per cent Fe₂O₃ (inferred) (Gagnon et al., 2018). The Michelin deposit has JORC-compliant (Australasian code for reporting of exploration results, mineral resources, and ore reserves) combined measured, indicated, and inferred resources of 42.7 Mt at 980 ppm U₃O₈ (Fig. 1; Paladin Energy Limited, 2019). Geological environments and mineral systems of known prospective Canadian settings are similar to those of global districts; however, the lack of a major discovery that could spur extensive exploration of, and training in, IOCG and affiliated deposits, combined with the Canadian focus on other deposit types, remote and often rugged terrain, moratoriums on uranium exploration, targeting of areas for preservation

and recreation, and lack of infrastructure in prospective settings have discouraged extensive greenfields exploration. Worldwide, government-supported field, gravity, magnetic, and magnetotelluric geophysical surveys have supported discoveries, for example extensive drilling around the Ernest Henry deposit in Australia for litigation purposes (Corriveau et al., 2010b), detailed gravity coverage in Scandinavia, or major joint government-academia research and geophysical surveys in Australia (Skirrow and Davidson, 2007; Skirrow et al., 2018). Australia has capitalized on knowledge gained across its mining districts to deploy prospectivity maps across its territory and launch many extensive geoscience programs that have strengthened existing exploration plays and opened new ground to exploration (Schofield, 2012; Schofield et al., 2014; Skirrow et al., 2019; Wise, 2019a, b; Katona and Fabris, 2022; Skirrow, 2022).

CONTEXTS OF THE GEM IOCG-GREAT BEAR PROJECT

The Land

The Great Bear magmatic zone overlaps with parts of the Sahtu Settlement Area; the North Slave Region, including the Wek'èzhii Management Area, Tẖçẖ-owned lands (the Tẖçẖ have both surface and subsurface rights on 39 000 km² of land, 3% of the Northwest Territories); the Tẖçẖ communities of Behchoḵ (formerly Rae-Edzo), Whaṯ (formerly Lac la Martre), Gamèṯ (formerly Rae Lakes), and Wekweèṯ (formerly Snare Lakes); the M̱q̱wẖ Gogha Dè Ṉi̱tḻèè area bordered by land claim settlement areas and traditional areas of neighbouring Aboriginal groups; the İdaà trail (the traditional trail between Great Bear Lake and Great Slave Lake); and many cultural sites. The Great Bear magmatic zone also extends under the sedimentary basin that is part of the Edaı̱ı̱la Area of Interest within the Northwest Territories Protected Areas Strategy, along the northeastern shore of Great Bear Lake. Land-use planning was underway during the GEM project (2008–2011) for the Sahtu Settlement Area (e.g. draft 3 of the land-use plan for

the Sahtu Settlement Area and Great Bear Lake Watershed Management Plan) and the Tẖçẖ-owned lands (Sahtu Land Use Planning Board, 2010, 2013; Tẖçẖ Government, 2013).

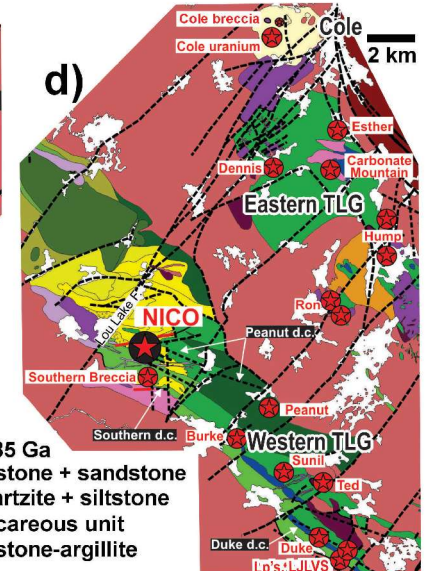
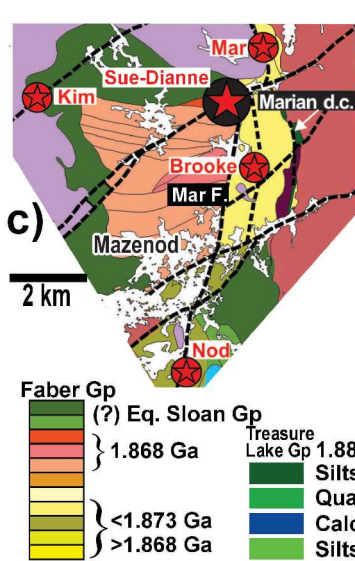
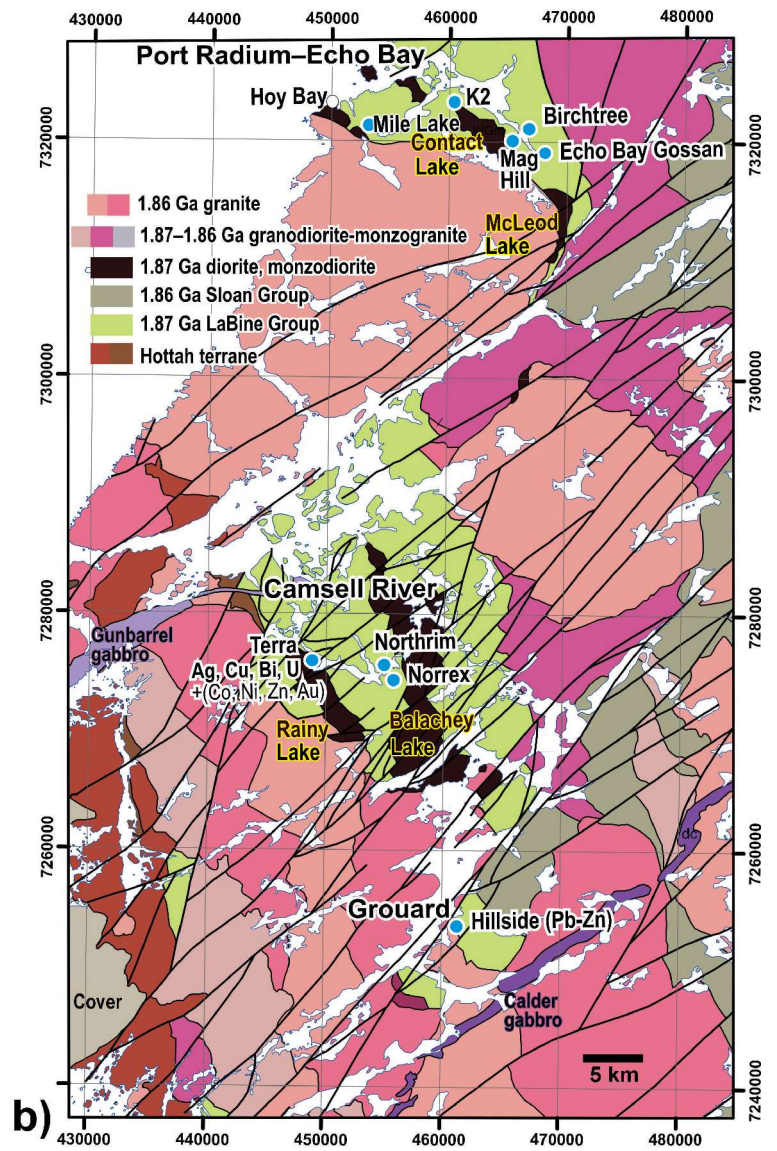
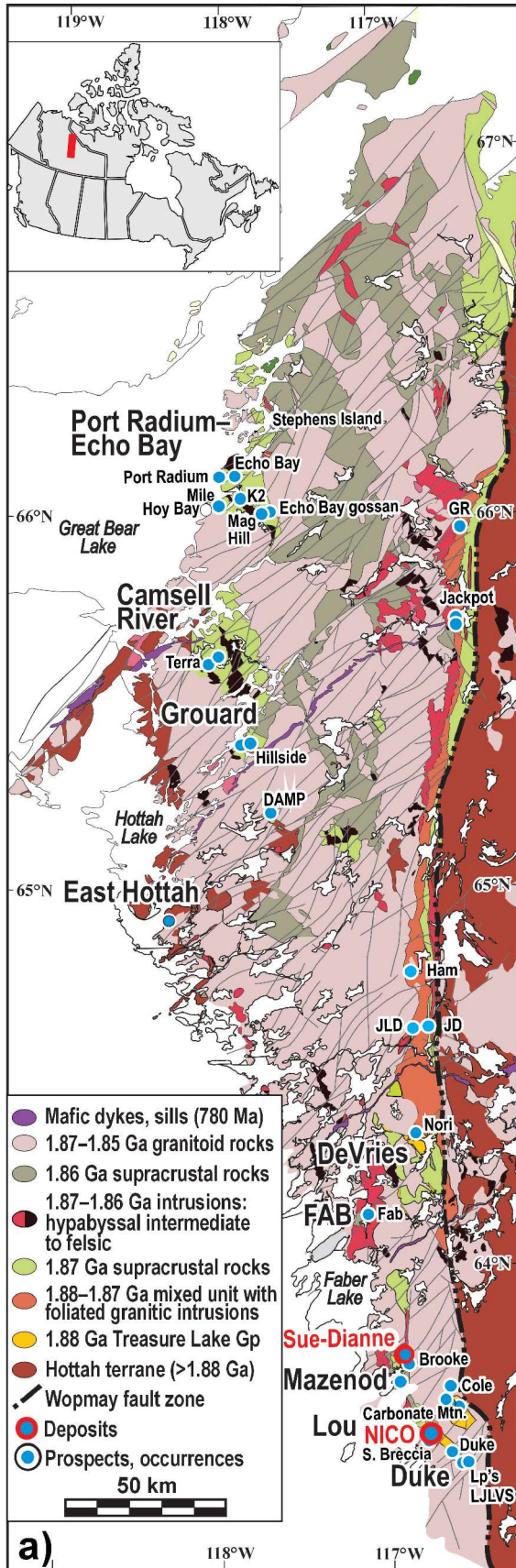
Geoscience and mineral exploration contexts

The Great Bear magmatic zone (Fig. 3a) is a north-trending geological belt exposed for 450 km between the Great Bear and Great Slave lakes; it extends further below younger sedimentary basins to the west, the south, and the northwest (Hildebrand et al., 1987, 2010a, b; Aspler et al., 2003; Hayward and Corriveau, 2014). The southern part of the belt (where exposed) hosts the Au-Co-Bi-Cu NICO and Cu-Ag-Au Sue-Dianne IOCG deposits (Fig. 3c, d; Goad et al., 2000a, b; Corriveau et al., 2010a; Mumin et al., 2010). Additional potential for IOA deposits was recognized early in the Camsell River and Port Radium–Echo Bay district (Fig. 3a, b; Badham and Morton, 1976; Hildebrand, 1986). At the time, the recognition of albitite in the immediate roof of subvolcanic intrusions, IOA mineralization above these albitite zones within volcanic rocks, and apical pyrite gossans led to the development of a zoned model, previously proposed for the Middle-lower Yangtze River metallogenic belt (Ningwu Research Group, 1978; Hildebrand, 1986; Reardon, 1992). The Great Bear magmatic zone was also a major past-mining district for uranium and silver (e.g. the Port Radium district along the northeastern shore of Great Bear Lake and the historical Rayrock uranium mine to the south).

At the start of the millennium, a new wave of mineral exploration by the private sector and collaborative research under the TGI program (Deep Search project) led to the recognition of significant IOCG potential in the Port Radium–Echo Bay district of the northern Great Bear magmatic zone (Mumin et al., 2007, 2010; Corriveau et al., 2010a, b). Based on this work, Gebert et al. (2007) recognized that the IOCG potential also extends to the basement of the subsequent overlying sedimentary basin in their assessment of nonrenewable resources in the 'Edaı̱ı̱la' peninsula.

Prior to GEM research, extensive lithological mapping of volcanic, sedimentary, and intrusive rocks across the Great Bear magmatic zone led to the understanding of the geodynamic evolution of the belt in terms of twentieth century

Figure 3. Geology and mineral occurrences of the Great Bear magmatic zone (*modified from Corriveau et al., 2016*). Inset locates the belt in Canada. **a)** Province-scale geology and location of the main deposits, prospects, and mineral occurrences. **b)** Geology and location of the main prospects and subvolcanic intrusions in the Port Radium–Echo Bay and the Camsell River and Grouard Lake iron oxide–alkali-calcic-altered (IOAA) systems. The 1.87 Ga volcanic and intrusive rocks of the Port Radium Echo Bay and Grouard Lake IOAA systems are tilted moderately to the northeast (Hildebrand, 1983; Hildebrand et al., 2014). **c)** Geology of the Mazenod district with the Sue-Dianne deposit located at the intersection of two regional faults (Gandhi et al., 2014; Montreuil et al., 2016a, b). Albitite is locally preserved to the south along the north-trending fault (Mar F.) that hosts the Sue-Dianne deposit. **d)** Geology of the Lou system that hosts the NICO deposit, the Chalco and Summit Peak (adjacent to the NICO deposit) prospects and the Southern Breccia albitite corridor mineral showings (Gandhi et al., 2014; Montreuil et al., 2015, 2016a, b). Fault network and deformation corridors (d.c.) are highlighted and labelled ones are described in Montreuil et al. (2016b). TLG = Treasure Lake Group



knowledge (Hildebrand, 1982, 1984; Hildebrand et al., 1987; Gandhi et al., 2001); however, many of the key geological and geophysical attributes of IOCG deposits and their ore systems remained overlooked throughout the belt, including the ‘productive’ alteration types (skarn, high- and low-temperature K-Fe, low-temperature Ca-Mg-Fe and K-skarn alteration facies) and potential continuum with other deposit types. The linkages among the seemingly disparate mineral showings had yet to be recognized and modern geoscience information on prospective areas was lacking (Corriveau et al., 2015, 2016, 2022d; Montreuil et al., 2016a, b; Bowdidge et al., 2014; Bowdidge and Dunford, 2015). Furthermore, many regional maps completed in the nineteen eighties by GSC staff were unpublished and the geodynamic settings required revisions based on advances worldwide in this field.

Optimizing the mineral potential of the Great Bear magmatic zone required extensive petrological alteration mapping of mineral systems, high-resolution geophysical surveys, multidisciplinary GEM and TGI research, and close collaboration with First Nation governments and land-use planners. Mapping was focused on the intense and pervasive zones of hydrothermal alteration (metasomatism) around known mineral occurrences and those with geophysical survey coverage (Corriveau, 2017a, b; Corriveau et al., 2022b). The metasomatic evolution of the systems, their geological attributes, mineralogy, composition, physical properties of rocks, and erosional drifts were thus studied by scientists from several GSC divisions (GSC-Pacific, GSC-Central, GSC-Northern, GSC-Québec) and the Northwest Territories Geological Survey (NTGS), in collaboration with colleagues from academia and the private sector, at both the national and international level, as well as with territorial and First Nations governments.

Logistical context

The poor infrastructure in the Great Bear magmatic zone has proven to be a major impediment to exploration and exploitation. In terms of logistics, historical airstrips have been decommissioned or poorly maintained, and their role in opening the North to development has been undervalued. The Th̄ch̄ Highway between Yellowknife and Whatì will slightly alleviate this by opening the southern Great Bear magmatic zone to exploration and fostering development of the NICO deposit (Fortune Minerals Limited, 2019).

Physiography of the land

Mineral systems that lead to the development of IOCG and affiliated deposits are triggered by the ascent of large fluid plumes channelled along structural corridors (e.g. Central Andes mineral systems related to the Atacama Fault and splays, and systems in the Cloncurry district and

Olympic Dam deposit in Australia; Sillitoe, 2003; Mumin et al., 2014; Skirrow et al., 2018; Ehrig and Clark, 2019). These systems develop metasomatic rock types with distinctive physical properties ranging from highly resistive to easily eroded. These characteristics can enhance differential erosion and lead to rugged landscapes with interconnected waterways and large watersheds. For example, the İdaà Trail is a traditional pathway of high cultural value that connects Great Slave Lake to Great Bear Lake along the exposed part of the Great Bear magmatic zone and the overlying Mackenzie sedimentary basin. The area is spatially associated with numerous IOCG and affiliated prospects (see distribution of Great Bear magmatic zone prospects in Bretzlaff and Kerswill, 2016) that formed along an ancient geological pathway for fluids and metals. The geological features that the historic trail follows is thus a potential host to mineral resources for the twenty-first century. Stunning landscapes and a potential for high biodiversity (e.g. Ruff et al., 2002) due to the extremely diverse rock compositions create highly valued wilderness targets for preservation such as the East Arm of Great Slave Lake, the traditional İdaà Trail, and the Wernecke Mountains in Yukon, among others. Nevertheless, the importance of the mineral potential of the belt as well as that of mineral exploration and extraction is well recognized globally and locally, including by the First Nation Denendeh Exploration and Mining Company (DEMCo) Ltd., which has acquired mineral property along the Camsell River (Bowdidge et al., 2014; Beaulieu, 2019).

RESEARCH ON THE GREAT BEAR MAGMATIC ZONE AS A CASE EXAMPLE

In the Great Bear magmatic zone, research activities were targeted to lay the geoscience foundation for a new cycle of mineral exploration across virgin areas, proximal to known deposits, areas with known mineral occurrences, and areas with past-producing mines. Research was highly multidisciplinary and encompassed: mineral systems geological mapping, petrology, litho-geochemistry, geochronology, mineral chemistry, and structural geology studies; till geochemistry and indicator mineral research; an airborne high-resolution magnetic survey; compilation, levelling, and integration of available aeromagnetic survey data; a local ground magnetotelluric survey and geophysical modelling methodology for targeting of mineral systems; measurement of the physical properties of rocks in the laboratory and in the field; remote predictive mapping; and publication of legacy geological maps. Knowledge was transferred through publications, short courses, presentations, research licences, community engagement, letters of agreement, yearly reports, meetings with land-use planners, comprehensive databases, and documentation of potential archeological sites.

These research themes led to the following:

- Development and testing of a practical and system-wide mineral deposit model, exploration methods, technologies, and mapping protocols through targeted mapping across the stunning field exposures of the Great Bear magmatic zone mineral systems. The mapping protocol for hydrothermal alteration and veins (Einaudi, 1997; Brimhall et al., 2006) and the means to label alteration (Gifkins et al., 2005) had to be modified for mapping the IOAA systems and their IOCG and affiliated mineralization using the alteration-facies approach described below (Corriveau et al., 2022b). Alteration mapping was supported by hand-held gamma-ray spectrometers and magnetic susceptibility meters, followed by cobaltinitrite staining of rock slabs to optimize identification of alteration facies, characterize paragenetic sequences and alteration intensity, and distinguish alteration from the common rocks. The ore-deposit model was developed through documentation of a regular sequence of alteration facies, from depth to surface and through time, and the repeated development of consistent mineral assemblages, mineral contents, textures, and structures from one system to the other, regardless of host rock types (Corriveau et al., 2016; Montreuil et al., 2016a, b; Percival et al., 2016).
- Geochronological constraints on development of the Great Bear magmatic zone IOAA systems and the coeval flare-up of magmatic and hydrothermal activities at 1.87 Ga (Ootes et al., 2010; Davis et al., 2011; Bennett et al., 2012; Acosta-Góngora et al., 2015a; Montreuil et al., 2016a, c). An in-depth study of the Hottah terrane established periods of magmatism during which these basement rocks were formed and how they are linked to the Great Bear magmatic events (Davis et al., 2015; Ootes et al., 2015).
- Improved understanding of known prospects, compilation of historical exploration data and recognition of new local IOCG and affiliated mineral potential, and new areas of interest for their exploration, including the mineral systems hosting the past-producing silver and uranium mines along the northeastern shore of Great Bear Lake (Ootes et al., 2008; Acosta-Góngora et al., 2011; Gandhi, 2013; Gandhi et al., 2013, 2018; Potter et al., 2013b; Bretzlaff and Kerswill, 2016; Montreuil et al., 2016b). The GEM geophysical surveys, compilations, and modelling parameters, combined with the extensive targeted petrological mapping, data acquired from the measurement of the physical properties of the rocks, and deposit model provided unprecedented resolution of the belt as well as new exploration targets for IOCG and affiliated deposits, including the identification of a significant conductor at 500 m depth below the NICO deposit (Craven et al., 2013; Hayward, 2013; Hayward et al., 2016) that led to renewed exploration and drilling (Fortune Minerals Limited, 2021).
- Demonstration of the ability of IOCG-bearing mineralizing systems to create affiliated deposit types such as IOCG variants with Co, Bi, Au, and low Cu contents; REE-rich IOA deposits; and albitite-hosted uranium deposits (Table 1; Corriveau et al., 2015, 2016, 2022c; Montreuil et al., 2015, 2016a, c; Potter et al. 2019). Concentrations of critical metals within these systems are particularly high in the Great Bear magmatic zone and global examples, highlighting the additional mineral potential of IOAA systems for critical metals (Skirrow et al., 2013; Corriveau et al., 2015, 2019a, b, 2022a; Denendeh Exploration and Mining Company (DEMCo) Ltd., unpub. data, 2015).
- Formulation of vectors to IOCG and affiliated mineralization based on a unifying ore-deposit model capable of predicting and explaining the multiple metal associations and alteration facies across IOAA systems globally (Corriveau et al., 2010a, b, 2016, 2018b, 2022c). This follows documentation of the broad-scale, chemically and geophysically distinctive haloes of intensely altered rocks that led to the identification of IOCG and affiliated deposits. The model explains why such haloes appear to differ from one prospect to the next.
- Collection of large data sets, including geochemistry, photographs, and descriptions of the evolution from alteration to mineralization and, in some cases, to ore deposits, extracting key diagnostic features of each alteration type and transient development to better understand metasomatic and mineralizing processes (Corriveau et al., 2015, 2022b; Montreuil et al., 2016a, b). The use of published data sets of mineral assemblages, textures, and structures of alteration that form the main corpus of the data used to formulate the new geological vectors to IOCG, and affiliated mineralization can hopefully ensure that exploration and government geologists recognize iron oxide and alkali-calcic alteration. Petrological information is key as some of the altered rocks can look like common rock types, but diagnostic field and geochemical features make it possible to recognize altered rocks (Corriveau et al., 2010a, b, 2016, 2022a, b, c, d, e; Blein et al., 2022).
- Development of new drift prospecting and till geochemistry exploration methodologies. Taking advantage of localized unconsolidated clay, sand, and gravel till deposits, the project revealed highly complex and variable chemical fingerprints related to known deposits and mineralization in these sediments, and contributed as well to the refinement of till geochemistry and indicator-mineral exploration methods (McMartin et al., 2009a, b, 2011a, b; Lypaczewski, 2012; Lypaczewski et al., 2013; Normandeau and McMartin, 2013; Normandeau, 2018; Normandeau et al., 2018). This research led to broader applications and comparison with signatures of global IOA and IOCG deposits (Dupuis et al., 2012; Sappin et al., 2014; Huang et al., 2017, 2019, 2022). The project also led to the identification of key minerals to analyze

from these sediments and the appropriate statistical methods to process results for exploration (Normandeau, 2018; Normandeau et al., 2018).

- Retrieval of all unpublished legacy geological maps and field data through collaboration with former GSC geologists, leading to publication of detailed regional geological maps from the Hottah Lake region (Leith Peninsula–Rivière Grandin area; Hildebrand, 2017) and Calder River map area (Hildebrand et al., 2014) as well as of two major geological compilation maps, with Hildebrand (2011) covering 1065 km² of the northern Great Bear magmatic zone and adjacent terranes, and Gandhi et al. (2014) covering the southern Great Bear magmatic zone. Furthermore, proprietary geophysical surveys were processed by Hayward et al. (2013, 2016). In parallel, Jackson and Ootes (2012) published a new regional map of the southern half of the central part of the Great Bear magmatic zone, leaving only the northern part of the central and Nunavut sections of the Great Bear magmatic zone to be mapped in the future.
- Publication of thematic geological maps of the Port Radium–Echo Bay district prospects and host alteration facies provided by the private sector (Mumin, 2015). These maps document the variety of metasomatites and breccia zones in the Breccia Island and Cross Fault Lake (Ivanov et al., 2015a, b), Camelback and Skinny Lake (Mumin et al., 2015a, b), Port Radium, Contact Plateau, South Uranium, and East Boundary Zone (Arbuckle et al., 2015a, b, c, d), Dowdell Peninsula (Rogge et al., 2015), and K1 prospect (Jones et al., 2015) regions. The area mapped in most detail is the Mag Hill transect that documents the depth to paleosurface evolution of the IOAA system across a pervasively and intensely metasomatized andesite sequence (Mumin et al., 2007, 2010; Corriveau et al., 2010b). An albitite corridor above a subvolcanic diorite intrusion evolved structurally and upwardly to pegmatitic albite-amphibole-magnetite-apatite metasomatites (high-temperature Na-Ca-Fe facies) and local amphibole veins (high-temperature Ca-Fe facies), then subsequently to the IOA mineralization of the Mag Hill prospect, which is structurally overlain by a 200 m long by 60 m thick hematite replacement body (Somarin et al., 2015b, c, d). Another transect illustrated the evolution of albitite to the polymetallic K-skarn-hosted Mile Lake prospect (Somarin et al., 2015a), whereas to the west, at Hoy Bay, the albitite zones evolved to magnetite, skarn, and hematite breccia (Elliott et al., 2015b). The Mag Hill and K1 prospects form the easterly and westerly boundary of the Contact Lake Belt, respectively (Mumin et al., 2015), whereas the epithermal lithocap and polymetallic prospect at Gossan Island represent the roof of the system (Elliott et al., 2015a).
- Acquisition of new geophysical aeromagnetic maps and compilation maps that cover the entire 450 km long study area and are based on several new geophysical surveys done in collaboration with the Northwest Territories Geological Survey (Harvey et al., 2009a, b, c, d, e, f, g, h, i, j, k; Hayward and Oneschuk, 2011; Kiss and Coyle, 2011a, b, c, d). Magnetic susceptibility measurements in the field allowed assessment of the intensity of magnetite-bearing alteration and mineralization. To this end, Lee (2012) conducted a curvature analysis of aeromagnetic data for quality control, geological mapping, and mineral resource assessment (*see also* Lee et al., 2013a, b). Other research included a comparison of magnetic susceptibility meters used in the field (Lee and Morris, 2013), development of an automatic network-extraction algorithm applied to magnetic survey data for the identification and extraction of geological lineaments (Lee et al., 2012a), followed by a curvature analysis to differentiate magnetic sources for geological mapping (Lee et al., 2013b), an assessment of the quality of aeromagnetic data using lineament analysis (Lee et al., 2013a), and development of a network-extraction tool for mineral exploration (Lee et al., 2012b).
- Publication of two special volumes, namely a joint GSC–United States Geological Survey special issue published in *Economic Geology* on IOCG and IOA deposits within the Southeast Missouri district and Great Bear magmatic zone (Slack et al., 2016) and a GSC-led global synthesis of mineral systems with IOCG and affiliated critical metal deposits, and applicable geological exploration and regional mapping tools, namely the Special Paper 52 published by the Geological Association of Canada (Corriveau et al., 2022e).
- Testing of GEM-TGI geological exploration tools during renewed geological mapping and research, in the first phase of the GEM program (GEM-1), proving their efficiency in poorly known areas and next to known deposits within the Great Bear magmatic zone. Geological mapping of the IOAA system hosting the Fab prospects affirmed the relevance of the alteration-facies model to exploration, yet proved to be time consuming (Potter et al., 2013b). Subsequently, chemical maps were produced (Montreuil et al., 2016b; Corriveau et al., 2022a) and proved to be an efficient method to display the evolution of the systems regionally as well as to assess mineral potential at the regional scale. Subsequently, the tools were refined through incorporation of case examples from the Romanet Horst in northern Quebec (GEM-2; Corriveau et al., 2014), the Bondy gneiss complex in the southwestern Grenville Province (Corriveau, 2013; Dufrechou, 2011; Dufrechou et al., 2011, 2014, 2015; Corriveau and Spry, 2014; Blein and Corriveau, 2017; Corriveau et al., 2018a), the Central Mineral Belt in Labrador (TGI; Acosta-Góngora et al., 2018a, 2019), the Wanapitei district in Ontario (collaboration with the private sector; Corriveau et al., 2022c), as well as examples from South Australia (TGI; with BHP-Olympic Dam, the Bureau de Recherches Géologiques et Minières, and the Geological Survey of South Australia; Corriveau et al., 2018b, 2019a, b, 2022a, d), China, and India (Blein et al.,

2022; Corriveau et al., 2022c). The process of broadening TGI case studies to global examples and refining exploration methods, technologies, strategies, and vectors to ore has enabled GEM and TGI research to incorporate an even larger spectrum of deposit types in the current IOAA ore-systems model and recognize that IOAA systems have iron oxide–poor to even iron-poor counterparts or components (Corriveau et al., 2022c). This breakthrough has led to the definition of a broader mineral-system umbrella, notably the metasomatic iron and alkali-calcic (MIAC) mineral system. It has significantly expanded the prospectivity of Canadian settings as well as increased the national expertise on multidisciplinary studies of IOCG deposits and favourable geological environments. For example, understanding the linkages among albitite-hosted mineralization and critical metal-rich deposit types based on GEM-2 research and private sector mineral exploration in the Romanet Horst of Quebec (Corriveau et al., 2014; Montreuil et al., 2014; McLaughlin et al., 2016) has led industry to explore other Canadian settings such as the Wanapitei Lake district of Ontario (Yarie and Wray, 2019). Outcomes have attracted an international audience (e.g. Fabris, 2019) and led to extensive collaboration with Australian state geological surveys (Corriveau et al., 2019a, b, 2020, 2021a, b). Global applications of the model and case examples (Blein et al., 2022; Corriveau et al., 2022a, c, d) have significantly expanded the understanding of the variety of iron oxide–bearing to iron oxide–poor deposit types and led to a new classification of deposit types for MIAC systems in Hofstra et al. (2021).

- Development of quality-control techniques based on proprietary exploration geochemical data from Great Bear magmatic zone and Central Mineral Belt in Labrador. The atypical rock types formed through IOAA metasomatism and documentation of evidence for the importance of optimal dissolution methods for bulk rock analysis must be considered (Corriveau et al., 2015; Acosta-Góngora et al., 2018a). Quality control of geophysical data was also undertaken (Hayward et al., 2013, 2016).
- Knowledge transfer among project participants (between 100 and 200 contributors) and through the completion of various Ph.D. (Dufrechou, 2011; Lee, 2012; Acosta-Góngora, 2014; Montreuil, 2016; Normandeau, 2018), M.Sc. (Byron, 2010; Robinson, 2013; Shakotko, 2014; Smar, 2015; De Toni, 2016; Duffett, 2019), and B.Sc. (Azar, 2007; Newton, 2011; Lypaczewski, 2012; Hamel, 2013) theses, as well as through yearly short courses attended by provincial and international government geologists, representatives from private sector companies and university faculties, and both graduate and undergraduate students. The short courses took place across Canada as well as in Sweden, Australia, and Chile, thus maximizing the impact of the research. The presentations are being published as contributions to the

GSC Scientific Presentations series and by Australian state geological surveys (Corriveau, 2017a, b; Corriveau et al., 2018b, c, 2019a, b, 2020, 2021a, b).

GREAT BEAR MAGMATIC ZONE IOAA SYSTEMS

Relationships between magmatism and IOAA systems

Previous work in the Great Bear magmatic zone by Hildebrand et al. (1987, 2010a, b) and Gandhi et al. (2001) documented in detail

- subaerial, volcanic explosive eruptions and flows that have led to a cluster of andesitic to rhyolitic volcanic centres with annular or elongate caldera-collapse structures (e.g. Camsell River district);
- collapse of a stratovolcano and sedimentation within the caldera structure leading to conglomerate infills (e.g. Port Radium–Echo Bay district);
- resurgent volcanic and plutonic activity, and renewed caldera collapse (e.g. Camsell River and Grouard districts); and
- intense hydrothermal activity at 1.87 Ga followed by a major 1.86 Ga ignimbritic flare-up event, coeval batholith emplacement, and terminal intrusions of A-type granite.

Work as part of the GEM project has helped advance regional knowledge across the Great Bear magmatic zone (Table 1). It has also revealed the strong similarities the Great Bear magmatic zone shares with the volcanoplutonic evolution of the Olympic Cu-Au Province of Australia and the IOCG deposits it hosts (Corriveau et al., 2022a, c, d, e), in addition to satisfying many of the criteria for terranes hosting large IOCG deposits, as developed in Skirrow (2010) and synthesized in Table 1. Research documented the shoshonitic character of some of the Great Bear magmatic zone 1.87 Ga volcanic rocks and high uranium contents associated with the 1.87 Ga magmatic events and 1.86 to 1.85 Ga plutons, thus substantiating the IOCG-U potential of the belt (Azar, 2007; Byron, 2010; Davis et al., 2011; Somarin and Mumin, 2012; Ootes et al., 2013; Montreuil et al., 2016a, c). Jackson et al. (2013) documented an extension of Great Bear magmatic zone magmatism to the east among reworked Archean rocks. Mumin et al. (2007) and Montreuil et al. (2016a, b) documented the andesitic nature of early 1.87 Ga magmatism in the southern Great Bear magmatic zone and the dioritic nature of some intrusions in the northern Great Bear magmatic zone, both of which were not recognized in previous works due to extensive potassic alteration. Mapping and research also demonstrated that the IOAA systems in the northern part of the belt host not only iron oxide–apatite deposits, as documented by Badham and Morton (1976) and Hildebrand (1986), but

also magnetite- to hematite-group iron oxide–copper-gold (IOCG) and K-skarn prospects, whereas Great Bear magmatic zone albitite-hosted uranium mineralization and cobalt-rich IOCG variants complement the IOCG deposits documented by Gandhi (1994) in the southern Great Bear magmatic zone, (Table 2; Mumin et al., 2007, 2010; Corriveau et al., 2010a, b, 2016, 2022a, b, c, d; Montreuil et al., 2013, 2015, 2016a, b, c; Potter et al., 2019, 2022).

The Great Bear magmatic zone IOAA systems were triggered by the ascent of regional-scale alkali-rich hypersaline fluid plumes that transformed the upper crust through a very regular sequence of alteration facies (Corriveau et al., 2010b, 2016, 2022c; Rusk et al., 2015). Fluids were shown to be largely derived from magmatic sources (Somarin and Mumin, 2014; Acosta-Góngora et al., 2015b; Kelly et al., 2020). Metals were sourced not only from the 1.87 Ga magma chambers, but also from interactions with the host rocks as the main fluid plume leached host rocks extensively during metasomatism, more particularly along albitite corridors, as determined by field, lithochemical, and isotopic studies (Mumin et al., 2007, 2010; Corriveau et al., 2010a, b, 2016, 2022a, b, c, d; Montreuil et al., 2015, 2016b, c; Potter et al., 2019; Kelly et al., 2020).

Evaporite units are a key source of saline fluids and sulphur in the formation of IOA and IOCG deposits (Xavier et al., 2008; Barton, 2014; Li et al., 2015). Where anhydrite and scapolite are present, they usually serve as proxies for the presence of evaporite units. In the Great Bear magmatic zone, scapolite is notably rare. On this basis, evaporite was interpreted as being largely absent, even though it is present in the adjacent East Arm Basin, which is genetically linked to the Great Bear magmatic zone (Potter et al., 2013a, 2017, 2020). The discovery of nodular albitite at DeVries Lake, with amphibole rims forming a chickenwire texture that resembles pseudomorphed nodular anhydrite in an evaporite unit, suggests that scapolite was replaced by albite in the Great Bear magmatic zone during intense metasomatism. Therefore, the absence of scapolite in most systems cannot be interpreted as a lack of evidence for evaporite per se (Corriveau et al., 2022b, c, d). In addition to evaporite units, sulphur can be sourced from other sedimentary rocks, as addressed by Acosta-Góngora et al. (2018b) in their study of the IOAA systems of the Great Bear magmatic zone.

Facies approach to alteration mapping

The fluid-rock reactions taking place as the main fluid plume ascends produce systematic suites of metasomatic mineral assemblages that are repeatedly associated in space and time, with distinct bulk chemical compositions induced by the evolving physical and chemical properties of the hydrothermal fluid plume. Though the suite of mineral assemblages is coherent at outcrop scale, the number of assemblages that form the coherent set is extremely high and their mineralogy, modal contents, textures, and structures are extremely varied, which can lead to highly complex outcrop

patterns. This complexity at outcrop to regional scales was resolved by focusing on the regular succession of suites of mineral assemblages observed from depth to surface along tilted transects and through crosscutting relationships across systems. These characteristics of the paragenetic suites allow the ‘facies’ approach of metamorphic petrology to be applied to alteration systems with IOCG and affiliated deposits in Canada and globally, including at the supergiant Olympic Dam deposit of Australia (Corriveau et al., 2016, 2022b, c, d).

The facies approach to mapping follows metamorphic petrological protocols (Carmichael, 1969, 1978; Pattison et al., 2005) by recognizing the mineral assemblages as the key building blocks of the mapping strategy. Mineralogy and textures define the mineral assemblages, and the suite of assemblages defines alteration facies and collectively provides information on the conditions under which they formed (Corriveau et al., 2010b, 2016, 2022b; Potter et al., 2013b; Montreuil et al., 2016c). Mapping minerals individually is discouraged in alteration facies mapping, just as it is in metamorphic petrological mapping, as the large number of variables make it difficult to anchor the regional and depth-to-surface progression of the metasomatism and metamorphism. In contrast, mapping individual minerals in hydrothermal alteration zones is the preferred practice in economic geology (Einaudi, 1997; Brimhall et al., 2006; Mumin, 2015; Cernuschi, 2017). Once mapped, the minerals in mineralization zones and deposits are subsequently interpreted to define alteration types and direct mapping of alteration assemblages is therefore discouraged. This approach was quickly found to be ill-suited for alteration mapping of the regional-scale IOAA systems because of the extreme variations in the suite of minerals, mineral contents, and mineral assemblages within a single outcrop or part of an outcrop. Conversely, the suites of mineral assemblages within outcrops and their relationships at system scale were shown to be repeatedly coherent across and among systems, thus satisfying the definition of an alteration facies (*see* examples and discussions in Corriveau et al., 2022b, d). As per the definition of metasomatic facies presented in Zharikov et al. (2007), each suite of metasomatic mineral assemblages that characterizes the sequence of alteration types within these systems is grouped as an alteration facies and the sum of the facies forms the system (Corriveau et al., 2022b, c, d). Although the systems formed in different host rock types (volcanic, sedimentary, plutonic, or metamorphic rocks), exhibit different morphologies (replacement, vein, breccia), and display varying intensities of alteration, the suite of assemblages and their alteration facies intrinsically lead to the same prograde metasomatic path and mineralization types (Fig. 4; Corriveau et al., 2022c, e).

The spectrum of mineral assemblages that crystallized under similar physicochemical conditions are grouped within a facies. Each facies has a diagnostic bulk composition, the variations of which reflect the mineralogy of the assemblages, the mineral contents, the intensity of alteration, and protolith

Table 2. Mineralization styles in the Great Bear magmatic zone (*modified from Mumin et al., 2010*).

	Mineralization style	Fe-oxides¹	Main metals	Accessory	Examples
Epithermal and vein-type mineralization and phyllic alteration-hosted mineralization					
1	Giant quartz vein and breccia complexes	Hem	Cu, U	Zn, Pb, Cu, Mn	Sloan and Mariner deposits, Rayrock mine ²
2	Quartz carbonate±hematite±sulpharsenide vein systems	Hem¹	U, Cu, Ag, Co, Ni, Bi, Pb	Zn, As, Au, Mn	Eldorado and Contact Lake mines ²
3	Epithermal veins	Hem	Cu, Ag, Au	Pb, Zn, Co, Bi, U, As, Mn	Echo Bay, Terra and Norex mines ² ; Thompson and Fab prospects
4	Phyllic alteration (disseminated and vein mineralization)	Hem	Ag	Cu, Au	SE Echo Bay gossan
Iron oxide–copper-gold (IOCG) and potassic skarn and cobalt-rich IOCG variants					
5	Phyllic-K-feldspar-hematite (LT K-Fe) alteration (polymetallic disseminated and vein mineralization)	Hem	Zn-Pb-Cu-Ag	Au	Echo Bay mine ² , Skinny Lake
6	K-feldspar-rich (K-felsite) alteration as host to copper and polymetallic veins	Hem, Mag	Cu		Summit Peak, Nod, Stephen's Island
7	Hydrothermal-structural breccia with polymetallic mineralization in K-feldspar-hematite (LT K-Fe)-phyllic alteration	Hem, Mag	Cu, Au, Ag, Co	As, Mn, U	K2, Stephen's Island
8	Hydrothermal hematite (LT Fe) ironstone	Hem	Fe		SE Echo Bay Fe zone
9	Cu-Au-Ag hydrothermal-structural breccia and replacement zones associated with iron oxide–K-feldspar (HT to LT K-Fe) alteration	Mag, Hem	Cu, Ag, Au	U	Sue-Dianne deposit
10	Volcaniclastic/tuff-hosted, iron oxide-sulphide-arsenide-biotite±K-feldspar (HT to LT K-Fe) replacement and breccia bodies	Mag, Hem	Zn, Pb, Ag, Cu, Co	Ni, As, Mn	Port Radium sulphides
11	K-feldspar-bearing skarn (K-skarn) in hydrothermal carbonate precursor host and alteration (andradite-vesuvianite-diopside-epidote-K-feldspar)	Mag, Hem	Cu, Zn, Pb, Ag, Mo, W	Mn	Mile Lake
12	Sediment-hosted amphibole-biotite-K-feldspar-iron oxide–arsenide-sulphide (HT Ca-K-Fe) stratabound replacement and localized breccia bodies	Mag, Hem	Co, Au, Bi, Cu	As, Te	NICO deposit, series of prospects south of Duke
Iron oxide–apatite (IOA) and skarn					
13	Stratabound hydrothermal magnetite±hematite ironstone (HT Ca-Fe)	Mag, Hem	Fe		Ron, Hump Lake, Peanut Lake
14	Hydrothermal magnetite-actinolite-apatite ironstone vein systems and breccias (IOA, HT Ca-Fe)	Mag, Hem	Fe, V, REE		Port Radium, Mag Hill, Fab, Mazenod Lake, Terra, Jackpot, McPhoo, Ron, Ham, JLD
15	Magnetite skarn: magnetite-pyroxene-garnet	Mag	Cu		Nod area prospects
16	Carbonate-hosted skarn: andradite-diopside-epidote	Mag, Hem	Zn, Pb, Cu	Ag	Carbonate Mountain Zn-Pb-Cu, Duke
Albitite-hosted uranium					
17	Albitite-hosted uranium	Mag, Hem	U	Cu, Mo	Southern Breccia, Cole, DAMP
¹ Hem, Mag = present in abundance (at least locally >15%) ² Past-producing mines HT = high-temperature LT = low-temperature					

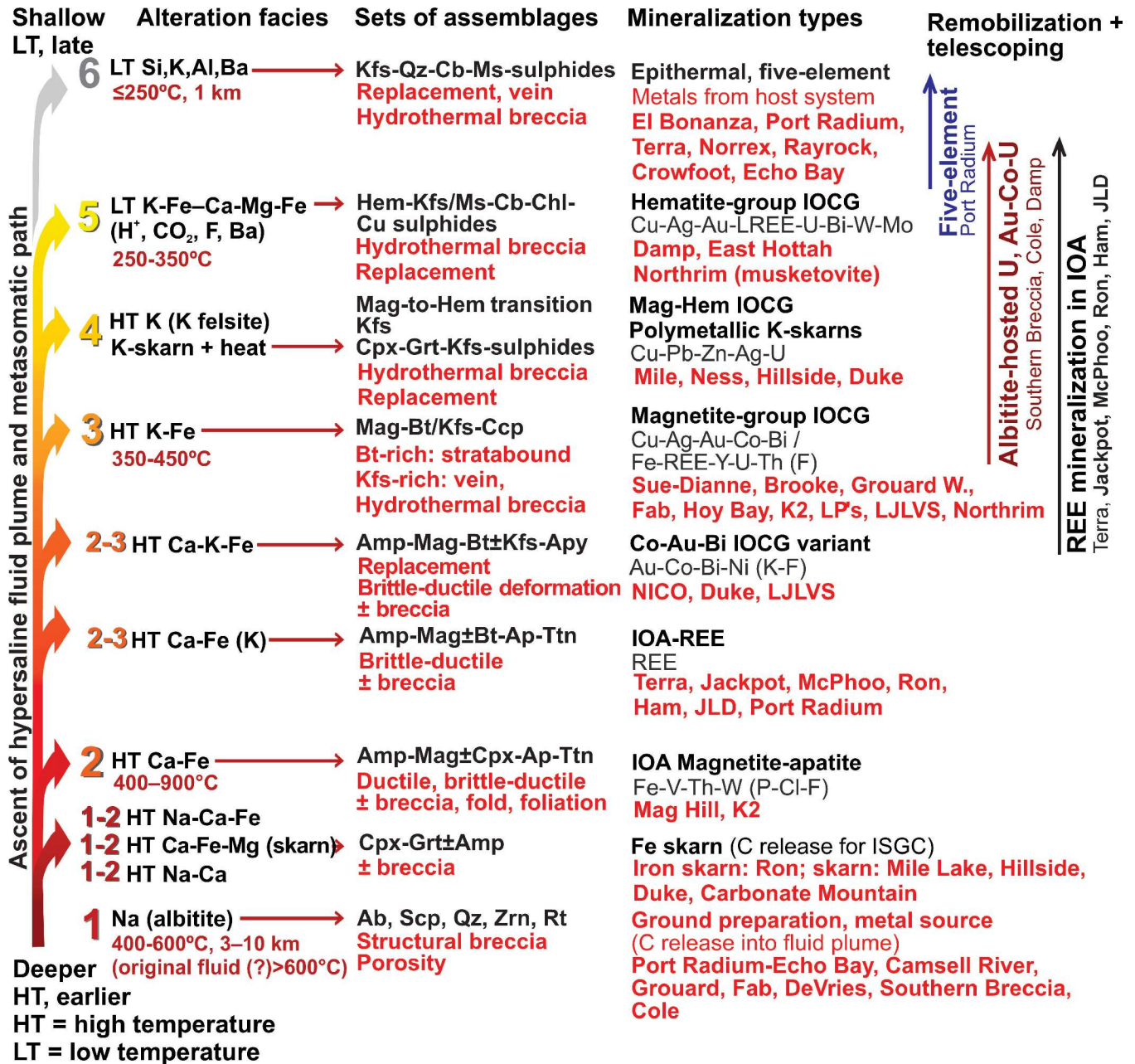


Figure 4. Prograde evolution of ore systems with iron-oxide and alkali-calcic alteration, showing the genetic linkage among some iron oxide-copper-gold, iron oxide-apatite, Fe skarn, albitite-hosted U, albitite-hosted orogenic Au-Co-U, Merlin-type Mo-Re, and five-element and vein-types of mineralization (modified from Corriveau et al., 2016). Mineral-name abbreviations from Whitney and Evans (2010).

modification. Rather than simply reflecting element enrichment or depletion, each alteration facies is a consequence of the systematic element partitioning between fluid and rock, and of the stability of the mineral assemblages as the magmatic-hydrothermal systems evolve. The mapping protocol for IOAA systems and the descriptive terminology required to support it was repeatedly tested, confirmed to be applicable globally, and to vector to mineralization (Corriveau et al., 2016, 2022a, b, c, d, e; Montreuil et al., 2016a, b, c). Digital geological mapping data sets have been built during the project, but technological limitations reduced mapping efficiency and data entry. Data sets and digital data-capture terminology are being optimized using current knowledge, experience, and expertise for future publication.

Metasomatic evolution of mineral systems

As documented in detail in Corriveau et al. (2022c), the prograde sequence of metasomatic facies and associated deposit types, induced by the evolution of the fluid column at regional scales as it ascends through the upper crust, follows a simple prograding order through time and from depth to surface (Fig. 4):

- Na alteration (albitite) and local skarn in carbonate units. The porous and fine-grained albitite that forms is easily fractured or brecciated and becomes a preferential host for later albitite-hosted uranium and orogenic Au-Co-U deposits. Skarn can be mineralized in Fe, Pb, and Zn in association with lower-temperature overprints.
- High-temperature Ca-Fe facies, which consists of a suite of assemblages with variable proportions of amphibole, magnetite, and apatite. This facies can evolve to IOA mineralization, especially above intermediate subvolcanic intrusions (Hildebrand, 1986; Zhao et al., 2022), and commonly has magmatic fluid sources (e.g. Somarin and Mumin, 2014). Iron oxide-apatite bodies represent the highest temperature core zone of the system, with fluid temperatures recorded up to 560°C in the Great Bear magmatic zone (Somarin and Mumin, 2014), though temperatures up to 800°C and locally 900°C in coeval skarn have been documented globally (e.g. Middle-lower Yangtze River metallogenic belt; Zeng, 2020). Temperatures are greater than those of fluids entrapped by the albitite potentially because the original high-temperature fluids interacted with country rocks in the initial stages of hydrothermal fluid convection and cooled down (Corriveau et al., 2016, 2022c, d). Within sedimentary rocks, stratabound high-temperature Ca-Fe alteration commonly evolves from amphibole-dominant to magnetite-dominant alteration and forms fairly homogeneous layers (Fig. 5a, b, c, d, e). Where alteration is extreme, IOA deposits can form and be associated with REE and nickel deposits (Clark et al., 2010; Ferreira Filho et al., 2021; Sappin and Perreault, 2021).
- Transitional high-temperature Ca-K-Fe facies that can lead to cobalt-rich variants of IOCG deposits and precipitate variable critical metals such as Bi, Co, and Ni, as defined by Natural Resources Canada (2021).
- High-temperature K-Fe facies with biotite, K-feldspar, and magnetite assemblages, leading to magnetite-group IOCG deposits. As K-feldspar becomes the dominant potassic phase, brecciation occurs and ore minerals precipitate largely in veins disseminated within iron-oxide breccia. This facies is commonly found in association with felsic intrusive suites (e.g. Montreuil et al., 2016a, c) and fluid sources are mixed (Baker et al., 2008). In such zones, magnetite commonly transitions into hematite and/or K-feldspar alteration at temperatures lower than approximately 450°C (Somarin and Mumin, 2014).
- K-felsite with K-feldspar; K-Ca-Mg (K-skarn) alteration with clinopyroxene, garnet, and K-feldspar; and polymetallic skarn can form independently or in association with magnetite-to-hematite-group IOCG deposits. Carbonate host rocks may or may not be required, early carbonate alteration is observed, and proximal intrusions are not an intrinsic characteristic of the development of the facies (Corriveau et al., 2016, 2022c, d).
- Low-temperature Fe-(Ca, Mg, Fe Co₂, hydrolytic) alteration ranges from a low-temperature K-Fe facies with K-feldspar, sericite, and hematite assemblages to a low-temperature Ca-Mg-Fe facies with carbonate, chlorite, and epidote end-members that lead to hematite-group IOCG deposits, albitite-hosted uranium or gold-cobalt, and a variety of other deposit types (Williams et al., 2005; Skirrow, 2010; Corriveau et al., 2016, 2022a, c, d). Low-temperature Fe-Si alteration is barren or gold-bearing (Schlegel and Heinrich, 2015). Iron oxide-copper-gold deposits can be enriched in uranium, light REEs, and other critical metals (Skirrow et al., 2013; Corriveau et al., 2022a).
- Epithermal alteration can be associated with a variety of epithermal and epizonal deposits (Mumin et al., 2010). Potassium-feldspar (potassic) alteration transitions into phyllic (quartz-sericite-pyrite or sericite) and sericitic alteration at less than 400 to 450°C, and phyllic into propylitic (chlorite, epidote, carbonate) at less than about 370°C (Somarin and Mumin, 2014). Propylitic alteration occurs as both prograde and retrograde phases, the latter persisting to temperatures under 200°C (Somarin and Mumin, 2014). Hydrothermal carbonate and quartz occur as structurally controlled veins, stockworks, breccia, and replacement zones within, and distal to, hydrothermal centres, and may superimpose any other assemblages as a result of retrograde alteration or through subsequent reactivation with circulation of fluids, including those related to overlying sedimentary basins (Trottier, 2019; Ehrig et al., 2021; Corriveau et al., 2022c). Tourmaline veins are common, but can also precipitate in various zones in association with earlier alteration facies (Kelly

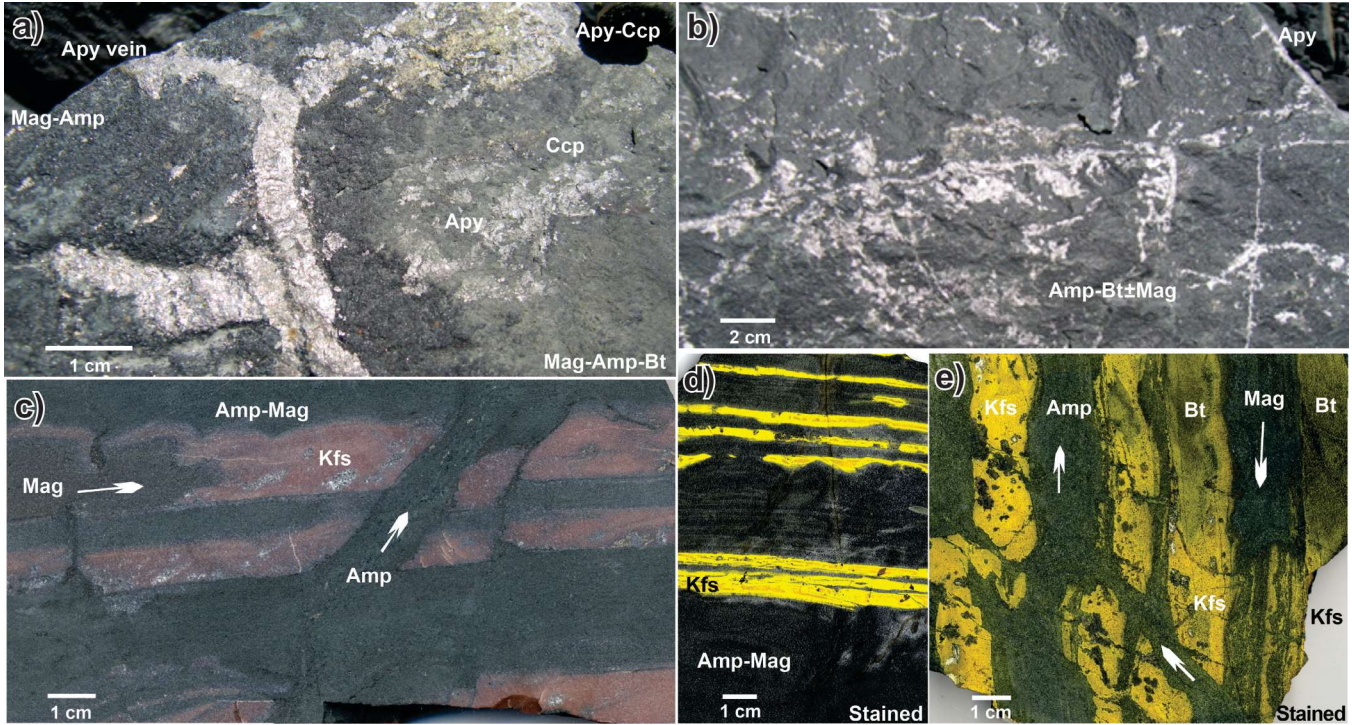


Figure 5. Cobaltian-arsenopyrite and associated ore minerals within pervasively high-temperature (HT) Ca-Fe and HT Ca-K-Fe altered metasedimentary rocks at the NICO deposit. **a), b)** Arsenopyrite±chalcopyrite ore in stratabound magnetite-hornblende-biotite-K-feldspar (HT Ca-K-Fe) alteration cut by arsenopyrite veins on outcrop CQA-08-0550. NRCan photos 2020-453 and 2020-454. **c)** Stratabound magnetite-amphibole (HT Ca-Fe) alteration in siltstone and K-feldspar alteration along wacke laminations replaced by renewed magnetite alteration along K-feldspar altered layers and that has been subsequently cut by an amphibole vein recording repetition of alteration facies within the deposit. NRCan photo 2020-455. **d)** Stained rock slab of the alteration shown in (c) from outcrop CQA-07-0480. NRCan photo 2020-456. **e)** Stained rock slab from outcrop CQA-07-0480, showing stratabound magnetite-amphibole (HT Ca-Fe) alteration in siltstone and K-feldspar alteration along wacke laminations replaced by renewed magnetite alteration of amphibole-biotite and K-feldspar alteration and that has been subsequently cut by an amphibole vein recording repetition of alteration facies within the deposit. NRCan photo 2020-457. All photographs by L. Corriveau. Apy = arsenopyrite, Ccp = chalcopyrite, Mag = magnetite, Amp = amphibole, Bt = biotite, Kfs = K-feldspar

et al., 2020). Fluorite is locally present in late-stage veins, but is most common at the low-temperature K-Fe alteration facies and Fe-dominant and K-poor variants (Mumin et al., 2010; Schlegel et al., 2020).

Examples of mineralization types

Deposits and mineralized tailings within high-temperature Ca-K-Fe and high-temperature K-Fe alteration facies

The Cu-Ag-Au Sue-Dianne deposit and Brooke, Summit Peak, and Chalco prospects are representative of magnetite-to-hematite group IOCG deposits that contain copper as the defining economic commodity, frequently in association with economic gold and silver, and localized uranium (Montreuil et al., 2016b). The Fab prospects have potential for magnetite group IOCG mineralization (Montreuil et al., 2016c), but appear to have limited extent based on the regional mapping done by Potter et al. (2013b) and the

geophysical modelling of Hayward (2013). The Great Bear magmatic zone mineral systems also form IOA prospects in the Port Radium–Echo Bay and Camsell River districts, with both districts exhibiting alteration facies and mineralization typical of IOCG and affiliated deposits (Mumin et al., 2007, 2010; Bowdidge et al., 2014; Bowdidge and Dunford, 2015). Mine tailings in these two districts remain mineralized with base and precious metals, critical metals, and uranium (e.g. average grade of tailings at the past-producing Eldorado mine is 154 g/t Ag, 0.079% U₃O₈, 0.27% Cu, 0.073% Co and 0.050% Ni; Alberta Star Development Corp., 2007).

The NICO deposit is a global example of cobalt-rich variants of IOCG deposits. Intense, iron oxide (magnetite-dominant)-hornblende±biotite±tourmaline, ±K-feldspar, ±carbonate alteration, veining, and brecciation occur along stratabound to discordant lenses within a thoroughly metasomatized metasedimentary sequence. Detailed characterization of alteration and cobalt-nitrate staining of rock slabs enabled the subdivision of alteration assemblages into multiple generations of amphibole-dominant, amphibole-magnetite, and

magnetite-dominant high-temperature Ca-Fe alteration facies as well as amphibole-biotite and amphibole-magnetite-biotite±K-feldspar high-temperature Ca-K-Fe alteration facies (Fig. 5a–e; Corriveau et al., 2016, 2022d). Mineralization at NICO is interpreted to have been optimized by the repetition of the two facies and their evolution to low-temperature K-Fe facies, forming in the process cobaltite, cobalt-rich loellingite, and cobalt-rich arsenopyrite with accessory pyrite and minor scheelite followed by arsenopyrite (with variable amounts of cobalt), native bismuth (±bismuthinite), gold, and lesser magnetite, marcasite, pyrite, followed by chalcopyrite, bismuthinite, and hematite (Goard et al., 2000a, b; Acosta-Góngora et al., 2015a, b).

Montreuil et al. (2016b) highlighted that a zone of high-temperature K-Fe alteration in the NICO orebody is richer in copper than the structurally overlying and earlier high-temperature Ca-K-Fe alteration facies. In addition, Corriveau et al. (2022d) illustrated that K-feldspar-rich zones occur within the deposit, although the K-feldspar is only visible through cobaltinitrite staining. Copper also occurs throughout the system in areas where fluids evolved from the high-temperature Ca-K-Fe to high-temperature and low-temperature K-Fe alteration facies and formed replacement zones or breccia bodies such as above the NICO deposit within the volcanic rocks (e.g. Chalco and Summit Peak prospects). Chalcopyrite was also discovered within the Southern Breccia corridor in association with uranium occurrences, including at the Eastern zone (Montreuil et al., 2015, 2016b). Resistivity and gravity anomalies occur below the Chalco prospect area and below the Eastern zone southeast of the NICO deposit at about 500 m depth, beyond current drilling depth (*see* Hayward et al., 2016). The bimodal porphyry intrusions share a direct spatial, and probable genetic, link with mineralization at the NICO deposit, based, among others, on the boron isotopic composition of tourmaline that was linked to the systems by syn- to postmetasomatism (1870–1868 Ma) porphyritic felsic dykes (Montreuil et al., 2016b; Kelly et al., 2020); however, the occurrence of tourmaline alteration associated with most alteration facies within IOAA systems should be noted. These relationships suggest that tourmaline crystallization most likely reflects magmatic-hydrothermal origins, wherein magmatic and pore fluids heated by the magmatism interact with host rocks as the fluid columns ascend (Kelly et al., 2020).

In sedimentary and volcanic rocks, iron oxide metasomatism can be extremely efficient at preserving the textures and structures of the host rocks and, in many instances, zones of high-temperature Ca-Fe alteration can be mistaken for iron formations or undivided ironstones. Iron oxide replacement zones were mapped reported as having been historically mapped as sedimentary banded iron-formations in the Great Bear magmatic zone (Aber Resources Ltd., 1993), in the Monakoff deposit of the Cloncurry district of Australia (Williams et al., 2015), in the Bafq district of Iran (Fig. 6 in Daliran et al., 2022), and in the Dahongshan

deposit of the Kangdian district of China (Fig. 4–5 in Zhao et al., 2022). The absence of quartz, jasper, and siliceous iron minerals; the presence of layers rich in amphibole (actinolite, hornblende), clinopyroxene, albite, or biotite, as well as of stratabound magnetite haloes along magnetite veins (Corriveau et al., 2022b); and geochemical signatures with elevated Ca, Hf, Mg, Nb, REE, Ta, Th, Ti, V, U, and Zr in an ironstone are all signs of iron-rich IOAA alteration.

Mineralization in skarn and K-skarn

Skarn (clinopyroxene-garnet dominant) and K-skarn (clinopyroxene-garnet-K-feldspar dominant) polymetallic sulphide mineralization formed within the Great Bear magmatic zone IOAA systems (Fig. 4; Table 2). Barren skarn occurs at Hoy Bay on the shore of Great Bear Lake. Barren and mineralized skarn occur at the Mile Lake prospect in the southwestern arm of Echo Bay, in the Grouard system (Hillside prospect), and at Carbonate Mountain (Mumin et al., 2007, 2010; Corriveau et al., 2010a, 2016, 2022b, d; Mumin, 2015; Montreuil et al., 2016b). Magnetite skarn hosts minor chalcopyrite-pyrite veins and disseminations northeast of the Nod prospect (Mumin et al., 2010; Hamilton, 2017). At Carbonate Mountain, sphalerite, chalcopyrite, galena, and pyrite occur in a small zone near the contact with the intrusion, hosted in a skarn assemblage of pyroxene (diopside), andradite, epidote, and K-feldspar. At the Duke prospect, chalcopyrite, cassiterite, sphalerite, and galena mineralization crystallized among low-temperature Ca-K alteration consisting of K-feldspar, pumpellyite, and epidote (De Toni, 2016). At the Mile Lake prospect, a crater-lake volcanoclastic and tuff assemblage within pyroclastic lapilli and breccia lenses hosts polymetallic sulphide mineralization that overprints an andradite-vesuvianite-diopside-epidote-K-feldspar K-skarn. Drilling results include a 9.9 m intersection grading 1.64% Cu, 1.00% Pb, 2.30% Zn, 42.0 g/t Ag, 0.07% Mo, and 0.16% W (Alberta Star Development Corp., 2006).

Low-temperature K-Fe alteration facies and associated mineralization

Massive hydrothermal hematite bodies and extensive iron-oxide breccia zones have now been documented throughout the Great Bear magmatic zone, extending the mineral potential of the Great Bear magmatic zone to the most prospective deposit types within IOAA systems, namely the hematite-group IOCG deposits. Extensive hematite breccia zones occur among clay- and K-feldspar-altered volcanic rocks within the Hottah system (Fig. 3a). Though barren, these breccia indicate potential for hematite-group mineralization at depth as the system has segments with magnetite alteration mineralized in sulphides and REE. Barren hematite breccia zones are also typical of the shallower part of hematite-group IOCG deposits (Olympic Dam and Prominent Hill deposit, and Oak Dam prospect,

Australia; Davidson et al., 2007; Ehrig et al., 2012; Schlegel and Heinrich, 2015). Renewed exploration at the Oak Dam prospect has led to the major Oak Dam West IOCG discovery and disclosure of best intercepts reaching 425 m at 3.04% Cu, 0.59 g/t Au, 346 ppm U_3O_8 , and 6.03 g/t Ag (BHP, 2018; King, 2019); a strong reminder of the importance of hematite breccias as vector to polymetallic mineralization based on the IOAA mineral system-model framework (Corriveau et al., 2022c).

In the Great Bear magmatic zone, the best example of massive hematite replacement lies structurally above the Mag Hill IOA prospect near the southeastern tip of Echo Bay in the Port Radium–Echo Bay district (Fig. 3b). In that location, a northwardly tilted porphyritic andesite sequence is progressively and upwardly replaced by albitite (Na), high-temperature Na-Ca-Fe alteration, an IOA body, and finally by a hematite ironstone lens up to several decametres thick and several hundred metres long with a near-massive hematite core. Locally preserved plagioclase phenocrysts are thoroughly replaced by quartz. The hematite lens occurs midway between the extensive magnetite-actinolite-apatite alteration that forms the high-temperature Ca-Fe alteration core of the Contact Lake Belt, and large, near paleosurface phyllic-potassic alteration zones at the southeast Echo Bay gossan (Fig. 3b). Associated K-feldspar alteration occurs along the contact of the hematite lens, indicative of a low-temperature K-Fe alteration zone that has evolved to a hematite-dominant quartz-bearing low-temperature Si-Fe facies — a feature present where such alteration matures to lower temperature facies (*see* Corriveau et al., 2022c, d).

Massive hematite with abundant pyrite occurs at depth (several hundred metres below surface) in the K2 system at Echo Bay, again in association with a low-temperature K-Fe alteration zone that has evolved to lower temperature facies. Here the hematite lens is in gradual contact with a magnetite-actinolite alteration zone and is associated with abundant sulphides, including minor amounts of chalcopyrite as well as biotite (Mumin et al., 2007, 2010). Hematite is also commonly present without magnetite in zones peripheral to hydrothermal magnetite-bearing bodies, as at NICO and Sue-Dianne deposits. In these deposits, the transition zones between magnetite and hematite stability contain the highest metal contents, as described above for the Summit Peak prospect. Hematite is also present as breccia matrix, veinlets, and disseminations in many epithermal zones and veins, including locally in the giant quartz veins previously mentioned.

Mineralized veins, metal remobilization, impacts of magmatism, and tectonic framework

Mineralized veins including giant quartz vein complexes are spatially associated with IOAA systems (e.g. Gandhi et al., 2000; Byron, 2010), which strongly

suggests a synmetasomatic origin for some components of the mineralized quartz veins and complexes in addition to long-lived fluid circulation and metal precipitation to form extensive polyphase quartz veins. Copper mineralization within veins commonly cuts high-temperature K-Fe alteration, such as in the Summit Peak Cu-Au-Ag IOCG prospect that occurs within extensively potassium-altered volcanic rocks above the unconformity with the tilted and metasomatized metasedimentary rocks hosting the Au-Co-Bi-Cu NICO deposit about 0.5 km to the northeast. A stringer-stockwork zone of pyrite plus chalcopyrite veining cuts K-feldspar and K-feldspar-magnetite-altered rhyodacite ignimbrite sheets (Montreuil et al., 2016b). The host K-feldspar alteration zone is associated with magnetite-K-feldspar high-temperature K-Fe replacement and breccia, with disseminated and vein-type chalcopyrite mineralization. Potassium-feldspar haloes form along magnetite veins (Montreuil et al., 2016b), which is typical of the K-feldspar and magnetite decoupling in this alteration facies (Corriveau et al., 2016, 2022b). Where hematite alters magnetite, chalcopyrite is more abundant. Local chalcopyrite, pyrite, magnetite, biotite, amphibole, and K-feldspar assemblages record a transition from high-temperature Ca-K-Fe to high-temperature K-Fe alteration facies and brecciation. A single surface trench returned values of 0.73% Cu over 44.0 m (Mumin, 1997), although drilling failed to intersect mineralization at depth.

Polycyclic episodic outgassing from subvolcanic magmas is normal for large volcano-plutonic systems (Myers et al., 2016). Caldera collapse and tectonic activity can also dramatically change fluid flow and cause ingress of low-temperature fluids from a variety of sources into the systems, including acidic, oxidized, and saline volcanic lake water. Among the geological findings of interest for the development of IOCG deposits in the Camsell River district are the presence of successive calderas, abundant evidence of synmetasomatic tectonic activity and magma emplacement, pulsating and telescoping of alteration facies, and potential presence of saline caldera lakes indicated by stromatolites in a localized carbonate unit between the two caldera-collapse structures of the Camsell River district that extends to the Grouard system (Fig. 3b; Hildebrand et al., 2010b; Mumin et al., 2014; Montreuil et al., 2016a; Corriveau et al., 2016, 2022b, c). The presence of saline caldera lakes capable of sustaining stromatolite growth might be particularly significant as Schlegel et al. (2018, 2020) attributed the high-grade copper-gold ore at the Prominent Hill IOCG deposit and rich metal endowment of the Olympic Dam deposit to the presence of oxidized, acidic, and saline volcanic lake water.

Multiple, superimposed hydrothermal cycles can cause alteration and mineralization to vary in terms of intensity and extent, as a function of proximity to the magmatic heat source, cooling rates (magmatic and geothermal), and fluid sources. This leads to numerous permutations of alteration facies with transitional, juxtaposed, overprinted, telescoped, and retrogressed assemblages as well as multiple cycles of brecciation, alteration, and mineralization such as at the

NICO deposit (Fig. 5a–e) and the K2 prospect (Mumin et al., 2010; Mumin, 2015; Corriveau et al., 2016, 2022b, c, d; Hayward et al., 2016; Montreuil et al., 2016a; Skirrow, 2022; Zhao et al., 2022).

Secondary hydrothermal convection cells and a retro-grading fluid system was proposed for the main stage of sulpharsenide mineralization at the NICO deposit (Goad et al., 2000a, b; Mumin and Camier, 2000; Mumin et al., 2000); however, the precipitation of arsenopyrite and cobalt-rich pyrite within IOAA systems during high-temperature Ca-K-Fe and biotite-rich high-temperature K-Fe alteration are now much better understood based on observations from the Ernest Henry and NICO deposits and are part of the prograde evolution of the mineral system (Fig. 4, 5a, b; Corriveau et al., 2016, 2022c, d). In addition, documentation of synmetasomatic magma emplacement at the NICO deposit and the adjacent Southern Breccia albitite corridor highlights how repeated heat ingress sustained development of the IOAA systems, whereas later stage dykes cut by arsenopyrite veins illustrate that renewed magma emplacement can cause remobilization of metals. Magmatic-sourced metals, repetition of alteration facies and associated metal precipitation, and remobilized metals at the NICO deposit produced locally complex zoning patterns (Corriveau et al., 2010a, b, 2016, 2019a, b, 2022a, c; Montreuil et al., 2015, 2016a, b). In addition, gold was remobilized and reconcentrated (gold-refining process) by bismuth melts during development of the high-temperature Ca-K-Fe and high-temperature K-Fe facies (Acosta-Góngora et al., 2015a, b).

In the Camsell River district, a series of fluidized magnetite breccia zones with albitite or apatite fragments cut albitite or albitized volcanoclastic rocks without the in situ transition from Na to amphibole-dominant high-temperature Ca-Fe alteration (Corriveau et al., 2022b, c, d). The field relationships at the Terra mine highlight that fluids can crystallize a vast amount of magnetite at the high-temperature Ca-Fe facies and that such metasomatic magnetite mushes can be fluidized. Fluidization may have been induced by faulting associated with the caldera-collapse events documented in the district by Hildebrand et al. (2010b), aided by decarbonation of host carbonate rocks during IOAA metasomatism, including carbonate rocks that precipitated after an earlier caldera collapse within a caldera lake (e.g. stromatolite-bearing carbonate rocks; Corriveau et al., 2022b). Magnetite breccia pipes and dykes with albitized clasts occur in the Cloncurry district and have been interpreted as the product of high-energy fluidization (e.g. Fig. 3a in Rusk et al., 2010). Fluidization of millerite- and pyrite-bearing IOA-nickel mineralization has been documented at the Jaguar deposit in the Carajás district, Brazil (Ferreira Filho et al., 2021). The deposit hosts nickel resources of 59 Mt at 0.95% Ni (Centaurus Metals Limited, 2021).

Extensive brittle deformation of early albitite along fault zones and brittle-ductile to ductile deformation during high-temperature Ca-Fe to high-temperature Ca-K-Fe

alteration facilitated pervasive alteration, metal transport, and precipitation (Fig. 4; Montreuil et al., 2015, 2016b). The high-temperature Ca-Fe to high-temperature Ca-K-Fe alteration facies are best developed along sedimentary sequences, as illustrated from the NICO deposit and the entire host sequence mapped by Gandhi et al. (2014), forming cobalt-rich variants of IOCG deposits at NICO, and a series of prospects and mineral occurrences in the Duke system (Fig. 3d; Montreuil et al., 2016b). At the NICO deposit, tectonic activity during metasomatism led to thrusting of the albitite corridor to higher structural levels, while the fluid plume had evolved to lower temperatures, which allowed precipitation of mineral assemblages at the high-temperature K-Fe facies (Corriveau et al., 2016; Hayward et al., 2016). This thrusting led to the precipitation of uranium within reduced magnetite-precipitating fluids in the high-temperature K-Fe facies within albitite (Montreuil et al., 2015; Potter et al., 2019, 2022). Fluid migration was facilitated by porosity in the albitite corridor and interconnectivity induced by damage during subsequent brecciation (Montreuil et al., 2012). High porosity associated with leaching of nearly all elements during albitization resulted in rocks and alteration zones with extremely low magnetic susceptibilities and densities in the Southern Breccia albitite corridor (Montreuil et al., 2012; Hayward et al., 2013, 2016; Enkin et al., 2016). Uranium was preferentially precipitated at the K-Fe facies in the Southern Breccia albitite corridor, whereas the NICO deposit remained barren in terms of uranium mineralization. In addition to eastward thrusting, northeast-trending normal faults differentially uplifted segments across the NICO deposit and Southern Breccia corridor (Enkin et al., 2012; Hayward et al., 2013, 2016). This preserved significant volcanic rocks and hematite-bearing breccia (e.g. Lou zone; Fig. 3d) to the north of the deposit, whereas adjacent, significantly less down-faulted blocks have widespread transitional magnetite to hematite attributes (Frank and Red Hot zones; Fig. 3d). To the southeast, the albitite of the eastern zone (Southern Breccia; Fig. 3d) dominates and is cut largely by magnetite-rich alteration with K-feldspar or biotite (Montreuil et al., 2015, 2016c). Based on the alteration-facies model, an area of copper-mineralized high-temperature K-Fe alteration zones structurally below earlier cobalt-mineralized high-temperature Ca-K-Fe alteration indicates that faulting may have preserved additional high-temperature K-Fe alteration within the region (Montreuil et al., 2016b; Corriveau et al., 2018c). The structural and alteration-facies framework described for the deposit and host IOAA system makes it possible to expand the mineral potential of the region (Hayward et al., 2013, 2016; Corriveau et al., 2016, 2019a, b, 2022c; Montreuil et al., 2016b; Potter et al., 2019, 2022). The new GEM-TGI geoscience framework for the region has led to renewed exploration and drilling (Fortune Minerals Limited, 2019, 2021).

Intrinsic development of quartz stockworks within IOAA systems is common and well documented at the Sue-Dianne deposit (Mumin et al., 2010). The IOAA systems also form a continuum with porphyry (Cu±Au) and epithermal

mineralization (Fig. 4; Mumin et al., 2010). If taken independently and out of context, such mineralization could easily be classified as unrelated, even though they form as part of the same large magmatic-hydrothermal events. The documentation of these systems has spearheaded new research on the continuum between these types of ore systems and the secular variations in their abundances, from the Precambrian to the Phanerozoic (Richards and Mumin, 2013a, b; Richards et al., 2017).

Remobilization of metals within the Great Bear magmatic zone IOAA systems has led to five-element and uranium-vein mineralization, both at 1.85 Ga during emplacement of the late-stage granitic suite and during the late Proterozoic, related to sedimentation and fluid circulation within the basin (Fig. 4; Badham, 1975; Davis et al., 2011; Gandhi et al., 2018; Trottier, 2019). Metal remobilization has been proposed in the Central Mineral Belt and Romanet Horst in Canada (McLaughlin et al., 2016; Sparkes, 2017; Acosta-Góngora et al., 2019) as well as at the Olympic Dam deposit (Macmillan et al., 2016; Cherry et al., 2018; Ehrig et al., 2021) and in the Cloncurry district of Australia, where some mineralization developed during a younger, low-latitude, meteoric fluid flow along a major fault zone (namely the Cloncurry Fault; Mark et al., 2004). The past-producing silver and uranium mines along the northeastern shore of Great Bear Lake have now been shown to be key exploration vectors for IOCG and affiliated deposits, including the Camsell River district currently explored by the Denendeh Exploration and Mining Company (Bowdidge et al., 2014; Bowdidge and Dunford, 2015; Beaulieu, 2019).

Critical metal endowment of IOAA systems has yet to be documented in detail, but processing of large geochemical data sets of altered and mineralized samples during GEM and TGI research highlights that endowment is significantly enriched with respect to continental crust and varies according to alteration facies and associated mineralization types (Fig. 4; Corriveau et al., 2016, 2019a, b, 2022a, c). Collectively, most critical metals listed in Fortier et al. (2018) and Natural Resources Canada (2021) can reach high values within IOAA systems and their deposits. In the GEM Great Bear magmatic zone database — largely derived from representative samples of alteration-type replacement, not mineralized, veins — maximum concentrations reach as high as (but are not necessarily contained within a single sample) 82 200 ppm As, 10 587 ppm Ba (excluding a pure barite vein), 31 ppm Be, 14 475 ppm Bi, 123 ppm Cd, 27 635 ppm Co, 1966 ppm Cr, 64 ppm Cs, 54 ppm Ga, 1.9 ppm Ge, 67 ppm Hf, 11 ppm In, 147 ppm Li, 589 ppm Nb, 1070 ppm Rb, 305 ppm Sb, 378 ppm Sc, 222 ppm Sn, 2574 ppm Sr, 162 ppm Ta, 26 ppm Te, 880 ppm Th, 2 ppm Tl, 7770 ppm U, and 1837 ppm V (Corriveau et al., 2015). Maximum rare-earth element concentrations are 7447 ppm La, 10 222 ppm Ce, 955 ppm Pr, 2845 ppm Nd, 318 ppm Sm, 32 ppm Eu, 218 ppm Gd, 41 ppm Tb, 254 ppm Dy, 51 ppm Ho, 144 ppm Er, 21 ppm Tm, 128 ppm Yb, 19 ppm Lu, and 1655 ppm Y (Corriveau et al., 2015). Similarly,

Bowdidge et al. (2014) and Bowdidge and Dunford (2015) documented high concentrations in critical metals from the Camsell River district prospects. Corriveau et al. (2022a) contrasted the critical metal contents of the Au-Co-Bi-Cu NICO deposit (and potential Sb, Se, Te credits from bismuth leach; R. Goad, pers. comm., 2020) to that of the Olympic Dam deposit.

LITHOGEOCHEMICAL TOOLS

Lithogeochemical discriminant tools developed in the course of the projects, as well as their integration with spectral and petrophysical measurements, aid in refining the characterization of alteration and element mobility from sources to deposits within IOAA systems and are critical for exploration, development of chemical and prospectivity maps, and mineral-potential assessments (Fabris et al., 2013; Montreuil et al., 2016b; Corriveau et al., 2017, 2022a; Blein et al., 2022; Fabris, 2022; Katona and Fabris, 2022). Lithogeochemistry has also proven helpful in understanding metasomatic processes, tectonic-magmatic disruption of the prograde metasomatic paths, and prognosticating faulting at the scale of systems and deposits (e.g. fault network across the Olympic Dam deposit; Ehrig and Clark, 2019). Alteration indices proposed by Benavides et al. (2008) allowed a first-order discrimination of the presence of IOCG geochemical signatures; however, the indices did not enable discrimination among alteration types and mineral systems. The AIOCG alteration indices and discriminant diagrams of Montreuil et al. (2013, 2016b) provided a means to characterize all the geochemical variations observed in IOCG-related ore systems. The elements that define the alteration facies are routinely and precisely analyzed by government, private sector, and academia, thus allowing reprocessing of large historical data sets to better guide mineral exploration across prospective settings (Blein et al., 2022).

The distinct chemical fingerprints of least altered and metasomatic rocks formed as the system evolves are best illustrated using molar proportions of the dominant cations in the facies, calculated from whole-rock analyses. The spectrum of rock compositions in each alteration facies is so distinct that once portrayed as coloured bars they represent a ‘barcode’ (Fig. 6; *see* Corriveau et al., 2016, 2017, 2018b, 2019a, b, 2022a; Montreuil et al., 2016b; Blein et al., 2022). Molar proportions of Na-Ca-Fe-K-Mg in least altered rocks are fairly uniform and comprise four or five dominant cations (except for rhyolite, which has only two). Conversely, one to three cations are dominant within IOAA facies, each with very diagnostic main cation(s). Variations in the relative proportions of the discriminant cations qualitatively record the intensity of alteration, the dominant minerals in the assemblage and, in some cases, the host rock types (Corriveau et al., 2018b, 2022a, c; Blein et al., 2022). As each facies has a distinct chemical signature, the proportions of Na, Ca, Fe, K and Mg or Si and Al in

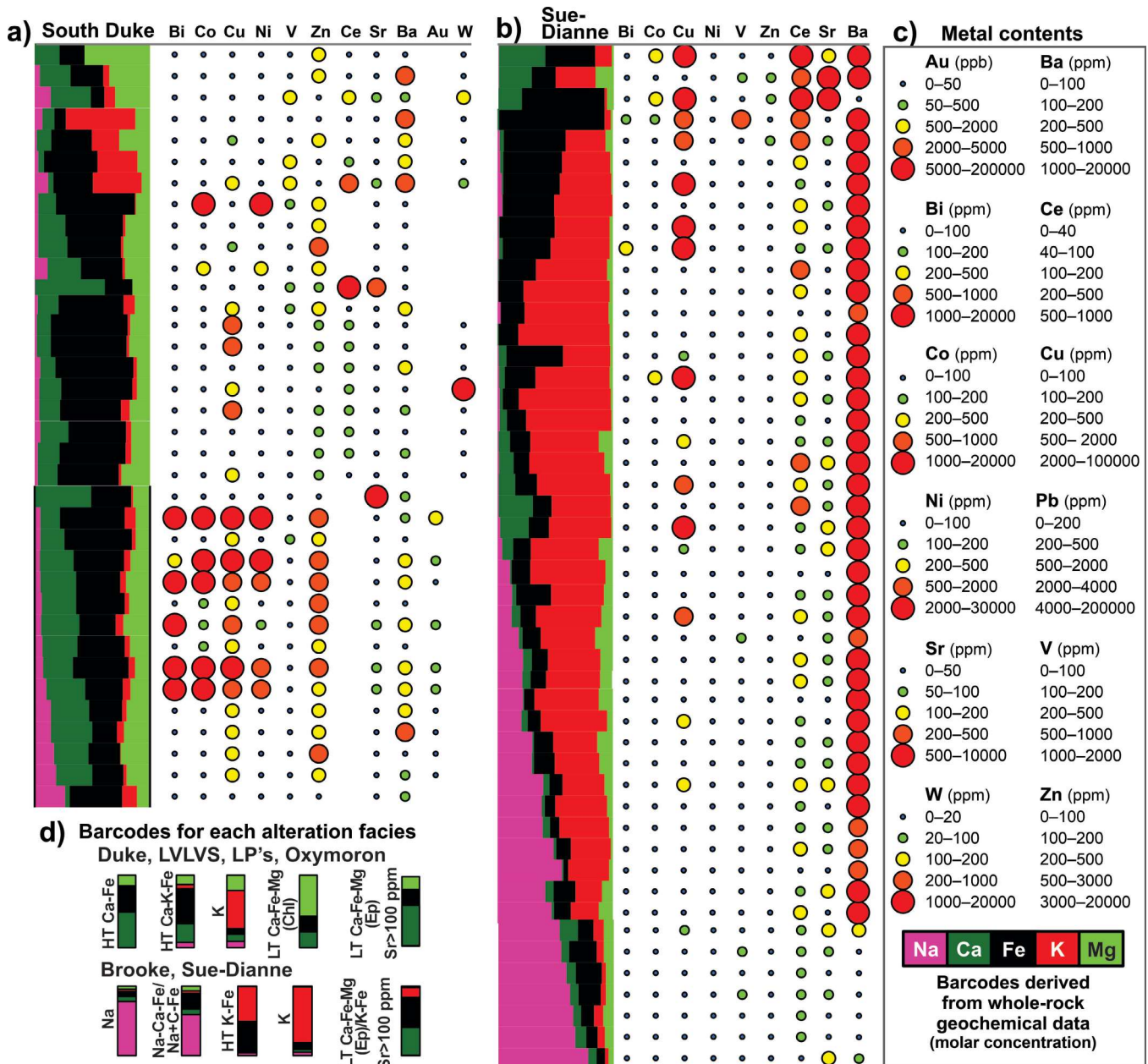


Figure 6. Chemical sections of the South Duke system and the Sue-Dianne deposit of the Mazenod system, illustrating the relationship between alteration facies and the molar proportion of the main cations (Na-Ca-Fe-K-Mg barcodes) as well as metal endowment. The metals Sr and Ba are plotted as intensity indicators of low-temperature (LT) Ca-Mg-Fe and K-Fe alteration, respectively. Geochemical analyses from Corriveau et al. (2015) and spatial distribution of barcodes from appendices in Montreuil et al. (2016b). Representative analyses of the **a)** South Duke system (Duke prospect and LVLVS, LP's, and Oxymoron showings; Montreuil et al., 2016b), **b)** Sue-Dianne deposit, and **c)** metal contents. The geochemical data sets for the South Duke system and Sue-Dianne deposit were complemented with analyses from Goad et al. (1996) and Camier (2002), respectively. **d)** Representative barcodes for each alteration facies. HT = high-temperature.

whole-rock analyses are useful proxies for the dominant mineralogy of the main alteration facies, which have distinct metal associations as illustrated in Figure 6.

Plotting molar barcodes along drill cores, on maps, in chemical discriminant diagrams, and as representative examples of systems (Fig. 6) significantly helps to assess the mineral potential of a region, recognize fault zones (including potential sense of displacement), indicate changes in host rock types (where alteration is mild to moderate), track alteration intensity, and interpret the evolution of systems at deposit to regional scales (e.g. Corriveau et al., 2016, 2022a, b, c; Montreuil et al., 2016b; Potter et al., 2020; Blein et al., 2022). In parallel, as IOAA systems have a very diagnostic evolution in silica and aluminum, the proportions of Na, Ca, Fe, K, and $(\text{Si}+\text{Al})/10$ help differentiate the IOAA facies from the epithermal caps and quartz±carbonate veins that form in the near surface, distal regions of these systems (spatial and timing relationships in Mumin et al., 2010; Davis et al., 2011; e.g. lithochemical footprint in Corriveau et al., 2018b, 2019a, b, 2022a, b, c; Blein et al., 2022).

Disruption to the prograde metasomatic path through heat or external fluid ingress resets the physicochemical conditions of the fluid plume and results in permutations of alteration facies (Fig. 5c–e). The juxtaposition, overprinting, telescoping, renewal, and retrogression of alteration facies can be identified and mapped in the field as well as through processing of geochemical data sets using variations in the cationic barcodes on the AIOCG diagram and along drill cores (Corriveau et al., 2022c; Potter et al., 2020). This process is particularly powerful where albitite has been telescoped to higher crustal levels or when volcanic and tectonic events have allowed ingress of low-temperature fluids within the fluid plume as well as brecciation, replacement, and mineralization by fertile K-skarn, high-temperature to low-temperature K-Fe and/or low-temperature Ca-Mg-Fe alteration, as observed in the Southern Breccia corridor and Mile Lake prospect region of the Great Bear magmatic zone, Romanet Horst, Wanapitei Lake district, and Central Mineral Belt (Corriveau et al., 2014, 2016, 2019a, b, 2022a, b, c, d; Hayward et al., 2016; Blein et al., 2022).

Plotting the molar barcodes on the chlorite-carbonate-pyrite index (CCPI) box plot developed by Large et al. (2001) as well as iron contents also helps discriminate the lithochemical footprints of volcanogenic massive sulphide, porphyry, epithermal, and sedimentary exhalative (SEDEX) ore systems from those of IOAA systems (Blein and Corriveau, 2017; Corriveau et al., 2018a, 2022a). The IOCG-related alteration facies (AIOCG) box plot of Montreuil et al. (2013), based on the AIOCG indices, have now been included within the ioGAS™ lithochemical package developed by Imdex Limited.

Trace-element geochemistry of magnetite has also been studied at the NICO deposit (Acosta-Góngora et al., 2014) and in several Great Bear magmatic zone mineral systems

(De Toni, 2016; Huang et al., 2017, 2019, 2022). The composition of magnetite varies based on the host alteration facies and associated mineralization, which allowed refinements to discriminant diagrams for use in mineral exploration; however, comparison of the magnetite chemistry to other deposit types highlighted some limitations in using such diagrams. A broader study by McMartin et al. (2009a, b, 2011a, b) documented the heavy-mineral detrital signature of the NICO Co-Au-Bi deposit. In addition, extensive characterization of apatite chemistry and zoning has been used to better understand metasomatic processes within IOAA systems and to optimize the use of apatite as a mineral indicator in drift exploration (Lypaczewski, 2012; Lypaczewski et al., 2013; Normandeau et al., 2018). The study of boron isotopes in tourmaline by Kelly et al. (2020) also documented significant changes in tourmaline chemistry (a proxy for fluid compositions) as alteration facies evolve within a system.

GEOPHYSICAL MODELLING

A major impediment to mineral exploration for IOCG deposits in Canada is the lack of detailed gravity and magnetotelluric surveys in prospective settings; these tools have been shown to play a key role in assessing prospectivity of settings with potential for IOCG and affiliated deposits as well as delineating exploration targets and deposits (Clark, 2014; Heinson et al., 2018; McCafferty et al., 2019; Wise, 2019a, b; Katona and Fabris, 2022). The 10 km data spacing of the Canadian national gravity survey is simply inadequate for prospecting purposes. Hayward et al. (2013) applied new geophysical techniques to IOCG systems and refined geophysical modelling protocols to fingerprint IOCG deposits and their favourable areas in the Great Bear magmatic zone. Their research and the complementary work of Kerswill et al. (2016a, b) allowed field crews to successfully prioritize areas for mapping as well as find areas with potential IOAA systems using new Northwest Territories Geological Survey and GSC geophysical surveys and a new compilation of high-resolution aeromagnetic data for the Great Bear magmatic zone (Hayward and Oneschuk, 2011). Maps of the total magnetic field, residual total magnetic field, and first vertical derivative of the magnetic field acquired in the course of the Hottah Lake aeromagnetic survey across parts of nineteen NTS sheets have been published at the 1:50 000 scale (Kiss and Coyle, 2011a, b, c, d). The new modelling capitalized on the detailed magnetic surveys to calculate pseudo-gravity and combined it with regional gravity and magnetic data (Hayward et al., 2013; Hayward and Corriveau, 2014). Large-scale hematite-group IOCG deposits that evolved to low-temperature, hematite-rich alteration facies (e.g. Olympic Dam and Prominent Hill in Australia) produce first and foremost a gravity anomaly, as hematite is the dominant iron oxide and early magnetite is commonly extensively replaced by hematite, decreasing the intensity of the original magnetic anomaly. Mineral potential assessments greatly rely on the

difference between the measured positive gravity anomalies and pseudogravity anomalies calculated from the magnetic data, with a larger difference indicating a more prospective target (assuming a mafic intrusion can be discarded). As a result, although the modelling of Hayward et al. (2013) made significant advances in geophysical prospecting, it may have underestimated the extent of the Hottah system, where a series of extensive hematite breccia have since been identified.

The intense mineralogical transformations associated with IOAA systems and development of extensive porosity in some of the alteration facies produce large petrophysical property variations (density, magnetic susceptibility, conductivity and resistivity; Enkin et al., 2016) that lead to high-amplitude geophysical anomalies in magnetic, gravity, and magnetotelluric surveys. The use of the molar barcodes on density-magnetic susceptibility diagrams illustrates that the large variations in the physical properties of the rocks are a function of alteration facies, intensity of alteration, and — where alteration is weaker — host rock types. The physical property relationships were integrated with aeromagnetic and gravity data in Hayward et al. (2013) and modelled in different ways to target prospective zones at local to regional scales across the Great Bear magmatic zone (Hayward, 2013; Hayward and Corriveau, 2014). The magnetotelluric inversion models across the mineral system hosting the NICO deposit unveiled new conductive zones in the region (Craven et al., 2013; Hayward et al., 2016). These conductors and integrated interpretation of three-dimensional aeromagnetic, gravity, and magnetotelluric surveys have identified zones of ground preparation for mineralization (albitization), areas with potential for IOA and affiliated rare-earth element mineralization, and IOCG mineralization in the mineral system that hosts the NICO deposit. In addition, major transcrustal fault zones and local fault zones have been identified, leading to a better understanding of the development of albitite-hosted uranium deposits as well as an improved understanding of the metasomatic and structural evolution of the systems that formed the NICO deposit (Corriveau et al., 2016, 2022c; Hayward et al., 2016).

Hayward and Corriveau (2014) have proposed a tectonic restoration model of the Great Bear magmatic zone that required characterization of the geophysical signature for the major lithotectonic units of the belt based on the regional aeromagnetic compilation. In the process, this research illustrated the original spatial distribution of IOAA systems across the belt and their subsequent segmentation through transcurrent shearing. A striking association between development of the large systems and emplacement of large A-type granite intrusions ca. 20 Ma after mineralization in an area that overlaps the edge of a younger sedimentary basin may be of some consequence to the understanding of the lithospheric architecture of the region, particularly in light of the recent advances in surface-wave tomography that link thick lithosphere edges with development of sedimentary basins and mineralization not only in Australia, but beyond (Hoggard and Richards, 2019; Hoggard et al., 2020).

CANADIAN AND GLOBAL IOAA MINERAL SYSTEMS STUDIED

Results from the Great Bear magmatic zone studies demonstrate the need for reassessing the metallogenic framework and mineral potential of areas hosting spatially associated showings and prospects with Ag, Au, Co, Cu, F, Fe, Mo, Nb, Ni, Pb, Pd, Pt, Re, REE, U, V, W, and/or Zn, particularly those with known regional iron and alkali-calcic enrichments such as IOA or Kiruna-type occurrences. These elements are all known to be economic resources in IOAA-related deposits (Corriveau et al., 2022c). Notable enrichments in Al, As, Ba, Cd, Rb, Sb, Sc, Se, Sn, Sr, Ta, Te, Th, Y, and Zr are also of interest (Corriveau et al., 2022a, c). Some of the occurrences may lead to *bona fide* IOCG deposits, whereas others may have formed affiliated deposits such as IOA, iron-rich Au-Co-Bi-Cu, polymetallic skarn, albitite-hosted uranium, molybdenum-rhenium, or gold-cobalt deposits, or continuum to epithermal and porphyry Cu-Au deposits (e.g. Great Bear, Andean, Chinese, and Australian (Olympic Dam) examples; Mumin et al., 2010; Kreiner and Barton, 2011; Ehrig et al., 2012; Li et al., 2015; Corriveau et al., 2022c). The relationship among albitite and subsequent uranium mineralization led to the launching of a GEM program activity targeting the mineral system hosting polymetallic prospects in the Romanet Horst of the Trans-Hudson Orogen. This study showed that mineral systems subjected to tectonic activity can have deep alteration facies, notably albitite, tectonically telescoped to higher structural levels. In the Romanet Horst, these facies were cut by low-temperature K-Fe and Ca-Mg-Fe alteration with associated Au, U, Co, Mo, and Cu mineralization, forming high-grade albitite-hosted mineralization along fault zones (Corriveau et al., 2014; Montreuil et al., 2014; McLaughlin et al., 2016; Blein et al., 2022). More particularly, Au, Co, Cu, and U mineralization, and Mo and REE enrichment in the Romanet Horst, are largely hosted within quartz and dolomite veins crosscutting and brecciating albitite corridors along bounding and transverse fault zones. These veins are associated with hydrolytic low-temperature K-Fe alteration (carbonate, chlorite, hematite, K-feldspar, white mica), silicification (quartz), sericitization and phyllic alteration (white mica, pyrite), low-temperature Ca-Mg-Fe (chlorite-epidote), carbonatization, and sulphate alteration (Corriveau et al., 2014; McLaughlin et al., 2016). Magnetite-bearing high-temperature Ca-Fe and K-Fe alteration with copper-sulphide mineralization occurs locally in the southwestern part of the horst (McLaughlin et al., 2016), within the deeper parts of the fault-bounded synclinorium that formed after tectonic inversion of the sedimentary rift basin and its mafic rocks, followed by normal faulting and exhumation (Konstantinovskaya et al., 2019). In contrast to Great Bear magmatic zone systems, a regular prograde transition across all facies and development of skarn, K-felsite, and K-skarn is not observed in the horst. Syntectonic and likely synmetasomatic magma emplacement of a batholith is only observed

tens of kilometres east of the Romanet Horst, although a few alkaline intrusions occur within the horst (Clark and Wares, 2004). Hence, the Romanet IOAA system seems to be missing coeval magmatism to sustain a high geothermal gradient. In association with tectonic activity, fluids could thus cool rapidly, leading to extensive overprints of early albitite by lower temperature alteration and metal precipitation. Similar types of gold-cobalt mineralized iron oxide-poor overprints on albitite (i.e. abundant chlorite) are widespread at the Scadding deposit in the Wanapitei Lake district (Yarie and Wray, 2019; Corriveau et al., 2022c).

Compilation of public and private sector geochemical data from the Central Mineral Belt of Labrador (Acosta-Góngora et al., 2018a) combined with data sets from the Romanet Horst (L. Corriveau and J.-F. Montreuil, unpub. data, 2014) and the Great Bear magmatic zone (Corriveau et al., 2015) permitted comparisons of Canadian settings with deposits from the Olympic Cu-Au Province in Australia, including the Olympic Dam deposit, in collaboration with the Bureau de Recherches Géologiques et Minières, the Geological Survey of South Australia and BHP-Olympic Dam. The Central Mineral Belt in Labrador (Fig. 1, 2) hosts multiple U±Cu±Mo±REE showings, prospects, and deposits (e.g. Michelin) in metamorphosed and variably hydrothermally altered Neoproterozoic to Mesoproterozoic, igneous and sedimentary rocks (Gower et al., 1982; Ryan, 1984; Kerr, 1994; Wilton, 1996; Sparkes and Kerr, 2008; Sparkes et al., 2016; Sparkes, 2017); however, the genetic link between regional- to deposit-scale metasomatic-hydrothermal alteration and the relationship to the U±Cu±Mo±REE mineralization remains poorly understood (Potter et al., 2016). Petrographic and geochemical data indicate that the regional-scale Na metasomatism predates the U±Cu±Mo±REE mineralization (Acosta-Góngora et al., 2019). In most cases, mineralization is constrained to later, structurally controlled hydrothermal alteration (e.g. high-temperature Ca-Fe and K-Fe), consistent with IOAA ore systems worldwide. The application of unsupervised machine-learning techniques (Acosta-Góngora et al., 2019) to geochemical data has also proven to be a useful tool in characterizing the alteration, identifying distinct types of uranium mineralization, as well as identifying new types of mineralization. In situ major- and trace-element analysis of uraninite grains from various occurrences indicates that high-temperature metasomatic fluids (>350°C) were responsible for primary uranium mineralization (Duffett, 2019; Duffett et al., 2020); however, distinct uraninite populations and geochronology record remobilization of metals by lower temperature hydrothermal fluids driven by felsic intrusive activity associated with younger orogenies. Using the molar barcodes and alteration facies, the Central Mineral Belt chemical footprints exhibit similarities with IOAA systems that form uranium and Au-Co±U deposits within albitite as well as IOCG mineralization in later K-Fe facies, with primary or early metal endowment remobilized during subsequent orogenesis and intrusive events. The molar barcodes of the Central Mineral Belt commonly include a low-temperature Ca-Mg-Fe alteration

of albitite, interpreted as low-temperature chlorite and carbonate alteration, veining, and breccia infilling of earlier albitite zones. Such low-temperature overprints can occur during prograde evolution of the systems, where albitite zones are uplifted and replaced by the low-temperature component of the fluid column, or during subsequent orogenic or magmatic activity. Compilations of industry and government geophysical surveys across the belt have provided a baseline for further research (Oneschuk et al., 2019a, b, c, d, e, f). The geological, metasomatic, and mineralization characteristics of the Great Bear magmatic zone and Central Mineral Belt also closely match the geological exploration criteria and footprint of magmatic fluid-driven mineralizing systems with high potential for world-class deposits presented by Skirrow (2010) for the Gawler Craton, which hosts the Olympic Cu-Au Province and Olympic Dam deposit (see Table 1 for a list of the criteria as applied to the Great Bear magmatic zone).

Collaboration with private sector and academia has shown that IOAA systems form a continuum with porphyry, epithermal, and polymetallic vein deposit types, significantly increasing the mineral potential of terranes prospective for IOCG deposits (Mumin et al., 2007, 2010; Somarin and Mumin, 2012, 2014; Corriveau et al., 2014; McLaughlin et al., 2016). In addition, the elevated uranium contents of pre- to post-IOAA volcanic and intrusive rocks have provided sources for primary as well as remobilized uranium mineralization (Somarin and Mumin, 2012; Ootes et al., 2013; Gandhi et al., 2018; Potter et al., 2019). The size, intensity of alteration, and extreme variety of potential metal endowments and deposit types in the documented mineral systems of the Great Bear magmatic zone rival those of world-class IOCG deposits. Although current knowledge does not permit accurate predictions of metal endowment (exploration is required for that), the development of the model has outlined more prospective settings in eastern Canada (e.g. Baldwin, 2019; Conliffe, 2019; Piette-Lauzière et al., 2019) and expanded exploration to high-grade metamorphic terranes (Corriveau et al., 2010a, 2018a; Corriveau and Spry, 2014; Trapy, 2018).

SPECIAL PUBLICATIONS THROUGH INTERNATIONAL COLLABORATIONS

Joint United States Geological Survey–GSC publication

Collaborations between the United States Geological Survey (USGS) and GSC, under the USGS Mineral Resources Program initially involved field examination of the Missouri district in light of the GEM results from the Great Bear magmatic zone. Joint research (e.g. Corriveau et al., 2017) led to the publication of a special issue of the journal *Economic Geology*, with 15 papers focused on the

geology and mineral deposits of Proterozoic IOAA systems in the St. Francois Mountains terrane of southeast Missouri, United States, and in the Great Bear magmatic zone of the Northwest Territories (Slack et al., 2016). Both metallogenic provinces are mostly unmetamorphosed, and deformational effects are minimal (except along the Wopmay fault zone in the Great Bear magmatic zone), even though they formed within Proterozoic pericratonic continental arcs.

Extensive U-Pb, Re-Os, and Ar/Ar geochronology of IOA deposits, REE-rich breccia pipes and volcanic host rocks in the southeast Missouri district have documented the coeval nature of volcanism, IOA, and IOCG mineralization as observed in the Great Bear magmatic zone (Ayuso et al., 2016; Day et al., 2016; Montreuil et al., 2016a, c; Neymark et al., 2016; Slack et al., 2016). Hofstra et al. (2016) documented the role of mafic magmatism in generating some of the isotopic and rare-gas signatures in Missouri, a role considered important in generating the A-type magmatism common to IOAA systems, which is a type of magmatism also observed in the Great Bear magmatic zone (Ootes et al., 2013, 2017).

Aleynikoff et al. (2016) and Harlov et al. (2016) demonstrated that REE-minerals precipitate within IOA deposits, but that higher REE ore grades form through remobilization of original REE endowment of IOA deposits during later stage fluid circulation related to subsequent magmatic events. Some of the remobilization processes observed in Missouri were also observed locally within the Great Bear magmatic zone (Normandeau et al., 2018). In addition, remobilization of original REE endowment of the Josette IOA deposit during orogenesis also led to potential REE ore (Sappin and Perreault, 2021; Corriveau et al., 2022a). These studies help explain why, in the Great Bear magmatic zone, high REE contents occur most commonly along the reworked IOAA systems of the Wopmay fault zone (e.g. Jackpot, Ham, and JLD prospects; Table 1; Fig. 3a; Corriveau et al., 2015).

Johnson et al. (2016) documented that, in addition to magmatic fluids, other fluids were also sourced from volcanic lake water (i.e. evaporated meteoric water mixed with volcanic gases). Calderas were considered a key factor in the generation of IOA and IOCG deposits in early models based on the geology of the Missouri district (Kisvarsanyi, 1981; Hauck, 1990) and are now resurfacing as a key component in the development of IOA and IOCG deposits (Ovalle et al., 2018; Schlegel et al., 2018, 2020). Considering these results, discovery of a localized stromatolite-bearing carbonate unit possibly deposited from a saline caldera lake at Grouard Lake in the Great Bear magmatic zone warrants further study.

By 2016, United States Geological Survey research had yet to discover albitite corridors in the Missouri district (Day et al., 2016; McCafferty et al., 2016). In contrast, extensive albitite corridors occur in the Great Bear magmatic zone and are considered a prerequisite in the development of

IOAA systems (Hildebrand, 1986; Montreuil et al., 2015; Corriveau et al., 2016, 2022d, c). The distinctive physical properties of albitite and large spatial extent of the zones produce widespread low-magnetic and low-density regions that present distinguishing characteristics in magnetic and gravity surveys (Montreuil et al., 2015; Enkin et al., 2016; Hayward et al., 2016). These results enabled McCafferty et al. (2019) to identify a zone of potential albitite at depth in the southeast Missouri metallogenic province.

Collaboration with the United States Geological Survey was furthered under the Critical Mineral Mapping Initiative and expanded to include Geoscience Australia, leading to reclassification of IOCG and affiliated deposits within a broader global deposit-type classification (Hofstra et al., 2021).

GSC collaboration with France, Australia, and China

To further the understanding of IOAA systems as well as the development of chemical tools for, and their application to, exploration, geological mapping, and mineral-potential mapping, the GSC worked with colleagues from Canadian, French, Australian, and Moroccan geological surveys and government (e.g. Clark et al., 2010; Pelleter et al., 2010; Skirrow, 2010, 2022; Blein et al., 2022; Fabris, 2022; Katona and Fabris, 2022; Potter et al., 2022), academia (e.g. Beaudoin and Dupuis, 2010; Daliran et al., 2010, 2022; Jébrak, 2010, 2022; Mumin et al., 2010; Chen and Zhao, 2022; Zhao et al., 2022), and the private sector (e.g. Lobo-Guerrero, 2010; Williams, 2010a, b) to produce two special volumes on IOCG and affiliated deposits (Corriveau and Mumin, 2010; Corriveau et al., 2022e). The 16 papers in Special Paper 52 of the Geological Association of Canada document mineral systems with IOCG and affiliated deposits globally, and more specifically outline the geological settings, alteration facies, breccia, and mineral chemistry using the Olympic Cu-Au Province and Cloncurry district (Australia), the Great Bear magmatic zone (Canada), the Central Andes (South America), the Bafq district (Iran), and the Kangdian district and Middle-lower Yangtze River metallogenic belt (China) as prime examples. Complementary information is sourced from the Norrbotten district (Sweden), Bayan Obo deposit, and Eastern Tianshan and Junggar districts (China), and Central Mineral Belt, Wanapitei Lake district, and Romanet Horst (Canada).

CONCLUDING REMARKS

The alteration facies-based mineral system model, alteration indices, and associated geochemical discriminant plot and molar barcodes developed in the course of the GEM and TGI programs now frame the extraordinary range of iron oxide-apatite, skarn, magnetite to hematite-group IOCG, iron-rich Au-Co-Bi-Cu, K-skarn, albitite-hosted uranium

and Au, Co, and U, five-element vein, and polymetallic vein-type deposits in a regional- to deposit-scale ore system. Case examples from Canada compare well with global analogues and have confirmed that additional types of deposits form within IOCG provinces, including those enriched in critical metals. Using alteration facies as metal pathways, practical alteration-mapping protocols were defined and combined with a consistent scientific language and tools such as cobaltinitrate staining, hand-held gamma-ray spectrometers, and magnetic susceptibility meters to map the extraordinary variety of mineral assemblages, morphologies, textures, structures, intensity of alteration, and space-time relationships among alteration, vein, breccia, host rocks, magmatism, and tectonic activity related to the genesis of IOCG and affiliated deposits. Large data sets of geochemical analyses were also published from two districts. In addition, mineral indicators for IOCG and affiliated deposits were significantly expanded, compared with global data sets, and supported by till geochemistry studies. Measurements of the physical properties of rocks (magnetic susceptibility, density, conductivity, porosity) significantly expanded global data sets, optimized geophysical data interpretation, contributed to novel modelling of mineral prospectivity, and allowed the identification of new targets ranging in size from deposit to province scales.

Knowledge gained during the GEM and TGI programs contributed to land-use planning through partnership with the Tłı̨ch̨o First Nations, renewed interest in exploring the Great Bear magmatic zone (Bowdidge et al., 2014; Fortune Minerals Limited, 2019, 2021), led to the development of exploration tools, and expanded knowledge of these systems through industry-focused short courses on IOCG and affiliated deposits nationally and internationally, and through publication of short-course volumes (e.g. Corriveau and Mumin, 2010), special volumes (Slack et al., 2016; Corriveau et al., 2022e), and scientific papers in collaboration with world experts from government, academia, and the private sector.

ACKNOWLEDGMENTS

The GEM IOCG/Great Bear project was achieved through close and sustained collaboration between the Geological Survey of Canada, the Northwest Territories Geological Survey (Central Wopmay Mapping Project), First Nations governments, academia, and private sector, as well as northern communities, governments, and organizations. The project conducted all its engagement activities through the leadership of the Northwest Territories Geological Survey. Collaboration with Northwest Territories Geological Survey geologists and managers also involved shared fieldwork and project implementation, liaison with Northwest Territories organizations, organization of courses for fieldwork, and joint scientific publications and presentations. The GEM program scientists also collaborated closely

with the Tłı̨ch̨o Government and the Sahtu Government, including through meetings and discussions with Tłı̨ch̨o and Sahtu First Nations land-use planners, Dillon Consulting, Wek'èezhii Land and Water Board representatives, Protected Areas Strategy Coordinators, and Traditional Knowledge Researchers. Formal collaborative agreements were implemented with the Community Government of Gamèti and Fortune Minerals Limited. During GEM-2, research related to the Romanet Horst was conducted through formal agreements with Energizer Resources Inc. and Honey Badger Exploration Inc.

The authors sincerely thank all project participants and managers from the GSC and Northwest Territories Geological Survey, in particular project co-leaders Kathleen Lauzière (GSC) and Val Jackson (formerly at the Northwest Territories Geological Survey), as well as Simon Hanmer, Daniel Lebel, Caroline Relf, Yves Michaud, Scott Cairns, and John Ketchum. They also wish to express their gratitude to the First Nations field assistants and cook, and the university students who joined them in the field; the Community Government of Gamèti and Whatì; the Tłı̨ch̨o Government and their Land Protection Department and Traditional Knowledge Researcher; the Jean Wettrade Gamèti School teachers and students; the Sahtu Government (including the Déline Land Corporation, the Déline Renewable Resource Council, the Sahtu Renewable Resource Board, and the Sahtu Secretariat Incorporated); and all other members of the First Nations, who provided vision, traditional and cultural knowledge, and significant input to the fieldwork as well as constantly following the project's scientific progress, never missing an opportunity to increase their knowledge and understand all the information provided in order to make informed decisions. The authors also thank the nearly one hundred Tłı̨ch̨o and Sahtu youths, elders, teachers, and other community members, who attended talks during the project community visits prior to the four field seasons of the GEM IOCG/Great Bear project. Their attendance and interest were extremely meaningful to, and gratifying for, the project participants. The authors are also grateful to members of the North Slave Métis Alliance, the Yellowknives Dene First Nation–Land and Environment, the Akaitcho Territory Government, and the City of Yellowknife for their interest in the GEM Great Bear/IOCG project.

The TGI metasomatic uranium project and current TGI MIAC research would not have been possible without the directions of Christine Hutton, Kathleen Lauzière, Geneviève Marquis, Yves Michaud, and Mike Villeneuve. The earlier TGI Deep Search research in the Great Bear magmatic zone was made possible by Daniel Lebel, John Lydon, and Wayne Goodfellow. Research in the Central Mineral Belt and Romanet Horst benefited from discussions and collaboration with colleagues of the Newfoundland and Labrador Geological Survey, in particular Greg Sparkes, James Conliffe, and Andy Kerr, as well as private sector collaborators.

Twelve universities across Canada and internationally conducted complementary research, in some cases funded by the Research Affiliate Program of Natural Resources Canada, but in most cases using their own research funds: INRS-ETE and the universities of Brandon, Alberta, McGill, McMaster, Laval, Iowa State, Western Ontario, Windsor, British Columbia, and Carleton. Private sector collaborators, in particular Fortune Minerals Limited, Diamonds North Resources Limited, Alberta Star Development Corporation, Honey Badger Exploration, NextSources Materials, Denendeh Exploration and Minerals Company (DEMCo) Limited, Hunter Bay Minerals Plc, and Cooper Minerals Inc. hosted some of the GEM and TGI crew, provided significant logistical support and in-kind funding, and/or donated proprietary geophysical and geochemical data and maps. The authors particularly appreciated the help provided by Fortune Minerals Limited, who included GEM program IOCG crew members within their own land-use permit renewal, enabling fieldwork in addition to providing free lodging, cooking, and office work facilities as well as sharing costs whenever possible, thus significantly increasing GEM outcomes, while respecting each other's mandates. Covello Consulting, Aurora Geosciences, GeoVector Management, Ivanhoe Australia, Clump Mountain Consulting (Patrick Williams), BHP-Olympic Dam, the Geological Survey of South Australia, as well as J. Clark, K. Ehrig, A. Fabris, S. Gandhi, R. Hildebrand, A.H. Mumin, A. Reid, and X.-F. Zhao were very helpful in broadening project participants' knowledge on the Great Bear magmatic zone, and Chinese and Australian IOCG districts, including during extensive visits to China and Australia. Overburden Drilling Management Limited (Nepean, Ontario) processed samples for drift-prospecting research, geochronology, and mineral chemistry. Knowledge transfer was greatly facilitated through the registration of hundreds of companies to the GEM- and TGI-related IOCG short courses and the keen interest of land-use planners associated with the Sahtu Land Use Plan, Tẖçẖ Land Use Plan, Great Bear Lake Watershed Management Plan, Taidene Nënë National Park Reserve, and Edaíjla Area of Interest within the Northwest Territories Protected Areas Strategy.

Several territorial and federal government agencies helped the project, including the Resource Management Office and Contaminants and Remediation Directorate of Indian and Northern Affairs Canada, Wek'èzhii Land and Water Board, Northwest Territories Geoscience Office of the Government of the Northwest Territories, (former) Indian and Northern Affairs Canada, Polar Continental Shelf, Prince of Wales Northern Heritage Centre, Aurora Research Institute, Environment and Natural Resources of the Government of the Northwest Territories, and archaeological database licencing office. Given the complex nature of fieldwork in the North, the authors acknowledge the professionalism of their amazing expeditor, Discovery Mining Services, as well as Air Tindi, Arctic Sunwest Charters, Aurora Geosciences, Great Slave Helicopter, Manitoulin Transport, Norpo Construction Limited, Tli Cho Landtran Limited, and Weaver and Devore Trading. The participation

of other government agencies, academia, and members of the private sector that have collaborated to the interpretation of the data or to the short courses, such as BHP-Olympic Dam, Bureau de Recherches Géologiques et Minières, Geological Survey of South Australia, Geoscience Australia, IFREMER (Institut Français de Recherche pour l'Exploitation de la Mer), Instituto Geológico y Minero de España, and Red Pine Exploration, is also appreciated.

Field-based research in the Great Bear magmatic zone was permitted under the Aurora Research Institute (Research Licence No. 14844, No. 14639, and No. 14548), whereas fieldwork was conducted under land-use permits (Class A number W2010J0004 and in part on W2009C0001 permit to Fortune Minerals Limited) granted by the Wek'èzhii Land and Water Board, in accordance with the Mackenzie Valley Resource Management Act, and followed all laws and regulations under this permitting process (fuel caching, waste disposal, water usage, engagement report, end of project report, etc.). The Northwest Territories archeological sites database agreements for fieldwork were No. DR2010–390 and No. DR2009–335, and field logistics were in part provided under the Polar Continental Shelf Program projects 010009, 50709, and 00410. Potential archeological sites were reported to the Land and Resources Manager and a Traditional Knowledge Researcher of the Tẖçẖ Government as well as to the Assessment Archaeologist of the Prince of Wales Northern Heritage Centre.

The authors thank Anthony Reid of the Geological Survey of South Australia, Dawn Kellett and Kathleen Lauzière from the Geological Survey of Canada, and Val Jackson, retired from the Northwest Territories Geological Survey, for their thorough reviews as well as Marie-France Dufour, scientific editor, for clarifying the text of this contribution. Their insightful comments were much appreciated.

REFERENCES

- Aber Resources Ltd., 1993. DeVries Lake property: reconnaissance mapping and prospecting; Northwest Territories Geoscience Office, Assessment Report 083158, 2 maps.
- Acosta-Góngora, P., 2014. Origins and geochemical characterization of the iron oxide-copper-gold deposits in the Great Bear magmatic zone, N.W.T., Canada; Ph.D. thesis, University of Alberta, Edmonton, Alberta, 283 p.
- Acosta-Góngora, P., Gleeson, S., Ootes, L., Jackson, V.A., Lee, M., and Samson, I., 2011. Preliminary observations on the IOCG mineralization at the DAMP, Fab, and Nori showings and Terra-Norex mines, Great Bear magmatic zone; Northwest Territories Geoscience Office, NWT Open Report 2011-001, 11 p.
- Acosta-Góngora, P., Gleeson, S.A., Samson, I., Ootes, L., and Corriveau, L., 2014. Trace element geochemistry of magnetite and its relationship to mineralization in the Great Bear magmatic zone, N.W.T., Canada; *Economic Geology*, v. 109, p. 1901–1928. <https://doi.org/10.2113/econgeo.109.7.1901>

- Acosta-Góngora, G.P., Gleeson, S.A., Samson, I., Ootes, L., and Corriveau, L., 2015a. Gold refining by bismuth melts in the iron oxide-dominated NICO Au-Co-Bi (\pm Cu \pm W) deposit, N.W.T., Canada; *Economic Geology*, v. 110, p. 291–314. <https://doi.org/10.2113/econgeo.110.2.291>
- Acosta-Góngora, P., Gleeson, S., Samson, I., Corriveau, L., Ootes, L., Taylor, B.E., Creaser, R.A., and Muehlenbachs, K., 2015b. Genesis of the Paleoproterozoic NICO iron oxide-cobalt-gold-bismuth deposit, Northwest Territories, Canada: evidence from isotope geochemistry and fluid inclusions; *Precambrian Research*, v. 268, p. 168–193. <https://doi.org/10.1016/j.precamres.2015.06.007>
- Acosta-Góngora, P., Duffett, C., Sparkes, G.W., and Potter, E.G., 2018a. Central Mineral Belt uranium geochemistry database, Newfoundland and Labrador; Geological Survey of Canada, Open File 8352, 8 p. <https://doi.org/10.4095/306562>
- Acosta-Góngora, P., Gleeson, S., Samson, I., Corriveau, L., Ootes, L., Jackson, S.E., Taylor, B.E., and Girard, I., 2018b. Origin of sulfur and crustal recycling of copper in polymetallic (Cu-Au-Co-Bi-U \pm Ag) iron-oxide-dominated systems of the Great Bear magmatic zone, N.W.T., Canada; *Mineralium Deposita*, v. 53, p. 353–376. <https://doi.org/10.1007/s00126-017-0736-6>
- Acosta-Góngora, P., Potter, E.G., Corriveau, L., Lawley, C.J.M., and Sparkes, G.W., 2019. Geochemistry of U \pm Cu \pm Mo \pm V mineralization, Central Mineral Belt, Labrador: differentiating between mineralization styles using a principal component analysis approach; *in Targeted Geoscience Initiative: 2018 report of activities*, (ed.) N. Rogers; Geological Survey of Canada, Open File 8549, p. 381–391. <https://doi.org/10.4095/313673>
- Alberta Star Development Corp., 2006. Alberta Star drilling intersects 42.0 gr/ton silver (Ag) over 9.9 meters (32.5 feet) and a new high grade poly-metallic discovery at Contact Lake; Alberta Star Development Corporation, news release, November 16, 2006. <www.sedar.com> [accessed January 11, 2022]
- Alberta Star Development Corp., 2007. Alberta Star achieves up to a 93% uranium recovery rate on gravity separation methods from the Eldorado silver & uranium tailings; Alberta Star Development Corporation, press release, April 30, 2007. <<https://elyseedevelopment.com/news/2007/alberta-star-achieves-up-to-a-93-uranium-recovery-rate-on-gravity-separation-methods-from-the-eldorado-silver-uranium-tailings/>> [accessed October 1, 2021]
- Aleinikoff, J.N., Selby, D., Slack, J.F., Day, W.C., Pillers, R.M., Cosca, M.A., Seeger, C.M., Fanning, C.M., and Samson, I.M., 2016. U-Pb, Re-Os, and Ar/Ar geochronology of REE-rich breccia pipes and associated host rocks from the Mesoproterozoic Pea Ridge Fe-REE-Au deposit, St. Francois Mountains, Missouri; *in Proterozoic iron oxide-apatite (\pm REE) and iron oxide-copper-gold and affiliated deposits of Southeast Missouri, U.S.A., and the Great Bear magmatic zone, Northwest Territories Canada*, (ed.) J. Slack, L. Corriveau, and M. Hitzman; *Economic Geology*, v. 111, p. 1883–1914.
- Apukhtina, O.B., Kamenetsky, V.S., Ehrig, K., Kamenetsky, M.B., Maas, R., Thompson, J., McPhie, J., Ciobanu, C.L., and Cook, N.J., 2017. Early, deep magnetite-fluorapatite mineralization at the Olympic Dam Cu-U-Au-Ag deposit, South Australia; *Economic Geology*, v. 112, p. 1531–1542. <https://doi.org/10.5382/econgeo.2017.4520>
- Arbuckle, B., Breen, W., Katsuragi, C., and Mumin, A.H., 2015a. Port Radium geology; Sheet 4 *in* Echo Bay IOCG thematic map series: geology, structure and hydrothermal alteration of a stratovolcano complex, Northwest Territories, Canada, (ed.) A.H. Mumin; Geological Survey of Canada, Open File 7807, 19 p., scale 1:3500. <https://doi.org/10.4095/296608>
- Arbuckle, B., Breen, W., and Mumin, A.H., 2015b. Contact Plateau geology; Sheet 11 *in* Echo Bay IOCG thematic map series: geology, structure and hydrothermal alteration of a stratovolcano complex, Northwest Territories, Canada, (ed.) A.H. Mumin; Geological Survey of Canada, Open File 7807, 19 p., scale 1:4000. <https://doi.org/10.4095/296615>
- Arbuckle, B., Breen, W., and Mumin, A.H., 2015c. Richardson pluton uranium anomaly; Sheet 17 *in* Echo Bay IOCG thematic map series: geology, structure and hydrothermal alteration of a stratovolcano complex, Northwest Territories, Canada, (ed.) A.H. Mumin; Geological Survey of Canada, Open File 7807, 19 p., scale 1:4000. <https://doi.org/10.4095/296621>
- Arbuckle, B., Etcheverry, D.J., Breen, W., and Mumin, H., 2015d. East Boundary Zone geology map; Sheet 6 *in* Echo Bay IOCG thematic map series: geology, structure and hydrothermal alteration of a stratovolcano complex, Northwest Territories, Canada, (ed.) A.H. Mumin; Geological Survey of Canada, Open File 7807, 19 p., scale 1:4000. <https://doi.org/10.4095/296610>
- Aspler, L.B., Pilkington, M., and Miles, W.F., 2003. Interpretations of Precambrian basement based on recent aeromagnetic data, Mackenzie Valley, Northwest Territories; Geological Survey of Canada, Paper 2003-C2, 11 p. <https://doi.org/10.4095/214184>
- Ayuso, R.A., Slack, J.F., Day, W.C., and McCafferty, A.E., 2016. Geochemistry, Nd-Pb isotopes, and Pb-Pb ages of the Mesoproterozoic Pea Ridge iron oxide-apatite-rare-earth element deposit, southeast Missouri, U.S.A.; *in Proterozoic iron oxide-apatite (\pm REE) and iron oxide-copper-gold and affiliated deposits of Southeast Missouri, U.S.A., and the Great Bear magmatic zone, Northwest Territories Canada*, (ed.) J. Slack, L. Corriveau, and M. Hitzman; *Economic Geology*, v. 111, p. 1935–1962.
- Azar, B., 2007. The lithogeochemistry of volcanic and subvolcanic rocks of the Fab Lake area, Great Bear magmatic zone, Northwest Territories, Canada; B.Sc. thesis, University of Toronto, Toronto, Ontario, 96 p.
- Babo, J., Spandler, C., Oliver, N., Brown, M., Rubenach, M., and Creaser, R.A., 2017. The high-grade Mo-Re Merlin deposit, Cloncurry District, Australia: paragenesis and geochronology of hydrothermal alteration and ore formation; *Economic Geology*, v. 112, p. 397–422.

- Badham, J.P.N., 1975. Mineralogy, paragenesis and origin of the Ag–Ni, Co arsenide mineralization, Camsell River, N.W.T., Canada; *Mineralium Deposita*, v. 10, p. 153–175. <https://doi.org/10.1007/BF00206530>
- Badham, J.P.N. and Morton, R.D., 1976. Magnetite-apatite intrusions and calc-alkaline magmatism, Camsell River, N.W.T.; *Canadian Journal of Earth Sciences*, v. 13, p. 348–354. <https://doi.org/10.1139/e76-037>
- Baker, T., Mustard, R., Fu, B., Williams, P.J., Dong, G., Fisher, L., Mark, G., and Ryan, C.G., 2008. Mixed messages in iron oxide-copper-gold systems of the Cloncurry district, Australia: insights from PIXE analysis of halogens and copper in fluid inclusions; *Mineralium Deposita*, v. 43, p. 599–608. <https://doi.org/10.1007/s00126-008-0198-y>
- Baldwin, G., 2019. The Highlands gold occurrences, eastern Cape Breton Highlands, Nova Scotia: an unrecognized IOCG district?; *Geological Association of Canada-Mineralogical Association of Canada, Abstracts*, v. 42, p. 58.
- Barton, M.D., 2014. Iron oxide(-Cu–Au–REE–P–Ag–U–Co) systems; *in Treatise on geochemistry (second edition)*, Volume 13, (ed.) H.D. Holland and K.K. Turekian; Elsevier, Amsterdam, Netherlands, p. 515–541.
- Beaudoin, G. and Dupuis, C., 2010. Iron oxides trace element fingerprinting of mineral deposit types; *in Exploring for iron oxide-copper-gold deposits: Canada and global analogues*, (ed.) L. Corriveau and A.H. Mumin; Geological Association of Canada, Short Course Notes 20, p. 111–125.
- Beaulieu, D., 2019. A Dene perspective on resource development in Canada for, by and among First Nations; *Geological Association of Canada–Mineralogical Association of Canada, Abstracts*, v. 42, p. 13.
- Benavides, J., Kyser, T.K., Clark, A.H., Stanley, C., and Oates, C.J., 2008. Exploration guidelines for copper-rich iron oxide-copper-gold deposits in the Mantoverde area, northern Chile: the integration of host-rock molar element ratios and oxygen isotope compositions; *Geochemistry: Exploration, Environment, Analysis*, v. 8, p. 343–367. <https://doi.org/10.1144/1467-7873/07-165>
- Bennett, V., Rivers, T., and Jackson, V., 2012. A compilation of U–Pb zircon preliminary crystallization and depositional ages from the Paleoproterozoic southern Wopmay orogen, Northwest Territories; *Northwest Territories Geoscience Office, NWT Open Report 2012-003*, 172 p.
- BHP, 2015. Annual report; BHP. <www.bhp.com/media-and-insights/reports-and-presentations/2015/09/2015-annual-reporting-suite> [accessed October 1, 2021]
- BHP, 2017. Annual report; BHP. <www.bhp.com/-/media/documents/investors/annual-reports/2017/bhpannualreport2017.pdf> [accessed October 1, 2021]
- BHP, 2018. BHP copper exploration program update, press release dated November 27th, 2018; BHP. <www.bhp.com/news/media-centre/releases/2018/11/bhp-copper-exploration-program-update> [accessed October 1, 2021]
- BHP, 2020. Annual report; BHP. <<https://www.bhp.com/-/media/documents/investors/annual-reports/2020/200915/bhpannualreport2020.pdf>> [accessed October 1, 2021]
- Blein, O. and Corriveau, L., 2017. Recognizing IOCG alteration facies at granulite facies in the Bondy gneiss complex of the Grenville Province; *in Proceedings of the 14th SGA Biennial Meeting; Society for Geology Applied to Mineral Deposits*, August 20–23, 2017, Québec, Quebec, p. 907–911.
- Blein, O., Corriveau, L., Montreuil, J.-F., Ehrig, K., Fabris, A., Reid, A., and Pal, D., 2022. Geochemical signatures of metasomatic ore systems hosting IOCG, IOA, albitite-hosted uranium and affiliated deposits: a tool for process studies and mineral exploration; *in Mineral systems with iron oxide-copper-gold (IOCG) and affiliated deposits*, (ed.) L. Corriveau, E.G. Potter, and A.H. Mumin; Geological Association of Canada, Special Paper 52, p. 263–298.
- Bowdidge, C. and Dunford, A., 2015. Camsell River property, Northwest Territories 86E09 and 86F12; *Northwest Territories Geological Survey, Assessment Report 033952*, 73 p.
- Bowdidge, C., Walker, E.C., and Dunford, A., 2014. DEMCo Ltd. report on 2014 exploration Camsell River property, NTS 86E09, 86F12, Northwest Territories, 117°55'18" to 118°09'44" West, 65°33'34" to 65°38'33" North; *Northwest Territories Geological Survey, Assessment Report 033596*, 110 p.
- Bretzlaff, R. and Kerswill, J.A., 2016. Mineral occurrences of the Great Bear magmatic zone; *Geological Survey of Canada, Open File 7959*, 7 p. <https://doi.org/10.4095/297587>
- Brimhall, G.H., Dilles, J.H., and Proffett, J.M., 2006. The role of geologic mapping in mineral exploration; Chapter 11 *in Wealth creation in the minerals industry: integrating science, business, and education*, (ed.) M.D. Doggett and J.R. Parry; Society of Economic Geologists, Special Publication, no. 12, p. 221–241.
- Burgess, H., Gowans, R.M., Hennessey, B.T., Lattanzi, C.R., and Puritch, E., 2014. Technical report on the feasibility study for the NICO gold–cobalt–bismuth–copper deposit, Northwest Territories, Canada; report prepared by Micon International Limited for Fortune Minerals Limited, National Instrument 43-101 Technical Report No. 1335, 385 p. <https://s1.q4cdn.com/337451660/files/doc_downloads/1335%20Nico%20Technical%20ReportLM.pdf> [accessed October 1, 2021]
- Burns, N., Davis, C., Diedrich, C., and Tagami, M., 2017. Salobo copper-gold mine, Carajás, Pará State, Brazil; report prepared for Wheaton Precious Metals Corporation, Technical Report, 126 p. <https://s21.q4cdn.com/266470217/files/doc_downloads/maps/salobo/Salobo-43-101-Dec-31-2017-FINAL.PDF> [accessed October 1, 2021]
- Byron, S.J., 2010. Giant quartz veins of the Great Bear magmatic zone, Northwest Territories, Canada; M.Sc. thesis, University of Alberta, Edmonton, Alberta, 146 p.
- Camier, J., 2002. The Sue-Dianne Fe-oxide Cu–Ag–Au breccia complex, southern Great Bear magmatic zone, Northwest Territories, Canada; M.Sc. thesis, University of Western Ontario, London, Ontario, 210 p.
- Carmichael, D., 1969. On the mechanism of prograde metamorphic reactions in quartz-bearing pelitic rocks; *Contributions to Mineralogy and Petrology*, v. 20, p. 244–267. <https://doi.org/10.1007/BF00377479>
- Carmichael, D., 1978. Metamorphic bathozones and bathograds: a measure of the depth of post-metamorphic uplift and erosion on the regional scale; *American Journal of Science*, v. 278, p. 769–797. <https://doi.org/10.2475/ajs.278.6.769>

- Centaurus Metals Limited, 2021. The Jaguar nickel sulphide project value-add scoping study, executive summary, May 2021; Centaurus Metals Limited, 39 p. <www.centaurus.com.au> [accessed June 28, 2021]
- Cernuschi, F., 2017. Integrated interpretation of Anaconda-style mapping and core logging, trace element geochemistry and short wave infrared spectroscopy for the exploration of porphyry copper deposits; Decennial Minerals Exploration Conferences (DMEC), workshop on Geochemical and infrared spectral mineralogical data integration for mineral exploration, October 27, 2017, Toronto, Canada, 41 p. <<http://www.dmecc.ca/Resources/Workshops/Geochemical-and-Infrared-Spectral-Data-Integration.aspx>> [accessed April 7, 2020]
- Chen, H. and Zhao, L., 2022. Iron oxide-copper-gold mineralization in the Central Andes: ore deposit geology and modelling; *in* Mineral systems with iron oxide-copper-gold (IOCG) and affiliated deposits, (ed.) L. Corriveau, E.G. Potter, and A.H. Mumin; Geological Association of Canada, Special Paper 52, p. 365–381.
- Cherry, A., Ehrig, K., Kamenetsky, V., McPhie, J., Crawley, J.L., and Kamenetsky, M., 2018. Precise geochronological constraints on the origin, setting and incorporation of ca. 1.59 Ga surficial facies into the Olympic Dam breccia complex, South Australia; *Precambrian Research*, v. 315, p. 162–178. <https://doi.org/10.1016/j.precamres.2018.07.012>
- Chorlton, L.B. (comp.), 2007. Generalized geology of the world: bedrock domains and major faults in GIS format; Geological Survey of Canada, Open File 5529, 48 p. <https://doi.org/10.4095/223767>
- Clark, D.A., 2014. Magnetic effects of hydrothermal alteration in porphyry copper and iron-oxide copper-gold systems: a review; *Tectonophysics*, v. 624–625, p. 46–65. <https://doi.org/10.1016/j.tecto.2013.12.011>
- Clark, T., and Wares, R., 2004. Synthèse lithotectonique et métallogénique de l'Orogène du Nouveau-Québec (Fosse du Labrador); Ministère des Ressources naturelles et de la Faune, Québec, Canada, MM 2004-01, 177 p.
- Clark, T., Gobeil, A., and Chevé, S., 2010. Alterations in IOCG-type and related deposits in the Manitou Lake area, Eastern Grenville Province, Québec; *in* Exploring for iron oxide copper-gold deposits: Canada and global analogues, (ed.) L. Corriveau and A.H. Mumin; Geological Association of Canada, Short Course Notes 20, p. 127–146.
- Conliffe, J., 2019. Possible iron-sulphide copper-gold mineralization in western Labrador, and the potential for IOCG exploration in the Labrador Trough; Geological Association of Canada–Mineralogical Association of Canada, Abstracts, v. 42, p. 73.
- Corriveau, L., 2007. Iron oxide copper-gold deposits: a Canadian perspective; *in* Mineral deposits of Canada: a synthesis of major deposit-types, district metallogeny, the evolution of geological provinces, and exploration methods, (ed.) W. Goodfellow; Geological Association of Canada, Mineral Deposits Division, Special Volume 5, p. 307–328.
- Corriveau, L., 2013. Architecture de la ceinture métasédimentaire centrale au Québec, Province de Grenville : un exemple de l'analyse de terrains de métamorphisme élevé; *Commission géologique du Canada, Bulletin* 586, 264 p. <https://doi.org/10.4095/226449>
- Corriveau, L., 2017a. Iron-oxide and alkali-calcic alteration ore systems and their polymetallic IOA, IOCG, skarn, albitite-hosted U±Au±Co, and affiliated deposits: a short course series. Part 1: introduction; Geological Survey of Canada, Scientific Presentation 56, 80 p. <https://doi.org/10.4095/300241>
- Corriveau, L., 2017b. Les systèmes minéralisateurs à oxydes de fer et altération à éléments alcalins (±calciques) et leurs gîtes IOA, IOCG, skarns, U±Au±Co (au sein d'albitites) et affiliés: une série de cours intensifs. Partie 1: introduction; Commission géologique du Canada, Présentation scientifique 57, 67 p. <https://doi.org/10.4095/300242>
- Corriveau, L. and Mumin, A.H., 2010. Exploring for iron oxide copper-gold deposits: the need for case studies, classifications and exploration vectors; *in* Exploring for iron oxide copper-gold deposits: Canada and global analogues, (ed.) L. Corriveau and A.H. Mumin; Geological Association of Canada, Short Course Notes 20, p. 1–12.
- Corriveau, L. and Spry, P., 2014. Metamorphosed hydrothermal ore deposits; *in* Treatise on geochemistry (second edition), Volume 13, (ed.) H.D. Holland and K.K. Turekian; Elsevier, Amsterdam, Netherlands, p. 175–194.
- Corriveau, L., Perreault, S., and Davidson, A., 2007. Prospectivity of the Grenville Province: a perspective, *in* Mineral deposits of Canada: a synthesis of major deposit-types, district metallogeny, the evolution of geological provinces, and exploration methods, (ed.) W. Goodfellow; Geological Association of Canada, Mineral Deposits Division, Special Volume 5, p. 819–848.
- Corriveau, L., Mumin, A.H., and Setterfield, T., 2010a. IOCG environments in Canada: characteristics, geological vectors to ore and challenges; *in* Hydrothermal iron oxide copper-gold and related deposits: a global perspective, (ed.) T.M. Porter; Porter Geoscience Consultancy Publishing, Adelaide, Australia, v. 4, p. 311–344.
- Corriveau, L., Williams, P.J., and Mumin, H., 2010b. Alteration vectors to IOCG mineralization from uncharted terranes to deposits; *in* Exploring for iron oxide copper-gold deposits: Canada and global analogues, (ed.) L. Corriveau and A.H. Mumin; Geological Association of Canada, Short Course Notes 20, p. 89–110.
- Corriveau, L., Nadeau, O., Montreuil, J.-F., and Desrochers, J.-P., 2014. Report of activities for the Core Zone: strategic geomapping and geoscience to assess the mineral potential of the Labrador Trough for multiple metals IOCG and affiliated deposits, Canada; Geological Survey of Canada, Open File 7714, 12 p. <https://doi.org/10.4095/295529>
- Corriveau, L., Lauzière, K., Montreuil, J.-F., Potter, E.G., Hanes, R., and Prémont, S., 2015. Dataset of geochemical data from iron oxide alkali-altered mineralizing systems of the Great Bear magmatic zone (N.W.T.); Geological Survey of Canada, Open File 7643, 24 p. <https://doi.org/10.4095/296301>
- Corriveau, L., Montreuil, J.-F., and Potter, E.G., 2016. Alteration facies linkages among IOCG, IOA and affiliated deposits in the Great Bear magmatic zone, Canada; *in* Proterozoic iron oxide-apatite (± REE) and iron oxide-copper-gold and affiliated deposits of Southeast Missouri, U.S.A., and the Great Bear magmatic zone, Northwest Territories, Canada, (ed.) J. Slack, L. Corriveau, and M. Hitzman; *Economic Geology*, v. 111, p. 2045–2072. <https://doi.org/10.2113/econgeo.111.8.2045>

- Corriveau, L., Potter, E.G., Acosta-Góngora, P., Blein, O., Montreuil, J.-F., De Toni, A.F., Day, W.C., Slack, J.F., and Ayuso, R.A., 2017. Petrological mapping and chemical discrimination of alteration facies as vectors to IOA, IOCG, and affiliated deposits within Laurentia and beyond; Proceedings of the 14th SGA Biennial Meeting; Society for Geology Applied to Mineral Deposits, August 20–23, 2017, Québec, Québec, p. 851–855.
- Corriveau, L., Blein, O., Gervais, F., Trapy, P.H., De Souza, S., and Fafard, D., 2018a. Iron-oxide and alkali-calcic alteration, skarn and epithermal mineralizing systems of the Grenville Province: the Bondy gneiss complex in the Central Metasedimentary Belt of Quebec as a case example – a field trip to the 14th Society for Geology Applied to Mineral Deposits (SGA) biennial meeting; Geological Survey of Canada, Open File 8349, 136 p. <https://doi.org/10.4095/311230>
- Corriveau, L., Potter, E.G., Montreuil, J.-F., Blein, O., Ehrig, K., and De Toni, A., 2018b. Iron-oxide and alkali-calcic alteration ore systems and their polymetallic IOA, IOCG, skarn, albitite-hosted U±Au±Co, and affiliated deposits: a short course series. Part 2: overview of deposit types, distribution, ages, settings, alteration facies, and ore deposit models; Geological Survey of Canada, Scientific Presentation 81, 154 p. <https://doi.org/10.4095/306560>
- Corriveau, L., Potter, E.G., Montreuil, J.-F., Blein, O., Ehrig, K., and De Toni, A., 2018c. Les systèmes minéralisateurs à oxydes de fer et altération à éléments alcalins (±calciques), et leurs gîtes IOA, IOCG, skarns, U±Au±Co (au sein d'albitites) et affiliés : une série de cours intensifs. Partie–2 – aperçu général des types de gîtes, distribution, âges, contextes, exemples, faciès d'altération et modèles métallogéniques; Commission géologique du Canada, Présentation scientifique 87, 190 p. <https://doi.org/10.4095/308269>
- Corriveau, L., Potter, E.G., Montreuil, J.-F., Blein, O., Ehrig, K., and Fabris, 2019a. Alteration facies of IOA, IOCG and affiliated deposits: understanding the similarities, recognising the diversity in these ore systems; Geological Survey of South Australia, GSSA Iron Oxide – Copper-Gold Mineral Systems Workshop 2019, 77 p. <http://www.energymining.sa.gov.au/_data/assets/pdf_file/0004/358708/REDCorriveau_IOCGworkshop_Alteration_Final.pdf> [accessed October 21, 2021].
- Corriveau, L., Potter, E.G., Montreuil, J.-F., Blein, O., Ehrig, K., Fabris, A., and Reid, A.J., 2019b. Alteration facies in 'IOCG terranes': a global view on mineral systems with IOCG and affiliated deposit types; Geological Survey of South Australia, Discovery Day 2019. <https://energymining.sa.gov.au/_data/assets/pdf_file/0010/355933/Corriveau_Discovery_Day_Nov2019_FINALRED.pdf> [accessed October 21, 2021]
- Corriveau, L., Potter, E.G., Montreuil, J.-F., Blein, O., Ehrig, K., Fabris, A., and Reid, A.J., 2020. Alteration facies in 'IOCG terranes': a global view on mineral systems with IOCG and affiliated deposit types; Geological Survey of South Australia, Discovery Day 2019, video, 35 minutes. <www.energymining.sa.gov.au/minerals/knowledge_centre/conferences_and_events/gssa_discovery_day_2019> [accessed October 21, 2021].
- Corriveau, L., Montreuil, J.-F., Blein, O., Potter, E.G., Ansari, M., Craven, J., Enkin, R., Fortin, R., Harvey, B., Hayward, N., Kellett, D., Ouellet, M., Paradis, S., Regis, D., Sappin, A.-A., Tschirhart, V., Pélouin S., Easton, R.M., Maity, B.,... Zhao, X.F., 2021a. Metasomatic iron and alkali calcic (MIAC) system frameworks: a TGI-6 task force to help de-risk exploration for IOCG, IOA and affiliated primary critical metal deposits; Geological Survey of Canada, Scientific Presentation 127, 105 p. <https://doi.org/10.4095/329093>
- Corriveau, L., Montreuil, J.-F., Blein, O., Potter, E.G., Fabris, A., and Reid, A., 2021b. Mineral systems with IOCG and affiliated critical metal deposits: from field geology and litho-geochemistry to deposit model, then back to the field; Geological Survey of Queensland–University of Queensland Exploration Webinar Series, Critical Minerals Collaborations, Online Workshop, April 29, 2021. <https://smi.uq.edu.au/project/gsq-uq-webinar-series#CMC_29apr2021> [accessed October 21, 2021].
- Corriveau, L., Montreuil, J.-F., Blein, O., Ehrig, K., Potter, E.G., Fabris, A., and Clark, J., 2022a. Mineral systems with IOCG and affiliated deposits: part 2 – geochemical footprints; *in* Mineral systems with iron oxide-copper-gold (IOCG) and affiliated deposits, (ed.) L. Corriveau, E.G. Potter, and A.H. Mumin; Geological Association of Canada, Special Paper 52, p. 159–204.
- Corriveau, L., Montreuil, J.-F., De Toni, A.F., Potter, E.G., and Percival, J.B., 2022b. Mapping mineral systems with IOCG and affiliated deposits: a facies approach; *in* Mineral systems with iron oxide-copper-gold (IOCG) and affiliated deposits, (ed.) L. Corriveau, E.G. Potter, and A.H. Mumin; Geological Association of Canada, Special Paper 52, p. 69–111.
- Corriveau, L., Montreuil, J.-F., Potter, E.G., Blein, O., and De Toni, A.F., 2022c. Mineral systems with IOCG and affiliated deposits: part 3 – metal pathways and ore deposit model; *in* Mineral systems with iron oxide-copper-gold (IOCG) and affiliated deposits, (ed.) L. Corriveau, E.G. Potter, and A.H. Mumin; Geological Association of Canada, Special Paper 52, p. 205–246.
- Corriveau, L., Montreuil, J.-F., Potter, E.G., Ehrig, K., Clark, J., Mumin, A.H., and Williams, P.J., 2022d. Mineral systems with IOCG and affiliated deposits: part 1 – metasomatic footprints of alteration facies; *in* Mineral systems with iron oxide-copper-gold (IOCG) and affiliated deposits, (ed.) L. Corriveau, E.G. Potter, and A.H. Mumin; Geological Association of Canada, Special Paper 52, p. 113–158.
- Corriveau, L., Mumin, A.H., and Potter, E.G., 2022e. Mineral systems with iron oxide-copper-gold (Ag-Bi-Co-U-REE) and affiliated deposits: introduction and overview; *in* Mineral systems with iron oxide-copper-gold (IOCG) and affiliated deposits, (ed.) L. Corriveau, E.G. Potter, and A.H. Mumin; Geological Association of Canada, Special Paper 52, p. 1–25.
- Craven, J., Roberts, B., Hayward, N., Stefanescu, M., and Corriveau, L., 2013. A magnetotelluric survey and preliminary geophysical inversion and visualization of the NICO IOCG deposit, Northwest Territories; Geological Survey of Canada, Open File 7465, 26 p. <https://doi.org/10.4095/292869>

- Daliran, F., Stosch, H.-G., Williams, P.J., Jamali, H., and Dorri, M.-B., 2010. Lower Cambrian iron oxide-apatite-REE (U) deposits of the Bafq district, east-central Iran; *in* Exploring for iron oxide copper-gold deposits: Canada and global analogues, (ed.) L. Corriveau and A.H. Mumin; Geological Association of Canada, Short Course Notes 20, p. 147–159.
- Daliran, F., Stosch, H.-G., Williams, P.J., Jamali, H., and Dorri, M.-B., 2022. Early Cambrian IOA-REE, U/Th and Cu(Au)-Bi-Co-Ni-Ag-As-sulphide deposits of the Bafq district, East-Central Iran; *in* Mineral systems with iron oxide copper-gold (IOCG) and affiliated deposits, (ed.) L. Corriveau, E.G. Potter, and A.H. Mumin; Geological Association of Canada, Special Paper 52, p. 409–424.
- Davidson, G.J., Paterson, H., Meffre, S., and Berry, R.F., 2007. Characteristics and origin of the Oak Dam East breccia-hosted, iron oxide-Cu-U-(Au) deposit: Olympic Dam region, Gawler Craton, South Australia; *Economic Geology*, v. 102, p. 1471–1498. <https://doi.org/10.2113/gsecongeo.102.8.1471>
- Davis, W., Corriveau, L., van Breemen, O., Bleeker, W., Montreuil, J.-F., Potter, E.G., and Pelleter, E., 2011. Timing of IOCG mineralizing and alteration events within the Great Bear magmatic zone; *in* 39th Annual Yellowknife Geoscience Forum Abstracts, (comp.) B.J. Fischer and D.M. Watson; Northwest Territories Geoscience Office, YKGSF Abstracts Volume, v. 2011, p. 97.
- Davis, W.J., Ootes, L., Newton, L., Jackson, V.A., and Stern, R.A., 2015. Characterization of the Paleoproterozoic Hottah terrane, Wopmay orogen using multi-isotopic (U-Pb, Hf and O) detrital zircon analyses: an evaluation of linkages to northwest Laurentian Paleoproterozoic domains; *Precambrian Research*, v. 269, p. 296–310. <https://doi.org/10.1016/j.precamres.2015.08.012>
- Day, W.C., Slack, J.F., Ayuso, R.A., and Seeger, C.M., 2016. Regional geologic and petrologic framework for iron oxide±apatite±rare-earth element and iron oxide-copper-gold deposits of the Mesoproterozoic St. Francois Mountains terrane, southeast Missouri, U.S.A.; *in* Proterozoic iron oxide-apatite (± REE) and iron oxide-copper-gold and affiliated deposits of Southeast Missouri, U.S.A., and the Great Bear magmatic zone, Northwest Territories, Canada, (ed.) J. Slack, L. Corriveau, and M. Hitzman; *Economic Geology*, v. 111, p. 1825–1858.
- de Melo, G.H.C., Monteiro, L.V.S., Xavier, R.P., Moreto, C.P.N., and Santiago, E., 2019. Tracing fluid sources for the Salobo and Igarapé Bahia deposits: implications for the genesis of the iron oxide copper-gold deposits in the Carajás Province, Brazil; *Economic Geology*, v. 114, p. 697–718. <https://doi.org/10.5382/econgeo.4659>
- De Toni, A.F., 2016. Les paragéneses à magnétite des altérations associées aux systèmes à oxydes de fer et altérations en éléments alcalins, zone magmatique du Grand lac de l'Ours; M.Sc. thesis, Institut national de la recherche scientifique, Québec, Quebec, 534 p.
- Decrée, S., Marignac, C., De Putter, T., Yans, J., Clauer, N., Dermech, M., Aloui, K., and Baele, J.-M., 2013. The Oued Belif hematite-rich breccia: a Miocene iron oxide Cu-Au-(U-REE) deposit in the Nefza mining district, Tunisia; *Economic Geology*, v. 108, p. 1425–1457. <https://doi.org/10.2113/econgeo.108.6.1425>
- Duffett, C.L., 2019. The evolution of metasomatic uranium ore systems in the Central Mineral Belt of Labrador; M.Sc. thesis, Carleton University, Ottawa, Ontario, 147 p.
- Duffett, C.L., Potter, E., Petts, D.C., Acosta-Gongóra, P., Cousens, B.L., and Sparkes, G.W., 2020. The evolution of metasomatic uranium ore systems in the Kitts–Post Hill belt of the Central Mineral Belt, Labrador; *Ore Geology Reviews*, v. 126, art. 103720, <https://doi.org/10.1016/j.oregeorev.2020.103720>
- Dufréchu, G., 2011. Implications tectoniques de structures transverses profondes interprétées à partir de données de champ potentiel, Province de Grenville, Canada; Ph.D. thesis, Institut national de la recherche scientifique, Québec, Quebec, 333 p.
- Dufréchu, G., Harris, L.B., Corriveau, L., and Antonoff, V., 2011. Gravity evidence for a mafic intrusion beneath a mineralized zone in the Bondy gneiss complex, Grenville Province, Quebec — exploration implications; *Journal of Applied Geophysics*, v. 75, p. 62–76. <https://doi.org/10.1016/j.jappgeo.2011.06.029>
- Dufréchu, G., Harris, L.B., and Corriveau, L., 2014. Tectonic reactivation of transverse basement structures in the Grenville orogen of SW Quebec, Canada: insights from potential field data; *Precambrian Research*, v. 241, p. 61–84. <https://doi.org/10.1016/j.precamres.2013.11.014>
- Dufréchu, G., Harris, L.B., Corriveau, L., and Antonoff, V., 2015. Regional and local controls on mineralization and pluton emplacement in the Bondy gneiss complex, Grenville Province, Canada interpreted from aeromagnetic and gravity data; *Journal of Applied Geophysics*, v. 116, p. 192–205. <https://doi.org/10.1016/j.jappgeo.2015.03.015>
- Dupuis, C., Sappin, A.-A., Pozza, M., Beaudoin, G., McMartin, I., and McClenaghan, M.B., 2012. Iron oxide compositions in till samples from the Sue-Dianne IOCG deposit, Northwest Territories and the Pipe Ni-Cu deposit, Manitoba; *Geological Survey of Canada, Open File 7310*, 8 p. <https://doi.org/10.4095/292141>
- Ehrig, K. and Clark, J., 2019. Insights into the structural evolution of Olympic Dam — the not so boring billion...; South Australian Exploration and Mining Conference, 29 November 2019, Adelaide, Australia, 22 p. <http://saemc.com.au/archives/2019/2019_19.ehrig.pdf> [accessed January 14, 2022].
- Ehrig, K., McPhie, J., and Kamenetsky, V.S., 2012. Geology and mineralogical zonation of the Olympic Dam iron oxide Cu-U-Au-Ag deposit, South Australia, *in* Geology and genesis of major copper deposits and districts of the world: a tribute to Richard H. Sillitoe, (ed.) J.W. Hedenquist, M. Harris, and F. Camus; *Economic Geology, Special Publication 16*, p. 237–267.
- Ehrig, K., Kamenetsky, V.S., McPhie, J., Apukhtina, O., Ciabanu, C.L., Cook, N., Kontonikas-Charos, A., and Krneta, S., 2017a. The IOCG-IOA Olympic Dam Cu-U-Au-Ag deposit and nearby prospects, South Australia; *in* Proceedings of the 14th SGA Biennial Meeting; Society for Geology Applied to Mineral Deposits, August 20–23, 2017, Québec, Quebec, p. 823–827.

- Ehrig, K., Kamenetsky, V.S., McPhie, J., Apukhtina, O., Cook, N., and Ciabanu, C.L., 2017b. Olympic Dam iron oxide Cu-U-Au-Ag deposit; *in* Australian ore deposits, (ed.) G.N. Phillips; Australasian Institute of Mining and Metallurgy, Melbourne, Australia, p. 601–610.
- Ehrig, K., Kamenetsky, V.S., McPhie, J., Macmillan, E., Thompson, J., Kamenetsky, M., and Maas, R., 2021. Staged formation of the supergiant Olympic Dam uranium deposit, Australia; *Geology*, v. 49, p. 1312–1316. <https://doi.org/10.1130/G48930.1>
- Einaudi, M.T., 1997. Mapping altered and mineralized rocks: an introduction to the Anaconda method; Department of Geological and Environmental Sciences, Stanford University, Stanford, California, 16 p. <https://www.academia.edu/36501875/MAPPING_ALTERED_AND_MINERALIZED_ROCKS_an_introduction_to_THE_ANACONDA_METHOD> [accessed April 3, 2020].
- Elliott, B., Mumin, H., and Arbuckle, B., 2015a. Gossan Island geology; Sheet 7 *in* Echo Bay IOCG thematic map series: geology, structure and hydrothermal alteration of a stratovolcano complex, Northwest Territories, Canada, (ed.) A.H. Mumin; Geological Survey of Canada, Open File 7807, scale 1:2600. <https://doi.org/10.4095/296611>
- Elliott, B., Morin, P., and Mumin, H., 2015b. Hoy Bay hydrothermal alteration; Sheet 9 *in* Echo Bay IOCG thematic map series: geology, structure and hydrothermal alteration of a stratovolcano complex, Northwest Territories, Canada, (ed.) A.H. Mumin; Geological Survey of Canada, Open File 7807, scale 1:1800. <https://doi.org/10.4095/296613>
- Enkin, R., Montreuil, J.F., and Corriveau, L., 2012. Differential exhumation and concurrent fluid flow at the NICO Au–Co–Bi–Cu deposit and Southern Breccia U–Th–REE–Mo anomaly, Great Bear magmatic zone, N.W.T. — A paleomagnetic and structural record; Geological Association of Canada–Mineralogical Association Canada, Joint Annual Meeting, Program with Abstracts, v. 35, p. 41.
- Enkin, R., Corriveau, L., and Hayward, N., 2016. Metasomatic alteration control of petrophysical properties in the Great Bear magmatic zone (Northwest Territories, Canada), *in* Proterozoic iron oxide-apatite (\pm REE) and iron oxide-copper-gold and affiliated deposits of Southeast Missouri, U.S.A., and the Great Bear magmatic zone, Northwest Territories Canada, (ed.) J. Slack, L. Corriveau, and M. Hitzman; *Economic Geology*, v. 111, p. 2073–2085.
- Fabris, A., 2019. IOCG in the spotlight; MESA Journal, news article, August 2019. <www.energymining.sa.gov.au/minerals/knowledge_centre/mesa_journal/news/iocg_in_the_spotlight> [accessed August 23, 2021].
- Fabris, A., 2022. Geochemical characteristics of IOCG deposits: examples from the Olympic Copper-Gold Province, South Australia; *in* Mineral systems with iron oxide-copper-gold (IOCG) and affiliated deposits, (ed.) L. Corriveau, E.G. Potter, and A.H. Mumin; Geological Association of Canada, Special Paper 52, p. 247–262.
- Fabris, A.J., Halley, S., van der Wielen, S., Keeping, T., and Gordon, G., 2013. IOCG-style mineralisation in the central eastern Gawler Craton, SA; characterisation of alteration, geochemical associations and exploration vectors; Department for Innovation, Manufacturing, Trade, Resources and Energy, South Australia, Adelaide, Report Book 2013/00014, 56 p.
- Fabris, A., Katona, L., Gordon, G., Reed, G., Keeping, T., Gouthas, G., and Swain, G., 2018a. Characterisation and mapping of Cu–Au skarn systems in the Punt Hill region, Olympic Cu–Au Province; MESA Journal, v. 87, p. 15–27.
- Fabris, A., Katona, L., Gordon, G., Reed, G., Keeping, T., Gouthas, G., and Swain, G., 2018b. Characterising and mapping alteration in the Punt Hill region: a data integration project; Department of the Premier and Cabinet, South Australia, Adelaide, Report Book 2018/00010, 604 p.
- Ferreira Filho, C.F., Ferraz de Oliveira, M.M., Mansur, E.T., and Rosa, W.D., 2021. The Jaguar hydrothermal nickel sulfide deposit: evidence for a nickel-rich member of IOCG-type deposits in the Carajás Mineral Province, Brazil; *Journal of South American Earth Sciences*, v. 111, art. 103501.
- Fortier, S.M., Nassar, N.T., Lederer, G.W., Brainard, J., Gambogi, J., and McCullough, E.A., 2018. Draft critical mineral list — summary of methodology and background information — U.S. Geological Survey technical input document in response to Secretarial Order No. 3359; United States Geological Survey, Open-File Report 2018-1021, 15 p. <https://doi.org/10.3133/ofr20181021>
- Fortune Minerals Limited, 2019. Fortune Minerals announces new discovery at NICO; Fortune Minerals Limited, press release, July 18th, 2019. <www.fortuneminerals.com> [accessed January 20, 2020]
- Fortune Minerals Limited, 2021. Fortune Minerals announces start of NICO drill program; Fortune Minerals Limited, press release, September 23rd, 2021. <<https://www.fortuneminerals.com/news/press-releases/press-release-details/2021/Fortune-Minerals-Announces-Start-of-NICO-Drill-Program/default.aspx>> [accessed October 21, 2021].
- Froude, T., 2006. Uranium mineralization in the Moran Lake area of the central mineral belt of Labrador: new models and developments from the Crosshair Exploration project; *Atlantic Geology*, v. 42, no. 2-3, p. 189.
- Gagnon, R., Buro, Y.A., Ibrango, S., Gagnon, D., Stapinsky, M., Del Carpio, S., and Laroche, E., 2018. Projet de terres rares Kwijjibo; Rapport technique National Instrument 43-101 révisé, 292 p. <www.sedar.com> [accessed July 2, 2021].
- Gandhi, S.S., 1994. Geological setting and genetic aspects of mineral occurrences in the southern Great Bear magmatic zone, Northwest Territories; *in* Studies of rare-metal deposits in the Northwest Territories, (ed.) W.D. Sinclair and D.G. Richardson; Geological Survey of Canada, Bulletin 475, p. 63–96. <https://doi.org/10.4095/194031>
- Gandhi, S.S., 2013. Report on the geological and mineral occurrence map of the Mazenod Lake–Lou Lake area, Northwest Territories; Geological Survey of Canada, Open File 7546, 44 p. <https://doi.org/10.4095/293348>
- Gandhi, S.S. and van Breemen, O., 2005. SHRIMP U–Pb geochronology of detrital zircons from the Treasure Lake Group — new evidence for Paleoproterozoic collisional tectonics in the southern Hottah terrane, northwestern Canadian Shield; *Canadian Journal of Earth Sciences*, v. 42, p. 833–845. <https://doi.org/10.1139/e05-021>
- Gandhi, S.S., Carrière, J.J., and Prasad, N., 2000. Implications of a preliminary fluid-inclusion study of giant quartz veins of the Northwest Territories; Geological Survey of Canada, Paper 2000-1C, 13 p. <https://doi.org/10.4095/211152>

- Gandhi, S.S., Mortensen, J.K., Prasad, N., and van Breemen, O., 2001. Magmatic evolution of the southern Great Bear continental arc, northwestern Canadian Shield: geochronological constraints; *Canadian Journal of Earth Sciences*, v. 38, p. 767–785. <https://doi.org/10.1139/e00-094>
- Gandhi, S., Potter, E., and Fayek, M., 2013. Polymetallic U-Ag veins at Port Radium, Great Bear magmatic zone, Canada: main botryoidal pitchblende stage cuts 1.74 Ga diabase dykes and has REE signatures diagnostic of unconformity-type deposits; Geological Survey of Canada, Open File 7493, 1 poster. <https://doi.org/10.4095/293118>
- Gandhi, S.S., Montreuil, J.-F., and Corriveau, L., 2014. Geology and mineral occurrences, Mazenod Lake–Lou Lake area, Northwest Territories; Geological Survey of Canada, Canadian Geoscience Map 148 (preliminary edition), scale 1:50 000. <https://doi.org/10.4095/292918>
- Gandhi, S.S., Potter, E.G., and Fayek, M., 2018. New constraints on genesis of the polymetallic veins at Port Radium, Great Bear Lake, Northwest Canadian Shield; *Ore Geology Reviews*, v. 96, p. 28–47. <https://doi.org/10.1016/j.oregeorev.2018.04.002>
- Gebert, J.S., Jackson, J.E., and O’Neil, C.E., 2007. Eadilla area of interest non-renewable resources assessment (phase I) Great Bear Lake area, Northwest Territories, Parts of NTS 86K, 86L, 86M, 86N and 96I; Northwest Territories Geoscience Office, NWT Open File 2007-06, 56 p.
- Gifkins, C., Herrmann, W., and Large, R., 2005. Altered volcanic rocks: a guide to description and interpretation; Centre for Ore Deposit Research, University of Tasmania, Hobart, Australia, 275 p.
- Goad, R.E., Mumin, A.H., and Mulligan, D.L., 1996. A report on the geology of the JBG1-7 claims, Marian River area, Mackenzie (south) district, Northwest Territories, Canada; Northwest Territories Geoscience Office, NORMIN Assessment Report 083776, 89 p.
- Goad, R.E., Mumin, A.H., Duke, N.A., Neale, K.L., and Mulligan, D.L., 2000a. Geology of the Proterozoic iron oxide-hosted, NICO cobalt-gold-bismuth, and Sue-Dianne copper-silver deposits, southern Great Bear magmatic zone, Northwest Territories, Canada; *in* Hydrothermal iron oxide copper-gold and related deposits: a global perspective, (ed.) T.M. Porter; Porter Geoscience Consultancy Publishing, Adelaide, Australia, v. 1, p. 249–267.
- Goad, R.E., Mumin, A.H., Duke, N.A., Neale, K.L., Mulligan, D.L., and Camier, W.J., 2000b. The NICO and Sue-Dianne Proterozoic, iron oxide-hosted, polymetallic deposits, Northwest Territories. Application of the Olympic Dam model in exploration; *Exploration and Mining Geology*, v. 9, p. 123–140. <https://doi.org/10.2113/0090123>
- Gower, C.F., Flanagan, M.J., Kerr, A., and Bailey, D.G., 1982. Geology of the Kaipokok Bay–Big River area, Central Mineral Belt, Labrador; Newfoundland and Labrador Department of Mines and Energy, Mineral Development Division, Report 82-7, 77 p.
- Hamel, F., 2013. Processus d’altération aux échelles régionales, locales, mégascopiques de systèmes IOCG dans le nord de la zone magmatique du Grand lac de l’Ours; B.Sc. thesis, Université Laval, Québec, Québec, 66 p.
- Hamilton, M., 2017. Geology, structure and geochemistry of the Mazenod Lake volcanic complex, Canada; M.Sc. thesis, Brandon University, Brandon, Manitoba, 232 p. <<https://irbu.arcabc.ca/islandora/object/irbu%3A47>> [accessed January 11, 2022].
- Harlov, D.E., Meighan, C., Kerr, I., and Samson, I.M., 2016. Mineralogy, chemistry, and fluid-aided evolution of the Pea Ridge Fe-oxide-(Y+REE) deposit, southeast Missouri, U.S.A., *in* Proterozoic iron oxide-apatite (\pm REE) and iron oxide-copper-gold and affiliated deposits of Southeast Missouri, U.S.A., and the Great Bear magmatic zone, Northwest Territories Canada, (ed.) J. Slack, L. Corriveau, and M. Hitzman; *Economic Geology*, v. 111, p. 1963–1984.
- Harvey, B.J.A., Kiss, F., and Carson, J.M., 2009a. Geophysical Series, NTS 86-F/5 and 86-F/6, airborne geophysical survey of the northern Great Bear magmatic zone, Northwest Territories/Série des cartes géophysiques, SNRC 86-F/5 et 86-F/6, levé géophysique aéroporté de la partie nord de la zone magmatique du Grand lac de l’Ours, Territoires du Nord-Ouest; Geological Survey of Canada, Open File 6289, scale 1:50 000. <https://doi.org/10.4095/248271>
- Harvey, B.J.A., Kiss, F., and Carson, J.M., 2009b. Geophysical Series, NTS 86-F/7 and 86-F/8, airborne geophysical survey of the northern Great Bear magmatic zone, Northwest Territories/Série des cartes géophysiques, SNRC 86-F/7 et 86-F/8, levé géophysique aéroporté de la partie nord de la zone magmatique du Grand lac de l’Ours, Territoires du Nord-Ouest; Geological Survey of Canada, Open File 6290, scale 1:50 000. <https://doi.org/10.4095/248272>
- Harvey, B.J.A., Kiss, F., and Carson, J.M., 2009c. Geophysical Series, NTS 86-F/9 and 86-F/10, airborne geophysical survey of the northern Great Bear magmatic zone, Northwest Territories/Série des cartes géophysiques, SNRC 86-F/9 et 86-F/10, levé géophysique aéroporté de la partie nord de la zone magmatique du Grand lac de l’Ours, Territoires du Nord-Ouest; Geological Survey of Canada, Open File 6291, scale 1:50 000. <https://doi.org/10.4095/248273>
- Harvey, B.J.A., Kiss, F., and Carson, J.M., 2009d. Geophysical Series, NTS 86-F/11 and 86-F/12, airborne geophysical survey of the northern Great Bear magmatic zone, Northwest Territories/Série des cartes géophysiques, SNRC 86-F/11 et 86-F/12, levé géophysique aéroporté de la partie nord de la zone magmatique du Grand lac de l’Ours, Territoires du Nord-Ouest; Geological Survey of Canada, Open File 6292, scale 1:50 000. <https://doi.org/10.4095/248274>
- Harvey, B.J.A., Kiss, F., and Carson, J.M., 2009e. Geophysical Series, NTS 86-F/13 and 86-F/14, airborne geophysical survey of the northern Great Bear magmatic zone, Northwest Territories/Série des cartes géophysiques, SNRC 86-F/13 et 86-F/14, levé géophysique aéroporté de la partie nord de la zone magmatique du Grand lac de l’Ours, Territoires du Nord-Ouest; Geological Survey of Canada, Open File 6293, scale 1:50 000. <https://doi.org/10.4095/248275>
- Harvey, B.J.A., Kiss, F., and Carson, J.M., 2009f. Geophysical Series, NTS 86-F/15 and 86-F/16, airborne geophysical survey of the northern Great Bear magmatic zone, Northwest Territories/Série des cartes géophysiques, SNRC 86-F/15 et 86-F/16, levé géophysique aéroporté de la partie nord de la zone magmatique du Grand lac de l’Ours, Territoires du Nord-Ouest; Geological Survey of Canada, Open File 6294, scale 1:50 000. <https://doi.org/10.4095/248276>

- Harvey, B.J.A., Kiss, F., and Carson, J.M., 2009g. Geophysical Series, NTS 86-K/1 and 86-K/2, airborne geophysical survey of the northern Great Bear magmatic zone, Northwest Territories/Série des cartes géophysiques, SNRC 86-K/1 et 86-K/2, levé géophysique aéroporté de la partie nord de la zone magmatique du Grand lac de l'Ours, Territoires du Nord-Ouest; Geological Survey of Canada, Open File 6295, scale 1:50 000. <https://doi.org/10.4095/248277>
- Harvey, B.J.A., Kiss, F., and Carson, J.M., 2009h. Geophysical Series, NTS 86-K/3 and 86-K/4, airborne geophysical survey of the northern Great Bear magmatic zone, Northwest Territories/Série des cartes géophysiques, SNRC 86-K/3 et 86-K/4, levé géophysique aéroporté de la partie nord de la zone magmatique du Grand lac de l'Ours, Territoires du Nord-Ouest; Geological Survey of Canada, Open File 6296, scale 1:50 000. <https://doi.org/10.4095/248278>
- Harvey, B.J.A., Kiss, F., and Carson, J.M., 2009i. Geophysical Series, NTS 86-K/5 and 86-K/6, airborne geophysical survey of the northern Great Bear magmatic zone, Northwest Territories/Série des cartes géophysiques, SNRC 86-K/5 et 86-K/6, levé géophysique aéroporté de la partie nord de la zone magmatique du Grand lac de l'Ours, Territoires du Nord-Ouest; Geological Survey of Canada, Open File 6297, scale 1:50 000. <https://doi.org/10.4095/248279>
- Harvey, B.J.A., Kiss, F., and Carson, J.M., 2009j. Geophysical Series, NTS 86-K/7, 86-K/8 and part of 86-J/5, airborne geophysical survey of the northern Great Bear magmatic zone, Northwest Territories/Série des cartes géophysiques, SNRC 86K/7, 86-K/8 et partie de 86-J/5, levé géophysique aéroporté de la partie nord de la zone magmatique du Grand lac de l'Ours, Territoires du Nord-Ouest; Geological Survey of Canada, Open File 6298, scale 1:50 000. <https://doi.org/10.4095/248280>
- Harvey, B.J.A., Kiss, F., and Carson, J.M., 2009k. Geophysical Series, NTS 86-F, parts of 86-E, 86-G, 86-J, 86-K, and 86-L, airborne geophysical survey of the northern Great Bear magmatic zone, Northwest Territories/Série des cartes géophysiques, SNRC 86-F, parties des 86-E, 86-G, 86-J, 86-K et 86-L, levé géophysique aéroporté de la partie nord de la zone magmatique du Grand lac de l'Ours, Territoires du Nord-Ouest; Geological Survey of Canada, Open File 6299, scale 1:50 000. <https://doi.org/10.4095/248249>
- Hauck, S.A., 1990. Petrogenesis and tectonic setting of Middle Proterozoic iron oxide-rich ore deposits: an ore deposit model for Olympic Dam-type mineralization; *in* The midcontinent of the United States – permissive terrane for an Olympic Dam-type deposit? (ed.) W.P. Pratt and P.K. Sims; United States Geological Survey, Bulletin 1932, p. 4–39.
- Hayward, N., 2013. 3D magnetic inversion of mineral prospects in the Great Bear magmatic zone, Northwest Territories; Geological Survey of Canada, Open File 7421, 43 p. <https://doi.org/10.4095/292662>
- Hayward, N. and Corriveau, L., 2014. Fault reconstructions using aeromagnetic data in the Great Bear magmatic zone, Northwest Territories, Canada; Canadian Journal of Earth Sciences, v. 51, p. 927–942. <https://doi.org/10.1139/cjes-2014-0035>
- Hayward, N. and Oneschuk, D., 2011. Geophysical Series, regional geophysical compilation project, Great Bear magmatic zone, Northwest Territories and Nunavut, NTS 85-M and N, and 86-C, D, E, F, K, and L/Série des cartes géophysiques, projet de compilation géophysique régionale, zone magmatique du Grand lac de l'Ours, Territoires du Nord-Ouest et Nunavut, SNRC 85-M et N, et 86-C, D, E, F, K et L; Geological Survey of Canada, Open File 6835; Northwest Territories Geoscience Office, NWT Open File 2011-05, scale 1:500 000. <https://doi.org/10.4095/289114>
- Hayward, N., Enkin, R.J., Corriveau, L., Montreuil, J.-F., and Kerswill, J., 2013. The application of rapid potential field methods for the targeting of IOCG mineralisation based on physical property data, Great Bear magmatic zone, Canada; Journal of Applied Geophysics, v. 94, p. 42–58. <https://doi.org/10.1016/j.jappgeo.2013.03.017>
- Hayward, N., Corriveau, L., Craven, J., and Enkin, R., 2016. Geophysical signature of the NICO Au-Co-Bi-Cu deposit and its iron oxide-alkali alteration system, Northwest Territories, Canada; *in* Proterozoic iron oxide-apatite (\pm REE) and iron oxide-copper-gold and affiliated deposits of Southeast Missouri, U.S.A., and the Great Bear magmatic zone, Northwest Territories, Canada, (ed.) J. Slack, L. Corriveau, and M. Hitzman; Economic Geology, v. 111, p. 2087–2109.
- Heinson, G., Didana, Y., Soeffky, P., Thiel, S., and Wise, T., 2018. The crustal geophysical signature of a world-class magmatic mineral system; Scientific Reports, v. 8, p. 10608. <https://doi.org/10.1038/s41598-018-29016-2>
- Hennessey, B.T. and Puritch, E., 2008. A technical report on a mineral resource estimate for the Sue-Dianne deposit, Mazonod Lake area, Northwest Territories, Canada; report prepared for Fortune Minerals Limited by Micon International Limited, National Instrument 43-101 Technical Report, 125 p. <www.sedar.com> [December 21, 2009].
- Hildebrand, R.S., 1982. Geology, Echo Bay–MacAlpine Channel area, district of Mackenzie, Northwest Territories; Geological Survey of Canada, Map 1546A, scale 1:50 000. <https://doi.org/10.4095/109234>
- Hildebrand, R.S., 1983. Bedrock geology, Rainy Lake and White Eagle Falls, District of Mackenzie, map; Geological Survey of Canada, Open File 930, scale 1:50 000. <https://doi.org/10.4095/129623>
- Hildebrand, R.S., 1984. Geology of the Rainy Lake–White Eagle Falls area, District of Mackenzie: early Proterozoic cauldrons, stratovolcanoes and subvolcanic plutons; Geological Survey of Canada, Paper 83-20, 42 p. <https://doi.org/10.4095/119735>
- Hildebrand, R.S., 1986. Kiruna-type deposits: their origin and relationship to intermediate subvolcanic plutons in the Great Bear magmatic zone, Northwestern Canada; Economic Geology, v. 81, p. 640–659. <https://doi.org/10.2113/gsecongeo.81.3.640>
- Hildebrand, R.S., 2011. Geological synthesis, Northern Wopmay/Coppermine Homocline, Northwest Territories–Nunavut; Geological Survey of Canada, Open File 6390; Northwest Territories Geoscience Office, NWT Open File 2010-011, scale 1:500 000. <https://doi.org/10.4095/287890>
- Hildebrand, R.S., 2017. Precambrian geology, Leith Peninsula–Rivière Grandin area, Northwest Territories; Geological Survey of Canada, Canadian Geoscience Map 153 (preliminary edition), scale 1:125 000. <https://doi.org/10.4095/297330>

- Hildebrand, R.S., Hoffman, P.F., and Bowring, S.A., 1987. Tectono-magmatic evolution of the 1.9 Ga Great Bear magmatic zone, Wopmay Orogen, northwestern Canada; *Journal of Volcanology and Geothermal Research*, v. 32, p. 99–118. [https://doi.org/10.1016/0377-0273\(87\)90039-4](https://doi.org/10.1016/0377-0273(87)90039-4)
- Hildebrand, R.S., Hoffman, P.F., and Bowring, S.A., 2010a. The Calderian orogeny in Wopmay orogen (1.9 Ga), northwestern Canadian Shield; *Geological Society of America, Bulletin*, v. 122, p. 794–814. <https://doi.org/10.1130/B26521.1>
- Hildebrand, R.S., Hoffman, P.F., Housh, T., and Bowring, S.A., 2010b. The nature of volcano-plutonic relations and shapes of epizonal plutons of continental arcs as revealed in the Great Bear magmatic zone, northwestern Canada; *Geosphere*, v. 6, p. 812–839. <https://doi.org/10.1130/GES00533.1>
- Hildebrand, R.S., Bowring, S., and Pelleter, K.F., 2014. *Geology, Calder River, Northwest Territories*; Geological Survey of Canada, Canadian Geoscience Map 154 (preliminary edition); Northwest Territories Geoscience Office, NWT Open Report 2013-003, scale 1:125 000. <https://doi.org/10.4095/292861>
- Hitzman, M.W. and Valenta, R.K., 2005. Uranium in iron oxide-copper-gold (IOCG) systems; *Economic Geology*, v. 100, p. 1657–1661. <https://doi.org/10.2113/gsecongeo.100.8.1657>
- Hitzman, M.W., Oreskes, N., and Einaudi, M.T., 1992. Geological characteristics and tectonic setting of Proterozoic iron oxide (Cu-U-Au-REE) deposits; *Precambrian Research*, v. 58, p. 241–287. [https://doi.org/10.1016/0301-9268\(92\)90121-4](https://doi.org/10.1016/0301-9268(92)90121-4)
- Hofstra, A.H., Meighan, C.J., Song, X.-Y., Samson, I., Marsh, E.E., Lowers, H.A., Emsbo, P., and Hunt, A.G., 2016. Mineral thermometry and fluid inclusion studies of the Pea Ridge iron oxide-apatite-rare-earth element deposit, Mesoproterozoic St. Francois Mountains terrane, southeast Missouri, U.S.A.; *in* Proterozoic iron oxide-apatite (\pm REE) and iron oxide-copper-gold and affiliated deposits of Southeast Missouri, U.S.A., and the Great Bear magmatic zone, Northwest Territories, Canada, (ed.) J. Slack, L. Corriveau, and M. Hitzman; *Economic Geology*, v. 111, p. 1985–2016.
- Hofstra, A., Lisitsin, V., Corriveau, L., Paradis, S., Peter, J., Lauzière, K., Lawley, C., Gadd, M., Pilote, J., Honsberger, I., Bastrakov, E., Champion, D., Czarnota, K., Doublier, M., Huston, D., Raymond, O., VanDerWielen, S., Emsbo, P., Granitto, M., and Kreiner, D., 2021. Deposit classification scheme for the Critical Minerals Mapping Initiative Global Geochemical Database: United States Geological Survey, Open-File Report 2021–1049, 60 p. <https://doi.org/10.3133/ofr20211049>
- Hoggard, M.J. and Richards, F.D., 2019. Source to sink: the impacts of mantle convection on sediment routing systems; *in* SGTSG and SGSEG 2019 abstracts: biennial meeting of the Specialist Group for Tectonics and Structural Geology and the Specialist Group in Solid Earth Geophysics, Convergence on the Coast, (ed.) S. Glorie, T. Wise, and R. Dutch; Department for Energy and Mining, South Australia, Report Book 2019/00019, p. 5.
- Hoggard, M.J., Czarnota, K., Richards, F.D., Huston, D., Jaques, L., and Ghelichkhan, S., 2020. Global distribution of sediment-hosted metals controlled by craton edge stability; *Nature Geoscience*, v. 13, p. 504–510.
- Hu, H., Li, J.W., Harlov, D.E., Lentz, D.R., McFarlane, C.R.M., and Yang, Y.H., 2020. A genetic link between iron oxide-apatite and iron skarn mineralization in the Jinniu volcanic basin, Daye district, eastern China: evidence from magnetite geochemistry and multi-mineral U-Pb geochronology; *Geological Society of America, Bulletin*, v. 132, p. 899–917. <https://doi.org/10.1130/B35180.1>
- Huang, X.-W., Beaudoin, G., Makvandi, S., Boutroy, E., Corriveau, L., and De Toni, A.F., 2017. Trace element composition of iron oxides from IOCG and IOA deposits, and relationships to hydrothermal alteration and deposit subtypes; *Proceedings of the 14th SGA Biennial Meeting*; Society for Geology Applied to Mineral Deposits, August 20–23, 2017, Québec, Quebec, p. 931–935.
- Huang, X.-W., Boutroy, E., Makvandi, S., Beaudoin, G., Corriveau, L., and De Toni, A.F., 2019. Trace element composition of iron oxides from IOCG and IOA deposits: relationship to hydrothermal alteration and deposit subtypes; *Mineralium Deposita*, v. 54, p. 525–552. <https://doi.org/10.1007/s00126-018-0825-1>
- Huang, X.-W., Beaudoin, G., De Toni, A.-F., Corriveau, L., Makanvi, S., and Boutroy, E., 2022. Iron-oxide trace element fingerprinting of iron oxide copper-gold and iron oxide-apatite deposits: a review; *in* Mineral systems with iron oxide-copper-gold (IOCG) and affiliated deposits, (ed.) L. Corriveau, E.G. Potter, and A.H. Mumin; Geological Association of Canada, Special Paper 52, p. 347–364.
- Huston, D.L., Blewett, R.S., Skirrow, R., McQueen, A., Wang, J., Jaques, L., and Waters, D., 2012. Foundations of wealth — Australia's major mineral provinces; *in* Shaping a nation: a geology of Australia, (ed.) R. Blewett; Australian University Press, p. 381–481. <http://doi.org/10.22459/SN.08.2012>
- Ivanov, G., Morin, P., Arbuckle, B., and Mumin, A.H., 2015a. Breccia Island geology; Sheet 5 *in* Echo Bay IOCG thematic map series: geology, structure and hydrothermal alteration of a stratovolcano complex, Northwest Territories, Canada, (ed.) A.H. Mumin; Geological Survey of Canada, Open File 7807, scale 1:1000. <https://doi.org/10.4095/296609>
- Ivanov, G., Marcotte, B., and Mumin, A.H., 2015b. Cross Fault Lake geology; Sheet 3 *in* Echo Bay IOCG thematic map series: geology, structure and hydrothermal alteration of a stratovolcano complex, Northwest Territories, Canada, (ed.) A.H. Mumin; Geological Survey of Canada, Open File 7807. <https://doi.org/10.4095/296607>
- Jackson, V.A. and Ootes, L., 2012. Preliminary geologic map of the south-central Wopmay Orogen, results from 2008 to 2011; Northwest Territories Geoscience Office, NWT Open Report 2012-004, scale 1:100 000.
- Jackson, V.A., van Breemen, O., Ootes, L., Bleeker, W., Bennett, V., Davis, W.D., Ketchum, J., and Smar, L., 2013. Ages of basement and intrusive phases of the Wopmay fault zone, south-central Wopmay Orogen, N.W.T.: a field-based U–Pb zircon study; *Canadian Journal of Earth Sciences*, v. 50, p. 979–1006. <https://doi.org/10.1139/cjes-2013-0046>
- Jébrak, M., 2010. Use of breccias in IOCG(U) exploration; *in* Exploring for iron oxide copper-gold deposits: Canada and global analogues, (ed.) L. Corriveau and A.H. Mumin; Geological Association of Canada, Short Course Notes 20, p. 79–88.

- Jébrak, M., 2022. Use of breccias in IOCG exploration: an updated review; *in* Mineral systems with iron oxide-copper-gold (IOCG) and affiliated deposits, (ed.) L. Corriveau, E.G. Potter, and A.H. Mumin; Geological Association of Canada, Special Paper 52, p. 315–324.
- Johnson, C.A., Day, W.C., and Rye, R.O., 2016. Oxygen, hydrogen, sulfur, and carbon isotopes in the Pea Ridge magnetite-apatite deposit, southeast Missouri, and sulfur isotope comparisons to other iron deposits in the region, *in* Proterozoic iron oxide-apatite (\pm REE) and iron oxide-copper-gold and affiliated deposits of Southeast Missouri, U.S.A., and the Great Bear magmatic zone, Northwest Territories Canada, (ed.) J. Slack, L. Corriveau, and M. Hitzman; *Economic Geology*, v. 111, p. 2017–2032.
- Jones, A.G., Ledo, J., Ferguson, I.J., Craven, J.A., Unsworth, M., Chouteau, M., and Spratt, J., 2014. The electrical resistivity of Canada's lithosphere and correlation with other parameters: contributions from LITHOPROBE and other programmes; *Canadian Journal of Earth Sciences*, v. 51, p. 573–617. <https://doi.org/10.1139/cjes-2013-0151>
- Jones, B., Mumin, A., and Mumin, A.H., 2015. K1 grid geology; Sheet 12 *in* Echo Bay IOCG thematic map series: geology, structure and hydrothermal alteration of a stratovolcano complex, Northwest Territories, Canada, (ed.) A.H. Mumin; Geological Survey of Canada, Open File 7807, scale 1:1600. <https://doi.org/10.4095/296616>
- Katona, L. and Fabris, A., 2022. Targeting for IOCG deposits using gravity and magnetic potential field data in the Gawler Craton, Australia; *in* Mineral systems with iron oxide-copper-gold (IOCG) and affiliated deposits, (ed.) L. Corriveau, E.G. Potter, and A.H. Mumin; Geological Association of Canada, Special Paper 52, p. 299–313.
- Kelly, C.J., Davis, W.J., Potter, E.G., and Corriveau, L., 2020. Geochemistry of hydrothermal tourmaline from IOCG occurrences in the Great Bear magmatic zone: implications for fluid source(s) and fluid composition evolution; *Ore Geology Reviews*, v. 118, art. no. 103329, 13 p. <https://doi.org/10.1016/j.oregeorev.2020.103329>
- Kerr, A., 1994. Early Proterozoic magmatic suites of the eastern Central Mineral Belt (Makkovik Province), Labrador: geology, geochemistry and mineral potential; Government of Newfoundland and Labrador, Department of Mines and Energy, Geological Survey, Report 94-03, 167 p.
- Kerswill, J.A., Hayward, N., and Oneschuk, D., 2016a. Knowledge-driven (KD) prospectivity model for IOCG deposits in the Great Bear magmatic zone, Northwest Territories and Nunavut, NTS 85-N and 86-C, F and K, and parts of NTS 85-M and 86-D, E and L; Geological Survey of Canada, Open File 8034, scale 1:500 000. <https://doi.org/10.4095/298693>
- Kerswill, J.A., Hayward, N., and Oneschuk, D., 2016b. Knowledge-driven (KD) prospectivity model for IOCG deposits in the Great Bear magmatic zone, Northwest Territories, parts of NTS 86-F, G, J and K; Geological Survey of Canada, Open File 8035, scale 1:150 000. <https://doi.org/10.4095/298694>
- King, J., 2019. Oak Dam – An early exploration opportunity; *in* South Australian Exploration and Mining Conference, Adelaide Convention Centre, November 27, 2020; SAEMC Online Proceedings Archive, 13 p. <http://saemc.com.au/archive/2019/2019_03_king.pdf> [accessed April 19, 2021].
- Kiss, F. and Coyle, M., 2011a. Residual total magnetic field, Hottah Lake aeromagnetic survey, parts of NTS 86-C/5, 12, -D/5, 6, 7, 8, 9, 10, 11, 12, Northwest Territories/Composante résiduelle du champ magnétique total, levé aéromagnétique de la région du lac Hottah, SNRC parties de 86-C/5, 12, 86-D/5, 6, 7, 8, 9, 10, 11, 12, Territoires du Nord-Ouest; Geological Survey of Canada, Open File 6851, scale 1:100 000. <https://doi.org/10.4095/288787>
- Kiss, F. and Coyle, M., 2011b. First vertical derivative of the magnetic field, Hottah Lake aeromagnetic survey, parts of NTS 86-C/5, 12, 86-D/5, 6, 7, 8, 9, 10, 11, 12, Northwest Territories/Dérivée première verticale du champ magnétique, levé aéromagnétique de la région du Lac Hottah, SNRC parties de 86-C/5, 12, 86-D/5, 6, 7, 8, 9, 10, 11, 12, Territoires du Nord-Ouest; Geological Survey of Canada, Open File 6852, scale 1:100 000. <https://doi.org/10.4095/288788>
- Kiss, F. and Coyle, M., 2011c. Residual total magnetic field, Hottah Lake aeromagnetic survey, parts of NTS 86-C/13, 86-D/13, 14, 15, 16, 86-E/1, 2, 3, Northwest Territories/Composante résiduelle du champ magnétique total, levé aéromagnétique de la région du Lac Hottah, SNRC parties de 86-C/13, 86-D/13, 14, 15, 16, 86-E/1, 2, 3, Territoires du Nord-Ouest; Geological Survey of Canada, Open File 6853, scale 1:100 000. <https://doi.org/10.4095/288789>
- Kiss, F. and Coyle, M., 2011d. First vertical derivative of the magnetic field, Hottah Lake aeromagnetic survey, parts of NTS 86-C/13, 86-D/13, 14, 15, 16, 86-E/1, 2, 3, Northwest Territories/Dérivée première verticale du champ magnétique, levé aéromagnétique de la région du Lac Hottah, SNRC parties de 86-C/13, 86-D/13, 14, 15, 16, 86-E/1, 2, 3, Territoires du Nord-Ouest; Geological Survey of Canada, Open File 6854, scale 1:100 000. <https://doi.org/10.4095/288790>
- Kisvarsanyi, E.B., 1981. Geology of the Precambrian St. Francois terrane, southeastern Missouri; Missouri Department of Natural Resources, Report of Investigations No. 64, 58 p.
- Konstantinovskaya, E., Ivanov, G., Feybesse, J.L., and Lescuyer, J.L., 2019. Structural features of the Central Labrador Trough: a model for strain partitioning, differential exhumation and late normal faulting in a thrust wedge under oblique shortening; *Geoscience Canada*, v. 46, p. 5–30. <https://doi.org/10.12789/geocanj.2019.46.143>
- Kreiner, D.C. and Barton, M.D., 2011. District-scale view of the upper levels of iron-oxide (-Cu-Au) ('IOCG') vein systems, Copiapó, Chile; Proceedings of the 11th GSA Biennial Meeting; Society for Geology Applied to Mineral Deposits, September 26–29, 2011, Antofagasta, Chile, p. 497–499.
- Large, R.R., Gemmill, J.B., Paulick, H., and Huston, D.L., 2001. The alteration box plot-A simple approach to understanding the relationship between alteration mineralogy and litho-geochemistry associated with volcanic-hosted massive sulfide deposits; *Economic Geology*, v. 96, p. 957–971. <https://doi.org/10.2113/gsecongeo.96.5.957>
- Lee, M., 2012. Curvature analysis of aeromagnetic data for quality control, geological mapping, and mineral resource assessment; Ph.D. thesis, McMaster University, Hamilton, Ontario, 187 p.

- Lee, M.D. and Morris, W.A., 2013. Comparison of magnetic-susceptibility meters using rock samples from the Wopmay Orogen, Northwest Territories, Canada; Geological Survey of Canada, Technical Note 5, 7 p. <https://doi.org/10.4095/292739>
- Lee, M., Morris, W., Harris, J., and Leblanc, G., 2012a. An automatic network-extraction algorithm applied to magnetic survey data for the identification and extraction of geologic lineaments; *The Leading Edge*, v. 31, p. 26–31. <https://doi.org/10.1190/1.3679324>
- Lee, M., Morris, W., Leblanc, G., and Harris, J., 2012b. Network extraction tool for mineral exploration: a case study from the Wopmay Orogen, Northwest Territories, Canada; *Exploration Geophysics*, v. 43, p. 116–124. <https://doi.org/10.1071/EG11045>
- Lee, M., Morris, W., Leblanc, G., and Harris, J., 2013a. Quality assurance of aeromagnetic data using lineament analysis; *Exploration Geophysics*, v. 44, p. 104–113. <https://doi.org/10.1071/EG12034>
- Lee, M., Morris, W., Leblanc, G., and Harris, J., 2013b. Curvature analysis to differentiate magnetic sources for geologic mapping; *Geophysical Prospecting*, v. 61, p. 572–585. <https://doi.org/10.1111/j.1365-2478.2012.01111.x>
- Li, W., Audétat, A., and Zhang, J., 2015. The role of evaporites in the formation of magnetite–apatite deposits along the Middle and Lower Yangtze River, China: evidence from LA-ICP-MS analysis of fluid inclusions; *Ore Geology Reviews*, v. 67, p. 264–278. <https://doi.org/10.1016/j.oregeorev.2014.12.003>
- Lobo-Guerrero, S.A., 2010. Iron oxide-copper-gold mineralization in the Greater Lufilian Arc, Africa; *in* Exploring for iron oxide copper-gold deposits: Canada and global analogues, (ed.) L. Corriveau and A.H. Mumin; Geological Association of Canada, Short Course Notes 20, p. 161–175.
- Lypaczewski, P., 2012. Cathodoluminescence characterization of apatite from the Sue-Dianne and Brooke IOCG mineralization system, Great Bear magmatic zone, Northwest Territories; B.Sc. thesis, McGill University, Montréal, Quebec, 32 p.
- Lypaczewski, P., Normandeau, P.X., Paquette, J., and McMartin, I., 2013. Petrographic and cathodoluminescence characterization of apatite from the Sue-Dianne and Brooke IOCG mineralization systems, Great Bear magmatic zone, Northwest Territories, Canada; Geological Survey of Canada, Open File 7319, 18 p. <https://doi.org/10.4095/292369>
- Macmillan, E., Cook, N.J., Ehrig, K., Ciobanu, C.L., and Pring, A., 2016. Uraninite from the Olympic Dam IOCG-U-Ag deposit: linking textural and compositional variation to temporal evolution; *American Mineralogist*, v. 101, p. 1295–1320. <https://doi.org/10.2138/am-2016-5411>
- Mark, G., Williams, P.J., and Boyce, A., 2004. Low-latitude meteoric fluid flow along the Cloncurry Fault, Cloncurry minerals province, NW Queensland, Australia: geodynamic and metallogenic implications; *Chemical Geology*, v. 207, p. 117–132. <https://doi.org/10.1016/j.chemgeo.2004.02.007>
- McCafferty, A.E., Phillips, J.D., and Driscoll, R.L., 2016. Magnetic and gravity gradiometry framework for Mesoproterozoic iron oxide-apatite and iron oxide-copper-gold deposits, southeast Missouri, U.S.A.; *in* Proterozoic iron oxide-apatite (\pm REE) and iron oxide-copper-gold and affiliated deposits of Southeast Missouri, U.S.A., and the Great Bear magmatic zone, Northwest Territories Canada, (ed.) J. Slack, L. Corriveau, and M. Hitzman; *Economic Geology*, v. 111, p. 1859–1882.
- McCafferty, A.E., Phillips, J.D., Hofstra, A.H., and Day, W.C., 2019. Crustal architecture beneath the southern Midcontinent (U.S.A.) and controls on Mesoproterozoic iron-oxide mineralization from 3D geophysical models; *Ore Geology Reviews*, v. 111, art. no. 102966, 21 p. <https://doi.org/10.1016/j.oregeorev.2019.102966>
- McLaughlin, B., Montreuil, J.-F., and Desrochers, J.-P., 2016. Exploration report (summer and fall 2014 drill program) on the Sagar Property, Romanet Horst, Labrador Trough, Quebec, Canada; report prepared for Energizer Resources Inc.; Ministère de l'Énergie et des Ressources naturelles du Québec, Assessment Report GM 69734, 65 p.
- McMartin, I., Corriveau, L., and Beaudoin, G., 2009a. Heavy mineral and till geochemical signatures of the NICO Co-Au-Bi deposit, Great Bear magmatic zone, Northwest Territories, Canada; *Proceedings of the 24th International Applied Geochemistry Symposium*, (ed.) D.R. Lentz, K.G. Thorne, and K.-L. Beal; Association of Applied Geochemists, June 1–4, 2009, Fredericton, New Brunswick, v. 2, p. 573–576.
- McMartin, I., Corriveau, L., Beaudoin, G., Averill, S., and Kjarsgaard, I., 2009b. Heavy mineral signature of the NICO Co-Au-Bi deposit, Great Bear magmatic zone, Northwest Territories, Canada; *in* Indicator mineral methods in mineral exploration, (ed.) B. McClenaghan and H. Thorleifson; Association of Applied Geochemists, 24th International Applied Geochemistry Symposium, June 1–4, 2009, Fredericton, New Brunswick, Workshop B, p. 71–81.
- McMartin, I., Corriveau, L., and Beaudoin, G., 2011a. An orientation study of the heavy mineral signature of the NICO Co-Au-Bi deposit, Great Bear magmatic zone, Northwest Territories, Canada; *Geochemistry: Exploration, Environment, Analysis*, v. 11, p. 293–307. <https://doi.org/10.1144/1467-7873/10-IM-023>
- McMartin, I., Corriveau, L., Beaudoin, G., Averill, S.A., and Kjarsgaard, I., 2011b. Results from an orientation study of the heavy mineral and till geochemical signatures of the NICO Co-Au-Bi deposit, Great Bear magmatic zone, Northwest Territories, Canada; Geological Survey of Canada, Open File 6723, 23 p. <https://doi.org/10.4095/289500>
- Montreuil, J.-F., 2016. Mobilité des éléments et formation de gîtes polymétalliques au sein des systèmes hydrothermaux à oxydes de fer et altération en alcalis, zone magmatique du Grand lac de l'Ours, Territoires du Nord-Ouest, Canada; Ph.D. thesis, Institut national de la recherche scientifique, Québec, Quebec, 550 p.
- Montreuil, J.-F., Corriveau, L., and Long, B., 2012. Porosity in albitites and the development of albitite-hosted U deposits: insights from x-ray computed tomography; CT Scan workshop, Development on non-medical environment, INRS, Québec, 550 p.

- Montreuil, J.-F., Corriveau, L., and Grunsky, E.C., 2013. Compositional data analysis of IOCG systems, Great Bear magmatic zone, Canada: to each alteration type its own geochemical signature; *Geochemistry: Exploration, Environment, Analysis*, v. 13, p. 229–247. <https://doi.org/10.1144/geochem2011-101>
- Montreuil, J.-F., Desrochers, J.-P., and Masters, J., 2014. Exploration report (July–August 2013) program on the Sagar property, Romanet Horst, Labrador Trough, Québec; Ministère de l'Énergie et des Ressources naturelles, Québec, GM 68408, 126 p.
- Montreuil, J.-F., Corriveau, L., and Potter, E.G., 2015. Formation of albitite-hosted uranium within IOCG systems: the Southern Breccia, Great Bear magmatic zone, Northwest Territories, Canada; *Mineralium Deposita*, v. 50, p. 293–325. <https://doi.org/10.1007/s00126-014-0530-7>
- Montreuil, J.-F., Corriveau, L., and Davis, W., 2016a. Tectonomagmatic evolution of the southern Great Bear magmatic zone (Northwest Territories, Canada) – implications on the genesis of iron oxide alkali-altered hydrothermal systems; *in* Proterozoic iron oxide-apatite (\pm REE) and iron oxide-copper-gold and affiliated deposits of Southeast Missouri, U.S.A., and the Great Bear magmatic zone, Northwest Territories Canada, (ed.) J. Slack, L. Corriveau, and M. Hitzman; *Economic Geology*, v. 111, p. 2111–2138.
- Montreuil, J.-F., Corriveau, L., Potter, E.G., and De Toni, A.F., 2016b. On the relation between alteration facies and metal endowment of iron oxide-alkali-altered systems, southern Great Bear magmatic zone (Canada); *in* Proterozoic iron oxide-apatite (\pm REE) and iron oxide-copper-gold and affiliated deposits of Southeast Missouri, U.S.A., and the Great Bear magmatic zone, Northwest Territories Canada, (ed.) J. Slack, L. Corriveau, and M. Hitzman; *Economic Geology*, v. 111, p. 2139–2168.
- Montreuil, J.-F., Potter, E.G., Corriveau, L., and Davis, W.J., 2016c. Element mobility patterns in magnetite-group IOCG systems: the Fab IOCG system, Northwest Territories, Canada; *Ore Geology Reviews*, v. 72, p. 562–584. <https://doi.org/10.1016/j.oregeorev.2015.08.010>
- Mumin, A.H., 1997. A qualifying report on the geology and mineralization of the NICO 1 (F28905), NICO 2 (F28906), NICO 3 (F50933), NICO 4 (F18965), NICO 5 (F18966), NICO 6 (F50155), NICO 7 (F50156), NICO 8 (F50157), NICO 9 (F50158), NICO 10 (F50159), NICO 11 (F51389), NICO 12 (F51390) claims, Marian River area, Mackenzie (South) District, Northwest Territories, Canada; Northwest Territories Geoscience Office, Assessment Report 084202, 61 p.
- Mumin, A.H. (ed.), 2015. Echo Bay IOCG thematic map series: geology, structure and hydrothermal alteration of a stratovolcano complex, Northwest Territories, Canada; Geological Survey of Canada, Open File 7807, 19 p. <https://doi.org/10.4095/296602>
- Mumin, A.H. and Camier, W.J., 2000. Proterozoic Fe-oxide hosted polymetallic mineralization associated with the Marion River Batholith, southern Great Bear magmatic zone, Northwest Territories; *GeoCanada 2000 – the Millennium Geoscience Summit Conference*; Geological Association of Canada–Mineralogical Association of Canada, Joint Annual Meeting, May 29–June 2, 2000, Calgary, Alberta, Program with Abstracts, v. 25.
- Mumin, A.H., Norman, P.E., Goad, R.E., and Camier, W.J., 2000. Metallogeny of the Proterozoic southern Great Bear magmatic zone; 28th Yellowknife Geoscience Forum Abstracts; Northwest Territories Geoscience Office, YKGSF Abstracts Volume, v. 2000, p. 56–57.
- Mumin, A.H., Corriveau, L., Somarin, A.K., and Ootes, L., 2007. Iron oxide copper-gold-type polymetallic mineralization in the Contact Lake Belt, Great Bear magmatic zone, Northwest Territories, Canada; *Exploration and Mining Geology*, v. 16, p. 187–208. <https://doi.org/10.2113/gsemg.16.3-4.187>
- Mumin, A.H., Somarin, A.K., Jones, B., Corriveau, L., Ootes, L., and Camier, J., 2010. The IOCG-porphry-epithermal continuum of deposit types in the Great Bear magmatic zone, Northwest Territories, Canada; *in* Exploring for iron oxide copper-gold deposits: Canada and global analogues, (ed.) L. Corriveau and A.H. Mumin; Geological Association of Canada, Short Course Notes 20, p. 59–78.
- Mumin, A.H., Phillips, A., Katsuragi, C.J., Mumin, A., and Ivanov, G., 2014. Geotectonic interpretation of the Echo Bay stratovolcano complex, northern Great Bear magmatic zone, Northwest Territories; Northwest Territories Geoscience Office, NWT Open File 2014-04, 25 p.
- Mumin, A., Phillips, J., and Mumin, A.H., 2015a. Skinny Lake geology; Sheet 16 *in* Echo Bay IOCG thematic map series: geology, structure and hydrothermal alteration of a stratovolcano complex, Northwest Territories, Canada, (ed.) A.H. Mumin; Geological Survey of Canada, Open File 7807, scale 1:4000. <https://doi.org/10.4095/296620>
- Mumin, A., Phillips, J., Katsuragi, C., and Mumin, A.H., 2015b. Glacier Lake East geology; Sheet 2 *in* Echo Bay IOCG thematic map series: geology, structure and hydrothermal alteration of a stratovolcano complex, Northwest Territories, Canada, (ed.) A.H. Mumin; Geological Survey of Canada, Open File 7807, scale 1:4000. <https://doi.org/10.4095/296606>
- Mumin, A.H., Lehmann, J., Corriveau, L., and Katsuragi, C., 2015. Contact Lake Belt hydrothermal alteration; Sheet 18 *in* Echo Bay IOCG thematic map series: geology, structure and hydrothermal alteration of a stratovolcano complex, Northwest Territories, Canada, (ed.) A.H. Mumin; Geological Survey of Canada, Open File 7807, scale 1:40 000. <https://doi.org/10.4095/296622>
- Myers, M.L., Wallace, P.J., Wilson, C.J.N., Morter, B.K., and Swallow, E.J., 2016. Prolonged ascent and episodic venting of discrete magma batches at the onset of the Huckleberry Ridge supereruption, Yellowstone; *Earth and Planetary Science Letters*, v. 451, p. 285–297. <https://doi.org/10.1016/j.epsl.2016.07.023>
- Natural Resources Canada, 2021. Canada's list of critical minerals; Natural Resources Canada, 5 p. <<https://www.nrcan.gc.ca/criticalminerals>> [accessed March 12, 2021].
- Newton, L., 2011. Metamorphism and provenance of the Holly Lake metamorphic complex, Hottah terrane, N.W.T.: a petrographic and SHRIMP U-Pb detrital zircon study; B.Sc. thesis, Dalhousie University, Halifax, Nova Scotia, 101 p.

- Neymark, L.A., Holm-Denoma, C.S., Pietruszka, A.J., Aleinikoff, J.N., Fanning, C.M., Pillers, R.M., and Moscati, R.J., 2016. High spatial resolution U-Pb geochronology and Pb-isotope geochemistry of magnetite-apatite ore from the Pea Ridge iron oxide-apatite (IOA) deposit, St. Francois Mountains, Southeast Missouri, U.S.A.; *in* Proterozoic iron oxide-apatite (\pm REE) and iron oxide-copper-gold and affiliated deposits of Southeast Missouri, U.S.A., and the Great Bear magmatic zone, Northwest Territories Canada, (ed.) J. Slack, L. Corriveau, and M. Hitzman; *Economic Geology*, v. 111, p. 1915–1933.
- Ningwu Research Group, 1978. Ningwu porphyry iron ore deposits; Geological Publishing House, Beijing, China (in Chinese), 196 p.
- Normandeau, P.X., 2018. Drift prospecting applied to iron oxide copper-gold deposit exploration in the Great Bear magmatic zone, Canada; Ph.D. thesis, McGill University, Montréal, Quebec, 226 p.
- Normandeau, P.X. and McMartin, I., 2013. Composition of till and bedrock across the Great Bear magmatic zone: field database and analytical results from the GEM IOCG-Great Bear project; Geological Survey of Canada, Open File 7307, 26 p. <https://doi.org/10.4095/292560>
- Normandeau, P.X., Harlov, D.E., Corriveau, L., Paquette, J., and McMartin, I., 2018. Characterization of fluorapatite within iron oxide alkali-calcic alteration systems of the Great Bear magmatic zone: a potential metasomatic process record; *The Canadian Mineralogist*, v. 56, p. 167–187. <https://doi.org/10.3749/canmin.1700035>
- Oliver, N.H.S., Mark, G., Pollard, P.J., Rubenach, M.J., Bastrakov, E., Williams, P.J., Marshall, L.C., Baker, T., and Nemchin, A.A., 2004. The role of sodic alteration in the genesis of iron oxide-copper-gold deposits: geochemistry and geochemical modelling of fluid-rock interaction in the Cloncurry district, Australia; *Economic Geology*, v. 99, p. 1145–1176. <https://doi.org/10.2113/gsecongeo.99.6.1145>
- Oneschuk, D., Kilfoil, G., and Hayward, N., 2019a. Residual total magnetic field, compilation of the Qipuuqqaq/Postville area, eastern-central Labrador, Newfoundland and Labrador, parts of NTS-13-J, K, N and O; Geological Survey of Canada, Open File 8642, scale 1:200 000. <https://doi.org/10.4095/315482>
- Oneschuk, D., Kilfoil, G., and Hayward, N., 2019b. First vertical derivative of the magnetic field, compilation of the Qipuuqqaq/Postville area, eastern-central Labrador, Newfoundland and Labrador, parts of NTS 13-J, K, N and O; Geological Survey of Canada, Open File 8643, scale 1:200 000. <https://doi.org/10.4095/315483>
- Oneschuk, D., Kilfoil, G., and Hayward, N., 2019c. Potassium, compilation of the Qipuuqqaq/Postville area, eastern-central Labrador, Newfoundland and Labrador, parts of NTS 13-J, K, N and O; Geological Survey of Canada, Open File 8644, scale 1:200 000. <https://doi.org/10.4095/315484>
- Oneschuk, D., Kilfoil, G., and Hayward, N., 2019d. Uranium, compilation of the Qipuuqqaq/Postville area, eastern-central Labrador, Newfoundland and Labrador, parts of NTS 13-J, K, N and O; Geological Survey of Canada, Open File 8645, scale 1:200 000. <https://doi.org/10.4095/315485>
- Oneschuk, D., Kilfoil, G., and Hayward, N., 2019e. Thorium, compilation of the Qipuuqqaq/Postville area, eastern-central Labrador, Newfoundland and Labrador, parts of NTS 13-J, K, N and O; Geological Survey of Canada, Open File 8646, scale 1:200 000. <https://doi.org/10.4095/315486>
- Oneschuk, D., Kilfoil, G., and Hayward, N., 2019f. Total count, compilation of the Qipuuqqaq/Postville area, eastern-central Labrador, Newfoundland and Labrador, parts of NTS 13-J, K, N and O; Geological Survey of Canada, Open File 8647, scale 1:200 000. <https://doi.org/10.4095/315487>
- Ootes, L., Jackson, V.A., and Corriveau, L., 2008. Assay results from the South Wopmay Bedrock Mapping Project (2006–2007 field seasons); Northwest Territories Geoscience Office, NWT Open Report 2008-008, 13 p.
- Ootes, L., Goff, S., Jackson, V., Gleeson, S., Creaser, R., Samson, I.M., Evensen, N., Corriveau, L., and Mumin, A.H., 2010. Timing and thermochemical constraints on multi-element mineralization at the Nori/RA Cu–Mo–U prospect, Great Bear magmatic zone, Northwest Territories, Canada; *Mineralium Deposita*, v. 45, p. 549–566. <https://doi.org/10.1007/s00126-010-0291-x>
- Ootes, L., Harris, J., Jackson, V.A., Azar, B., and Corriveau, L., 2013. Uranium-enriched bedrock in the central Wopmay Orogen: implications for uranium mineralization; *in* Geological environments hosting uranium deposits, (ed.) E.G. Potter, C.W. Jefferson, and D. Quirt; *Exploration and Mining Geology*, v. 21, p. 85–103.
- Ootes, L., Davis, W.J., Jackson, V.A., and van Breemen, O., 2015. Chronostratigraphy of the Hottah terrane and Great Bear magmatic zone of Wopmay Orogen, Canada, and exploration of a terrane translation model; *Canadian Journal of Earth Sciences*, v. 52, p. 1062–1092. <https://doi.org/10.1139/cjes-2015-0026>
- Ootes, L., Snyder, D., Davis, W.J., Acosta-Góngora, P., Corriveau, L., Mumin, A.H., Gleeson, S.A., Samson, I.M., Montreuil, J.-F., Potter, E.G., and Jackson, V.A., 2017. A Paleoproterozoic Andean-type iron oxide copper-gold environment, the Great Bear magmatic zone, Northwest Canada; *Ore Geology Reviews*, v. 81, p. 123–139. <https://doi.org/10.1016/j.oregeorev.2016.09.024>
- Ovalle, J.T., La Cruz, N.L., Reich, M., Barra, F., Simon, A.C., Konecke, B.A., Rodriguez-Mustafa, M.A., Deditius, A.P., Childress, T.M., and Morata, D., 2018. Formation of massive iron deposits linked to explosive volcanic eruptions; *Scientific Reports*, v. 8, art. no. 14 855. <https://doi.org/10.1038/s41598-018-33206-3>
- Paladin Energy Limited, 2019. Michelin project, Labrador, Canada; Paladin Energy Limited. <www.paladinenergy.com.au/project/michelin-canada> [accessed September 1, 2019].
- Pattison, D.R.M., St-Onge, M.R., and Bégin, N.J., 2005. Preface; *in* Truth and beauty in metamorphism: a tribute to Dugald M. Carmichael, (ed.) D.R.M. Pattison, M.R. St-Onge, N.J. Bégin, and R.F. Martin; *The Canadian Mineralogist*, v. 43, p. 1–10.

- Pelleter, E., Gasquet, D., Cheillets, A., and Mouttaqi, A., 2010. Alteration processes and impacts on regional-scale element mobility and geochronology, Tamlalt–Menhouhou deposit, Morocco; *in* Exploring for iron oxide copper-gold deposits: Canada and global analogues, (ed.) L. Corriveau and A.H. Mumin; Geological Association of Canada, Short Course Notes 20, p. 177–185.
- Percival, J.B., Potter, E.G., Lauzière, K., Ijewliw, O., Bilot, I., Hunt, P., English, M.L.R., Olejarz, A.D., Laudadio, A.B., Enright, A., Robillard, K.-L., and Corriveau, L., 2016. Mineralogy, petrography and autoradiography of selected samples from the Contact Lake and NICO areas, Great Bear magmatic zone, Northwest Territories (IOCG-GEM Project); Geological Survey of Canada, Open File 7755, 48 p. <https://doi.org/10.4095/297677>
- Perreault, S. and Lafrance, B., 2015. Kwyjibo, a REE-enriched iron oxides-copper-gold (IOCG) deposit, Grenville Province, Québec; *in* Symposium on strategic and critical materials proceedings, (ed.) G.J. Simandl and M. Neetz, November 13–14, 2015, Victoria, British Columbia; British Columbia Ministry of Energy and Mines, British Columbia Geological Survey, Paper 2015-3, p. 139–145.
- Piette-Lauzière, N., Graziani, R., Larson, K.P., and Kellett, D.A., 2019. Reactivation of the Eastern Highlands shear zone, Cape Breton Island, Appalachian Orogen; *in* Targeted Geoscience Initiative: 2018 report of activities, (ed.) N. Rogers; Geological Survey of Canada, Open File 8549, p. 295–305. <https://doi.org/10.4095/313663>
- Pollard, P.J., Taylor, R.G., Peters, L., Matos, F., Freitas, C., Saboia, L., and Huhn, S., 2019. ⁴⁰Ar–³⁹Ar dating of Archean iron oxide Cu–Au and Paleoproterozoic granite-related Cu–Au deposits in the Carajás Mineral Province, Brazil: implications for genetic models; *Mineralium Deposita*, v. 54, p. 329–346. <https://doi.org/10.1007/s00126-018-0809-1>
- Porter, T.M., 2010. Current understanding of iron oxide associated–alkali altered mineralised systems. Part 1 — an overview; *in* Hydrothermal iron oxide copper-gold and related deposits: a global perspective, (ed.) T.M. Porter; Porter Geoscience Consultancy Publishing, Adelaide, Australia, v. 3, p. 5–32.
- Potter, E.G., Corriveau, L., and Kerswill, J.K., 2013a. Potential for iron oxide-copper–gold and affiliated deposits in the proposed national park area of the East Arm, Northwest Territories: insights from the Great Bear magmatic zone and global analogs; *in* Mineral and energy resource assessment for the proposed Thaidene Nene National Park reserve, East Arm of Great Slave Lake, Northwest Territories, (ed.) D.F. Wright, B.A. Kjarsgaard, E.J. Ambrose, and G.F. Bonham-Carter; Geological Survey of Canada, Open File 7196, p. 477–493. <https://doi.org/10.4095/292468>
- Potter, E.G., Montreuil, J.-F., Corriveau, L., and De Toni, A., 2013b. Geology and hydrothermal alteration of the Fab Lake region, Northwest Territories; Geological Survey of Canada, Open File 7339, 26 p. <https://doi.org/10.4095/292562>
- Potter, E.G., Corriveau, L., and Sparkes, G.W., 2016. Metal pathways and traps in polymetallic (U±Fe, Cu, Au, REE) metasomatic ore systems; *in* Targeted Geoscience Initiative, 2016 report of activities, (ed.) N. Rogers; Geological Survey of Canada, Open File 8199, p. 99–102. <https://doi.org/10.4095/299619>
- Potter, E.G., Corriveau, L., and Kjarsgaard, B.A., 2017. East Arm basin–Great Bear magmatic zone linkages and iron oxide-copper-gold (IOCG) mineral potential; Proceedings of the 14th SGA Biennial Meeting; Society for Geology Applied to Mineral Deposits, August 20–23, 2017, Québec, Quebec, p. 879–883.
- Potter, E.G., Montreuil, J.-F., Corriveau, L., and Davis, W., 2019. The Southern Breccia metasomatic uranium system of the Great Bear magmatic zone, Canada: iron oxide-copper-gold (IOCG) and albitite-hosted uranium linkages; Chapter 5 *in* Ore deposits: origin, exploration, and exploitation, (ed.) S. Decrée and L. Robb; American Geophysical Union, Geophysical Monograph 242, p. 109–130. <https://doi.org/10.1002/9781119290544.ch5>
- Potter, E.G., Corriveau, L., and Kjarsgaard, B., 2020. Paleoproterozoic iron oxide apatite (IOA) and iron oxide-copper-gold (IOCG) mineralization in the East Arm Basin, Northwest Territories, Canada; *Canadian Journal of Earth Sciences*, v. 57, p. 167–183. <https://doi.org/10.1139/cjes-2018-0171>
- Potter, E.G., Acosta-Góngora, P., Corriveau, L., Montreuil, J.-F., and Yang, Z., 2022. Uranium enrichment processes in iron oxide and alkali-calcic alteration systems as revealed by uraninite trace element chemistry; *in* Mineral systems with iron oxide-copper-gold (IOCG) and affiliated deposits, (ed.) L. Corriveau, E.G. Potter, and A.H. Mumin; Geological Association of Canada, Special Paper 52, p. 325–345.
- Rantala, E., Seppä, V.-M., and Brown, M., 2021. Mineral resource estimate NI 43-101 technical report — Rajapalot; report prepared for Mawson Gold Limited, 175 p. < <https://mawsongold.com/assets/docs/reports/210826-Mineral-Resource-Estimate-NI-43-101-Technical-Report--Rajapalot.pdf> > [accessed October 23, 2021].
- Reardon, N.C., 1992. Magmatic-hydrothermal systems and associated magnetite–apatite–actinolite deposits, Echo Bay, Northwest Territories; M.Sc. thesis, University of Ottawa, Ottawa, Ontario, 154 p.
- Reid, A., 2019. The Olympic Cu–Au Province, Gawler Craton: a review of the lithospheric architecture, geodynamic setting, alteration systems, cover successions and prospectivity; *Minerals*, v. 9, p. 371. <https://doi.org/10.3390/min9060371>
- Reid, A.J. and Fabris, A., 2015. Influence of pre-existing low metamorphic grade sedimentary successions on the distribution of copper-gold mineralisation in the Olympic Cu–Au Province, Gawler Craton; *Economic Geology*, v. 110, p. 2147–2157. <https://doi.org/10.2113/econgeo.110.8.2147>
- Richards, J.P. and Mumin, A.H., 2013a. Lithospheric fertilization and mineralization by arc magmas: genetic links and secular differences between porphyry copper±molybdenum±gold and magmatic-hydrothermal iron oxide copper-gold deposits; *in* Tectonics, metallogeny, and discovery: the North American Cordillera and similar accretionary settings, (ed.) M. Colpron, T. Bissig, B.G. Rusk, and J.F.H. Thompson; Society of Economic Geologists, Special Publication 17, p. 277–299.
- Richards, J.P. and Mumin, A.H., 2013b. Magmatic-hydrothermal processes within an evolving Earth: iron oxide-copper-gold and porphyry Cu±Mo±Au deposits; *Geology*, v. 41, p. 767–770. <https://doi.org/10.1130/G34275.1>

- Richards, J.P., Lopez, G.P., Zhu, J., Creaser, R.A., Locock, A.J., and Mumin, A.H., 2017. Contrasting tectonic settings and sulfur contents of magmas associated with Cretaceous porphyry Cu-Au and intrusion-related iron oxide-Cu-Au deposits in northern Chile; *Economic Geology*, v. 112, p. 295–318. <https://doi.org/10.2113/econgeo.112.2.295>
- Robinson, G., 2013. Nature of potassium metasomatism at the Au-Co-Bi NICO deposit, N.W.T.; M.Sc. thesis, University of Western Ontario, London, Ontario, 267 p.
- Rogge, D.M., Jones, B., and Mumin, A.H., 2015. Dowdell Peninsula geology; Sheet 8 in Echo Bay IOCG thematic map series: geology, structure and hydrothermal alteration of a stratovolcano complex, Northwest Territories, Canada, (ed.) A.H. Mumin; Geological Survey of Canada, Open File 7807, scale 1:7000. <https://doi.org/10.4095/296612>
- Ruff, E.C., Mumin, A.H., Webb, D.R., and Piercey-Normore, M.D., 2002. Discovery of Porpidia ursus metal indicator lichens in the Great Bear magmatic zone, N.W.T.; Geological Association of Canada–Mineralogical Association of Canada, Joint Annual Meeting, Program with Abstracts, v. 28.
- Rusk, B., Oliver, N., Blenkinsop, T., Zhang, D., Williams, P., Cleverley, J., and Habermann, H., 2010. Physical and chemical characteristics of the Ernest Henry iron oxide copper gold deposit, Cloncurry, Queensland, Australia; implications for IOCG genesis; in *Hydrothermal iron oxide copper-gold and related deposits: a global perspective*, v. 3, (ed.) T.M. Porter; PGC Publishing, Adelaide, p. 201–218.
- Rusk, B., Emsbo, P., Xavier, R.P., Corriveau, L., Oliver, N., and Zhang, D., 2015. A comparison of fluid origins and compositions in iron oxide-copper-gold and porphyry-Cu (Mo-Au) deposits; Proceedings of the PACRIM 2015 Congress; Australasian Institute of Mining and Metallurgy, March 18–22, 2015, Hong Kong, China, p. 271–280.
- Ryan, B., 1984. Regional geology of the central part of the Central Mineral Belt, Labrador; Government of Newfoundland and Labrador, Department of Mines and Energy, Mineral Development Division, Memoir 3, 185 p.
- Sahtu Land Use Planning Board, 2010. Sahtu land use plan, plain language summary; Sahtu Land Use Planning Board, Northwest Territories. <<https://www.sahtulanduseplan.org>> [accessed April 28, 2011]
- Sahtu Land Use Planning Board, 2013. Sahtu land use plan; Sahtu Land Use Planning Board. <<https://www.sahtulanduseplan.org>> [accessed October 21, 2021]
- Sappin, A.-A. and Perreault, S., 2021. Drill core pictures and description of samples collected from the REE Kwyjibo deposit (SOQUEM warehouse, Val d’Or, QC – October 2015); Geological Survey of Canada, Open File 8794, 14 p. <https://doi.org/10.4095/328274>
- Sappin, A.-A., Dupuis, C., Beaudoin, G., Pozza, M., McMartin, I., and McClenaghan, M.B., 2014. Optimal ferromagnetic fraction of iron oxides in till samples along ice-flow paths: case studies from the Sue-Dianne and Thompson deposits, Canada; *Geochemistry: Exploration, Environment, Analysis*, v. 14, p. 315–329. <https://doi.org/10.1144/geochem2013-212>
- Schandl, E.S. and Gorton, M.P., 2007. The Scadding gold mine, east of the Sudbury Igneous Complex, Ontario: an IOCG-type deposit?; *The Canadian Mineralogist*, v. 45, p. 1415–1441. <https://doi.org/10.3749/canmin.45.6.1415>
- Schlegel, T.U. and Heinrich, C.A., 2015. Lithology and hydrothermal alteration control the distribution of copper grade in the Prominent Hill iron oxide-copper-gold deposit (Gawler Craton, South Australia); *Economic Geology*, v. 110, p. 1953–1994. <https://doi.org/10.2113/econgeo.110.8.1953>
- Schlegel, T.U., Wagner, T., Wälle, M., and Heinrich, C.A., 2018. Hematite breccia-hosted iron oxide copper-gold deposits require magmatic fluid components exposed to atmospheric oxidation: evidence from Prominent Hill, Gawler Craton, South Australia; *Economic Geology*, v. 113, p. 597–644. <https://doi.org/10.5382/econgeo.2018.4564>
- Schlegel, T.U., Wagner, T., and Fusswinkel, T., 2020. Fluorite as indicator mineral in iron oxide-copper-gold systems: explaining the IOCG deposit diversity; *Chemical Geology*, v. 548, art. 119674.
- Schofield, A. (ed.), 2012. An assessment of the uranium and geothermal prospectivity of the southern Northern Territory; *Geoscience Australia, Record 2012/51*, 214 p.
- Schofield, A., Huston, D., Gallagher, R., and Kemp, C., 2014. Iron oxide-copper-gold potential of the southern Arunta region; *Geoscience Australia, Record 76423*, 7 p.
- Shakotko, P., 2014. 1.9 Ga paleo-unconformity, Beaverlodge Ridge; M.Sc. thesis, University of Saskatchewan, Saskatoon, Saskatchewan, 150 p.
- Sillitoe, R.H., 2003. Iron oxide-copper-gold deposits: an Andean view; *Mineralium Deposita*, v. 38, p. 787–812. <https://doi.org/10.1007/s00126-003-0379-7>
- Sillitoe, R.H., Magaranov, G., Mladenov, V., and Creaser, R.A., 2020. Rosen, Bulgaria: a newly recognized iron oxide-copper-gold district; *Economic Geology*, v. 115, p. 481–488. <https://doi.org/10.5382/econgeo.4731>
- Skirrow, R.G., 2010. “Hematite-group” IOCG±U ore systems: tectonic settings, hydrothermal characteristics, and Cu-Au and U mineralizing processes; in *Exploring for iron oxide copper-gold deposits: Canada and global analogues*, (ed.) L. Corriveau and A.H. Mumin; Geological Association of Canada, Short Course Notes 20, p. 39–57.
- Skirrow, R.G., 2022. Hematite-group IOCG±U deposits: an update on their tectonic settings, hydrothermal characteristics, and Cu-Au-U mineralizing processes; in *Mineral systems with iron oxide-copper-gold (IOCG) and affiliated deposits*, (ed.) L. Corriveau, E.G. Potter, and A.H. Mumin; Geological Association of Canada, Special Paper 52, p. 27–51.
- Skirrow, R.G. and Davidson, G., 2007. A special issue devoted to Proterozoic iron oxide Cu-Au-(U) and gold mineral systems of the Gawler Craton: preface; *Economic Geology*, v. 102, p. 1373–1375. <https://doi.org/10.2113/gsecongeo.102.8.1373>
- Skirrow, R.G., and Walshe, J.L., 2002. Reduced and oxidized Au-Cu-Bi iron oxide deposits of the Tennant Creek inlier, Australia: an integrated geologic and chemical model; *Economic Geology*, v. 97, p. 1167–1202. <https://doi.org/10.2113/gsecongeo.97.6.1167>
- Skirrow, R.G., Huston, D.L., Mernagh, T.P., Thorne, J.P., Dulfer, H., and Senior, A.B., 2013. Critical commodities for a high-tech world: Australia’s potential to supply global demand; *Geoscience Australia, Canberra*, 118 p.

- Skirrow, R.G., van der Wielen, S.E., Champion, D.C., Czarnota, K., and Thiel, S., 2018. Lithospheric architecture and mantle metasomatism linked to iron oxide Cu-Au ore formation: multidisciplinary evidence from the Olympic Dam region, South Australia; *Geochemistry, Geophysics, Geosystems*, v. 19, p. 2673–2705. <https://doi.org/10.1029/2018GC007561>
- Skirrow, S.G., Murr, J., Schofield, A., Huston, D.L., van der Wielen, S., Czarnota, K., Coghlan, R., Highet, L.M., Connolly, D., Doublier, M., and Duan, J., 2019. Mapping iron oxide Cu-Au (IOCG) mineral potential in Australia using a knowledge-driven mineral systems-based approach; *Ore Geology Reviews*, v. 113, p. 103011. <https://doi.org/10.1016/j.oregeorev.2019.103011>
- Slack, J., 2013. Descriptive and geoenvironmental model for cobalt–copper–gold deposits in metasedimentary rocks; United States Geological Survey, Scientific Investigations Report 2010-5070-G, 218 p. <http://doi.org/10.3133/sir20105070g>
- Slack, J., Corriveau, L., and Hitzman, M., 2016. A special issue devoted to Proterozoic iron oxide-apatite (\pm REE) and iron oxide-copper-gold and affiliated deposits of Southeast Missouri, U.S.A., and the Great Bear magmatic zone, Northwest Territories, Canada; Preface *in* Proterozoic iron oxide-apatite (\pm REE) and iron oxide-copper-gold and affiliated deposits of Southeast Missouri, U.S.A., and the Great Bear magmatic zone, Northwest Territories Canada, (ed.) J. Slack, L. Corriveau, and M. Hitzman; *Economic Geology*, v. 111, p. 1803–1814.
- Smar, L., 2015. Complex P-T-t-d history of supracrustal rocks of the metamorphic internal zone of the southern Wopmay Orogen, N.W.T.; M.Sc. thesis, University of British Columbia, Vancouver, British Columbia, 171 p.
- Somarin, A.K. and Mumin, A.H., 2012. The Paleoproterozoic high heat production Richardson granite, Great Bear magmatic zone, Northwest Territories, Canada: source of U for Port Radium; *Resource Geology*, v. 62, p. 227–242. <https://doi.org/10.1111/j.1751-3928.2012.00192.x>
- Somarin, A.K. and Mumin, A.H., 2014. P–T-composition and evolution of paleofluids in the Paleoproterozoic Mag Hill IOCG hydrothermal system, Contact Lake belt, Northwest Territories, Canada; *Mineralium Deposita*, v. 49, p. 199–215. <https://doi.org/10.1007/s00126-013-0482-3>
- Somarin, A.K., Breen, W., Arbuckle, B., and Mumin, A.H., 2015a. East Mile Lake geology; Sheet 10 *in* Echo Bay IOCG thematic map series: geology, structure and hydrothermal alteration of a stratovolcano complex, Northwest Territories, Canada, (ed.) A.H. Mumin; Geological Survey of Canada, Open File 7807, scale 1:2200. <https://doi.org/10.4095/296614>
- Somarin, A.K., Jones, B., Mumin, A., Breen, W., and Mumin, A.H., 2015b. Mag Hill–Central Block, geology and hydrothermal alteration; Sheet 14 *in* Echo Bay IOCG thematic map series: geology, structure and hydrothermal alteration of a stratovolcano complex, Northwest Territories, Canada, (ed.) A.H. Mumin; Geological Survey of Canada, Open File 7807, scale 1:1600. <https://doi.org/10.4095/296618>
- Somarin, A.K., Mumin, A., Jones, B., Breen, W., and Mumin, A.H., 2015c. Mag Hill–Northeast Block, geology and hydrothermal alteration; Sheet 13 *in* Echo Bay IOCG thematic map series: geology, structure and hydrothermal alteration of a stratovolcano complex, Northwest Territories, Canada, (ed.) A.H. Mumin; Geological Survey of Canada, Open File 7807, scale 1:1600. <https://doi.org/10.4095/296617>
- Somarin, A.K., Mumin, A., Jones, B., Breen, W., and Mumin, A.H., 2015d. Mag Hill–Southwest Block, geology and hydrothermal alteration; Sheet 15 *in* Echo Bay IOCG thematic map series: geology, structure and hydrothermal alteration of a stratovolcano complex, Northwest Territories, Canada, (ed.) A.H. Mumin; Geological Survey of Canada, Open File 7807, scale 1:1600. <https://doi.org/10.4095/296619>
- Sparkes, G., 2017. Uranium mineralization within the Central Mineral Belt of Labrador: a summary of the diverse styles, settings and timing of mineralization; Newfoundland and Labrador Department of Resources, Open File LAB/1684, 198 p.
- Sparkes, G. and Kerr, A., 2008. Diverse styles of uranium mineralization in the Central Mineral Belt of Labrador: an overview and preliminary discussion; Newfoundland and Labrador Department of Natural Resources, Geological Survey, Report 08-1, p. 193–227.
- Sparkes, G., Dunning, G., Fonkwe, M., and Langille, A., 2016. Age constraints on the formation of the iron oxide-rich hydrothermal breccias of the Moran Lake area: evidence for potential IOCG-style mineralization within the Central Mineral Belt of Labrador; Newfoundland and Labrador Department of Natural Resources, Geological Survey, Report 16-1, p. 71–90.
- Sparkes, G.W., Dunning, G.R., and Langille, A., 2017. The Michelin deposit: an example of albitite-hosted uranium mineralization within the Central Mineral Belt of Labrador; Newfoundland and Labrador Department of Natural Resources, Geological Survey, Report 17-1, p. 219–238.
- Spratt, J.E., Jones, A.G., Jackson, V.A., Collins, L., and Avdeeva, A., 2009. Lithospheric geometry of the Wopmay orogen from a Slave craton to Bear Province magnetotelluric transect; *Journal of Geophysical Research*, v. 114, issue B1, 18 p. <https://doi.org/10.1029/2007JB005326>
- Th̄çh̄q̄ Government, 2013. Th̄çh̄q̄ Wenek̄'e/Th̄çh̄q̄ land use plan; Th̄çh̄q̄ Government, 66 p. <<https://www.tl̄ich̄o.ca/government/departments/culture-lands-protection/lands-protection>> [accessed June 13, 2013].
- Trapy, P.-H., 2018. Modélisation d'équilibre de phase prédictive des faciès d'altération associés aux gîtes à oxydes de fer-cuivre-or dans les terrains de hauts grades métamorphiques; M.Sc. thesis, École polytechnique de Montréal, Montréal, Quebec, 138 p.
- Trottier, C.R.M., 2019. Fluid inclusion, stable and radiogenic isotope, and geochronological investigation of the polymetallic “five-element” vein deposit at the Eldorado Mine, Port Radium, Northwest Territories, Canada; M.Sc. thesis, Saint Mary's University, Halifax, Nova Scotia, 186 p.

- Wade, C.E., Reid, A., Wingate, M.T.D., Jagodzinski, E.J., and Barovich, K., 2012. Geochemistry and geochronology of the ca. 1585 Ma Benagerie Volcanic Suite, southern Australia: relationship to the Gawler Range Volcanics and implications for the petrogenesis of a Mesoproterozoic silicic large igneous province; *Precambrian Research*, v. 206–207, p. 17–35. <https://doi.org/10.1016/j.precamres.2012.02.020>
- Wheeler, J.O., Hoffman, P.F., Card, K.D., Davidson, A., Sanford, B.V., Okulitch, A.V., and Roest, W.R., 1996. Geological map of Canada/Carte géologique du Canada; Geological Survey of Canada, Map 1860A, scale 1:5 000 000. <https://doi.org/10.4095/208175>
- Whitney, D.L. and Evans, B.W., 2010. Abbreviations for names of rock-forming minerals; *American Mineralogist*, v. 95, p. 185–187. <https://doi.org/10.2138/am.2010.3371>
- Wilde, A., 2013. Towards a model for albitite-type uranium; *Minerals*, v. 3, p. 36–48. <https://doi.org/10.3390/min3010036>
- Wilde, A., Otto, A., Jory, J., MacRae, C., Pownceby, M., Wilson, N., and Torpy, A., 2013. Geology and mineralogy of uranium deposits from Mount Isa, Australia: implications for albitite uranium deposit models; *Minerals*, v. 3, p. 258–283.
- Williams, M.R., Holwell, D.A., Lilly, R.M., Case, G.N.D., and McDonald, I., 2015. Mineralogical and fluid characteristics of the fluorite-rich Monakoff and E1 Cu–Au deposits, Cloncurry region, Queensland, Australia: implications for regional F–Ba-rich IOCG mineralisation; *Ore Geology Reviews*, v. 64, p. 103–127.
- Williams, P.J., 2010a. Classifying IOCG deposits; *in Exploring for iron oxide copper-gold deposits: Canada and global analogues*, (ed.) L. Corriveau and A.H. Mumin; Geological Association of Canada, Short Course Notes 20, p. 13–21.
- Williams, P.J., 2010b. “Magnetite-group” IOCGs with special reference to Cloncurry and Northern Sweden: settings, alteration, deposit characteristics, fluid sources, and their relationship to apatite-rich iron ores; *in Exploring for iron oxide copper-gold deposits: Canada and global analogues*, (ed.) L. Corriveau and A.H. Mumin; Geological Association of Canada, Short Course Notes 20, p. 23–38.
- Williams, P.J., Barton, M.D., Johnson, D.A., Fontboté, L., de Haller, A., Mark, G., Oliver, N.H.S., and Marschik, R., 2005. Iron-oxide copper-gold deposits: geology, space-time distribution, and possible modes of origin; *Economic Geology*, 100th Anniversary Volume, p. 371–405.
- Wilton, D.H.C., 1996. Metallogeny of the Central Mineral Belt and adjacent Archean basement, Labrador; Government of Newfoundland and Labrador, Department of Mines and Energy, Geological Survey and Mineral Resources, Report 8, p. 178.
- Wise, T., 2019a. IOCG prospectivity modelling of the Olympic Cu–Au Province; Geological Survey of South Australia, Department for Energy and Mining, DIGIMAP 00093, scale 1:2 000 000.
- Wise, T., 2019b. Prospectivity modelling of the Olympic Cu–Au Province; *MESA Journal*, v. 90, p. 36–41.
- Xavier, R.P., Wiedenbeck, M., Trumbull, R.B., Dreher, A.M., Monteiro, L.V.S., Rhede, D., de Araújo, C.E.G., and Torresi, I., 2008. Tourmaline B-isotopes fingerprint marine evaporites as the source of high-salinity ore fluids in iron oxide copper-gold deposits, Carajás Mineral Province (Brazil); *Geology*, v. 36, p. 743–746. <https://doi.org/10.1130/G24841A.1>
- Xavier, R.P., Moreto, C.P.N., Monteiro, L.V.S., Melo, G.H.C., Toledo, P., Hunger, R.B., Delinardo da Silva, M., Previato, M., Jesus, S.S.G.P., and Huhn, S.B., 2017. Geology and metallogeny of Neoproterozoic and Paleoproterozoic copper systems of the Carajás domain, Amazonian Craton, Brazil; *Proceedings of the 14th SGA Biennial Meeting; Society for Geology Applied to Mineral Deposits*, August 20–23, 2017, Québec, Quebec, p. 899–902.
- Yarie, Q. and Wray, N., 2019. National Instrument 43-101 technical report for the SPJ project; MacDonald Mines Exploration Ltd., 108 p. <www.sedar.com> [accessed January 11, 2022].
- Zeng, L., 2020. Formation mechanism and genetic model of iron-oxide apatite deposits in the Ningwu district, China; Ph.D. thesis, China University of Geosciences, Wuhan, China, 270 p.
- Zhao, X.-F., Chen, H., Zhao, L., and Zhou, M.-F., 2022. Linkages among IOA, skarn, and magnetite-group IOCG deposits in China: from deposit studies to mineral potential assessment; *in Mineral systems with iron oxide-copper-gold (IOCG) and affiliated deposits*, (ed.) L. Corriveau, E.G. Potter, and A.H. Mumin; Geological Association of Canada, Special Paper 52, p. 383–407.
- Zharikov, V.A., Pertsev, F.N., Rusinov, V.L., Callegari, E., and Fettes, D.J., 2007. Metasomatism and metasomatic rocks; *in Metamorphic rocks: a classification and glossary of terms – Recommendations by the IUGS Subcommittee on the Systematics of Metamorphic Rocks*, (ed.) D. Fettes and J. Desmons; Cambridge University Press, Cambridge, United Kingdom, 17 p. <<https://stuff.mit.edu/afs/athena.mit.edu/course/12/12.115/OldFiles/www/12.114%20Papers/BGS/Metamorphic/DetailedMetamorphic/9%20Metasomatism%20and%20metasomatic%20rocks.pdf>> [accessed January 31, 2013].

Record of Precambrian orogenic unroofing preserved in fluvial strata of western Nunavut

A. Ielpi^{1*}, R.H. Rainbird², and W.J. Davis²

Ielpi, A., Rainbird, R.H., and Davis, W.J., 2024. Record of Precambrian orogenic unroofing preserved in fluvial strata of western Nunavut; in Canada's northern shield: new perspectives from the Geo-mapping for Energy and Minerals program, (ed.) S.J. Pehrsson, N. Wodicka, N. Rogers, and J.A. Percival; Geological Survey of Canada, Bulletin 612, p. 99–114. <https://doi.org/10.4095/332496>

Abstract: Fluvial sandstone in the Kilohigok and Elu basins of western Nunavut record deposition related to the amalgamation and tenure of the Nuna supercontinent. The ca. 1.9 Ga Burnside River Formation was sourced by erosional unroofing of the nearly coeval Thelon Orogen, about 250 km away, in a regime of crustal flexure. This proximally sourced sandstone contains abundant clustered channel forms that point to high-magnitude discharge and sediment yield in weakly mobile channels. By comparison, the ca. 1.6 Ga Ellice Formation was sourced by the erosional unroofing of the ca. 1.8 Ga Trans-Hudson Orogen, about 1000 km away, in a geodynamic regime of thermally driven sagging. The distally sourced Ellice Formation contains some rare and nonclustered channel forms that point to lesser discharge and sediment yield in mobile channels. Provenance analysis and plate models support links between the fluvial style of the Burnside River and Ellice formations and orogenic unroofing facilitated by Hadley-cell atmospheric circulation at tropical paleolatitudes.

Résumé : Dans les bassins de Kilohigok et d'Elu, dans l'ouest du Nunavut, des grès fluviaux témoignent de la sédimentation associée à l'assemblage et à l'existence du supercontinent Nuna. Les matériaux de la Formation de Burnside River, qui remonte à environ 1,9 Ga, proviennent de la dénudation par érosion de l'orogène de Thelon, d'un âge à peu près semblable et éloigné d'environ 250 km, dans un régime de flexure crustale. Ces grès à source proximale renferment d'abondantes formes de chenaux groupés, qui sont l'indication de forts débits et de grandes charges de sédiments dans des chenaux peu mobiles. En contrepartie, la Formation d'Ellice, qui remonte à environ 1,6 Ga, tire ses matériaux de la dénudation par érosion de l'orogène trans-hudsonien, distant d'environ 1000 km et âgé d'environ 1,8 Ga, dans un régime géodynamique d'affaissement de source thermique. La Formation d'Ellice, aux matériaux de provenance distale, contient peu de formes de chenaux et ceux-ci ne sont pas groupés, ce qui indique des débits plus faibles et des charges moindres de sédiments dans des chenaux mobiles. L'analyse de la provenance et les modèles de plaques soutiennent les liens entre le style fluvial des formations de Burnside River et d'Ellice et la dénudation orogénique, qui a été facilitée par la circulation atmosphérique liée aux cellules de Hadley aux paléolatitudes tropicales.

¹Harquail School of Earth Sciences, Laurentian University, Sudbury, Ontario P3E 2C6

²Geological Survey of Canada, 601 Booth Street, Ottawa, Ontario K1A 0E8

*Corresponding author: A. Ielpi (email: aielpi@laurentian.ca)

INTRODUCTION

The erosional unroofing of orogenic edifices is widely recognized as a primary control on the delivery of detritus toward sedimentary basins downslope of mountain ranges (Summerfield and Hulton, 1994; Walling and Webb, 1996; Willett, 1999; Syvitski et al., 2003; Garzanti et al., 2007). Through self-sustained isostatic uplift and removal of progressively lower crustal panels (Beaumont et al., 1992; Hoffman and Grotzinger, 1993), erosional orogenic unroofing was responsible for global-scale mass transfer of sediment (Syvitski et al., 2003). The highest rates of sediment yield were recorded in the forelands of young orogenic belts facing moist atmospheric circulation systems (Métivier et al., 1999; Syvitski et al., 2014).

The modes and tempos of orogenic unroofing are dictated by an orogen's width, crustal thickness, and associated metamorphic gradients as well as by the prevailing climate and biogeomorphic setting at the time (Beaumont et al., 1992; Hoffman and Grotzinger, 1993; Willett, 1999; Syvitski et al., 2003). An overarching goal of Precambrian geology is to decipher secular trends in planetary, crustal, and surface processes through the study of Earth's rock record. Questions linger about the evolution of orogenic style through time (e.g. Percival et al., 2012; Weller and St-Onge, 2017) as well as the influence of diverse micro- and macroscopic biotic communities on surface weathering (Eriksson et al., 1998; Long, 2011; Ielpi et al., 2018a). A topic of particular interest to sedimentologists is the comparison between fluvial strata deposited before and after the early Paleozoic radiation of macroscopic life — and, specifically, vascular vegetation — across Earth's continents (Davies and Gibling, 2010; Santos et al., 2017; Ielpi 2018; Ganti et al., 2019; Ielpi and Lapôtre, 2020). Fluvial strata are important for their ability to record information about provenance and physical processes at the time of deposition.

This paper presents a summary of three field seasons of study (2014–2016) in the Kilohigok and Elu basins of western Nunavut, Arctic Canada (Fig. 1), as part of the second phase of the Geo-mapping for Energy and Minerals program of the Geological Survey of Canada. Studies included thematic sedimentology of terrigenous sandstone deposits, characterization of their provenance, and assessment of their potential for uranium enrichment. Here the focus is on a sedimentological and depositional-architectural characterization of two well preserved Paleo- to Mesoproterozoic sandstone units of the Burnside River and Ellice formations. Aspects of sedimentation in two basin tracts interpreted to be occupying proximal and distal locations to their upland source areas are discussed, and the relationship between depositional style as well as patterns of orographic precipitation and orogenic unroofing are assessed. This study ultimately serves to demonstrate that, once integrated with provenance data, fluvial sedimentary records can be interrogated to test and refine extant paleogeographic and paleoclimate models.

GEOLOGICAL SETTING

Laurentia, the ancestral core of North America, preserves an assemblage of crustal blocks that are inferred to have amalgamated during a time of global orogenesis at ca. 2.1 to 1.8 Ga (Hoffman, 1988; Zhao et al., 2002; Pehrsson et al., 2016), and that resulted from the collision of pre-existing crustal blocks, including the Superior, Hearne, Sask, Wyoming, Rae, and Slave cratons (Bleeker, 2003; Pehrsson et al., 2013). Products of this amalgamation are a set of highly deformed and metamorphosed sutures between pre-existing cratons (inferred to represent the roots of now deeply eroded orogenic belts; e.g. Berman et al., 2013) and widespread, poorly deformed, and weakly metamorphosed sandstone, shale, and carbonate strata (inferred to represent, in turn, the remnants of large sedimentary basins developed during supercontinent amalgamation, tenure, and breakup (e.g. Young et al., 1979; Rainbird et al., 1996; Davidson, 2008). Causal links between the repeated erosional unroofing of orogens in the Canadian Shield and the development of large syn- to postorogenic basins are supported by provenance analysis (McCormick, 1992; Rainbird and Young, 2009; Rainbird et al., 2017).

Sedimentary basins preserved on the Slave Craton in western Nunavut include the Kilohigok and Elu basins (Fig. 1), which record fluvial-eolian to shallow-marine deposition at ca. 2.0 to 1.8 Ga and 1.6 to 1.3 Ga, respectively (Campbell, 1979; Campbell and Cecile, 1981; Grotzinger and McCormick, 1988; Bowring and Grotzinger, 1992; Heaman et al., 1992; Ielpi and Rainbird, 2015, 2016). Theories proposed to explain the development of such basins included failed rifting and intracratonic extension (Hoffman, 1973; Campbell and Cecile, 1981). The Kilohigok Basin is hypothesized to have been a foreland basin, produced by crustal flexure accompanying loading of the Rae Craton (upper plate) onto the Slave Craton during the Thelon Orogeny (Grotzinger and Gall, 1986; Grotzinger and McCormick, 1988; Tirrul and Grotzinger, 1990). The Elu Basin is considered to be one of a family of intracontinental basins formed by thermal subsidence following the Hudsonian Orogeny and amalgamation of the Nuna supercontinent (Rainbird and Young, 2009; Rainbird et al., 2014; Ielpi and Rainbird, 2015).

Basin stratigraphy

The Kilohigok and Elu basins together encompass about 10 km of strata exposed for about 800 km along strike (Campbell and Cecile, 1976; Campbell, 1981; Grotzinger and McCormick, 1988), although a composite stratigraphic section can only be reconstructed in the central Bathurst Inlet area (Fig. 2). Sedimentary rocks in the region are mainly underlain by late Archean (ca. 2700–2580 Ma; Sherlock et al., 2012) granitoid rocks, gneiss, and intervening metasedimentary and metavolcanic panels (Culshaw and van Breeman, 1990; Sherlock et al., 2012). In the Kilohigok Basin, fluvial to tide-dominated shallow-marine conditions

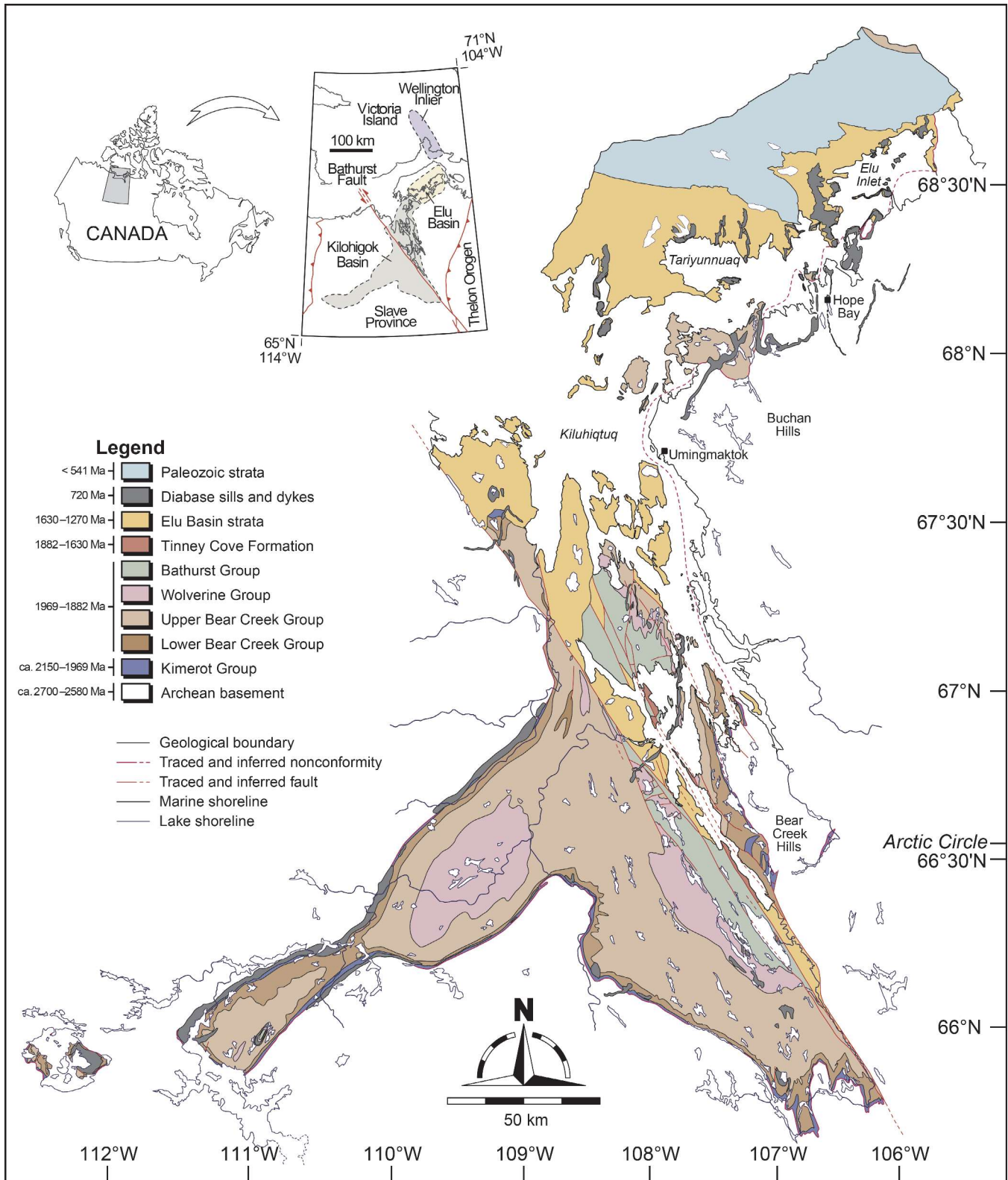


Figure 1. Geographic and geological setting of the Kilohigok and Elu basins, western Nunavut (modified from Campbell and Cecile, 1976; Ielpi et al., 2017a).

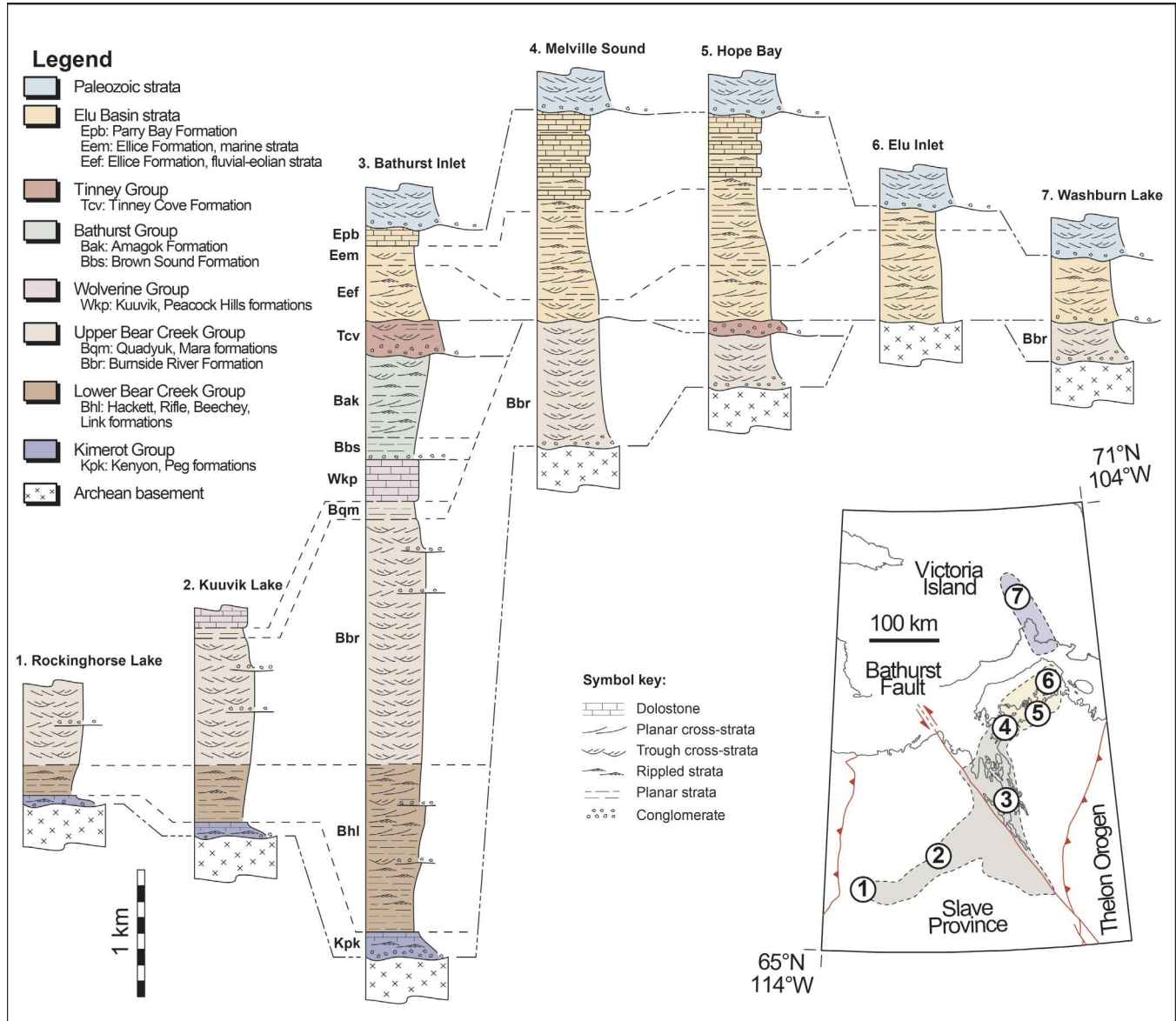


Figure 2. Simplified stratigraphic sections through the Kilohigok and Elu basins, western Nunavut (*modified from Campbell and Cecile 1976, 1981; Grotzinger and McCormick, 1988; Ielpi and Rainbird, 2015, 2016*). The stratigraphic profile mimics grain-size-controlled weathering profiles on outcrop.

along a stable platform margin are recorded at ca. 2150 to 1969 Ma (Bowring and Grotzinger, 1992; Bradley, 2008; Sheen et al., 2019) by conglomerate, sandstone, and dolostone of the Kimerot Group (Fig. 3a; Grotzinger and Gall, 1986). Although the geodynamic significance of the Kimerot Group and broadly correlative successions preserved on the Slave Craton (e.g. the East Arm Basin; Sheen et al., 2019) is being re-evaluated, these units have previously been interpreted to represent rifting and drifting along a Slave Craton passive margin (Grotzinger and Gall, 1986). The overlying Bear Creek, Wolverine, and Bathurst groups (1969–1882 Ma; Bowring and Grotzinger, 1992) are composed of a largely clastic succession that transitions upsection from deep- to shallow-marine facies (Fig. 3b), and thick terrestrial sandstone, with minor

conglomerate (e.g. the Burnside River Formation; Fig. 3c, d). These groups are inferred to represent crustal flexure and foredeep development in response to collision between the Slave and Rae cratons (Grotzinger and McCormick, 1988; Grotzinger et al., 1989; Tirrul and Grotzinger, 1990), an inference substantiated by geochronological constraints pointing to nearly synchronous Thelon Orogeny and Bear Creek Group deposition (Bowring and Grotzinger, 1992; Berman et al., 2015).

The transition from Kilohigok Basin to Elu Basin deposition is placed at the regionally unconformable boundary between the Bathurst Group and overlying Tinney Cove Formation (the latter dated at 1882 to 1630 Ma; Bowring

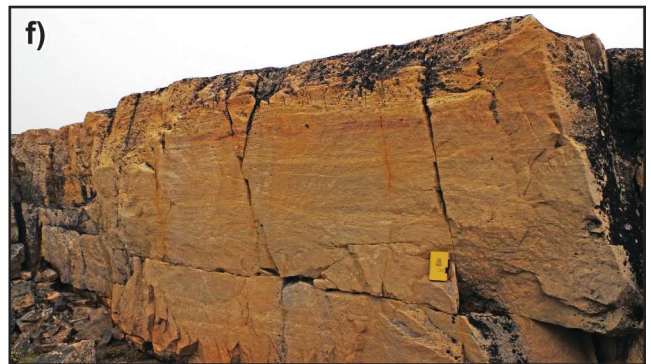


Figure 3. Representative field photographs of the stratigraphy in the Kilohigok and Elu basins, western Nunavut: **a**) intertidal stromatolitic dolostone, Peg Formation, Kimerot Group; lens cap for scale (about 5 cm in diameter and circled in yellow); NRCan photo 2019-739; **b**) deep-marine (i.e. below wave base) shale and sandstone, lower Bear Creek Group; marker for scale (10 cm long); NRCan photo 2019-752; **c**) extrabasinal pebble-conglomerate of alluvial fan origin, Burnside River Formation, upper Bear Creek Group; lens cap for scale (about 5 cm in diameter and circled in yellow); NRCan photo 2019-753; **d**) cross-stratified sandstone of fluvial origin, Burnside River Formation, upper Bear Creek Group; field book for scale (about 10 cm long and circled in yellow); NRCan photo 2019-757; **e**) intrabasinal scree-slope breccia (individual clasts are derived from the underlying Burnside River Formation), Tinney Cove Formation; hammer for scale (about 30 cm long); NRCan photo 2019-740; **f**) planar-bedded and cross-stratified fluvial sandstone, Ellice Formation, Elu Basin; field book for scale (about 9 cm long); NRCan photo 2019-756; **g**) cross-stratified sandstone and planar-bedded dolostone of shallow-marine origin, Ellice Formation, Elu Basin; field book for scale (about 9 cm long); NRCan photo 2019-754; **h**) inter- to subtidal stromatolitic dolostone, Parry Bay Formation, Elu Basin; field book for scale (about 9 cm long); NRCan photo 2019-755. All photographs by A. Ielpi.

and Grotzinger, 1992). The Tinney Cove Formation records the localized deposition of scree-slope breccia and conglomerate units overlain by immature terrestrial sandstone (Fig. 3e; Campbell, 1978). Although inferring a geodynamic setting from such geographically and stratigraphically limited deposits is fraught with uncertainty, the Tinney Cove Formation can be tentatively related to extensional block-faulting of older Kilohigok Basin strata in the aftermath of the amalgamation of the supercontinent Nuna (Rainbird et al., 2014). Such a hypothesis is consistent with the stratigraphic development of the overlying Elu Basin strata (bracketed between 1630 and 1270 Ma; Heaman et al., 1992; Rainbird et al., 2014), which is proposed to record thermally driven intraplate sagging and the establishment of a widespread terrestrial to nearshore-marine depression (e.g. Ellice Formation; Fig. 3f–h; Rainbird et al., 2014; Ielpi and Rainbird, 2015).

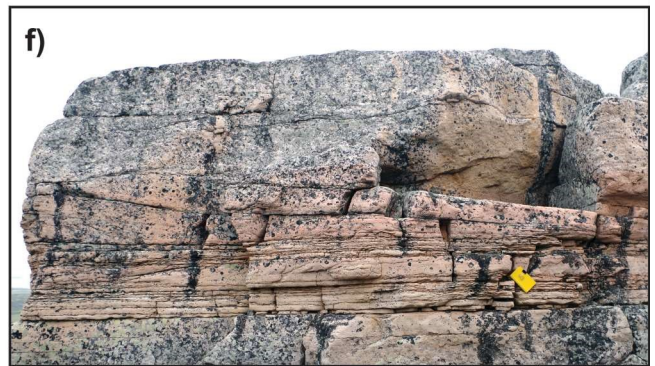
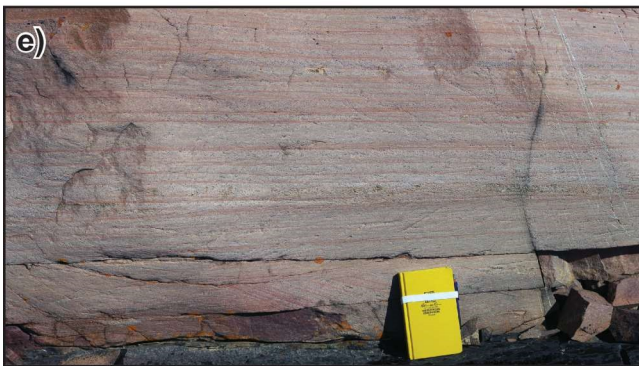
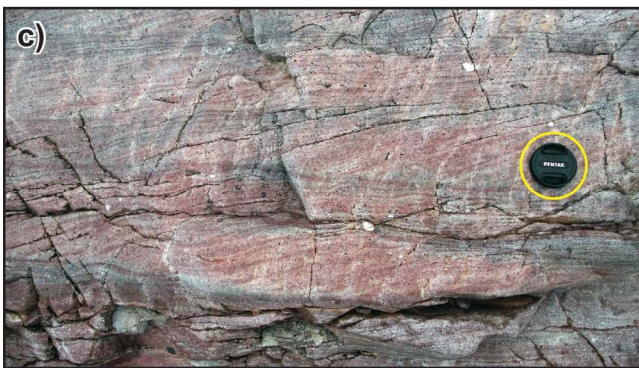
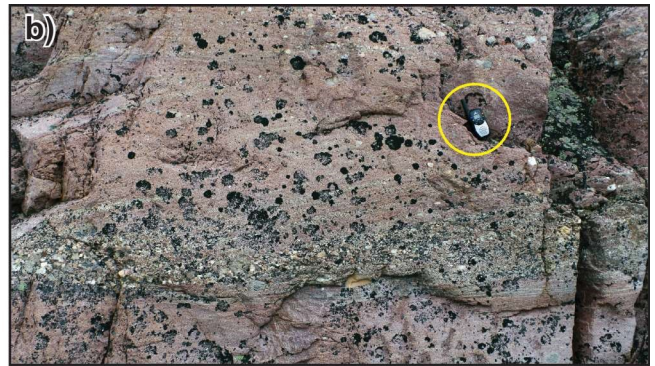
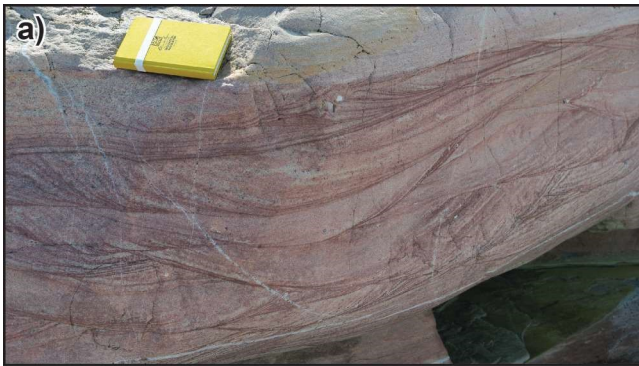
SEDIMENTOLOGY

Thick and regionally extensive fluvial sandstone units like the Burnside River and Ellice formations often exhibit a limited number of sedimentary facies in outcrop (Miall, 1996). Such sedimentary facies point to shared physical processes that are common to most fluvial systems irrespective of their planform (Brierley and Hickin, 1991; Ethridge, 2011). It is rather the appreciation of depositional architecture, at scales varying from that of metres to kilometres, and paleoflow analysis that allow for the eventual inference

of (pre-vegetation) fluvial style (Long, 2011; Hartley et al., 2015; Ielpi et al., 2018b). Details about the methodological approaches employed to collect sedimentological, depositional architecture, and paleoflow data sets are contained in previous publications, to which the reader is referred (e.g. Ielpi and Rainbird, 2015, 2016; Ielpi et al., 2015, 2017a).

Analysis of the fluvial deposits of both the Burnside River and Ellice formations has revealed the common occurrence of the following facies. Cross-stratified sandstone (Fig. 3d, f, 4a), pebbly in places (Fig. 4b) and with foresets dipping at 5° to 20°, is by far the most abundant (~80% of inferred volume). Cross-sets present a predominantly trough-like (Fig. 4a) and, less frequently, planar (Fig. 4c) geometry, and range in thickness from 0.1 to approximately 1.5 m. Monotonous bedsets of cross-stratified sandstone reach up to tens of metres in thickness. In places, such crossbeds bear submetre-scale soft-sediment deformation such as, for example, overturned and dissected foresets (Fig. 4d) or, less frequently, water-escape cusped structures. Crossbeds are interpreted as a record of the accretion and migration of dunes in subcritical flow regime (Collinson et al., 2006), and their widespread occurrence in Precambrian environments is related to deposition by sustained, perennial flows in relatively deep (>1 m) fluvial channels (Todd and Went, 1991; Nicholson, 1993; Long, 2006). Soft-sediment deformation is a common feature of prevegetation fluvial sandstone units and, when at the submetre scale, is associated with flow-induced bed shearing or dewatering soon after high bedload yield (Owen, 1995; Owen and Santos, 2014; Ielpi and Ghinassi, 2015).

Figure 4. Sedimentary facies observed in the Burnside River and Ellice formations, western Nunavut: **a**) trough cross-stratified sandstone; field book for scale (about 9 cm long); NRCan photo 2019-744; **b**) trough cross-stratified sandstone, pebbly in places; hand-held radio for scale (about 10 cm long and circled in yellow); NRCan photo 2019-745; **c**) planar-cross-stratified sandstone; lens cap for scale (about 5 cm in diameter and circled in yellow); NRCan photo 2019-746; **d**) cross-stratified sandstone with flow-induced sheared foresets (highlighted by dashed lines); field book for scale (about 9 cm long); NRCan photo 2019-747; **e**) planar-stratified sandstone; field book for scale (about 9 cm long); NRCan photo 2019-748; **f**) assemblage of planar-stratified and low-angle cross-stratified sandstone; field book for scale (about 9 cm long); NRCan photo 2019-749; **g**) current ripples preserved on a bedding plane; field book for scale (about 9 cm long); NRCan photo 2019-750; **h**) wave ripples preserved on a bedding plane; field book for scale (about 9 cm long); NRCan photo 2019-751. All photographs by A. Ielpi.



Second in order of abundance (~15% of inferred volume) is an assemblage of planar cross-stratified sandstone (Fig. 4e), pebbly in places or, rarely, arranged in wavy- and lenticular-bedded sets, and low-angle cross-stratified sandstone (i.e. foreset dipping <5°; Fig. 4f). Bedsets of planar cross-stratified and low-angle cross-stratified sandstone reach up to just under a metre in thickness. Their occurrence signifies deposition of low-relief dunes and flat-lying traction carpets in either transcritical or supercritical flow regime (represented by low-angle cross-sets and planar sets, respectively; Collinson et al., 2006). An interpretation of high-flow-strength bedforms such as antidunes preserved as wavy- and lenticular-bedded sets is also viable (Fielding, 2006). Accordingly, their occurrence in Precambrian fluvial sandstone units is traditionally interpreted to indicate episodes of ephemeral discharge (Røe, 1987; Lebeau and Ielpi, 2017) in shallow (<1 m deep) channels.

Fluvial strata of the Burnside River and Ellice formations also contain rare (~5% of inferred volume) tabular beds of rippled sandstone, a few centimetres to a decimetre thick (exceptionally up to 2 m thick). Ripples mainly point to unidirectional flow (Fig. 4g), although centimetre-thick layers preserving wave-ripple morphology (Fig. 4h) have also been observed. These deposits represent subcritical flow-regime deposition in ripple-bed configuration (Collinson et al., 2006) and are typically attributed to waning-flood and shallowing-water discharge stages (Sønderholm and Tirsgaard, 1998). The less common preservation of wave-ripple forms accordingly suggests bed reworking in wind-stressed shallow ponds that were located beside active fluvial channels (Fralick and Zaniewski, 2012).

Finally, it is important to point out that, beside the preponderance of fluvial deposits, both the Burnside River and Ellice formations contain a portion of supermature and very well sorted, fine-grained quartz arenite. These deposits feature quartz grains with frosted surface, pin-stripe stratification that is characterized by locally inversely graded laminae, within large-scale sets of crossbeds with basal deflation lags. All these features are classically related to eolian transport (Chakraborty, 1991; Cain and Mountney, 2009). Although the sedimentological features of eolian facies appear comparable in the two formations, architectural analysis of large exposures of the eolian strata using satellite imagery highlighted different relationships with adjoining fluvial strata. In the Burnside River Formation, eolian deposits appear to have been limited to simple dunes developed atop interfluvies, i.e. locally developed flat surfaces found in-between entrenched channels (Ielpi and Rainbird, 2016). By comparison, areally more extensive eolian deposits of the Ellice Formation display a complex internal interstratification and were related to comparatively mature dune fields developed over larger basin tracts flanking fluvial-channel belts (Ielpi and Rainbird, 2015).

PALEOFLOW ANALYSIS

A large data set of paleoflow vectors collected from both the Burnside River and Ellice formations points to northwestward shedding of detritus (present co-ordinates; Fig. 5), a recurring theme in many Proterozoic sandstone units preserved on the Canadian Shield (Rainbird and Young, 2009; Rainbird et al., 2014, 2017). Specifically, paleoflow data from the Burnside River Formation exposed in northern Kiluhiquaq (formerly Bathurst Inlet) and Tariyunnuaq (formerly Melville Sound) indicate focused to mildly dispersed unimodal transport over the north-northeastern to west-northwestern quadrants, yet notably with a cluster of paleoflow data pointing to opposite, eastward paleoflow, in the southwestern corner of the sampled area (Fig. 5). Paleoflow data from the Ellice Formation, exposed in Tariyunnuaq and Elu Inlet, point instead to mildly dispersed, unimodal transport toward the north-northwestern to west-southwestern quadrants (Fig. 5).

DEPOSITIONAL ARCHITECTURE

A remarkable feature of the study area is the abundance of exposures where undeformed sections, hundreds of metres thick and several kilometres wide, can be observed (e.g. Fig. 6a). Such exceptional quality of exposure allowed the examination of depositional geometry at a scale that typically remains unresolved in Precambrian basins. Full details on the depositional architecture of the Burnside River and Ellice formations are published elsewhere (Ielpi and Rainbird, 2015, 2016) and here, only details relevant to their style of channellization are reported.

Several architectural elements were recognized with the aid of satellite-based imagery and oblique aerial photography; these included laterally continuous sand sheets, large-scale cross-stratified fluvial-bar complexes, and, perhaps most notably, active-channel forms in both formations (the latter a feature thought to be uncommon in Precambrian fluvial strata; Davies and Gibling, 2010). Channel forms consist of sand bodies floored by scoop-shaped erosional surfaces and composed of sedimentary facies pointing to the direction of active flow (as opposed to abandonment intervals; cf. Toonen et al., 2012). The discrimination between channel forms and other architectural elements, such as valley fills, relied on criteria discussed by Gibling (2006) and Gibling et al. (2011), such as: 1) the identification of fluvial bars within the channel forms, approximating the thickness of the latter; 2) the lack of stratigraphic correlation between individual channel scours; and 3) the scalar disambiguation from observed valley fills, which consistently displayed 10- to 100-fold wider geometry.

Fifty-two active channel forms were recognized in the Burnside River Formation. These channel forms are observed in distinct, narrow clusters (Fig. 6a) and are contained within stratigraphic sections underlain by a basin-floor unconformity that displays up to 250 m of relief 15 km along strike.

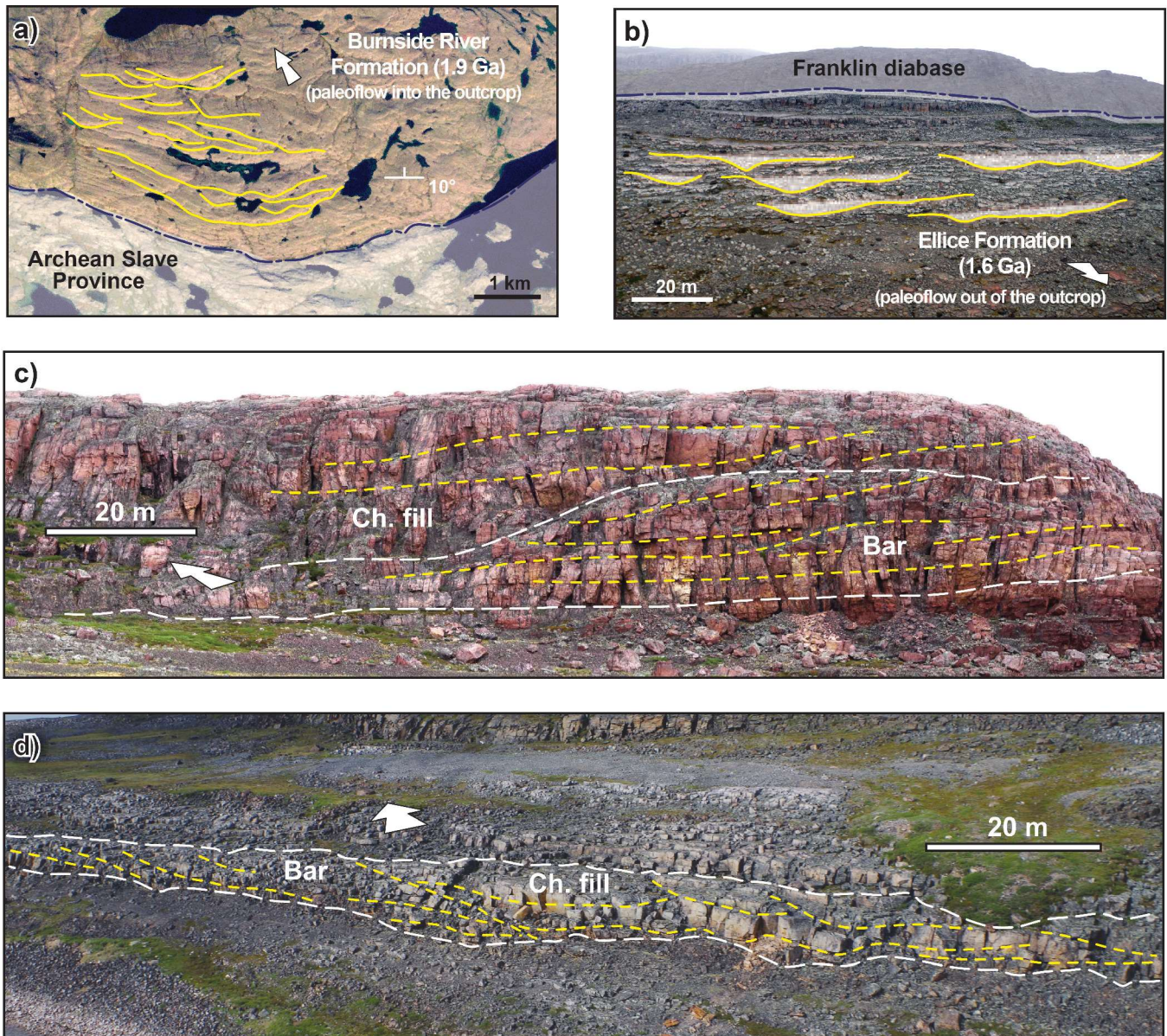


Figure 6. Depositional architecture of channel forms observed in the Burnside River and Ellice formations, western Nunavut (Ielpi et al., 2017b), including **a)** a satellite view of a cluster of channel forms in the lower stratigraphic portion of the Burnside River Formation, with individual channel forms delineated by yellow lines (note erosional relief along the unconformity with basement rocks); **b)** an oblique aerial photograph of channel forms of the Ellice Formation delineated by yellow lines and grey shading. Interpreted architectural panels showing representative examples of fluvial sediment bars (Bar) and fluvial channel fill (Ch. fill) from **c)** the Burnside River Formation and **d)** the Ellice Formation, with the white and yellow dashed lines indicating architectural-element boundaries and stratification patterns, respectively.

Such channel forms are 5 to 102 m thick and 92 to 1106 m wide. Accordingly, their aspect ratio (i.e. width to thickness) ranges from 9 to 83, averaging 37 (Ielpi et al., 2017b). Fluvial bars observed therein are less than 25 m thick and point to downstream accretion and migration, a feature consistent with dominantly low-sinuosity, weakly mobile channels characterized by a straight to braided planform (Fig. 6c). By comparison, eight active-channel forms were recognized in the Ellice Formation, within sections underlain by a basin-floor unconformity that displays up to 30 m of relief 20 km along strike. The channel forms of the Ellice Formation are not clustered (Fig. 6b), 50 cm to 7 m thick, and 5 to 400 m wide (Ielpi et al., 2017b). Their aspect ratio ranges from 6 to 57, averaging 21. Fluvial bars observed therein are less than 4 m thick and point to mixed modes of accretion and migration (dominantly downstream-lateral; Fig. 6d), which is consistent with mobile, low- to intermediate-sinuosity channels characterized by a wandering planform.

DISCUSSION AND CONCLUSIONS

Provenance

Inferences about the provenance of the Burnside River and Ellice formations are formulated based on regional basin analysis, paleoflow distribution, and detrital-zircon geochronology. Several features are consistent with a genetic link between the growth of the Thelon tectonic zone and the development of a foredeep in the Kilohigok Basin, including thickness trends, intrabasin unconformities, and kinematic indicators consistent with syndepositional crustal flexure and northwestward foredeep migration (Grotzinger and Gall, 1986; Grotzinger and McCormick, 1988; Grotzinger et al., 1989; Tirrul and Grotzinger, 1990). Combining the above with observed paleoflow trends (Fig. 5) leads to the formulation of a preferred hypothesis according to which much of the detritus from the Burnside River Formation is directly derived from erosion of the Thelon Orogen (Ielpi et al., 2017b). This inference is corroborated by upward compositional trends observed throughout the formation, such as a shift from monomictic to oligomictic conglomerate, the appearance of intrabasinal detritus, and an increase in feldspar content (Ielpi and Rainbird, 2016). Geochronological data presented in McCormick (1992) showed an important detrital-zircon age mode from the Burnside River Formation synchronous with peak metamorphism and deformation during the Thelon Orogeny (1.97–1.99 Ga), as well as older detrital ages (2.3–2.4 Ga) that the authors tentatively related to sediment sourcing from the Queen Maud Block, a crustal block exposed to the east of the Thelon Orogen and interpreted as part of the Rae Craton.

A number of regional aspects help to establish correlations between the Ellice Formation and other Canadian Shield sandstone units of similar vintage, e.g. the Barrenland Group of the Thelon Basin, the Athabasca group of the eponymous basin, and the Mountain Lake and Dismal Lakes groups of

the Hornby Bay Basin (Hadlari et al., 2006; Rainbird and Davis, 2007; Rainbird et al., 2007; Ramaekers, 2010; Hahn et al., 2013). Based on shared lithostratigraphic and inferred depositional development, and basin shape, size, and thickness, Fraser et al. (1970) first inferred that such sandstone units may represent the erosional remnants of a once wider deposit that blanketed the Canadian Shield — a hypothesis supported by, among others, Gall (1994), Rainbird et al. (2007), and Rainbird and Young (2009). Such aspects are consistent with the establishment of a pancontinental depositional realm that best fits with a sag basin sustained by thermal subsidence within a supercontinent interior (e.g. Armitage and Allen, 2010). Rainbird et al. (2014) also presented detrital-zircon geochronological data from a single Ellice Formation sample, which demonstrated a composite age spread with multiple peaks at 2.6 to 2.2 Ga, a dominant peak at 1.82 Ga, and a youngest peak at ca. 1.65 Ga. These age groups were interpreted to represent, respectively, both first-cycle and reworked detritus from Archean crystalline rocks and early Paleoproterozoic cover successions (2.6–2.2 Ga), and an important contribution from the erosion of syn- to postorogenic magmatic rocks of Hudsonian affinity (1.82–1.65 Ga) (Rainbird et al., 2014). Therefore, consistent with northwestward paleoflow data (Fig. 5) and detrital zircon ages from correlative successions, the Ellice Formation is interpreted as a far-travelled and, possibly, in part polycyclic product of unroofing of the Trans-Hudson Orogen (cf. Ielpi et al., 2017b).

Fluvial record of orogenic unroofing

Based on the available provenance data (McCormick, 1992; Rainbird et al., 2014), fluvial strata preserved in the Burnside River and Ellice formations may be related to drainage systems located about 250 km and 1000 km from their upland sediment source, respectively. Differences in their architectural style and paleochannel depths, estimated from the thickness of preserved fluvial bars (Nicholson, 1993; Chakraborty, 1999; Ielpi, 2018) are related to deposition in river tracts located in relative proximity and far away from their upper catchment basin.

Commonly preserved and well clustered channel forms in the Burnside River Formation are contained within stratigraphic sections floored by significant basement topography — features overall consistent with valley-confined fluvial systems (Heller and Paola, 1996; Ethridge, 2011). This inference is corroborated by the depositional style of fluvial bars preserved within channel forms, which points to low-sinuosity channels characterized by restricted lateral mobility (Bianchi et al., 2015; Ielpi et al., 2016). Furthermore, the relatively large scale of preserved channels (comparable in both width and inferred depth with modern ‘large rivers’; *sic* Latrubesse, 2015) points to drainage being focused in fluvial conduits capable of passing high-magnitude discharge and sediment supply. As originally proposed by Hoffman and Grotzinger (1993), such high-magnitude discharge and

sediment supply may have been sustained by orographic precipitation and enhanced orogenic unroofing on the windward side of the Thelon mountain range (Fig. 7a), which would have been impacted by northeasterly trade-wind circulation at near-equatorial latitudes (Pehrsson et al., 2016). Despite the relatively humid climate found on the windward side of mountain ranges, eolian strata in those locations can develop as architecturally simple dunes limited to interfluves protected by erosion (Mountney and Russell, 2009).

The lack of firm geochronological constraints on the deposition of the Elu Basin strata (for which a permissible age window of about 400 Ma exists; Rainbird et al., 2014) hinders a precise paleolatitudinal positioning of the Ellice Formation's fluvial system. Laurentia is nevertheless inferred to have remained at near-equatorial latitudes from 1.63 to 1.27 Ga (Pehrsson et al., 2016), although moist trade-wind circulation could have been somewhat weakened while transecting the vast interior of the Nuna supercontinent (Fig. 7b). Accordingly, far-travelled detritus is consistent with the occurrence of rarely preserved channel forms characterized by shallower depth and both higher sinuosity and mobility than the Burnside River Formation's counterparts. Together with the observation of gentle basement topography, these features are consistent with a mid-size, unconfined fluvial system, where drainage and sediment supply are progressively reduced downstream due to hydrological loss (related, in turn, to evaporation within a dry continental interior or within-basin infiltration; Cain and Mountney, 2009) and fractionation along bifurcating channels (Latrubesse, 2015; Weissmann et al., 2015). Consistent with

the hypothesis of deposition in a somewhat drier continental interior is the occurrence in the Ellice Formation of larger and architecturally complex eolian strata sets, which point to climate-controlled development of extensive dune fields adjacent to fluvial channel belts (e.g. Rogala et al., 2007).

Noteworthy corollaries to this analysis are that: 1) causal links can be tested between fluvial style, orogenic unroofing, and prevailing trade-wind generated by Hadley-cell circulation established as early as 1.9 Ga; 2) questions linger regarding the weakening and drying of trade-wind circulation across pre-vegetation supercontinent interiors; and 3) by the time of the Elu Basin's deposition, the orographic relief of the Thelon mountain range would have diminished enough to allow for the bypass of Hudsonian detritus to the Elu Basin.

ACKNOWLEDGMENTS

Fieldwork in the Kilohigok and Elu basins was supported by the second phase of the Geo-mapping for Energy and Minerals program led by the Geological Survey of Canada, part of Natural Resources Canada; the Strategic Investments in Northern Economic Development program, led by the Canadian Northern Development Agency; and the Canada-Nunavut Geoscience Office. Assistance in the field by J.W. Greenman and C.G. Creason is kindly acknowledged. This paper benefited from thorough reviews by R. McNaughton and Q. Gall. The lead author's fieldwork

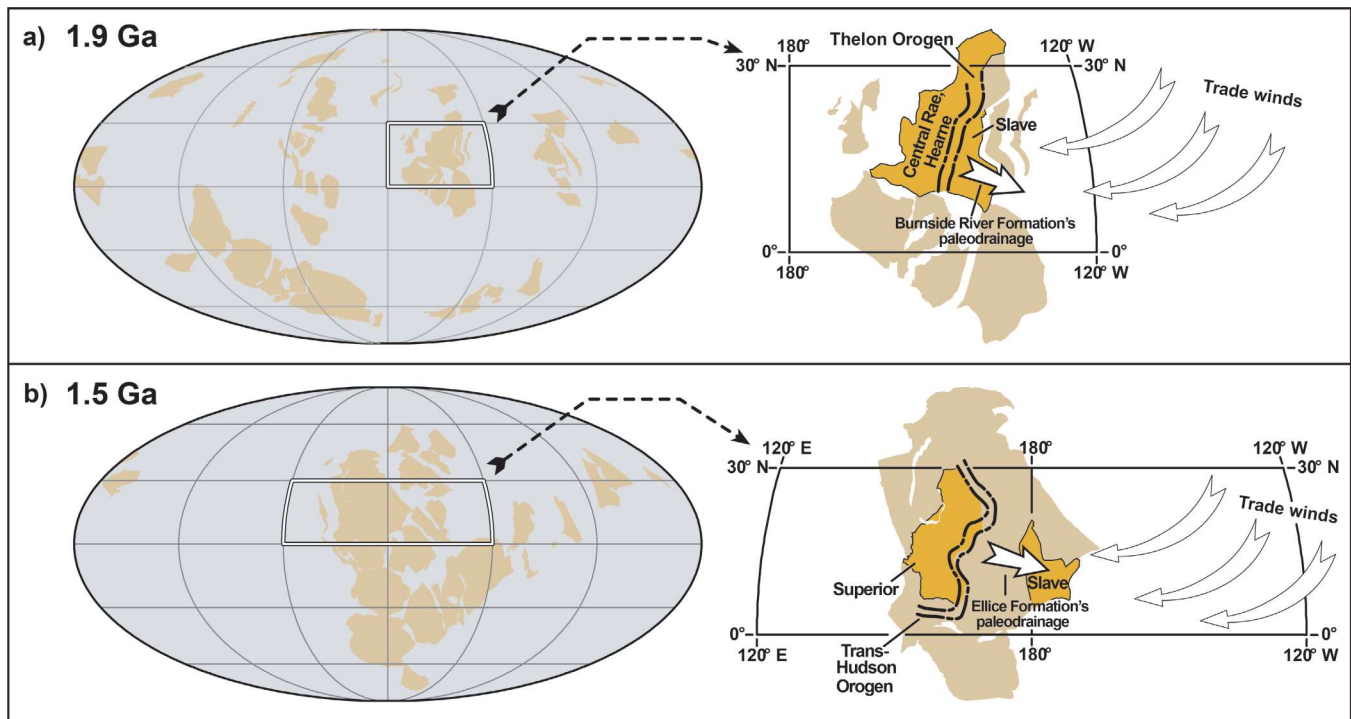


Figure 7. Paleogeographic reconstruction (adapted from Pehrsson et al., 2016), showing spatial relationships between orogenic ranges and trade-wind circulation at approximately the time of deposition of **a)** the Burnside River Formation and **b)** Ellice Formation in western Nunavut. See text for discussion.

in Arctic Canada is also supported by a Discovery Grant and a Strategic Partnership Grant provided by the Natural Sciences and Engineering Research Council of Canada.

REFERENCES

- Armitage, J.J. and Allen, P., 2010. Cratonic basins and the long-term subsidence history of continental interiors; *Journal of the Geological Society*, v. 167, p. 61–70. <https://doi.org/10.1144/0016-76492009-108>
- Beaumont, C., Fullsack, P., and Hamilton, J., 1992. Erosional control of active compressional orogens; *in* Thrust tectonics, (ed.) R.R. McClay; Springer, Dordrecht, Germany, p. 1–18. https://doi.org/10.1007/978-94-011-3066-0_1
- Berman, R.G., Pehrsson, S.J., Davis, W.J., Ryan, J.J., Qui, H., and Ashton, K.E., 2013. The Arrowsmith orogeny: geochronological and thermobarometric constraints on its extent and tectonic setting in the Rae craton, with implications for pre-Nuna supercontinent reconstruction; *Precambrian Research*, v. 232, p. 44–69. <https://doi.org/10.1016/j.precamres.2012.10.015>
- Berman, R.G., Davis, W.J., Whalen, J.B., McCurdy, M.W., Craven, J.A., Roberts, B.J., McMartin, I., Percival, J.A., Rainbird, R.H., Ielpi, A., Mitchell, R., Sanborn-Barrie, M., Nadeau, L., Girard, É., Carr, S., and Pehrsson, S.J., 2015. Report of activities for the geology and mineral potential of the Chantrey–Thelon area: GEM-2 Thelon tectonic zone, Montesor belt and Elu Basin projects; Geological Survey of Canada, Open File 7964, 19 p. <https://doi.org/10.4095/297302>
- Bianchi, V., Ghinassi, M., Aldinucci, M., Boaga, J., Brogi, A., and Deiana, R., 2015. Tectonically driven deposition and landscape evolution within upland incised valleys: Ambra Valley fill, Pliocene–Pleistocene, Tuscany, Italy; *Sedimentology*, v. 62, p. 897–927. <https://doi.org/10.1111/sed.12165>
- Bleeker, W., 2003. The late Archean record: a puzzle in ca. 35 pieces; *Lithos*, v. 71, p. 99–134. <https://doi.org/10.1016/j.lithos.2003.07.003>
- Bowring, S.A. and Grotzinger, J.P., 1992. Implications of new chronostratigraphy for tectonic evolution of Wopmay Orogen, northwest Canadian Shield; *American Journal of Science*, v. 292, p. 1–20. <https://doi.org/10.2475/ajs.292.1.1>
- Bradley, D.C., 2008. Passive margins through earth history; *Earth-Science Reviews*, v. 91, p. 1–26. <https://doi.org/10.1016/j.earscirev.2008.08.001>
- Brierley, G.J. and Hickin, E.J., 1991. Channel planform as a non-controlling factor in fluvial sedimentology: the case of the Squamish River floodplain, British Columbia; *Sedimentary Geology*, v. 75, p. 67–83. [https://doi.org/10.1016/0037-0738\(91\)90051-E](https://doi.org/10.1016/0037-0738(91)90051-E)
- Cain, S.A. and Mountney, N.P., 2009. Spatial and temporal evolution of a terminal fluvial fan system: the Permian Organ Rock Formation, South-east Utah, USA; *Sedimentology*, v. 56, p. 1774–1800. <https://doi.org/10.1111/j.1365-3091.2009.01057.x>
- Campbell, F.H.A., 1978. Geology of the Helikian rocks of the Bathurst Inlet area, Coronation Gulf, Northwest Territories; *in* Current Research, Part A; Geological Survey of Canada, Paper 78-1A, p. 97–106. <https://doi.org/10.4095/103872>
- Campbell, F.H.A., 1979. Stratigraphy and sedimentation in the Helikian Elu Basin and Hiukitak Platform, Bathurst Inlet–Melville Sound, Northwest Territories; Geological Survey of Canada, Paper 79-8, 18 p. <https://doi.org/10.4095/105323>
- Campbell, F.H.A., 1981. Stratigraphy and tectono-depositional relationships of the Proterozoic rocks of the Hadley Bay area, Northern Victoria Island, District of Franklin; *in* Current Research, Part A; Geological Survey of Canada, Paper 81-1A, p. 15–22. <https://doi.org/10.4095/109525>
- Campbell, F.H.A. and Cecile, M.P., 1976. Geology of the Kilohigok Basin, Bathurst Inlet, Northwest Territories; Geological Survey of Canada, Open File 332, scale 1:506 880. <https://doi.org/10.4095/129445>
- Campbell, F.H.A. and Cecile, M.P., 1981. Evolution of the Early Proterozoic Kilohigok Basin, Bathurst Inlet–Victoria Island, Northwest Territories; *in* Proterozoic basins of Arctic Canada, (ed.) F.H.A. Campbell; Geological Survey of Canada, Paper 81-10, p. 103–131. <https://doi.org/10.4095/109385>
- Chakraborty, T., 1991. Sedimentology of a Proterozoic erg: the Venkatpur Sandstone, Pranhita–Godvari Valley, south India; *Sedimentology*, v. 38, p. 301–322. <https://doi.org/10.1111/j.1365-3091.1991.tb01262.x>
- Chakraborty, T., 1999. Reconstruction of fluvial bars from the Proterozoic Mancheral Quartzite, Pranhita–Godavari Valley, India; *in* Fluvial sedimentology VI, (ed.) N.D. Smith and J. Rogers; International Association of Sedimentologists, Special Publication 28, p. 451–466. <https://doi.org/10.1002/9781444304213.ch31>
- Collinson, J.D., Mountney, N.P., and Thompson, D.B., 2006. Sedimentary structures; Terra Publishing, Enfield, United Kingdom, 292 p.
- Culshaw, N. and van Breeman, O., 1990. A zoned low P–high T complex at the level of anatexis—structural and plutonic patterns in metasediments of the Archean Yellowknife Supergroup, near Bathurst Inlet, N.W.T., Canada; *Precambrian Research*, v. 48, p. 1–20. [https://doi.org/10.1016/0301-9268\(90\)90054-T](https://doi.org/10.1016/0301-9268(90)90054-T)
- Davidson, A., 2008. Late Paleoproterozoic to mid-Neoproterozoic history of northern Laurentia: an overview of central Rodinia; *Precambrian Research*, v. 160, p. 5–22. <https://doi.org/10.1016/j.precamres.2007.04.023>
- Davies, N.S. and Gibling, M.R., 2010. Cambrian to Devonian evolution of alluvial systems: the sedimentological impact of the earliest land plants; *Earth-Science Reviews*, v. 98, p. 171–200. <https://doi.org/10.1016/j.earscirev.2009.11.002>
- Eriksson, P.G., Condie, K.C., Tirsgaard, H., Mueller, W.U., Altermann, W., Miall, A.D., Aspler, L.B., Catuneanu, O., and Chiarenzelli, J.R., 1998. Precambrian clastic sedimentation systems; *Sedimentary Geology*, v. 120, p. 5–53. [https://doi.org/10.1016/S0037-0738\(98\)00026-8](https://doi.org/10.1016/S0037-0738(98)00026-8)
- Ethridge, F.G., 2011. Interpretation of ancient fluvial channel deposits: review and recommendations; *in* From river to rock record: the preservation of fluvial sediments and their subsequent interpretation, (ed.) S.K. Davidson, S. Leleu, and C.P. North; Society for Sedimentary Geology, SEPM Special Publication 97, p. 9–35. <https://doi.org/10.2110/sepm.sp.097.009>

- Fielding, C.R., 2006. Upper flow regime sheets, lenses and scour fills: extending the range of architectural elements for fluvial sediment bodies; *Sedimentary Geology*, v. 190, p. 227–240. <https://doi.org/10.1016/j.sedgeo.2006.05.009>
- Fralick, P. and Zaniewski, K., 2012. Sedimentology of a wet, pre-vegetation floodplain assemblage; *Sedimentology*, v. 59, p. 1030–1049. <https://doi.org/10.1111/j.1365-3091.2011.01291.x>
- Fraser, J.A., Donaldson, J.A., Fahrig, W.F., and Tremblay, L.P., 1970. Helikian basins and geosynclines of the northwestern Canadian Shield; in *Symposium on basins and geosynclines of the Canadian Shield*, (ed.) A.J. Baer; Geological Survey of Canada, Paper 70-40, p. 213–238. <https://doi.org/10.4095/105255>
- Gall, Q., 1994. The Proterozoic Thelon paleosol, Northwest Territories, Canada; *Precambrian Research*, v. 68, p. 115–137. [https://doi.org/10.1016/0301-9268\(94\)90068-X](https://doi.org/10.1016/0301-9268(94)90068-X)
- Ganti, V., Whittaker, A., Lamb, M.P., and Fischer, W.W., 2019. Low-gradient, single-thread rivers prior to greening of the continents; *Proceedings of the National Academy of Sciences of the United States of America*, v. 116, p. 11652–11657.
- Garzanti, E., Doglioni, C., Vezzoli, G., and Andò, S., 2007. Orogenic belts and orogenic sediment provenance; *The Journal of Geology*, v. 115, p. 315–334. <https://doi.org/10.1086/512755>
- Gibling, M.R., 2006. Width and thickness of fluvial channel bodies and valley fills in the geological record: a literature compilation and classification; *Journal of Sedimentary Research*, v. 76, p. 731–770. <https://doi.org/10.2110/jsr.2006.060>
- Gibling, M.R., Fielding, C.R., and Sinha, R., 2011. Alluvial valleys and alluvial sequences: towards a geomorphic assessment; in *From river to rock record: the preservation of fluvial sediments and their subsequent interpretation*, (ed.) S. Davidson, S. Leleu, and C.P. North; Society for Sedimentary Geology, SEPM Special Publication 97, p. 423–447. <https://doi.org/10.2110/sepm.097.423>
- Grotzinger, J.P. and Gall, Q., 1986. Preliminary investigations of early Proterozoic Western River and Burnside River formations: evidence for foredeep origin of Kilohigok Basin, N.W.T., Canada; in *Current Research, Part A*; Geological Survey of Canada, Paper 86-1A, p. 95–106. <https://doi.org/10.4095/120355>
- Grotzinger, J.P. and McCormick, D.S., 1988. Flexure of the Early Proterozoic lithosphere and the evolution of Kilohigok Basin (1.9 Ga), Northwest Territories; in *New frontiers in basin analysis*, (ed.) K.L. Kleinspehn and C. Paola; Springer-Verlag, New York, New York, p. 405–430.
- Grotzinger, J.P., Adams, R.D., McCormick, D.S., and Myrow, P., 1989. Sequence stratigraphy, correlations between the Wopmay Orogen and Kilohigok Basin, and further investigations of the Bear Creek Group (Goulburn Supergroup), District of Mackenzie, N.W.T.; in *Current Research, Part C*; Geological Survey of Canada, Paper 89-1C, p. 107–119. <https://doi.org/10.4095/126836>
- Hadlari, T., Rainbird, R.H., and Donaldson, A.J., 2006. Alluvial, eolian and lacustrine sedimentology of a Paleoproterozoic half-graben, Baker Lake Basin, Nunavut, Canada; *Sedimentary Geology*, v. 190, p. 47–70. <https://doi.org/10.1016/j.sedgeo.2006.05.005>
- Hahn, K., Rainbird, R.H., and Cousens, B., 2013. Sequence stratigraphy, provenance, C and O isotopic composition, and correlation of the late Paleoproterozoic–early Mesoproterozoic upper Hornby Bay and lower Dismal Lakes groups, N.W.T. and Nunavut; *Precambrian Research*, v. 232, p. 209–225. <https://doi.org/10.1016/j.precamres.2012.06.001>
- Hartley, A.J., Owen, A., Swan, A., Weissmann, G.S., Holzweber, B.I., Howell, J., Nichols, G., and Scuderi, L., 2015. Recognition and importance of amalgamated sandy meander belts in the continental rock record; *Geology*, v. 43, p. 679–682. <https://doi.org/10.1130/G36743.1>
- Heaman, L.M., LeCheminant, A.N., and Rainbird, R.H., 1992. Nature and timing of Franklin igneous event, Canada: implications for a Neoproterozoic mantle plume and break-up of Laurentia; *Earth and Planetary Science Letters*, v. 109, p. 117–131. [https://doi.org/10.1016/0012-821X\(92\)90078-A](https://doi.org/10.1016/0012-821X(92)90078-A)
- Heller, P.C. and Paola, C., 1996. Downstream changes in alluvial architecture: an exploration of controls on channel stacking patterns; *Journal of Sedimentary Research*, v. 66, p. 297–306.
- Hoffman, P.F., 1973. A discussion on the evolution of the Precambrian crust — evolution of an early Proterozoic continental margin: the Coronation geosyncline and associated aulacogens of the northwestern Canadian shield; *Royal Society of London, Philosophical Transactions, ser. A*, v. 273, p. 547–581. <https://doi.org/10.1098/rsta.1973.0017>
- Hoffman, P.F., 1988. United plates of America, birth of a craton: early Proterozoic assembly and growth of Laurentia; *Annual Review of Earth and Planetary Sciences*, v. 16, p. 543–603. <https://doi.org/10.1146/annurev.earth.16.050188.002551>
- Hoffman, P.F. and Grotzinger, J.P., 1993. Orographic precipitation, erosional unloading, and tectonic style; *Geology*, v. 21, p. 195–198. <https://doi.org/10.1130/0091-7613%281993%29021%3C0195%3A0PEUAT%3E2.3.CO%3B2>
- Ielpi, A., 2018. River functioning prior to the rise of land plants: a uniformitarian outlook; *Terra Nova*, v. 30, p. 341–349. <https://doi.org/10.1111/ter.12349>
- Ielpi, A. and Ghinassi, M., 2015. Planview style and palaeodrainage of Torridonian channel belts: Applecross Formation, Stoer Peninsula, Scotland; *Sedimentary Geology*, v. 325, p. 1–16. <https://doi.org/10.1016/j.sedgeo.2015.05.002>
- Ielpi, A. and Lapôte, M.G.A., 2020. A tenfold slowdown in river meander migration driven by plant life; *Nature Geoscience*, v. 13, p. 82–86. <https://doi.org/10.1038/s41561-019-0491-7>
- Ielpi, A. and Rainbird, R.H., 2015. Architecture and morphodynamics of a 1.6 Ga fluvial sandstone: Ellice Formation of Elu Basin, Arctic Canada; *Sedimentology*, v. 62, p. 1950–1977. <https://doi.org/10.1111/sed.12211>
- Ielpi, A. and Rainbird, R.H., 2016. Reappraisal of Precambrian sheet-braided rivers: evidence for 1.9 Ga deep-channelled drainage; *Sedimentology*, v. 63, p. 1550–1581. <https://doi.org/10.1111/sed.12273>
- Ielpi, A., Rainbird, R.H., Greenman, J.W., and Creason, C.G., 2015. The 1.9 Ga Kilohigok paleosol and Burnside River Formation, western Nunavut: stratigraphy and gamma-ray spectrometry; *Canada-Nunavut Geoscience Office, Summary of Activities 2015*, p. 1–10.

- Ielpi, A., Ventra, D., and Ghinassi, M., 2016. Deeply channelled Precambrian rivers: remote sensing and outcrop evidence from the 1.2 Ga Stoer Group of NW Scotland; *Precambrian Research*, v. 281, p. 291–311. <https://doi.org/10.1016/j.precamres.2016.06.004>
- Ielpi, A., Michel, S., Greenman, J.W., and Lebeau, L.E., 2017a. Stratigraphy, gamma-ray spectrometry and uranium prospectivity of the Kilohigok paleosol, Bear Creek Hills, western Nunavut; Canada-Nunavut Geoscience Office, Summary of Activities 2017, p. 37–48.
- Ielpi, A., Rainbird, R.H., Ventra, D., and Ghinassi, M., 2017b. Morphometric convergence between Proterozoic and post-vegetation rivers; *Nature Communications*, v. 8, art. no. 15250. <https://doi.org/10.1038/ncomms15250>
- Ielpi, A., Fralick, P., Ventra, D., Ghinassi, M., Lebeau, L.E., Marconato, A., Meek, R., and Rainbird, R.H., 2018a. Fluvial floodplains prior to greening of the continents: stratigraphic record geodynamic setting, and modern analogues; *Sedimentary Geology*, v. 372, p. 140–172. <https://doi.org/10.1016/j.sedgeo.2018.05.009>
- Ielpi, A., Ghinassi, M., Rainbird, R.H., and Ventra, D., 2018b. Planform sinuosity of Proterozoic rivers: a craton to channel-reach perspective; *in* Fluvial meanders and their sedimentary products in the rock record, (ed.) M. Ghinassi, L. Colomera, N.P. Mountney, and A.J.H. Reesink; International Association of Sedimentologists, Special Publication 48, p. 81–118.
- Latrubesse, E.M., 2015. Large rivers, megafans and other Quaternary avulsive fluvial systems: a potential “who’s who” in the geological record; *Earth-Science Reviews*, v. 146, p. 1–30. <https://doi.org/10.1016/j.earscirev.2015.03.004>
- Lebeau, L.E. and Ielpi, A., 2017. Fluvial channel-belts, floodbasins, and aeolian ergs in the Precambrian Meall Dearg Formation (Torridonian of Scotland): inferring climate regimes from pre-vegetation clastic rock records; *Sedimentary Geology*, v. 357, p. 53–71. <https://doi.org/10.1016/j.sedgeo.2017.06.003>
- Long, D.F.G., 2006. Architecture of pre-vegetation sandy braided perennial and ephemeral river deposits in Paleoproterozoic Athabasca Group, northern Saskatchewan, Canada as indicators of Precambrian fluvial style; *Sedimentary Geology*, v. 190, p. 71–95. <https://doi.org/10.1016/j.sedgeo.2006.05.006>
- Long, D.G.F., 2011. Architecture and depositional style of fluvial systems before land plants: a comparison of Precambrian, early Paleozoic and modern river deposits; *in* From river to rock record: the preservation of fluvial sediments and their subsequent interpretation, (ed.) S. Davidson, S. Leleu, and C.P. North; Society for Sedimentary Geology, SEPM Special Publication 97, p. 37–61. <https://doi.org/10.2110/sepm.097.037>
- McCormick, D.S., 1992. Evolution of an early Proterozoic alluvially dominated foreland basin, Burnside Formation, Kilohigok Basin, N.W.T., Canada; Ph.D. thesis, Massachusetts Institute of Technology, Cambridge, Massachusetts, 547 p.
- Métivier, F., Gaudemer, Y., Tapponier, P., and Klein, M., 1999. Mass accumulation rates in Asia during the Cenozoic; *Geophysical Journal International*, v. 137, p. 280–318. <https://doi.org/10.1046/j.1365-246X.1999.00802.x>
- Miall, A.D., 1996. *The geology of fluvial deposits*; Springer-Verlag, Berlin, Heidelberg, Germany, 582 p.
- Mountney, N.P. and Russell, A.J., 2009. Aeolian dune-field development in a water table-controlled system: Skeidarársandur, Southern Iceland; *Sedimentology*, v. 56, p. 2107–2131. <https://doi.org/10.1111/j.1365-3091.2009.01072.x>
- Nicholson, P.G., 1993. A basin reappraisal of the Proterozoic Torridon Group, northwest Scotland; *in* Tectonic controls and signatures in sedimentary successions, (ed.) L. Frostick and R.J. Steel; International Association of Sedimentologists, Special Publication 20, p. 183–202.
- Owen, G., 1995. Soft-sediment deformation in upper Proterozoic Torridonian sandstones (Applecross Formation) at Torridon, northwest Scotland; *Journal of Sedimentary Research*, v. A65, p. 495–504.
- Owen, G. and Santos, M.G.M., 2014. Soft-sediment deformation in a pre-vegetation river system: the Neoproterozoic Torridonian of NW Scotland; *Proceedings of the Geologists’ Association*, v. 125, p. 511–523. <https://doi.org/10.1016/j.pgeola.2014.08.005>
- Pehrsson, S.J., Berman, R.G., Eglinton, B., and Rainbird, R.H., 2013. Two Neoproterozoic supercontinents revisited: the case for a Rae family of cratons; *Precambrian Research*, v. 232, p. 27–43. <https://doi.org/10.1016/j.precamres.2013.02.005>
- Pehrsson, S.J., Eglinton, B.M., Evans, D.A.D., Huston, D., and Reddy, S.M., 2016. Metallogeny and its links to orogenic style during the Nuna supercontinent cycle; *in* Supercontinent cycles through earth history, (ed.) Z.X. Li, D.A.D. Evans, and J.B. Murphy; Geological Society, Special Publications, v. 424, p. 83–94.
- Percival, J.A., Skulski, T., Sanborn-Barrie, M., Stott, G.M., Leclair, A.D., Corkery, M.T., and Boily, M., 2012. Geology and tectonic evolution of the Superior Province, Canada; Chapter 6 *in* Tectonic styles in Canada: the LITHOPROBE perspective, (ed.) J.A. Percival, F.A. Cook, and R.M. Clowes; Geological Association of Canada, Special Paper 49, p. 321–378.
- Rainbird, R.H. and Davis, W.J., 2007. U-Pb detrital zircon geochronology and provenance of the late Paleoproterozoic Dubawnt Supergroup; linking sedimentation with tectonic reworking of the western Churchill Province, Canada; *Geological Society of America, Bulletin*, v. 119, p. 314–328. <https://doi.org/10.1130/B25989.1>
- Rainbird, R.H. and Young, G.M., 2009. Colossal rivers, massive mountains and supercontinents; *Earth*, v. 54, p. 52–61.
- Rainbird, R.H., Jefferson, C.W., and Young, G.M., 1996. The early Neoproterozoic sedimentary Succession B of northwestern Laurentia: correlations and paleogeographic significance; *Geological Society of America, Bulletin*, v. 108, p. 454–470. [https://doi.org/10.1130/0016-7606\(1996\)108%3c0454:TENSSB%3e2.3.CO%3b2](https://doi.org/10.1130/0016-7606(1996)108%3c0454:TENSSB%3e2.3.CO%3b2)
- Rainbird, R.H., Stern, R.A., Rayner, N.M., and Jefferson, C.W., 2007. Age, provenance, and regional correlation of the Athabasca Group, Saskatchewan and Alberta, constrained by igneous and detrital zircon geochronology; *in* EXTECH IV: geology and uranium EXploration TECHnology of the Proterozoic Athabasca Basin, Saskatchewan and Alberta, (ed.) C.W. Jefferson and G. Delaney; Geological Survey of Canada, Bulletin 588, p. 193–209. <https://doi.org/10.4095/223761>

- Rainbird, R.H., Ielpi, A., Long, D.G.F., and Donaldson, J.A., 2014. Similarities and paleogeography of late Paleoproterozoic sandstone deposits on the Canadian Shield: product of Hudsonian orogenesis; Geological Society of America Annual Meeting 2014; Geological Society of America, Abstracts with Programs, v. 46, p. 89.
- Rainbird, R.H., Rayner, N.M., Hadlari, T., Heaman, L.M., Ielpi, A., Turner, E.C., and MacNaughton, R.B., 2017. Zircon provenance data record the lateral extent of pancontinental, early Neoproterozoic rivers and erosional unroofing history of the Grenville orogen; Geological Society of America, Bulletin, v. 129, p. 1408–1423. <https://doi.org/10.1130/B31695.1>
- Ramaekers, P., 2010. Revision of the stratigraphy of the Proterozoic Hornby Bay Group, Nunavut; *in* GeoCanada 2010 — Working with the Earth; Canadian Society of Petroleum Geologists–Canadian Society of Exploration Geophysicists–Canadian Well Logging Society Conference, Program with Abstracts, v. 2020, p. 1–3.
- Røe, S.-L., 1987. Cross-strata and bedforms of probable transitional dune to upper-stage plane-bed origin from a Late Precambrian fluvial sandstone, northern Norway; *Sedimentology*, v. 34, p. 89–101. <https://doi.org/10.1111/j.1365-3091.1987.tb00562.x>
- Rogala, B., Fralick, P.W., Heaman, L.M., and Metsaranta, R., 2007. Lithostratigraphy and chemostratigraphy of the Mesoproterozoic Sibley Group, northwestern Ontario, Canada; *Canadian Journal of Earth Sciences*, v. 44, p. 1131–1149. <https://doi.org/10.1139/e07-027>
- Santos, M.G.M., Mountney, N.P., and Peakall, J., 2017. Tectonic and environmental controls on Palaeozoic fluvial environments: reassessing the impacts of early land plants on sedimentation; *Journal of the Geological Society*, v. 174, p. 393–404. <https://doi.org/10.1144/jgs2016-063>
- Sheen, A., Heaman, L.M., Kjarsgaard, B., Ootes, L., Pearson, G., and Creaser, R.A., 2019. Athapuscow aulacogen revisited: geochronology and geochemistry of the 2046 Ma Union Island Group mafic magmatism, East Arm of Great Slave Lake, Northwest Territories, Canada; *Precambrian Research*, v. 321, p. 85–102. <https://doi.org/10.1016/j.precamres.2018.11.012>
- Sherlock, R.L., Shannon, A., Hebel, M., Lindsay, D., Madsen, J., Sandeman, H., Hrabí, B., Mortensen, J.K., Tosdal, R.M., and Friedman, R., 2012. Volcanic stratigraphy, geochronology, and gold deposits of the Archean Hope Bay greenstone belt, Nunavut, Canada; *Economic Geology*, v. 107, p. 991–1042. <https://doi.org/10.2113/econgeo.107.5.991>
- Sønderholm, M. and Tirsgaard, H., 1998. Proterozoic fluvial styles: response to changes in accommodation space (Rivieradal sandstones, eastern North Greenland); *Sedimentary Geology*, v. 120, p. 257–274. [https://doi.org/10.1016/S0037-0738\(98\)00035-9](https://doi.org/10.1016/S0037-0738(98)00035-9)
- Summerfield, M.A. and Hulton, N.J., 1994. Natural controls on fluvial denudation rates in major world drainage basins; *Journal of Geophysical Research*, v. 99, p. 13871–13883. <https://doi.org/10.1029/94JB00715>
- Syvitski, J.P.M., Peckman, S.D., Hilberman, R., and Mulder, T., 2003. Predicting the terrestrial flux of sediment to the global ocean: a planetary perspective; *Sedimentary Geology*, v. 162, p. 5–24. [https://doi.org/10.1016/S0037-0738\(03\)00232-X](https://doi.org/10.1016/S0037-0738(03)00232-X)
- Syvitski, J.P.M., Cohen, S., Kettner, A.J., and Brakenridge, G.R., 2014. How important and different are tropical rivers? — an overview; *Geomorphology*, v. 227, p. 5–17. <https://doi.org/10.1016/j.geomorph.2014.02.029>
- Tirru, R. and Grotzinger, J.P., 1990. Early Proterozoic collisional orogeny along the northern Thelon tectonic zone, Northwest Territories, Canada: evidence from the foreland; *Tectonics*, v. 9, p. 1015–1036. <https://doi.org/10.1029/TC009i005p01015>
- Todd, S.P. and Went, D.J., 1991. Lateral migration of sand-bed rivers: examples from the Devonian Glashabeg Formation, SW Ireland and the Cambrian Alderney Sandstone Formation, Channel Islands; *Sedimentology*, v. 38, p. 997–1020. <https://doi.org/10.1111/j.1365-3091.1991.tb00368.x>
- Toonen, W.H.J., Kleinmans, M.G., and Cohen, K.M., 2012. Sedimentary architecture of abandoned channel fills; *Earth Surface Processes and Landforms*, v. 37, p. 459–472. <https://doi.org/10.1002/esp.3189>
- Walling, D.E. and Webb, B.W., 1996. Erosion and sediment yield: a global overview; *in* Erosion and sediment yield: global and regional perspectives, (ed.) D.E. Walling and B.W. Webb; International Association of Hydrological Sciences, Publication 236, p. 3–19.
- Weissmann, G.S., Hartley, A.J., Scuderi, L.A., Nichols, G.J., Owen, A., Wright, S., Felicia, A.I., Holland, F., and Anaya, F.M.L., 2015. Fluvial geomorphic elements in modern sedimentary basins and their potential preservation in the rock record: a review; *Geomorphology*, v. 250, p. 187–219. <https://doi.org/10.1016/j.geomorph.2015.09.005>
- Weller, O.M. and St-Onge, M.R., 2017. Record of modern-style plate tectonics in the Palaeoproterozoic Trans-Hudson orogeny; *Nature Geoscience*, v. 10, p. 305–311. <https://doi.org/10.1038/ngeo2904>
- Willett, S.D., 1999. Orogeny and orography: the effects of erosion on the structure of mountain belts; *Journal of Geophysical Research, Solid Earth*, v. 104, p. 28957–28981. <https://doi.org/10.1029/1999JB900248>
- Young, G.M., Jefferson, C.W., Delaney, G.D., and Yeo, G.M., 1979. Middle to late Proterozoic evolution of the northern Canadian Cordillera and Shield; *Geology*, v. 7, p. 125–128. [https://doi.org/10.1130/0091-7613\(1979\)7%3c125:MALPEO%3e2.0.CO%3b2](https://doi.org/10.1130/0091-7613(1979)7%3c125:MALPEO%3e2.0.CO%3b2)
- Zhao, G., Cawood, P.A., Wilde, S., and Sun, M., 2002. Review of global 2.1–1.8 Ga orogens: implications for a pre-Rodinia supercontinent; *Earth-Science Reviews*, v. 59, p. 125–162. [https://doi.org/10.1016/S0012-8252\(02\)00073-9](https://doi.org/10.1016/S0012-8252(02)00073-9)

Crustal architecture and evolution of the central Thelon tectonic zone, Nunavut: insights from Sm-Nd and O isotope analysis, U-Pb zircon geochronology, and targeted bedrock mapping

R.G. Berman^{1*}, B.E. Taylor¹, W.J. Davis¹, M. Sanborn-Barrie¹, and J.B. Whalen¹

Berman, R.G., Taylor, B.E., Davis, W.J., Sanborn-Barrie, M., and Whalen, J.B., 2024. Crustal architecture and evolution of the central Thelon tectonic zone, Nunavut: insights from Sm-Nd and O isotope analysis, U-Pb zircon geochronology, and targeted bedrock mapping; in Canada's northern shield: new perspectives from the Geo-mapping for Energy and Minerals program, (ed.) S.J. Pehrsson, N. Wodicka, N. Rogers, and J.A. Percival; Geological Survey of Canada, Bulletin 612, p. 115–158. <https://doi.org/10.4095/332497>

Abstract: New isotopic analyses (Sm-Nd, O, and U-Pb), targeted geological mapping, and previously published whole-rock geochemical data and high-resolution aeromagnetic surveys define ten crustal domains across the central Thelon tectonic zone. In the eastern Slave Craton, granitoid rocks in the Overby Lake domain are more isotopically evolved than in the Tinney Hills domain and include tonalite dated at 2.71 Ga. The 400 km long main leucogranite belt separates most early (ca. 2.07–1.95 Ga) Thelon tectonic zone plutonic belts from the Queen Maud Block. Oxygen isotopes support its formation via melting of a sedimentary source during peak metamorphism, which coincides with three, new 1.925–1.91 Ga leucogranite ages. Modelling of Nd-Sm isotopes indicates Neoproterozoic crust as basement to early Thelon tectonic zone plutonic belts. Detrital zircon geochronology suggests a 2.5 Ga basement component that is not recognized in exposed crustal domains, but is compatible with the Dharwar Craton, which can be paleomagnetically reconstructed adjacent to the Slave Craton at 2.2 Ga.

Two tectonic models are discussed for the evolution of the Thelon tectonic zone in the convergent margin tectonic setting indicated by the whole-rock geochemistry and mantle-like oxygen isotopic compositions of plutonic rocks. In one model, ca. 2.1 Ga extension precedes east-dipping subduction, which leads to 1.97 Ga collision of the Slave Craton with a composite Thelon tectonic zone basement–Rae Craton, upper plate. The second model proposes a ca. 2.05 Ga Slave–microcontinent (Thelon tectonic zone basement) collision, followed by a polarity flip with west-dipping subduction, leading to ca. 1.95 Ga collision of the Rae Craton.

Résumé : De nouvelles analyses isotopiques (Sm-Nd, O et U-Pb), de la cartographie géologique ciblée, des données géochimiques sur roche totale déjà publiées ainsi que des levés aéromagnétiques à haute résolution permettent de définir dix domaines crustaux dans la partie centrale de la zone tectonique de Thelon. Dans la partie orientale du craton des Esclaves, des roches granitoïdes contenues dans le domaine d'Overby Lake sont plus évoluées sur le plan isotopique que celles présentes dans le domaine de Tinney Hills et comprennent de la tonalite datée à 2,71 Ga. La ceinture principale de leucogranite, longue de 400 km, sépare les ceintures plutoniques plus précoces (env. 2,07-1,95 Ga) de la zone tectonique de Thelon du bloc de Queen Maud. Les isotopes de l'oxygène appuient la formation de cette ceinture de leucogranite par la fusion d'une source sédimentaire lors de la culmination du métamorphisme, qui coïncide avec trois nouveaux âges de leucogranite compris dans l'intervalle 1,925-1,91 Ga. La modélisation des isotopes Nd-Sm indique qu'une croûte néoarchéenne constitue le socle des ceintures plutoniques précoces de la zone tectonique de Thelon. La géochronologie des zircons détritiques suggère l'existence d'une composante de socle de 2,5 Ga qui n'a pas été relevée dans les domaines crustaux exposés en surface, mais qui est compatible avec le craton de Dharwar, lequel était adossé au craton des Esclaves à 2,2 Ga d'après les reconstitutions paléomagnétiques.

Nous analysons deux modèles tectoniques concernant l'évolution de la zone tectonique de Thelon dans un cadre tectonique de marge de convergence indiqué par la géochimie sur roche totale et les compositions isotopiques de l'oxygène des roches plutoniques aux apparentements mantelliques. Dans l'un des modèles, une extension à environ 2,1 Ga a précédé une subduction suivant une surface inclinée vers l'est, ce qui a mené à une collision à 1,97 Ga du craton des Esclaves avec un ensemble composite formé du socle de la zone tectonique de Thelon et du craton de Rae, qui constituait la plaque supérieure de la zone de subduction. Dans le second modèle, une collision entre le craton des Esclaves et un microcontinent (socle de la zone tectonique de Thelon) à environ 2,05 Ga a été suivie par une inversion de polarité de la subduction suivant une surface inclinée vers l'ouest, ce qui a mené à une collision à environ 1,95 Ga avec le craton de Rae.

¹Geological Survey of Canada, 601 Booth Street, Ottawa, Ontario K1A 0E8

*Corresponding author: R. Berman (email: Rob.Berman@nrcan-rncan.gc.ca)

INTRODUCTION

The Thelon tectonic zone is a major geophysical and geological feature separating the Slave and Rae cratons in the Canadian Shield (Fig. 1), yet its significance is controversial. Gibb and Thomas (1977) modelled its regional gravity expression as an east-dipping suture. Similarities in aeromagnetic response (Fig. 2) and preliminary plutonic ages led Hoffman (1988) to correlate the Thelon tectonic

zone with the Taltson magmatic zone and propose they represented a ca. 2.0 Ga continental arc on the western flank of the Churchill Province (referred to here as the ‘Rae Craton’) prior to collision of the Slave Craton and Buffalo Head terrane (Fig. 1). A geochemical and samarium-neodymium (Sm-Nd) isotope study of major plutonic phases in the northern Taltson magmatic zone supported this interpretation (Thériault, 1992). In contrast, Chacko et al. (2000) and De et al. (2000) interpreted geochemical and oxygen-isotope analyses of Taltson magmatic zone plutonic

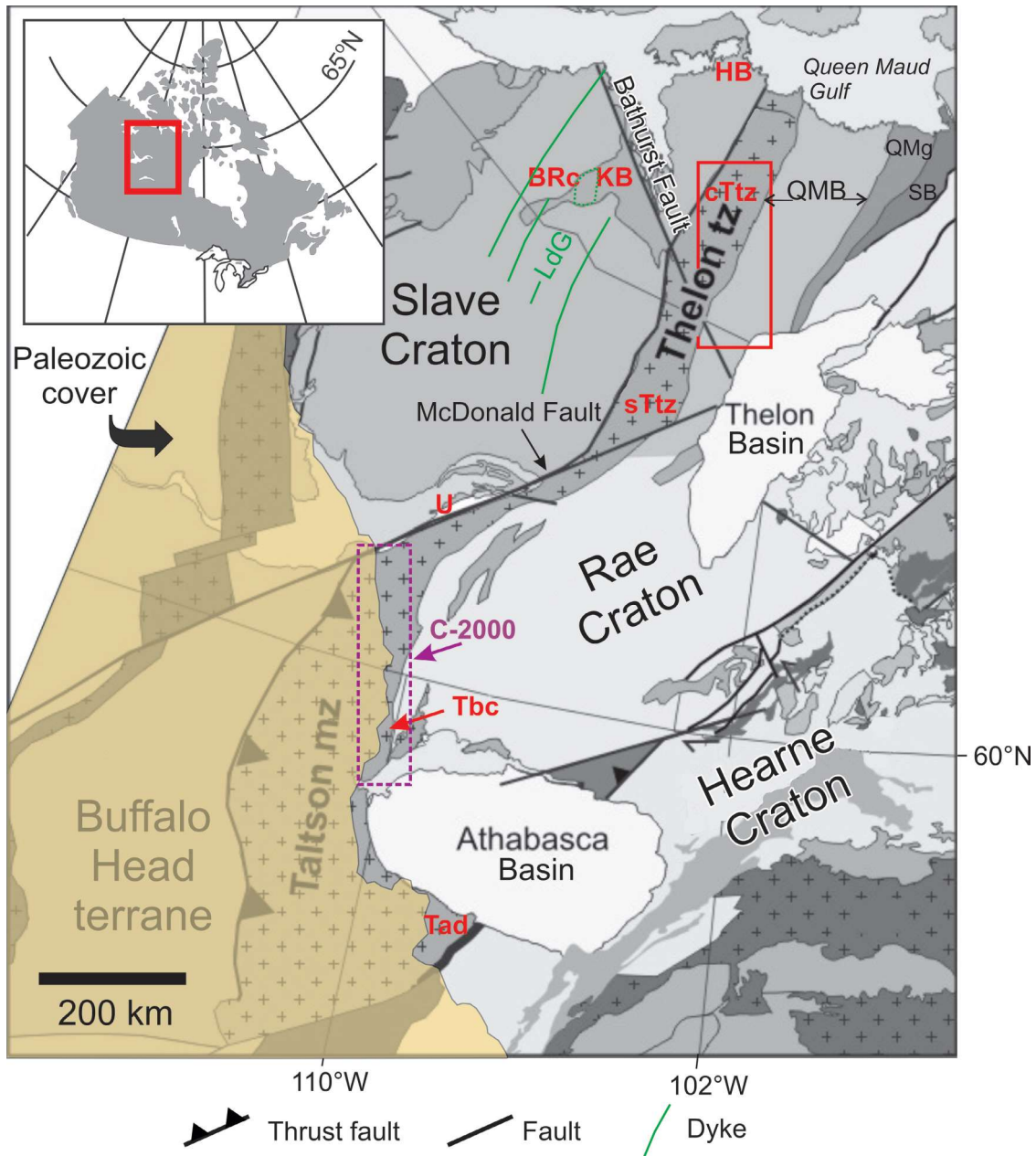


Figure 1. Regional geology (*modified from Wheeler et al., 1996*) of a portion of the Canadian Shield (see inset) showing the location of the study area in the central Thelon tectonic zone (cTtz) and a study in the Taltson magmatic zone by Chacko et al. (2000; rectangle labelled ‘C-2000’). BRc = Booth River complex, HB = Hope Bay belt, KB = Kilohigok Basin, LdG = Lac de Gras dykes, QMB = Queen Maud Block, QMg = Queen Maud granitoid suite, SB = Sherman Basin, sTtz = southern Thelon tectonic zone, Tad = Taltson domain, Tbc = Taltson basement complex, U = Union Island Group.

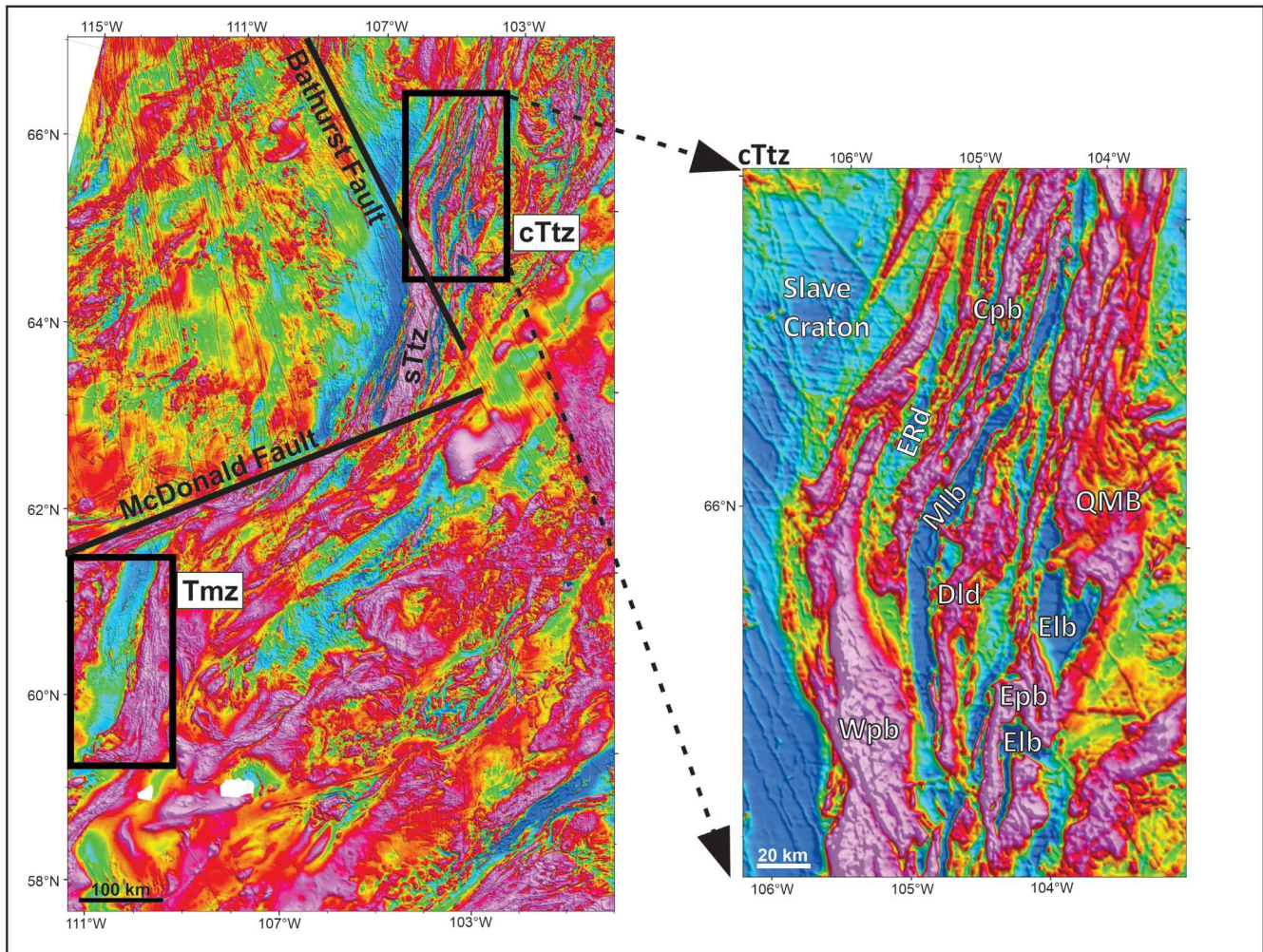


Figure 2. Aeromagnetic total-field map of the Talston magmatic zone (Tmz) and Thelon tectonic zone (outlined by black rectangles) area (Natural Resources Canada, 2013). Enlarged inset illustrates the magnetic fabric of the central Thelon tectonic zone (cTtz). Crustal domains include the Central plutonic belt (Cpb), Duggan Lake domain (DLd), Eastern leucogranite belt (Elb), Eastern plutonic belt (Epb), Ellice River domain (ERd), Main leucogranite belt (Mlb), Queen Maud Block (QMB), and Western plutonic belt (Wpb).

rocks to indicate an intracontinental setting, far from a plate boundary. Similarly, Thompson (1989) suggested that metamorphic patterns in the Thelon tectonic zone reflect orogenesis following crustal thinning in an intra-cratonic setting, a scenario aligned with the proposed earlier (ca. 2.35 Ga) accretion of the Slave Craton to the Rae Craton during the Arrowsmith Orogeny (Schultz et al., 2007). More recently, Card et al. (2014) concluded that the Talston magmatic zone does not correlate with the Thelon tectonic zone and proposed the latter may have been built on the northern extension of the Buffalo Head terrane, rather than the Rae Craton.

Evaluation of tectonic models requires a base-level understanding of geological relationships. Whereas bedrock mapping and supporting geochronology are available for the Talston magmatic zone in Alberta and the Northwest Territories (Bostock et al., 1987, 1991; Bostock and van Breemen, 1994; McDonough et al., 2000; McNicholl et al., 2000;

Card et al., 2014), detailed understanding of the Thelon tectonic zone was restricted to its western portion (Frith, 1982; Thompson, 1986; Henderson et al., 1999), and hindered by availability of limited geochronological data (van Breemen et al., 1987; Henderson et al., 1999). The present paper addresses these problems by presenting Sm-Nd, O, and U-Pb isotope analyses from the central Thelon tectonic zone (cTtz, Fig. 1) in the context of recently completed geological mapping (Berman et al., 2018) and high-resolution aeromagnetic surveys (Kiss, 2014a, b; Coyle, 2017a, b), and integrating them with lithogeochemistry (Whalen et al., 2018). The results allow definition of distinct crustal domains in the central Thelon tectonic zone that place first-order controls on economic potential in the region (Berman et al., 2018), yield insights into the petrogenesis of Thelon tectonic zone plutonic rocks, enable further assessment of the relationship between the Thelon tectonic zone and the Talston magmatic zone, and provide a basis for re-evaluating tectonic models for the evolution of western Laurentia.

REGIONAL GEOLOGICAL SETTING

The Thelon tectonic zone comprises a north-northeast-trending belt of meta-igneous and subordinate meta-supracrustal rocks flanked by the Archean Slave Craton to the west and the Archean Rae Craton to the east (Fig. 1). It extends more than 500 km northward from the McDonald Fault to Queen Maud Gulf (Fig. 1) and affects the western coast of Boothia Peninsula (Frisch and Hunt, 1993; Sanborn-Barrie and Regis, 2020). Although the Thelon tectonic zone has been interpreted as the northern continuation of the Taltson magmatic zone (Fig. 1; Bostock et al., 1987; Hoffman, 1988; Ross et al., 1991; Ross, 2002), others have argued against this correlation on the basis of age contrasts (Card et al., 2014; Berman et al., 2015a, b; Davis et al., 2021), litho-geochemistry (Whalen et al., 2018), and pre-1.84 Ga strike difference (Card et al. 2014).

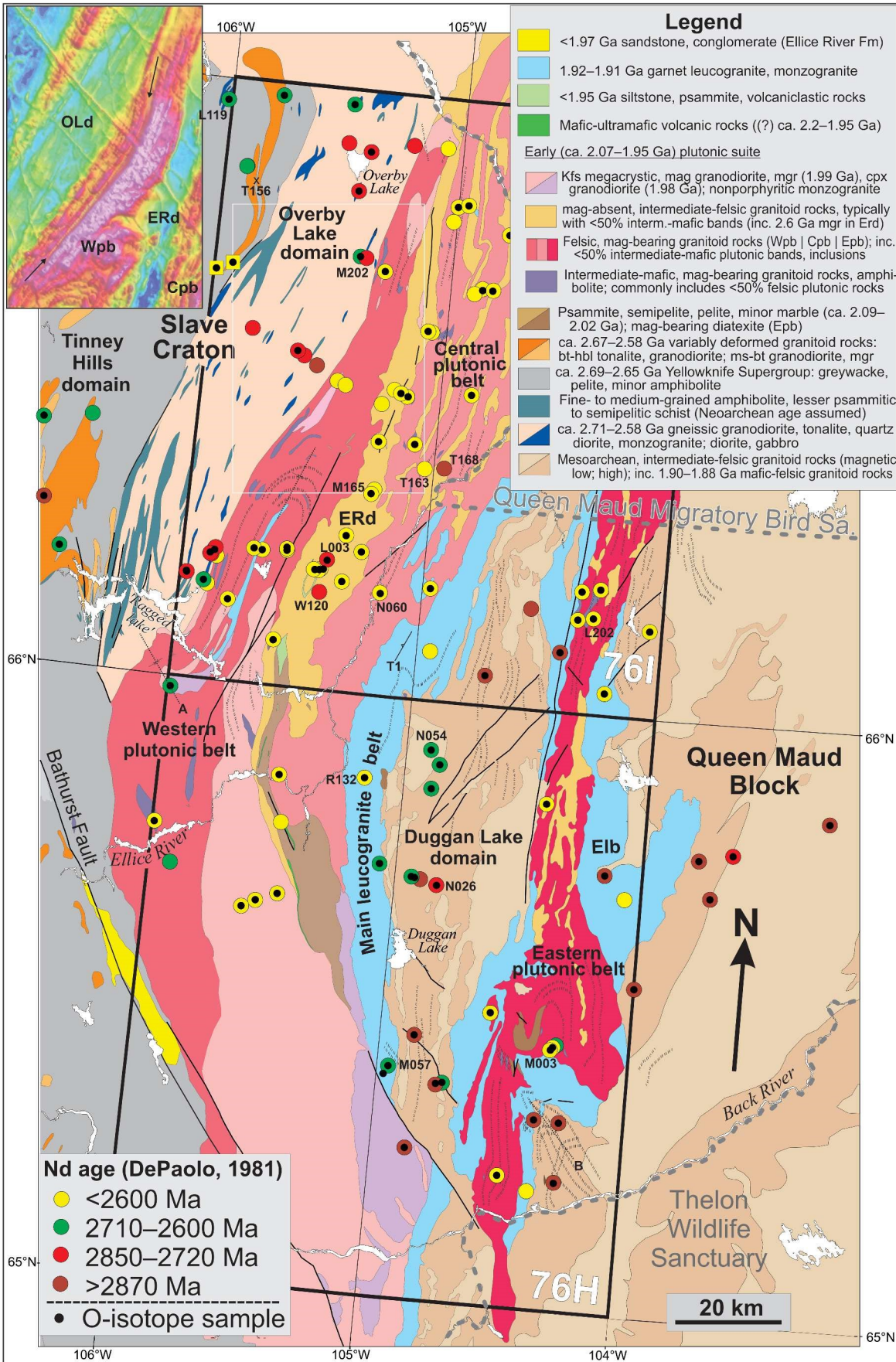
Early geological investigations of the Thelon tectonic zone, based on reconnaissance grid mapping by helicopter (Fraser, 1964; Wright, 1967), recognized that the western limit of the zone, referred to as the ‘Thelon front’, varied depending on whether it was defined on a lithological, metamorphic, or structural basis. Bedrock mapping of the southern (Henderson et al., 1982) and central (Thompson et al., 1985, 1986) Thelon tectonic zone (Fig. 1) led to interpretation of the Thelon tectonic zone as structurally and metamorphically reworked Slave Craton, showing evidence of superimposed late Archean and Proterozoic tectonometamorphic events. In the southern Thelon tectonic zone, Paleoproterozoic, amphibolite- to granulite-facies plutonic rocks were dated at ca. 1.95 to 1.925 Ga (Henderson et al., 1999). In the central Thelon tectonic zone (Fig. 1, 3), Frith (1982) interpreted widespread granitoid migmatite as Archean and part of the Slave Craton. Frith and van Breemen (1990) subsequently established a ca. 1.99 Ga age for a regionally extensive K-feldspar megacrystic granodiorite. Thompson et al. (1985, 1986) recognized that the western Thelon tectonic zone (designated Bathurst terrane) was characterized by abundant Yellowknife Supergroup metapelitic rocks of lower- to upper-amphibolite facies and was distinct from the Ellice River terrane, in which supracrustal rocks are far subordinate to migmatitic plutonic rocks, overall metamorphic grade is higher, and orthopyroxene is widespread within ca. 2.02 to 1.91 Ga plutonic rocks (van Breemen et al., 1987). Culshaw (1991) interpreted structural constraints to indicate

west-vergent thrusting related to Slave–Rae convergence, followed by east-vergent, dextral transpression driven by indentation of the Slave Craton. A convergent setting has been interpreted to characterize the Kilohigok Basin (KB, Fig. 1), a sequence of platformal (Kimerot Group) and foredeep (Bear Creek Group) deposits (Grotzinger and McCormick, 1988) that accumulated on the Slave lower plate during collisional loading by the Rae upper plate (Hoffman, 1988; Tirrul and Grotzinger, 1990) at 1.97 Ga (Bowring and Grotzinger, 1992). Lithological offsets along the McDonald (Fig. 1, 2) and Bathurst (Fig. 2, 3) faults are attributed to ca. 1.84 to 1.75 Ga postcollisional indentation by the Slave Craton (Hoffman, 1988; Henderson and van Breeman, 1991; Ma et al., 2020).

The region south of the McDonald Fault (Fig. 1) records a complex Paleoproterozoic history. Buffalo Head terrane comprises ca. 2.32 to 2.28 Ga plutonic rocks (Villeneuve et al., 1993), the isotopic compositions of which are consistent with development via arc magmatism on the southwestern Rae margin (Thériault and Ross, 1991). Younger (ca. 2.19–2.09 Ga), more juvenile plutonism in the Chinchaga domain (west of the Buffalo Head terrane in Fig. 1; Villeneuve et al., 1993) suggests continued magmatic growth of this margin (Bostock and van Breemen, 1994; Ross, 2002; Ashton et al., 2013). Buffalo Head terrane is interpreted to have rifted off the Rae Craton and returned following ca. 1.99 to 1.96 Ga continental arc magmatism recorded by early Taltson plutonic rocks (Ross et al., 1991; Thériault, 1992; Card et al., 2014).

Prior to this second phase of the Geo-mapping for Energy and Minerals program, bedrock mapping projects had not investigated the eastern side of the Thelon tectonic zone adjacent to the Queen Maud Block (QMB, Fig. 1) of the western Rae Craton. The Queen Maud Block is dominated by Mesoarchean granitoid rocks with widespread U-Pb crystallization ages ranging from 3.26 to 2.98 Ga (Tersmette, 2012; Davis et al., 2014; Berman et al., work in progress, 2022). Younger plutonism is documented at 2.7 Ga (two localities; Tersmette, 2012) and at ca. 2.52 to 2.45 Ga (Queen Maud granitoid suite, QMg in Fig. 1) along its eastern flank (Schultz et al., 2007; Tersmette, 2012; Davis et al., 2013, 2014). Widespread reworking during the 2.4 to 2.35 Ga Arrowsmith Orogeny (Schultz et al., 2007; Tersmette, 2012; Berman et al., 2005, 2013) is considered to reflect a collisional event, considered by some to have involved the Slave Craton (Schultz et al., 2007; Tersmette, 2012).

Figure 3. Simplified geology of the central Thelon tectonic zone, based on interpretation of high-resolution aeromagnetic survey data (inset; Kiss, 2014a, b; Coyle, 2017a, b), isotopic constraints (this paper; W.J. Davis, unpub. data, 2021), and targeted field mapping (Berman et al., 2015b, 2016). Dashed-dotted curves show foliation traces; bold dotted lines show prominent late fold axes; T1 is location of east-vergent thrusts, and A, B is location of axes of late folds. Sample locations are colour-coded with respect to Nd model ages listed in Table A-1. Oxygen-isotope data (Table A-1) were collected at a subset of these locations (small black circles). References to published U-Pb zircon crystallization ages are given in Table A-1. Inset shows high-resolution aeromagnetic survey across the boundary (arrows) between the Overby Lake domain (OLd) and Western plutonic belt (Wpb). Cpb = Central plutonic belt, Elb = Eastern leucogranite belt, Epb = Eastern plutonic belt, ERd = Ellice River domain, inc. = include, interm. = intermediate, mgr = monzogranite; Kfs = potassium feldspar, cpx = clinopyroxene, mag = magnetite, bt = biotite, hbl = hornblende, ms = muscovite.



GEOLOGY OF THE CENTRAL THELON TECTONIC ZONE

This study reports results of targeted bedrock mapping, which extends earlier mapping of the boundary between the Thelon tectonic zone and Slave Craton eastward to the boundary between the Thelon tectonic zone and Queen Maud Block (Fig. 3). Geological domains in the central Thelon tectonic zone (Fig. 3) are defined on the basis of geological (Berman et al., 2018) and geochemical (Whalen et al., 2018) constraints, combined with high-resolution aeromagnetic data (Kiss, 2014a, b) and U-Pb zircon ages (van Breemen et al., 1987, Frith and van Breemen, 1990; Davis et al., 2013, 2014; W.J. Davis, unpub. data, 2021; this study). Samarium-neodymium and oxygen isotope data further characterize these domains and place important constraints on tectonic models for this region.

The central Thelon tectonic zone is considered to comprise ten crustal domains, including four Archean and six Paleoproterozoic domains (Fig. 2, 3). From west to east, these informally named domains are: 1) Tinney Hills domain of the eastern Slave Craton; 2) Overby Lake domain at the eastern edge of the Slave Craton; 3) Western plutonic belt; 4) Ellice River domain; 5) Central plutonic belt; 6) Main leucogranite belt; 7) Duggan Lake domain; 8) Eastern plutonic belt; 9) East leucogranite belt; and 10) Queen Maud Block (of the western Rae Craton).

The Tinney Hills domain represents the eastern edge of the Bathurst terrane, as identified in Thompson et al. (1985, 1986). It is dominated by Archean metapelitic rocks of the Yellowknife Supergroup intruded by ca. 2.66 Ga tonalite (Berman and Camacho, 2020) and ca. 2.59 Ga two-mica granitoid rocks (Culshaw and van Breemen, 1990; Berman and Camacho, 2020). The metamorphic grade increases eastward, from lower- to upper-amphibolite facies, culminating northeast of the Bathurst Fault in the Overby Lake domain (Fig. 3), which corresponds to the western side of the Ellice River terrane of Thompson et al. (1985, 1986). The Overby Lake domain comprises strongly foliated, migmatitic granitoid gneisses which host thin strands of biotite- and/or amphibole-bearing lithological units and sparse metapelitic rocks. The latter have historically been considered to be high-grade Yellowknife Supergroup rocks, hence a deeper crustal level of the Slave Craton (Thompson et al., 1986). Tonalitic to granodioritic plutonic rocks in the Overby Lake domain are metaluminous and generally less potassic, magnesian, and aluminous than Tinney Hill domain granitoid rocks (Whalen et al., 2018). These differences call into question the relationship between the Overby Lake domain and Tinney Hill domain, a point addressed in this paper with new geochronology as well as Sm-Nd and O isotopic data. Steeply dipping, shallowly lineated high-strain zones occur along the boundary between the Tinney Hill domain and Overby Lake domain and are particularly well exposed in the in the area of ‘Ragged lake’ (unofficial name; Fig. 3). This approximately 7 km wide region of mylonitic rocks, designated the ‘main boundary zone’ by Thompson

(1992), records a complex history of predominantly dextral transpression (Thompson, 1992). This ‘main boundary zone’ occurs about 13 km west of orthopyroxene-bearing, ca. 2.02 to 1.91 Ga plutonic rocks, which have been interpreted to mark the boundary between the Rae and Slave cratons (Hoffman, 1988; Tirrul and Grotzinger, 1990; Culshaw, 1991). The Overby Lake domain narrows and terminates south of ‘Ragged lake’ (Fig. 3), possibly reflecting tectonic escape of a portion of this domain.

On the eastern flank of the Thelon tectonic zone, the Queen Maud Block consists of Mesoarchean (ca. 3.2–2.9 Ga) upper amphibolite- to granulite-facies diorite to monzogranite (Tersmette, 2012; Davis et al., 2013, 2014; Berman et al., 2015a, b). These rocks are typically moderately deformed, with foliations that vary from steep to shallower in the east (Berman et al., 2015a, b). Evidence of 2.45 to 2.34 Ga reworking during the Arrowsmith Orogeny is consistently recorded in U-Pb zircon and monazite systematics (Tersmette, 2012; Davis et al., 2014; Berman et al., 2015a, work in progress, 2022). Mesoarchean rocks of the Duggan Lake domain (Fig. 3) are separated from the Queen Maud Block by the Paleoproterozoic Eastern plutonic belt (described below). The Duggan Lake domain is correlated with the Queen Maud Block, based on tonalite and monzogranite with 3.2 to 3.1 Ga U-Pb zircon crystallization ages, ca. 3.4 to 3.1 Ga Nd model ages, and ca. 2.35 Ga metamorphic zircon ages (Davis et al., 2014; Berman et al., work in progress, 2022), ages indistinguishable from those recorded in the Queen Maud Block. Two geochemically distinct and areally restricted plutonic suites occur mainly in the western Queen Maud Block (including the Duggan Lake domain; Whalen et al., 2018). High-Zr, post-tectonic (A-type) quartz monzonite to monzogranite with ages of ca. 1.90 to 1.89 Ga (W.J. Davis, unpub. data, 2021) cut the Duggan Lake domain and occur as a dyke cutting granulite-facies fabrics in the Central plutonic belt. Variably foliated, low- to moderate-Zr monzogranite to alkali feldspar granite with preliminary ages of ca. 1.93 to 1.92 Ga (W.J. Davis, unpub. data, 2021) cut the Duggan Lake domain and western Queen Maud Block.

Forming the western boundary of the Duggan Lake domain is the Main leucogranite belt, which is approximately 10 wide and characterized by very low aeromagnetic response (Fig. 2). Based on regional aeromagnetic data (Natural Resources Canada, 2013), it extends more than 400 km from the McDonald Fault northeast to Queen Maud Gulf (Fig. 1). In the central Thelon tectonic zone, this domain comprises strongly foliated, peraluminous, garnet±sillimanite±spinel leucogranite (Fig. 4a), with lesser garnet-sillimanite diatexite and garnet-free monzogranite. At one locality, garnet leucogranite has been dated at 1.908 ± 0.002 Ga (van Breemen et al., 1987); ages at three other locations are presented in this paper.

The region between Archean rocks of the Slave and Rae cratons is dominated by ca. 2.01 to 1.98 Ga, commonly orthopyroxene-bearing plutonic rocks. Three discrete, linear, high-amplitude aeromagnetic anomalies distinguish the Western, Central, and Eastern plutonic belts from the

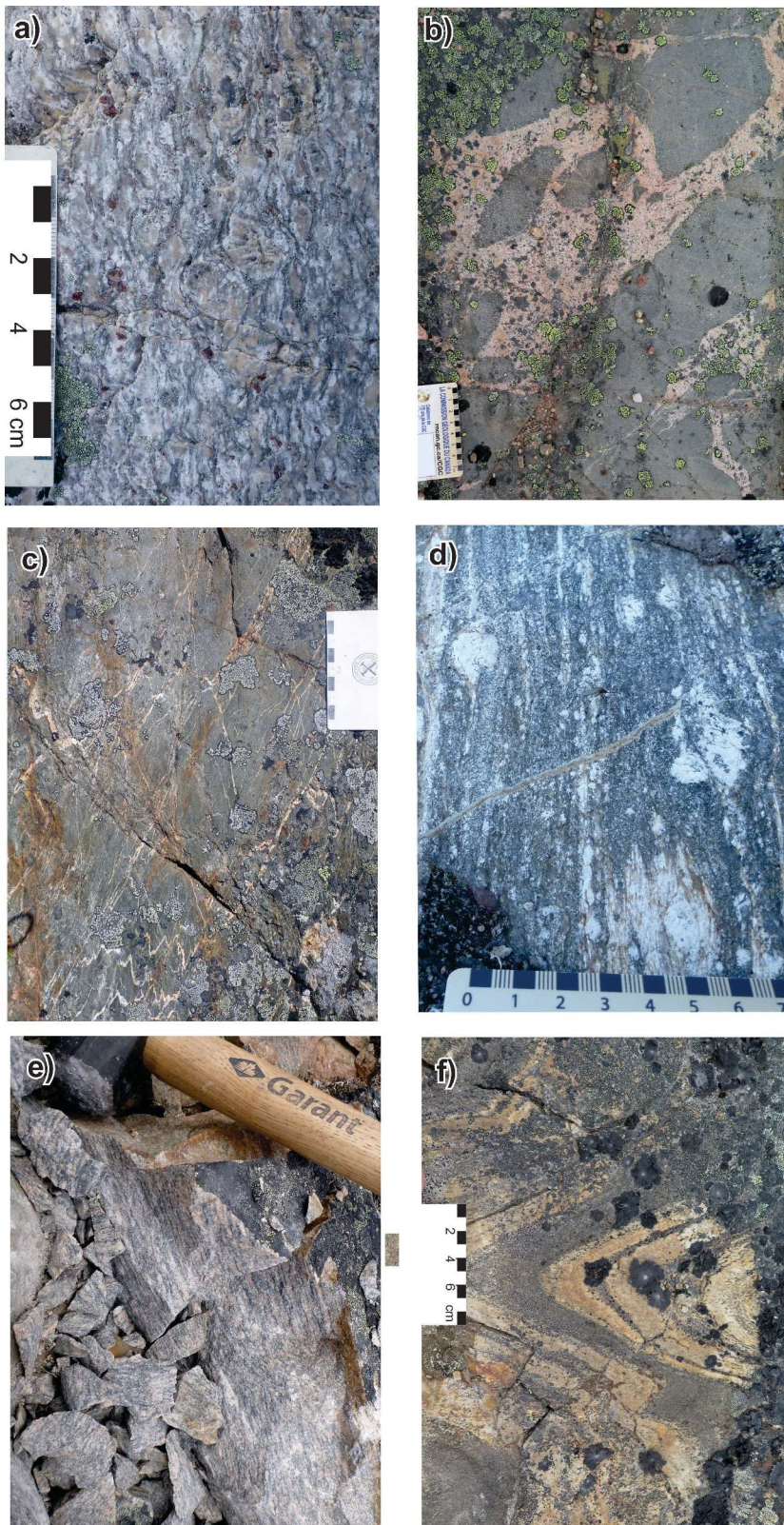


Figure 4. Field photographs of Thelon tectonic zone rocks. **a)** Highly strained garnet leucogranite (geochronology sample M003A) typical of the Main leucogranite belt and Eastern leucogranite belt. Photograph by M. Sanborn-Barrie. NRCan photo 2020-830. **b)** Diorite intruded by monzogranite sample W101 in the Western plutonic belt; card for scale is in centimetres. Photograph by O. Weller. NRCan photo 2020-831. **c)** Lower amphibolite-facies komatiitic metavolcanic rock (M074) interlayered with intermediate-mafic volcanic rocks from the southern part of the Ellice River domain. Photograph by M. Sanborn-Barrie. NRCan photo 2020-832. **d)** Porphyroclastic, mylonitic quartz monzonite (shear fabric orientation of $354^{\circ}/75^{\circ}$, sample M150A) within a high-strain zone approximately 1 km wide along the boundary between the Western plutonic belt and the Overby Lake domain; card for scale is in centimetres. Photograph by M. Sanborn-Barrie. NRCan photo 2020-833. **e)** Well foliated monzogranite (geochronology sample M202A) from the Overby Lake domain; hammer for scale is 31 cm long. Photograph by M. Sanborn-Barrie. NRCan photo 2020-834. **f)** Folded, layered gneiss comprising (?) Neoproterozoic monzogabbro and monzogranite ((?) ca. 1.99 Ga) from station W120 in the northern part of the Ellice River domain. Photograph by O. Weller. NRCan photo 2020-835. Note that samples W101, M074, and M150A, which were not part of this study, can be accessed by contacting the first author of this paper or a custodian of archival samples at the Geological Survey of Canada.

Ellice River domain, which also includes ca. 2.0 Ga plutons (Fig. 2, 3). Plutonic rocks in each of these belts comprise a spectrum of calc-alkaline compositions from gabbro to alkali-feldspar granite (Whalen et al., 2018). Early mafic plutonism is established by the common occurrence in all plutonic belts of diorite and quartz diorite xenoliths in monzogranite or granodiorite (Fig. 4b). Crystallization ages determined in the Western plutonic belt vary from 2.03 ± 0.005 Ga for clinopyroxene-bearing quartz monzonite (Davis et al., 2014) to 1.99 ± 0.004 Ga for monzogranite (Davis et al., 2014) and 1.978 ± 0.002 Ga for clinopyroxene granodiorite (Frith and van Breemen, 1990). Variably deformed, ca. 1.99 Ga K-feldspar megacrystic granodiorite (Table A-1; Frith and van Breemen, 1990; W.J. Davis, unpub. data, 2021) dominates the southern part of the Western plutonic belt. The presence of well foliated monzogranite, dated at 2.005 ± 0.005 Ga (Davis et al., 2013), suggests that the Eastern plutonic belt is similar in age to the Western plutonic belt; however, a 2.06 Ga granodiorite (sample L202A; Table A-1) has also been dated in the Eastern plutonic belt (W.J. Davis, unpub. data, 2021). Late, map-scale isoclinal folds occur in the Eastern plutonic belt, where it widens in the south (Fig. 3). In several locations, the Eastern plutonic belt is spatially associated with magnetite-bearing diatexite (Berman et al., 2018) interpreted to be derived from iron-rich metasedimentary rocks. Preliminary ages for the Central plutonic belt indicate slightly younger plutonism (ca. 1.98–1.96 Ga; Table A-1; W.J. Davis, unpub. data, 2021) than in the Western plutonic belt and Eastern plutonic belt, although contact metamorphism at 2.0 Ga in metapelitic rocks of the Central plutonic belt and Western plutonic belt (Berman et al., 2015b) suggests that plutonism had initiated in the Central plutonic belt by this time.

The Ellice River domain is a low-amplitude magnetic domain between the Western plutonic belt and Central plutonic belt (Fig. 2, 3). This domain comprises ca. 2.07 to 1.98 Ga plutonic rocks (Table A-1; W.J. Davis, unpub. data, 2021), one locality of ca. 2.6 Ga orthogneiss (sample L003 discussed below; Davis et al., 2014), and coherent strands of metasedimentary and metavolcanic rocks. Two Paleoproterozoic sedimentary sequences are documented in the southern Ellice River domain. An older, psammitic to pelitic sequence (assemblage 1) deposited between ca. 2.09 Ga and ca. 2.0 Ga contains prominent detrital zircon modes of ca. 2.32, 2.17, and 2.11 Ga, with sparse Meso- and Neoproterozoic zircons (Davis et al., 2021). Considered correlative with the Mary Francis (James, 1989, Henderson and van Breemen 1991) and Rutledge River (Bostock and van Breemen, 1994) groups, assemblage 1 is interpreted to record extension and potential rifting of the western margin of the Rae Craton (Davis et al., 2021). Assemblage 2 was deposited after 1.95 Ga and is dominated by ca. 2.02 to 1.95 Ga detrital zircons derived from unroofed Thelon tectonic zone plutonic rocks, as well as several Neoproterozoic zircons. Discontinuous strands of undated, ultramafic and mafic volcanic rocks (Fig. 4c) less than 1 km wide, preserved in the lower grade southern Ellice River domain, are spatially associated locally with polymetallic geochemical

anomalies (e.g. Ag, Cu, Ni, Pb, U, Zn; McCurdy et al., 2013). The absence of exposed contacts between the different supracrustal rocks obscures relationships between the volcanic assemblages and the dated clastic sequences.

The Thelon tectonic zone has experienced multiple episodes of deformation, interpreted to reflect northwest-directed thrusting driven by convergence between the Slave and Rae cratons, followed by dextral transpression during indentation of the Slave Craton (Tirrul, 1985; Hoffman, 1988; Culshaw, 1991; Ma et al., 2020). In the Slave Craton–Tinney Hills domain, Neoproterozoic west-northwest-striking fabrics are preserved, with Paleoproterozoic deformation manifested as thin-skinned, northwest-vergent basement-cover thrusts on its western flank (Tirrul, 1985; Tirrul and Grotzinger, 1990) and as narrow, discontinuous shear zones on its eastern flank (Culshaw, 1991). Farther east, Neoproterozoic fabrics are transposed into the dominant north-northeast strike of the Thelon tectonic zone (Thompson et al., 1985, 1986), with deformation intensity higher in the Overby Lake domain, where widely distributed zones of straight gneiss approximately 100 m to 1 km wide are characterized by steep, west-dipping foliations, shallow lineations, and dextral kinematics (Culshaw, 1991). Most of the Thelon tectonic zone plutonic domains also display steep, west-dipping foliations and shallow lineations. Evidence of thrusting has been recognized primarily in the Main leucogranite belt (east-vergent, location T1 in Fig. 3; Culshaw, 1991). Late ductile deformation is manifested in a variably developed, northwest-striking foliation parallel to the trend of several map-scale folds (*see* locations A, B in Fig. 3). The sinistral, strike-slip Bathurst Fault (Fig. 3) has been interpreted as an escape structure (Culshaw, 1991; Ma et al., 2020) formed during Slave Craton indentation, subsequent to an earlier stage of ductile, transpression separating regions with opposite vergence (Culshaw, 1991).

Basement to the Thelon tectonic zone plutonic suite is not readily apparent. Intense structural transposition and limited outcrop obscure the nature of primary contacts between ca. 2.0 Ga plutonic belts and the various crustal domains. Moreover, similar rock types (quartz diorite, granodiorite, monzogranite), magnetic characteristics, and variable strain obscure the distinction between Paleoproterozoic intrusions in the Western plutonic belt and their potential basement. The boundary between the Western plutonic belt and the Overby Lake domain is defined by high-resolution aeromagnetic data that display a muted lineament within a broad magnetic high (inset, Fig. 3). Sixteen traverses in areas of good outcrop across the boundary between the Western plutonic belt and Overby Lake domain revealed only one high-strain zone, a feldspar-porphycroclastic mylonite zone approximately 1 km wide in granodiorite-monzonite (Fig. 4d). The absence of a throughgoing high-strain zone along the domain boundary is suggestive of a primary intrusive relationship between the Western plutonic belt and the Overby Lakes domain, which has been reworked, although a cryptic fault cannot be ruled out. In the eastern Thelon tectonic zone, high-resolution aeromagnetic data clearly define the boundary of the Eastern plutonic belt and Queen Maud Block–Duggan Lake domain

(Fig. 2, 3). In contrast to moderate to steep foliations, which characterize plutonic rocks of the Eastern plutonic belt, Duggan Lake domain, and Main leucogranite belt, several outcrops along the poorly exposed eastern boundary of the Eastern plutonic belt display subhorizontal foliations, characterized by thin, high-strain zones, consistent with structural emplacement of the Eastern plutonic belt on Mesoarchean basement rocks. This conclusion is supported by geochronological results for an Eastern leucogranite belt metasedimentary rock (sample EA-265 from Davis et al., 2013), the detrital zircon population of which suggests exhumation of the adjacent Eastern plutonic belt (ca. 2.0–1.94 Ga detrital zircon ages) was not accompanied by that of Queen Maud Block crust (ca. 2.5 Ga, not Mesoarchean detrital zircon).

Five main metamorphic events are recognized in the central Thelon tectonic zone (Davis et al., 2015; Mitchell et al., 2017; Berman et al., 2018): 1) ca. 2.58 Ga in the Tinney Hills domain; 2) ca. 2.43 to 2.35 Ga in the Duggan Lake domain and Queen Maud Block; 3) ca. 2.0 Ga in the Central plutonic belt, Eastern plutonic belt, and northern Ellice River domain; 4) 1.92 to 1.89 Ga upper amphibolite- to granulite-facies metamorphism documented in all domains; and 5) ca. 1.82 Ga lower amphibolite-facies metamorphism recognized mainly in the southern Ellice River domain.

RESULTS

Appendix A presents the methodology used to obtain all isotopic and geochronological data discussed below.

Sm-Nd isotopes

Table A-1 presents Sm-Nd isotopic data for 131 samples spanning the central Thelon tectonic zone and its boundary regions (Fig. 3). Analyses are mainly of plutonic rocks discussed below, and also include six undated supracrustal rocks. It is important to note that calculated depleted mantle model ages (T_{DM} ; DePaolo, 1981) for polymetamorphic rocks, such as the Queen Maud Block and Thelon tectonic zone plutonic rocks studied here, have an inherent uncertainty stemming from the possibility that they underwent one or more melting episodes that may have changed their Sm/Nd ratios (and thus their model age). Nevertheless, calculated model ages provide a useful general characterization and basis for comparison of crustal domains. Table A-1 presents ϵ_{Nd} values calculated at determined or estimated ages, as well as at 1950 Ma to facilitate comparisons between ca. 2.0 and 1.9 Ga rocks.

With few exceptions, model ages of plutonic rocks fall into one of the four following groups that distinguish Archean domains from Paleoproterozoic domains within the Thelon tectonic zone (Table 1; Fig. 3):

Queen Maud Block–Duggan Lake domain

Samples of Mesoarchean crust in the western Queen Maud Block and the Duggan Lake domain consist mainly of tonalite (4) and granodiorite (5), in addition to monzogabbro (1), monzogranite (1), and syenogranite (1). The samples have a range of T_{DM} ages that vary from 3.61 to 2.87 Ga (Fig. 3; Table 1, A-1). For the seven dated samples in these domains, ca. 3.25 to 2.9 Ga crystallization ages correspond to ϵ_{Nd} values between -1.4 and $+4.2$ (Table 1, A-1). These relatively juvenile samples define a range of crustal evolution curves (dark shaded region, Fig. 5) with which to compare younger domains.

Overby Lake domain

Overby Lake domain plutonic rock samples are mainly tonalite (9) and granodiorite (3), in addition to diorite (2), quartz diorite (1), and monzogranite (1). Samples show a range in T_{DM} ages from 2.88 to 2.70 Ga, with most samples between 2.85 and 2.72 Ga (Fig. 3; Table 1, A-1). Dated samples (Table A-1) define a range of ϵ_{Nd} values between -0.4 (at 2.6 Ga) and 2.5 (at 2.7 Ga). Other, undated samples, have ϵ_{Nd} values within this range, assuming 2.65 Ga crystallization ages (Table 1; Fig. 5).

Tinney Hills domain

The plutonic rock samples from the Tinney Hills domain include peraluminous, muscovite-bearing alkali-feldspar granite, syenogranite, and monzogranite (4), and metaluminous granodiorite and quartz monzodiorite (3). Samples have T_{DM} ages ranging from 2.71 to 2.60 Ga, except for two-mica syenogranite sample A288 ($T_{DM} = 2.89$ Ga; Fig. 3; Table 1, A-1). Assuming crystallization ages of 2.6 Ga, ϵ_{Nd} values vary between $+1.8$ and $+2.8$ (except for sample A288), indicating these samples are somewhat more juvenile than samples of the Overby Lake domain (Table 1; Fig. 5).

Thelon tectonic zone plutonic belts

Paleoproterozoic plutonic rocks are divided into early (2.07–1.95 Ga) and late (1.93–1.88 Ga) groups. Early Thelon tectonic zone granitoid rocks have Nd model ages between 2.64 and 2.19 Ga (Fig. 3; Table 1, A-1), with Paleoproterozoic model ages (i.e. <2.5 Ga) for over 70% of the samples (Table A-1). Corresponding $\epsilon_{Nd}(2.0$ Ga) values vary between -4.5 and 0.2 , with 85% of samples in a tight range from -3.2 to -0.9 (Table A-1). There are no systematic differences between the four plutonic belts.

The two oldest samples (L202A, Eastern plutonic belt; M165A, Ellice River domain), with crystallization ages of ca. 2.07 to 2.06 Ga (Table 1, A-1), are among the most juvenile ($\epsilon_{Nd}(t) = -0.6, -0.3$, respectively) of the early Thelon tectonic zone plutonic rocks (Fig. 5).

Table 1. Crustal domain characteristics.

Domain	Magnetic	Lithologies (in order of abundance)	Age (Ga)	T _{DM} (Ga)	δ ¹⁸ O _{WR}	εNd(initial)
Thelon tectonic zone						
Wpb	High	mgr, gdi, di, qmdi, qm, sygr, qdi (qm)	2.01–1.98 (2.03)	2.52–2.27 (2.43)	5.7–8.7 (6.9)	–4.2 to –1.7 (–1.6)
ERd	Low	mgr, qdi, qmdi, gdi, mga, ton, qdi, qm (sygr)	2.0–1.95 (2.07)	2.58–2.32 (2.28)	6.1–9.8	–3.7 to –0.9 (–0.3)
Cpb	High	di, gdi, mgr, qmdi, sygr, afs, mga, qm, ton	1.98–1.96	2.57–2.29	6.5–9.3	–4.3 to –2.3
Cpb	Low	di, gdi, mgr, qdi, qmdi		2.51–2.19	8.0–10.6	
Epb	High	di, qdi, ga, gdi, qm, ton (gdi)	2.01 (2.06)	2.60–2.40 (2.39)	5.9–7.9	–2.7 to –2.0 (–0.6)
Mlb	Low	grt, sil-sp, lgr, mgr	1.92–1.91	2.63–2.52	10.5–11.6	–6.1 to –4.3
Elb	Low	grt, sil-sp, lgr, mgr	1.93–1.91	2.59–2.46	10.5–11.6	–5.6 to –4.8
Slave						
THd	Low	gdi, afs, qmdi, ga, di, mgr, qdi, qga, sygr, ton	2.66–2.58	2.71–2.60 (2.89)	7.8–10.8	1.8 to 2.8 (0.5)
OLd	Low-med	ton, gdi, di, mgr, qdi	2.71–2.58	2.88–2.70	5.6–7.8	–0.4 to 2.5
QMB, DLd		gdi, ton, qdi, di, mga, mgr, mnz, qga, sygr	3.25–2.97	3.61–2.87	5.2–9.6	–3.0 to 4.2
Lithology abbreviations: afs = alkali feldspar granite, di = diorite, ga = gabbro, gdi = granodiorite, lgr = leucogranite, mga = monzogabbro, mgr = monzogranite, mnz = monzonite, qdi = quartz diorite, qga = quartz gabbro, qm = quartz monzonite, qmdi = quartz monzodiorite, ton = tonalite, sygr = syenogranite Mineral abbreviations: grt = garnet, sil = sillimanite, sp = spinel Domain abbreviations: Cpb = Central plutonic belt, DLd = Duggan Lake domain, Elb = Eastern leucogranite belt, Epb = Eastern plutonic belt, ERd = Ellice River domain, Mlb = Main leucogranite belt, OLd = Overby Lake domain, QMB = Queen Maud Block, THd = Tinney Hills domain, Wpb = Western plutonic belt Age = U-Pb zircon crystallization age T _{DM} = DePaolo (1981): range shown for Wpb, ERd, Cpb-low does not include several older results discussed in text Values in parentheses reflect the few older samples						

Late (1.93–1.88 Ga) plutonic rocks are more isotopically evolved than the early suite. They are characterized by model ages mostly between 2.51 to 2.78 Ga, with two samples yielding 2.95 to 3.01 Ga model ages (Table 1, A-1; Fig. 5). Leucogranites and high-Zr granitoid rocks display an overlapping, narrow range of ε_{Nd} values (–6.2 to –4.3). Normal-Zr, 1.9 Ga granitoid rocks have lower ε_{Nd} values of –13.0 to –7.1 that partly coincide with the crustal evolution range of Mesoarchean crust (Queen Maud Block, Duggan Lake domain; Fig. 3) that they intrude. This group largely consists of monzogranite and alkali-feldspar granite; however, at one Duggan Lake domain outcrop, monzodiorite (sample J023C in Whalen et al., 2018) is mingled with ca. 1.92 Ga monzogranite, indicating a component of mafic plutonism at this time.

Two additional groups are represented in the data set:

- Four samples of basaltic komatiite from the southern Ellice River domain display back-arc geochemical characteristics (Whalen et al., 2018), but have no direct age constraints. Their occurrence near metasedimentary rocks of assemblage 1 suggests they may be of similar age (ca. 2.1–2.0 Ga). Three of four samples are juvenile, with εNd(2100 Ma) values of up to +3.2 (Fig. 5; Table A-1).

- Metasedimentary samples in the Ellice River domain have model ages of 2.77 Ga (assemblage 1 metapelite; εNd(1950 Ma) = –6.0) and 2.54 Ga (assemblage 2 metapsammite; εNd(1950 Ma) = –3.7). The more juvenile isotopic composition of the latter is consistent with detrital zircon populations indicating sourcing of 2.0 to 1.99 Ga Thelon tectonic zone plutons (Davis et al., 2021) with 2.57 to 2.19 Ga model ages.

U-Pb geochronology

Uranium-lead data for biotite monzogranite from the Overby Lake domain and three leucogranite samples from the Main leucogranite belt and Eastern leucogranite belt, acquired using the Sensitive High-Resolution Ion Microprobe (SHRIMP), are presented (*see* Table A-2) to extend characterization of the Overby Lake domain and further constrain the timing of leucogranite generation.

Overby Lake domain

Sample M202A is a moderately foliated, medium-grained biotite monzogranite (Fig. 4e) collected from a monzogranite to granodiorite layer approximately 1 m wide that is interpreted to cut foliated to gneissic hornblende diorite near the eastern Overby Lake domain boundary.

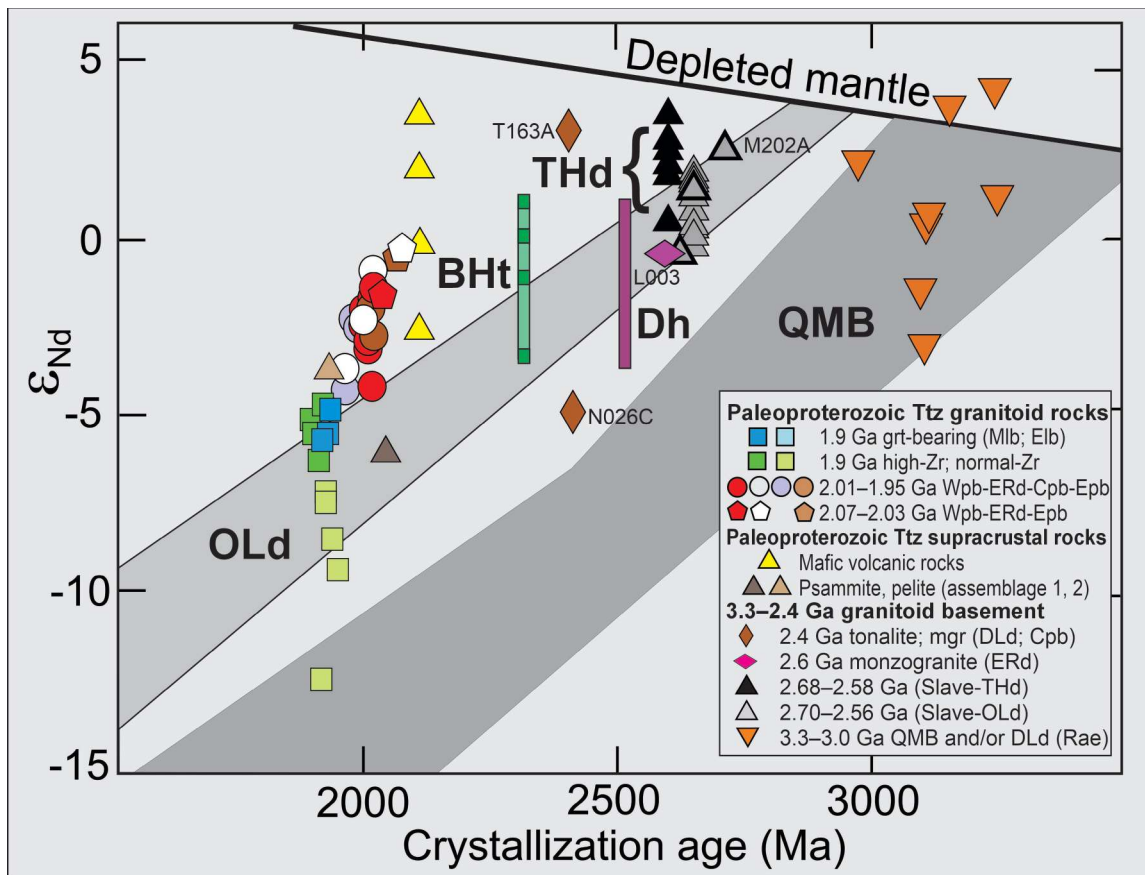


Figure 5. Diagram of ϵ_{Nd} (1950 Ma) versus time for central Thelon tectonic zone (Ttz) and adjacent basement rocks; for clarity, the plot includes only Paleoproterozoic Thelon tectonic zone plutonic rocks with available U-Pb zircon ages. Shaded crustal evolution fields for the Queen Maud Block (QMB) and Overby Lake domain (OLd) have boundaries defined by the Sm/Nd isotopic composition of limiting samples in these groups. Also shown are the range of ϵ_{Nd} values for samples from the ca. 2.33 to 2.32 Ga Buffalo Head terrane (BHT; green bar (4 samples); Villeneuve et al., 1993) and ca. 2.52 Ga Closepet granite of the Dharwar Craton (Dh; purple bar (7 samples); Dey, 2013). Cpb = Central plutonic belt, DLd = Duggan Lake domain, Elb = Eastern leucogranite belt, Epb = Eastern plutonic belt, ERd = Ellice River domain, Mlb = Main leucogranite belt, THd = Tinney Hills domain, Wpb = Western plutonic belt; grt = garnet, mgr = monzogranite.

Zircon grains in this sample are characterized by elongate euhedral prisms with well developed, annular growth zoning. Many grains show evidence of metamictization and alteration that accentuate the growth zoning. Analyses have yielded U concentrations of 70 to 800 ppm. Nineteen of twenty-four analyses define a weighted mean age of 2712 ± 4 Ma (MSWD = 2.3; Fig. 6a), with some degree of excess scatter. Rejected analyses (5) have younger $^{207}\text{Pb}/^{206}\text{Pb}$ ages between 2694 and 2637 Ma, which is consistent with a small degree of Paleoproterozoic Pb loss at ca. 1.9 to 1.7 Ga. The crystallization age of the rock is interpreted as 2712 ± 4 Ma.

Leucogranite units

Sample M003A is a medium-grained, intensely foliated $138^\circ/36^\circ$ leucogranite with prominent quartz ribbons from the east (Fig. 3). It contains approximately 3 modal per cent

garnet and 2% biotite. Zircon grains are dominantly equant with rounded morphology and poorly developed terminations. Backscatter images of grain interiors show minor evidence for growth zoning. The zircons have U contents of 670 to 1510 ppm, ytterbium (Yb) contents of 40 to 100 ppm, and Th/U ratios less than 0.19. Twenty of twenty-one analyses yielded a weighted mean $^{207}\text{Pb}/^{206}\text{Pb}$ age of 1925 ± 3 Ma (MSWD = 1.8; Fig. 6b), which is interpreted as the time of leucogranite crystallization. Two slightly older analyses with ages of 1965 and 1944 Ma were rejected as statistical outliers.

Sample R132A is a medium- to coarse-grained, strongly deformed ($L > S$) syenogranite from the central part of the Main leucogranite belt (Fig. 3), with less than 2 modal per cent garnet and 1% biotite. Zircons in this sample are euhedral to subhedral prismatic grains with length to breadth ratios of approximately 2:1 to 3:1. All grains are strongly altered, which is consistent with their generally high U abundances

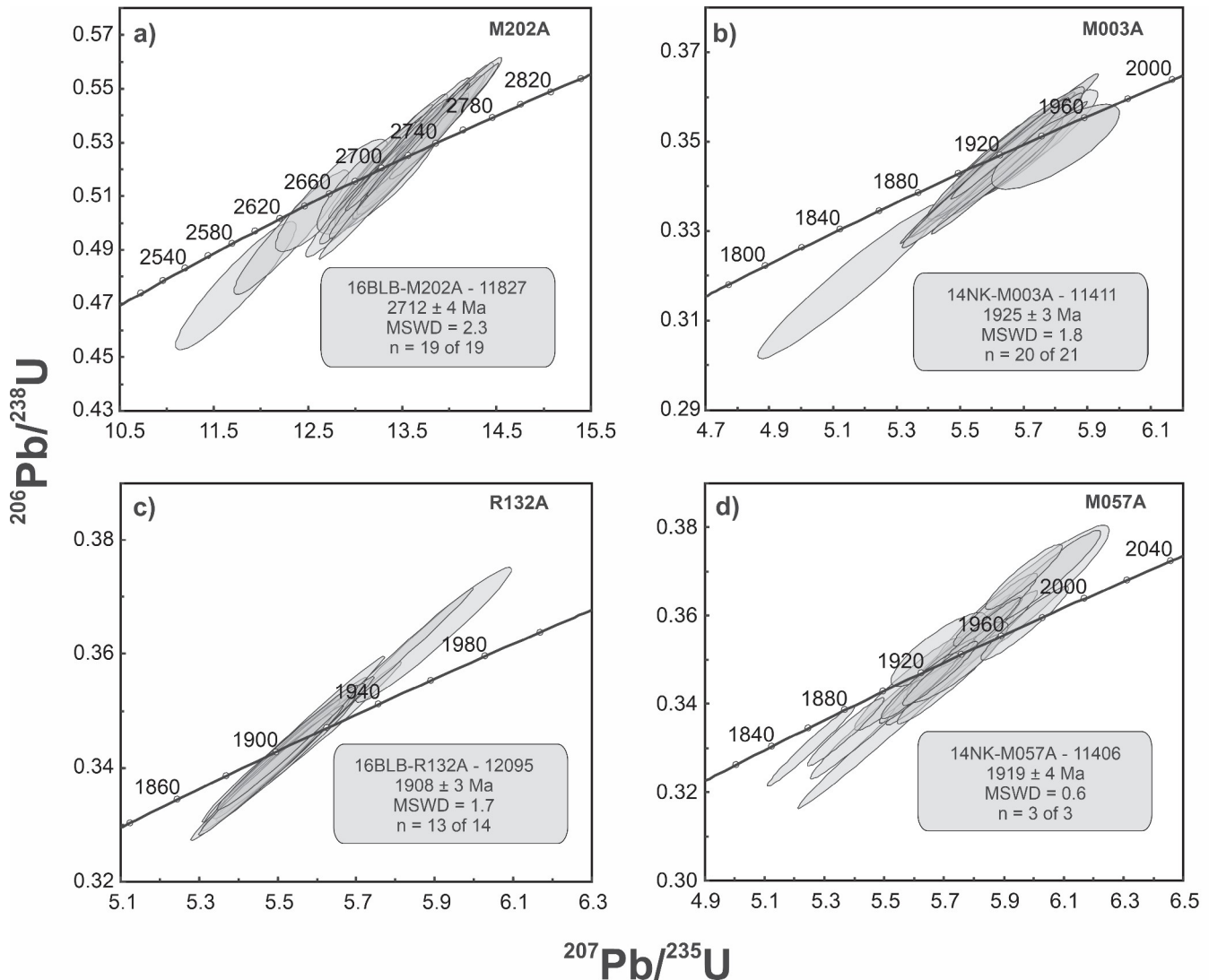


Figure 6. Concordia diagrams showing results of Sensitive High-Resolution Ion Microprobe (SHRIMP) analyses for samples from the Thelon tectonic zone: **a)** Overby Lake domain monzogranite sample M202A; **b)** Eastern leucogranite belt sample M003A; **c)** Main leucogranite belt sample R132A; **d)** Main leucogranite belt sample M057A.

of 900 to 1600 ppm. The analyzed grains are compositionally similar, with Th/U ratios between 0.06 and 0.18 and high hafnium (Hf) contents ranging approximately from 11 000 to 15 600 ppm. The weighted mean $^{207}\text{Pb}/^{206}\text{Pb}$ age of fourteen analyses yielded a value of 1909 ± 3.4 Ma (MSWD = 2.9; Fig. 6c). The high MSWD indicates some excess scatter in the data and a better fit is met if one reversely discordant analysis, which shows anomalous characteristics including relatively high Zr_2O sensitivity and U/UO ratio outside of calibration range, is rejected from the calculation. The refined age of 1908 ± 3 Ma (MSWD = 1.7) is taken as the crystallization age of the leucogranite.

Sample M057A is a coarse-grained, moderately foliated ($206^\circ/78^\circ$) alkali-feldspar granite from the Main leucogranite belt (Fig. 3), with approximately 4 modal per cent garnet, less than 1% spinel, and less than 1% biotite, mostly rimming garnet and/or ilmenite. Zircons in this sample are highly

altered and consist of euhedral to subhedral grains typically exhibiting medium to fine oscillatory zoning. Two distinct chemical subgroups are documented. A high Th/U group (0.16–0.49) has moderate Hf contents (9000–13 000 ppm), low U (370–2800 ppm), and variable $^{207}\text{Pb}/^{206}\text{Pb}$ ages ranging from 1954 to 1916 Ma (Fig. 6d). A low Th/U group (<0.10) has generally higher Hf (12 000–17 000 ppm) and U (1200–7000 ppm) contents, and $^{207}\text{Pb}/^{206}\text{Pb}$ ages of 1967 to 1884 Ma. Many of the latter analyses have high common Pb contents indicative of metamictization and alteration, which is consistent with their high U (>1000 ppm) contents. The higher Th/U group generally yields older ages than the low Th/U group, which is chemically similar to the uniformly low Th/U (<0.18) zircon populations in leucogranite samples R132A and M003A. Six of the seven youngest analyses of the low Th/U group yielded a weighted mean $^{207}\text{Pb}/^{206}\text{Pb}$ age of 1921 ± 6 Ma (MSWD = 3.7), which is considered to reflect magmatic crystallization. Three of these analyses have low

common Pb contents, indicative of minimal alteration, and yielded a weighted mean $^{207}\text{Pb}/^{206}\text{Pb}$ age of 1919 ± 4 Ma (MSWD = 0.6), which is interpreted as the best estimate of the crystallization age of the leucogranite. The high Th/U zircons in this sample are interpreted to reflect partially reset inherited or earlier metamorphic grains.

Oxygen isotopes

The 96 samples selected for whole-rock oxygen isotope ($\delta^{18}\text{O}_{\text{WR}}$) analysis comprise plutonic rocks from sample suites collected throughout the central Thelon tectonic zone (black dot localities in Fig. 3; Table A-1). The samples

represent a subset of those used for Sm-Nd analyses (Fig. 3; Table A-1) and whole-rock geochemical analyses (Whalen et al., 2018).

The sample set spans a range in measured SiO_2 contents from 47.0 to 77.1 weight per cent for Paleoproterozoic rocks (Fig. 7a; Whalen et al., 2018) and from 47.3 to 75.3 weight per cent for Archean rocks (Fig. 8; Whalen et al., 2018). Most rocks are moderately to strongly foliated and partially recrystallized. For simplicity, these samples are referred to collectively as ‘granitoid rocks’ (sensu lato) and encompass quartz-bearing plutonic rocks that range in composition from gabbro to alkali-feldspar granite. Most are of intermediate composition (quartz monzonite–granodiorite). The plutonic rocks (Table A-1) represent a full range of aluminum saturation indices

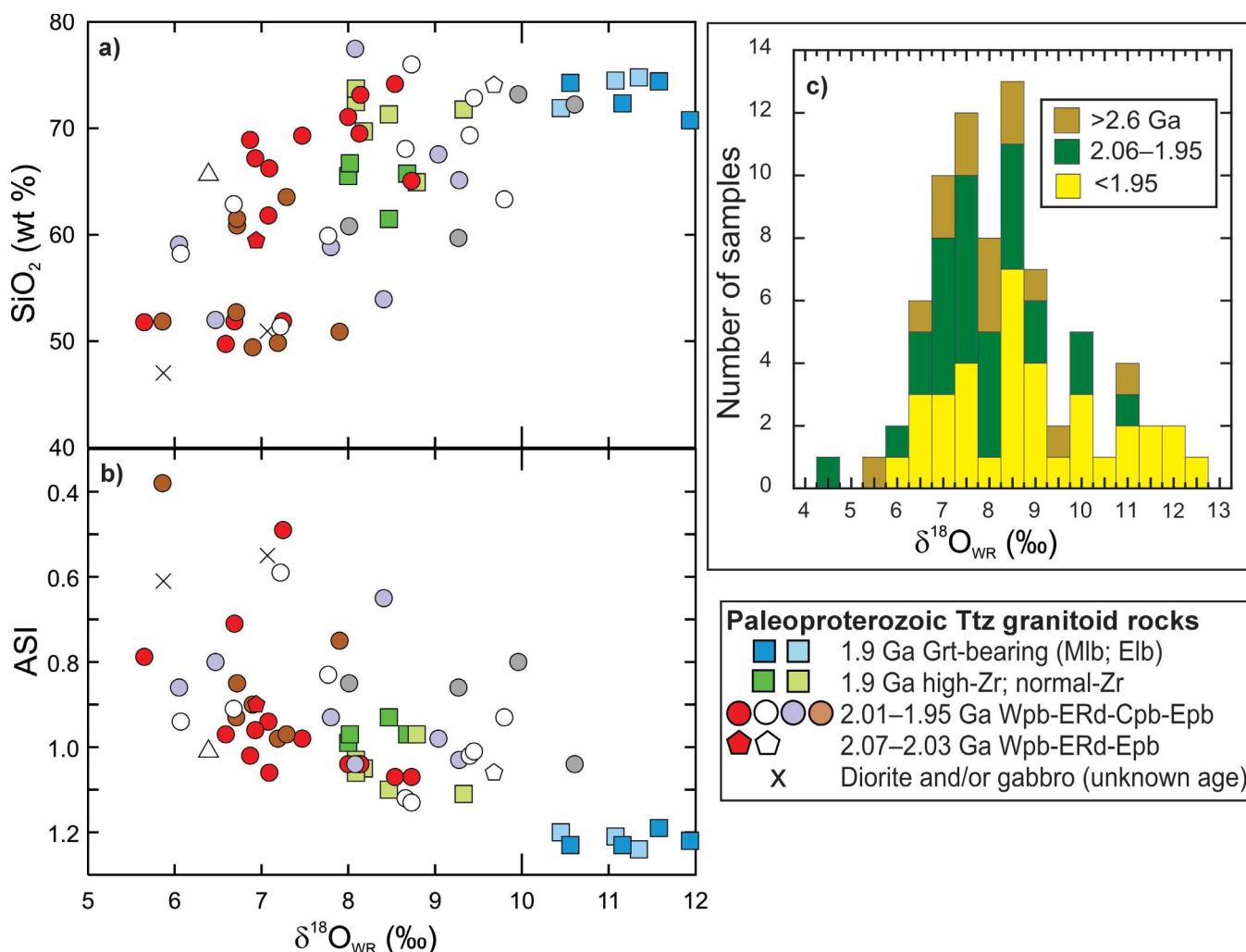


Figure 7. Correlation between samples of Paleoproterozoic Thelon tectonic zone (Ttz) plutonic rocks, shown using: **a)** a diagram of SiO_2 contents (in weight per cent) versus whole-rock $\delta^{18}\text{O}$ (in parts per thousand relative to V-SMOW), illustrating the influence of magmatic processes; **b)** a diagram of aluminum saturation index ($\text{ASI} = \text{molecular Al}/(\text{Ca}+\text{Na}+\text{K}-1.67*\text{P})$) versus whole-rock $\delta^{18}\text{O}$, illustrating the influence of source-rock composition; **c)** a histogram plot of whole-rock $\delta^{18}\text{O}$, illustrating a change from isotopically lighter to heavier granitoid rocks with time. Cpb = Central plutonic belt, Elb = Eastern leucogranite belt, ERd = Ellice River domain, Epb = Eastern plutonic belt, Mlb = Main leucogranite belt, Wpb = Western plutonic belt.

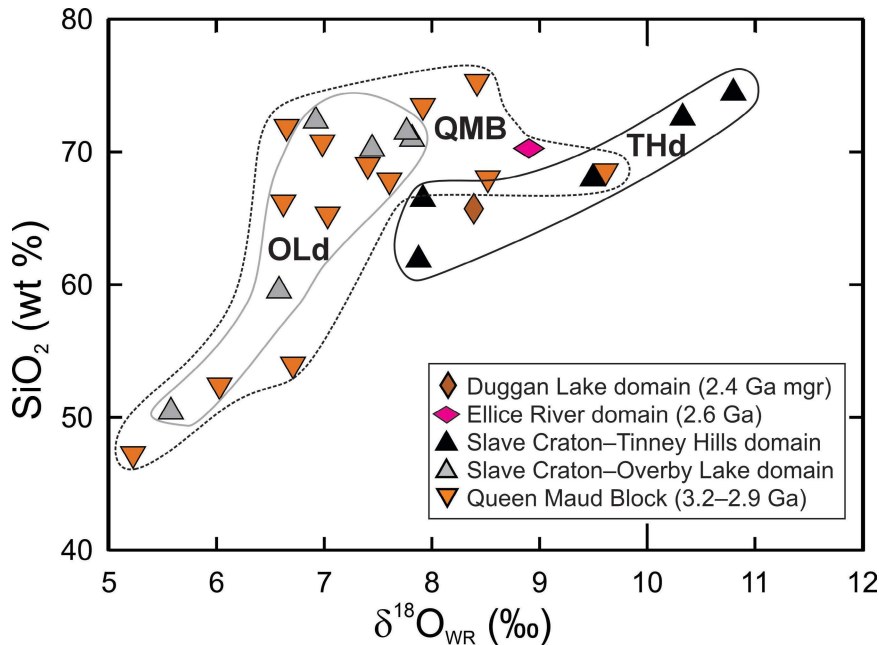


Figure 8. Diagram of SiO_2 contents (in weight per cent) versus whole-rock $\delta^{18}\text{O}$ (in parts per thousand relative to V-SMOW) for Archean rocks in the Thelon tectonic zone. mgr = monzogranite, OLd = Overby Lake domain, QMB = Queen Maud Block, THd = Tinney Hills domain.

($\text{ASI} = \text{molecular Al}/(\text{Ca}+\text{Na}+\text{K}-1.67*\text{P})$), from peralkaline ($\text{ASI} = 0.8$) through subaluminous ($\text{ASI} < 1.0$), and from metaluminous ($\text{ASI} \approx 1.0$) to peraluminous ($\text{ASI} > 1.1$). Most samples are subaluminous to metaluminous, except for strongly peraluminous samples of Paleoproterozoic leucogranites (Fig. 7b) and several of the Archean rocks with the highest SiO_2 contents in the Tinney Hills domain (Fig. 8; Whalen et al, 2018). As a whole, the samples display a positive correlation between whole-rock $\delta^{18}\text{O}_{\text{WR}}$ and weight per cent SiO_2 (Fig. 7a, 8), and ASI (e.g. Fig. 7b).

The values for $\delta^{18}\text{O}_{\text{WR}}$ show a similar wide range of variation (Table A-1) for Paleoproterozoic rocks (5.7–11.9; Fig. 7b) as for Archean rocks (5.2–10.8; Fig. 8). Two samples with strong epidote overprints show values less than 5 (quartz monzonite W173A, Ellice River domain; granodiorite L202A, Eastern plutonic belt); these are attributed to the effects of hydrothermal alteration and are not considered further. The distribution of $\delta^{18}\text{O}_{\text{WR}}$ values (Fig. 7c) is similar for early (2.07–1.95 Ga) Paleoproterozoic and Archean granitoid rocks, which both have average $\delta^{18}\text{O}_{\text{WR}}$ values between 7.5 and 8‰. In contrast, results for late (ca. 1.93–1.88 Ga) granitoid rocks are skewed toward heavier $\delta^{18}\text{O}_{\text{WR}}$ values (Fig. 7c) by the leucogranite group which has $\delta^{18}\text{O}_{\text{WR}}$ values of 10.5 to 11.9‰ (Fig. 7a–c; Table A-1).

DISCUSSION

The isotopic data set presented here, integrated with bedrock mapping results and high-resolution aeromagnetic data, facilitate discrimination of crustal domains in the central Thelon tectonic zone, where intense deformation and structural transposition, as well as limited exposure, make it difficult to trace lithological units along strike.

Collectively the data establish the continuity and extent of ten crustal domains, four dominated by Archean rocks with Nd model ages older than 2.6 Ga and six Paleoproterozoic domains with model ages generally younger than 2.57 Ga (Fig. 3; Table A-1). These domains and implications for their tectonic evolution are discussed below.

Nature and distribution of Archean rocks

Queen Maud Block (Rae Craton)

In the eastern Thelon tectonic zone, contrasting aeromagnetic characteristics (Fig. 2) distinguish Mesoproterozoic basement in the western Queen Maud Block and Duggan Lake domain (Fig. 3) from Paleoproterozoic plutonic rocks of the Eastern plutonic belt (magnetic high) and the Main leucogranite belt (magnetic low). These aeromagnetic distinctions are supported by the distribution of Nd model ages, which are generally less than 2.6 Ga in magnetic domains correlated with the Eastern plutonic belt and Main leucogranite belt (Table A-1), but greater than 3 Ga in the Queen Maud Block and Duggan Lake domain (Table A-1). These differences in Nd model ages correspond to U-Pb zircon crystallization ages of 3.28 to 2.98 Ga in the Queen Maud Block and Duggan Lake domain (Table 1) and Paleoproterozoic ages in the Eastern plutonic belt and Main leucogranite belt (Table A-1).

Tinney Hills and Overby Lake domains (Slave Craton)

Samarium-neodymium isotopes (Table A-1) show that the eastern boundary of the Slave Craton is marked by a sharp change in model ages that range from older than 2.7 Ga in the Overby Lake domain to younger than 2.53 Ga

in the Western plutonic belt (Fig. 3), although two localities in the latter have higher T_{DM} ages of 2.63 and 2.64 Ga. This isotopic boundary coincides with an aeromagnetic lineament in the central part of NTS map area 76I (inset, Fig. 3). Farther north and south, where a distinct aeromagnetic lineament is not evident, the eastern boundary of the Overby Lake domain is established by these Nd model-age differences. The western boundary of the Overby Lake domain with the Tinney Hills domain is established by the presence in the Tinney Hills domain of metapelitic rocks of the Yellowknife Supergroup as well as of high-strain zones mapped in the ‘Ragged lake’ area (Fig. 3; Thompson, 1992).

Available geochronology indicates that, although the Overby Lake domain and Tinney Hills domain both host ca. 2.6 Ga plutonic rocks, the Overby Lake domain contains older plutonic rocks not recognized in the Tinney Hills domain. The ca. 2.71 Ga crystallization age of Overby Lake domain monzogranite determined in this study (2.712 ± 0.004 Ga; sample M202A Table A-1; Fig. 6a) is within error of the age of granodiorite farther west in this domain (2.705 ± 0.006 Ga; sample R114A; Berman and Camacho, 2020). In contrast, the oldest crystallization age determined in the Tinney Hills domain is 2.66 ± 0.004 Ga obtained for metaluminous tonalite (sample T156; Fig. 3; Berman and Camacho, 2020), which is compatible with

the oldest plutonic ages (ca. 2.68–2.66 Ga) documented in greenstone belts of the eastern Slave Craton (van Breemen et al., 1992). Younger granitoid rocks in the Overby Lake domain have ages (2.61–2.59 Ga; Berman and Camacho, 2020) similar to those of two ca. 2.6 Ga two-mica granites in the Tinney Hills domain, approximately 20 km west of the area shown in Figure 3 (Culshaw and van Breemen, 1990).

The Tinney Hills and Overby Lake domains exhibit several geochemical and isotopic differences. In the Overby Lake domain, metaluminous, medium- K_2O tonalite and granodiorite dominate (Whalen et al., 2018), $\delta^{18}O_{WR}$ values are less than 7.8‰, and most $\epsilon_{Nd}(2650 \text{ Ma})$ values range from -0.4 to 1.9 (Fig. 5; Table A-1). In contrast, although Tinney Hills domain granitoid rocks include peraluminous compositions (Whalen et al., 2018) and are more magnesian (Fig. 9a), more potassic (Fig. 9b), and have heavier $\delta^{18}O_{WR}$ values (7.9–10.8; Fig. 8), most have less evolved Nd isotopic compositions ($\epsilon_{Nd}(2650 \text{ Ma})$ of 1.8 to 2.8; Fig. 5). Although these geochemical and isotopic differences are not insignificant, they can be explained by interaction of Tinney Hills domain granitoid rocks with Yellowknife Supergroup metasedimentary rocks that they intrude (Fig. 3). Given the occurrence of ca. 2.6 Ga plutonic rocks in both domains, it may be that the Tinney Hills domain represents a higher structural level of the Slave Craton than the Overby

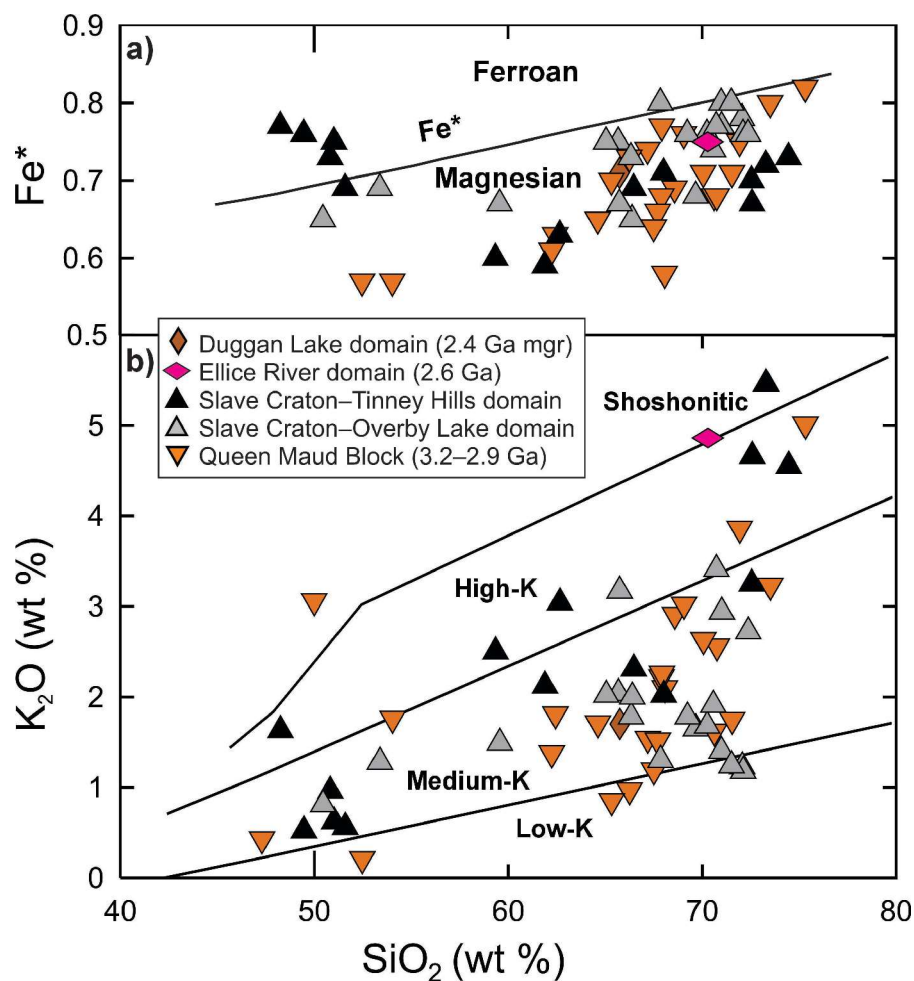


Figure 9. Geochemical differences of Archean Thelon tectonic zone basement rocks, shown using: **a)** a diagram of Fe^* ($= Fe/(Fe+Mg)$) versus SiO_2 contents (in weight per cent); **b)** K_2O versus SiO_2 contents. Note that Overby Lake domain granitoid rocks are distinctly less potassic than Tinney Hill domain and Rae Craton granitoid rocks. mgr = monzogranite.

Lake domain as interpreted by Thompson et al. (1986), and consistent with the lower metamorphic grade of the Tinney Hills domain. The ca. 2.71 Ga crystallization ages determined for two plutonic rocks in the Overby Lake domain are similar to volcanic ages in the Hope Bay Block (HB, Fig. 1; Sherlock et al., 2012) and Kam group (Bleeker and Hall, 2007) of the Yellowknife supracrustal belt. The age similarity of the Hope Bay and Kam group volcanic rocks, which are structurally offset, led Bleeker and Hall (2007) to suggest the Hope Bay Block may have rifted off the Slave Craton (central Slave basement complex) and subsequently re-amalgamated. As regional aeromagnetic data indicate correlation of the Overby Lake domain with the Hope Bay Block to the north (Stubley, 2005), their suggestion could account for the high-strain boundary between the Tinney Hills and Overby Lake domains. If reassembly of these blocks occurred by the time of ca. 2.6 Ga plutonism, it would corroborate the interpretation by Thompson et al. (1985, 1986) of a Neoproterozoic structural component within the central Thelon tectonic zone.

Basement to Thelon tectonic zone plutonism

Uranium-lead geochronological data obtained in the central Thelon tectonic zone have identified only two samples with pre-2.1 Ga crystallization ages. Accordingly, the character, extent, and affinity of crust into which the Thelon tectonic zone plutonic suite was emplaced remain elusive. Orthogneiss sample L003, in the Ellice River domain, consists of alternating dioritic and monzogranitic bands. The bulk orthogneiss yielded a crystallization age of 2591 ± 27 Ma (Davis et al., 2014), Nd model age of 2.79 Ga, and $\epsilon_{\text{Nd}}(2600 \text{ Ma})$ value of -0.4 (Table A-1). Folded orthogneiss 6 km along strike of sample L003 (Fig. 3) similarly consists of monzogabbro (sample W120C; Fig. 4f) with monzogranite (sample W120B) bands; the isotopic composition of monzogabbro sample W120C (2.74 Ga model age; $\epsilon_{\text{Nd}}(2600 \text{ Ma}) = 1.2$; Table A-1) closely corresponds to sample L003. The congruence of isotopic data from these outcrops in the Ellice River domain with ca. 2.6 Ga granitoid rocks in the Overby Lake domain (Table A-1; Fig. 5) suggests they may represent Overby Lake domain crust. Field relationships do not resolve whether these rocks were tectonically emplaced after Thelon tectonic zone plutonism or whether they were intruded by Thelon tectonic zone plutons. At one locality in the Central plutonic belt, ca. 2.41 Ga quartz monzonite sample T163A (Fig. 3; Table A-1; Berman and Camacho, 2020) has a juvenile isotopic composition ($T_{\text{DM}} = 2.4$ Ga; $\epsilon_{\text{Nd}}(2408 \text{ Ma}) = -2.9$). Two kilometres away, the 2.88 Ga T_{DM} value of diorite sample T168 indicates interaction with significantly more evolved crust; the age of sample T168 is unknown, but may also be ca. 2.4 Ga.

Compared to the few samples discussed above, isotopic data collected for early Thelon tectonic zone plutonic rocks yield younger T_{DM} ages of 2.19 to 2.57 Ga. To explore the nature of the basement rocks into which the early Thelon

tectonic zone suite was emplaced, Nd isotopic compositions of early Thelon tectonic zone plutons are used as crustal probes. This requires a petrological model for the genesis of early Thelon tectonic zone plutonic rocks, which is first addressed before returning to the question of the affinity of basement to these belts.

Tectonic setting and petrogenesis of early Thelon tectonic zone plutonic rocks

Neodymium isotopic results (Table A-1) provide an important complement to zircon geochronology in establishing the continuity of Paleoproterozoic plutonic rocks between the Western plutonic belt and the Eastern plutonic belt, with the notable exception of the Duggan Lake domain (Fig. 3). Available zircon geochronology indicates crystallization ages dominantly between ca. 2.01 and 1.98 Ga (Table A-1; Davis et al., 2014; Berman et al., 2018). The occurrence of a significant number of ca. 2.03 to 2.02 Ga detrital zircons in Ellice River domain assemblage 2 (Davis et al., 2021), which also yields 1.99 and 1.95 Ga modes, suggests the main pulse of Thelon tectonic zone plutonism may have been established by 2.03 Ga, the crystallization age of quartz monzonite (sample L2; Davis et al., 2014) in the Western plutonic belt. Isolated occurrences in two plutonic belts of 2.07 Ga granodiorite (sample L202A in the Eastern plutonic belt; $T_{\text{DM}} = 2.39$ Ga) and 2.06 Ga syenogranite (sample M165A in the Ellice River domain; $T_{\text{DM}} = 2.28$ Ga) indicate that Thelon tectonic zone magmatism initiated as early as 2.07 Ga. Two samples (sample M032 in the Ellice River domain; $T_{\text{DM}} = 2.48$ Ga; sample L160 in the Central plutonic belt; $T_{\text{DM}} = 2.57$) with respective crystallization ages of 1.953 and 1.955 Ga (Davis et al., 2021) provide a lower limit on plutonism in the central Thelon tectonic zone.

Thelon tectonic zone plutonic rocks exhibit a broad spectrum of compositions (Whalen et al., 2018), from diorite to alkali-feldspar granite, with field relationships documenting mafic magmatism prior to (Fig. 4b), as well as contemporaneously with, felsic magmatism (Whalen et al., 2018). Whole-rock geochemical data for 2.03 to 1.95 Ga Thelon tectonic zone plutonic rocks indicate a convergent margin setting. Major element features consistent with arc magmatism include their magnesian and calc-alkalic to calcic character, and the significant proportion of intermediate (quartz diorite, quartz monzodiorite) compositions relative to more felsic slab-failure magmatism (Whalen et al., 2018). A convergent margin setting is also reflected in negative Nb anomalies (Whalen et al., 2018) and trace-element contents of felsic rocks (Fig. 10a) supporting the interpretation of an arc setting, with or without slab-failure magmatism (Whalen et al., 2018); only two samples display 'within-plate' compositions (Fig. 10a). Geochemical signatures of 2.07 to 2.06 Ga plutonic rocks show no significant differences from the ca. 2.03 to 1.95 Ga plutonic rocks (Fig. 10a). This indicates that subduction-generated magmatism may have initiated as early as 2.07 Ga; however, recycling of similar basement geochemical signatures (Fig. 10a) cannot be ruled out.

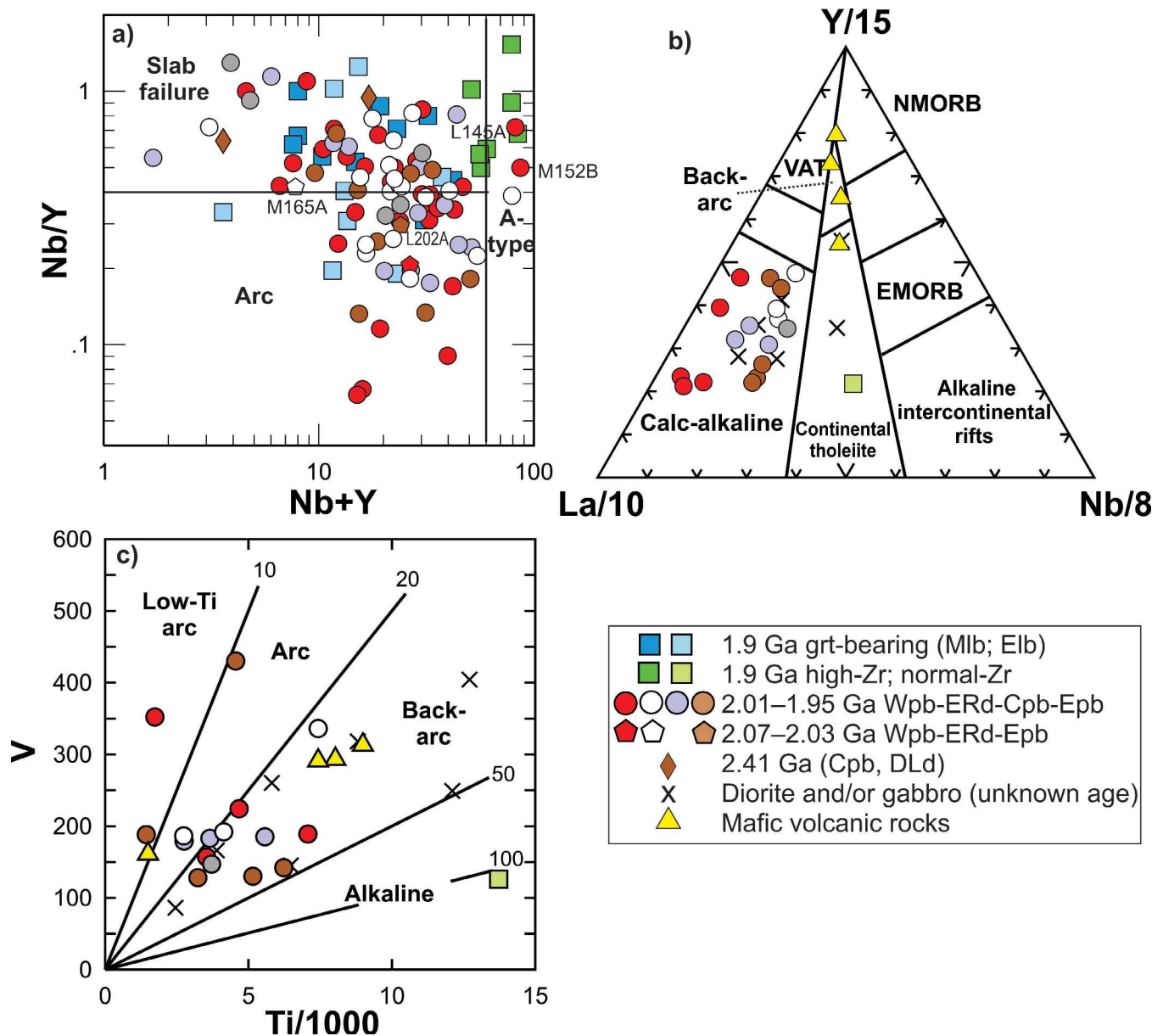


Figure 10. Tectonic discrimination diagrams for Paleoproterozoic Thelon tectonic zone rocks: **a)** Nb/Y versus (Nb+Y) diagram (Whalen and Hildebrand, 2019); **b)** ternary Y-La-Nb diagram for mafic rocks (Cabanis and Lecolle, 1989); **c)** Ti versus V diagram for mafic rocks (Shervais, 1982). Cpb = Central plutonic belt, DLd = Duggan Lake domain, Elb = Eastern leucogranite belt, EMORB = E-type mid-ocean-ridge basalt, Epb = Eastern plutonic belt, ERd = Ellice River domain, Mlb = Main leucogranite belt, NMORB = normal mid-ocean-ridge basalt, VAT = volcanic arc tholeiite, Wpb = Western plutonic belt; grt = garnet.

In parallel with felsic plutonic rocks, early mafic granitoid rocks have ‘calc-alkaline’ compositions (Fig. 10b; Cabanis and Lecolle, 1989), though some have V/Ti ratios suggestive of a transitional arc to back-arc setting (Fig. 10c; Shervais, 1982). A back-arc setting is also consistent with several undated samples with higher than transitional V/Ti ratios, but much lower Ti (<10 000 ppm) than typical rift suites (Fig. 10c; Shervais, 1982). Although the overall Thelon tectonic zone suite exhibits SiO₂ values ranging from 47 to 78 weight per cent (Fig. 7; Whalen et al., 2018), the absence of approximately 53 to 59 weight per cent SiO₂ samples in

the Western plutonic belt (n = 22) and Eastern plutonic belt (n = 10) could either highlight an SiO₂ gap associated with bimodal rift magmatism or reflect a sampling bias; however, rift magmatism is not supported by the geochemical characteristics noted above. Nor is it suggested by the trend with age among early Thelon tectonic zone granitoid rocks from more juvenile to more evolved ε_{Nd} values (Fig. 5), which is the opposite of that expected in a rift setting, where younger plutons would be expected to have less interaction with basement wall rocks.

Oxygen-isotope data presented in this paper (Fig. 11a) offer further support for a convergent margin tectonic setting, where magmas invariably acquire a significant isotopic mantle component. Studies of arc magmatism in the Andean Cordillera demonstrated that $\delta^{18}\text{O}_{\text{WR}}$ values of volcanic rocks vary from close to mantle values ($\delta^{18}\text{O}_{\text{MANTLE}} \approx 5.7\text{‰}$; Kyser, 1986; Matthey et al., 1994), where overlying continental crust is thin in the south, to 7 to 8‰, where continental crust is thickest in the Central Volcanic Zone (Fig. 11a; James 1982; Longstaffe et al., 1983; Harmon et al., 1984). Similarly, continental margin batholiths display $\delta^{18}\text{O}_{\text{WR}}$ values dominantly lower than 8.5‰ (Fig. 11a; Driver et al., 2000). In contrast, $\delta^{18}\text{O}_{\text{WR}}$ values are significantly greater (predominantly $>8.5\text{‰}$) for granitoid rocks formed in an intracontinental setting (Fig. 11b; Driver et al., 2000), where sedimentary rocks are more abundant in magma-source regions and a significant mantle component is generally not recognized (Fleck and Criss, 1985; Brandon and Lambert, 1994; Driver et al., 2000). In comparison to these well documented differences, early (2.07 to 1.95 Ga) granitoid rocks have a mean $\delta^{18}\text{O}_{\text{WR}}$ value of 7.6‰ (n = 44), with lower mean values for the Western plutonic belt (7.3‰) and Eastern plutonic belt (6.6‰), and seven samples within 1‰ of the average mantle value (Table A-1). The distribution of these compositions, with over 50% of all samples, and 90% of Western plutonic belt and Eastern plutonic belt samples, having $\delta^{18}\text{O}_{\text{WR}}$ values less than 7.5‰ is similar to, but shifted approximately 1‰ lower (i.e. closer to mantle values) than, those of continental margin batholiths (Fig. 11a; Driver et al., 2000)

and volcanic rocks from the Central Volcanic Zone of the Andes (Fig 11a). These comparisons strongly support a convergent margin origin for Thelon tectonic zone plutonic rocks.

Constraints on Thelon tectonic zone petrogenesis

Spanning a broad range of $\delta^{18}\text{O}_{\text{WR}}$ values from approximately 5.5 to 10.5‰, the compositions of early Thelon tectonic zone granitoid rocks help constrain their petrogenetic evolution. Two end-member processes, magmatic fractionation and assimilation-fractional crystallization (AFC; Taylor and Sheppard, 1986), can be considered to account for the increase in $\delta^{18}\text{O}_{\text{WR}}$ with SiO_2 in early Thelon tectonic zone plutonic compositions (Fig. 12). Whereas an increase in $\delta^{18}\text{O}$ of 2 to 3‰ in the melt may accompany the closed-system process of crystal fractionation (Taylor and Sheppard, 1986), much larger increases in $\delta^{18}\text{O}$ values are possible during open-system AFC (Fig. 12). Open-system modification of a crystallizing melt can also describe melt hybridization in the source region due to the occurrence of variable proportions of melted crust. The compositions of Eastern plutonic belt granitoid rocks are well represented by closed-system fractionation (Fig. 12), with some mixing at source indicated by the spread in $\delta^{18}\text{O}_{\text{WR}}$ values in samples characterized by low SiO_2 contents. With several minor exceptions, most Western plutonic belt samples also follow the closed-system trend. The $\delta^{18}\text{O}_{\text{WR}}$ values for many Central

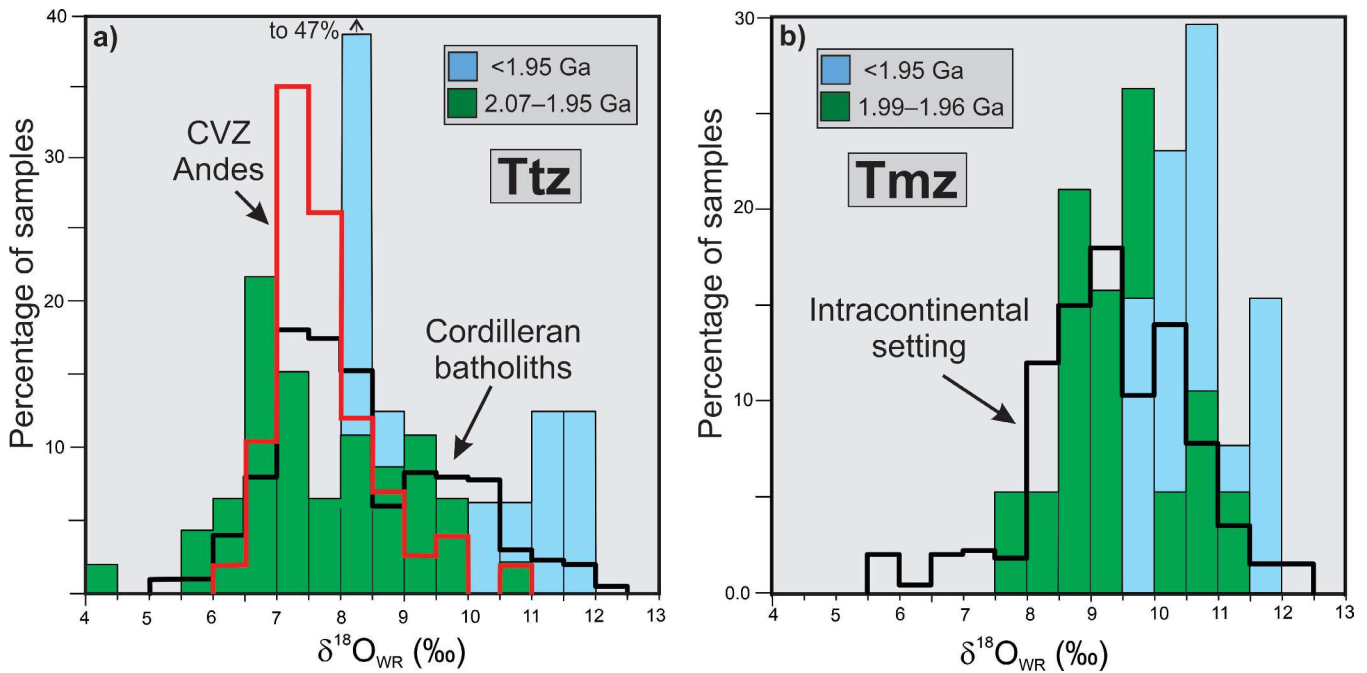


Figure 11. Histograms of whole-rock $\delta^{18}\text{O}$ (in parts per thousand relative to V-SMOW) of ‘early’ and ‘late’ granitoid rocks from **a)** the Thelon tectonic zone (Ttz), compared to continental arc granitoid rocks (black line; Driver et al., 2000) and arc volcanic rocks from the Central Volcanic Zone (CVZ) in the Andes (red line, based on data of James, 1982; Longstaffe et al., 1983; and Harmon et al., 1984); **b)** the Taltson magmatic zone (Tmz; De et al., 2000), compared to intracontinental granitoid rocks (black line; Driver et al., 2000)

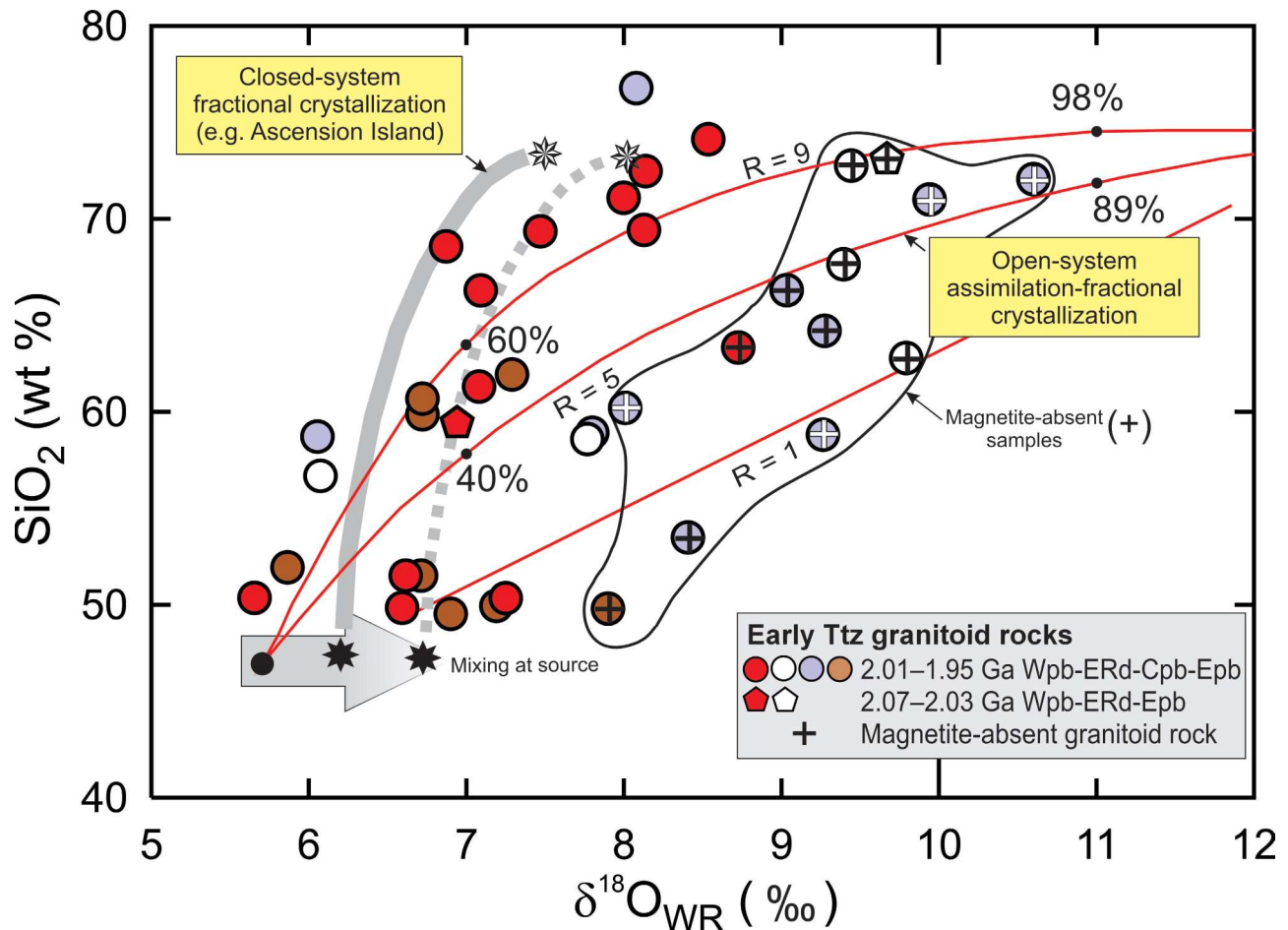


Figure 12. Diagram of SiO_2 contents (in weight per cent) versus whole-rock $\delta^{18}\text{O}$ (in parts per thousand relative to V-SMOW) for Proterozoic granitoid rocks of the Thelon tectonic zone (Ttz), comparing results from this study with closed-system (thick solid and dashed grey curves; black stars indicate the starting compositions and white stars, the end compositions for the model) and open-system oxygen-isotope models (red curves; black dot shows starting composition for the model; after Taylor, Jr., 1980). Differences in path curvature of model curves correspond to different ratios (R factors) of crystallized magma to assimilated crust. The percentages of crystallization for two hypothetical, hybrid magmas are indicated along each curve. Samples without magnetite are shown with plus signs (white plus sign for samples from Central plutonic belt aeromagnetic lows). Cpb = Central plutonic belt, Epb = Eastern plutonic belt, ERd = Ellice River domain, Wpb = Western plutonic belt.

plutonic belt and Ellice River domain samples follow the model open-system AFC path (Fig. 12), extending to high values (9.9–10.6‰), more than 1 to 2‰ higher than those of the Western plutonic belt or Eastern plutonic belt (Fig. 12, 13). These results indicate the Central plutonic belt and Ellice River domain granitoid rocks evolved in a lithologically more heterogeneous setting with a greater component of sedimentary rocks, possibly at somewhat higher crustal levels containing more supracrustal rocks.

The Nd and O isotopic data (Table A-1) provide constraints on the nature of the assimilated material (Fig. 14). In the continental arc setting interpreted for early Thelon tectonic zone plutonic rocks, juvenile mantle-derived melts are envisioned to pond in the lower crust, assimilating isotopically evolved basement rocks and derived partial

melts via melting, assimilation, storage, and homogenization (MASH) processes (Hildreth and Moorbath, 1988; Ducea et al., 2015). The compositions of most early Thelon tectonic zone plutonic rocks outline an average MASH-derived melt composition (grey field, Fig. 14), with $\epsilon_{\text{Nd}}(1950 \text{ Ma})$ values of -3.8 to -1.3 and $\delta^{18}\text{O}_{\text{WR}}$ values of 5.5 to 7.5‰, intermediate to evolved Archean crustal domains, and juvenile mantle compositions (Fig. 5). Two early Thelon tectonic zone plutonic rocks with a $\delta^{18}\text{O}_{\text{WR}}$ less than 7.5‰ have ϵ_{Nd} values outside this range (Fig. 14). These are interpreted to reflect basement-rock heterogeneity and/or different proportions of basement and mantle-derived melts interacting in the MASH zone. Many early Thelon tectonic zone plutonic rocks have higher $\delta^{18}\text{O}_{\text{WR}}$, but similar $\epsilon_{\text{Nd}}(1950 \text{ Ma})$ values compared to the average melt range (Fig. 14). These samples could reflect source-rock heterogeneity (consistent with the range

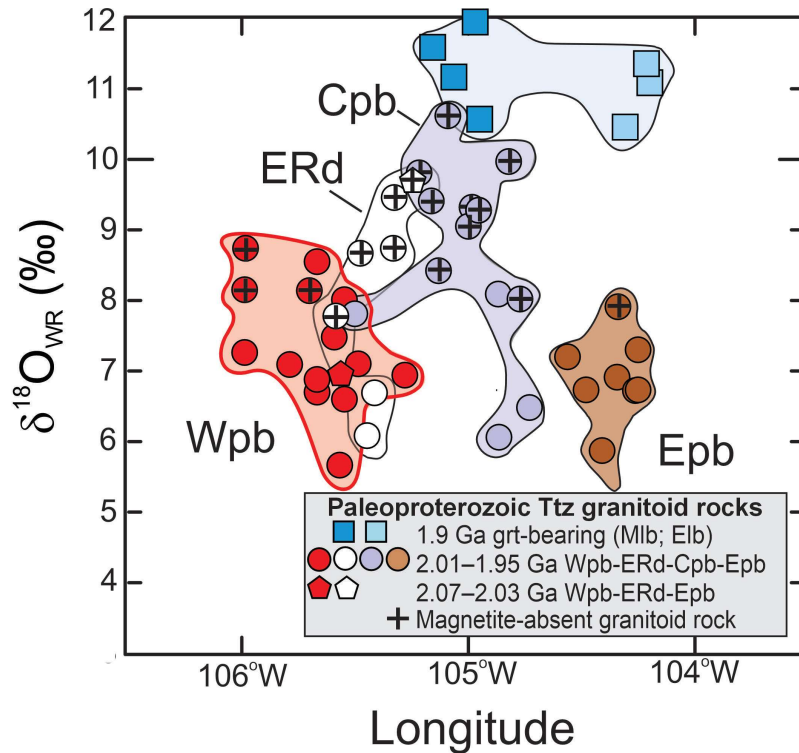


Figure 13. Diagram of whole-rock $\delta^{18}\text{O}$ (in parts per thousand relative to V-SMOW) versus longitude across the Thelon tectonic zone (Ttz), for early (2.07–1.95 Ga) granitoid rocks and ca. 1.9 Ga leucogranites. Note that plutonic rocks in the central portion of the Thelon tectonic zone are enriched in $\delta^{18}\text{O}_{\text{WR}}$. Cpb = Central plutonic belt, Elb = Eastern leucogranite belt, Epb = Eastern plutonic belt, ERd = Ellice River domain, Mlb = Main leucogranite belt, Wpb = Western plutonic belt; grt = garnet.

of $\delta^{18}\text{O}_{\text{WR}}$ values of Archean rocks with low- SiO_2 contents shown in Figure 7a, fractionated melts, and/or assimilation of evolved sedimentary rocks in the MASH zone (path A, Fig. 14). Assimilation of evolved sedimentary material (Archean sedimentary rocks or Paleoproterozoic Ellice River domain assemblage 1 ($\epsilon_{\text{Nd}}(1950 \text{ Ma}) = -7.2$; Table A-1) at higher crustal levels after ascent from the MASH source zone would be described by open-system, curved paths similar to path B in Figure 14 (e.g. Trumbull et al., 2004). This process, while not dominant, may have affected some samples with more negative $\epsilon_{\text{Nd}}(1950 \text{ Ma})$ and higher $\delta^{18}\text{O}_{\text{WR}}$ values (e.g. ca. 1.95 Ga granodiorite sample M032 and tonalite sample L160; ca. 2.01 Ga monzogranite sample M138A); moreover, one sample, L160, contains a single ca. 2.3 Ga inherited zircon that potentially reflects assimilation of assemblage 1 supracrustal rocks. One dated sample (ca. 1.985 Ga granodiorite sample W134A) has elevated $\delta^{18}\text{O}_{\text{WR}}$ (8.7‰) values, but a more juvenile composition ($\epsilon_{\text{Nd}}(1950 \text{ Ma}) = -1.5$). The uncommon occurrence of young, ca. 2.07 to 2.03 Ga inherited zircons in this sample suggests that its juvenile composition reflects interaction with early Thelon tectonic zone plutonic rocks of similar age.

Regional variations in oxygen-isotope compositions, with distinctly higher $\delta^{18}\text{O}_{\text{WR}}$ values in the Central plutonic belt and Ellice River domain compared to the Western plutonic belt and Eastern plutonic belt (Fig. 13), provide an explanation for the different aeromagnetic characteristics of these crustal domains (Fig. 2, 3). In contrast to dominantly magnetite-bearing plutonic rocks with $\delta^{18}\text{O}_{\text{WR}}$ values less than approximately 8‰, samples with the highest $\delta^{18}\text{O}_{\text{WR}}$ values all lack magnetite (samples with the '+' symbol superposed in Fig. 12, 13). This relationship suggests that destabilization of magnetite

in Thelon tectonic zone magmas resulted from the reducing effect of assimilation of graphite-bearing sedimentary rocks that occur as enclaves and pendants in all plutonic belts, but are most abundant in the Central plutonic belt and Ellice River domain. Isotopic modification by secondary processes has not been recognized. Magnetite-absent samples with $\delta^{18}\text{O}_{\text{WR}}$ values greater than 8‰ comprise 50% of analyzed Ellice River domain samples, all samples from Central plutonic belt magnetic low areas, and no samples from Central plutonic belt magnetic high areas (Fig. 3; Table A-1). This correlation supports assimilation of sedimentary rocks as the dominant process controlling the distribution of regions with low aeromagnetic response (Fig. 2, 3).

Isotopic constraints on basement to early Thelon tectonic zone plutonic rocks

Given the scarcity of exposures of rocks predating ca. 2 Ga in the central Thelon tectonic zone (*see above*), potential basement to the Thelon tectonic zone plutonic belts is evaluated here using the Nd isotopic compositions of early Thelon tectonic zone plutons as crustal probes. Across the central Thelon tectonic zone (Fig. 15), values of $\epsilon_{\text{Nd}}(2000 \text{ Ma})$ in Archean domains decrease from the Tinney Hills domain (mostly -7 to -4) to the Overby Lake domain (mostly -10 to -6), and more profoundly in the western part of the Rae Craton (Queen Maud Block; mostly -16 to -10). Early (ca. 2.03–1.95 Ga) Thelon tectonic zone plutonic rocks in all four domains (Western plutonic belt, Ellice River domain, Central plutonic belt, Eastern plutonic belt) yield model ages of 2.57 to 2.19 Ga and a restricted range of

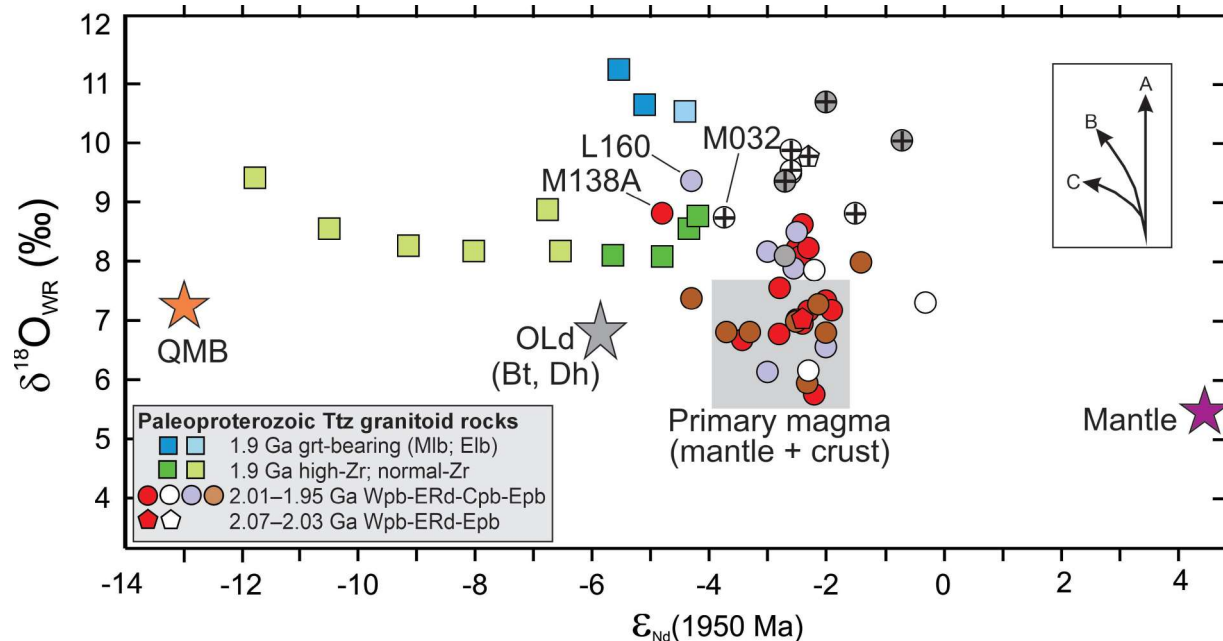


Figure 14. Diagram of whole-rock $\delta^{18}\text{O}$ (in parts per thousand relative to V-SMOW) versus $\epsilon_{\text{Nd}}(1950 \text{ Ma})$ for Thelon tectonic zone (Ttz) plutonic rocks, and average values of Archean domains and mantle (plus symbols indicate samples without magnetite). Average $\epsilon_{\text{Nd}}(1950 \text{ Ma})$ for Overby Lake domain (OLd) also applies to Boothia terrane (Bt) and Dharwar Craton (Dh; Dey, 2013). Schematic trajectories (upper right) reflect assimilation of sedimentary material of similar age within the MASH (melting, assimilation, storage, homogenization) zone (path A); melting and/or assimilation of evolved sedimentary rocks (path B); and variable admixture of Archean crust with oxygen-isotope composition similar to Thelon tectonic zone plutonic rocks (path C). Unusually low values of $\delta^{18}\text{O}_{\text{WR}}$ for two samples indicate a history of hydrothermal alteration. Cpb = Central plutonic belt, Elb = Eastern leucogranite belt, Epb = Eastern plutonic belt, ERd = Ellice River domain, QMB = Queen Maud Block, Mlb = Main leucogranite belt, Wpb = Western plutonic belt; grt = garnet.

more juvenile values of $\epsilon_{\text{Nd}}(2000 \text{ Ma})$, mostly between -4 and -2 (Fig. 15). In marked contrast to the basement-rock variations, the Paleoproterozoic plutonic rock values show no systematic change with geographic location (Fig. 15), which supports the interpretation that all four plutonic belts interacted with, or were derived from, basement rocks of similar isotopic composition.

Five possibilities are considered for potential basement to ca. 2 Ga Thelon tectonic zone plutonic rocks: 1) Archean Overby Lake domain exposed on the flanks of the central Thelon tectonic zone; 2) Archean Queen Maud Block exposed on the flanks of the central Thelon tectonic zone; 3) Boothia terrane, a ca. 2.56 to 2.48 Ga crustal block recently documented on Boothia Peninsula (northeast of area shown in Fig. 1; Sanborn-Barrie and Regis, 2020); 4) Buffalo Head terrane, hypothesized to have extended north of the McDonald Fault into the Thelon tectonic zone (Fig. 1; Ross et al., 1991; Card et al., 2014; Davis et al., 2021); and 5) Dharwar Craton in southern India, which paleomagnetic data allow was proximal to the eastern Slave Craton during ca. 2.21 Ga mafic dyke emplacement (*see* Fig. 14 in Kumar et al., 2012). Mass-balance calculations were used to evaluate these alternatives, based on the assumption that arc plutonic rocks can be modelled as approximately even

mixtures (Hildreth and Moorbath, 1988; Ducea et al., 2015) of juvenile mantle-derived melts (10 ppm Nd; Patchett and Bridgwater, 1984) and lower crust, as represented by the middle- to upper-crust samples collected from each domain. To the extent that these samples underwent earlier melting events, the lower crust would have a higher Sm/Nd ratio and more juvenile composition than inferred from collected samples. Notwithstanding this uncertainty, calculated lower-crust proportions are 25 to 35% for Queen Maud Block crust (average values: Nd = 18.5 ppm; $\epsilon_{\text{Nd}}(2000 \text{ Ma}) = -12.5$) and 40 to 60% for Overby Lake domain crust (average values: Nd = 19 ppm; $\epsilon_{\text{Nd}}(2000 \text{ Ma}) = -7.5$). The Overby Lake domain results apply as well to samples with overlapping ϵ_{Nd} values from the eastern Dharwar Craton (Fig. 5; Dey, 2013) and Boothia terrane (M. Sanborn-Barrie and D. Regis, unpub. data, 2021). The ca. 2.3 Ga Buffalo Head terrane is isotopically heterogeneous, with $\epsilon_{\text{Nd}}(2300 \text{ Ma})$ values between -3.4 and $+1.0$ (4 samples; Fig. 5; Thériault and Ross, 1991), which have been interpreted to reflect variable hybridization of evolved Archean crust by juvenile magma (Ross et al., 1991). As three samples (with $\epsilon_{\text{Nd}}(2300 \text{ Ma})$ of -1.3 , $+0.2$, and $+1.0$) are too juvenile to yield Thelon tectonic zone plutonic rock compositions via mixing with mantle-derived melts (Fig. 5), Buffalo Head terrane is not considered viable as a basement possibility.

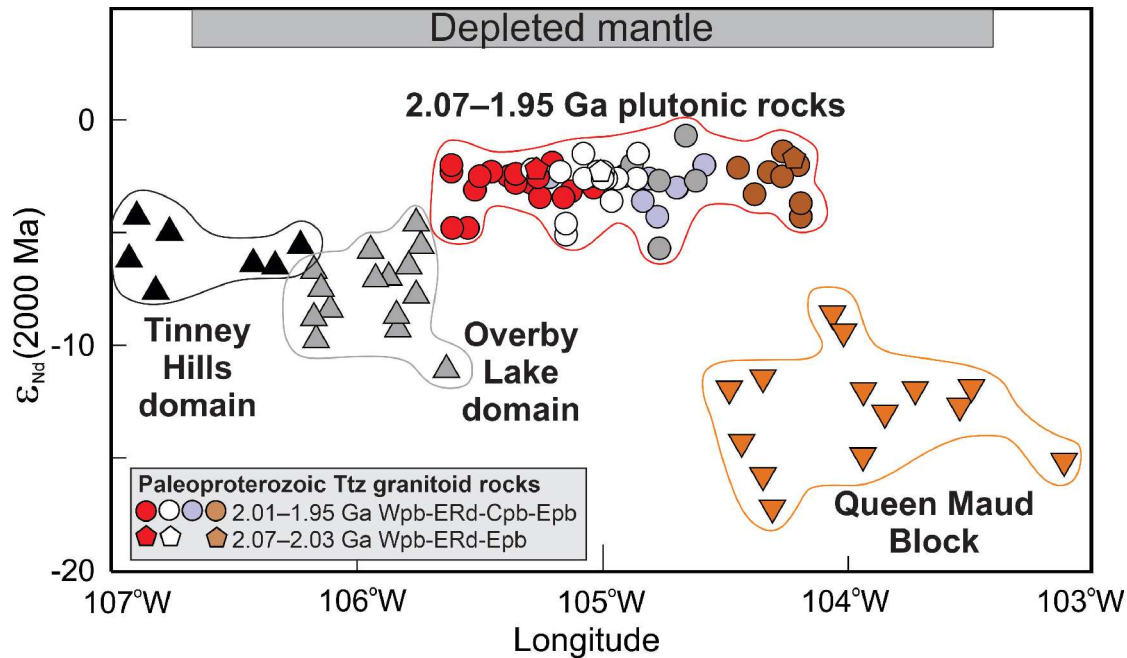


Figure 15. Variations in ϵ_{Nd} (2000 Ma) with respect to geographic location (longitude) across the central Thelon tectonic zone (Ttz). Sample locations were projected along strike to approximate an east-west cross-section. Cpb = Central plutonic belt, Epb = Eastern plutonic belt, ERd = Ellice River domain, Wpb = Western plutonic belt.

Although the isotopic constraints summarized above would allow for the Overby Lake domain, Boothia terrane, or Dharwar Craton to be interpreted as the potential lower crustal component of Thelon tectonic zone plutonic rocks, detrital zircon geochronology allows further discrimination between these possibilities. Assemblage 2 metapsammite in the Ellice River domain is dominated by ca. 2.02 to 1.99 Ga detrital zircons likely derived from exhumed Thelon tectonic zone plutonic rocks (Davis et al., 2021) and yields a ca. 2.54 to 2.49 Ga age mode (3 grains) along with one ca. 2.3 Ga detrital zircon. This sample lacks Mesoarchean detrital zircons, consistent with Nd isotopic constraints that establish the Queen Maud Block did not form the lower crustal basement of the Thelon tectonic zone. Plutonic rocks of the ca. 2.52 to 2.45 Ga Queen Maud granitoid suite (QMg, Fig. 1; Schultz et al., 2007; Davis et al., 2014) correspond well to the ca. 2.5 Ga detrital age mode; however, the absence of Mesoarchean detrital zircons in the studied sample argues against a source region that would have required traversing the Queen Maud Block. Similarly, the absence of ca. 2.7 and 2.6 Ga detrital zircons does not support the Overby Lake domain potentially being the basement to Thelon tectonic zone plutonic rocks, as also interpreted from the absence of zircon of Slave Craton age in assemblage 1 of the Ellice River domain (Davis et al., 2021). This, in turn, suggests that isolated Overby Lake domain-like outcrops (L003, W120) described above in the Ellice River domain may have been structurally juxtaposed, potentially during ca. 1.9 Ga east-vergent thrusting that is interpreted to have juxtaposed the Eastern plutonic belt and Queen Maud Block.

Boothia terrane is characterized by 2.56 to 2.54 Ga granodiorite cut by ca. 2.49 to 2.48 Ga mafic plutonic rocks (Sanborn-Barrie and Regis, 2020). If Boothia terrane extended south into the central Thelon tectonic zone, it would be expected to comprise 2.56 to 2.54 Ga crust without 2.49 to 2.48 Ga rocks that appear to reflect rifting and mafic magmatism along strike of the contemporaneous Queen Maud granitoid suite (Fig. 1). The ca. 2.56 to 2.54 Ga age of the Boothia terrane thus appears older than the ca. 2.5 Ga detrital zircons that are most precisely dated by two 2.51 to 2.49 Ga grains (Davis et al., 2021).

A closer correspondence to these detrital ages is provided by the ca. 2.53 to 2.51 Ga Closepet batholith and ca. 2.5 Ga anatectic granites (Jayananda et al., 1995) of the eastern Dharwar Craton, where ca. 2.6 Ga plutonic rocks have not been documented. Another potential link is the ca. 2.37 Ga giant dyke swarm of the Dharwar Craton (Kumar et al., 2012), which is age-correlative with the ca. 2.37 to 2.35 Ga Perry River gabbro in the eastern Queen Maud Block (Berman et al., work in progress, 2022). Kumar et al. (2012) cast doubt on a Slave–Dharwar connection based on the different orientation of Neoproterozoic structures in these blocks; however, this argument does not apply if the Dharwar Craton accreted to the Rae Craton after Neoproterozoic deformation and prior to ca. 2.21 Ga mafic dyke intrusion. In summary, although the Dharwar Craton appears to provide a plausible solution to available constraints, the combined data set is not conclusive. Thus, in the ensuing discussion, reference will be made to the Thelon tectonic zone basement (bTtz).

The Main leucogranite belt: age, isotopic composition, and petrological significance

The Main leucogranite belt comprises an approximately 10 km wide domain of peraluminous, syenogranitic plutonic rocks in the central Thelon tectonic zone, the distinctive low aeromagnetic response of which (Fig. 2) can be traced from the McDonald Fault to Queen Maud Gulf (Fig. 1). Its approximate length of 400 km along the western boundary of the Queen Maud Block (Fig. 2, 3) underscores the tectonic importance of this crustal domain. The most salient characteristics of the Main leucogranite belt that can be used to constrain tectonic models for its evolution are summarized here (*see* ‘Implications for the tectonic evolution of the Thelon tectonic zone’ section).

The Main leucogranite belt shares many features with leucogranites formed during contractional deformation and the peak of metamorphism in collisional orogens worldwide (Brown and Solar, 1998; Nabelek and Liu, 2004; Searle, 2013). In the Main leucogranite belt, leucogranite crystallization occurred between 1919 ± 3 Ma (sample M057A) and 1908 ± 3 Ma (sample R132A), coinciding closely with the timing of deformation and peak metamorphism determined by monazite geochronology (Mitchell et al., 2017; Berman et al., 2018). Leucogranite ages in the Eastern leucogranite belt are consistent with those in the Main leucogranite belt, although the nominal ages of two samples (sample M003A at 1925 ± 3 Ma (this study); sample 55-EA-265 at 1905 ± 4 Ma (Davis et al., 2013)) indicate crystallization may have taken place over a somewhat wider time span.

Isotopic and petrological studies of Himalayan leucogranites indicate they formed by melting of metapelite sourced in the underthrust Indian continent (Inger and Harris, 1993; Patiño Douce and Harris, 1998). Derivation of Main leucogranite belt plutonic rocks is linked to a sedimentary source based on their high ASI values (>1.1) and heavy oxygen-isotope signatures (>10 ‰), both of which contrast markedly with the compositions of early Thelon tectonic zone plutonic rocks (Fig. 7). Neodymium-isotope compositions of Thelon tectonic zone leucogranite ($\epsilon_{\text{Nd}}(1900 \text{ Ma}) = -5$ to -4.5) lie between those of Overby Lake domain crust and early Thelon tectonic zone plutonic rocks (Fig. 5), suggesting sediments were sourced in the exhumed Thelon tectonic zone basement (similar isotopically to the Overby Lake domain; *see* above) and ca. 2 Ga Thelon tectonic zone plutonic rocks. The latter source is supported by the few inherited zircons in leucogranite of the Main leucogranite belt that are all ca. 1.97 to 1.94 Ga in age (e.g. sample M057A, Table A-1).

A much-debated question pertains to the source of the heat needed to produce leucogranites in collisional orogens, where there is little evidence of heat advection by mantle-derived mafic magmatism (Harrison et al., 1998; Nabelek and Liu, 2004; Searle, 2013). Phase-equilibrium experiments pertaining to leucogranite genesis (Patiño Douce and Beard, 1995) demonstrate that muscovite and biotite dehydration melting above 750 and 800°C, respectively, produces melts

that closely match observed peraluminous (and low FeO, MgO, CaO) compositions, whereas hydrous melting at lower temperatures yields trondhjemitic melts. Some authors advocated greater than 750°C temperatures can be achieved by radiogenic heating of the Greater Himalayan sediments (Searle, 2013), whereas others have argued that an additional heat source is required, such as frictional heating (Nabelek and Liu, 2004).

The heat-source problem for leucogranite formation is accentuated in the Thelon tectonic zone, where leucogranites lack muscovite, have only minor biotite (which is often texturally linked to retrograde melt crystallization), and the spinel-quartz assemblage is commonly observed. Quantitative petrological modelling indicates formation of Main leucogranite belt leucogranites on pressure-temperature paths that reach peak conditions above the stability of biotite at 850 to 900°C (5 to 6 kbar), with spinel forming at high temperature on the prograde or retrograde P-T path. Furthermore, the unusually high temperatures responsible for leucogranite formation in the belt were widely attained across the central Thelon tectonic zone, not just in the Main leucogranite belt (Mitchell et al., 2017; Berman et al., 2018). Four factors are considered to have contributed to providing the heat for these high temperatures at mid-crustal levels: 1) crustal thickening of radiogenic lithological units (early Thelon tectonic zone plutonic rocks, of which a high proportion contain a significant amount of potassium (Whalen et al., 2018); accretionary wedge sediments derived from early Thelon tectonic zone plutonic rocks; sedimentary rocks of assemblage 1 with a high potassium content); 2) thickening of crust that had been pre-warmed during the preceding, voluminous ca. 2.01 to 1.95 Ga plutonism; 3) crustal thickening that incorporated hot back-arc regions (Hyndman, 2010) formed during east- and west-dipping subduction during the thickening process; and 4) mafic magmatism documented in the Duggan Lake domain (e.g. sample J023C in Whalen et al., 2018). Additional contributions localized to the Main leucogranite belt may have been slab breakoff during the continental collision driving crustal thickening, and frictional heating along the tectonic boundary between the Queen Maud Block and Thelon tectonic zone basement (e.g. Nabelek and Liu, 2004).

Comparison of the Thelon tectonic zone with the Taltson magmatic zone

The Thelon tectonic zone has been correlated with the Taltson magmatic zone on the basis of the continuity of similarly aged (ca. 2.0–1.9 Ga), north-striking plutonic rocks with high-amplitude aeromagnetic response (Fig. 1, 2; Hoffman, 1988; Ross et al., 1991). Evaluation of this correlation is particularly important to understand whether tectonic models proposed for one orogenic belt can be applied to both zones (e.g. Chacko et al., 2000). Card et al. (2014) suggested that the early (ca. 1.98 Ga) Taltson magmatic zone plutonic belt in the Taltson domain south of the Athabasca Basin (Fig. 1) was northwest-trending following 1.94 to

1.92 Ga metamorphism, whereas the Taltson magmatic zone west of the Athabasca Basin had been transposed into a north-striking belt during indentation of the Slave Craton (Fig. 1). They suggested, in part, that the difference in primary orientations of the Taltson magmatic zone and Thelon tectonic zone argued against their correlation.

Whalen et al. (2018) reached the same conclusion on the basis of a geochemical and geochronological comparison between the early Thelon tectonic zone and Taltson magmatic zone plutonic rocks. Specifically, available crystallization ages indicate that Thelon tectonic zone plutonism had initiated by ca. 2.07 to 2.03 Ga and was well established by ca. 2.01 Ga (Table A-1; Davis et al., 2014; Berman et al., 2018), significantly earlier than the oldest (ca. 1.99 Ga) Taltson magmatic zone plutonic rocks that have been dated (Thériault, 1992; Card et al., 2014). The Thelon tectonic zone also includes a much greater proportion of intermediate plutonic rocks with convergent margin trace-element signatures (Whalen et al., 2018). Both of these features are lacking in magmatic rocks from the northwestern Taltson magmatic zone (Whalen et al., 2018), although they are present in granitoid rocks of the southeastern Taltson magmatic zone (Card et al., 2014).

Comparison of the Thelon tectonic zone oxygen-isotope data (Table A-1) with Taltson magmatic zone isotope data (Chacko et al., 2000; De et al., 2000) further strengthens the conclusion that these belts are not along-strike equivalents. ‘Early’ and ‘late’ granitoid rocks from the Taltson magmatic zone yield rather symmetrical $\delta^{18}\text{O}_{\text{WR}}$ distributions averaging 9.26‰ and 9.88‰, respectively (Fig. 11b). Notably, only one of the early Taltson magmatic zone samples has a $\delta^{18}\text{O}_{\text{WR}}$ value of less than 8.0‰ (Fig. 11b). The similarity of these data, in addition to geochemical and Nd isotopic data, to those obtained from granitoid rocks from the Cordilleran interior (Fig. 11b) formed the basis of the interpretation of Taltson magmatic zone magmatism occurring in an intracontinental setting rather than at a plate boundary (Chacko et al., 2000; De et al., 2000). In marked contrast to early plutonic rocks in the Taltson magmatic zone, the Thelon tectonic zone oxygen-isotope compositions are dominated by $\delta^{18}\text{O}_{\text{WR}}$ values below 8‰ (Fig. 11a, b). Unfortunately, oxygen-isotope data are not available to extend this comparison to the earliest (1.99–1.97 Ga) Taltson magmatic zone plutonic rocks (Thériault, 1992; McDonough et al., 2000). These plutonic rocks may be isotopically similar to early Thelon tectonic zone plutonic rocks, which would strengthen the case for a magmatic arc component to the northwestern Taltson magmatic zone, as concluded by Card et al. (2014).

Implications for the tectonic evolution of the Thelon tectonic zone

Whole-rock major and trace-element geochemical data for plutonic rocks across the central Thelon tectonic zone (e.g. Fig. 10a, b) indicate a convergent margin setting for ca. 2.03 to 1.95 Ga Thelon tectonic zone plutonism (Whalen et al., 2018), possibly initiating as early as 2.07 Ga (samples

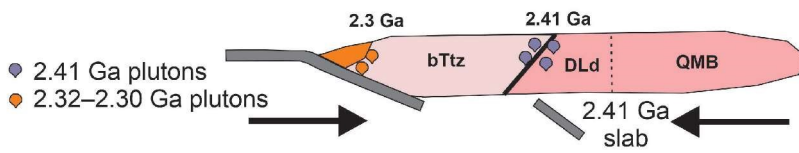
M165A, L202A; Fig. 10a; Table A-1). Further support for this tectonic setting derives from the similarity between oxygen-isotope compositions of central Thelon tectonic zone plutonic rocks and those of documented continental margin magmatic rocks (Fig. 11a). A convergent margin setting is also consistent with paleomagnetic data, indicating the Slave and Rae cratons were not contiguous at 2.19 Ga, although it has yet to be demonstrated that the paleomagnetic pole of the Rae Craton is primary (LeCheminant et al., 1997).

Two tectonic models are discussed below that account, with varying degrees of success, for the evolution of the Thelon tectonic zone in a convergent margin setting. Both are relatively simple end members that do not attempt to incorporate additional collisions that might account for the post-tectonic (A-type) geochemical signature of two ca. 1.99 Ga Western plutonic belt samples (L145A, M152B, Fig. 10a; R.G. Berman, unpub. data, 2021) or slab-breakoff magmatism that has been interpreted as a component of early Thelon tectonic zone plutonic rocks (Fig. 10a; Whalen et al., 2018). Arc and slab-failure magmatism are best distinguished by their pre- and post-collisional character (Hildebrand and Whalen, 2014); however, the deformation history of early Thelon tectonic zone plutonic rocks is obscured by profound reworking that occurred after 1.95 Ga.

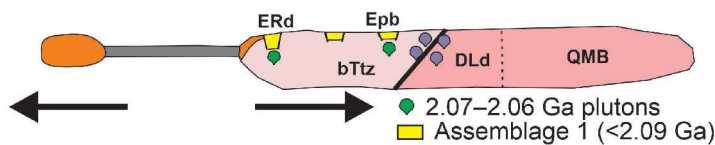
Model 1 (Fig. 16a–e) is essentially that proposed by Hoffman (1988), in which east-dipping subduction and ca. 2.03 to 1.98 Ga arc magmatism were terminated by the collision of the Slave and Rae cratons at ca. 1.97 Ga. In the analogous model presented in Figure 16c, east-dipping subduction occurs beneath a composite upper plate consisting of Thelon tectonic zone basement and the Queen Maud Block. Juxtaposition of these contrasting crustal blocks is considered to have occurred at ca. 2.41 Ga (Fig. 16a), the age of tonalite and quartz monzonite on the western flank of the Queen Maud Block (sample N026C; Duggan Lake domain) and in the Central plutonic belt (sample T163A), respectively, which both have trace-element signatures characteristic of a convergent margin setting (i.e. arc and/or slab failure; Fig. 10a). Accretion is interpreted to have driven inversion of the Sherman Basin (Fig. 1; Schultz et al., 2007) and high-grade, ca. 2.39 to 2.35 Ga metamorphism (Arrowsmith Orogeny) documented across the Queen Maud Block (Schultz et al., 2007; Tersmette, 2012; Davis et al., 2013, 2014; Berman et al., 2015a). Following a hiatus in magmatism, ca. 2.3 Ga plutonic activity resumed on the western flank of the Thelon tectonic zone basement, in parallel with magmatic construction of the 2.32 to 2.26 Ga Buffalo Head terrane south of the present-day McDonald Fault on the western flank of the southwestern Rae Craton (Fig. 1; Thériault and Ross, 1991; McNicoll et al., 2000).

The ca. 2.2 to 2.1 Ga period is well known globally as a significant time of emplacement of mafic dyke swarms and large igneous provinces (LIPs) associated with the breakup or attempted breakup of Neoproterozoic supercontinents and/or supercratons during the early Paleoproterozoic (French et al., 2004; Ernst and Bleeker, 2010; Nagaraju et al., 2018). Rifting at this time has been proposed along the southwestern margin

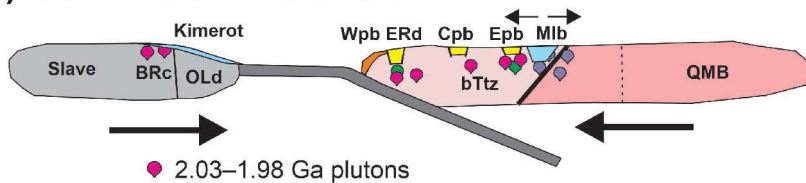
a) ca. 2.41–2.30 Ga:



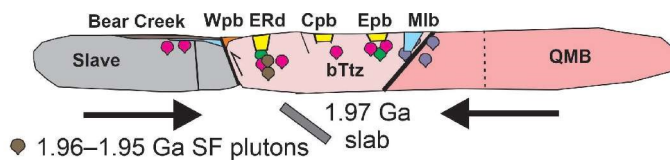
b) ca. 2.20–2.06 Ga:



c) ca. 2.03–1.98 Ga:



d) ca. 1.97–1.95 Ga:



e) ca. 1.94–1.90 Ga:

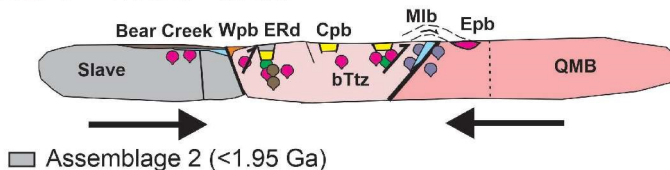


Figure 16. Schematic representation of model 1 (in part *modified from Hoffman, 1988*), illustrating five time periods in the tectonic evolution of the central Thelon tectonic zone: **a)** collision of the Thelon tectonic zone basement (bTtz) and Queen Maud Block (QMB) at ca. 2.41 Ga following east-dipping subduction and ca. 2.3 Ga magmatic accretion analogous to Buffalo Head terrane south of present-day McDonald Fault; **b)** extensional phase with ca. 2.2 to 2.15 Ga rifting of ca. 2.3 Ga crust off Thelon tectonic zone basement, post-2.09 Ga deposition of Ellice River domain (ERd) assemblage 1, and ca. 2.07 to 2.06 Ga Thelon tectonic zone plutonism; **c)** east-dipping subduction producing arc magmatism in Thelon tectonic zone basement, ca. 2.025 Ga intrusion of Booth River alkaline complex (BRc), exhumation and erosional exposure of Booth River complex prior to deposition of Kimerot Platform, and opening of back-arc basin in Thelon tectonic zone basement (ancestral basin to Main leucogranite belt (Mlb)); **d)** collision of Slave Craton and Thelon tectonic zone basement at 1.97 Ga, deposition of Bear Creek Group in foreland basin, and 1.96 to 1.95 Ga Thelon tectonic zone slab-failure (SF) plutonism; **e)** crustal thickening, regional high-temperature metamorphism, leucogranite formation, thrust emplacement of Eastern plutonic belt (Epb) on Queen Maud Block, followed by exhumation and erosion of Thelon tectonic zone plutonic rocks into assemblage 2 sediments. Cpb = Central plutonic belt, DLd = Duggan Lake domain, OLd = Overby Lake domain, Wpb = Western plutonic belt.

of the Rae Craton at ca. 2.15 Ga, leading to development of the Rutledge River Basin (Bostock and van Breemen, 1994) and potential separation of the Buffalo Head terrane from the southwestern Rae Craton (Bostock and van Breemen, 1994; McNicoll et al., 2000). Similarly, Davis et al. (2021) proposed that assemblage 1 sedimentary rocks of the Ellice River domain were deposited during rifting of the hypothesized northern extension of the Buffalo Head terrane off the Rae Craton, leaving remnant Thelon tectonic zone basement and 2.3 Ga (Buffalo Head) crust along the central Thelon tectonic zone margin (Fig. 16b) as a potential local source of 2.3 Ga detrital zircons in assemblage 1. This model accounts for the two known occurrences of ca. 2.3 Ga plutonic rocks in the western Thelon tectonic zone (Fig. 1; southern Thelon tectonic zone in Roddick and van Breemen, 1994; northern Thelon tectonic zone on Prince of Wales Island in Frisch and Hunt, 1993). A third

locality, where ca. 2.32 Ga post-tectonic granite and gabbro occur in the Queen Maud Block (Tersmette, 2012) may record distal effects of convergent margin magmatism.

In model 1, ca. 2.03 to 1.98 Ga continental arc magmatism occurs above an east-dipping subduction zone, and a back-arc basin sourcing these plutonic rocks within the Thelon tectonic zone basement would have the appropriate Nd isotopic composition of the sedimentary precursor to the Main leucogranite belt basin (Fig. 16c). Arc magmatism is terminated by collision at ca. 1.97 Ga (Fig. 16d), the age of a volcanic tuff layer near the base of the Bear Creek Group in the Kilohigok Basin (Fig. 1). This sedimentary sequence is interpreted to have been deposited in a foreland basin above the drowned passive margin (Kimerot Group; Grotzinger and McCormick, 1988; Tirrul and Grotzinger, 1990; Bowring and Grotzinger, 1992). Two plutonic rocks dated at 1.955 Ga

(samples L160, M032; Table A-1) may represent slab-failure magmatism (Fig. 16d), which is documented to occur up to about 15 Ma after collision in Phanerozoic orogenic belts (Hildebrand and Whalen, 2014). Continued convergence leads to inversion of the back-arc basin and development of the Main leucogranite belt (Fig. 16e), as well as structural emplacement of the Eastern plutonic belt on the Queen Maud Block (Fig. 16e).

Results of recent work in the central Thelon tectonic zone pose several challenges to model 1. Firstly, thermal models of continental collision zones predict peak metamorphic conditions typically 20 to 30 Ma after the onset of crustal thickening (Ruppel and Hodges, 1994; Jamieson et al., 1998; Zhang et al., 2004; Medvedev and Beaumont, 2006) and studies in collisional orogens support the duration of this time lag (e.g. Nabelek and Liu, 2004; Kohn, 2014). In contrast, the metamorphic peak across the central Thelon tectonic zone, which coincides closely with the ca. 1.925 to 1.91 Ga age of leucogranites (Mitchell et al., 2017; Berman et al., 2018), occurs about 45 to 60 Ma after the proposed time of collision. Evidence of a preceding, ca. 1950 to 1940 Ma metamorphic episode is limited (Mitchell et al., 2017; Berman et al., 2018), but could potentially have been recorded at higher structural levels than currently exposed in the central Thelon tectonic zone. Secondly, whereas a Slave–Rae collision at ca. 1.97 Ga should lead to cooling ages in the eastern Slave Craton (lower plate) that are significantly younger than 1.97 Ga, the $^{40}\text{Ar}/^{39}\text{Ar}$ age of biotite in a granodiorite near the boundary between the Overby Lake domain and the Tinney Hills domain is 1.977 ± 0.004 Ga (Camacho et al., 2020). This result aligns with K–Ar data for the Healey Lake area of the eastern Slave Craton, where 2.03 ± 0.019 to 1.96 ± 0.019 Ga hornblende cooling ages (4 of 10 samples) were considered to potentially reflect excess Ar (Henderson and van Breemen, 1991). Further $^{40}\text{Ar}/^{39}\text{Ar}$ analysis is needed to test these cooling age constraints. Lastly, interpretation of ca. 2.07 to 2.06 Ga plutonic rocks (M165A, L202A; Table A-1) as late extensional magmatic

products (Fig. 16b) is not indicated by their geochemical similarity to ca. 2.03 to 1.95 Ga plutonic rocks (Fig. 10a), but could be explained by significant basement recycling.

Model 2 (Fig. 17a–f) invokes a component of west-dipping subduction during the Thelon Orogeny to address the above issues. Although the ca. 2.4 to 2.3 Ga evolution could follow that of model 1 (Fig. 16a), variations are considered here that would allow Thelon tectonic zone basement to be Dharwar Craton. As with model 1, the primary relationship between the Queen Maud Block and Thelon tectonic zone basement is interpreted to have formed at ca. 2.41 Ga, during the Arrowsmith Orogeny (Fig. 17a). In model 2, the Slave Craton accretes at ca. 2.3 Ga following east-dipping subduction (Fig. 17a). This terminates ca. 2.3 Ga magmatism on the western flank of the Thelon tectonic zone basement, while magmatic growth of the Buffalo Head terrane continues unimpeded south of the present-day McDonald Fault until ca. 2.26 Ga. Accretion of the Slave Craton juxtaposes the Overby Lake domain lower crust of the Slave Craton with the Thelon tectonic zone basement (Fig. 17b) prior to ca. 2.21 Ga emplacement of potentially correlative mafic dykes in the Slave and Dharwar cratons (Kumar et al., 2012). In model 2, extension at ca. 2.2 to 2.15 Ga leads to rifting of the Slave Craton from the Overby Lake domain and rifting of the Queen Maud Block from the Thelon tectonic zone basement (Fig. 17b). This leaves the Overby Lake domain attached to the Thelon tectonic zone basement and opens ocean basins between the Slave Craton and Overby Lake domain, as well as between the Thelon tectonic zone basement and Queen Maud Block (including the Duggan Lake domain); closure of the latter at ca. 1.95 Ga produces the Main leucogranite belt (Fig. 17e, f).

Model 2 proposes that east-dipping subduction beneath the Thelon tectonic zone basement was established by ca. 2.07 to 2.06 Ga (Fig. 17c), the age of the oldest Thelon tectonic zone plutonic rocks (samples L202A, M165A), the convergent margin geochemical signatures of which are indistinguishable from those of ca. 2.03 to 1.95 Ga plutonic


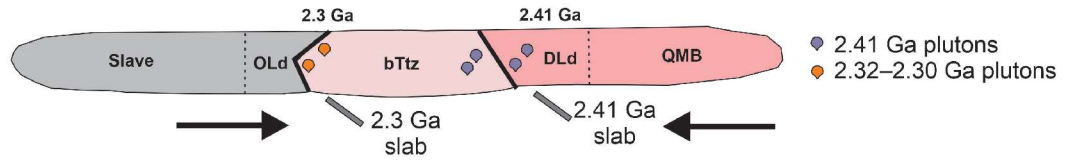
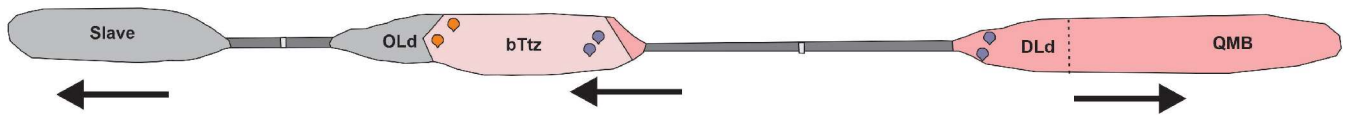


Figure 17. Schematic representation of model 2 illustrating six time periods in the tectonic evolution of the central Thelon tectonic zone: **a)** collision of Thelon tectonic zone basement (bTtz) and Queen Maud Block (QMB) at ca. 2.41 Ga following east-dipping subduction and collision of Slave Craton and Thelon tectonic zone basement at ca. 2.3 Ga following east-dipping subduction; **b)** extensional phase with ca. 2.2 to 2.15 Ga rifting of Thelon tectonic zone basement off Queen Maud Block (initiation of ancestral basin to Main leucogranite belt (MLb)) and Slave Craton off composite Thelon tectonic zone basement and Overby Lake domain (OLd); **c)** convergent margin with ca. 2.15 to 2.055 Ga arc magmatism in the upper plate (Overby Lake domain–Thelon tectonic zone basement), deposition of Ellice River domain (ERd) assemblage 1 (yellow) in retro-arc or back-arc setting; **d)** subduction polarity flip leading to Thelon tectonic zone continental arc magmatism via west-dipping subduction beneath composite Slave Craton–Thelon tectonic zone basement upper plate, accretionary wedge formation; back-arc setting for ca. 2.045 Ga Union Island Group volcanism (U), 2.025 Ga Booth River complex (BRc) magmatism and Kimerot Group deposition; **e)** deposition of Bear Creek Group (Kilohigok Basin) in retro-arc foreland basin, initiated by subduction flattening; further growth of accretionary wedge; **f)** collision of Queen Maud Block and Thelon tectonic zone basement at 1.95 to 1.94 Ga, slab failure, crustal thickening, burial of accretionary wedge and pelagic sediments on the boundary between the Thelon tectonic zone and Queen Maud Block, regional high-temperature metamorphism, leucogranite formation, thrust emplacement of Eastern plutonic belt (Epb) on Queen Maud Block, followed by exhumation and erosion of Thelon tectonic zone plutonic rocks into assemblage 2 sediments. Cpb = Central plutonic belt, DLd = Duggan Lake domain, Wpb = Western plutonic belt.

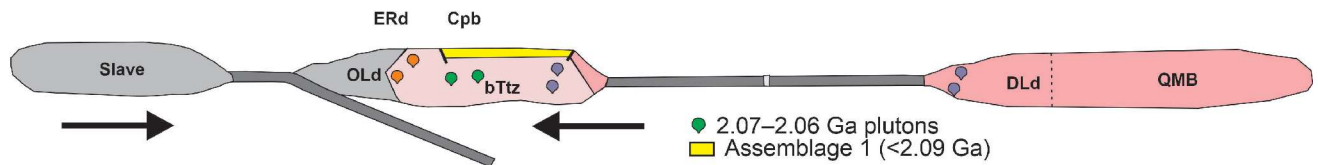
a) ca. 2.41–2.30 Ga:



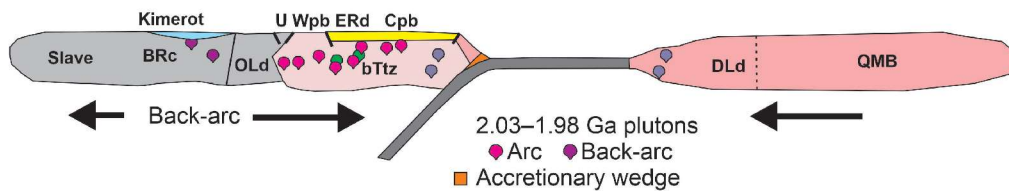
b) ca. 2.20–2.15 Ga:



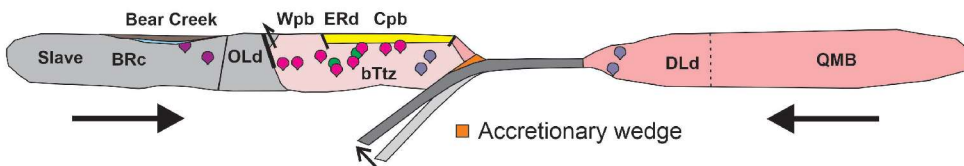
c) ca. 2.15–2.055 Ga:



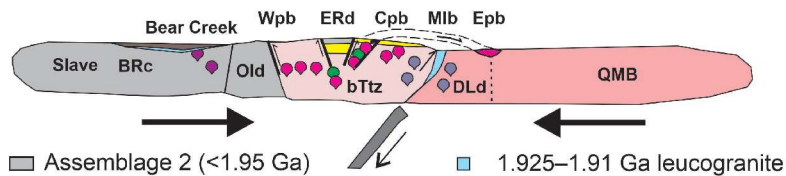
d) ca. 2.05–1.98 Ga:



e) ca. 1.97–1.95 Ga:



f) ca. 1.95–1.90 Ga:



rocks (Fig. 10a; Whalen et al., 2018). The apparent absence of early arc-related Thelon tectonic zone plutonic rocks in the Overby Lake domain may be explained by the paucity of geochronological control, by a fore-arc setting for the Overby Lake domain, or by the Slave Craton not accreting at ca. 2.3 Ga (i.e. as in model 1). Continental arc magmatism may have been established earlier, by ca. 2.1 to 2.09 Ga, which is the age of detrital zircons observed in assemblage 1 of the Ellice River domain as well as correlative samples farther south (e.g. Mary Francis gneiss and Rutledge River Basin in Davis et al., 2021). This aligns with ca. 2.2 to 2.1 Ga accretionary models for the western Rae Craton advocated by some workers (Ross et al., 1991; Bostock and van Breemen, 1994; Ashton et al., 2013) and puts deposition of assemblage 1 in a retro-arc or back-arc basin formed on the composite Thelon tectonic zone basement (Fig. 17c), a setting that could account for the back-arc chemistry of undated mafic volcanic rocks that are spatially associated with assemblage 1 (Berman et al., 2018). Davis et al. (2021) argued against a connection between the Ellice River domain and the Slave Craton based on the absence of Slave provenance in detrital zircons of assemblage 1. To accommodate this constraint, model 2 (assuming the 2.4 to 2.3 Ga history shown in Figure 17a, b) proposes the boundary between the Overby Lake domain and the Thelon tectonic zone basement was reactivated as a normal fault restricting Slave detritus from entering the basin of the Ellice River domain (Fig. 17c).

Bostock and van Breemen (1994) postulated a ca. 2.08 Ga collisional event in the Taltson magmatic zone based on 2.08–2.05 Ga metamorphic zircon and monazite in Rutledge River Basin metasedimentary rocks. Similarly, model 2 proposes collision of the Slave Craton with the composite Thelon tectonic zone basement–Overby Lake domain block at ca. 2.05 Ga (Fig. 17d). Subsequent reversal in the polarity of subduction places the eastern Slave Craton in an extensional back-arc setting that could account for: 1) ca. 2.046 ± 0.001 Ga mafic and alkaline magmatism in the Union Island Group (Fig. 1; Sheen et al., 2019); 2) deposition of the Kimerot Group of the Kilohigok Basin, rather than on a short-lived (2.025–1.97 Ga) passive margin (model 1; Hoffman, 1988); and 3) the ca. 2.025 Ga Booth River complex and the Lac de Gras mafic dykes (Fig. 1). The latter approach the scale of some LIP magmatic events (Ernst and Bleeker, 2010), which have been proposed to occur in an upper plate, back-arc setting (Wang et al., 2015). Model 2 accounts for ca. 2.03–1.96 Ga cooling ages in the eastern Slave Craton (Henderson and van Breemen, 1991; Camacho et al., 2020) as a contact metamorphic effect of potential ca. 2.03–1.95 Ga plutonism in an upper plate, back-arc setting.

West-dipping subduction requires that oceanic crust separate the Thelon tectonic zone basement from the Queen Maud Block (i.e. Fig. 17b, c) prior to its consumption during ca. 2.03 to 1.95 Ga arc magmatism (Fig. 17d). In model 2, Bear Creek Group strata of the Kilohigok Basin represent a retro-arc foreland basin, potentially initiated by increased coupling of the lower and upper plates caused by subduction

flattening (Fig. 17e). Collision of the Queen Maud Block (Fig. 17f) occurs after 1.953 Ga, the age of the youngest Thelon tectonic zone plutonic rock (Fig. 16e). The Main leucogranite belt demarcates the suture between the Thelon tectonic zone basement and Queen Maud Block (Fig. 17f), and the accretionary wedge (Fig. 17d, e) provides the sedimentary source of appropriate isotopic composition (*see above*). Crustal thickening is characterized by east-vergent thrusting (observed in the Main leucogranite belt; interpreted for Eastern plutonic belt emplacement; Fig. 17f), which is kinematically linked to the preceding west-dipping subduction. With high-grade metamorphism and leucogranite formation dated at 1.925 to 1.910 Ga (Mitchell et al., 2017; Berman et al., 2018), onset of crustal thickening at 1.95 to 1.94 Ga is congruent with the 20 to 30 Ma thermal time lag of radiogenic heating in thickened crust that is both predicted (e.g. Ruppel and Hodges, 1994; Jamieson et al., 1998; Zhang et al., 2004; Medvedev and Beaumont, 2006) and commonly observed in collisional orogens (Nabelek and Liu, 2004; Kohn, 2014).

SUMMARY AND CONCLUSIONS

Significant progress has been achieved in understanding the architecture and evolution of the central Thelon tectonic zone through Sm-Nd, O, and U-Pb isotope analyses interpreted in the context of targeted geological mapping, whole-rock geochemical data, and high-resolution aeromagnetic surveys. Two newly recognized crustal domains flank the main Thelon tectonic zone plutonic belts. Compared to the Tinney Hills domain, the Overby Lake domain comprises plutonic rocks with distinct geochemistry, slightly older Nd model ages, and some older (ca. 2.71 Ga) tonalite and granodiorite, but it also shares a significant ca. 2.6 Ga magmatic history. It may have rifted off the Slave Craton and returned, consistent with an earlier interpretation of an Archean deformation event in the Thelon tectonic zone. The Main leucogranite belt is a 400 km long tectonic domain separating most Thelon tectonic zone plutonic belts from Mesoarchean crust of the Queen Maud Block. Oxygen isotopes and petrological modelling support its formation via melting of a sedimentary source during peak metamorphism, which closely coincides with three new 1.925 to 1.910 Ga leucogranite age determinations. Shallow high-strain zones and detrital zircon constraints point to structural juxtapositioning of the Eastern plutonic belt and Queen Maud Block. Neodymium-isotope modelling is most compatible with Neoproterozoic crust being the largely unexposed basement to Thelon tectonic zone plutonic belts. The ca. 2.51 to 2.49 Ga component of detrital zircons in Ellice River domain assemblage 2, which is dominated by exhumed Thelon tectonic zone plutonic rocks, points to a crustal block like the Dharwar Craton as potential basement to the Thelon tectonic zone, rather than the Overby Lake domain. The possibility of the Buffalo Head terrane as basement to the Thelon tectonic zone is not supported due to its heterogeneity and more juvenile compositions.

A convergent margin tectonic setting for Thelon tectonic zone plutonic rocks is indicated by their whole-rock geochemistry and oxygen-isotope compositions (Table A-1) similar to other continental margin magmatic rocks. Two models are discussed for the evolution of the central Thelon tectonic zone. In model 1, ca. 2.07 to 2.06 Ga plutonic rocks reflect the latter stage of extension associated with deposition of assemblage 1 (youngest detrital zircon <2.09 Ga), and the collision between the Slave and Rae cratons occurs at 1.97 Ga, following east-dipping subduction. In model 2, ca. 2.07 to 2.06 Ga plutonic rocks form during east-dipping subduction that is terminated by ca. 2.05 Ga collision of the Slave Craton with the Thelon tectonic zone basement (microcontinent). Following reversal in the subduction polarity, ca. 2.03 to 1.95 Ga Thelon tectonic zone plutonism is terminated by collision with the Rae Craton (Queen Maud Block) at ca. 1.95 to 1.94 Ga. Significant differences between these models include

- the convergent margin geochemistry of ca. 2.07 to 2.06 Ga plutonic rocks is consistent with model 2, whereas model 1 requires their geochemistry to reflect crustal recycling;
- available $^{40}\text{Ar}/^{39}\text{Ar}$ and K-Ar cooling ages greater than 1.97 Ga in the eastern Slave Craton are consistent with model 2, whereas model 1 requires a number of samples to have been affected by excess argon; and
- thermal modelling and empirical observations indicating a 20 to 30 Ma gap between collision and peak metamorphism is compatible with model 2, whereas model 1 requires evidence for ca. 1.95 to 1.94 Ga metamorphism to have been largely removed by erosion and/or metamorphic overprinting.

The two models can be tested with geochronological and geochemical analyses of additional ca. 2.1 to 2.03 Ga plutonic and sedimentary rocks, $^{40}\text{Ar}/^{39}\text{Ar}$ geochronology of samples from the eastern Slave Craton, and thermal modelling of the metamorphic evolution of the central Thelon tectonic zone.

ACKNOWLEDGMENTS

The authors gratefully acknowledge assistance with 2014 and 2016 bedrock mapping provided by colleagues (Pierre Brouillette, Sharon Carr, Alfredo Comacho, Étienne Girard, Leo Nadeau, and Owen Weller), and students (Tim Chadwick, Michelle English, Dusty Liikane, and Svieda Ma), as well as logistical support provided by Great Slave Helicopters, Air Tindi, Sabina Gold, Ltd. via John Laitin at their Goose Lake camp, as well as Sarah Harper (cook) and Bobby Klengenber (wildlife monitor/camp assistant). They also thank Jacques Pinard for sample preparation, Pat Hunt for scanning electron microscopy assistance, Tom Pestaj for support in operating the

Sensitive High-Resolution Ion Microprobe (SHRIMP), as well as C. Card, S. Pehrsson, and D. Regis, for constructive reviews. This contribution was supported by the Geo-Mapping for Energy and Minerals (GEM-2) program.

REFERENCES

- Ashton, K.E., Hartlaub, R.P., Bethune, K.M., Heaman, L.M., Rayner, N., and Niebergall, G.R., 2013. New depositional age constraints for the Murmac Bay Group of the southern Rae Craton, Canada; *Precambrian Research*, v. 232, p. 70–88. <https://doi.org/10.1016/j.precamres.2012.05.008>
- Berman, R.G. and Camacho, A., 2020. U-Pb zircon ages of plutonic rocks in the eastern Slave craton and adjacent Thelon tectonic zone, Nunavut, determined by laser ablation inductively coupled multi-collector mass spectrometry; *Geological Survey of Canada, Open File 8703*, 20 p. <https://doi.org/10.4095/321633>
- Berman, R.G., Sanborn-Barrie, M., Stern, R.A., and Carson, C., 2005. Tectonometamorphism at ca. 2.35 and 1.85 Ga in the Rae domain, western Churchill Province, Nunavut, Canada: insights from structural, metamorphic and in situ geochronological analysis of the southwestern Committee Bay belt; *Canadian Mineralogist*, v. 43, p. 409–442. <https://doi.org/10.2113/gscanmin.43.1.409>
- Berman, R.G., Pehrsson, S., Davis, W.J., Ryan, J., Qiu, H., and Ashton, K.E., 2013. The Arrowsmith orogeny: new insights from in situ SHRIMP geochronology of the southwestern and central Rae craton; *Precambrian Research*, v. 232, p. 44–69. <https://doi.org/10.1016/j.precamres.2012.10.015>
- Berman, R.G., Nadeau, L., Percival, J.A., Harris, J.R., Girard, E., Whalen, J.A., Davis, W.J., Kellett, D., Jefferson, C.W., Camacho, A., and Bethune, K., 2015a. Geo-Mapping Frontiers' Chantrey project: bedrock geology and multidisciplinary supporting data of a 550 kilometre transect across the Thelon tectonic zone, Queen Maud block, and adjacent Rae craton; *Geological Survey of Canada, Open File 7698*, 39 p. <https://doi.org/10.4095/296202>
- Berman, R.G., Nadeau, L., McMartin, I., McCurdy, M., Craven, J., Girard, E., Sanborn-Barrie, M., Carr, S., Pehrsson, S., Whalen, J., Davis, W.J., Roberts, B., and Grenier, A., 2015b. Report of activities for the geology and mineral potential of the Chantrey–Thelon area: GEM-2 Thelon tectonic zone project, Montessoro belt and Elu Basin projects; *Geological Survey of Canada, Open File 7694*, 14 p. <https://doi.org/10.4095/297302>
- Berman, R.G., Sanborn-Barrie, M., Nadeau, L., Brouillette, P., Camacho, A., Davis, W.J., McCurdy, M.W., McMartin, I., Weller, O.M., Chadwick, T., Liikane, D.A., and Ma, S., 2016. Report of activities for the geology and mineral potential of the Chantrey–Thelon area: GEM-2 Rae project; *Geological Survey of Canada, Open File 8129*, 12 p. <https://doi.org/10.4095/299386>
- Berman, R.G., Davis, W.J., Sanborn-Barrie, M., Whalen, J.B., Taylor, B., McMartin, I., McCurdy, M.W., Mitchell, R., Ma, S., Coyle, M., Roberts, B., and Craven, J., 2018. Report of 2017 activities: Chantrey–Thelon activity, Thelon tectonic zone project; *Geological Survey of Canada, Open File 8372*, 19 p. <https://doi.org/10.4095/306622>

- Bindeman, I., 2008. Oxygen isotopes in mantle and crustal magmas as revealed by single crystal analysis; *Reviews in Mineralogy and Geochemistry*, v. 69, p. 445–478. <https://doi.org/10.2138/rmg.2008.69.12>
- Bindeman, I.N., Eiler, J.M., Yogodzinski, G.M., Tatsumi, Y., Stern, C.R., Grove, T.L., Portnyagin, M., Hoernle, K., and Danyushevsky, L.V., 2005. Oxygen isotope evidence for slab melting in modern and ancient subduction zones; *Earth and Planetary Science Letters*, v. 235, p. 480–496. <https://doi.org/10.1016/j.epsl.2005.04.014>
- Bleeker, W. and Hall, B., 2007. The Slave craton: geological and metallogenic evolution; *in* *Mineral deposits of Canada: a synthesis of major deposit-types, district metallogeny, the evolution of geological provinces, and exploration methods*, (ed.) W.D. Goodfellow; Geological Association of Canada, Special Publication 5, p. 849–879.
- Borthwick, J. and Harmon, R.S., 1982. A note regarding ClF_3 as an alternative to BrF_5 for oxygen isotopic analysis; *Geochimica et Cosmochimica Acta*, v. 46, p. 1665–1668. [https://doi.org/10.1016/0016-7037\(82\)90321-0](https://doi.org/10.1016/0016-7037(82)90321-0)
- Bostock, H.H. and van Breemen, O., 1994. Ages of detrital and metamorphic zircons from a pre-Taltson magmatic zone basin at the western margin of Churchill Province; *Canadian Journal of Earth Sciences*, v. 31, p. 1353–1364. <https://doi.org/10.1139/e94-118>
- Bostock, H.H., van Breemen, O., and Loveridge, W.D., 1987. Proterozoic geochronology in the Taltson magmatic zone, N.W.T.; *in* *Radiogenic age and isotopic studies: report 1*; Geological Survey of Canada, Paper 87-2, p. 73–80. <https://doi.org/10.4095/122751>
- Bostock, H.H., van Breemen, O., and Loveridge, W.D., 1991. Further geochronology of plutonic rocks in northern Taltson Magmatic Zone, District of Mackenzie, N.W.T.; *in* *Radiogenic age and isotopic studies, report 4*; Geological Survey of Canada, Paper 90-2, p. 67–78. <https://doi.org/10.4095/131938>
- Bowring, S.A. and Grotzinger, J.P., 1992. Implications of new chronostratigraphy for tectonic evolution of Wopmay orogen, northwest Canadian Shield; *American Journal of Science*, v. 292, p. 1–20. <https://doi.org/10.2475/ajs.292.1.1>
- Brandon, A.D. and Lambert, R.S.J., 1994. Crustal melting in the Cordilleran Interior: the mid-Cretaceous White Creek batholith in the southern Canadian Cordillera; *Journal of Petrology*, v. 35, p. 239–269. <https://doi.org/10.1093/petrology/35.1.239>
- Brown, M. and Solar, G.S., 1998. Granite ascent and emplacement during contractional deformation in convergent orogens; *Journal of Structural Geology*, v. 20, no. 9/10, p. 1365–1393.
- Cabanis, B. and Lecolle, M., 1989. Le diagramme $\text{La}/10 - \text{Y}/15 - \text{Nb}/8$: un outil pour la discrimination des séries volcaniques et la mise en évidence des processus de mélange et/ou de contamination crustale; *Comptes Rendus de l'Académie des Sciences Paris*, v. 309, p. 2023–2029.
- Camacho, A., Berman, R.G., and Sanborn-Barrie, M., 2020. $^{40}\text{Ar}/^{39}\text{Ar}$ hornblende and biotite cooling ages for metaplutonic rocks of the central Thelon tectonic zone, Nunavut; Geological Survey of Canada, Open File 8625, 77 p. <https://doi.org/10.4095/315135>
- Card, C.D., Bethune, K.M., Davis, W.J., Rayner, N., and Ashton, K., 2014. The case for a distinct Taltson orogeny: evidence from northwest Saskatchewan, Canada; *Precambrian Research*, v. 255, p. 245–265. <https://doi.org/10.1016/j.precamres.2014.09.022>
- Chacko, T., De, S.K., Creaser, R.A., and Muehlenbachs, K., 2000. Tectonic setting of the Taltson magmatic zone at 1.9–2.0 Ga: a granitoids-based perspective; *Canadian Journal of Earth Sciences*, v. 37, p. 1597–1609. <https://doi.org/10.1139/e00-029>
- Coyle, M., 2017a. Residual total magnetic field, aeromagnetic survey of the Overby-Duggan area, part of NTS 076-I south, Nunavut; Geological Survey of Canada, Open File 8281, scale 1:100 000. <https://doi.org/10.4095/304673>
- Coyle, M., 2017b. Residual total magnetic field, aeromagnetic survey of the Overby-Duggan area, part of NTS 076-I north, Nunavut; Geological Survey of Canada, Open File 8282, scale 1:100 000. <https://doi.org/10.4095/304674>
- Culshaw, N., 1991. Post-collisional oblique convergence along the Thelon tectonic zone, north of the Bathurst Fault, N.W.T., Canada; *Journal of Structural Geology*, v. 13, p. 501–516. [https://doi.org/10.1016/0191-8141\(91\)90040-P](https://doi.org/10.1016/0191-8141(91)90040-P)
- Culshaw, N.G. and van Breemen, O., 1990. A zoned low P-high T complex at the level of anatexis; structural and plutonic patterns in metasediments of the Archean Yellowknife Supergroup, near Bathurst Inlet, N.W.T., Canada; *Precambrian Research*, v. 48, p. 1–20. [https://doi.org/10.1016/0301-9268\(90\)90054-T](https://doi.org/10.1016/0301-9268(90)90054-T)
- Davis, W., Berman, R.G., and MacKinnon, A., 2013. U-Pb geochronology of archival rock samples from the Queen Maud block, Thelon tectonic zone and Rae Province, Kitikmeot Region, Nunavut, Canada; Geological Survey of Canada, Open File 7409, 42 p. <https://doi.org/10.4095/292663>
- Davis, W.J., Berman, R.G., Nadeau, L., and Percival, J.A., 2014. U-Pb Zircon geochronology of a transect across the Thelon tectonic zone, Queen Maud region, and adjacent Rae Craton, Kitikmeot Region, Nunavut, Canada; Geological Survey of Canada, Open File 7652, 41 p. <https://doi.org/10.4095/295177>
- Davis, W.J., Pehrsson, S.J., and Percival, J.A., 2015. Results of a U-Pb zircon geochronology transect across the southern Rae Craton, Northwest Territories, Canada; Geological Survey of Canada, Open File 7655, 74 p. <https://doi.org/10.4095/295610>
- Davis, W., Sanborn-Barrie, M., Berman, R.G., and Pehrsson, S., 2021. Timing and provenance of Paleoproterozoic supra-crustal rocks in the central Thelon tectonic zone, Canada: implications for the tectonic evolution of western Laurentia from ca. 2.1 to 1.9 Ga; *Canadian Journal of Earth Sciences*, v. 58, no. 4, p. 378–395. <https://doi.org/10.1139/cjes-2020-0046>
- De, S.K., Chacko, T., Creaser, R.A., and Muehlenbachs, K., 2000. Geochemical and Nd–Pb–O isotope systematics of granites from the Taltson magmatic zone, NE Alberta: implications for Early Proterozoic tectonics in western Laurentia; *Precambrian Research*, v. 102, p. 221–249. [https://doi.org/10.1016/S0301-9268\(00\)00068-1](https://doi.org/10.1016/S0301-9268(00)00068-1)
- DePaolo, D.J., 1981. Neodymium isotopes in the Colorado Front Range and crust-mantle evolution in the Proterozoic; *Nature*, v. 291, p. 193–196. <https://doi.org/10.1038/291193a0>
- Dey, S., 2013. Evolution of Archaean crust in the Dharwar craton: the Nd isotope record; *Precambrian Research*, v. 227, p. 227–246. <https://doi.org/10.1016/j.precamres.2012.05.005>

- Driver, L.A., Creaser, R.A., Chacko, T., and Erdmer, P., 2000. Petrogenesis of the Cretaceous Cassiar batholith, Yukon–British Columbia, Canada: implications for magmatism in the North American Cordilleran Interior; *Geological Society of America Bulletin*, v. 112, p. 1119–1133. [https://doi.org/10.1130/0016-7606\(2000\)112%3c1119:POTCCB%3e2.0.CO%3b2](https://doi.org/10.1130/0016-7606(2000)112%3c1119:POTCCB%3e2.0.CO%3b2)
- Ducea, M., Saleeby, J., and Bergantz, G., 2015. The architecture, chemistry, and evolution of continental magmatic arcs; *Annual Review of Earth and Planetary Sciences*, v. 43, p. 299–331. <https://doi.org/10.1146/annurev-earth-060614-105049>
- Elliott, B.A., Peck, W.H., Råmo, O.T., Vaasjoki, M., and Nironen, M., 2005. Magmatic zircon oxygen isotopes of 1.88–1.87 Ga orogenic and 1.65–1.54 Ga anorogenic magmatism in Finland; *Mineralogy and Petrology*, v. 85, p. 223–241. <https://doi.org/10.1007/s00710-005-0087-3>
- Ernst, R.E. and Bleeker, W., 2010. Large igneous provinces (LIPs), giant dyke swarms, and mantle plumes: significance for breakup events within Canada and adjacent regions from 2.5 Ga to the present; *Canadian Journal of Earth Sciences*, v. 47, p. 695–739. <https://doi.org/10.1139/E10-025>
- Fleck, R.J. and Criss, R.E., 1985. Strontium and oxygen isotopic variations in Mesozoic and Tertiary plutons of central Idaho; *Contributions to Mineralogy and Petrology*, v. 90, p. 291–308. <https://doi.org/10.1007/BF00378269>
- Fraser, J., 1964. Geological notes on northeastern District of Mackenzie, Northwest Territories; Geological Survey of Canada, Paper 63-40, 16 p. <https://doi.org/10.4095/101050>
- French, J.E., Heaman, L.M., Chacko, T., and Rivard, B., 2004. Global mafic magmatism and continental breakup at 2.2 Ga; evidence from the Dharwar Craton, India; *Annual Meeting, Geological Society of America, Abstracts with Programs*, v. 36, 340 p.
- Frisch, T. and Hunt, P.A., 1993. Reconnaissance U-Pb geochronology of the crystalline core of the Boothia Uplift, District of Franklin, Northwest Territories; *in Radiogenic age and isotopic studies, report 7*; Geological Survey of Canada, Paper 93-2, p. 3–22. <https://doi.org/10.4095/193328>
- Frith, R.A., 1982. Geology, Beechey Lake–Duggan Lake, District of Mackenzie; Geological Survey of Canada, Open File 851, scale 1:125 000. <https://doi.org/10.4095/129738>
- Frith, R.A. and van Breemen, O., 1990. U-Pb zircon age from the Himag plutonic suite, Thelon tectonic zone, Churchill structural province, Northwest Territories; *in Radiogenic age and isotopic studies, report 3*; Geological Survey of Canada, Paper 89-2, p. 49–54. <https://doi.org/10.4095/129069>
- Gibb, R.A. and Thomas, M.D., 1977. The Thelon front: a cryptic suture in the Canadian Shield; *Tectonophysics*, v. 38, p. 211–222. [https://doi.org/10.1016/0040-1951\(77\)90211-6](https://doi.org/10.1016/0040-1951(77)90211-6)
- Grotzinger, J.P. and McCormick, D.S., 1988. Flexure of the early Proterozoic lithosphere and the evolution of Kilohigok Basin (1.9 Ga), Northwest Canadian Shield; *in Frontiers in sedimentary petrology – new perspectives in basin analysis*, (ed.) K.L. Kleinspehn and C. Paola; Springer-Verlag, New York, New York, p. 405–430.
- Harmon, R.S., Barriero, B.A., Moorbath, S., Hoefs, J., Francis, P.W., Thorpe, R.S., Deruelle, B., McHugh, J., and Viglino, J.A., 1984. Regional O-, Sr-, and Pb-isotope relationships in late Cenozoic calc-alkaline lavas of the Andean Cordillera; *Geological Society of London, Journal*, v. 141, p. 803–822. <https://doi.org/10.1144/gsjgs.141.5.0803>
- Harrison, T.M., Grove, M., Lovera, O.M., and Catlos, E.J., 1998. A model for the origin of Himalayan anatexis and inverted metamorphism; *Journal of Geophysical Research*, v. 103, p. 27017–27032. <https://doi.org/10.1029/98JB02468>
- Henderson, J.B. and van Breemen, O., 1991. K-Ar (hornblende) data from the Healey Lake area, District of Mackenzie: a potential time constraint on the intracratonic indentation of the Slave Province into the Thelon Tectonic zone; *in Radiogenic age and isotopic studies, report 4*; Geological Survey of Canada, Paper 90-2, p. 61–66. <https://doi.org/10.4095/131937>
- Henderson, J., Thompson, P., and James, D., 1982. The Healey Lake map area and the Thelon Front problem, District of Mackenzie; *in Current Research, Part A*; Geological Survey of Canada, Paper 82-1A, p. 191–195. <https://doi.org/10.4095/111264>
- Henderson, J., James, D., and Thompson, P., 1999. Geology, Healey Lake–Artillery Lake, Northwest Territories–Nunavut; Geological Survey of Canada, Open File 3819, scale 1:250 000. <https://doi.org/10.4095/210957>
- Hildebrand, R.S. and Whalen, J.B., 2014. Arc and slab-failure magmatism in Cordilleran batholiths II – the Cretaceous Peninsular Ranges batholith of southern and Baja California; *Geoscience Canada*, v. 41, p. 399–458. <https://doi.org/10.12789/geocanj.2014.41.059>
- Hildreth, W. and Moorbath, S., 1988. Crustal contributions to arc magmatism in the Andes of Central Chile; *Contributions to Mineralogy and Petrology*, v. 98, p. 455–489. <https://doi.org/10.1007/BF00372365>
- Hoffman, P.F., 1988. United plates of America: the birth of a craton. Early Proterozoic assembly and growth of Laurentia; *Annual Review of Earth and Planetary Sciences*, v. 16, p. 543–603. <https://doi.org/10.1146/annurev.ea.16.050188.002551>
- Hyndman, R.D., 2010. The consequences of Canadian Cordillera thermal regime in recent tectonics and elevation; a review; *Canadian Journal of Earth Sciences*, v. 47, p. 621–632. <https://doi.org/10.1139/E10-016>
- Inger, S. and Harris, N.B.W., 1993. Geochemical constraints on leucogranite magmatism in the Langtang Valley, Nepal Himalaya; *Journal of Petrology*, v. 34, p. 345–368. <https://doi.org/10.1093/petrology/34.2.345>
- James, D.E., 1982. A combined O, Sr, Nd, and Pb isotopic and trace element study of crustal contamination in Central Andean lavas, I. Local geochemical variations; *Earth and Planetary Science Letters*, v. 57, p. 47–62. [https://doi.org/10.1016/0012-821X\(82\)90172-8](https://doi.org/10.1016/0012-821X(82)90172-8)
- James, D.T., 1989. Geology of the Thelon tectonic zone in the Moraine Lake area, District of Mackenzie, Northwest Territories: the definition and significance of lithological, structural and metamorphic changes across the boundary between the Slave and Churchill provinces; Ph.D. thesis, Queen's University, Kingston, Ontario, 399 p.

- Jamieson, R.A., Beaumont, C., Fullsack, P., and Lee, B., 1998. Barrovian regional metamorphism; where's the heat?; *in* What drives metamorphism and metamorphic reactions?, (ed.) P.J. Treloar and P.J. O'Brien; Geological Society of London, Special Publications, v. 138, p. 23–51.
- Jayananda, M., Martin, H., Peucat, J.J., and Mahabaleswar, B., 1995. Late Archaean crust-mantle interactions: geochemistry of LREE-enriched mantle derived magmas. Example of the Closepet batholith, southern India; *Contributions to Mineralogy and Petrology*, v. 119, p. 314–329. <https://doi.org/10.1007/BF00307290>
- Kiss, F., 2014a. Residual total magnetic field, aeromagnetic survey of the Duggan Lake area, part of NTS 76-H/N, Nunavut; Geological Survey of Canada, Open File 7521, scale 1:100 000. <https://doi.org/10.4095/293654>
- Kiss, F., 2014b. Residual total magnetic field, aeromagnetic survey of the Duggan Lake area, part of NTS 76-I/S, Nunavut; Geological Survey of Canada, Open File 7523, scale 1:100 000. <https://doi.org/10.4095/293656>
- Kohn, M.J., 2014. Himalayan metamorphism and its tectonic implications; *Annual Review of Earth and Planetary Sciences*, v. 42, p. 381–419. <https://doi.org/10.1146/annurev-earth-060313-055005>
- Kumar, A., Hamilton, M., and Halls, H.C., 2012. A Paleoproterozoic giant radiating dyke swarm in the Dharwar Craton, southern India; *Geochemistry Geophysics Geosystems*, v. 13, 12 p. <https://doi.org/10.1029/2011GC003926>
- Kyser, T.K., 1986. Stable isotope variations in the mantle; *in* Stable isotopes in high temperature processes, (ed.) J.W. Valley, H.P. Taylor, Jr., and J.R. O'Neil; *Reviews in Mineralogy*, v. 16, p. 141–164.
- LeCheminant, A.N., Buchan, K.L., van Breemen, O., and Heaman, L.M., 1997. Paleoproterozoic continental break-up and reassembly: evidence from 2.19 Ga diabase dyke swarms in the Slave and Western Churchill provinces, Canada; *Geological Association of Canada, Programs with Abstracts*, v. 22, p. A86.
- Liu, X., Fan, H.R., Santosh, M., Hu, F.D.-F., Yang, K.-F., Li, Q.-L., Yang, Y.-H., and Liu, Y., 2012. Remelting of Neoproterozoic relict volcanic arcs in the Middle Jurassic: implication for the formation of the Dexing porphyry copper deposit, Southeastern China; *Lithos*, v. 150, p. 85–100. <https://doi.org/10.1016/j.lithos.2012.05.018>
- Longstaffe, F.J., Clark, A., McNutt, R.H., and Zentilli, M., 1983. Oxygen isotopic compositions of central Andean plutonic and volcanic rocks, latitudes 26°–29° south; *Earth and Planetary Science Letters*, v. 64, p. 9–18. [https://doi.org/10.1016/0012-821X\(83\)90048-1](https://doi.org/10.1016/0012-821X(83)90048-1)
- Ludwig, K.R., 2003. User's manual for Isoplot 3.00: a geochronological toolkit for Microsoft® Excel®; Berkeley Geochronology Center, Special Publication 4, 71 p.
- Ludwig, K., 2009. SQUID 2: A User's Manual; Berkeley Geochronology Center, Special Publication 5.
- Ma, S., Kellett, D.A., Godin, L., and Jercinovic, M.J., 2020. Localisation of the brittle Bathurst fault on pre-existing fabrics: a case for structural inheritance in the northeastern Slave craton, western Nunavut, Canada; *Canadian Journal of Earth Sciences*, v. 57, no. 6, p. 725–746. <https://doi.org/10.1139/cjes-2019-0100>
- Mattey, D., Lowry, D., and Macpherson, C., 1994. Oxygen isotope composition of mantle peridotite; *Earth and Planetary Science Letters*, v. 128, p. 231–241. [https://doi.org/10.1016/0012-821X\(94\)90147-3](https://doi.org/10.1016/0012-821X(94)90147-3)
- McCurdy, M.W., Berman, R.G., Kerr, D.E., and Vaive, J.E., 2013. Geochemical, mineralogical and kimberlite indicator mineral data for silts, heavy mineral concentrates and waters, Duggan Lake area, Nunavut (NTS 76H and 76I South); Geological Survey of Canada, Open File 7471, 22 p. <https://doi.org/10.4095/293044>
- McDonough, M.R., McNicoll, V.J., Schetselaar, E.M., and Grover, W., 2000. Geochronological and kinematic constraints on crustal shortening and escape in a two-sided oblique-slip collisional and magmatic orogen, Paleoproterozoic Taltson magmatic zone, northeastern Alberta; *Canadian Journal of Earth Sciences*, v. 37, p. 1549–1573. <https://doi.org/10.1139/e00-089>
- McNicoll, V.J., Thériault, R.J., and McDonough, M.R., 2000. Taltson basement gneissic rocks: U-Pb and Nd isotopic constraints on the basement to the Paleoproterozoic Taltson magmatic zone, northeastern Alberta; *Canadian Journal of Earth Sciences*, v. 37, p. 1575–1596. <https://doi.org/10.1139/e00-034>
- Medvedev, S. and Beaumont, C., 2006. Growth of continental plateaus by channel injection: models designed to address constraints and thermomechanical consistency; *Geological Society of London, Special Publications*, v. 268, p. 147–164. <https://doi.org/10.1144/GSL.SP.2006.268.01.06>
- Mitchell, R.K., Berman, R.G., Davis, W.J., and Carr, S., 2017. Paleoproterozoic metamorphism of the Thelon tectonic zone and margins of the Slave and Rae Archaean cratons - insights into the nature and timing of the Slave–Rae collision; *Geological Association of Canada, Programs with Abstracts*, v. 40, p. 265.
- Nabelek, P.I. and Liu, M., 2004. Petrologic and thermal constraints on the origin of leucogranites in collisional orogens; *Transactions of the Royal Society of Edinburgh, Earth Sciences*, v. 95, p. 73–85. <https://doi.org/10.1017/S0263593300000936>
- Nagaraju, E., Parashuramulu, V., Kumar, A., and Srinivas, S., 2018. Paleomagnetism and geochronological studies on a 450 km long 2216 Ma dyke from the Dharwar craton, southern India; *Physics of the Earth and Planetary Interiors*, v. 274, p. 222–231.
- Natural Resources Canada, 2013. Kitikmeot area (NTS 076-P); *in* Geoscience Data Repository for Geophysical Data, Magnetic-Radiometric-EM, Natural Resources Canada. <<http://gdr.agg.nrcan.gc.ca/gdrdap/dap/search-eng.php>> [accessed January 10, 2022].
- Patchett, P.J. and Bridgwater, D., 1984. Origin of continental crust of 1.9–1.7 Ga age defined by Nd isotopes in the Ketilidian terrain of South Greenland; *Contributions to Mineralogy and Petrology*, v. 87, p. 311–318. <https://doi.org/10.1007/BF00381287>
- Patiño Douce, A.E. and Beard, J., 1995. Dehydration-melting of biotite gneiss and quartz amphibolite from 3 to 15 kbar; *Journal of Petrology*, v. 36, p. 707–738. <https://doi.org/10.1093/petrology/36.3.707>

- Patiño Douce, A.E. and Harris, N.B.W., 1998. Experimental constraints on Himalayan anatexis; *Journal of Petrology*, v. 39, p. 689–710. <https://doi.org/10.1093/ptro/39.4.689>
- Richard, P., Shimizu, N., and Allègre, C.J., 1976. $^{143}\text{Nd}/^{146}\text{Nd}$, a natural tracer: an application to oceanic basalts; *Earth and Planetary Science Letters*, v. 31, p. 269–278. [https://doi.org/10.1016/0012-821X\(76\)90219-3](https://doi.org/10.1016/0012-821X(76)90219-3)
- Roddick, J.C. and van Breemen, O., 1994. U-Pb zircon dating: a comparison of ion microprobe and single grain conventional analyses; *in* Current Research 1994-F; Geological Survey of Canada, p. 1–9. <https://doi.org/10.4095/195164>
- Ross, G.M., 2002. Evolution of Precambrian continental lithosphere in Western Canada: results from Lithoprobe studies in Alberta and beyond; *Canadian Journal of Earth Sciences*, v. 39, no. 3, p. 413–437. <https://doi.org/10.1139/e02-012>
- Ross, G.M., Parrish, R.R., Villeneuve, M.E., and Bowring, S.A., 1991. Geophysics and geochronology of the crystalline basement of the Alberta Basin, western Canada; *Canadian Journal of Earth Sciences*, v. 28, p. 512–522. <https://doi.org/10.1139/e91-045>
- Ruppel, C. and Hodges, K.V., 1994. Role of horizontal thermal conduction and finite time thrust emplacement in simulation of pressure-temperature-time paths; *Earth and Planetary Science Letters*, v. 123, p. 49–60. [https://doi.org/10.1016/0012-821X\(94\)90256-9](https://doi.org/10.1016/0012-821X(94)90256-9)
- Sanborn-Barrie, M. and Regis, D., 2020. 2.56 to 1.87 Ga evolution of the Rae cratonic margin: micro- to macro-scale constraints from Boothia Peninsula-Somerset Island, Nunavut; *Geoconvention 2020* (abstract). <<https://geoconvention.com/2020-abstract-archive>> [accessed November 24, 2021]
- Schultz, M.E.J., Chacko, T., Heaman, L.M., Sandeman, H.A., Simonetti, A., and Creaser, R.A., 2007. Queen Maud block: a newly recognized Paleoproterozoic (2.4–2.5 Ga) terrane in northwest Laurentia; *Geology*, v. 35, p. 707–710. <https://doi.org/10.1130/G23629A.1>
- Searle, M., 2013. Crustal melting, ductile flow, and deformation in mountain belts: cause and effect relationships; *Lithosphere*, v. 5, p. 547–554. <https://doi.org/10.1130/RF.L006.1>
- Sheen, A.I., Heaman, L.M., Kjarsgaard, B., Ootes, L., Pearson, D.G., and Creaser, R.A., 2019. Athapuscow aulacogen revisited: geochronology and geochemistry of the 2046 Ma Union Island Group mafic magmatism, East Arm of Great Slave Lake, Northwest Territories, Canada; *Precambrian Research*, v. 321, p. 85–102. <https://doi.org/10.1016/j.precamres.2018.11.012>
- Sherlock, R.L., Shannon, A., Hebel, M., Lindsay, D., Madsen, J., Sandeman, H., Hrabi, B., Mortensen, J.K., Tosdal, R.M., and Friedman, R., 2012. Volcanic stratigraphy, geochronology, and gold deposits of the Archean Hope Bay greenstone belt, Nunavut, Canada; *Economic Geology*, v. 107, p. 991–1042.
- Shervais, J.W., 1982. Ti-V plots and the petrogenesis of modern and ophiolitic lavas; *Earth and Planetary Science Letters*, v. 59, p. 101–118. [https://doi.org/10.1016/0012-821X\(82\)90120-0](https://doi.org/10.1016/0012-821X(82)90120-0)
- Stern, R.A., 1997. The GSC Sensitive High-Resolution Ion Microprobe (SHRIMP): analytical techniques of zircon U-Th-Pb age determinations and performance evaluation; *in* Radiogenic age and isotopic studies, report 10; Geological Survey of Canada, Paper 97-F, p. 1–31. <https://doi.org/10.4095/209089>
- Stern, R.A. and Amelin, Y., 2003. Assessment of errors in SIMS zircon U–Pb geochronology using a natural zircon standard and NIST SRM 610 glass; *Chemical Geology*, v. 197, p. 111–142. [https://doi.org/10.1016/S0009-2541\(02\)00320-0](https://doi.org/10.1016/S0009-2541(02)00320-0)
- Stubble, M.P., 2005. Slave Craton: interpretive bedrock compilation; Northwest Territories Geoscience Office, NWT-NU Open File 2005-01: digital files and 2 maps.
- Taylor, H.P., Jr., 1980. The effects of assimilation of country rocks by magma on $^{18}\text{O}/^{16}\text{O}$ and $^{87}\text{Sr}/^{86}\text{Sr}$ systematics in igneous rocks; *Earth and Planetary Science Letters*, v. 47, p. 243–254. [https://doi.org/10.1016/0012-821X\(80\)90040-0](https://doi.org/10.1016/0012-821X(80)90040-0)
- Taylor, H.P., Jr., and Sheppard, S.M.F., 1986. Igneous rocks: I. Processes of isotopic fractionation and isotope systematics; *in* Stable isotopes in high temperature processes, (ed.) J.W. Valley, H.P. Taylor, Jr., and J.R. O’Neil; *Reviews in Mineralogy*, v. 16, p. 227–272. <https://doi.org/10.1515/9781501508936-013>
- Tersmette, D., 2012. Geology, geochronology, thermobarometry, and tectonic evolution of the Queen Maud block, Churchill Craton, Nunavut, Canada; M.Sc. thesis, University of Alberta, Edmonton, Alberta, 161 p.
- Thériault, R.J., 1992. Nd isotopic evolution of the Taltson magmatic zone, Northwest Territories, Canada: insights into early Proterozoic accretion along the western margin of the Churchill Province; *The Journal of Geology*, v. 100, p. 465–475. <https://doi.org/10.1086/629598>
- Thériault, R.J. and Ross, G.M., 1991. Nd isotopic evidence for crustal recycling in the ca. 2.0 Ga subsurface of Western Canada; *Canadian Journal of Earth Sciences*, v. 28, no. 8, p. 1140–1147. <https://doi.org/10.1139/e91-104>
- Thompson, D.L., 1992. Proterozoic evolution of the northern Thelon tectonic zone; Ph.D. thesis, Princeton University, Princeton, New Jersey, 311 p.
- Thompson, P.H., 1986. Geology, Tinney Hills–Overby Lake (west half), District of Mackenzie, Northwest Territories; Geological Survey of Canada, Open File 1316, scale 1:125 000. <https://doi.org/10.4095/130101>
- Thompson, P.H., 1989. An empirical model for metamorphic evolution of the Archaean Slave Province and adjacent Thelon tectonic zone, north-western Canadian Shield; *in* Evolution of metamorphic belts, (ed.) J.S. Daly, R.A. Cliff, and B.W.D. Yardley; Geological Society of London, Special Publications, v. 43, p. 245–263. <https://doi.org/10.1144/GSL.SP.1989.043.01.17>
- Thompson, P.H., Culshaw, N., Thompson, D.L., and Buchanan, J.R., 1985. Geology across the western boundary of the Thelon Tectonic Zone in the Tinney Hills–Overby Lake (west half) map area, District of Mackenzie; *in* Current Research, Part A; Geological Survey of Canada, Paper 85-1A, p. 555–572. <https://doi.org/10.4095/120152>
- Thompson, P.H., Culshaw, N., Buchanan, J.R., and Manojlovic, P., 1986. Geology of the Slave Province and Thelon tectonic zone in the Tinney Hills–Overby Lake (west half) map area, District of Mackenzie; *in* Current Research, Part A; Geological Survey of Canada, Paper 86-1A, p. 275–289. <https://doi.org/10.4095/120372>

- Tirrul, R., 1985. Nappes in the Kilohigok Basin and their relationship to the Thelon tectonic zone, District of Mackenzie; *in* Current Research, Part A; Geological Survey of Canada, Paper 85-1A, p. 407–420. <https://doi.org/10.4095/120189>
- Tirrul, R. and Grotzinger, J.P., 1990. Early Proterozoic collisional orogeny along the northern Thelon tectonic zone, Northwest Territories, Canada, evidence from the foreland; *Tectonics*, v. 9, p. 1015–1036. <https://doi.org/10.1029/TC009i005p01015>
- Trumbull, R.B., Harris, C., Frindt, S., and Wigand, M., 2004. Oxygen and neodymium isotope evidence for source diversity in Cretaceous anorogenic granites from Namibia and implications for A-type granite genesis; *Lithos*, v. 73, p. 21–40. <https://doi.org/10.1016/j.lithos.2003.10.006>
- van Breemen, O., Thompson, P.H., Hunt, P.A., and Culshaw, N., 1987. U-Pb zircon and monazite geochronology from the northern Thelon tectonic zone, District of Mackenzie; *in* Radiogenic age and isotopic studies, report 1; Geological Survey of Canada, Paper 87-2, p. 81–93. <https://doi.org/10.4095/122752>
- van Breemen, O., Davis, W.J., and King, J.E., 1992. Temporal distribution of granitoid plutonic rocks in the Archean Slave Province, northwest Canadian Shield; *Canadian Journal of Earth Sciences*, v. 29, p. 2168–2199.
- Villeneuve, M.E., Ross, G.M., Thériault, R.J., Miles, M., Parrish, R.R., and Broome, J., 1993. Tectonic subdivision and U-Pb geochronology of the crystalline basement of the Alberta Basin, western Canada; Geological Survey of Canada, Bulletin 447, 93 p. <https://doi.org/10.4095/77642>
- Wang, Y., Santosh, M., Zhaohua, L., and Jinhua, H., 2015. Large igneous provinces linked to supercontinent assembly; *Journal of Geodynamics*, v. 85, p. 1–10. <https://doi.org/10.1016/j.jog.2014.12.001>
- Wei, C.-S., Zheng, Y.-F., Zhao, Z.-F., and Valley, J.W., 2002. Oxygen and neodymium isotope evidence of recycling of juvenile crust in northeast China; *Geology*, v. 30, p. 375–378. [https://doi.org/10.1130/0091-7613\(2002\)030%3c0375:OANIEF%3e2.0.CO%3b2](https://doi.org/10.1130/0091-7613(2002)030%3c0375:OANIEF%3e2.0.CO%3b2)
- Whalen, J.B., Berman, R.G., Davis, W.J., Sanborn-Barrie, M., and Nadeau, L., 2018. Bedrock geochemistry of the Thelon tectonic zone; Geological Survey of Canada, Open File 8234, 49 p. <https://doi.org/10.4095/306385>
- Whalen, J. and Hildebrand, R. 2019. Trace element discrimination of arc, slab failure, and A-type granitic rocks; *Lithos*, v. 348, p. 1–29.
- Wheeler, J.O., Hoffman, P.F., Card, K.D., Davidson, A., Sanford, B.V., Okulitch, A.V., and Roest, W.R., 1996. Geological map of Canada; Geological Survey of Canada, Map 1860A, 3 sheets, scale 1:5 000 000. <https://doi.org/10.4095/208175>
- Wright, G.M., 1967. Geology of the southeastern Barren Grounds, parts of Mackenzie and Keewatin, operations Keewatin, Baker, Thelon; Geological Survey of Canada, Memoir 350, 91 p. <https://doi.org/10.4095/101544>
- Zhang, H., Harris, N., Parrish, R.R., Kelley, S., Zhang, L., Rogers, N., Argles, T., and King, J., 2004. Causes and consequences of protracted melting of the mid-crust exposed in the North Himalayan antiform; *Earth and Planetary Science Letters*, v. 228, p. 195–212. <https://doi.org/10.1016/j.epsl.2004.09.031>

Appendix A

Methodology

Sm-Nd isotopes

Isotopic analyses (Table A-1) were performed at the Isotope Geochemistry and Geochronology Research Centre, Department of Earth Sciences, Carleton University (Ottawa, Ontario). Silicate rock powders were spiked with a mixed $^{148}\text{Nd}/^{149}\text{Sm}$ spike solution before being dissolved in an acid mixture of about 29 M HF and 16 M HNO_3 . The samples were then dried on a hotplate before being redissolved in 8 M HNO_3 and 6 M HCl sequentially. The dried residues of samples were dissolved in 2.5 M HCl and then loaded into borosilicate glass chromatography columns from Bio-Rad Laboratories, Inc. containing 3.0 mL of Dowex® AG® 50W-X8 cation exchange resin. The columns were then washed with 23 mL of 2.5 M HCl before the rare-earth elements were eluted using 9 mL of 6 M HCl. Rare-earth element fractions were dissolved in 0.26 M HCl and then loaded in Ln resin chromatographic columns from Eichrom Technologies Inc. containing Teflon powder coated with di(2-ethylhexyl) orthophosphoric acid (HDEHP; Richard et al., 1976). Neodymium was eluted using 0.26 M HCl, followed by elution of samarium using 0.5 M HCl. Isotope ratios were measured using a Thermo/Finnigan Triton™ multicollector thermal ionization mass spectrometer manufactured by Thermo Scientific™ at temperatures of 1500 to 1650°C after samples were loaded with H_3PO_4 in a double rhenium filament assembly. The isotope ratios were normalized to $^{146}\text{Nd}/^{144}\text{Nd} = 0.72190$. An in-house Nd standard was routinely measured with $^{143}\text{Nd}/^{144}\text{Nd} = 0.511831 \pm 0.000011$ (2σ) over a period of three years; this value is an equivalent of $^{143}\text{Nd}/^{144}\text{Nd} = 0.511861 \pm 0.000009$ (2σ) for the La Jolla Nd standard. The Sm and Nd concentrations were measured precisely within 1%. Analyses of the United States Geological Survey standard BCR-2 yielded Nd = 28.53 ppm, Sm = 6.618 ppm, and $^{143}\text{Nd}/^{144}\text{Nd} = 0.512643 \pm 0.000011$ ($n = 13$, 2σ). Total procedural blanks for Nd are less than 50 picograms.

Oxygen-isotope ratios

Oxygen-isotope ratios (Table A-1) were determined on aliquots of 10 to 15 mg of whole-rock powder at the University of Western Ontario (London, Ontario) by fluorination using ClF_3 (Borthwick and Harmon, 1982). Other geochemical analyses (Berman et al., 2015a; Whalen et al., 2018) used the same whole-rock powders. Calculation of the isotopic compositions of the melts from the oxygen-isotope compositions of resistant phenocrysts or accessory minerals, such as zircon or clinopyroxene, has become more common in the study of plutonic (e.g. Elliott et al., 2005) and volcanic (e.g. Wei et al., 2002; Bindeman et al., 2005; Liu et al., 2012)

rocks; however, the possibility of phenocryst modification during, and subsequent to, magma evolution warrants caution (Bindeman, 2008). In deformed, metamorphosed rocks in particular, the phenocryst-based approach can be problematic. Whole-rock oxygen-isotope analysis was used in this study as an estimate of the isotopic composition of the magma.

All results are reported relative to the V-SMOW (Vienna standard mean ocean water) standard in parts per thousand (‰). Long-term duplication of in-house standards indicates typical reproducibility of 0.2‰ (F. Longstaffe, pers. comm., 2018). Results for duplicates of selected Thelon tectonic zone whole-rock samples were within this range, except for several samples that differed by 0.3‰.

Zircon geochronology

The samples dated in this study (Table A-2) were processed at the Radiogenic Isotope Geochemistry and Geochronology Laboratory of the Geological Survey of Canada (Ottawa, Ontario), using the Sensitive High-Resolution Ion Microprobe (SHRIMP). The samples were crushed by mechanical disaggregation and heavy minerals separated using a Wilfley table; this operation was followed by heavy liquid separation. Zircon was sorted using a Frantz isodynamic magnetic separator and then, following analytical procedures described by Stern and Amelin (2003), cast in epoxy mounts 2.5 cm in diameter (along with fragments of the Geological Survey of Canada (GSC) laboratory reference zircon; z6266, with $^{206}\text{Pb}/^{238}\text{U}$ age = 559 Ma). The mid-sections of the zircons were exposed using 9, 6, and 1 μm diamond compound, and the internal features of the zircons (such as zoning, structures, alteration, etc.) were characterized in backscattered electron (BSE) mode utilizing a Zeiss Evo 50 scanning electron microscope. The SHRIMP count rates at eleven masses YbO, Zr, HfO, ^{204}Pb , background, ^{206}Pb , ^{207}Pb , ^{208}Pb , ^{238}U , ^{248}ThO , ^{254}UO were sequentially measured with a single electron multiplier corrected for a dead time of 20 ns. Analytical procedures are modified from those described by Stern (1997) with data processing accomplished using SQUID2 (version 2.5; Ludwig, 2009). The 1σ external errors of $^{206}\text{Pb}/^{238}\text{U}$ ratios reported in the data table incorporate the error in calibrating the standard. Common Pb correction utilized the Pb composition of the surface blank (Stern, 1997). Ytterbium and hafnium concentration data were calculated using sensitivity factors derived from standard z6266 with values of 229 and 8200 ppm, respectively. A secondary internal reference zircon (z1242) was analyzed to monitor accuracy of the measured $^{207}\text{Pb}/^{206}\text{Pb}$ ratios and correct for any instrumental mass bias; no mass bias was applied to the data. Isoplot v. 3.00 (Ludwig, 2003) was used to generate concordia plots and calculate regression ages and weighted means. The error ellipses on the concordia diagrams and the weighted mean errors are reported at the 95% confidence interval.

Table A-1. Results of Sm-Nd and O isotope analyses.

Sample	Year	Group	Rock description	Nd (ppm)	Sm (ppm)	¹⁴³ Nd/ ¹⁴⁴ Nd	¹⁴³ Nd/ ¹⁴⁴ Nd (initial)	$\epsilon_{Nd}(T)$	$\epsilon_{Nd}(1.95 Ga)$	T_{DM} (Ga)	$\delta^{18}O$ (‰)	Age (Ma)	Ref	Latitude (°N)	Longitude (°W)
J023A	2014	1.9 Ga-high Zr	cg, n/w-foi bt-hbl monzogranite	87.9	15.9	0.1094	0.511273	-5.5	-4.8	2.61	8.0	1890	5	65.856	104.884
N048A	2014	1.9 Ga-high Zr	cg, un-foi, hbl-bt monzogranite	88.2	14.9	0.1019	0.511134	-6.2	-5.6	2.62	8.0	1900	5	65.896	104.858
N054A	2014	1.9 Ga-high Zr	cg, n/w-foi, hbl-bt quartz monzonite	86.1	15.4	0.1079	0.511277	-5.1	-4.3	2.56	8.5	1890	5	65.920	104.900
N060A	2014	1.9 Ga-high Zr	mg, w-foi, hbl-bt monzogranite	67.6	11.9	0.1066	0.511268	-4.7	-4.2	2.54	8.7	1910	5	66.171	105.170
J023D	2014	1.9 Ga-low Zr	cg, w-foi, bt alkali-feldspar granite	171.4	20.2	0.0712	0.510492	-11.3	-10.5	2.75	8.5	1900	est	65.856	104.884
J023E	2014	1.9 Ga-low Zr	mg-cg, w-foi, bt-hbl monzogranite	46.9	7.8	0.1005	0.511059	-7.2	-6.8	2.69	8.8	1915	5	65.856	104.884
J024A	2014	1.9 Ga-low Zr	cg, m-foi, bt syenogranite	17.7	2.6	0.0871	0.510756	-10.0	-9.3	2.78		1900	est	65.698	104.605
L032	2012	1.9 Ga-low Zr	mg, s-foi, bt monzogranite	29.9	4.5	0.0914	0.510877	-8.4	-8.0	2.72	8.1	1930	5	65.785	103.640
M046A	2014	1.9 Ga-low Zr	cg, un-foi, bt monzogranite	31.9	4.0	0.0765	0.510629	-9.3	-9.1	2.70	8.2	~1940	5	65.369	104.734
N015BA2	2014	1.9 Ga-low Zr	cg, m-s-foi, bt metatexite	22.4	3.4	0.0923	0.510669	-13.0	-12.3	3.01		1900	est	66.169	104.545
N017A	2014	1.9 Ga-low Zr	cg, m-s-foi, bt monzogranite	32.0	3.6	0.0679	0.510652	-7.1	-6.5	2.51	8.1	1915	5	66.148	104.048
N025D	2014	1.9 Ga-low Zr	cg, un-foi, bt alkali-feldspar granite	10.3	1.5	0.0887	0.510652	-12.4	-11.8	2.95	9.3	1910	5	65.705	104.923
85-M109A	1985	Cpb	mg, w-foi, bt-opx granodiorite	10.5	1.5	0.0870	0.511096	-1.9	-2.6	2.35		2000	est	66.802	105.008
J102A	2016	Cpb	fg-mg, m-foi, hbl-bt-opx quartz monzodiorite	45.0	7.8	0.1053	0.511312	-2.5	-3.0	2.45	6.1	1990	5	66.693	104.867
L160	2016	Cpb	mg-cg, m-foi, bt tonalite	31.2	5.7	0.1105	0.511312	-4.3	-4.3	2.57	9.3	1955	5	66.187	104.967
L175A02	2016	Cpb	cg, w/m-foi, cpx-opx-bt monzogabbro	22.0	4.5	0.1234	0.511569	-2.0	-2.5	2.50	8.4	2000	est	66.502	105.134
N061A	2014	Cpb	mg, w-foi hbl-bt quartz monzodiorite	53.0	11.4	0.1300	0.511652	-2.3	-2.6	2.55	7.8	1980	5	65.854	105.504
T175A01	2016	Cpb	fg, w/m-foi opx-bt diorite	21.2	4.5	0.1272	0.511644	-1.6	-2.0	2.48	6.5	2000	est	66.787	104.733
T202A02	2016	Cpb	cg, m-foi, bt monzogranite	5.7	0.5	0.0542	0.510654	-2.1	-3.0	2.29	8.1	2000	est	66.516	104.871
J105	2016	Cpb-mag low	cg, w-foi, bt monzogranite	8.3	0.9	0.0666	0.510933	0.2	-0.7	2.19	10.0	2000	est	66.691	104.825
L188A01	2016	Cpb-mag low	fg-cg, m-foi, bt quartz monzodiorite	26.5	5.2	0.1194	0.511507	-2.2	-2.7	2.50	9.3	2000	est	66.829	104.958

Table A-1. (cont.)

Sample	Year	Group	Rock description	Nd (ppm)	¹⁴⁷ Sm/ ¹⁴⁴ Nd	¹⁴³ Nd/ ¹⁴⁴ Nd	¹⁴³ Nd/ ¹⁴⁴ Nd (initial)	$\epsilon_{Nd}(T)$	$\epsilon_{Nd}(1.95 Ga)$	$T_{DM}(Ga)$	$\delta^{18}O(‰)$	Age (Ma)	Ref	Latitude (°N)	Longitude (°W)
T174A01	2016	Cpb-mag low	fg-mg, m/s-foI quartz diorite	19.7	4.0	0.1219	0.511540	-2.2	-2.7	2.51	8.0	2000	est	66.786	104.775
W177A02	2016	Cpb-mag low	mg, un-foI, bt granodiorite	9.1	1.3	0.0865	0.511121	-1.3	-2.0	2.31	10.6	2000	est	66.421	105.094
C062A	2014	Epb	mg-cg, w-foI, hbl-bt gabbro	11.2	2.3	0.1229	0.511582	-1.7	-2.1	2.47	7.2	2000	est	65.492	104.565
D008A	2014	Epb	fg, m/s-foI, bt-opx-cpx diorite	17.9	4.0	0.1337	0.511710	-1.9	-2.3	2.56	5.9	2000	est	65.847	104.412
J114A	2016	Epb	mg-cg, w-foI, cpx-hbl-bt diorite	31.1	7.2	0.1408	0.511852	-1.0	-1.4		7.9	2000	est	66.205	104.341
J121A	2016	Epb	mg-cg, m-foI, cpx-hbl-bt diorite	32.3	5.9	0.1100	0.511422	-1.5	-2.0	2.39	6.7	2000	est	66.210	104.265
M201A	2016	Epb	cg, w-foI, bt quartz diorite	32.0	6.3	0.1194	0.511478	-2.7	-3.3	2.55	6.7	2005	5	65.222	104.482
N012A	2014	Epb	cg, w-foI hbl-bt monzogabbro	28.7	5.4	0.1129	0.511435	-2.0	-2.5	2.45	6.9	2000	5	66.157	104.345
R105A1	2016	Epb	fg, s-foI, bt quartz monzonite	113.3	13.2	0.0707	0.510803	-3.4	-4.3	2.40	7.3	2000	est	65.434	104.252
R105B1	2016	Epb	fg-mg, s-foI, opx-bt-hbl quartz diorite	25.2	5.1	0.1218	0.511489	-3.2	-3.7	2.60	6.7	2000	est	65.434	104.252
L202A	2016	Epb >2.01 Ga	fg-mg, s-foI, hbl granodiorite	24.3	4.6	0.1140	0.511489	-0.6	-1.7	2.39	4.2	2060	5	66.161	104.286
L151A01	2016	ERd	mg-cg, un-foI, bt monzogranite	28.6	3.7	0.0771	0.510973	-1.8	-2.6	2.32		2000	est	66.920	105.069
L170A01	2016	ERd	mg, w-foI, bt monzogranite	45.3	6.8	0.0901	0.511088	-2.9	-3.6	2.42		2000	est	66.511	105.195
L173A02	2016	ERd	cg, s-foI hbl-bt monzogranite	55.5	9.4	0.1028	0.511298	-2.0	-2.6	2.41	9.4	2000	est	66.507	105.166
M104A01	2016	ERd	mg-cg, w-foI, hbl-bt quartz diorite	16.5	3.8	0.1385	0.511777	-1.8	-2.2		7.8	2000	est	66.077	105.589
M117A	2016	ERd	cg, m-foI hbl-opx-bt granodiorite	25.0	4.7	0.1127	0.511427	-2.3	-2.6	2.45	9.8	1980	5	66.242	105.220
M120	2016	ERd	fg-mg, s-foI, bt-hbl quartz monzodiorite	79.7	14.3	0.1087	0.511393	-1.7	-2.3	2.41		2000	est	66.237	105.264
M166A	2016	ERd	cg, w-foI, bt tonalite	34.9	5.6	0.0979	0.511252	-1.7	-2.3	2.37		2000	est	66.343	105.236
M178	2016	ERd	cg, w-foI, bt monzogabbro	14.8	3.1	0.1286	0.511688	-1.0	-1.5	2.44		2000	est	66.612	105.062
T130A02	2016	ERd	cg, w-foI, bt monzogranite	5.2	0.7	0.0786	0.510990	-1.8	-2.6	2.32	9.5	2000	est	66.185	105.330
W111A03	2016	ERd	mg, m-s-foI, hbl-bt quartz monzodiorite	26.9	5.1	0.1142	0.511463	-1.7	-2.3	2.43	6.1	2000	est	66.200	105.450
W120B	2016	ERd	mg, s-foI, bt monzogranite	25.9	4.3	0.1007	0.511144	-4.5	-5.1	2.58		2000	est	66.163	105.422

Table A-1. (cont.)

Sample	Year	Group	Rock description	Nd (ppm)	Sm (ppm)	¹⁴⁷ Sm/ ¹⁴⁴ Nd	¹⁴³ Nd/ ¹⁴⁴ Nd	¹⁴³ Nd/ ¹⁴⁴ Nd (initial)	$\epsilon_{Nd}(T)$	$\epsilon_{Nd}(1.95 Ga)$	T _{DM} (Ga)	$\delta^{18}O$ (‰)	Age (Ma)	Ref	Latitude (°N)	Longitude (°W)
W134A	2016	ERd	cg, m/s- <i>fol</i> (gneissic), <i>bt</i> granodiorite	29.8	5.1	0.1027	0.511354	0.510037	-1.1	-1.5	2.33	8.7	1985	5	66.261	105.334
W173A	2016	ERd	<i>fg</i> , <i>s-<i>fol</i></i> , <i>bt-hbl</i> quartz monzodiorite	37.8	6.9	0.1095	0.511383	0.509978	-2.1	-2.6	2.44	3.9	2000	est	66.423	105.240
W110B	2016	ERd	<i>fg</i> , <i>s-<i>fol</i></i> , monzogranite dyke (post-tectonic)	58.1	10.2	0.1061	0.511375	0.510013	-3.4	-2.0	2.37	6.1	1830	est	66.199	105.434
M032	2014	ERd hypabyssal	<i>fg</i> - <i>mg</i> , <i>s-<i>fol</i></i> <i>hbl</i> - <i>bt</i> microgranodiorite	33.4	5.6	0.1011	0.511220	0.509922	-3.7	-3.7	2.48	8.7	1953 ± 3	3	65.775	105.481
M180A02	2016	ERd hypabyssal	<i>mg</i> , <i>w-<i>fol</i></i> , <i>hbl</i> - <i>bt</i> microdiorite	15.2	3.8	0.1507	0.512031	0.510097	-0.3	-0.3		7.2	1950	est	66.615	105.077
M165A	2016	ERd >2.01 Ga	<i>cg</i> , <i>w-<i>fol</i></i> , <i>bt</i> syenogranite	53.3	6.0	0.0678	0.510868	0.509945	-0.3	-2.3	2.28	9.7	2070	5	66.335	105.249
L003	2012	ERd ~ 2.6 Ga	<i>cg</i> , <i>m-<i>s-<i>fol</i></i></i> , <i>bt</i> monzogranite	48.3	7.0	0.0879	0.510757	0.509255	-0.4	-9.5	2.79	8.9	2591 ± 27	2	66.220	105.402
W120C	2016	ERd ~ (?) 2.6 Ga	<i>mg</i> , <i>m-<i>fol</i></i> , <i>cpx-hbl</i> monzogabbro	39.2	8.3	0.1284	0.511527	0.509879	1.2	-4.6	2.74		2600	est	66.163	105.422
S049A	2014	ERd psammite assemblage 1/2	pelite (and- <i>grt</i>)	30.0	5.3	0.1062	0.511109	0.509640	-5.4	-7.2	2.77		2100	est	65.766	105.460
M108A	2016	ERd psammite assemblage 2	<i>fg</i> , <i>s-<i>fol</i></i> <i>bt-hbl</i> psammite	38.9	7.2	0.1122	0.511364	0.509924	-3.7	-3.7	2.54	6.4	<1954 ± 5	3	66.202	105.425
M029A	2014	ERd volcanic	<i>fg</i> , <i>s-<i>fol</i></i> <i>hbl</i> - <i>bt</i> basaltic komatiite	11.2	3.7	0.1991	0.512768	0.510213	1.9	1.9			2100	est	65.778	105.466
M075A3	2014	ERd volcanic	<i>fg</i> , <i>s-<i>fol</i></i> <i>hbl</i> - <i>bt</i> basaltic komatiite	9.4	3.0	0.1958	0.512787	0.510274	3.2	3.1			2100	est	65.779	105.467
M077	2016	ERd volcanic	<i>fg</i> , <i>s-<i>fol</i></i> <i>hbl</i> - <i>bt</i> basaltic komatiite	9.4	2.9	0.1851	0.512461	0.510085	-0.3	-0.6			2100	est	65.778	105.473
S044A	2014	ERd volcanic	<i>fg</i> , <i>m-<i>fol</i></i> <i>hbl</i> - <i>bt</i> basaltic komatiite	23.8	4.6	0.1175	0.511413	0.509905	-2.5	-4.1	2.64		2100	est	65.754	105.439
J027A	2014	Lgr-east	<i>mg</i> - <i>cg</i> , <i>w-<i>fol</i></i> , <i>grt-sp</i> tonalite	35.7	4.4	0.0748	0.510817	0.509856	-5.8	-5.0	2.46		1900	est	65.701	104.055
L039	2012	Lgr-east	<i>cg</i> , <i>s-<i>fol</i></i> (gneissic), <i>sp-sil</i> alkali-feldspar granite	26.4	4.4	0.1020	0.511198	0.509923	-5.0	-4.4	2.53	11.4	1900	est	66.038	104.215
M003A	2014	Lgr-east	<i>fg</i> , <i>s-<i>fol</i></i> , <i>grt</i> - <i>bt</i> syenogranite	74.5	10.5	0.0849	0.510978	0.509905	-4.8	-4.4	2.46	10.5	1925 ± 3	0	65.438	104.310
N019B	2014	Lgr-east	<i>fg</i> , <i>s/m-<i>fol</i></i> , <i>grt</i> - <i>bt</i> syenogranite	21.6	3.7	0.1043	0.511198	0.509859	-5.6	-5.0	2.59		1900	est	65.200	104.361
M057A	2014	Lgr-main	<i>cg</i> , <i>un-<i>fol</i></i> , <i>grt</i> alkali-feldspar granite	44.6	7.5	0.1017	0.511161	0.509883	-5.6	-5.1	2.58	10.6	1919 ± 4	0	65.390	104.953
M162A01	2016	Lgr-main	<i>mg</i> - <i>cg</i> , <i>m-<i>fol</i></i> , <i>bt</i> syenogranite	14.3	3.3	0.1383	0.511619	0.509845	-5.7	-5.3			1900	est	65.254	104.859
N008A1	2014	Lgr-main	<i>mg</i> , <i>w-<i>fol</i></i> <i>grt-sil</i> monzogranite	24.9	4.8	0.1162	0.511414	0.509923	-4.3	-3.7	2.56		1900	est	66.083	104.943

Table A-1. (cont.)

Sample	Year	Group	Rock description	Nd (ppm)	Sm (ppm)	$^{143}\text{Nd}/^{144}\text{Nd}$	$^{147}\text{Sm}/^{144}\text{Nd}$	$^{143}\text{Nd}/^{144}\text{Nd}$	$^{143}\text{Nd}/^{144}\text{Nd}$ (initial)	$\epsilon_{\text{Nd}}(\text{T})$	$\epsilon_{\text{Nd}}(1.95 \text{ Ga})$	T_{DM} (Ga)	$\delta^{18}\text{O}$ (‰)	Age (Ma)	Ref	Latitude (°N)	Longitude (°W)
N024A	2014	Lgr-main	cg, m/s-foI, grt-bt-sil syenogranite	41.9	7.2	0.1044	0.511170	0.509858	0.509858	-6.1	-5.5	2.63	11.2	1900	est	65.723	105.067
R132A	2016	Lgr-main	mg-cg, s-foI grt syenogranite	15.6	2.3	0.0890	0.510996	0.509854	0.509854	-5.7	-5.1	2.52	11.6	1908 ± 3	0	65.863	105.160
J026A	2014	DLd	mg, w-foI, bt tonalite	15.4	2.0	0.0800	0.510479	0.509452	0.509452	4.4	-13.0	2.95		3100	est	65.738	104.148
L038	2012	DLd	fg-mg, m-foI, opx-bt monzogranite	21.6	2.8	0.0789	0.510248	0.509011	0.509011	0.7	-17.2	3.20	6.7	3117 ± 28	1	66.050	104.709
M025A	2014	DLd	cg, m-foI, opx-bt granodiorite	26.2	4.3	0.0997	0.510664	0.508614	0.508614	0.4	-14.3	3.23	7.4	3111 ± 51	4	65.443	104.861
M044A	2014	DLd	mg, w-foI, hbl-opx monzogabbro	22.3	4.8	0.1299	0.511198	0.508970	0.508970	-1.4	-11.4	3.43	6.7	3100	5	65.366	104.756
M044B	2014	DLd	fg-mg, w-foI, opx granodiorite	8.9	1.2	0.0788	0.510320	0.508628	0.508628	4.2	-15.8	3.11	7.6	3248 ± 5.3	4	65.366	104.756
N013A	2014	DLd	mg, w-foI, cpx-sp diorite	4.5	1.1	0.1414	0.511490	0.508499	0.508499	-0.3	-8.6		5.2	3100	est	66.100	104.409
N025C	2014	DLd	mg-cg, w-foI, opx-bt tonalite	47.8	9.7	0.1228	0.511081	0.508566	0.508566	-0.9	-11.9	3.36	7.9	3100	est	65.705	104.923
J128A	2016	QMB	cg, n/w-foI, opx-bt granodiorite	9.5	1.2	0.0764	0.510484	0.509503	0.509503	3.8	-12.0	2.87	7.0	2965 ± 5	4	65.218	104.256
L031	2012	QMB	cg, s-foI, bt-hbl granodiorite	17.4	3.8	0.1324	0.511166	0.508447	0.508447	-3.0	-12.7	3.61	9.6	3108 ± 58	2	65.772	103.775
L033	2012	QMB	mg-cg, w-foI, bt-hbl tonalite	22.1	2.8	0.0770	0.510329	0.508751	0.508751	3.7	-15.2	3.06	8.5	3158 ± 42	2	65.848	103.257
M072A	2014	QMB	fg, w-foI, opx-bt tonalite	18.6	3.7	0.1187	0.511027	0.508480	0.508480	1.2	-12.0	3.29	6.6	3246 ± 51	4	65.551	103.997
N032A	2014	QMB	cg, m-foI, bt syenogranite	14.1	2.6	0.1120	0.510945	0.508652	0.508652	0.8	-11.9	3.19	8.4	3100	est	65.711	103.718
T188B01	2016	QMB	fg-mg, w-foI, opx-bt quartz gabbro	3.9	0.9	0.1407	0.511440	0.509635	0.509635	-1.0	-9.4		6.0	3100	est	65.320	104.354
T193A01	2016	QMB	mg, m-foI, bt-opx calcic tonalite	17.5	2.7	0.0923	0.510536	0.509351	0.509351	0.7	-14.9	3.19	7.0	3100	est	65.317	104.258
N058B	2014	(?)2.15 Ga - DLd	mg, w-foI, bt gabbro	11.8	3.3	0.1681	0.512275	0.510118	0.510118	0.8	0.1		5.9	(?)2150	est	65.706	104.933
N026C	2014	2.4 Ga - DLd	mg-cg, w-foI, bt-opx tonalite	10.9	1.5	0.0853	0.510622	0.509268	0.509268	-4.9	-11.5	2.90	8.4	2408 ± 4	4	65.696	104.828
T163A	2016	2.4 Ga - Cpb	cg, m-foI, opx-bt quartz monzonite	25.0	3.7	0.0899	0.511083	0.509929	0.509929	2.6	-3.6	2.43		2405 ± 25	6	66.385	105.038
T168A01	2016	(?)2.4 Ga - Cpb	fg-cg, w-foI opx diorite	18.0	3.9	0.1311	0.511504	0.509821	0.509821	-1.9	-5.7	2.88		(?)2400	est	66.389	104.956
N025E	2014	(?)2.4 Ga - Cpb	fg, w-foI, bt-opx monzogabbro	18.2	4.0	0.1339	0.511559	0.509174	0.509174	-1.7	-5.4	2.87	7.1	(?)2400	est	65.705	104.923
85-M015	1985	Slave-OLd	mg, s-foI, bt tonalite	11.6	2.3	0.1206	0.511306	0.509758	0.509758	0.0	-7.0	2.88		2650	est	66.539	105.528
85-M018	1985	Slave-OLd	mg-cg, m/s-foI bt-hbl tonalite	10.7	1.9	0.1077	0.511135	0.509252	0.509252	1.0	-7.1	2.77		2650	est	66.551	105.594
85-M019-1	1985	Slave-OLd	mg, un-foI, bt tonalite	5.6	1.1	0.1136	0.511275	0.509289	0.509289	1.8	-5.8	2.72	7.8	2650	est	66.560	105.619

Table A-1. (cont.)

Sample	Year	Group	Rock description	Nd (ppm)	Sm (ppm)	¹⁴⁷ Sm/ ¹⁴⁴ Nd	¹⁴³ Nd/ ¹⁴⁴ Nd	¹⁴³ Nd/ ¹⁴⁴ Nd (initial)	$\epsilon_{Nd}(T)$	$\epsilon_{Nd}(1.95 \text{ Ga})$	T_{DM} (Ga)	$\delta^{18}O$ (‰)	Age (Ma)	Ref	Latitude (°N)	Longitude (°W)
85-M27A	1985	Slave-OLD	mg, w/m-fof, bt granodiorite	7.0	1.2	0.1000	0.510967	0.509219	0.4	-8.4	2.81		2650	est	66.588	105.821
85-N147	1985	Slave-OLD	mg, s-fof, hbl-bt tonalite	52.5	7.0	0.0805	0.510649	0.509241	0.8	-9.8	2.76		2650	est	66.205	105.890
L128B03	2016	Slave-OLD	fg-mg, w-fof, bt diorite	11.2	3.2	0.1738	0.512313	0.510082	1.5	-0.6		5.6	2650	est	66.175	105.973
L133A01	2016	Slave-OLD	mg, w-fof, hbl-bt tonalite	29.2	5.0	0.1028	0.511091	0.509772	1.9	-6.7	2.70		2650	est	66.164	105.901
L142A01	2016	Slave-OLD	mg, s-fof, bt tonalite	20.4	2.4	0.0716	0.510464	0.509545	0.3	-11.1	2.79		2650	est	66.920	105.212
M146B01	2016	Slave-OLD	mg-cg, w-fof, bt-hbl tonalite	12.4	2.7	0.1307	0.511506	0.509828	0.4	-5.6	2.86		2650	est	66.725	105.367
M202A	2016	Slave-OLD	mg, s-fof, bt monzogranite	8.0	1.7	0.1249	0.511482	0.509879	2.5	-4.6	2.70	6.9	2712 ± 4	0	66.727	105.392
R112	2016	Slave-OLD	mg-cg, s-fof, bt tonalite	21.5	2.7	0.0756	0.510608	0.509638	1.7	-9.3	2.71	7.8	2658 ± 17	6	66.978	105.482
R114A	2016	Slave-OLD	fg, m-fof, bt granodiorite	14.8	2.3	0.0923	0.510852	0.509668	1.6	-8.7	2.77		2711 ± 6	6	66.913	105.490
R116	2016	Slave-OLD	mg-cg, m-fof, bt tonalite	16.2	2.5	0.0935	0.510915	0.509714	1.4	-7.8	2.72	7.5	2650	est	66.902	105.391
R118	2016	Slave-OLD	mg, m/s-fof hbl quartz diorite	26.3	4.8	0.1106	0.511203	0.509783	1.3	-6.5	2.75	6.6	2650	est	66.835	105.428
T143A	2016	Slave-OLD	mg, n/w-fof, bt	29.3	4.9	0.1015	0.510968	0.509665	-0.9	-8.8	2.85		2595 ± 4	6	66.220	105.901
T146A01	2016	Slave-OLD	mg, w-fof, hbl-bt diorite	24.0	4.3	0.1074	0.511110	0.509732	0.7	-7.5	2.80		2650	est	66.213	105.865
83-A288	1983	Slave-THd	cg, w-fof, ms alkali-feldspar granite	8.3	2.0	0.1437	0.511736	0.509892	0.5	-4.3	2.89	10.8	2600	est	66.272	106.597
84-N305	1984	Slave-THd	mg-cg, w-fof, bt-ms granodiorite	45.9	7.8	0.1021	0.511110	0.509799	1.8	-6.2	2.66	9.5	2600	est	66.405	106.635
84-N312A	1984	Slave-THd	fg-mg, m-fof bt-ms alkali-feldspar granite	12.7	2.6	0.1219	0.511424	0.509859	1.3	-5.0	2.71		2600	est	66.419	106.435
C100B01	2016	Slave-THd	fg, m/s-fof, hbl-bt gabbro	30.2	8.1	0.1627	0.512234	0.510147	1.5	0.7		6.3	2150	est	66.681	105.991
C105B02	2016	Slave-THd	fg, m-fof, grt-hbl quartz gabbro	17.3	5.0	0.1752	0.512448	0.510200	2.2	1.7		7.7	2150	est	66.693	105.924
L112A01	2016	Slave-THd	mg-cg, s-fof bt granodiorite	22.7	3.9	0.1046	0.511171	0.509829	2.1	-5.6	2.63	7.9	2600	est	66.980	105.783
L119A02	2016	Slave-THd	cg, n/w-fof, hbl-bt quartz monzodiorite	32.7	5.8	0.1063	0.511151	0.509786	1.2	-6.4	2.71	7.9	2600	est	66.966	106.017
N001A	2014	Slave-THd	fg, s-fof, ms-bt syenogranite	58.9	7.3	0.0749	0.510686	0.509402	2.7	-7.6	2.60	10.3	2600	est	66.193	106.503
R109A01	2016	Slave-THd	cg, un-fof, bt monzogranite	10.4	1.8	0.1023	0.511097	0.509784	1.4	-6.5	2.68		2600	est	66.857	105.909
85-M008	1985	Wpb	cg, n/w-fof, bt-hbl quartz diorite	54.6	10.1	0.1118	0.511386	0.509922	-2.6	-3.2	2.49		2000	est	66.511	105.397
85-M009	1985	Wpb	cg, w-fof, hbl-bt quartz monzodiorite	35.2	6.5	0.1118	0.511372	0.509908	-2.9	-3.5	2.51		2000	est	66.515	105.434
D023A	2014	Wpb	mg-cg, w-fof, bt granodiorite	33.6	4.0	0.0726	0.510948	0.509993	-1.1	-1.9	2.27	7.1	2000	est	65.647	105.490
J032A	2014	Wpb	mg-cg, s-fof monzogranite	56.6	9.7	0.1032	0.511295	0.509937	-2.2	-2.8	2.42	7.5	2000	est	65.636	105.595

Table A-1. (cont.)

Sample	Year	Group	Rock description	Nd (ppm)	¹⁴⁷ Sm/ ¹⁴⁴ Nd	¹⁴³ Nd/ ¹⁴⁴ Nd	¹⁴³ Nd/ ¹⁴⁴ Nd (initial)	$\epsilon_{Nd}(T)$	$\epsilon_{Nd}(1.95 Ga)$	T _{DM} (Ga)	$\delta^{18}O$ (‰)	Age (Ma)	Ref	Latitude (°N)	Longitude (°W)
J035A	2014	Wpb	cg, s- <i>fol</i> , hbl- <i>bt</i> monzogranite	48.4	0.0920	0.511170	0.509953	-1.7	-2.4	2.36	8.0	2010	5	65.641	105.550
J035B	2014	Wpb	fg, m- <i>fol</i> , hbl- <i>bt</i> diorite	40.4	0.1128	0.511386	0.509900	-2.9	-3.4	2.52	6.6	2000	5	65.641	105.550
L001	2012	Wpb	cg, m- <i>fol</i> , opx- <i>bt</i> monzogranite	23.2	0.1016	0.511289	0.509958	-2.0	-2.5	2.40	8.1	1991 ± 4	2	66.225	105.706
L134A	2016	Wpb	cg, m- <i>fol</i> , bt- <i>hbl</i> granodiorite	18.7	0.0888	0.511096	0.509927	-2.4	-3.1	2.39		2000	est	66.159	105.874
L140A	2016	Wpb	mg-cg, m- <i>fol</i> (gneissic), hbl- <i>bt</i> quartz monzodiorite	32.9	0.1099	0.511405	0.509994	-1.8	-2.3	2.42	7.1	2000	est	66.136	105.792
M042	2014	Wpb	fg, s- <i>fol</i> bt monzogranite	39.1	0.1140	0.511330	0.509867	-4.3	-4.8	2.64		2000	est	65.690	105.909
M138A	2016	Wpb	cg, un- <i>fol</i> , cpx- <i>bt</i> - <i>hbl</i> monzogranite	25.1	0.1127	0.511315	0.509869	-4.2	-4.8	2.63	8.7	2010	5	65.982	105.987
M152A	2016	Wpb	mg, m- <i>fol</i> , pink, bt- <i>hbl</i> monzogranite	35.1	0.0871	0.511078	0.509961	-2.4	-3.0	2.37		1990	5	66.706	105.284
M152B	2016	Wpb	cg, s- <i>fol</i> bt- <i>hbl</i> monzogranite	83.3	0.1052	0.511335	0.509984	-2.1	-2.5	2.41	6.9	1990 ± 5	6	66.706	105.284
T147A	2016	Wpb	mg-cg, s- <i>fol</i> hbl granodiorite	29.1	0.1072	0.511361	0.509985	-1.9	-2.5	2.42		2000	est	66.206	105.850
W142A	2016	Wpb	cg, w- <i>fol</i> cpx- <i>hbl</i> - <i>bt</i> diorite	102.6	0.1115	0.511404	0.509973	-2.2	-2.8	2.46	6.7	2000	est	66.224	105.672
W142B	2016	Wpb	cg, w- <i>fol</i> , bt granodiorite	40.5	0.0648	0.510824	0.509993	-1.5	-2.4	2.28	6.9	2000	est	66.224	105.672
W142C	2016	Wpb	cg, w- <i>fol</i> opx- <i>bt</i> monzogranite	7.1	0.0794	0.511007	0.509989	-1.7	-2.4	2.32	8.5	2000	est	66.224	105.672
W164A02	2016	Wpb	cg, w- <i>fol</i> , bt monzogranite	37.5	0.1057	0.511353	0.509997	-1.7	-2.3	2.40	8.1	2000	est	65.755	105.991
W164B02	2016	Wpb	fg-mg, n/w- <i>fol</i> , hbl diorite	13.4	0.1352	0.511746	0.510011	-1.6	-2.0		7.3	2000	est	65.755	105.991
M157A	2016	Wpb	cg, w- <i>fol</i> , hbl- <i>bt</i> diorite	22.1	0.1159	0.511491	0.510003	-1.4	-2.2	2.43	5.7	2010	5	66.227	105.569
L002	2012	Wpb >2.01 Ga	mg, s- <i>fol</i> , cpx- <i>hbl</i> - <i>bt</i> quartz monzonite	51.7	0.1109	0.511413	0.509931	-1.6	-2.4	2.43	6.9	2029 ± 4	2	66.230	105.566

Sample prefixes are 12NK- (2012; data from Berman et al., 2015a), 14NK- (2014), 16BLB- (2016); TZ- (1984, 1985)

Group abbreviations: Cpb = Central plutonic belt, DLd = Duggan Lake domain, Epb = Eastern plutonic belt, ERd = Ellice River domain, Lgr = Leucogranite, Old = Overby Lake

domain, QMB = Queen Maud Block, THd = Tinney Hills domain, Wpb = Western plutonic belt

Descriptive abbreviations: fg = fine grained, mg = medium grained, cg = coarse grained; un-*fol* = unfoliated, n/w-*fol* = non- to weakly foliated, w-*fol* = weakly foliated,

m-*fol* = moderately foliated, s-*fol* = strongly foliated

Mineral abbreviations: bt = biotite, hbl = hornblende, opx = orthopyroxene, cpx = clinopyroxene, and = andesite, grt = garnet, sp = spinel, sil = sillimanite, ms = muscovite

T_{DM} = DePaolo (1981) model age (not calculated for samples with ¹⁴³Nd/¹⁴⁴Nd > 0.135)

$\delta^{18}O = \delta^{18}O_{WR}$ in ‰ (per mil) relative to V-SMOW (Vienna Standard Mean Ocean Water) standard

Age = zircon crystallization age: unpublished (rounded to nearest 5 Ma; typical errors are ± <5 Ma)

Ref = zircon age reference: 0 = this paper; 1 = Davis et al. (2013), 2 = Davis et al. (2014); 3 = Davis et al. (2021); 4 = R.G. Berman, W.J. Davis, M. Sanborn-Barrie, J.A. Percival,

J. Whalen, and L. Nadeau, work in progress, 2022; 5 = W.J. Davis, unpub. data, 2021 (unpublished U-Pb SHRIMP ages); 6 = Berman and Camacho (2020); est = estimated

Table A-2. Results of U-Pb analyses using Sensitive High-Resolution Ion Microprobe (SHRIMP).

Spot name	IP#	U (ppm)	Th (ppm)	Th/U	Yb (ppm)	Hf (ppm)	$\pm 204\text{Pb}/206\text{Pb}$	$f(206)^{204}$	$^{206}\text{Pb}^*$ (ppm)	$^{208}\text{Pb}/^{206}\text{Pb}$	$\pm 208\text{Pb}/206\text{Pb}$	$^{207}\text{Pb}/^{235}\text{U}$	$\pm 207\text{Pb}/235\text{U}$	$^{206}\text{Pb}/^{238}\text{U}$	$\pm 206\text{Pb}/238\text{U}$	Corr Coeff	$^{207}\text{Pb}/^{206}\text{Pb}$	$\pm 207\text{Pb}/206\text{Pb}$	$^{207}\text{Pb}/^{206}\text{Pb}$	$\pm 207\text{Pb}/206\text{Pb}$	Disc. (%)				
16BLB-M202A																									
11827-003.1	863	168	39	0.24	0.79	10404	1.1E-4	24	0.19	73.6	0.075	3.4	13.041	1.8	0.5092	1.7	0.965	0.1857	0.5	2653	38	2705	8	+2.3	
11827-004.1	863	185	146	0.82	0.40	7775	2.4E-5	45	0.04	83.4	0.231	1.5	13.590	1.7	0.5253	1.7	0.976	0.1876	0.4	2722	38	2721	6	0.0	
11827-005.1	863	151	64	0.44	0.60	8265	1.3E-5	71	0.02	68.1	0.123	2.4	13.389	1.8	0.5262	1.7	0.970	0.1846	0.4	2725	38	2694	7	-1.4	
11827-006.1	863	268	68	0.26	0.55	218	3.4E-5	32	0.06	119.6	0.074	2.3	13.252	1.7	0.5187	1.7	0.982	0.1853	0.3	2694	37	2701	5	+0.3	
11827-007.1	863	201	94	0.48	0.50	8217	9.5E-6	71	0.02	90.5	0.135	2.0	13.544	1.7	0.5235	1.7	0.977	0.1876	0.4	2714	38	2722	6	+0.3	
11827-009.1	863	223	85	0.39	0.51	7994	1.3E-5	58	0.02	99.2	0.109	3.9	13.234	2.0	0.5176	1.7	0.842	0.1854	1.1	2689	37	2702	18	+1.6	
11827-015.1	863	805	225	0.29	0.31	12911	8.0E-6	38	0.01	367.6	0.083	1.9	13.661	1.6	0.5314	1.6	0.994	0.1865	0.2	2747	36	2711	3	-1.6	
11827-025.1	863	337	145	0.44	0.52	374	8408	-1.5E-5	45	-0.03	152.8	0.122	1.6	13.632	1.7	0.5274	1.7	0.984	0.1875	0.3	2731	37	2720	5	-0.5
11827-026.1	863	273	196	0.74	0.35	200	8868	-1.4E-5	50	-0.02	122.6	0.214	1.3	13.259	1.7	0.5232	1.7	0.982	0.1838	0.3	2713	37	2687	5	-1.2
11827-038.1	863	45	11	0.24	1.45	82	8598	-1.9E-13	9999	0.00	18.6	0.076	5.8	11.727	2.2	0.4770	2.1	0.927	0.1783	0.8	2514	43	2637	14	+5.6
11827-040.1	863	648	147	0.23	0.39	431	13281	2.9E-6	71	0.01	292.6	0.070	3.6	13.428	1.6	0.5256	1.6	0.992	0.1853	0.2	2723	36	2701	3	-1.0
11827-045.1	863	177	52	0.31	3.84	193	10203	-1.1E-5	71	-0.02	78.3	0.085	2.7	13.185	1.8	0.5142	1.7	0.974	0.1860	0.4	2675	37	2707	7	+1.4
11827-052.1	863	175	79	0.47	0.53	492	7847	-1.1E-5	71	-0.02	80.8	0.129	2.1	13.861	1.8	0.5373	1.7	0.974	0.1871	0.4	2772	38	2717	7	-2.5
11827-055.1	863	200	34	0.18	0.79	188	10720	2.4E-5	45	0.04	88.7	0.052	13.0	13.287	1.7	0.5162	1.7	0.975	0.1867	0.4	2683	37	2713	6	+1.4
11827-056.1	863	206	69	0.35	0.58	222	8853	4.8E-6	100	0.01	95.2	0.100	2.3	13.952	1.7	0.5392	1.7	0.977	0.1877	0.4	2780	38	2722	6	+0.5
11827-061.1	863	282	95	0.35	2.12	268	10300	6.8E-6	71	0.01	126.9	0.100	1.9	13.559	2.9	0.5232	2.9	0.994	0.1880	0.3	2713	63	2724	5	-2.6
11827-063.1	863	271	130	0.49	0.43	277	8914	3.6E-6	100	0.01	124.3	0.146	1.8	13.791	1.7	0.5336	1.7	0.982	0.1874	0.3	2757	37	2720	5	-1.7
11827-064.1	863	246	44	0.18	0.70	212	11417	1.3E-3	6	2.22	107.7	0.055	6.7	12.738	1.9	0.5105	1.7	0.885	0.1810	0.9	2659	37	2662	15	+0.1
11827-065.1	863	447	245	0.57	2.46	226	10257	1.8E-4	21	0.31	199.7	0.173	1.5	13.320	1.7	0.5204	1.6	0.977	0.1856	0.4	2701	36	2704	6	+0.1
11827-069.1	863	205	132	0.67	2.81	217	8244	5.1E-5	30	0.09	93.7	0.189	1.6	13.622	1.7	0.5320	1.7	0.976	0.1857	0.4	2750	38	2704	6	-2.1
11827-070.1	863	241	242	1.04	0.34	187	7782	1.6E-5	50	0.03	110.4	0.298	1.2	13.706	1.7	0.5326	1.7	0.979	0.1866	0.3	2752	38	2713	6	-1.8
11827-097.1	863	356	107	0.31	0.45	365	10878	7.9E-6	58	0.01	159.8	0.088	1.8	13.327	1.7	0.5223	1.6	0.964	0.1850	0.5	2709	36	2699	8	-0.5
11827-101.1	863	69	27	0.41	0.97	139	7957	1.4E-5	100	0.02	29.5	0.120	3.7	12.312	2.0	0.4969	1.9	0.944	0.1797	0.7	2601	40	2650	11	+2.3
11827-102.1	863	229	116	0.52	0.46	209	8122	4.2E-6	100	0.01	104.1	0.149	1.7	13.622	1.7	0.5292	1.7	0.979	0.1867	0.3	2738	38	2713	6	-1.1
14NK-M003A																									
11411-003.1	781	1726	134	0.08	0.62	49	10416	8.4E-6	35	0.01	509.3	0.024	1.8	5.601	2.1	0.3436	2.1	0.988	0.1182	0.3	1904	34	1930	6	+1.6
11411-004.1	781	1187	110	0.10	0.37	67	10975	8.5E-6	35	0.01	350.0	0.030	1.9	5.592	1.4	0.3434	1.3	0.960	0.1181	0.4	1903	22	1928	7	+1.5
11411-005.1	781	989	123	0.13	0.42	50	12629	5.9E-5	21	0.10	296.8	0.038	2.5	5.676	1.9	0.3493	1.8	0.990	0.1179	0.3	1931	31	1924	5	-0.4
11411-006.1	781	1687	83	0.05	0.42	61	11337	9.7E-6	29	0.02	495.4	0.016	2.4	5.549	1.7	0.3419	1.7	0.997	0.1177	0.1	1896	29	1922	3	+1.5
11411-006.2	781	887	124	0.14	0.37	58	11082	6.6E-6	58	0.01	262.3	0.045	2.0	5.628	1.4	0.3442	1.3	0.955	0.1186	0.4	1907	22	1935	7	+1.7

Table A-2. (cont.)

Spot name	IP#	U (ppm)	Th (ppm)	Th/U ± Th/U	Yb (ppm)	Hf (ppm)	$\frac{^{204}\text{Pb}}{^{206}\text{Pb}} \pm \frac{^{204}\text{Pb}}{^{206}\text{Pb}}$	$f(206)^{204}$	$^{206}\text{Pb}^*$ (ppm)	$\frac{^{206}\text{Pb}}{^{206}\text{Pb}} \pm \frac{^{206}\text{Pb}}{^{206}\text{Pb}}$	$\frac{^{208}\text{Pb}}{^{206}\text{Pb}} \pm \frac{^{208}\text{Pb}}{^{206}\text{Pb}}$	$\frac{^{207}\text{Pb}}{^{238}\text{U}} \pm \frac{^{207}\text{Pb}}{^{238}\text{U}}$	$\frac{^{206}\text{Pb}}{^{238}\text{U}} \pm \frac{^{206}\text{Pb}}{^{238}\text{U}}$	Corr Coeff	$\frac{^{207}\text{Pb}}{^{206}\text{Pb}} \pm \frac{^{207}\text{Pb}}{^{206}\text{Pb}}$	$\frac{^{206}\text{Pb}}{^{238}\text{U}} \pm \frac{^{206}\text{Pb}}{^{238}\text{U}}$	$\frac{^{206}\text{Pb}}{^{238}\text{U}} \pm \frac{^{206}\text{Pb}}{^{238}\text{U}}$	$\frac{^{207}\text{Pb}}{^{206}\text{Pb}} \pm \frac{^{207}\text{Pb}}{^{206}\text{Pb}}$	Disc. (%)	
11411-007.1	781	1156	60	0.05	0.61	10804	9.1E-6	58	0.02	340.9	0.016	5.590	1.3	0.3432	1.3	0.986	0.1181	1928	4	+1.6
11411-008.1	781	858	92	0.11	1.18	10806	8.8E-6	41	0.02	253.6	0.035	5.655	1.8	0.3442	1.8	0.994	0.1192	1944	4	+2.2
11411-009.1	781	1163	40	0.04	5.40	11842	2.1E-5	26	0.04	347.3	0.010	5.645	1.8	0.3475	1.7	0.969	0.1178	1923	8	+0.1
11411-011.1	781	1608	76	0.05	3.48	12418	4.7E-6	100	0.01	476.3	0.014	5.634	1.3	0.3448	1.1	0.898	0.1185	1934	10	+1.5
11411-012.1	781	971	62	0.07	13.48	11333	1.1E-5	45	0.02	289.1	0.020	5.624	1.7	0.3465	1.7	0.991	0.1177	1922	4	+0.2
11411-014.1	781	1508	76	0.05	0.55	11759	6.6E-6	50	0.01	451.5	0.016	5.657	1.3	0.3486	1.3	0.990	0.1177	1922	3	-0.4
11411-014.2	781	1286	96	0.08	0.85	12849	1.4E-5	35	0.02	387.6	0.022	5.695	1.0	0.3509	1.0	0.972	0.1177	1939	16	-1.0
11411-016.1	781	1363	47	0.04	0.81	14029	1.4E-4	13	0.25	373.3	0.009	5.151	2.3	0.3187	2.2	0.963	0.1172	1934	34	+7.8
11411-017.1	781	1784	51	0.03	1.53	13679	5.7E-6	45	0.01	537.0	0.009	5.729	1.5	0.3504	1.3	0.904	0.1186	1935	11	-0.1
11411-018.1	781	1165	106	0.09	0.49	13633	8.8E-6	41	0.02	337.0	0.029	5.473	1.0	0.3368	1.0	0.977	0.1179	1924	4	+3.2
11411-018.2	781	1055	113	0.11	0.47	13651	7.7E-6	58	0.01	311.7	0.033	5.635	1.1	0.3438	1.1	0.980	0.1189	1939	4	+2.0
11411-019.1	781	1079	121	0.12	0.50	13333	1.5E-5	38	0.03	323.3	0.033	5.800	1.4	0.3488	1.1	0.783	0.1206	1965	16	+2.1
11411-021.1	781	1211	121	0.10	0.46	13952	6.0E-7	50	0.00	361.6	0.031	5.612	1.0	0.3477	1.0	0.973	0.1171	1912	4	-0.7
11411-022.1	781	1583	101	0.07	0.51	13771	6.9E-6	58	0.01	468.0	0.020	5.610	1.7	0.3441	1.7	0.980	0.1182	1930	6	+1.4
11411-023.1	781	671	121	0.19	0.47	13662	6.8E-6	71	0.01	199.8	0.066	5.661	1.5	0.3466	1.3	0.894	0.1184	1933	12	+0.9
11411-025.1	781	1408	105	0.08	0.47	13430	7.8E-6	71	0.01	422.1	0.023	5.681	1.4	0.3491	1.3	0.968	0.1180	1927	6	-0.2
11411-026.1	781	1414	65	0.05	1.15	13445	1.8E-6	100	0.00	420.4	0.015	5.634	1.1	0.3462	1.0	0.985	0.1180	1926	3	+0.6
16BLB-R132A																				
12095-078.1	879	1618	150	0.10	0.36	13836	1.4E-5	25	0.02	483.4	0.028	5.637	1.3	0.3479	1.3	0.993	0.1175	1924	21	-0.3
12095-084.1	879	1615	146	0.09	0.33	12164	3.7E-6	45	0.01	504.2	0.028	5.898	1.4	0.3635	1.3	0.970	0.1177	1921	23	-4.7
12095-100.1	879	1662	114	0.07	1.11	15180	1.4E-5	22	0.02	512.5	0.019	5.794	1.4	0.3591	1.4	0.995	0.1170	1978	24	-4.0
12095-007.1	879	1094	166	0.16	0.35	13961	1.6E-5	29	0.03	320.8	0.046	5.481	1.3	0.3414	1.3	0.988	0.1164	1894	21	+0.5
12095-022.1	879	1099	115	0.11	0.42	14544	2.8E-5	22	0.05	325.2	0.031	5.540	1.4	0.3446	1.4	0.989	0.1166	1905	23	-0.2
12095-021.1	879	986	147	0.15	0.37	13565	1.6E-5	30	0.03	289.3	0.044	5.519	1.3	0.3416	1.3	0.987	0.1172	1894	21	+1.2
12095-041.1	879	1337	234	0.18	0.60	13861	1.3E-5	29	0.02	395.5	0.062	5.550	1.4	0.3442	1.4	0.991	0.1169	1907	24	+0.2
12095-025.1	879	1361	203	0.15	0.83	14057	1.0E-5	32	0.02	406.2	0.045	5.574	1.5	0.3475	1.5	0.993	0.1163	1922	24	-1.3
12095-032.1	879	800	104	0.13	0.73	13587	2.0E-5	29	0.03	233.9	0.039	5.494	1.4	0.3406	1.4	0.988	0.1170	1911	23	+1.3
12095-051.1	879	1437	35	0.03	0.71	15658	3.3E-6	33	0.01	421.6	0.007	5.486	1.3	0.3415	1.3	0.992	0.1165	1904	3	+0.6
12095-036.1	879	928	115	0.13	0.42	13883	8.1E-5	23	0.05	273.5	0.038	5.528	1.4	0.3431	1.4	0.988	0.1168	1902	23	+0.4
12095-055.1	879	932	129	0.14	0.38	13702	1.6E-5	30	0.03	271.1	0.042	5.458	1.4	0.3386	1.3	0.989	0.1169	1910	22	+1.8
12095-056.1	879	962	138	0.15	0.63	13618	8.4E-6	41	0.01	280.6	0.046	5.483	1.4	0.3397	1.4	0.990	0.1171	1912	22	+1.6
12095-061.1	879	858	54	0.06	0.59	11355	1.6E-5	32	0.03	253.4	0.019	5.524	1.3	0.3437	1.3	0.986	0.1166	1905	21	0.0

Table A-2. (cont.)

Spot name	IP#	U (ppm)	Th (ppm)	Th/U ± Th/U (ppm)	Yb (ppm)	Hf (ppm)	$\frac{^{204}\text{Pb}}{^{206}\text{Pb}} \pm \frac{^{204}\text{Pb}}{^{206}\text{Pb}}$	$f(206)^{204}$	$\frac{^{206}\text{Pb}^*}{^{206}\text{Pb}}$ (ppm)	$\frac{^{208}\text{Pb}^*}{^{206}\text{Pb}}$	$\frac{^{207}\text{Pb}}{^{206}\text{Pb}} \pm \frac{^{207}\text{Pb}}{^{206}\text{Pb}}$	$\frac{^{206}\text{Pb}}{^{238}\text{U}}$	$\frac{^{207}\text{Pb}}{^{206}\text{Pb}} \pm \frac{^{207}\text{Pb}}{^{206}\text{Pb}}$	$\frac{^{206}\text{Pb}}{^{238}\text{U}}$	$\frac{^{207}\text{Pb}}{^{206}\text{Pb}} \pm \frac{^{207}\text{Pb}}{^{206}\text{Pb}}$	Disc. (%)									
14NK-M057A																									
11406-005.1	778	3117	105	0.03	0.60	253	13779	4.2E-5	34	0.07	924.7	0.011	6.2	5.641	1.2	0.3454	1.1	0.968	0.1185	0.3	1912	19	1933	5	+1.2
11406-009.1	778	5697	240	0.04	1.78	727	14051	2.7E-4	3	0.47	1618.5	0.014	2.4	5.253	1.1	0.3307	1.1	0.983	0.1152	0.2	1842	18	1893	4	+2.5
11406-013.1*	778	2117	30	0.01	1.01	525	16351	-1.6E-6	71	0.00	640.9	0.004	4.8	5.680	1.1	0.3525	1.0	0.846	0.1169	0.6	1946	16	1909	11	-2.3
11406-019.1*	778	2566	135	0.05	0.40	571	14718	4.6E-15	9999	0.00	813.2	0.016	1.8	5.966	0.9	0.3689	0.8	0.929	0.1173	0.3	2024	14	1915	6	-6.6
11406-021.1	778	2806	633	0.23	2.21	94	15628	2.4E-5	17	0.04	836.0	0.070	2.0	5.716	0.8	0.3468	0.8	0.985	0.1195	0.1	1919	14	1949	3	+1.8
11406-031.1	778	2812	182	0.07	3.12	148	13901	3.2E-5	12	0.06	846.9	0.020	2.3	5.756	1.8	0.3506	1.8	0.978	0.1191	0.4	1938	30	1942	7	+0.3
11406-033.1	778	545	208	0.39	4.11	127	9673	1.5E-4	11	0.26	168.4	0.125	1.4	5.571	2.7	0.3383	2.6	0.994	0.1194	0.3	1879	43	1948	5	+4.1
11406-035.1	778	607	260	0.44	0.29	169	11132	8.1E-6	50	0.01	180.8	0.136	1.3	5.684	0.9	0.3471	0.9	0.953	0.1188	0.3	1921	14	1938	5	+1.0
11406-035.1.2	778	703	293	0.43	0.22	205	10316	7.0E-5	16	0.12	203.8	0.128	1.1	5.491	1.8	0.3376	1.8	0.983	0.1179	0.3	1875	29	1925	6	+3.0
11406-043.1	778	3991	109	0.03	0.36	414	15111	6.0E-6	20	0.01	1215.7	0.009	1.8	5.762	1.3	0.3546	1.3	0.998	0.1178	0.1	1957	22	1924	1	-2.0
11406-048.1	778	3137	228	0.08	1.59	752	12797	6.0E-7	71	0.00	994.6	0.022	2.9	6.042	1.2	0.3691	1.1	0.944	0.1187	0.4	2025	20	1937	7	-5.3
11406-048.2	778	1165	114	0.10	1.57	356	12573	6.4E-6	41	0.01	363.2	0.031	3.7	5.761	1.4	0.3528	1.4	0.970	0.1184	0.3	1948	23	1933	6	-0.9
11406-049.1	778	3196	85	0.03	2.35	188	14120	2.4E-4	4	0.42	916.7	0.007	14.0	5.369	1.0	0.3339	0.9	0.965	0.1166	0.3	1857	15	1905	5	+2.9
11406-050.1	778	371	175	0.49	0.66	157	10674	1.2E-5	50	0.02	110.3	0.148	1.5	5.716	1.2	0.3459	1.2	0.963	0.1199	0.3	1915	20	1954	6	+2.3
11406-064.1	778	901	139	0.16	21.43	220	13143	3.8E-6	71	0.01	275.9	0.048	4.3	5.821	0.9	0.3563	0.9	0.967	0.1185	0.2	1965	15	1933	4	-1.9
11406-065.1	778	973	150	0.16	0.56	224	13069	-5.0E-6	71	-0.01	287.9	0.047	2.5	5.617	0.9	0.3443	0.9	0.940	0.1183	0.3	1907	15	1931	6	+1.4
11406-066.1*	778	2100	61	0.03	3.04	417	15341	1.9E-15	9999	0.00	638.8	0.009	2.2	5.739	1.3	0.3541	1.3	0.996	0.1175	0.1	1954	21	1919	2	-2.1
11406-075.1	778	3151	33	0.01	6.66	665	15125	6.2E-6	78	0.01	970.4	0.004	8.2	5.968	1.0	0.3585	0.9	0.947	0.1207	0.3	1975	16	1967	6	-0.5
11406-076.1	778	3956	87	0.02	0.74	565	17491	3.5E-4	10	0.60	1188.3	0.007	24.3	5.743	1.2	0.3497	1.1	0.882	0.1191	0.6	1933	18	1943	10	+0.6
11406-083.1	778	2711	148	0.06	0.96	108	11602	6.8E-4	7	1.17	846.9	0.013	21.2	5.955	2.0	0.3636	1.9	0.934	0.1188	0.7	1999	33	1938	13	-3.7
11406-085.1	778	6556	565	0.09	4.42	1070	14077	1.8E-4	5	0.31	2036.0	0.026	3.5	5.869	1.0	0.3615	0.9	0.942	0.1177	0.3	1989	16	1922	6	-4.1
11406-086.1	778	1613	698	0.45	2.55	331	9912	2.7E-6	45	0.00	477.8	0.136	2.0	5.577	1.3	0.3448	1.2	0.954	0.1173	0.4	1910	21	1916	7	+0.4

Spot name follows the convention x-y-z; where x = sample number, y = grain number, and z = spot number. Multiple analyses in an individual spot are labelled as x-y-z-z.

Spot labels in bold font were used in age calculation. Asterisks identify low common Pb-analyses.

IP# refers to mount and session number.

Uncertainties are reported at 1 σ and are calculated by numerical propagation of all known sources of error using SQUID2 version 2.5. Uncertainties in ages are 1 σ absolute in Ma.

$f(206)^{204}$ refers to mole fraction of total ^{206}Pb that is due to common Pb, calculated using the ^{204}Pb -method; common-Pb composition used is the surface blank

* refers to radiogenic Pb (corrected for common Pb)

9999 is used in calculations to approximate value approaching infinite error

Corr Coeff = Correlation coefficient

Discordance (Disc.) relative to origin = $100 \cdot (1 - \frac{^{206}\text{Pb}}{^{238}\text{U}} / \frac{^{207}\text{Pb}}{^{206}\text{Pb}} \text{ age})$

Calibration standard z6266; U = 910 ppm; Yb = 69.85; Hf = 8100 ppm; age = 559 Ma; $\frac{^{206}\text{Pb}}{^{238}\text{U}} = 0.09059$

Sessional calibration uncertainties are as follows (internal added to each analysis, external uncertainty of calibration):

Session IP778: 0.83%, 0.25%; IP879: 1.26%, 0.4%; IP781: 0.8%, 0.18%; IP863: 1.58, 0.38%

Th/U calibration: F = 0.03900 \cdot UO + 0.85600

All analyses with a ~16 μm spot size except for sample 11411 at 12 μm

$^{207}\text{Pb}/^{206}\text{Pb}$ ratios were monitored by sessional analyses of reference zircon z1242 with an age of 2679 Ma. IP778: 2678 \pm 3 Ma; IP879: 2682 \pm 4 Ma; IP863: 2681 \pm 6 Ma; IP781: 2676 \pm 4 Ma.

No instrumental mass fractionation (IMF) correction required except for session IP781 for which an IMF value of 1.003 was used.

Overview of the geology of the Montresor belt, Nunavut

J.A. Percival^{1*}, V. Tschirhart¹, and W.J. Davis¹

Percival, J.A., Tschirhart, V., and Davis, W.J., 2024. Overview of the geology of the Montresor belt, Nunavut; in Canada's northern shield: new perspectives from the Geo-mapping for Energy and Minerals program, (ed.) S.J. Pehrsson, N. Wodicka, N. Rogers, and J.A. Percival; Geological Survey of Canada, Bulletin 612, p. 159–162. <https://doi.org/10.4095/332498>

Abstract: The Montresor belt, Nunavut, was originally described as a synform of Paleoproterozoic metasedimentary rocks resting unconformably on Archean basement. Heterogeneous units of the lower Montresor group are imbricated with granitoid basement units. In the more homogeneous upper Montresor group, aeromagnetic patterns are interpreted to reflect distal polyphase deformation during the Trans-Hudson Orogeny, several phases of which have been recognized in the Montresor belt.

Résumé : La ceinture de Montresor, au Nunavut, a été décrite à l'origine comme une synforme de roches métasédimentaires du Paléoprotérozoïque reposant en discordance sur un socle archéen. Les unités hétérogènes du groupe de Montresor inférieur sont imbriquées avec des unités granitoïdes du socle. Dans le groupe de Montresor supérieur, plus homogène, les configurations aéromagnétiques seraient le reflet des effets distaux de la déformation polyphasée associée à l'orogénèse trans-hudsonienne, dont plusieurs phases ont été reconnues dans la ceinture de Montresor.

¹Geological Survey of Canada, 601 Booth Street, Ottawa, Ontario K1A 0E8

*Corresponding author: J.A. Percival (email: john.percival@nrcan-mcan.gc.ca)

Manuscript accepted December 8, 2022

Originally described as a synformal keel of Paleoproterozoic metasedimentary rocks unconformable on Archean basement (Frisch, 2000), the Montesor belt has a more complex history in light of modern geological and geophysical information. Similar to the Amer belt 100 km to the south (Patterson, 1986), heterogeneous units of the lower Montesor group (Percival et al., 2015a) are imbricated with granitoid basement units. In the more homogeneous upper Montesor group, aeromagnetic patterns are interpreted to reflect distal polyphase deformation during the Trans-Hudson Orogeny (Pehrsson et al., 2013; Percival and Tschirhart, 2017).

The Montesor group is considered part of the Rae cover sequence (Rainbird et al., 2010), a broad platformal basin deposited after the 2.5 to 2.3 Ga Arrowsmith Orogeny

(Berman et al., 2013) and affected by the 1.89 to 1.80 Ga Trans-Hudson Orogeny. A broadly correlative stratigraphic sequence has been deduced from deformed and metamorphosed units in the Montesor, Amer, and Ketyet River belts, although geochronological control is sparse and uncertainties remain (Jefferson et al., 2023; this volume).

Units of the lower Montesor group include quartz arenite, carbonate, and mudstone-wacke at greenschist to amphibolite facies, best exposed in a structural footwall complex at the northeastern margin of the belt (Fig. 1). Fault contacts preclude definition of stratigraphic relationships between these units, which also occur sporadically at the belt margins to the southwest (Percival et al., 2015b). In adjacent structural panels of the footwall complex, age constraints are

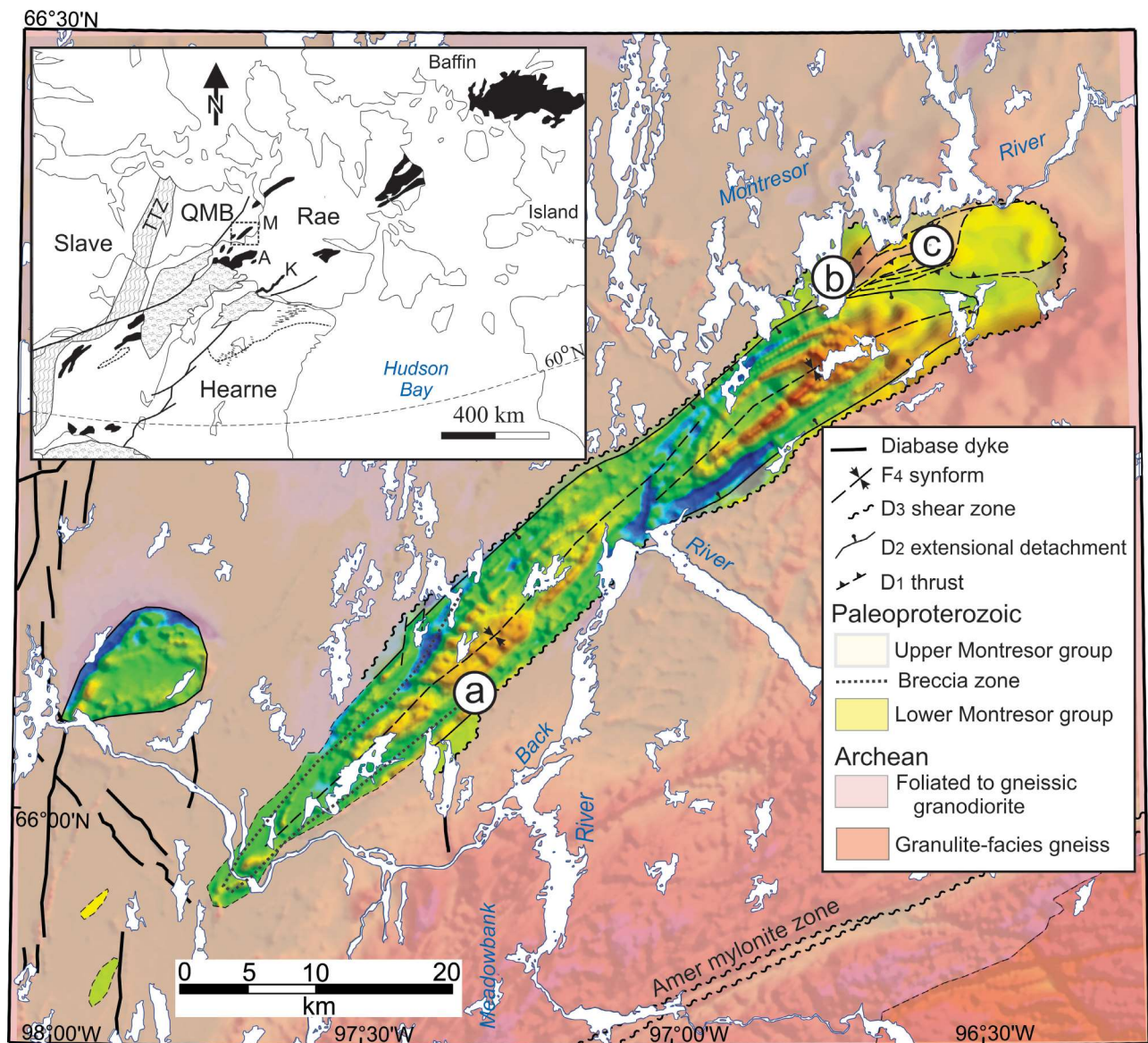


Figure 1. Generalized geology of the Montesor belt underlain by a reduced-to-pole, total field aeromagnetic map. Upper Montesor group is transparent. Locations a, b, and c refer to ongoing work described in text. Inset: black units are Rae cover sequence and probable correlative sequences: A = Amer belt; K = Ketyet River belt; M = Montesor belt; QMB = Queen Maud Block; TTV = Thelon tectonic zone.

provided by detrital zircons in quartz arenite, which yielded a maximum depositional age of 2194 ± 14 Ma (refined to 2189 ± 4 Ma; W.J. Davis, unpublished data), and a minimum age of 2045 ± 13 Ma provided by zircon in a gabbroic dyke cutting mudstone-wacke (Percival et al., 2017).

The upper Montresor group is dominated by massive to thinly laminated siltstone with minor dolomite at low metamorphic grade. Stratigraphic markers are not evident, but aeromagnetic anomalies match bedding trends and the regional synformal structure (Fig. 1). Positive anomalies correspond to heavy-mineral-rich layers (detrital apatite, magnetite, tourmaline, zircon). The youngest detrital zircon from one such bed yielded an age of 1924 ± 6 Ma, providing a maximum depositional age for the unit (Percival et al., 2017). Of the three age modes in the detrital zircon spectrum (3.8–3.1, 2.55–2.35, 2.05–1.924 Ga), all can be attributed to western Rae margin basement units to the west (Queen Maud Block, Sherman Basin, and Thelon magmatic suite, respectively (Davis et al., 2014, 2021)). In light of the western provenance, it is likely that these rocks were deposited just prior to the 1.92 to 1.89 Ga (Berman et al., 2018) pulse of Thelon tectonic zone magmatism.

Several phases of Trans-Hudson deformation have been recognized in the Montresor belt. The D_1 thrusts imbricated lower Montresor and basement units, as well as upper Montresor strata as interpreted from offsets of aeromagnetic markers. A synmetamorphic D_2 extensional detachment was inferred at the base of the upper Montresor, and D_3 shear zones bound the lower Montresor at its base. A close, north-dipping F_4 synform produced the present map pattern. Monazite in low-grade upper Montresor schist constrains metamorphism to 1848 ± 8 Ma, whereas monazite inclusions in peak-metamorphic (3 kbar, 575°C) garnet from a lower Montresor pelite have a range of ages between 1870 and 1837 ± 9 Ma (Dziawa et al., 2019).

Work continues on several aspects of Montresor geology (Fig. 1): breccia units at the southwestern end of the belt form an extensive pseudostratigraphic unit traceable as an aeromagnetic low (location a) (Tschirhart et al., 2015). Petrographic evidence indicates intense hydrothermal alteration and progressive overprinting of mineral assemblages amphibole \rightarrow albite \rightarrow k-feldspar-hematite. Trace-element analysis is planned to determine whether the zone might relate to an endowed IOCGU (iron-oxide-copper-gold-uranium) system; skarns consisting of diopside±tremolite occur in carbonate units within the footwall complex in the northeast (location b). Their origin and possible linkage to mineralized skarn systems are under investigation; impact spherules in mudstone of the footwall complex (location c) (Percival et al., 2021) provide evidence of a global event ca. 2.1 Ga. The nature and origin of the spherules, as well as their possible significance in Earth's atmospheric and biological evolution, continue to be explored.

ACKNOWLEDGMENTS

The authors wish to acknowledge S. Pehrsson for encouraging us to make this contribution, M. Plouffe for continued support, and GSC Scientific Publishing Services (P. Champagne, B. Couture, E. Inglis, N. Morisset, and S. Stewart) for editorial improvements.

REFERENCES

- Berman, R.G., Pehrsson, S., Davis, W.J., Ryan, J.J., Qui, H., and Ashton, K.E., 2013. The Arrowsmith Orogeny: geochronological and thermobarometric constraints on its extent and tectonic setting in the Rae Craton, with implications for pre-Nuna supercontinent reconstruction; *Precambrian Research*, v. 232, p. 44–69. <https://doi.org/10.1016/j.precamres.2012.10.015>
- Berman, R.G., Davis, W.J., Sanborn-Barrie, M., Whalen, J.B., Taylor, B.E., McMartin, I., ... Craven, J.A., 2018. Report of activities for the GEM-2 Chantrey–Thelon activity: Thelon Tectonic Zone project, Nunavut; Geological Survey of Canada, Open File 8372, 19 p. <https://doi.org/10.4095/306622>
- Davis, W.J., Berman, R.G., Nadeau, L., and Percival, J., 2014. U-Pb zircon geochronology of a transect across the Thelon tectonic zone, Queen Maud region, and adjacent Rae Craton, Kitikmeot region, Nunavut, Canada; Geological Survey of Canada, Open File 7652, 41 p. <https://doi.org/10.4095/295177>
- Davis, W.J., Sanborn-Barrie, M., Berman, R.G., and Pehrsson, S., 2021. Timing and provenance of Paleoproterozoic supracrustal rocks in the central Thelon tectonic zone, Canada: implications for the tectonic evolution of western Laurentia from ca. 2.1 to 1.9 Ga; *Canadian Journal of Earth Sciences*, v. 58, no. 4, p. 378–395. <https://doi.org/10.1139/cjes-2020-0046>
- Dziawa, C., Gaidies, F., and Percival, J., 2019. Conditions and timing of low-pressure-high-temperature metamorphism in the Montresor belt, Rae Province, Nunavut; *Canadian Journal of Earth Sciences*, v. 56, no. 6, p. 654–671. <https://doi.org/10.1139/cjes-2018-0184>
- Frisch, T., 2000. Precambrian geology of Ian Calder Lake, Cape Barclay, and part of Darby Lake map areas, south-central Nunavut; Geological Survey of Canada, Bulletin 542, 51 p., 2 sheets, scale 1:250 000. <https://doi.org/10.4095/211320>
- Jefferson, C.W., Rainbird, R.H., Young, G.M., White, J.C., Tschirhart, V., and Creaser, R.A., 2023. The Paleoproterozoic Amer supergroup, Amer fold belt, Nunavut: stratigraphy, structure, correlations, and uranium metallogeny; *Canadian Journal of Earth Sciences*, e-First. <https://doi.org/10.1139/cjes-2022-0077>
- Patterson, J.G., 1986. The Amer belt: remnant of an Aphebian foreland fold and thrust belt; *Canadian Journal of Earth Sciences*, v. 23, no. 12, p. 2012–2023. <https://doi.org/10.1139/e86-186>
- Pehrsson, S.J., Berman, R.G., and Davis, W.J., 2013. Paleoproterozoic orogenesis during Nuna aggregation: a case study of reworking of the Rae Craton, Woodburn Lake, Nunavut; *Precambrian Research*, v. 232, p. 167–188. <https://doi.org/10.1016/j.precamres.2013.02.010>

- Percival, J.A. and Tschirhart, V., 2017. Trans-Hudsonian far-field deformation effects in the Rae foreland: an integrated geological–3D magnetic model; *Tectonophysics*, v. 699, p. 82–92. <https://doi.org/10.1016/j.tecto.2017.01.021>
- Percival, J.A., Tschirhart, V., Ford, A., and Dziawa, C., 2015a. Report of activities for geology and mineral potential of the Chantrey–Thelon area: GEM-2 Montresor project; Geological Survey of Canada, Open File 7707, 15 p. <https://doi.org/10.4095/295673>
- Percival, J.A., Tschirhart, V., Davis, W.J., Berman, R.G., and Ford, A., 2015b. Geology, Montresor River area, Nunavut, parts of NTS 66-H and NTS 66-I; Geological Survey of Canada, Canadian Geoscience Map 231 (preliminary edition), scale 1:100 000. <https://doi.org/10.4095/296915>
- Percival, J.A., Davis, W.J., and Hamilton, M.A., 2017. U–Pb zircon geochronology and depositional history of the Montresor group, Rae Province, Nunavut, Canada; *Canadian Journal of Earth Sciences*, v. 54, no. 5, p. 512–528. <https://doi.org/10.1139/cjes-2016-0170>
- Percival, J.A., Davis, B., Berman, R., Petts, D., Jackson, S., Harrison, M., and Bell, E., 2021. Impact spherules in ca. 2.1 Ga black shale of the Montresor belt, Nunavut: significance in early Paleoproterozoic history; *GAC–MAC 2021 Abstracts*, v. 44, no. 4; *Geoscience Canada*, v. 48, p. 221–222. <https://doi.org/10.12789/geocanj.2021.48.181>
- Rainbird, R.H., Davis, W.J., Pehrsson, S.J., Wodicka, N., Rayner, N., and Skulski, T., 2010. Early Paleoproterozoic supracrustal assemblages of the Rae Domain, Nunavut, Canada: intracratonic basin development during supercontinent break-up and assembly; *Precambrian Research*, v. 181, no. 1-4, p. 167–186. <https://doi.org/10.1016/j.precamres.2010.06.005>
- Tschirhart, V., Percival, J.A., and Jefferson, C.W., 2015. Geophysical models of the Montresor metasedimentary belt and its environs, central Nunavut, Canada; *Canadian Journal of Earth Sciences*, v. 52, no. 10, p. 833–845. <https://doi.org/10.1139/cjes-2015-0008>

Geology and metallogeny of the northeast Thelon Basin region, Nunavut, and comparison with the Athabasca Basin, Saskatchewan

C.W. Jefferson^{1*}, S.J. Pehrsson¹, V. Tschirhart¹, T.D. Peterson¹, L.B. Chorlton¹, K.M. Bethune², J.C. White³, W.J. Davis¹, V.J. McNicoll¹, R.C. Paulen¹, and N. Rayner¹

Jefferson, C.W., Pehrsson, S.J., Tschirhart, V., Peterson, T.D., Chorlton, L.B., Bethune, K.M., White, J.C., Davis, W.J., McNicoll, V.J., Paulen, R.C., and Rayner, N., 2024. Geology and metallogeny of the northeast Thelon Basin region, Nunavut, and comparison with the Athabasca Basin, Saskatchewan; in Canada's northern shield: new perspectives from the Geo-mapping for Energy and Minerals program, (ed.) S.J. Pehrsson, N. Wodicka, N. Rogers, and J.A. Percival; Geological Survey of Canada, Bulletin 612, p. 163–281. <https://doi.org/10.4095/332499>

Abstract: Based on extensive remapping of the northeast Thelon Basin region in Nunavut, uranium exploration criteria are adapted from those of the Athabasca Basin in Saskatchewan, as basin-specific paradigms. The Athabasca Basin straddles the Rae and Hearne cratons and the Taltson magmatic zone, whereas the Thelon Basin rests entirely within the Rae Craton. In the Athabasca Basin, four unconformity-bounded siliciclastic sequences with different paleocurrents record a complex depositional history, whereas the Thelon Formation is a single, albeit cyclic siliciclastic unit with unimodal paleocurrents. Beneath the Athabasca Basin, amphibolite-grade, conductive graphitic-pyritic-Paleoproterozoic units localize all major deposits. Conductor analogues below the Thelon Basin are barren, impermeable, black slate of anchizone to lower-greenschist-facies grade. Instead, the Thelon uranium deposit host rocks are Neoproterozoic pyritic greywacke and epiclastic rocks that range in metamorphic grade from lower- to upper-amphibolite facies. Similar mineralogical sources, saline brines, alteration (fluorapatite, aluminum-phosphate-sulphate minerals, chlorite, clays, and desilicification), and reactivated intersecting faults focused unconformity-type uranium mineralization in each basin. Previously published ages for pre-ore fluorapatite cements of the Athabasca and Thelon basins (1638 versus 1688 to 1667 Ma, respectively) reaffirm their independent diagenetic–hydrothermal histories.

Résumé : En se fondant sur une recartographie étendue de la partie nord-est de la région du bassin de Thelon, au Nunavut, nous avons adapté les critères d'exploration de l'uranium propres au bassin d'Athabasca, en Saskatchewan, pour qu'ils soient spécifiques aux particularités du bassin de Thelon. Le bassin d'Athabasca chevauche les cratons de Rae et de Hearne ainsi que la zone magmatique de Taltson, alors que le bassin de Thelon repose entièrement à l'intérieur des limites du craton de Rae. Dans le bassin d'Athabasca, quatre séquences silicoclastiques délimitées par des discordances révélant des paléocourants variables témoignent d'une histoire sédimentaire complexe, alors que la Formation de Thelon est une unité silicoclastique unique, bien que cyclique, dévoilant des paléocourants unimodaux. Tous les grands gisements situés sous le bassin d'Athabasca sont confinés à des unités graphitiques-pyriteuses conductrices, qui sont métamorphosées au faciès des amphibolites et remontent au Paléoprotérozoïque. Des zones conductrices analogues sous le bassin de Thelon sont formées d'ardoise noires stériles, imperméables, qui présentent un degré de métamorphisme variant de l'anchizone au faciès des schistes verts inférieur. Par ailleurs, les roches hôtes des gîtes d'uranium du bassin de Thelon sont des grauweekes pyriteux et des roches époclastiques du Néoproterozoïque dont le degré de métamorphisme varie de la partie inférieure à la partie supérieure du faciès des amphibolites. Des sources minéralogiques, des saumures salines et des altérations (fluorapatite, minéraux de phosphate-sulfate d'aluminium, chlorite, argiles et désilicification) semblables ainsi que des failles transversales réactivées ont concentré la minéralisation uranifère de type gîte associé à une discordance dans chaque bassin. Les âges publiés antérieurement pour les ciments de fluorapatite antérieurs à la minéralisation dans les bassins d'Athabasca et de Thelon (1638 Ma dans le premier cas et de 1688 à 1667 Ma dans le second) confirment de nouveau l'indépendance de l'histoire diagénétique-hydrothermale de chacun des bassins.

¹Geological Survey of Canada, 601 Booth Street, Ottawa, Ontario K1A 0E8

²Department of Geology, University of Regina, 3737 Wascana Parkway, Regina, Saskatchewan S4S 0A2

³Department of Geology, University of New Brunswick, P.O. Box 4400, Fredericton, New Brunswick E3B 5A3

*Corresponding author: C.W. Jefferson (email: charlie.jefferson@nrcan-mcan.gc.ca)

INTRODUCTION

Guiding hypothesis

The Uranium project, begun in 2009 as part of the first phase of the Geo-Mapping for Energy and Minerals (GEM-1) program, was guided by the following hypothesis: “Can exploration criteria from the Athabasca Basin such as hydrothermal alteration, reactivated faults, and basement geology be adapted to the poorly explored Thelon and other northern Paleoproterozoic basins?” (Fig. 1; Jefferson et al., 2011a, b, c). This study focuses on new knowledge of the Thelon Basin, with a review of Athabasca Basin knowledge for comparison. Such exploration criteria embrace

the geological, geophysical, and geochemical knowledge required to understand the source-transport-trap attributes of unconformity-related uranium deposits in the Athabasca and correlative basins (e.g. Miller and LeCheminant, 1985; Gandhi, 1989; Kyser et al., 2000; Renac et al., 2002; Jefferson et al., 2007a, b, c; Alexandre et al., 2009; Cuney and Brisbin, 2010). The aim of this project was to bring such knowledge of the Thelon Basin closer to that gathered on the Athabasca Basin and now well beyond that summarized in Jefferson and Delaney (2007). The study region (Fig. 2, 3a) comprises a large area of basement rocks surrounding and underlying the northeast Thelon Basin, as well as its main basin fill, the Thelon Formation, and its cover.

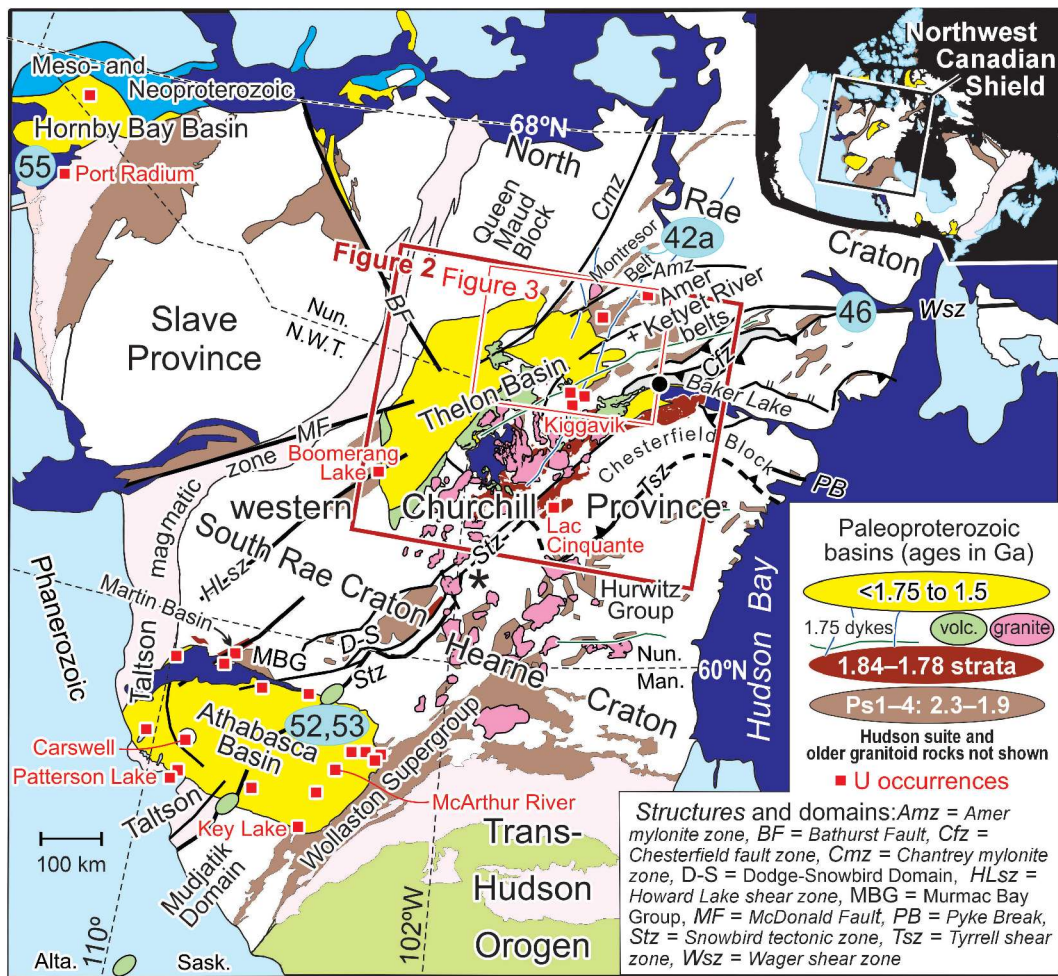


Figure 1. Context of the Dubawnt Supergroup (brown, green, and yellow units within the bold red outline of Fig. 2), whose stratigraphy is detailed in Figure 4a. Its lower unit, the Baker Lake Group (dark brown), hosts the Lac Cinquante uranium deposit (labelled) and roughly equates to the Martin group north of the Athabasca Basin. The middle, Wharton Group (pale green) includes the volcanic (volc.) component of the 1.75 Ga Kivalliq igneous suite that also has equivalents beneath the Athabasca Basin. The upper, Barrenland Group (yellow) fills the Thelon Basin, roughly equivalent to the Athabasca Basin. Numbered blue circles are geochronology sites outside of Figure 2 that are listed in Table 2. Asterisk (*) denotes 1.75 Ga Nueltin granite pancakes overlying Snowbird tectonic zone faults and fault intersections. *Adapted from* Jefferson et al. (2013), with selected data from Sanborn-Barrie et al. (2014), Lawley et al. (2016), Regis et al. (2017), Wodicka et al. (2017), Therriault et al. (2018), and Therriault (2019).

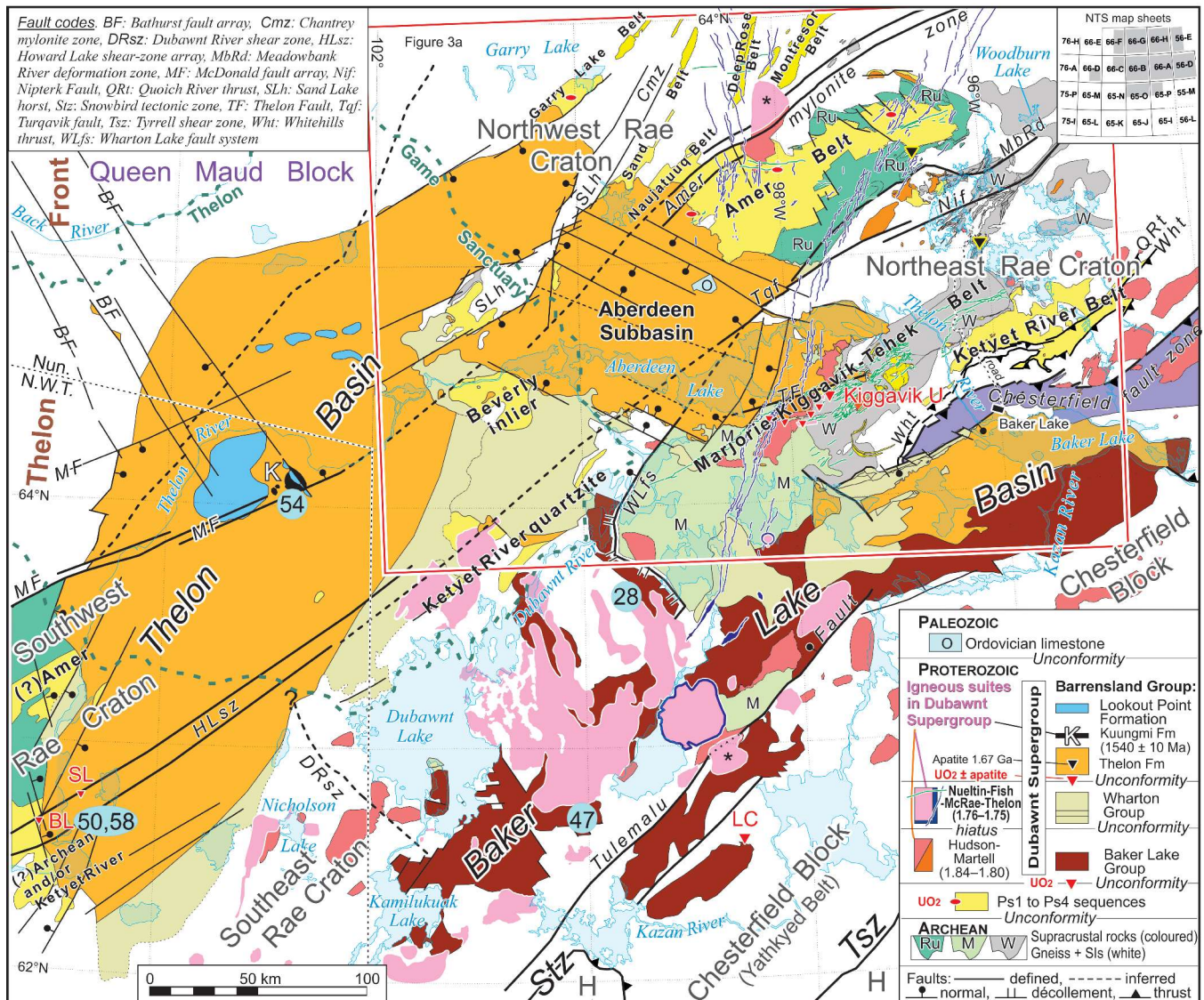


Figure 2. Geology and selected mineral occurrences of the Dubawnt Supergroup region, Nunavut (geology after Tella et al., 2005; Rainbird et al., 2007; Jefferson et al., 2011c; Pehrsson et al., 2014a; and Skulski et al., 2018). Uranium occurrences are labelled in the most detailed figures that show them; Boomerang Lake (BL), Lac Cinquante (LC), Screech Lake (SL) are shown here. In unit legend and on map, Woodburn Lake group (W) is represented undivided, except the Rumble (Ru) and Aberdeen assemblages; the latter is part of the Marjorie (M) terrane, shown undivided here. Also shown are the Hearne Craton (H) and Snow Island suite (SIs). Faults are labelled in the more detailed figures, except those in upper left legend. Numbered blue circles outside the area of Figure 3a (red rectangle) are geochronology sites listed in Table 2. Asterisk (*) denotes 1.75 Ga Nueltin granite pancakes overlying faults. Shading in NTS key = study area.

Definitions of geological areas of focus and terminology

Geological areas of focus

Data acquisition in the study area was designed to improve understanding of uranium metallogeny on a regional scale, to provide context for site-specific studies of unconformity-related and other types of uranium deposits (see ‘Previous and parallel studies’ section). One of the

most important aspects of these complex uranium deposits is basement geology (e.g. Jefferson et al., 2007a, b, c; Cuney, 2010; Cuney and Brisbin, 2010). Knowledge of the basement geology is as paramount for exploration beneath the Thelon Basin as it is beneath the Athabasca Basin, especially because the only significant occurrences in the Thelon Basin region are within basement rocks at or near the surface (Miller and LeCheminant, 1985; Fuchs and Hilger, 1989; Hunter et al., 2012, 2014; Grare et al., 2018). Therefore, a comprehensive regional mapping approach was taken

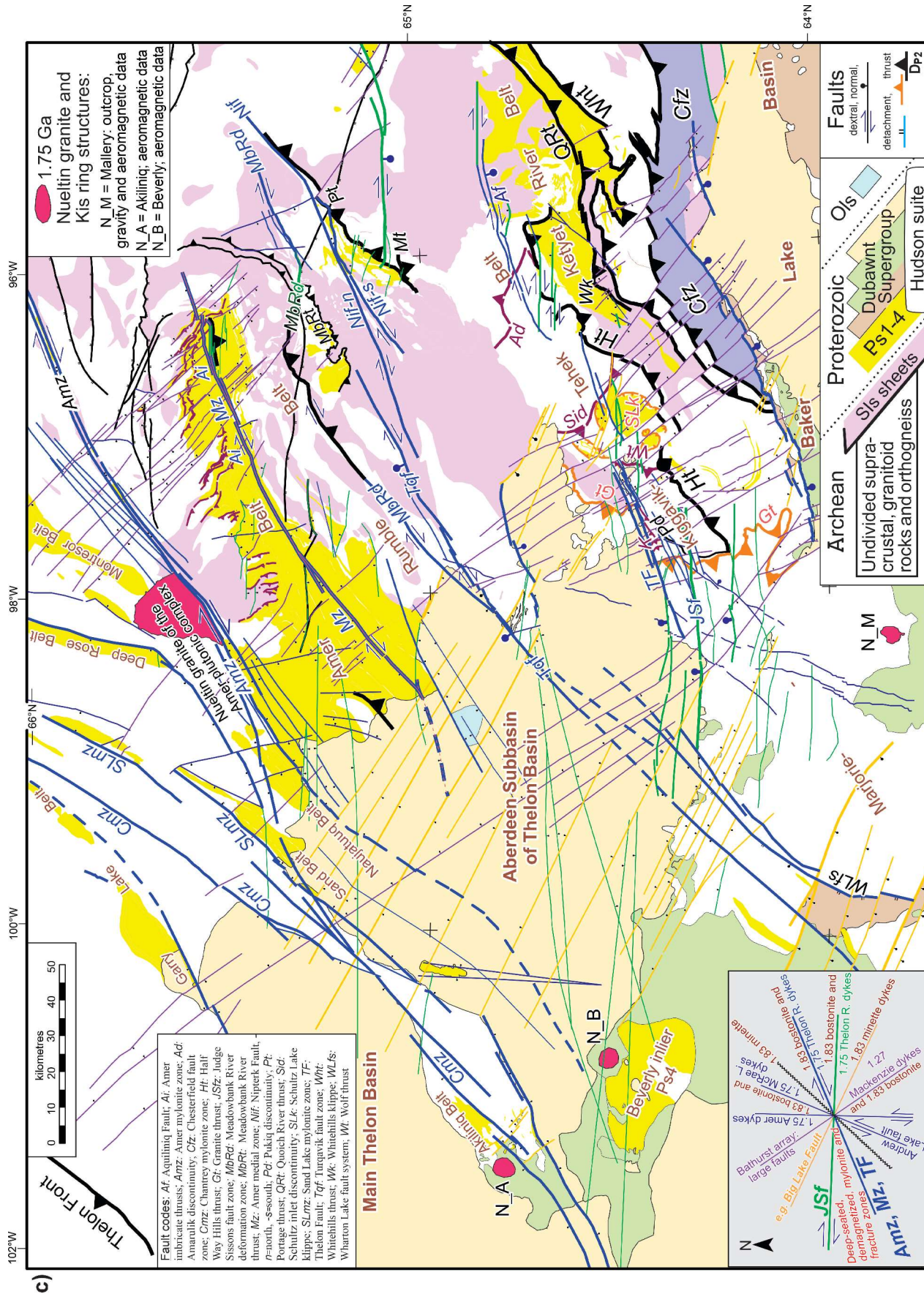


Figure 3. (cont.) c) Faults and 1.75 Ga ring structures of the Aberdeen Subbasin region in the same area as Figures 3a and 3b. Faults are colour coded to the Riedel-shear schema (lower left, explained in Fig. 9 and text). The areas of Snow Island suite selectively shown here are mainly laterally extensive tectonic sheets, including klippe, in the order of hundreds of metres to several kilometres thick. Kis = Kivalliq igneous suite, Ols = Ordovician limestone.

in this study to achieve new contiguous integrated geoscience maps for four full NTS map sheets and parts of eight additional map sheets (56-D W, 56-E W, 65-O N, 65-P NW, 66-A, 66-B, 66-C NE, 66-D SE, 66-F E, 66-G, 66-H; Fig. 2) at scales ranging from 1:250 000 to 1:1000. Selected, variably detailed maps of localities with exceptional exposures enhanced thematic knowledge that led to a better understanding of basement-hosted uranium deposits as well as of the entire geological and resource endowment of this overall poorly exposed region.

Because the Thelon Game Sanctuary covers most of the Thelon Basin (Fig. 2, 3a), the only parts of the Thelon Basin that are available for uranium research and exploration are at the southern tip and in the northeastern part of the basin. The Aberdeen Subbasin is defined here as the northeastern part of the Thelon Basin around Aberdeen Lake, separated from the main Thelon Basin by the Sand Lake horst and extending eastward as far as Schultz Lake. In these studies, the geological framework of the Aberdeen Subbasin and its surrounding region, all transected by the lower portion of the Thelon River, has been updated, hence the use of the generalized term ‘northeast Thelon Basin region’ (Fig. 3a).

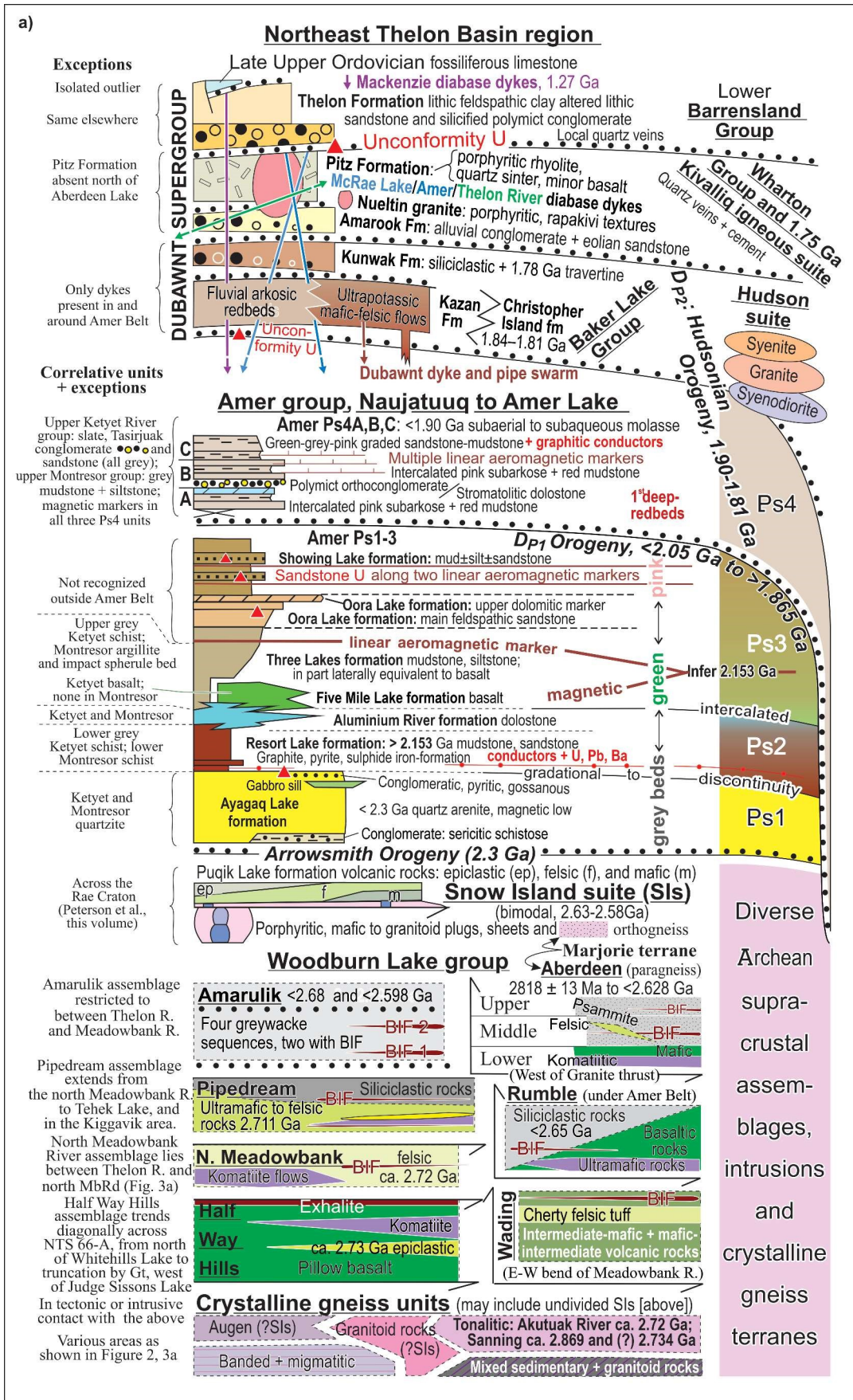
Much of the early exploration in the Aberdeen Subbasin targeted conductors of the Amer group that extend under the Thelon Formation (e.g. Young, 1979). The Amer Belt is here defined as a northeast-trending grand synform of post-Archean, pre-1.83 Ga strata (cover sequences Ps1 through Ps4, Fig. 3a, 4a (see ‘New developments in geology of the northeast Thelon Basin region’ section) that extends from near Meadowbank River in the northeast, to the Beverly Lake area in the southwest. The original contiguous exposure of the grand synform as outlined by Tella (1984, 1994) extends from the northern side of the Aberdeen Subbasin to a broad closure, halfway between upper and lower Amer Lake and the northern portion of Meadowbank River. Tschirhart et al. (2014, 2017) and Jefferson et al. (2015) traced the grand synform continuously beneath the Aberdeen Subbasin to where it emerges in the Beverly inlier, south of Beverly Lake and along the banks of the Thelon River. There it was described by LeCheminant et al. (1984) in some detail. At its broadest point along the northern edge of the Aberdeen Subbasin, the Amer grand synform extends 70 km from the Neoproterozoic Rumble Belt (see ‘Woodburn Lake group: Neoproterozoic supracrustal rocks’ section) to the western side of the contiguous Nauyasuq Belt.

The Amer mylonite zone delimits the northwestern side of the grand synform between there and the Amer plutonic complex. The Amer Belt necks to about 15 km southwest of upper and lower Amer Lake and broadens across a major 145° normal fault to a width of 30 km, spanning lower and upper Amer Lake. The Rumble assemblage wraps around the northeastern closure of the synclinorium in outcrop, and underlies its northeastern (Tschirhart et al., 2013d) and broadest (Tschirhart et al., 2014) portions at depth. Across its broadest point, the grand synform comprises three major synforms and two culminations. Of these, Tschirhart et al. (2014) modelled the flat-bottomed Tahiratuaq synform, the complex Quartzite culmination, and part of the R22 synform northwest of the culmination (Fig. 3a). These two second-order synforms, separated by a complex antiformal culmination, extend the length of the Amer grand synform, as mapped by Jefferson et al. (2015) throughout the outcrop area and by Tschirhart et al. (2014, 2017) in the subsurface.

The Ketyet River Belt comprises large to small, contiguous to structurally isolated areas of post-Archean to pre-1.83 Ga strata that extend from the Judge Sissons (JS, Fig. 3a, c) pluton in the southwest, through the Schultz Lake klippe, to the Quoich River area in the northeast. The belt includes structural slivers in the Akutuak River gneiss and a number of outliers tightly infolded with Archean units as far northwest as the Meadowbank River deformation zone (Fig. 3a, c). It has many stratigraphic and structural similarities with the Amer Belt (see ‘Early Paleoproterozoic cover sequences: Amer, Ketyet River, Montresor, and western belts’ section), but does not extend under the Thelon Formation to any great extent.

Frisch (1992, 2000) mapped the Montresor Belt as a single large synform of Paleoproterozoic strata from a sharp cutoff at the Back River, northwestward about 70 km to a bend in the Montresor River. Maps by Percival et al. (2015b, 2017, 2019) show that the northeastern part of the lower Montresor group is a basement-involved imbricate zone that is also folded as part of the northeastern closure of this synform. Other studies by Tella (1994), Tschirhart et al. (2015), and Pilkington and Tschirhart (2017) support the overall configuration of Frisch (2000). Jefferson et al. (2015) mapped the southwestern extension of the Montresor Belt from the Back River to as far as the Nueltin granite of the Amer plutonic complex. The methods used to map that

Figure 4. a) Stratigraphic column (not to scale) of the northeast Thelon Basin region (Fig. 2, 3a). The upper portion, ‘Northeast Thelon Basin region’ outlines the Dubawnt Supergroup within the area of Figure 2. The middle portion, ‘Amer group, Nauyasuq to Amer Lake (after Jefferson et al., 2023), applies to the northern portion of Figures 3a–c, with correlation notes pertaining to the Ketyet River Belt (southern portion of Fig. 3a, b) and the Montresor Belt (northern portion of Fig. 2, 3a, b). The lower portions: ‘Snow Island suite’, ‘Woodburn Lake group’, and ‘Crystalline gneiss units’, apply to the entire study region (Fig. 2, 3a) and include new data from Hunter et al. (2018) for the Aberdeen assemblage of the Woodburn Lake group. The Marjorie terrane is defined in the text. The four Woodburn Lake group assemblages on the left are in geochronological and structural order, whereas those on the right are too poorly known or too complex to place in order. Tables 1 and 2 provide descriptions and references for all of these units and correlations, with selected aspects discussed further in the text. BIF = banded iron-formation, Gt = Granite thrust, MbRd = Meadowbank River deformation zone.



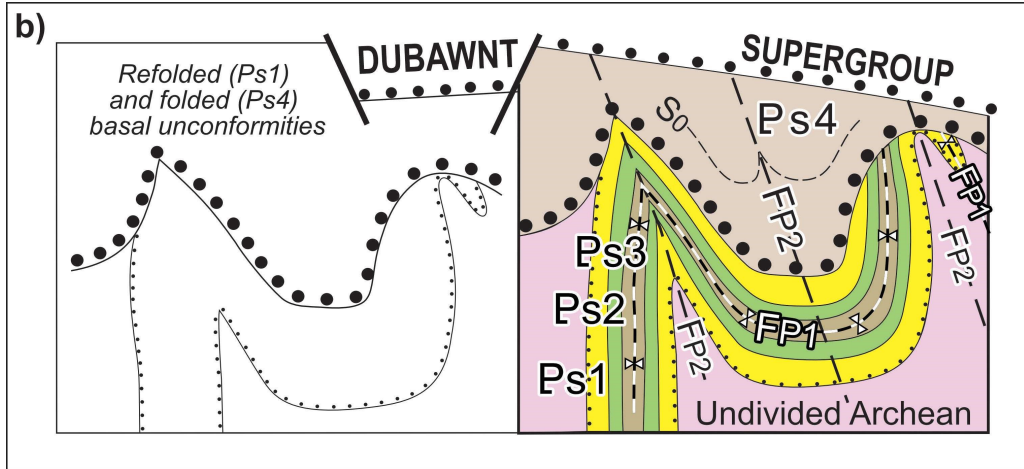


Figure 4. (cont.) b) Structural-stratigraphic schema for the first two major folding events (F_{P1} and F_{P2}) in the northeast Thelon Basin region (Fig. 2, 3a). For explanation of how this schema helps differentiate the early Paleoproterozoic stratigraphic sequences Ps1, Ps2, and Ps3 from Ps4 shown in part a), see ‘Structure and metamorphism’ section.

extension are detailed under ‘Sequences Ps1, Ps2, Ps3, and Ps4 in the Ketyet River, Montresor, and western belts’ section below.

Stratigraphic units and structures like those of the southwestern Montresor Belt are exposed in the Akiliniq, Deep Rose, Garry Lake, Naujatuuq, and Sand belts. The Garry Lake, Naujatuuq, and Sand belts all extend beneath the Thelon Formation and their sequence Ps4 units host conductors. The Naujatuuq Belt, being contiguous with the western Amer Belt across the Amer mylonite zone, serves as a type locality for the uppermost Amer group unit, as well as a lithological look-alike of the upper Montresor group (see ‘Early Paleoproterozoic cover sequences: Amer, Ketyet River, Montresor, and western belts’ section). Although Tella (1994) mapped much of the Naujatuuq Belt as ‘quartzite’, it is mainly pinkish grey-green, fine-grained sandstone to siltstone rhythmites. Although narrow units of sequence Ps1 quartzite overlain by sequence Ps2 schist flank these belts, the bulk of their strata are rhythmically graded, fine-grained sandstone to mudstone characteristic of sequence Ps4 and include graphitic conductors previously thought to be restricted to sequence Ps2.

The Schultz Lake intrusive complex (SLic, Fig. 3a) is a frequently referenced landmark feature for many facets of this study. It is a massive, gently northwest-dipping laccolith of Hudson suite granite and Martell syenite hundreds of metres thick that forms three large rectilinear surface exposures over a 150 km long, southwest trend from Tebesjuak Lake in the southwest to Schultz Lake in the northeast (Fig. 3a). Miller and Peterson (2015) detailed it extensively in outcrop and petrogenetically, and Tschirhart et al. (2013b) configured it geographically and structurally by integrated geological-geophysical modelling constrained by outcrop

lithology and rock property data (for details on its age and host rocks, see ‘Marjorie terrane’ and ‘Hudson suite’ sections below).

Because the only significant unconformity-related uranium deposits known in the northeast Thelon Basin region are hosted by Neoproterozoic supracrustal rocks (above), it is of paramount importance to understand these belts not only in outcrop, but also where they extend beneath the Aberdeen Subbasin. Three such Neoproterozoic supracrustal belts are defined below (see ‘Woodburn Lake group: Neoproterozoic supracrustal rocks’ section): the ca. 2.71 Ga Pipedream assemblage, the ca. 2.65 Ga Rumble assemblage, and the ca. 2.75–2.60 Ga Aberdeen assemblage (after Aberdeen Lake supracrustal belt of Hunter et al., 2018) that was intruded by, and is structurally intercalated with, 2.6 Ga Snow Island suite orthogneiss (Hunter et al., 2021) as part of the Marjorie terrane.

Terminology

Terminology of sedimentary and metasedimentary rocks varies herein depending on the purpose and context of the description. Units are described mainly in terms of field appearance. Metamorphic terms include ‘quartzite’ for highly indurated and vitreous quartz arenite or even feldspathic or lithic quartz arenite, as in the Archean sequences and sequence Ps1. The term ‘quartzite’ is used for vitreous-appearing metamorphosed quartz arenite, where bedding is generally transposed and difficult to discern without close observation. ‘Quartzite’ is not used to refer to any other metamorphosed sandstone, such as metagreywacke or metaarkose. In the case of fine-grained metasedimentary rocks, the same unit may in places be described as mudstone, slate,

phyllite, or schist depending on its appearance, state of metamorphic recrystallization, and the degree of preservation of primary features.

‘Strata’ is an even more generalized term, referring to all stratified earth materials, including carbonate and unconsolidated sediment such as till and varved clay. The term ‘siliciclastic strata’ refers to an undivided range of clastic sedimentary rocks ranging from conglomerate to mudstone in grain size, and from alluvial to eolian to turbiditic in depositional setting. Siliciclastic strata can range from highly deformed to flat lying, and from unmetamorphosed to paragneissic, providing there is sufficient diagnostic information to indicate a sedimentary origin with some certainty.

The term ‘sandstone’ generally refers to medium-grained siliciclastic rocks with high proportions of feldspar, lithic fragments and/or clay. Weakly deformed to undeformed sandstone, preserved well enough to recognize primary sedimentary structures, is described mainly by its composition (e.g. quartz arenite for a sandstone with greater than 90% detrital quartz). Lithic feldspathic sandstone has less than 90% detrital quartz and subequal proportions of rock fragments and feldspar in the framework. Both quartz arenite and lithic feldspathic sandstone are present in sequence Ps4 of the Amer Belt and quartz arenite predominates in the younger Amarook Formation, whereas only the clay-altered feldspathic lithic arenite is present in the Thelon Formation. Maroon desiccation-cracked mudstone, siltstone, and pink sandstone are common components of sequence Ps4 and younger strata, but rare in older strata. Some older siliciclastic strata, for example in the Showing Lake formation, are salmon-pink on weathered surfaces but grey-green internally — these are not redbeds.

‘Greywacke’ is used for all grey, compositionally immature siliciclastic rocks that generally have recognizable graded bedding. Greywacke turbidite is well indurated feldspathic lithic grey sandstone grading to dark grey mudstone. Metagreywacke denotes more highly deformed and metamorphosed rocks of similar composition, in which the bedding has been smeared out parallel to foliation and grading is very difficult to define. The same greywacke composition at even higher metamorphic grade is termed paragneiss.

Primary thicknesses of units in the Archean and early Paleoproterozoic sequences cannot be determined because of thickening and/or local thinning caused by structural repetition and/or local strike-slip faulting during their intense polyphase deformation histories. The resulting internal variability of strikes and dips further increases uncertainty. For these reasons, thicknesses of units are approximated in terms of ‘map width’. ‘Map width’ is the horizontal distance measured orthogonally from one side to the other side of a unit in plan view.

Place names used in this report are a mixture of formal and informal names. Here and in Jefferson et al. (2023) and C.W. Jefferson, R.H. Rainbird, G.M. Young, S.S. Gandhi,

J.C. White, V. Tschirhart, D. Lemkow, and L.B. Chorlton (work in progress, 2023), Inuit lake names are used, with reference to Pelly and Nales (2004), for geographic reference in the Amer Belt (Inuit lake names stand alone, without the word ‘lake’ because ‘lake’ is part of the meaning of the single Inuktitut word). Inuit place names are also maintained for units named by Zaleski (2005) and Zaleski and Pehrsson (2005). Informal place names introduced by the exploration industry appear in single quotes and the generic component is designated by a lower-case letter (e.g. ‘Rumble lake’).

Methods

This project acquired knowledge using a comprehensive, multidisciplinary, and metallogenic approach. This project built upon, and followed methods from, two predecessor programs: the Athabasca Uranium Multidisciplinary Study (EXTECH IV) and the Northern Uranium for Canada project (NUC). The Secure Canadian Energy Supply Program supported publication of the EXTECH IV final volume (Jefferson and Delaney, 2007) and managed the NUC project that assessed geological settings of all known significant Canadian uranium occurrences (Gandhi et al., 2015). The EXTECH IV and NUC projects, together with prior and parallel studies such as those cited in the ‘Guiding hypothesis’ section, developed a set of exploration parameters to test in the Thelon Basin. The NUC project also supported the first three years of fieldwork in the Aberdeen Subbasin region (defined above). In 2009, the NUC project became the GEM-1 Uranium project, thereby sustaining and enhancing the work reported here. An opening 2009 field trip by the second author introduced all project participants and industry collaborators to the existing knowledge framework (summarized in Pehrsson et al., 2013a). Preliminary results reported by Jefferson et al. (2011a, b, c) also summarized existing knowledge, with an emphasis on Thelon Basin stratigraphy, and outlined the collaborative consortium membership, project-planning process, and methodologies in use. The focus of this project is uranium metallogeny; the most important aspect of that is basement geology (Jefferson et al., 2007a, b, c). Knowledge of the basement geology is of as paramount importance for exploration beneath the Thelon Basin as it is for exploration beneath the Athabasca Basin, especially because the only significant occurrences in the Thelon Basin region are within basement rocks at or near the surface (Miller and LeCheminant, 1985; Fuchs and Hilger, 1989; Hunter et al., 2012, 2014; Grare et al., 2018). Therefore, a comprehensive, regional mapping approach was taken to produce new, contiguous, integrated geoscience maps of four full NTS map sheets and parts of eight additional map sheets (56-D W, 56-E W, 65-O N, 65-P NW, 66-A, 66-B, 66-C NE, 66-D SE, 66-E E, 66-F E, 66-G, 66-H; Fig. 2) at scales ranging from 1:250 000 to 1:1000. The GEM-1 traverses were designed to test, calibrate, and research problem areas identified in existing regional to detailed maps, both published (*see* ‘Previous and parallel studies’ section) and unpublished (*see* ‘Acknowledgments’ section).

Because of the huge area under study, it was impossible logistically to remap every belt in any detail, so remote predictive mapping was employed for the regional compilation. Key assets were high-quality, detailed previous maps, such as those generated by Urangesellschaft Canada Limited (shared by AREVA Resources Canada, now Orano Canada Inc.) and Westmin Resources Limited (Young, 1979). Because of their internal consistency, it was possible to recalibrate these to the new and developing knowledge base. These resources thereby became dependable data sources that reduced the need for detailed new mapping in those areas; however, new, variably detailed maps were created, of selected localities with exceptional exposures, that enhanced thematic knowledge and thereby led to a better understanding of the basement-hosted uranium deposits as well as the entire geological and resource endowment of this overall poorly exposed region. This methodology emphasized field relationships, especially structural geology integrated with lithostratigraphy and geophysics, to create robust maps and lithostratigraphic schema at various scales, with university-based laboratory studies and geochronology at the Geological Survey of Canada (GSC) and the University of Manitoba to calibrate key geological entities and type localities.

Airborne geophysical data, and remote data collected by satellite and from helicopter, are additional indispensable and also consistent assets that were used extensively for remote predictive mapping, calibrated by targeted outcrop transects, ground geophysical data, and the above-mentioned existing geological maps. Under the Northeastern Thelon Basin Region consortium agreement, eight companies shared aeromagnetic and gamma-ray data, and participated in a federal-territorial-industry co-ordinating committee that prioritized where the GSC should acquire new data to fill knowledge gaps. Consortium members also provided logistical support and geological knowledge, including group field trips and joint field traverses. Tschirhart et al. (2011a) stitched and leveled the aeromagnetic data, published as a series of individual maps by Harvey et al. (2011). Tschirhart (2013) also collected extensive rock property and gravity data along key transects to help develop two-dimensional cross-sections and thereby better understand major structures such as folds, faults, and their continuation beneath the Thelon Basin. In addition, Thomas (2012) analyzed gravity and rock property data collected in the 1990s along regional transects parallel to the Meadowbank River. Tschirhart et al. (2013a) collected new gravity data and analyzed two transects of the Schultz Lake klippe (Fig. 3a) in similar fashion. As in EXTECH IV, geophysical data and interpretations made it possible to project geoscience knowledge from basement exposures outside of the northeast Thelon Basin to beneath it, as well as beneath lakes and till cover (Tschirhart et al., 2013b, c, d, 2014, 2017).

The map units of the northeast Thelon Basin region are summarized in Tables 1 and 2, and Figure 4a (lithological), and the first two major fold generations in Figure 4b (*see* ‘Structure and metamorphism’ section below). Previous regional mapping and new, targeted metallogenic studies

were mainly relied upon to update the Dubawnt Supergroup in the more distant surrounding parts of the Kivalliq Region of Nunavut (Fig. 2). In the main study area (Fig. 3a–d), metallogenically oriented, map-based research revised the attributes and distribution of all rock packages.

Studies of the igneous suites (e.g. Peterson et al., 2011, 2014, 2015a, b, c, this volume; Scott et al., 2012, 2015) were integral to the northeast Thelon Basin uranium project. Before these works, there was considerable uncertainty as to classification and genesis of many of the granitoid rock units in the area of Figure 3a. Until very recently, one remaining deep uncertainty related to amphibolite-biotite-banded tonalitic to granodioritic Archean gneiss exposed in the Turqavik horst (informal because the name ‘Turqavik’ is an informal construct (G. Drever, pers. comm., 2006), along the northern side of Schultz Lake, and in the horst that exposes the Schultz Lake intrusive complex (Fig. 3a) (*see* ‘Recommendations for further work’ section below). This undivided Archean gneiss had been informally dubbed the ‘grandfather gneiss’ (source unknown), whereas Hunter et al. (2018) proposed it to be a highly metamorphosed variant of the Snow Island suite. New geochronology on this gneiss, both directly and indirectly through inherited zircon from the Schultz Lake intrusive complex (Scott et al., 2015; Hunter et al., 2021), demonstrates that this gneiss is a highly deformed and partially melted portion of the Snow Island suite (*see* ‘Marjorie terrane’ section below).

Additional knowledge gaps addressed by this project include structural geology (e.g. MacIsaac, 2011; McEwan, 2012; Calhoun et al., 2014; Anand and Jefferson, 2017a, b); drift prospecting for Kiggavik-style, unconformity-related uranium deposits (Robinson et al., 2014, 2016); remote sensing using satellite imagery and aerial photographs to map surficial materials (LaRocque et al., 2012; Shelat et al., 2012a, b; A. LaRocque, B. Leblon, C.W. Jefferson, and J. Harris, work in progress, 2023); and geochronology (Table 2). The geochronology data listed in Table 2 were selected to represent the range of ages available for the various rock units and do not include all available analyses, some of which are unpublished. The use of detrital zircon ages to determine the maximum age of siliciclastic units is tempered by experience of the youngest zircon grains in many units being far older than the likely age of such units, given their stratigraphic and structural context. Such ages are denoted by an asterisk (*) in Table 2 and some are discussed below on a case-by-case basis.

In terms of project development and fieldwork, these activities benefited from strong collaborations at both management and working levels among federal, territorial, and industrial partners. The eastern portions of the study area, as introduced by Pehrsson et al. (2013a), provided excellent exposures for training purposes at the start of this project, even though the focus is on lode gold in that area. Knowledge shared during a 2009 consortium field trip led by S. Pehrsson also became the starting point for structural and stratigraphic updates of the Paleoproterozoic Amer Belt (Calhoun et al., 2014;

Table 1. Geological events in the Aberdeen Subbasin region. Stratigraphic, structural (including Riedel shear), and alteration (after Table 1 of Anand and Jefferson 2017a, C.W. Jefferson, R.H. Rainbird, G.M. Young, S.S. Gandhi, J.C. White, V. Tschirhart, D. Lemkow, and L.B. Chorlton, work in progress, 2023).

Event ¹	Age ² (Ga)	Name, description, tectonic and/or depositional setting and/or event	Belt-specific manifestation and characteristics; related and distal events	Metallogenic and/or diagenetic events	Stress and Riedel-shear orientations	References
D _{P13}	?	Uplift; Ordovician preserved in graben as an epicratonic outlier of Hudson Bay Basin.	Aberdeen faults reactivated, single outlier in Aberdeen Subbasin (Fig. 1).	U remobilized.	σ_1 (T faults) $\sim 120^\circ$.	Jefferson et al. (2015); C.W. Jefferson, R.H. Rainbird, G.M. Young, S.S. Gandhi, J.C. White, V. Tschirhart, D. Lemkow, and L.B. Chorlton, work in progress (2023).
D _{P12}	0.447	Ordovician limestone: marine transgression over shallow marine platform.	Epeiric sea, rich fossil record, limestone, dolomitized during diagenesis.	Hydrocarbons likely infiltrated basement.	(?) Extensional passive margin	Bolton and Nowlan (1979).
D _{P11}	Ca. 0.53	Postrift subsidence: marine transgression.	Alteration of uraninite associated with coffinite at Andrew Lake deposit.	U remobilized.	Not determined.	Shabaga et al. (2017).
D _{P13}	Ca. 1.04	Post-Grenville crustal relaxation and breakup of Rodinia.	Mini-roll-front 'Stage 3' uraninite at Bong deposit; vein style 'U1' at Andrew Lake deposit.	U remobilized.	Not determined.	Alexandre et al. (2009), Sharpe et al. (2015), Shabaga et al. (2017).
D _{P12}	Ca. 1.12	Grenville Orogeny – distal effects.	U disseminated along previous foliation planes - 'Stage 2' uraninite at Bong deposit; common resetting age of Athabasca uranium deposits.	U remobilized and thermally reset.	$\sigma_1 \sim 160^\circ$.	Alexandre et al. (2009), Sharpe et al. (2015).
D _{P11}	Ca. 1.27	Mackenzie dykes: hypabyssal; plume origin centred in Coppermine River area.	Dyke swarms spatially associated with and obliquely cut reactivated Bathurst fault cluster from D _{P4} to D _{P8} .	U remobilized and thermally reset.	$\sigma_1 \sim 140-160^\circ$.	LeCheminant and Heaman (1989), Alexandre et al. (2009), Buchan and Ernst (2013).
D _{P10}	Ca. 1.46–1.33	U-age resetting of uraninite and precious-metal deposits across Canadian Shield, possibly related to plume transecting the craton, and/or the Berthoud Orogeny.	Thermal and hydrogeological event; affected U-Pb ages of uraninite, Re-Os, K-Ar, ⁴⁰ Ar/ ³⁹ Ar on illite, and other such easily reactivated isotopic systems of uranium and precious-metal deposits.	U, Au, Ag remobilized, alteration clay minerals reset.	$\sigma_1 \sim$ vertical.	Fuchs and Hilger (1989), Turner et al. (2003), Alexandre et al. (2009), Bridge et al. (2013), Shabaga et al. (2017), Gandhi et al. (2018).
D _{P9}	<1.54	Lookout Point Formation: regional cratonic subsidence, marine transgression, dolomitization, and silicification.	Uppermost Barrensland Group; marine stromatolitic carbonate correlates with Carswell Formation of the Athabasca Supergroup.	U-thermal or diagenetic resetting.	Unknown, suspect as for D _{P8} .	Gall et al. (1992), Ramaekers et al. (2007).
D _{P8}	1.54	Kuungmi Formation: subsidence and eruption of ultrapotassic mafic lavas focused at intersection of reactivated Bathurst and McDonald faults. Extension by the Bathurst fault array extended across the Rae Craton. Douglas Formation black shale deposited in Athabasca Basin.	Upper Barrensland Group; subaerial flows. Reactivated D _{P4} T faults incremented horsts and grabens, e.g. Lone Gull horst uplifted U deposits. SLic had mid-crustal 1.83 Ga origin, brought up by Granite thrust, then D _{P8} horst along T faults. Other such horsts include Sand Lake, Turqavik, and the exposed basement belts between Baker Lake and Thelon basins.	Silicification and calcite alteration, U remobilized ca. 1.5 Ga, as 'Stage 1' disseminated uraninite at Bong deposit, Thelon Basin; not Athabasca.	$\sigma_1 \sim 140^\circ$; D $\sim 075^\circ$; P $\sim 055^\circ$.	Kuungmi Fm: Chamberlain et al. (2010). <i>Fault intersection</i> idea from P. Ramaekers (pers. comm., 2007), here defined by aeromagnetic data. <i>Overlaps U ages</i> from Sharpe et al. (2015). <i>Douglas Fm:</i> Creaser and Stasiuk (2007).

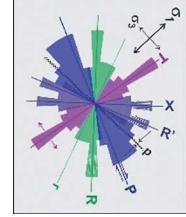


Table 1. (cont.)

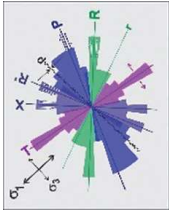
Event ¹	Age ² (Ga)	Name, description, tectonic and/or depositional setting and/or event	Belt-specific manifestation and characteristics; related and distal events	Metallogenic and/or diagenetic events	Stress and Riedel-shear orientations	References
D _{P7b}	1.63–1.54	Primary uraninite deposited in overall dextral reactivated brittle faults over deep ductile zones. Stress fields within faults rotated ~10–20° clockwise, mostly during extensional reactivation. Deep Rose dykes ³ bent into Chantrey mylonite zone. Overlaps D _{P7a} . Gentle folds beside Thelon and Bong faults.	Kiggavik Main Zone U pods dip steeply NW along 055° faults between 075° faults. Tatiggaq and Qavvik U pods dip steeply SE at intersections of P and T micro-shears over major deep ductile zone. Anand and Jefferson (2015a) reoriented Figure 5 of Fuchs and Hilger (1989) to determine current structural orientations. Overall compression and fault reactivation from Racklan Orogeny to the west.	Primary uraninite and tristramite replaced fluorapatite; quartz was dissolved; fault zones bleached, clay altered and oxidized (hematite + limonite).		Fuchs and Hilger (1989), Hunter et al. (2012, 2014), Alexandre et al. (2009), Davis et al. (2011, 2012), Sharpe et al. (2015), Anand and Jefferson (2017a, b), <i>Racklan reactivation</i> : Pehrsson et al. (2013b).
D _{P7a}	1.688, 1.67, 1.667, 1.644, 1.638	Fluorapatite cement patchy and along faults in Thelon, Athabasca, and Hornby Bay basins. Gentle dextral reactivation of fault arrays that had been established and reactivated during D _{P4} through D _{P7} before complete lithification. Felsic tuff in Athabasca Basin, bimodal Narakay volcanic rocks, Hornby Bay Basin.	Thelon Formation folded into open synclines and anticlines along the Thelon Fault: elongate syncline north of Kiggavik and multiple folds N of 'Unconformity lake'. Reactivated faults brittle in cemented rock, soft sediment in upper Thelon sand, focused diagenetic and hydrothermal alteration before and during D _{P7b} . Fluorapatite ages distinct between basins.	Fluorapatite: 1688 ± 14 Ma at Boomerang Lake, 1667 ± 5 Ma in Aberdeen Subbasin, 1638 ± 5 Ma in Athabasca Basin, undated in Hornby Bay Basin.	$\sigma_1 \sim 110\text{--}130^\circ$ Thelon Fault 075°, Turqavik fault at 055°; Aberdeen array at 120°; horsts and/or grabens at 070° and 140°.	<i>Fluorapatite</i> : Miller et al. (1989), Rainbird et al. (2003b), Gall and Donaldson (2006), Davis et al. (2011, 2012). <i>1.644 Ga felsic tuff</i> : Rainbird et al. (2003b). <i>1.66 Ga Narakay lavas</i> : Bowring and Ross (1985).
D _{P6c}	n.a.	Deep Rose mafic dykes intruded in NW corner of study area.	Known only from linear aeromagnetic highs ³ trending ~070 to 115°, curving into Chantrey Fault.	Unknown.		Jefferson et al. (2015).
D _{P6b} ; Thelon Formation deposited	1.7–1.63	Regional thermal subsidence + gentle dextral transextension formed marked to subtle extensional subbasins. All fault arrays from D _{P4} and D _{P5} reactivated, forming intersecting horsts (e.g. Turqavik + Chantrey) and grabens. Thelon Formation deposited in three upward-fining siliciclastic sequences and base locally cemented.	Initiation of the Barrensland Group . D-, P-, and R-shears reactivated, dip-slip>dextral (e.g. Judge Sissons, Bong, Thelon fault arrays). Dip-slip>sinistral for R'- and X-shears. Basal talus breccias flanked conglomerate-based giant (~20 km) alluvial channels draped by desiccation-cracked red mudstone. The upper sequence records marine transgression. All of Thelon Fm cut by brittle and soft sediment faults and clastic dykes.	Thelon Fm silicified along conglomerate beds (aquifers) and fault zones, e.g. sides of Turqavik horst and south margin of Thelon Fault. Overall clay altered and bleached.		Gall et al. (1992), Hiatt et al. (2003), Rainbird et al. (2003a), Davis et al. (2011), Jefferson et al. (2011a, b, c, 2012, 2013, 2015, 2023).

Table 1. (cont.)

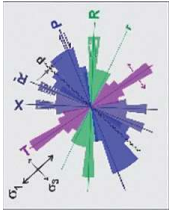
Event ¹	Age ² (Ga)	Name, description, tectonic and/or depositional setting and/or event	Belt-specific manifestation and characteristics; related and distal events	Metallogenic and/or diagenetic events	Stress and Riedel-shear orientations	References
D _{P6a}	<1.7	Broad uplift and subaerial erosion at the Matonabee unconformity surface.	Erosion, oxidative (hematitic-ironitic) paleoweathering, peneplanation.	U leached from underlying sources.	σ_1 ~vertical.	Ross and Chiarenzelli (1985), Gall et al. (1992), Gall (1994), Jefferson et al. (2023).
D _{P5c} ; Kivalliq igneous suite (Kis); upper Wharton Group deposited	1.77 to possibly ca. 1.69	Nuelin gabbro to granite; Pitz Formation bimodal volcanic rocks; 3 swarms of diabase dykes; McRae Lake (1000 km along R'-shears), Thelon River (700 km along P- and R'-shears) and Amer (>150 km along X-shears) ³ . Counterclockwise rotation of successive McRae Lake dykes along ~030–350° R'- to X-shears records sinistral rotation of principle stress over time. Pelly Bay dykes may be coeval with Thelon River dykes.	Intracontinental bimodal co-magmatic suites. Silicification and large quartz veins affect Pitz lavas, and underlying Amarook Formation, strongest along P- and R'-shears. Upper Pitz Formation includes preatmagmatic breccia beds and hot spring deposits, including microstromatolites. Large shallow rapikivi granite pancakes and fingers covered and were cut by their reactivated fault conduits. Broad, linear, deep gravity lows align with intrusive and extrusive phases along dextral transtensional and normal surface faults. Faults initiated during D _{P5c} reactivated during D _{P7} through D _{P11} .	Silicification is main alteration phase. Major quartz-vein systems ⁴ initiated: crack-seal quartz veins host hydrothermal Ag + Au at Mallery Lake and possibly elsewhere.	σ_1 ~120–150°. T at ~120–150°; gravity lows at 030, 050, and 120°; D at 075°; granite fingers at ~160°; Mallery Lake veins + Ag + Au follow P- and R'-shears at 075° and 110° ³ .	Kis: Jefferson et al. (2013) and Peterson et al. (2015a). D _{P5c} = the original D _{P5} of Pehrsson et al. (2013a). Mallery Lake Ag-Au: Turner et al. (2001, 2003); placed in Kis context by Peterson et al. (2014, 2015a, b) and Scott et al. (2015). If Pelly Bay dykes (Bleeker et al., 2010) are coeval with Thelon R. dykes then Thelon Fm <1.69 Ga.
D _{P5b} lower Wharton Group deposited	1.785–1.77	Amarook Formation . Silicified polymict alluvial conglomerate to fluvial and eolian feldspathic quartzite. Overall thermal subsidence + dextral transextension reactivated D _{P4} structures as dip-slip and low-angle extensional faults forming sedimentary basins.	Local block faults with small offsets, quartz pebble-dominated polymict alluvial conglomerate and sandstone; broad eolian sand basins between. Early diagenetic hematite. Possible initiation or reactivation of low-angle Pukiq structural discontinuity ⁵ and Wharton Lake Fault. Most eolian units in the region are Amarook Formation based on silicification and context.	Silicification pervasive, includes drusy quartz in matrix, cherty quartz in matrix and along bedding laminae, and quartz veins, forming aquitards.		Amarook: Rainbird and Hadlari (2000); eolian aspect: Jefferson et al. (2015). Early D _{P5} : Pehrsson et al. (2013a). The Pukiq discontinuity ⁵ could be a strained unconformity, or a detachment, now or during D _{P3} .
D _{P5a}	1.785–1.77	Broad uplift, subaerial erosion, and paleoweathering.	Deep erosion, oxidative paleoweathering (earthy hematization), peneplanation.	U leaching and transport.	Gentle NW-SE compression. Unknown.	Gall (1994), Rainbird et al. (2006).

Table 1. (cont.)

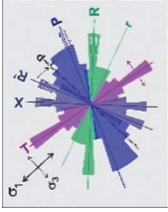
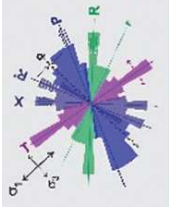
Event ¹	Age ² (Ga)	Name, description, tectonic and/or depositional setting and/or event	Belt-specific manifestation and characteristics; related and distal events	Metallogenic and/or diagenetic events	Stress and Riedel-shear orientations	References
D _{P4} b + end of upper Baker Lake Group	1.81–1.785 Ga overlap D _{P3}	Late Hudsonian reactivation of regional, deep-seated dextral fault systems, some with oblique thrust and reverse components. Master dextral (D) faults include: Amer mylonite zone, Amer Belt medial zone, Thelon Fault, Judge Sissons Fault, and Nutaaq Fault. Steeply plunging major kink folds are between master faults. Regional normal Bathurst fault array defines X (extensional) orientation. Sinistral Andrew Lake Fault is R' (antithetic). Kunwak Formation conglomeratic sandstone capped by 1785 ± 3 Ma calcite travertine.	Major D faults are an échelon and splayed into numerous left-stepping en échelon, ENE-trending P-shears and ESE-trending R-shears. Compressional P faults should have a convex-upward shape, but few have this shape because of later extensional reactivation. Strong ductile S-C fabric developed near the D faults; farther away, the strain is localized along brittle subsidiary P-shears with narrow ductile fabric envelopes. Little fabric is preserved along the R- and X/R-shears. Regional-scale kink folds occur between D faults. NNE- and NW-trending upright folds, crenulation cleavage, kink bands and short dextral axial planar faults developed mainly near D faults.	Possibly more alteration and mineralization as in D _{P3} .	σ ₁ ~120–135°. 065–075° D faults. Steep and upright kink folds, crenulation cleavage + minor faults. 	= D _{P4} of Pehrsson et al. (2013a). <i>Age of Kunwak calcite travertine</i> : Rainbird et al. (2006).
D _{P4} a (unsure if truly a discrete event)	1.80–1.78	West-dipping Granite thrust ⁶ truncated Half Way thrust and juxtaposed Marjorie terrane para- and orthogneiss (previously intruded by SLIC during D _{P2} -D _{P3}) over imbricate zone ⁶ of 2.6 Ga Pukik Lake fm with Ketyet River quartzite. Wolf and Schultz Inlet thrusts may also have developed at this time.	Drill core at Andrew Lake deposit shows E-vergent isoclinal folds and thrusts in banded orthogneiss and supracrustal gneiss of the Marjorie terrane. Wolf thrust is a well exposed hematitized mylonite zone. Schultz Inlet thrust inferred beneath string of lakes: subhorizontal Pipedream metagreywacke on west is juxtaposed with steeply dipping upper Amarulik assemblage on east (Fig. 6).	Unknown.	s ₁ ~090–110°. 	Unpublished data of Urangesellschaft (1980s) and C.W. Jefferson (field notes 2006–2012, e.g. Andrew Lake DDH 10-03 and Sleek core). <i>Detailed gravity + aeromagnetic models</i> : Tschirhart et al. (2013b); spatial analysis in ArcGIS.

Table 1. (cont.)

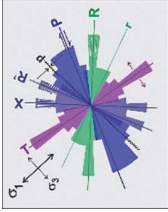
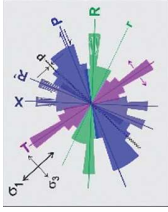
Event ¹	Age ² (Ga)	Name, description, tectonic and/or depositional setting and/or event	Belt-specific manifestation and characteristics; related and distal events	Metallogenic and/or diagenetic events	Stress and Riedel-shear orientations	References
D _{P3} , upper Baker Lake Group, Hudson suite continued	Ca. 1.82–1.78; overlap D _{P4}	SE-NW extension caused subhorizontal chevron fold trains and detachment faults. Unroofing exposed the Kinngaaquik igneous complex . Pressure drop and partial melting filled dilatant faults with Hudson granite + Martell syenite laccoliths to thin sills and ovoid plugs, the margins of which commonly inherited S _{P2} . Dubawnt bostonite to minette dykes and shonkinite plugs continued along with Christopher Island formation ultrapotassic volcanic rocks intercalated with Kazan formation arkose and conglomerate.	Axial planes of SE-vergent, open to tight fold trains dip gently SE at Meadowbank mine. Bostonite and minette flows are interbedded with siliclastic rocks and texturally resemble hypabyssal plugs and dykes ³ . Retrograde metamorphism during D _{P3} included chlorite alteration of amphibole and biotite. Major detachment faults include Wharton Lake fault system west of SLic that accommodated Kunwak Fm of Baker Lake Group; faults bounding Baker Lake Basin accommodated the entire Baker Lake and Wharton groups + Thelon Formation. Margins of granitoid sheets and sills inherit S _{P2} from host rocks. Detachment at this time is one possible explanation for the enigmatic Pukiq discontinuity (Fig. 6, 8). ⁶	Minette + bostonite dykes flanked by calcite-chlorite-albite alteration + uranium. Granitoid rocks contain high-heat producing Th-U-K and are potential U source, but in refractory minerals, hard to leach.	σ_1 050–070° 	As in Pehrsson et al. (2013a). Includes <i>Wharton Lake fault system</i> (Peterson et al., 2010, 2014). <i>Kinngaaquik core complex</i> : Zaleski et al. (2001b); Zaleski and Pehrsson (2005), Pehrsson et al. (2013a).
D _{P2} -b+c+d: lower Baker Lake Group, Hudson suite initiates	Ca. 1.84–1.82; overlaps D _{P3} and D _{P4}	Transpression: pull-apart basins along major dextral shear zones accommodated subaerial South Channel and Kazan conglomerate and sandstone, and ultrapotassic bimodal volcanism of Christopher Island formation (Cif) in Baker Lake Basin while D_{P2}-a-b folding and Hudson granite and Martell syenite intrusion propagated toward the NW. Multiple orientations of Dubawnt minette and bostonite dykes (intrusive equivalents of the Cif).	Slightly overlaps main folding north of Baker Lake (below) but Baker Lake Group is unfolded. 120° U veins may follow transposed beds and/or R-shears ⁴ . Ultrapotassic magmatism ca. 1.84–1.81 Ga included flows, conjugate dykes ³ and mixed Hudson granite–Martell syenite. Crack-seal veins ⁴ filled transtensional cracks. Minette and bostonite dykes are foliated along ~070° F _{P2} fold axes; massive along ~130 and 180° Riedel-shear arrays. Alteration of Lac Cinquante conductors that may be primary graphitic Archean epiclastic and tuffaceous units.	Lac Cinquante unconformity uranium at basal unconformity. Metasomatic U with calcite-chlorite-albite alteration flanks minette dykes cutting Kazan Formation.	σ_1 ~140–165° 	Hudson suite: van Breemen et al. (2005), Rainbird et al. (2006), Peterson et al. (2010), and Scott et al. (2015). Includes: <i>SLic</i> (Miller and Peterson, 2015), <i>Amer plutonic complex</i> (see 'Magmatism' section), <i>Lone Gulf and Granite Grid</i> plugs (Scott et al., 2015). <i>Lac Cinquante U</i> is from Bridge et al. (2013). <i>Metasomatic U</i> in Kazan is from Stanton (1979).

Table 1. (cont.)

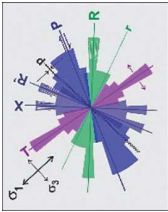
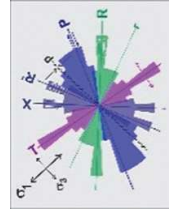
Event ¹	Age ² (Ga)	Name, description, tectonic and/or depositional setting and/or event	Belt-specific manifestation and characteristics; related and distal events	Metallogenic and/or diagenetic events	Stress and Riedel-shear orientations	References
D ₂ b: main Hudsonian Orogeny, heating of crust (overlaps Snowbird Orogeny)	Ca. 1.86–1.83; D _{P3} overlaps	Compression: S _{P2} , F _{P2} (e.g. Whitehills synform), reverse faults and thrusts (e.g. Nipterk, Half Way Hills, and Quoich River thrusts), and kippen (e.g. Snow Island suite granite sheets and Schultz Lake outlier). Set the stage for extensional development of the Baker Lake Basin + Kinggaauk igneous complex, and in situ formation of Hudson granite (D _{P2} b + D _{P2} c + D _{P2} d).	NW-vergent, inclined folds and reverse faults to thrusts and SE-dipping S _{P2} fabrics affected typically broad and flat-bottomed; antiforms tightly rounded, many broken by reverse faults. Refolded F _{P1} form type-2 and type-3 interference patterns. Regional M_{P2} metamorphism was low pressure, greenschist through amphibolite to partial melting. ‘Syenodiorite’ of the Kinggaauk complex comprises older monzodiorite to syenite phases cut by high-level Hudson granite.	Granitoid rocks contain high-heat-producing Th-U-K and are potential U source, but the U crystallized in refractory minerals, resistant to weathering, alteration, and leaching.	 <p>$\sigma_1 \sim 145\text{--}165^\circ$.</p>	Kjarsgaard et al. (1997), Zaleski et al. (1999, 2001b, 2005), Hadlari et al. (2004), Zaleski and Pehrsson (2005), McEwan (2012), Pehrsson et al. (2013a), Jefferson et al. (2015, 2023).
D ₂ a + deposition of sequence Ps4 (overlaps end of Snowbird Orogeny and start of main Hudsonian Orogeny)	Ca. 1.865–1.85	Molasse and flysch filled foreland basins (sequence Ps4 of Ketyet River, Amer, and Montrosor groups). Polymict conglomerate beds with predeformed clasts in Amer and Ketyet River belts separate sandstone and mudstone sequences derived from three possible orogens: early Hudsonian Snowbird, Thelon, and/or Taltson. Chesterfield fault zone emplaced granulite-facies 2695 ± 4 Ma gneiss northwesterly over 2.72 Ga Akutuak tonalitic gneiss from about 1.865 to 83 Ga.	Ps4 facies vary. Ketyet River group dark shale was interrupted by proximal subaqueous polymict conglomeratic debris flows and covered by arkosic sandstone with magnetic markers. Amer group distal arkosic red sand and mudstone with desiccation cracks was interrupted by thin stromatolitic dolostone and polymict conglomerate, and overlain by grey pelagic turbidites with disseminated magnetite marker beds (not cherty BIF) and local graphitic shales. Upper Montrosor group shallow-marine mudstones also contain magnetic marker beds, where magnetite is part of a transported heavy-mineral suite including zircon, monazite, and tourmaline.	Detrital magnetite in heavy-mineral beds (noneconomic) and locally continuous graphitic pyritic conductors (weakly metamorphosed aquitards).	 <p>$\sigma_1 \sim 130\text{--}160^\circ$.</p>	Zaleski et al. (2001a, b), Berman et al. (2007), Rainbird et al. (2010), (youngest detrital zircon 1.90 Ga in Amer Belt; 2.59 Ga in Ketyet River Belt), Pehrsson et al. (2013a), Jefferson et al. (2015, 2023); C.W. Jefferson, R.H. Rainbird, G.M. Young, S.S. Gandhi, J.C. White, V. Tschirhart, D. Lemkow, and L.B. Chorlton (work in progress, 2023), Percival et al. (2017) (youngest detrital zircon 1924 ± 6 Ma).
Erosion	Ca. 1.875 to ca. 1.855	Tectonic hiatus, uplift and erosion, part of >100 Ma time interval from sequence Ps1 to just before deposition of sequence Ps4.	Regional basal unconformity beneath Itza Lake formation truncates D _{P1} structures, but is not exposed. Pukiq discontinuity may have been extensional then ⁶ .	Not applicable.		Mapping by Jefferson et al. (2015), Anand and Jefferson (2017a, b), Percival et al. (2017).

Table 1. (cont.)

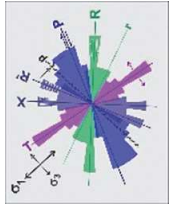
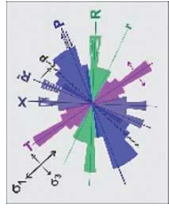
Event ¹	Age ² (Ga)	Name, description, tectonic and/or depositional setting and/or event	Belt-specific manifestation and characteristics; related and distal events	Metallogenic and/or diagenetic events	Stress and Riedel-shear orientations	References
D _{P1a} , D _{P1b} , D _{P1C}	<1.9 to ca. 1.865	Basement-involved thin-skinned translation, isoclinal and sheath folding, thrusting, and décollements. Bedding transposed and translated (D _{P1a}) subparallel to foliation (S _{P1a}), thrusts, décollements, and enigmatic structural discontinuities. Metamorphism (M _{P1}) anchizone to greenschist. The most likely driver was the 1.9–1.865 Ga Snowbird Orogeny.	Vergences highly varied: NE in Amer Belt, SW at 'Ukaiik lake' and Schultz Lake klippe, S at Meadowbank mine, E-NE in Pukij imbricate zone ⁵ . Enigmatic discontinuity between sequence Ps1 quartzite and 2.6 Ga Sls with no basal paleoweathered basement or conglomerate in the Pukij imbricate zone, Akliniq Hills, and the Montresor + Garry Lake belts. Metamorphism ranged from anchizone to lower greenschist facies. Did late relaxation start the Pukij discontinuity as a décollement? The 1.98–1.91 Ga Talison Orogeny is considered too distal to have had a direct influence.	Unknown	$\sigma_1 \sim 035\text{--}070^\circ$. 	Pehrsson et al. (2013a). Detail: McEwan (2012), Calhoun et al. (2014). Ages: Rainbird et al. (2010). Talison Orogen: Bethune et al. (2013), Card et al. (2014). Snowbird Orogen: Thiessen et al. (2020). Thelon Orogen: Hoffman (1989), Berman et al. (2015a, b), Percival et al. (2017). See 'Structure and metamorphism' section in text.
Ultramafic to felsic event	Ca. 2.05 to 2.0	Ultramafic-mafic-syenite-granite magmatism with high magnetic susceptibility. Recorded in both primary intrusive outcrops and detrital zircon suites across much of the study area.	2045 ± 13 Ma gabbro sill in lower Montresor, plugs with strong aeromagnetic anomalies under SW Thelon Basin (drillhole JP1), outcrops in Penylan Domain of SW Rae Craton; possibly the sill in northern Amer Belt. One of the defining components of sequence Ps4 detrital zircon suites.	Ultramafic to mafic sills + plugs may have potential for Ni-Cu-PGE and Cr .	Unknown.	Davis et al. (2015), Percival et al. (2017), W. Bleeker (unpub. data, 2018, 2019), Regis et al. (2017). Youngest detrital zircons summarized in Table 2.
Deposition of sequence Ps3 + impact event	2.153–2.045	Linear SW-NE basalt eruption recorded tectonic instability and faulting at high angles to previous shelf margin. Grey Ps3 mudstone above carbonate in Montresor belt preserves ca. 2.1 Ga spherules from an interstellar asteroid strike. Higher strata located only in the Amer Belt record a series of shallow-marine, but anoxic transgressions and regressions in upper sequence Ps3 of the Amer Belt . Sequence Ps3 strata are partly represented in Ketyet River and Montresor belts .	Basal sequence Ps3 tholeiitic basalt geochemically resembles the 2153 ± 4 Ma Schultz Lake gabbro and may have fed iron into upper Three Lakes fm aeromagnetic markers hosted by grey mudstone and/or schist (mid-Ps3 sequence, Amer Belt). Arkosic quartz arenite of the Oora Lake formation grades up from the Three Lakes formation, has an upper, tan, dolomitic sandstone marker, and is overlain by alternating argillite-sandstone (Showing Lake formation). Mainly the basalt portion of sequence Ps3 is present (discontinuously) in Ketyet River group, nonmagnetic lower Ps3 mudstone in Montresor belt hosts 2.045 Ga gabbro and a higher Ps3 mudstone hosts 2.05 Ga impact spherules.	Strong magnetite marker in lower sequence Ps3. Two stratabound disseminated U + Cu + magnetite marker units in Showing Lake formation argillite and sandstone. Both markers present only in the Amer Belt .	$\sigma_1 \sim 070^\circ$. 	Young (1979), Jefferson et al. (2015, 2023); Patterson et al. (2012), Percival et al. (2017, 2019), Rainbird et al. (2010). <i>Stratigraphic details and proposed new correlations between Amer, Montresor, and Ketyet River belts</i> are in Figure 4; Jefferson et al. (2023); C.W. Jefferson, R.H. Rainbird, G.M. Young, S.S. Gandhi, J.C. White, V. Tschirhart, D. Lemkow, and L.B. Chorlton, work in progress (2023)

Table 1. (cont.)

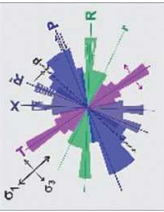
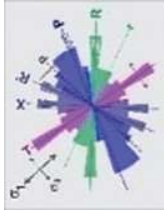
Event ¹	Age ² (Ga)	Name, description, tectonic and/or depositional setting and/or event	Belt-specific manifestation and characteristics; related and distal events	Metallogenic and/or diagenetic events	Stress and Riedel-shear orientations	References
Deposition of Ps1 and Ps2.	Ca .2.19–2.154	Subaerial to epicratonic to marginal marine facies deepened westerly; lateral facies changes were NW-SE. The SW-NE trending carbonate units record faulting at high angles to the overall shelf margin. The Amer medial zone and Nipiterk structural zones originated syndepositionally. Sequences Ps1-2 are in all three of the Amer, Ketyet River, and Montresor belts .	Sequence Ps1 aluminous schist and conglomerate at base, grading to quartzite, topped by conglomerate. Sequence Ps2 lower black shale is polymetallic, top marked by siliceous dolostone in Amer Belt and dolomitic tuff in Ketyet River Belt. Detrital zircons in Montresor Ps1 quartzite indicate deposition after 2.194 Ga based on detrital zircons derived from Thelon Orogen to the west. The youngest detrital zircons and clasts found in the Amer and Ketyet River sequence Ps1 are limited to the proximal 2.6 Ga SIs sources.	Upper Ps1 conglomerate heavy minerals elevated in U, Th, and REE. Stratatound disseminated U + Cu in lower Wollaston Supergroup has no equivalent here.	$\sigma_1 \sim 005-030^\circ$. 	Young (1979), Hadjari et al. (2004), Rainbird et al. (2010), Patterson et al. (2012), Jefferson et al. (2012), Percival et al. (2017). <i>Stratigraphic details and proposed correlations</i> are in Figure 4; Jefferson et al. (2023); C.W. Jefferson, R.H. Rainbird, G.M. Young, S.S. Gandhi, J.C. White, V. Tschirhart, D. Lemkow, and L.B. Chorlton, work in progress (2023). Wollaston U+Cu described by Yeo and Delaney (2007).
D _{Py}	2.2–2.1	Accretionary event along west-southwestern margin of Rae Craton.	Recorded by detrital zircons in sequence Ps1 quartzite of Montresor Belt and upper Murmac Bay group; later by sequence Ps4 of Montresor, Amer, and Ketyet River belts (Table 2).			Hoffman (1989), Ashton et al. (2013), Percival et al. (2017).
Erosion	2.3–2.2	Arrowsmith mountains became bevelled, basin space developed with regional extension.	Deep paleoweathering under low-oxygen conditions produced aluminous paleosol, now schist.	Not applicable.		Young (1979), Knox (1980), Patterson (1986).
D _{Px}	2.37–2.3	Arrowsmith Orogeny on W side of Rae Craton. Great Slave Lake shear zone dextral 070° transform fault. No record of this event in the study region.	Regional compression with high-grade metamorphism along the western flank of Rae Craton. During this time the Bathurst Fault was a sinistral R' shear and the Great Slave Lake shear zone was a dextral R shear, as were ancestral forms of many other shear zones in the region.	Not assessed.	$\sigma_1 \sim 110^\circ$. 	Berman et al. (2013, 2015a). <i>Kinematics</i> from Figure 16 of Berman et al. (2013). <i>Detrital zircon data</i> from Percival et al. (2017).
Ps0	2.45–2.39	Sherman group: metapelite and metagreywacke (south tip in extreme NW of study area; hiatus elsewhere in the region).	Sherman Basin = depositional trough between Slave and Rae cratons, now part of the Queen Maud Block.	Not assessed.	Not assessed.	Schultz et al. (2007), Tersmette (2012).

Table 1. (cont.)

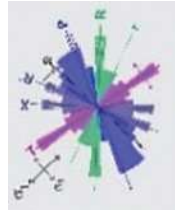
Event ¹	Age ² (Ga)	Name, description, tectonic and/or depositional setting and/or event	Belt-specific manifestation and characteristics; related and distal events	Metallogenic and/or diagenetic events	Stress and Riedel-shear orientations	References
D _{A2C}	2.63–2.58	Snow Island suite magmatic event affected a large part of the just-amalgamated Rae Craton; possibly from shallow subduction and/or mafic underplating. Deposition of the upper Aberdeen, then Amarulik assemblages.	Bimodal gabbro to granite intrusions and comagmatic volcanic strata blanketed the lower assemblages of the Woodburn Lake and Keyet River groups. Synvolcanic and detrital zircons also made their way into the upper Aberdeen and Amarulik depositional basins.	Layered ultramafic intrusions may have Ni-Cu-PGE and/or Cr potential.	Unknown; pre-D _{P1} fabrics not discernable.	LeCheminant and Roddick (1991), Jefferson et al. (2015), Peterson et al. (2015c, this volume).
Overlap		Local unconformities, geographic gaps.	(?) Part of Pukiq structural discontinuity ⁶	Not applicable.		See text and caption to Figure 4.
D _{A2b} , Late Woodburn Lake group	Ca. 2.67, 2.628, 2.611, 2.598	Extension, intra- (Amarulik sequences A3 and A4) + marginal (upper Marjorie) sequences within and adjacent to early-amalgamated Woodburn Lake group microcraton.	Detrital zircon grains from greywacke of Amarulik sequence A3 and turbiditic paragneiss of the Aberdeen and Rumble assemblages have multiple sources, the youngest overlapping the SIs in age.	Possibly coeval with and/or sourced from early Snow Island suite volcanism.	Unknown; pre-D _{P1} fabrics not discernable.	Jefferson et al. (2015), Robinson et al. (2016), McNicoll (2020, site 23 Table 2), Davis et al. (2021, site 33 Table 2).
D _{A2a} (early)	Unknown	Collisional deformation, during successive amalgamation of the various early assemblages of the Woodburn Lake group, up to the lower Amarulik. Woodburn Lake microcraton amalgamated with others e.g. Committee Bay belt, in approximate NE-SW convergence.	Local outcrops with cryptic pre-D _{P1} structures are obscured by Paleoproterozoic overprints. Inferred s ₁ assumes that the Amarulik and Schultiz Inlet structural discontinuities developed NE-SW compression. Relationships with gneissic basement are unknown as these were upthrown during Hudsonian Orogeny.	Unknown.	(?) σ ₁ ~090° 	Janvier et al. (2015a, b); Figure 5, this paper.

Table 1. (cont.)

Event ¹	Age ² (Ga)	Name, description, tectonic and/or depositional setting and/or event	Belt-specific manifestation and characteristics; related and distal events	Metallogenic and/or diagenetic events	Stress and Riedel-shear orientations	References
Early Woodburn Lake group (WLg) and Akutuak tonalite	Ca. 3.05 to ca. 2.65	WLg interpreted to have formed in a microcratonic rift flanked by basement gneiss, in an oceanic plateau or crust setting, as volcanic arcs, and/or as an assembly thereof. Detrital and igneous zircon ages range from 3.05–2.72 Ga (Table 2). Akutuak gneiss ca. 2.72 Ga.	Disparate assemblages (Fig. 4a) were juxtaposed during D _{A2} . Rumble Belt (Fig. 3a) includes undivided rocks resembling Pipedream assemblage, but with metagreywacke as young as 2.65 Ga. The Marjorie mafic-felsic package is the oldest (2.754 Ga) of the Woodburn Lake group. The Akutuak and Sanning tonalite to quartz diorite gneiss units possibly were subvolcanic intrusions.	Oceanic plateau and island-arc magmatism with subvolcanic intrusions; epiclastic-hosted BIF contains Au ⁷ ; exhalite has Au-VMS ⁸ potential.	Unknown.	
D _{A1}	(?) >2.74 Ga or 2866 ±6–5 Ma	Early shortening and thickening – inferred, but unexposed in the map area unless the Sanning tonalite gneiss was basement to the above.	Contractional basement gneiss predated deposition of the Woodburn Lake group. Deformation cryptic because of Paleoproterozoic reworking.	If <2.74 Ga, it could be subvolcanic and support VMS potential	Unknown.	

1. This table integrates all geological events that directly or indirectly affected the northeast Thelon Basin region study area: deposition/erosion, magmatism, diagenesis, deformation, metamorphism, mineralization, and distal events. It includes lithostratigraphy and aspects of metallogeny known to the authors, with a strong emphasis on uranium.

2. Geochronology is detailed in Table 2 with references therein.

3. Dykes form an échelon patterns that mimic, but commonly transect those of the fault systems they follow, and have no preferred step direction (cf. dyke and Riedel-shear orientations in Fig. 9).

4. Similar crack-seal quartz veins are abundant along the Thelon, Bong, and Judge Sissons fault zones. Silicified and brecciated Amarook Formation underlies the Thelon Formation along the Thelon and Turqavik faults.

5. Stromatolitic chert breccias located south of western end of the Thelon Fault record synvolcanic siliceous hot-water systems of the Pitz Formation that are interpreted as being coeval with the quartz veins + cement in underlying units.

6. The Pukiq structural discontinuity (Fig. 6, 8) description and hypotheses are in the text.

7. Granite thrust and Pukiq imbricate zone (Fig. 8) descriptions and hypotheses are in the text.

7. Meadowbank and Amaruq gold mines (Sherlock et al., 2004; Pehrsson et al., 2013a; Côté-Mantha et al., 2015; Gosselin and Dubé, 2015; Janvier et al., 2015a, b; Valette et al., 2019).

8. Volcanogenic massive sulphide (VMS) deposits with precious-metal enrichment, such as the Greyhound property northwest of Whitehills Lake (Aura Silver Resources Inc., 2018).
BIF = banded iron-formation, Kis = Kivalliq igneous suite, SIs = Snow Island suite, SLic = Schultz Lake intrusive complex

Table 2. Selected geochronology in the southern portion of the Aberdeen Subbasin region and some key representative ages in the northern Canadian Shield. Site locations are in the most detailed maps for those locations, keyed by site number (column 1) to figure number (column 2). Blue circles with these site numbers show these locations in the relevant figures.

Site	Fig. no.	Age \pm error*	Method \pm mineral	Rock type, unit name	Geographic location, structural setting	References**
59	3a	Ca. 448 Ma (late Ordovician)	Paleontology	Limestone: finely crystalline, flaggy, fossiliferous	Outlier on Thelon Formation, ~55 km north of Aberdeen Lake	Upper Maysvillian to Richmondian age by Bolton and Nowlan (1979) on two samples of Donaldson (1965)
58	n.a.	1.28–1.27 Ga	U-Pb zircon	Diabase dykes (Mackenzie igneous event)	Clusters of 140° faults across entire area	LeChemiant and Heaman (1989), Buchan and Ernst (2013)
57	8a	1.4 Ga	U-Pb uraninite	Lone Gull uranium deposit	Kiggavik U camp (same granite as site 49)	Fuchs and Hilger (1989)
56	3a	1434 \pm 23 Ma	Sm–Nd errorchron	Ca. 1.75 Ga vein quartz reset metasomatically	3 phase quartz veins at Mallery Lake cutting Pitz Formation	Turner et al. (2003); reinterpreted by Peterson et al. (2015a)
55	1	1.74–1.59 Ga and 1453 \pm 18 Ma	U-Pb uraninite	Uraninite veins at Port Radium–Eldorado deposit	East shore of Great Bear Lake. Veins cut 1.74 Ga dykes, in turn cut by 1.74 Ga sills	Gandhi et al. (2018)
54	2	1540 \pm 30 Ma	SIMS U-Pb baddelyite	Ultrapotassic mafic flow (Kuungmi Formation)	Centre of Thelon Basin, overlies Lookout Point Fm dolostone	JP07-63C; Chamberlain et al. (2010)
53	1	1638 \pm 5 Ma	U-Pb apatite	U-rich fluorapatite cement, multiple sites	Up to and including Wolverine Point Fm, Athabasca Basin	Rainbird et al. (2003b); JP03-03/z8406, DDH HK12; Davis et al. (2011)
52	1	1644 \pm 13 Ma	U-Pb zircon	Felsic tuff (Wolverine Point Fm)	Central Athabasca Basin	Rainbird et al. (2003b, 2007)
51	3a	1667 \pm 5 Ma	U-Pb apatite	U-rich fluorapatite cement from 5 sites	Aberdeen Subbasin, in sandstone and at unconformity	Davis et al. (2011) (multiple samples); is it coeval with Kiggavik apatite cut by U ₃ O ₈ ?
50	2	1688 \pm 14 Ma	U-Pb apatite	U-rich fluorapatite cement; replaced by tristramite	Boomerang Lake prospect; BL-83-21, 98.91 m; no U ₃ O ₈	Davidson and Gandhi (1989), Beyer et al. (2010), Davis et al. (2012)
49	8a	1748 \pm 9.4 Ma; 1806 \pm 41 Ma	U-Pb zircon	Lone Gull granite stock, two textural domains (mineralized Hudson and Nueltin granite)	Kiggavik Main Zone (uranium); 17.3 and 75.5 m in DDH	09PHAJ39/z10064 and 08JP052A/z10068; Scott et al. (2015)
48	8a	1758.5 \pm 44 and 1837.8 \pm 7.7 Ma	U-Pb titanite; zircon	Porphyritic hypabyssal Martell syenite intruding western Pipedream assemblage	Bong DDH 49 at 145 m (under Bong uranium deposit)	10JP-116a, z-10647; Scott et al. (2015): 1758.5 Ma from metasomatic titanite, 1837.8 Ma from magmatic zircons
47	2	1785 \pm 3 Ma	Pb-Pb calcite	Calcite travertine (upper Kunwak formation)	Top of conglomeratic sandstone in Baker Lake Basin	89PHA-40; z5601; Rainbird et al. (2006)
46	1	1808 \pm 2 and 1837 \pm 7 Ma (same site)	U-Pb zircon	Massive to mylonitized granite (Hudson suite)	'Base Camp granite' intrudes, and is cut by, Wager shear zone at Paliak Islands	1808 \pm 2 Ma: 5-HAS-94-2; Henderson and Roddick (1990). 1837 \pm 7 Ma: 16WGA-M047A01; Therriault et al. (2018)
45	6	1835 \pm 1 Ma	U-Pb monazite	Coarse-grained, massive granite (Hudson suite)	3 m E-trending dyke cuts wacke NE of Amarulik Lake	91HSA-2/z2594; Roddick et al. (1992)

Table 2. (cont.)

Site	Fig. no.	Age \pm error*	Method \pm mineral	Rock type, unit name	Geographic location, structural setting	References**
44	8a	1839.7 \pm 9.3 Ma	U-Pb zircon	Syenogranite, Schultz Lake intrusive complex (Hudson suite)	Extensive 200 m thick granodiorite to syenite slab intrudes Aberdeen assemblage.	09PHA-018/z10067; Scott et al. (2015)
43	8a	1840 \pm 11 Ma	U-Pb zircon, titanite	Small monzogranite plug (Hudson suite)	Granite Grid area, northwest of Bong deposit	09PHA-J33A/z10066z; Scott et al. (2015)
42a, b	1, 3a	<1923.8 \pm 5.9 Ma; <1.95 Ga	U-Pb detrital zircon	Pink arkosic sandstone with detrital magnetite; black carbonaceous quartzite	NE-central Montresor belt, upper unit; Sand belt conductor, margin of Aberdeen Subbasin	z11290, Percival et al. (2017); z7806, Rainbird et al. (2010) respectively
41a, b, c, d	3a	<1.90, 1.91, 1.92, and 2.06 Ga	U-Pb detrital zircon	Pink, red, brown and tan arkose, Amer group (sequence Ps4)	N-central, central Medial zone, NE oval and along Amer mylonite zone, Amer Belt	z8983 and z8985 (Rainbird et al., 2010); 10JP009/z10511 and 10JP056/z10513 (Davis, 2021) respectively
40	6	<2.05 Ga	U-Pb detrital zircon	Grey lithic sandstone in polymict conglomerate, Tasirjuak Fm (sequence Ps4)	NE shore Whitehills Lake, in Whitehills synform, Ketyet River Belt	z6465; Rainbird et al. (2010); '<2.0 Ga' of Pehrsson et al. (2002)
39	7b	<2397 \pm 6 Ma *** (1 grain)	U-Pb detrital zircon	Dark grey pelitic schist with highly transposed lamination (sequence Ps2)	Grey schist belt, 'Nipterk lake' area near quartz arenite	10JPM030-B02/z10488; highly discordant ²⁰⁷ Pb/ ²⁰⁶ Pb; all other grains Archean (McEwan, 2012)
38	6	2153 \pm 5 Ma	U-Pb baddeleyite	Metagabbro cutting Neoproterozoic greywacke (interpreted = sequence Ps2 basalt)	NTS 66A, Schultz Lake, baddeleyite has metamorphic zircon corona	88-LAA-T73-1/z1465; LeCheminant and Roddick (one fraction, unpublished, cited in Hadlari et al., 2004)
37	6	<2.50 Ga***	U-Pb detrital zircon	Polymict conglomerate between quartzite and basalt (upper sequence Ps1)	NW limb of Whitehills F _{P2} synform at river draining Whitehills Lake	Unknown sample no., analyses done at Memorial University; informal reference in Pehrsson et al. (2002)
36	6	<2.59 Ga***	U-Pb detrital zircon	Arenite, green, sublithic + conglomerate (upper sequence Ps1)	Core of F _{P1} syncline, below basalt, NW of Whitehills Lake	z7814; Rainbird et al. (2010); new mapping: single transition from quartzite to basalt, isoclinally folded
35	8a	<2.72 Ga***	U-Pb detrital zircon	Polymict monazite-rich conglomerate (upper sequence Ps1)	Schultz Lake klippe. Ordered here because at top of PqzK	08JP066D1/z10512; Davis (2021)
34	7a	<2623.3 \pm 5.0 Ma***	U-Pb zircon	SIs granite clast in basal conglomerate (base of sequence Ps1)	Core of Ukalik Lake synform, granite cobble cut out for dating	PQB-37-04A/z8405; Davis (2021)

Table 2. (cont.)

Site	Fig. no.	Age \pm error*	Method \pm mineral	Rock type, unit name	Geographic location, structural setting	References**
33	6	$<2598 \pm 20$ Ma	U-Pb detrital zircon	Lithic-feldspathic greywacke (sequence A3 of Amarulik assemblage)	Northwest portion of Amarulik basin, quarry on mine road.	ZB98-132CZ/z5554. Also has 2611 ± 20 and 2639 ± 10 Ma grains; Davis (2021)
32	3a	2595.7 ± 3 Ma	U-Pb zircon	Plagioclase porphyritic, hornblende-biotite-magnetite quartz monzodiorite (SIs)	East edge of small lake, on linear aeromagnetic high, Chantrey mylonite zone	12NKL008/10969; Davis et al., 2014 (station 12JP105 of this study). Composition ranges from diorite to tonalite.
31b	8a	2603.6 ± 3 Ma	U-Pb zircon	Rhyolite, quartz-K-feldspar-phyric (Pukiq Lake formation)	'Rhyolite lake', Granite Grid east, north of Bong deposit, highly foliated	11JP373/z10802; Davis (2021)
31a	8a	Ca. 2.607 Ga	U-Pb detrital zircon	Quartz-K-feldspar-phyric epiclastic rock (Pukiq Lake formation)	AREVA DDH GG21, Granite Grid, hanging wall of Bong deposit	12JP040/z10810; Appendix A, Figure A-6; plot from data of McNicoll (2020)
30	3a	$2606 +4/-3$ Ma	U-Pb zircon	Quartz diorite to granite with agmatite (SIs)	South of Judge Sissons Lake, foliated, large domal pluton	J.C. Roddick, unpublished data, age no. 2 in Hadlari et al. (2004)
29	3a, 6	$2608 +28/-10$ Ma	U-Pb zircon, discordant	Monzogranite, foliated (SIs)	Whale-shaped lake between Thelon Fault and Schultz Lake	A.N. LeCheminant and J.C. Roddick, unpublished data, age no. 4 in Hadlari et al. (2004)
28	2	$2610 +11/-13$ Ma	U-Pb zircon	Quartz-K-feldspar porphyritic dacite lapilli tuff	North of Pukiq Lake (type locality)	83LAA-T188/z697; LeCheminant and Roddick (1991)
27	3a	$2610 +2.7/-2.1$ Ma	U-Pb zircon	Foliated granite, porphyry dyke apophyses + many inclusions (SIs)	8.7 km NE of 'Farside lake'; west edge of Tehek plutonic complex, actually klippe sheet	ZB96-204AZ/z4587; Davis and Zaleski (1998); Tehek plutonic complex <i>after</i> Schau et al. (1982)
26	6	2612 ± 4 Ma	U-Pb zircon	Coarse unfoliated granite (SIs)	Klippe on Woodburn Lake group, west side of 'Third Portage lake'	91HSA-2/z2594; Roddick et al. (1992)
25	7a	$2620 +3/-2$ Ma	U-Pb zircon	Foliated quartz-K-feldspar porphyry (SIs)	1.5 km southeast of 'Nipterk lake'; dyke cuts quartzite	z4414 and 4425; Davis and Zaleski (1998) (ZB96-128AZ)
24	3a	2621 ± 2 Ma	U-Pb zircon	Weakly foliated granite (SIs)	Klippe on Woodburn Lake group, SW corner Pipedream Lake	K406/z1466; Ashton (1988); 2629 ± 2 Ma in Tella (1994)
23	3a	<2.628 Ga and ca. 2672 Ga	U-Pb detrital zircon	Graded epiclastic paragneiss (Aberdeen assemblage)	Between Aberdeen, Marjorie, and Mallery lakes, near sites 11 and 12	11JP009/z10807; see Appendix A, Figure A-5 for relative abundances of ages (plot from data of McNicoll, 2020).
22	7a	2628.7 ± 1.2 Ma	U-Pb zircon	Foliated quartz-K-feldspar-phyric rhyolite lapilli tuff (Pukiq Lake Formation)	Isoclinal F1 infold in Ketyet River quartzite, N corner of F2 synform, wrapped by 'Ukalik lake'	ZB99-042dz/z6326; Zaleski (2005), Davis et al. (2021)
21	6	2627 ± 1 Ma	U-Pb zircon	Felsic porphyry sill and tuff (Pukiq Lake formation)	Transects Tern Lake 1 km N of Meadowbank mine	ZB99-443az/z6388; Davis et al. (2021)

Table 2. (cont.)

Site	Fig. no.	Age \pm error*	Method \pm mineral	Rock type, unit name	Geographic location, structural setting	References**
20	3a	<2.65 Ga	U-Pb detrital zircon	Greywacke (Rumble assemblage)	Hosts BIF, volcanic and chemical strata, Amaruq Au deposit	Valette et al. (2019)
19	3a	<2649 \pm 10 Ma	U-Pb detrital zircon	Paragneiss (Aberdeen assemblage)	Upper sequence of Hunter et al. (2018); close to Qavvik U occurrence	GC-204967; psammopelitic gneiss of Hunter et al. (2018). Similar to 11JP009
18	3a	<2653 \pm 14 Ma	U-Pb detrital zircon	Paragneiss (Aberdeen assemblage)	Supracrustal raft in Hudson granite, core of Tatiggaq prospect.	GC-204973; psammopelitic gneiss of Hunter et al. (2018)
17	3a	<2654 \pm 7 Ma	U-Pb detrital zircon	Paragneiss (Aberdeen assemblage)	Upper sequence (Hunter et al. 2018); ~7 km S of site 23 (11JP009)	GC-204952; psammopelitic gneiss of Hunter et al. (2018). Close to 11JP009 (no. 23)
16	6	<2.680 Ga	U-Pb detrital zircon	Quartz-pebbly feldspathic lithic wacke (sequence A1 of Amarulik assemblage)	Northeast corner of 'Third Portage lake', near big basal BIF	PQB-MDB-2011-06/z10574; Appendix A, Figure A-4; plot from data of McNicoll (2020)
15	6	<2.725 Ga***	U-Pb detrital zircon	Lithic quartz-feldspar wacke (possibly sequence A3 of Amarulik assemblage)	East corner Amarulik basin, on peninsula in northern 'Tasiraraujaq'	ZB98-455AZ/z5556; Davis (2021), AAMwq lithology and geology from Zaleski et al. (2005)
14	6	<2769 \pm 11 Ma***	U-Pb detrital zircon	Metagreywacke, southeast of Amarulik Lake (possibly sequence A3 of Amarulik assemblage)	Southeast of site 13 ("metadacite" of Roddick et al., 1992)	89HSA-74/z1868; 4 discordant points on discordia diagram by Roddick et al. (1992)
13	6	<2739 \pm 2; <2787 \pm 9 Ma***	U-Pb detrital titanite; zircon	Epiclastic, southeast of Amarulik Lake ((?) sequence A3 of Amarulik assemblage)	'Metadacite' of Roddick et al. (1992)	89HSA-75/z1869; also z3300; z3299; Roddick et al. (1992)
12	3a	2679.6 \pm 2.5 Ma	U-Pb zircon	Felsic gneiss (Aberdeen assemblage)	Middle package of Hunter et al (2018), located near site 23 (11JP009)	GC-204954, felsic gneiss of Hunter et al. (2018). 150 m SE of GC-204953
11	3a	<2687 \pm 7 Ma	U-Pb detrital zircon	Paragneiss (Aberdeen assemblage)	Middle package of Hunter et al. (2018), located close to site 23 (11JP009)	GC-204953, psammopelitic gneiss of Hunter et al. (2018). 150 m NW of GC-204954
10	7a	<2.686 Ga	U-Pb detrital zircon	Metagreywacke, Jim zone Au (Pipedream assemblage)	Between 'Ukalik lake' and north Meadowbank River	11PHA041/z10809; Appendix A, Figure A-3; plot from data of McNicoll (2020)
9	8a	<2.686 Ga	U-Pb detrital zircon	Metagreywacke at Kiggavik (Pipedream assemblage west)	West side of Kiggavik camp (Lone Gull) drill camp, part host of U deposits	11JP398A01/z10808; Appendix A, Figure A-2; plot from data of McNicoll (2020)

Table 2. (cont.)

Site	Fig. no.	Age \pm error*	Method \pm mineral	Rock type, unit name	Geographic location, structural setting	References**
8	3a	2695 \pm 4 Ma	U-Pb zircon, discordant	Syenogranite, foliated, Chesterfield fault zone	South end of Long Lake, NW side of Baker Lake Basin	A.N. LeCheminant and J.C. Roddick, unpublished data, age listed in Hadlari et al. (2004)
7	3a, 6	<2.706 Ga	U-Pb detrital zircon	Metagreywacke (type Pipedream assemblage)	7 km northeast of Meadowbank Au mine; 5.2 km east of Tern Lake	10JPM078/z10971; Appendix A, Figure A-1; plot from data of McNicoll (2020)
6	6	2710 \pm 3.5/-2.2	U-Pb zircon	Similar ages on same felsic meta-volcanic rocks (Pipedream assemblage)	8.5 km NNE of North Portage BIF and Au deposit	ZB96-223AZ/z4413; Davis and Zaleski (1998)
5b	6	2711 \pm 3 Ma	U-Pb zircon	Blue quartz-plagioclase-phyric massive dacite (Pipedream assemblage)	Footwall 400 m E of North Portage deposit	GC02; z6669; Sherlock et al. (2004) (upper intercept, MSWD = 2.47)
5a	6	2.711 Ga host; 2.717 Ga at fault	U-Pb zircon	Intermediate-felsic + felsic volcanoclastic rocks (Pipedream assemblage)	Meadowbank Au mine; outcrops and open pits	Janvier et al. (2015a); Janvier et al. (2015b); Fig. 2 legend: 2a-2b-2c, 3a = 2.711 Ga; uncoded = 2.717 Ga). Concordia diagram upper intercept
4	3a	2719 \pm 1, 2718 \pm 3.1/-2.2 Ma	U-Pb zircon	Quartz-plagioclase porphyritic felsic tuff (North Meadowbank assemblage)	z5493 south of quartzite; z5513 between komatiites, west of Meadowbank River	zb98-449Az/z5493; zb98-448AZ/z5513, respectively. Nutiplilik of Zaleski (2005); ages from Davis et al. (2021)
3	6	2734.2 \pm 1.8 Ma	U-Pb zircon	Felsic flows and tuffs in mafic-dominated succession (Half Way Hills assemblage)	Between Thelon River and Whitehills synform	zb99-449az/z5918; Davis et al. (2021); context Zaleski et al. (2005, Map 2069a)
2	3a	2754.4 \pm 9.7 Ma	U-Pb zircon	Felsic and mafic gneiss (lower Aberdeen assemblage)	Lower Aberdeen assemblage, west of Schultz Lake intrusive complex	GC-204970 (felsic gneiss), GC-204972 (mafic gneiss); lower sequence of Hunter et al. (2018)
1b	6	2869 \pm 6 Ma	U-Pb zircon	Sanning tonalite as below	Northern part of same oval as below	zb00-118cz/z6691; Davis et al. (2021)
1a	6	2869 \pm 6 Ma	U-Pb zircon	Sanning tonalite: (?)basement and/or (?) 2.734 subvolcanic intrusion	NE end of ovals between Woodburn Lake group and Whitehills quartzite	zb99-420cz/z5917; Davis et al. (2021) (2.87 Ga of Zaleski et al., 2001b)

* The ordering of samples in this table is by geochronological age where possible, but in the case of obviously inherited zircon, e.g. site 42, or detrital zircon suites interpreted as incomplete, e.g. sites 34–37, the position is based on lithostratigraphy.

** z no. is the unique sample identifier in the Canadian Geochronology Knowledgebase (<https://www.nrcan.gc.ca/maps-tools-publications/tools/geodetic-reference-systems/canadian-geochronology-knowledgebase/18211>), accessed October 25, 2020.

*** Maximum detrital zircon or clast age is much older than the likely age of host unit (see 'Methods' section).

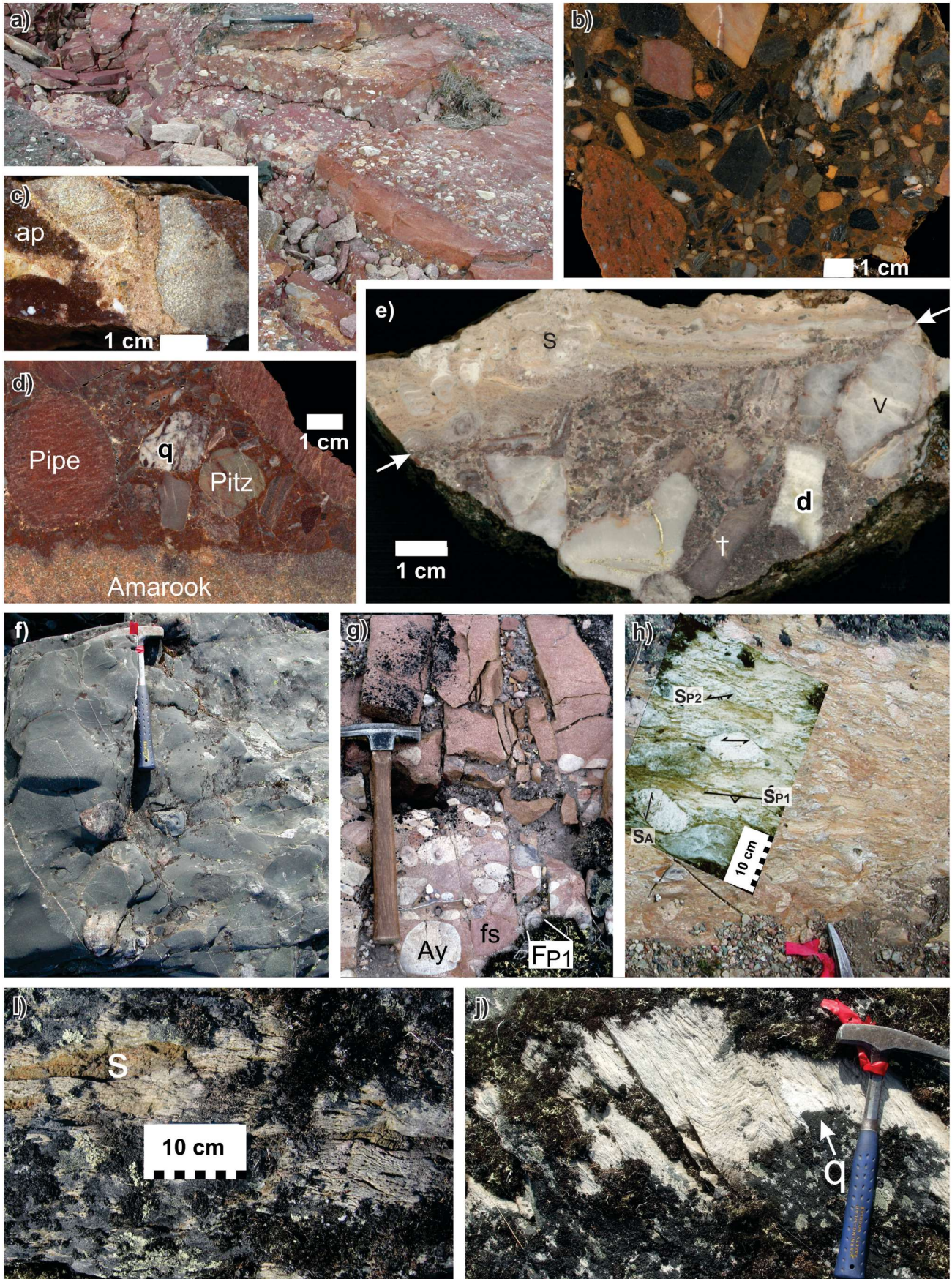
BIF = banded iron-formation, MSWD = mean square of weighted deviates, SIMS = secondary-ion mass spectrometry, SIs = Snow Island suite

Jefferson et al., 2015, 2023; C.W. Jefferson, R.H. Rainbird, G.M. Young, S.S. Gandhi, J.C. White, V. Tschirhart, D. Lemkow, and L.B. Chorlton, work in progress, 2023).

The Amer and Ketyet River belts were the main focus of the present Paleoproterozoic studies, whereas only limited data were collected from the Montresor Belt and much derived from other workers, principally Frisch (1992, 2000) and Percival et al. (2017). For clarity of description and analysis, the areas of the Amer, Ketyet River, Montresor, and other Paleoproterozoic belts are defined with reference to Figures 2 and 3a (see also 'Definitions of geological areas of focus and terminology' section above). This study provides limited, but critical new data and reassesses existing information on the Montresor Belt and five more westward Paleoproterozoic belts that resemble the Montresor Belt: Akiliniq, Deep Rose, Garry Lake, Naujatuq, and Sand.

The methodology used in GEM-1 mapping relied on extensive fieldwork to build a multidisciplinary ArcGIS® spatial geodatabase using Ganfeld 2004 (<https://science.gc.ca/site/science/en/educational-resources/history-geological-survey-canada-175-objects/165-ganfeld-2004>; accessed March 3, 2023), calibrated to specialized laboratory studies depending on the scientific focus. The focus in this study was mainly on real-time spatial integration of data from, and co-ordinating scientifically between, all members of the GEM-1 mapping team and the eight partners in the consortium. It was thus possible to develop working maps and thereby target favourable outcrop areas to calibrate key lithological (e.g. conglomerate types, Fig. 5) and geophysical markers; for example, iron-formation, some basalt, and other linear units with abundant disseminated magnetite, magnetic dykes and demagnetized fault zones, and radioactive sources as detailed by Peterson

Figure 5. Conglomerate and breccia as key marker units in the Aberdeen Subbasin region, *after* Jefferson et al. (2012). Images are in approximate stratigraphic order, with youngest at top right and oldest at bottom right (see text for further contextual information). **a)** Interbedded brick red mudstone and polymict conglomerate, a typical facies within the undeformed basal conglomerate assemblage of the Thelon Formation (hammer is 36 cm long). Photograph by C.W. Jefferson. NRCan photo 2020-886. **b)** Ferricrete breccia: iron-oxide-cemented postglacial fault talus located near the reactivated Medial fault zone on the northern side of upper Amer Lake. Sample collected by D. MacIsaac. Photograph by C.W. Jefferson. NRCan photo 2020-881. **c)** Intraformational conglomerate of the Thelon Formation cemented by uranium-bearing fluorapatite (ap) from near Spruce Grove Lake, in the Beverly Lake area. Photograph by I. Bilot. NRCan photo 2020-882. **d)** Locally derived nature of the polymict basal Thelon Formation conglomerate, with rounded clasts of red hematitized Neoproterozoic Pipe assemblage (Pipe), vein quartz (q), rhyolite of the Pitz Formation (Pitz), and the edge of a large angular block of silicified feldspathic quartzite of the Amarook Formation. Photograph by C.W. Jefferson. NRCan photo 2020-887. **e)** Upper Pitz Formation: horizontally laminated stratiform chert stromatolite onlapping silcrete breccia at a microunconformity (arrows) that dips toward the left and represents the edge of a hot spring pool. Columnar microstromatolites (s, upper left) grew beside the stratiform stromatolite laminae on upper right. Fragments within the siliceous breccia include vein quartz (v), drusy quartz (d), and tiny chert stromatolites (t) like those in the overlying pool deposit (see also Fig. 8b, d of Peterson et al., 2015a). Photograph by I. Bilot. NRCan photo 2020-883. **f)** Polymict conglomerate within slate of the lower Tasirjuak formation, the sequence Ps4 component of the Ketyet River group, exposed between the western shoreline of Whitehills Lake and a ridge of Ketyet River sequence Ps1 quartzite. Prominent rounded clasts of granitoid gneiss, quartzite, argillite, and dolostone below the 36 cm hammer are embedded in a compressed framework of larger to smaller, flat, grey slate and shaly sandstone intraclasts. Photograph by C.W. Jefferson. NRCan photo 2020-885. **g)** Upper part of polymict conglomerate grading up to salmon red sandstone at the base of Amer sequence Ps4B. Clasts include well rounded Ayagaq quartzite (Ay) (some predeformed (F_{p1})) and a high proportion of subrounded blocks of feldspathic sandstone (fs) resembling the underlying Amer sequence Ps4A strata. Hammer for scale is 34 cm. Photograph by G.M. Young. NRCan photo 2020-880. **h)** Basal polymict sequence Ps1 conglomerate, Ketyet River group, at geochronology site 34 (Table 2, Fig. 7a). Photograph by C.W. Jefferson. NRCan photo 2020-890. Rectilinear photograph overlay (reoriented from Fig. 4a of Pehrsson et al., 2013a) shows range of clast and matrix foliations visible prior to cuts in outcrop for removal of granite clast dated at 2.62 Ga; granite clast with foliation acquired prior to incorporation in this conglomerate is indicated (S_A). First Proterozoic (S_{p1}) and second Proterozoic (S_{p2}) foliations are so labelled. Photograph by S.J. Pehrsson. NRCan photo 2020-889. **i)** Polymict conglomerate at the interface between the sequence Ps1 quartzite and the first infold of sequence Ps3 basalt west of geochronology site 40 (Fig. 6). The normally intervening sequence Ps2 fine-grained siliciclastic unit is not present at this locality. The grey-green impure quartz arenite matrix is typical of the upper sequence Ps1 quartzite in the Whitehills Lake area, whereas the common scoria clasts (s) of this outcrop are atypical. Additional clasts not shown include vein quartz and Pukiq Lake formation porphyritic rhyolite. Photograph by C.W. Jefferson. NRCan photo 2020-884. **j)** Dispersed quartz pebbles to cobbles (q) in pale greenish and tan, coarse-grained quartzite, basal sequence in the Amarulik assemblage (northern sequence A1, geochronology site 16, 2, Fig. 6) Hammer for scale is 36 cm. Photograph by Y. Shelat. NRCan photo 2020-888



et al. (2011), Tschirhart et al. (2013a, b, c, d, 2014, 2017), and Morris et al. (2017). In poorly traversed areas, such as the southwestern portion of the Amarulik assemblage, spatial analysis of multiple remotely sensed data sets became the main basis for defining regional map units and the structural breaks between them (Fig. 6). Highly detailed mapping was also conducted by using aerial photographs, both 1:50 000 scale high-altitude and numerous low-level helicopter photographs geo-registered and rubbersheeted in ArcGIS, linked with detailed traverses and spot landings. In particular, superb exposures in the ‘Nipterk lake–Ukalik lake’ (unofficial names) (Zaleski, 2005) postglacial washout area provide unequalled areal knowledge about facies relationships and deformation in recessive supracrustal rocks, including the distinguishing of individual graded quartzite beds outlined by black slate partings, metre- to decametre-scale D_{p1} isoclinal folds, and multiply reactivated Riedel-shear structures (Fig. 7a–c). The work in the ‘Nipterk lake’ area confirmed a general working rule that quartzite, the most resistant rock in the region, can reasonably be expected to be mapped using aerial photographs and satellite imagery exactly where exposed, but is not to be inferred where not visible — this includes water bodies in places.

Petrology-defined mineralogical (e.g. Robinson et al., 2014, 2016) and microstructural (e.g. Calhoun et al., 2014) attributes helped calibrate and document field-based mapping criteria. Petrochemical analysis of igneous rocks (e.g. Peterson et al., 2015a, b, c; Scott et al., 2015) was successful in defining several suites that greatly simplified the map pattern. Geochronology of detrital, igneous, and diagenetic minerals (e.g. Table 2, Appendices A, B; Davis et al., 2011, 2021; McNicoll, 2020; Davis, 2021) provided essential constraints to pin the various igneous and sedimentary suites in sequence, as well as to link deformation and metamorphism (e.g. Pehrsson et al., 2013a).

Mapping relied heavily on extrapolation of knowledge between sparse outcrops with the aid of geophysical imagery and modelling, as well as Landsat and airphoto interpretation. A few well exposed localities and transects were mapped in great detail to serve as references for stratigraphy and structural style, and to calibrate geophysical data. Integrated geophysical data and interpretations were critical for calibrating and mapping the extents, shapes, and

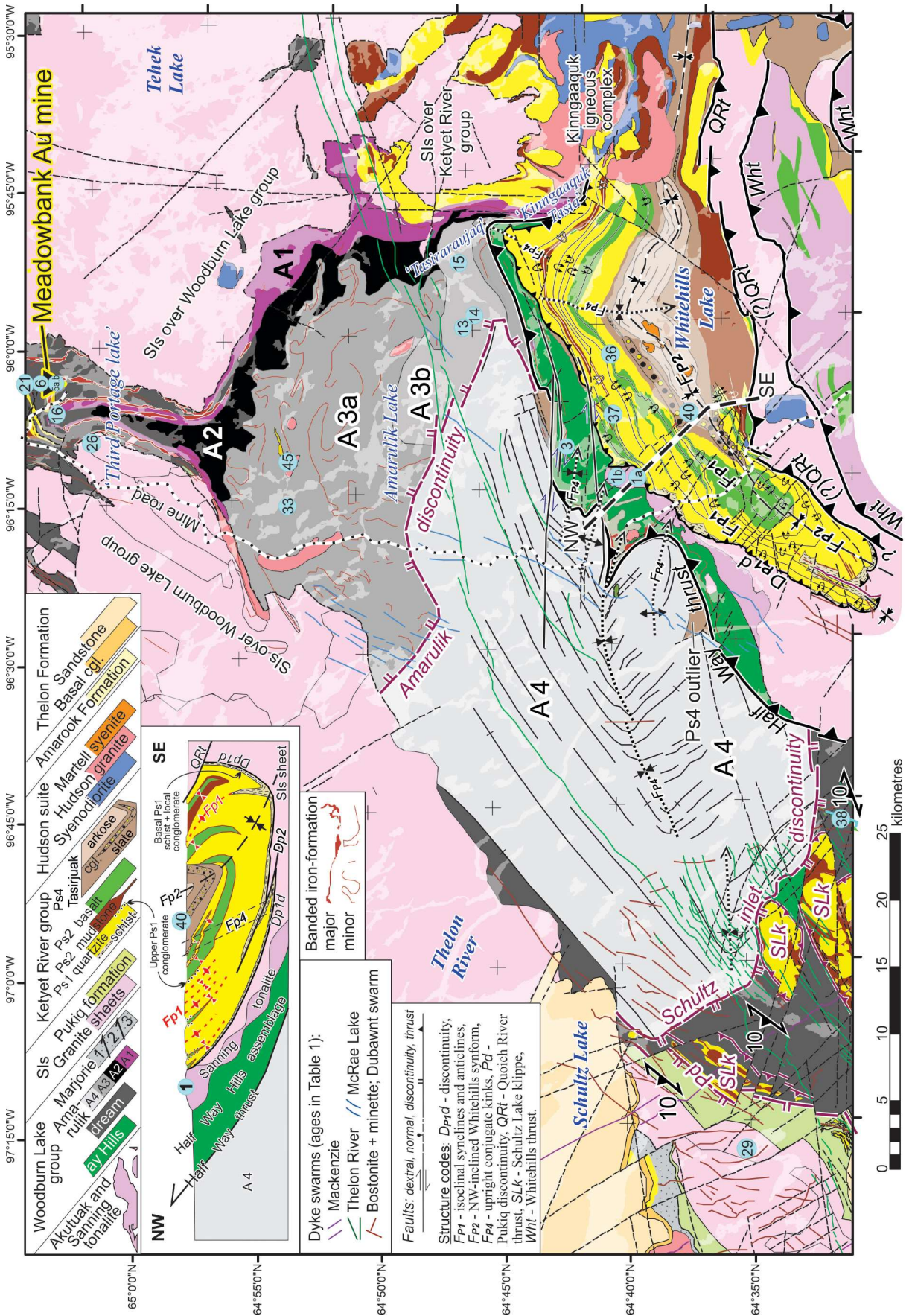
structures of basement rock units, both outside and underlying the northeast Thelon Basin, including reactivated fault systems (e.g. Tschirhart et al., 2011b, 2013a, b, c, d, 2014, 2017; Thomas, 2012). Geophysical reprocessing and modelling enhanced the value of raw, leveled aeromagnetic data through edge detection (e.g. Tschirhart et al., 2013a, b, c, d, 2017). Tschirhart (*see* Jefferson et al., 2013) adapted the Keating coefficient to identify small intrusions of Nueltin granite with outer comagmatic rings of Mallery gabbro (Peterson et al., 2015b), interpreted as eruption centres for the Pitz Formation (Kivalliq igneous suite) along fault zones in the Kivalliq Region of Nunavut. Based on these geophysical constraints, the present maps show geological boundaries continuing beneath lakes and sedimentary cover, especially the Amarook and Thelon formations. In many places, underlying geological units and structures can also be traced beneath sheets of 2.6 and 1.75 Ga granite. The structural paradigms followed herein are based on detailed outcrop mapping, but geophysics is a powerful tool for extrapolating structures and uranium-prospective magnetic units along strike beneath cover as well as to determine their three-dimensional geometries at depth after calibration of bulk rock properties with outcrop data.

Previous and parallel studies

The Thelon Basin has been far less studied than the Athabasca Basin, yet remains tantalizing in its promise, as reflected by reconnaissance uranium exploration programs covering much of the current study area in the late 1970s and early 1980s (e.g. Young, 1979; Miller and LeCheminant, 1985). The Thelon Game Sanctuary covers much of the main Thelon Basin (Fig. 2) and, as a result, the exploration surged from 1970 to the early 1980s and again in 2000 to 2012 targeted the northeast Thelon Basin and the southern tip around Boomerang Lake (Davidson and Gandhi, 1989). These are the areas that provide the most knowledge and easiest logistical access.

These exploration programs focused on the remarkable geological similarities between unconformity-related uranium environments of the Thelon Basin and the highly productive Athabasca Basin, as reviewed by Miller and LeCheminant (1985), Fuchs et al. (1986), Fuchs and Hilger (1989), and

Figure 6. Geology of the Neoproterozoic Amarulik basin (*after* Taylor, 1985; Roddick et al., 1992; Henderson and Henderson, 1994; Hrabí et al., 2003; Hadlari et al., 2004; Pehrsson et al., 2004, 2013a; Sherlock et al., 2004; Zaleski and Pehrsson, 2005; Shelat et al., 2012a, b; Tschirhart et al., 2011a; LaRocque et al., 2012; Janvier et al., 2015a, b; L.B. Aspler, A.R. Miller, and A.N. LeCheminant, unpub. comp., 2010). Numbered blue dots locate geochronology sites listed in Table 2. Faults are either labelled directly or coded as in legend (inset). Labels A1 through A4 denote the four sequences of the Amarulik assemblage discussed in the text. Iron-formations in sequence A3a and projected beneath Snow Island suite (SIs) sheets are interpreted mainly from aeromagnetic data with few outcrop constraints. Representative fold axes in quartzite, basalt, and sequence Ps4 units illustrate the degree of structural thickening. Dashed black and white line trending northwest shows location of schematic, down-plunge-projected, northwest-southeast cross-section through the Half Way thrust and Whitehills Lake F_{p2} synform (upper left inset, below map-unit legend). cgl. = conglomerate.



Gandhi (1989). Exploration also targeted stratabound, sandstone-hosted uranium in basement rocks beside the Athabasca Basin (Wollaston Supergroup; Yeo and Delaney, 2007) and the northeast Thelon Basin (Amer group; e.g. Blackwell, 1978, Young, 1979). Matthews et al. (1997) further set out integrated geophysical-geochemical-geological models and techniques used to explore unconformity-related uranium prospects in both the Athabasca and Thelon basins. The exploration surge from around 2005 through to 2012 further advanced how the unconformity model applies to the Thelon Basin region (Jefferson et al., 2011b), as well as tested other uranium environments, such as sandstone uranium in the Amer group (Jefferson et al., 2011b, 2015, 2023; C.W. Jefferson, R.H. Rainbird, G.M. Young, S.S. Gandhi, J.C. White, V. Tschirhart, D. Lemkow, and L.B. Chorlton, work in progress, 2023). Each exploration surge also trained fresh cadres of graduate students and uranium-exploration experts. The latest surge generated large, high-resolution geophysical data sets, which the GEM-1 consortium preserved and integrated (Tschirhart et al., 2011a).

The GEM-1 Uranium project built on important previous, and parallel, thematic and regional studies. Tella (1984, 1994) and Patterson (1986) published the first comprehensive maps of the Amer Belt. Hadlari et al. (2004) mapped and compiled legacy data for the first modern geological map of the Schultz Lake area at the 1:250 000 scale, while Zaleski (2005), Zaleski and Pehrsson (2005), and Pehrsson et al. (2013a) summarized many map products in the region from Whitehills Lake (the Inuit name for that lake, ‘Tasirjuak’ (unofficial name) (Zaleski and Pehrsson, 2005), is used later in this paper to name a stratigraphic unit) to the eastern Amer Belt. They also pointed out areas of superb outcrop deserving more detailed study, such as around ‘Nipterk’ and ‘Ukalik’ lakes (Fig. 7a–c). Hiatt et al. (2003) documented three upward-fining sequences of Thelon Basin stratigraphy that Davis et al. (2011) corroborated through the same quantitative grain-size analysis as applied to the Athabasca Basin (Ramaekers et al., 2007). Beyer et al. (2010) detailed the basement geology, unconformity-related uranium trends and paragenesis in the Boomerang Lake area. Detailed mapping, geochronology, structural geology, and fluid inclusion results of Hunter et al. (2018, 2021) provided new understanding in areas south of Aberdeen Lake (rectangle labelled ‘Hunter 2018’ in Fig. 3a) and was extrapolated to south of

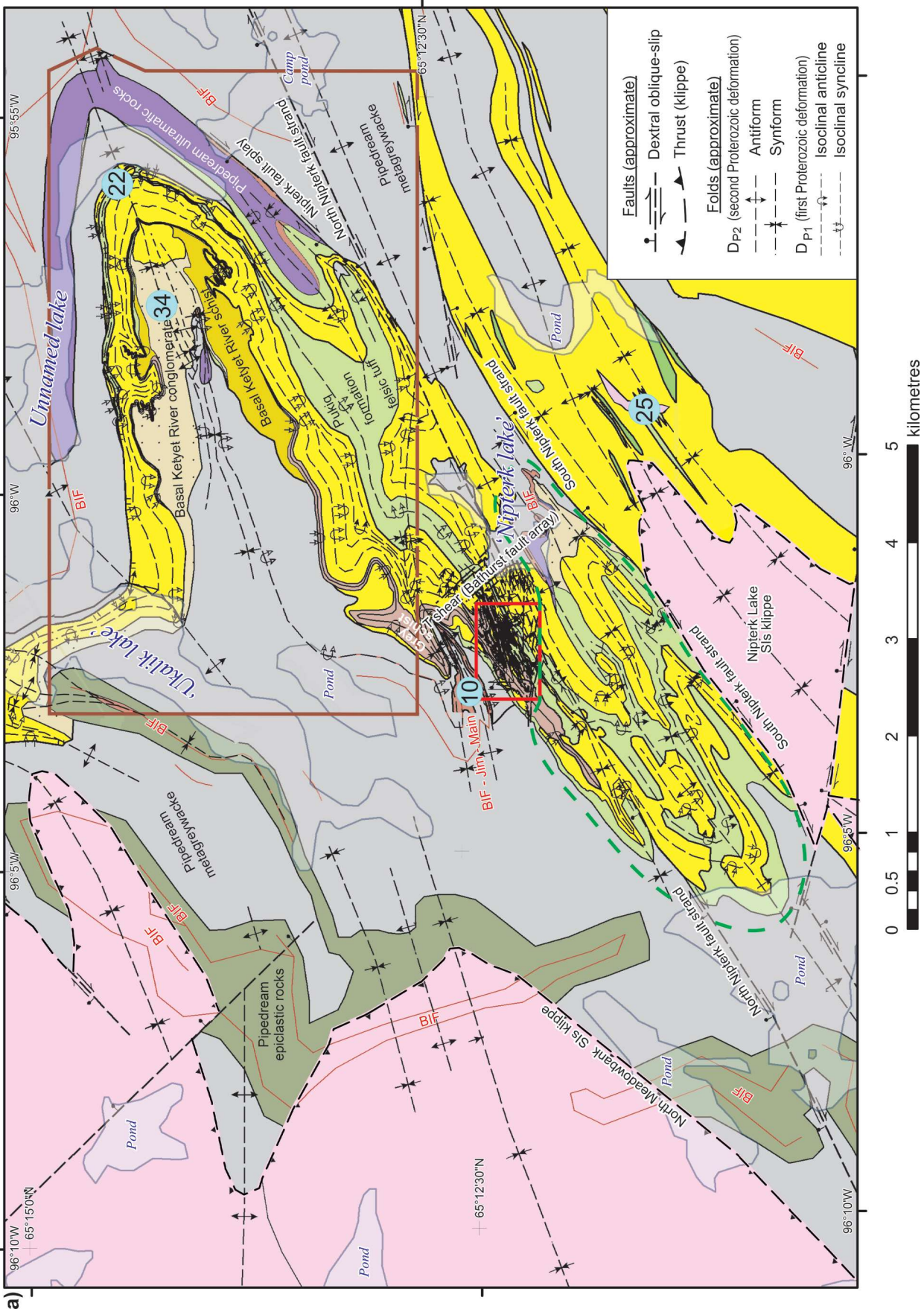
Schultz Lake, where GEM-1 knowledge had been based on reconnaissance geological-geophysical traverses and maps by LeCheminant et al. (1983) and Hadlari et al. (2004).

For the remaining parts of the Thelon Basin and adjacent basement terranes, historical regional maps and preliminary reports provided meticulous baseline information and insights into the regional geology. For example, Peterson et al. (2014) updated LeCheminant (1981) as part of this project. The compilation by Patterson and LeCheminant (1985) is the only source of map knowledge in places such as the northeastern Turqavik horst (Fig. 3a, b) and, together with Donaldson (1965), provides insights in many other places. Peterson (2006) and Peterson and LeCheminant (1996) documented the core igneous components of the Dubawnt Supergroup in their map context. Schau et al. (1982) and Hadlari et al. (2004) mapped units of granitoid gneiss that constitute the Chesterfield fault zone, with descriptions specific enough to allow partitioning of some units into the Snow Island suite and others into the Hudson granitoid suite (*see* ‘Magmatism’ section). Berman et al. (2007) added high-pressure metamorphism and tectonic understanding of the Chesterfield fault zone (*see* ‘Structure and metamorphism’ section), whereas the bulk of the Chesterfield gneiss remains of unknown age and parentage — the subjects of ongoing research. The outcrop mapping of Taylor (1985) precisely documented dykes, myriad outcrops, and major lithological contacts that no others have since traced by ‘boots on the ground’ in the Whitehills Lake region, as did LeCheminant et al. (1983, 1984) in much of the region south of Aberdeen and Beverly lakes. Regional stratigraphic and petrographic studies by Donaldson (1965, 1966), Cecile (1973), Gall (1992, 1994) and Gall et al. (1992) are all dependably integrated into the current stratigraphic scheme.

A seismic reflection study by Overton (1979) provides depth constraints covering all of the Thelon Basin and integrates well in its northeastern portion with the results of Tschirhart et al. (2014). Metallogenic comparisons between the Athabasca and Thelon basins by Miller and LeCheminant (1985), Fuchs et al. (1986), Fuchs and Hilger (1989), Gandhi (1989), and Kyser et al. (2000) remain valid, with the comparisons here providing more parameters and precision.

While the NUC and GEM-1 Uranium projects were underway, industry members of the consortium (Jefferson et al., 2011b) supported many independent graduate student projects

Figure 7. Detailed Archean–Paleoproterozoic geology of the ‘Nipterk lake’–‘Ukalik lake’ area lakes area, exported from ArcGIS® geodatabase (C.W. Jefferson and L.B. Chorlton, work in progress, 2023). Numbered blue dots locate geochronology sites listed in Table 2. Legend for fault and fold symbols appears on Figure 7a. **a)** Map at 1:50 000 scale of the ‘Ukalik lake’ F_{p2} fold (area outlined in brown *after* McEwan, 2012) to the ‘Nipterk lake’ washout (red rectangle detailed in Fig. 7b, c). Pipedream banded iron-formation (BIF) hosted by epiclastic rocks is geophysically extrapolated beneath a tectonic sheet of Snow Island suite (SIs) along the western side of the map. Complex folds involving Pukiq Lake formation rhyolite tuff and Ketyet River group quartzite southwest of ‘Nipterk lake’ (area outlined by green dashed line) are interpreted from limited ground data, air photographs, and Landsat imagery (remaining geology *after* Zaleski, 2005; Pehrsson et al., 2013a).



a)

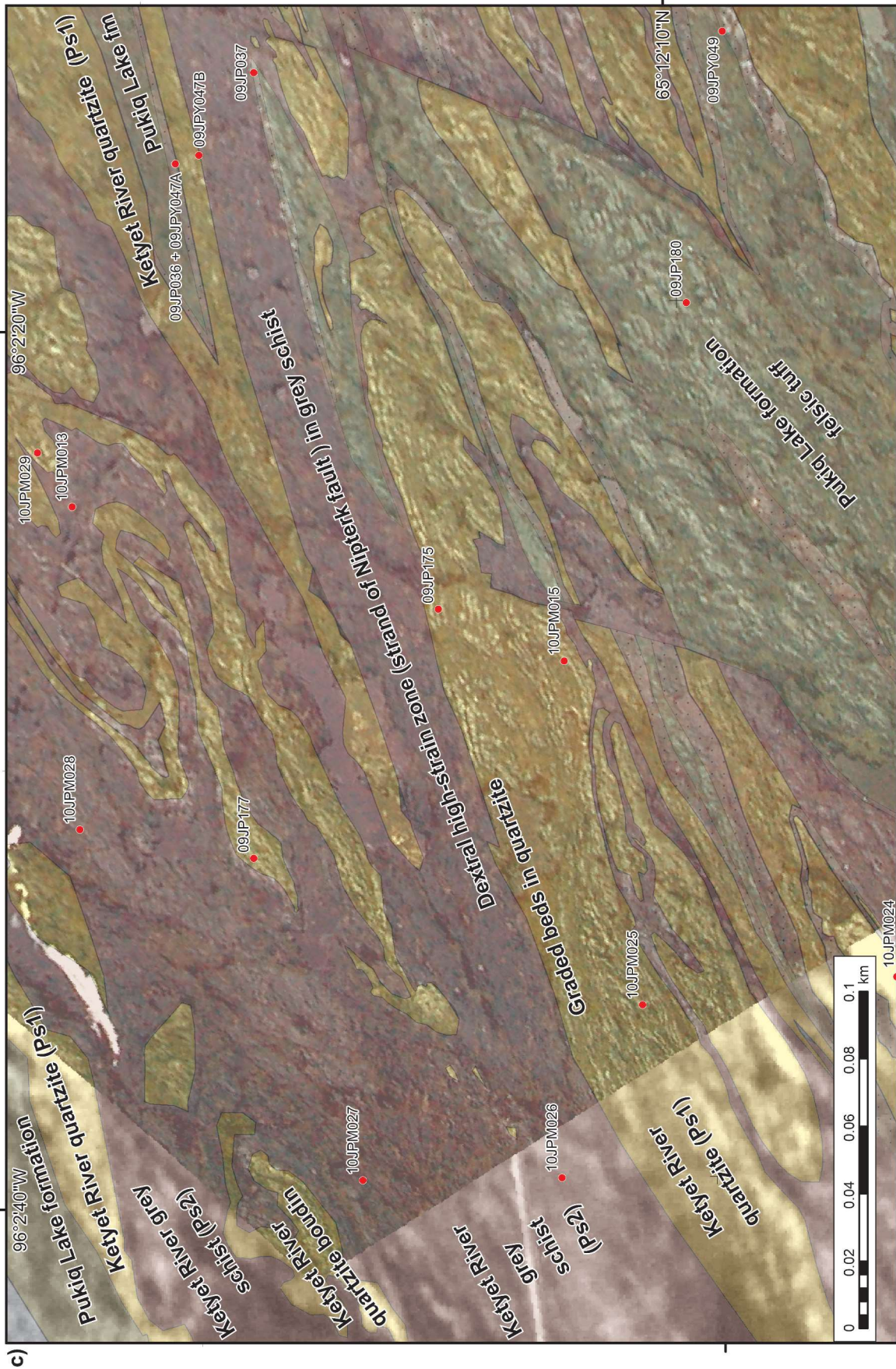


Figure 7. (cont.) c) Detail at 1:1500 scale of the approximately 90% exposed core of the 'Nipterk lake' washout. The same geology polygons as in Figure 7b are outlined as transparent overlays on part of NRCan photo 2021-954 taken from a helicopter. The photograph was rubbersheeted and geo-registered in ArcGIS with the same regional air photographs as in Figure 7b completing the western part of this detailed map base (part of NRCan photo 2021-955). Labelled stations 09JPY (Y. Shelat) and 10JPM (B. McEwan) show sample locations; 09JP stations denote centres of this and other photographs taken from a helicopter and used for remote mapping. Photographs by C. W. Jefferson.

on their claim groups. Comprehensive mapping, as well as petrochemistry and geochronology studies (Hunter et al., 2012, 2014, 2018, 2021), shed considerable light on the composition, ages, and structural complexities of Archean supracrustal rocks south of Aberdeen Lake, between the Schultz Lake intrusive complex and Marjorie Lake (black rectangle Fig. 3a). Studies by Riegler (2014) and Riegler et al. (2014, 2016a, b) examined the alteration related to the uranium deposits in the Kiggavik–Andrew Lake structural trend, while Johnstone (2017) and D. Johnstone, K. Bethune, D. Quirt, and A. Benedicto (unpub. rept. no. 15-CND-92-04 of AREVA Resources Canada Inc., 2015) studied the lithostratigraphic and structural controls of uranium mineralization in the Kiggavik deposits. Later independent work, such as by Grare et al. (2018), provided additional knowledge of the Kiggavik uranium exploration camp as a whole, while focusing on new deposit-specific research on the Contact occurrence (Fig. 8). Like Hunter et al. (2014), by putting the original faults of Fuchs and Hilger (1989) for the Lone Gull (now Kiggavik Main Zone) deposit into modern context, Anand and Jefferson (2017a) recognized Riedel-shear arrays (Fig. 9a, b) as critical to understanding fault controls of uranium mineralization. Grare et al. (2018) expanded Riedel-shear analysis to the scale of the entire Kiggavik uranium camp (approximately the area of Fig. 8).

At the same time as the northeast Thelon Basin consortium developed, first the NUC and then the GEM-1 Uranium project supported new research on uranium environments elsewhere in the Canadian Shield, many projects being undertaken in collaboration with the exploration industry. These include the “Beaverlodge Uranium District” (Tracey et al., 2009, 2010), the Great Bear magmatic zone (Potter et al., 2013, 2019, 2020, 2022; Montreuil et al., 2015, 2016; Corriveau et al., 2016; Gandhi et al., 2018; Corriveau and Potter, this volume), Lac Cinquante (Bridge et al., 2013), and the Athabasca Basin (Reid et al., 2014, 2016; Reid, 2018). Over the Athabasca Basin in Saskatchewan, the largest contiguous government geophysical survey in Canada was also completed during GEM-1 by partnering with the Saskatchewan Geological Survey. Subsequent Targeted Geoscience Initiative and GEM-1 projects also integrated the GEM-1 Uranium project knowledge (e.g. Pehrsson et al., 2014a, b; Potter and Wright, 2015; Wright and Potter, 2015). These parallel studies provide additional context and analogues with which to better understand the Thelon Basin. Especially important are key parameters for uranium exploration (*see* ‘Alteration and metallogenic comparisons of the Athabasca Basin and Thelon Basin regions’ section) and major resetting events, such as the extensive 1.4 Ga resetting of uranium- and gold-occurrence ages across the Canadian Shield (Table 2; *see also* ‘Comparative ages of sedimentation and diagenesis’ section).

In surrounding basement terranes, considerable gold endowment is being mined at the Meadowbank and Amaruq deposits operated by Agnico Eagle Mines Limited (Pehrsson et al., 2004, 2013a; Côté-Mantha et al., 2015; Janvier et al., 2015a, b). Although not uranium deposits, these sites provide

excellent training areas for understanding basement-hosted uranium because of their extensive drilling operations and outcrop exposures. Enhancing the understanding of lithology, structure, and metamorphism of gold-producing assemblages also improves exploration and mining strategies for basement-hosted uranium deposits.

NEW DEVELOPMENTS IN GEOLOGY OF THE NORTHEAST THELON BASIN REGION

Table 1 summarizes the tectonic (D_{p1} through D_{p13} and D_{ph1} through D_{ph3}) and magmatic events, depositional sequences, alteration, and metallogeny of the Aberdeen Subbasin region. Figure 4a provides context for Figure 4b that illustrates D_{p1} and D_{p2} in this region. The main rock packages include various granitoid gneiss units of unknown ages and origins; an assortment of Neoproterozoic supracrustal packages constituting the informal Woodburn Lake group; four early Paleoproterozoic supracrustal sequences (Ps1–Ps4) that correlate across the study area; the Baker Lake, Wharton, and Barrenland groups of the Dubawnt Supergroup; and a small outlier of Ordovician dolostone. Three large igneous provinces (*see* ‘Magmatism’ section below) punctuated and contributed key extrusive components to the Archean and Paleoproterozoic depositional records. This section briefly describes all of the supracrustal packages and magmatic suites, as well as their distinguishing textural and structural characteristics, and expands these descriptions where new information is available since that reported by Pehrsson et al. (2013a).

Woodburn Lake group: Neoproterozoic supracrustal rocks

Background and geographic definition of Neoproterozoic supracrustal belts

The relatively well preserved Neoproterozoic volcano-sedimentary belts in the study region comprise seven assemblages (Fig. 3b, 4a), all included in the Woodburn Lake group by previous workers. This group was named, but left essentially undefined by Fraser (1988), and little published information is available about supracrustal rocks in the area around Woodburn Lake itself (northeast corner of Fig. 3a, b), mapped by Skulski et al. (2018) as “Adx: paragneiss, migmatite, metatexite and diatexite, locally dated at ca. <2.69 >2.60 Ga.” As introduced by Fraser (1988), supracrustal rocks included in the Woodburn Lake group extended only as far northeast as the ‘Fractal lake’–‘Farside lake’ (unofficial names)—north Meadowbank River area, with only scattered “Anp: biotite-quartz schist/gneiss, paragneiss” (Skulski et al., 2018) recognized around Woodburn Lake. The group is thus loosely understood as comprising all recognizably Neoproterozoic supracrustal rocks in the study region, and it is unknown which, if any, of the currently

known assemblages is present at Woodburn Lake itself. Nevertheless, geophysical trends, especially distinct linear aeromagnetic highs, here interpreted as iron-formation and ultramafic rocks outlining large folds (Fig. 3b, d), suggest that the Pipedream assemblage continues much farther to the northeast than previously mapped (e.g. Fraser, 1988; Skulski et al., 2018), through and well past Woodburn Lake itself, albeit at high metamorphic grades. Based on aeromagnetic data and a gravity transect interpreted by Thomas (2012), much of the Pipedream assemblage underlies broad thrust sheets of the Snow Island suite in the northeastern part of the study area.

Collectively, the Woodburn Lake group assemblages range in age from 2.75 to after 2.6 Ga. Hunter et al. (2018) compared the Neoproterozoic supracrustal assemblages of the Rae Craton and noted that most have a 2.75 to 2.73 Ga mafic-ultramafic volcanic lower assemblage and psammitic to pelitic middle and upper assemblages ranging to as young as 2.6 Ga. None of these belts correlate in detail. The Woodburn Lake group as defined by Pehrsson et al. (2013b), the Committee Bay Belt (Sanborn-Barrie et al., 2014), and the Mary River group also have second 2.72 to 2.71 Ga ultramafic to felsic metavolcanic assemblages with associated psammite and iron-formation that are unrepresented in the Aberdeen assemblage and two other areas. Analysis of the Woodburn Lake group assemblages shows that they each have independent geochemical and geochronological evolutions.

The Woodburn Lake group is thus not a group in the stratigraphic sense, but rather a collage of diverse assemblages, which have been tectonically assembled, first internally and then collectively into apparently contiguous belts. The Woodburn Lake ‘group’ name is nevertheless retained for convenience, as it is deeply embedded in the literature. Coined by Fraser (1988) for supracrustal rocks thought to be Archean, it originally included extensive quartzite units and associated strata that are now known as the early Paleoproterozoic Ketyet River group. Pehrsson et al. (2013a) excluded Paleoproterozoic quartzite from the Woodburn Lake group and set out structural criteria to help differentiate the Neoproterozoic from the early Paleoproterozoic (*see below*). They named five ‘sequences’ of the Woodburn Lake group: the Half Way Hills, Wading Lake (here termed just Wading), North Meadowbank, Pipedream, and Amarulik. Work during this project further confirmed that laterally extensive white quartzite units of the Ketyet River group unconformably overlie the 2.6 Ga Pukiq Lake formation (Peterson et al., this volume; *see ‘Snow Island suite’ section below*) and thus postdate the earlier-than 2.6 Ga Woodburn Lake group (*see ‘Early Paleoproterozoic cover sequences: Amer, Ketyet River, Montesor, and western belts’ section below*). The Archean quartzite is differentiated lithologically from the Proterozoic quartzite by its thin and discontinuous geometry, waxy yellowish colour, and by intercalation with felsic to ultramafic metavolcanic rocks and greywacke, which are not present in the Paleoproterozoic cover sequences.

The ‘sequence’ descriptions by Pehrsson et al. (2013a) incorporated previous studies (e.g. Kjarsgaard et al., 1997; Zaleski et al., 1999, 2001a) that ascertained limited volcanic architecture and stratigraphic facing-direction data. Given that mappable stratigraphy has not been established within any of these packages, the term ‘assemblage’ is used here instead, following Jefferson et al. (2015). Jefferson et al. (2015) changed the term ‘sequence’ of Pehrsson et al. (2013a) to ‘assemblage’ for the Neoproterozoic packages, also because these rock packages are broken into individual map units based on only limited geochronology, structural breaks, and basic lithological variations rather than by mappable unconformities or other sequence boundaries. Paleoproterozoic and earlier deformation have obscured the primary lithostratigraphic ordering of their volcanic and sedimentary facies. One exception may be the Amarulik assemblage that unconformably overlies the Pipedream assemblage and can be divided geophysically and lithologically into four internal sequences (Fig. 6).

The original five Woodburn Lake group assemblages are differentiated in Figure 3b and their geometric relationships are cartooned in Figure 4a. The contacts between the Amarulik, Pipedream, and Half Way Hills assemblages as context for the Amarulik assemblage are mapped in Figure 6. Considerable detailed field and laboratory study would be required to develop Archean sequence stratigraphy within all of the other Woodburn Lake group assemblages. Summary lithological characteristics of existing and new Neoproterozoic assemblages are provided in Figure 4a and Table 1. The following descriptions introduce the new assemblages and more lithological detail, only where the knowledge synthesized by Pehrsson et al. (2013a) is incremented.

Jefferson et al. (2015) introduced the Rumble assemblage, incorporating map data from Young (1979), Tella (1994), Zaleski (2005), and new GEM results (e.g. Jefferson et al., 2011a, c; Patterson et al., 2012; Tschirhart et al., 2013d; Calhoun et al., 2014; Peterson et al., 2015c, this volume). Hunter et al. (2018) established the three supracrustal packages here included in the Aberdeen *assemblage* and considered them to be independent of the Woodburn Lake group and other Neoproterozoic belts in the Rae Craton, as detailed below. On the other hand, their ‘independent’ interpretation, with which the present authors agree, also applies to all the other assemblages of the Woodburn Lake group, therefore independence is not a valid reason to exclude the Aberdeen assemblage from the Woodburn Lake group. Tschirhart et al. (2013b, 2017) and Jefferson et al. (2015) had previously included the rocks of the Aberdeen assemblage (black rectangle in Fig. 3a) as part of the Marjorie Hills assemblage, here renamed the ‘Marjorie terrane’ (Fig. 3b, 4a) (*see revised definition of Marjorie terrane below*). Because Hunter et al. (2018, 2021) were able to map three distinct age packages of Neoproterozoic supracrustal rocks in the portion of the Marjorie terrane south of Aberdeen Lake, it is useful to retain the term Aberdeen as a distinct assemblage of the Woodburn Lake group.

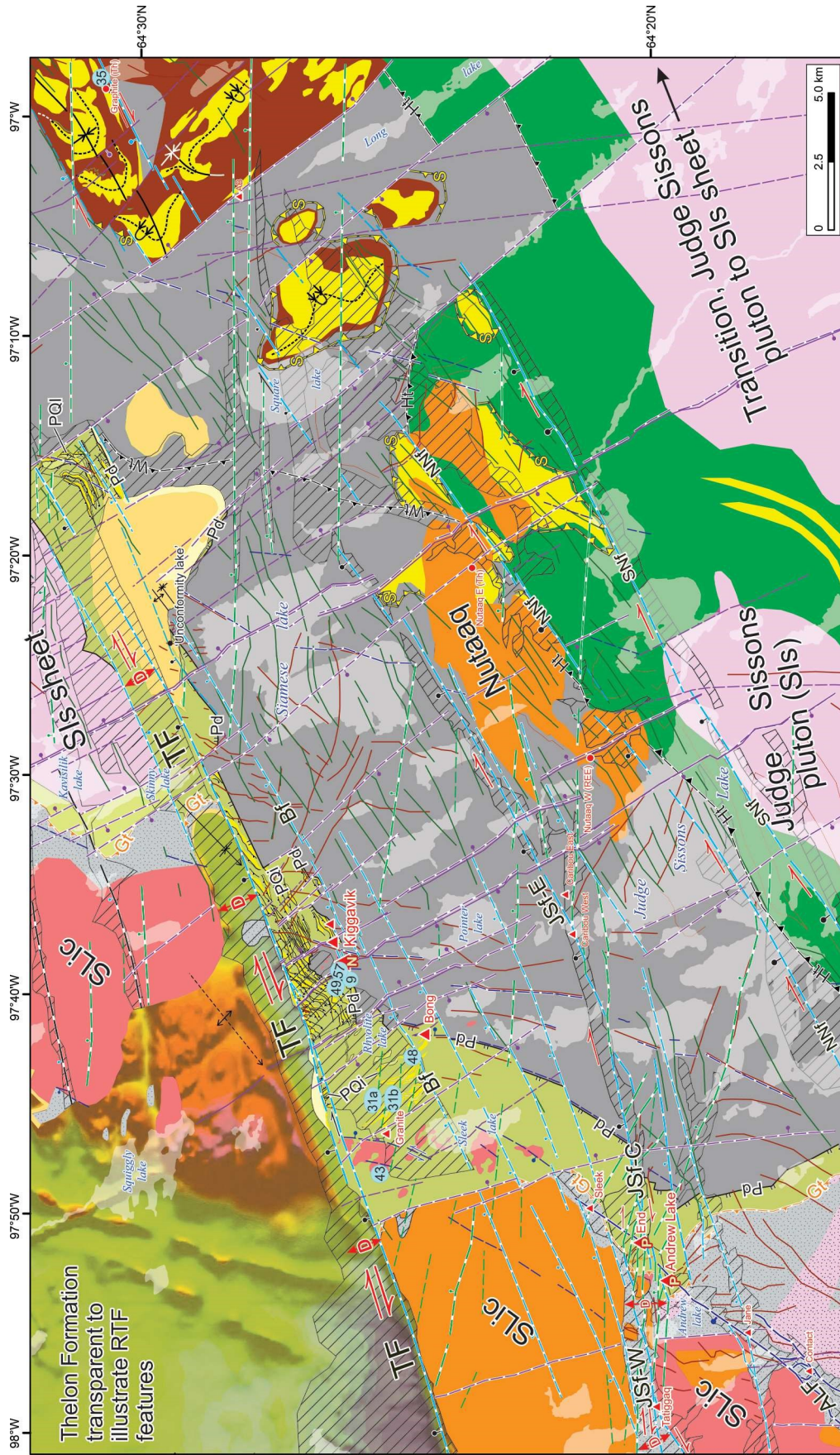


Figure 8. a) Generalized geology of the Kiggavik uranium camp and adjacent parts of the northeast Thelon Basin (after Anand and Jefferson, 2017a). Context shown in Figure 3a. Geology in the area including Tatiggaq, Contact, Sleek, and Caribou East uranium occurrences is after Grare et al. (2018). Half Way thrust is extrapolated from the Half Way Hills area (Fig. 6). The labels SLic (Schultz Lake intrusive complex) and Nutaq denote mixed Hudsonian (1.83 Ga) granite and syenite altered by the 1.75 Ga Kivalliq igneous suite (see 'Magmatism' section). The Riedel-shear elements are colour coded to faults on the map and explained in Figure 9 and the text. Transparent Thelon Formation in northwest corner illustrates the way residual total field (RTF) imagery enables remote mapping of dykes, faults, and other magnetic units such as the SLic. Legend (Fig. 8b) shows selected map units, mineral occurrences, and structural elements. BIF = banded iron-formation, D = demagnetized zone.

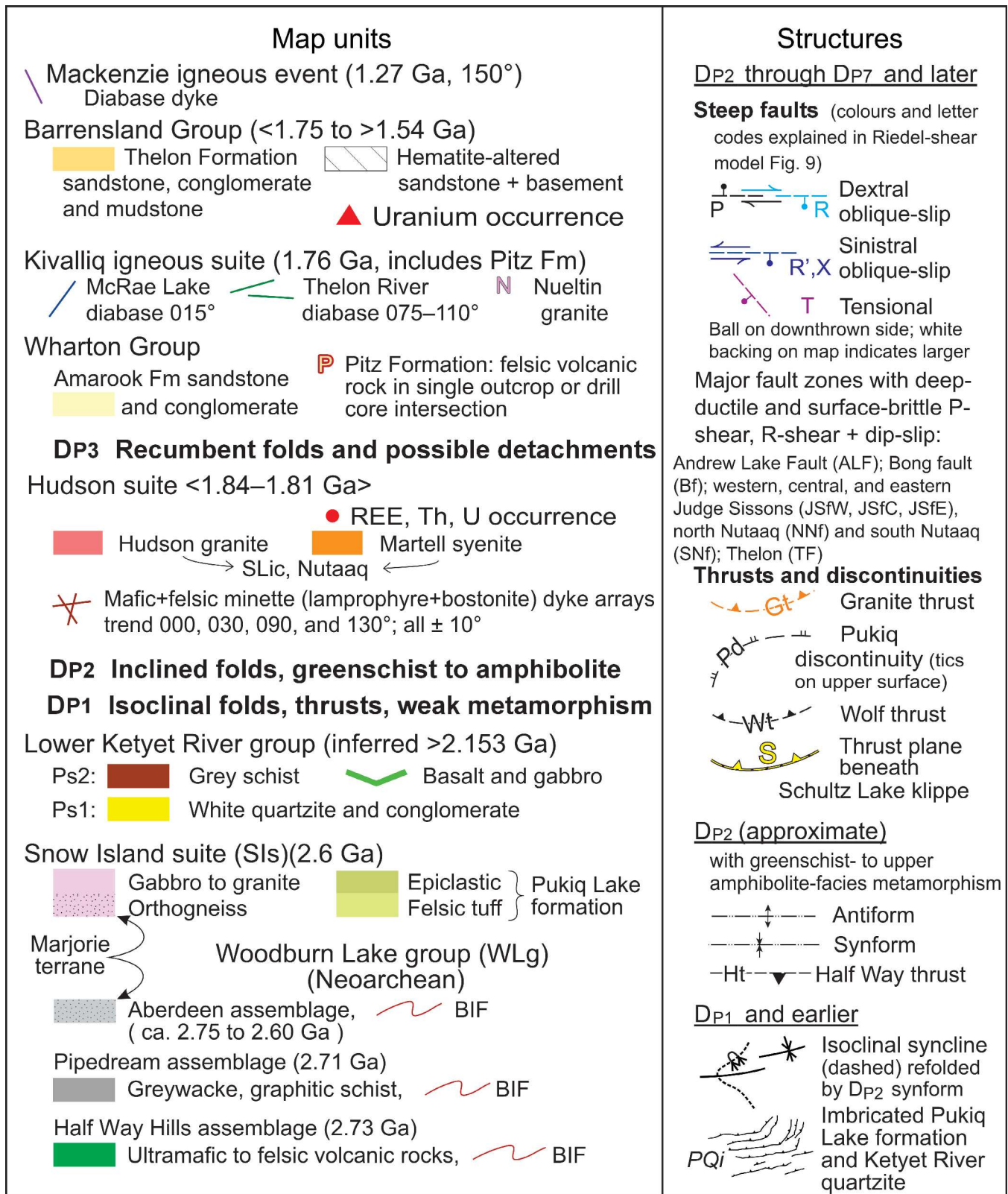


Figure 8. (cont.) b) Legend for Figure 8a.

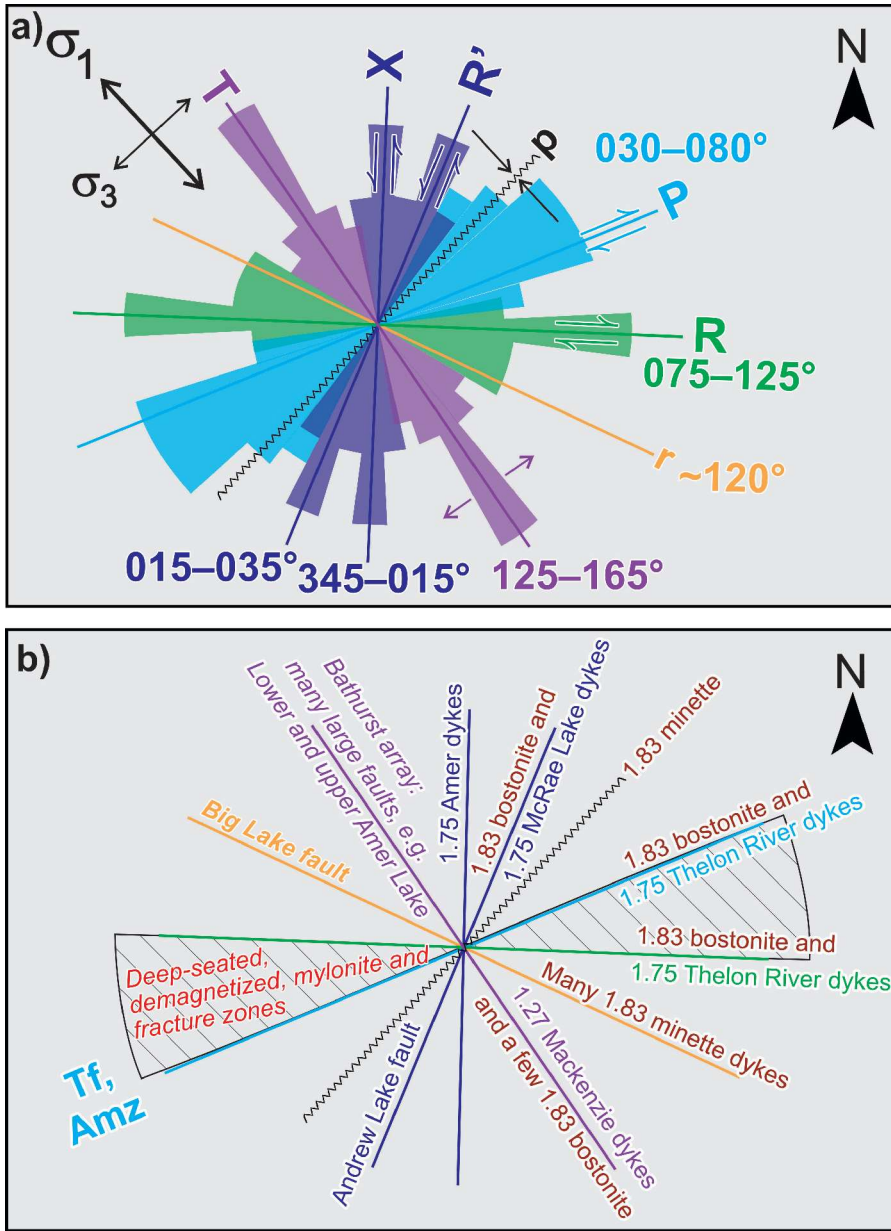


Figure 9. Summary of Riedel-shear elements in the northeast Aberdeen Subbasin region (after Anand and Jefferson, 2017a, b), exemplified in Figures 3c, 7b, and 8a. **a)** Riedel elements shown as lines (qualitative modes) and rose diagrams (qualitative relative abundances of orientations, with approximate ranges labelled in degrees). **b)** Examples of faults and dykes occupying Riedel-shear orientations (numbers represent approximate ages in Ga). Amz = Amer mylonite zone, TF = Thelon Fault.

For better understanding of the spatial distribution of these Neoproterozoic assemblages, the Marjorie–Kiggavik–Tehek Belt is defined here as the geographic area of Neoproterozoic supracrustal rocks that extends from the Marjorie Lake region in the southwest, through the Kiggavik uranium camp (Fig. 8), up to and including the western Tehek Lake area (Fig. 2, 3a). The Neoproterozoic rocks in this belt include all or parts of four assemblages: all of the Half Way Hills assemblage, the western block and marginal slivers of the eastern Pipedream assemblage, all of the Aberdeen assemblage, and all of the Amarulik assemblage. Using the term ‘Woodburn Lake supracrustal belt’ as diagrammed by Theriault et al. (2018) is confusing because it excludes the Rumble assemblage that is also part of the Woodburn Lake group, and it includes a north–south component distinguished here as the ‘Meadowbank River Belt’. It is useful to define the Rumble Belt as a separate entity because

the Rumble assemblage underlies the Paleoproterozoic Amer Belt, whereas other assemblages of the Woodburn Lake group underlie the Paleoproterozoic Ketyet River Belt. Furthermore, the Rumble Belt is separated from the rest of the Woodburn Lake group by a major tectonic break, which is described below.

The Meadowbank River Belt is separated from the Marjorie–Kiggavik–Tehek Belt, because the former extends northward and is rich in gold, but the latter trends northeast and hosts the largest known uranium occurrences. The Meadowbank River Belt (Fig. 3a) stretches from around the Meadowbank mine, up to, but not crossing, the Meadowbank River deformation zone. It comprises most of the originally defined Pipedream assemblage of Pehrsson et al. (2013a), as well as all of the North Meadowbank and Wading assemblages.

Neoproterozoic strata of the Meadowbank River Belt are separated from, yet contiguous to, the Marjorie–Kiggavik–Tehek Belt via a narrow structural neck south of the Meadowbank gold mine and west of Tehek Lake.

The extensive en échelon fault system of the Turqavik fault through the Meadowbank River deformation zone constitutes the mapping divide between the Rumble Belt and the Meadowbank River Belt. The Rumble Belt extends parallel to, and north of, that en échelon fault system, and wraps beneath the Amer Belt grand synclinorium (Fig. 3a, b; Jefferson et al., 2013). Neoproterozoic rocks around Woodburn Lake itself and along the Quoich River are essentially unstudied and not assigned here to any assemblage, but appear to be on trend with the Rumble and Meadowbank River belts, respectively. The following descriptions further position the seven Neoproterozoic assemblages temporally with respect to Tables 1 and 2, and geographically with reference to Figures 3a, b, 6, and 8.

First five Neoproterozoic supracrustal assemblages

Half Way Hills assemblage

The ca. 2.734 Ga Half Way Hills assemblage occupies the hanging wall of the Half Way thrust, where it structurally overlies outliers of sequence Ps4 conglomerate and sandstone resting on the Amarulik assemblage. It includes komatiitic to dacitic volcanic and epiclastic rocks, and highly magnetic iron-formation associated with extensive, gossanous iron-carbonate alteration. The type area extends from the Thelon River northeast to ‘Tasiraraujaq’ (unofficial name) (Fig. 6). Here, its southwestern portion is flanked on the southeast by 2.6 Ga Snow Island suite granite and the Sanning tonalite that may have been either basement or a synvolcanic intrusion (see ‘Magmatism’ section). Its northeastern portion is flanked by quartzite of the Ketyet River group, separated by a high-strain zone here interpreted as the base of the Whitehills klippe. The thrust, the assemblage, and the high-strain zone all wrap around the noses of sharp macroscopic F_{p4} kink folds. Southwest of the Thelon River, the Half Way thrust continues to carry the Half Way Hills assemblage in its hanging wall as far as the Granite thrust (Fig. 3a, b). Throughout this southwestern portion, the western block of the Pipedream assemblage is in the footwall.

North Meadowbank assemblage

The North Meadowbank assemblage comprises komatiite, felsic volcanic, and epiclastic rocks, as well as minor banded iron-formation. Rhyolite of the North Meadowbank assemblage was dated as ca. 2.72 Ga at geochronology site 4 (Table 2, Fig. 3a), south of the Meadowbank River deformation zone (Fig. 3a, c). The southeastern side of the North Meadowbank assemblage appears to structurally overlie the undated Wading

assemblage, because a linear aeromagnetic anomaly associated with iron-formation in the Wading assemblage continues from south to north beneath the North Meadowbank assemblage.

Wading assemblage

The Meadowbank River thrust places a sheet of Snow Island suite over the southeastern side of the Wading assemblage, west of the Meadowbank River deformation zone. The undated Wading assemblage comprises thinly intercalated felsic, felsic to intermediate, and intermediate to mafic flows and tuff, with strongly magnetic cherty iron-formation that serves as a structural marker beneath water and till cover. The Wading assemblage roughly follows the east-northeast leg of the north Meadowbank River and is transected diagonally by the Meadowbank River deformation zone. The eastern portion of this deformation zone constitutes the southeast boundary of the Wading assemblage against the northern end of the Pipedream assemblage. The northern limit of the Wading assemblage on the northern side of the Meadowbank River deformation zone reaches amphibolite-facies metamorphism in the hanging walls of extensive, folded, northward-directed thrust sheets of the Snow Island suite, estimated as 1000 m thick (2613 ± 1 Ma ‘Pencil’ granite of Davis et al., 2021). These relationships are shown in Figure 3b (after Fig. 3 of Pehrsson et al., 2013a).

Pipedream assemblage

The ca. 2.71 Ga (geochronology site 5a, 5b, and 6, Table 2) Pipedream assemblage comprises ultramafic to felsic volcanic and epiclastic rocks, greywacke with multiple iron-formations, and minor quartz arenite and conglomerate. It is one of the most extensive Neoproterozoic packages (Fig. 3b), extending southward from at least the Meadowbank River deformation zone through the ‘Nipterk lake’–‘Ukalik lake’ area (Fig. 7a), around and to the east of the Meadowbank mine (centre of a broad type area), continuing south and east as inliers beneath sheets of Snow Island suite in the Tehek Lake area, wrapping round the eastern portion of the Amarulik Basin, and a separate western block underlying much of the area between the Amarulik Basin and the Granite thrust (Fig. 8). Structural trends suggest that its Meadowbank River Belt portion may extend northeastward into the area around Woodburn Lake, although no map of that area has been published since Fraser (1988). In its type area, it wraps around the narrow, north-trending synform cored by Amarulik assemblage through ‘Third Portage lake’ (unofficial name) (Fig. 6). A structurally separate portion of the Pipedream assemblage, west of the Amarulik assemblage, comprises mainly pyritic greywacke and is the basement host for much of the Kiggavik, Bong, Andrew Lake, and End Grid uranium deposits. Similar felsic volcanic ages (Davis et al., 2021) characterize the Pipedream assemblage along the Meadowbank River Belt. Similar yet distinct detrital zircon assemblages are present in the type area of the Pipedream

assemblage, at the Kiggavik uranium deposits and the Jim zone gold occurrence (geochronology sites 7, 9, and 10, respectively, of Table 2 and Appendix A; McNicoll, 2020). All three greywacke samples yielded peaks near 2.72, 2.81, and 2.90 Ga. The type area and Jim zone samples also have peaks at 2.95 to 3.00 Ga, and the type sample also has smaller peaks at 3.00 to 3.05 Ga and at 3.26 Ga. The ca. 2.72 Ga peaks provide the same approximate maximum age for each of the three Pipedream greywacke samples, whereas the older peaks illustrate different provenances for each geographic locality.

Amarulik assemblage

The Amarulik assemblage is the fifth introduced by Pehrsson et al. (2013a) and remains the youngest known part of the Woodburn Lake group. Remote predictive mapping under this project shows promise for subdivision of the Amarulik assemblage into four internal sequences (A1 through A4, Fig. 6), the contacts between which have not been observed in outcrop. Provisionally, sequence A1 comprises coarse-grained, greyish-greenish-white lithic feldspathic quartzite to wacke with local quartz-pebbly beds (Fig. 5j; <2.68 Ga, geochronology site 16, Table 2) and thick, highly magnetic iron-formation hosted by greywacke. Some of sequence A1, as mapped in Figure 6, may include undivided Pipedream assemblage. Sequence A2 includes poorly exposed slate and fine greywacke with very low magnetic susceptibility. Sequence A3 is dominantly thinly bedded greywacke (<2598 ± 20 Ma, geochronology site 33, Table 2), with common thin aeromagnetically traceable iron-formation (A3a), and local epiclastic and intraformational breccia beds (A3a and A3b). Other detrital zircon results in Table 2 suggested to be sequence A3 (geochronology site 13, 14, 15, 16) are of uncertain context and interpretation, but are included there for completeness. Sequence A4 comprises mainly straight, thick, graded beds of greywacke with slaty tops and no iron-formation.

The structural styles of the Amarulik assemblage sequences help distinguish between them, in concert with their lithological attributes. Both outcrops and aeromagnetic traces of the iron-formation in sequence A3a document complex internal folds (Fig. 6) that are disharmonic with respect to the semi-parallel sequences A1 and A2. These lower two sequences also form the limbs of a tight synform, cored by Amarulik assemblage sequence A2 that extends finger-like to the north of the main Amarulik Basin (Fig. 3b, 6). Thin turbidite beds in sequence A3 are transposed parallel to slaty cleavage that resembles S_{p1} schistosity in Paleoproterozoic cover sequences. The continuous, mainly straight, thick beds of sequence A4 are readily traceable from the air and define only very large D_{p4} kink folds that also deform the Half Way thrust (F_{p4} , Fig. 6), but are not seen in sequence A3. Because of these structural differences, the presence of a structural discontinuity through a band of thick till cover obscuring this contact is inferred. The aeromagnetic data suggest that sequence A4 extends beneath sequence A3 along a structural

discontinuity. Sequence A4 is separated from the western Pipedream assemblage by the inferred Schultz Inlet discontinuity, with the Pipedream appearing to structurally overlie it. Based on its geometric context and structural simplicity at both outcrop and regional scales, sequence A4 is interpreted to be younger than sequence A3, and possibly the youngest Neoproterozoic siliciclastic unit in the study region, although no geochronological data were acquired in sequence A4. The northwestern side of the Amarulik assemblage is poorly constrained. The stratigraphic and structural architecture of the Amarulik assemblage thus poses multiple questions that could be answered with further study.

The Rumble assemblage

The Rumble assemblage (new name introduced by Jefferson et al., 2015) is located north of the Turqavik horst and the Meadowbank River deformation zone (Fig. 3a, c). It is positioned in Figure 4a beside the Pipedream assemblage because the two assemblages share many lithological elements, including ultramafic rocks, greywacke, and iron-formation-hosted gold (Annesley, 1990; Zaleski, 2005). The Rumble assemblage appears to be more metamorphosed, whereas its greywacke has a younger detrital zircon age (<2.65 Ga, geochronology site 20, Table 2) than the Pipedream assemblage greywacke.

The recently opened Amaruq gold mine (Côté-Mantha et al., 2015; Valette et al., 2019) is hosted by Rumble assemblage iron-formation that is cherty and associated with komatiite. The Amaruq deposits have similarities with both the Meadowbank and the Meliadine gold deposits; for example, they are located near the structural juxtaposition of two geochemically and lithologically distinct volcano-sedimentary complexes (Valette et al., 2020). Structurally complex ore at the Amaruq mine records multiple mineralization events, the earliest of which may have been Archean (Lauzon et al., 2020).

From a uranium-host perspective, the pyritic greywacke of the Rumble assemblage, where it underlies or is proximal to the Thelon Formation, may be as prospective as pyritic greywacke of the Pipedream and Aberdeen assemblages. The Rumble Belt is very poorly known southwest of the above-described Amaruq deposit. East of there, it was mapped by Zaleski (2005). Ground data in the southwestern portion of the Rumble Belt are limited to sparse stations from Young (1979), Patterson and LeCheminant (1985), Tella (1994), and helicopter stops during the GEM-1 program. Geophysical and satellite data, and detailed photographs taken from helicopter extended the limited ground data to tightly constrain its contacts with the Amer Belt, but the differentiation in the present study between the Snow Island suite and the Rumble assemblage in the main part of the southwest Rumble Belt is speculative. The Rumble assemblage wraps around, and is an underlying component of, the grand synclinorium that constitutes the Amer Belt (Fig. 3b). Typically, the Pukij Lake formation and/or Snow Island suite granitoid rocks

(see ‘Magmatism’ section) separate the Rumble assemblage from the Amer group, but the basal conglomerate of the Ayagaq Lake formation also directly overlies the Rumble assemblage in a number of places (Jefferson et al., 2023).

Marjorie terrane

The Marjorie terrane (new name after ‘Marjorie Hills assemblage’ of Tschirhart et al. (2014, 2015) and Jefferson et al. (2015)) comprises three packages of paragneiss that form the Aberdeen assemblage (Hunter et al., 2018, 2021) plus the discordant and structurally intercalated orthogneiss facies of the Snow Island suite between the Wharton Lake fault system and the Granite thrust. The Marjorie terrane and Aberdeen assemblage are discussed more thoroughly than the other components of the Woodburn Lake group for several reasons. Firstly, Hunter et al. (2012, 2014, 2018, 2021) have shown that the Aberdeen assemblage expands the area of potential for basement-hosted, unconformity-related uranium deposits. Secondly, they have proposed a different tectonic evolution for the Aberdeen assemblage than for the other assemblages of the Woodburn Lake group. Lastly, the Marjorie terrane differs from the other Neoproterozoic portions of the study area in that both supracrustal and Snow Island suite granitoid rocks in this terrane together underwent gneissification and partial melting, such that primary igneous and sedimentary features are only locally preserved, not a characteristic of the rest of the Woodburn Lake group (similarities and differences are detailed below).

The Marjorie terrane extends about 200 km from beneath Schultz Lake in the north to south of Tebesjuak Lake (Fig. 2). In outcrop, the Marjorie terrane extends from the southern side of Schultz Lake, through the southeastern corner of NTS 66-B and down into NTS area 65-O (Fig. 2). There, Peterson et al. (2014) mapped large expanses of ‘Marjorie Hills’ assemblage around Tebesjuak and Mallery lakes, and in a southern inlier abutting the Tulemalu Fault. Between Schultz Lake and Princess Mary Lake, the banded orthogneiss component of the Snow Island suite and mafic phases of the Aberdeen assemblage structurally overlie the western Pipedream and Half Way Hills assemblages along the Granite thrust (Fig. 3a–c). Highly magnetic banded orthogneiss of the Turqavik horst separates the Marjorie terrane from the Rumble Belt. Tschirhart et al. (2014, 2015) geophysically extrapolated the then ‘Marjorie Hills assemblage’ beneath the eastern part of the Aberdeen Subbasin and found it to be geophysically indistinguishable from the Pipedream assemblage around the Kiggavik uranium deposits. Drill core intersections of basement to the Thelon Formation in the eastern Aberdeen Subbasin, previously assigned to undifferentiated Woodburn Lake group (Davis et al., 2011; Jefferson et al., 2011c), are here recognized as lower Aberdeen assemblage mafic paragneiss, consistent with the geophysical modelling and outcrop mapping done south of there by Hunter et al. (2018, 2021). Tschirhart et al. (2017) modelled the Turqavik horst as extending southwest

under the Thelon Formation, and wedging out in the same direction, leaving the southern tip of the Rumble Belt separated from the Marjorie terrane by the northern part of the Wharton Lake fault system (WLfs, Fig. 3c).

Hunter et al. (2018) documented multiple internal lithological, age, and structural components of the Aberdeen assemblage in the area south of Aberdeen Lake. Hunter et al. (2012, 2014) showed this belt to be a favourable site for basement-hosted unconformity-related uranium mineralization. This includes their Tatiggaq occurrence located within a raft of upper paragneiss included in Hudson suite granite and Martell syenite of the Schultz Lake intrusive complex. They also showed that the Aberdeen assemblage contains broadly similar supracrustal rock types, ages, and structures compared to other assemblages of the Woodburn Lake group, albeit with a temporal gap at 2.72 to 2.71 Ga. The psammitic and pelitic gneiss contains 1 to 2% disseminated pyrite (Hunter et al., 2018), similar to the Pipedream metagreywacke (e.g. Riegler et al., 2014).

In contrast, the other Neoproterozoic supracrustal assemblages generally preserve primary features (although structurally transposed); they are unconformably overlain by crystal tuff of the Pukiq Lake formation (extrusive phase of the Snow Island suite); they are intruded by discrete plugs to plutons of weakly deformed Snow Island suite granite with agmatitic margins; and they are structurally overlain by slabs of well preserved Snow Island suite granite ranging in thickness from hundreds to thousands of metres that show strong lateral aeromagnetic variations (see ‘Snow Island suite’ section below). In addition, the three paragneiss packages of the Aberdeen assemblage were intruded by, structurally intercalated with, and overlie, quartzofeldspathic orthogneiss of the Snow Island suite (Hunter et al., 2018, 2021), and together these para- and orthogneiss units host the Schultz Lake intrusive complex. Compositionally, the paragneiss includes pelite, psammite, felsic and mafic tuff and intrusions, and ultramafic rocks including komatiite with relict spinifex. As noted by Hunter et al. (2018, p. 116), “Partial melting, less than 15% outcrop exposure, and amphibolite-facies metamorphism have destroyed most primary structures, so distinguishing original lithological units in the field can be challenging.”

On a regional scale, a number of attributes distinguish the Aberdeen assemblage of the Marjorie terrane from the rest of the Woodburn Lake group. Firstly, this terrane is entirely highly metamorphosed such that partial melting is characteristic. Secondly, it was at a deep to mid-crustal level during intrusion of the Hudson granite, because sills 200 to 300 m thick that constitute the Schultz Lake intrusive complex are unique to this assemblage. Thirdly, the 1.83 to 1.81 Ga Dubawnt minette dykes (Peterson and LeCheminant, 1996) show two features unique to the Marjorie terrane: having cusp and lobe structures along dyke margins that record plastic deformation of wall rocks during intrusion, and having been magmatically mingled with the thick Hudson granite slabs of the Schultz Lake intrusive complex — an

exposed example of how the Martell syenite formed (Miller and Peterson, 2015; Scott et al., 2015). Elsewhere in the region the minette dykes have sharp straight margins and record only limited interaction with Hudson granite. Fourthly, its lenticular fabric is evident in hand specimen, here interpreted as a form of S-C fabric, based on petrography showing intersecting translational shear surfaces (C, possibly S_{p1}) with foliation (S, possibly S_{p2}). Lastly, the paragneiss is multiply intercalated with granodioritic quartzofeldspathic orthogneiss that characteristically includes chlorite-altered biotite-hornblende layers and has been dated indirectly and directly as 2.6 Ga Snow Island suite (details below).

The portion of the Marjorie terrane mapped in detail by Hunter et al. (2018) (black rectangle southwest of Kiggavik U in Fig. 3a) comprises three paragneiss packages of the Aberdeen assemblage repeated by south- to southeast-directed folds and thrusts, as summarized below. Geochronology from Hunter et al. (2018) is compiled here as geochronology sites 2, 11, 12, 17, 18, and 19 of Table 2 and Figure 3a, with the one result from this study presented as site 23. The 2.75 Ga (geochronology site 2) lower supracrustal package comprises komatiitic gneiss, tonalite-trondhjemite-granodiorite gneiss, and Fe-tholeiitic mafic gneiss. Mafic paragneiss south of Schultz Lake (unit 'Am' of Hadlari et al., 2004) is highly deformed, metamorphosed, and metasomatized, and so is provisionally included in the lower package of Hunter et al. (2018).

The middle Aberdeen supracrustal package consists of later than 2.687 Ga (detrital zircon, geochronology site 11) paragneiss, iron-formation, and 2679.6 ± 2.5 Ma (crystallization age, geochronology site 12) felsic gneiss. The upper Aberdeen package of paragneiss comprises mainly thick, weakly graded beds of psammitic to epiclastic gneiss, dated at later than 2.65 Ga by Hunter et al. (2018) and 2.672 to after 2.628 Ga (geochronology site 23 (sample 11JP009), Table 2, Fig. 3a). There is likely very detailed structural intercalation of the middle and upper supracrustal packages, because sample 11JP009 with upper supracrustal package ages was mapped as middle supracrustal package and is located within 100 m of the samples analyzed by Hunter et al. (2018) to represent the middle supracrustal package.

Hunter et al. (2018, 2021) have shown that all three packages of the Aberdeen assemblage are structurally intercalated with quartzofeldspathic orthogneiss dated at a single locality as part of the Snow Island suite. This orthogneiss is a characteristic component of the Marjorie terrane. It is not observed intercalated with any other Neoproterozoic assemblages. Hunter et al. (2021) obtained an age of 2601.7 ± 4.2 Ma on a pink granitic orthogneiss with relict potassium feldspar phenocrysts at the northern end of Marjorie Lake. They used the same term 'quartzofeldspathic orthogneiss' for this rock as for the rest of the orthogneiss in their study area and inferred that this age applies to all of the banded gneiss in this region, mapping it all as 'Snow Island suite'. Hunter et al. (2021) reported no geochemical comparisons; however, the orthogneiss compositions they obtained are similar to those of the Snow Island

suite published by Peterson et al. (2015c) (R.C. Hunter, pers. comm., 2021). The eastern, 'grandfather gneiss' component of the orthogneiss is more granodioritic to quartz dioritic in composition (*see* 'Recommendations for further work' section below).

Most of the aeromagnetically traceable iron-formation of the Aberdeen assemblage appears to be located within the middle psammitic paragneiss, although Hunter et al. (2018) described iron-formation as also being present in the upper psammitic paragneiss. The banded iron-formation occupies intervals with thin graded beds of psammite to graphitic metapelite as opposed to the thicker psammitic graded beds. The iron-formation is magnetically continuous and comprises garnet-magnetite-metachert. Together with the relatively low background residual total field magnetic signature of supracrustal rocks, the irregular linear aeromagnetic highs of iron-formation help to differentiate the paragneiss from the orthogneiss in the Marjorie terrane (Fig. 3a, d). Low magnetic signatures along hematitized reactivated fault zones (Morris et al., 2017) make it difficult to distinguish granite from supracrustal rocks in those locations. Remote predictive mapping using these criteria extends the Aberdeen assemblage west and south of the area mapped by Hunter et al. (2018) (Fig. 3a, b), where demagnetized fault zones are less evident.

The three supracrustal packages of the Aberdeen assemblage together range in age from older than the rest of the Woodburn Lake group to overlapping the initiation of the 2.62 to 2.58 Ga Snow Island suite bimodal intrusive and extrusive magmatism. The lower ultramafic to felsic package is similar in composition to, but older than, the 2734.2 ± 1.8 Ma (geochronology site 3, Table 2; Davis et al., 2021) ultramafic to intermediate Half Way Hills assemblage. The middle supracrustal package is lithologically distinct from, but similar in age to, the later than 2.680 Ga detrital zircon result of McNicoll (2020) (geochronology site 16, Table 2) for the basal quartz-pebbly wacke to quartzite unit of the Amarulik assemblage. The later than 2.65 Ga detrital zircon age limit found in three paragneiss samples of the upper supracrustal package (geochronology sites 17, 18, 19, Table 2) by Hunter et al. (2018) is the same as that for metagreywacke of the Rumble assemblage (geochronology site 20, Table 2). The later than 2.628 Ga shoulder of the detrital zircon population of geochronology site 23 from this study overlaps with the initiation of the Snow Island suite, whereas the youngest detrital zircon ages from the middle sequence of the Amarulik assemblage (2598 ± 20 Ma; geochronology site 33, Table 2) are in the middle of the Snow Island suite time span.

Amalgamation of the Woodburn Lake group

The Woodburn Lake group assemblages have geometric relationships reworked by the Hudsonian Orogeny (Pehrsson et al., 2013a) that can only suggest their complex history of Neoproterozoic amalgamation. For the Aberdeen assemblage, Hunter et al. (2018) interpreted their lower 2.75 Ga package

of ultramafic to mafic volcanic rocks to have formed as an oceanic plateau or oceanic crust between older microcratons. Successive microcraton-margin flysch deposits constitute their middle and upper siliciclastic sequences. The upper siliciclastic sequence includes a small proportion of zircon of early Snow Island suite age, but whether it is in contact with any primary Snow Island suite units is uncertain. The structural style in the Marjorie terrane also differs from the rest of the study area, with structures interpreted by Hunter et al. (2018) as Hudsonian being southeast vergent, diametrically opposed to the northwest vergence of the rest of the study area. How and when the entire Marjorie terrane came together and was accreted to the rest of the Woodburn Lake group are unknown, as the Granite thrust appears to have juxtaposed this terrane from the west and south *after* the northwest-directed D_{p2} Half Way thrust formed.

The primary relationship of the island-arc-like (Aura Silver Resources Inc., 2018; J. Franklin, pers. comm., 2011), 2.734 Ga Half Way Hills assemblage to the rest of the Woodburn Lake group is similarly unknown, as it was emplaced over the Pipedream and Amarulik assemblages along the Hudsonian Half Way thrust prior to development of the Granite thrust. The Half Way thrust may represent a primary accretionary suture that became reactivated during Hudsonian compression. The contacts between the Rumble, North Meadowbank, Wading, and Pipedream assemblages all trend about 070° and are now late Hudsonian dextral fault zones, although north–south directed primary accretion is suggested.

The undated Wading assemblage (Wading Lake belt in Fig. 3 of Pehrsson et al. 2013b) comprises plagioclase and amphibole-phyric basalt, andesite, dacite, cherty felsic tuff, and iron-formation that are locally cut by diorite plugs. The Wading assemblage is lithologically distinct from the 2.72 Ga North Meadowbank assemblage that comprises komatiite, komatiitic basalt, rhyolite flows and domes, and felsic volcanoclastic rocks. These compositionally discrete, but structurally adjacent belts are interpreted to have formed in separate volcanic arcs that later collided. Strong linear aeromagnetic anomalies associated with outcrops of Wading iron-formation are continuous northward beneath a broadened bend in the northern Meadowbank River and outcropping volcanoclastic rocks of the North Meadowbank assemblage, suggesting that the North Meadowbank assemblage structurally overlies the Wading assemblage. Northward-directed D_{p2} thrusting and dextral D_{p4} faulting along the Meadowbank River deformation zone have partially obscured the above primary relationships.

The 2.71 Ga Pipedream assemblage forms much of the core of the Woodburn Lake group, with detrital zircon assemblages recording different source terranes in its northern, western, and southeastern components; however, extension of the Pipedream assemblage to the undated area around Woodburn Lake, as presented here, is speculative. In any case, the extensive graded metagreywacke with iron-formation

represents deep-water turbiditic sedimentation in a large basin, possibly on the flanks of an emergent volcanic arc, or in a back-arc setting.

The Amarulik assemblage, the youngest at later than 2.68 Ga to after 2.58 Ga, occupies an interior position between two portions of the Pipedream assemblage on the northeast and southwest, and the Half Way assemblage on the southeast, possibly representing a multiphased interior rift basin within the Woodburn Lake group microcraton. Of the four mapped sequences (A1 through A4) described above, the later than 2.68 Ga detrital zircon age of sequence A1 suggests that its deposition preceded the Snow Island suite event. The 2598 ± 20 Ma, 2611 ± 20 Ma, and 2639 ± 10 Ma detrital zircon grains recovered from sequence A3 (Fig. B-1, Appendix B; Davis, 2021) represent derivation from multiple ages of Snow Island suite products. Thus, Amarulik sequence A3 may in part have been coeval with later stages of the Snow Island suite event. The age and origin of the undated sequence A4, structurally discordant with all adjacent Neoproterozoic packages as described above, are partially constrained by its geometry and the unconformably overlying sequence Ps4 sandstone and conglomerate in the footwall of the Half Way thrust (Fig. 6). Criss-crossing dykes of presumed Snow Island suite granite intrude inferred A4 metagreywacke along the northwest side of the Amarulik basin.

No Neoproterozoic supracrustal rocks were documented beneath the Montresor Belt (Percival et al., 2017) — only the thick slab of foliated to gneissic Snow Island suite granodiorite that is structurally intercalated with, and underlies, it; however, biotite schist and amphibolite described by Dziawa et al. (2019) is very similar to inclusions observed in the undated garnet-muscovite leucogranite of Frisch (2000) in the course of this study. This schist may be Archean, if the leucogranite is part of the Snow Island suite. Other than the possibly Archean schist, this leaves a gap in the Neoproterozoic record between the northern part of the study area and the Committee Bay Belt farther north.

The latter, as described by Sanborn-Barrie et al. (2014), differs in many ways from the Woodburn Lake group and the structurally involved early Paleoproterozoic belts of the study area, except for the dominance of mafic–ultramafic volcanic rocks in the oldest Neoproterozoic supracrustal sequences and the presence of iron-formation-hosted gold deposits in their middle assemblages. Ultramafic rocks are a defining component of all three sequences in the Committee Bay group, and are kilometres thick in the lower sequence, but are only a few tens of metres thick in the Woodburn Lake group. The 2.71 Ga middle supracrustal sequence of the Committee Bay group comprises intermediate volcanic rocks, abundant semipelite and psammite with auriferous iron-formation, and much quartzite. In contrast, the Pipedream assemblage is dominantly felsic volcanic with minor komatiite and intermediate rocks, overlain by extensive epiclastic and greywacke strata that host auriferous iron-formation, and only minor thin beds of quartzite.

Most of the quartzite in the Committee Bay Belt has been confirmed as Archean, whereas most of the quartzite in the study area is now known to be Paleoproterozoic and much of it overlies the 2.6 Ga Pukioq Lake formation. There is no mention of 2.6 Ga felsic volcanic rocks in the Committee Bay group. Postdepositional histories also differ — the 2.35 Ga Arrowsmith Orogeny (Berman et al., 2013) strongly affected the Committee Bay Belt (Sanborn-Barrie et al., 2014), but left no metamorphic or deformation record in the Montesor, Amer, or Ketyet River belts. Peterson et al. (this volume) describe consistent differences between Snow Island suite manifestations in the north, south, and central Rae Craton, whose boundaries must have already been in existence and played a significant role during the Snow Island suite event.

Early Paleoproterozoic cover sequences: Amer, Ketyet River, Montesor, and western belts

Background

The inclusion of all of the Amer, Ketyet River, Montesor, Nauyatuuq, Deep Rose, Sand, Garry, and Akiliniq belts in this study is based on the knowledge that similar Paleoproterozoic strata underlie the Athabasca Basin, where they host or localize most of the uranium deposits there. All but one (Akiliniq) of the forenamed belts extend beneath the northeast Thelon Basin and, therefore, are prospective targets that need to be understood for uranium metallogeny. Rainbird et al. (2010) reviewed the history of nomenclature, age interpretations, and correlations of early Paleoproterozoic strata across the Rae and Hearne cratons, and provided the first tectonostratigraphic framework to understand these strata in terms of four assemblages that they compared across this vast region. With a focus on the Ketyet River group, and separating it from the Archean Woodburn Lake group, Pehrsson et al. (2013a) recast these Paleoproterozoic assemblages in terms of sequences: Ps1, Ps2, Ps3, and Ps4. They moreover erected the first comprehensive structural-metamorphic framework in the region that helps resolve the lithostratigraphic complexities of the Ketyet River and Amer groups. They recognized an early Paleoproterozoic deformation event (D_{p1}) that affected only the first three sequences and thereby helps differentiate them from the fourth. The undated D_{p1} involved isoclinal folding and basement-involved thrusting with weak metamorphic effects. Deformation event D_{p1} is tentatively interpreted as a distal manifestation of the 1.9 to 1.865 Ga Snowbird Orogeny (Berman et al., 2007). The D_{p1} event affects only the Archean sequences, and sequences Ps1, Ps2, and Ps3. In contrast, D_{p2} reflects the overlapping main-stage ca. 1.87 to 1.81 Ga Hudsonian Orogeny, with variable metamorphism. D_{p2} affects all four Paleoproterozoic sequences (Fig. 4b).

Data acquired during this project show that the stratigraphic and structural architecture of the contiguous portion of the Amer Belt, as defined above, provides a more complete

stratigraphic record than the Ketyet River group, and thus serves as the type area to redefine and recalibrate the above-introduced four sequences (Jefferson et al., 2015, 2023; C.W. Jefferson, R.H. Rainbird, G.M. Young, S.S. Gandhi, J.C. White, V. Tschirhart, D. Lemkow, and L.B. Chorlton, work in progress, 2023). Young (1979) introduced eight formation-scale lithostratigraphic units constituting the Amer group, in ascending order: 1) conglomerate and quartzite, 2) black sulphidic graphitic slate with immature sandstone, 3) carbonate, 4) basalt (infolded with the quartzite and carbonate), 5) dark siltstone, 6) arkosic quartz arenite, 7) interbedded arkose and drab mudstone hosting stratabound uranium occurrences, and 8) molasse of feldspathic [sic] sandstone and red mudstone with locally stromatolitic carbonate and minor conglomerate. Jefferson et al. (2023) and C.W. Jefferson, R.H. Rainbird, G.M. Young, S.S. Gandhi, J.C. White, V. Tschirhart, D. Lemkow, and L.B. Chorlton (work in progress, 2023) fully describe these formations, organize them into two groups and propose to raise the Amer group to supergroup status.

Rainbird et al. (2010) had amalgamated, but also re-ordered Young's (1979) stratigraphic sequencing of these eight Amer formations to construct the above-noted four lithotectonic assemblages. In ascending stratigraphic position, the Rainbird et al. (2010) ordering became: 1) undivided conglomerate and quartz arenite; 2) quartz arenite intercalated with carbonate±mafic volcanic rocks; 3) a combined succession of dark shale, carbonate, siltstone, and sandstone; and 4) immature marine sandstone, including turbidite. Their reordering was based on lack of recognition of the fold closures and changes in facing directions that Young (1979) had mapped. Even though Pehrsson et al. (2013a) were the first to document the presence of F_{p1} compounded by F_{p2} , they surprisingly also missed the Paleoproterozoic fold repetitions of quartzite with basalt, and thus maintained the intercalation interpretation in converting those four lithotectonic assemblages into their four stratigraphic sequences: sequence Ps1 consisting of conglomerate on paleoregolith, quartz arenite, minor iron-formation and shale; sequence Ps2 consisting of intercalated feldspathic quartz arenite, oligomictic quartz-pebble conglomerate and basalt; sequence Ps3 consisting of carbonate-cemented feldspathic sandstone, sulphidic shale, and conglomerate; and sequence Ps4 consisting of clastic, coarsening-upward slate to conglomerate (flysch to molasse).

New definitions of sequences Ps1, Ps2, Ps3, and Ps4 in the Amer Belt

Tschirhart et al. (2013d, 2017), Calhoun et al. (2014), Jefferson et al. (2011a, 2015, 2023), and C.W. Jefferson, R.H. Rainbird, G.M. Young, S.S. Gandhi, J.C. White, V. Tschirhart, D. Lemkow, and L.B. Chorlton (work in progress, 2023), updated the relative and absolute ages of the four sequences, remapped the type localities for each formation within the Amer Belt type area in greater detail with the aid of

new geophysical data (Tschirhart et al., 2011a), and revised the map units that belong to each sequence by reinstating the original lithostratigraphic order of the *eight informal formations* set out by Young (1979). These changes in understanding of the four sequences are based on validation and more complete application of the deformation paradigm by Pehrsson et al. (2013a) for the Ketyet River group, here and by White et al. (2021, 2023) applied equally to the contiguous Amer Belt. The four revised sequences retain the Ps1 through Ps4 codes of Pehrsson et al. (2013a), with informal formation names for the Amer Belt as follows:

Sequence Ps1 is the *Ayagaq Lake formation* of basal conglomerate on paleoregolith, a main body of quartzite, and an upper varied package of impure quartzite and conglomerate.

Sequence Ps2 excludes quartzite and includes the *Resort Lake formation* consisting of dark shale and gossanous iron-formation (formerly sequence Ps1), siltstone, and immature sandstone (formerly sequence Ps3); and the *Aluminium River formation* of siliceous dolostone (formerly sequence Ps3).

Sequence Ps3 now includes four map units in ascending stratigraphic order: *Five Mile Lake formation* consisting of basalt tuff and flows; *Three Lakes formation*, of grey siltstone and wacke; *Oora Lake formation*, of arkose with an upper carbonate marker; and *Showing Lake formation*, of intercalated siltstone and arkose, with uranium occurrences. In more highly metamorphosed and deformed sections, the fine-grained siliciclastic rocks of the lower portion of sequence Ps2 are indistinguishable lithologically from the fine-grained siliciclastic rocks of sequence Ps3. Thickness and context are key, in that the fine-grained siliciclastic rocks of sequence Ps2 are bracketed between quartzite and carbonate or between quartzite and basalt, and range in map width from about 1 to 30 m. Sequence Ps3 differs by ranging from hundreds of metres to kilometres in map width and overlying carbonate and/or basalt. In the absence of carbonate and basalt, thick sections of fine-grained clastic strata overlying quartzite that record D_{p1} are mapped as undivided sequences Ps2 and Ps3, or just sequence Ps3. In the Schultz Lake klippe (Fig. 6, 8a), laminated slate of sequence Ps2 is indistinguishable from laminated slate of sequence Ps3, except that the Ps2 slate is separated from the Ps3 slate by dolomitic tuff hosting a gabbro sill.

Sequence Ps4 comprises weakly deformed (no D_{p1} folds or faults) feldspathic sandstone, siltstone, mudstone, conglomerate, and dolostone (the *Itza Lake formation* of Young (1979); renamed ‘Tahiratuaq group’ by Jefferson et al. (2023)). In places where the second Paleoproterozoic deformation and metamorphism (D_{p2} and M_{p2}) are intense, such as the eastern part of the Ketyet River Belt, intrinsic distinction of sequences Ps2 and Ps3 from sequence Ps4 is challenging, except that iron-formation and thick carbonate units are indicative of sequence Ps2. This fourth sequence is the same as the fourth assemblage of Rainbird et al. (2010) and the fourth sequence of Pehrsson et al. (2013a).

In the above-defined Amer Belt, Jefferson et al. (2023) and C.W. Jefferson, R.H. Rainbird, G.M. Young, S.S. Gandhi, J.C. White, V. Tschirhart, D. Lemkow, and L.B. Chorlton (work in progress, 2023) group the formations in sequences Ps1 through Ps3 as a lower package that uniquely experienced D_{p1} deformation (hereafter the informal ‘Amer sequences Ps1–3’); sequence Ps4 is the upper package of the Amer group that did not experience D_{p1} (hereafter the informal ‘Amer sequence Ps4’). Because of the profound structural differences between the lower and upper packages, and the mapped regional unconformity between them, the Amer group should logically be a supergroup (Jefferson et al., 2023; C.W. Jefferson, R.H. Rainbird, G.M. Young, S.S. Gandhi, J.C. White, V. Tschirhart, D. Lemkow, and L.B. Chorlton, work in progress, 2023). Similar revisions are required for the Ketyet River and Montresor groups.

Particular attention is drawn to the Amer sequence Ps4, with weak deformation, good preservation of primary sedimentary structures, and a middle conglomerate. These key *structural and clast compositional* aspects are in common with those of sequence Ps4 in the Ketyet River Belt (hereafter referred to as ‘Ketyet River sequence Ps4’). Three subunits of formational rank make up the Amer sequence Ps4 (Jefferson et al., 2023). The lowest, Amer sequence Ps4A, comprises about 500 m of interbedded pink and grey quartz arenite, feldspathic sandstone with polymodal festoon crossbeds, ripple marks, and interbeds, as well as intraclasts of purple and red mudstone. It overlies different parts of the Amer sequences Ps1 to Ps3, from the Showing Lake formation down to the Ayagaq quartzite, as well as the Neoproterozoic Rumble assemblage. The unexposed basal contact is a mapped angular unconformity, but there is no indication of a basal conglomerate. A thin unit of interbedded desiccation-cracked red mudstone and orange- and buff-weathering, locally stromatolitic dolostone caps the Amer sequence Ps4A in several places; in other places, some of the upper sandstone beds are dolomitic. The Amer sequence Ps4A has one linear aeromagnetic marker.

The base of the middle subunit, Amer sequence Ps4B, is marked in outcrop by polymict conglomerate unconformably overlying either orange stromatolite or calcareous sandstone of the lower package. The overlying redbed succession has three linear aeromagnetic markers, the first being just above the conglomerate. Like the Showing Lake formation (*see* ‘Distinguishing structural, lithological, and geophysical characteristics of sequences Ps1, Ps2, Ps3, and Ps4’ section below), these markers are subdued in the residual total field maps, but are accentuated in filtered and reprocessed maps such as the tilt-derivative image, which enhances short wavelength, near-surface anomalies. The conglomerate comprises rounded cobbles to boulders of white and pink, bedded and massive, metamorphosed quartzite up to 30 cm in diameter, as well as pebbles of pink porphyritic rhyolite (interpreted as Pukiq Lake formation) and locally derived orange-weathering dolostone, green and buff mudstone,

lithic feldspathic sandstone, and pink orthoquartzite. Some of the quartzite cobbles contain previous folds and fabrics (Fig. 5g). Where its upper contact is exposed, the conglomerate grades upward into salmon pink arkose. The bulk of the Amer sequence Ps4B is interbedded pink feldspathic sandstone and quartz arenite, also with polymodal crossbeds, ripple marks, and deep red mudstone as interbeds and intra-clasts. All of these rock types resemble the Amer sequence Ps4A; however, the Amer sequence Ps4B is distinguished by overlying the conglomerate and stromatolite subunits as well as having three more linear aeromagnetic markers that outline major F_{p2} folds, consistent with limited data from a few areas of good outcrop. The Amer sequence Ps4B is 7 to 10 km in map width.

Very similar strata to the Amer sequences Ps4A and Ps4B are exposed in the western part of the Beverly inlier of the Amer Belt, including a conglomerate with up to 50 cm diameter rounded clasts of quartzite, vein quartz, brown siltstone, granite (Snow Island suite), feldspar porphyry (Pukiq Lake formation), and jasper (top of sequence A in LeCheminant et al. (1984), equivalent to base of Amer sequence Ps4B). Their overlying 'sequence B' in the same area comprises at least 500 m of rhythmically interbedded 1) reddish-brown, fine- to coarse-grained, poorly sorted feldspathic wacke; 2) dark reddish-brown, mudcracked siltstone-mudstone; and 3) pale pink, medium- to coarse-grained, trough-cross-bedded quartz arenite. This is essentially the same facies as the Amer sequence Ps4B, except the latter mudstone beds are deep maroon. LeCheminant et al. (1984) provided detailed descriptions, measured sections, and photographic illustrations of these facies.

The Amer sequences Ps4A and Ps4B redbeds are remarkably similar to redbeds of the Kazan Formation (Baker Lake Group), Amarook Formation (Wharton Group), and Thelon Formation (Barrensland Group). They are not in contact with the Kazan Formation, but are cut by 1.83 to 1.81 Ga minette dykes that are petrochemically the same as minette flows of the Christopher Island formation that is interdigitated with the Kazan, South Channel, and Angikuni formations to make up the lower part of the Baker Lake Group. Detailed mapping along the northeastern margin of the Aberdeen Subbasin (Young, 1979; Jefferson et al., 2015; C.W. Jefferson, R.H. Rainbird, G.M. Young, S.S. Gandhi, J.C. White, V. Tschirhart, D. Lemkow, and L.B. Chorlton, work in progress, 2023) shows that the Amer sequences Ps4A and Ps4B redbeds occupy a large open syncline named the 'Tahiratuaq synform' because its axis passes just northeast of 'Tahiratuaq' (unofficial name) and it involves not only the sequence Ps4 strata, but also the sequence Ps1 to Ps3 and underlying Archean strata, as well as the Snow Island suite (Jefferson et al., 2023). This large synform is documented both by dips of bedding and fabrics, and by geophysical modelling (Tschirhart et al., 2014, 2017).

The Amarook Formation overlies the Amer sequence Ps4 with angular unconformity and is in turn overlain with angular unconformity by the Thelon Formation.

The Amer sequence Ps4C comprises decimetre-scale rhythmites of lithic arkosic sandstone grading up to mudstone, cut by abundant ptlygmatically folded sandstone dykelets, punctuated by a number of conductive, black, graphitic and sulphidic slate intervals. The sandstone ranges in colour from pale pink to grey-green and the siltstone to mudstone is green to dark grey-green, with the reddest sandstone being near the top of the unit. Small, low-angle crossbeds are common in the fine-grained sandstone to siltstone portions of the graded beds. These features together suggest deep-water turbidite sedimentation during active tectonism. Some of the fine-grained crossbeds may have been generated by contourite-forming currents.

The Amer sequence Ps4C is known from both drill core and good exposures in the western corner of the contiguous Amer Belt, along and west of the Amer mylonite zone, in the Nauyatuuq Belt (Fig. 3a). A log of drillhole RHC-07-01 by the former Western Uranium Corporation that cored the eastern part of that belt is in Appendix B of C.W. Jefferson, R.H. Rainbird, G.M. Young, S.S. Gandhi, J.C. White, V. Tschirhart, D. Lemkow, and L.B. Chorlton (work in progress, 2023). The drill-intersected stratigraphic thickness is at least 330 m, the hole having ended within this unit. By comparison with the modelled thicknesses of the Tahiratuaq (1 km of sequences Ps4A and Ps4B; Tschirhart et al., 2014) and Montresor (800 m of sequence Ps4; see Percival and Tschirhart, 2017) synclines, the Amer sequence Ps4C is estimated to be 600 to 800 m thick in the Nauyatuuq Belt.

The contact relationship of Amer sequence Ps4C with Amer sequence Ps4B has not been studied, but is constrained to be close to the Amer mylonite zone by the presence of Amer sequence Ps4B along the Amer mylonite zone at geochronology site 41d (Fig. 3a, Table 2). This study did not examine the sparse outcrops between geochronology site 41d and Nauyatuuq Lake. Neither did Tella (1984, 1994) distinguish them from outcrops in the Nauyatuuq or Amer belts. The Nauyatuuq Belt (Amer sequence Ps4C) has linear aeromagnetic markers that are stronger than those of the Amer sequence Ps4B, yet similar in intensity, but discontinuous compared to those of sequence Ps4 of the Montresor Belt. The Amer sequence Ps4C exhibits faint F_{p2} cleavage and records anchizone to lowest greenschist-facies metamorphism. The graphitic conductors drilled by the former Western Uranium Corporation (D. Bowden, pers. comm., July 25, 2008) and logged by the first author (DDH RHC 07-01, 02, 03; Appendix B in C.W. Jefferson, R.H. Rainbird, G.M. Young, S.S. Gandhi, J.C. White, V. Tschirhart, D. Lemkow, and L.B. Chorlton, work in progress, 2023) are sheared, and are interpreted as weak carbonaceous mudstone beds that focused flexural slip during D_{p2} and later deformations.

Sequences Ps1, Ps2, Ps3 and, Ps4 in the Ketyet River, Montresor, and western belts

Sequences Ps1 through Ps4 defined in the Amer Belt extend in different ways to the Ketyet River, Montresor, and western belts (Fig. 3a, 4a, 6; Jefferson et al., 2023; C.W. Jefferson, R.H. Rainbird, G.M. Young, S.S. Gandhi, J.C. White, V. Tschirhart, D. Lemkow, and L.B. Chorlton, work in progress, 2023). In the Ketyet River Belt, the area around Whitehills Lake provides the largest contiguous exposures at low metamorphic grades in the belt, and thus serves as the type area for the belt. The sequence Ps1 conglomerate and main quartzite unit are remarkably similar to those of the Amer Belt. The sequence Ps2 carbonate unit is mostly absent in the Ketyet River Belt, except for a thin calcareous schist in the Schultz Lake klippe (McEwan, 2012), a dolomitic limestone unit in the core of a quartzite synform east of Quoich River (Fraser, 1988), and dissected outliers in the Akutuak River gneiss. Basalt is the only confirmed representative of sequence Ps3 in the Ketyet River group around Whitehills Lake and, like that of the Amer Belt, is discontinuous (Fig. 6) — it is present in the southern part of the Whitehills Lake synform, but not in the north. The sequence Ps3 mafic event is also represented by a gabbro sill hosted by calcareous tuff in the Schultz Lake klippe, but is absent from most of the other outliers. Fine-grained strata east of Whitehills Lake are higher in metamorphic grade and have not been examined in this study, but lack basalt. These may include some sequence Ps3 versus sequence Ps4 (Fig. 6 of Pehrsson et al., 2013a), but lack the aeromagnetic markers or uranium occurrences that characterize sequence Ps3 of the Amer group. The Ketyet River sequence Ps2 iron-formation ranges from hematite to pyritic siderite in composition, whereas that of the Amer group is pyritic. The Ketyet River sequence Ps2 also includes conductors, such as along the eastern side of the Schultz Lake klippe (P. Wollenberg, pers. comm., 2009). The basal discontinuity of the Schultz Lake klippe is also a conductive zone, but the source of that low resistivity is unclear (Tschirhart et al., 2013a).

The southwestern extension of the Montresor Belt was mapped during this study to complete NTS map sheets 66-G and 66-H, and to help understand those western Paleoproterozoic belts underlying the northern main Thelon Basin and the Aberdeen Subbasin that have been explored for uranium. As part of this research, basic understanding of the geology of the main part of the Montresor Belt was also acquired from the literature and discussions in 2021 and 2022 with J. Percival and T. Frisch, the latter also sharing his field notebooks and photographs of key outcrops. As described by Frisch (2000) and Percival et al. (2017), the sequence Ps1 quartzite unit there is very similar to that of the Amer and Ketyet River belts. These authors do not record isoclinal folds in sequences Ps1 to Ps3 such as documented in this study, however Frisch (2000) did mention thrusting (*see* sequence Ps2 in the next paragraph). Frisch (2000, p. 26) also described a basal conglomerate as

“southeasterly dipping, rusty brown-weathering, dark biotite phyllite containing rounded clasts, up to 5 cm long, of white quartz and granitic rock and crosscut by quartz veins resting on garnet-muscovite leucogranite (unit Amg) that bears traces of arsenopyrite.” He assigned this to the base of the upper Montresor group, but later he described overlying “grey quartzite with long lenses and layers, commonly 0.6 m thick, of very fine-grained dark schist containing trace native copper” (Frisch, 2000, p. 41). This is unlike any basal sequence Ps1 unit seen in the Amer or Ketyet River groups, but is then overlain by the typical pink and grey rocks of the meta-arkosic upper Montresor group. It is puzzling that Percival et al. (2015b) showed the undated garnet-muscovite leucogranite as a Paleoproterozoic intrusive body (Pgm unit) that truncates both lower and upper Montresor group strata, whereas Frisch (2000) interpreted it as Archean.

The sequence Ps2 carbonate unit of the Montresor group (AMt and Ad units in Frisch, 1992) lies directly on the sequence Ps1 quartzite (AMo and Aq units in Frisch, 1992), with no equivalent of the Resort Lake formation being reported. Schist mapped to the southeast where units AMt and AMo are absent may include highly metamorphosed sequence Ps2 mudstone, but is more likely to be Archean. The sequence Ps1 quartzite and sequence Ps2 carbonate units become discontinuous toward the southwest along both sides of the Montresor Belt, and the last mapped exposures are about midway along the belt (Frisch, 1992, 2000). The last outcrops of quartzite and carbonate on the southeastern side of the belt (northeast of Mount Meadowbank), appear to be structurally repeated (Frisch, 1992, 2000) in the style of D_{P1} . Similarly, quartzite and carbonate are shown as structurally repeated with ca. 2.6 Ga foliated to gneissic granodiorite at the northeastern end of the belt (Percival et al., 2015a, b, 2017). These structural repetitions, and the angular truncation of the northeastern thrusts by the basal contact of the upper Montresor group, are consistent with them being D_{P1} , prior to deposition of the sequence Ps4 strata of the upper Montresor group.

There are no reports of sequence Ps3 basalt overlying quartzite or dolostone in the Montresor Belt. An approximately 200 m wide thrust sliver of greenschist-facies-grade wacke and semipelitic mudstone at the northeastern end of the belt has been assigned to sequence Ps3, based on the interpretation by Percival et al. (2017) that it is younger than the dolostone, and the knowledge that it hosts a ca. 2.1 Ga layer of impact spherules (Percival et al., 2019). The mudstone bed hosting the spherule layer is apparently younger than the basalt that constitutes the base of sequence Ps3 in the Amer and Ketyet River belts (*see* ‘Geochronology of sequences Ps1, Ps2, and Ps3’ section below). The 2045 ± 13 Ma gabbro sill (Percival et al., 2017) nearby within the wacke and semipelitic unit provides a minimum age. Equivalents of the gabbro sill and impact spherule bed have not been documented in the other belts, although gabbroic bodies in the north-central Amer and northern Sand belts offer comparative research opportunities. The presence or absence of

linear aeromagnetic markers in the Montresor sequence Ps3 at the northeastern end of the belt is unknown at this time because the high-resolution aeromagnetic survey (Miles and Oneschuk, 2013) did not cover that part of the belt (Fig. 3d).

In the main part of the Montresor Belt, fine-grained sandstone to mudstone of the upper Montresor group directly overlies the quartzite and dolostone with little of sequence Ps3 being recognizable, except for a thin dark phyllitic to schistose layer between them in some places (Frisch, 2000). The upper ‘meta-arkose’ unit is here assigned to sequence Ps4 because it is only weakly metamorphosed and deformed, with well preserved crossbeds, fine laminations, ripple marks, and delicate clastic textures in thin section. The pink and grey colour is also consistent with sequence Ps4 strata in the Amer and Nauyasuq belts. An additional key similarity is the presence of polymict conglomerate within the lower part of the upper Montresor sequence Ps4. Frisch (2000, p. 26) described it as follows:

Conglomerate occurs in the meta-arkose unit near the western margin of the Montresor belt about 2 km north of the southern border of the Ian Calder Lake map area. The conglomerate forms a lense [*sic*] a few hundred metres long and up to 20 m thick. It consists of well rounded clasts, up to 20 cm across, of white quartz and pink granite in a matrix of grey calcareous arkose. The matrix is inequigranular with clasts, 1–5 mm across, of quartz, feldspar (chiefly microcline) and aggregates of sutured quartz grains in a feldspathic and sericitic groundmass; carbonate is patchily distributed in the matrix. Rocks stratigraphically above and below the conglomerate are calcareous arkose.

This conglomerate and the enclosing arkose are remarkably similar to those described above at the interface between units Ps4A and Ps4B of Amer Belt sequence Ps4. Neither conglomerate nor arkose like these are present in sequence Ps3 of the Amer Belt.

A rhombic unit of muscovite-andalusite-sillimanite-garnet schist, indicating middle amphibolite-facies conditions (3.3 kbar (330 MPa), 575°C) at 1861 to 1844 Ma (Berman et al., 2015a; Dziawa et al., 2019) was interpreted by Frisch (Am unit; 1992, 2000) as partly fault bounded and older than the quartzite. Following that interpretation, the Am unit could be an Archean inclusion in the Snow Island suite (Ak unit of Frisch, 1992). On the other hand, Percival et al. (2017) assigned all of these schistose units to the lower Montresor group (their unit P_{Mp}). The greater than 2 km map width of the rhombic schist unit is consistent with it being sequence Ps3, although no quartzite is exposed between it and the Snow Island suite and there are no linear aeromagnetic anomalies within it. Instead, this schist unit is coincident with a broad linear aeromagnetic low that separates the lowest aeromagnetic high of the upper Montresor group from the moderate magnetic high demarking the Snow Island suite. Farther northeast, this magnetic low

corresponds to the quartzite and carbonate units and, to the southwest, the magnetic low corresponds to mainly garnet-muscovite granite, with inclusions of schist and amphibolite (generalized as lower Montresor group in Fig. 3a). The magnetic low of the schist is much less pronounced than a deep magnetic low within the upper Montresor strata, associated with a stratabound zone of breccia, hydrothermal alteration, and alkaline igneous rock types ranging in apparent composition from ultramafic to felsic (Percival et al., 2015a, b; Tschirhart et al., 2015).

Both the moderate magnetic low and the undated unit of garnet-muscovite granite veined by pegmatite are present on both sides of the synform (Amg unit of Frisch, 1992, 2000), just north of the Back River. The geometry of the garnet-muscovite granite as mapped by Frisch (1992), and the schistose conglomerate that rests upon it (Frisch, 2000), are consistent with it being unconformably overlain by the Montresor group and wrapping beneath the Montresor synform as one part of the Snow Island suite spectrum. On the other hand, Percival et al. (2015b) extended the garnet-muscovite granite as far south as latitude 65°50'N and reinterpreted it as Paleoproterozoic, cutting the Montresor group. It appears to correspond to unit Pg of Tella (1994), described as white to pink, coarse-grained porphyritic granite and pegmatite that extend southwest to the Amer plutonic complex on both sides of the extended Montresor Belt. Outcrops of this granite examined in the study area have abundant inclusions of schist and amphibolite. Outside of the garnet-muscovite granite, the dated Snow Island suite commonly includes hornblende-biotite granodiorite gneiss with K-feldspar augen (Ak unit) and hornblende-biotite augen gneiss (At unit) (two of a number of components distinguished by Frisch, 1992, 2000). Percival et al. (2017) generalized all of these Snow Island suite phases as “ca 2.6 Ga foliated to gneissic granodiorite.” The Snow Island suite phases on the northwestern side of the synform have low to moderate magnetic expression, whereas the K-feldspar porphyritic Snow Island suite on the southeastern side has a moderate to high magnetic expression, increasing toward the Amer mylonite zone and dissected by linear magnetic lows associated with multiple strands of the mylonite.

As noted above under the ‘Geological areas of focus’ section, Jefferson et al. (2015) and this study extrapolate the above information to continue the Montresor Belt and its single broad synform southwesterly as far as the Amer plutonic complex. Data sources include previous publications, aerial reconnaissance, outcrop sampling, as well as visual inspection of Landsat, residual total field, and tilt-derivative geophysical maps. Although Frisch (1992, 2000) stopped mapping the belt at latitude 66°N, Tschirhart et al. (2015) showed that the distinct linear aeromagnetic highs of the upper Montresor group continue across the Back River and pinch out about 8.8 km southwest of it. Just south of latitude 66°N, the river makes a distinct U bend that is coincident with a set of major 145°, northeast-side-down normal faults that coincide with offsets of the linear aeromagnetic markers

of sequence Ps4. Although the sequence Ps4 markers pinch out, the underlying muscovite-andalusite-sillimanite-garnet schist of the lower Montresor group continues, as evidenced by the ongoing aeromagnetic low and sparse outcrops of schist shown by Tella (1994) and Percival et al. (2017), and as documented at several stations of this study. No quartzite is exposed, and it is here interpreted to be absent, south of where last mapped by Frisch (1992), well north of the Back River. The garnet-muscovite granite and pegmatite do continue southwest of the Back River, where they include large rafts of schist and amphibolite, and remain coincident with the aeromagnetic low. If the schist inclusions are the same lithology as the purported sequence Ps3 schist farther northeast, then a date on the garnet-muscovite granite would provide a minimum age for the schist. About 28 km southwest of the Back River, two large outcrops and coincident irregular linear aeromagnetic highs document a 20 km long outlier of pristine, subhorizontal upper Montresor sequence Ps4 in the core of the extrapolated Montresor synform. The elevated aeromagnetic signature of sequence Ps4 terminates about 5 km northeast of the Amer plutonic complex. The sequence Ps4 outcrops were mapped by Tella (1994) as 'quartzite', but this study (station 11JP164) showed them to be a broad area of subhorizontal, fine-grained arkosic sandstone and siltstone, with no apparent cleavage, but well preserved ripple-drift crosslaminae. This sequence Ps4 unit is correlated as an outlier of the upper Montresor group, just as Frisch (1992) and Percival et al. (2017) included an area of arkosic siliciclastic rocks west of the Montresor Belt as an outlier of the upper Montresor group. The aeromagnetic low interpreted as schist wraps around the southwestern closure of the sequence Ps4 portion of the synform, coincident with a large outcrop area of schist and amphibolite adjacent to the Nueltin granite. The southwestern tip of the Montresor synform is transected obliquely by the northernmost strand of the Amer mylonite zone (Fig. 3a, c).

The western belts (Akiliniq, Deep Rose, Garry Lake, Nauyasuuq, and Sand) all feature thin (80–200 m) to discontinuous sequence Ps1 quartzite and lack the sequence Ps2 carbonate and sequence Ps3 basalt, except for small outcrops in the northern Sand Belt. A 50 to 100 m sequence Ps2 unit of rusty-weathering, ferruginous, fine-grained sandstone and mudstone, with local hematitic iron-formation, typically overlies the quartzite. The dominant unit in these belts is hundreds of metres of sequence Ps4 pinkish-green feldspathic sandstone, siltstone, mudstone, and arkose (Tella, 1984, 1994; LeCheminant et al., 1984; Miller, 1995). Graded beds predominate, recording turbiditic sedimentation. Centimetre-scale crossbeds and clastic dykes are well preserved. The sandstone beds are grey to pink, whereas the mudstone interbeds are grey-green. An outlier of the northern Sand Belt, north of the study area, exposes weakly deformed, ripple-marked, dolomitic calcilutite. Multiple graphitic slate interbeds are present within the turbiditic sandstone-siltstone facies, particularly toward the base of sequence Ps4 (Miller, 1995; logs of RHC07-01, 02, 03 by C.W. Jefferson, R.H. Rainbird, G.M. Young, S.S. Gandhi,

J.C. White, V. Tschirhart, D. Lemkow, and L.B. Chorlton, work in progress, 2023). Linear magnetic marker units are present only in the Nauyasuuq and Deep Rose belts, where they have a similar appearance, but have not been modelled geophysically. Sequence Ps4 directly overlies gneissic basement throughout much of the Garry Lake Belt and parts of the Deep Rose, Nauyasuuq, and Sand belts.

The original sequence Ps4 in the Ketyet River Belt, as defined by Pehrsson et al. (2013a), comprises dark slate (Ketyet River sequence Ps4A) and polymict conglomerate (sequence Ps4B; Tasirjuak conglomerate of Zaleski and Pehrsson, 2005) that is intercalated with the upper part of the slate. An upper unit of subarkose (unit APWqm of Zaleski and Pehrsson, 2005), formerly thought to underlie the conglomerate, is here reassigned to overlie the conglomerate in the core of the Whitehills synform, as Ketyet River sequence Ps4C. It has linear aeromagnetic markers that define the core of the F_{p4} -kinked Whitehills F_{p2} synform (Fig. 6). The Ketyet River sequence Ps4C is intruded by a set of syenite plugs exposed on islands in Whitehills Lake. Syenite boulders to cobbles within the Ketyet River sequence Ps4B differ petrographically from the Martell syenite and are considered as derived from an older intrusive unit. The following synopses of the four Paleoproterozoic sequences in each belt include the criteria used to assign strata to a particular sequence.

Distinguishing structural, lithological, and geophysical characteristics of sequences Ps1, Ps2, Ps3, and Ps4

Criteria to distinguish between the four Paleoproterozoic cover sequences are their unique combinations of 1) primary lithology and colour, 2) sedimentary structures, 3) geophysical signatures, 4) stratigraphic position (not possible without unravelling the effects of the D_{p1} and D_{p2} events), and 5) tectonic fabrics and folds at scales from outcrop to thin section. This section focuses on the first four attributes and covers the structural and metamorphic attributes sufficiently to put the first four into context. The section entitled 'Structure and metamorphism' provides context and more details on the tectonic fabrics and folds. Descriptions of lateral variations in these sequences presented below complement the correlations described and cartooned by Jefferson et al. (2023).

The sequence Ps1 quartzite is white, highly indurated, vitreous, resistant to weathering, and has very low magnetic susceptibility. Where the quartzite is present, it forms topographic highs and is readily mapped by aerial photography and satellite imagery. It is the most resistant supracrustal unit in the region. As a rule, if the quartzite is not exposed, it is not present, as confirmed by drilling to basement in a number of places such as the Garry Lake Belt (Miller, 1995).

Bedding in the quartzite is transposed subparallel to D_{p1} muscovite foliation (most evident along stylolitized bedding-plane partings). Bedding is very difficult to recognize

in outcrop without close inspection, but is commonly clear at a distance, such as from helicopter. One photographed example of a helicopter view is the rhythmically graded, tabular quartzite beds with black slate interbeds at ‘Nipterk lake’ (Fig. 7c). Sedimentologically, those are interpreted as turbidite deposits. More commonly, the quartz arenite to feldspathic quartz arenite displays fluvial to shallow-marine trough crossbeds and ripple marks. Rare giant crossbeds such as documented by Young (1979) in the south-southwest Amer Belt are likely eolian.

The map width of the undivided sequence Ps1 quartzite+conglomerate is highly variable and, toward the north and west of the study area, it is discontinuous. In the Montresor Belt, the quartzite unit is continuous and about 1 km in map width, only around its northeastern portion, becoming thinner and discontinuous toward the southwest. The last sequence Ps1 exposures are at about longitude 96°50'W on the southeastern limb and longitude 96°40'W on the northwestern limb (Frisch, 1992). No quartzite is exposed past these points for the remaining southwestern end of the belt. In the Garry Lake Belt, only a few localities of quartzite are known, and it overlies quartz-feldspar-biotite gneiss, porphyroblastic K-feldspar augen gneiss (Snow Island suite), and foliated granite (Miller, 1995). Quartzite units are continuous in the Amer and Ketyet River belts. It thus seems that the Ps1 quartzite was originally a nearly continuous sheet across the region, but was eroded after D_{p1} in the western Montresor Belt and most of the Deep Rose and Garry Lake belts prior to deposition of sequence Ps4. Quartzite map widths in the region range from 1 m (e.g. Fig. 7a–c) to 15 km or more. The wider map widths are a result of structural repetition by intense D_{p1} isoclinal folds and open to tight D_{p2} refolds (e.g. Fig. 4b, 6). The primary depositional thickness is estimated to range from no greater than 1 m to perhaps 1 km, as can be seen clearly in the ‘Nipterk lake’ area (Fig. 7a–c).

In well exposed sections of the Amer and Ketyet River belts, the white quartzite grades down into pale tan schistose quartzite and polymict conglomerate that rests on, and includes, clasts of the underlying Archean unit, such as 2.6 Ga Snow Island suite granite (e.g. geochronology site 34, Table 2; Fig. 5h), 2.6 Ga rhyolite (Pukiq Lake formation), or an assemblage of the Woodburn Lake group (various volcanic rocks, iron-formation, greywacke, and vein quartz). At geochronology site 4 (Fig. 3a), basal sequence Ps1 conglomerate overlies and incorporates clasts of the 2.72 Ga North Meadowbank assemblage. Petrography of the amphibolite-facies-grade basal muscovite schist in the northeast Amer Belt reveals highly foliated and flattened pebbles, including abundant Pukiq Lake formation rhyolite, the schistosity of which is parallel to that of the enclosing muscovite-rich, lithic–feldspathic quartz arenite matrix. The identical lithology, including pebble types, is only weakly deformed in the southwestern portion of the Amer Belt (Jefferson et al., 2023; C.W. Jefferson, R.H. Rainbird, G.M. Young, S.S. Gandhi, J.C. White, V. Tschirhart, D. Lemkow, and L.B. Chorlton, work in progress, 2023).

In the Montresor Belt, Frisch (2000) documented a basal sequence Ps1 conglomerate and phyllite to schist at only one locality (‘Cu’ in Fig. 3a). Elsewhere, Percival et al. (2017) described an exposed basal contact at the northeastern end of the belt as a ductile high-strain zone between amphibolite-facies schist above and gneissic to mylonitic granitoid rocks below. They showed several contacts between quartzite and Snow Island suite granitoid gneiss in this area, in some places isolating slivers of quartzite, in others placing quartzite on quartzite. They described no outcrop-scale folds. A ductile high-strain zone is also present at the base of the quartzite in much of the Whitehills synform (Fig. 6), and at the northeastern end of the Amer Belt (Patterson, 1986). At the southern end of the Whitehills synform, a locally preserved lens of highly schistose basal conglomerate overlies Snow Island suite granite, whereas the rest of the basal contact around that synform is isoclinally folded and transposed sericitic schist to mylonite (Taylor, 1985; Zaleski and Pehrsson, 2005) in contact with Snow Island suite granite or Sanning tonalite. The schistose basal contacts in the Amer and Ketyet River belts are interpreted as products of flexural slip focused at the contacts between the sedimentary rocks and the thick, massive Snow Island suite slabs that wrap beneath, and form highly competent layers within, the F_{p2} synforms and antiforms.

In localities with complex F_{p1} to F_{p2} interference patterns, such as ‘Nipterk lake’ (Fig. 7a), the Pukiq Lake formation is the immediate substrate for the Paleoproterozoic quartzite. There, this felsic tuff is isoclinally infolded (D_{p1}) and refolded (D_{p2}) along with the quartzite, obscuring their primary stratigraphic relationship. Along the southeastern side of the Thelon Fault in the Kiggavik uranium exploration camp, Anand and Jefferson (2017a, b) showed that mylonitized and lineated quartzite as well as Pukiq Lake formation are structurally intercalated at millimetre to decametre scales (PQi in Fig. 8), and no conglomerate is preserved. More information on the PQi and other examples where the basal unconformity assemblage is highly strained are in the section entitled ‘Types of structural discontinuities’ below.

The transition from sequence Ps1 to Ps2 is highly varied and unlike any other upward transition in the early Paleoproterozoic of the study region. One common feature in most of the Amer and Ketyet River belts is the development of gossans at this transition (see ‘Alteration and metallogenic comparisons of the Athabasca Basin and Thelon Basin regions’ section below). In the ‘Nipterk lake’ area (Fig. 7a–c), the quartzite unit becomes very thin, individual quartzite beds are thin, graded, and separated by thin layers of sequence Ps2 grey schist. Deformation there is extreme (Fig. 7b, c). In the southwest Amer Belt (Jefferson et al., 2023; C.W. Jefferson, R.H. Rainbird, G.M. Young, S.S. Gandhi, J.C. White, V. Tschirhart, D. Lemkow, and L.B. Chorlton, work in progress, 2023), fine-grained rhythmically bedded quartzite with muscovite schist partings passes abruptly upward into rusty-weathering mudstone of sequence Ps2. In the Schultz Lake klippe area of the

Ketyet River Belt (western part of Fig. 6 and eastern part of Fig. 8), the upper portion of the sequence Ps1 quartzite becomes coarser grained and forms decimetre- to metre-scale graded beds with local ball-and-pillow structures. The upper graded beds are separated by carbonaceous slate ('e' horizon of the Bouma turbidite cycle) and become progressively thinner upward, until the lithology is entirely black carbonaceous slate of sequence Ps2. The black slate hosts pods of polymict conglomerate interpreted as submarine channel deposits. In the northeast Amer Belt and parts of the Ketyet River Belt, such as the Whitehills Lake synform, the quartzite grades upward to pale grey-green feldspathic quartz arenite and polymict conglomerate, and is overlain in most places by sequence Ps2 lithic, fine-grained clastic rocks, then basalt. The upper part of the sequence Ps1 polymict conglomerate has a rusty pyritic matrix, locally includes angular scoria lapilli (Fig. 5i), and is separated from the overlying sequence Ps3 basalt flows by very thin sequence Ps2 tuffaceous mudstone in the Whitehills Lake synform. The grey-green quartzite and scoria lapilli are evidence that basalt eruption was diachronous, starting in places at the same time as continued deposition of the upper quartzite and conglomerate (*see* discussion of sequence Ps3 below). The sequence Ps2 slate encloses lenses of polymict conglomerate in the northern Schultz Lake klippe. The upper conglomerate has elevated radioactivity in places, such as the 'Graphite' uranium occurrence (geochronology site 35, northeast corner of Fig. 8) explored by the Forum Uranium Corporation. Thorium is more abundant than uranium in these occurrences, a result of paleoplacer accumulations of monazite and zircon.

Sequence Ps2 comprises mainly fine-grained siliciclastic strata stratigraphically intercalated with, and overlying, the quartzite (e.g. Ketyet River grey schist at 'Nipterk lake', Fig. 7a–c). Sequence Ps2 graphitic mudstone in the Amer Belt hosts strong conductors that have been the target of much exploration drilling (e.g. Young, 1979; G. Drever, pers. comm., 2006; M. McLaren, pers. comm., 2008). Such conductors are likely present in sequence Ps2 of the Ketyet River (P. Wollenberg, pers. comm., 2009) and Montresor belts (inference). In places such as the northeast Amer Belt, a middle feldspathic lithic sandstone unit (unit 8 of Patterson, 1986) forms a low, but mappable ridge. The fine-grained siliciclastic strata grade up through impure to pure dolostone, with recrystallized chert layers and boudins in parts of the Amer and easternmost Ketyet River belts. In the Montresor Belt, no graphitic mudstone has been recognized at the transition between the quartzite and the dolostone, but as it is very recessive, its presence is suspected there too. The sequence Ps2 dolostone unit in the Montresor Belt is identical in appearance to that of the Amer Belt (J. Patterson, pers. comm., 2009). The Aluminium River formation of the Amer group is the type example. The fine-grained siliciclastic and dolostone units are typically highly strained and bedding is transposed, with no primary sedimentary structures preserved. Map widths of lower sequence Ps2 fine-grained siliciclastic strata range from zero to hundreds of metres. In

the Whitehills Lake area, the thickness of the Ps2 mudstone sequence (commonly termed 'grey schist') is one metre or less, increasing to several tens of metres where the basalt is absent (Fig. 6). In the 'Nipterk lake' area, the grey schist is thicker than the conglomerate and quartzite (Fig. 7b, c) and is the youngest Paleoproterozoic unit preserved there. The sequence Ps2 carbonate unit is discontinuous in all three belts. In the Amer and Ketyet River belts, the presence or absence of the carbonate unit is characteristically a linear feature, interpreted as a result of primary deposition or nondeposition (Jefferson et al., 2023; C.W. Jefferson, R.H. Rainbird, G.M. Young, S.S. Gandhi, J.C. White, V. Tschirhart, D. Lemkow, and L.B. Chorlton, work in progress, 2023). In the Montresor, Garry Lake, and Akiliniq belts, the presence or absence of the carbonate unit may be in part depositional, and in part due to differential erosion prior to deposition of sequence Ps4.

Sequence Ps3 begins in some places with mafic tuff and metre-thick flows gradationally overlying sequence Ps2 dolostone or fine-grained siliciclastic rocks. In other places, the basalt is absent and fine-grained siliciclastic rocks of sequence Ps3 gradationally overlie the dolostone. In most exposures of the Ketyet River group, no dolostone is present and the locally termed 'grey schist' unit may include both of sequences Ps2 and Ps3. The basalt is carbonate-rich and has high magnetic susceptibility, forming a powerful linear aeromagnetic marker unit with high density (Tschirhart et al., 2013d). Distinct swallow-tail plagioclase phenocrysts are diagnostic and carbonate-filled amygdalae are well preserved in both the Ketyet River and Amer belts. Basalt flows in both the Amer and Ketyet River belts form laterally continuous markers in the southern Whitehills Lake area, a small belt on the western side of the north Meadowbank River, and along the southeastern side of the Amer Belt (Jefferson et al., 2015, 2023; C.W. Jefferson, R.H. Rainbird, G.M. Young, S.S. Gandhi, J.C. White, V. Tschirhart, D. Lemkow, and L.B. Chorlton, work in progress, 2023). The basalt is positioned stratigraphically above, and intercalated with, dolostone and/or fine-grained siliciclastic rocks of sequence Ps2. In both belts, the basalt is nowhere in contact with the sequence Ps3 fine-grained siliciclastic strata, but Jefferson et al. (2015, 2023) and C.W. Jefferson, R.H. Rainbird, G.M. Young, S.S. Gandhi, J.C. White, V. Tschirhart, D. Lemkow, and L.B. Chorlton (work in progress, 2023) infer it to be laterally equivalent to a highly magnetic marker about midway in the Three Lakes formation of the lower part of sequence Ps3. Basalt is absent in the northern part of the Whitehills Lake synform, most other places in the Ketyet River Belt, the northwestern part of the Amer Belt, all of the Montresor Belt, and from all of the western belts, except a small part of the northern Sand Belt.

The sequence Ps3 mudstone facies includes a strong linear, upper magnetic marker unit in the Three Lakes formation of the Amer Belt. There, Calhoun et al. (2014) documented the aeromagnetic source as densely disseminated euhedral

(metamorphic) magnetite. Only in the Amer Belt, the middle of sequence Ps3 is a marker unit of laminated quartz arenite to trough-crossbedded calcareous arkose — the informal Oora Lake formation — with gradational lower and upper contacts. Additionally, only in the Amer Belt, the upper part of sequence Ps3 comprises intercalated green-grey argillite and calcareous arkose, with two laterally extensive units of magnetic sandstone that host disseminated uraninite, pyrite, and magnetite — the informal Showing Lake formation. These units, and their type and reference sections, are detailed by Jefferson et al. (2023) and C.W. Jefferson, R.H. Rainbird, G.M. Young, S.S. Gandhi, J.C. White, V. Tschirhart, D. Lemkow, and L.B. Chorlton (work in progress, 2023).

The linear magnetic marker units of the Three Lakes and Five Mile Lake formations (lower part of sequence Ps3) in the Amer Belt are of comparable amplitude to those in sequence Ps4 of the Montresor Belt (Tschirhart et al., 2015), but differ fundamentally in terms of 1) the D_{p1} versus D_{p2} structures they outline, 2) the fabrics in the host strata, and 3) their lithological context and mineral petrography. Magnetic markers in the Amer sequence Ps4 are much weaker, being clearly evident only on images of tilt derivatives, but have not been documented petrographically. Those in the Ketyet sequence Ps4 have not been calibrated in any way except by visual analysis of residual total field images, but are visually similar in amplitude to those of the Montresor sequence Ps4. The magnetic phase of the Amer sequence Ps3 is euhedral (metamorphic) magnetite ranging from 10 to 70 μm (it is the only mineral of this grain size as there are no detrital heavy minerals) and it cuts across the more finely crystalline, strongly foliated host phyllite (Fig. 6 of Calhoun et al., 2014). In petrographic contrast, the weakly foliated Montresor sequence Ps4 magnetic beds comprise angular less than 50 μm detrital magnetite as a component of heavy mineral bands accompanying zircon, apatite, and tourmaline of similar grain size (Fig. 3c of Percival and Tschirhart, 2017). The magnetic phase in the Five Mile Lake basalt is much coarser crystalline igneous-metamorphic titanomagnetite. The Showing Lake formation contains two magnetic marker units, both being distinct, but moderate on residual total field images, whereas markers of both the Three Lakes and Five Mile Lake formations are prominent on residual total field images. The Showing Lake formation markers are accentuated and can be traced individually and continuously on the images of tilt derivatives, where they help define complex D_{p1} isoclinal folds (Tschirhart et al., 2013d; Calhoun et al., 2014; Jefferson et al., 2023; C.W. Jefferson, R.H. Rainbird, G.M. Young, S.S. Gandhi, J.C. White, V. Tschirhart, D. Lemkow, and L.B. Chorlton, work in progress, 2023).

A fourth and key difference for explorationists is that the two magnetic markers in the upper Amer sequence Ps3 (Showing Lake formation) are the locus of strat-
around sediment-hosted uranium occurrences, unknown in the Montresor and Ketyet River belts (see ‘Alteration

and metallogenic comparisons of the Athabasca Basin and Thelon Basin regions’ section below). In both the middle and upper Amer sequence Ps3 markers, the magnetic minerals appear to have had a chemical sedimentary-diagenetic origin and were modified by metamorphic recrystallization. The sequence Ps3 magnetic marker beds outline isoclinal F_{p1b} and F_{p1c} folds that were refolded by F_{p2} (Calhoun et al., 2014; White et al., 2021, 2023). Tschirhart et al. (2017) documented multiple linear aeromagnetic anomalies *within* the sequence Ps4 strata of the Amer Belt, then termed the ‘Itza Lake formation’, after fieldwork had been completed, so it was not possible to target them for sampling. These linear aeromagnetic anomalies are very subtle on residual total field images, but quite distinct on tilt-derivative images (Jefferson et al., 2023; C.W. Jefferson, R.H. Rainbird, G.M. Young, S.S. Gandhi, J.C. White, V. Tschirhart, D. Lemkow, and L.B. Chorlton, work in progress, 2023). They had been previously misinterpreted (Jefferson et al., 2015) as sequence Ps3 magnetic markers visible through the overlying sequence Ps4 strata. The sequence Ps4 magnetic markers in the Amer Belt are remarkably continuous on images of tilt derivatives and, linked with outcrop data of Young (1979), define multiple F_{p2} folds, but not F_{p1} folds (Jefferson et al., 2023; C.W. Jefferson, R.H. Rainbird, G.M. Young, S.S. Gandhi, J.C. White, V. Tschirhart, D. Lemkow, and L.B. Chorlton, work in progress, 2023). Except for basalt, no magnetic markers are known below sequence Ps4 in the Ketyet River Belt, but multiple strong and continuous linear aeromagnetic markers in a newly recognized uppermost sequence Ps4 lithic arkosic sandstone unit help define the axis of the main F_{p2} Whitehills synform (Fig. 6). Again, the sequence Ps4 aeromagnetic markers of the Ketyet River Belt have not been sampled for analysis of their magnetite.

The fundamental field criteria for differentiating sequence Ps4 from the first three Paleoproterozoic cover sequences are: the mapped unconformity at the base of sequence Ps4 (see ‘Basal contact of sequence Ps4’ section below), the molasse and flysch rock types (distinct rhythmic interbedding of sandstone and mudstone in either alluvial or marine [turbiditic] settings), and their intrinsic structural attributes — *pristinely preserved primary sedimentary structures and textures*, and *weak tectonic* structures. Sequence Ps4 across the region shows great diversity of sedimentary facies that result from diverse depositional environments, and thus are not useful for sequence stratigraphy, except inasmuch as they define unconformities, similar provenance, and distinct grain-size excursions (conglomerates) that mark internal sequence boundaries. Bedding in sequence Ps4 is transected by a single, relatively weak S_{p2} fabric that is axial planar to F_{p2} . There are no isoclinal folds at any scale, whereas these are ubiquitous in sequences Ps1 to Ps3 (see ‘Structure and metamorphism’ section). A remarkable local attribute of sequence Ps4 in the central and southwestern Amer Belt and the Garry Lake Belt is the dominance of true redbeds — deep to bright red desiccation-cracked mudstone, rhythmically interbedded with, and included as intraclasts within,

the salmon-pink lithic feldspathic sandstone. These could easily be confused with redbeds of the Dubawnt Supergroup (R. Rainbird, pers. comm., 2021), were it not for their detrital zircon ages and their deformation during D_{p2} . The paleodiagenetic redbed attribute depends on subaerial to shallow subaqueous deposition, so is not present in deep subaqueous (below wave base) sequence Ps4 facies of the Ketyet River and Montresor belts, nor is it present in deep-water turbidite facies of the uppermost part of sequence Ps4 in the Amer Belt. Geochronology of detrital zircon (below) provides important corroboration of the young age of sequence Ps4, as well as provenance constraints.

The depositional environment of sequence Ps4 is much more varied than those of the units of sequences Ps1 through Ps3 that individually tend to have uniform depositional records throughout each one, with the sequence Ps1 to Ps2 transition being the most varied of those. Sequence Ps4 on the other hand varies laterally from deep subaqueous to subaerial alluvial, yet all sequence Ps4 samples produced similar detrital zircon profiles (Appendix B, Fig. 2). Sequence Ps4 in the Ketyet River Belt was all deposited in deep water, below wave base, as indicated by the presence of centimetre-scale graded bedding and finer laminae in dark grey to black slate. The contained lenses of grey polymict conglomerate (Fig. 5f) are interpreted as submarine-channel deposits. In contrast, the lower two sequence Ps4 units in the Amer Belt are dominated by redbeds interpreted as subaerial-alluvial through shallow-marine deposits. In the lower portion of the Amer sequence Ps4, some sections with widely scattered paleocurrents and stromatolitic dolostone facies support an intertidal to very shallow-marine interpretation, whereas other sections with unimodal paleocurrents and desiccation cracks in deep red mudstone support alluvial deposition. The polymict conglomerate (Fig. 5g) that overlies an orange stromatolite biostrome has an intact framework and grades upward to red lithic feldspathic sandstone, consistent with tectonic uplift, provenance of both distal basement rocks to locally derived sandstone and orange dolostone blocks, and their accumulation in an alluvial thalweg. A similar depositional setting is suggested for the sequence Ps4 conglomerate enclosed in arkose, as described by Frisch (2000) for the Montresor Belt.

The magnetic marker units in the southwestern part of the contiguous Amer Belt may thus be intertidal to shallow marine, suggesting that the magnetic marker beds in the uppermost Ketyet River sequence Ps4 (exposed only on islands) should be re-examined for the possibility of intercalated redbeds. These shallow-marine to subaerial molasse deposits could have started accumulating in the Amer Belt on a subsiding foreland bulge in front of a prograding mountain belt, while sequence Ps4 in the Ketyet River Belt was initially deposited in very deep water, then gradually filled the basin, thus creating possibly shallow-marine to emergent environments. The turbiditic upper portion of sequence Ps4 in the northwest Amer Belt includes black graphitic slate conductors (references provided at end of 'New

definitions of sequences Ps1, Ps2, Ps3, and Ps4 in the Amer Belt' section) and abundant crosscutting sandstone dykelets, characteristic of deep-water sedimentation during active tectonism, recording continued deepening as the prograding D_{p2} foreland basin migrated to the Amer Belt region.

Frisch (2000) and Percival et al. (2017) also found the depositional environment in the Montresor sequence Ps4 to be shallow water (pinkish-grey crossbedded siltstone with abundant dolostone interbeds), consistent with earlier depositional sequences in the Montresor Belt; however, these are not brightly coloured redbeds and there are no reported desiccation cracks, suggesting a continuously submerged environment influenced by shallow subtidal currents, or contourite-forming currents and/or ephemeral paleocurrents associated with turbidite flows. A large, flat-lying outcrop of Montresor sequence Ps4 siltstone observed by the first author at latitude 65.79°N, longitude 97.84°W (station 11JP164) preserves undeformed, centimetre-scale, ripple-drift crossbeds directed toward 160°. The scattered paleocurrents of the Amer sequence Ps4 (Young, 1979; C.W. Jefferson, R.H. Rainbird, G.M. Young, S.S. Gandhi, J.C. White, V. Tschirhart, D. Lemkow, and L.B. Chorlton, work in progress, 2023) do not constrain whether the area of the Amer Belt might have been a part of the same basin as sequence Ps4 in the Ketyet River and/or Montresor belts.

Basal contact of sequence Ps4

Sequence Ps4 unconformably overlies the F_{p1} isoclinally folded and D_{p1} thrust sequences Ps1 through Ps2 or Ps3. Map patterns in both the Ketyet River (e.g. Fig. 6) and Amer (Jefferson et al. 2015; C.W. Jefferson, R.H. Rainbird, G.M. Young, S.S. Gandhi, J.C. White, V. Tschirhart, D. Lemkow, and L.B. Chorlton, work in progress, 2023) belts, as well as in outcrops at Whitehills Lake, define the profound, deeply crosscutting nature of this angular unconformity. The base of sequence Ps4 directly overlies Archean basement gneiss in a number of places: e.g. Garry Lake (Miller, 1995), the northern side of the Amer Belt (northwest of geochronology site 41a, Fig. 3a), and overlying Neoproterozoic rocks of the Amarulik assemblage in the footwall of the Half Way thrust (Fig. 6). The basal unconformity is well exposed west of geochronology site 40 at Whitehills Lake (Fig. 6), where slate directly overlies overturned, isoclinally folded sequence Ps1 quartzite with no conglomerate, recording quiescent onlap in a deep basinal environment. The basal unconformity has not been observed precisely in outcrop in the Amer Belt, where it is defined geometrically, but in places it is constrained within metres. For example, a decametre-scale subhorizontal outlier of ripple-marked feldspathic sandstone west of upper Amer Lake rests on the steeply dipping contact between isoclinally folded sequence Ps1 quartzite and sequence Ps2 schist (Jefferson et al., 2015; C.W. Jefferson, R.H. Rainbird, G.M. Young, S.S. Gandhi, J.C. White, V. Tschirhart, D. Lemkow, and L.B. Chorlton, work in progress, 2023).

For the most part, the basal sequence Ps4 unconformity is regional, map-defined, and angular, cutting deeply across underlying and D_{p1} -deformed sequences Ps3 through Ps1 to the Archean. In the Montresor, Deep Rose, Garry Lake, and northwestern Amer belts, the fine-grained sequence Ps4 strata successively overlie sequence Ps2 carbonate, sequence Ps1 quartzite, 2.6 Ga foliated granite, and Woodburn Lake group or undated paragneiss and orthogneiss (Fig. 3a). In the Garry Lake and other western Paleoproterozoic belts at the northern edge of the Aberdeen Subbasin, preservation of quartzite beneath sequence Ps4 is highly varied to nil. In the absence of quartzite, the best definition of the base of the Garry Lake sequence Ps4 is a continuous conductor in a lower graphitic metapelite that Miller (1995) included in the upper Amer group (Amer sequence Ps4). The scale over which sequence Ps4 overlies and truncates underlying sequences Ps1 through Ps3 strata is such that it cannot be a detachment fault, consistent with the Whitehills Lake exposures of an undeformed basal contact gently draping highly D_{p1} deformed sequences Ps1 through Ps2 strata. Similarly, it may be hypothesized that the sequences Ps1 and Ps2 strata were never deposited in the areas where they are absent beneath sequence Ps4. Such a hypothesis is inconsistent with the typical lateral continuity demonstrated by sequence Ps1 in most places, the one exception being in superb exposures at 'Nipterke lake', where the quartzite exhibits lateral pinch-outs into sequence Ps2 or Ps3 mudstone across a mapped distance of 200 m, but is regionally continuous. Discontinuities such as at the scale seen in the Garry Lake Belt (Miller, 1995) and the Montresor Belt (Frisch, 1992) speak to erosion prior to deposition of sequence Ps4. Finally, the fact that sequence Ps4 contains cobbles to boulders of predeformed sequence Ps1 and Snow Island suite in both the Amer and Ketyet River belts demonstrates pre-sequence Ps4 erosion cut down through sequence Ps1 into the Archean basement.

Percival et al. (2015a, b; 2017) interpreted the discontinuity at the base of the upper Montresor group strata as a detachment fault, even though Tschirhart et al. (2015) had not ruled out the unconformity interpretation. The detachment fault of Percival et al. (2015b) is extrapolated around the nose of the Montresor synform (Fig. 4 of Percival et al., 2017), showing that whatever the origin of this structure, it predates formation of the main Montresor synform (their F4, here reinterpreted as F_{p2} like all the other large structures of this style in the region; F_{p4} , as defined by Pehrsson et al. (2013a), comprises kink folds such as illustrated in Fig. 6). The actual structural break is not exposed and so there are no kinematic indicators to substantiate their interpretation, however the difference in metamorphic grade between the lower (middle-amphibolite facies generated at 1861–1844 Ma, Berman et al., 2015b; Dziawa et al., 2019) and upper (middle-greenschist facies) Montresor group strata across a distance of less than 100 m requires a fault with significant dip-slip offset (Percival et al. 2015a, b, 2017) or a major time gap between the lower and upper Montresor group strata, with the metamorphism pre-dating the faulting and folding of the upper Montresor group.

The geometry of the dip-slip fault interpreted by Percival et al. (2015a, b, 2017) is incompatible with dip-slip motion inward around all three sides of the synform — unless the fault was an early slide emplacing the younger sequence Ps4 on the older Archean basement and sequences Ps1 through Ps3. As noted above, the Montresor sequence Ps4 progressively cuts out sequences Ps1 to Ps3 strata toward the southwest, which is unlikely with such a slide. The present authors prefer to interpret this angular discontinuity as an unconformity, with the metamorphic difference between Montresor sequences Ps1 through Ps3 and Ps4 being less in other parts of the synform. The southeastern side of the belt could well have been down-dropped to the north by a set of northeast-trending P-shears following clearly visible linear topographic lows, as documented elsewhere in the region. Foliated outcrops at this contact, such as reported by Frisch (2000), can be interpreted as a result of either P-shears or, if parallel to bedding, of F_{p2} flexural slip, similar to the highly strained basal contacts of the Amer and Ketyet River groups described above. In places such as the southeastern margin of the Montresor Belt, straight linear 060 to 070° P-shears can be readily interpreted from the existing mapped faults coupled with Landsat imagery. Further supporting the unconformity interpretation, the basal discontinuity of sequence Ps4 at the northeastern end of the Montresor Belt clearly cuts across D_{p1} imbricate thrusts that repeat basement Snow Island suite, sequence Ps1 quartzite, sequence Ps2 dolostone, and the sequence Ps3 wacke that hosts the 2045 ± 13 Ma gabbro sill (localities 2 and 3 in Fig. 4 of Percival et al., 2017). These basement-involved D_{p1} imbricate thrusts do not affect the upper Montresor group sequence Ps4. The Montresor D_{p1} thrusts affect only the basement and sequences Ps1 through Ps3 — the same sequences as in the Amer Belt.

Polymict conglomerate is located some 20 to 100 m or more above the base of sequence Ps4 in all three belts. This includes the Tasirjuak conglomerate of Zaleski and Pehrsson (2005; Fig. 5f in this study), the conglomerate overlying a stromatolite biostrome and overlain by red feldspathic lithic sandstone in the contiguous Amer Belt (Fig. 5g; Jefferson et al., 2023), conglomerate in upper Amer group correlatives along the Thelon River southwest of Beverly Lake (Fig. 3a) (top of sequence A of LeCheminant et al., 1984), and conglomerate enclosed in pink and grey arkose at the southwestern end of the Montresor Belt as described by Frisch (2000, p. 26; see full description by Frisch in 'Sequences Ps1, Ps2, Ps3 and Ps4 in the Ketyet River, Montresor, and western belts' section). Conglomerate is not known at the base of sequence Ps4; instead, slate directly overlies isoclinally folded quartzite in the Ketyet River Belt, sandstone-mudstone rests on Archean to sequence Ps3 strata in the Amer Belt, and phyllite to schist is commonly at the base of the Montresor sequence Ps4. Extrabasinal clasts of the intra-Ps4 conglomerate in all three belts include well rounded, previously folded and foliated, vitreous quartzite interpreted as sequence Ps1; porphyritic felsic volcanic rocks interpreted as Pukiq Lake formation; and pink granite interpreted as Snow Island suite. The Tasirjuak conglomerate cobbles of foliated granitoid rocks (Pehrsson et al.,

2013a) are illustrated in Figure 5f. Locally derived, not previously deformed, intraformational clasts characteristic of the local sequence Ps4 are more abundant than the tectonized clasts in the Amer and Ketyet River conglomerate units. Those in the Ketyet River Belt are mainly slate, whereas those in the Amer Belt include feldspathic sandstone, mudstone, and undeformed quartz arenite, consistent with the local enclosing rock types. Sparse orange-weathering, apparently local dolostone clasts are also present in the Amer and Ketyet River sequence Ps4 conglomerate. Those in the Amer Belt may be derived from desiccation-cracked stromatolitic dolostone that directly underlies the conglomerate (Young, 1979).

The basal contact of sequence Ps4 in the Amer Belt is interpreted as a mapped angular unconformity (*see above*), even though no basal conglomerate is known. Young (1979) came to this conclusion based on polymict conglomerate within the upper Amer group containing rounded quartzite boulders. Similar contacts at the base of sequence Ps4 have been interpreted as either a structural discontinuity (Montresor group in Percival et al., 2015a, b, 2017; Dziawa et al., 2019) or an unconformity (Montresor group in Frisch, 2000; Ketyet River group in Pehrsson et al., 2013a). The contact in the Ketyet River group is particularly instructive because it is well enough constrained in outcrop to define a locally irregular unconformable contact involving weakly deformed dark slate directly overlying highly deformed sequence Ps1 quartzite, with no conglomerate, on the inside western limb of the Whitehills synform (here the term ‘synform’ is still used, even though in sequence Ps4 this is the first fold event, because the lower strata involved in this major fold all display F_{p1} isoclinal folds). The black mud protolith appears to have been simply draped over the irregular surface of eroded, isoclinally folded quartzite.

The presence of deformed sequence Ps1 clasts in the Tasirjuak conglomerate shows that deep, but discontinuous erosion of the lower units of the Ketyet River group took place after D_{p1} (*see description of quartzite discontinuity above*); however, the absence of basal sequence Ps4 conglomerate in all three belts indicates that no local, erosional fault uplifts were present in this area immediately prior to deep epeirogenic subsidence that created the sequence Ps4 flysch to molasse basins. Thus, the previously eroded quartzite subsided below wave-base before any clastic sediment arrived in this location, after which dark muds accumulated under anoxic quiet-water conditions. Only later did conglomerate enter the sequence Ps4 basin as submarine-channel deposits derived from the advancing mountain front in the area of the Chesterfield fault zone. The conglomerate forms lenticular bodies in the order of 1 to 5 m thick and is succeeded by more black slate. Arkosic sandstone overlies the slate and has distinct linear aeromagnetic markers that define the core of the synform (Fig. 6), just as they do in the Amer sequence Ps4.

The stratigraphic style of the Ketyet River group sequence Ps4 is characteristic of foreland-basin flysch and molasse, as noted by Pehrsson et al. (2013a), with the conglomerate

representing a major syndepositional tectonic pulse. The same tectonic-stratigraphic interaction is recorded in the Amer Belt, also termed ‘molasse’ (Young, 1979), except that the basin-deepening event there was not as extreme. Initial deposits of grey phyllite with flute casts (Jefferson et al., 2023) are relatively thin and known from only one locality; elsewhere the lowest exposed beds are highly oxygenated, shallow-marine to alluvial quartz arenite, arkosic sandstone, and deep red desiccation-cracked mudstone. As in the Ketyet River Belt, conglomerate was introduced part way through deposition of the finer grained molasse. In the Amer Belt, the conglomerate overlies a shallow-marine orange stromatolite biostrome in several places and calcareous arkose in others. The stromatolites are well preserved, with gentle dips and weak fabric. In the upper Montresor molasse, the phyllitic base of sequence Ps4 and its arkose-enclosed polymict conglomerate similarly support the subtle foreland unconformity model for the base of the Montresor sequence Ps4.

Geochronology of sequences Ps1, Ps2, and Ps3

Although the lithological criteria for distinguishing sequences Ps1, Ps2, and Ps3 are clear (*see above*), their depositional ages are weakly constrained in the Amer and Ketyet River belts. The youngest clasts in sequence Ps1 conglomerate are 2.6 Ga Snow Island suite granite (geochronology site 34, Table 2; Pehrsson et al., 2013a; Davis, 2021). The youngest detrital zircon grains in the succeeding quartzite and conglomerate are 2.72 to 2.50 Ga (geochronology site 35–37, Table 2; Appendix B), within a narrow spectrum only as old as 3.0 Ga (spectra in Appendix B). Sequence Ps1 in these belts shows no structural or metamorphic evidence of the ca. 2.35 Ga Arrowsmith Orogeny (Berman et al., 2013), hence sequence Ps1 in the Amer and Ketyet River belts is interpreted as younger than 2.35 Ga. The youngest detrital zircon cluster in Ps1 of the Montresor Belt is 2.194 ± 0.014 Ga (Percival et al., 2017), consistent with the post-Arrowsmith interpretation of the Ps1 sequence in the Amer and Ketyet River belts.

The only existing constraining age on sequences Ps2 and Ps3 in the Amer and Ketyet River belts is the 2153 ± 5 Ma (site 38, Table 2; Fig. 6) age of the ‘Schultz Lake metagabbro’ plug and sheets that crosscut the Neoproterozoic western Pipedream assemblage with gentle northward dip, is tenuous, but worthy of consideration. There are no detrital zircon data for lithostratigraphically confirmed sequence Ps2 or Ps3 units in the Amer and Ketyet River belts, which is understandable given the fine-grained nature of much of these units and the general difficulty in obtaining datable zircon from them. The reason this 2153 ± 5 Ma age may be relevant to stratigraphy is that Patterson et al. (2012) found the metagabbro to be geochemically similar to Paleoproterozoic basalt of both the Amer and Ketyet River belts, in that all are continental tholeiite with elevated light rare-earth elements (LREEs) and no felsic phases, in contrast to the Archean

basalts that are calc-alkaline with low LREEs and a spectrum ranging from mafic to felsic. The present authors also found that within the Proterozoic mafic data set, the basalt and gabbro samples from the Amer group and the basement-hosted Schultz Lake metagabbro have parallel REE patterns, but different abundances, with the Schultz Lake metagabbro lying between the Amer basalt and gabbro, whereas the Ketyet River basalt has more strongly fractionated REEs. They also found significant differences between the Paleoproterozoic major-element compositions of each belt that are sufficient to require independent local generation of magmas. This is consistent with the localized nature of the sequence Ps3 basalt eruption, established through detailed lithostructural mapping. Varying degrees of carbonate alteration and metamorphic recrystallization likely contributed to these geochemical differences. The medium crystalline equigranular Schultz Lake metagabbro sheet that discordantly cuts Neoproterozoic metagreywacke is texturally very similar to concordant gabbro sills within sequences Ps2 and Ps3 slate and calcareous tuff in the Schultz Lake klippe, just 10 km to the west, whereas both are very different from finely crystalline plagioclase porphyritic flows and sills in the Whitehills Lake and Amer Belt areas. Even though Patterson et al. (2012) could not conclude that the Paleoproterozoic basalt is cogenetic, the 2153 ± 5 Ma age of the Schultz Lake metagabbro is the only result yet obtained for a unimodal tholeiitic mafic rock in the study area. Given that basalt marks the base of sequence Ps3 and assuming the age obtained for the Schultz Lake metagabbro is relevant, sequence Ps2 is older than 2.153 Ga and the rest of sequence Ps3 in the Amer and Ketyet River belts is between 2.153 Ga and the maximum age of sequence Ps4. Patterson et al. (2012) and Percival et al. (2017) considered the 2.19 Ga Tulemalu dyke swarm (Tella et al., 2001, 2005; Buchan and Ernst, 2013) as a possible correlative of the sequence Ps3 basalt, but that swarm is geographically far removed, and the age is very close to that of the youngest tightly controlled group of detrital zircon in the Montresor sequence Ps1 (2.194 ± 0.014 Ga, Percival et al., 2017). This makes the Tulemalu dyke swarm too old to be related to Ps3 volcanism, assuming all of the sequence Ps1 quartzite units are similar in age. Given that the methodology of this project emphasized field relationships and sequence analysis, this age constraint does not prove or disprove the lithostratigraphic correlation of sequence Ps3 basalt between the Amer and Ketyet River groups.

Pehrsson et al. (2013a, p. 176) attempted to constrain the ages of sequences Ps2 and Ps3 by considering that “ D_{P1} structures define an early fold-thrust belt that is younger than 1.93 Ga, the maximum depositional age of the Ketyet River group assemblage 3 (Rainbird et al., 2010).” This fold and fabric analysis is useful for differentiating fine-grained siliciclastic rocks of sequences Ps2 and Ps3 from those of sequence Ps4 because the latter postdates and therefore lacks D_{P1} recumbent isoclinal folds and S_{P1} fabrics. Minor clarifications on the above quoted analysis include 1) Rainbird et al. (2010) reported later than 1.95 and later than 1.91 Ga, not after 1.93 Ga as maximum ages for units in

their assemblage 3; 2) much of their assemblage 3 is actually sequence Ps2 (the first fine-grained siliciclastic strata above the sequence Ps1 quartzite) or sequence Ps4 (as reassigned here); and 3) none of the strata purported to be sequence Ps3 in the Ketyet River Belt have the combined lithological, metallogenic, and geophysical attributes of sequence Ps3 in the Amer Belt (*see* below). All D_{P1} -deformed fine-grained siliciclastic rocks in the Ketyet River Belt are in mapped contact with the upper feldspathic sandstone to conglomerate member of the sequence Ps1 quartzite (and underlie sequence Ps3 basalt where the basalt is present) and are thereby assigned to sequence Ps2 (Fig. 4a, 6).

Another uncertainty regarding the above sequence Ps3 assignment by Pehrsson et al. (2013a) is that sample z7806 of Rainbird et al. (2010) (geochronology site 42b, Table 2; Appendix B) yielded a single 1.95 Ga detrital zircon. They tentatively assigned it to the Resort Lake formation (the base of sequence Ps2), but problematically, its location is not in the contiguous Amer Belt, nor can its lithostratigraphic position be confirmed with available data. The later than 1.95 Ga sample was taken from outcrop in the core of the synformal Sand Belt, north of Sand Lake (Fig. 3a), 40 km northwest of the Amer Belt and separated from the Amer Belt by the Amer mylonite zone. Jefferson et al. (2023) re-assigned the later than 1.95 Ga unit to sequence Ps4 based on the limited deformation of the sample, the detrital zircon spectrum being similar to others from sequence Ps4 (Appendix B), and the presence of similar graphitic conductors observed within sequence Ps4 in nearby drill core (Jefferson et al., 2023; C.W. Jefferson, R.H. Rainbird, G.M. Young, S.S. Gandhi, J.C. White, V. Tschirhart, D. Lemkow, and L.B. Chorlton, work in progress, 2023) and in sequence Ps4 of the Garry Lake Belt (Miller, 1995).

The Montresor Belt provides the best age constraints for sequences Ps1 through Ps3, as reported by Percival et al. (2017, 2019). There, the sequence Ps1 subarkosic quartz arenite yielded a broad range of detrital zircon ages, including a few 3.6 to 3.2 Ga grains, with a tightly constrained peak centred on 2.19 Ga (2194 ± 14 Ma), not present in any of the other sequence Ps1 samples shown in Appendix B. Percival et al. (2017) could find no likely source for the 2.19 Ga zircon, suggesting a possible local source given their abundance. Another curious feature of this population is that 2190 Ma is the peak of a broad (>150 Ma) range of ages from compositionally similar zircon, not a single-event source (J. Percival, pers. comm., 2021). They speculated that magmatism represented by the 2190 Ma Tulemalu dykes (Tella et al., 2001; Buchan and Ernst, 2013) may have had an associated felsic component that yielded the 2.19 Ga detrital zircon.

The present authors support the hypothesis of a local source for the 2.19 Ga zircon, given its absence in the Amer and Ketyet River belts; however, the linking of this age with the 2.19 Ga Tulemalu dykes and with the Ps3 basalt in the Amer and Ketyet River belts is inconsistent with the stratigraphic context and composition of the flows in both the

Ketyet River and Amer belts, as they *overlie* the sequence Ps1 quartzite, have no known felsic components, and are geochemically similar (*see above*) to the 2153 ± 5 Ma (A.N. LeCheminant and J.C. Roddick, unpub. data, cited in Hadlari et al., 2004) Schultz Lake metagabbro. If the Amer and Ketyet River basalt units are 2.19 Ga, and a contemporaneous (but unknown) felsic source fed the Montresor quartz arenite, then the quartzite units cannot correlate (highly unlikely). One way out of this conundrum is that the sequence Ps3 mafic event may have been highly diachronous, extending in different places from 2.19 to 2.15 Ga. Another puzzle noted by Percival et al. (2017) is the lack of sequence Ps1 detrital zircon derived from the 2.35 Ga Arrowsmith Orogen to the west (Berman et al., 2013) in contrast to their presence in the upper Montresor strata. The Arrowsmith-age detrital zircon are also common in sequence Ps4 samples from the Amer and Ketyet River belts (Appendix B).

There is no sequence Ps3 basalt in the Montresor Belt like that of the Amer and Ketyet River belts; however, parts of both the Amer and Ketyet River belts also lack basalt, reinforcing the local nature of the sequence Ps3 eruptions. Percival et al. (2017) bracketed the structural sliver of fine-grained siliciclastic rocks in the northeast Montresor footwall complex between the later than 2.19 Ga quartzite and the 2.05 Ga (2045 ± 13 Ma) gabbro sill, consistent with the 2153 ± 5 Ma Schultz Lake metagabbro and overlying sequence Ps3 siliciclastic rocks. The structural uncertainty discussed by Percival et al. (2017) as a reason to reject this straightforward solution hinged on their own structural complexity and the intercalated stratigraphic interpretation of the Amer Belt (Rainbird et al., 2010) that has been discarded and corrected back to that of Young (1979) through extensive mapping (Jefferson et al., 2015, 2023; White et al., 2023) and integrated geophysical analysis (Tschirhart et al., 2013d, 2017). Percival et al. (2019) provided further support for the interpretation of lower fine-grained siliciclastic rocks in the Montresor Belt as sequence Ps3, with their discovery of a ca. 2.1 Ga (U-Pb zircon) spherule bed interpreted as representing condensate from an interstellar asteroid impact. The spherules occupy a 7 cm bed in weakly deformed and metamorphosed mudstone dated at 1.85 Ga that Percival et al. (2017) had interpreted as sequence Ps2. This spherule bed thus appears to be younger than the 2153 ± 5 Ma Schultz Lake metagabbro and older than the youngest detrital zircon grains from sequence Ps4 siliciclastic rocks in all three belts (2.05 to 1.90 Ga, Appendix B and discussed in the following section).

Geochronology of sequence Ps4

The detrital zircon assemblages of the upper units in the Montresor, Amer, and Ketyet River belts are broadly similar and tend to have age clusters over a much broader age range than the sequences Ps1 to Ps3 units, however each locality presents distinct differences from the others (Table 2; Appendix B). Percival et al. (2017) obtained U-Pb detrital

zircon ages of 3.8 to 2.65 Ga, 2.55 to 2.25 Ga, and 2.1 to 1.92 Ga in the upper unit of the Montresor Belt. They assigned one concordant grain with an age of 1923.8 ± 5.9 Ma as representing the maximum depositional age of the upper unit. In the contiguous Amer Belt, detrital zircon ages in four samples assigned to sequence Ps4 are in the range of 3.12 to 1.92, 3.52 to 2.06, 3.05 to 1.90, and 3.71 to 1.91 Ga (geochronology sites 41c, 41d, 41a, 41b, Table 2, Appendix B). The ‘Resort lake’ sample of Rainbird et al. (2010) has a similar age range, from 3.74 to 1.95 Ga (geochronology site 42b, Table 2, Appendix B). In the Ketyet River Belt, one sample of sequence Ps4 (‘Upper Succession,’ Table 1 in Rainbird et al., 2010) yielded a range of detrital zircon ages from 3.73 to 2.00 Ga (Appendix B), although they listed later than 2.05 Ga as the maximum age (Table 2). All of these spectra represent a wide range of older Archean ages up to 2.7 Ga, the 2.35 Ga Arrowsmith Orogeny, and the 2.05 to 2.0 Ga magmatic event (Table 2, Fig. B-1; *see* ‘2.05 to 2.0 Ga magmatic event’ section below). Remarkably, the upper Montresor group sample of Percival et al. (2017) yielded no Snow Island suite ages (2.62 to 2.58 Ga; Peterson et al., this volume), whereas all of the sequence Ps4 samples from the Amer and Ketyet River belts and the southwestern outlier of the Montresor Belt (geochronology site 42B) strongly represent the Snow Island suite.

Percival et al. (2017) did not recognize a depositional contact between the upper and lower Montresor strata, instead interpreting the contact as an extensional discontinuity based on the much lower metamorphic grade of the upper versus the lower strata and the schist that separates the lower from the upper strata; however, neither has a precise depositional contact yet been found in the Amer Belt despite much more extensive mapping, and the structural geometry does not allow for an extensional discontinuity. Instead, the contact is spatially constrained in a large number of areas that require sequence Ps4 to unconformably overlie rocks ranging from the Archean, through sequence Ps1 quartzite to the upper sequence Ps3 units. Only in the Ketyet River Belt has a precise depositional contact been recognized in outcrop (*see* ‘Basal contact of sequence Ps4’ section above). Furthermore, the metamorphic grades in the Montresor Belt are highly varied, ranging from the highly metamorphosed schist at the southern end of the belt to the weakly deformed and greenschist-facies metamorphosed host of the 2.05 Ga gabbro sill (Percival et al., 2017), as well as the 2.1 Ga spherule bed (Percival et al., 2019). In summary, the detrital zircon-age spectrum for the upper Montresor strata, with the youngest at 1.924 Ga, places it comfortably within the range of sequence Ps4 documented for the Amer Belt (Table 2; Appendix B). As noted by Percival et al. (2017), the detrital zircon spectrum of the upper Montresor group (here assigned to Ps4) represents a much more varied provenance than the various detrital zircon spectra of samples from the sequence Ps1 quartzite. This same observation applies to sequence Ps4 in the Amer and Ketyet River belts (Fig. B-2).

Thus, the only modification here brought to the interpretation by Percival et al. (2017) is that the upper sequence in the Montresor, Amer, and Ketyet River belts is sequence Ps4, not Ps3. Percival et al. (2017) stated that the presence of detrital zircon in the 1.91 to 1.89 Ga range is typical of assemblage 4 (sequence Ps4) units (LaFlamme et al., 2014; Partin et al., 2014; Wodicka et al., 2014); however, the present authors would expand that typical young zircon range for sequence Ps4 to include 2.0 Ga, as discussed by Rainbird et al. (2010), with the Amer Belt here supported as the type area for sequence Ps4 (Jefferson et al., 2023). The broad older spectra of detrital zircon results are also characteristic of sequence Ps4 and stand in contrast to the much narrower age spectra of sequence Ps1 samples (compare Fig. B-1 versus Fig. B-2). The upper Montresor group 1.924 Ga detrital zircon is essentially in the same range as the youngest detrital zircon grains from the Amer and Ketyet River sequence Ps4. The youngest detrital zircons in the Amer sequence Ps4 are 1.91 and 1.90 Ga. The youngest detrital zircon in the Ketyet River sequence Ps4 is 2.0 Ga, within the above ‘typical’ range. Furthermore, the assignment of the upper Ketyet River Belt to sequence Ps4 is independently defined by structural and contextual field criteria (*see above*; Pehrsson et al., 2013a). In a strict sense, the youngest detrital zircon ages for each belt (1.924, 1.90, and 2.00 Ga) provide the current ‘local maximum’ ages for sequence Ps4 sedimentation in the Montresor, Amer, and Ketyet River belts respectively. Given the above-noted broadly similar age spectra for all three belts, zircon in the 1.90 Ga range may yet be found in parts of the respective sequence Ps4 strata of the Montresor and Ketyet River belts.

Detrital zircon provenance of sequence Ps4

This discussion is prefaced with the above sedimentological characterization of sequence Ps4 strata as molasse and flysch that filled one or more foreland basins. Secondly, their alluvial and/or marine depositional systems could have transported sediment either along the axis of a foreland basin, and/or across that axis from advancing mountains. Lastly, these sedimentological discussions are intimately dependent upon the tectonic evolution of the depositional region, as summarized in the ‘Structure and metamorphism’ section below.

Percival et al. (2017, p. 524) noted that the age spectrum in the upper Montresor Belt

is generally attributed to derivation of sediment from the west, where sources include Paleo- to Mesoarchean gneiss (Davis et al. 2013, 2014), 2.5–2.3 Ga plutonic and metasedimentary rocks (Sherman Group) of the Queen Maud block (Schultz et al. 2007; Tersmette 2012; Davis et al. 2014) and Taltson magmatic zone (McNicoll et al. 2000), as well as 2.03–1.89 Ga plutonic and metamorphic rocks of the Thelon

orogen (van Breemen et al. 1987; Bostock and van Breemen 1994; McDonough et al. 2000; Davis et al. 2014; Berman et al. 2015a, b).

The 2.05 to 2.0 Ga magmatic event of the south Rae Craton is here added to these possible sources (*see* ‘Magmatism’ section below).

There is no known ca. 2.05 to 1.89 Ga magmatic arc in the collision zone to the southeast (i.e. proximal Snowbird tectonic zone) that could have provided sources of the sequence Ps4 detrital zircon. This argues against a southern source for sequence Ps4 in the Ketyet River and Amer belts, also favouring the western derivation hypothesis. These ages are best recorded southwest of the study area, in the Thelon Orogen and Taltson magmatic zone (Hoffman, 1989; Bostock and van Breemen, 1994), in the western Beaverlodge Domain (Bethune et al., 2013; Card et al., 2014), and in the Snowbird–Dodge Domain. Most detrital zircon suites in sequence Ps4 of the Ketyet River, Amer, and Montresor belts also feature single-zircon ages going back to 3.3 Ga, very strong peaks at 2.6 Ga (Snow Island suite, except the Montresor Belt), some to strong representation of the ca. 2.35 Ga Arrowsmith Orogeny (Berman et al., 2013), and multigrain clusters at 2.05 Ga (Appendix B; Rainbird et al., 2010; Percival et al., 2017), all supporting a southwestern provenance.

The upper unit of the Montresor Belt yielded a strong peak of detrital zircon grains from 2.1 to 1.95 Ga and a 2045 ± 13 Ma gabbro sill intrudes a lower fine-grained clastic unit (Percival et al., 2017). Sequence Ps4 of the Ketyet River and Amer groups also sampled the 2.05 to 2.0 Ga igneous event (*see* ‘2.05 to 2.0 Ga magmatic event’ section below), but to a minor degree, with one to five detrital zircon grains in this age range. In four samples, a single 2.06 to 2.0 Ga zircon is the youngest one found (Table 2; Rainbird et al., 2010).

The 2.05 to 1.9 Ga sequence Ps4 detrital zircon could have been transported from the south Rae Craton, along the axis of a broad foreland basin developed during the latter part of the Snowbird phase (1.9–1.865 Ga; Berman et al., 2007) of the Hudsonian Orogeny, whereas the more abundant 2.6 Ga zircon could have been shed across the axis, from locally exposed Snow Island suite such as in the Chesterfield fault zone. The present authors prefer this hypothesis for the Tasirjuak formation (sequence Ps4 in the Ketyet River Belt) and for the Tahiratuaq group (sequence Ps4 in the Amer Belt). Alternatively, or in addition, the sequence Ps4 strata could have filled the distal foreland basin of the earlier Taltson Orogen, which at that time trended roughly east. The Taltson Orogen was then tightly folded during the Hudsonian Orogeny to become part of the current southwest–northeast grain of the Rae Craton (Card et al., 2007). Percival et al. (2017) interpreted the upper Montresor strata to have been sourced from the Thelon magmatic zone to the west, as the Thelon Front was also active during the upper Montresor depositional time window (sequence Ps4, ca.

1.865 to 1.85 Ga, Table 1). In this scenario, the Montesor depositional basin was located in the distal foreland of the Thelon Front.

Correlations of sequences Ps1 through Ps4 of the above three basins with other cover sequences in the western Churchill Province, such as the Nonacho, Hurwitz, and Wollaston groups are discussed by Rainbird et al. (2010), Percival et al. (2017), and Jefferson et al. (2023). In addition, the section entitled ‘Alteration and metallogenic comparisons of the Athabasca Basin and Thelon Basin regions’ includes examples from the Wollaston Supergroup.

Late Paleoproterozoic Dubawnt Supergroup

The Dubawnt Supergroup comprises the Baker Lake, Wharton, and Barrenslund groups; all of which are undeformed except by faulting and minor local upright folds along some faults (Fig. 2, 4a). Rainbird et al. (2003a) reviewed and interpreted these groups in terms of three major depositional sequences. Peterson et al. (2010) noted that the volcanic strata intercalated within the first two of these sequences are products of two large igneous provinces (LIPs; *see* ‘Magmatism’ section below). Rainbird and Davis (2007) calibrated the ages of these sequences. The present section briefly explains the stratigraphic context of the two LIPs and their interrelationships with terrestrial siliciclastic sedimentation. The Baker Lake Group fills mainly the Baker Lake Basin that extends in a series of subbasins from Baker Lake in the northwest to Dubawnt and Kamilukuak lakes in the southwest, flanked by the Kazan River along much of its southeastern margin, with western outliers along the Dubawnt River. The Baker Lake Group overlaps the northwestern boundary of the Chesterfield Block of the Rae Craton along the Tulemalu and related faults. The south-westernmost portion of the Baker Lake Group straddles the cryptic boundary between the north and south Rae Craton along the Dubawnt River shear zone (Fig. 2). Nowhere does the Baker Lake Group rest on the Hearne Craton. The Wharton and Barrenslund groups successively unconformably overlap the Baker Lake Group within the western Baker Lake Basin; the Wharton Group forms flat-lying cover west of the Dubawnt River; and the bulk of the Thelon Formation fills the separate Thelon Basin farther west.

The first large igneous province in the Dubawnt Supergroup comprises the Christopher Island formation volcanic rocks and related minette (lamprophyre) and bostonite (felsic ultrapotassic) dykes (Dubawnt minettes of Peterson et al., 2002; Peterson, 2006). The Christopher Island formation is intercalated with siliciclastic strata of the South Channel, Angikuni, Kazan, and Kunwak formations (Aspler et al., 1999; Rainbird et al., 2006). The Christopher Island formation and siliciclastic strata together constitute the Baker Lake Group. Rainbird et al. (2006) bracketed Baker Lake Group deposition between an 1833.2 ± 2.4 Ma lower felsic minette flow of the Christopher Island formation and a 1783 ± 3 Ma calcite travertine near the top of the

Kunwak formation. This first-order supracrustal sequence is temporally equivalent to the 1.84 to 1.81 Ga Hudson suite granite and Martell syenite that are mingled with, and cut by, the mafic to felsic Dubawnt minette dykes that are temporally equivalent to the Christopher Island formation (Scott et al., 2015).

The Amarook Formation unconformably overlies the Baker Lake Group, constitutes the first unit of the Wharton Group (Rainbird and Hadlari, 2000), and marks an hiatus between the first and second large igneous province of the Dubawnt Supergroup (Fig. 4a). In addition to the thin polymict conglomerate of the basal Amarook Formation, key diagnostic features include eolian crossbeds and cementation by both clear and cryptocrystalline quartz. The Amarook Formation is exposed in many sections from the northwestern side of the Baker Lake Basin to around the northern and eastern margins of the Aberdeen Subbasin. It differs from the dominantly shallow-marine Ayagaq Lake formation in being essentially subaerial with well developed red mudstone and neither folds nor cleavage, although locally tilted by block faulting. A typical sequence consists of a thin basal breccia, an eolian feldspathic quartzite unit, and an alluvial unit of interbedded polymict conglomerate and slightly feldspathic quartzite with minor red mudstone. Angular unconformities and the presence of previously silicified blocks of Amarook Formation sandstone in the base of the Thelon Formation (Fig. 5d) help to distinguish the former from the latter. C.W. Jefferson, R.H. Rainbird, G.M. Young, S.S. Gandhi, J.C. White, V. Tschirhart, D. Lemkow, and L.B. Chorlton (work in progress, 2023) provide detailed descriptions of a number of Amarook Formation exposures, such as the Dune lake area, previously assigned by Jackson et al. (1984) to the Thelon Formation before the Amarook Formation was defined by Rainbird and Hadlari (2000).

The Pitz Formation abruptly overlies the Amarook Formation with interpreted disconformity (Rainbird and Hadlari, 2000), constitutes the upper part of the Wharton Group, and is the extrusive portion of the second large igneous province of the Dubawnt Supergroup — the Kivalliq igneous suite. The Pitz Formation is restricted to south of Aberdeen Lake, where it blankets much of the area (Fig. 3a). The upper member of the Pitz Formation comprises intercalated conglomerate and sandstone, with the conglomerate consisting of 30% volcanic rocks of the lower Pitz Formation, 60% sedimentary rocks including the Amarook Formation, and 10% granitoid and volcanic basement rocks (Rainbird and Hadlari, 2000). Rainbird and Hadlari (2000) established this upper member in the Baker Lake Basin south of Baker Lake. They also reassigned to this upper member strata south of Aberdeen Lake that LeCheminant et al. (1983) had assigned to the basal Thelon Formation. Similarly, Jefferson et al. (2013) reassigned volcanic-rock-rich conglomeratic strata exposed along the eastern margin of the main Thelon Basin to the upper Pitz Formation that Cecile (1973) had assigned to the basal Thelon Formation. Geophysically, it is characterized by a mottled moderately high/moderately

low pattern that masks underlying aeromagnetic signatures trending into the Pitz Formation cover strata from adjacent basement exposures.

The Barrenland Group (Fig. 2, 4a, Table 1) comprises the siliciclastic redbed Thelon Formation (e.g. Fig. 5a), thin 1540 ± 30 Ma ultrapotassic mafic flows and tuffs of the Kuungmi Formation (Gall et al., 1992; Peterson, 1995; Chamberlain et al., 2010), and silicified dolostone of the Lookout Point Formation (Gall et al., 1992). Hiatt et al. (2003), Palmer et al. (2004), Davis et al. (2011), Jefferson et al. (2011a, c, 2015), and C.W. Jefferson, R.H. Rainbird, G.M. Young, S.S. Gandhi, J.C. White, V. Tschirhart, D. Lemkow, and L.B. Chorlton (work in progress, 2023) provide the most recent descriptions of the Thelon Formation, including references to previous work and evidence for reactivated faulting before, during, and after sedimentation.

The mainly flat-lying Thelon Formation was originally arkosic lithic sandstone, but diagenesis converted it to a mainly quartz-grain framework in a clay matrix (A.R. Miller, unpub. rept., 1996). Depositionally, it is dominantly alluvial, including basal kilometre-wide shallow channels floored by boulder to pebble conglomerate, in turn draped by red, desiccation-cracked mudstone (Fig. 5a). Hiatt et al. (2003) and Palmer et al. (2004) defined three upward-fining sequences based on sedimentological attributes and identified conglomerate as a favourable facies for diagenetic to hydrothermal fluid flow. Davis et al. (2011) corroborated the upward-fining sequences with quantitative grain-size analysis using the same methodology as Ramaekers et al. (2007) established for the Athabasca Basin. The basal conglomerate of the Thelon Formation is highly varied in clast composition and cobble-to-boulder grade, tending toward dominance by the local basement rocks, be they granitoid, Pitz Formation volcanic rocks, or Amarook Formation sandstone. Where the Thelon Formation overlies the Amarook Formation, large blocks of silicified feldspathic arenite identical to eolian beds of the Amarook Formation are a highly diagnostic component. This coarse polymict conglomerate and the large blocks of Amarook Formation help to distinguish the Thelon Formation from underlying conglomerate of the basal Amarook Formation and from upper Pitz Formation strata that are dominantly pebble-to-cobble grade and rich in porphyritic volcanic clasts of the lower Pitz Formation. In this study, the boulder conglomerate reported by Cecile (1973) is used to revise the eastern side of the main Thelon Basin between Aberdeen Lake and the southern tip of the basin (Fig. 2), such that the Thelon Formation unconformably overlies and excludes the upper Pitz Formation alluvial facies.

An upper conglomerate of the Thelon Formation in the eastern part of the Aberdeen Subbasin is also polymict, but dominated by quartz pebbles 5 to 20 cm in diameter, with common rounded red mudstone intraclasts. This upper conglomerate is well exposed because it is preferentially silicified, forming local plateaus in the area around geochronology site 51 (Fig. 3a). Very large trough crossbeds

in the cobbly sandstone are visible from the air and record unimodal fluvial flow toward the west. The unimodal paleocurrents, coarse grain size, and large dimensions of the troughs, ranging up to 20 m across and 5 m in depth, suggest that this conglomerate formed in the main thalweg of a very large river system. Drill core analysis suggests that this conglomerate forms the base of the second upward-fining sequence defined by Hiatt et al. (2003). The downstream, lateral equivalent of this conglomerate, where logged by the first author in the centre of the Aberdeen Subbasin (e.g. the DPR drill sites shown by Hiatt et al., 2003), contains only pebble-grade quartz and is unsilicified, but retains relatively large crossbeds.

Paleocurrent data from Donaldson (1965), Cecile (1973), and this project are overall unimodal, with subordinate orthogonal directions in finer grained facies. Together these data support the ‘big river’ concept of Rainbird et al. (2003a) in terms of a major alluvial system that trended west from the vicinity of Baker Lake toward the Sand Lake horst then curved south through the main part of the Thelon Basin and curved west again toward the East Arm of Great Slave Lake (see slide 6 of Jefferson et al., 2011a). Tributaries flowed into this main channel from the south, east, and west. The western side of the Thelon Basin was bounded by residual uplands over the area of the Thelon front.

This interpretation implies that the current shape of the Thelon Basin is fundamentally depositional. On the other hand, the distribution of outliers, and paleoweathered and hydrothermally altered basement rocks, show that the thinner marginal areas of the original Thelon Basin, now eroded, were quite extensive. The Thelon Formation is aeromagnetically transparent, hence the effectiveness of aeromagnetic and gravity data when used to remotely map basement units beneath it (Tschirhart et al., 2011b, 2013a, 2014), as simplified in Figure 3a.

Phanerozoic strata

Lithified strata covering the Thelon Basin are limited to an outlier of gently dipping, fossiliferous, late Ordovician (ca. 448 Ma) limestone documented by Bolton and Nowlan (1979) (geochronology site 59, Table 2). Remote predictive mapping refined the gentle northwestward dip of these strata as being restricted to a four-sided graben, using integrated RADARSAT and Landsat data (LaRocque et al., 2012). The graben faults are also constrained along strike in places by drill core, lineament, and aeromagnetic analysis (Tschirhart et al., 2013c, 2017; Jefferson et al., 2015).

Widespread Quaternary sediment covers some 95% of the bedrock with variable thicknesses of red and olive-grey till, and reworked products thereof (LaRocque et al., 2012; McMartin et al., 2021). Their distributions and compositions reflect the interplays between multiple ice-flow directions; postglacial fluvial, lacustrine, and marine processes; and the nature of bedrock beneath these deposits. For example, the till is very sandy over the Thelon Formation. The multiple

ice-flow directions documented by Aylsworth and Shilts (1989), Aylsworth et al. (1990), McMartin et al. (2008), and Robinson et al. (2014, 2016) extend in more or less the same geometric relationships across the northeast Thelon Basin region (Grunsky et al., 2009; LaRocque et al., 2012; Shelat et al., 2012a, b). The first major preserved transport direction was northwesterly, as documented by striae on roches moutonnées, consistent with drumlins and crag-and-tail structures in the order of 3 km long and 500 m wide. The northwesterly trending crag-and-tail structures are best developed on the northwestern side of high-standing, silicified faults such as the Thelon Fault. The next major ice flow was westerly and built secondary ice constructional features over the still-preserved drumlins in the southern part of the study area. The effects of this westward ice-flow direction increase southward into the core of the major Dubawnt Lake ice stream (McMartin et al., 2021). This ice stream formed highly elongate drumlins, with no trace of the northerly drumlins that may have formed there on the northwestern side of the Keewatin ice divide (McMartin et al., 2008; Stokes et al., 2013; Geological Survey of Canada, 2017a, b; McMartin, 2017). These transport directions informed the design of a drift prospecting study by Robinson et al. (2014, 2016) in the Kiggavik uranium exploration area (*see* ‘Alteration and metallogenic comparisons of the Athabasca Basin and Thelon Basin regions’ section).

Magmatism

Magmatism in the northeast Thelon Basin region comprises elements of three large igneous provinces and a mafic event. These four magmatic events are presented below in their stratigraphic context.

Archean granitoid magmatism predating the Snow Island suite

Little is known about Archean granitoid magmatism predating the Snow Island suite (*see* below). The Sanning tonalite yields the oldest igneous U-Pb zircon age in the region, 2869 \pm 6/–5 Ma (geochronology site 1a, Table 2), and structurally underlies the Half Way Hills assemblage as a series of lozenge-shaped bodies (inset in Fig. 6). The lozenges may represent either 2.734 Ga subvolcanic intrusions into the base of the 2734.2 \pm 1.8 Ma (geochronology site 3, Table 2) Half Way Hills assemblage, with inherited zircon (Pehrsson et al., 2013a) or boudinaged 2.87 Ga granitoid basement to the Half Way Hills assemblage (Davis and Zaleski, 1998; Davis et al., 2021). The name ‘Sanning’ is applied here as an informal identifier, after the nearby ‘Sanningajukuluk’ (unofficial name) (Zaleski et al., 2001b).

The Akutuak River gneiss (Schau et al., 1982; Hadlari et al., 2004) is tonalite–quartz diorite in composition. It was thrust northward over (along the Quoich River thrust), and refolded with, the Snow Island suite and Ketyet River group cover along the southern side of Whitehills Lake (Fig. 3a, 6).

An age of ca. 2.72 Ga has been obtained from a locality south of Whitehills Lake (Pehrsson et al., 2013a). Being the same age as the Half Way Hills assemblage suggests that it is part of a subvolcanic intrusive suite, although it is separated from the Half Way Hills volcanic rocks by the Quoich River thrust and the Whitehills synform that is floored by the Snow Island suite. The presumed Archean gneiss exposed in the Turkavik horst is geophysically more similar to the Schultz Lake intrusive complex than the Snow Island suite orthogneiss, having a high, but magnetic expression transected by reticulate demagnetized fault and fracture zones on residual total field maps (Fig. 3d). The Turkavik gneiss, which is poorly known and undated, has the potential to be either yet another form of the Snow Island suite (*see* ‘Marjorie terrane’ section above) or an older gneiss, like the Akutuak River or Chesterfield.

The Chesterfield fault zone (Schau et al., 1982; Hadlari et al., 2004; Berman et al., 2007) is a sinuous 10 to 20 km wide belt of highly metamorphosed, south-dipping, medium- to coarse-grained granitoid rocks of foliated to gneissic texture, with numerous gneissosity-parallel mylonite zones. Compositions include granite, syenogranite, granodiorite, and tonalite, with minor diorite and gabbro. It trends northeast from the northern margin of the Baker Lake Basin that truncates it, curves into an east–west section north of Baker Lake, and bends northeastward again toward Wager Bay, east of the study area (Fig. 2, 3a) (Wodicka et al., 2017). Zircon crystallized at 2695 \pm 4 Ma in a portion of the gneiss just north of where it is cut off by the Baker Lake Basin (A.N. LeCheminant and J.C. Roddick, unpub. data, cited in Hadlari et al., 2004). The Chesterfield fault zone is interpreted as a crustal-scale, northward-directed thrust fault that brought granulite-facies Archean gneiss up over the Akutuak River gneiss during the collisional Snowbird phase of the Hudsonian Orogeny, from about 1.9 to 1.865 Ga (Berman et al., 2007).

Snow Island suite

The Snow Island suite (SIs, Fig. 3a) gabbro to granite intruded much of the Rae Craton during the period from about 2.62 to 2.58 Ga and were generated by melting of crustal rocks — convecting mantle, Mesoproterozoic lower lithosphere, and Neoproterozoic Rae Craton crust that included varying amounts of supracrustal rocks (Peterson et al., 2015c, this volume). Snow Island suite granitoid rocks typically contain centimetre-scale potassium feldspar phenocrysts and their contact margins contain abundant xenoliths of the adjacent Neoproterozoic supracrustal rocks. Most of the Snow Island suite granitoid rocks are weakly foliated, although they range into banded augen gneiss in places, such as northern Marjorie Lake, and banded quartzofeldspathic and amphibolitic gneiss, which is in discordant contact with the older Aberdeen assemblage (Hunter et al., 2021), and forms much of the Marjorie terrane (*see* ‘Marjorie terrane’ section above), as well as the granitoid gneiss between the Amer mylonite zone and the Thelon front (Berman et al., 2015a, b). The bimodal Pukik Lake formation, the extrusive component of the Snow Island

suite, covered much of the central Rae Craton within the area of Figure 2 with thin felsic pyroclastic rocks and sills, and minor mafic flows, but is absent from the north and south Rae Craton as well as the Hearne Craton (Peterson et al., 2015c, this volume). The Snow Island suite was the first major magmatic event in the Rae Craton that moved uranium and heat sources to its upper crust. Recognition of widespread granitoid and felsic volcanic units in the study area (Fig. 3a) as aged 2.62 to 2.58 Ga (LeCheminant and Roddick, 1991) and their petrochemical classification as the craton-scale Snow Island suite (Peterson et al., 2015c, this volume) has resolved huge areas of previously undefined map units.

The Snow Island suite compositional spectrum includes ultramafic phases (Peterson et al., this volume). The complex magmatic processes involved for some mafic to ultramafic phases is illustrated by an outcrop of 2595.7 ± 3 Ma monzodiorite (geochronology site 32, Table 2; station 12JP105 = 12NKL008 of Davis et al., 2014) along the Chantrey mylonite zone (Fig. 3a) that includes gabbro with magmatic trough-crossbedding and planar layering preserved as stoped blocks enclosed in massive monzodiorite. The outcrop is also transected by multiple late-stage diffuse plagioclase veins and dykes of metasomatic granodiorite (Peterson et al., this volume). The nickel-copper-platinum potential of the Snow Island suite is discussed below (*see* 'Alteration and metallogenic comparisons of the Athabasca Basin and Thelon Basin regions' section).

The Snow Island suite began the transition from Archean microcontinents to the Paleoproterozoic Rae Craton. Amalgamation of five of the Woodburn Lake group assemblages and the lower part of the Amarulik assemblage, and apparently the Aberdeen assemblage, took place either just before, and/or in part during, Snow Island suite magmatism. In the 'Nipterik lake' area, the Pukiq Lake formation overlies the Pipedream assemblage and is in turn overlain by conglomerate and quartzite of the Ketyet River group. The contact between the Pipedream assemblage and the Pukiq Lake formation is highly strained — it may be purely tectonic or a tectonized unconformity. The contact between the Pukiq Lake formation and the Ketyet River group is also highly strained, but interpreted as an unconformity, based on the presence of clasts of both dated granite (2.62 Ga, geochronology site 34, Table 2) and undated, but distinctive rhyolite of the Snow Island suite within the basal conglomerate (Fig. 5h). Along the margins of the Amer Belt, deep-seated Snow Island suite granitoid plutons and the Rumble assemblage that these intrude are separated from overlying Paleoproterozoic quartzite by highly strained felsic and mafic volcanic rocks of the Pukiq Lake formation (Jefferson et al., 2015; Peterson et al., 2015c, this volume). In the Akiliniq Hills (western part of Fig. 3a), a broad and thick subhorizontal tectonic sheet of Snow Island suite granitoid rock is overlain by about 75 m of Pukiq Lake formation — intercalated schistose tuff and weakly foliated porphyry sills dated at 2581 ± 10 –9 Ma (LeCheminant and Roddick, 1991). The contact with the overlying sequence Ps1 quartzite is a high-strain zone. The Pukiq Lake formation in other

areas is unconformably overlain by, and commonly incorporated as pebbles within, the basal conglomerate of sequence Ps1 (e.g. geochronology site 34, Table 2). Abundant clasts of distinctive Pukiq Lake formation rhyolite are also present in the upper sequence Ps1 conglomerate and again in the sequence Ps4 conglomerate.

In the eastern part of the study area, tectonic sheets of Snow Island suite granitoid rocks (Fig. 3c) structurally overlie much of the Woodburn Lake group. These sheets are hundreds of metres to several kilometres thick (Thomas, 2012; Davis et al., 2021). Their basal contacts with Woodburn Lake group units are moderately dipping to subhorizontal mylonite zones (Kjarsgaard et al., 1997; Pehrsson et al., 2013a; Davis et al., 2021). The lateral extents of these sheets range from hundreds to thousands of square kilometres. Sheets of Snow Island suite granitoid rocks wrap around and beneath grand F_{p2} synclinoria of early Paleoproterozoic cover strata in the Montresor, Amer, and Ketyet River belts, and define large F_{p2} structures in the area of Pipedream and Tehek lakes (Fig. 6), and along the Meadowbank River Belt (Fig. 3a, 7a). Little is understood about the structural relationships between these eastern tectonic sheets and the deep-seated plugs to plutons of Snow Island suite granitoid rocks that dominate the western portion of the study area. The area between the deep Judge Sissons pluton and the Snow Island suite sheet that underlies the Whitehills Lake synform (Fig. 8) provides an opportunity to study this transition geophysically.

The temporal and geographic range of the Snow Island suite clearly postdates some assemblages of the Woodburn Lake group, but overlaps that of others. The Pipedream, Rumble, and Half Way Hills assemblages are all intruded by small plugs to large plutons, and overthrust by thick sheets of Snow Island suite diorite to granite. Contact zones of the large, deep Snow Island suite plutons contain abundant supracrustal inclusions typically in the Half Way Hills and Rumble assemblages. The Wading and North Meadowbank assemblages are overthrust by Snow Island suite sheets, but do not have large Snow Island suite plutons.

Much of the orthogneiss component of the Marjorie terrane was not originally recognized by Peterson et al. (2015c) as Snow Island suite, due to its distinctly banded appearance in outcrop and drill core. Partial-melt leucosomes are 1 to 2 cm thick, comprising medium crystalline quartz and feldspar with sparse disseminated hornblende and biotite. Adjacent paleosome layers are 5 to 10 mm thick with up to 50% layer-parallel biotite-hornblende. The 'background' quartzofeldspathic gneiss layers are in the order of 5 cm thick, with 5 to 10% biotite and hornblende in a quartzofeldspathic crystalline matrix. As described by Hunter et al. (2021), this extensive quartzofeldspathic orthogneiss is in discordant contact with the older Aberdeen assemblage rocks and is interpreted as part of the Snow Island suite; they interpreted the larger amphibolitic portions as inclusions. They dated one sample of potassium feldspar augen gneiss at the northern end of Marjorie Lake at 2601.7 ± 4.2 Ma,

and this is similar to augen gneiss elsewhere in the study area that is included in the Snow Island suite. This more granitic representative of the Snow Island suite orthogneiss has similar quartzofeldspathic leucosomes, but the biotite-hornblende paleosomes are in the order of millimetres thick and the ‘background’ contains relict potassium feldspar phenocrysts. Their geochronology of two samples of the Schultz Lake intrusive complex produced not only Hudsonian ages, but also Snow Island suite ages on inherited zircon (*see* ‘Hudson suite’ section below for details on the Schultz Lake intrusive complex).

The Marjorie terrane is in limited contact with the relatively well preserved crystal-tuff porphyry of the Pukiq Lake formation. Small occurrences of aphanitic rhyolite with quartz and K-feldspar phenocrysts typical of the Pukiq Lake formation overlie highly metamorphosed Marjorie orthogneiss and mafic paragneiss west of the Schultz Lake intrusive complex. The contrast in metamorphic grade suggests structural juxtaposition of the relatively well preserved crystal-tuff textures of the Pukiq Lake formation above the gneiss. The upper package of the Aberdeen assemblage includes a minor 2.628 Ga peak of detrital zircon that is almost within the age range of the Snow Island suite (geochronology site 23, Table 2). The 2.65 Ga youngest detrital zircon of the Rumble assemblage (geochronology site 20, Table 2) is also close to the maximum documented age of the Snow Island suite. The third Amarulik assemblage includes detrital zircon as young as 2598 ± 20 Ma, which corresponds to the middle of the Snow Island suite age range (geochronology site 33, Table 2; Appendix B).

Much of the highly foliated gneiss in the region is now recognized as Snow Island suite, including most, if not all, orthogneiss with low magnetic expression northwest of the Amer Belt, but some orthogneiss remains uncertain in origin. The orthogneiss of the Turqavik horst superficially resembles the Snow Island suite orthogneiss portion of the Marjorie terrane in outcrop, but the former has a relatively uniform, low to moderate aeromagnetic expression, whereas the Turqavik gneiss has a high aeromagnetic expression transected by a network of linear aeromagnetic lows, which are interpreted as demagnetized fault and fracture zones. Geophysically, the Turqavik gneiss strongly resembles the Schultz Lake intrusive complex, however it is a foliated gneiss, not fresh granite and syenite like that of the Schultz Lake intrusive complex. A small outlier of Snow Island suite foliated granite overlies the Turqavik gneiss southeast of the location of Figure 10a (*see* Fig. 3). The outlier and the contact between the Turqavik gneiss and the less deformed Snow Island suite sheet to the northeast are after Patterson and LeCheminant (1985).

2.05 to 2.0 Ga magmatic event

In the western part of the south Rae Craton (Fig. 1), there are numerous ultramafic to felsic intrusions of this age range. An age of 2.04 Ga (W. Bleeker, A.N. LeCheminant,

and M. Hamilton, pers. comm., 2017) was obtained on a highly magnetic mafic–ultramafic body intersected in the JP1 drillhole below the southwest Thelon Basin, on strike with the Porter Domain of Davis et al. (2015). In the adjacent Penylan Domain, Davis et al. (2015) and Regis et al. (2017) reported ages of 2.05 to 2.03 Ga for massive to variably foliated syenogranite to monzogranite, spatially associated with a mafic anorthosite–gabbrodiorite complex. Individual mafic plugs have yielded similar ages within the McCann Domain (W.J. Davis, unpub. data, 2020). The only place this mafic event is documented near the study area is in the northeastern portion of the Montresor Belt, where a 2045 ± 13 Ma gabbro sill intrudes a lower, fine-grained clastic unit (Percival et al., 2017). A transposed amphibolite sill or dyke in quartzite of the central northwest Amer Belt is a possible candidate to test for this event, being geochemically distinct from the Five Mile Lake basalt (Patterson et al., 2012), but has so far yielded only a metamorphic age of 1.83 Ga (U–Pb zircon; W. Bleeker and M. Hamilton, unpub. data, 2018).

Hudson suite

The Hudson suite in the study area comprises mid-crustal sills to kilometre-thick slabs, dykes, and discrete vertically extensive plugs. Most sills and dykes in the study area, exemplified by observations in drill core and outcrop around the Kiggavik camp, are in the order of 1 to 10 m thick, with the Schultz Lake intrusive complex being a major exception (*see* below). The discrete Hudson Suite plugs in the Kiggavik area tend to be situated along extensional portions of fault zones and at the intersections of steep faults. The exposed plugs west of the Granite occurrence and extending south of ‘Sleek lake’ (unofficial name) (western side of Fig. 8) are relatively small, ranging from about 100 m to 2 km in diameter. The Lone Gull pluton is at least 250 by 350 m across its gently undulating top; it peaks within about 90 m of the surface and broadens at depth (Fuchs et al., 1986). Exposed granitoid bodies above that pluton are Hudson granite sills and pegmatite dykes, and Dubawnt minette sills and dykes. Textures of the discrete granitoid exposures (including granitic aplite and pegmatite, and porphyritic microcrystalline syenite), the sharp and straight boundaries of dykes and sills, and the lack of partial melting in the host rocks, all suggest relatively shallow emplacement depths, albeit still ‘mid-crustal’ because of the lack of contact metamorphism. Contact metamorphism around a few bodies, such as granite of the Kinngaaquk igneous complex (Fig. 6) indicates upper crustal emplacement. Inclusions are rare, except for the Schultz Lake intrusive complex (*see* below). Examples of larger discrete plugs include the southern part of the Amer plutonic complex (Fig. 3a, defined below in ‘Kivalliq igneous suite’ section), several plugs between the northeastern Turqavik fault and Meadowbank River deformation zone (Fig. 3a), and granite of the Kinngaaquk igneous complex (Fig. 6). Poorly defined Hudson granite bodies are present in the Akutuak River and Chesterfield gneiss terranes, whereas well defined discrete plugs cut the Baker Lake Group (southeastern part of Fig. 3a). Inherited zircon in granite

to syenite of the Hudson suite reflect their geological settings, with 2720 to 2650 Ma being the most common range (van Breemen et al., 2005). Local middle to early Archean crust is recorded by 3.5 to 3.0 Ga inherited zircon in the area of the Nunavut–Manitoba border (van Breemen et al., 2005) and 3.3 Ga zircon in syenite of the ‘Nipterk lake’ area (McEwan, 2012). The oldest inherited zircon of the Kiggavik area east of the Granite thrust are 2700 ± 8 Ma in the Bong porphyritic syenite, 2788 ± 8 Ma in a 1 m thick monzogranite sill beside the Lone Gull discovery outcrop, and 2793 ± 9 Ma in a heterogeneous syenite dyke cutting that sill (Scott et al., 2015).

The Schultz Lake intrusive complex (defined in ‘Geological areas of focus’ section above), is a massive, mixed-magmatic, subhorizontal slab hundreds of metres thick, which intrudes and contains inclusions of both ortho- and supracrustal gneiss of the Marjorie terrane in the hanging wall of the Granite thrust and which extends over a northeast-southwest strike length of at least 150 km. The Granite thrust delineates the eastern side of the complex and the western side of the Kiggavik uranium camp that is hosted by the western block of the Pipedream assemblage; however, the Granite thrust does not delimit the potential for basement-hosted, unconformity-related uranium deposits. An enclave of upper Aberdeen assemblage paragneiss within the Schultz Lake intrusive complex hosts the Tatiggaq uranium occurrence, and two others are located within contiguous Aberdeen assemblage paragneiss west of it (Hunter et al., 2012, 2014, 2018, 2021). Scott et al. (2015) dated a syenogranite component at 1839.7 ± 9.3 Ma, and Hunter et al. (2021) obtained ages of 1832.9 ± 9.6 Ma and 1831 ± 11 Ma on two samples of the Schultz Lake intrusive complex. A key component of the geochronology results by Hunter et al. (2021) is the abundant inherited zircon suite, dominated by the age range of the Snow Island suite: 2592.4 ± 7.1 Ma and 2580 ± 21 Ma for their two samples, respectively. These inherited zircon ages are consistent with most individual inherited zircon ages reported by Scott et al. (2015) for the Schultz Lake intrusive complex, although those include some as old as 2.75 Ga. The likelihood of the 2.6 Ga inherited zircon of the Schultz Lake intrusive complex representing the age of the orthogneiss is favoured by the unusual abundance of gneiss inclusions in the Schultz Lake intrusive complex. These include locally abundant small blocks of Snow Island suite orthogneiss (Miller and Peterson, 2015) to large subhorizontal rafts of Aberdeen Lake supracrustal rocks (Hunter et al., 2012, 2014, 2018, 2021), with the latter being possible sources of the 2.7 Ga and older zircon. Scott et al. (2015) and Hunter et al. (2021) also found weak expressions of the 1.75 Ga Kivalliq igneous event in the Schultz Lake intrusive complex, but no older Archean ages.

The older magmatic component of the Kinngaaq complex, weakly foliated to massive monzodiorite to syenite, forms thick sheets separating thinner, highly strained layers of Ketyet River group sequence Ps2. Thicker slabs of massive Hudson granite cut both and are rimmed by a contact

metamorphic aureole where they cut sequence Ps2 slate. The patchy and nebulous textures in the early monzodiorite to syenite phase indicate magma mingling (Zaleski and Pehrsson, 2005), a feature also noted in the younger Martell syenite, suggesting that the as yet undated syenodiorite may be an early phase of the Martell syenite. This is consistent with observations by Miller and Peterson (2015) that the syenite phase largely predates the granite phase of the Hudsonian Schultz Lake intrusive complex. The overall circular shape of both components of the Kinngaaq complex and the tectonized contacts of this sheet-like to reticulate body (Zaleski and Pehrsson, 2005) suggest that extension and domal uplift took place during intrusion of both the syenodiorite and the granite phases.

Peterson et al. (2010) described the 1.84 to 1.81 Ga Hudson suite of granite and syenite (Peterson et al., 2002, 2010; van Breemen et al., 2005) as part of a large igneous and sedimentary province because it intruded synchronously with deposition of the Baker Lake Group. Its later syenitic component is a result of contamination by shonkonitic magmas. The extrusive components of shonkinite — ultrapotassic mafic and felsic minette flows of the Christopher Island formation (Peterson and LeCheminant, 1996; Peterson et al., 2002; Peterson, 2006; Scott et al., 2015) — are intercalated with siliciclastic rocks of the Baker Lake Group (Rainbird et al., 2003a, 2006; Hadlari and Rainbird, 2011). The Dubawnt minette dykes (Peterson et al., 2002) are widespread across much of the southern study region (Peterson and LeCheminant, 1996), occur along multiple Riedel-shear trends (Fig. 8, 9a, b; Anand and Jefferson, 2017a, b), transect parts of the Amer Belt, especially around the Amer plutonic complex and across sequence Ps4 in the Tahiratuaq synform (Fig. 3a; Jefferson et al., 2015), and have remarkably similar textures to Christopher Island formation mafic and felsic minette flows, as well as some Martell syenite plugs (Scott et al., 2015). Exposures show that shonkonitic magmas transported upward by these dykes transected mid-crustal Hudson suite sills to thick slabs, with mingling resulting in the Martell syenite (Scott et al., 2015). Coarsely crystalline mafic ultrapotassic rocks are rarely exposed as deep-intrusive shonkinite and mafic minette pipes that are expressed as small diameter, but intense circular aeromagnetic highs (Coyle and Kiss, 2012) between Chesterfield Inlet and Wager Bay (Wodicka et al., 2017). Circular aeromagnetic highs 100 to 1500 m in diameter transecting the Tahiratuaq synform of the Amer Belt have central peaks that are similar in amplitude to the linear magnetic highs over the nearby Mackenzie dykes (*see* residual total field image in Fig. 3d). One of these circular magnetic highs is associated with outcrop of a ‘granitoid’ plug described as radiometrically anomalous by Young (1979). These are interpreted as comparable to shonkinite plugs north of Baker Lake (Wodicka et al., 2017) that have higher amplitude aeromagnetic highs than the Keating anomalies modelled in that area by Tschirhart (2017). The circular magnetic highs in the Amer Belt are thus labelled as ‘(?)Shonkinite’ in Figure 3a, and would benefit from petrographic and petrophysical study.

The depositional age range of the undeformed and non-metamorphosed Baker Lake Group spans that of the Hudson suite, the second Paleoproterozoic deformation (*see* 'D_{p1} and D_{p2} — folds, structural discontinuities, and fabrics as expressed in cover sequences Ps1 to Ps3 versus sequence Ps4' section below), and metamorphism of adjacent basement terranes (Pehrsson et al., 2013a). The Hudson suite and Dubawnt minette magmatism also moved considerable potassium, thorium, and uranium to higher crustal levels in the study region. Through erosion, these intrusions contributed radioactive elements within refractive heavy minerals that rivers transported to contemporaneous and later siliciclastic basins. The high background radioactivity of the Hudson suite and the locally abundant Dubawnt minette dykes (Peterson et al., 2011) have been distractions to uranium prospecting, especially the dykes because they are not exploration targets in themselves (Jefferson et al., 2015). On the other hand, the large intrusions may have contributed to an elevated geothermal gradient, especially where blanketed by an insulating sedimentary pile. Potter et al. (2020) showed that in northern Saskatchewan and Alberta, the Clearwater, Hudson, Nueltin, and other such felsic intrusive suites all have high radiogenic heat production, and are thus termed 'high-heat granites'.

Kivalliq igneous suite

The bimodal 1.77 to 1.74 Ga Kivalliq igneous suite (Peterson et al., 2002, 2015a, b; Scott et al., 2012, 2015) was the last large igneous event prior to deposition of the Athabasca and Thelon basins and extends from south of the Athabasca Basin to southern Greenland (Peterson et al., 2015a). In the area of the Dubawnt Supergroup (Fig. 1, 2), intrusive phases extend southwestward as far as Nicholson Lake (McGregor et al., 2018), northwestward to the Amer plutonic complex, and eastward as far as Hudson Bay (Jefferson et al., 2013). The plutonic components include Nueltin granite stocks, to pancake-shaped intrusions that are variably highly magnetic to magnetically translucent, and highly magnetic gabbro bodies that form basal and marginal parts of some granite intrusions, as well as separate elongate intrusions. The major-element compositions of felsic phases in the Kivalliq igneous suite are very similar to those of Hudson suite granite (Scott et al., 2015), but trace-element ratios can be used to consistently distinguish between the two suites, particularly by lake-sediment geochemistry (Grunsky et al., 2012; Hayward et al., 2013; McCurdy et al., 2013).

The Pitz Formation in the middle part of the Dubawnt Supergroup (*see* above; Fig. 4a) is the extrusive component of the Kivalliq igneous suite, comprising bimodal and intermingled flows, subvolcanic sills, tuffs to breccias, and epiclastic rocks. Several trends of diabase dyke swarms (Fig. 2, 3a, c) complete this large igneous province. Peterson et al. (2015b) dated a southern, coarse-grained feeder of the 020°-trending McRae Lake dyke swarm at 1753.6 ± 2 Ma.

The geochemically very similar, but undated 070°- to 110°-trending Thelon River dykes occupy faults that dextrally offset the McRae Lake dykes, and are thus somewhat younger, possibly young enough to be contemporaneous with the 1.69 Ga, 090°-trending Pelley Bay dykes (Bleeker et al., 2010). Additional dykes tentatively included in the Kivalliq igneous suite trend about 160° to 180° around the Amer plutonic complex and are here termed 'Amer dykes'. Their existence is inferred solely from linear aeromagnetic anomalies, and they have not been observed in outcrop. The Deep Rose dykes are similarly inferred solely from linear aeromagnetic anomalies, but differ from all others in having sinuous trajectories trending overall eastward. The Deep Rose linear anomalies trend without offset across all faults in the region, from Garry Lake to the Montessor Belt and northwestern Amer Belt, and do not appear to be part of the Riedel-shear system described below (*see* 'Riedel-shear analysis of steeply dipping faults in the study region' section).

All phases of the Kivalliq igneous suite and some deep plutons of the Hudson suite are spatially associated with fault systems (*see* 'Tectonics and structure during sedimentation of the two basins' section below). The Amer plutonic complex (Apc_H + Apc_N, Fig. 3a) is defined here because it is a special case where all three granitoid suites (Snow Island suite, Hudson suite, and Kivalliq igneous suite) are spatially associated with each other and with the Amer mylonite zone. One of the large subsurface Snow Island suite plutons in the area of the Aberdeen Subbasin (Tschirhart et al., 2017) trends obliquely across and beneath the northeastern margin of the Aberdeen Subbasin, west of 'Tahiratuq' (Inuit place name for the informal 'Itza lake' in Fig. 3a; Pelly and Nales, 2004). The characteristically pronounced and broad aeromagnetic anomaly of this pluton continues northward to underlie the mylonite zone and bends northeastward along the mylonite zone to the northern edge of Figure 3 in Tschirhart et al. (2017). This Snow Island suite pluton is only defined geophysically, with its apex buried more than a kilometre below the surface (Fig. 6 in Tschirhart et al., 2017). At the northeastern end of the Snow Island suite anomaly, south of the Amer mylonite zone, a well exposed granitoid and syenite complex of the Hudson suite (Apc_H, Fig. 3a) was originally mapped and dated by Tella (1984, 1994). Here the Hudson suite granite to syenite is cut and surrounded by numerous aphanitic mafic minette dykes of the Dubawnt swarm (Peterson et al., 2011). Geophysically, this part of the Amer plutonic complex is dominated by the powerful aeromagnetic signature of the deep-seated Snow Island suite pluton, with only the minette dykes being clearly distinguishable as linear aeromagnetic anomalies. Some of the Hudson suite granite is exposed within the mylonite zone, where it appears to have been injected as magma during movement along the mylonite zone, reminiscent of the 1837 ± 7 Ma (Therriault et al., 2018) to 1808 ± 2 Ma (Henderson and Roddick, 1990) 'Base Camp' granite (geochronology site 46, Fig. 1, Table 2) that cuts, and is cut by, the Wager shear zone. On the northern side of the Amer

mylonite zone, a discrete and moderately well exposed body of Nueltin rapikivi granite (Apc_N, Fig. 3a), with uniformly very high magnetic susceptibility, constitutes the northern part of the Amer plutonic complex. The surface outcrop pattern and the sharp termination of the aeromagnetic anomaly on all sides is characteristic of a tabular surface body, like many of the Nueltin rapikivi granite shapes in the Kivalliq Region (Jefferson et al., 2013; Peterson et al., 2015a). The present authors hypothesize that the rapikivi granite came up along the Amer mylonite zone when the fault was reactivated in extension and the viscous porphyritic magma likely spread out over the fault as a large pancake, much like those still preserved above such faults in the southern Kivalliq Region (asterisk (*) in Fig. 1, 2). This hypothesis includes the corollary that subsequent north-side-down dip-slip movement on the Amer mylonite zone resulted in erosion of the southern half of the rapikivi granite pancake, whereas the northern half was preserved as it appears today.

Although some of the minette dykes in the Amer plutonic complex have anomalous uranium-thorium values (Peterson et al., 2011), these are directly related to magmatic processes and not to hydrothermal alteration systems such as form unconformity uranium deposits. Elsewhere however, some granitoid intrusive phases are spatially, temporally, and genetically linked to uranium and precious-metal mineralization (*see* 'Alteration and metallogenic comparisons of the Athabasca Basin and Thelon Basin regions' section below).

Structure and metamorphism

This study builds on the structural-stratigraphic framework set out by Pehrsson et al. (2013a, b), in particular the four phases of Paleoproterozoic deformation (D_{p1} through D_{p4}) in the Meadowbank River region. Table 1 slightly modifies these events, further extends the deformational evolution to the top of the stratigraphic column (D_{p5} through D_{p13} and D_{ph1} to D_{ph3} , inclusive), and adds periods of erosion, as well as events that are expressed only as faulting and/or fault reactivation. Table 1 also breaks down major events into multiple components, beginning with D_{p1a} , b and c, following Calhoun et al. (2014). Table 1 refers to Figures 3c, 4, and 6 to 10a, b for specific examples. This structural evolution is important for distinguishing the Paleoproterozoic cover sequences (*see* 'Distinguishing structural, lithological, and geophysical characteristics for sequences Ps1, Ps2, Ps3, and Ps4' section above) because it determined the settings and conditions for transport, deposition, and preservation of the Paleoproterozoic cover sequences, discussed above in the section entitled 'Detrital zircon provenance of sequence Ps4'. Structural analyses in this project did not include Archean deformation, known only from very detailed drill core studies of the Meadowbank mine area (e.g. Janvier et al., 2015a, b) and not mappable for any great distances in outcrop.

Types of structural discontinuities

Structural discontinuities include uncontroversial thrusts and klippe that stacked older strata over younger (*see* ' D_{p1} and D_{p2} vergences' section below) and readily classifiable steeply dipping faults (*see* 'Riedel-shear analysis of steeply dipping faults in the study region' section), but also a number of subhorizontal to moderately dipping and folded high-strain zones that are of less certain origin. Examples of this latter category follow, some being laterally extensive and requiring different interpretations in different places, with others being poorly understood local discontinuities that require further study.

Laterally extensive high-strain zones are common along parallel contacts between early Paleoproterozoic units with contrasting rheology, for example between sequence Ps1 quartzite and basement, between sequence Ps1 quartzite and sequence Ps2 carbonate and sequence Ps3 basalt, and between sequence Ps4 and the underlying strata. The first two examples do not result in truncation of one unit by another, but trend parallel to their mutual contact for great distances. The basal sequence Ps4 example involves significant truncation of underlying units on a local to regional scale, and is interpreted mainly as a profound regional unconformity, discussed above in the 'Basal contact of sequence Ps4' section.

The first two examples of high-strain zones can be interpreted in different ways, but are not thrusts, nor are they detachments. Calhoun et al. (2014) considered some of these highly foliated zones to be a result of deformation they identified as D_{p1a} , a subhorizontal, purely translational event. Jefferson et al. (2015) considered the foliation in some such places to be a result of flexural slip during D_{p1} and/or D_{p2} . Consideration of the effects of intense isoclinal folding in quartzite during D_{p1b} and D_{p1c} , compared to the lack of internal shortening in the kilometres-thick underlying Snow Island suite bodies, indicates that translation must have been the most important factor in places such as the Whitehills synform (Fig. 6).

On the other hand, especially in the southwestern part of the Amer Belt, pristine exposures of the basal sequence Ps1 contact overlain by relatively undeformed quartzite show that neither D_{p1} nor D_{p2} caused structural discontinuity everywhere along the base of sequence Ps1. Along the northwestern panel of the Amer Belt, kilometre-scale imbricate thrusts expose this basal contact in a number of places, where again it is intact, albeit highly foliated, showing that the translational strain there was accommodated by thrusting within the basement units. Where the unit below the quartzite is felsic tuff of similar rheology to the quartzite, such as in the 'Ukalik–Nipterk' lakes area (Fig. 7a), the Akiliniq Hills (Fig. 8 of Jefferson et al., 2015), and the north Meadowbank River area (Fig. 3, 5 of Pehrsson et al., 2013a), the unconformity surface is isoclinally folded and refolded by D_{p1} as well as D_{p2} , and is simply an intact zone of intense foliation because of the aluminous composition.

Some examples of poorly understood local discontinuities, shown in Figures 3a, 6, and 8, include the Pukiq (Pd, discussed in Anand and Jefferson, 2017a), Amarulik, and Schultz Inlet discontinuities (*see* ‘First five Neoproterozoic supracrustal assemblages’ section), and the Schultz Lake klippe (Hadlari et al., 2004). None of these discontinuities are exposed. Mapping (McEwan, 2012) and geophysical modelling (Tschirhart et al., 2013a) of the Schultz Lake klippe suggest a subhorizontal discontinuity between an isoclinally D_{p1} -folded and open D_{p2} -refolded sequence Ps1 to Ps2 and structurally underlying subhorizontally foliated metagreywacke and basalt of the Neoproterozoic Pipedream and Half Way Hills assemblages. In places, the geophysical discontinuity appears to be within the Neoproterozoic rocks. The lack of a basal unconformity and the structural disharmony between the Paleoproterozoic and Neoproterozoic rocks preclude the Schultz Lake klippe being a depositional outlier, such as the several isolated patches of Ketyet River group that preserve their basal unconformity assemblage along the Meadowbank River Belt (Fig. 3a).

D_{p1} and D_{p2} — folds, structural discontinuities, and fabrics as expressed in cover sequences Ps1 to Ps3 versus sequence Ps4

Studies done as part of GEM-1 validated and provided additional styles and subcomponents of the D_{p1} through D_{p4} structural schema and of Pehrsson et al. (2013a) for both the Amer Belt (Calhoun et al., 2014; Jefferson et al., 2015, 2023; C.W. Jefferson, R.H. Rainbird, G.M. Young, S.S. Gandhi, J.C. White, V. Tschirhart, D. Lemkow, and L.B. Chorlton, work in progress, 2023) and a number of localities in the Kiggavik uranium camp to Meadowbank River area (Fig. 3c, 6, 7a–c, 8; McEwan, 2012). The M_{p1} through M_{p3} metamorphic phases from Pehrsson et al. (2013a) are also adopted here, while noting additional criteria for distinguishing M_{p1} from M_{p2} . Figure 4b generalizes the distinctive styles of F_{p1} versus F_{p2} , the first two Proterozoic folding events produced by D_{p1} and D_{p2} , respectively, in the study region. These distinctive styles are diagnostic in the Amer, Ketyet River, and Montresor belts, and predate the Dubawnt Supergroup.

The Ps1, Ps2, and Ps3 units, together with the Archean units, were isoclinally folded in the study area during an early Paleoproterozoic deformation event termed ‘ D_{p1} ’ by Pehrsson et al. (2013a). They interpreted the 1.9 to 1.865 Ga Snowbird Orogeny of Berman et al. (2007) as the driver for D_{p1} . The type region for this deformation in the Ketyet River Belt stretches from Whitehills Lake (Fig. 6) to ‘Ukalik lake’ (Fig. 7a). In the Amer Belt, the type areas are at the northeastern end, where Calhoun et al. (2014) documented at least four phases of D_{p1} : subhorizontal translation, isoclinal folding, followed by refolding, and significant basement-involved imbricate thrusting. The thrusts all verge

northeasterly and are restricted to the northern limb of the Amer grand synform (Jefferson et al., 2015). The documentation by Calhoun et al. (2014) and White et al. (2023) is graphic and clear, spectacular in terms of D_{p1a} , D_{p1b} , and D_{p1c} being present in a single, elegant thin-section photomicrograph. A key aspect of D_{p1} in the study area is its low metamorphic grade, despite intense structural manifestations (*see* ‘Timings and origins of D_{p1} and D_{p2} in the northeast Thelon region’ section below). Together with sequence Ps4, the sequences Ps1 through Ps3 strata and D_{p1} structures were then refolded, metamorphosed, faulted, and intruded by the Hudson granitoid suite and Dubawnt minette dyke swarm during the 1.87 to 1.80 Ga Hudsonian Orogeny (D_{p2} of this paper). In the above-noted type areas, the key evidence for what constitutes D_{p1} and how it predates D_{p2} includes: 1) refolding of all D_{p1} structures (fabrics, folds, refolds, and thrusts) by open F_{p2} folds and broad D_{p2} thrusts that verge northwesterly; 2) the variation in vergences and localization of D_{p1} structures from one locality to another, ranging from northeastward to southeastward to southwestward; and 3) the presence of prefolded clasts of sequence Ps1 quartzite in conglomerate of sequence Ps4 that is in turn folded by F_{p2} open synforms and tight to broken antiforms. This schema is summarized in Figure 4b.

Clarification on what may be included in D_{p1} structures is required for the Marjorie terrane and the Montresor Belt (*see* below). Hunter et al. (2018, 2021) described southeast-vergent isoclinal folds and thrusts that structurally repeat the three paragneiss packages of the Aberdeen assemblage, together with the Snow Island suite orthogneiss of the Marjorie terrane. Whereas they assigned these to ‘F2’, citing evidence of previous structures, these folds and thrusts are in turn folded by north-vergent asymmetric folds that are more consistent in orientation, style (flat-bottomed synforms and peaked antiforms), and vergence with the regional F_{p2} structures that dominate the eastern part of the study area and that decrease in intensity toward the west. The isoclinal folds and thrusts within the Marjorie terrane are here assigned to D_{p1} , as they are consistent in style and vergence with other D_{p1} structures, particularly those in the Amer Belt where Calhoun et al. (2014) documented three phases, thereby accounting for the earlier structures noted by Hunter et al. (2018).

In the Montresor Belt, Percival et al. (2015a, b, 2017) and this study have documented the lack of intrinsic deformation (outcrop- and hand-specimen-scale fabrics and folds) of the upper Montresor group strata, consistent with the absence of D_{p1} structures therein. According to Pehrsson et al. (2013a), the lack of D_{p1} structures is a key criterion for Paleoproterozoic strata being sequence Ps4, yet Percival and Tschirhart (2017) and Percival et al. (2017) assigned them to sequence Ps3 because of the presence of magnetic markers and a relatively fine clastic lithology that they thought correlated with sequence Ps3 in the Amer Belt. The present authors dispute that proposed correlation (*see* ‘Distinguishing structural, lithological, and geophysical characteristics of

sequences Ps1, Ps2, Ps3, and Ps4' section). Once Percival et al. (2015a, b) had decided on sequence Ps3 for the upper Montresor strata, that misinterpretation propagated through subsequent interpretations of otherwise useful data. For example, Percival and Tschirhart (2017) interpreted D_{p1} thrusts from geophysical modelling of magnetically defined bedding discontinuities in the upper (sequence Ps4) Montresor group. In their model, they considered the 1.85 Ga metamorphic monazite in the upper strata to date D_{p1} in that area, even though the 1.85 Ga age is more consistent with deformation and metamorphism related to the Hudsonian Orogeny. The 1.85 Ga age postdates the 1.9 to 1.865 Ga range of the Snowbird Orogeny (Berman et al., 2007) and is more likely to be an early manifestation of the 1.834 ± 5 Ma monazite peak (Pehrsson et al., 2013a) that dates D_{p2} in the Meadowbank River–Whitehills Lake area.

The following alternative interpretations for the aeromagnetic discontinuities defined by Percival and Tschirhart (2017) take into account the straight to gently curved nature of the beds and discontinuities that are consistent with D_{p2} , but not D_{p1} structures. Firstly, they may be intraformational unconformities, consistent with the above evidence of intraformational erosion of the Amer sequence Ps4A beneath conglomerate at the base of the Amer sequence Ps4B. Secondly, the aeromagnetic discontinuities may be pre-lithification slump structures (mentioned in Tschirhart et al., 2015), as these strata were deposited during a tectonically active time. This is consistent with slump structures and sandstone dykelets documented in drill core of the upper part of sequence Ps4 along strike to the southwest (Jefferson et al., 2023; C.W. Jefferson, R.H. Rainbird, G.M. Young, S.S. Gandhi, J.C. White, V. Tschirhart, D. Lemkow, and L.B. Chorlton, work in progress, 2023). Thirdly, the aeromagnetic discontinuities may be out-of-syncline reverse faults generated during development of the F_{p2} Montresor synform. Lastly, the discontinuities may represent syn- D_{p3} extensional faults.

Whatever the origin of these upper Montresor group discontinuities, whether pre- or postlithification, they are only intraformational, simple planar features, albeit being folded by the F_{p2} Montresor synform. The structural style of these discontinuities is inconsistent with the style of D_{p1} structures in the Amer and Ketyet River belts — those include intense, imbricate basement-involved thrusts refolded by F_{p2} and the isoclinal F_{p1a} and F_{p1b} folds within sequences Ps1 through Ps3 (Fig. 4b), as documented by Pehrsson et al. (2013a) for the Ketyet River Belt and as documented for the Amer Belt by Tschirhart et al. (2013d), Calhoun et al. (2014), Jefferson et al. (2015, 2023), and C.W. Jefferson, R.H. Rainbird, G.M. Young, S.S. Gandhi, J.C. White, V. Tschirhart, D. Lemkow, and L.B. Chorlton (work in progress, 2023). In particular, Jefferson et al. (2015, 2023) showed F_{p2} -refolded accordion D_{p1} folds in the Ayagaq Lake sequence Ps1 quartzite, and Calhoun et al. (2014) and White et al. (2023) illustrated that the schistosity S_{p1a} and S_{p1b} can be traced through F_{p1b} and F_{p1c} in a single thin section. The

Amer Belt D_{p1} folds are consistent with what McEwan (2012) and Pehrsson et al. (2013a) documented for D_{p1} in the Ketyet River Belt (e.g. Fig. 7a). The Amer D_{p1} imbricate thrusts that repeat Archean basement over sequences Ps1 through Ps3 have good analogues at the northwestern end of the Montresor Belt, and both imbricate thrust belts are refolded by F_{p2} ; however, neither such structures nor such fabrics are present in outcrops or samples of the upper Montresor group (*see* 'Basal contact of sequence Ps4' section above). If such structures or such fabrics were indeed present, they would also likely be outlined by the Montresor aeromagnetic data (cf. Tschirhart et al., 2013d; Calhoun et al., 2014), but they are not.

D_{p1} and D_{p2} vergences

The D_{p1} vergences differ markedly from place to place in the study area. The D_{p1} thrust configurations and associated stretching lineations indicate vergence toward the northeast in several discrete structural panels, one being the 80 km long stretch of imbricate basement-sole thrusts spanning the northwestern panel and northeastern tip of the Amer Belt (Fig. 3a). These thrusts trend southeast and dip about 35° southwest, placing Neoproterozoic Rumble greywacke or Snow Island suite granite and rhyolite over the Amer sequences Ps1 through Ps3 in some 22 imbricates on the order of 1 to 3 km thick (Jefferson et al., 2015). These imbricate thrusts are refolded along southwest-plunging F_{p2} axes. Another well documented northeast-verging example is the 60 km long Pukiq imbricate zone (PQi, Fig. 8) along the southern side of the Thelon Fault. Hundreds of imbricates comprise upright panels of sequence Ps1 quartzite resting on Pukiq Lake formation rhyolite ranging from millimetres to tens of metres in thickness. Both quartzite and mylonite are highly strained to mylonitized, with mullions and stretching lineations plunging gently toward about 250° , with suggestions of sheath folds (Anand and Jefferson, 2017a, b). Here too, the imbricate slices are refolded along southwest-plunging F_{p2} axes. In the area between geochronology site 29 and Schultz Lake (Fig. 3a, southwestern Fig. 6), amphibolite-grade quartzite overlies mafic gneiss of the lower Aberdeen assemblage that in turn overlies mylonitized Pukiq Lake formation, all with stretching lineations plunging 10 to 15° toward 250° .

Vergences interpreted from D_{p1} fold analyses are less certain and range from diametrically opposed to orthogonal at different localities. The D_{p1} folds verge northeastward in the Amer Belt, both in terms of well exposed, large, northeast-overturned isoclinal folds along the two limbs of the grand synclinorium (Jefferson et al., 2015, 2023; C.W. Jefferson, R.H. Rainbird, G.M. Young, S.S. Gandhi, J.C. White, V. Tschirhart, D. Lemkow, and L.B. Chorlton, work in progress, 2023) and in terms of multiply refolded isoclinal folds at outcrop to thin-section scale in fine-grained strata of sequence Ps3 (Calhoun et al., 2014; Jefferson et al., 2023; C.W. Jefferson, R.H. Rainbird, G.M. Young, S.S. Gandhi, J.C. White, V. Tschirhart, D. Lemkow, and L.B. Chorlton,

work in progress, 2023). On the other hand, reconstructed D_{p1} vergences in the ‘Ukalik lake’ area (Fig. 7a) and in the Schultz Lake klippe (Fig. 8) appear to have been toward the southwest (McEwan, 2012; Pehrsson et al., 2013a). Out-of-sequence-style stacking of sequences Ps1 and Ps2 of the Ketyet River group along the Quoich River in the hanging wall of the D_{p2} Quoich River thrust suggests south vergence (Fig. 6 of Pehrsson et al., 2013a).

The D_{p2} fold and thrust vergences are uniformly toward the northwest across the study area, except in the Marjorie terrane and the Akiliniq Belt where they verge east-southeasterly. The D_{p2} folds and thrusts throughout the study area re-fold and/or break the D_{p1} structures (Fig. 4b; Pehrsson et al., 2013a; Jefferson et al., 2015). The F_{p2} antiforms tend to be much tighter than the F_{p2} synforms. Many antiforms are tight kinks like that on the left of Figure 4b; kink-shaped minor antiforms are also common at the centres of typically broad, flat F_{p2} synforms, such as the Whitehills (Fig. 6) and Tahiratuq synclinoria. Other F_{p2} antiforms are rounded and still others broken into high-angle reverse faults to low-angle klippen. Along the southern side of the Aberdeen Subbasin, the Aberdeen assemblage is amphibolite-facies grade and has two fabrics, one of which may be transposed D_{p1} . This lenticular fabric is folded into flat-bottomed synforms and peaked antiforms that are much like F_{p2} folds in the Paleoproterozoic sequences, except their axes trend northwesterly and dip southeasterly.

M_{p1} versus M_{p2} — further distinctions between cover sequences Ps1 to Ps3 and sequence Ps4

Metamorphism across the study area is extrapolated from the results of Pehrsson et al. (2013a) in the Woodburn Lake to Meadowbank River area with the aid of belt-specific sources cited below. In the Ketyet River Belt, M_{p1} is defined by D_{p1} fabrics characterized by low- to mid-greenschist-facies mineral assemblages at unknown pressures and ages. The M_{p2} regional metamorphism of Pehrsson et al. (2013a) is broadly coeval with D_{p2} , ranges from mid-greenschist to amphibolite facies and peaked at ca. 570°C, with a minimum pressure of 2.7 kbar (270 000 kPa) by 1834 ± 5 Ma. Peak pressure was 5 kbar (500 000 kPa) at 540°C, with temperatures reaching as high as 600 to 650°C in places. They cited thermal modelling of relatively low heat-producing rocks in the Committee Bay Belt by Berman et al. (2010) as being directly applicable to the Woodburn Lake region, indicating an approximately 30 Ma time lag between the onset of crustal thickening at ca. 1870 Ma and the 1834 ± 5 Ma monazite growth. Regional metamorphism increases significantly from southwest to northeast along the Ketyet River Belt.

Metamorphism from D_{p1} fabrics in the Amer Belt is similar in range to that of the Ketyet River Belt, and also undated. The variable effects of D_{p2} deformation and M_{p2} metamorphism are evident both along and across strike of the contiguous Amer Belt. At the northeastern end of the

Amer Belt, kyanite and sillimanite are developed in places (Patterson, 1986). Calc-silicate minerals are best developed at the interface between quartz and carbonate within the sequence Ps2 dolostone. The carbonate-altered sequence Ps3 basalt is also much more recrystallized toward the northeast. Toward the southwest, the basalt uniformly preserves better primary textures and the dolostone is cryptocrystalline with no calc-silicates, even though still highly strained. The basal unconformity sequence also changes appearance from southwest to northeast. In the southwest, the basal conglomerate is very well preserved with only moderate foliation, the polymict nature is clear in outcrop, and the basal unconformity is distinct and well exposed in a number of places, with conglomerate directly overlying paleoweathered Snow Island suite (Young, 1979; Jefferson et al., 2023; C.W. Jefferson, R.H. Rainbird, G.M. Young, S.S. Gandhi, J.C. White, V. Tschirhart, D. Lemkow, and L.B. Chorlton, work in progress, 2023). In contrast the basal conglomerate and the unconformity assemblages flanking the northeastern end of the Amer Belt is a zone of schist that grades almost imperceptibly into basement below and quartzite above. Only close inspection can pinpoint the unconformity, and only quartz clasts are readily identifiable without turning to hand lens and thin section to document the same primary pebble compositions as in the southwest. Iron-oxide minerals in sequences Ps1 to Ps3 are recrystallized to euhedral magnetite throughout much of the Amer Belt, as noted for the magnetic marker beds, but pink colours reflect dusty hematite in the lower part of the sequence Ps1 quartzite in the southwest. In addition to the increase in metamorphic grade along the axis from southwest to northeast, the grade also increases across the Amer medial zone, with much higher grades on the northwestern side than the southeastern side. The quartzite is also more strongly stylolitized on the northwestern side of the grand synform, with the S_{p1} muscovite partings partitioned into pillars and pits along bedding planes. These metamorphic differences reflect a deeper crustal level on the northwestern side, as shown in the restriction of basement-involved D_{p1} thrusts to that side. The metamorphic grade in the basement northeast of the final closure of the Amer grand synform also increases from south to north (Tella and Heywood, 1978). In all of the Paleoproterozoic belts, except southeast of the Quoich River thrust (Fig. 3a, c), the sequence Ps4 strata are much lower in metamorphic grade than the sequence Ps1 to Ps3 strata. This is considered to be a result of both lack of D_{p1} and their higher structural level. The sequence Ps4 strata are located in the cores of synforms and they are generally not preserved, or are restricted in distribution, toward the higher grade northeastern ends of the belts. The low metamorphic grade of sequence Ps4 in a large rhombic graben of sequence Ps4 in the north-central Amer Belt is consistent with it being down-dropped. In the Ketyet River Belt, sequence Ps4 strata become more metamorphosed toward the northeast, between the Whitehills and Quoich River thrusts, and structural criteria that help in distinguishing sequence Ps4 from sequences Ps1 to Ps3 siliciclastic rocks become difficult to apply in that direction.

The metamorphic contrast between lower and upper strata in the Montresor Belt is so distinct that Percival et al. (2015a, b, 2017) interpreted it as a tectonic discontinuity. They described the higher levels of the upper Montresor strata as weakly deformed and metamorphosed only to middle-greenschist facies, dated locally by metamorphic monazite at 1847 ± 15 Ma (Percival et al., 2015b). In contrast, the footwall complex of the Montresor Belt comprises quartzite, carbonate, and schist that reached middle-amphibolite-facies conditions at 1861 to 1844 Ma (Berman et al., 2015b; Dziawa et al., 2019). The high-strain zone separating the lower Montresor group from underlying granitoid gneiss and mylonite also yielded metamorphic monazite with a U-Pb age of 1850 ± 5 Ma that Percival et al. (2015b, 2017) interpreted as their D3, predating the development of the major Montresor synform (their D4). To put their deformation chronology into the context of this study area (Table 1), their D4 would be reinterpreted as a classic F_{p2} synform produced by D_{p2b} compression. Their D3 shear zones are reinterpreted as products of $D_{p2b+c+d}$ transpression, followed by D_{p3} extension and D_{p4b} reactivation of regional deep-seated dextral fault systems (major P-shears like those shown in Fig. 3c). This reinterpretation is based on geometry — their above-noted 1.85 Ga shear zones are straight and not folded by their D4 (D_{p2b} in this study) major folds. The D_{p3} -extension component of the straight shear zones in this study is compatible with the deep-seated extensional model set out in Percival and Tschirhart (2017). One other clarification relates to the above 1.85 Ga metamorphic ages that Percival et al. (2017) related to the Snowbird phase of the Hudsonian Orogeny. Whereas Percival and Tschirhart (2017) attributed the 1.85 Ga age to D_{p1} , Pehrsson et al. (2013a) demonstrated that D_{p1} was most likely driven by the 1.9 to 1.865 Ga Snowbird Orogeny (Berman et al., 2007), well before 1.85 Ga. In both orogenies, these ages represent peak metamorphism, and the actual orogenic deformation and thickening would have begun up to 30 Ma earlier.

Metamorphic contrasts between sequence Ps4 and the underlying sequence Ps1 are less pronounced in the Garry Lake Belt, where Miller (1995) found that chlorite-grade greenschist-facies hydromuscovite-clinocllore defines the weak penetrative fabric in his ‘upper Amer Group’ strata (sequence Ps4) and the quartzite resembles that of the Amer Belt. Far to the southwest, LeCheminant et al. (1984) found metamorphism in the sequence Ps1 and Ps2 units of the Akiliniq Hills to range from anchizone through lowermost greenschist facies, whereas the upper Amer group strata along the Thelon River nearby are pristine. In the Meadowbank River area, Pehrsson et al. (2013a) determined that M_{p1} metamorphism from D_{p1} fabrics is low- to mid-greenschist facies, with pressures unknown. In the Whitehills Lake synform, the sequences Ps1 through Ps3 strata have undivided upper-greenschist $M_{p1} + M_{p2}$, and the slaty cleaved sequence Ps4 has chlorite-grade greenschist M_{p2} , the main distinction between sequence Ps4 and older strata there being the folds and fabrics described above.

The current quantitatively calibrated and dated M_{p2} metamorphism in the study region is Hudsonian, whether it was regional due to crustal burial beneath thrust stacks or local due to high-level Hudsonian (1.84–1.81 Ga) intrusions. In the Ketyet River and Montresor belts, metamorphism also increases toward the northeast, where it attains upper-greenschist to mid-amphibolite grade (see Pehrsson et al., 2013a; Percival et al., 2017). On the other hand, the sliver of sequence Ps3 at the northeastern end of the Montresor Belt is only lower greenschist-facies grade where it contains the impact spherules (Percival et al., 2019). Higher metamorphic grades are associated with structurally uplifted or unroofed panels, or with large, high-level Hudson granite bodies, such as in the extensional Kinngaaquik igneous complex.

Structural and metamorphic distinctions between sequence Ps4 strata and the older Paleoproterozoic strata

Structural and metamorphic attributes are the defining evidence that sequence Ps4 postdates sequences Ps1 to Ps3 in all Paleoproterozoic belts of this study. The uppermost units (sequence Ps4) in these belts are nearly pristine, with open flat-bottomed F_{p2} synforms and sharply peaked antiforms (Fig. 4b), as well as weak penetrative foliation at high angles to bedding. Flat-lying desiccation-cracked siltstone interbedded with ripple-marked and crossbedded quartz arenite to lithic feldspathic sandstone in sequence Ps4 of the Amer Belt are slightly deformed by flattening parallel to steeply dipping S_{p2} cleavage. Well developed slaty cleavage of D_{p2} characterizes sequence Ps4 slate and conglomerate of the Ketyet River Belt around Whitehills Lake, but that is the earliest cleavage therein. Pehrsson et al. (2013a) showed that the sequence Ps1 quartzite clasts in the Tasirjuak conglomerate are predeformed, with both isoclinal folds and bedding transposed parallel to foliation, in contrast to the weakly deformed conglomerate matrix and intraclasts. Frisch (2000), Percival and Tschirhart (2017), Percival et al. (2017), Jefferson et al. (2023), and C.W. Jefferson, R.H. Rainbird, G.M. Young, S.S. Gandhi, J.C. White, V. Tschirhart, D. Lemkow, and L.B. Chorlton (work in progress, 2023) reported that the upper Montresor siltstone is also only weakly deformed, with well preserved primary sedimentary structures and textures in a monotonous, kilometres-thick flysch sequence, broken only by the arkose-enclosed polymict conglomerate at the southwestern end of the area mapped by Frisch (2000).

LeCheminant et al. (1984) illustrated and described in detail some hundreds of metres of spectacular exposures of sequence Ps4 along the Thelon River, on the northwestern side of the Beverly inlier. These rocks are so well preserved, with no apparent cleavage, that only their steep dips convincingly distinguish them from redbeds of the subhorizontal Amarook, Pitz, and Thelon formations in that area. Although the base of sequence Ps4 is not exposed there, the desiccation cracks, trough-crossbedded quartz arenite,

sandstone-mudstone rhythmites and calcareous arkose are remarkably similar to molasse of the Amer sequences Ps4A and Ps4B. Similar lithofacies are also present in sequence Ps4 south of the Akiliniq Hills (LeCheminant et al., 1984). These are more deformed, yet with a single foliation that transects bedding at a high angle, much like the Amer, Ketyet River, and Montresor sequence Ps4 units. The underlying sequences Ps1 through Ps2 strata have bedding transposed parallel to foliation and, together with Akiliniq sequence Ps4, form a southeast-vergent (LeCheminant et al., 1984) F_{p2} fold. Thus, in all localities of the study region, the sequence Ps4 strata lack the D_{p1} penetrative fabrics and structures that are clear and penetrative at microscopic to map scales in all of sequences Ps1 through Ps3 (McEwan, 2012; Pehrsson et al., 2013a; Calhoun et al., 2014; Jefferson et al., 2015, 2023; C.W. Jefferson, R.H. Rainbird, G.M. Young, S.S. Gandhi, J.C. White, V. Tschirhart, D. Lemkow, and L.B. Chorlton, work in progress, 2023).

As noted above, the lower-greenschist to anchizone redbed Ps4 lithofacies is so well preserved that it strongly resembles redbeds in the Dubawnt Supergroup. The Baker Lake and Wharton groups are not metamorphosed, except where cut by large mafic minette dykes, are generally flat lying, and have no fabrics. These attributes, unconformities, and other superposition metrics such as clast types in basal conglomerate, detrital zircon geochronology, and context within specific belts determined by mapping are key to distinguishing these strata from those of sequence Ps4, especially the redbeds.

Timing of emplacement of Snow Island suite thrust sheets

Most of the thick thrust sheets of Snow Island suite granite were emplaced prior to the main folding event of D_{p2} , as the sheets outline megascopic F_{p2} folds in the eastern part of the study area, as detailed above. Figure 8 of Pehrsson et al. (2013a) interpreted the thrust at the base of one thick sheet south of ‘Nipterk lake’ as being D_{p1} , with their D_{p1} being considered a result of the 1.9 to 1.865 Ga Snowbird phase (Berman et al., 2007) of the Hudsonian Orogeny. In this paper, the concept of D_{p1} deformation being related to the Snowbird event and distinct from the Hudsonian D_{p2} (see ‘Timing and origins of D_{p1} and D_{p2} in the northeast Thelon region’ section below) is retained. The emplacement of Snow Island suite sheets during early to mid-Hudsonian D_{p2} thrusting is consistent with Figure 7 of Pehrsson et al. (2013a) that illustrated mylonite at the base of a 2.63 Ga monzogranite, where they stated that kinematics and older-over-younger stacking are consistent with northwest-vergent thrusting during D_{p2} deformation. Similar observations by Kjarsgaard et al. (1997) and Davis et al. (2021) also support emplacement of Snow Island suite thrust sheets in a north-northwestward direction during Hudsonian D_{p2} deformation.

Riedel-shear analysis of steeply dipping faults in the study region

Anand and Jefferson (2017a, b), Hunter et al. (2014), Johnstone (2017), Grare et al. (2018), and D. Johnstone, K. Bethune, D. Quirt, and A. Benedicto (unpub. rept. no. 15-CND-92-04 of AREVA Resources Canada Inc., 2015) all recognized that steeply dipping faults fit the Riedel-shear model (Fig. 3c, 9a, b) that helps to understand their relationships with hydrothermal alteration and uranium mineralization (Fig. 8, 9a, b). Anand and Jefferson (2017a, b) and D. Johnstone, K. Bethune, D. Quirt, and A. Benedicto (unpub. rept. no. 15-CND-92-04 of AREVA Resources Canada Inc., 2015) further recognized the prospectivity of gently dipping structural discontinuities where they intersect with steeply dipping structures. Anand and Jefferson (2017b) noted that each dyke swarm follows and provides linear magnetic markers of the Riedel-shear arrays.

Figure 3c shows specific yet still regional details of the interplay between strike-slip faults, folds, and low-angle faults at a regional scale. It is based on detailed mapping (e.g. Fig. 6, 7a–c, 8) that exemplifies the conceptual schema reported in Figure 15 of Pehrsson et al. (2013a) for their D_{p3} and D_{p4} events (here promoted to D_{p4} and D_{p5} , respectively). The key difference here is that most of those faults were demonstrably active by D_{p2} and many were reactivated multiple times since D_{p5} deformation (see ‘Post-Dubawnt Supergroup fault reactivation’ section below). Faults that initially were dip-slip extensional during deposition became thrust and reverse faults during D_{p2} deformation and ultimately strike-slip faults during subsequent events, such as the D_{p4} stage of the Hudsonian Orogeny (Pehrsson et al., 2013a; this study) and the 1.63 to 1.54 Ga Racklan Orogeny (Pehrsson et al., 2013b). Only selected folds are traced on maps in this paper, although Figure 3c summarizes the main elements across the study area.

Figure 3c is generalized, but nevertheless represents variations in density of the different fault arrays. The Bathurst array of extensional faults in particular forms clusters, as do the Mackenzie dykes that are spatially associated with it. The P-shears also form clusters, in part reflecting the detail of local mapping, but also reflecting deep underlying ductile fault zones (Anand and Jefferson, 2017a, b). Figure 10 illustrates the complexity of some surface P-shears, cross faults, and fault-controlled sedimentation of the Thelon Formation — in this case where the single Turqavik fault splits into two — its continuation along the northwestern edge of the Turqavik horst, and a northeast-trending structure that can be traced into the Meadowbank River deformation zone.

Development of accommodation space for the Baker Lake Group (lower Dubawnt Supergroup) was spanned by Hudsonian magmatism, strike-slip (D_{p2} and D_{p4}) and extensional (D_{p3}) deformation with M_{p2} to M_{p3} metamorphism. These deformation events took place across the study

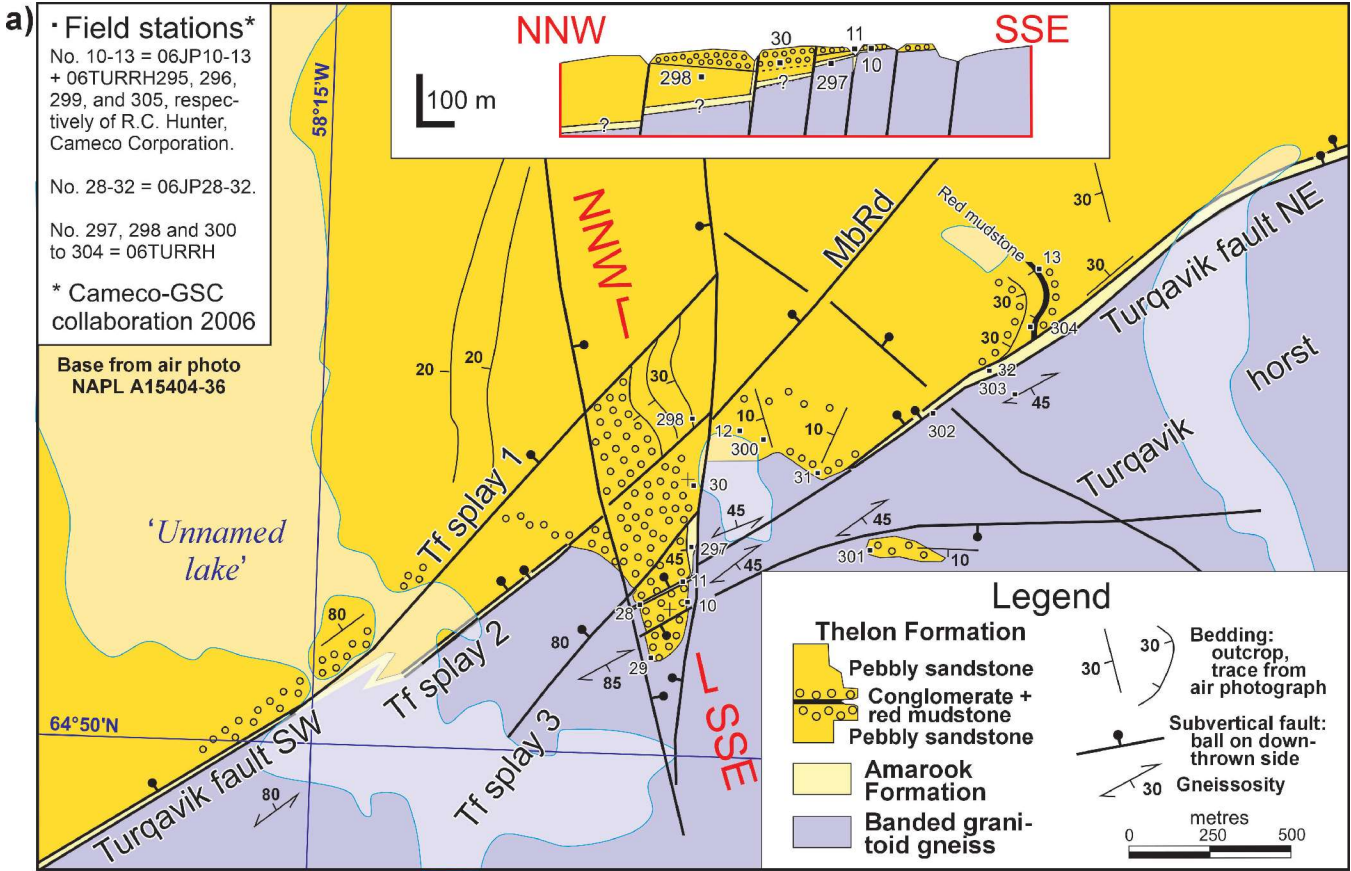


Figure 10. Detailed geology and cross-section of the Turqavik fault near 'Rumble lake'. **a)** Geology of the area outlined in Figure 3a (10). A south-southeast–north-northwest cross-section (top inset) transects the Turqavik fault where the Meadowbank River deformation zone (MbRd) is one of several counterclockwise splays from the Turqavik fault (Tf splay 1, 2, 3). Geological relationships are described further in the text.

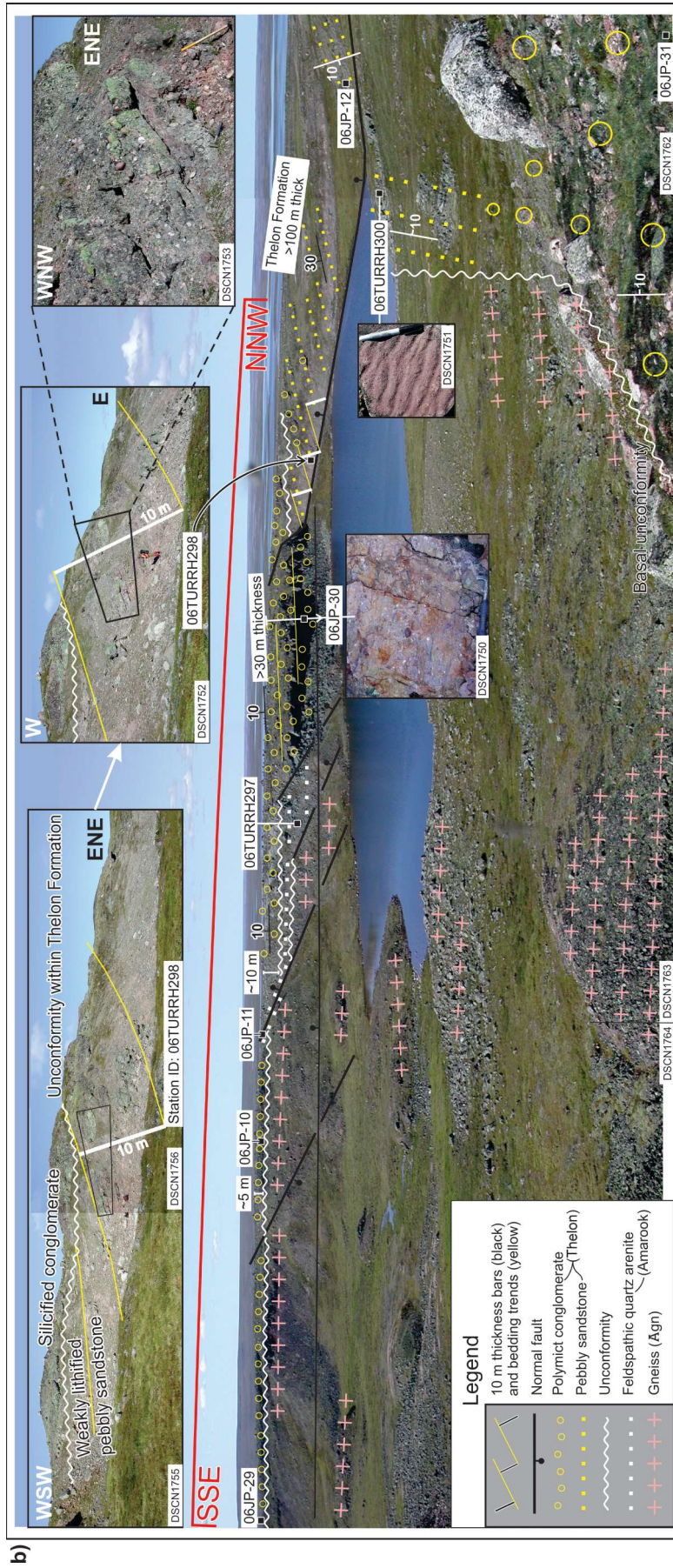
area (Fig. 2, 3a, c). Swarms of Dubawnt minette dykes, equivalent to the minette flows, are intense in places such as south of Aberdeen Lake and around the Amer plutonic complex, suggesting that the Baker Lake Group was deposited in these areas, especially the Christopher Island formation, before deep erosion. Strain was partitioned between en échelon dextral faults. For example, considerable thrust-involved shortening took place on the northwestern side of the Amer medial zone (Fig. 3a, c), but none on its southern side. This transfer of strain between en échelon strike-slip faults is fractal, from outcrop scale (e.g. Fig. 7a–c) up to that of the entire Rae Craton (Fig. 1, 2).

Timing of fault development and reactivation from before D_{p1} to the present

Some faults shown in this paper, e.g. the Medial fault zone of the Amer Belt (Fig. 3a, c) and the Thelon Fault (Fig. 3a, c, 8), were active at least by D_{p1} and many are suspected to have been present during deposition of the early Paleoproterozoic cover sequences (Jefferson et al., 2023; C.W. Jefferson, R.H. Rainbird, G.M. Young, S.S. Gandhi, J.C. White,

V. Tschirhart, D. Lemkow, and L.B. Churlton, work in progress, 2023). Early faults also became inactive through time; for example, early strands of the Amer mylonite zone (Tella and Heywood, 1978) are truncated by 1.75 Ga Nueltin granite of the Amer plutonic complex, but the Nueltin granite body is itself truncated by the youngest main strand that is a graben along much of its length (Fig. 3a, c) and was active long afterward as a dip-slip fault. Fault zones also change in style as the host rocks change, the Nipiterk Fault (Fig. 3c, 7a–c) being an example detailed below.

The major faults within the study area experienced differing offsets along their length, both in magnitude and style, and the offset of many faults is passed on to spatially related faults. The Thelon Fault (Fig. 3a, c, 8) exemplifies this and is particularly significant because it is the northern boundary of the Kiggavik uranium camp. It is well enough documented (Tschirhart et al., 2013b, c; Anand and Jefferson, 2017a, b; Johnstone, 2017; Grare et al., 2018; Hunter et al., 2021; D. Johnstone, K. Bethune, D. Quirt, and A. Benedicto, unpub. rept. no. 15-CND-92-04 of AREVA Resources Canada Inc., 2015) to be formalized here. It is named after the Thelon River and the Thelon Formation. Its immediate southern



side ranges from an imbricated complex of Pukiq Lake formation and Ketyet River quartzite north of the Kiggavik camp, to Schultz Lake intrusive complex west of there, and Marjorie terrane farther west. It trends 060° and dips about 70° northwest, with down-dip slickensides on hematitic gouge indicating northwest-side down. Across the Thelon Fault, the Schultz Lake intrusive complex has an apparent dextral offset of 15 km, much of which is actually dip-slip, given the Schultz Lake intrusive complex dips gently westward (Tschirhart et al., 2013b). The western portion of the fault loses definition within the Thelon Formation beneath Aberdeen Lake, and the eastern end of the fault loses definition where its offset is transferred to a series of thrusts and 090° dextral and dip-slip faults transecting the Schultz Lake klippe. The preservation of metre-scale boulder conglomerate, much coarser than elsewhere in the Thelon Formation, and slivers of Amarook Formation along the interface between the Thelon Formation and basement show that the Thelon Fault was active during deposition of the Thelon Formation. Much of the Amarook Formation along the fault is a milled and silicified tectonic breccia. Silicification of both the Amarook and Thelon formations records multiple events of siliceous fluid flow along the Thelon Fault associated with the Kivalliq igneous suite (Peterson et al., 2010, 2015a) (*see* detailed analysis of epithermal veins along the Judge Sissons and Thelon faults in Hunter et al., 2021). A deep demagnetized zone (D, Fig. 8) represents ductile deformation at depth beneath the brittle outcropping features of the Thelon Fault (Anand and Jefferson, 2017a, b).

The Turqavik fault is another well documented example of reactivation, having experienced successive episodes of dextral motion before deposition of the Thelon Formation, then dip-slip motion during deformation, and subsequently renewed strike- and dip-slip motion over time. The Turqavik fault connects en échelon with the Meadowbank River deformation zone (Fig. 3c). This entire fault system includes dip-slip, strike-slip, and reverse offsets depending on the previously established structural breaks that were reactivated during D_{p2} through D_{p5} deformation events and the directions of maximum compression vis-à-vis the orientation of the pre-existing reactivated fault. The faults also form interconnected to disconnected networks, wherein offsets were passed from one strand to the next, with strands terminating at null points and the deformation accommodated by either folds and/or smaller faults between major faults.

The Nipterk Fault is one such major structure that comprises multiple strands and appears to be a southern en échelon continuation of some of the dextral offset transferred eastward from the Turqavik fault (Fig. 3c). The transfer zone between the Turqavik and Nipterk faults is poorly exposed and essentially unmapped. In better exposed locations along and to the east of the Meadowbank River, some of the Nipterk fault strands are clearly defined by major lithological changes across them, especially a southern one that separates a klippe sheet of Snow Island suite granite south of the fault from complexly interfolded Neoproterozoic and early Paleoproterozoic strata north

of the fault (Fig. 7a). A set of northern strands passes through the ‘Nipterk lake’ area (Fig. 7a–c) and appears to be partitioned along highly elongate and asymmetrical limbs of D_{p1} isoclinal folds, as outlined by sequence Ps1 quartzite of the Ketyet River group. One of many strands that pass through the ‘Nipterk lake’ washout is localized along a 300 m wide unit of highly sheared Ketyet River grey schist (dextral high-strain zone, Fig. 7c). Sharp contacts on its northern and southern margins are defined by outcrops of the complexly folded (D_{p1}) tripartite sequence of the Pukiq Lake formation, Ketyet River quartzite (sequence Ps1), and Ketyet River grey schist (sequence Ps2) (Fig. 7b, c). Other evidence of high strain throughout the ‘Nipterk lake’ washout area includes boudins of quartzite within grey schist and ubiquitous truncated D_{p1} folds.

Depositionally, the Ketyet River group in the ‘Nipterk lake’ area records an early Paleoproterozoic depositional trough, in which many of the structurally repeated quartzite units are very thin with graded bedding. In places, the quartzite is absent, with sequence Ps1 being represented only by 1 to 3 m of matrix-rich schistose conglomerate sandwiched between Pukiq Lake formation and relatively thick Ketyet River grey schist (sequence Ps2). Sedimentary laminae in the grey schist are completely transposed, whereas the quartzite bedding remains distinct, albeit transposed parallel to D_{p1} schistosity. The spatial correlation of these clearly depositional-facies changes with later shear zones is interpreted as a result of syndepositional faults, here and elsewhere, that have since been highly reactivated and disguised by major D_{p1} , D_{p2} , and later shear zones.

Low-angle structural discontinuities are among the most difficult to interpret. Some discontinuities explain extension that created accommodation space for sedimentation, with the Wharton Lake fault system (Fig. 2, 3a, b) being a prime example. This fault system forms a boundary between the undeformed Kunwak formation on the west-southwest and the gently west-dipping highly foliated, highly metamorphosed, and partially melted Marjorie terrane on the east. Peterson et al. (2014) detailed the southern continuation of this low-angle fault system where it wraps 90° counterclockwise around Tebesjuak Lake (northeast of geochronology site 28; Fig. 2). Many similarities between this structure and shallow décollements in the Basin and Range area of the western United States were pointed out by A.N. LeCheminant (pers. comm., 2017). One such example is the Salmon basin detachment fault of Lewis and Burmeister (2013). Further examples of structure and sedimentation are presented in the section entitled ‘Dubawnt Supergroup: structure, sedimentation, and LIPs’ below.

The north-northwest-directed Half Way thrust (Half Way Hills thrust in Pehrsson et al., 2013a) is well defined in its namesake area (Fig. 6), and is extrapolated westward as far as the Granite thrust (Fig. 3a, c), assuming that basalt and major iron-formation as far west as Judge Sissons Lake define its hanging wall as basalt and iron-formation of the Half Way Hills assemblage, with greywacke in its footwall

belonging to the western Pipedream assemblage. The Half Way thrust, as with other D_{p2} structures, is folded by D_{p4} kinks (Fig. 6).

A discontinuity is also required in the Whitehills Lake area between the Ketyet River group and the underlying Snow Island suite sheet because far more structural shortening is documented by isoclinal F_{p1} folds in the Ketyet River group than in the massive Snow Island suite sheet. This discontinuity is interpreted as D_{p1} in origin, but is interpreted to have been reactivated by flexural slip during D_{p2} deformation. This discontinuity is represented by a highly foliated sericitic schist and was first mapped as a thrust by Taylor (1985).

The Granite thrust (Fig. 3a, c, 8) is relatively well defined spatially and geometrically, but is not exposed, and its interpretation here as a thrust is based mainly on its geometry, one logged drillhole intersection, and the much higher metamorphic grade of the hanging wall compared to the footwall. Constraints include surface mapping of highly metamorphosed gneiss and the deep-seated extensive Schultz Lake intrusive complex (1.83 Ga Hudson suite) to the west, with greenschist-facies metavolcanic and metasedimentary units (imbricated Pukiq Lake formation and Ketyet River quartzite) intruded by small, high-level, granite-aplite and subvolcanic syenite plugs to the east. Drill core intersections of the Marjorie terrane Snow Island suite orthogneiss and Schultz Lake intrusive complex together with geophysical models (Tschirhart et al., 2013b) indicate a gentle westward dip. This thrust is one of the younger structures in the study area, as it truncates the D_{p2} Half Way thrust, but further studies are required to constrain precise age and kinematics. Thus, the timing of assembly of the Marjorie terrane with the other Neoproterozoic belts hinges on the age of the Granite thrust.

The gently undulating Pukiq discontinuity separates the western Pipedream assemblage from the structurally overlying panel of mylonitized and imbricated Ketyet River quartzite and Pukiq Lake formation rhyolite (Fig. 3a, 8; Anand and Jefferson, 2017a, b; Johnstone, 2017; D. Johnstone, K. Bethune, D. Quirt, and A. Benedicto, unpub. rept. no. 15-CND-92-04 of AREVA Resources Canada Inc., 2015). Strong extension lineations suggest easterly, low-angle translation of the imbricate panel over greywacke of the Pipedream assemblage. The west-dipping Wolf Fault lies within the same greywacke. The Schultz Lake klippe, first suggested as such by Hadlari et al. (2004), manifests geologically as an area of Ketyet River quartzite and grey schist with complex D_{p1} and D_{p2} structures that are not evident in the immediately surrounding Pipedream and Half Way Hills assemblages of greywacke (McEwan, 2012) and basalt (Fig. 8), respectively. Geophysically, the Schultz Lake klippe is a subhorizontal structure, separated by a low-resistivity zone from more deeply underlying greywacke and a deep Snow Island suite pluton, the domal top of which is modelled as being about 100 to 200 m below surface

(Tschirhart et al., 2013a). The origin and emplacement kinematics of this discontinuity, which appears to be located within the Pipedream assemblage, await further study.

Two low-angle structures shown in Figure 6 are based mainly on geometric relationships, because they are located in very poorly exposed areas, and arose from spatial analysis after fieldwork was completed. The Schultz Inlet discontinuity is drawn mainly along water-covered areas and separates steeply dipping, thick-bedded greywacke (Amarulik assemblage sequence A4) to the northeast from subhorizontally transposed strata of the Pipedream assemblage. Greywacke of Amarulik assemblage sequence A4 lacks iron-formation, has remarkably straight, thick-graded bedding clearly kinked by D_{p4} , and appears to lack D_{p1} and D_{p2} folds, although it has a strong schistose foliation interpreted as S_{p2} , oriented at a high angle to bedding. The Amarulik discontinuity (also named after Amarulik Lake) is not exposed, but spatial analysis of satellite imagery and clear differences in structural style constrain it to the approximate location shown. It underlies a zone of thick till that separates the above-described Amarulik assemblage sequence A4 outcrops from outcrops of chaotically deformed, thin- and transposed-bedded, slaty greywacke with abundant iron-formation of Amarulik assemblage sequence A3a. The sharply defined geophysical anomalies of the complexly folded iron-formation in the latter sequence A3a are consistent with it being structurally above, albeit older than, Amarulik assemblage sequence A4.

Timings and origins of D_{p1} and D_{p2} in the northeast Thelon region

Pehrsson et al. (2013a) first recognized D_{p1} events as limited to the Archean and sequences Ps1 to Ps3 and not affecting sequence Ps4. As D_{p1} predated deposition of sequence Ps4 with detrital zircon as young as 1.9 Ga, they proposed that D_{p1} deformation took place during the Snowbird event, an early (1.9–1.865 Ga) accretionary phase of the Hudsonian Orogeny (Berman et al., 2007; Thiessen et al., 2020). They further proposed that continuation of the Snowbird collision shed detritus northwestward to fill a foreland trough in the Whitehills Lake area with sequence Ps4 flysch that incorporated eroded D_{p1} -affected rocks. Jefferson et al. (2015, 2023) and C.W. Jefferson, R.H. Rainbird, G.M. Young, S.S. Gandhi, J.C. White, V. Tschirhart, D. Lemkow, and L.B. Chorlton (work in progress, 2023) expanded the deep proximal foreland interpretation of the Ketyet River sequence Ps4, northwestward into the Amer Belt, where it is manifested as both deep-water flysch and alluvial redbed molasse (*see* Table 1 and ‘Early Early Paleoproterozoic cover sequences: Amer, Ketyet River, Montesor, and western belts’ section above).

Soon after deposition, sequence Ps4 became caught up in the advancing Hudsonian Orogeny. Sequence Ps4 was first regionally folded and thrustured at upper crustal levels during

the early stages of northwest-vergent D_{p2} deformation. This deformation is inferred to have started at about 1.87 Ga, 30 Ma before peak metamorphism at 1834 ± 5 Ma (Pehrsson et al., 2013a, with reference to Berman et al., 2010). Because sequence Ps4 rested mainly in the upper part of a crustal pile, peak metamorphism in sequence Ps4 rarely exceeded lower-greenschist-facies metamorphism. The only Hudsonian magmatic products to transect the folded sequence Ps4 are undeformed hypabyssal minette dykes, Martell syenite plugs, and possible shonkinite pipes. At Whitehills Lake, Martell syenite plugs intrude the Ketyet River sequence Ps4C in the core of the Whitehills synform and Hudson granite cuts fine-grained clastic rocks east of the lake that may include sequence Ps4 (see Table 1 and ‘Early Paleoproterozoic cover sequences: Amer, Ketyet River, Montresor, and western belts’ section above). A minette swarm transects the R22 (R, Fig. 3a) uranium prospect, sequence Ps4 in the Tahiratuq synform, and the Medial zone of the Amer Belt without offset (Fig. 3a). Although the R22 minette dykes are undated, they are petrochemically related (Peterson et al., 2011) to minette flows in the Baker Lake Basin that range in age from 1.83 to 1.81 Ga (Rainbird et al., 2003a, 2006), suggesting a 1.83 to 1.81 Ga upper age limit on folding and strike-slip deformation along the Amer medial zone.

An added recognition is that the Dubawnt minette dykes geologically separate the redbeds of sequence Ps4 from the younger redbeds of the Baker Lake Group that are bracketed between the 1.83 to 1.81 Ga minette flows. The following distinctions support this separation in age between sequence Ps4 and the Baker Lake Group. The minette dykes in the Baker Lake Basin are in the order of 5 to 10 m thick and associated with sodic hydrothermal alteration and uranium mineralization in the adjacent Kazan Formation redbeds, suggesting that the dykes intruded soon after sedimentation (Stanton, 1979). In contrast, the minette dykes that cut the Amer Belt are only 1 to 3 m thick and have little if any adjacent hydrothermal alteration, indicating that the host strata were well lithified with low porosity long before the time of intrusion.

Parallel studies of the Dodge–Snowbird Domain (Thiessen et al., 2020) and Murmac Bay group (Card et al., 2007, 2014; Bethune et al., 2013) southwest of the study area (Fig. 1) provide analogies for the origins and extents of D_{p1} and D_{p2} events in the study area. Many elements of D_{p1} in the Dodge–Snowbird and western Beaverlodge domains are represented by D_{p1} in the Amer Belt, as detailed by Calhoun et al. (2014): early low-angle translation, northeast-vergent folding and refolding, lack of magmatism, gravity-driven translation of cover rocks over basement, as well as low-angle translation within the deforming sedimentary pile. In those areas and in much of the study area the D_{p1} structures are orthogonal to the D_{p2} structures; however, the deformation in those southern regions was too far removed (400 to 700 km) from the northeast Thelon Basin region to have been directly involved in the development of D_{p1} and D_{p2} structures in the study area.

Dubawnt Supergroup: structure, sedimentation, and LIPs

In this section, the accommodation and preservation of three successive groups of the Dubawnt Supergroup as a result of regional to local strike- and dip-slip faulting are reviewed. The stratigraphic and temporal associations of these groups with large igneous provinces (LIPs) are discussed above. The first group, the Baker Lake Group, developed in two stages (Rainbird and Davis, 2007; Hadlari and Rainbird, 2011). The first stage filled a series of elongate, deep, asymmetric sub-basins of northwest-dipping half-graben style, with four thick sequences of intercalated minette volcanic (Christopher Island formation) and arkosic siliciclastic rocks (South Channel, Angikuni, and Kazan formations). The second stage of subsidence accommodated the youngest and thinnest sequence of the Baker Lake Group — the Kunwak formation, comprising conglomerate, felsic minette domes, and associated calcite travertine, and largely confined to the interior of the Baker Lake Basin half-graben (Hadlari and Rainbird, 2011), with a major exception to the west and southwest, where the Kunwak formation appears to be the only unit of the Baker Lake Group present (see below).

The Granite thrust and a major late 140°-striking fault, largely covered by till and Princess Mary Lake, cut off the southwestern end of the main Baker Lake Basin. The Marjorie terrane to the west underlies the broad, 000°- to 020°-trending Marjorie horst. The Wharton Lake fault system (Fig. 2, 3a, c) delimits the western side of the Marjorie horst, flanked by an apparently thick package of the Kunwak formation that fills an east-dipping half-graben underlying the southern part of Wharton Lake and continuing to the southeast. The Granite thrust delineates the eastern side of the Marjorie horst (Fig. 3b; not to be confused with the Marjorie–Kiggavik–Tehek Belt labelled in Fig. 3a). The Marjorie horst narrows northeast of the Thelon Fault to become a northwest-dipping panel in the hanging wall of the Granite thrust and then terminates against the Turqavik horst (Fig. 3b). The western contact of the Kunwak package at Wharton Lake is unstudied, but the map pattern suggests an unconformity that overlaps gneiss, quartzite, and Snow Island suite granite west of Wharton Lake. Based on gently dipping lineations observed in the 1980s (LeCheminant, 1981), A.N. LeCheminant (pers. comm., 2012) suggested that the Wharton Lake fault system is a low-angle slide structure that accommodated significant extension toward the west, consistent with the half-graben interpretation for the Kunwak accumulation.

Based on comparisons of metamorphic ages with magmatic and volcanic ages (e.g. Pehrsson et al., 2013a), the Baker Lake Group depositional events spanned the ages of D_{p2} compressive deformation and metamorphism in basement terranes flanking the Baker Lake Basin. The entire history of the Baker Lake Basin is therefore interpreted as a series of classic pull-apart basins that developed during overall dextral transpressional orogenesis. Hadlari and Rainbird (2011)

comprehensively discussed alternative theories that focus on the half-graben style of the basin, with a significant master fault along the southeastern side and smaller faults on the northwestern side. The primary development of the basin was obscured by renewed faulting during deposition of the Thelon Formation that resulted in accumulation of Thelon Formation sandstone toward the northwestern side of the basin, accommodated by renewed offset along smaller faults within the larger Baker Lake Basin, and no sedimentation along the former southeast-side master fault.

Active faulting and deformation ceased at the end of the Hudsonian Orogeny and the entire study region became quiescent. A prolonged period of peneplanation and oxidative paleoweathering predated gentle regional subsidence that accommodated eolian sands covering a thin regolith (Amarook Formation of the Wharton Group). Moderate local faulting, interpreted from local conglomeratic alluvial deposits higher in the Amarook Formation, was possibly a result of differential uplift and local faulting caused by magma injection at the start of the 1.75 Ga Kivalliq event. Tectonism during magmatism and sedimentation of the Kivalliq large igneous province left a number of structural features that record reactivation of previously established fault systems, as outlined in Jefferson et al. (2013). Nueltin granite plugs and pancakes intruded preferentially along fault zones (e.g. finger shapes northeast of Dubawnt Lake and round plutons along the trend of subbasins constituting the overall Baker Lake Basin shown in Fig. 2; see circular anomalies N_A, N_B, and the exposed Mallery plug N_M described in detail in Peterson et al., 2015a, b). Preservation of the high-level pancake-shaped intrusions was affected by renewed movement on those same faults (Jefferson et al., 2013), with some pancake-shaped intrusions being thinner on one side of the fault or preserved only on one side (Apc_N in Fig. 3a; 'Nueltin granite of the Amer plutonic complex' in Fig. 3c). The circular anomalies representing volcanic centres form arrays that coincide with fault zones and overall are restricted to a wedge interpreted as a craton-scale graben that predated development of the Thelon Basin. The areas of preservation of the Pitz Formation are restricted to a large blanket south of Aberdeen Lake, westward under the main Thelon Basin, and lesser areas along the northwestern side of the Baker Lake Basin. These represent fault reactivations that redeveloped existing and new grabens under weak, but resumed dextral transpression.

Another major period of quiescence, peneplanation, and deep oxidative paleoweathering postdated the Wharton Group and the second large igneous province. Gall (1992, 1994) interpreted this pre-Thelon Formation paleosol as part of the Matonabee unconformity that extended across the northwestern Canadian Shield. The Barrenland Group, equivalent to the Athabasca Supergroup, constitutes the upper third of the Dubawnt Supergroup and lacks igneous rocks except for the Kuungmi lavas. The Thelon Formation, preserved in the western Baker Lake Basin and forming the dominant fill of the Thelon Basin (Fig. 2), yields evidence of significant

transtensional faulting before, during, and after sedimentation, with the best knowledge base being of the Aberdeen Subbasin (Fig. 3a–c). The relationships between faulting and sedimentation are discussed below, with reference to Figure 3c for the overall subbasin.

At the regional scale, the Aberdeen Subbasin is interpreted as a pull-apart structure caused by differential extension between major strike-slip faults: the 030°- to 045°-striking Chantrey mylonite zone to the west, the sub-parallel Turqavik fault transecting the subbasin, and the 060°- to 090°-striking Thelon Fault to the east. These faults are significantly reactivated, previously existing faults, with brittle to ductile structures exposed at surface, transitioning to deep-seated demagnetized shear zones at depth. Well exposed parts of the Turqavik fault are discussed in the 'Tectonics and structure during sedimentation of the two basins' section below, with reference to Figures 1, 2, and 3c. Multiple orientations of other pre-existing faults were also reactivated around, and within, the Aberdeen Subbasin during this process. New faults also developed, in particular a 100° to 140° array (yellow-orange lines, Fig. 3c) that steps down toward the northeast on the southwestern side of the Subbasin and toward the southwest on the northeastern side of the Subbasin. Outcrops along the northeastern margin of the subbasin include paleofault scarps of this orientation (yellow-orange line at 65°N and 98°W in Fig. 3c) with a very coarse paleotalus breccia of silicified Amarook Formation arkose overlapped by nonsilicified conglomerate of the Thelon Formation, much like at 'Unconformity lake' (unofficial name) (Fig. 8; Fig. 7 of Anand and Jefferson, 2017b).

Post-Dubawnt Supergroup fault reactivation

Preservation of the Thelon Basin required continued or retained subsidence through subsequent geological events. The extension of many basement faults as distinct topographic lineaments across the Thelon Basin and the en échelon off-sets of individual Mackenzie dykes, where they cross faults, show that many faults were reactivated after lithification of the Thelon Formation. Even later reactivation is shown by the preservation of the Ordovician limestone in a small graben between 050° and 140° faults; by the presence of fresh, post-glacial ferricrete breccia (Fig. 5b) beside a reactivated fault strand of the Amer medial zone (Fig. 3a, c); a fault and fold system along the axis of the Amer grand synform (Fig. 3b) north of upper Amer Lake; by postglacial topographic scarps, such as along the Thelon Fault (Fig. 8) and Turqavik fault (Fig. 10a); and by the presence of pockmarks in lakes.

Pockmarks are decimetre- to metre-scale mud volcanoes that generate low-amplitude sediment cones in lake-bottom mud. Some of these actively vent radon throughout the year, resulting in ice-free sites with natural radiometric anomalies, such as at 'Screech lake' (unofficial name) (northeast of Boomerang Lake, Fig. 2). The continuous release of small amounts of gas and water through these vents shows the potential for groundwater flow along reactivated faults,

despite the presence of permafrost. The first author has observed pockmarks like those at ‘Screech lake’ in a number of lakes in the northeast Thelon Basin study area, including northwestern ‘Rumble lake’ (Fig. 3a) and the southern part of the Schultz Lake klippe (SLk Fig. 3a).

THEMATIC COMPARISONS OF THE THELON AND ATHABASCA BASINS

The following comparisons are roughly in order by decreasing age, beginning with basement compositions and magmatic events, followed by structural geology preceding and during sedimentation of the Thelon and Athabasca basins. The comparisons continue with diagenesis and hydrothermal processes that led to, and constrained, the locations and sizes of their respective uranium endowments. Table 1 summarizes the *events* in chronological order, oldest at bottom and youngest at top, whereas Table 3 summarizes the *comparisons* in the opposite order of oldest at top and youngest at bottom. The first-order comparisons between the two regions are based mainly on this study and on information presented in the EXTECH IV bulletin that was co-published by the GSC, Saskatchewan Geological Society, and Mineral Deposits Division of the Geological Association of Canada (Jefferson and Delaney, 2007). Particularly relevant papers were those of Card et al. (2007), Ramaekers et al. (2007), and Yeo and Delaney (2007), with reference to Figures 1, 2, and 11 of this paper. More recent studies provide additional citations on a case-by-case basis.

Basement domains and rock types

Archean and early Paleoproterozoic basement

The Athabasca Basin blankets the intersections of three major cratonic domains. The western Hearne Craton comprises the Wollaston and Mudjatik supracrustal domains that underlie the eastern third of the Athabasca Basin. The south Rae Craton underlies the north-central sixth of the Athabasca Basin and is lithologically diverse, comprising the fault-bounded Nolan, Zemlak, Beaverlodge (Martin Basin), Ena, Train Lake, Dodge, and Tantato domains. The Taltson magmatic zone includes extensive linear supracrustal belts, abuts the Zemlak Domain in the north and wraps around the other domains of the Rae Craton beneath the western and southwestern Athabasca Basin (Tschirhart et al., 2021), abutting the Mudjatik Domain of the Hearne Craton along the Virgin River shear zone. The Taltson magmatic zone and the Taltson Orogeny in the Murmac Bay Group (MBG, Fig. 1) are distinct from the Thelon Orogen that took place farther to the northwest, in the reworked collision zone between the Slave and Rae cratons (Card et al., 2014).

In contrast, the Thelon Basin rests only on rocks of the Rae Craton. The Thelon Formation unconformably overlaps the Wharton and Baker Lake groups in the northwestern part

of the Baker Lake Basin. The suture between the south Rae and south Hearne cratons follows the Snowbird tectonic zone (Stz, Fig. 1, 2), east of the Thelon Formation, with the Hearne Craton representing a possible distal, eastern provenance area. At Angikuni Lake, the northeast trajectory of the Snowbird tectonic zone loses definition, and northeast-continuing faults such as the Tulemalu are mainly extensional, related to development of the Baker Lake Basin (Hadlari and Rainbird, 2011). Starting at Angikuni Lake, the north-dipping Tyrrell shear zone (Tsz, Fig. 1, 2) separates the Chesterfield Block of the Rae Craton from the structurally underlying northern Hearne Craton. Here, the Chesterfield Block represents the main basement detrital provenance area for most of the Baker Lake Basin. The eastern portion of the Tyrrell shear zone is a complex imbricate zone involving early Paleoproterozoic (?) sequence Ps4 and Neoproterozoic strata (Lawley et al., 2016) that represent additional possible sources of detritus for the Dubawnt Supergroup in the Baker Lake Basin.

In both regions, the Archean comprises both granitoid gneiss and supracrustal belts. The Archean supracrustal belts around the Athabasca Basin are highly metamorphosed and interleaved with gneiss (Card et al., 2007), with little representation of the 2.6 Ga Snow Island suite (Peterson et al., this volume). In contrast, the Archean around the Thelon Basin comprises diverse assemblages of Neoproterozoic supracrustal rocks in the Woodburn Lake group and a high proportion of Snow Island suite foliated granite, with older basement gneiss being restricted to the Akutuak River and Chesterfield gneiss belts.

Favourable basement host rocks for unconformity-related uranium deposits

Card et al. (2007) interpreted the basement beneath the Athabasca Basin to consist of rocks that outcrop within the Rae and Hearne cratons. Pyritic-graphitic conductors spatially underlie and/or host all of the major basement-hosted unconformity-related uranium deposits in the Athabasca Basin (Jefferson et al., 2007a, b, c). Most such conductors consist of fine-grained siliciclastic schist at amphibolite-facies grade and are key lithological components of the basement supracrustal assemblages in all three domains. An exception is the Patterson Lake corridor, where the conductive, ore-hosting graphitic-pyritic shears are located within orthogneiss or altered ultramafic–mafic intrusions (Armitage, 2013; Card, 2017; Tschirhart et al., 2018; Potter et al., 2020).

The Neoproterozoic Woodburn Lake group of the northeast Thelon Basin region includes graphitic schist with conductors that have been drilled south of Schultz Lake (Heart Lake core logged by first author). The weakly mineralized amphibolite-facies grade, graphitic metapelite zone at Boomerang Lake (F conductor trend, Fig. 2 of Beyer et al., 2010) may also be Archean in age. The subparallel, but nonmineralized

conductor (G trend, Fig. 2 of Beyer et al., 2010) has very low metamorphic grade and is spatially associated with quartzite, here correlated with the Paleoproterozoic sequence Ps1 quartzite of the Amer or Ketyet River belts (Fig. 2). Although Card et al. (2007) did not recognize Archean supracrustal rocks in drill core, it is possible that some conductors under the northeastern and eastern Athabasca Basin could be associated with Archean supracrustal belts of the Beaverlodge, Tantato, and Mudjatik domains (Fig. 1).

Conductive Paleoproterozoic units below the Thelon Basin are mainly slate grade and impermeable, despite intense polyphase folds and thrusts. Drilling has not resulted in discovery of any significant uranium occurrences associated with conductors (G. Drever, pers. comm., 2008). Instead, the best-known uranium deposits (Kiggavik Main, Kiggavik Centre, Kiggavik East, Bong, End, and Andrew Lake (Jefferson et al., 2007a, b, c; Gandhi et al., 2015)) in the Aberdeen Subbasin region (Fig. 2, 3a, 8) are hosted mainly in pyritic greywacke and epiclastic rocks of Neoproterozoic age — the Pipedream assemblage and Pukiq Lake formation. Hunter et al. (2012, 2014) described several discoveries (Ayra, Qavvik, and Tatiggaq) hosted by pyritic paragneiss of the upper two Aberdeen assemblages. The Neoproterozoic metasedimentary hosts appear to be most prospective where intruded and altered by Hudson suite and Kivalliq igneous suite magmatic and hydrothermal systems.

Basement magmatic suites

The pre-1.74 Ga basement terranes of both basins contain records of three bimodal LIPs that are predominantly felsic in terms of volume as exposed. Each magmatic suite represents a potential source of uranium as discussed below. The first of these was the 2.6 Ga Snow Island suite that affected large portions of the Rae Craton, but not the adjacent Hearne Craton (Peterson et al., 2015c, this volume). In the case of the Thelon Basin, the Snow Island suite surrounds and underlies the basin, and the distribution of the Pukiq Lake formation rhyolite beneath most of the Paleoproterozoic sequence Ps1 quartzite suggests that the Pukiq Lake formation blanketed much, if not all, of the craton in the Thelon Basin region before uplift and erosion after the Hudsonian Orogeny. The dominant felsic component of this bimodal volcanic unit represents a widespread, readily dissolved source of uranium brought to the surface at 2.6 Ga. The volumetrically far larger granitoid rocks of this suite represent an immense reservoir of uranium and thorium, albeit mainly in refractory minerals, although monazite is demonstrably leachable (*see* ‘Alteration and metallogenic comparisons of the Athabasca Basin and Thelon Basin regions’ section below). In the case of the Athabasca Basin, the main basement block containing the Snow Island suite is the south Rae Craton, with a few 2.6 Ga zircon ages in drill core from the Mudjatik Domain (western Hearne Craton; Fig. 1 in Peterson et al., this volume). Furthermore, paleocurrent and provenance analysis (e.g. Ramaekers et al., 2007) showed that the eastern Athabasca Basin received

little detritus from this wedge of the Rae Craton. In contrast, the Fair Point Formation, restricted to the Jackfish Subbasin in the western part of the Athabasca Basin, was sourced in part from the northeast. This provenance region includes the south Rae Craton and is reflected in a substantial population of 2.61 to 2.52 Ga detrital zircon in the Fair Point Formation (Rainbird et al., 2007). In the case of the Thelon Formation, erosional products of the surrounding Snow Island suite should comprise a significant proportion of its basin fill and, indeed, ca 2.6 Ga zircon constitutes the largest population in the lower two sequences (Palmer et al., 2004).

Granitoid rocks of the 1.84 to 1.81 Ga Hudson suite are present on all sides and beneath both basins. The Thelon Formation also sourced from the extensive ultrapotassic Dubawnt minette dyke swarm and Christopher Island formation, whereas the Athabasca Basin sourced from only the much smaller and less potassic lamprophyre dykes and mafic flows in the Beaverlodge Domain north of the basin. The 1.84 to 1.81 Ga magmatism represents a second major movement of deep crustal sources of uranium to the surface, albeit mainly in refractory minerals, but here again the monazite was demonstrably leached (*see* ‘Alteration and metallogenic comparisons of the Athabasca Basin and Thelon Basin regions’ section below). Sedimentary depocentres of the Athabasca and Thelon basins are mostly offset from the depocentres of the 1.84 to 1.81 Ga strike-slip siliciclastic and volcanic basins that developed during Hudsonian deformation. Paleocurrent data of Ramaekers et al. (2007) indicated that the Athabasca Basin received little recycled detritus from the 1.83 Ga Martin Basin, except along its northern edge. Nonetheless, detrital zircon of 1.84 to 1.81 Ga age are abundant in the Manitou Falls Formation of the eastern Athabasca Basin, as are ca. 2.58 Ga zircon interpreted as derived from the Hearne Craton (Rainbird et al., 2007). On the other hand, the Baker Lake Basin, with its voluminous ultrapotassic and uranium-thorium-rich volcanic strata, was located ‘upstream’ to the east during Thelon Basin sedimentation, although little coarse clastic material can be specifically identified as sourced from the Baker Lake Group. Thus, it is somewhat surprising that 1.84 to 1.81 Ga detrital zircon represent only a tiny population in the Thelon Formation (Palmer et al., 2004).

The 1.75 Ga Kivalliq igneous suite represents a third possible magmatic source of uranium brought to the surface by hypabyssal intrusions and volcanism. Around the Athabasca Basin, there is scant lithological evidence of the Kivalliq igneous suite in outcrop, however Peterson et al. (2015a, b) documented geochronological evidence in several places and C.D. Card (pers. comm., 2015) pointed out a number of magnetic ring structures like those documented by Jefferson et al. (2013) and Tschirhart (2017) for the Kivalliq Region of Nunavut. Nevertheless, detrital zircon studies by Rainbird et al. (2007) in the Athabasca Supergroup and Palmer et al. (2004) for the Thelon Formation yielded scant results of this age in the Athabasca Basin and none in the Thelon Basin, respectively.

Table 3. Geological and geophysical comparisons between the Athabasca and Thelon basins, with oldest attributes at the top and youngest at the bottom (*after* Miller and LeCheminant, 1985; Gandhi, 1989; Jefferson et al., 2007a, Table 3). The section entitled 'Thematic comparisons of the Thelon and Athabasca basins' provides detail on the more favourable attributes for uranium mineralization. Figure 11 illustrates some of these metallogenic similarities and differences between the two basins.

Attributes	Athabasca	Thelon
Uranium-bearing igneous basement rocks (names in text)	Snow Island, Hudsonian, and Kivalliq granitoid rocks	Snow Island, Hudson, and Kivalliq suite granitoid rocks and Pitz Formation volcanic rocks
Uranium as one element of polymetalliferous carbonaceous metapelite in basement rocks of district	In Wollaston Supergroup (Yeo and Delaney, 2007). General geographic spatial association with U deposits, amphibolite-facies metamorphism facilitated alteration (Reid et al., 2014; Reid, 2018).	In Archean Pipedream assemblage and Paleoproterozoic Amer, Montesor, Ketyet River, and western belts, but not associated with U. Slate grade to lower-greenschist facies. Fine grain size = unaltered, therefore tight.
Stratabound uranium, copper and magnetite in sandstone	Cu > U in Janice Lake formation (Yeo and Delany, 2007; Forum Energy Metals, 2021)	U > Cu in Showing Lake fm, Amer group only (Young, 1979; Gandhi et al., 2015; Jefferson et al., 2015, 2023; C.W. Jefferson, R.H. Rainbird, G.M. Young, S.S. Gandhi, J.C. White, V. Tschirhart, D. Lemkow, and L.B. Chorlton, work in progress, 2023)
Bimodal 1.75 Ga Kivalliq igneous suite (Kis) (see silicification next row)	Kis yes, but cryptic igneous products (Card, 2014; Peterson et al., 2015a).	Abundant granite, minor gabbro, extensive diabase dykes, bimodal volcanic strata (Peterson et al., 2015a); alteration of Hudson suite (Scott et al., 2015).
Pre-ore (1.75 Ga) basement alteration and surficial silica hotspots associated with Kis	'Quartzite ridges' represent long-lived conduits for fluid flow (Card, 2014). Chert stromatolite fragments in flank breccia (Yeo et al., 2007).	Silicification 1.75 Ga focused along fault zones, e.g. Thelon and Judge Sissons. Pristine chert stromatolites (Fig. 5e; Peterson et al., 2015a).
Other favourable basement host rocks and events (Thelon names explained in text)	Amphibolite- to granulite-facies grade metasedimentary gneiss of Taltson magmatic zone in Carswell and Patterson Lake areas.	Greenschist-facies grade pyritic metagreywacke (Pipedream, Amarulik assemblages) + felsic epiclastic rocks (Pukiq Lake fm) + amphibolite-facies grade paragneiss (Marjorie terrane)
Matonabee unconformity at base of basin (Gall, 1992)	Deeply paleoweathered: hematitized, clay altered	Deeply paleoweathered: hematitized, clay altered
Maximum age of sedimentation	Ca. 1.75–1.69 Ga	Ca. 1.75–1.69 Ga
Intersecting fault arrays, reactivated before, during, and after sedimentation	Fractal Riedel-shear arrays (Wright and Potter, 2014; Tschirhart et al., 2017) + low-angle reverse (e.g. Györfi et al., 2007)	Fractal Riedel-shear arrays (Fig. 9; Anand and Jefferson, 2017a, b) + low-angle detachments (e.g. Pukiq Fault, Fig. 8)
Fault-controlled local subbasins associated with deposits	McClellan Lake, McArthur River, Key Lake, not Cigar Lake. Based entirely on drill and open-pit data.	Present; no known associated deposits beneath main expanses of Thelon Formation, but Ayra occurrence underlies small outlier that may record a subbasin.
Sandstone and conglomerate originally arkosic redbeds	Now mostly pale tan to grey, but quartz overgrowths preserve hematite; still redbeds at base.	Overall pale pink-tan colour preserved, redbeds best preserved in finer sections, especially at base.

Table 3. (cont.)

Attributes	Athabasca	Thelon
Youngest sedimentation	<ca. 1.54 Ga	<ca. 1.54 Ga
Quantitative stratigraphy unique to each basin, except both mainly siliciclastic and topped by carbonate. Units preceding carbonate very different, but same age in both basins.	Unconformities bound Fair Point, Read-Smart, Manitou Falls, and Lazenby Lake fms. Deep red beds only in Read and Smart fms. Douglas Fm carbonaceous mudstone 1.54 Ga (Creaser and Stasiuk, 2007).	Simpler stratigraphy with only Thelon (3 upward-fining siliciclastic sequences), gap of unexposed possible unit(s), Kuungmi ultrapotassic mafic lavas 1.54 Ga (Chamberlain et al., 2010)
Cap carbonate formations	Marine-shelf stromatolitic Carswell dolostone prograded over euxinic shale basin, not much silicification. Well preserved albeit overturned.	Marine shelf stromatolitic Lookout Point dolostone prograded over subaerial potassic-mafic lavas and tuffs. Silicified and karst brecciated.
Basinwide clay alteration	Dickite + illite, strong bleaching and dequartzification.	Illite, moderate bleaching and dequartzification.
Illite incorporates Mg and Fe in basement-alteration settings		
Eolian sandstone	Suggested in places by bimodal grain-size distribution; no large eolian crossbeds observed.	With one possible exception, eolian crossbeds are all in Amaroook Fm, unconformably below Thelon Fm.
Syn-ore basement alteration (APS = aluminum phosphate sulphate)	Chlorite-illite±sericite-dravite-APS-fluorapatite, SiO ₂ removal	Chlorite-illite±sericite-APS 1, 2, 3-fluorapatite, SiO ₂ removal
APS depleted in U and heavy REEs occupy sandstone matrix along altered heavy mineral laminae (Mwenifumbo and Bernius, 2007; Davis et al., 2011). Locally replaces basement monazite (Madore et al., 2000). See also above.		
U-fluorapatite cement (Davis et al., 2011, 2012; Miller et al., 1989; Rainbird et al., 2003b, 2007).	1638 ± 5 Ma in basement through sandstone, up to and including the 1644 ± 13 Ma Wolverine Point Fm.	1667 ± 5 Ma in basement through Thelon Fm in Aberdeen Subbasin; 1688 ± 14 Ma at Boomerang Lake.
Peak diagenetic and/or hydrothermal temperatures	~240°C	~200°C
Corroded zircon grains near ore	Local	Unknown
Regional well preserved detrital zircon grains		
Bleaching and clay-alteration fronts		
Uranium hosted by sandstone or unconformity assemblage	Yes, generally above basement-hosted deposits.	Boomerang Lake is weak example.
Basement-hosted uranium	Largest deposits	The only known deposits
Significant deposits	Largest and highest grades in world.	1 to 3 orders of magnitude smaller.

The Hudson and Kivalliq LIPs also had associated site-specific hydrothermal alteration effects, the descriptions of which are included in the 'Alteration and metallogenic comparisons of the Athabasca Basin and Thelon Basin regions' section below.

Comparative stratigraphy of the Athabasca Supergroup and Barrenland Group

Although there have been many stratigraphic advances in the Athabasca Basin (Fig. 1) since Ramaekers et al. (2007) and Yeo et al. (2007), those papers remain sufficiently current for the purpose of comparing the Athabasca Supergroup with the Barrenland Group of the western Baker Lake Basin and the Thelon Basin. After prolonged peneplanation and paleoweathering across the entire western

Canadian Shield (D_{p6a} , Table 1; Matonabbee unconformity of Gall, 1992), multiple sequences of similarly arkosic lithic quartzose sandstone filled the Athabasca and Thelon basins (D_{p6b} , Table 1). At even a gross scale, their multiple clastic sequence boundaries and the minor volcanic and carbonate components reflect complex and different depositional histories. These resulted from different tectonic and structural histories that are compared in the next section.

Four major siliciclastic sequences constitute the Athabasca Supergroup that fills the Athabasca Basin. Each sequence fines upward, each has significantly different subbasin configurations and paleocurrent patterns, and each rests on basinwide unconformities. The Wolverine Point Formation, basal unit of the third major sequence, includes minor felsic tuff dated at 1644 ± 13 Ma (geochronology site 52, Table 2; Rainbird et al., 2003b, 2007). Together the four sequences fill a single

basin with no major lateral breaks. The maximum thickness at any one place is about 1500 m, although the aggregate of the maximum thicknesses of the four sequences is far greater.

The Barrenland Group of the Baker Lake and Thelon basins is the main equivalent of the Athabasca Supergroup. The Thelon Formation, the basal siliciclastic and main unit of the Barrenland Group, constitutes a single major sequence with three upward-fining subsequences and no internal unconformities, and is best compared with the initial two sequences of the Athabasca Supergroup. It fills three subbasins separated by major basement horsts described below. It is the only formation of the Barrenland Group in the western Baker Lake Basin and Aberdeen Subbasin, and it constitutes most of the large western oval of the Thelon Basin. Its paleocurrents trace a single, large fluvial system that flowed west-northwestward through the Baker Lake and Aberdeen subbasins, then curved southwest to follow the axis of the main western basin. Subsidiary paleocurrents vector toward this axis from both sides (Jefferson et al., 2011a).

The Thelon Formation paleocurrent trends follow the axes of greatest seismic thickness as contoured by Overton (1979). Although he presented his stratigraphic thicknesses as undivided Dubawnt Group (now Dubawnt Supergroup), analyses such as those done by Davis et al. (2011) and Tschirhart et al. (2013c, 2014, 2017), and drill core logged by the first author showed that the Overton (1979) undivided thicknesses for the Thelon Basin are essentially those of the Thelon Formation. The point of greatest thickness (>1800 m) is within the Thelon Basin and coincides with the sole outcrops of the Kuungmi ultrapotassic lavas. These in turn also coincide with the intersection of the McDonald and Bathurst faults (Fig. 1) — the apex of the Slave indenter (first pointed out by P. Ramaekers, pers. comm., 2007). Thus, it can be inferred that those two major fault systems influenced the depth of the Thelon Basin, especially where they intersect. Most of the Thelon Basin at that point is inferred to be Thelon Formation.

In the area of the Aberdeen Subbasin, outcrops around its margins suggest that more than the Thelon Formation contributed to its fill. On the southern margin, unknown thicknesses of sequence Ps4 (in the Beverly Lake area), Amarook Formation, and Pitz Formation are inferred at depth. On its northern margin, no Pitz Formation is exposed and therefore none is inferred at depth. On the other hand, the Amarook Formation is exposed in many places along the northern and eastern sides. One drillhole intersects the Amarook Formation (Davis et al., 2011), and many drillholes intersect limited sections of the Amer sequences Ps1 to Ps3 and Amer sequence Ps4 (Appendix B of C.W. Jefferson, R.H. Rainbird, G.M. Young, S.S. Gandhi, J.C. White, V. Tschirhart, D. Lemkow, and L.B. Churlton, work in progress, 2023). As shown by Tschirhart et al. (2014, 2017), the seismic velocities of the Amarook Formation and the underlying Amer sequence Ps4 strata are indistinguishable. Therefore, the individual stratigraphic contributors

to the undivided depths determined by Overton (1979) in the three areas of preserved Thelon Formation can only be crudely inferred from the adjacent outcrops and the limited drill intersections.

Nevertheless, drill core logs from the Aberdeen Subbasin and the Boomerang Lake area enabled Hiatt et al. (2003) to define three upward-fining siliciclastic sequences in the Aberdeen Subbasin. Davis et al. (2011) quantified those sequences by grain-size analysis using the same techniques established for the Athabasca Basin by Ramaekers et al. (2007) and refined by Bosman and Ramaekers (2015). Quantitative logs (C.W. Jefferson, L.B. Churlton, T.D. Peterson, B.J. McEwan, L. Calhoun, J.M.J. Scott, S.J.V. Robinson, R.H. Rainbird, and D. MacIsaac, work in progress, 2023) of limited drill core at the southern end of the main Thelon Basin document siliciclastic strata that have a more distal aspect than those of the Aberdeen Subbasin or the eastern flank of the main Thelon Basin as interpreted from descriptions by Cecile (1973). In the Boomerang Lake area, unique attributes include sparse and thin basal pebble conglomerate, limited vertical grain-size variations in the arenaceous facies, and the presence of sparse white clay intraclasts that are reminiscent of the upper Manitou Falls Formation of the Athabasca Basin. Such intraclasts are unknown in the Aberdeen Subbasin.

Jefferson et al. (2023) and C.W. Jefferson, R.H. Rainbird, G.M. Young, S.S. Gandhi, J.C. White, V. Tschirhart, D. Lemkow, and L.B. Churlton (work in progress, 2023) exclude eolian quartzite bodies located around the margins of the Aberdeen Subbasin from the Thelon Formation and assign them to the older Amarook Formation, based on angular unconformities and silicification of the Amarook Formation at all such locations. No felsic tuff like that of the Wolverine Point Formation has yet been discovered in the Thelon Formation, but one possible location to look for it would be in the very poorly exposed region in the western main Thelon Basin, stratigraphically below the Lookout Point and Kuungmi formations.

Other than the above noted studies, very little is known about the Thelon Formation in the main Thelon Basin, and there is no knowledge of its contact relationship with overlying strata. The 1.54 Ga Kuungmi Formation (geochronology site 54, Table 2), comprising about 10 m of ultrapotassic mafic tuffs and lavas, is age-equivalent to the approximately 300 m thick Douglas Formation of carbonaceous mudstone and fine quartzite in the Athabasca Basin. Both basins are capped by stromatolitic dolostone (Carswell Formation in the Athabasca Basin, Lookout Point Formation in the Thelon Basin). Fortunately preserved, but structurally disrupted in the Ordovician Carswell meteorite-impact structure (Alwmark et al., 2017) in the western Athabasca Basin ('Carswell' in Fig. 1), the primary lithofacies of the Carswell Formation are well preserved in fine detail. Hendry and Wheatley (1985) described some 500 m of stromatolitic, oolitic, and micritic to rudite dolostone, the contact of which with the Douglas Formation is faulted, but seems gradational

due to the presence of sand grains in the lower Carswell member. They also presented evidence for past evaporites. In contrast, the Lookout Point Formation is only approximately 40 m thick and comprises siliceous dolostone, with poorly preserved stromatolites and some interbedded quartzite. Recrystallization is intense and much of the outcrop consists of siliceous breccia, suggesting paleokarst collapse.

Based on these first-order summaries, there are no equivalents of the stratigraphically lower Amarook or Pitz formations in the Athabasca Basin, although there is evidence of the Kivalliq igneous suite (*see below*). The Thelon Formation, as exposed, appears to preserve a much simpler sedimentary record than the four major siliciclastic sequences known from the Athabasca Basin. For example, neither obvious erosional boundaries nor angular unconformities separate the three upward-fining sequences established by Hiatt et al. (2003) in the Aberdeen Subbasin, and the paleocurrent trends all support flow toward the centre of basins and along the basin axis, toward the west then southwest (Jefferson et al., 2011a). Many questions remain; for example, could the Fair Point Formation of the western Athabasca Basin be epiclastic in part and, if so, equivalent to epiclastic rocks of the upper Pitz Formation?

Tectonics and structure during sedimentation of the two basins

Major shear-zone trajectories originate from or change across both the Athabasca Basin (Ramaekers et al., 2007) and the Thelon Basin (Fig. 1, 2; P. Ramaekers, pers. comm., 2007). These changes in trajectories and relative offsets help explain the development of accommodation space at various times and places. Dip-slip offsets during reactivation of these faults are clear for each basin, particularly in their basal units. For example, the Dawn Lake and Key Lake open pits in the Athabasca Basin each expose subbasins developed in close proximity to where the reactivated faults host uranium deposits (e.g. Collier and Yeo, 2001; Bernier, 2004; Györfi et al., 2007; Hajnal et al., 2007; Jefferson et al., 2007a, b, c; Long 2007). The vertical fault offsets along these subbasins are only in the order of several metres and pebble sizes are limited to a few centimetres at most, but flanking, wedge-shaped, paleotalus deposits with sieve textures and lateral restriction of basal fluvial sandstone members (e.g. Long, 2007) clearly show that the faults were active during sedimentation.

In the Thelon Basin, the scale of syndepositional faulting was much more significant. Basal polymict conglomerate ranges up to large boulder size, paleoriver channels in the order of 100 m across are preserved, and differential stratigraphic thicknesses across paleofault scarps range in size from hundreds of metres to kilometres. Examples include the Turqavik fault (Fig. 3a, c, 10a, b) and the Thelon Fault (Fig. 3a, c, 8a; Davis et al., 2011; Jefferson et al., 2011a, c; Tschirhart et al., 2013b). The coarsest boulder conglomerate is located right along the Thelon Fault that marks the contact

between the Thelon Formation to the north and a much older imbricate fault zone of Archean and Paleoproterozoic rocks to the south (PQi, Fig. 8). Clearly, the Thelon and Turqavik faults were active during sedimentation. Tectonic activity continued while the upper Thelon Formation was still unconsolidated, as evidenced by small clastic dykes with geopetal structures and locally cemented by fluorapatite (Davis et al., 2011). Thelon Basin fault offsets were much greater, and sedimentation was much more proximal in the Aberdeen Subbasin than anywhere in the Athabasca Basin, given the diverse lithology preserved in the Thelon Formation conglomerate (Fig. 5d) and the onlapping of silicified conglomerate over lower, weakly lithified sandstone members as well as up onto basement gneiss (Fig. 10a, b; previously noted by Donaldson, 1965).

Reactivated intersecting faults initially controlled accommodation space and paleotopography, later focused chlorite-clay alteration of both basement rocks and basin fill, and over time defined the preserved extent and depth of the Thelon Basin (*see* ‘Comparative stratigraphy of the Athabasca Supergroup and Barrenland Group’ section above). Ultimately, some fault intersections controlled the formation and preservation of uranium deposits in clay-alteration envelopes. The fault systems of both basins include sub-vertical fractal arrays geometrically explained in terms of Riedel shear (Fig. 9a, b; *see* ‘Structure and metamorphism’ section above) under overall dextral conditions. The steep faults intersect low-angle compressional and extensional structures, thereby creating complex vertical and horizontal fluid pathways. In both areas, post-1.75 Ga hydrothermal alteration followed the multiply reactivated complex fault systems. Pseudo-three-dimensional analysis in the Athabasca Basin clearly delineated such fault intersections along the sequence P2 fault, showing their relationship to ore pods at the McArthur River deposit (Fig. 1 of Györfi et al., 2007). Original detailed mapping and drill core analysis by Fuchs and Hilger (1989) showed similar structural controls at the Lone Gull (now Kiggavik Main Zone) deposit south of the Thelon Fault (geochronology site 57, Fig. 8), which Anand and Jefferson (2017a) integrated with a regional-scale interpretation of Riedel-shear arrays.

The above noted fault structures being reactivated during sedimentation show clear spatial associations with emplacement of ore in the Athabasca Basin. The basement-hosted uranium deposits of the Kiggavik camp, south of the Thelon Fault, have lost their cover of Thelon Formation, although they do retain alteration assemblages very similar to those of basement-hosted deposits in the Athabasca Basin. The Kiggavik deposits also are clearly developed along multiply reactivated fault systems. In both basins, the reactivated faults are arranged in systematic Riedel-shear patterns (Fig. 9a, b; e.g. by Wright and Potter (2014, 2015) for the Athabasca Basin and by Hunter et al. (2014), Anand and Jefferson (2017a, b), and Grare et al. (2018) for the Thelon Basin region).

The Athabasca Basin forms a coherent oval package with minor outliers, such as the Reilly Basin on its southeastern corner (Fig. 2b of Ramaekers et al., 2007). On the other hand, alteration associated with its basal unconformity assemblage locally extends well beyond the basin along reactivated fault systems, such as southwest of the Key Lake deposit (K. Wheatley, oral presentation, November 2007) and in the Patterson Lake area (Fig. 1) (Armitage, 2013; Tschirhart et al., 2018). Explorationists interpret this alteration as showing that the Athabasca Basin once covered a much wider area under which unconformity deposits could have formed. The most spectacular vindication of such interpretations is the discovery of the Triple R deposit in the Patterson Lake corridor, well south of the basin edge (Armitage, 2013). In addition, the Arrow deposit in the same trend extends from depths of 110 to 980 m below surface, well below depths of erosion around much of the Athabasca Basin (<<https://www.nexgenenergy.ca/projects/arrow/>> [accessed July 29, 2020]).

In contrast, the Thelon Basin is broken into three major parts by large horsts and there are numerous small outliers (Fig. 3a–c). The 020° Marjorie horst (Fig. 3b) and a horst exposing the 060° Marjorie–Kiggavik–Tehek Belt (Fig. 3a) separate the large area of Thelon Formation in the northwestern part of the Baker Lake Basin from that of the Aberdeen Subbasin. The Turqavik and Marjorie horsts partially separate a smaller fault-bounded subbasin underlying Schultz Lake from the main Aberdeen Subbasin. The major northeast-trending Sand Lake horst mostly separates the main Thelon Basin from the Aberdeen Subbasin.

The 60 km wide horst along the 060° Marjorie–Kiggavik–Tehek Belt (Fig. 3a) exposes the Neoproterozoic Marjorie–Kiggavik–Tehek Belt with its basement-hosted uranium occurrences, one of which (Ayra: Ay, Fig. 3a) underlies a small, thin outlier of the Thelon Formation (Hunter et al., 2014, 2018). In the Kiggavik camp, the Lone Gull deposit and the multiple additional discoveries of basement-hosted uranium deposits are all associated with alteration (*see below*), similar to that of basement-hosted unconformity-related deposits under the Athabasca Basin. Like the Patterson Lake corridor (Potter et al., 2020), such alteration must have developed under the cover of now-eroded Thelon Formation. Taken all together, the three large subbasins of Thelon Formation with relatively uniform westward paleocurrents, the many small outliers of Thelon Formation, and the alteration associated with unconformity-style basement-hosted uranium deposits all document the much greater original extent of continuous Thelon Basin cover in the study region.

Similarly, the fault-preserved outlier of fossiliferous Ordovician limestone in the Aberdeen Subbasin (geochronology site 59, Fig. 3a, c, Table 2) is likely the remnant of a continuous sheet of limestone that once covered much of the study region. As shown by raised beaches, a postglacial marine incursion covered much of the Aberdeen Subbasin during the Holocene (McMartin et al., 2008, 2017, 2021; Grunsky et al., 2009; LaRocque et al., 2012).

Comparative ages of sedimentation, diagenesis, and hydrothermal alteration

The ages of initial sedimentation in both the Thelon and Athabasca basins are imprecise, simply postdating the last-known basement magmatic activity (Table 1). Rainbird et al. (2007) suggested that sedimentation in the Athabasca Basin began during or after the 1.78 to 1.73 Ga Yavapai–Mazatzal Orogen. Consistent with their suggestion, the Kivalliq igneous suite can now be used to provide a maximum age for initiation of sedimentation (*see* ‘Magmatism’ section above). Ages on the Kivalliq igneous suite in the study area range from 1.77 Ga to 1.75 Ga. If the Thelon River dykes are the same generation as the similarly oriented 1.69 Ga Pelly Bay dykes on Boothia Peninsula (Bleeker et al., 2010), then that provides an even later start of sedimentation. Given time gaps typical of stratigraphic records, Table 1 arbitrarily uses later than 1.7 Ga as the start of Thelon Formation sedimentation, after development of the Matonabbee unconformity across much of the Canadian Shield.

The next datable event in both basins was the precipitation of uranium-bearing fluorapatite cement. In the Athabasca Basin, the fluorapatite cement developed contemporaneously with a felsic volcanic event recorded in the Wolverine Point Formation. The fluorapatite age of 1638 ± 5 Ma reported by Davis et al. (2011) for cements ranging from the base of the Read Formation, up to, and including, the Wolverine Point Formation, are within error of 1644 ± 13 Ma zircon grains from felsic tuff within the Wolverine Point Formation (geochronology site 52, Table 2; Rainbird et al., 2003b, 2007). Fluorapatite cementation took place about midway through development of the Athabasca Basin and predated uranium mineralization.

Fluorapatite ages in the Thelon Basin are 33 to 44 Ma older than those of the Athabasca Basin: 1688 ± 14 Ma at its southern tip (Boomerang Lake occurrence; geochronology site 50, Table 2) and 1667 ± 5 Ma for all fluorapatite from base to top of the Thelon Formation in the Aberdeen Subbasin (geochronology site 51, Table 2). Undated uraninite that replaced undated fluorapatite at the Kiggavik Main Zone (Lone Gull) deposit (Robinson et al., 2016), and replacement tristramite at Boomerang Lake (Beyer et al., 2010; Davis et al., 2012) suggest the same paragenetic sequence as in the Athabasca Basin, yet starting 33 to 44 Ma earlier. This assumes that the undated fluorapatite at the Kiggavik uranium deposits is the same age as the fluorapatite cement in the Thelon Formation.

Alexandre et al. (2009) documented an extended sequence of mineralization events in the Athabasca Basin: later than 1.75 Ga erosion and paleoweathering prior to sandstone deposition, an average $^{40}\text{Ar}/^{39}\text{Ar}$ age of 1675 ± 15 Ma for pre-ore illite and chlorite alteration, and a U–Pb age of 1588 ± 15 Ma for primary uranium precipitation plus associated illite alteration. They noted periodic resetting of the $^{40}\text{Ar}/^{39}\text{Ar}$ and U–Pb isotopic systems used to date the different minerals. They interpreted this resetting as caused by a

succession of distal events — the ca. 1.6 to 1.5 Ga Mazatzal Orogeny, 1.4 Ga Berthoud Orogeny, 1.27 Ga Mackenzie mafic dykes, 1.15 to 1 Ga Grenville Orogeny, and 1 to 0.85 Ga breakup of Rodinia. Their $^{40}\text{Ar}/^{39}\text{Ar}$ ages of pre-ore illite and chlorite alteration actually range from 1692 ± 11 Ma for sandstone-hosted prospects in the western Athabasca Basin to 1665 ± 11 Ma for basement-hosted deposits in the eastern Athabasca Basin. Accepting the published error margins, these clay-alteration ages are substantively older than the 1638 ± 5 Ma fluorapatite age reported by Davis et al. (2011), suggesting that sandstone cementation by fluorapatite was an intermediate step between clay alteration and uraninite precipitation. It is puzzling that Alexandre et al. (2009) made no mention of apatite in the paragenesis of the Athabasca Basin uraninite ores. The U-Pb age of 1588 ± 15 Ma for primary uranium precipitation in the Athabasca Basin is older than the 1.54 Ga Re-Os age on the Douglas Formation obtained by Creaser and Stasiuk (2007). It is compatible with age constraints for the Eldorado U-Co-Ni-Cu-Ag veins at Port Radium, Northwest Territories. Gandhi et al. (2018) constrained the primary age of the five-element Eldorado veins as postdating the 1.74 Ga Cleaver dykes and predating the 1.59 Ga Western Channel diabase sheets that also cut the Hornby Bay Group, equivalent to the Athabasca and Thelon formations.

Geochronology data for the Thelon Basin are much more limited and uncertain, as the U-Pb systems in uraninite there have all been reset. The oldest mineralization-related U-Pb age is the relict 1.5 Ga obtained by Sharpe et al. (2015) on uraninite from the Bong deposit that was reset at 1.1 and 1.0 Ga. Shabaga et al. (2017) described four mineralization events at the Andrew Lake deposit, all interpreted here as resetting of an unknown primary phase. They determined their sequence of phases by a combination of textural and geochronological methods. Their phase 1 is vein-style uraninite at 1031 ± 23 Ma associated with illite and hematite; their phase 2 is altered ca. 530 Ma uraninite associated with coffinite; their phase 3 is younger than 1 Ma altered uraninite and centimetre-scale uraninite ‘roll-fronts’; and their phase 4, an undated phase of boltwoodite that altered uraninite. Shabaga et al. (2017) also reported $^{40}\text{Ar}/^{39}\text{Ar}$ illite ages associated with uraninite of 941 ± 31 and 1330 ± 36 Ma. These modern geochronological results have led to a better understanding of the 1.4 Ga resetting event noted above for the Athabasca Basin and the classic Eldorado vein deposits at Great Bear Lake (Hornby Bay Basin region). Bridge et al. (2013) determined a strong 1.4 Ga U-Pb resetting age for the same uraninite that yielded a primary 1.83 Ga U-Pb age for the Lac Cinquante deposit of the southern Baker Lake Basin (Fig. 2). The early geochronology results of Fuchs and Hilger (1989) on the Kigavviq (Lone Gull) Main Zone deposit also reflect the 1.4 Ga resetting event (geochronology site 57, Table 2). Peterson et al. (2010, 2014, 2015a, b) further considered the 1.4 Ga event to have reset isotopic systems of the Mallery Lake Ag-Au prospect (geochronology site 56,

Fig. 2; Table 2). Peterson et al. (2010, 2014, 2015a, b) reinterpreted the Ag-Ag-bearing quartz veins as a primary metallotect of the 1.75 Ga Kivalliq igneous suite.

Alteration and metallogenic comparisons of the Athabasca Basin and Thelon Basin regions

Table 3 and Figure 11 summarize uranium metallogenic similarities and differences between the Athabasca Basin and Thelon Basin regions, with emphasis on the northeastern portion of the latter. Most of the uranium metallotects of the Athabasca Basin region are present in the Thelon Basin region, but with significant differences, resulting in markedly different exploration priorities and strategies for each. From a geochemical source perspective, both provenance regions were rich in uranium, but distinctly different (*see* ‘Tectonics and structure during sedimentation of the two basins’ section above). Alteration and metallogenic comparisons are presented in order by age, starting with the Archean. Table 1 provides a chronological geological reference for the Thelon Basin region; for the Athabasca Basin region, the reader is referred to the compendium volume published following the EXTECH IV project (Jefferson and Delaney, 2007) and specific references cited below.

Although uranium metallogeny is the focus of this study, the metallogeny of Archean domains has a bearing on uranium exploration, in terms of critical mass that may improve logistics and providing additional targets that improve the chances of discovery. Whereas no major mineral resources are known from the Archean in the vicinity of the Athabasca Basin, there are major producing gold mines in the Aberdeen Subbasin region that are the current and sustained economic drivers. These drivers support geological research as well as broader mineral exploration in the Kivalliq Region of Nunavut. Up to the start and during the GEM-1 Uranium project, understanding of basement geology benefited enormously from knowledge gained by research on the gold deposits. Furthermore, there are many similarities between lode-gold deposits and basement-hosted uranium deposits, the most important being structural attributes at the deposit scale.

Gold deposits in the Woodburn Lake group are hosted by Archean iron-formation, with theories on their origins ranging from primary syndepositional concentration to synmetamorphic Hudsonian in age, including some combinations of the two (Hrabi et al., 2003; Sherlock et al., 2004; Pehrsson et al., 2013a; Côté-Mantha et al., 2015; Gosselin and Dubé, 2015; Janvier et al., 2015a, b; Lawley et al., 2016; Valette et al., 2019). Regardless of such questions, the presence of iron-formation as a host is paramount, and the extreme structural complexity of the Meadowbank and Amaruq deposits in the study area shows that meticulous

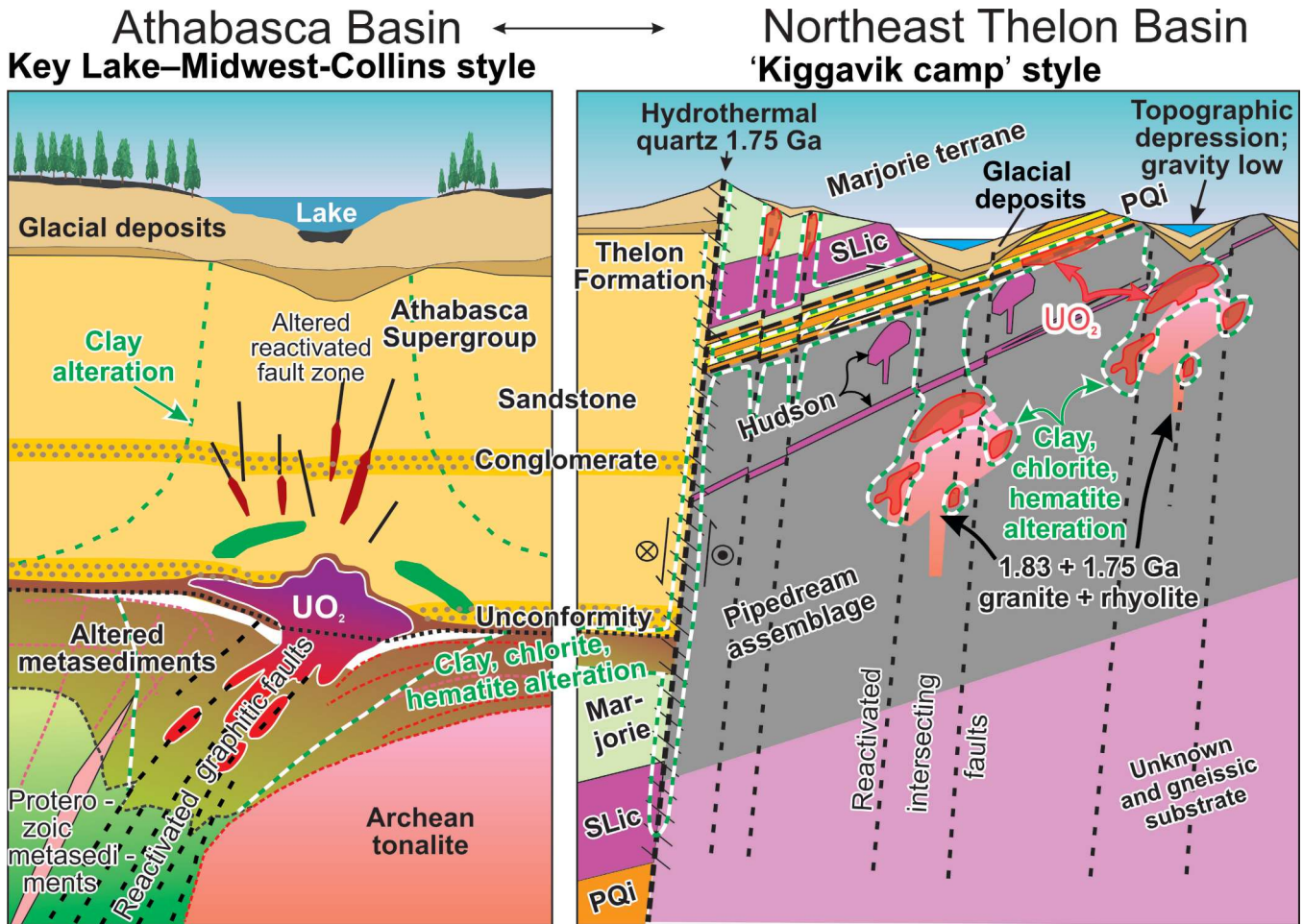


Figure 11. Empirical comparison of uranium-deposit models for the Athabasca and Thelon basins. The Athabasca Basin model is after Jefferson et al. (2007c). The Thelon Basin model is based on the Kiggavik uranium camp, consistent with Fuchs and Hilger (1989), Riegler (2014), Riegler et al. (2014, 2016a, b), and P. Wollenberg (pers. comm., 2006 through 2012). The Pukiq imbricate zone (PQi) is after D. Johnstone, K. Bethune, D. Quirt, and A. Benedicto (unpub. rept. no. 15-CND-92-04 of AREVA Resources Canada Inc. (2015), Anand and Jefferson (2017a), and Johnstone (2017)). The Schultz Lake intrusive complex (SLic) of Figures 3a and 8, and other granitoid bodies, are cartooned after Tschirhart et al. (2013b). The '1.83 + 1.75 Ga granite + rhyolite' are after Scott et al. (2015). The dextral strike-slip component of the Thelon Fault is also represented by the small circled symbols (dot = left-backward fault displacement, x = right-forward fault displacement).

geological assessment and grade control have gone into the development of and sustained production from these large and high-grade, but complicated deposits.

From the perspective of an outside observer reviewing the above literature, one key empirical parameter appears to be common to the Meadowbank and Amaruq deposits, but is absent from adjacent nonmineralized iron-formation: the presence of exhalative and epiclastic strata as the immediate hosts of the auriferous iron-formation. The potential for volcanogenic massive sulphide and gold deposits in the region east of the northeast Thelon Basin is also being explored in the Half Way Hills assemblage at the Greyhound property, northwest of Whitehills Lake (Aura Silver Resources Inc., 2018). The iron-formation in the Half Way Hills greenstone belt is associated with significant

proportions of iron-carbonate alteration and epiclastic rocks. A key difference from northern Saskatchewan is that such greenstone-belt-style gold metallogeny is absent from the basement terranes that underlie and immediately surround the Athabasca Basin.

The presence of highly magnetic, mafic to ultramafic phases of the Snow Island suite raises the question of nickel, copper, platinum (Ni-Cu-PGE) and chrome (Cr) potential in the basement of both basins. The Thye and Axis gabbros on the northern side of the Athabasca Basin have very high contents of Sc-Cr-Ni (Acosta-Góngora et al., 2018) and are considered part of the Snow Island suite (Peterson et al., this volume). As for the Thelon Basin, a remarkable outcrop northwest of Sand Lake along the Chantrey mylonite zone exposes igneous layering and trough crossbedding, multiple

crosscutting magma phases, blocks of layered mafic rock enclosed in massive monzodiorite, and metasomatized phases in a portion of the Snow Island suite that has multiple elongate zones of high magnetic susceptibility (Peterson et al., this volume). Such primary igneous-sedimentary structures are common in host rocks of Ni-Cu-PGE deposits that formed by convective cooling processes; however, the exposed portions of the Snow Island suite are dominantly granitoid rocks and most source rocks for the powerful magnetic highs in the Snow Island suite are buried deeply. Most of the exposed Snow Island suite lacks the fundamental attributes of geological settings that host Ni-Cu-PGE and Cr deposits such as, for example, tholeiitic magmas, a high-volume rift-related flood basalt province, a major astrobleme, or komatiites (Eckstrand, 1995).

On the other hand, Barrie (1995) noted that the late Archean Lac des Îles ultramafic intrusion is nearly coeval with, and is likely, an early phase of adjacent granite. More recently, Lavigne et al. (2005) noted that traditional prospecting involving systematic ground transects across intense magnetic anomalies found the Lac des Îles palladium deposit in a nonmagnetic early gabbroic phase of the 2690 ± 0.9 Ma Shelby Lake batholith — a monzodioritic part of a sanukitoid suite located directly south of, and not related to, the Lac des Îles intrusive complex. The Shelby Lake gabbro bodies show evidence of repeated magmatic injection and brecciation, such as displayed at the outcrop northwest of Sand Lake. Intriguingly, both Lac des Îles and the Chantrey mylonite zone localities include mylonitic fault zones, but the gabbro in both places is essentially undeformed. Opportunity beckons for detailed litho-geochemical study and prospecting of mafic phases of the sanukitoid Snow Island suite (Peterson et al., this volume) in locations such as near Sand Lake.

Uranium occurrences are numerous in basins precursor to both the Athabasca and Thelon basins, yet with a number of differences. The early Paleoproterozoic (ca. 2.19–1.85 Ga) is well represented in both regions. In the Athabasca Basin region, these include the Murmac Bay group, the copper-preponderant and uranium prospects in the Janice Lake formation of the Wollaston Supergroup (Yeo and Delaney, 2007; Forum Energy Metals, 2021), supracrustal components of the Taltson magmatic zone (Card et al., 2007), and metasedimentary rocks of the Snowbird–Dodge and eastern Zemlak domains (Thiessen et al., 2020). In the Thelon Basin region, the equivalent strata are described above in the section entitled ‘Early Paleoproterozoic cover sequences: Amer, Ketyet River, Montresor, and western belts’. In particular, these include stratabound uranium+magnetite-preponderant and copper occurrences of the Showing Lake formation (Young, 1979; Miller and LeCheminant, 1985; Gandhi et al., 2015; Jefferson et al., 2015, 2023; C.W. Jefferson, R.H. Rainbird, G.M. Young, S.S. Gandhi, J.C. White, V. Tschirhart, D. Lemkow, and L.B. Chorlton, work in progress, 2023).

For the Amer Belt, Jefferson et al. (2015, 2023) and C.W. Jefferson, R.H. Rainbird, G.M. Young, S.S. Gandhi, J.C. White, V. Tschirhart, D. Lemkow, and L.B. Chorlton (work in progress, 2023) provide contextual stratigraphic and geophysical evidence to support previous interpretations of uranium occurrences in the upper part of sequence Ps3 of the Showing Lake formation as stratabound, sandstone-hosted, and diagenetic (Knox, 1980; Gandhi, 1995; Gandhi et al., 2015). Work by Blackwell (1978) of Cominco Ltd. also highlighted the importance of deformation in generating southwest-plunging, cigar-shaped concentrations of uranium within this overall stratabound context. He also noted the presence of copper- and iron-sulphide minerals and magnetite within these uranium occurrences. Structural analysis by Calhoun et al. (2014) showed how elongated uranium pods might form, by analogy with elongate lenticular sandstone beds hosted by argillaceous beds affected by combined D_{p1} and D_{p2} events. Serial sections of conglomerate clasts of this study also document cigar-shaped cobbles. Jefferson et al. (2023) and C.W. Jefferson, R.H. Rainbird, G.M. Young, S.S. Gandhi, J.C. White, V. Tschirhart, D. Lemkow, and L.B. Chorlton (work in progress, 2023) highlight the close spatial association of the Amer uranium occurrences with linear magnetic markers and the petrographic corroboration of magnetite as part of the mineral paragenesis, along with uraninite and copper sulphide minerals. Such uranium occurrences are unknown in the Ketyet River and Montresor belts and are not present in sequence Ps4 of any of these belts. Given the amount of uranium prospecting that has taken place in this region since 1968, it is unlikely that such occurrences are preserved anywhere else in this region, other than in the upper strata of sequence Ps3 (Showing Lake formation) of the Amer Belt.

Carbonaceous sulphidic conductors have long been a focus for drilling in the Athabasca Basin (e.g. Jefferson et al., 2007c). Although not every conductor is associated with viable deposits therein, considerable exploration success has resulted from including this parameter (Jefferson et al., 2007c), up to, and including, the discovery of the Patterson Lake corridor (e.g. Armitage, 2013). This is also one of the key comparative features that focused early exploration in the southern tip of the Thelon Basin at Boomerang Lake (Davidson and Gandhi, 1989; Beyer et al., 2010), in the Aberdeen Subbasin (Young, 1979), and in the Amer (unpublished assessment reports) and Garry Lake (Miller, 1995) belts, well away from the Thelon Basin. Many of the drillholes logged in the Aberdeen Subbasin (Jefferson et al. 2011b, c, 2015) targeted such conductors that can be traced geophysically into the basal sequence Ps2 unit of the Amer Belt (Young, 1979; Jefferson et al., 2015, 2023; Tschirhart et al., 2017). The contrast with the Athabasca Basin is that no significant uranium deposits have yet been found beneath the Thelon Basin in this way. Jefferson et al. (2023) and C.W. Jefferson, R.H. Rainbird, G.M. Young, S.S. Gandhi, J.C. White, V. Tschirhart, D. Lemkow, and L.B. Chorlton (work in progress, 2023) note that the carbonaceous units

in the Amer Belt are at slate grade and hydrodynamically tight, not being conducive to fluid flow and alteration. Furthermore, they now realize that graphitic conductors are present not only in sequence Ps2, but also within the upper part of sequence Ps4 near the Amer mylonite zone (*see* references at the end of ‘New definitions of sequences Ps1, Ps2, Ps3, and Ps4 in the Amer Belt’ section) and at the base of sequence Ps4 in the Garry Lake Belt, where it was a target of uranium exploration (Miller, 1995). Reid (2018) noted that recrystallization of basement host rocks, including the graphitic conductors, is a favourable factor for fluid flow, for mineral alteration, and therefore for uranium mineralization.

The conductors in both the Amer and Ketyet River belts also include other metallotects. The sequence Ps2 graphitic unit in the Ketyet River group is a biotitic pelite to semipelite, locally associated with conglomerate of the upper sequence Ps1 quartzite unit. It is medium grey to black, fine-grained, commonly gossanous, sulphidic and graphitic, with transposed thin bedding of 2 to 40 cm width, local dark cherty layers transitional to iron-formation, and strong schistosity. This is unit APwpt of Zaleski and Pehrsson (2005). Their ‘No. 1 Mineral Occurrence’, located east of Whitehills Lake, and at the contact between this unit and the quartzite, is a gossanous sulphidic zone in schistose quartzite and iron-formation with anomalous Pb and Cu carried by pyrite, pyrrhotite, and galena. Gossans are particularly well developed over siderite- and sulphide-facies iron-formation infolded with this 1 to 2.5 km wide, east–west belt, and are present in other sequence Ps2 localities of the Ketyet River group. The lithological variations within, as well as the gossan development at the base of this unit, are very similar to those of the Resort Lake formation of the Amer group (Jefferson et al., 2015, 2023; C.W. Jefferson, R.H. Rainbird, G.M. Young, S.S. Gandhi, J.C. White, V. Tschirhart, D. Lemkow, and L.B. Chorlton, work in progress, 2023) and the ferruginous siliciclastic unit of LeCheminant et al. (1984) in the Akiliniq Belt that includes hematite iron-formation much like that in sequence Ps2 of the Schultz Lake klippe (this study).

The next age of uranium comparisons is between intracratonic redbed sequences of the Baker Lake Basin, mainly east of the Thelon Basin, and the Martin Basin, north of the Athabasca Basin (Fig. 1). Miller (1980) comprehensively compared the lithology and metallogeny of the two basins, and that correlation still stands (Card et al., 2007). These correlative basins developed transextensionally to extensionally and were filled during the Hudsonian Orogeny (ca. 1.84–1.78 Ga). Miller (1980) detailed three types of uranium associations along the southeastern side of Baker Lake Basin: 1) fracture-hosted in the Dubawnt Supergroup and basement gneiss (U-Cu-Ag-Au-Se or U-Cu-Pb-Mo-Zn), 2) diatreme breccias cutting basement gneiss (U-Cu-Zn), and 3) disseminations and microfracture fillings in altered arkose peripheral to minette dykes (U-Cu-Ag). Stanton (1979) interpreted the last as having formed in response to thermally

driven fluid flow beside the larger minette dykes. She noted that the Kazan formation arkosic beds were preferentially mineralized rather than the intercalated conglomerate beds that had been cemented by calcite and chlorite during early diagenesis. The Martin Basin lacks a thick arkose sequence and uranium occurrences of the three styles described above.

Both the Baker Lake and Martin basins host unconformity-related uranium deposits. Bridge et al. (2013) studied the Lac Cinquante (Fig. 2) deposits that fill crack-seal veins in relatively straight, conductive Archean metatuff layers between pillowed mafic to dacitic metavolcanic units. These carbonaceous sulphidic conductors and their contained uranium occurrences are partly covered by basal breccia to conglomerate of the South Channel and Angikuni formations and, in places, directly covered by Christopher Island formation volcanic rocks. Uraninite U-Pb dating yielded two groupings in a gash vein. The least-altered grains gave a discordant U-Pb age of 1828 ± 29 Ma, whereas altered uraninite grains gave a U-Pb age of 1437 ± 31 Ma. These ages support classification of Lac Cinquante as an unconformity-related, vein-style deposit, given the spatial association of the mineralization to the basal unconformity of the Baker Lake Group and the oldest date on a felsic minette flow of the interlayered Christopher Island formation in that area (1833.2 ± 2.4 Ma, U-Pb zircon; Rainbird et al., 2006).

The Martin Basin is filled by redbeds, but contains mafic volcanic rocks (Sparrow basalt) that are not ultrapotassic (Miller, 1980), yet exhibit some similarities with the Christopher Island formation (Morelli et al., 2009). Although there are minette dykes in the area of the Martin Basin, the basin lacks the equivalents of the Christopher Island formation lavas in the Baker Lake Basin. There are varying degrees of Sparrow basaltic magma mixed with Dubawnt-like minette dykes in the Martin Basin region, although it may be that the glimmerite source of those minettes was diminished at depth for unknown reasons. Key metallogenic similarities include the alteration assemblages associated with vein-style, basement-hosted uranium occurrences in both basins: albite, calcite, and chlorite. Key differences are the lack of breccia and minette dyke as well as sandstone-hosted uranium styles in the Martin Basin. Nevertheless, the subject of sodic alteration associated with these uranium deposits remains topical in the Martin Basin (Ashton et al., 2013; Kennicott et al., 2015) as well as in the Athabasca Basin (Chi et al., 2018). Bridge et al. (2013) compared the unconformity-related, Lac Cinquante style to that of the “Beaverlodge Uranium District” of northern Saskatchewan. Miller (1980) and Card et al. (2007) had also noted geological and metallogenic similarities between the Baker Lake and Martin basins. Thus, the Beaverlodge uranium deposits have many characteristics of unconformity-related deposits, especially in terms of practical empirical analysis (Beaverlodge-type U±polymetallic (A-2) ore-deposit model of Rogers (2015)), even though alternative genetic models are also available (e.g. Ashton et al., 2013).

One of the most visible alteration products in the Kivalliq Region, and also present in the basement to the Athabasca Basin, is silicification related to the 1.75 Ga Kivalliq igneous suite (Peterson et al., 2015a). This is expressed in numerous ways, most dramatically by vein-quartz systems associated with multiple fault orientations, but mainly the P, R, and R' directions of Riedel shear (Fig. 9a, b). Grare et al. (2018) described these vein systems in great detail as their 'Fracturing stage 2, quartz breccia' that they associated with the first stage of oxidation. Like Riegler (2014) and Riegler et al. (2014), Grare et al. (2018) concluded that this alteration predated the unconformity-related uranium mineralization and alteration in the Kiggavik project area. Grare et al. (2018) also recognized that the fault arrays emphasized by the quartz breccia were reactivated multiple times and some of these reactivated faults controlled unconformity-related uranium deposition; this was also proposed by Anand and Jefferson (2017a). Riegler (2014) and Grare et al. (2018) recognized both drusy and crosscutting cryptocrystalline quartz from the uranium deposit areas. Turner et al. (2001) described epithermal Au-Ag mineralization hosted by crack-seal veins of alternating drusy and cryptocrystalline quartz. In the Athabasca Basin, a distinctive basement ridge of hydrothermal quartz extends along a string of uranium deposits, including the Wheeler River and McArthur River (Card, 2014). This paleotopographic feature follows a distinct break in isopachs of the Read and Manitou Falls formations.

Granitoid phases of the Kivalliq igneous suite are spatially and temporally associated with precious-metal and uranium mineralization (e.g. Charbonneau and Swettenham, 1986; Jefferson et al., 2013; Scott et al., 2012, 2015; Peterson et al., 2015a). Peterson et al. (2015a) proposed that potential for Au-Ag associated with such quartz veins and breccias extends to multiple other localities in the Kivalliq Region of Nunavut, by analogy with the extent of 1.75 Ga Kivalliq igneous suite magmatism. They further noted the presence of submillimetre-laminated microcolumnar chert stromatolites within phreatic breccia of the Pitz Formation (Fig. 5e). Card (2014) interpreted major quartz ridges beneath the eastern Athabasca Basin as silicified pelitic gneiss and vein quartz (not quartzite of the Wollaston Supergroup). These are best developed along a linear fault zone in the Key Lake–Wheeler River–McArthur River deposits corridor. Yeo et al. (2007) described cryptomicrobial stromatolites in chert clasts of a breccia flanking this quartz ridge. The microscopic stromatolites from quartz ridges in the Athabasca Basin are similar in context and composition to the above-described chert stromatolites in the 1.75 Ga Pitz Formation. In the Patterson Lake corridor, silicification of the basement gneiss and ultramafic to mafic units can be traced in drill core from minor alteration to near complete replacement of the host rocks (Card and Noll, 2016; Card, 2017, E. Potter, pers. comm., March 24, 2020).

This silicification event is extended to embrace the drusy and cryptocrystalline cement that pervades the Amarook Formation, and to downward-tapering millimetre-scale quartz

veins that salt the unconformity surface between the hematitized Pipedream assemblage and the Amarook Formation at 'Unconformity lake' (Fig. 8, east of the Kiggavik deposit). This silicification was previously interpreted by Ross and Chiarenzelli (1985) as silcretes developed during paleoweathering, however the hydrothermal and hot spring association is very strong and the silicification transects depositional boundaries. Silicification is very difficult to date, but field relationships provide key constraints such as the pervasive stratabound nature of silicification in the Amarook Formation, versus more localized silicification in the Thelon Formation. Multiply reactivated fault zones are typical sites of multiple quartz-vein development. These are present in both the eastern (Alexandre et al., 2009) and western (Rabiei et al., 2019) Athabasca Basin, and in both the southwest (Beyer et al., 2010) and northeast (Anand and Jefferson, 2017a, b; Grare et al., 2018) Thelon Basin regions.

The primary driver of uranium exploration in both the Athabasca and Thelon basins has been the recognition of unconformity-type uranium deposits in the former (e.g. Hoeve and Sibbald, 1978) and the continued improvement in knowledge regarding that deposit model, both empirically and genetically, in both basins (e.g. Miller and LeCheminant, 1985; Gandhi, 1989; Matthews et al., 1997; Kyser et al., 2000; Renac et al., 2002; Jefferson et al., 2007a, b, c; Alexandre et al., 2009; Cuney and Brisbin, 2010). In terms of alteration, both the Athabasca and Thelon basin fills represent effectively blank canvases on which multiple diagenetic to hydrothermal alteration events have painted their signatures. As noted by Jefferson et al. (2007a, b, c), sedimentation of the four unconformity-bounded sequences of the Athabasca Basin spanned 200 Ma, with each sequence experiencing a unique diagenetic trajectory as well as affecting the previous sequences. Unconformity-bounded sequences have not been recognized in the Thelon Basin, and it appears that a single diagenetic trajectory is recorded in the Aberdeen Subbasin. The Athabasca and Thelon basins experienced slightly different clay-mineral alteration and the early alteration events took place at different times in each basin. Illite and chlorite dominate the regional clay-alteration mineralogy in both basins, but the Athabasca Basin includes dickite (Renac et al., 2002); however, on a regional scale, the intense clay alteration left both basins with quartz as the dominant residual framework mineral. Only petrographic, microprobe, and geochemical detective work could infer the original arkosic lithic nature of these strata (e.g. Miller and LeCheminant, 1985; A.R. Miller, unpub. rept., 1996).

Because of basinwide diagenetic alteration, zircon and tourmaline are the only detrital heavy minerals that are abundant in both basins. These heavy minerals commonly form laminae with associated aluminum-phosphate-sulphate (APS) minerals (described further below) and disseminated, finely crystalline hematite. In some samples, the disseminated hematite is concentrated in clots that are similar in size and concentrated along the same laminae as the preserved tourmaline and zircon. Better preserved hematite pseudomorphs of

heavy minerals in the Thelon Formation have rounded shapes visible in hand specimen and thin section. In both basins, the gross distribution of dark hematite at hand-specimen scale outlines both planar laminae and small festoon-shaped crossbed laminae in outcrop and drill core. The hematite concentrations along sedimentary laminae are distinct from the much later, pervasive hematite and limonite stains that commonly form Liesegang rings, some of which superficially resemble depositional crossbeds, but actually cut across planar depositional laminae.

Millimetre-scale cubes of APS are concentrated along the same heavy mineral laminae as the hematite in both Thelon and Athabasca sandstone, as well as in the alteration assemblages around basement-hosted deposits of both basins. These have been ascribed to various mineral names in the APS spectrum, such as goyazite and crandallite (Madore et al., 2000; Gaboreau et al., 2007; Jefferson et al., 2007a, b, c; Mwenifumbo and Bernius, 2007; Riegler et al., 2016a). Riegler et al. (2016a, p. 219) described three compositionally distinct phases of APS related to the following: “(1) paleoweathering of continental surfaces prior to the basin occurrence, (2) diagenetic processes during the burial history of the lower unit of the Thelon Formation sandstone, and (3) hydrothermal alteration processes that accompanied the uranium deposition in the basement rocks and partially overlap the sedimentary-diagenetic mineral parageneses.” Gall and Donaldson (2006) described similar morphologies of APS minerals in the Hornby Bay Basin, and noted that, although they locally occur in the same places, their paragenetic sequence is uncertain. The tendency of APS cubes to impinge locally on fluorapatite in Hornby Bay Group sandstone led them to suggest that the APS postdated fluorapatite; in any case, both appear to postdate illite. On the other hand, Jefferson et al. (2007a, b, c) focused on the observation of APS replacing altered monazite in basement to the Athabasca Basin (Madore et al., 2000). From this, Jefferson et al. (2007a, b, c) proposed that alteration of monazite in heavy mineral layers produced the relict thorium-enriched APS-rich layers documented by Mwenifumbo and Bernius (2007), while releasing uranium and phosphate that could form fluorapatite. In both the Athabasca and Thelon basins, fluorapatite is the immediate precursor to the earliest uraninite. The APS minerals are undated, but context suggests that the alteration of monazite during peak diagenesis may have contributed at least some of the uranium and phosphate that formed fluorapatite and, ultimately, the uranium deposits in each basin. An unusual occurrence of large, zoned APS minerals in the area of the Centennial deposit, in the south-central Athabasca Basin, records a late hydrothermal remobilization event possibly related to intrusion of the Mackenzie diabase dykes (Reid et al., 2016).

Silicification, although a hallmark of the 1.75 Ga Kivalliq igneous event, also later affected parts of the Thelon and Athabasca basins. Selective silicification of some sandstone in the Athabasca Basin created hydrodynamic barriers (aquitards of Hiatt et al., 2003 and Hiatt and Kyser, 2007) that were

inevitably breached by reactivated faults, but still constrained fluid flow. Silicification in the Thelon Basin is dominantly along fault zones, resulting in topographic ridges such as along the Thelon, Turqavik, and 120° ‘r’ faults (yellow-orange lines, Fig. 3c) that played a large role in development and preservation of the Aberdeen Subbasin. Silicification also preferentially affected the basal Thelon Formation conglomerate and the conglomeratic sandstone at the base of its second upward-fining sequence. These resistant units tend to form local plateaus. Given the silicification along faults, some of the basement-hosted quartz veins in the northeast Thelon Basin region likely postdate the 1.75 Ga Kivalliq event and thus would be part of the quartz-breccia paragenesis documented by Grare et al. (2018).

Desilicification characterized intense alteration zones around Athabasca Basin deposits such as Cigar Lake, the clay-alteration envelopes of which (Hoeve and Quirt, 1984) also served as impermeable barriers that preserved the deposits from the time of their formation until the present (Percival et al., 1993). Similar desilicification and clay alteration (illite±sidoite±hematite±APS minerals) are integral parts of ore paragenesis at the Kiggavik deposits (Riegler, 2014; Riegler et al., 2014, 2016a), as well as being recognized in the Thelon sandstone (Renac et al., 2002; A.R. Miller, unpub. rept., 1996). Silicification in strata above ore deposits of the Athabasca Basin takes the form of drusy quartz at the outer margins of desilicification and clay-alteration haloes (Percival et al., 1993), as well as diffuse subhorizontal stratabound zones such as modelled by Craven et al. (2007). Renac et al. (2002) found similar timing, salinity, and isotopic compositions of peak-diagenetic fluids in both basins, but differences in their mineralogy, with illite dominant in the Thelon Basin, but both dickite and illite being quantitatively represented in the Athabasca Basin, along with minor dravite and goyasite. Post-peak diagenetic assemblages in the Thelon Formation include potassium feldspar and sudoite as replacements of illite (not found in the Athabasca Basin) interpreted as due to late infiltration of saline brine.

Uranium-rich fluorapatite cement, which is present in both the Athabasca and Thelon basins, generates measurable airborne radiometric and ground uranium anomalies. The cement postdates xenotime, but Rainbird et al. (2007) were unable to obtain any ages on the xenotime due to very low uranium contents; however, this does suggest that uranium-bearing diagenetic fluids first started circulating within these basins during deposition of the uraniferous fluorapatite — *after* the development of early diagenetic xenotime. Chi et al. (2019) documented uranium-rich fluid inclusions throughout the Athabasca Basin, supporting the notion that uranium-rich diagenetic brines pervaded these basins during peak diagenesis. In the Thelon Basin, large areas of fluorapatite cement underlie significant airborne radiometric uranium anomalies and have been targets of extensive drilling. Early studies by Miller et al. (1989) documented brick-red fluorapatite cement in numerous places around the Aberdeen Subbasin, especially

in the basal unconformity assemblage, in the form of apatite-cemented breccia and conglomerate (e.g. Fig. 5c). In the Thelon Basin, the fluorapatite patches extend from the bottom to the top of the three Thelon Formation sandstone sequences. In the Athabasca Basin, the fluorapatite cements fault zones cutting the lower two clastic sequences and forms stratabound layers associated with felsic tuff in the second unit of the third sequence (Wolverine Point Formation) (Rainbird et al., 2007).

According to geochronological data in the Athabasca Basin (*see* discussion in ‘Comparative ages of sedimentation and diagenesis’ section above), the earliest illite-chlorite alteration predated the fluorapatite cement by some 31 Ma, and the earliest uranium mineralization postdated the fluorapatite by some 85 Ma. These temporal relationships are consistent with paragenetic observations. Illite is associated with, but not included in, APS minerals (Jefferson et al., 2007a, b, c; Mwenifumbo and Bernius, 2007). The fluorapatite cement encloses and therefore postdates illite. In the Thelon Basin, uraninite replaces fluorapatite at the Kiggavik Main Zone (Lone Gull) deposit (Robinson et al., 2016) and trisramite replaces fluorapatite at Boomerang Lake (Beyer et al., 2010; Davis et al., 2012). Assuming that the basement-hosted Lone Gull fluorapatite is the same generation as the fluorapatite cement in the Thelon Formation, the fluorapatite age of 1667 ± 5 Ma in the Aberdeen Subbasin represents a plausible maximum age for mineralization, despite the reset uraninite U-Pb systems. The statistically different apatite ages of the two basins, yet their similar uranium-deposit-related alteration sequences, indicate temporally and spatially independent, but sequentially similar diagenetic and early metallogenic events, followed by very similar resetting events that affected correlative sedimentary basins spanning the Canadian Shield.

Within the deposit-specific alteration zones, quartz dissolution and deep clay alteration of mafic to felsic silicate minerals is common to basement host rocks in the Thelon and Athabasca basins, but the expression of such alteration in the overlying sandstone is known so far only for the Athabasca Basin, due to the fact it has been more extensively explored. Thus, basement-alteration zoning is a key component of the exploration paradigms for both basins (Fig. 11). Alteration has been mapped in three dimensions for both camps using lithological (e.g. Riegler et al., 2014 for the Kiggavik uranium camp; *see* summaries in Jefferson et al., 2007a, b, c for the Athabasca deposits) and geophysical core logs (e.g. Matthews et al., 1997; Mwenifumbo and Bernius, 2007). Audiomagnetotelluric transects have contributed to improving knowledge of alteration in the Athabasca sandstone as well as in the basement (Craven et al., 2007) — the altered fault zones are resistivity lows. Gravity lows are first-order exploration anomalies for both basins (Matthews et al., 1997; Thomas and Wood, 2007; Tschirhart et al., 2014), although the precise location of resources within these large target areas depends on three-dimensional geological analysis of drill core.

Carbonaceous material is commonly found as disseminated haloes above and around unconformity deposits, and intimately associated with uranium-oxide mineralization in both the Athabasca (McCready et al., 1999; Wilson et al., 2007) and Thelon (Riegler et al., 2016b) basins, as well as in the “Beaverlodge Uranium District” (thucholite of Tremblay, 1972). Proposed origins of these hydrocarbons in the Athabasca Basin range from the migration of newly generated hydrocarbons, first from the Douglas Formation and second from Cretaceous strata, then being altered to pyrobitumen by radioactive decay (Wilson et al., 2007), to abiotic synthesis (e.g. McCready et al., 1999; Sangély et al., 2003; Paná et al., 2007). Regardless, their common presence is a factor to include in empirical models.

In terms of surficial prospecting for uranium, Robinson et al. (2014, 2016) approximated the net glacial-distribution direction from the two main ice flows as toward the north-west and sampled in that quadrant ‘down-ice’ of the Kiggavik uranium deposits to test whether heavy minerals in till could be used to track unconformity-related uranium deposits. Robinson et al. (2016) found no durable sand-sized uranium tracer minerals, but raised the possibility of separating anomalously heavy lead- and uranium-rich fluorapatite grains from silt-sized heavy mineral concentrates. Their microprobe study showed that lead- and uranium-rich fluorapatite was partially replaced by uraninite and thus may be a diagnostic part of the uranium-deposit paragenesis.

Robinson et al. (2014, 2016) also studied whether precious metals entrained from sources up-ice of a uranium deposit might then appear to have been derived from that uranium deposit. As a result, they detected a number of gold anomalies up-ice to the south and southeast of the Kiggavik uranium deposit, as had McMartin et al. (2008). Some of these minor gold anomalies possibly reflect iron-formation sources, but one in particular at station 10PTA047 (‘047’ in red, south of the Fig. 8 outline in Fig. 3a) is associated with rhyolite that occupies a north–south fault zone. This occurrence may thus be an expression of the 1.75 Ga Kivalliq igneous suite.

In the Athabasca Basin, Potter and Wright (Potter and Wright, 2015; Wright and Potter, 2015) assessed regional surficial geochemical data sets and noted subtle, but consistently detectable trace-element-*ratio* patterns that follow Riedel-shear trends. These are more intense where spatially associated with known, deep uranium deposits. In both the Athabasca and Thelon basins, reactivated fault systems form comparable Riedel-shear arrays, affect both basement rocks and the basin-filling siliciclastic strata, and served as fluid-flow pathways that focused alteration and uranium mineralization. The above-noted presence of active mud volcanoes (pockmarks) in lake-bottom sediments, some of which actively vent radon (e.g. ‘Screech lake’, Fig. 2) suggests that surficial geochemical methods may be as effective in the Thelon Basin as in the Athabasca Basin.

The technology introduced by Potter and Wright (Potter and Wright, 2015; Wright and Potter, 2015) is thus worthy of further refinement and testing.

Recommendations for further work

Many questions cry out for answers. Very few publicly available data are available for the newly recognized Pipedream assemblage traced by linear aeromagnetic highs into the area around Woodburn Lake. The readily traceable linear markers in that area (Fig. 3d) are interpreted as iron-formation (Fig. 3b), although they may include ultramafic units. The main part of the Aberdeen assemblage has been mapped in some detail by Hunter et al. (2018, 2021) and is generalized in Figure 3a. In addition, linear aeromagnetic highs calibrated as iron-formation extend west of their map area; thus, the Aberdeen assemblage is extrapolated into that area. Indistinct linear aeromagnetic highs farther south, coincident with moderately low background values in the residual total field image, suggest that more Aberdeen assemblage is present in the Marjorie terrane south of the large outlier of Pitz Formation. The southern extrapolation of the Aberdeen assemblage shown in Figure 3a should be tested by outcrop mapping.

Geochronology knowledge gaps could be addressed through targeted studies, for many of which the samples are in hand. The present authors predict that detrital zircon geochronology of the fourth sequence of the Amarulik assemblage will obtain some of the youngest Neoproterozoic ages in the region. The eastern portion of the Marjorie terrane orthogneiss has been dated only by inference at ca. 2.58 Ga based on a dominant inherited zircon population in the Schultz Lake intrusive complex (Hunter et al., 2021) and should be dated directly. Many samples of sandstone units in the overall fine-grained sequences Ps2 to Ps3 strata provide opportunities for dating, in particular for the uranium-copper-magnetite-bearing Showing Lake formation. An age on the garnet muscovite granite underlying the southwestern part of the Montresor synform could establish its relationship to the Snow Island or Hudson suites and provide a minimum age of its schist inclusions. Geochronology of the fluorapatite that is replaced by uraninite in the Lone Gull deposit (Robinson et al., 2016) would provide a lower age limit on uranium mineralization and test the hypothesis that the basinwide syndepositional fluorapatite cement dated by Davis et al. (2011) in the Thelon Formation is of the same generation. Attempts to date have been foiled by the abundance of common lead. A more robust age is needed on the Schultz Lake metagabbro sheet (references in Table 2), and comprehensive petrochemical analysis and comparison of sequence Ps3 basalt across the region are needed to follow up on Patterson et al. (2012). Amygdular portions of the Kuungmi lavas yielded the 1540 ± 30 Ma baddelyite result of Chamberlain et al. (2010); the amygdular zones in the Five Mile Lake and Keteyet River basalts could be tested in the same way.

A number of intriguing geophysical features have yet to be examined on the ground. Field visits to the circular aeromagnetic anomalies transecting the Tahiratuq synform ('(?) Shonkinite', Fig. 3a, d) could verify whether these are shonkinite or another type of intrusion, possibly kimberlite. Field sampling and modelling of linear aeromagnetic anomalies in the Naujatuuq and Deep Rose belts, and sequence Ps4C in the core of the Whitehills synform are needed to determine the sources of these structural markers (Fig. 3d, 6). Numerous GSC core samples obtained from Western Uranium Corporation drill holes RHC-07-01, 02, and 03 are available for possible petrophysical calibration of the Naujatuuq anomalies, but visits to islands in Whitehills Lake would be required in the case of the anomalies in the core of the Whitehills synform. Apparent major detachments (labelled 'Unexplained, (?)related' and 'Woodburn Lake detachment', Fig. 3d) warrant further study.

Isotopic study of fluid inclusions in quartz could further test the relationships between precious-metal prospects at Mallery Lake (Turner et al., 2001, 2003) and various products of the Kivalliq igneous suite (Peterson et al., 2010, 2015a), including chert microstromatolites in the Pitz Formation southeast of Aberdeen Lake (Fig. 5e); the epithermal-style comb, crustiform, banded chalcedony, cockade, and lattice-bladed textures in quartz veins along the Judge Sissons and Thelon faults (Hunter et al., 2021); and the epithermal quartz ridges of the Athabasca Basin (Card, 2014). Samples from this GEM project are publicly available for further study from all of these putative 1.75 Ga quartz-vein and chert localities.

Metamorphic conundrums abound. How and when was the Marjorie terrane uplifted from mid-crustal levels, during intrusion of 1.83 to 1.81 Ga Hudsonian granite slabs and minette dykes, to the same level as adjacent terranes for the 1.76 to 1.74 Ga epithermal faulting and Kivalliq igneous events? Tschirhart et al. (2013b) explored different hypotheses for the nature of the faulting along the eastern side of the Marjorie terrane and proposed the Granite thrust, whereby the Marjorie terrane was emplaced eastward over the Pipedream and Half Way Hills assemblages, cutting off previous northwest-directed Hudsonian structures such as the Half Way thrust. Hunter et al. (2018, 2021) did not recognize the Granite thrust and showed the Pipedream and Half Way Hills assemblages as the same as the middle and lower packages of the Aberdeen assemblage, respectively; however, their map configuration is inconsistent with geochronology summarized here and with their own correlation diagram that recognizes the Pipedream and Half Way Hills assemblages as different in age from the middle and lower Aberdeen assemblages, respectively. The Wharton Lake fault system that uplifted the western side of the Marjorie terrane is interpreted as a low-angle extensional feature associated with accommodation of the thick pile of Kunwak formation siliciclastic rocks (A. LeCheminant, pers comm., 2016). Pehrsson et al. (2013a) predicted such uplifts during their D_{P3} extensional deformation; Tschirhart et al. (2015),

and Percival and Tschirhart (2017) modelled them for the Montresor Belt; and major extensional detachments in the northeastern corner of the study area are interpreted from aeromagnetic data (Fig. 3d). The nature and interrelationships of the Granite thrust, mylonitic Pukiiq Lake formation rhyolite and imbricates with Ketyet River quartzite east of it, the inferred Pukiiq detachment (Fig. 8), and the Wharton Lake fault system are worthy of further such research.

How sequence Ps4 can be of such low metamorphic grade compared to the middle amphibolite-facies grade of sequences Ps1 to Ps3 within 100 m or less has been explained by Percival et al. (2017) as a folded dip-slip fault wrapping around the main Montresor synform, whereas reinterpretation here suggests the metamorphic contrast is restricted to the southeastern side of that synform and associated with major dip-slip P-shears. The metamorphic contrast on the north-western side of the Montresor Belt is much less, as described by Frisch (2000) for the copper occurrence there ('Cu', top edge of Fig. 3a). This question is not resolved. In the north central Amer Belt, a high metamorphic contrast exists for the graben of sequence Ps4 redbeds that yielded 1.9 Ga detrital zircon from geochronology site 41a (Fig. 3a, Table 2). The drop in metamorphic grade from a mid-amphibolite sill with 1.83 Ga metamorphic zircon (W. Bleeker and M. Hamilton, unpub. data, 2018) in sequences Ps1 through Ps2 adjacent to that graben requires at least 10 km of fault offset (J. Percival, pers. comm., May 21, 2021), unlikely even though the bounding faults of that graben are significant.

Uncertainty also remains with respect to banded-gneiss units. Most of the nondescript granodioritic orthogneiss northwest of the Amer Belt (Agn, Fig. 3a) now appears to be Snow Island suite (Berman et al., 2015a). The amphibolite-biotite-banded tonalitic to granodioritic orthogneiss in the horst that exposes the Schultz Lake intrusive complex (Fig. 3a) is now believed to be Snow Island suite (Hunter et al., 2021) by inference from inherited zircon in the Schultz Lake intrusive complex. This granodioritic orthogneiss with biotite-hornblende mafic layers has been ignored by researchers, this project included, because of its perceived lack of exploration potential. The similar appearing granodioritic gneiss of the Turqavik horst has a very high aeromagnetic expression in contrast to that hosting the Schultz Lake intrusive complex — is the Turqavik gneiss also Snow Island suite? Given the potential for Ni-Cu-PGE mineralization in the Snow Island suite, more U-Pb ages and geochemical analyses of the Turqavik gneiss and eastern parts of the gneiss that hosts the Schultz Lake intrusive complex would help clarify their origin, mineral potential, and relationships to supracrustal rocks in the region.

SUMMARY AND CONCLUSIONS

Existing and new data for the Amer, Ketyet River, south-western Montresor, and five westerly Paleoproterozoic belts were compiled during the GEM-1 Uranium project. These

data support revisions and correlations of the stratigraphic sequences of each belt, consistent with the eight-formation lithostratigraphic succession proposed by Young (1979) for the Amer Belt. This amends the four Paleoproterozoic cover sequences of the central Rae Craton (Rainbird et al., 2010; Pehrsson et al., 2013a) as follows: sequence Ps1 is quartzite and conglomerate; sequence Ps2, mudstone and carbonate; sequence Ps3, basalt, mudstone, and sandstone with (only in the upper sequence Ps3 unit of the Amer Belt) stratabound uranium occurrences; and sequence Ps4, lithic feldspathic sandstone, mudstone, and carbonate with a marker unit of polymict conglomerate in the lower part of all three belts. Graphitic conductors are present in sequences Ps2 and Ps4 (references at the end of 'New definitions of sequences Ps1, Ps2, Ps3, and Ps4 in the Amer Belt' section). The structural paradigm set out by Pehrsson et al. (2013a) was also tested and confirmed by White et al. (2021, 2023). Sequences Ps1, Ps2, and Ps3 experienced intense deformation with weak metamorphism from after the 2.05 Ga mafic igneous event to before 1.865 Ga (end of Snowbird D_{p1} event), whereas sequence Ps4, together with all older strata, were subject only to Hudsonian deformation and metamorphism from earlier than 1.835 Ga to after 1.81 Ga (D_{p2} - D_{p4}). This updated knowledge of basement rocks underlying the Thelon Formation provides essential context for understanding the metallogeny of uranium as well as gold in this region.

The GEM-1 Uranium project has shown that exploration criteria from the Athabasca Basin such as hydrothermal alteration, reactivated faults, and basement geology can be adapted to the less well explored Thelon Basin, as theorized in the guiding hypothesis. Some broad similarities include

- basement terranes of both basins include widespread 2.60, 1.83, and 1.75 Ga intrusive and extrusive magmatic events, the latter two with similar volcanic rocks and alteration products;
- multiple complex sequences of arkosic lithic sandstone filled each basin after ca. 1.7 Ga, sourced from uranium-rich terranes and capped by stromatolitic dolostone;
- multiple diagenetic events pervasively altered their strata, leaving quartz as the dominant framework mineral and clay as the matrix;
- intersecting-reactivated fault systems initially controlled sedimentation and paleotopography, then focused saline hydrothermal fluid flow that generated chlorite-clay and other alteration of both basement rocks and basin fill, producing local geochemical anomalies and silicified zones;
- the geophysically translucent strata show only faint representation of the geochemical anomalies, such as U-Th-K, in gamma ray data;

- intersecting reactivated fault systems that localize deposits included both subvertical fractal Riedel-shear arrays with overall dextral transextensional indicators and low-angle compressional to extensional structures;
- alteration of monazite preferentially released uranium into peak diagenetic saline fluids, leaving behind thorium-bearing APS minerals;
- uranium-bearing fluorapatite locally cemented the lower sequences in each basin at the same time as, or slightly after, the APS minerals, and clearly after regional diagenetic illite;
- multiple stages of uranium mineralization and remobilization began about 100 Ma after the fluorapatite events and continued through the Phanerozoic; and
- basement-hosted alteration assemblages have gravity lows and serve as detailed exploration vectors.

Fundamental differences between these basins include their tectonic settings, detrital source terranes and prospective basement host rocks, as well as their detailed depositional and diagenetic sequences. Firstly, the Athabasca Basin straddles the Taltson magmatic zone, the south Rae and the Hearne cratons, including boundary zones such as the Snowbird tectonic zone, and all of these basement regions include amphibolite-facies grade, conductive graphitic-pyritic units to localize the major deposits. In contrast, the Thelon Basin rests entirely within the Rae Craton, the conductive Paleoproterozoic units of which are mainly slate grade and impermeable. The smaller and lower grade deposits of the Thelon Basin region occupy pyritic greywacke and epiclastic rocks of Neoproterozoic age rather than conductive graphitic schist. Secondly, the three major magmatic suites are reflected differently in the two basins. In the Athabasca Basin, its four unconformity-bounded sequences sampled detrital zircon from different hinterlands over time: Snow Island suite in sequence 1, Hudson granite to Martell syenite and Archean terranes in sequences 2 to 4, with sparse input from the 1.75 Ga Kivalliq igneous suite only in sequence 3. For the Thelon Basin, the Archean Woodburn Lake group and Snow Island suite contributed most of the detrital zircon, whereas the Hudson suite contributed little and the Kivalliq igneous suite none. On the other hand, both basins show potential localizing effects of individual Hudson and Kivalliq igneous suite intrusions. Thirdly, the siliciclastic sequences and volcanic components do not correlate between basins. Fourthly, the fluorapatite cement is ca. 1688 ± 14 Ma in the south Thelon Basin and 1667 ± 5 Ma in the northeast Thelon Basin, but 1638 ± 5 Ma across the Athabasca Basin, documenting temporally and spatially independent early stages of their successive diagenetic-hydrothermal alteration and ore-forming events. Lastly, geochronology of deposit-related alteration minerals by $^{40}\text{Ar}/^{39}\text{Ar}$ and the uraninite itself by U-Pb analysis is far advanced in the Athabasca Basin, with a plausible primary uranium-mineralization event at 1588 ± 15 Ma having been

reset by a series of subsequent distal events. Uranium-lead dating in the Thelon Basin region has so far been unable to ‘see through’ the resetting events despite their similar mineral parageneses. In summary, most of the uranium-exploration criteria of the Athabasca Basin apply to the Thelon Basin, but differ in detail, requiring markedly different strategies.

ACKNOWLEDGMENTS

The elders, as well as the associations of hunters and trappers and their members, in the communities of Baker Lake, Chesterfield Inlet and Rankin Inlet, and the Kivalliq Inuit Association (Luis Manzo and Veronica Tattuinee), provided a sounding board for project proposals, advice on where to find certain rocks, and guidance and approval on proceeding to do fieldwork in their ancestral lands. They also provided numerous place names for reference localities. The Nunavut Water Board and Government of Nunavut, in particular Eric Prosh, Linda Ham, and Ronnie Suluk, provided guidance similar to that of the elders from their perspectives as policy managers and field officer, respectively. Karen Costello generously advised on much of the community and industry consultations, as well as regulatory requirements, from the perspective of the former Indian and Northern Affairs Canada.

Lesley Chorlton has been an essential partner in building the spatial geodatabase of knowledge for the northeast Thelon Basin region (publication in progress) that is synthesized in this paper. Tom Skulski shared an early version of his regional compilation (Skulski et al., 2018) in 2009, thereby providing considerable initial guidance in both regional geoscience and a substantial ArcGIS® geodatabase framework for the study area. Cameco Corporation (Garth Drever) and AREVA Resources Canada (Thomas Riegler) respectively shared detailed digital geological maps of the Amer Belt (*see* Young, 1979) and the Kiggavik exploration camp (courtesy of Urangesellschaft Canada Limited). Similarly, Tony LeCheminant shared an unpublished geology map of the Schultz Lake area that had been compiled by Larry Aspler in the 1990s. It includes outcrop observations by Alan Donaldson, Alan Miller, and Tony LeCheminant. These unpublished maps comprise outcrop-scale field observations that contributed great value to this project.

The authorship of this paper represents the GEM-1-supported scientific leaders who spearheaded new knowledge of the Marjorie–Kiggavik–Tehek Belt, and of key elements relevant to the entire Aberdeen Subbasin region. Scientific leaders who focused mainly on the Amer Belt region — Rob Rainbird, Grant Young, and Joe White — are co-authors of two journal papers cited herein and a Geological Survey of Canada bulletin in progress on that region. They contributed strongly to that key component of this overall GEM-1 study. Beth McClenaghan stepped in to supervise Scott Robinson when a flood prevented Roger Paulen from joining the authors in the field. Brigitte Leblon, Armand

LaRocque, Dave Lentz, and Yask Shelat contributed analyses of RADARSAT imagery integrated with outcrop data that helped find outcrops to plan traverses, to define large structures, and map the extent of the Ordovician dolostone. Darrel Long catalogued valuable photographic (e.g. Fig. 5g) and written documentation by Grant Young. The excellent work of many students funded through the GEM-1 program is acknowledged here, in addition to citations of their theses and publications.

Considerable scientific leadership and collaboration by industry were formalized by letters of agreement between eight exploration companies, Nunavut Tunngavik Incorporated, and the GSC. AREVA Resources Canada (now Orano Canada Inc.), Bayswater Uranium Corporation, Cameco Corporation, Forum Uranium Corporation, Mega Uranium Ltd., Titan Uranium Inc., Uranium North Resources Corporation, and Western Uranium Company Limited (now Western Uranium and Vanadium Company Limited) all shared geophysical data, geological knowledge, and logistical support. Orano and Forum geologists (e.g. Dave Quirt, Thomas Riegler, Ken Wheatley, and Peter Wollenberg) continued informal joint research, discussions, and student support long after the agreements had expired. Beth Hillary, Deborah Lemkow, Angela Ford, Igor Bilot, Jacques Pinard, many undergraduate student assistants, logistical support by Boris Kotelewetz and Helen Moffat through Baker Lake Lodge and Ookpik Aviation, and staff of the industry partners provided enormous support over the years since 2006. Rebecca Hunter, Eric Potter, Natasha Wodicka, and John Percival provided highly constructive critical reviews that greatly improved the manuscript. Comprehensive and thorough technical editing by Marie-France Dufour and Evelyn Inglis, and layout by Paul Champagne, enhanced clarity and consistency of the final product.

REFERENCES

- Acosta-Góngora, P., Pehrsson, S.P., Knox, B., Regis, D., Hulbert, L., Creaser, R.A., and Ashton, K., 2018. Neoproterozoic convergent margin Ni-Cu mineralization? Axis Lake and Nickel King Ni-Cu deposits in the south Rae Province craton of the Canadian Shield; *Precambrian Research*, v. 316, p. 305–323.
- Alexandre, P., Kyser, K., Thomas, D., Polito, P., and Marlatt, J., 2009. Geochronology of unconformity-related uranium deposits in the Athabasca Basin, Saskatchewan, Canada and their integration in the evolution of the basin; *Mineralium Deposita*, v. 44, p. 41–59. <https://doi.org/10.1007/s00126-007-0153-3>
- Alwmark, C., Bleeker, W., LeCheminant, A.N., Page, L., and Schersten, A., 2017. An Early Ordovician ^{40}Ar - ^{39}Ar age for the ~50 km Carswell impact structure, Canada; *Geological Society of America Bulletin*, v. 129, p. 1442–1449. <https://doi.org/10.1130/B31666.1>
- Anand, A. and Jefferson, C.W., 2017a. Reactivated fault systems and their effects on outcrop patterns of thin-skinned early thrust imbrications in the Kiggavik uranium camp, Nunavut; Geological Survey of Canada, Open File 7895, 9 p. <https://doi.org/10.4095/302776>
- Anand, A. and Jefferson, C.W., 2017b. Outcropping and remotely predicted lineaments, faults, fractures and dykes in the Kiggavik uranium camp of Nunavut; Geological Survey of Canada, Open File 7896, 8 p. <https://doi.org/10.4095/302777>
- Annesley, I.R., 1990. Petrochemistry of the Woodburn Lake group komatiitic suite, Amer Lake, N.W.T., Canada; Ph.D. thesis, University of Ottawa, Ottawa, Ontario, 404 p.
- Armitage, A.R., 2013. Technical report on the Patterson Lake, Patterson Lake South and Clearwater West properties, Northern Saskatchewan; 43-101 report for Fission Uranium Corp. and Fission Energy Corp, 132 p. <https://www.fission3corp.com/wp-content/uploads/2013/04/as_FCU-PLS_PL_CW-Technical-Report-18Mar2013.pdf> [accessed September 2019]
- Ashton, K.E., 1988. Precambrian geology of the southeastern Amer Lake area (66H/1), near Baker Lake, N.W.T.; Ph.D. thesis, Queen's University, Kingston, Ontario, 335 p.
- Ashton, K.E., Chi, G., Rayner, N.M., and McFarlane, C., 2013. Geological history of granitic rocks hosting uranium mineralization in the Ace-Fay-Verna-Dubyna Mines area, Beaverlodge Uranium District; *in* Summary of Investigations 2013, Volume 2; Saskatchewan Geological Survey, Saskatchewan Ministry of the Economy, Miscellaneous Report 2013-4.2, Paper A-1, 23 p.
- Aspler, L.B., Chiarenzelli, J.R., Cousens, B.L., and Valentino, D., 1999. Precambrian geology, northern Angikuni Lake, and a transect across the Snowbird tectonic zone, western Angikuni Lake, Northwest Territories (Nunavut); *in* Current Research 1999-C; Geological Survey of Canada, p. 107–118. <https://doi.org/10.4095/210176>
- Aura Silver Resources Inc., 2018. Aura provides update on the 2018 Greyhound exploration program; Press Release #18-12, December 3, 2018. <www.aurasilver.com/news/2018> [accessed September 25, 2019]
- Aylsworth, J.M. and Shilts, W.W., 1989. Glacial features around the Keewatin Ice Divide: districts of Mackenzie and Keewatin; Geological Survey of Canada, Paper 88-24, 21 p. <https://doi.org/10.4095/127320>
- Aylsworth, J.M., Cunningham, C.M., and Shilts, W.W., 1990. Surficial geology, Schultz Lake, District of Keewatin, Northwest Territories; Geological Survey of Canada, Preliminary Map 43-1989, scale 1:125 000. <https://doi.org/10.4095/130943>
- Barrie, C.T., 1995. Magmatic platinum group elements; *in* Geology of Canadian mineral deposit types, (ed.) O.R. Eckstrand, W.D. Sinclair, and R.I. Thorpe; Geological Survey of Canada, Geology of Canada, no. 8, p. 605–614 (*also* Geological Society of America, The geology of North America, v. P-1). <https://doi.org/10.4095/208044>
- Berman, R.G., Davis, W.J., and Pehrsson, S., 2007. Collisional Snowbird tectonic zone resurrected: growth of Laurentia during the 1.9 Ga accretionary phase of the Hudsonian orogeny, *Geology*; Geological Society of America Bulletin, v. 35, p. 911–914. <https://doi.org/10.1130/G23771A.1>

- Berman, R.G., Sanborn-Barrie, M., Rayner, N.M., Carson, C., Sandeman, H.A., and Skulski, T., 2010. Petrological and in situ SHRIMP geochronological constraints on the tectonometamorphic evolution of the Committee Bay belt, Rae Province, Nunavut; *Precambrian Research*, v. 181, p. 1–20. <https://doi.org/10.1016/j.precamres.2010.05.009>
- Berman, R.G., Pehrsson, S., Davis, W.J., Ryan, J.J., Qui, H., and Ashton, K.E., 2013. The Arrowsmith orogeny: geochronological and thermobarometric constraints on its extent and tectonic setting in the Rae craton, with implications for pre-Nuna supercontinent reconstruction; *Precambrian Research*, v. 232, p. 44–69. <https://doi.org/10.1016/j.precamres.2012.10.015>
- Berman, R.G., Nadeau, L., Percival, J.A., Harris, J., Girard, É., Whalen, J.B., Davis, W.J., Kellett, D., Jefferson, C.W., Camacho, A., and Bethune, K., 2015a. Geo-Mapping Frontiers' Chantrey project: bedrock geology and multidisciplinary supporting data of a 550 kilometre transect across the Thelon tectonic zone, Queen Maud block, and adjacent Rae Craton; Geological Survey of Canada, Open File 7698, 39 p. <https://doi.org/10.4095/296202>
- Berman, R.G., Davis, W.J., Whalen, J.B., McCurdy, M.W., Craven, J.A., and Roberts, B.J., 2015b. Report of activities for the geology and mineral potential of the Chantrey-Thelon area: GEM-2 Thelon tectonic zone, Montresor belt and Elu basin projects; Geological Survey of Canada, Open File 7964, 19 p. <https://doi.org/10.4095/297302>
- Bernier, S., 2004: Stratigraphy of the Late Paleoproterozoic Manitou Falls Formation, in the vicinity of the McArthur River uranium deposit, Athabasca Basin, Saskatchewan, Canada; M.Sc. thesis, Laurentian University, Sudbury, Ontario, 184 p.
- Bethune, K.M., Berman, R.G., Rayner, N., and Ashton, K.E., 2013. Structural, petrological and U–Pb SHRIMP geochronological study of the western Beaverlodge domain: implications for crustal architecture, multi-stage orogenesis and the extent of the Taltson orogen in the SW Rae craton, Canadian Shield; *Precambrian Research*, v. 232, p. 89–118. <https://doi.org/10.1016/j.precamres.2013.01.001>
- Beyer, S.R., Kyser, K., Hiatt, E.E., and Fraser, I., 2010. Geological evolution and exploration geochemistry of the Boomerang Lake unconformity-type uranium prospect, Northwest Territories, Canada; *Society of Economic Geologists, Special Publication 15*, p. 675–702.
- Blackwell, J.D., 1978. Amer Option, Year-end Report 1977, Cominco Ltd.: Mineral Assessment Report 061789, Indian and Northern Affairs Canada, Yellowknife, Assessment Report 061789, 18 p.
- Bleeker, W., Hamilton, M., Ryan, J., and Ernst, R., 2010. Pelly Bay dykes: A new magmatic event for northern Laurentia at 1692 Ma; *in* Reconstruction of supercontinents back to 2.7 Ga using the large igneous province (LIP) record: with implications for mineral deposit targeting, hydrocarbon resource exploration, and earth system evolution, 6 p. <www.supercontinent.org> [accessed April 15, 2011]
- Bolton, T.E. and Nowlan, G.S., 1979. A Late Ordovician fossil assemblage from an outlier north of Aberdeen Lake, District of Keewatin; *in* Contributions to Canadian Paleontology, (ed.) P.J. Griffin; Geological Survey of Canada, Bulletin 321, p. 1–26. <https://doi.org/10.4095/106171>
- Bosman, S.A. and Ramaekers, P., 2015. Athabasca Group + Martin Group = Athabasca Supergroup? Athabasca Basin multiparameter drill log compilation and interpretation, with updated geological map; *in* Summary of Investigations 2015, Volume 2; Saskatchewan Geological Survey, Saskatchewan Ministry of the Economy, Miscellaneous Report 2015-4.2, Paper A-5, 13 p.
- Bostock, H.H. and van Breemen, O., 1994. Ages of detrital and metamorphic zircons and monazites from a pre-Taltson magmatic zone basin at the western margin of Rae Province; *Canadian Journal of Earth Sciences*, v. 31, p. 1353–1364. <https://doi.org/10.1139/e94-118>
- Bowring, S.A. and Ross, G.M., 1985. Geochronology of the Narakay Volcanic Complex: implications for the age of the Coppermine Homocline and Mackenzie igneous events; *Canadian Journal of Earth Sciences*, v. 22, p. 774–781.
- Bridge, N.J., Banerjee, N.R., Pehrsson, S., Fayek, M., Finnigan, C.S., Ward, J., and Berry, A., 2013. The Lac Cinquante uranium deposit, western Churchill Province, Nunavut, Canada; *Exploration and Mining Geology*, v. 21, p. 27–50.
- Buchan, K.L. and Ernst, R.E., 2013. Diabase dyke swarms of Nunavut, Northwest Territories, and Yukon, Canada; Geological Survey of Canada, Open File 7464, 24 p. <https://doi.org/10.4095/293149>
- Calhoun, L., White, J.C., Jefferson, C.W., Patterson, J., and Tschirhart, V., 2014. Integrated geodatabase study of the complexly deformed U-hosting Paleoproterozoic Amer Group, Nunavut; Geological Survey of Canada, Scientific Presentation 19, 26 p. <https://doi.org/10.4095/293108>
- Card, C., 2014. Altered pelitic gneisses and associated “quartzite ridges” beneath the southeastern Athabasca Basin: alteration facies and their relationship to uranium deposits along the Wollaston–Mudjatik transition; *in* Summary of Investigations 2013, Volume 2; Saskatchewan Geological Survey, Saskatchewan Ministry of the Economy, Miscellaneous Report 2013-4.2, Paper A-4, 23 p.
- Card, C., 2017. Distribution and significance of crystalline rocks in the Patterson Lake uranium exploration corridor of northwest Saskatchewan; *in* Summary of Investigations 2017, Volume 2; Saskatchewan Geological Survey, Saskatchewan Ministry of the Economy, Miscellaneous Report 2017-4.2, Paper A-11, 18 p.
- Card, C. and Noll, J., 2016. Host-rock protoliths, pre-ore metasomatic mineral assemblages and textures, and exotic rocks in the western Athabasca Basin: ore-system controls and implications for the unconformity-related uranium model; *in* Summary of Investigations 2016, Volume 2; Saskatchewan Geological Survey, Saskatchewan Ministry of the Economy, Miscellaneous Report 2016-4.2, Paper A-8, 19 p.
- Card, C.D., Pană, D., Portella, P., Thomas, D.J., and Annesley, I.R., 2007. Basement rocks to the Athabasca Basin, Saskatchewan and Alberta; *in* EXTECH IV: Geology and Uranium EXploration TECHnology of the Proterozoic Athabasca Basin, Saskatchewan and Alberta, (ed.) C.W. Jefferson and G. Delaney; Geological Survey of Canada, Bulletin 588, p. 69–87. <https://doi.org/10.4095/223745>

- Card, C.D., Bethune, K.M., Davis, W.J., Rayner, N., and Ashton, K.E., 2014. The case for a distinct Taltson orogeny: evidence from northwest Saskatchewan, Canada; *Precambrian Research*, v. 255, pt. 1, p. 245–265. <https://doi.org/10.1016/j.precamres.2014.09.022>
- Cecile, M.P., 1973. Lithofacies analysis of the Proterozoic Thelon Formation, Northwest Territories (including computer analysis of field data); M.Sc. thesis, Carleton University, Ottawa, Ontario, 119 p.
- Chamberlain, K.R., Schmitt, A.K., Swapp, S.M., Harrison, T.M., Swoboda-Colberg, N., Bleeker, W., Peterson, T.D., Jefferson, C.W., and Khudoley, A.K., 2010. In-situ U-Pb (IN_SIMS) micro-baddeleyite dating of mafic rocks: method with examples; *Precambrian Research*, v. 183, p. 379–387. <https://doi.org/10.1016/j.precamres.2010.05.004>
- Charbonneau, B.W. and Swettenham, S.S., 1986. Gold occurrences in radioactive calc-silicate float at Sandybeach Lake, Nueltin Lake area, District of Keewatin; *in Current Research, Part A; Geological Survey of Canada, Paper 1986-A*, p. 803–808. <https://doi.org/10.4095/120457>
- Chi, G., Li, Z., Chu, H., Bethune, K.M., Quirt, D.H., Ledru, P., Normand, C., Card, C., Bosman, S., Davis, W.J., and Potter, E.G., 2018. A shallow-burial mineralization model for the unconformity-related uranium deposits in the Athabasca Basin; *Economic Geology*, v. 113, no. 5, p. 1209–1217. <https://doi.org/10.5382/econgeo.2018.4588>
- Chi, G., Chu, H., Petts, D., Potter, E.G., and Williams-Jones, A.E., 2019. Uranium-rich diagenetic fluids provide the key to unconformity-related uranium mineralization in the Athabasca Basin; *Nature Scientific Reports*, v. 9, p. 5530. <https://doi.org/10.1038/s41598-019-42032-0>
- Collier, B. and Yeo, G.M., 2001. Stratigraphy of the Paleoproterozoic Manitou Falls B Member at the Deilmann pit, Key Lake, Saskatchewan; *in Summary of Investigations 2001, Volume 2; Saskatchewan Geological Survey, Saskatchewan Energy and Mines, Report 2001-4.2*, p. 297–305.
- Corriveau, L., Montreuil, J.-F., and Potter, E.G., 2016. Alteration facies linkages among IOCG, IOA and affiliated deposits in the Great Bear magmatic zone, Canada; *in Proterozoic iron oxide-apatite (\pm REE) and iron oxide-copper-gold and affiliated deposits of Southeast Missouri, U.S.A., and the Great Bear magmatic zone, Northwest Territories, Canada*, (ed.) J. Slack, L. Corriveau, and M. Hitzman; *Economic Geology*, v. 111, p. 2045–2072.
- Côté-Mantha, O., Gosselin, G., Vaillancourt, D., and Blackburn, A., 2015. Amaruq: a new gold discovery in Nunavut, Canada; *in Proceedings, NewGenGold 2015; Pan Pacific Perth*, November 17–18, p. 41–56.
- Coyle, M. and Kiss, F., 2012. Residual total magnetic field, aeromagnetic survey of the Tehery Lake area, NTS 56-A/SW, 56-B/SE, and parts of 56-A/NW and 56-B/NE, Nunavut / Composante résiduelle du champ magnétique total, levé aéromagnétique de la région du Lac Tehery, SNRC 56-A/SW, 56-B/SE et parties de 56-A/NW et 56-B/NE, Nunavut; Geological Survey of Canada, Open File 7203, scale 1:100 000. <https://doi.org/10.4095/291780>
- Craven, J.A., McNeice, G., Powell, B., Koch, R., Annesley, I.R., Wood, G., Mwenifumbo, C.J., Unsworth, M.J., and Xiao, W., 2007. Audio-magnetotelluric studies at the McArthur River mining camp and Shea Creek area, northern Saskatchewan; *in EXTECH IV: Geology and Uranium EXploration TECHnology of the Proterozoic Athabasca Basin, Saskatchewan and Alberta*, (ed.) C.W. Jefferson and G. Delaney; Geological Survey of Canada, Bulletin 588, p. 413–424. <https://doi.org/10.4095/223785>
- Creaser, R.A. and Stasiuk, L.D., 2007. Depositional age of the Douglas Formation, northern Saskatchewan, determined by Re-Os geochronology; *in EXTECH IV: Geology and Uranium EXploration TECHnology of the Proterozoic Athabasca Basin, Saskatchewan and Alberta*, (ed.) C.W. Jefferson and G. Delaney; Geological Survey of Canada, Bulletin 588, p. 341–346. <https://doi.org/10.4095/223779>
- Cuney, M., 2010. Evolution of uranium fractionation processes through time: driving the secular variation of uranium deposit types; *Economic Geology*, v. 105, p. 553–569. <https://doi.org/10.2113/gsecongeo.105.3.553>
- Cuney, M. and Brisbin, D., 2010. SEG-PDAC 2010 Uranium geology and deposit types course; Society of Economic Geologists and Prospectors and Developers Association of Canada, Toronto, March 5–6, 2010, 311 p.
- Davidson, G.I. and Gandhi, S.S., 1989. Unconformity-related U-Au mineralization in the Middle Proterozoic Thelon sandstone, Boomerang Lake prospect, Northwest Territories, Canada; *Economic Geology*, v. 84, p. 143–157. <https://doi.org/10.2113/gsecongeo.84.1.143>
- Davis, W.J., 2021. U-Pb zircon age data for supracrustal samples from the White Hills Lake to Amer Lake area, Rae Province, Nunavut, Canada; Geological Survey of Canada, Open File 8807, 6 p. <https://doi.org/10.4095/328453>
- Davis, W.J. and Zaleski, E., 1998. Geochronological investigations of the Woodburn Lake group, western Churchill Province, Northwest Territories: preliminary results; *in Radiogenic age and isotopic studies, report 11; Geological Survey of Canada, Current Research 1998-F*, p. 89–97. <https://doi.org/10.4095/210060>
- Davis, W.J., Gall, Q., Jefferson, C.W., and Rainbird, R.H., 2011. Fluorapatite in the Paleoproterozoic Thelon Basin: structural-stratigraphic context, in situ ion microprobe U-Pb ages, and fluid-flow history; *Geological Society of America, Bulletin*, v. 123, no. 5-6, p. 1056–1073. <https://doi.org/10.1130/B30163.1>
- Davis, W.J., Gandhi, S.S., Enright, A., Gall, Q., Hunt, P., and Jefferson, C.W., 2012. Age of diagenetic apatite cements from the unconformity-type Boomerang Lake uranium occurrence, Paleoproterozoic Thelon Basin, Nunavut; *Geological Association of Canada–Mineralogical Association of Canada, Abstracts*, v. 35, p. 33.
- Davis, W., Berman, R.G., and MacKinnon, A., 2013. U-Pb geochronology of archival rock samples from the Queen Maud block, Thelon tectonic zand Rae Craton, Kitikmeot Region, Nunavut, Canada; Geological Survey of Canada, Open File 7409, 42 p. <https://doi.org/10.4095/292663>

- Davis, W.J., Berman, R.G., Nadeau, L., and Percival, J.A., 2014. U-Pb zircon geochronology of a transect across the Thelon tectonic zone, Queen Maud region, and adjacent Rae Craton, Kitikmeot Region, Nunavut, Canada; Geological Survey of Canada, Open File 7652, 41 p. <https://doi.org/10.4095/295177>
- Davis, W.J., Pehrsson, S.J., and Percival, J.A., 2015. Results of a U-Pb zircon geochronology transect across the southern Rae Craton, N.W.T., Canada: 2009–2014; Geological Survey of Canada, Open File 7655, 74 p. <https://doi.org/10.4095/295610>
- Davis, W.J., Zaleski, E., and Emon, Q., 2021. U-Pb geochronology of volcanic and plutonic rocks from the White Hills Lake to Meadowbank River area, Rae Province, Nunavut, Canada; Geological Survey of Canada, Open File 8766, 11 p. <https://doi.org/10.4095/327936>
- Donaldson, J.A., 1965. The Dubawnt Group, districts of Keewatin and Mackenzie; Geological Survey of Canada, Paper 64-20, 11 p. <https://doi.org/10.4095/101035>
- Donaldson, J. A., 1966. Geology, Schultz Lake, District of Keewatin; Geological Survey of Canada, Preliminary Map 7-1966, scale 1:253 440. <https://doi.org/10.4095/107734>
- Dziawa, C., Gaidies, F., and Percival, J., 2019. Conditions and timing of low-pressure–high-temperature metamorphism in the Montresor belt, Rae Province, Nunavut; Canadian Journal of Earth Sciences, v. 56, no. 6, p. 654–671. <https://doi.org/10.1139/cjes-2018-0184>
- Eckstrand, O.R., 1995. Nickel-copper sulphide; in Geology of Canadian mineral deposit types, (ed.) O.R. Eckstrand, W.D. Sinclair, and R.I. Thorpe; Geological Survey of Canada, Geology of Canada, no. 8, p. 584–605 (also Geological Society of America, The geology of North America, v. P-1). <https://doi.org/10.4095/208042>
- Forum Energy Metals, 2021. Exploring Saskatchewan’s Wollaston Copperbelt: Janice Lake Sedimentary Copper Project (Rio Tinto Canada Option). <<https://www.forumenergymetals.com/projects/overview/>> [accessed May 5, 2021]
- Fraser, J.A., 1988. Geology, Woodburn Lake, District of Keewatin, Northwest Territories; Geological Survey of Canada, Map 1656A, scale 1:250 000. <https://doi.org/10.4095/126936>
- Frisch, T., 1992. Geology, Ian Calder Lake, District of Keewatin, Northwest Territories; Geological Survey of Canada, Map 1780A, scale 1:250 000. <https://doi.org/10.4095/183920>
- Frisch, T., 2000. Precambrian geology of Ian Calder Lake, Cape Barclay, and part of Darby Lake map areas, south-central Nunavut; Geological Survey of Canada, Bulletin 542, 51 p. <https://doi.org/10.4095/211320>
- Fuchs, H.D. and Hilger, W., 1989. Kiggavik (Lone Gull): an unconformity related uranium deposit in the Thelon Basin, Northwestern Territories, Canada; in Uranium resources and geology of North America, (ed.) E. Muller-Kahle; International Atomic Energy Agency, Technical Document, IAEA-TECDOC-500, p. 429–454.
- Fuchs, H., Hilger, W., and Prosser, E., 1986. Geology and exploration history of the Lone Gull property; in Uranium deposits of Canada, (ed.) L. Evans; Canadian Institute of Mining and Metallurgy, Special Volume 33, p. 286–292.
- Gaboreau, S., Cuney, M., Quirt, D., Patrier, P., and Mathieu, R., 2007. Significance of aluminum phosphate-sulfate minerals associated with U unconformity-type deposits: the Athabasca basin, Canada; The American Mineralogist, v. 92, no. 2-3, p. 267–280. <https://doi.org/10.2138/am.2007.2277>
- Gall, Q., 1992. The early Proterozoic Thelon paleosol as part of the Matonabee unconformity, northwestern Canadian Shield; in Mineralogical and geochemical records of paleoweathering, (ed.) J.M. Schmitt and Q. Gall; International Geoscience Programme 317, Mémoires des sciences de la Terre, École des mines de Paris, v. 18, p. 163–174.
- Gall, Q., 1994. The Proterozoic Thelon paleosol, Northwest Territories, Canada; Precambrian Research, v. 68, no. 1-2, p. 115–137. [https://doi.org/10.1016/0301-9268\(94\)90068-X](https://doi.org/10.1016/0301-9268(94)90068-X)
- Gall, Q. and Donaldson, J.A., 2006. Diagenetic fluorapatite and aluminum phosphate-sulphate in the Paleoproterozoic Thelon Formation and Hornby Bay Group, northwestern Canadian Shield; Canadian Journal of Earth Sciences, v. 43, no. 5, p. 617–629. <https://doi.org/10.1139/e06-011>
- Gall, Q., Peterson, T.D., and Donaldson, J.A., 1992. A proposed revision of early Proterozoic stratigraphy of the Thelon and Baker Lake basins, Northwest Territories; in Current Research, Part C; Geological Survey of Canada, Paper 92-1C, p. 129–137. <https://doi.org/10.4095/132856>
- Gandhi, S.S., 1989. Geology and uranium potential of the Thelon Basin and adjacent basement in comparison with the Athabasca Basin region; in Uranium resources and geology of North America, (ed.) E. Muller-Kahle; International Atomic Energy Agency, Technical Document, IAEA-TECDOC-500, p. 411–428.
- Gandhi, S.S., 1995. An overview of the exploration history and genesis of Proterozoic uranium deposits in the Canadian Shield; Exploration and Research for Atomic Minerals, v. 8, p. 1–47.
- Gandhi, S.S., Prasad, N., Chorlton, L.B., Richer, C., and Lentz, D.R., 2015. Canadian U-Th-REE deposit and occurrence database; Geological Survey of Canada, Open File 7854, 9 p. <https://doi.org/10.4095/297481>
- Gandhi, S.S., Potter, E.G., and Fayek, M., 2018. New constraints on genesis of the polymetallic veins at Port Radium, Great Bear Lake, Northwest Canadian Shield; Ore Geology Reviews, v. 96, p. 28–47. <https://doi.org/10.1016/j.oregeorev.2018.04.002>
- Geological Survey of Canada, 2017a. Surficial geology, Schultz Lake, Nunavut, NTS 66-A, Geological Survey of Canada, Canadian Geoscience Map 324, (preliminary edition, Surficial Data Model, v. 2.3 conversion of Map 43-1989), scale 1:125 000. <https://doi.org/10.4095/305328>
- Geological Survey of Canada, 2017b. Surficial geology, Aberdeen Lake, Nunavut, NTS 66-B, Geological Survey of Canada, Canadian Geoscience Map 323 (preliminary edition, Surficial Data Model, v. 2.3 conversion of Map 44-1989), scale 1:125 000. <https://doi.org/10.4095/304279>
- Gosselin, P. and Dubé, B., 2015. World lode gold deposit database; Geological Survey of Canada, Open File 7930, 27 p. <https://doi.org/10.4095/297322>

- Grare, A., Benedicto, A., Lacombe, O., Trave, A., Ledru, P., Blain, M., and Robbins, J., 2018. The Contact uranium deposit, Kiggavik Project, Nunavut (Canada): tectonic history, structural constraints and timing of mineralization; *Ore Geology Reviews*, v. 93, p. 141–167. <https://doi.org/10.1016/j.oregeorev.2017.12.015>
- Grunsky, E., Harris, J., and McMartin, I., 2009. Predictive mapping of surficial materials, Schultz Lake area (NTS 66A), Nunavut, Canada; *in* Remote sensing and spectral geology, (ed.) R. Bedell, A.P. Crosta, and E. Grunsky; *Reviews in Economic Geology*, v. 16, p. 177–198.
- Grunsky, E.C., McCurdy, M.W., Pehrsson, S.J., Peterson, T.D., and Bonham-Carter, G.F., 2012. Predictive geologic mapping and assessing the mineral potential in NTS 65A/B/C, Nunavut, with new regional lake sediment geochemical data; *Geological Survey of Canada*, Open File 7175, 1 poster. <https://doi.org/10.4095/291920>
- Györfi, I., Hajnal, Z., White, D.J., Takács, E., Reilkoff, B., Annesley, I.R., Powell, B., and Koch, R., 2007. High-resolution seismic survey from the McArthur River region: contributions to mapping the complex P2 uranium ore zone, Athabasca Basin, Saskatchewan; *in* EXTECH IV: Geology and uranium EXploration TECHnology of the Proterozoic Athabasca Basin, Saskatchewan and Alberta, (ed.) C.W. Jefferson and G. Delaney; *Geological Survey of Canada*, Bulletin 588, p. 397–412. <https://doi.org/10.4095/223784>
- Hadlari, T. and Rainbird, R.H., 2011. Retro-arc extension and continental rifting: a model for the Paleoproterozoic Baker Lake Basin, Nunavut; *Canadian Journal of Earth Sciences*, v. 48, no. 8, p. 1232–1258. <https://doi.org/10.1139/c11-002>
- Hadlari, T., Rainbird, R.H., and Pehrsson, S.J., 2004. Geology, Schultz Lake, Nunavut; *Geological Survey of Canada*, Open File 1839, scale 1:250 000. <https://doi.org/10.4095/215673>
- Hajnal, Z., Takács, E., White, D.J., Györfi, I., Powell, B., and Koch, R., 2007. Regional seismic signature of the basement and crust beneath the McArthur River mine district, Athabasca Basin, Saskatchewan; *in* EXTECH IV: Geology and uranium EXploration TECHnology of the Proterozoic Athabasca Basin, Saskatchewan and Alberta, (ed.) C.W. Jefferson and G. Delaney; *Geological Survey of Canada*, Bulletin 588, p. 389–396. <https://doi.org/10.4095/223783>
- Harvey, B.J.A., Coyle, M., Buckle, J.L., Carson, J.M., and Hefford, S.W., 2011. Geophysical Series, airborne geophysical survey of the northeast Thelon Basin, Nunavut, NTS 66 A, parts of 66 B, 66 C, 66 G and 66 H / Série des cartes géophysiques, levé géophysique aéroporté de la partie nord-est du Bassin de Thelon, Nunavut, SNRC 66 A, parties des 66 B, 66 C, 66 G et 66 H; *Geological Survey of Canada*, Open File 6510, scale 1:250 000. <https://doi.org/10.4095/288204>
- Hayward, N., Harris, J.R., Grunsky, E., Beauchemin, M., Jefferson, C., and Peterson, T., 2013. Geo-mapping Frontiers: predictive geology map of the Ennadai region, Nunavut; *Geological Survey of Canada*, Open File 7485, 21 p. <https://doi.org/10.4095/293261>
- Henderson, J.R. and Henderson, M.N., 1994. Geology, Whitehills-Tehek lakes area, District of Keewatin, Northwest Territories; *Geological Survey of Canada*, Open File 2923, scale 1:100 000. <https://doi.org/10.4095/194832>
- Henderson, J.R. and Roddick, J.C., 1990. U-Pb age constraint on the Wager shear zone, District of Keewatin, N.W.T.; *in* Radiogenic age and isotopic studies, report 3; *Geological Survey of Canada*, Paper 89-2, p. 149–152. <https://doi.org/10.4095/129080>
- Hendry, H.E. and Wheatley, K.L., 1985. The Carswell Formation, northern Saskatchewan: stratigraphy, sedimentology and structure; *in* The Carswell structure uranium deposits, Saskatchewan, (ed.) R. Lainé, D. Alonso, and M. Svab; *Geological Association of Canada*, Special Paper 28, p. 87–103.
- Hiatt, E. and Kyser, K., 2007. Sequence stratigraphy, hydrostratigraphy, and mineralizing fluid flow in the Proterozoic Manitou Falls Formation, eastern Athabasca Basin, Saskatchewan; *in* EXTECH IV: Geology and uranium EXploration TECHnology of the Proterozoic Athabasca Basin, Saskatchewan and Alberta, (ed.) C.W. Jefferson and G. Delaney; *Geological Survey of Canada*, Bulletin 588, p. 489–506. <https://doi.org/10.4095/223793>
- Hiatt, E.E., Kyser, K., and Dalrymple, R.W., 2003. Relationships among sedimentology, stratigraphy, and diagenesis in the Proterozoic Thelon Basin, Nunavut, Canada: implications for paleo-aquifers and sedimentary-hosted mineral deposits; *Journal of Geochemical Exploration*, v. 80, no. 2-3, p. 221–240. [https://doi.org/10.1016/S0375-6742\(03\)00192-4](https://doi.org/10.1016/S0375-6742(03)00192-4)
- Hoeve, J. and Quirt, D.H., 1984. Mineralization and host rock alteration in relation to clay mineral diagenesis and evolution of the Middle-Proterozoic, Athabasca Basin, northern Saskatchewan, Canada; *Saskatchewan Research Council*, Technical Report 187, 187 p.
- Hoeve, J. and Sibbald, T., 1978. On the genesis of Rabbit Lake and other unconformity-type uranium deposits in northern Saskatchewan, Canada; *Economic Geology*, v. 73, p. 1450–1473. <https://doi.org/10.2113/gsecongeo.73.8.1450>
- Hoffman, P.F., 1989. Precambrian geology and tectonic history of North America; *in* The geology of North America — an overview, (ed.) A.W. Bally and A.R. Palmer; *Geological Society of America*, The geology of North America, v. A, p. 447–512. <https://doi.org/10.1130/DNAG-GNA-A.447>
- Hrabi, R.B., Barclay, W.A., Fleming, D., and Alexander, R.B., 2003. Structural evolution of the Woodburn Lake group in the area of the Meadowbank gold deposit, Nunavut; *Geological Survey of Canada*, Current Research 2003-C27, 10 p. <https://doi.org/10.4095/214396>
- Hunter, R., Lafrance, B., Lesperance, J., and Zaluski, G., 2012. The Qavvik-Tatiggaq Trend: an evolving unconformity-related uranium corridor of the northeast Thelon Basin, Nunavut; *Geological Association of Canada–Mineralogical Association of Canada*, Abstracts, v. 35, p. 60.
- Hunter, R., Lafrance, B., and Thomas, D., 2014. Structural controls on unconformity-type uranium mineralization with comparisons to the newly discovered Tatiggaq Zone, northeast Thelon Basin, Nunavut, Canada; *Geological Association of Canada–Mineralogical Association of Canada*, Abstracts, v. 40, p. 3.

- Hunter, R.C., Lafrance, B., Heaman, L.M., Zaluski, G., and Thomas, D., 2018. Geology, litho-geochemistry and new LA-ICP-MS U-Pb geochronology of the Aberdeen Lake area, Nunavut: new insights into the Neoproterozoic tectonic evolution of the central Rae Domain; *Precambrian Research*, v. 310, p. 114–132. <https://doi.org/10.1016/j.precamres.2018.02.024>
- Hunter, R.C., Lafrance, B., Heaman, L.M., and Thomas, D., 2021. Long-lived deformation history recorded along the Precambrian Thelon and Judge Sissons faults, northeastern Thelon Basin, Nunavut; *Canadian Journal of Earth Sciences*, v. 58, p. 433–457. <https://doi.org/10.1139/cjes-2020-0108>
- Janvier, V., Castonguay, S., Mercier-Langevin, P., Dubé, B., McNicoll, V., Pehrsson, S., Malo, M., De Chavigny, B., and Côté-Mantha, O., 2015a. Preliminary results of the geology of the Portage deposit, Meadowbank gold mine, Churchill Province, Nunavut; Geological Survey of Canada, Current Research 2015-2, 21 p. <https://doi.org/10.4095/295532>
- Janvier, V., Castonguay, S., Mercier-Langevin, P., Dubé, B., Malo, M., McNicoll, V.J., Creaser, R.A., de Chavigny, B., and Pehrsson, S.J., 2015b. Geology of the banded iron-formation-hosted Meadowbank gold deposit, Churchill Province, Nunavut; *in Targeted Geoscience Initiative 4: Contributions to the understanding of Precambrian lode gold deposits and implications for exploration*, (ed.) B. Dubé and P. Mercier-Langevin; Geological Survey of Canada, Open File 7852, p. 255–269. <https://doi.org/10.4095/296646>
- Jefferson, C.W. and Delaney, G. (ed.), 2007. EXTECH IV: Geology and uranium EXploration TECHNOlogy of the Proterozoic Athabasca Basin, Saskatchewan and Alberta; Geological Survey of Canada, Bulletin 588, 644 p. <https://doi.org/10.4095/223742>
- Jefferson, C.W., Thomas, D.J., Gandhi, S.S., Ramaekers, P., Delaney, G., Brisbin, D., Cutts, C., Portella, P., and Olson, R.A., 2007a. Unconformity-associated uranium deposits of the Athabasca Basin, Saskatchewan and Alberta; *in EXTECH IV: Geology and uranium EXploration TECHNOlogy of the Proterozoic Athabasca Basin, Saskatchewan and Alberta*, (ed.) C.W. Jefferson and G. Delaney; Geological Survey of Canada, Bulletin 588, p. 23–68. <https://doi.org/10.4095/223744>
- Jefferson, C.W., Thomas, D.J., Gandhi, S.S., Ramaekers, P., Delaney, G., Brisbin, D., Cutts, C., Quirt, D., Portella, P., and Olson, R.A., 2007b. Unconformity-associated uranium deposits of the Athabasca Basin, Saskatchewan and Alberta; *in Mineral deposits of Canada: a synthesis of major deposit-types, district metallogeny, the evolution of geological provinces, and exploration methods*, (ed.) W.D. Goodfellow; Geological Association of Canada, Mineral Deposits Division, Special Publication 5, p. 273–305.
- Jefferson, C.W., Thomas, D., Quirt, D., Mwenifumbo, C.J., and Brisbin, D., 2007c. Empirical models for Canadian unconformity associated uranium deposits; *in Proceedings of Exploration 07*, (ed.) B. Milkereit; Fifth Decennial International Conference on Mineral Exploration, p. 741–769.
- Jefferson, C.W., Chorlton, L.B., Pehrsson, S.J., Peterson, T., Wollenberg, P., Scott, J., Tschirhart, V., McEwan, B., Bethune, K., Calhoun, L., White, J.C., Leblon, B., LaRocque, A., Shelat, Y., Lentz, D., Patterson, J., Riegler, T., Skulski, T., Robinson, S., ... Tschirhart, P., 2011a. Northeast Thelon region: geomapping for uranium in Nunavut; Geological Survey of Canada, Open File 6962, 38 p. <https://doi.org/10.4095/289037>
- Jefferson, C.W., Hunter, R., McLaren, M., Peterson, T., Skulski, T., Rainbird, R., Young, G.M., Gandhi, S.S., and Costello, K., 2011b. Northeastern Thelon Basin uranium region: geological compilation for geophysical consortium planning; Geological Survey of Canada, Open File 6950, 1 poster. <https://doi.org/10.4095/288801>
- Jefferson, C.W., Pehrsson, S., Peterson, T., Chorlton, L., Davis, W., Keating, P., Gandhi, S., Fortin, R., Buckle, J., Miles, W., Rainbird, R., LeCheminant, A., Tschirhart, V., Tschirhart, P., Morris, W., Scott, J., Cousens, B., McEwan, B., Bethune, K., ... Riegler, T., 2011c. Northeast Thelon region geoscience framework – new maps and data for uranium in Nunavut; Geological Survey of Canada, Open File 6949, 1 poster. <https://doi.org/10.4095/288791>
- Jefferson, C.W., Anand, A., Rainbird, R., Pehrsson, S., Davis, W., Peterson, T., McEwan, B., Bethune, K., Calhoun, L., White, J.C., and Patterson, J., 2012. Conglomerates in the uraniferous northeast Thelon Basin region, Nunavut: guides for unravelling >800 Ma of sequence stratigraphy and metallogeny; Geological Association of Canada–Mineralogical Association of Canada, Abstracts, v. 35, p. 63.
- Jefferson, C.W., Peterson, T., Tschirhart, V., Davis, W., Scott, J.M.J., Reid, K., Ramaekers, P., Gandhi, S.S., Bleeker, W., Pehrsson, S., Morris, W.A., Fayek, M., Potter, E., Bridge, N., Grunsky, E., Keating, P., Ansdell, K., and Banerjee, N., 2013. LIPs and Proterozoic uranium (U) deposits of the Canadian Shield; Geological Survey of Canada, Open File 7352, 56 p. <https://doi.org/10.4095/292377>
- Jefferson, C.W., White, J.C., Young, G.M., Patterson, J., Tschirhart, V.L., Pehrsson, S.J., Calhoun, L., Rainbird, R.H., Peterson, T.D., Davis, W.J., Tella, S., Chorlton, L.B., Scott, J.M.J., Percival, J.A., Morris, W.A., Keating, P., Anand, A., Shelat, Y., and MacIsaac, D., 2015. Outcrop and remote predictive geology of the Amer Belt and basement beside and beneath the northeast Thelon Basin, in parts of NTS 66-A, B, C, F, G and H, Kivalliq Region, Nunavut; Geological Survey of Canada, Open File 7242, 1 poster. <https://doi.org/10.4095/296825>
- Jefferson, C.W., Rainbird, R.H., Young, G.M., White, J.C., Tschirhart, V., and Creaser, R.A., 2023. The Paleoproterozoic Amer supergroup, Amer Fold Belt, Nunavut: stratigraphy, structure, correlations, and uranium metallogeny; *in Understanding the Precambrian: a collection of papers in celebration of Grant McAdam Young*; Canadian Journal of Earth Sciences, 35 p. (posted Open Access 21 November 2022). <https://doi.org/10.1139/cjes-2022-0077>
- Johnstone, D.D., 2017. Lithostratigraphic and structural controls of uranium mineralization in the Kiggavik East Zone, Centre Zone, and Main Zone deposits, Thelon Basin, Nunavut; M.Sc. thesis, University of Regina, Regina, Saskatchewan, 178 p.

- Kennicott, J., Chi, G., and Ashton, K., 2015. Field and petrographic study of albitization associated with uranium mineralization in the Beaverlodge uranium district of northern Saskatchewan; *in* Summary of Investigations 2015, Volume 2; Saskatchewan Geological Survey, Saskatchewan Ministry of the Economy, Miscellaneous Report 2015-4.2, Paper A-4, 24 p.
- Kjarsgaard, B.A., Kerswill, J.A., and Jenner, G.A., 1997. Lithostratigraphy and metallogenic implications of komatiite-banded iron-formation-felsic volcanic rocks of the Archean Woodburn Lake group, Pipedream Lake, central Churchill Province, Northwest Territories; *in* Current Research 1997-C; Geological Survey of Canada, p. 101–110. <https://doi.org/10.4095/208636>
- Knox, A.W., 1980. The geology and uranium mineralization of the Aphebian Amer Group, southwest of Amer Lake, District of Keewatin, N.W.T.; M.Sc. thesis, University of Calgary, Calgary, Alberta, 159 p.
- Kyser, K., Hiatt, E., Renac, C., Durocher, K., Holk, G., and Deckart, K., 2000. Diagenetic fluids in Paleo- and Mesoproterozoic sedimentary basins and their implications for long protracted fluid histories; Chapter 19 *in* Fluids and basin evolution, (ed.) K. Kyser; Mineralogical Association of Canada, Short Course Series, v. 28, p. 225–262.
- LaFlamme, C., McFarlane, C.R.M., Corrigan, D., and Wodicka, N., 2014. Origin and tectonometamorphic history of the Repulse Bay block, Melville Peninsula, Nunavut: exotic terrane or deeper level of the Rae craton; *Canadian Journal of Earth Sciences*, v. 51, p. 1097–1122. <https://doi.org/10.1139/cjes-2014-0040>
- Lavigne, M.J., Michaud, M.J., and Rickard, J., 2005. Discovery and geology of the Lac Des Iles Palladium deposits; Chapter 17 *in* Exploration for platinum-group elements deposits, (ed.) J.E. Mungall; Mineralogical Association of Canada, Short Course Series, v. 35, p. 369–390.
- LaRocque, A., Leblon, B., Harris, J., Jefferson, C.W., Tschirhart, V., and Shelat, Y., 2012. Use of multi-beam RADARSAT-2 dual-polarization C-HH and C-HV imagery for surficial geology mapping in Nunavut, Canada; *Canadian Journal of Remote Sensing*, v. 38, no. 3, p. 281–305. <https://doi.org/10.5589/m12-020>
- Lauzon, M.-C., Mercier-Langevin, P., Valette, M., Beaudoin, G., De Souza, S., Côté-Mantha, O., and Simard, M., 2020. Ore mineralogy and mineral chemistry of the Whale Tail zone, Amaruq gold deposit, Nunavut; *in* Targeted Geoscience Initiative 5: Contributions to the understanding of Canadian gold systems, (ed.) P. Mercier-Langevin, C.J.M. Lawley, and S. Castonguay; Geological Survey of Canada, Open File 8712, p. 267–279. <https://doi.org/10.4095/326044>
- Lawley, C.J.M., McNicoll, V., Sandeman, H., Pehrsson, S., Simard, M., Castonguay, S., Mercier-Langevin, P., and Dubé, B., 2016. Age and geological setting of the Rankin Inlet greenstone belt and its relationship to the gold endowment of the Meliadine gold district, Nunavut, Canada; *Precambrian Research*, v. 275, p. 471–495. <https://doi.org/10.1016/j.precamres.2016.01.008>
- LeCheminant, A.N., 1981. Geology, Tebesjuak Lake, District of Keewatin; Geological Survey of Canada, Open File 728, scale 1:200 000. <https://doi.org/10.4095/129725>
- LeCheminant, A.N. and Heaman, L.M., 1989. Mackenzie igneous events, Canada: Middle Proterozoic hotspot magmatism associated with ocean opening; *Earth and Planetary Science Letters*, v. 96, no. 1-2, p. 38–48. [https://doi.org/10.1016/0012-821X\(89\)90122-2](https://doi.org/10.1016/0012-821X(89)90122-2)
- LeCheminant, A.N. and Roddick, J.C., 1991. U-Pb zircon evidence for widespread 2.6 Ga felsic magmatism in the central District of Keewatin, N.W.T.; *in* Radiogenic age and isotopic studies, report 4; Geological Survey of Canada, Paper 90-2, p. 91–99. <https://doi.org/10.4095/131941>
- LeCheminant, A.N., Ashton, K.E., Chiarenzelli, J., Donaldson, J.A., Best, M.A., Tella, S., and Thompson, D.L., 1983. Geology of Aberdeen Lake map area, District of Keewatin: preliminary report; *in* Current Research, Part A; Geological Survey of Canada, Paper 83-1A, p. 437–448. <https://doi.org/10.4095/111480>
- LeCheminant, A.N., Jackson, M.J., Galley, A.G., Smith, S.L., and Donaldson, J.A., 1984. Early Proterozoic Amer Group, Beverly Lake map area, District of Keewatin; *in* Current Research, Part B; Geological Survey of Canada, Paper 84-1B, p. 159–172. <https://doi.org/10.4095/119571>
- Lewis, R.S. and Burmeister, R.F., 2013. The Salmon basin detachment fault in the Wimpey Creek area, east-central Idaho; *Northwest Geology*, v. 42, p. 337–342.
- Long, D.G.F., 2007. Topographic influences on the sedimentology of the Manitou Falls Formation, eastern Athabasca Basin, Saskatchewan; *in* EXTECH IV: Geology and uranium EXploration TECHnology of the Proterozoic Athabasca Basin, Saskatchewan and Alberta, (ed.) C.W. Jefferson and G. Delaney; Geological Survey of Canada, Bulletin 588, p. 267–280. <https://doi.org/10.4095/223771>
- MacIsaac, D.A., 2011. Paleoproterozoic supracrustal deformation, Amer Lake, Nunavut; B.Sc. thesis, Department of Geology, University of New Brunswick, Fredericton, New Brunswick, 43 p.
- Madore, C., Annesley, I., and Wheatley, K., 2000. Petrogenesis, age, and uranium fertility of peraluminous leucogranites and pegmatites of the McClean Lake / Sue and Key Lake / P-Patch deposit areas, Saskatchewan; *Geological Association of Canada–Mineralogical Association of Canada, Program with abstracts*, v. 25, extended abstract no. 1041, 4 p.
- Matthews, R., Koch, R., and Leppin, M., 1997. Advances in integrated exploration for unconformity uranium deposits in western Canada; *in* Proceedings, Integrated exploration case histories, (ed.) A.G. Gubins; Exploration 97: Fourth Decennial International Conference on Mineral Exploration, Paper 130, p. 993–1024.
- McCready, A.J., Annesley, I.R., Parnell, J., and Richardson, L.C., 1999. Uranium-bearing carbonaceous matter, McArthur River uranium deposit, Saskatchewan; *in* Summary of Investigations 1999, Volume 2; Saskatchewan Geological Survey, Saskatchewan Energy and Mines, Miscellaneous Report 99-4.2, p. 110–120.
- McCurdy, M.W., Campbell, J.E., Böhm, C.O., Trommelen, M.S., and Syme, E.C., 2013. Regional lake sediment geochemical data, Kasmere Lake–Nueltin Lake area, Manitoba (NTS 64-K, 64-N, 64-O); Geological Survey of Canada, Open File 7309, 17 p. <https://doi.org/10.4095/292267>

- McDonough, M.R., McNicoll, V.J., Schetselaar, E.M., and Grover, T.W., 2000. Geochronological and kinematic constraints on crustal shortening and escape in a two-sided oblique-slip collisional and magmatic orogen, Paleoproterozoic Taltson magmatic zone, northeastern Alberta; *Canadian Journal of Earth Sciences*, v. 37, p. 1549–1573. <https://doi.org/10.1139/e00-089>
- McEwan, B.J., 2012. Structural style and regional comparison of the Paleoproterozoic Ketyet River group in the region north-northwest of Baker Lake, Nunavut; M.Sc. thesis, University of Regina, Regina, Saskatchewan, 121 p.
- McGregor, M., McFarlane, C.R.M., and Spray, J.G., 2018. In situ LA-ICP-MS apatite and zircon U–Pb geochronology of the Nicholson Lake impact structure, Canada: shock and related thermal effects; *Earth and Planetary Science Letters*, v. 504, p. 185–197. <https://doi.org/10.1016/j.epsl.2018.10.006>
- McMartin, I., 2017. Till provenance across the terminus of the Dubawnt Lake ice stream, central Nunavut; *Geological Survey of Canada, Current Research 2017-1*, 13 p. <https://doi.org/10.4095/299744>
- McMartin, I., Dredge, L.A., and Aylsworth, J.M., 2008. Surficial geology, Schultz Lake South, Nunavut; Geological Survey of Canada, Map 2120A, scale 1:100 000. <https://doi.org/10.4095/224825>
- McMartin, I., Tremblay, T., and Godbout, P.-M., 2017. Report of 2017 field activities for the GEM-2 Rae glacial history activity in the Kivalliq region, Nunavut; Geological Survey of Canada, Open File 8320, 14 p. <https://doi.org/10.4095/306006>
- McMartin, I., Godbout, P.-M., Campbell, J.E., Tremblay, T., and Behnia, P., 2021. A new map of glacial features and glacial landsystems in central mainland Nunavut, Canada; *Boreas*, v. 50, 25 p. <https://doi.org/10.1111/bor.12479>
- McNicoll, V., 2020. U-Pb detrital-zircon geochronology of the Woodburn Lake group, Nunavut; Geological Survey of Canada, Open File 8720, 4 p. <https://doi.org/10.4095/326019>
- McNicoll, V., Thériault, R.J., and McDonough, M.R., 2000. Taltson basement gneissic rocks: U–Pb and Nd isotopic constraints on the basement to the Paleoproterozoic Taltson magmatic zone, northeastern Alberta; *Canadian Journal of Earth Sciences*, v. 37, p. 1575–1596. <https://doi.org/10.1139/e00-034>
- Miles, W. and Oneschuk, D., 2013. Northeastern Thelon–Garry Lake, NU, aeromagnetic compilation, parts of NTS 55, 65, 66 and 76, Nunavut; Geological Survey of Canada, Open File 7461, scale 1:500 000. <https://doi.org/10.4095/292809>
- Miller, A.R., 1980. Uranium geology of the eastern Baker Lake Basin, District of Keewatin, Northwest Territories; Geological Survey of Canada, Bulletin 330, 63 p. <https://doi.org/10.4095/119463>
- Miller, A.R., 1995. Polymetallic unconformity-related uranium veins in Lower Proterozoic Amer Group, Pelly Lake map area, northern Thelon Basin, Churchill Province, Northwest Territories; *in Current Research 1995-C*; Geological Survey of Canada, p. 151–161. <https://doi.org/10.4095/202914>
- Miller, A.R. and LeCheminant, A.N., 1985. Geology and uranium metallogeny of Proterozoic supracrustal successions, central District of Keewatin, N.W.T. with comparisons to northern Saskatchewan; *in Geology of uranium deposits*, (ed.) T.I.I. Sibbald and W. Petruk; Canadian Institute of Mining and Metallurgy, Special Volume 32, p. 167–185.
- Miller, A.R. and Peterson, T.D., 2015. Geology and petrology of the Schultz Lake intrusive complex and its relationship to unconformity uranium deposits: Schultz Lake, NTS 66A/5 and Aberdeen Lake, 66B/8, Western Churchill Province; Geological Survey of Canada, Open File 7858, 160 p. <https://doi.org/10.4095/296600>
- Miller, A.R., Cumming, G.L., and Krstic, D., 1989. U-Pb, Pb-Pb, and K-Ar isotopic study and petrography of uraniferous phosphate bearing rocks in the Thelon Formation, Dubawnt Group, Northwest Territories, Canada; *Canadian Journal of Earth Sciences*, v. 26, p. 867–880. <https://doi.org/10.1139/e89-070>
- Montreuil, J.-F., Corriveau, L., and Potter, E.G., 2015. Formation of albitite-hosted uranium within IOCG systems: the Southern Breccia, Great Bear magmatic zone, Northwest Territories, Canada; *Mineralium Deposita*, v. 50, p. 293–325. <https://doi.org/10.1007/s00126-014-0530-7>
- Montreuil, J.-F., Corriveau, L., Potter, E.G., and De Toni, A.F., 2016. On the relation between alteration facies and metal endowment of iron oxide-alkali-altered systems, southern Great Bear magmatic zone (Canada); *in Proterozoic iron oxide-apatite (\pm REE) and iron oxide-copper-gold and affiliated deposits of Southeast Missouri, U.S.A., and the Great Bear magmatic zone, Northwest Territories, Canada*, (ed.) J. Slack, L. Corriveau, and M. Hitzman; *Economic Geology*, v. 111, p. 2139–2168.
- Morelli, R.M., Hartlaub, R.P., Ashton, K.E., and Ansdell, K.M., 2009. Evidence for enrichment of subcontinental lithospheric mantle from Paleoproterozoic intracratonic magmas: geochemistry and U-Pb geochronology of Martin Group igneous rocks, western Rae Craton, Canada; *Precambrian Research*, v. 175, p. 1–15. <https://doi.org/10.1016/j.precamres.2009.04.005>
- Morris, W.A., Tschirhart, V., and Jefferson, C.W., 2017. Fracture framework mapping from magnetics: a SLIC example; 15th SAGA Biennial Conference and Exhibition, Extended Abstracts, 6 p.
- Mwenifumbo, C.J. and Bernius, G.R., 2007. Crandallite-group minerals: host of thorium enrichment in the eastern Athabasca Basin, Saskatchewan; *in EXTECH IV: Geology and uranium EXploration TEChnology of the Proterozoic Athabasca Basin, Saskatchewan and Alberta*, (ed.) C.W. Jefferson and G. Delaney; Geological Survey of Canada, Bulletin 588, p. 521–532. <https://doi.org/10.4095/223795>
- Overton, A., 1979. Seismic reconnaissance survey of the Dubawnt Group, districts of Keewatin and Mackenzie; *in Current Research, Part B*; Geological Survey of Canada, Paper 79-1B, p. 397–400. <https://doi.org/10.4095/105448>
- Palmer, S.E., Kyser, T.K., and Hiatt, E.E., 2004. Provenance of the Proterozoic Thelon Basin, Nunavut, Canada, from detrital zircon geochronology and detrital quartz oxygen isotopes; *Precambrian Research*, v. 129, p. 115–140. <https://doi.org/10.1016/j.precamres.2003.10.010>

- Paná, D., Creaser, R.A., Muehlenbachs, K., and Wheatley, K., 2007. Basement geology in the Alberta portion of the Athabasca Basin: context for the Maybelle River area; *in* EXTECH IV: Geology and uranium EXploration TECHnology of the Proterozoic Athabasca Basin, Saskatchewan and Alberta, (ed.) C.W. Jefferson and G. Delaney; Geological Survey of Canada, Bulletin 588, p. 135–153. <https://doi.org/10.4095/223749>
- Partin, C.A., Bekker, A., Corrigan, D., Modeland, S., Francis, D., and Davis, D.W., 2014. Sedimentological and geochemical basin analysis of the Paleoproterozoic Penrhyn and Piling groups of Arctic Canada; *Precambrian Research*, v. 251, p. 80–101. <https://doi.org/10.1016/j.precamres.2014.06.010>
- Patterson, J.G., 1986. The Amer Belt: remnant of an Aphebian foreland fold and thrust belt; *Canadian Journal of Earth Sciences*, v. 23, p. 2012–2023. <https://doi.org/10.1139/e86-186>
- Patterson, J.G. and LeCheminant, A.N., 1985. A preliminary geological compilation map of the northeastern Barren Grounds, parts of the Districts of Keewatin and Franklin; Geological Survey of Canada, Open File 1138, scale 1:1 000 000. <https://doi.org/10.4095/129971>
- Patterson, J., Jefferson, C.W., Kjarsgaard, B.A., Pehrsson, S., McEwan, B., Calhoun, L., Bethune, K., White, J., and Tschirhart, V., 2012. Differentiation of Neoarchean from Paleoproterozoic basalt in the uraniumiferous Amer and Whitehills belts, northeast Thelon Region, Nunavut; Geological Association of Canada–Mineralogical Association of Canada, Abstracts, v. 35, p. 103.
- Pehrsson, S.J., Jenner, G., and Kjarsgaard, B.A., 2002. The Ketyet River group: correlation with Paleoproterozoic supracrustal sequences of northeastern Rae and implications for Proterozoic orogenesis in the western Churchill Province; Geological Association of Canada–Mineralogical Association of Canada, Program with abstracts, v. 27, p. 90.
- Pehrsson, S.J., Wilkinson, L., and Zaleski, E., 2004. Geology, Meadowbank gold deposit area, Nunavut; Geological Survey of Canada, Open File 4269, scale 1:20 000. <https://doi.org/10.4095/215550>
- Pehrsson, S.J., Berman, R., and Davis, W.J., 2013a. Paleoproterozoic orogenesis during Nuna aggregation: a case study of reworking of the Archean Rae craton, Woodburn Lake, Nunavut; *Precambrian Research*, v. 232, p. 167–188. <https://doi.org/10.1016/j.precamres.2013.02.010>
- Pehrsson, S.J., Ramaekers, P., Fayek, M., Eglinton, B.E., Rainbird, R., and St-Onge, M., 2013b. Extent and metallogenic significance of the Racklan-Forward orogen in Canada; Geological Association of Canada–Mineralogical Association of Canada, Abstracts, v. 36, p. 160.
- Pehrsson, S.J., Currie, M., Ashton, K.E., Harper, C.T., Paul, D., Paná, D., Berman, R.G., Bostock, H., Corkery, T., Jefferson, C.W., and Tella, S., 2014a. Bedrock geology compilation and regional synthesis of south Rae and parts of Hearne domains, Churchill Province, Northwest Territories, Saskatchewan, Nunavut, Manitoba and Alberta; Geological Survey of Canada, Open File 5744, scale 1:550 000. <https://doi.org/10.4095/292232>
- Pehrsson, S.J., Percival, J.A., Davis, W.J., McCurdy, M.W., Berman, R.G., Hillary, E.M., Kiss, F., MacKinnon, A., and Jefferson, C.W., 2014b. Operation GEM South Rae: Reconnaissance geology of the most poorly known part of the Churchill Province, Northwest Territories and Nunavut; Geological Survey of Canada, Open File 7410, 25 p. <https://doi.org/10.4095/293762>
- Pelly, D. and Nales, F., 2004. Hanningajuq: Inuit traditional place names, Garry Lake, Pelly Lake region; Baker Lake Hunters and Trappers Organization, 1 sheet, scale 1:1 000 000.
- Percival, J.A. and Tschirhart, V., 2017. Trans-Hudsonian far-field deformation effects in the Rae foreland: an integrated geological-3D magnetic model; *Tectonophysics*, v. 699, p. 82–92. <https://doi.org/10.1016/j.tecto.2017.01.021>
- Percival, J.B., Bell, K., and Torrence, J.K., 1993. Clay mineralogy and isotope geochemistry of the alteration halo at the Cigar Lake uranium deposit; *Canadian Journal of Earth Sciences*, v. 30, p. 689–704. <https://doi.org/10.1139/e93-056>
- Percival, J.A., Tschirhart, V., Ford, A., and Dziawa, C., 2015a. Report of activities for geology and mineral potential of the Chantrey–Thelon area: GEM-2 Montesor project; Geological Survey of Canada, Open File 7707, 12 p. <https://doi.org/10.4095/295673>
- Percival, J.A., Tschirhart, V., Davis, W., Berman, R.G., and Ford, A., 2015b. Geology, Montesor River area, Nunavut, parts of NTS 66-H and NTS 66-I; Geological Survey of Canada, Canadian Geoscience Map 231 (preliminary edition), scale 1:100 000. <https://doi.org/10.4095/296915>
- Percival, J.A., Davis, W.J., and Hamilton, M.A., 2017. U–Pb zircon geochronology and depositional history of the Montesor group, Rae Province, Nunavut, Canada; *Canadian Journal of Earth Sciences*, v. 54, p. 512–528. <https://doi.org/10.1139/cjes-2016-0170>
- Percival, J.A., Davis, B., Petts, D., Jackson, S., Berman, R., Shalchi, B., Harrison, M., and Bell, E., 2019. Rae impact spherules: aftermath of a 2.1 Ga exoplanet strike; Goldschmidt Conference, August 18–23, 2019, Goldschmidt Abstracts, no. 2617, 1 p.
- Peterson, T.D., 1995. A potassic phreatomagmatic volcanic centre in the Thelon Basin (Northwest Territories): implications for diamond exploration; *in* Current Research 1995-C; Geological Survey of Canada, p. 19–26. <https://doi.org/10.4095/202901>
- Peterson, T.D., 2006. Geology of the Dubawnt Lake area, Nunavut-Northwest Territories; Geological Survey of Canada, Bulletin 580, 56 p. <https://doi.org/10.4095/221939>
- Peterson, T.D. and LeCheminant, A.N., 1996. Ultrapotassic rocks of the Dubawnt Supergroup, District of Keewatin, N.W.T.; *in* Searching for diamonds in Canada, (ed.) A.N. LeCheminant, D.G. Richardson, R.N.W. Dilabio, and K.A. Richardson; Geological Survey of Canada, Open File 3228, p. 97–100. <https://doi.org/10.4095/210976>
- Peterson, T.D., van Breemen, O., Sandeman, H., and Cousens, B., 2002. Proterozoic (1.85–1.75 Ga) igneous suites of the Western Churchill Province: granitoid and ultrapotassic magmatism in a reworked Archean hinterland; *Precambrian Research*, v. 119, p. 73–100. [https://doi.org/10.1016/S0301-9268\(02\)00118-3](https://doi.org/10.1016/S0301-9268(02)00118-3)

- Peterson, T., Pehrsson, S., Jefferson, C., Scott, J., and Rainbird, R., 2010. The Dubawnt Supergroup, Canada: a LIP with a LISP; Large Igneous Provinces Commission, December 2010 LIP of the month, 32 p. <<http://www.largeigneousprovinces.org/LOM.html>> [accessed March 3, 2012].
- Peterson, T.D., Scott, J.M.J., and Jefferson, C.W., 2011. Uranium-rich bostonite-carbonatite dykes in Nunavut: recent observations; Geological Survey of Canada, Current Research 2011-11, 12 p. <https://doi.org/10.4095/288751>
- Peterson, T.D., Scott, J.M.J., LeCheminant, A.N., Chorlton, L.B., and D'Aoust, B.M.A., 2014. Geology, Tebesjuak Lake, Nunavut; Geological Survey of Canada, Canadian Geoscience Map 158 (preliminary edition), scale 1:250 000. <https://doi.org/10.4095/293892>
- Peterson, T.D., Scott, J.M.J., LeCheminant, A.N., Jefferson, C.W., and Pehrsson, S.J., 2015a. The Kivalliq Igneous Suite: anorogenic bimodal magmatism at 1.75 Ga in the western Churchill Province, Canada; Precambrian Research, v. 262, p. 101–119. <https://doi.org/10.1016/j.precamres.2015.02.019>
- Peterson, T.D., Scott, J.M.J., LeCheminant, A.N., Tschirhart, V., Chorlton, L.B., Davis, W.J., and Hamilton, M.A., 2015b. Nueltin granites and mafic rocks in the Tebesjuak Lake map area, Nunavut: new geochronological, petrological, and geophysical data; Geological Survey of Canada, Current Research 2015-5, 23 p. <https://doi.org/10.4095/296163>
- Peterson, T.D., Jefferson, C.W., and Anand, A., 2015c. Geological setting and geochemistry of the ca. 2.6 Ga Snow Island suite in the central Rae Domain of the Western Churchill Province, Nunavut; Geological Survey of Canada, Open File 7841, 29 p. <https://doi.org/10.4095/296599>
- Pilkington, M. and Tschirhart, V., 2017. Practical considerations in the use of edge detectors for geological mapping using magnetic data; Geophysics, v. 82, no. 3, p. J1–J8. <https://doi.org/10.1190/geo2016-0364.1>
- Potter, E.G. and Wright, D.M., 2015. TGI-4 unconformity-related uranium deposits synthesis: tools to aid deep exploration and refine the genetic model; in Targeted Geoscience Initiative 4: unconformity-related uranium systems, (ed.) E.G. Potter and D.M. Wright; Geological Survey of Canada, Open File 7791, p. 1–13. <https://doi.org/10.4095/295777>
- Potter, E.G., Montreuil, J.-F., Corriveau, L., and De Toni, A., 2013. Geology and hydrothermal alteration of the Fab Lake region, Northwest Territories; Geological Survey of Canada, Open File 7339, 26 p. <https://doi.org/10.4095/292562>
- Potter, E.G., Montreuil, J.-F., Corriveau, L., and Davis, W.J., 2019. The Southern Breccia metasomatic uranium system of the Great Bear magmatic zone, Canada: iron oxide-copper-gold (IOCG) and albitite-hosted uranium linkages; in Ore deposits: origin, exploration, and exploitation, (ed.) S. Decrée and L. Robb; American Geophysical Union, Geophysical Monograph 242, p. 109–130. <https://doi.org/10.1002/9781119290544.ch5>
- Potter, E.G., Tschirhart, V., Powell, J.W., Kelly, C.J., Rabiei, M., Johnstone, D., Craven, J.A., Davis, W.J., Pehrsson, S., Mount, S.M., Chi, G., and Bethune, K.M., 2020. Targeted Geoscience Initiative 5: integrated multidisciplinary studies of unconformity-related uranium deposits from the Patterson Lake corridor, northern Saskatchewan; Geological Survey of Canada, Bulletin 615, 37 p. <https://doi.org/10.4095/326040>
- Potter, E.G., Acosta-Góngora, P., Corriveau, L., Montreuil, J.-F., and Yang, Z., 2022. Uranium enrichment processes in iron oxide and alkali-calcic alteration systems as revealed by uraninite trace element chemistry; in Mineral systems with iron oxide-copper-gold (IOCG) and affiliated deposits, (ed.) L. Corriveau, E.G. Potter, and A.H. Mumin; Geological Association of Canada, Special Paper 52, p. 325–345.
- Rabiei, M., Chi, G., Potter, E., Tschirhart, V., Feng, R., MacKay, C., Frostad, S., McElroy, R., Ashley, R., and McEwan, B., 2019. Evolution of hydrothermal fluids in the Patterson Lake Corridor, southwestern Athabasca Basin: significance for uranium mineralization; in Geological Association of Canada–Mineralogical Association of Canada, Abstracts, v. 42, p. 163.
- Rainbird, R.H. and Davis, W.J., 2007. U-Pb detrital zircon geochronology and provenance of the late Paleoproterozoic Dubawnt Supergroup: linking sedimentation with tectonic reworking of the western Churchill Province, Canada; Geological Society of America Bulletin, v. 119, p. 314–328. <https://doi.org/10.1130/B25989.1>
- Rainbird, R.H. and Hadlari, T., 2000. Revised stratigraphy and sedimentology of the Paleoproterozoic Dubawnt Supergroup at the northern margin of Baker Lake Basin, Nunavut; Geological Survey of Canada, Current Research 2000-C8, 9 p. <https://doi.org/10.4095/211102>
- Rainbird, R.H., Hadlari, T., Aspler, L.B., Donaldson, J.A., LeCheminant, A.N., and Peterson, T.D., 2003a. Sequence stratigraphy and evolution of the Paleoproterozoic intracontinental Baker Lake and Thelon basins, western Churchill Province, Nunavut, Canada; Precambrian Research, v. 125, p. 21–53. [https://doi.org/10.1016/S0301-9268\(03\)00076-7](https://doi.org/10.1016/S0301-9268(03)00076-7)
- Rainbird, R.H., Rayner, N., and Stern, R.A., 2003b. SHRIMP U-Pb geochronology of apatite cements and zircon bearing tuff clasts in sandstones from the Athabasca Group, Athabasca Basin, northern Saskatchewan and Alberta; Saskatchewan Industry and Resources Open House, Abstracts, p. 6.
- Rainbird, R.H., Davis, W.J., Stern, R.A., Peterson, T.D., Smith, S.R., Parrish, R.R., and Hadlari, T., 2006. Ar-Ar and U-Pb geochronology of a late Paleoproterozoic rift basin: support for a genetic link with Hudsonian Orogenesis, western Churchill province, Nunavut, Canada; The Journal of Geology, v. 114, p. 1–17. <https://doi.org/10.1086/498097>
- Rainbird, R.H., Stern, R.A., Rayner, N., and Jefferson, C.W., 2007. Age, provenance, and regional correlation of the Athabasca Group, Saskatchewan and Alberta, constrained by igneous and detrital zircon geochronology; in EXTECH IV: Geology and uranium EXploration TECHnology of the Proterozoic Athabasca Basin, Saskatchewan and Alberta, (ed.) C.W. Jefferson and G. Delaney; Geological Survey of Canada, Bulletin 588, p. 193–209. <https://doi.org/10.4095/223761>
- Rainbird, R.H., Davis, W.J., Pehrsson, S.J., Wodicka, N., Rayner, N., and Skulski, T., 2010. Early Paleoproterozoic supracrustal assemblages of the Rae domain, Nunavut, Canada: intracratonic basin development during supercontinent break-up and assembly; Precambrian Research, v. 181, p. 167–186. <https://doi.org/10.1016/j.precamres.2010.06.005>

- Ramaekers, P., Jefferson, C.W., Yeo, G.M., Collier, B., Long, D.G.F., Catuneanu, O., Bernier, S., Kupsch, B., Post, R., Drever, G., McHardy, S., Jiricka, D., Cutts, C., and Wheatley, K., 2007. Revised geological map and stratigraphy of the Athabasca Group, Saskatchewan and Alberta; *in* EXTECH IV: Geology and uranium EXploration TECHnology of the Proterozoic Athabasca Basin, Saskatchewan and Alberta, (ed.) C.W. Jefferson and G. Delaney; Geological Survey of Canada, Bulletin 588, p. 155–192. <https://doi.org/10.4095/223754>
- Regis, D., Martel, E., Davis, W.J., and Pehrsson, S.J., 2017. U-Pb zircon geochronology of metaplutonic rocks across the southern Rae province, Northwest Territories; Geological Survey of Canada, Open File 8254, 37 p. <https://doi.org/10.4095/302772>
- Reid, K.D., 2018. Geological setting and fluid history of the Centennial unconformity-related uranium deposit, and implications of post Mackenzie diabase fluid events; Ph.D. thesis, Department of Geological Sciences, University of Saskatchewan, Saskatoon, Saskatchewan, 287 p.
- Reid, K.D., Ansdell, K., Jiricka, D., Witt, G., and Card, C., 2014. Regional setting, geology, and paragenesis of the Centennial unconformity-related uranium deposit, Athabasca Basin, Saskatchewan, Canada; *Economic Geology*, v. 109, no. 3, p. 539–566. <https://doi.org/10.2113/econgeo.109.3.539>
- Reid, K.D., Ansdell, K., Creighton, S., and Potter, E.G., 2016. Composition of large zoned aluminium phosphate sulfate minerals: implications for fluid evolution in the Centennial uranium deposit area, Athabasca Basin, Saskatchewan, Canada; *Canadian Mineralogist*, v. 54, no. 5, p. 1205–1228. <https://doi.org/10.3749/canmin.1500052>
- Renac, C., Kyser, T.K., Durocher, K., Drever, G., and O'Connor, T., 2002. Comparison of diagenetic fluids in the Proterozoic Thelon and Athabasca basins, Canada: implications for protracted fluid histories in stable intracratonic basins; *Canadian Journal of Earth Sciences*, v. 39, p. 113–132. <https://doi.org/10.1139/e01-077>
- Riegler, T., 2014. Système d'altération et minéralisation en uranium le long du faisceau structural Kiggavik–Andrew Lake (Nunavut, Canada): modèle génétique et guides d'exploration; Ph.D. thesis, Université de Poitiers, Poitiers, France, 244 p.
- Riegler, T., Lescuyer, J.-L., Wollenberg, P., Quirt, D., and Beaufort, D., 2014. Alteration related to uranium deposits in the Kiggavik-Andrew Lake structural trend, Nunavut Canada; new insights from petrography and clay mineralogy; *Canadian Mineralogist*, v. 52, p. 27–45. <https://doi.org/10.3749/canmin.52.1.27>
- Riegler, T., Beaufort, M.F., Allard, T., Pierson-Wickmann, A.-C., and Beaufort, D., 2016a. Nanoscale relationships between uranium and carbonaceous material in alteration halos around unconformity-related uranium deposits of the Kiggavik camp, Paleoproterozoic Thelon Basin, Nunavut, Canada; *Ore Geology Reviews*, v. 79, p. 382–391. <https://doi.org/10.1016/j.oregeorev.2016.04.018>
- Riegler, T., Quirt, D., and Beaufort, D., 2016b. Spatial distribution and compositional variation of APS minerals related to uranium deposits in the Kiggavik-Andrew Lake structural trend, Nunavut, Canada; *Mineralium Deposita*, v. 51, no. 2, p. 219–236. <https://doi.org/10.1007/s00126-015-0595-y>
- Robinson, S.V.J., Paulen, R.C., Jefferson, C.W., McClenaghan, M.B., Layton-Matthews, D., Quirt, D., and Wollenberg, P., 2014. Till geochemical signatures of the Kiggavik uranium deposit, Nunavut; Geological Survey of Canada, Open File 7500, 156 p. <https://doi.org/10.4095/293857>
- Robinson, S.V.J., Jefferson, C.W., Paulen, R.C., Layton-Matthews, D., Joy, B., and Quirt, D., 2016. Till and bedrock heavy mineral signatures of the Kiggavik uranium deposits, Nunavut; Geological Survey of Canada, Open File 7771, 70 p. <https://doi.org/10.4095/297563>
- Roddick, J.C., Henderson, J.R., and Chapman, H.J., 1992. U-Pb ages from the Archean Whitehills-Tehek lakes supracrustal belt Churchill Province, District of Keewatin, Northwest Territories; *in* Radiogenic age and isotopic studies, report 6; Geological Survey of Canada, Paper 92-2, p. 31–40. <https://doi.org/10.4095/134162>
- Rogers, M.C., 2015. Saskatchewan descriptive mineral deposit models; Saskatchewan Ministry of the Economy, Saskatchewan Geological Survey, Open File 2014-2 (second edition), 147 p.
- Ross, G.M. and Chiarenzelli, J.R., 1985. Paleoclimatic significance of widespread Proterozoic silcretes in the Bear and Churchill provinces of the northwestern Canadian Shield; *Journal of Sedimentary Petrology*, v. 55, p. 196–204.
- Sanborn-Barrie, M., Davis, W.J., Berman, R.G., Rayner, N., Skulski, T., and Sandeman, H., 2014. Neoproterozoic continental crust formation and Paleoproterozoic deformation of the central Rae craton, Committee Bay belt, Nunavut; *Canadian Journal of Earth Sciences*, v. 51, p. 635–667. <https://doi.org/10.1139/cjes-2014-0010>
- Sangély, L., Michels, R., Chaussidon, M., Brouand, M., Cuney, M., Richard, L., and Huault, V., 2003. Origin of carbonaceous matter in discordance-type uranium ore-deposit of Saskatchewan (Canada): clues to a biogenic synthesis; *in* Proceedings of Uranium Geochemistry 2003, International Conference, (ed.) M. Cuney; Unité Mixte de Recherche CNRS 7566 G2R, Université Henri Poincaré, April 13–16, 2003, Nancy, France, p. 323–326.
- Schau, M., Tremblay, F., and Christopher, A., 1982. Geology of Baker Lake map area, District of Keewatin: a progress report; *in* Current Research, Part A; Geological Survey of Canada, Paper 82-1A, p. 143–150. <https://doi.org/10.4095/111258>
- Schultz, M.E.J., Chacko, T., Heaman, L.M., Sandeman, H.A., Simonetti, A., and Creaser, R.A., 2007. Queen Maud block: a newly recognized Paleoproterozoic (2.4–2.5 Ga) terrane in northwest Laurentia; *Geology*, v. 35, p. 707–710. <https://doi.org/10.1130/G23629A.1>
- Scott, J.M.J., Peterson, T.D., and McCurdy, M.W., 2012. U, Th, REE occurrences within Nueltin granite at Nueltin Lake, Nunavut: recent observations; Geological Survey of Canada, Current Research 2012-1, 11 p. <https://doi.org/10.4095/289393>
- Scott, J.M.J., Peterson, T.D., Davis, W.J., Jefferson, C.W., and Cousens, B.L., 2015. Petrology and geochronology of Paleoproterozoic intrusive rocks, Kiggavik uranium camp, Nunavut; *Canadian Journal of Earth Sciences*, v. 52, no. 7, p. 495–518. <https://doi.org/10.1139/cjes-2014-0153>

- Shabaga, B.M., Fayek, M., Quirt, D., Jefferson, C.W., and Camacho, A., 2017. Mineralogy, geochronology, and genesis of the Andrew Lake uranium deposit, Thelon Basin, Nunavut, Canada; *Canadian Journal of Earth Sciences*, v. 54, no. 8, p. 850–868. <https://doi.org/10.1139/cjes-2017-0024>
- Sharpe, R., Fayek, M., Quirt, D., and Jefferson, C.W., 2015. Geochronology and genesis of the Bong uranium deposit, Thelon Basin, Nunavut, Canada; *Economic Geology*, v. 110, p. 1759–1777. <https://doi.org/10.2113/econgeo.110.7.1759>
- Shelat, Y., Leblon, B., La Rocque, A., Harris, J., Jefferson, C., Lentz, D., and Tschirhart, V., 2012a. Effects of incidence angles on mapping accuracy of surficial geology in Umiujalik Lake area, Nunavut, using multi-beam RADARSAT-2 polarimetric images. Part 1. Nonpolarimetric analysis; *Canadian Journal of Remote Sensing*, v. 38, no. 3, p. 383–403. <https://doi.org/10.5589/m12-030>
- Shelat, Y., Leblon, B., La Rocque, A., Harris, J., Jefferson, C., Lentz, D., and Tschirhart, V., 2012b. Effects of incidence angles on mapping accuracy of surficial geology in Umiujalik Lake area, Nunavut using multi-beam RADARSAT-2 polarimetric images. Part 2. Polarimetric analysis; *Canadian Journal of Remote Sensing*, v. 38, no. 3, p. 404–423. <https://doi.org/10.5589/m12-031>
- Sherlock, R., Pehrsson, S., Logan, A.V., Hrabí, R.B., and Davis, W.J., 2004. Geological setting of the Meadowbank gold deposits, Woodburn Lake Group, Nunavut; *Exploration and Mining Geology*, v. 13, no. 1–4, p. 67–107. <https://doi.org/10.2113/gsemg.13.1-4.67>
- Skulski, T., Paul, D., Sandeman, H., Berman, R.G., Chorlton, L., Pehrsson, S.J., Rainbird, R.H., Davis, W.J., and Sanborn-Barrie, M., 2018. Bedrock geology of the central Rae Craton and eastern Queen Maud Block, western Churchill Province, Nunavut; Geological Survey of Canada, Canadian Geoscience Map 307, scale 1:550 000. <https://doi.org/10.4095/308348>
- Stanton, R.A., 1979. Genesis of uranium-copper occurrence 74–1E, Baker Lake, Northwest Territories; M.Sc. thesis, University of Western Ontario, London, Ontario, 167 p.
- Stokes, C.R., Spagnolo, M., Clark, C.D., Ó Cofaigh, C., Lian, O.B., and Dunstone, R.B., 2013. Formation of mega-scale glacial lineations on the Dubawnt Lake Ice Stream bed: 1. size, shape and spacing from a large remote sensing dataset; *Quaternary Science Reviews*, v. 77, p. 190–209. <https://doi.org/10.1016/j.quascirev.2013.06.003>
- Taylor, F.C., 1985. Geology, Half Way Hills area, District of Keewatin, Northwest Territories; Geological Survey of Canada, Map 1602A, scale 1:50 000. <https://doi.org/10.4095/120472>
- Tella, S., 1984. Geology of the Amer Lake (NTS 66H), Deep Rose Lake (NTS 66G), and parts of the Pelly Lake (NTS 66F) map areas, District of Keewatin, N.W.T.; Geological Survey of Canada, Open File 1043, scale 1:250 000. <https://doi.org/10.4095/129891>
- Tella, S., 1994. Geology, Amer Lake (66 H), Deep Rose Lake (66 G), and parts of Pelly Lake (66 F); Geological Survey of Canada, Open File 2969, scale 1:250 000. <https://doi.org/10.4095/194789>
- Tella, S. and Heywood, W.W., 1978. The structural history of the Amer mylonite zone, Churchill structural province, District of Keewatin; *in* Current Research, Part C; Geological Survey of Canada, Paper 78-1C, p. 79–88. <https://doi.org/10.4095/104594>
- Tella, S., Hanmer, S., Sandeman, H.A., Ryan, J.J., Mills, A., Davis, W.J., Berman, R.G., Wilkinson, L., and Kerswill, J.A., 2001. Geology, MacQuoid Lake-Gibson Lake-Akunak Bay area, Nunavut; Geological Survey of Canada, Map 2008A, scale 1:100 000. <https://doi.org/10.4095/212827>
- Tella, S., Paul, D., Davis, W.J., Berman, R.G., Sandeman, H.A., Peterson, T.D., Pehrsson, S.J., and Kerswill, J.A., 2005. Bedrock geology compilation and regional synthesis, parts of Hearne domain, Nunavut; Geological Survey of Canada, Open File 4729 (revised edition), scale 1:250 000. <https://doi.org/10.4095/221124>
- Tersmette, D.B., 2012. Geology, geochronology, thermobarometry, and tectonic evolution of the Queen Maud block, Churchill craton, Nunavut, Canada; M.Sc. thesis, University of Alberta, Department of Earth and Atmospheric Sciences, Edmonton, Alberta, 170 p.
- Therriault, I., 2019. Structural characterisation and geochronological constraints on the Wager shear zone, northwestern Hudson Bay, Nunavut; M.Sc. thesis, The University of British Columbia, Vancouver, British Columbia, 213 p. <https://doi.org/10.14288/1.0378539>
- Therriault, I., Steenkamp, H.M., Larson, K.P., and Cottle, J.M., 2018. Geochronological constraints on deformation in the Wager shear zone, northwestern Hudson Bay, Nunavut; *in* Summary of Activities 2018, Canada-Nunavut Geoscience Office, p. 1–14. <<http://cngo.ca/summary-of-activities/2018/>> [accessed March, 2019].
- Thiessen, E.J., Gibson, H.D., Regis, D., Pehrsson, S., Ashley, K.T., and Smit, M.A., 2020. The distinct metamorphic stages and structural styles of the 1.94–1.86 Ga Snowbird Orogen, Northwest Territories, Canada; *Journal of Metamorphic Geology*, v. 38, p. 963–992. <https://doi.org/10.1111/jmg.12556>
- Thomas, M.D., 2012. Shallow crustal structure in Meadowbank River–Tehek Lake area: insights from gravity and magnetic modelling; Geological Survey of Canada, Open File 7308, 42 p. <https://doi.org/10.4095/292157>
- Thomas, M.D. and Wood, G., 2007. Geological significance of gravity anomalies in the area of McArthur River uranium deposit, Athabasca Basin, Saskatchewan; *in* EXTECH IV: Geology and uranium EXPloration TECHnology of the Proterozoic Athabasca Basin, Saskatchewan and Alberta, (ed.) C.W. Jefferson and G. Delaney; Geological Survey of Canada, Bulletin 588, p. 441–464. <https://doi.org/10.4095/223744>
- Tracey, G.M., Lentz, D.R., Olson, R.A., and Ashton, K.E., 2009. Geology and associated vein- or shear zone-hosted uranium mineralization of the 46 Zone and Hab Mine areas, Beaverlodge Uranium District, northern Saskatchewan; *in* Summary of Investigations 2009; Saskatchewan Geological Survey, Saskatchewan Energy and Mines, Miscellaneous Report 2009-4.2, 18 p.

- Tracey, G.M., Lentz, D.R., Olson, R.A., and Ashton, K.E., 2010. Vein- and shear zone-hosted uranium mineralization of the 46 Zone and Hab Mine areas, Beaverlodge Uranium District, Northern Saskatchewan: preliminary petrology and geochemical results; *GeoCanada 2010*, extended abstract, 4 p.
- Tremblay, L.P., 1972. Geology of the Beaverlodge mining area, Saskatchewan; Geological Survey of Canada, Memoir 367, 265 p. <https://doi.org/10.4095/101489>
- Tschirhart, V., 2013. Geophysical and geological integration and interpretation of the northeast Thelon Basin, Nunavut; Ph.D. thesis, McMaster University, Hamilton, Ontario, 180 p.
- Tschirhart, V., 2017. Keating correlation coefficient results over the Tehery Lake area, Nunavut, NTS 56-B and parts of 55-N, O, P, 56-A, C, F, G and H; Geological Survey of Canada, Open File 8099, scale 1:250 000. <https://doi.org/10.4095/299252>
- Tschirhart, V., Morris, W.A., and Oneschuk, D., 2011a. Geophysical series, geophysical compilation project, Thelon Basin, Nunavut, NTS 66A, B, and parts of 65N, O, P, 66C, F, G and H / Série des cartes géophysiques, projet de compilation géophysique, Bassin de Thelon, Nunavut, SNRC 66A, B, et parties des 65N, O, P, 66C, F, G et H; Geological Survey of Canada, Open File 6944, scale 1:300 000. <https://doi.org/10.4095/288806>
- Tschirhart, V., Morris, W.A., Ugalde, H., and Jefferson, C.W., 2011b. Preliminary 3D geophysical modelling of the Aberdeen sub-basin, northeast Thelon Basin region, Nunavut; Geological Survey of Canada, Current Research 2011-4, 12 p. <https://doi.org/10.4095/287165>
- Tschirhart, P.A., Morris, W.A., and Jefferson, C.W., 2013a. Geophysical modeling of the Neoproterozoic Woodburn Lake and Paleoproterozoic Ketyet River groups, and plutonic rocks in central Schultz Lake map area, Nunavut; Geological Survey of Canada, Current Research 2013-2, 19 p. <https://doi.org/10.4095/292116>
- Tschirhart, V., Morris, W.A., and Jefferson, C.W., 2013b. Framework geophysical modelling of granitoid vs. supracrustal basement to the northeast Thelon Basin around the Kiggavik uranium camp, Nunavut; *Canadian Journal of Earth Sciences*, v. 50, p. 667–677. <https://doi.org/10.1139/cjes-2012-0149>
- Tschirhart, V., Morris, W.A., and Jefferson, C.W., 2013c. Faults affecting northeast Thelon Basin: improved basement constraints from source edge processing of aeromagnetic data; *in* Uranium in Canada: geological environments and exploration developments, (ed.) E. Potter, D. Quirt, and C.W. Jefferson; *Exploration and Mining Geology*, Special Issue, v. 21, p. 105–113.
- Tschirhart, V., Morris, W.A., Jefferson, C.W., Keating, P., White, J.C., and Calhoun, L., 2013d. 3D geophysical inversions of the northeast Amer Belt and their relationship to the geologic structure; *Geophysical Prospecting*, v. 61, p. 547–560. <https://doi.org/10.1111/j.1365-2478.2012.01098.x>
- Tschirhart, V., Morris, W.A., and Jefferson, C.W., 2014. Unconformity surface architecture of the northeast Thelon Basin, Nunavut, derived from integration of magnetic source depth estimates; *Society of Exploration Geophysicists and American Association of Petroleum Geologists; Interpretation*, v. 2, no. 4, p. SJ117–SJ132. <https://doi.org/10.1190/INT-2014-0001.1>
- Tschirhart, V., Percival, J.A., and Jefferson, C.W., 2015. Geophysical models of the Montresor metasedimentary belt and its environs, central Nunavut, Canada; *Canadian Journal of Earth Sciences*, v. 52, p. 833–845. <https://doi.org/10.1139/cjes-2015-0008>
- Tschirhart, V., Jefferson, C.W., and Morris, W.A., 2017. Basement geology beneath the northeast Thelon Basin, Nunavut: insights from integrating new gravity, magnetic and geological data; *Geophysical Prospecting*, v. 65, no. 2, p. 617–636. <https://doi.org/10.1111/1365-2478.12430>
- Tschirhart, V.L., Potter, E.G., Powell, J.W., Johnstone, D., Rabiei, M., Bethune, K.M., Chi, G., and Duffett, C.L., 2018. Reactivated basement faults and uranium-rich fluid pathways in the Athabasca Basin: new insights from the Patterson Lake corridor, northwestern Saskatchewan; *in* Targeted Geoscience Initiative: 2017 report of activities, volume 1, (ed.) N. Rogers; Geological Survey of Canada, Open File 8358, p. 89–93. <https://doi.org/10.4095/306434>
- Tschirhart, V., Pehrsson, S., Card, C., Potter, E.G., Powell, J., and Paná, D., 2021. Interpretation of buried basement in the southwestern Athabasca Basin, Canada, from integrated geophysical and geological datasets; *in* Thematic collection: uranium fluid pathways, (ed.) E. Potter, V. Tschirhart, and J. Powell; *Geochemistry: Exploration, Environment, Analysis*, v. 21, no. 1, art. geochem2019-061, 17 p. <https://doi.org/10.1144/geochem2019-061>
- Turner, W.A., Richards, J.P., Nesbitt, B.E., Muchlenbachs, K., and Biczok, J.L., 2001. Proterozoic low-sulfidation epithermal Au-Ag mineralization in the Mallery Lake area, Nunavut, Canada; *Mineralium Deposita*, v. 36, p. 442–457. <https://doi.org/10.1007/s001260100181>
- Turner, W.A., Heaman, L.M., and Creaser, R.A., 2003. Sm–Nd fluorite dating of Proterozoic low-sulfidation epithermal Au–Ag deposits and U–Pb zircon dating of host rocks at Mallery Lake, Nunavut, Canada; *Canadian Journal of Earth Sciences*, v. 40, p. 1789–1804. <https://doi.org/10.1139/e03-061>
- Valette, M., De Souza, S., Mercier-Langevin, P., McNicoll, V.J., Wodicka, N., Creaser, R.A., Côté-Mantha, O., and Simard, M., 2019. Geological setting of the 5.2 M oz. Au Amaruq banded iron-formation-hosted gold deposit, Churchill Province, Nunavut; *in* Targeted Geoscience Initiative: 2018 report of activities, (ed.) N. Rogers; Geological Survey of Canada, Open File 8549, p. 83–87. <https://doi.org/10.4095/313643>
- Valette, M., De Souza, S., Mercier-Langevin, P., Côté-Mantha, O., Simard, M., Wodicka, N., McNicoll, V.J., and Barbe, P., 2020. Lithological and tectonic controls on banded iron-formation-associated gold at the Amaruq deposit, Churchill Province, Nunavut, and implications for exploration; *in* Targeted Geoscience Initiative 5: Contributions to the understanding of Canadian gold systems, (ed.) P. Mercier-Langevin, C.J.M. Lawley, and S. Castonguay; Geological Survey of Canada, Open File 8712, p. 251–266. <https://doi.org/10.4095/326042>
- van Breemen, O., Thompson, P.H., Hunt, P.A., and Culshaw, N., 1987. U–Pb zircon and monazite geochronology from the northern Thelon Tectonic zone, District of Mackenzie; *in* Radiogenic age and isotopic studies, report 1; Geological Survey of Canada, Paper 87-2, p. 81–93. <https://doi.org/10.4095/122752>

- van Breemen, O., Peterson, T.D., and Sandeman, H.A., 2005. U–Pb zircon geochronology and Nd isotope geochemistry of Proterozoic granitoids in the western Churchill Province: intrusive age pattern and Archean source domains; *Canadian Journal of Earth Sciences*, v. 42, p. 339–377. <https://doi.org/10.1139/e05-007>
- White, J.C., Calhoun, L., and Jefferson, C.W., 2021. Paradoxical mid-crustal displacements and stratigraphic continuity: tectonic evolution of the Paleoproterozoic Amer belt, Nunavut, Canada; *Geological Association of Canada–Mineralogical Association of Canada, Abstracts*, v. 44, p. 307.
- White, J.C., Calhoun, L., and Jefferson, C.W., 2023. Paradoxical mid-crustal displacements and stratigraphic continuity: structural evolution of the northeastern Paleoproterozoic Amer belt, Nunavut, Canada; *Canadian Journal of Earth Sciences*, v. 60, p. 1078–1103. <https://doi.org/10.1139/cjes-2022-0083>
- Wilson, N.S.F., Stasiuk, L.D., and Fowler, M.G., 2007. Origin of organic matter in the Proterozoic Athabasca Basin of Saskatchewan and Alberta, and significance to unconformity-associated uranium deposits; *in* EXTECH IV: Geology and uranium EXploration TECHnology of the Proterozoic Athabasca Basin, Saskatchewan and Alberta, (ed.) C.W. Jefferson and G. Delaney; Geological Survey of Canada, Bulletin 588, p. 325–341. <https://doi.org/10.4095/223778>
- Wodicka, N., St-Onge, M.R., Corrigan, D., Scott, D.J., and Whalen, J.B., 2014. Did a proto-ocean basin form along the southeastern Rae cratonic margin? Evidence from U–Pb geochronology, geochemistry (Sm–Nd and whole-rock), and stratigraphy of the Paleoproterozoic Piling Group, northern Canada; *Geological Society of America, Bulletin*, v. 126, p. 1625–1653. <https://doi.org/10.1130/B31028.1>
- Wodicka, N., Steenkamp, H.M., Peterson, T.D., McMartin, I., Day, S.J.A., and Tschirhart, V.L., 2017. Report of 2017 activities for the geology and economic potential of the Tehery–Wager area, Nunavut: GEM-2 Rae project; Geological Survey of Canada, Open File 8318, 20 p. <https://doi.org/10.4095/305979>
- Wright, D.M. and Potter, E.G., 2014. Regional surface rock geochemistry, Athabasca Basin, Saskatchewan; Geological Survey of Canada, Open File 7614, 33 p. <https://doi.org/10.4095/293915>
- Wright, D.M. and Potter, E.G., 2015. Application of regional geochemical datasets to uranium exploration in the Athabasca Basin, Saskatchewan; *in* Targeted Geoscience Initiative 4: unconformity-related uranium systems, (ed.) E.G. Potter and D.M. Wright; Geological Survey of Canada, Open File 7791, p. 14–20. <https://doi.org/10.4095/295778>
- Yeo, G.M. and Delaney, G., 2007. The Wollaston Supergroup, stratigraphy and metallogeny of a Paleoproterozoic Wilson cycle in the Trans-Hudson Orogen, Saskatchewan; *in* EXTECH IV: Geology and uranium EXploration TECHnology of the Proterozoic Athabasca Basin, Saskatchewan and Alberta, (ed.) C.W. Jefferson and G. Delaney; Geological Survey of Canada, Bulletin 588, p. 89–118. <https://doi.org/10.4095/223746>
- Yeo, G.M., Percival, J.B., Jefferson, C.W., Ickert, R., and Hunt, P., 2007. Environmental significance of oncoids and crypto-microbial laminates from the late Paleoproterozoic Athabasca Group, Saskatchewan and Alberta; *in* EXTECH IV: Geology and uranium EXploration TECHnology of the Proterozoic Athabasca Basin, Saskatchewan and Alberta, (ed.) C.W. Jefferson and G. Delaney; Geological Survey of Canada, Bulletin 588, p. 315–324. <https://doi.org/10.4095/223777>
- Young, G.M., 1979. Report on the geology of the western part of the Amer Belt (NTS sheets 66G1, G2, H5, H6 and parts of G8 and H4), Keewatin District; Appendix 2 *in* Mineral Assessment Report 081047, prepared by E. Nutter for Western Mines Ltd. (operator); Department of Indian Northern Affairs, Yellowknife, 37 p.
- Zaleski, E., 2005. Geology, Meadowbank River area, Nunavut; Geological Survey of Canada, Map 2068A, scale 1:50 000. <https://doi.org/10.4095/220495>
- Zaleski, E. and Pehrsson, S., 2005. Geology, Half Way Hills and Whitehills Lake area, Nunavut; Geological Survey of Canada, Map 2069A, scale 1:50 000. <https://doi.org/10.4095/220576>
- Zaleski, E., L’Heureux, R., Duke, N., Wilkinson, L., and Kerswill, J.A., 1999. Geology, Woodburn Lake group, Meadowbank River area, Kivalliq Region, Nunavut; Geological Survey of Canada, Open File 3709, scale 1:50 000. <https://doi.org/10.4095/210633>
- Zaleski, E., Davis, W.J., and Sandeman, H.A., 2001a. Continental extension, mantle magmas and basement/cover relationships; Fourth International Archaeological Symposium, Perth, Australia, Extended abstracts, p. 374–376.
- Zaleski, E., Pehrsson, S.J., Davis, W.J., Greiner, E., L’Heureux, R., Duke, N., and Kerswill, J.A., 2001b. Geology, Half Way Hills to Whitehills Lake area, Nunavut; Geological Survey of Canada, Open File 3697, scale 1:50 000. <https://doi.org/10.4095/212057>
- Zaleski, E., Pehrsson, S.J., and Wilkinson, L., 2005. Geology, Amarulik and Tehek lakes area, Nunavut; Geological Survey of Canada, Map 2070A, scale 1:50 000. <https://doi.org/10.4095/220579>

Appendix A

Detrital zircon geochronology plots for parts of the Amarulik, Aberdeen, and Pipedream assemblages of the Woodburn Lake group and the Paleoproterozoic sequence Ps4

The following representations of detrital-zircon-provenance profiles in the form of probability-density plots (red) superimposed on frequency histograms (blue) are based on data published in McNicoll (2020). Table 2 of this paper lists the maximum depositional ages interpreted from these plots. Table 2 also explains and denotes the map figure number for the geological setting of each sample. The alphanumeric codes are field-officer sample numbers; the z number is the index used in the Canadian Geochronology Knowledgebase (<https://www.nrcan.gc.ca/maps-tools-publications/tools/geodetic-reference-systems/canadian-geochronology-knowledgebase/18211>). Further details are provided in the text.

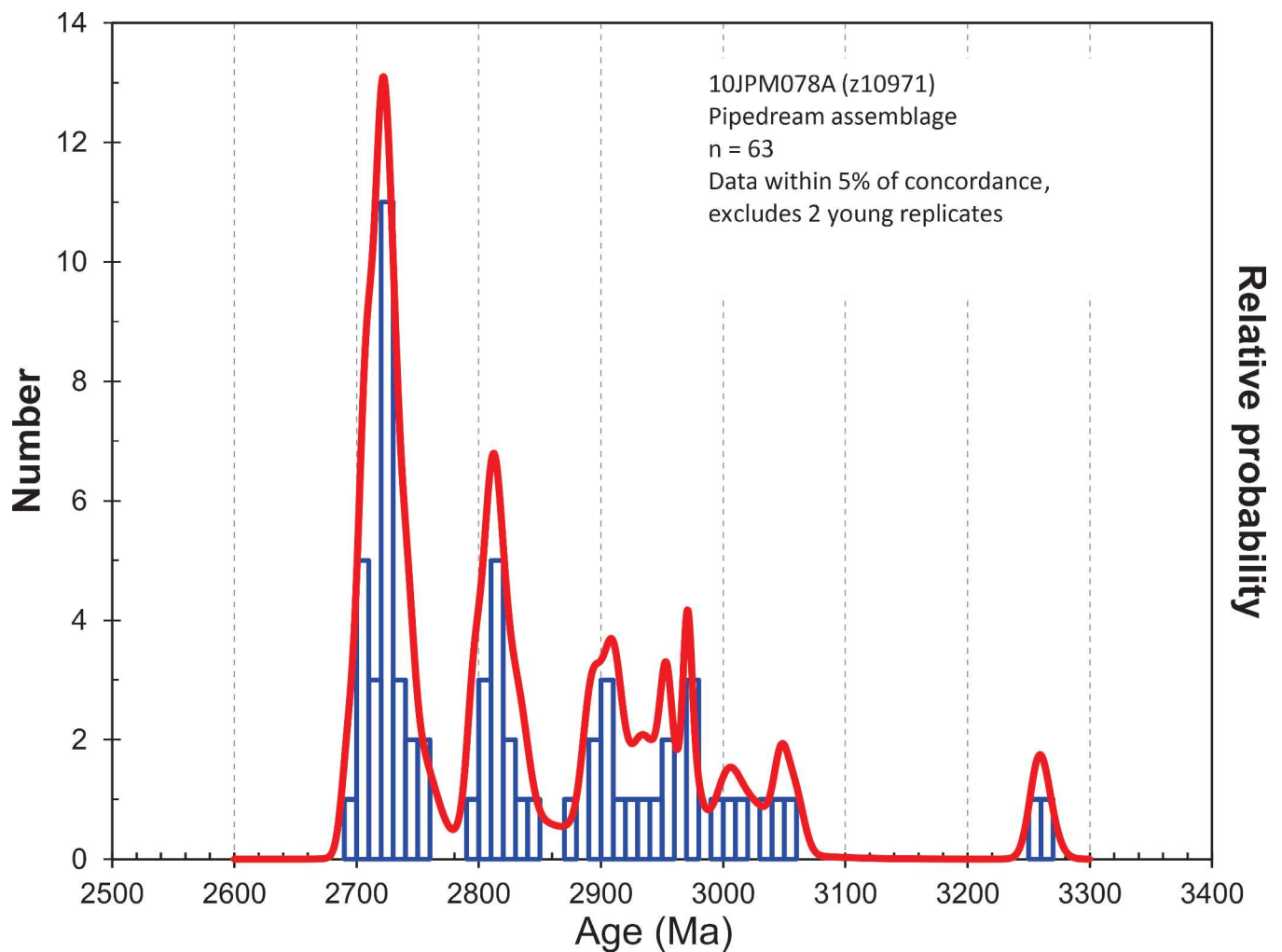


Figure A-1. Greywacke at type area of Pipedream assemblage (geochronology site 7, Table 2).

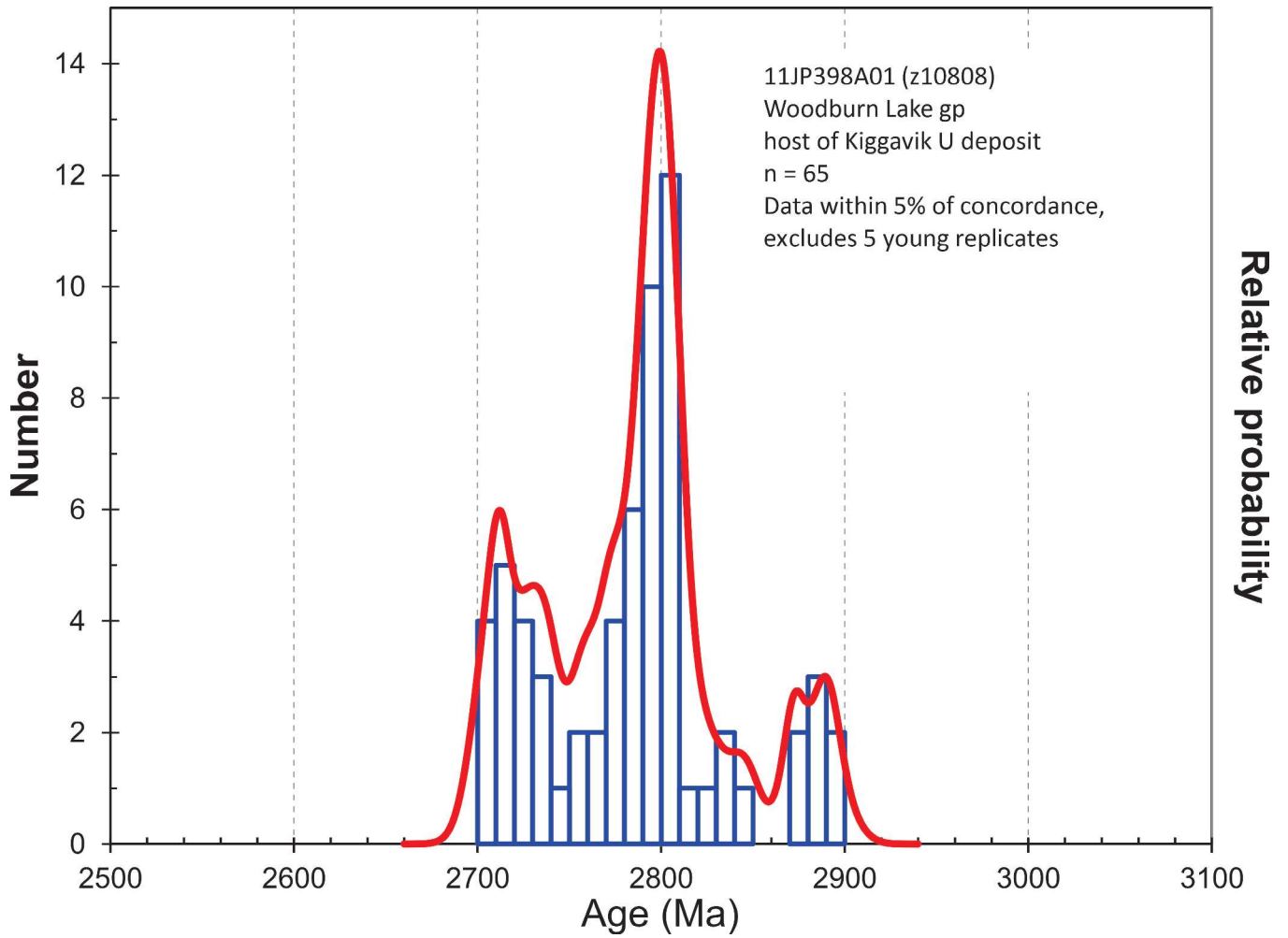


Figure A-2. Greywacke of western Pipedream assemblage at the Kiggavik Main Zone (Lone Gull) uranium deposit (geochronology site 9, Table 2).

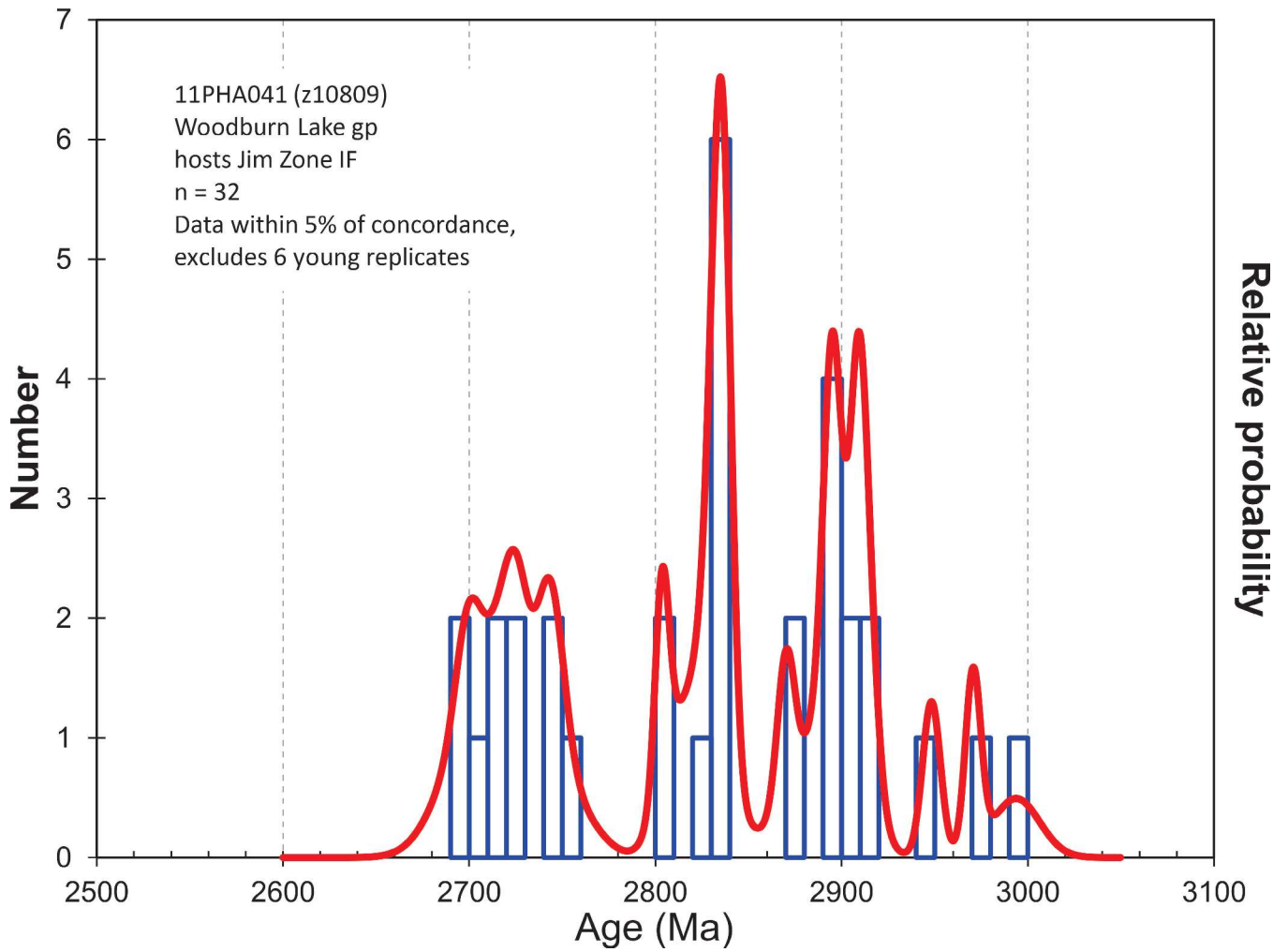


Figure A-3. Greywacke of Pipedream assemblage at Jim zone gold occurrence in iron-formation (IF; geochronology site 10, Table 2).

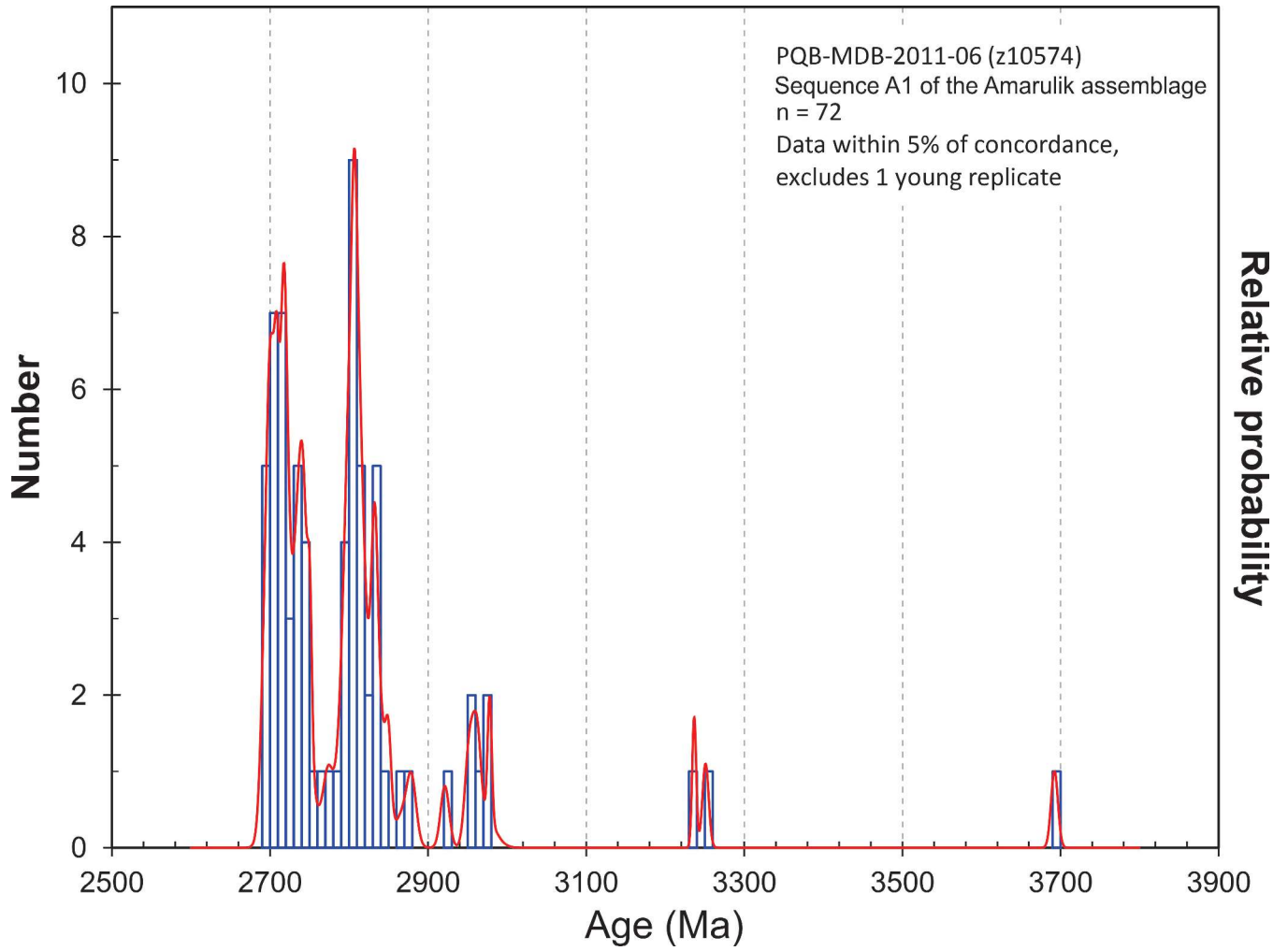


Figure A-4. Quartz-pebbly, coarse-grained, feldspathic, lithic quartz wacke in sequence A1 of the Amarulik assemblage (geochronology site 16, Table 2).

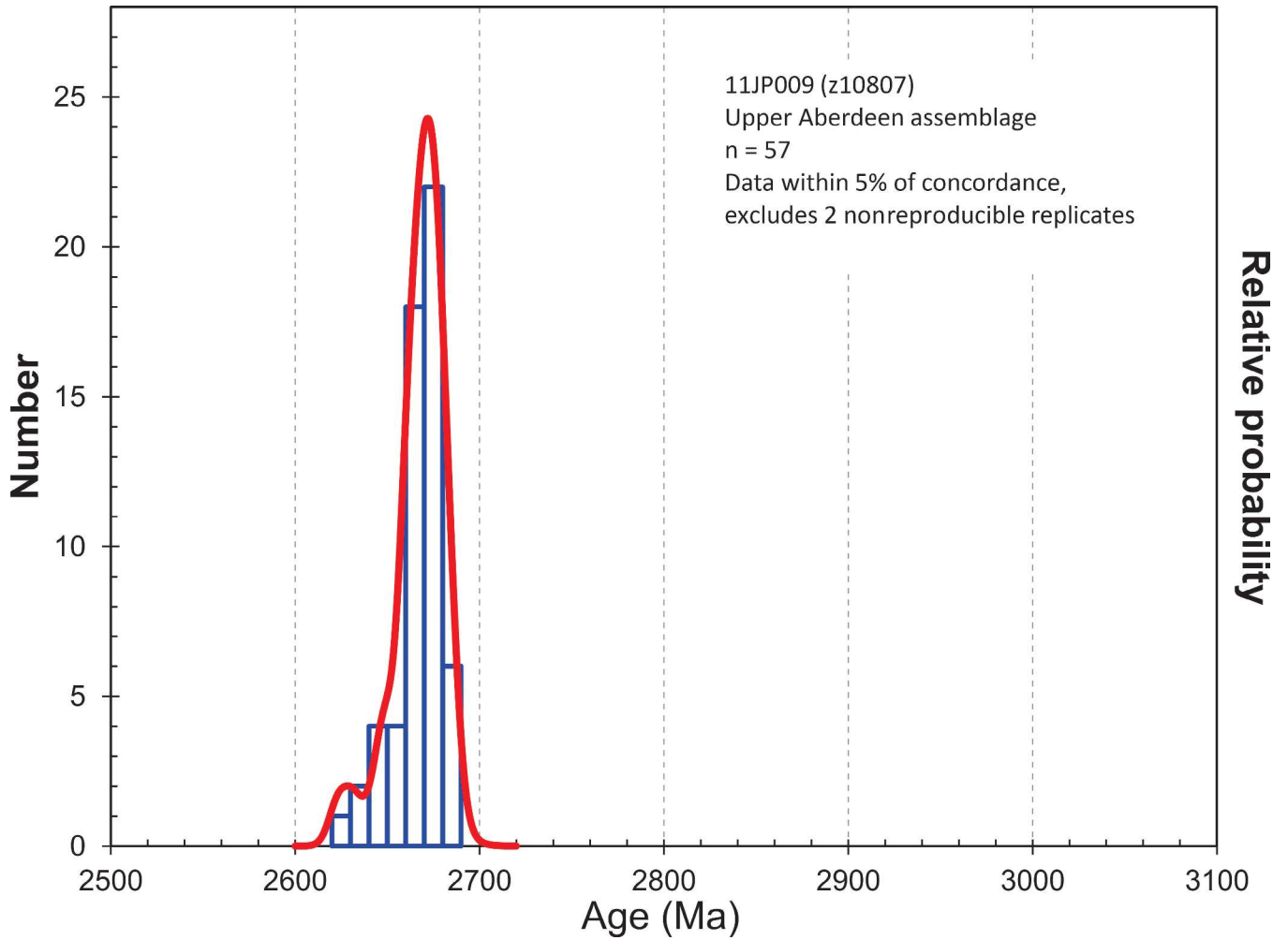


Figure A-5. Metasedimentary gneiss, middle or upper package of the Aberdeen assemblage, west of the Schultz Lake intrusive complex (geochronology site 23, Table 2).

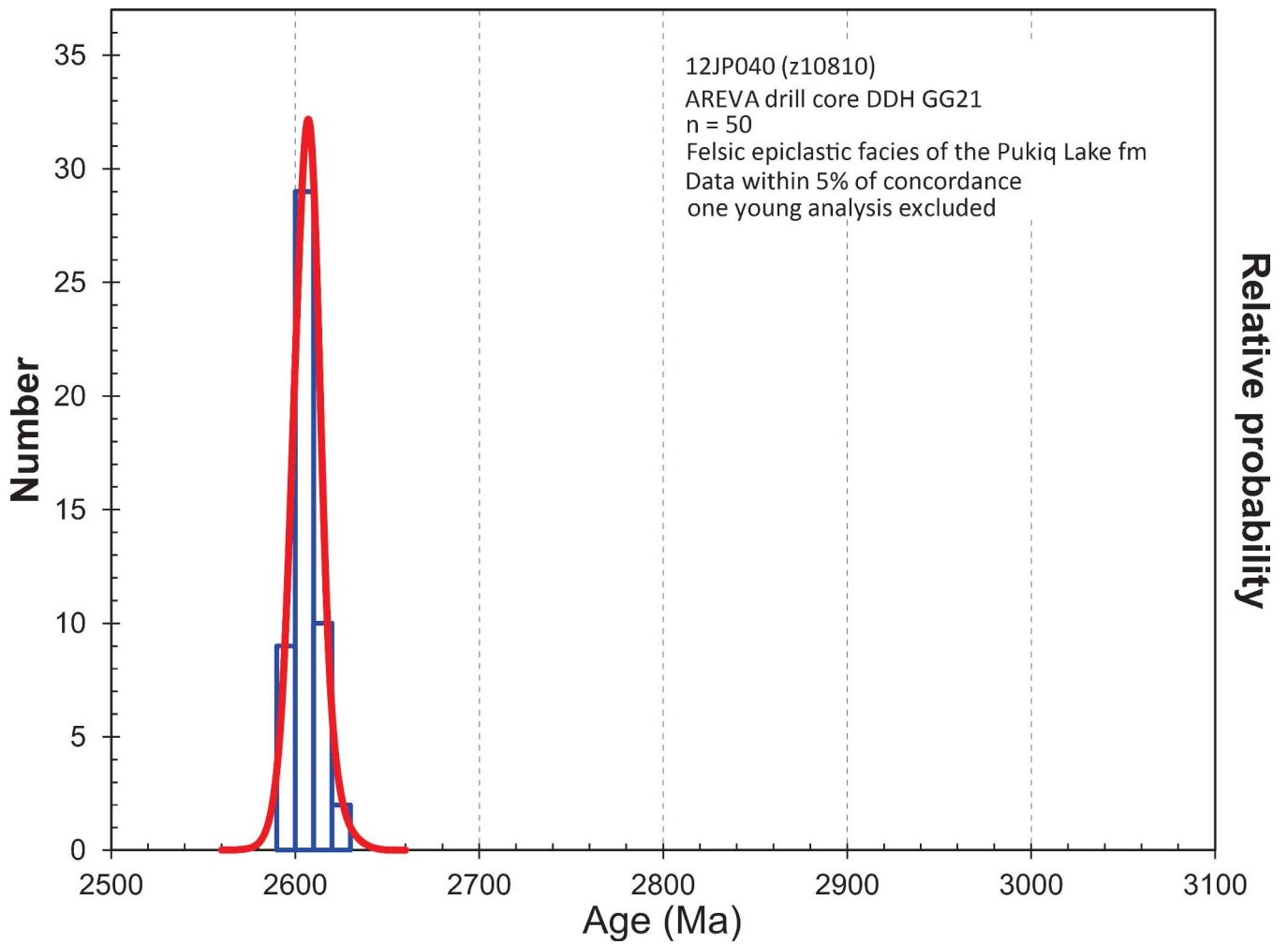


Figure A-6. Felsic epiclastic facies of Pukiq Lake formation in Bong drill core (geochronology site 31a, Table 2).

Appendix B

Detrital zircon geochronology plots for the Amarulik sequence A3, and sequences Ps1 and Ps4

Figures B-1 and B-2 show stacked detrital-zircon-provenance profiles: frequency histograms (blue), all but one with the same vertical 'Zircon count' scales, and relative probability density plots (red). The first two-digit number in selected sample descriptions is keyed to Table 2 that summarizes maximum ages, sample descriptions, and site positions in figures. Samples without the two-digit prefix in their descriptions are not listed in Table 2, although the descriptions provide approximate locations. The alphanumeric codes are field-officer sample numbers; the z number is the index used in the Canadian Geochronology Knowledgebase (<<https://www.nrcan.gc.ca/maps-tools-publications/tools/geodetic-reference-systems/canadian-geochronology-knowledgebase/18211>>). Geological events for reference are shown as coloured bars, labelled in lower left and explained as follows (*see* details in the text):

Hudson = Hudson suite (Peterson et al., 2002, 2010; van Breemen et al., 2005);

Taltson = Taltson magmatic zone and Thelon Orogen (Hoffman, 1989; Bostock and van Breemen, 1994);

Gabbro = 2045 ± 13 Ma gabbro sill in lower Montresor group (Percival et al., 2017) and 2.05 to 2.0 Ga ultramafic to felsic intrusions in the western part of the south Rae Craton (Davis et al., 2015; Regis et al., 2017; W. Bleeker, A.N. LeCheminant, and M. Hamilton, pers. comm., 2017);

Impact = 2.1 Ga spherule bed interpreted to represent condensate from an interstellar asteroid impact (Percival et al., 2019);

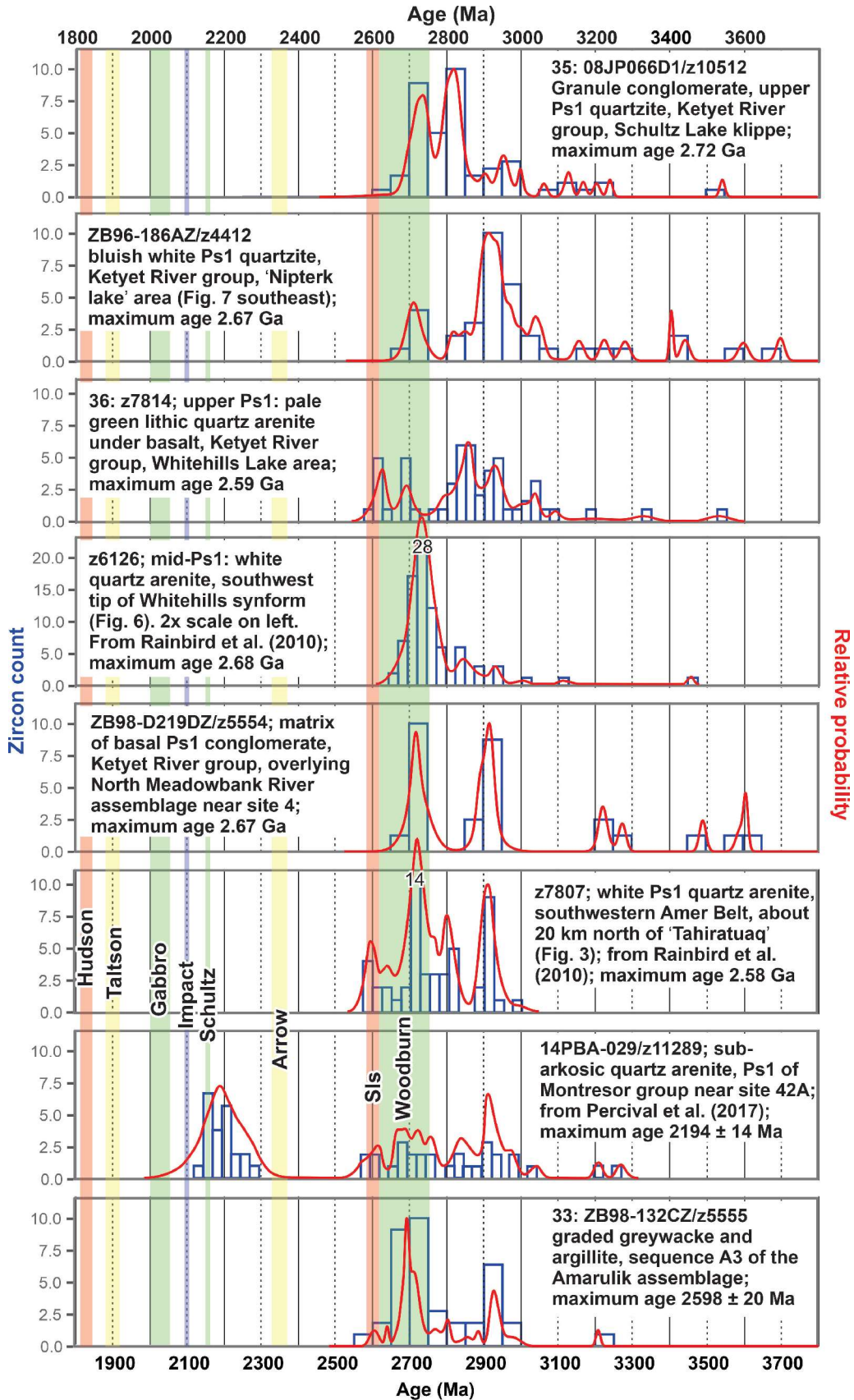
Schultz = 2153 ± 5 Ma 'Schultz Lake metagabbro' (geochronology site 38, Table 2) interpreted to represent the age of sequence Ps3 basalt;

Arrow = 2.35 Ga Arrowsmith Orogeny (Berman et al., 2013);

SIs = 2.62 to 2.58 Ga Snow Island suite (Peterson et al., 2015c, this volume);

Woodburn = Woodburn Lake group (Fraser, 1988): seven assemblages collectively range from 2.75 to later than 2.6 Ga.

Figure B-1. Detrital zircon geochronology plots of the Amarulik sequence A3 and sequence Ps1. Unattributed plots are derived from data in Davis (2021). The other plots are rescaled from Rainbird et al. (2010) and Percival et al. (2017), as cited. The numbers 14 and 28 denote the two peak zircon counts that exceed the uniform vertical scale chosen in order to display this group of results in one chart. SIs = Snow Island suite.



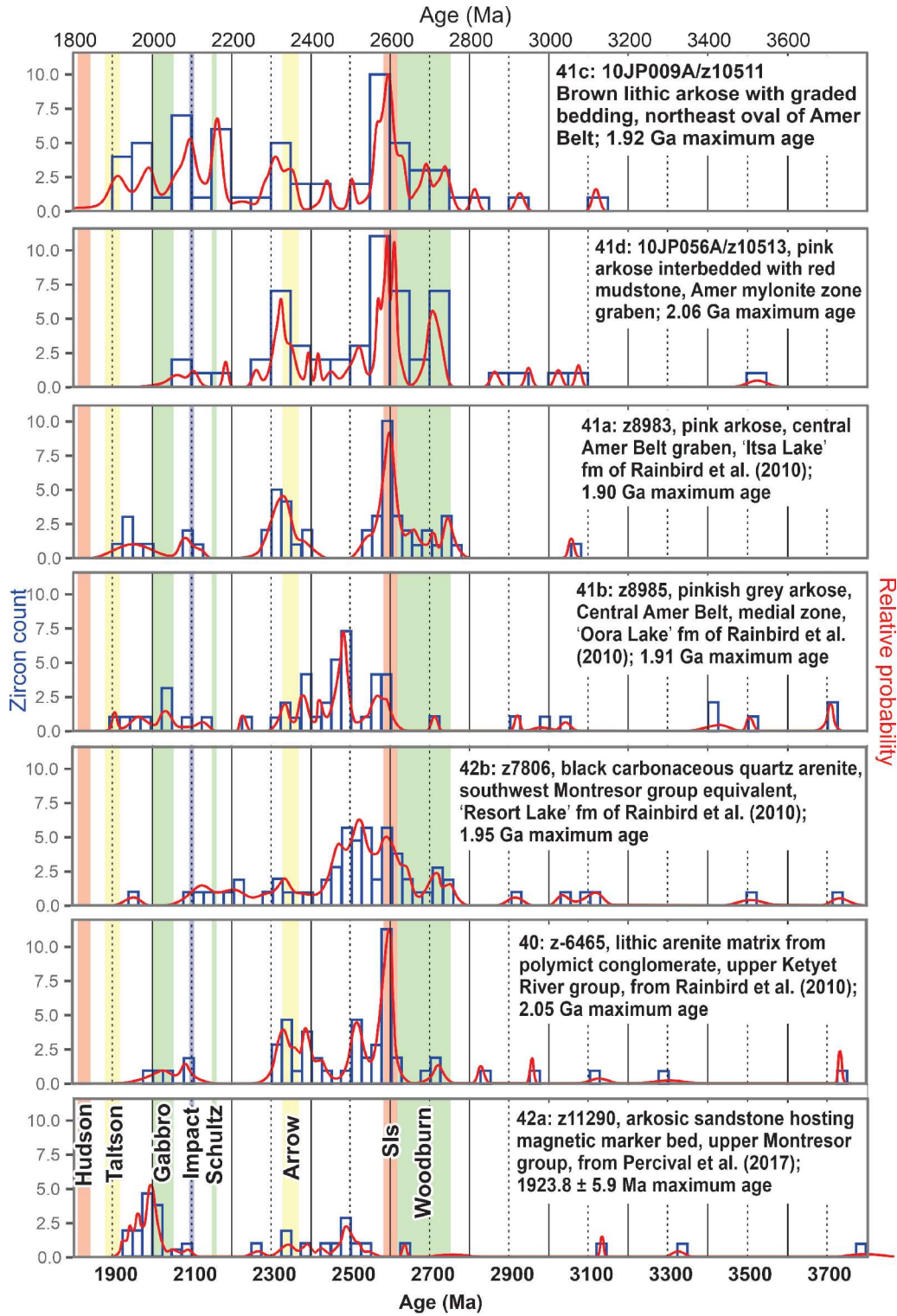


Figure B-2. Detrital zircon geochronology plots of sequence Ps4. The top two are derived from data in Davis (2021). The remaining plots are rescaled from Rainbird et al. (2010) and Percival et al. (2017), as cited. Sis = Snow Island suite.

New crustal subdivision and architecture of the south Rae Craton, Northwest Territories: a synthesis

S.J. Pehrsson^{1*}

Pehrsson, S.J., 2024. New crustal subdivision and architecture of the south Rae Craton, Northwest Territories: a synthesis; in Canada's northern shield: new perspectives from the Geo-mapping for Energy and Minerals program, (ed.) S.J. Pehrsson, N. Wodicka, N. Rogers, and J.A. Percival; Geological Survey of Canada, Bulletin 612, p. 283–287. <https://doi.org/10.4095/332500>

Abstract: South Rae Craton has historically been the most poorly known part of the Canadian Shield. Last mapped in the early 1950s, it was thought to comprise old high-grade granitic gneiss and Archean metasedimentary belts and felsic plutons that had not been affected significantly by the Snowbird or Trans-Hudson orogenies.

A new, two-year mapping transect across south Rae Craton was undertaken by the Geological Survey of Canada and Northwest Territories Geological Survey in 2015–2017. Results are summarized in four new 1:250 000 scale maps and presented in reports, Open Files, and external journal publications available through GEOSCAN showing that south Rae Craton comprises nine distinct crustal domains bounded by newly recognized crustal-scale shear zones with a protracted history of deformation and reactivation between 2.5 Ga to ca. 1.7 Ga.

Résumé : Le craton de Rae Sud a été, par le passé, la partie la moins bien connue du Bouclier canadien. Cartographié pour la dernière fois au début des années 1950, on le croyait composé d'anciens gneiss granitiques de fort degré de métamorphisme ainsi que de ceintures métasédimentaires de l'Archéen et de plutons felsiques qui n'avaient pas été touchés de manière significative par les orogénèses de Snowbird ou trans-hudsonienne.

Un nouveau transect cartographique recoupant le craton de Rae Sud, échelonné sur une période de deux ans, a été entrepris par la Commission géologique du Canada et la Commission géologique des Territoires du Nord-Ouest en 2015-2017. Les résultats sont résumés à l'aide de quatre nouvelles cartes à l'échelle de 1/250 000 et présentés dans des rapports, des dossiers publics et des publications de revues externes disponibles par l'entremise de GEOSCAN. Ils montrent que le craton de Rae Sud comprend neuf domaines crustaux distincts délimités par des zones de cisaillement à l'échelle de la croûte nouvellement reconnues, qui révèlent une longue histoire de déformation et de réactivation entre 2,5 Ga et environ 1,7 Ga.

¹Geological Survey of Canada, 601 Booth Street, Ottawa, Ontario K1A 0E8

*Corresponding author: S.J. Pehrsson (email: sally.pehrsson@nrcan-rncan.gc.ca)

South Rae Craton in the Northwest Territories (N.W.T.), situated between the Hearne Craton, Taltson-Thelon Orogen, and Thelon Basin (Fig. 1), has historically been the most poorly known part of the Canadian Shield. Last mapped in the early 1950s at only 1:500 000 scale, it was thought to comprise old high-grade granitic gneiss interspersed with Archean metasedimentary belts and felsic plutons that had not been affected significantly by the Snowbird or Trans-Hudson orogenies. With few crustal formation or metamorphic ages available for most of the region, its relationship and tectonic architecture compared to the rest of Rae Craton was poorly understood.

A new, two-year mapping transect across south Rae Craton in Northwest Territories from its margin with Hearne Craton at Kasba Lake to Porter Lake, southeast of the Great Slave Lake shear zone, was undertaken by the Geological Survey of Canada and Northwest Territories Geological Survey in 2015–2017 following a reconnaissance survey in 2012 (Pehrsson et al., 2015). The region studied (Fig. 1) encompasses the Snowbird Tectonic zone between Rae and Hearne cratons, the previously studied Snowbird domain of Rae Craton (Martel et al., 2008), and undifferentiated gneisses. Results are summarized in four new 1:250 000 scale maps (Martel et al., 2020a–d) and presented in Reports

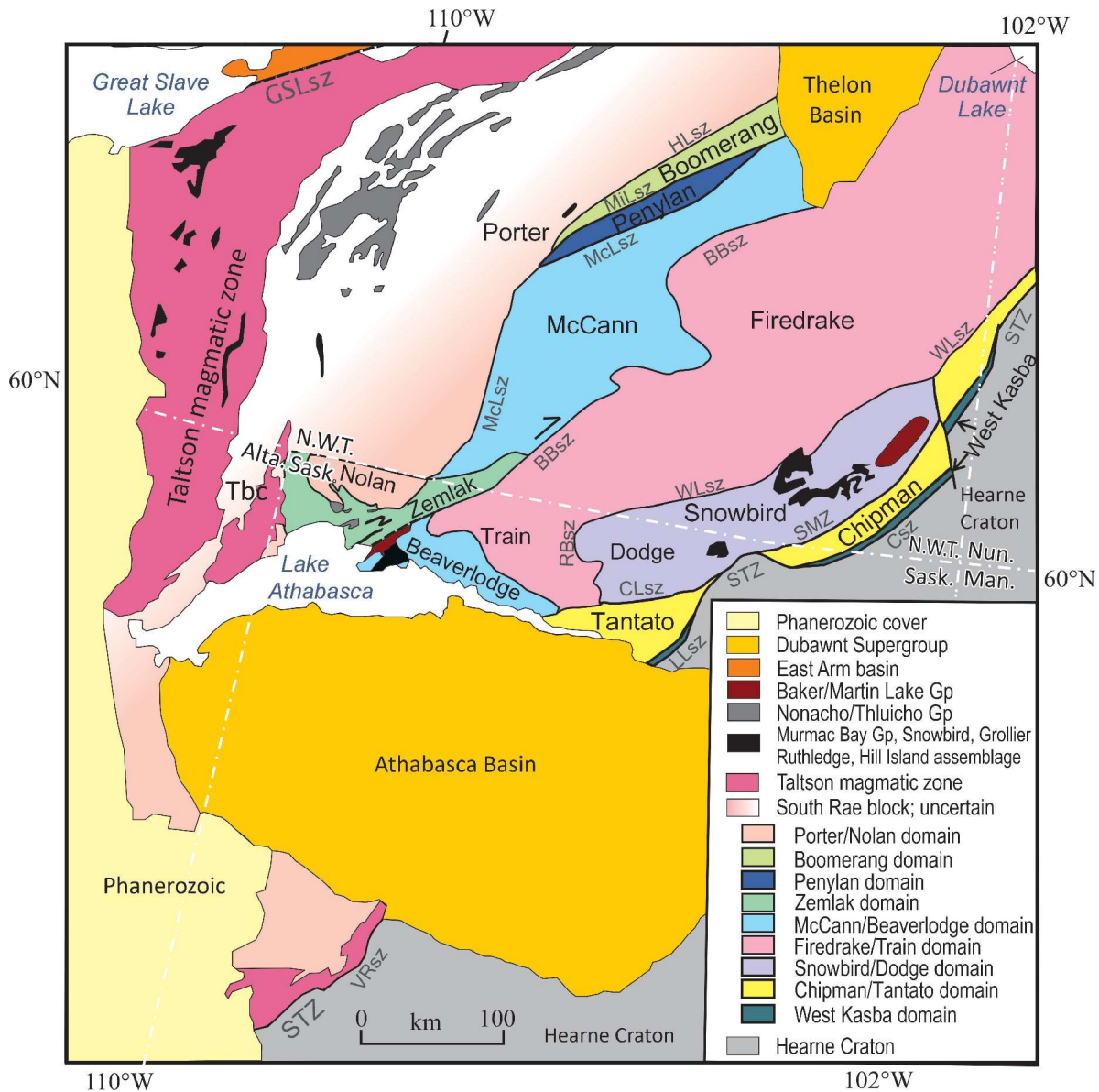


Figure 1. Domains of the south Rae block of the Rae Craton, Nunavut and Saskatchewan. Tbc: Taltson basement complex; GSLsz: Great Slave Lake shear zone; BBSz: Black Bay shear zone; WLSz: Wholdaia Lake shear zone; HLSz: Howard Lake shear zone; MILsz: Miller Lake shear zone; McLsz: McArthur Lake shear zone; SMZ: Striding Mylonite Zone; STZ: Snowbird Tectonic Zone; CLsz: Cora lake shear zone; LLsz: Legs Lake shear zone; Csz: Chipman shear zone; VRsz: Virgin River shear zone; RBsz: Ryckman Bay shear zone. Modified from Martel et al. (2020a–d).

of Activities (Pehrsson et al., 2015; Percival et al., 2016), Open Files, and external journal publications available through GEOSCAN.

New U-Pb geochronological, isotopic, and tectono-metamorphic studies show that south Rae Craton comprises nine distinct crustal domains bounded by newly recognized crustal-scale shear zones with a protracted history of deformation and reactivation between 2.5 Ga and ca. 1.7 Ga (Fig. 1, 2; Martel et al., 2018). In contrast to previous models, much of south Rae Craton is late Neoproterozoic to early Paleoproterozoic in age, with evidence for Paleo-Mesoarchean crustal contamination restricted to areas west of the MacArthur Lake shear zone (Fig. 1; Penylan, Boomerang, and Porter domains) that include rocks potentially correlative with the Taltson basement complex (Peterson et al., in press). All domains record ca. 2.7–2.6 Ga crust formation (Fig. 2) with important, newly identified greenstone belts and subaerial volcanic rocks preserved in the Boomerang domain. This pattern suggests that, like north Rae Craton, south Rae domains were largely

assembled during the 2.62–2.58 Ga Snow Island event (Peterson et al., this volume). Ca. 2.55–2.3 Ga Archean to Paleoproterozoic intermediate-felsic plutonism is found in Snowbird, Firedrake, and McCann domains (Fig. 2), and post-2.3 Ga, all domains except Chipman record nearshore to marine sedimentation, with formation of a moderate to deep marine clastic and volcanic basin along West Kasba domain. Paleoproterozoic magmatism, including ca. 2.29–2.0 Ga mafic dyke swarms and layered complexes, as well as ca. 1.9 Ga arc-like plutons, highlights a significantly different cratonic core than previously postulated, and one that saw attempted break-up during Siderian-Rhyacian time (Pehrsson et al., 2013).

The tectonometamorphic record of south Rae is highly complex (Fig. 2). Ca. 2.55–2.5 Ga MacQuoid orogenesis, at moderate pressure, amphibolite to granulite facies, is restricted to Archean basement of the West Kasba, Chipman, and Snowbird domains near the Snowbird Tectonic zone suture with Hearne Craton. The ca. 2.4–2.3 Ga Arrowsmith Orogeny is recorded in moderate-pressure, high-temperature

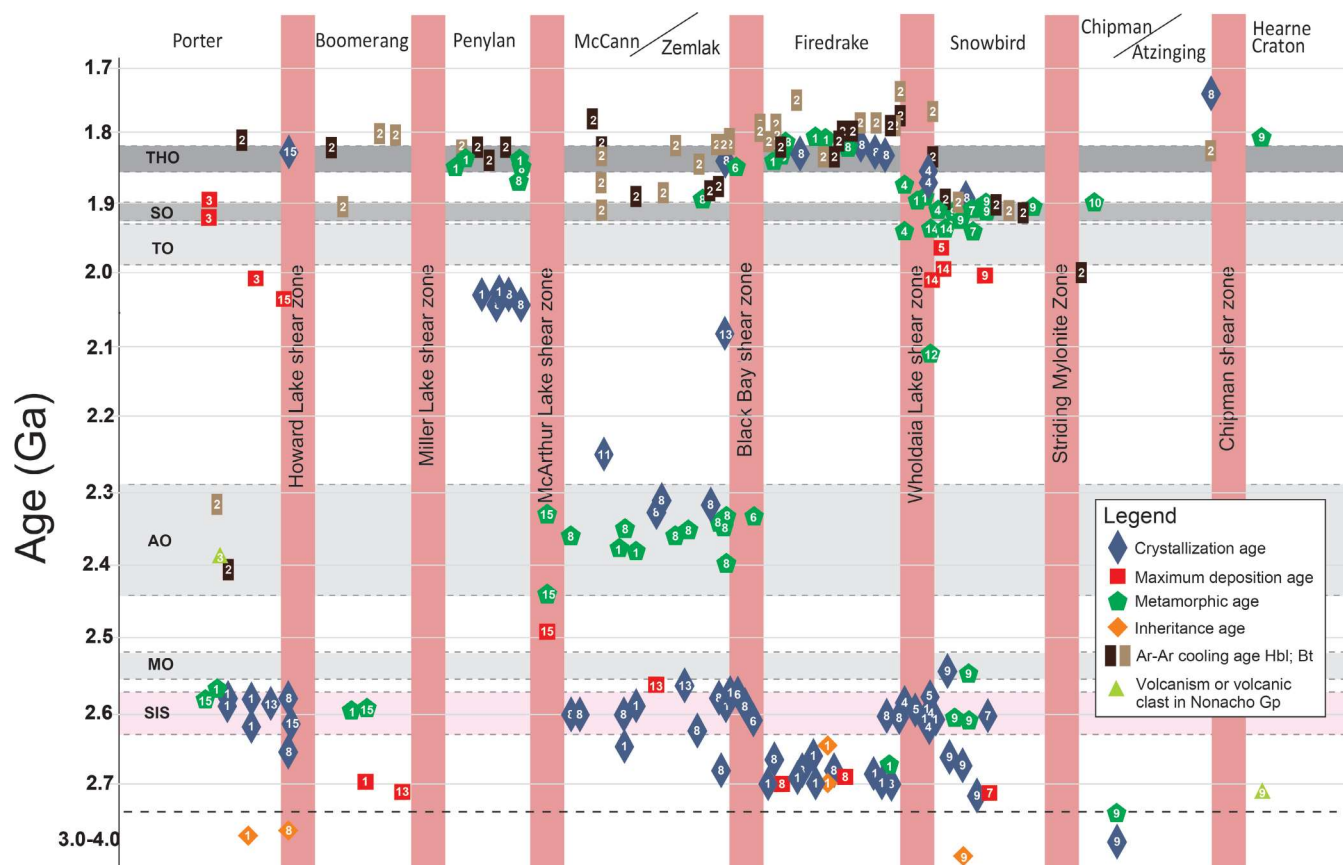


Figure 2. Compilation of new and existing ages for the south Rae Craton domain subdivisions in Northwest Territories. This summary includes igneous, volcanic, metamorphic, cooling, and maximum deposition ages obtained during the GEM-2 South Rae mapping project and previous projects (GEM-1, Western Churchill Project and other studies). Numbers in symbols refer to the source of data: 1: Regis et al., 2017; 2: Regis and Kellett, 2018; 3: Neil, 2017; 4: Thiessen et al., 2017; 5: Thiessen et al., 2018; 6: Jamison, 2018; 7: Regis et al., 2017; 8: Davis et al., 2015; 9: Martel et al., 2008; 10: Flowers et al., 2006; 11: Mowbray and Pehrsson, 2019; 12: Thiessen et al., 2018; 13: unpublished ages (See Martel et al. 2020a–d); 14: Thiessen et al., 2020; 15: Thiessen et al., 2022. THO: Trans-Hudson Orogeny; SO: Snowbird Orogeny; TO: Taltson Orogeny; AO: Arrowsmith Orogeny; MO: MacQuoid Orogeny; SIS: Snow Island Suite; Hbl: hornblende; Bt: biotite.

granulite gneiss west of the Black Bay shear zone and formed the dominant regional structure of the McCann and Zemlak domains. Based on preservation of rocks with ca. 2.4 Ga cooling ages west of Porter Lake in Porter domain and 5–7 kbar conditions at ca. 2.36 Ga in McCann domain, Thiessen et al. (2022) proposed that the Howard Lake shear zone (HLsz) was active as a major crustal structure since ca. 2.3 Ga, and has been reactivated repeatedly in a ductile regime right up to Trans-Hudson time at 1.80 Ga.

Effects of the ca. 1.9 Ga Snowbird Orogeny are the most widespread in south Rae Craton (Martel et al., 2008; Martel et al., 2020a–d; Regis et al., 2021). West Kasba, Chipman, Snowbird, and Firedrake domains all record ca. 1.9 Ga tectonometamorphism that formed fabrics that were folded or locally transposed during the Trans-Hudson Orogeny. Most major structures, including Howard Lake, Miller Lake, Black Bay, Wholdaia Lake, and Chipman shear zones, were active at ca. 1.9 Ga. Black Bay shear zone accommodated east-vergent thrusting of McCann domain over Firedrake Domain, with coronitic, ca. 1.9 Ga high pressures recorded in Paleoproterozoic fertile mafic units that intruded the McCann granulite-facies rocks, such as the Orpheus and Penylan suites. Wholdaia Lake and Chipman shear zones were also part of an east-vergent thrust stack at 1.9 Ga, which exhumed progressively deeper crustal levels westward.

Extension of the thickened south Rae Craton architecture occurred during both Snowbird and Trans-Hudson time (Regis et al., 2021), with the latter particularly prominent in the uplift of mid- to deep crustal Firedrake and Penylan domains on the Howard Lake, MacArthur, Black Bay, and Wholdaia shear zones.

Testable correlations of these new domains and structures into Northern Saskatchewan and Nunavut have been proposed (Fig. 2) and define a linear crustal-block geometry resulting from the combined effects of the Arrowsmith collisional orogeny to the west, accretion of the Hearne Microcontinent to the east, and final closure of the Manikewan Ocean during ca. 1.83 Ga collision of the Superior Plate. The prominent cycles of thickening and collapse between 1.9 and 1.80 Ga can thus be viewed as a response of the near (Snowbird) and far (Trans-Hudson)-field Rae upper plate during closure of the Manikewan Ocean and assembly of the Nuna Supercontinent (Regis et al., 2021; Pehrsson et al., 2023).

ACKNOWLEDGMENTS

This project was supported by GEM-2 and NSERC research grants to D. Gibson and Shoufa Lin. Discussions with Rob Berman, Ken Ashton, and Colin Card are gratefully acknowledged and Natasha Wodicka is warmly thanked for her timely and excellent review.

REFERENCES

- Davis, W.J., Pehrsson, S.J., and Percival, J.A., 2015. Results of a U-Pb zircon geochronology transect across the southern Rae craton, Northwest Territories, Canada; Geological Survey of Canada, Open File 7655, 74 p. <https://doi.org/10.4095/295610>
- Flowers, R.M., Bowring, S.A., and Williams, M.L., 2006. Timescales and significance of high-pressure, high-temperature metamorphism and mafic dike anatexis, Snowbird tectonic zone, Canada. *Contributions to Mineralogy and Petrology* v. 151, p. 558–581. <https://doi.org/10.1007/s00410-006-0066-7>
- Jamison, D., 2018. Deformation history of the Black Bay Fault, Northwest Territories, Canada: unpublished M.Sc. thesis, University of Waterloo, Waterloo, Ontario, 145 p.
- Martel, E., van Breemen, O., Berman, G., and Pehrsson, S., 2008. Geochronology and tectonometamorphic history of the Snowbird Lake area, Northwest Territories, Canada: new insights into the architecture and significance of the Snowbird tectonic zone; *Precambrian Research*, v. 161, p. 201–230. <https://doi.org/10.1016/j.precamres.2007.07.007>
- Martel, E., Pehrsson, S.J., Percival, J., Acosta-Góngora, P., Thiessen, E., Regis, D., Jamison, D., Neil, B., and Knox, B., 2018. Geology and mineral potential of the southern Rae Craton, Northwest Territories, NTS 75-G and H; Geological Survey of Canada, Open File 8194, 1 poster. <https://doi.org/10.4095/306542>
- Martel, E., Pehrsson, S.J., Jamison, D., Thiessen, E.J., Pierce, K.L., Acosta-Góngora, P., and Davis, W.J., 2020a. Geology of the Abitau Lake area, south Rae Craton, Northwest Territories (NTS 75B); Northwest Territories Geological Survey, NWT Open File 2020-01, scale 1:250 000.
- Martel, E., Pehrsson, S.J., Regis, D., Thiessen, E.J., Jamison, D., Percival, J., Pierce, K.L., and Acosta-Góngora, P., 2020b. Geology of the McCann Lake area, south Rae Craton, Northwest Territories (NTS 75G); Northwest Territories Geological Survey, NWT Open File 2020-02, scale 1:250 000.
- Martel, E., Pehrsson, S.J., Regis, D., Thiessen, E.J., Jamison, D., Percival, J., Pierce, K.L., and Acosta-Góngora, P., 2020c. Geology of the Rennie Lake area, south Rae Craton, Northwest Territories (NTS 75H); Northwest Territories Geological Survey, NWT Open File 2020-03, scale 1:250 000.
- Martel, E., Pehrsson, S.J., Thiessen, E.J., Jamison, D., Pierce, K.L., Acosta-Góngora, P., and Davis, W.J., 2020d. Geology of the Wholdaia Lake area, south Rae Craton, Northwest Territories (NTS 75A); Northwest Territories Geological Survey, NWT Open File 2020-04, scale 1:250 000.
- Mowbray, B. and Pehrsson, S.J., 2019. Geochemistry, petrology, and aeromagnetic mapping of the Orpheus dykes, South Rae craton, Northwest Territories; Geological Survey of Canada, Open File 8340, 28 p. <https://doi.org/10.4095/311306>
- Neil, B., 2017. Depositional age, provenance and tectonic significance of the Porter Lake and Lynx Lake outliers, south Rae craton, Northwest Territories. B.Sc. Honours Thesis. Simon Fraser University, Burnaby, British Columbia, 123 p.

- Pehrsson, S.J., Berman, R., Eglington, B., and Rainbird, R., 2013. Two Neoproterozoic supercontinents revisited: the Rae family of cratons and their implications for alternate pre-Nuna configurations; *Precambrian Research*, v. 232, p. 27–43. <https://doi.org/10.1016/j.precamres.2013.02.005>
- Pehrsson, S.J., Campbell, J.E., Martel, E., McCurdy, M.W., Agosta-Góngora, P., Thiessen, E., Jamieson, D., Lauzon, G., Buller, G., Falck, H., and Dyke, A.S., 2015. Report of 2015 activities for the geologic and metallogenic framework of the south Rae Craton, southeast Northwest Territories: GEM 2 South Rae quaternary and bedrock project; Geological Survey of Canada, Open File 7958, 24 p. <https://doi.org/10.4095/297387>
- Pehrsson, S.J., Eglington, B., Rainbird, R., Regis, D., Ramaekers, P., and Jefferson, C., 2023. Extent and significance of the Racklan-Forward orogen in Canada: far-field interior reactivation during Nuna assembly; *in* *Journal of the Geological Society of London*, v. 531. <https://doi.org/10.1144/SP531-2022-307>
- Percival, J., Martel, E., Pehrsson, S.J., Acosta-Gongora, P., Regis, D., Thiessen, E., Jamison, D., Neil, B., and Knox, B., 2016. Report of 2016 activities for the geologic and metallogenic framework of the South Rae craton, southeast Northwest Territories: GEM 2 South Rae quaternary and bedrock project; Geological Survey of Canada, Open File 8142, 17 p. <https://doi.org/10.4095/299469>
- Peterson, T., Pehrsson, S.J., Martel, E., and Percival, J., in press. Lithochemistry and Sm-Nd isotopes in the GEM2/South Rae study area, 2012–2016; Geological Survey of Canada, Open File 8510, 52 p.
- Regis, D. and Kellett, D.A., 2018. $^{40}\text{Ar}/^{39}\text{Ar}$ hornblende and biotite cooling ages for metamorphic rocks from the southern Rae Craton, Northwest Territories; Geological Survey of Canada, Open File 8438, 1 .zip file. <https://doi.org/10.4095/311217>
- Regis, D., Martel, E., Davis, W., and Pehrsson, S.J., 2017. U-Pb zircon geochronology of metaplutonic rocks across the southern Rae Province, Northwest Territories; Geological Survey of Canada, Open File 8254, 37 p. <https://doi.org/10.4095/302772>
- Regis, D., Pehrsson, S., Martel, E., Thiessen, E., Peterson, T., and Kellett, D., 2021. Post-1.9 Ga evolution of the south Rae Craton (Northwest Territories, Canada): a Paleoproterozoic orogenic collapse system; *Precambrian Research*, v. 355, art. no. 106105, 29 p. <https://doi.org/10.1016/j.precamres.2021.106105>
- Thiessen, E., Gibson, H.D., Regis, D., Pehrsson, S.J., 2018. Deformation and extensional exhumation of 1.9 Ga high-pressure granulites along the Wholdaia Lake shear zone, south Rae craton, Northwest Territories, Canada; *Lithosphere* vol. 10, no. 5, p. 641–661. <https://doi.org/10.1130/L704.1>
- Thiessen, E.J., Gibson, H.D., Regis, D., and Pehrsson, S.J., 2019. Deformation and extensional exhumation of Paleoproterozoic high-pressure granulites along the Wholdaia Lake shear zone, south Rae craton, Northwest Territories. *Lithosphere*, v. 10, no. 5, p. 641–661. <https://doi.org/10.1130/L704.1>
- Thiessen, E. J., Gibson, H. D., Regis, D., Pehrsson, S. J., Ashley, K. T., and Smit, M.A., 2020. The distinct metamorphic stages and structural styles of the 1.94–1.86 Ga Snowbird Orogen, Northwest Territories, Canada; *Journal of Metamorphic Geology* v. 38, no. 9, p. 963–992. <https://doi.org/10.1111/jmg.12556>
- Thiessen, E., Gibson, H.D., Pehrsson, S.J., and Regis, D., 2022. A lithospheric-scale Arrowsmith (2.4 Ga) detachment system with major Trans-Hudson (1.8 Ga) reactivation documented in the Howard Lake shear zone, Rae craton, Canada; *Precambrian Research*, v. 376, no. 106683, 21 p. <https://doi.org/10.1016/j.precamres.2022.106683>

An overview of Archean and Proterozoic history of the Tehery Lake–Wager Bay area, central Rae Craton, Nunavut

N. Wodicka^{1*}, H.M. Steenkamp², T.D. Peterson¹, I. Therriault³, J.B. Whalen¹, V. Tschirhart¹, C.J.M. Lawley¹, C. Guilmette², D.A. Kellett⁴, O.M. Weller⁵, W. Garrison⁶, J. Kendrick⁷, and W.J. Davis¹

Wodicka, N., Steenkamp, H.M., Peterson, T.D., Therriault, I., Whalen, J.B., Tschirhart, V., Lawley, C.J.M., Guilmette, C., Kellett, D.A., Weller, O.M., Garrison, W., Kendrick, J., and Davis, W.J., 2024. An overview of Archean and Proterozoic history of the Tehery Lake–Wager Bay area, central Rae Craton, Nunavut; in Canada's northern shield: new perspectives from the Geo-mapping for Energy and Minerals program, (ed.) S.J. Pehrsson, N. Wodicka, N. Rogers, and J.A. Percival; Geological Survey of Canada, Bulletin 612, p. 289–293. <https://doi.org/10.4095/332501>

Abstract: This short contribution describes the Archean and Proterozoic history of the central Rae Craton in the Tehery Lake–Wager Bay area, Nunavut. The study area comprises six lithotectonic domains separated by large-scale structures: the Gordon Domain, Lunan Domain, Daly Bay complex, Douglas Harbour Domain, Kummel Lake Domain, and Ukkusiksalik Domain. These domains can be differentiated on the basis of metamorphic assemblages, Nd model and U–Pb ages, absence or presence of specific lithologies, and/or geophysical characteristics. Links between these domains and neighbouring areas of the central Rae Craton, the timing of assembly of domains and terranes, and the effects of the Snowbird and Trans-Hudson orogenies are briefly described.

Résumé : Cette courte contribution décrit l'histoire archéenne et protérozoïque de la partie centrale du craton de Rae dans la région de lac Tehery-baie Wager, au Nunavut. La région d'étude comprend six domaines lithotectoniques séparés par des structures à grande échelle : le domaine de Gordon, le domaine de Lunan, le complexe de Daly Bay, le domaine de Douglas Harbour, le domaine de Kummel Lake et le domaine d'Ukkusiksalik. Ces domaines peuvent être différenciés en se fondant sur les assemblages métamorphiques, les âges modèles Nd et U–Pb, l'absence ou la présence de lithologies particulières et/ou les caractéristiques géophysiques. Les liens entre ces domaines et les régions voisines du craton de Rae central, la chronologie de l'assemblage des domaines et des terranes, ainsi que les effets des orogènes de Snowbird et trans-hudsonienne sont brièvement décrits.

¹Geological Survey of Canada, 601 Booth Street, Ottawa, Ontario K1A 0E8

²Département de géologie et de génie géologique, Université Laval, 1065, avenue de la Médecine, Québec, Québec G1V 0A6

³Department of Earth, Environmental and Geographic Sciences, University of British Columbia – Okanagan, 1177 Research Road, Kelowna, British Columbia V1V 1V7

⁴Geological Survey of Canada, 1 Challenger Drive, P.O. Box 1006, Dartmouth, Nova Scotia B2Y 4A2

⁵Department of Earth Sciences, University of Cambridge, Downing Street, Cambridge, CB2 3EQ United Kingdom

⁶Nova Scotia Department of Energy and Mines, Geoscience and Mines Branch, P.O. Box 698, Halifax, Nova Scotia B3J 2T9

⁷Department of Earth and Planetary Sciences, McGill University, 3450 University Street, Montréal, Quebec H3A 0E8

*Corresponding author: N. Wodicka (email: natasha.wodicka@NRCan-RNCan.gc.ca)

This contribution presents an overview of the Archean and Proterozoic history of the central Rae Craton in the Tehery Lake–Wager Bay area, Nunavut, stemming from bed-rock mapping, U-Pb geochronology, whole-rock and Sm-Nd isotope geochemistry, metamorphic petrology, and geophysical studies conducted under the Geo-mapping for Energy and Minerals program (N. Wodicka, H.M. Steenkamp, T. Peterson, and J.B. Whalen, unpub. U-Pb, Sm-Nd, Lu-Hf, and geochemical data, 2012–2019; Ferderber, 2013; Steenkamp et al., 2015, 2016, 2023a, b, c; Wodicka et al., 2015, 2016, 2017a, b; W. Garrison, unpub. B.Sc. research project, 2016; Tschirhart et al., 2016, this volume; Therriault et al., 2018, 2023; Therriault, 2019; Peterson et al., this volume; H.M. Steenkamp, N. Wodicka, and C.J.M. Guilmette, unpub. paper, 2023).

The study area comprises six lithotectonic domains with distinct lithological, metamorphic, isotopic, and/or geophysical characteristics, separated by large-scale structures (Fig. 1). The easternmost Gordon Domain on the west coast of Roes Welcome Sound south of Wager Bay contains Meso- to Neoproterozoic (2.86, 2.71–2.68, 2.62–2.60 Ga) tonalite to monzogranite gneiss and plutonic rocks with 3.29–2.76 Ga Nd model ages, whereas the Lunan Domain to the west comprises Neoproterozoic (2.71–2.70, 2.58 Ga) granitoid gneiss and plutonic rocks with generally younger 2.97–2.72 Ga Nd model ages. Owing to complex structural overprinting, the boundary between the two domains cannot be clearly delineated, but it closely coincides with the ca. 2.70 Ga Lorillard supracrustal sequence, top-to-the-west reverse-sense high-strain zones, a north-trending magnetic and gravity lineament at depth, and a transition zone with both old and relatively young Nd model ages (3.09–2.75 Ga). The Lorillard belt shares age, lithological, and geochemical characteristics with greenstone belts of the Chesterfield Block (e.g. Davis et al., 2006; Sandeman et al., 2006; Acosta-Góngora et al., 2018a) to the south, and was likely amalgamated with the Lunan and Gordon domains outboard of the proto-Rae Craton prior to 2.62 to 2.58 Ga Snow Island suite arc magmatism (Peterson et al., this volume). The combined Chesterfield–Tehery terranes, together with the Snowbird Domain to the southwest of the study area, are inferred to have initially collided with an oceanic arc (Axis Lake gabbro; Acosta-Góngora et al., 2018b) at ca. 2.62 Ga, along or near the trace of the Chesterfield shear zone, and then with the proto-Rae Craton at ca. 2.605 Ga (Peterson et al., this volume).

Two large granulite-facies domains defining gravity highs occur in the southern part of the study area. The Kummel Lake Domain to the southwest comprises Neoproterozoic (2.71–2.70 Ga) granodiorite to monzogranite gneiss and gabbroic anorthosite with folded panels of supracrustal rocks (Kummel Lake belt). Inverse modelling of the regional gravity data, combined with structural data, illustrates that the Kummel Lake Domain dips shallowly to moderately northward beneath the upper amphibolite-facies rocks of the Lunan–Lorillard–Gordon domains, thereby resembling

a metamorphic core complex. The Kummel Lake Domain shares age, lithological, and metamorphic characteristics with the Uvauk complex and a granulite suite (Tella, 1993; Mills et al., 2007) immediately to the south of the study area. By contrast, the Daly Bay complex to the southeast is a dominantly Paleoproterozoic (1.92–1.91 Ga) mafic granulite domain, with northeast-verging map-scale synforms and inward-dipping sheared margins, that was tectonically juxtaposed over amphibolite-facies Archean orthogneiss of the Gordon Domain by north-directed thrusting. Later extensional normal-oblique shearing may explain the preservation of a greenschist- to lower amphibolite-facies Paleoproterozoic (<1.975 Ga) supracrustal assemblage (Kingmirit belt) structurally beneath the granulite-facies rocks.

The Douglas Harbour Domain, separated from the Lunan–Lorillard–Gordon domains to the south by the Chesterfield shear zone and bounded to the north by the Wager shear zone, comprises dominantly Meso- and Neoproterozoic (2.90, 2.69 Ga) granodiorite to monzogranite gneissic and plutonic rocks, including 2.61 Ga K-feldspar porphyritic monzogranite. Folded, thick-skinned thrust sheets preserving stacked repetitions of Archean basement gneiss and Paleoproterozoic, lower Ketyet River group–equivalent supracrustal rocks (Pennington belt), together with low to middle amphibolite-facies metamorphic assemblages, distinguish this domain from adjacent ones south of the Chesterfield shear zone. The northernmost Ukkusiksalik Domain shares lithological similarities with the Douglas Harbour Domain, including two supracrustal sequences of differing age (the Paliak belt of probable Archean age and the Paleoproterozoic Pennington belt); however, this domain may represent the southwesternmost extent of the Repulse Bay Block, bounded to the northwest by a large 2.61 Ga Snow Island suite monzogranite body and to the south by the Wager shear zone. The latter structure may have initially formed as an oceanic transform fault in the Archean (Peterson et al., this volume), but was most recently active as a dextral strike-slip shear zone during the Paleoproterozoic at 1.835–1.826 and 1.75–1.74 Ga (Therriault et al., 2018, 2023).

The Archean and Paleoproterozoic rocks of the Tehery Lake–Wager Bay area were extensively deformed and metamorphosed during the ca. 1.94–1.90 Ga Snowbird and/or 1.88–1.80 Ga Trans-Hudson orogenies, partly overprinting earlier tectonometamorphic events (ca. 2.7, 2.6, and 2.55 Ga) in Archean rocks. The ca. 1.84 to 1.81 Ga syn- to early post-orogenic monzogranite to monzonite plutons, sills, and dykes of the Hudson suite cut through all rock units, except the granulite-facies rocks of the Daly Bay complex and Mesoproterozoic Mackenzie dykes. Medium- to coarse-grained ultrapotassic intrusions (1.825 Ga) in the Lunan Domain and in the transition zone between the Lunan and Gordon domains likely represent the deep-crustal equivalent of the Martell syenite suite.

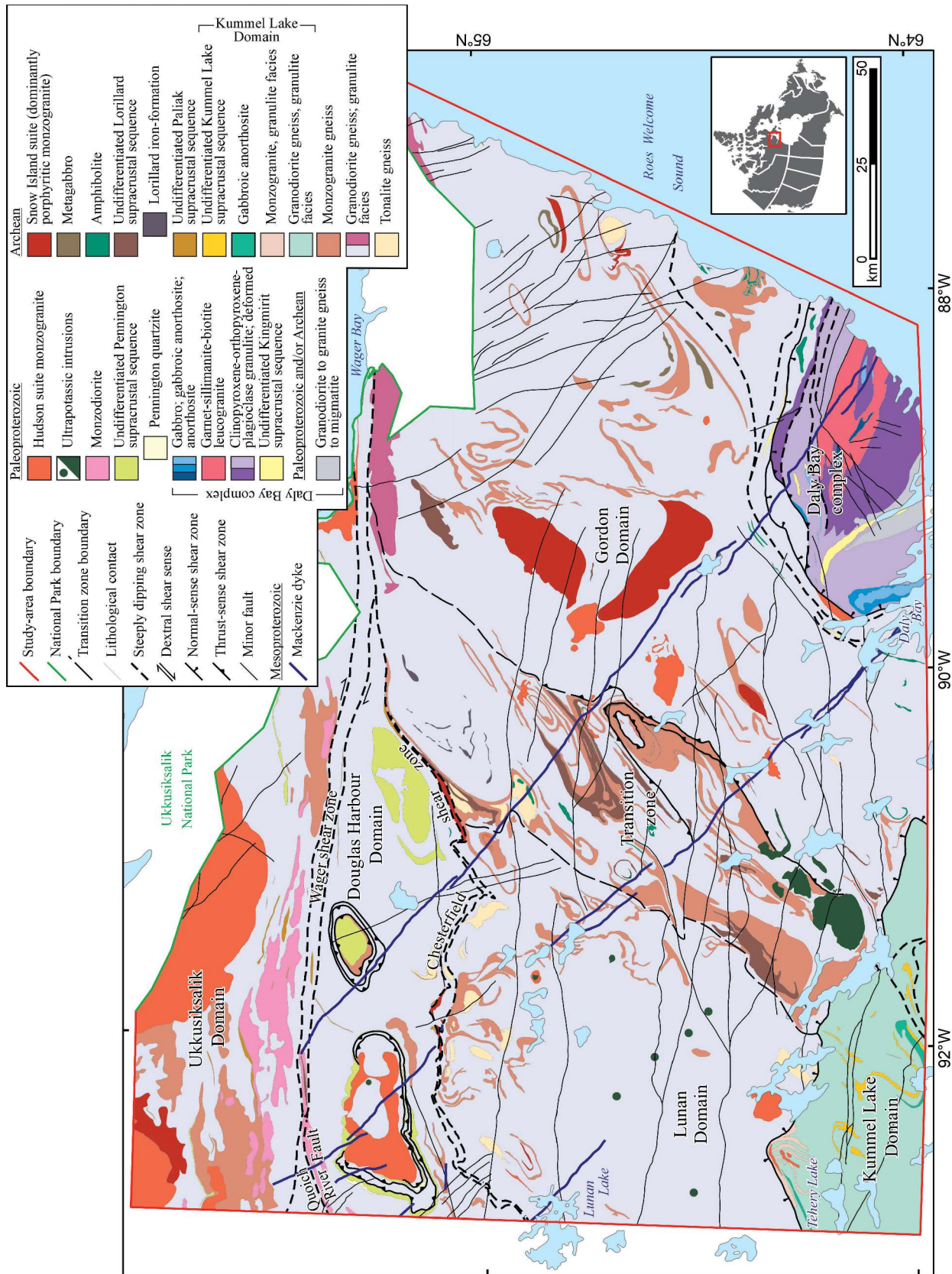


Figure 1. Geological map of the Tehery Lake–Wager Bay area in the central Rae Craton showing the different lithotectonic domains bounded by large-scale structures (after Steenkamp et al., 2023a, b, c). Inset map shows the location of the study area in Canada.

Future studies in the Tehery Lake–Wager Bay area could be aimed at

- increasing the understanding of the role of major structures in the assembly of the different domains during the Archean, Paleoproterozoic sedimentary accumulation and preservation, and/or exhumation of high-grade rocks during the Trans-Hudson Orogeny;
- increasing the knowledge of the full mineral potential of the study area, only briefly documented in previous publications;
- defining the tectonic processes responsible for Archean crustal growth and metamorphism that initially reworked the central Rae Craton in the Tehery Lake–Wager Bay and surrounding areas, particularly at ca. ≥ 2.7 Ga.

ACKNOWLEDGMENTS

This contribution was produced as part of the Geo-mapping for Energy and Minerals program (2012–2019). Sally Pehrsson is thanked for a constructive review of the manuscript.

REFERENCES

- Acosta-Góngora, P., Pehrsson, S.J., Sandeman, H.A., Martel, E., and Peterson, T.D., 2018a. The Ferguson Lake deposit: an example of Ni-Cu-Co-PGE mineralization emplaced in a back-arc basin setting?; *Canadian Journal of Earth Sciences*, v. 55, p. 958–979. <https://doi.org/10.1139/cjes-2017-0185>
- Acosta-Góngora, P., Pehrsson, S.P., Knox, B., Regis, D., Hulbert, L., Creaser, R.A., and Ashton, K., 2018b. Neorchean convergent margin Ni-Cu mineralization? Axis Lake and Nickel King Ni-Cu deposits in the south Rae Province craton of the Canadian Shield; *Precambrian Research*, v. 316, p. 305–323. <https://doi.org/10.1016/j.precamres.2018.07.016>
- Davis, W.J., Hanmer, S., Tella, S., Sandeman, H.A., and Ryan, J.J., 2006. U-Pb geochronology of the MacQuoid supracrustal belt and Cross Bay plutonic complex: key components of the northwestern Hearne subdomain, western Churchill Province, Nunavut, Canada; *Precambrian Research*, v. 145, p. 53–80. <https://doi.org/10.1016/j.precamres.2005.11.016>
- Ferderber, J., Kellett, D.A., and Wodicka, N., 2013. Exploring the Tehery region: correlating supracrustal sequences using detrital zircon geochronology, Rae Craton, Nunavut; Geological Survey of Canada, Open File 7424, 1 sheet. <https://doi.org/10.4095/292709>
- Mills, A.J., Berman, R.G., Davis, W.J., Tella, S., Carr, S., Roddick, C., and Hanmer, S., 2007. Thermobarometry and geochronology of the Uvauk complex, a polymetamorphic Neorchean and Paleoproterozoic segment of the Snowbird tectonic zone, Nunavut, Canada; *Canadian Journal of Earth Sciences*, v. 44, p. 245–266. <https://doi.org/10.1139/e06-080>
- Sandeman, H.A., Hanmer, S., Tella, S., Armitage, A.A., Davis, W.J., and Ryan, J.J., 2006. Petrogenesis of Neorchean volcanic rocks of the MacQuoid supracrustal belt: a back-arc setting for the northwestern Hearne subdomain, western Churchill Province, Canada; *Precambrian Research*, v. 144, p. 40–165. <https://doi.org/10.1016/j.precamres.2005.11.001>
- Steenkamp, H.M., Wodicka, N., Lawley, C.J.M., Peterson, T.D., and Guilmette, C., 2015. Overview of bedrock mapping and results from portable X-ray fluorescence spectrometry in the eastern part of the Tehery Lake–Wager Bay area, western Hudson Bay, Nunavut; *in* Summary of activities 2015; Canada-Nunavut Geoscience Office, p. 121–134.
- Steenkamp, H.M., Wodicka, N., Weller, O.M., and Kendrick, J., 2016. Overview of bedrock mapping in the Tehery Lake–Wager Bay area, western Hudson Bay, Nunavut; *in* Summary of activities 2016; Canada-Nunavut Geoscience Office, p. 27–40.
- Steenkamp, H.M., Wodicka, N., Lawley, C.J.M., Peterson, T., Garrison, W., Therriault, I., Kendrick, J., Weller, O.M., and Tschirhart, V., 2023a. Bedrock geology, Daly Bay area, Kivalliq, Nunavut, NTS 56-A, 46-D west, 46-E southwest, and 56-H south; Geological Survey of Canada, Canadian Geoscience Map 458, scale 1:150 000. <https://doi.org/10.4095/331888>
- Steenkamp, H.M., Wodicka, N., Lawley, C.J.M., Peterson, T., Weller, O.M., Kendrick, J., and Tschirhart, V., 2023b. Bedrock geology, Armit Lake area, Kivalliq, Nunavut, NTS 56-B and 56-C east; Geological Survey of Canada, Canadian Geoscience Map 459, scale 1:150 000. <https://doi.org/10.4095/331889>
- Steenkamp, H.M., Wodicka, N., Weller, O.M., Kendrick, J., Therriault, I., Peterson, T., Lawley, C.J.M., and Tschirhart, V., 2023c. Bedrock geology, Wager Bay area, Kivalliq, Nunavut, parts of NTS 56-F and 56-G; Geological Survey of Canada, Canadian Geoscience Map 460, scale 1:150 000. <https://doi.org/10.4095/331890>
- Tella, S., 1993. Geology, Chesterfield Inlet, District of Keewatin, Northwest Territories; Geological Survey of Canada, Open File 2756, scale 1:250 000. <https://doi.org/10.4095/183967>
- Therriault, I., 2019. Structural characterisation and geochronological constraints on the Wager shear zone, northwestern Hudson Bay, Nunavut; M.Sc. thesis, University of British Columbia Okanagan, Kelowna, British Columbia, 228 p.
- Therriault, I., Steenkamp, H.M., Larson, K.P., and Cottle, J.M., 2018. Geochronological constraints on deformation in the Wager shear zone, northwestern Hudson Bay, Nunavut; *in* Summary of activities 2018; Canada-Nunavut Geoscience Office, p. 1–14.
- Therriault, I., Larson, K.P., Steenkamp, H.M., Apen, F.E., Graziani, R., Soret, M., Guilmette, C., and Cottle, J.M., 2023. Characterization of the Wager shear zone, Nunavut, Canada: insights from microstructures and geochronology; *Canadian Journal of Earth Sciences*, v. 60, p. 78–96. <https://doi.org/10.1139/cjes-2022-0031>

- Tschirhart, V.L., Wodicka, N., and Steenkamp, H.M., 2016. Shallow crustal structure of the Tehery Lake–Wager Bay area, western Hudson Bay, Nunavut, from potential-field datasets; *in* Summary of activities 2016; Canada-Nunavut Geoscience Office, p. 41–50.
- Wodicka, N., Steenkamp, H.M., Lawley, C.J.M., Peterson, T.D., Guilmette, C., Girard, É., and Buenviaje, R., 2015. Report of activities for the bedrock geology and economic potential of the Tehery–Wager area: GEM-2 Rae project; Geological Survey of Canada, Open File 7970, 14 p. <https://doi.org/10.4095/297294>
- Wodicka, N., Steenkamp, H.M., Weller, O.M., Kendrick, J., Tschirhart, V.L., Peterson, T.D., and Girard, É., 2016. Report of 2016 activities for the bedrock geology and economic potential of the Tehery–Wager area: GEM-2 Rae project; Geological Survey of Canada, Open File 8149, 21 p. <https://doi.org/10.4095/299392>
- Wodicka, N., Steenkamp, H.M., Peterson, T., Whalen, J., and Lawley, C.J.M., 2017a. Neoproterozoic to Paleoproterozoic evolution of the south-central Rae margin, Tehery-Wager area, Nunavut: insights from field mapping, U-Pb geochronology, and Sm-Nd isotope data; Geological Association of Canada–Mineralogical Association of Canada, Program with Abstracts, v. 40, p. 423.
- Wodicka, N., Steenkamp, H.M., Peterson, T.D., McMartin, I., Day, S.J.A., and Tschirhart, V.L., 2017b. Report of 2017 activities for the geology and economic potential of the Tehery-Wager area, Nunavut: GEM-2 Rae project; Geological Survey of Canada, Open File 8318, 20 p. <https://doi.org/10.4095/305979>

Geophysical contributions to a synthesis of western Churchill geology and metallogeny, Northwest Territories, Nunavut, and Saskatchewan

V. Tschirhart^{1*}, S.J. Pehrsson¹, N. Wodicka¹, J.A. Percival¹,
C.W. Jefferson¹, T.D. Peterson¹, and R.G. Berman¹

Tschirhart, V., Pehrsson, S.J., Wodicka, N., Percival, J.A., Jefferson, C.W., Peterson, T.D., and Berman, R.G., 2024. Geophysical contributions to a synthesis of western Churchill geology and metallogeny, Northwest Territories, Nunavut, and Saskatchewan; in Canada's northern shield: new perspectives from the Geo-mapping for Energy and Minerals program, (ed.) S.J. Pehrsson, N. Wodicka, N. Rogers, and J.A. Percival; Geological Survey of Canada, Bulletin 612, p. 295–325. <https://doi.org/10.4095/332502>

Abstract: The geophysical data sets available for the western Churchill Province have had a bearing on the understanding of its structure, evolution, and metal endowment. New data were acquired and interpreted during the Geo-mapping for Energy and Minerals (GEM) program (2008–2020). Regional, high-resolution aeromagnetic, and targeted gravity and magnetotelluric surveys were collected in GEM, in conjunction with geological mapping projects, in order to provide control on bedrock features beneath widespread glacial overburden and flat-lying sedimentary basins. Quantitative estimates of three-dimensional geometry were obtained in key areas through geophysical models, integrating the geophysical characteristics with local rock-property measurements. These geophysical data sets contributed to new knowledge and interpretations in three related research fields: location and nature of Rae Craton's boundaries within the western Churchill Province; definition of internal Rae architecture; and identification of reactivated structures controlling gold and uranium mineralization. The new data, models, and emerging tectonic and metallogenic frameworks will serve as guides for future exploration in this remote, complex, challenging region.

Résumé : Les ensembles de données géophysiques disponibles pour la Province de Churchill occidentale ont eu une influence sur la compréhension de sa structure, de son évolution et de sa richesse en métaux. Le programme Géocartographie de l'énergie et des minéraux (GEM) (2008-2020) a permis l'acquisition et l'interprétation de nouvelles données. Des levés aéromagnétiques régionaux à haute résolution, ainsi que des levés gravimétriques et magnétotelluriques ciblés, ont été réalisés dans le cadre du programme GEM, parallèlement à des projets de cartographie géologique, afin de repérer les entités du socle rocheux se trouvant sous la couverture étendue de matériaux glaciaires et les couches à stratification horizontale des bassins sédimentaires. Nous avons obtenu des estimations quantitatives de la géométrie tridimensionnelle dans des zones clés grâce à des modèles géophysiques intégrant les caractéristiques géophysiques et les mesures des propriétés des roches de la région. Ces ensembles de données géophysiques ont contribué à l'actualisation des connaissances et des interprétations dans trois domaines de recherche connexes : l'emplacement et la nature des limites du craton de Rae dans la Province de Churchill occidentale; la définition de l'architecture interne du craton de Rae; et la détermination de structures réactivées exerçant un contrôle sur les minéralisations aurifères et uranifères. Les nouvelles données, les modèles et les cadres tectoniques et métallogéniques émergents permettront d'orienter l'exploration future dans cette région éloignée, complexe et pleine de défis.

¹Geological Survey of Canada, 601 Booth Street, Ottawa, Ontario K1A 0E8

*Corresponding author: V. Tschirhart (email: victoria.tschirhart@nrcan-rncan.gc.ca)

INTRODUCTION

Regional, publically available gravity and magnetic data sets are widely used in mineral exploration and geological mapping programs throughout the world. Lateral changes in the physical properties mapped by these methods — magnetic susceptibility and density — may be the result of different lithological, structural, metamorphic, or mineralogical characteristics, or reflect the cumulative deformation and alteration history of the crust. By incorporating additional parameters such as bedrock maps, rock physical properties, and geochronological and geochemical data sets, the geophysical interpretations can be linked to ground observations. As such, regional geophysical data sets are valuable in remote locations where field costs are high, glacial overburden may be extensive, and detailed ground-truthing may not be possible. Fortunately, key reference localities can be established to calibrate geophysical responses with geological observations in order to extrapolate interpretations over broad areas. Airborne geophysical surveys are a particularly cost-effective means of covering vast tracts of land with systematic data sets. Furthermore, where used with multiple geoscience observations, regional geophysical data sets help answer fundamental questions about the tectonic framework, lithology, and three-dimensional (3-D) structure of the crust (e.g. Cook et al., 2012).

Prior to initiation of the Geo-mapping for Energy and Minerals (GEM) program, many parts of the northern Canadian Shield, in particular the western Churchill Province, comprising the Rae and Hearne cratons and Chesterfield Block (Fig. 1), were underexplored as a result of inaccessibility and coarse geoscience information. Existing potential field data sets included regional ground gravity stations that resolved features more than 25 km, and sparse high-resolution gravity transects. Aeromagnetic coverage acquired prior to 1980 comprised predominantly 805 m spaced (0.5 mile) lines. Such low-resolution data made all but the most rudimentary interpretations tenuous. Bedrock in northern Canada is largely obscured by glacial overburden, making aeromagnetic maps an essential tool for geological mapping and mineral exploration. To generate new knowledge, assess the resource potential of the landmass, and to support bedrock mapping programs under GEM, the Geological Survey of Canada (GSC) has been updating, infilling, and modernizing geophysical data sets over key regions (Fig. 2). This initiative included the acquisition of 24 airborne geophysical surveys (Table 1) over the areas included in this synthesis volume, a series of ground gravity surveys across key geological transects (Thomas, 2012; Tschirhart et al., 2013a, b, d, 2015, 2016, 2017), and several magnetotelluric surveys (Spratt et al., 2011, 2012a, 2013a, b, 2014; Roberts et al., 2015). For interpretations and surveys on parts of the western Churchill province not discussed herein (i.e. on Baffin Island), the reader is directed to the references in Table 1.

This contribution summarizes select integrated interpretations, potential-field geophysical innovations, and modelling products generated for parts of the Rae Craton, Hearne Craton, and Chesterfield Block produced under the GEM-1 and GEM-2 programs until early 2020. The authors first introduce the key areas of interest and provide an overview of the geophysical activities in these regions completed under GEM. This is followed by a discussion of the regional implications. By comparing distinct, but comprehensive integrated interpretations, the authors highlight regional-scale linkages to better understand the 3-D crustal structure and mineral endowment of this remote region.

REGIONAL GEOLOGICAL SETTING

The Canadian Shield region north of 60°N encompasses the 3.5–2.5 Ga Rae and 3.0–2.65 Ga Hearne cratons, comprising the western Churchill province, the 4.0–2.5 Ga Slave Craton, parts of the northern Superior Craton, and younger Paleoproterozoic orogens that welded them (Hoffman, 1988; Wheeler et al., 1996; Fig. 1). The authors herein summarize the prime interest, the Rae Craton; for summaries of the Hearne and Slave craton geology, the reader is referred respectively to Davis et al. (2004), Hanmer et al. (2004), and Helmstaedt and Pehrsson (2012). A summary of post-1.6 Ga mafic magmatic events in the northern Canadian Shield can be found in Buchan and Ernst (this volume).

The Rae Craton, within which the present authors include the Chesterfield Block (Berman et al., 2007), underlies most of the study region and extends from beneath Phanerozoic cover in Saskatchewan and Alberta through mainland Nunavut, Northwest Territories, and central Baffin Island (Fig. 1; Berman et al., 2005). It predominantly comprises Meso- to Neoproterozoic plutonic and volcano-sedimentary rocks, including a widespread magmatic suite, the 2.62–2.58 Ga Snow Island Suite (Peterson et al., 2015a, this volume). The subsequent reworking of the Rae Craton is complex (Berman, 2010), involving five major tectono-metamorphic events: the 2.56–2.52 Ga MacQuoid Orogeny which affected the Committee Bay and Chesterfield blocks (Davis et al., 2006); the 2.50–2.35 Ga Arrowsmith Orogeny which reworked the western Rae Craton margin from Saskatchewan to Baffin Island (Berman et al., 2013a); the 2.0–1.92 Ga Taltson-Thelon Orogeny, which involved accretion of the Slave and Buffalo Head terranes to the west (Chacko et al., 2000; Ross, 2002; Berman et al., 2016; Whalen et al., 2018); the 1.92–1.88 Ga Snowbird Orogeny, which accreted the Hearne Craton to the east (Berman et al., 2007; Thiessen et al. 2018), and variable effects of the widespread 1.87–1.80 Ga Trans-Hudson Orogeny (Pehrsson et al., 2013; Regis et al., 2021). An extensive Paleoproterozoic cover sequence, deposited ca. 2.29–1.88 Ga, overlies the crystalline basement (Rainbird et al., 2010). The component Amer, Ketyet River, Montresor, and Chantrey groups formed part of a broad, epicratonic sedimentary system that extended to the Piling and Penrhyn groups of the northeastern Rae

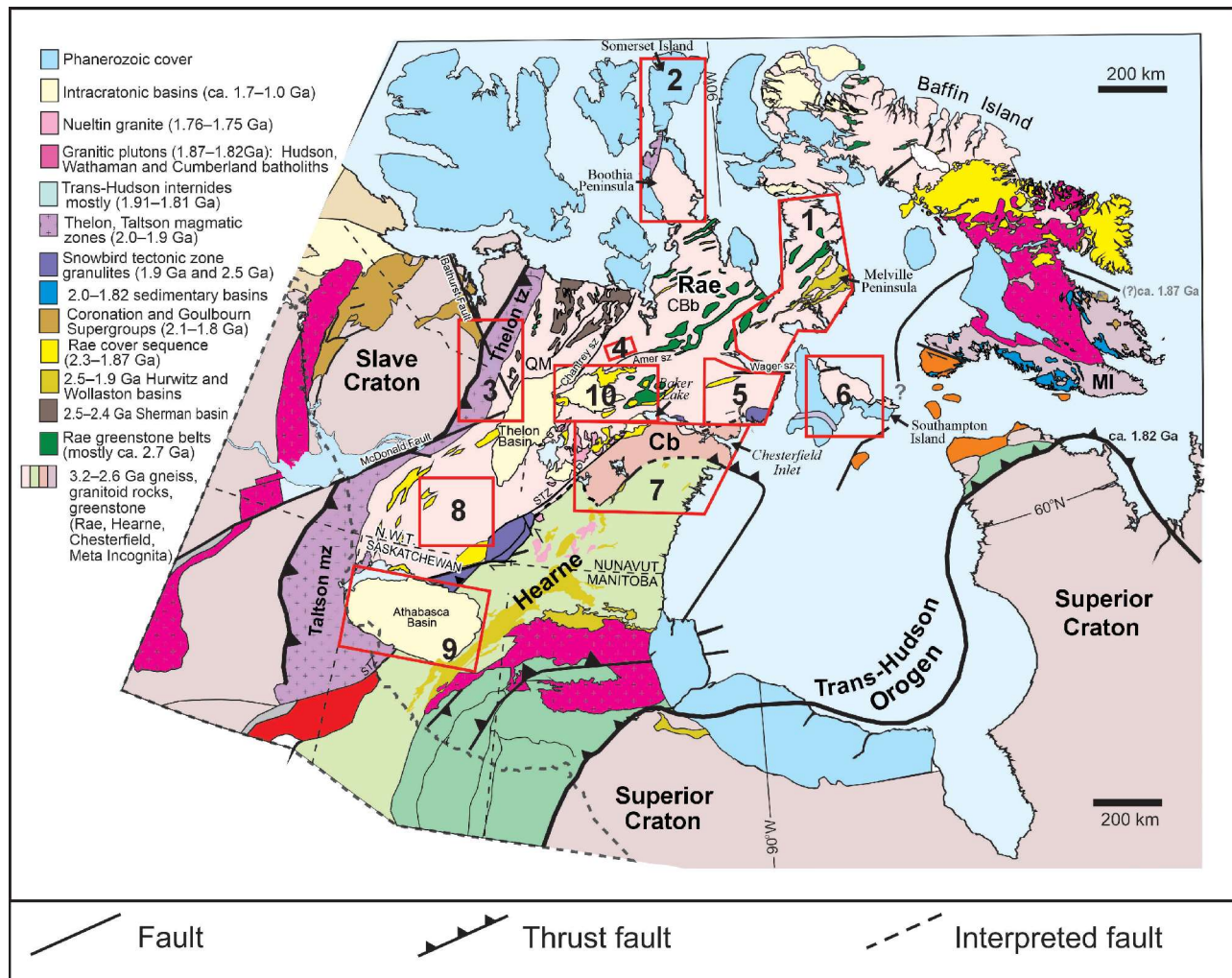


Figure 1. Simplified geological map of the western Churchill Province and surrounding crustal blocks, *modified from Berman et al. (2005)*. Areas discussed in text shown by red boxes: 1 = Melville Peninsula; 2 = Boothia Peninsula and Somerset Island; 3 = Thelon tectonic zone; 4 = Montresor Belt; 5 = Tehery Lake and Wager Bay; 6 = Southampton Island; 7 = Chesterfield Inlet; 8 = south Rae Craton; 9 = Athabasca Basin; 10 = Thelon Basin. Abbreviations: Amer sz = Amer shear zone; Chantrey sz = Chantrey shear zone; Cb = Chesterfield Block; CBb = Committee Bay Block; MI = Meta Incognita microcontinent; QM = Queen Maud Block; STZ = Snowbird tectonic zone; Taltson mz = Taltson magmatic zone; Thelon tz = Thelon tectonic zone; Wager sz = Wager shear zone. Note geology southwest of dashed line is covered by the Phanerozoic Western Canada Sedimentary Basin.

Craton, where an incipient ocean basin may have formed (Wodicka et al., 2014; Percival et al., 2017). Owing to effects of the Trans-Hudson Orogeny, only remnants of the Rae cover sequence are preserved in elongate northeast-trending, synformal belts.

The Chesterfield Block comprises 2.75–2.64 Ga back arc–like supracrustal belts (Sandeman et al., 2006; Acosta-Góngora et al., 2018) and collided with the Rae Craton at or prior to 2.6 Ga (Berman et al., 2007). Its southern boundary may be demarcated by the Tyrrell shear zone, and the ca. 1.8 Ga Happy Lake and Panartoq Points shear zones (Pehrsson, this volume), which thrust the domain over the Hearne Craton. The cryptic ca. 1.90 Ga Snowbird tectonic zone (Berman et al., 2007) bounds the Rae Craton to the

east, separating Rae Craton and Chesterfield Block from the Hearne Craton, and is excised by the younger Happy Lake and Panartoq structures.

Two major Paleoproterozoic magmatic suites were intruded into the Rae Craton at the end of, and following, the Trans-Hudson Orogeny. The 1.85–1.80 Ga Hudson granite suite (van Breemen et al., 2005) was emplaced late-syntectonically and has been interpreted as the product of intracrustal melting during thickening (Peterson et al., 2002). The 1.77–1.73 Ga Kivalliq igneous suite, including the Nueltin rapikivi granite, mafic dykes, and bimodal volcanic rocks within the Wharton Group, extend from Somerset Island to southern Saskatchewan (Hayward et al., 2013; Peterson et al., 2015c).

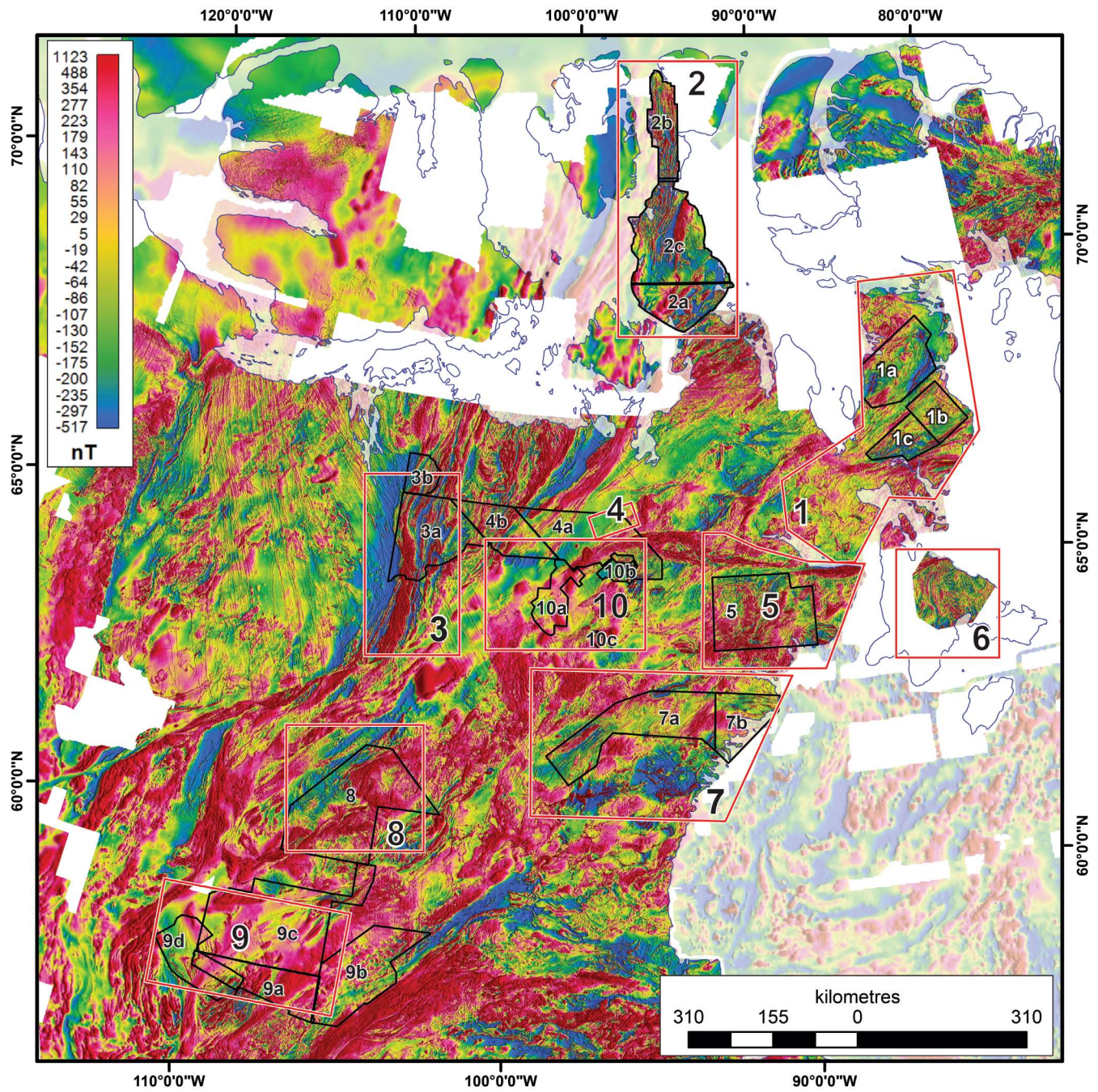


Figure 2. Residual total-field map. Project areas discussed in text outlined by red boxes and labelled as in Figure 1. Black boxes and white labels show GEM-1 and GEM-2 airborne survey locations discussed in the text from Table 1.

Table 1. Aeromagnetic surveys in the western Churchill Province flown under GEM.

Label	Program	Survey name	Data	Year	Spacing (m)	Project	Publications
1a	GEM-1	Sarcpa Lake	Mag	2009	400	Melville Peninsula	Corrigan et al., 2013; Spratt et al., 2013a, b; LaFlamme et al., 2014
1b	GEM-1	Miertsching Lake East	Mag, Rad	2009	400	Melville Peninsula	Corrigan et al., 2013; Spratt et al., 2013a, b; LaFlamme et al., 2014
1c	GEM-1	Miertsching Lake West	Mag, Rad	2009	400	Melville Peninsula	Corrigan et al., 2013; Spratt et al., 2013a, b; LaFlamme et al., 2014
2a	GEM-2	Northern Boothia Peninsula	Mag	2013	400	Boothia	Sanborn-Barrie et al., 2018
2b	GEM-2	Somerset Island	Mag	2014	400	Boothia	Sanborn-Barrie et al., 2018
2c	GEM-2	Northern Boothia Peninsula II	Mag	2016	400	Boothia	Sanborn-Barrie et al., 2018
3a	GEM-2	Duggan Lake I and II	Mag	2014	400	Chantrey-Thelon	Roberts et al., 2015; Berman et al., 2018; Ma, 2018
3b	GEM-2	Overby-Duggan	Mag	2017	400	Chantrey-Thelon	Roberts et al., 2015; Berman et al., 2018; Ma, 2018
4a	GEM-2	Garry Lake	Mag	2012	400	Chantrey-Thelon	Percival et al., 2015; Tschirhart et al., 2015; Percival and Tschirhart, 2017
4b	GEM-2	Pelly Lake	Mag	2012	400	Chantrey-Thelon	Roberts et al., 2015; Berman et al., 2018; Ma, 2018
5	GEM-2	Tehery Lake	Mag	2012	400	Tehery-Wager	Wodicka et al., 2016, 2017; Tschirhart et al., 2016
7a	GEM-1	Chesterfield Inlet, block AB	Mag	2009	400	Chesterfield	Pehrsson et al., 2014a, b
7b	GEM-1	Chesterfield Inlet, block C	Mag	2009	400	Chesterfield	Pehrsson et al., 2014a, b
8	GEM-2	NTGO-GSC South Rae Craton	Mag	2012	400	South Rae	Percival et al., 2016; Jamison et al., 2017; Martel et al., 2018; Mowbray and Pehrsson, 2019
9a	GEM-1	Southern Athabasca Basin	Mag, Rad	2008	400	Athabasca	Card et al., 2010
9b	GEM-1	Eastern Athabasca Basin	Mag, Rad	2009	400	Athabasca	Card et al., 2010
9c	GEM-1	N.W. Athabasca Basin	Mag, Rad	2010	400	Athabasca	Card et al., 2010
9d	TGI-5	Marguerite River	Mag	2017	400	Athabasca	Potter et al., 2020; Tschirhart et al., 2021
10a	GEM-1	N.E. Thelon Basin area 1-2-3	Mag, Rad	2009	400	Northeast Thelon	Calhoun et al., 2014; Hayward et al., 2013; Tschirhart et al., 2011a, 2013a, b, c, d, 2014, 2017; Tschirhart, 2014; Peterson et al., 2015a, b, c, this volume; Jefferson et al., 2015; this volume
10b	GEM-1	N.E. Thelon Basin area 6	Mag, Rad	2009	400	Northeast Thelon	Calhoun et al., 2014; Hayward et al., 2013; Tschirhart et al., 2011a, 2013a, b, c, d, 2014, 2017; Tschirhart, 2014; Peterson et al., 2015a, b, c, this volume; Jefferson et al., 2015; this volume
10c	GEM-1	N.E. Thelon Basin area 5	Mag, Rad	2009	400	Northeast Thelon	Calhoun et al., 2014; Hayward et al., 2013; Tschirhart et al., 2011a, 2013a, b, c, d, 2014, 2017; Tschirhart, 2014; Peterson et al., 2015a, b, c, this volume; Jefferson et al., 2015; this volume
	GEM-1	NTGO-GSC - Minto Inlier	Mag, Rad	2010	400	Victoria Island	
	GEM-1	NTGO-GSC - N. Great Bear Magmatic Zone	Mag, Rad	2009	400	Great Bear	Hayward et al., 2013; Hayward et al., 2014; Enkin et al., 2016; Hayward et al., 2016
	GEM-1	Great Island - Seal River	Mag, Rad	2008	400	Great Island	Anderson et al., 2009, 2010
	GEM-1	Cumberland Peninsula A	Mag	2008	400	Baffin Island	*
	GEM-1	Cumberland Peninsula B	Mag	2008	400	Baffin Island	*
	GEM-2	Amittok Lake	Mag	2015	400	Baffin Island	*
	GEM-2	McKeand River	Mag	2015	400	Baffin Island	*

*Baffin publications summarized in Dafoe and Bingham-Koslowski (2022)

Mag = magnetics, Rad = radiometrics

Following Trans-Hudson orogenesis and regional exhumation and cooling (Kellett et al., 2020), older Archean basement and Paleoproterozoic cover of the western Churchill Province were overlain by the Dubawnt (Rainbird et al., 2003) and Athabasca supergroups (Ramaekers et al., 2007), which occur in intracontinental basins. The Dubawnt Supergroup comprises three unconformity-bounded, largely clastic sequences: the 1840–1785 Ma Baker Lake, 1780–1750 Ma Wharton, and 1700–1500 Ma Barrenslund groups. The Barrenslund Group is exposed in Thelon Basin (Fig. 1) and includes the Thelon, Kuungmi, and Lookout Point formations. The Dubawnt Supergroup is broadly stratigraphically and tectonically similar to the 1760–1500 Ma Athabasca Supergroup (Ramaekers et al., 2007) of the Athabasca Basin in Saskatchewan, host to the world's highest grade, large tonnage uranium deposits (Fig. 1).

GEOPHYSICAL DATA SETS

The interpretation and modelling process was based on multiple geophysical data sets described below. The regional aeromagnetic data were acquired as part of Canada's National Aeromagnetic Surveying program that began in 1947, which included systematic surveys over Canada along 805 m (0.5 mile) spaced lines acquired at a nominal terrain clearance of about 300 m. These data were gridded to 200 m using minimum curvature (Fig. 2). More modern surveys acquired during GEM-1 and -2 (Table 1) were, for the most part, flown along 400 m spaced lines (Table 1).

From 1944 to present, the Earth Physics Branch (now part of the GSC), Surveys and Mapping Branch and the GSC have been acquiring ground gravity stations at an average spacing of 10–15 km. The ground gravity data were corrected for latitude, instrument drift, elevation, and Earth's tides, followed by application of Free Air and Bouguer corrections. The data were reduced to a Bouguer slab density of 2.67 g/cm³ and gridded to 2 km using minimum curvature. The isostatic residual was removed using the methodology defined in Jobin et al. (2017) (Fig. 3). In addition, during GEM, a number of detailed surveys were conducted and interpreted across key transects (Thomas, 2012; Tschirhart et al., 2013a, b, d, 2015, 2017; Tschirhart, 2014) to provide information on the geometry of shallow crustal features. Individual transects and data reduction are described in the aforementioned publications. Many of the archival gravity stations include density information (available through the Canadian Geoscience Data Repository). Rock properties provide the linkage between geological and geophysical information. To constrain the interpretations and modelling products produced under GEM, additional magnetic susceptibility and density data were acquired (Thomas, 2012; Tschirhart, 2014; Enkin et al., 2016; Tschirhart et al., 2017; Enkin, 2018) on archival and new samples. These data are available through the Canadian Geoscience Data Repository (<http://gdr.agg.nrcan.gc.ca/gdrdap/dap/search-eng.php>) or in Enkin (2018).

Long period and broadband magnetotelluric (MT) stations were established along several transects within the study area (Fig. 3). The acquisition, processing, and preliminary results are outlined in Spratt et al. (2011, 2012a, b, 2013a, b) and Roberts et al. (2015).

Geophysical-geological interpretation: an example from the northeast Thelon Basin

Despite the reconnaissance nature of regional potential field data sets, meaningful unique geological solutions can be generated from them. An example of the integration of geological and geophysical information is presented for the northeast Thelon Basin. Stratigraphically and tectonically similar to the Athabasca Basin, the northeast Thelon Basin (Fig. 1) is similarly prospective for unconformity-related uranium deposits in and around the Kiggavik camp (Fig. 4) and was the subject of extensive geological and geophysical studies under the GEM Uranium project (*see* overview by Jefferson et al., this volume). Following compilation, leveling, and stitching of nine industry surveys (Tschirhart et al., 2011), three airborne magnetic and radiometric surveys were flown to infill the gaps between the high-resolution industry surveys (Table 1) provided by a collaborative consortium that shared their airborne geophysical data (Jefferson et al., 2011). This resulted in an extensive compilation of high-resolution and/or modern airborne coverage over most of the northeast Thelon Basin (Fig. 2, 4). The new compilation, coupled with bedrock mapping, ground gravity transects, and rock property measurements, formed the backbone of numerous geophysical interpretations in the region. The initial studies (Tschirhart et al., 2013a, b, d) were conducted outside the northeast Thelon Basin margins, with the structural style and geophysical characteristics of the rock packages providing the information for the later interpretations of the sub-Thelon basement (Tschirhart et al., 2014, 2017; Tschirhart and Pehrsson, 2016).

Tschirhart et al. (2013d) demonstrated the value of partially constrained inversions in the northeastern Amer synform (Fig. 4, area 1; Fig. 5a), a broad fold and thrust belt stretching over 100 km and underlying the central axis of the northeast Thelon Basin. The belt is of interest as stratabound uranium occurrences are associated with linear magnetic markers in the Amer group and conductive graphitic units also have the potential to host deposits below the Thelon Formation cover (Davidson and Gandhi, 1989). Near the northeastern end of the Amer synform, sparse exposure resulted in limited structural data and speculative geological interpretations with multiple possible geometric configurations (Calhoun et al., 2014). Distinct concentric oval magnetic anomalies in this area form an elongate, aeromagnetic bulls-eye, interpreted as a canoe-shaped synform. Follow-up modelling generated two-dimensional geometries of synthetic inverse models that mimic the isolated anomaly within the bulls-eye. In the absence of geological controls, the 2-D models were incorporated into a reference model,

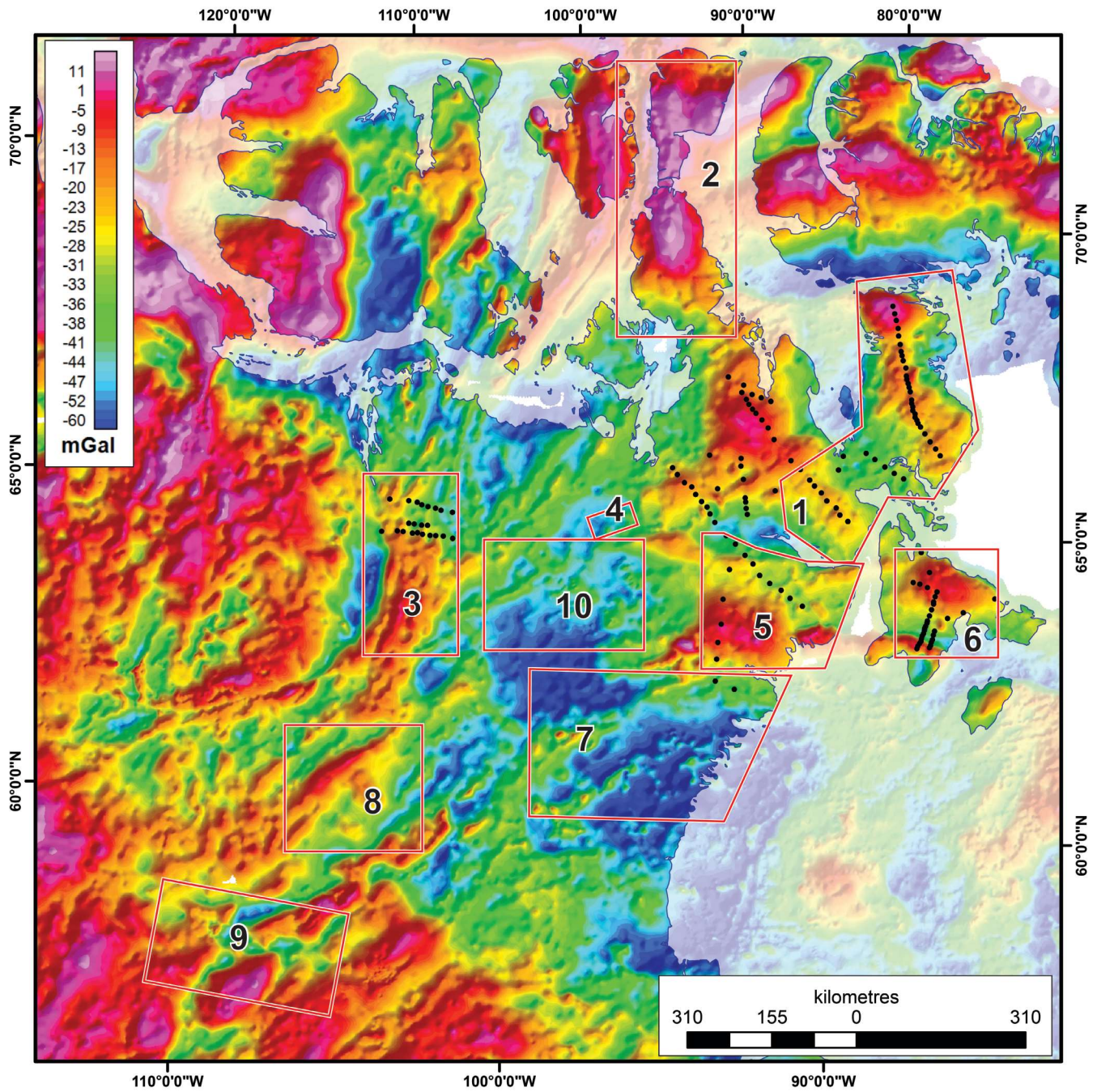


Figure 3. Isostatic residual Bouguer gravity map. Project areas discussed in text outlined by red boxes and labelled as in Figure 1. GEM MT stations plotted as black dots.

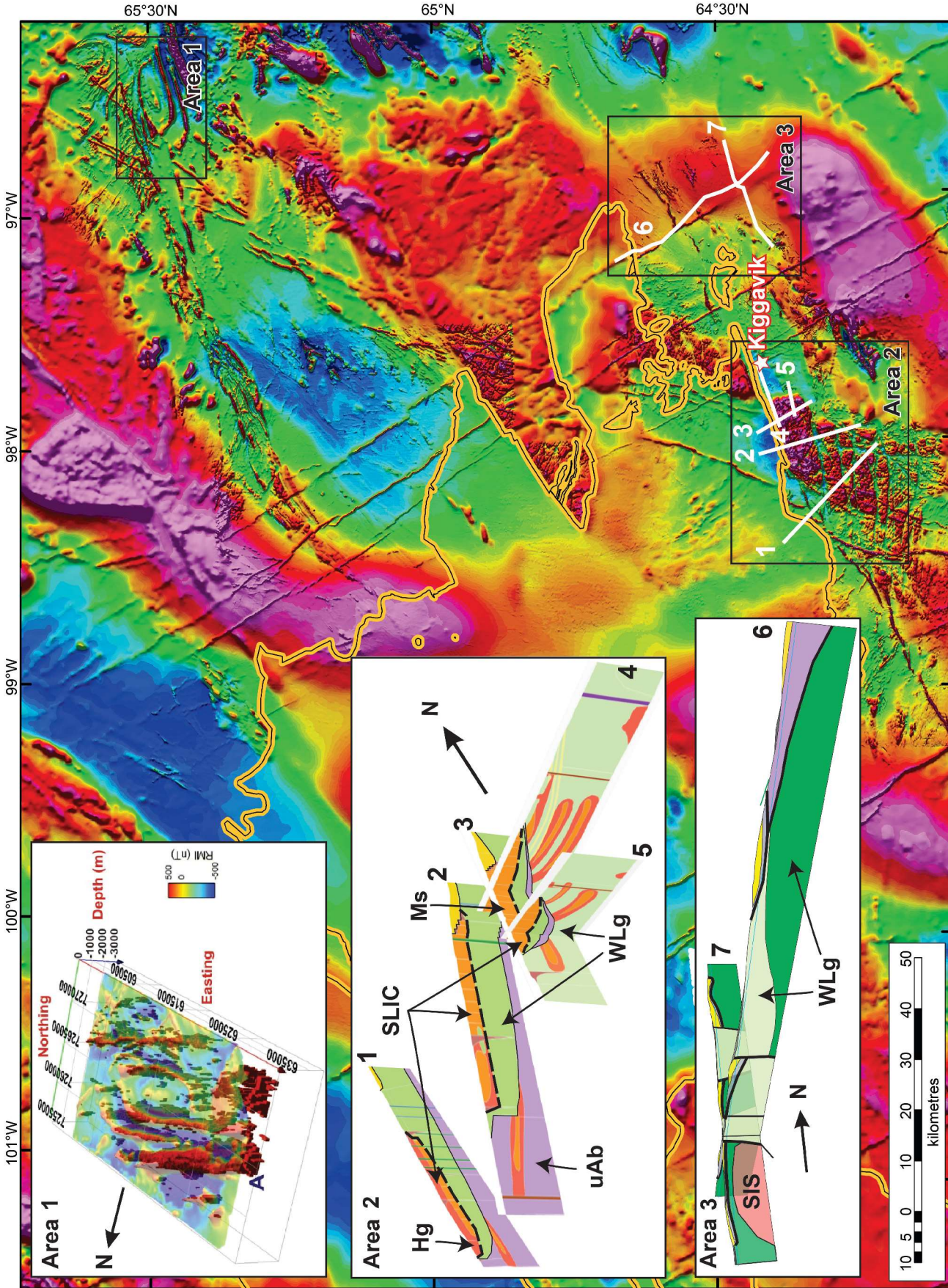


Figure 4. Merged residual total-field map of the northeast Thelon Basin as outlined in orange. Areas discussed in text and visualized in the panels are outlined by black boxes; gravity transects are denoted by white lines and labelled as in the panels. The 2-D and 3-D modelling results are after Tschirhart et al., 2013d. In area 2 the dashed line delineates the thrust surface of the Shultz Lake intrusive complex; Tschirhart et al., 2013b; area 3 is from Tschirhart et al., 2013a. Hg = Hudson granite; Ms = Martell syenite; SIS = Snow Island Suite; SLIC = Shultz Lake intrusive complex; WLg = Woodburn Lake group; uAb = undifferentiated Archean basement.

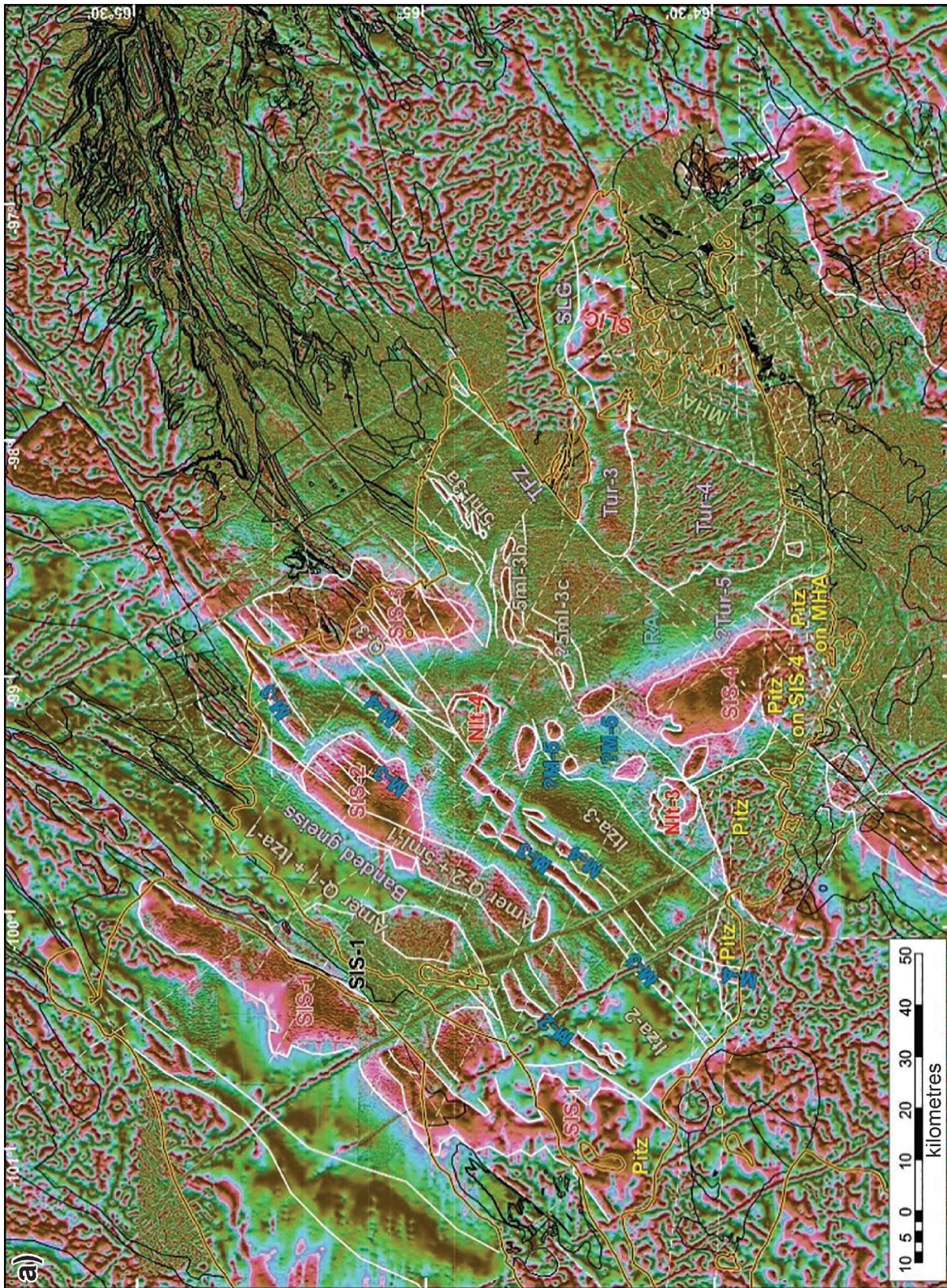


Figure 5. a) Enhanced image of the northeast Thelon Basin and surrounding region using tilt derivative displayed at 60% transparency over greyscale Theta. The previously mapped geological contacts and labels outside the Thelon Basin are in black (after Jefferson et al., 2015). Outline of Thelon Formation is plotted as thin black line on thick orange line. Select faults are plotted as dashed white lines. Newly mapped geophysical units outlined in white are labelled as follows: 5ml = Five Mile Lake formation; Itza = Itza lake formation; Amer Q = Ayagaq lake formation; Nlt = Nueltin granite; MHA = Marjorie Hills Assemblage; SIS = Snow Island Suite; M = mafic intrusive; SLIC = Shultz Lake intrusive complex; TFZ = Turqavik fault zone; Tur = Turqavik; RA = Rumble Assemblage; SLG = Shultz Lake graben.



Figure 5. b) Remote predictive map of the geology at the unconformity surface beneath the Thelon Basin. Surrounding geology is after Jefferson et al. (2015). Outline of Thelon Formation is shown by thin black line on thick orange line. White lines are selected reactivated faults, yellow lines are reactivated faults within uranium-prospective basement units, and red lines are intersecting reactivated faults in uranium-prospective basement units. Figure from Tschirhart et al. (2017). See Fig. 5c for legend.

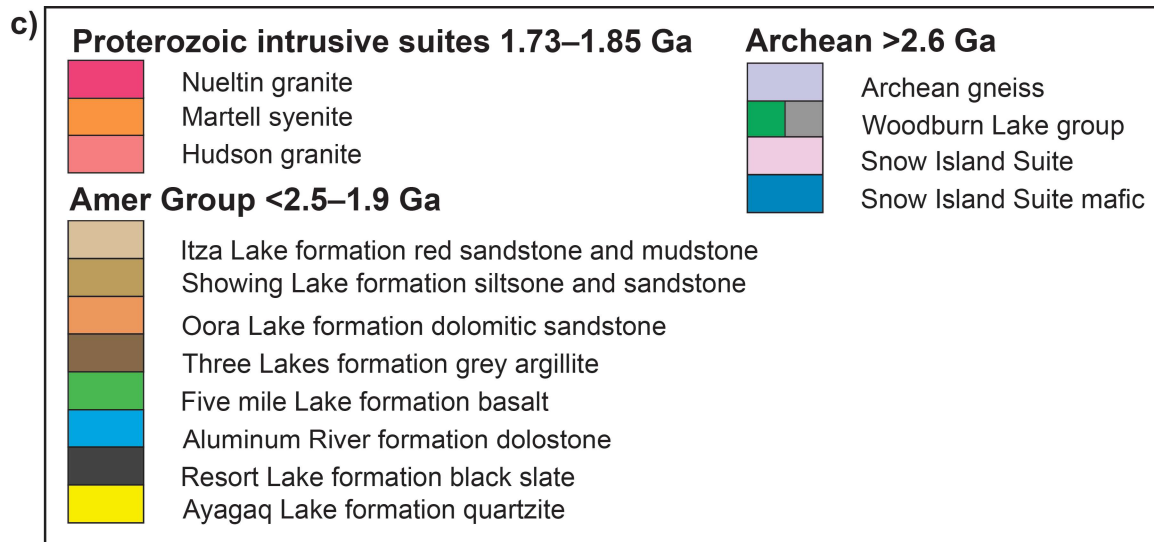


Figure 5. c) Legend for Figure 5b.

which forms the input in the inversion algorithm (Tschirhart et al., 2013d). A major innovation of Tschirhart et al. (2013d) was the integration of geophysically derived constraints that maintain structure at depth and verify the concept of a partially constrained inversion (Fig. 4, area 1; Fig. 5a).

The Schultz Lake intrusive complex unconformably underlies the Barrenland Group in the northeast Thelon Basin. To constrain its geometry and framework (Fig. 4, area 2) with respect to nearby ore-hosting metasedimentary rocks, Tschirhart et al. (2013b) used joint gravity and magnetic forward modelling that incorporated magnetic susceptibility, density, and geological mapping constraints. The Schultz Lake intrusive complex comprises 1.83 Ga Hudson granite and Martell syenite and is expressed on the aeromagnetic map as an abrupt high, crosscut by intersecting demagnetized fault zones, some of which host uranium deposits in supracrustal enclaves (Hunter et al., 2012). Through an iterative process with project geologists, the data were used to test three hypotheses regarding the shape of the complex. The best-fit model indicates a 200–300 m thick, gently west-dipping, sheet-like body that intruded and encloses highly metamorphosed Neoproterozoic supracrustal rocks of the Woodburn Lake group (Fig. 4, area 2). The composite sheet was modelled as a thrust package structurally emplaced over weakly metamorphosed Neoproterozoic supracrustal rocks, themselves cut by high-level equivalents of Hudson granite. The timing of the thrust postdates intrusion of the Hudson granite bodies in both panels.

South of the Schultz Lake intrusive complex and Thelon Basin, Tschirhart et al. (2013a) used ground gravity, aeromagnetic, electromagnetic, and remote-sensing data sets to constrain the subsurface geological contacts of a basement klippe. Inversions of the magnetic data defined several dyke arrays, and forward modelling defined a deep-seated intrusion interpreted to belong to the 2.6 Ga Snow Island

Suite (SIS on Fig. 4, area 3; Peterson et al., 2015a, b, c). The forward modelling brought to attention the nature and geometry of broad positive magnetic anomalies associated with Snow Island Suite plutons, some of the contacts of which are exposed, but others deeply buried. Tschirhart et al. (2013a) presented the first thickness estimate of the pluton. Another widespread manifestation of the Snow Island Suite is as tectonically emplaced, nonmagnetic sheets that structurally overlie Neoproterozoic supracrustal rocks as modelled by Thomas (2012) (Pehrsson et al., 2013) and form the immediate substrate for Paleoproterozoic strata such as the Amer, Ketyet River, and Montresor belts (Jefferson et al., this volume).

Closer to the Thelon Basin margins, the location and timing of faults that controlled the development of the basin were explored using a new approach based on the Blakely and Simpson (1986) algorithm as implemented in the geophysical software Geosoft Oasis montaj™. For every magnetic peak, the algorithm calculates a strike and dip direction based on the trend of adjacent maxima and source geometry, respectively. Because the dip direction is a function of the downslope gradient of the magnetic source body, it is always perpendicular to the strike and pointing away from the magnetic source body. Gridding the dip direction resulted in the definition of blocks of similar magnetic-lithological character separated by magnetic lineaments marking fault offsets. Used in corroboration with a digital elevation model, these lineaments were matched with surface geological features to deduce fault timing and reactivation (Tschirhart et al., 2013c).

The interpreted structures from Tschirhart et al. (2013c) served as input for modelling the basal architecture of the northeast Thelon Basin, as described in Tschirhart et al. (2014). Because the sedimentary sequences of the Thelon Basin are nonmagnetic, any anomalies within the basin margins are attributed to the underlying basement rocks.

Limited drillhole intersections and sparse seismic refraction data provide the only documented unconformity depths (Overton, 1979), so Tschirhart et al. (2014) utilized a combination of automatic and inverse source depth routines to compute depth estimates on idealized source bodies corresponding to known basement units. By constructing numerous intersecting profiles that incorporated all known and calculated depth estimates, a pseudo-3-D model of the basin was constructed. The model illustrated a highly variable basement topography, including northwest-trending horst and graben structures and east-northeast- to northeast-trending faults, similar to the uranium-hosting Judge Sisson Fault. The deepest parts of the basin are buried by approximately 950 m (>2100 m in Tschirhart and Pehrsson, 2016) of siliciclastic strata. The northwest-southeast fault system, termed the Mackenzie fault array by Tschirhart et al. (2014) (and subsequently, the Bathurst fault array in Tschirhart and Pehrsson (2016) and Tschirhart et al. (2017)), appears to be the dominant set of structures controlling the geometry (and depth) of the basin. Forward modelling of gravity and magnetic data in the southwest Thelon Basin (Tschirhart and Pehrsson, 2016) noted a similar association with northwest-trending structures that primarily controlled basin geometry and the locations of fault-bounded depocenters.

The 3-D geophysical interpretations (including forward and inverse modelling products) further allowed for discrimination of the geometry of buried supracrustal packages such as the Amer belt (Tschirhart et al., 2017). The calibration of magnetic anomalies with rock packages described above allowed for the construction of a map of buried geology predicted by geophysical data (Fig. 4, 5a) in the northeast Thelon Basin (Tschirhart et al., 2017) that served as a training area for additional studies in the southwestern part of the basin (Tschirhart and Pehrsson, 2016). When combined with the pseudo-3-D model, the interpretive products identified areas most prospective for unconformity-related uranium mineralization to focus future exploration efforts (Tschirhart and Pehrsson, 2016; Tschirhart et al., 2017). Prospective features include intersecting reactivated faults, fertile basement units, and minimal burial depths, such as the buried intersecting faults northeast of the Schultz Lake intrusive complex and in the central Thelon over interpreted Woodburn Lake group (Fig. 5a). The results of the broader GEM Uranium project were enabled by integrating multiple geoscientific data sets (Jefferson et al., this volume). Furthermore, the integrated use of geophysics and geology optimized time in the field.

PROJECT AREAS

In the following sections, results from selected regions investigated in the western Churchill Province until early 2020 under GEM are briefly reviewed.

Melville Peninsula

Located in the eastern part of the region covered in this synthesis, Melville Peninsula of the north Rae Craton displays tectonic and geological settings prospective for precious- and base-metal mineralization and diamondiferous kimberlite (area 1 on Fig. 1, 2, 3; Corrigan et al., 2013; Spratt et al., 2013a). Aeromagnetic surveys and three subsequent field seasons of geological mapping resulted in updated geological maps (Table 1; Corrigan et al., 2013), in which Melville Peninsula was divided into four distinct lithotectonic domains: the Archean Northern Granulite, Prince Albert and Repulse Bay blocks, and overlying Penrhyn Group of Paleoproterozoic age. These domains predominantly comprise reworked Archean orthogneiss, Archean and Paleoproterozoic supracrustal belts (Prince Albert Group and Penrhyn Group, respectively), and mafic to felsic plutonic rocks. An abrupt Bouguer gravity gradient in the regional data marks the domain boundary between the Northern Granulite Block, a prominent Bouguer gravity high, and the Prince Albert Block (dashed line separating NGb and PAb on Fig. 6a). Like much of the Rae Craton, the dominant magnetic fabric strikes northeast, likely reflecting Paleoproterozoic reworking during the Trans-Hudson Orogeny (Fig. 2; Berman et al., 2005, 2015; Corrigan et al., 2013).

The Prince Albert and Repulse Bay blocks are separated by high-strain rocks of the Lyon Inlet boundary zone (LIBZ on Fig. 6a, b). On the aeromagnetic map, the boundary zone is the northern limit of curvilinear, east-northeast-striking positive magnetic anomalies (not shown here, but Fig. 2b in LaFlamme et al., 2014). This zone coincides with a near-vertical, low-resistivity magnetotelluric anomaly (Spratt et al. 2013a). Spratt et al. (2013a, 2014) also noted a change in the mantle structure or composition (*see also* Snyder et al., 2015; Liu et al., 2016) between these two blocks, coinciding with the surface trace. This boundary has alternatively been interpreted as a Neoproterozoic suture zone (Skulski et al., 2014), an exhumation-related structure accommodating uplift of the deep-crustal Repulse Bay Block (LaFlamme et al., 2014, 2017), or an older feature reactivated in the Proterozoic (Peterson et al., this volume).

Boothia Peninsula and Somerset Island

The Boothia Peninsula–Somerset Island region is located in the northwestern part of the synthesis region (Table 1; area 2 on Fig. 1, 2, 3). Magnetic lows and subdued responses on the aeromagnetic map are predominantly correlated with nonmagnetic belts of metasedimentary rocks that are crosscut by curvilinear, high-amplitude magnetic highs corresponding to intermediate to mafic metaplutonic rocks (Sanborn-Barrie et al., 2018). Magnetic susceptibility measurements (H. Ugalde, unpub. data, 2018) indicate that high magnetic susceptibility values correspond to mafic intrusive

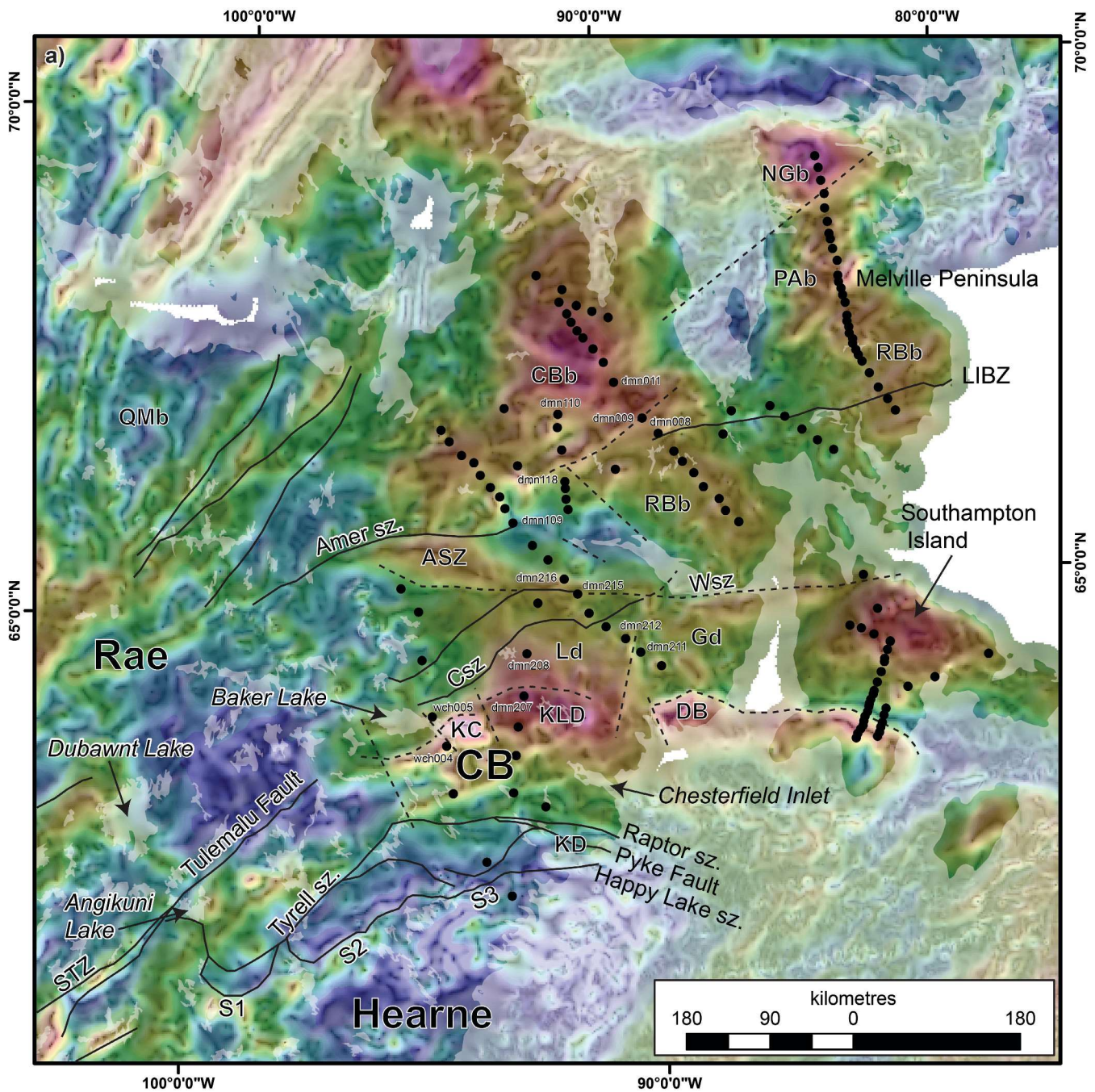


Figure 6. a) Horizontal gradient magnitude of the Bouguer gravity anomalies displayed at 50% greyscale transparency over the isostatic residual Bouguer gravity data. Solid black lines represent select major faults from Tella et al. (2007), Pehrsson et al. (2014b), and Skulski et al. (2018). Black dots are MT stations and labels, as discussed in the text. Dashed black lines represent interpreted structures and domain boundaries discussed in text. ASZ = Amer shear zone; CB = Chesterfield Block; CBb = Committee Bay Block; Csz = Chesterfield shear zone; DB = Daly Bay; Gd = Gordon domain; KC = Kramanitaur Complex; KD = Kaminuriak domain; KLD = Kummel Lake domain; Ld = Lunan domain; LIBZ = Lyon Inlet boundary zone; NGb = Northern Granulite Block; PAb = Prince Albert block; QMb = Queen Maud Block; RBb = Repulse Bay Block; STZ = Snowbird tectonic zone; sz. = shear zone; Wsz = Wager shear zone. S1, S2, S3 = possible southern limits of the Chesterfield Block (Berman et al., 2007).

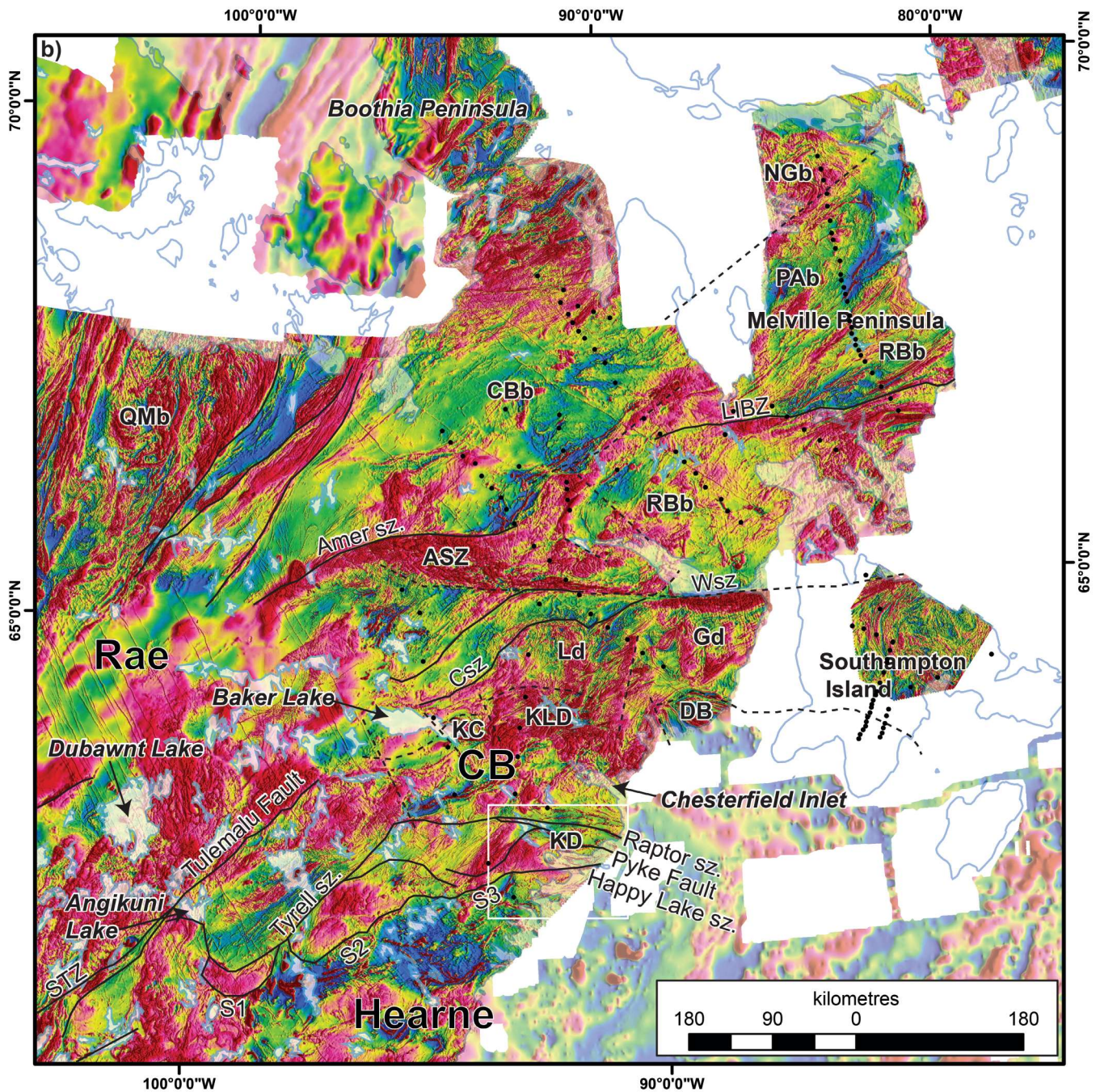


Figure 6. b) Residual total field. Solid black lines represent select major faults from Tella et al. (2007), Pehrsson et al. (2014b), and Skulski et al. (2018). Black dots are MT stations and labels, as discussed in the text. Dashed black lines represent interpreted structures and domain boundaries discussed in text. ASZ = Amer shear zone; CB = Chesterfield Block; CBb = Committee Bay Block; Csz = Chesterfield shear zone; DB = Daly Bay; Gd = Gordon domain; KC = Kramanitaur Complex; KD = Kaminuriak domain; KLD = Kummel Lake domain; Ld = Lunan domain; LIBZ = Lyon Inlet boundary zone; NGb = Northern Granulite Block; PAb = Prince Albert Block; QMb = Queen Maud Block; RBb = Repulse Bay Block; STZ = Snowbird tectonic zone; sz. = shear zone; Wsz = Wager shear zone. S1, S2, S3 = possible southern limits of the Chesterfield Block (Berman et al., 2007). White-outlined area is shown in Figure 7.

rocks, whereas felsic and intermediate intrusive rocks have similar, lower values. Polyphase deformation is widespread across the region and this is reflected in the magnetic patterns as abrupt truncations, lateral displacement, attenuation effects, and curvilinear fold interference patterns (Sanborn-Barrie et al., 2018). Boothia Peninsula is transected by the regional, southwest-striking, moderately northwest-dipping Sanagak Lake shear zone that extends at least 160 km (Sanborn-Barrie et al., 2018, 2019a).

Thelon tectonic zone

Separating the Rae Craton from the Slave Craton in the east, the Thelon tectonic zone (area 3 on Fig. 1, 2, 3) has been considered to represent either a 2.03–1.96 Ga arc prior to the Slave-Rae collision (Hoffman, 1988) or an intracratonic mountain belt formed subsequent to Slave-Rae accretion (Chacko et al., 2000; Schultz et al., 2007). Geophysically, the Thelon tectonic zone comprises a series of north- to north-northeast-trending magnetic lineaments that extend 550 km from the McDonald Fault to north of the Queen Maud Gulf (Table 1; Fig. 2, area 3; Berman et al., 2016, 2018). The detailed nature of the interaction between the Slave and Rae cratons remains elusive, and the crustal architecture poorly understood. Owing to the paucity of bedrock exposure, the aeromagnetic surveys were key in outlining high-amplitude, linear anomalies corresponding to ca. 2.0 Ga Western, Central, and Eastern plutonic belts (survey 3a on Fig. 2) of magmatic arc geochemical character (Whalen et al., 2018), as well as a nonmagnetic, ca. 1.90 Ga leucogranite belt, and the margins of the Slave and Rae cratons (Berman et al., 2018). Subtle features in the high-resolution data over the western plutonic belt outline a curvilinear anomaly corresponding to a quartz diorite to monzogranite suite that overlaps the boundary with the Slave Craton (Berman et al., 2018). The aeromagnetic data further aided the interpretation of intersecting the Thelon tectonic zone structures with those of the Bathurst fault system (Ma, 2018), which extends northeastward beneath the Thelon Basin. There, Ma (2018) documented progressive strain localization and fluid-rock interaction, which are important for mobilizing and localizing hydrothermal fluid flows (Ma, 2018; Ma et al., 2020).

Two regional magnetotelluric transects provided constraints on the geometry of the Slave-Rae boundary at depth (Roberts et al., 2015; locations shown as black dots within area 3 on Fig. 3). The 3-D inversion results suggested an east-dipping Rae-Slave boundary, consistent with Nd-Sm isotopic variations (Berman et al., 2018); however, within the crust the geometry is complex (Roberts et al., 2015; Berman et al., 2018). In the Rae Craton, the upper 10 km of the conductivity cross-section is correlative with resistive, ca. 2.0–1.90 Ga plutonic rocks, such as leucogranite. Below 10 km, the Rae Craton is underlain by highly conductive zones, interpreted to reflect either deeply buried

metasedimentary rocks or alternatively, graphite-grain boundary films developed during granulite-facies metamorphic conditions (Roberts et al., 2015). An upper crustal high-conductivity region underlying the Ellice River supracrustal belt may reflect sulphide enrichment also documented in stream sediment surveys (McCurdy et al., 2013; Berman et al., 2018). Beneath the Slave Craton, the lower crust (>20 km depths) appears to be more resistive than corresponding levels in the Rae Craton (Roberts et al., 2015). Taken together, the geophysical data indicate steep structures and complex geometry, resulting from multiple intrusive, metamorphic, and deformational events.

Montresor belt

Paleoproterozoic Montresor group metasedimentary rocks occur in a narrow syncline about 100 km north of the Amer group (area 4 on Fig. 1, 2, 3), with which they have been correlated (Rainbird et al., 2010; Percival et al., 2017). Magnetic marker horizons outline structures in the belt and are similar to those documented in the Amer group (Tschirhart et al., 2013d, 2017; Percival and Tschirhart, 2017). Elevated levels of copper, silver, and gold were identified in a hydrothermal breccia within the syncline, the first example of this mineralization style recognized in the region (Percival et al., 2015). To determine the spatial extents and subsurface geometry of the demagnetized hydrothermal breccia, Tschirhart et al. (2015) derived the apparent susceptibility from the magnetic data using an approximate method. These approximate values on the syncline limbs were scaled using sparse magnetic susceptibility measurements from outcrops. The scaled apparent susceptibility values served as constraints for magnetic forward models that illustrated the geometry of the limbs and demagnetized zones, including a narrow vertical zone extending from the surface exposure of the hydrothermal breccia. Forward modelling of the regional gravity data in Tschirhart et al. (2015) further recognized an extensional detachment (and potential metamorphic core complex) corresponding to the Amer shear zone. This study was expanded in Percival and Tschirhart (2017) in which five additional forward models were constructed across the northeastern syncline (Fig. 5 in Percival and Tschirhart, 2017). By graphically restoring the limbs of the late syncline to their pre- F_3 state, forward models revealed early (D_1) thrusts and later (D_2) extensional faults, the latter related to the late-orogenic extensional phase of the Trans-Hudson Orogeny (Percival et al., 2015, 2017; Percival and Tschirhart, 2017). Tschirhart et al. (2015) postulated that depending on timing, the extensional event that exhumed the interpreted core complex could have controlled the geometry of the deposition of the 1.85–1.50 Ga Dubawnt Supergroup, distributed in northeast-trending fault-bounded troughs, consistent with the interpretations of Hadlari and Rainbird (2011).

Tehery Lake and Wager Bay

Southwest of Melville Peninsula, the Tehery Lake–Wager Bay area (Table 1; area 5 on Fig. 1, 2, 3) is dominated by Meso- to Neoproterozoic gneissic rocks, folded Archean and Paleoproterozoic supracrustal belts, and felsic to ultramafic plutonic rocks belonging to several plutonic suites, including the ca. 2.6 Ga Snow Island, ca. 1.85–1.80 Ga Hudson, and ca. 1.83–1.82 Ga Martell suites (Steenkamp et al., 2015, 2016; Wodicka et al., 2016, 2017; Peterson et al., this volume). The Snowbird tectonic zone has been historically interpreted to transect the southern portion of the project area based on potential field anomalies that suggest highly magnetic, dense rocks (Hoffman, 1988). Bedrock mapping, combined with surficial studies, identified potential for base- and precious-metal mineralization, primarily in the Archean supracrustal rocks in the vicinity of the Chesterfield shear zone, and diamondiferous kimberlite outside previously known kimberlite fields (Steenkamp et al., 2015; Wodicka et al., 2016; McMartin et al., 2019). In addition to redefining the distribution of Archean versus Paleoproterozoic supracrustal rocks in complexly deformed regions, this work documented the style and deformation of major Paleoproterozoic structures, including the Wager Bay and Chesterfield shear zones (Tschirhart et al., 2016; Wodicka et al., 2017; Therriault et al., 2017). Furthermore, new geophysical maps (Fig. 3, 6a, b) illustrate that gravity highs in the southern Tehery Lake–Wager Bay region do not correspond to geometrically consistent structures as would be predicted for the originally defined Snowbird tectonic zone. Rather, inverse models of the regional gravity data illustrate that the granulite-facies Daly Bay and Kummel Lake domains, bordering Chesterfield Inlet and Hudson Bay, have different subsurface geometries (Wodicka et al., 2017). Whereas the ca. 1.9 Ga Daly Bay complex is carried on a steep east-dipping thrust, the Kummel Lake domain is modelled as dipping northward below amphibolite-facies gneissic rocks, resembling a metamorphic core complex. A linear structure visible on both the upward-continued magnetic data and regional gravity data, demarcates the boundary between the isotopically distinct Gordon and Lunan domains (Wodicka et al., 2017; Fig. 6a, b). On a more detailed scale, source depth routines and forward models of the modern aeromagnetic data in the Gordon domain allowed the geometry of the 2.6 Ga Borden Complex, a compositionally distinct Snow Island pluton, to be defined as sheet-like (Wodicka et al., 2017; Peterson et al., this volume).

Magnetotelluric investigations in the Tehery Lake region are described by Spratt et al. (2014). Three regional profiles indicate generally resistive upper crust and conductive lower crust, but provide relatively sparse definition of upper crustal features in the Wager–Tehery region.

Southampton Island

Southampton Island in northwestern Hudson Bay (area 6 on Fig. 1, 2, 3) is underlain predominantly by high-grade gneiss, mainly of plutonic origin with subordinate metasedimentary units, as well as sparse mafic-ultramafic intrusions (Berman et al., 2011; Sanborn-Barrie et al., 2014b). Paleozoic strata cover the southwestern part of the island. Where exposed, shield rocks are dominated by curvilinear magnetic anomalies (Fig. 2) and a positive gravity response (Fig. 3) that characterize Mesoarchean to Paleoproterozoic plutonic and supracrustal rocks that were intensely deformed together and refolded at the crustal scale. South of the Wager shear zone (Fig. 6b), Southampton Island displays a discontinuity between magnetic anomalies over the Precambrian plutonic rock-dominated basement exposed in the eastern half of the island and the region covered by Paleozoic sedimentary rocks to the southwest (Spratt et al., 2012b; Fig. 1). To image potential crustal-scale structures that explain the discontinuity, long period and broadband magnetotelluric data were collected to examine the deep lithosphere (Spratt et al., 2012b). These authors observed more complex structures in the upper crust below the Paleozoic cover, including a narrow east-trending resistive crust that they correlated with mafic granulite-facies rocks exposed in a small window in the southwest. The present authors and Spratt et al. (2014) follow Hoffman (1988) and Gordon and Heywood (1987) in correlating this discontinuity with the Daly Bay complex to the west. Strong, west-northwest-striking magnetic and gravity anomalies support this interpretation. Spratt et al. (2012b) further noted northward thickening of Rae Craton crust from about 30 km below Southampton Island to about 40 km below Melville Peninsula, consistent with tectonic models that propose southeastward underthrusting of Rae mantle beneath a wedge of Meta Incognita microcontinent exposed on southern Baffin Island (Fig. 1; Corrigan et al., 2009; Berman et al., 2013b; Snyder et al., 2013).

Chesterfield Inlet

Particularly extensive drift cover obscures complex bedrock features in the Chesterfield Inlet area (area 7 on Fig. 1, 2, 3) that nevertheless has been the focus of extensive gold exploration. Upgraded aeromagnetic coverage has facilitated geological interpretation relevant to both regional-scale Churchill architecture and mineralized structures (Table 1; Fig. 6b, 7; Pehrsson et al., 2014a). The Chesterfield Block was recognized as a tectonic entity by virtue of its distinct units (Sandeman et al., 2006; Acosta-Góngora et al., 2018), and deformation history involving accretion to the margin of the Rae Craton prior to 2.61 Ga (Berman et al., 2007). These rocks underwent additional deformation at 2.56–2.50 Ga (Davis et al., 2006) and deposition of Paleoproterozoic sedimentary and volcanic rocks (Lawley et al., 2016), prior to

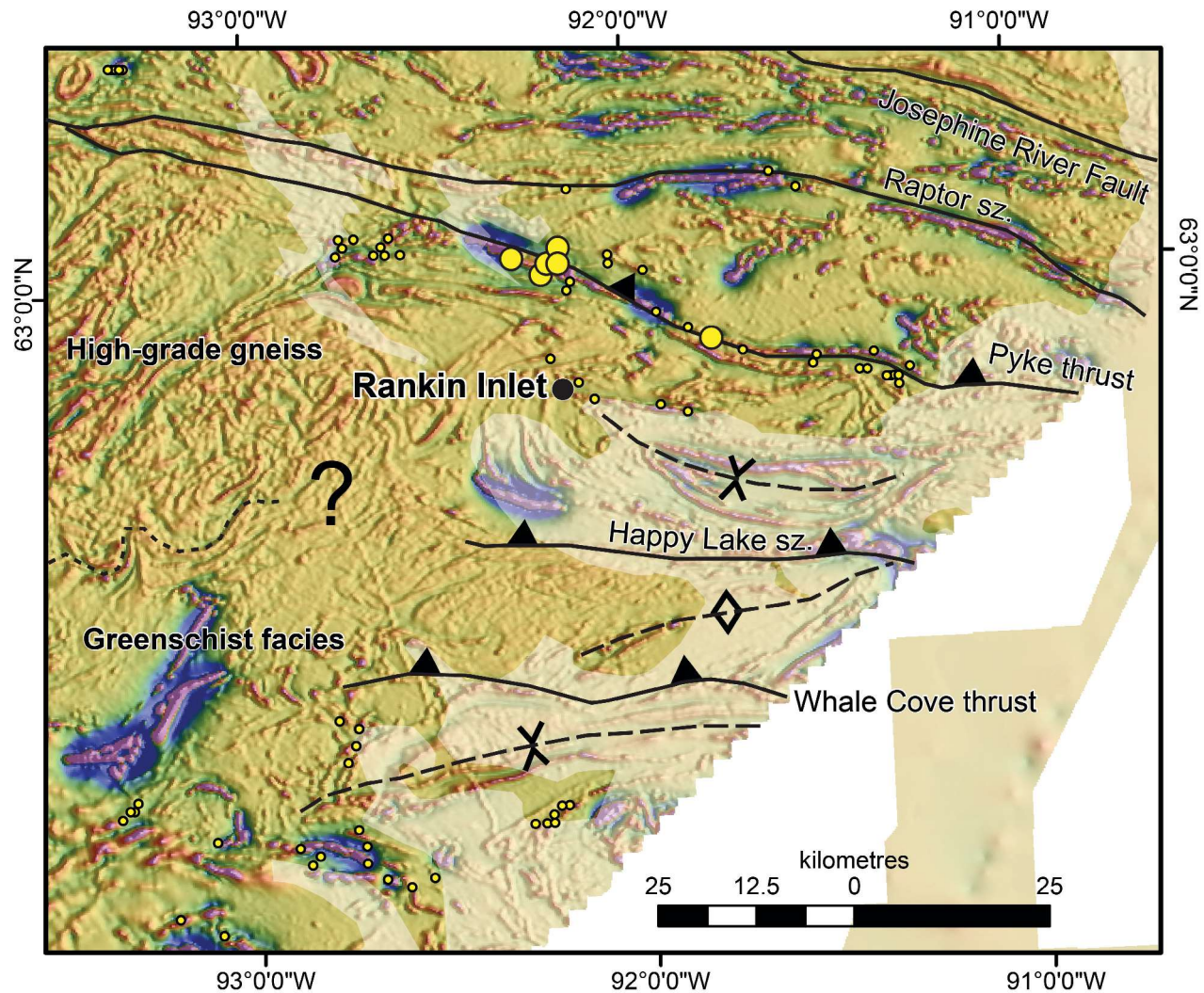


Figure 7. First vertical derivative of the magnetic field of the Rankin Inlet area showing the distribution of gold deposits (large yellow circles), and occurrences and showings (small yellow circles) in relation to faults and shear zones (solid black lines) and folds (dashed black lines) (after Pehrsson et al., 2014a). sz. = shear zone.

amalgamation with the Hearne at ca. 1.91 Ga and reworking at 1.85 Ga (Davis et al., 2006). Integration of the regional high-resolution aeromagnetic data with previous structural and stratigraphic studies outlined a new feature — the Kaminuriak domain, which underlies the most heavily drift-covered region. It is characterized by curvilinear magnetic features defining large refolded folds with 20–70 km long axial surfaces. This pattern is structurally bounded by the Raptor shear zone to the north and the Happy Lake shear zone to the south (Fig. 6b). Combining recent geological results near Rankin Inlet (Lawley et al., 2015, 2016) and Happy (Berman et al., 2007) and Yathkyed (Acosta-Góngora et al., 2018) lakes illustrates that the Kaminuriak domain comprises Chesterfield Block Archean and Paleoproterozoic crust that is transposed and regionally folded during late extrusion and south-vergent thrusting of the domain over the Hearne Craton (Pehrsson, this volume).

Orogenic gold deposits, occurrences, and showings of the Chesterfield Inlet area are hosted by Archean volcano-sedimentary units along prominent shear zones, particularly the Pyke Fault (Fig. 7; Carpenter et al., 2005). Faults and shear zones have protracted deformation histories culminating in reactivation and mineralizing fluid ingress between 1.9 and 1.85 Ga (Carpenter and Duke, 2004; Lawley et al., 2015). Current exploration models for the region identify the Chesterfield Block and Rae Archean supracrustal packages, along with reactivated shear zones, as key elements in gold prospectivity (Pehrsson et al., 2013, 2014a; Lawley et al., 2015; Janvier et al., 2015). Significantly, the Chesterfield aeromagnetic survey illustrates that the Pyke break is a splay to the Raptor shear zone that bounds the Kaminuriak domain to the north (Fig. 6b, 7). Such second-order structural features are commonly considered the most prospective for orogenic gold mineralization (Goldfarb et al., 2005; Dubé et al., 2015).

South Rae

South of the western Thelon Basin, preliminary studies in the south Rae region (area 8 on Fig. 1, 2, 3) documented unrecognized mineral potential in a particularly poorly understood part of Churchill province that had previously only been mapped during early GSC reconnaissance (1:500 000 to 1:2 500 000 scale; Harris et al., 2013a–o). A modern aeromagnetic survey (Table 1) tied to similar surveys in adjacent mapped parts of northern Saskatchewan and southeast Northwest Territories allowed completion of 1:250 000 scale maps in three field seasons (e.g. Martel et al., 2018). In conjunction with bedrock mapping, the integrated aeromagnetic coverage enabled distinction of five geophysically and isotopically defined domains, named Porter, Boomerang, Penylan, McCann, and Firedrake, each with a characteristic magmatic and 2.6–1.80 Ga tectono-metamorphic history (Percival et al., 2016; Regis et al., 2017; Martel et al., 2018; Thiessen et al., 2020; Pehrsson, this volume) and transected by sparse dyke swarms (Mowbray and Pehrsson, 2019). The domains strike predominantly northeast and notably display distinctive aeromagnetic signatures that reflect the variable intensity of moderate- to high-pressure, crustal-scale reworking during the Snowbird and Trans-Hudson orogenic phases. The characteristic geophysical expression of several domains allows correlation with other parts of the Rae Craton–Chesterfield Block. For instance, the McCann domain and its ca. 2.55 Ga metasedimentary rocks that were metamorphosed and deformed during the ca. 2.3 Ga Arrowsmith Orogeny are characterized by the same widespread smooth magnetic low as the contemporaneous Sherman Basin of the Queen Maud Block (Schultz et al., 2007). Similarly, the Firedrake domain displays the same large, regional, complex re-fold pattern of distinctly linear magnetic features that is observed in the Kaminuriak domain (Fig. 6b). Both are significant regions that were exhumed from the mid-crust during late Trans-Hudson time (Martel et al., 2018), suggesting that this pattern may stem from crustal flow processes during extensional collapse of an orogenic plateau (Regis et al., 2021).

The individual geological domains of south Rae Craton are bounded by extensive, newly recognized ductile and brittle-ductile shear zones that correspond to textural discontinuities on the magnetic maps and derivative products (shown in Jamison, 2018; Thiessen et al., 2018; and Martel et al., 2018). Several of these boundary zones are spatially associated with rare-earth element (REE)–prospective syenite bodies (Jamison et al., 2017).

Athabasca Basin

The Athabasca Basin (area 9 on Fig. 1, 2, 3) in the southern part of the synthesis area hosts world-class uranium deposits and is the premier exploration region in Canada for unconformity-associated uranium deposits (Jefferson and Delaney,

2007). Nonmagnetic sedimentary rocks cover the majority of the deposits, such that aeromagnetic surveys, coupled with other multiparameter geophysical transects, are essential to interpreting the geology of the crystalline basement that hosts the uranium deposits. To maximize resolution, systematic airborne magnetic and radiometric surveys were completed to modern standards (Table 1) over the Saskatchewan portion of the Athabasca Basin, in collaboration with Saskatchewan Industry and Resources, resulting in the largest contiguous modern aeromagnetic and radiometric data set in Canada (Card et al., 2010). In 2017, through the Targeted Geoscience Initiative (TGI) Uranium project, the coverage was expanded to include the southwestern Athabasca Basin (box 9d on Fig. 2; Table 1), including parts of Alberta and south of the basin margins. The Athabasca Basin geophysical compilations provided fundamental information for industry operating in the basin to help assess the uranium resource potential of areas buried by Athabasca Supergroup cover. In conjunction with drill-core information and rock-property information, improved resolution in the southwestern Athabasca Basin allowed for redefinition of the location and distribution of felsic intrusive bodies, and identified several major crustal structures that may have played a role in localizing hydrothermal fluid movement (Fig. 8; Tschirhart et al., 2019, 2021). Moreover, the airborne magnetic surveys showed discrete, isolated circular anomalies (Kiss and Tschirhart, 2017a–o) that have the potential to correspond to kimberlite pipes.

DISCUSSION

Geophysical information is used most effectively to constrain geological models. These connect through rock physical properties, and models will continue to improve as the rock-property database expands. Geophysical methods provide essential depth constraints on 3-D geological models, whether illuminating crystalline bedrock through a thin veneer of glacial sediments, thicker sections of Proterozoic strata or Phanerozoic cover, or imaging crust- or lithosphere-scale features. Over the decades as regional aeromagnetic coverage became available for the western Churchill region, geophysics has contributed to definition and resolution of geological problems at a range of scales. During the GEM-1 and GEM-2 programs, acquisition and interpretation of high-resolution aeromagnetic surveys were integral components of a modern geoscientific approach. In the following sections, the authors highlight the impact of geophysical insights into the evolving picture of geological evolution and the inexorably linked enterprise of mineral exploration; however, domain-by-domain analysis may be required to take account of the protracted and variably reworked nature of the Rae Craton, which limits the applicability of data from adjacent domains and adds layers of complexity to interpretations.

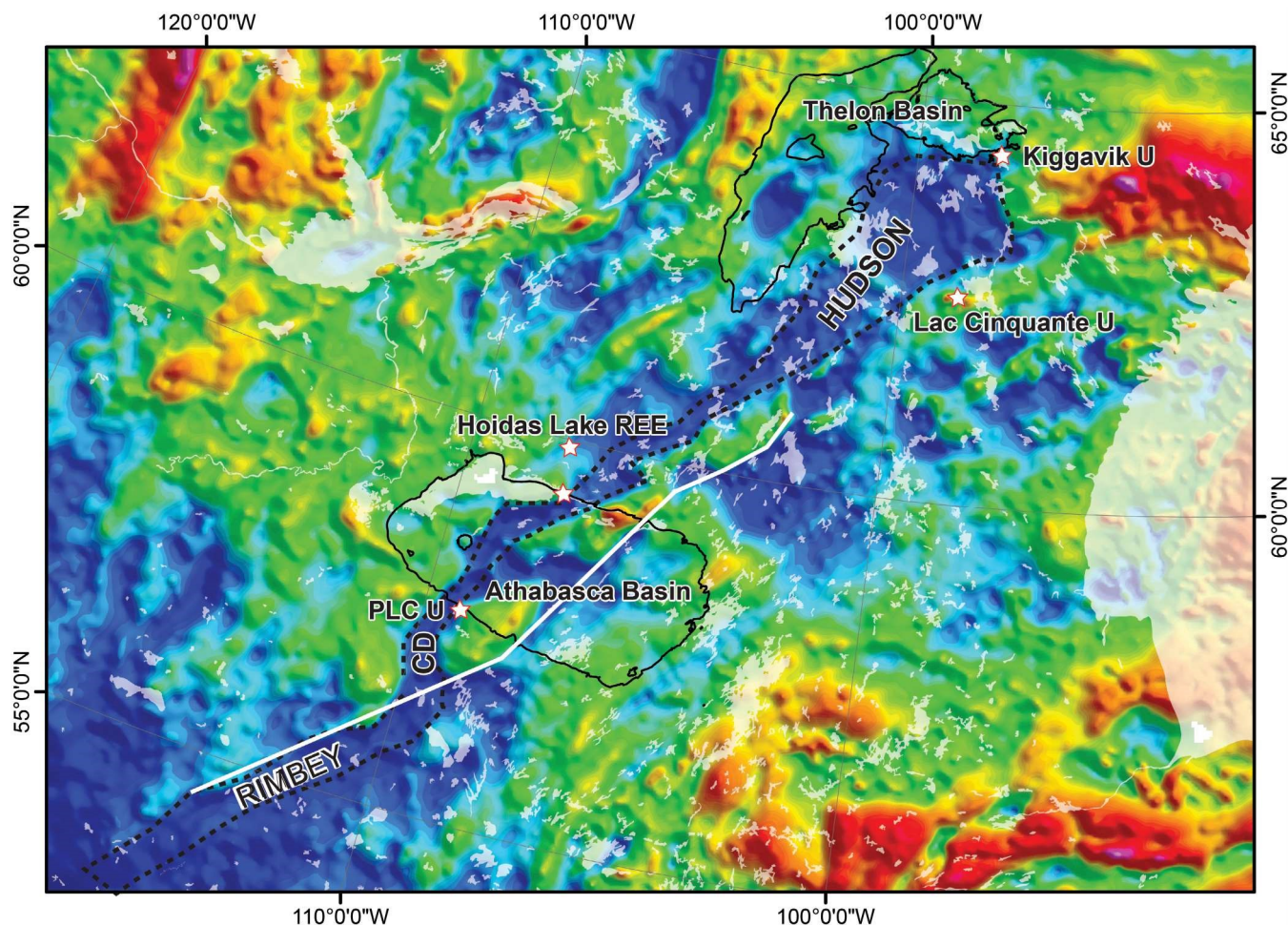


Figure 8. Location of uranium and REE deposits and occurrences over the Bouguer gravity. Thelon and Athabasca basins outlined in black. White line delineates location of mapped Snowbird tectonic zone; dashed black line outlines Bouguer gravity low.

Rae Craton boundaries

The western and southeastern boundaries of the Rae Craton are exposed in the northwestern Canadian Shield and were investigated by GEM projects. Gibb and Thomas (1977) first drew attention to the gravity signature of the Slave–Churchill boundary, localized along the Thelon tectonic zone. Their interpretation of higher density Churchill crust led Hoffman (1988) to propose an exhumed Thelon tectonic zone–age Rae plateau, the Queen Maud Block. Debate on the nature of this boundary has grown with acquisition of new information, including models involving an intracontinental magmatic belt (Thompson, 1989; Chacko et al., 2000). Recent work integrating new geophysical and bedrock mapping illustrates a complex 2.06–1.9 Ga tectono-magmatic history of continental-arc magmatism at a consuming margin (Berman et al., 2016, 2018; Whalen et al., 2018). This boundary is characterized by steeply dipping conductive zones that extend through the crust, however their origin as graphitic metasedimentary layers or high-grade metamorphic zones is uncertain (Roberts et al., 2015).

The northern extension of the Thelon tectonic zone is poorly constrained beneath Paleozoic cover and water. Previous extrapolations projected the Thelon tectonic zone through Boothia Peninsula–Somerset Island (Fig. 6b; Wheeler et al., 1996), however recent work (Sanborn-Barrie et al., 2018) excludes this possibility, requiring a more westerly trajectory through an area of sparse geophysical coverage.

At its southeastern margin, the Rae Craton is bordered by the Snowbird tectonic zone, defined originally as a line of gravity and magnetic anomalies and interpreted as a suture within the Churchill Province (Walcott and Boyd, 1971). Hoffman (1988) inferred the zone to be the Paleoproterozoic boundary between the Archean Rae and Hearne cratons. The Snowbird tectonic zone can be traced from southern Alberta (Pilkington et al., 2000) to the Angikuni Lake area (Fig. 6a, b). Over much of this length it is expressed geophysically as a chain of positive gravity anomalies corresponding to granulite-facies granitoid gneiss intruded by gabbro-anorthosite, typical of mid- to lower crust (Gordon and Lawton, 1995;

Sanborn-Barrie et al., 2001, 2019b; Berman et al., 2007; Mills et al., 2007), although recent studies demonstrate that high-pressure rocks of the Snowbird Orogeny occur far to the west of the Snowbird tectonic zone as originally defined (Regis et al., 2019; Pehrsson, this volume). The magnetic anomalies from Angikuni Lake to Baker Lake are subdued in comparison to the anomalies north of the Tulemalu Fault by the overlapping Baker Lake Basin, which contains low-density sedimentary and igneous rocks (Fig. 2; Tschirhart et al., 2013b, 2017; Peterson et al., 2015c). The northern dense and highly magnetic features north of Baker Lake along Chesterfield Inlet (Fig. 6a, b) originally ascribed to the Snowbird tectonic zone have more recently been shown to be of differing age and origin (Gordon and Lawton, 1995; Sanborn-Barrie et al., 2001, 2019b; Berman et al., 2007; Mills et al., 2007).

A joint magnetotelluric-teleseismic profile detailed deep structural discontinuities supporting juxtaposition of the two terranes (Jones et al., 2002). Structural-petrological studies at the southwestern exposures of the Snowbird tectonic zone in Saskatchewan (Hanmer et al., 1995; Mahan and Williams, 2005) have been interpreted as indicative of Archean assembly; however, subsequent work has revealed a complex interface consistent with ca. 1.9 Ga assembly during the Snowbird accretionary phase of the Trans-Hudson Orogeny (Berman et al., 2007; Thiessen et al., 2018).

Several GEM projects provide insight into the enigmatic northeastern extension of the Snowbird zone east of Dubawnt Lake where it lacks a pronounced magnetic and gravity signature (Fig. 6a). Several interpretations of its eastern extents have emerged in the Chesterfield–Wager Bay region (Jones et al., 2002; Berman et al., 2007; Spratt et al., 2012b), where relationships among shear zones, exhumed high-pressure rocks, layered igneous complexes, and terrane architecture are complex (Spratt et al., 2014; Skulski et al., 2018) and only separable from older (2.6, 2.55 Ga) and younger (1.85 Ga) structures and events by detailed geochronological work (e.g. Thiessen et al., 2018; Sanborn-Barrie et al., 2019b; Regis et al., 2019). Recent interpretations place the Snowbird tectonic zone along the major west-dipping Tyrell shear zone (Berman et al., 2007; Fig. 6a, b). Comparison of Figures 2, 3 (area 7), and 6a shows a zone of linear, positive anomalies (Fig. 6a: S1, S2, S3) on the most southerly of Berman et al.'s (2007) proposed trajectories, coincident with the southern margin of the Kaminuriak domain. A subtle break in the mantle and crust resistivity subjacent to anomaly S3 was modelled in an early magnetotelluric profile (Jones et al., 2002), and is supported by more recent magnetotelluric models (Fig. 11d *in* Spratt et al., 2014), as well as teleseismic definition of their eastward extension in Hudson Bay (Gilligan et al., 2016; Liddell et al., 2018).

In the sparsely exposed Chesterfield Inlet–Wager Bay region, elucidation of the complex fault geometry and its association with lode gold showings and deposits was enabled by field observations guided by high-resolution aeromagnetic maps (Pehrsson et al., 2014a; Wodicka et al.,

2017). Similarly, gravity profiles defined the 3-D geometry of granulite complexes and some shear zones (Tschirhart et al., 2016), contributing to regional kinematic analysis. The emerging picture of Snowbird tectonism involves a 1.9 Ga collision between the Rae Craton–Chesterfield Block, the approximately 200 km wide southeastern margin of which underwent burial, structural and metamorphic reworking, and variable compressional and extensional exhumation during accretion of the relatively intact Hearne Craton (Pehrsson, this volume).

Internal Rae Craton architecture

Most of the Rae Craton is characterized by a pervasive northeast-oriented structural grain evident in the aeromagnetic data (Fig. 2), attributed to the cumulative effects of the Trans-Hudson and older deformation events. Whereas some internal domains of the Rae Craton have distinct aeromagnetic and/or gravity expressions, other, more structurally overprinted domains have more cryptic boundaries, evident only through contrasting isotopic character (Peterson et al., 2010; Regis et al., 2019; Kellett et al., 2020). Conversely, some prominent linear aeromagnetic features correspond to ductile shear zones of relatively minor tectonic significance.

The south Rae Craton region represents a distinct structural style in which shear zones separate domains of variable aeromagnetic intensity and amplitude (Pehrsson et al., 2014b, 2015; Percival et al., 2016). The shear zones are commonly curvilinear, ductile and brittle-ductile structures of low magnetic intensity that were active between ca 1.9 and 1.8 Ga (Regis et al., 2017, 2019, 2021; Kellett et al., 2020). Based on the variable metamorphic ages and pressures of individual domains, the shear zones appear to represent discontinuities among blocks with different burial and exhumation histories (Regis et al., 2017, 2021; Thiessen et al., 2018). Although most domains consist predominantly of Archean (ca. 2.6 Ga) rocks, some (e.g. Porter, Boomerang) underwent minor Paleoproterozoic reworking, whereas McCann shows a strong Arrowsmith (2.4–2.3 Ga) overprint, Firedrake exhibits a strong Trans-Hudsonian (1.85 Ga) resetting, and Snowbird domain, a thorough Snowbird (1.9 Ga) structural-metamorphic reworking (Regis et al., 2017, 2019, 2021).

Structural style in the central Rae Craton region is dominated by the superimposed effects of the Snowbird and Trans-Hudson events. The Rae Craton cover sequence, deposited between the Arrowsmith and Snowbird events, acts as a monitor of internal strain within the Rae Craton. Structural studies of these rocks, in concert with aeromagnetic interpretation, have illustrated a polyphase fold and thrust belt geometry and associated ca. 1.83 Ga high-temperature, moderate pressure metamorphism (Patterson, 1986; Pehrsson et al., 2013; Calhoun et al., 2014; Percival and Tschirhart, 2017; Dziawa et al., 2019), locally superimposed by late extensional structures (Percival et al., 2015; Wodicka et al., 2017). The regional pattern of individually isolated Rae Craton cover outliers, separated by broad granitic and

granulitic massifs west of the Committee Bay–Woodburn greenstone belts, may reflect these late Trans-Hudson structures, including a ductile phase of movement on the prominent Amer shear zone.

To the northeast, the Committee Bay belt is characterized by northeast-trending, southeast-dipping structures (Fig. 6b) and ca. 1.86–1.82 Ga metamorphism (Sanborn-Barrie et al., 2014a) that overprint ca. 2.35 Ga fabrics attributed to the Arrowsmith Orogeny. In the adjacent Tehery-Wager region to the east, polydeformed sequences represent penetrative Trans-Hudson Orogen deformation superimposed on Archean structures. Domains of contrasting metamorphic grade (e.g. Kummel Lake and Daly Bay) are bounded by continuous lineaments on the horizontal gradient of the Bouguer gravity anomaly map (dashed lines bounding DB and KLD, Fig. 6a), suggestive of truncations juxtaposing significantly different exposure levels. Late extension may be responsible for differential uplift of blocks (Wodicka et al., 2016; Tschirhart et al., 2016).

In the Melville region further to the northeast (area 1 on Fig. 1, 2, 3), northeasterly structural, aeromagnetic, and gravity trends reflect variable effects of Trans-Hudson deformation and metamorphism (Fig. 6a, b). Areas dominated by the less than 1.897 Ga Penhryn Group (Partin et al., 2014) and the Repulse Bay Block (LaFlamme et al., 2014) underwent amphibolite- to granulite-facies metamorphism between 1.84 and 1.82 Ga (LaFlamme et al., 2017), whereas the Prince Albert Block to the north retains Archean fabrics. The magnetotelluric inversions have delineated the subsurface boundary between the Prince Albert Block, with thicker lithosphere and moderate resistivity, and the Repulse Bay Block, with high resistivity and thinner lithosphere (Spratt et al., 2013a). Geological mapping identified the absence of 2.6 Ga Snow Island Suite rocks in the Repulse Bay and Prince Albert blocks and thus suggested accretion to the Rae Craton after 2.6 Ga (Peterson et al., this volume). The proposed contact in Peterson et al. (this volume) is demarcated by a notable gravity lineament between Committee Bay Block and Repulse Bay Block (Fig. 6a) and slight break in the mantle resistivity structure in Profile 2 and Profile 3 from Spratt et al. (2014).

Metallogenic implications

One of the most challenging goals of the GEM program has been to understand the distribution of mineral resources and their tectonic controls across the Rae Craton. Whereas the protracted orogenic history that affected the Rae Craton provided multiple opportunities for reactivation of major crustal structures, only some of these events channelled mineralizing fluids along some structures. Therefore, defining the geophysical attributes of structures that host uranium and gold deposits of the Rae Craton has been a significant contribution (e.g. Lawley et al., 2015, 2016; Jamison et al., 2017; Ma, 2018; Martel et al., 2018; Tschirhart et al., 2019, 2021; Ma et al., 2020; Jefferson et al., this volume).

Gold deposits and showings of the Rae Craton exhibit the attributes of orogenic gold systems, including spatial association with faults and shear zones (Fig. 7; Sherlock et al., 2004; Carpenter et al., 2005; Davies et al., 2010; Pehrsson et al., 2013, 2014a; Lawley et al., 2015, 2016; Janvier et al., 2015). Most deposits — Meadowbank, Meliadine, Three Bluffs, as well as numerous gold showings — occur in volcanic-dominated sequences of Archean age reworked during Paleoproterozoic tectonism (1.9–1.8 Ga). The deposits occur along regional-scale or second-order faults that acted as conduits for mineralizing fluids (Fig. 7; Lawley et al., 2015). In the Meliadine camp, faults and shear zones likely relate to terrane suturing between the Chesterfield Block–Rae Craton and Hearne Craton to the south (Pehrsson et al., 2014a; Lawley et al., 2016). In this largely drift-covered region, interpretation of high-resolution aeromagnetic data has identified additional gold-prospective corridors (Pehrsson et al., 2014a) that are not as evident on the legacy data sets.

Similar concepts of fault reactivation and fluid channeling apply to uranium metallogeny within the Rae Craton (Jefferson and Delaney, 2007; Jefferson et al., this volume). A recent example of the metallogenic link between basement structure reactivation and uranium is the regional-scale Patterson Lake corridor south of the Athabasca Basin. In this region, basement features of the Clearwater domain (Stern et al., 2003), including ductile shear zones, high heat-producing intrusions, and basin growth faults, are associated with uranium mineralization in the overlying Athabasca Basin (Fig. 8; Tschirhart et al., 2021). Ashton et al. (2018) noted that the prominent linear gravity low associated with the Clearwater domain extends northeastward, and geophysical products presented here demonstrate their continuity into the Baker Lake area, south of the northeastern Thelon Basin (Fig. 8) and co-location with the major mineralized faults of the south Rae Craton (McCurdy et al., 2016; Jamison et al., 2017; Thiessen et al., 2020). Both unconformity-style and basement-hosted uranium deposits and occurrences, as well as rare-earth element (REE) anomalies (Acosta-Góngora et al., 2017) occur along this trend that parallels the trace of the 1.84–1.81 Ga Baker Lake Group basin depocentres and related magmatism (Peterson et al., 2002; Percival et al., 2016; Card, 2018). The association between ca 1.85–1.80 Ga intrusions, including alkaline rocks (Card, 2018) and elevated U-Th-REE contents makes Ashton et al.'s (2018) suggestion of a potential genetic link between the intrusions and younger U mineralization intriguing.

In the Kiggavik uranium camp (Fig. 4, 5, 8), linkages can be made between reactivated basement faults at regional to deposit scales, basin development, hydrothermal fluid flow, and uranium occurrences around the northeastern Thelon Basin (Tschirhart et al., 2013c; Tschirhart and Pehrsson, 2016; Jefferson et al., this volume). These spatial and process linkages were established by integration of geophysical and geological data acquired under the GEM program (Tschirhart et al., 2011).

Given the possible conductive mantle pathways noted by Spratt et al. (2014) below Hudson-age intrusions in the Committee Bay and Repulse Bay blocks (Fig. 6a), it is notable that Peterson et al. (2002) proposed that these suites host mantle melts and major metasomatic components. Significantly, the metasomatizing fluids could provide linkage to the observed low crustal resistivity magnetotelluric response. Furthermore, Tschirhart et al. (2013b) modelled eastern extensions of Hudson magmatism (Shultz Lake intrusive complex) underlying the Kiggavik uranium deposit, again demonstrating the potential for mineralization where 1.8 Ga magmatism, reactivated crustal structures, and basin fluid-reduction processes intersected.

In the Thelon tectonic zone and northeast Thelon regions, Ma (2018) noted that all known uranium occurrences are located at the intersections of hydrothermally altered, east-northeast- and northeast-trending brittle fault systems (including the northeast-trending McDonald fault array) that are localized along earlier ductile shear zones (Tschirhart et al., 2017; Anand and Jefferson, 2017; Hunter et al., 2018). Ma's (2018) research on the Bathurst Fault in the Thelon tectonic zone (Fig. 1) documented brittle deformation after 1840 Ma, fluid-rock interaction, and thus enhanced basement permeability. Preliminary age constraints on deposition of sediments in the northeast Thelon Basin are compatible with the temporal constraints on ductile deformation in the Bathurst fault system (ca. 1850–1830 Ma; Ma et al., 2020). Overprinting of the brittle deformation occurred after ca. 1810 Ma (Hunter et al., 2018). As the intersection of the Bathurst fault array and MacDonald Fault coincides with the Thelon Basin depocentre (Jefferson et al., 2015; Tschirhart et al., 2014, 2017; Tschirhart and Pehrsson, 2016), this establishes significant potential in the basin's underexplored western and northern margins, owing to possible fluid pathways for uranium mineralization along the Bathurst fault array. This is particularly true along its intersection with additional deep-seated structures such as the McDonald Fault and Howard Lake fault zone (Tschirhart and Pehrsson, 2016).

SUMMARY AND OUTSTANDING PROBLEMS

Numerous studies have demonstrated the utility of high-resolution aeromagnetic maps in resolving near-surface features at a range of scales. Regional features such as the Rae Craton boundaries — the Thelon tectonic zone and Snowbird tectonic zone — are evident even at the coarse resolution of regional maps. Much finer resolution is required to follow these boundaries through complexly intruded, deformed, and metamorphosed zones. For example, magmatism in the Thelon tectonic zone extended over tens of millions of years, and was accompanied by granulite-facies

metamorphism, local basin development, and both ductile and brittle deformation, producing a variety of detailed and/or complex aeromagnetic features (Berman et al., 2018; Whalen et al., 2018). Conversely, the trajectory of the Snowbird tectonic zone east of Dubawnt Lake is obscure on regional aeromagnetic maps. High-resolution maps, in concert with detailed geological interpretation, show a complex boundary zone characterized by thrust and transcurrent faults, folds, and rock packages of different ages and origins (Pehrsson et al., 2014a; Lawley et al., 2016), yielding no single feature with clear geophysical expression.

Magnetotelluric data sets proved vital for understanding the deep lithospheric structure of the Rae Craton and the relationship to surface geological features. For example, when interpreted alongside higher resolution data sets such as aeromagnetic data, key crustal breaks were identified such as the break between the Repulse Bay and Committee Bay blocks. The gravity data further contributed to this enhanced understanding by identifying subsurface density contrasts that demarcated terrain boundaries (e.g. Repulse Bay and Prince Albert blocks in Melville Peninsula) and low-density intrusive centres (e.g. 1.85–1.80 Ga Hudson granite suite). Whereas not all features are present in all geophysical data sets, when used in concert they offer the ability to probe the nature of major geological features by visualizing features at a variety of scales and highlighting physical property contrasts related to the metamorphic, structural, geological, and alteration histories. Unfortunately, numerous geological models are permitted by the current level of knowledge of the Rae Craton boundaries in the third dimension, based on sparse gravity and magnetotelluric data sets. This uncertainty regarding the dip and continuity of major crustal features remains an obstacle to broad understanding of tectonic evolution, although the long-lived nature and attendant complexity may preclude tracing these features to mantle depths using existing geophysical methods.

Features related to gold and uranium mineralization are commonly at a finer scale and have been successfully imaged geophysically by modern data in concert with geological models. For example, uranium metallogenic models view reactivated faults in the basement beneath Proterozoic sedimentary basins as channels for mineralizing fluids (Jefferson and Delaney, 2007; Potter et al., 2020). Geophysical models of the sub-Thelon basement show the distribution of key features, including reactivated structures and intrusive units with potential linkage to uranium mineralization processes (Tschirhart et al., 2013b, c, 2014; Tschirhart and Pehrsson, 2016; Potter et al., 2020). Exploration of the basal units of thick, flat-lying sedimentary basins remains a challenging enterprise. Derivative products on modern aeromagnetic data sets (e.g. Fig. 7) clearly delineate structural breaks related to gold mineralization in the Chesterfield Inlet region, emphasizing the importance of updating the aeromagnetic survey coverage in prospective terrains.

ACKNOWLEDGMENTS

This contribution was produced as part of the Geomapping for Energy and Minerals program and ongoing research in the Uranium activity of the Targeted Geoscience Initiative program. Brad Harvey is thanked for his technical support. Discussions with Jeremy Powell and Eric Potter provided appreciated insight. Comments and reviews from Nathan Hayward and Richard Smith improved the quality of the manuscript.

REFERENCES

- Acosta-Góngora, P., Pehrsson, S.J., Martel, E., Lauzon, G., and Jamison, D., 2017. South Rae Project: preliminary field observations (2015) and lake sediment analysis, Northwest Territories and Saskatchewan; Geological Survey of Canada, Scientific Presentation 67, 2017, 47 p. <https://doi.org/10.4095/302765>
- Acosta-Góngora, P., Pehrsson, S.J., Sandeman, H.A., Martel, E., and Peterson, T.D., 2018. The Ferguson Lake deposit: an example of Ni-Cu-Co-PGE mineralization emplaced in a back-arc basin setting; Canadian Journal of Earth Sciences, v. 55, p. 958–979. <https://doi.org/10.1139/cjes-2017-0185>
- Anand, A. and Jefferson, C.W., 2017. Outcropping and remotely predicted lineaments, faults, fractures and dykes in the Kiggavik uranium camp of Nunavut; Geological Survey of Canada, Open File 7896, 1 poster. <https://doi.org/10.4095/302777>
- Anderson, S.D., Böhm, C.O., Syme, E.C., Carlson, A.R. and Murphy, L.A., 2009. Far North Geomapping Initiative: geological investigations in the Great Island area, Manitoba (parts of NTS 54L13, 54M4, 64I15, 16, 64P1, 2); in Report of Activities 2009; Manitoba Innovation, Energy and Mines, Manitoba Geological Survey, p. 132–147.
- Anderson, S.D., Böhm, C.O., and Syme, E.C., 2010. Precambrian geology of the Seal River region, Manitoba (parts of NTS 54L, M, 64I, P); Manitoba Geological Survey, Preliminary Map PMAP2010-1, scale 1:75 000.
- Ashton, K., Card, C., and Rayner, N., 2018. A new U-Pb age for the Hudson granites and lamprophyre dykes in the southern Rae Province of Saskatchewan; Summary of Investigations 2018, Volume 2, Saskatchewan Geological Survey, Saskatchewan Ministry of Energy and Resources, Miscellaneous Report 2018-4.2, Paper A-6, 15 p. and 2 appendices.
- Berman, R.G., 2010. Metamorphic map of the western Churchill Province; Geological Survey of Canada, Open File 5279, scale 1:2 500 000. <https://doi.org/10.4095/287320>
- Berman, R.G., Sanborn-Barrie, M., Stern, R.A., and Carson, C.J., 2005. Tectono- metamorphism at ca. 2.35 and 1.85 Ga in the Rae domain, western Churchill Province, Nunavut, Canada: insights from structural, metamorphic and in situ geochronological analysis of the southwestern Committee Bay belt; Canadian Mineralogist, v. 43, p. 409–442. <https://doi.org/10.2113/gscanmin.43.1.409>
- Berman, R., Davis, W., and Pehrsson, S., 2007. Collisional Snowbird tectonic zone resurrected: Growth of Laurentia during the 1.9 Ga accretionary phase of the Hudsonian orogeny; Geology, v. 35, p. 911–914. <https://doi.org/10.1130/G23771A.1>
- Berman, R.G., Rayner, N., Sanborn-Barrie, M., and Chakungal, J., 2011. New constraints on the tectonothermal history of Southampton Island, Nunavut, provided by in situ SHRIMP geochronology and thermobarometry; Geological Survey of Canada, Current Research 2011-6, 14 p. <https://doi.org/10.4095/287287>
- Berman, R.G., Pehrsson, S., Davis, W.J., Ryan, J.J., Qui, H., and Ashton, K.E., 2013a. The Arrowsmith orogeny: Geochronological and thermobarometric constraints on its extent and tectonic setting in the Rae craton, with implications for pre-Nuna supercontinent reconstruction; Precambrian Research, v. 232, p. 44–69. <https://doi.org/10.1016/j.precamres.2012.10.015>
- Berman, R.G., Sanborn-Barrie, M., Rayner, N., and Whalen, J., 2013b. The tectonometamorphic evolution of Southampton Island, Nunavut: insight from petrologic modeling and in situ SHRIMP geochronology of multiple episodes of monazite growth; Precambrian Research, v. 232, p. 140–166. <https://doi.org/10.1016/j.precamres.2012.08.011>
- Berman, R.G., Davis, W.J., Corrigan, D., and Nadeau, L., 2015. Insights into the tectonothermal history of Melville Peninsula, Nunavut, provided by in situ SHRIMP geochronology and thermobarometry; Geological Survey of Canada, Current Research 2015-4, 22 p. <https://doi.org/10.4095/295852>
- Berman, R.G., Sanborn-Barrie, M., Nadeau, L., Brouillette, P., Camacho, A., Davis, W.J., McCurdy, M.W., McMartin, I., Weller, O.M., Chadwick, T., Liikane, D.A., and Ma, S., 2016. Report of activities for the geology and mineral potential of the Chantrey-Thelon area: GEM-2 Rae project; Geological Survey of Canada, Open File 8129, 12 p. <https://doi.org/10.4095/299386>
- Berman, R.G., Davis, W.J., Sanborn-Barrie, M., Whalen, J.B., Taylor, B.E., McMartin, I., McCurdy, M.W., Mitchell, R.K., Ma, S., Coyle, M., Roberts, B., and Craven, J.A., 2018. Report of activities for the GEM-2 Chantrey-Thelon activity: Thelon Tectonic Zone project, Nunavut; Geological Survey of Canada, Open File 8372, 19 p. <https://doi.org/10.4095/306622>
- Blakely, R.J. and Simpson, R.W., 1986. Approximating edges of source bodies from magnetic or gravity anomalies; Geophysics, v. 51, p. 1494–1498. <https://doi.org/10.1190/1.1442197>
- Calhoun, L., White, J.C., Jefferson, C.W., Patterson, J., and Tschirhart, V., 2014. Integrated geodatabase study of the complexly deformed U-hosting Paleoproterozoic Amer Group, Nunavut; Geological Survey of Canada, Scientific Presentation 19, 26 p. <https://doi.org/10.4095/293108>
- Card, C.D., 2018. The Patterson Lake alkaline igneous complex: evidence for deep-seated structural control in the Patterson Lake corridor, and implications for mineral exploration; in Summary of Investigations 2018, Volume 2, Saskatchewan Geological Survey, Saskatchewan Ministry of Energy and Resources, Miscellaneous Report 2018-4.2, Paper A-9, 19 p.

- Card, C.D., Bosman, S.A., Slimmon, W.L., Delaney, G., Heath, P., Gouthas, G. and Fairclough, M., 2010. Enhanced geophysical images and multi-scale edge (worm) analysis for the Athabasca region; Geological Survey of Saskatchewan, Open File 2010-46, 2 p.
- Carpenter, R.L. and Duke, N.A., 2004. Geological setting of the West Meliadine gold deposits, Western Churchill Province, Nunavut, Canada; *Exploration and Mining Geology*, v. 13, p. 49–65. <https://doi.org/10.2113/gsemg.13.1-4.49>
- Carpenter, R.L., Duke, N.A., Sandeman, H.S., and Stern, R., 2005. Relative and absolute timing of gold mineralization along the Meliadine Trend, Nunavut, Canada: evidence for Paleoproterozoic gold hosted in an Archean greenstone belt; *Economic Geology and the Bulletin of the Society of Economic Geologists*, v. 100, p. 567–576. <https://doi.org/10.2113/gsecongeo.100.3.567>
- Chacko, T., De, S.K., Creaser, R.A., and Muehlenbachs, K., 2000. Tectonic setting of the Taltson Magmatic zone at 1.9 to 2.0 Ga: a granitoid-based perspective; *Canadian Journal of Earth Sciences*, v. 37, p. 1597–1609. <https://doi.org/10.1139/e00-029>
- Cook, F.A., Percival, J.A., and Clowes, R.M., 2012. Tectonic styles in Canada: LITHOPROBE perspectives on the evolution of the North American continent; *in* *Tectonic styles in Canada: the LITHOPROBE perspective*, (ed.) J.A. Percival, F.A. Cook, and R.M. Clowes; Geological Association of Canada, Special Paper no. 49, p. 467–498.
- Corrigan, D., Pehrsson, S., Wodicka, N., and De Kemp, E., 2009. The Palaeoproterozoic Trans-Hudson Orogen: a prototype of modern accretionary processes; *in* *Ancient orogens and modern analogues*, (ed.) J.B. Murphy, J.D. Keppie, and A.J. Hynes; Geological Society, London, Special Publications 327, p. 457–479.
- Corrigan, D., Nadeau L., Brouillette, P., Wodicka, N., Houlié, M.G., Tremblay, T., Machado, G., and Keating, P., 2013. Overview of the GEM Multiple Metals — Melville Peninsula project, central Melville Peninsula, Nunavut; Geological Survey of Canada, Current Research 2013-19, 17 p. <https://doi.org/10.4095/292862>
- Dafoe, L.T. and Bingham-Koslowski, N. (ed.), 2022. Geological synthesis of Baffin Island (Nunavut) and the Labrador–Baffin Seaway; Geological Survey of Canada, Bulletin 608, 2 .zip files. <https://doi.org/10.4095/314542>
- Davidson, G.I. and Gandhi, S.S., 1989. Unconformity-related U-Au mineralization in the Middle Proterozoic Thelon sandstone, Boomerang Lake prospect, Northwest Territories, Canada; *Economic Geology and the Bulletin of the Society of Economic Geologists*, v. 84, p. 143–157.
- Davies, T., Richards, J.P., Creaser, R.A., Heaman, L.M., Chacko, T., Simonetti, A., Williamson, J., and McDonald, D.W., 2010. Paleoproterozoic age relationships in the Three Bluffs Archean iron formation-hosted gold deposit, Committee Bay Greenstone Belt, Nunavut, Canada; *Exploration and Mining Geology*, v. 19, p. 55–80. <https://doi.org/10.2113/gsemg.19.3-4.55>
- Davis, W.J., Hanmer, S., and Sandeman, H.A., 2004. Temporal evolution of the Neoproterozoic Central Hearne supracrustal belt: rapid generation of juvenile crust in a suprasubduction zone setting; *Precambrian Research*, v. 134, p. 85–112. <https://doi.org/10.1016/j.precamres.2004.02.002>
- Davis, W.J., Hanmer, S., Tella, S., Sandeman, H.A., and Ryan, J.J., 2006. U–Pb geochronology of the MacQuoid supracrustal belt and Cross Bay plutonic complex: key components of the northwestern Hearne subdomain, western Churchill Province, Nunavut, Canada; *Precambrian Research*, v. 145, p. 53–80. <https://doi.org/10.1016/j.precamres.2005.11.016>
- Dubé, B., Mercier-Langevin, P., Castonguay, S., McNicoll, V.J., Bleeker, W., Lawley, C.J.M., De Souza, S., Jackson, S.E., Dupuis, C., Gao, J-F, Bécu, V., Pilote, P., Goutier, J., Beakhouse, G.P., Yergeau, D., Oswald, W., Janvier, V., Fontaine, A., Pelletier, M., ... Lauzière, K., 2015. Precambrian lode gold deposits - a summary of TGI-4 contributions to the understanding of lode gold deposits, with an emphasis on implications for exploration; *in* *Targeted Geoscience Initiative 4: Contributions to the understanding of Precambrian lode gold deposits and implications for exploration*, (ed.) B. Dubé and P. Mercier-Langevin; Geological Survey of Canada, Open File 7852, p. 1–24. <https://doi.org/10.4095/296625>
- Dziawa, C., Gaidies, F., and Percival, J., 2019. Conditions and timing of low-pressure–high-temperature metamorphism in the Montesor Belt, Rae Province, Nunavut; *Canadian Journal of Earth Sciences*, v. 56, p. 654–671. <https://doi.org/10.1139/cjes-2018-0184>
- Enkin, R.J., 2018. Canadian rock physical property database: first public release; Geological Survey of Canada, Open File 8460, 68 p. <https://doi.org/10.4095/313389>
- Enkin, R.J., Corriveau, L., and Hayward, N., 2016. Metasomatic alteration control of physical properties in the Great Bear magmatic zone (Northwest Territories, Canada); *Economic Geology and the Bulletin of the Society of Economic Geologists*, v. 111, p. 2073–2085.
- Gibb, R.A. and Thomas, M.D., 1977. The Thelon front: a cryptic suture in the Canadian shield; *Tectonophysics*, v. 38, p. 211–222. [https://doi.org/10.1016/0040-1951\(77\)90211-6](https://doi.org/10.1016/0040-1951(77)90211-6)
- Gilligan, A., Bastow, I.D., and Darbyshire, F.A., 2016. Seismological structure of the 1.8 Ga Trans-Hudson Orogen of North America; *Geochemistry Geophysics Geosystems*, v. 17, p. 2421–2433. <https://doi.org/10.1002/2016GC006419>
- Goldfarb, R.J., Baker, T., Dubé, B., Groves, D.I., Hart, C.J.R., and Gosselin, P., 2005. Distribution, character, and genesis of gold deposits in metamorphic terranes; *in* *One hundredth anniversary volume 1905-2005*; (ed.) J.W. Hedenquist, J.F.H. Thompson, R.J. Goldfarb, and J.P. Richards, *Economic geology and the bulletin of the Society of Economic Geologists*, p. 407–450 <https://doi.org/10.5382/AV100.14>
- Gordon, T.M. and Heywood, W.W., 1987. Geology, Daly Bay area, District of Keewatin, Northwest Territories; Geological Survey of Canada, Map 1652A, scale 1:250 000. <https://doi.org/10.4095/126317>
- Gordon, T.M. and Lawton, D.C., 1995. Geometry of the allochthonous Daly Bay Complex, Northwest Territories: a model constrained by geology and a three-dimensional gravity interpretation; *Canadian Journal of Earth Sciences*, v. 32, p. 1292–1302. <https://doi.org/10.1139/e95-105>
- Hadlari, T. and Rainbird, R.H., 2011. Retro-arc extension and continental rifting: a model for the Paleoproterozoic Baker Lake Basin, Nunavut; *Canadian Journal of Earth Sciences*, v. 48, p. 1232–1258. <https://doi.org/10.1139/e11-002>

- Hanmer, S., Williams, M., and Kopf, C., 1995. Striding-Athabasca mylonite zone: implications for the Archean and Early Proterozoic tectonics of the western Canadian Shield; *Canadian Journal of Earth Sciences*, v. 32, p. 178–196. <https://doi.org/10.1139/e95-015>
- Hanmer, S., Sandeman, H.A., Davis, W.J., Aspler, L.B., Rainbird, R.H., Ryan, J.J., Relf, C., and Peterson, T., 2004. Geology and Neoproterozoic tectonic setting of the Central Hearne supracrustal belt, Western Churchill Province, Nunavut, Canada; *Precambrian Research*, v. 134, p. 63–83. <https://doi.org/10.1016/j.precamres.2004.04.005>
- Harris, J.R., Hillary, E.M., Percival, J.A., Buller, G., Buenviaje, R., Bazor, D., Baer, S., Kiessling, G.M., Pehrsson, S.J., Davis, W., Berman, R.G., Wodicka, N., Beauchemin, M., Coyne, M., and Therriault, A.M., 2013a. Geo-mapping Frontiers: updated information on the regions covered by Operations Baker, Bathurst, Keewatin, Northern Keewatin, Thelon and Wager; Nunavut and Northwest Territories: GIS components; Geological Survey of Canada, Open File 7434, 31 p. <https://doi.org/10.4095/292744>
- Harris, J.R., Hillary, E.M., Percival, J.A., Buller, G., Buenviaje, R., Bazor, D., Baer, S., Kiessling, G.M., Pehrsson, S.J., Davis, W., Berman, R.G., Wodicka, N., Beauchemin, M., Coyne, M., and Therriault, A.M., 2013b. Geo-mapping Frontiers: updated information on the regions covered by Operations Baker, Bathurst, Keewatin, Northern Keewatin, Thelon and Wager; Nunavut and Northwest Territories: photos of archived samples; Open File 7435, 31 p. <https://doi.org/10.4095/292745>
- Harris, J.R., Hillary, E.M., Percival, J.A., Buller, G., Buenviaje, R., Bazor, D., Baer, S., Kiessling, G.M., Pehrsson, S.J., Davis, W., Berman, R.G., Wodicka, N., Beauchemin, M., Coyne, M., and Therriault, A.M., 2013c. Geo-mapping Frontiers: updated information on the regions covered by Operations Baker, Bathurst, Keewatin, Northern Keewatin, Thelon and Wager; Nunavut and Northwest Territories: Landsat; Geological Survey of Canada, Open File 7436, 31 p. <https://doi.org/10.4095/292746>
- Harris, J.R., Hillary, E.M., Percival, J.A., Buller, G., Buenviaje, R., Bazor, D., Baer, S., Kiessling, G.M., Pehrsson, S.J., Davis, W., Berman, R.G., Wodicka, N., Beauchemin, M., Coyne, M., and Therriault, A.M., 2013d. Geo-mapping Frontiers: updated information on the regions covered by Operations Baker, Bathurst, Keewatin, Northern Keewatin, Thelon and Wager; Nunavut and Northwest Territories: geophysics; Geological Survey of Canada, Open File 7437, 31 p. <https://doi.org/10.4095/292747>
- Harris, J.R., Hillary, E.M., Percival, J.A., Buller, G., Buenviaje, R., Bazor, D., Baer, S., Kiessling, G.M., Pehrsson, S.J., Davis, W., Berman, R.G., Wodicka, N., Beauchemin, M., Coyne, M., and Therriault, A.M., 2013e. Geo-mapping Frontiers: updated information on the regions covered by Operations Baker, Bathurst, Keewatin, Northern Keewatin, Thelon and Wager; Nunavut and Northwest Territories: legacy fieldnotes; Geological Survey of Canada, Open File 7438, 31 p. <https://doi.org/10.4095/292748>
- Harris, J.R., Hillary, E.M., Percival, J.A., Buller, G., Buenviaje, R., Bazor, D., Baer, S., Kiessling, G.M., Pehrsson, S.J., Davis, W., Berman, R.G., Wodicka, N., Beauchemin, M., Coyne, M., and Therriault, A.M., 2013f. Geo-mapping Frontiers: updated information on the regions covered by Operations Baker, Bathurst, Keewatin, Northern Keewatin, Thelon and Wager; Nunavut and Northwest Territories: legacy traverse maps north of 68 degrees; Geological Survey of Canada, Open File 7439, 31 p. <https://doi.org/10.4095/292749>
- Harris, J.R., Hillary, E.M., Percival, J.A., Buller, G., Buenviaje, R., Bazor, D., Baer, S., Kiessling, G.M., Pehrsson, S.J., Davis, W., Berman, R.G., Wodicka, N., Beauchemin, M., Coyne, M., and Therriault, A.M., 2013g. Geo-mapping Frontiers: updated information on the regions covered by Operations Baker, Bathurst, Keewatin, Northern Keewatin, Thelon and Wager; Nunavut and Northwest Territories: legacy traverse maps, NTS 46; Geological Survey of Canada, Open File 7440, 31 p. <https://doi.org/10.4095/292750>
- Harris, J.R., Hillary, E.M., Percival, J.A., Buller, G., Buenviaje, R., Bazor, D., Baer, S., Kiessling, G.M., Pehrsson, S.J., Davis, W., Berman, R.G., Wodicka, N., Beauchemin, M., Coyne, M., and Therriault, A.M., 2013h. Geo-mapping Frontiers: updated information on the regions covered by Operations Baker, Bathurst, Keewatin, Northern Keewatin, Thelon and Wager; Nunavut and Northwest Territories: legacy traverse maps, NTS 55 and 56; Geological Survey of Canada, Open File 7441, 31 p. <https://doi.org/10.4095/292751>
- Harris, J.R., Hillary, E.M., Percival, J.A., Buller, G., Buenviaje, R., Bazor, D., Baer, S., Kiessling, G.M., Pehrsson, S.J., Davis, W., Berman, R.G., Wodicka, N., Beauchemin, M., Coyne, M., and Therriault, A.M., 2013i. Geo-mapping Frontiers: updated information on the regions covered by Operations Baker, Bathurst, Keewatin, Northern Keewatin, Thelon and Wager; Nunavut and Northwest Territories: legacy traverse maps, NTS 65; Geological Survey of Canada, Open File 7442, 31 p. <https://doi.org/10.4095/292752>
- Harris, J.R., Hillary, E.M., Percival, J.A., Buller, G., Buenviaje, R., Bazor, D., Baer, S., Kiessling, G.M., Pehrsson, S.J., Davis, W., Berman, R.G., Wodicka, N., Beauchemin, M., Coyne, M., and Therriault, A.M., 2013j. Geo-mapping Frontiers: updated information on the regions covered by Operations Baker, Bathurst, Keewatin, Northern Keewatin, Thelon and Wager; Nunavut and Northwest Territories: legacy traverse maps, NTS 66; Geological Survey of Canada, Open File 7443, 31 p. <https://doi.org/10.4095/292753>
- Harris, J.R., Hillary, E.M., Percival, J.A., Buller, G., Buenviaje, R., Bazor, D., Baer, S., Kiessling, G.M., Pehrsson, S.J., Davis, W., Berman, R.G., Wodicka, N., Beauchemin, M., Coyne, M., and Therriault, A.M., 2013k. Geo-mapping Frontiers: updated information on the regions covered by Operations Baker, Bathurst, Keewatin, Northern Keewatin, Thelon and Wager; Nunavut and Northwest Territories: legacy traverse maps, NTS 75 and 76; Geological Survey of Canada, Open File 7444, 31 p. <https://doi.org/10.4095/292754>

- Harris, J.R., Hillary, E.M., Percival, J.A., Buller, G., Buenviaje, R., Bazor, D., Baer, S., Kiessling, G.M., Pehrsson, S.J., Davis, W., Berman, R.G., Wodicka, N., Beauchemin, M., Coyne, M., and Therriault, A.M., 2013l. Geo-mapping Frontiers: updated information on the regions covered by Operations Baker, Bathurst, Keewatin, Northern Keewatin, Thelon and Wager; Nunavut and Northwest Territories: National Reference Collection maps and tables, NTS 55 and 56; Geological Survey of Canada, Open File 7445, 31 p. <https://doi.org/10.4095/292755>
- Harris, J.R., Hillary, E.M., Percival, J.A., Buller, G., Buenviaje, R., Bazor, D., Baer, S., Kiessling, G.M., Pehrsson, S.J., Davis, W., Berman, R.G., Wodicka, N., Beauchemin, M., Coyne, M., and Therriault, A.M., 2013m. Geo-mapping Frontiers: updated information on the regions covered by Operations Baker, Bathurst, Keewatin, Northern Keewatin, Thelon and Wager; Nunavut and Northwest Territories: National Reference Collection maps and tables, NTS 65; Geological Survey of Canada, Open File 7446, 31 p. <https://doi.org/10.4095/292756>
- Harris, J.R., Hillary, E.M., Percival, J.A., Buller, G., Buenviaje, R., Bazor, D., Baer, S., Kiessling, G.M., Pehrsson, S.J., Davis, W., Berman, R.G., Wodicka, N., Beauchemin, M., Coyne, M., and Therriault, A.M., 2013n. Geo-mapping Frontiers: updated information on the regions covered by Operations Baker, Bathurst, Keewatin, Northern Keewatin, Thelon and Wager; Nunavut and Northwest Territories: National Reference Collection maps and tables, NTS 66; Geological Survey of Canada, Open File 7447, 31 p. <https://doi.org/10.4095/292757>
- Harris, J.R., Hillary, E.M., Percival, J.A., Buller, G., Buenviaje, R., Bazor, D., Baer, S., Kiessling, G.M., Pehrsson, S.J., Davis, W., Berman, R.G., Wodicka, N., Beauchemin, M., Coyne, M., and Therriault, A.M., 2013o. Geo-mapping Frontiers: updated information on the regions covered by Operations Baker, Bathurst, Keewatin, Northern Keewatin, Thelon and Wager; Nunavut and Northwest Territories: National Reference Collection maps and tables, NTS 75 and 76; Geological Survey of Canada, Open File 7448, 31 p. <https://doi.org/10.4095/292758>
- Hayward, N. and Corriveau, L., 2014. Fault reconstructions using aeromagnetic data in the Great Bear magmatic zone, Northwest Territories, Canada; *Canadian Journal of Earth Sciences*, v. 51, no. 10, p. 927–942. <https://doi.org/10.1139/cjes-2014-0035>
- Hayward, N., Corriveau, L., Craven, J.A. and Enkin, R.J., 2016. Geophysical signature of the NICO Au-Co-Bi-Cu deposit and its iron oxide-alkali alteration system, Northwest Territories, Canada; *Economic Geology*, v. 111, no. 8, p. 2087–2109. <https://doi.org/10.2113/econgeo.111.8.2087>
- Hayward, N., Harris, J.R., Grunsky, E., Beauchemin, M., Jefferson, C., and Peterson, T., 2013. Geo-mapping Frontiers: predictive geology map of the Ennadai region, Nunavut; Geological Survey of Canada, Open File 7485, 21 p. <https://doi.org/10.4095/293261>
- Helmstaedt, H.H. and Pehrsson, S.J., 2012. Geology and tectonic evolution of the Slave Province – a post Lithoprobe perspective; Chapter 7 in *Tectonic styles in Canada: the Lithoprobe perspective*, (ed.) J.A. Percival, F.A. Cook, and R.M. Clowes; Geological Association of Canada, Special Paper, v. 49, p. 379–466.
- Hoffman, P., 1988. United plates of America, the birth of a craton: early Proterozoic assembly and growth of Laurentia; *Annual Review of Earth and Planetary Sciences*, v. 16, p. 543–603. <https://doi.org/10.1146/annurev.ea.16.050188.002551>
- Hunter, R., Lafrance, B., Lesperance, J., and Zaluski, G., 2012. The Qavvik-Tatiggaq Trend: an evolving unconformity-related uranium corridor of the northeast Thelon Basin, Nunavut (abstract); in *Geological Association of Canada–Mineralogical Association of Canada Joint Annual Meeting*, St. John's, Newfoundland and Labrador, Abstracts, v. 35, p. 60.
- Hunter, R.C., Lafrance, B., Heaman, L.M., Zaluski, G., and Thomas, D., 2018. Geology, litho-geochemistry and new LA-ICP-MS U-Pb geochronology of the Aberdeen Lake area, Nunavut: new insights into the Neoproterozoic tectonic evolution of the central Rae Domain; *Precambrian Research*, v. 310, p. 114–132.
- Jamison, D., 2018. Deformation history of the Black Bay Fault, Northwest Territories; M.Sc. thesis, University of Waterloo, Waterloo, Ontario, 133 p.
- Jamison, D., Acosta-Góngora, P., Knox, B.K., Pehrsson, S.J., and Lin, S., 2017. Deformation history of the Black Bay Fault and associated mineralization, Northwest Territories; Geological Survey of Canada, Scientific Presentation 69, 1 poster. <https://doi.org/10.4095/304197>
- Janvier, V., Castonguay, S., Mercier-Langevin, P., Dubé, B., Malo, M., McNicoll, V.J., Creaser, R.A., de Chavigny, B., and Pehrsson, S.J., 2015. Geology of the banded iron formation-hosted Meadowbank gold deposit, Churchill Province, Nunavut; in *Targeted Geoscience Initiative 4: Contributions to the understanding of Precambrian lode gold deposits and implications for exploration*, (ed.) B. Dubé and P. Mercier-Langevin; Geological Survey of Canada, Open File 7852, p. 255–269. <https://doi.org/10.4095/296646>
- Jefferson, C.W. and Delaney, G., 2007. EXTECH IV: Geology and Uranium EXploration TECHnology of the Proterozoic Athabasca Basin, Saskatchewan and Alberta, Geological Survey of Canada, Bulletin 588, 645 p. <https://doi.org/10.4095/223742>
- Jefferson, C.W., Hunter, R., McLaren, M., Peterson, T., Skulski, T., Rainbird, R., Young, G.M., Gandhi, S.S., and Costello, K., 2011. Northeastern Thelon Basin Uranium Region: Geological compilation for geophysical consortium planning; Geological Survey of Canada, Open File 6950, 1 poster. <https://doi.org/10.4095/288801>
- Jefferson, C.W., White, J.C., Young, G.M., Patterson, J., Tschirhart, V., Pehrsson, S.J., Calhoun, L., Rainbird, R.H., Peterson, T.D., Davis, W.J., Tella, S., Chorlton, L.B., Scott, J.M.J., Percival, J.A., Morris, W.A., Keating, P., Anand, A., Shelat, Y., and MacIsaac, D., 2015. Outcrop and remote predictive geology of the Amer Belt and basement beside and beneath the northeast Thelon Basin, in parts of NTS 66-A, B, C, F, G and H, Kivalliq Region, Nunavut; Geological Survey of Canada, Open File 7242, 1 poster. <https://doi.org/10.4095/296825>
- Jobin, D.M., Veronneau, M., and Miles, W., 2017. Isostatic residual gravity anomaly map, Canada / Carte des anomalies isostatiques résiduelles du champ de gravité, Canada; Geological Survey of Canada, Open File 8076, scale 1:7 500 000. <https://doi.org/10.4095/299556>

- Jones, A.G., Snyder, D., Hanmer, S., Asudeh, I., and White, D., 2002. Magnetotelluric and teleseismic study across the Snowbird Tectonic Zone: a Neoproterozoic mantle suture? *Geophysical Research Letters*, v. 29, issue 17, p. 10-1–10-4. <https://doi.org/10.1029/2002GL015359>
- Kellett, D.A., Pehrsson, S., Skipton, D.R., Regis, D., Camacho, A., Schneider, D.A., and Berman, R., 2020. Thermochronological history of the northern Canadian Shield; *Precambrian Research*, v. 342. <https://doi.org/10.1016/j.precamres.2020.105703>
- Kiss, F. and Tschirhart, V., 2017a. Residual total magnetic field, aeromagnetic survey of the Marguerite River area, Alberta, parts of NTS 74-L north and 74-L south; Geological Survey of Canada, Open File 8259, 1 sheet, scale 1:100 000. <https://doi.org/10.4095/302744>
- Kiss, F. and Tschirhart, V., 2017b. Residual total magnetic field, aeromagnetic survey of the Marguerite River area, Alberta, parts of NTS 74-E north and 74-E south; Geological Survey of Canada, Open File 8260, 1 sheet, scale 1:100 000. <https://doi.org/10.4095/302747>
- Kiss, F. and Tschirhart, V., 2017c. Residual total magnetic field, aeromagnetic survey of the Marguerite River area, Saskatchewan, parts of NTS 74-F south; Geological Survey of Canada, Open File 8261, 1 sheet, scale 1:100 000. <https://doi.org/10.4095/302748>
- Kiss, F. and Tschirhart, V., 2017d. Residual total magnetic field, aeromagnetic survey of the Marguerite River area, Saskatchewan, parts of NTS 74-F north; Geological Survey of Canada, Open File 8262, 1 sheet, scale 1:100 000. <https://doi.org/10.4095/302749>
- Kiss, F. and Tschirhart, V., 2017e. Residual total magnetic field, aeromagnetic survey of the Marguerite River area, Saskatchewan, parts of NTS 74-K south; Geological Survey of Canada, Open File 8263, 1 sheet, scale 1:100 000. <https://doi.org/10.4095/302750>
- Kiss, F. and Tschirhart, V., 2017f. First vertical derivative of the magnetic field, aeromagnetic survey of the Marguerite River area, Alberta, parts of NTS 74-L north and 74-L south; Geological Survey of Canada, Open File 8264, 1 sheet, scale 1:100 000. <https://doi.org/10.4095/302751>
- Kiss, F. and Tschirhart, V., 2017g. First vertical derivative of the magnetic field, aeromagnetic survey of the Marguerite River area, Alberta, parts of NTS 74-E north and 74-E south; Geological Survey of Canada, Open File 8265, 1 sheet, scale 1:100 000. <https://doi.org/10.4095/302752>
- Kiss, F. and Tschirhart, V., 2017h. First vertical derivative of the magnetic field, aeromagnetic survey of the Marguerite River area, Saskatchewan, parts of NTS 74-F south; Geological Survey of Canada, Open File 8266, 1 sheet, scale 1:100 000. <https://doi.org/10.4095/302753>
- Kiss, F. and Tschirhart, V., 2017i. First vertical derivative of the magnetic field, aeromagnetic survey of the Marguerite River area, Saskatchewan, parts of NTS 74-F north; Geological Survey of Canada, Open File 8267, 1 sheet, scale 1:100 000. <https://doi.org/10.4095/302754>
- Kiss, F. and Tschirhart, V., 2017j. First vertical derivative of the magnetic field, aeromagnetic survey of the Marguerite River area, Saskatchewan, parts of NTS 74-K south; Geological Survey of Canada, Open File 8268, 1 sheet, scale 1:100 000. <https://doi.org/10.4095/302755>
- Kiss, F. and Tschirhart, V., 2017k. Tilt angle of the magnetic field, aeromagnetic survey of the Marguerite River area, Alberta, parts of NTS 74-L north and 74-L south; Geological Survey of Canada, Open File 8269, 1 sheet, scale 1:100 000. <https://doi.org/10.4095/302756>
- Kiss, F. and Tschirhart, V., 2017l. Tilt angle of the magnetic field, aeromagnetic survey of the Marguerite River area, Alberta, parts of NTS 74-E north and 74-E south; Geological Survey of Canada, Open File 8270, 1 sheet, scale 1:100 000. <https://doi.org/10.4095/302757>
- Kiss, F. and Tschirhart, V., 2017m. Tilt angle of the magnetic field, aeromagnetic survey of the Marguerite River area, Saskatchewan, parts of NTS 74-F south; Geological Survey of Canada, Open File 8271, 1 sheet, scale 1:100 000. <https://doi.org/10.4095/302758>
- Kiss, F. and Tschirhart, V., 2017n. Tilt angle of the magnetic field, aeromagnetic survey of the Marguerite River area, Saskatchewan, parts of NTS 74-F north; Geological Survey of Canada, Open File 8272, 1 sheet, scale 1:100 000. <https://doi.org/10.4095/302759>
- Kiss, F. and Tschirhart, V., 2017o. Tilt angle of the magnetic field, aeromagnetic survey of the Marguerite River area, Saskatchewan, parts of NTS 74-K south; Geological Survey of Canada, Open File 8273, 1 sheet, scale 1:100 000. <https://doi.org/10.4095/302760>
- LaFlamme, C., McFarlane, C.R.M., Corrigan, D., and Wodicka, N., 2014. Origin and tectonometamorphic history of the Repulse Bay block, Melville Peninsula, Nunavut: exotic terrane or deeper level of the Rae craton; *Canadian Journal of Earth Sciences*, v. 51, p. 1097–1122. <https://doi.org/10.1139/cjes-2014-0040>
- LaFlamme, C., McFarlane, C.R.M., Fisher, C.M., and Kirkland, C.L., 2017. Multi-mineral geochronology: insights into crustal behaviour during exhumation of an orogenic root; *Contributions to Mineralogy and Petrology*, v. 172, p. 9. <https://doi.org/10.1007/s00410-017-1331-7>
- Lawley, C.J.M., Creaser, R.A., Jackson, S.E., Yang, Z., Davis, B.J., Pehrsson, S.J., Dube, B., Mercier-Langevin, P., and Vaillancourt, D., 2015. Unraveling the Western Churchill Province Paleoproterozoic gold metallogeny: constraints from Re-Os arsenopyrite and U-Pb xenotime geochronology and LA-ICP-MS arsenopyrite trace element chemistry at the BIF-hosted Meliadine gold district, Nunavut, Canada; *Economic Geology and the Bulletin of the Society of Economic Geologists*, v. 110, p. 1425–1454. <https://doi.org/10.2113/econgeo.110.6.1425>
- Lawley, C.J.M., McNicoll, V., Sandeman, H., Pehrsson, S., Simard, M., Castonguay, S., Mercier-Langevin, P., and Dubé, B., 2016. Age and geological setting of the Rankin Inlet greenstone belt and its relationship to the gold endowment of the Meliadine gold district Nunavut, Canada; *Precambrian Research*, v. 275, p. 471–495. <https://doi.org/10.1016/j.precamres.2016.01.008>

- Liddell, M.V., Bastow, I., Rawlinson, N., Darbyshire, F., Gilligan, A., and Watson, E., 2018. Precambrian plate tectonics in northern Hudson Bay: evidence from P and S wave seismic tomography and analysis of source side effects in relative arrival-time data sets; *Journal of Geophysical Research. Solid Earth*, v. 123, issue 7, p. 5690–5709. <https://doi.org/10.1029/2018JB015473>
- Liu, J., Riches, A.J.V., Pearson, D.G., Luo, Y., Kienlen, B., Kjarsgaard, B.A., Stachel, T., and Armstrong, J.P., 2016. Age and evolution of the deep continental root beneath the central Rae craton, northern Canada; *Precambrian Research*, v. 272, p. 168–184. <https://doi.org/10.1016/j.precamres.2015.11.001>
- Ma, S., 2018. Structural style and timing and deformation on the Bathurst fault in the eastern Slave craton, western Nunavut, Canada; M.Sc. thesis, Queen's University, Kingston, 255 p.
- Ma, S.M., Kellett, D.A., Godin, L., and Jercinovic, M.J., 2020. Localisation of the brittle Bathurst fault on pre-existing fabrics: a case for structural inheritance in the northeastern Slave craton, western Nunavut, Canada; *Canadian Journal of Earth Sciences* June 2020, v. 57, no. 6. <https://doi.org/10.1139/cjes-2019-0100>
- Mahan, K.H. and Williams, M.L., 2005. Reconstruction of a large deep-crustal terrane: implications for the Snowbird tectonic zone and early growth of Laurentia; *Geology*, v. 33, p. 385–388. <https://doi.org/10.1130/G21273.1>
- Martel, E., Pehrsson, S.J., Percival, J., Acosta-Góngora, P., Thiessen, E., Regis, D., Jamieson, D., Neil, B., and Knox, B., 2018. Geology and mineral potential of the southern Rae Craton, Northwest Territories, NTS 75-G and H; Geological Survey of Canada, Open File 8194, 1 poster. <https://doi.org/10.4095/306542>
- McCurdy, M.W., Berman, R.G., Kerr, D.E., and Vaive, J.E., 2013. Geochemical, mineralogical and kimberlite indicator mineral data for silts, heavy mineral concentrates and waters, Duggan Lake area, Nunavut (NTS 76-H and 76-I South); Geological Survey of Canada, Open File 7471, 22 p. <https://doi.org/10.4095/293044>
- McCurdy, M.W., Pehrsson, S.J., Falck, H., Day, S.J.A., and Campbell, J.E., 2016. Geochemical data for lake sediments and surface waters, Abitau Lake area, Northwest Territories (NTS 75-B); Geological Survey of Canada, Open File 8082, 19 p. <https://doi.org/10.4095/299389>
- McMartin, I., Randour, I., and Wodicka, N., 2019. Till composition across the Keewatin Ice Divide in the Tehery-Wager GEM-2 Rae project area, Nunavut; Geological Survey of Canada, Open File 8563, 42 p. <https://doi.org/10.4095/314707>
- Mills, A., Berman, R.G., Davis, W.J., Tella, S., Carr, S.D., Roddick, C., and Hanmer, S., 2007. Thermobarometry and geochronology of the Uvauk Complex: a polymetamorphic Neoproterozoic and Paleoproterozoic segment of the Snowbird tectonic zone, Nunavut, Canada; *Canadian Journal of Earth Sciences*, v. 44, no. 2, p. 245–266. <https://doi.org/10.1139/e06-080>
- Mowbray, B. and Pehrsson, S.J., 2019. Geochemistry, petrology, and aeromagnetic mapping of the Orpheus dykes, South Rae craton, Northwest Territories; Geological Survey of Canada, Open File 8340, 28 p. <https://doi.org/10.4095/311306>
- Overton, A., 1979. Seismic reconnaissance survey of the Dubawnt Group, districts of Keewatin and Mackenzie; *in* Current research, Part B, Geological Survey of Canada, Paper 79-1B, p. 397–400. <https://doi.org/10.4095/105448>
- Partin, C.A., Bekker, A., Corrigan, D., Modeland, S., Francis, D., and Davis, D.W., 2014. Sedimentological and geochemical basin analysis of the Paleoproterozoic Penrhyn and Piling groups of Arctic Canada; *Precambrian Research*, v. 251, p. 80–101. <https://doi.org/10.1016/j.precamres.2014.06.010>
- Patterson, J.G., 1986. The Amer Belt: remnant of an Aphebian foreland fold and thrust belt; *Canadian Journal of Earth Sciences*, v. 23, p. 2012–2023. <https://doi.org/10.1139/e86-186>
- Pehrsson, S.J., Berman, R.G., and Davis, W.J., 2013. Paleoproterozoic orogenesis during Nuna aggregation: a case study of reworking of the Rae craton, Woodburn Lake, Nunavut; *Precambrian Research*, v. 232, p. 167–188. <https://doi.org/10.1016/j.precamres.2013.02.010>
- Pehrsson, S.J., Coyle, M., and Berman, R., 2014a. The GEM Chesterfield gold project: understanding controls on western Churchill gold endowment from the bottom up; Geological Survey of Canada, Open File 7490, 31 p. <https://doi.org/10.4095/293763>
- Pehrsson, S.J., Currie, M., Ashton, K.E., Harper, C.T., Paul, D., Pana, D., Berman, R.G., Bostock, H., Corkery, T., Jefferson, C.W., and Tella, S., 2014b. Bedrock geology compilation south Rae and western Hearne provinces, Churchill Province, Northwest Territories, Saskatchewan, Nunavut, Manitoba, and Alberta; Geological Survey of Canada, Open File 5744, scale 1:550 000. <https://doi.org/10.4095/292232>
- Pehrsson, S.J., Campbell, J.E., Martel, E., McCurdy, M.W., Acosta-Gongora, P., Thiessen, E., Jamieson, D., Lauzon, G., Buller, G., Falck, H., and Dyke, A.S., 2015. Report of 2015 activities for the geologic and metallogenic framework of the south Rae Craton, southeast Northwest Territories: GEM 2 south Rae Quaternary and Bedrock project; Geological Survey of Canada, Open File 7958, 24 p. <https://doi.org/10.4095/297387>
- Percival, J.A. and Tschirhart, V., 2017. Trans-Hudsonian far-field deformation effects in the Rae foreland: an integrated geological-3D magnetic model; *Tectonophysics*, v. 699, p. 82–92. <https://doi.org/10.1016/j.tecto.2017.01.021>
- Percival, J.A., Tschirhart, V., Ford, A., and Dziawa, C., 2015. Report of field activities for the geology and mineral potential of the Chantrey-Thelon area: GEM-2 Montresor project; Geological Survey of Canada, Open File 7707, 15 p. <https://doi.org/10.4095/295673>
- Percival, J.A., Martel, E., Pehrsson, S.J., Acosta-Gongora, P., Regis, D., Thiessen, E., Jamieson, D., Neil, B., and Knox, B., 2016. Report of 2016 bedrock activities for the geologic and metallogenic framework of the south Rae Craton, southeast NWT: GEM 2 South Rae Quaternary and Bedrock project; Geological Survey of Canada, Open File 8142, 17 p. <https://doi.org/10.4095/299469>
- Percival, J.A., Davis, W.J., and Hamilton, M.A., 2017. U-Pb zircon geochronology and depositional history of the Montresor group, Rae Province, Nunavut, Canada; *Canadian Journal of Earth Sciences*, v. 54, p. 512–528. <https://doi.org/10.1139/cjes-2016-0170>

- Peterson, T.D., Van Breeman, O., Sandeman, H., and Cousens, B., 2002. Proterozoic (1.85–1.75 Ga) igneous suites of the Western Churchill Province: granitoid and ultrapotassic magmatism in a reworked Archean hinterland; *Precambrian Research*, v. 119, p. 73–100. [https://doi.org/10.1016/S0301-9268\(02\)00118-3](https://doi.org/10.1016/S0301-9268(02)00118-3)
- Peterson, T.D., Pehrsson, S.J., Skulski, T., and Sandeman, H., 2010. Compilation of Sm-Nd isotope analyses of igneous suites, western Churchill Province; Geological Survey of Canada, Open File 6439, 18 p. <https://doi.org/10.4095/285360>
- Peterson, T.D., Jefferson, C.W., and Anand, A., 2015a. Geological setting and geochemistry of the ca. 2.6 Ga Snow Island Suite in the central Rae Domain of the Western Churchill Province, Nunavut; Geological Survey of Canada, Open File 7841, 29 p. <https://doi.org/10.4095/296599>
- Peterson, T.D., Scott, J.M.J., LeCheminant, A.N., Tschirhart, V.L., Chorlton, L.B., Davis, W.J., and Hamilton, M.A., 2015b. Nueltin granites and mafic rocks in the Tebesjuak Lake map area, Nunavut: new geochronological, petrological, and geophysical data; Geological Survey of Canada, Current Research 2015-5, 23 p. <https://doi.org/10.4095/296163>
- Peterson, T.D., Scott, J.M.J., LeCheminant, A.N., Jefferson, C.W., and Pehrsson, S.J., 2015c. The Kivalliq Igneous Suite: anorogenic bimodal magmatism at 1.75 Ga in the western Churchill Province, Canada; *Precambrian Research*, v. 262, p. 101–119. <https://doi.org/10.1016/j.precamres.2015.02.019>
- Pilkington, M., Miles, W., Ross, G., and Roest, W.R., 2000. Potential-field signatures of buried Precambrian basement in the Western Canada Sedimentary Basin; *Canadian Journal of Earth Sciences*, v. 37, p. 1453–1471. <https://doi.org/10.1139/e00-020>
- Potter, E.G., Tschirhart, V., Powell, J.W., Kelly, C.J., Rabiei, M., Johnstone, D., Craven, J.A., Davis, W.J., Pehrsson, S., Mount, S.M., Chi, G., and Bethune, K.M., 2020. Targeted Geoscience Initiative 5: integrated multidisciplinary studies of unconformity-related uranium deposits from the Patterson Lake corridor, northern Saskatchewan; Geological Survey of Canada, Bulletin 615, 37 p. <https://doi.org/10.4095/326040>
- Rainbird, R.H., Hadlari, T., Aspler, L.B., Donaldson, J.A., LeCheminant, A.N., and Peterson, T.D., 2003. Sequence stratigraphy and evolution of the paleoproterozoic intracontinental Baker Lake and Thelon basins, western Churchill Province, Nunavut, Canada; *Precambrian Research*, v. 125, p. 21–53. [https://doi.org/10.1016/S0301-9268\(03\)00076-7](https://doi.org/10.1016/S0301-9268(03)00076-7)
- Rainbird, R.H., Davis, W.J., Pehrsson, S., Wodicka, N., Rayner, N., and Skulski, T., 2010. Early Paleoproterozoic supracrustal assemblages of the Rae domain, Nunavut, Canada: intracratonic basin development during supercontinent break-up and assembly; *Precambrian Research*, v. 181, p. 167–186. <https://doi.org/10.1016/j.precamres.2010.06.005>
- Ramaekers, P., Jefferson, C.W., Yeo, G.M., Collier, B., Long, D.G.F., Drever, G., McHardy, S., Jiricka, D., Cutts, C., Wheatley, K., Catuneanu, O., Bernier, S., Kupsch, B., and Post, R.T., 2007. Revised geological map and stratigraphy of the Athabasca group, Saskatchewan and Alberta; in EXTECH IV: Geology and Uranium EXploration TECHnology of the Proterozoic Athabasca Basin, Saskatchewan and Alberta, (ed.) C.W. Jefferson and G. Delaney; Geological Survey of Canada, Bulletin 588, p. 155–191. <https://doi.org/10.4095/223754>
- Regis, D., Martel, E., Davis, W.J., and Pehrsson, S.J., 2017. U-Pb zircon geochronology of metaplutonic rocks across the southern Rae province, Northwest Territories; Geological Survey of Canada, Open File 8254, 37 p. <https://doi.org/10.4095/302772>
- Regis, D., Davis, W.J., Ryan, J.J., Berman, R.G., Pehrsson, S., Joyce, N.L., and Sandeman, H.A., 2019. Multiple burial–exhumation episodes revealed by accessory phases in high-pressure granulite-facies rocks (Rae craton, Nunavut, Canada); *Contributions to Mineralogy and Petrology*, v. 174, p. 41. <https://doi.org/10.1007/s00410-019-1572-8>
- Regis, D., Pehrsson, S.J., Martel, E., Thiessen, E., Peterson, T., and Kellett, D., 2021. Post-1.9 Ga evolution of the south Rae craton (Northwest Territories, Canada): A Paleoproterozoic orogenic collapse system; *Precambrian Research*, v. 355, article 106105. <https://doi.org/10.1016/j.precamres.2021.106105>
- Roberts, B., Craven, J.A., Berman, R.G., and Roots, E., 2015. Preliminary results of a Magnetotelluric survey in the Chantrey-Thelon area; GEM-2 Thelon tectonic zone project; Geological Survey of Canada, Open File 7931, 29 p. <https://doi.org/10.4095/297426>
- Ross, G.M., 2002. Evolution of Precambrian continental lithosphere in Western Canada: results from Lithoprobe studies in Alberta and beyond; *Canadian Journal of Earth Sciences*, v. 39, p. 413–437. <https://doi.org/10.1139/e02-012>
- Sanborn-Barrie, M., Carr, S.D., and Theriault, R., 2001. Geochronological constraints on metamorphism, magmatism and exhumation of deep-crustal rocks of the Kramanitaur Complex, with implications for the Paleoproterozoic evolution of the Archean western Churchill Province, Canada; *Contributions to Mineralogy and Petrology*, v. 141, p. 592–612. <https://doi.org/10.1007/s004100100262>
- Sanborn-Barrie, M., Davis, W.J., Berman, R.G., Rayner, N., Skulski, T., and Sandeman, H., 2014a. Neoproterozoic continental crust formation and Paleoproterozoic deformation of the central Rae craton, Committee Bay belt, Nunavut; *Canadian Journal of Earth Sciences*, v. 51, p. 635–667. <https://doi.org/10.1139/cjes-2014-0010>
- Sanborn-Barrie, M., Chakungal, J., James, D.T., Rayner, N., and Whalen, J.B., 2014b. Precambrian bedrock geology, Southampton Island, Nunavut; Geological Survey of Canada, Canadian Geoscience Map 132, scale 1:250 000. <https://doi.org/10.4095/293328>
- Sanborn-Barrie, M., Regis, D., Ford, A., Osinchuk, A., and Drayson, D., 2018. Report of activities for the GEM-2 Boothia Peninsula–Somerset Island Project: integrated geoscience of the Northwest Passage, Nunavut; Geological Survey of Canada, Open File 8339, 16 p. <https://doi.org/10.4095/306597>
- Sanborn-Barrie, M., Regis, D., and Ford, A., 2019a. Integrated Geoscience of the Northwest Passage, Nunavut; GEM-2 Boothia Peninsula–Somerset Island Project, report of activities 2018; Geological Survey of Canada, Open File 8557, 17 p. <https://doi.org/10.4095/314501>
- Sanborn-Barrie, M., Camacho, A., and Berman, R., 2019b. High-pressure, ultrahigh-temperature 1.9 Ga metamorphism of the Kramanitaur Complex, Snowbird Tectonic Zone, Rae Craton; *Contributions to Mineralogy and Petrology*, v. 174, no. 14, 26 p. <https://doi.org/10.1007/s00410-019-1547-9>

- Sandeman, H.A., Davis, W.J., Hanmer, S., Tella, S., Ryan, J.J., and Armitage, A., 2006. Petrogenesis of Neoproterozoic volcanic rocks of the MacQuoid supracrustal belt: back-arc setting for the northwestern Hearne subdomain, western Churchill Province, Canada; *Precambrian Research*, v. 144, p. 140–165. <https://doi.org/10.1016/j.precamres.2005.11.001>
- Schultz, M., Chacko, T., Heaman, L.M., Sandeman, H., Simonetti, A., and Creaser, R.A., 2007. The Queen Maud Block: a newly recognized Paleoproterozoic (2.4–2.5 Ga) terrane in northwest Laurentia; *Geology*, v. 35, p. 707–710. <https://doi.org/10.1130/G23629A.1>
- Sherlock, R., Pehrsson, S., Logan, A.V., Hrabí, R.B., and Davis, W.J., 2004. Geological setting of the Meadowbank gold deposits, Woodburn Lake Group, Nunavut; *Exploration and Mining Geology*, v. 13, p. 67–107. <https://doi.org/10.2113/gsemg.13.1-4.67>
- Skulski, T., Spratt, J.E., Craven, J.A., Jones, A.G., and Snyder, D.B., 2014. Deep crustal structure of the Rae Craton, mainland Nunavut; *in* Program with Abstracts, Annual Meeting of the Geological Association of Canada–Mineralogical Association of Canada, May 21–23, 2014, Fredericton, New Brunswick, p. 253.
- Skulski, T., Paul, D., Sandeman, H., Berman, R.G., Chorlton, L., Pehrsson, S.J., Rainbird, R.H., Davis, W.J., and Sanborn-Barrie, M., 2018. Bedrock geology, central Rae Craton and eastern Queen Maud Block, western Churchill Province, Nunavut; Geological Survey of Canada, Canadian Geoscience Map 307, scale 1:550 000. <https://doi.org/10.4095/308348>
- Snyder, D.B., Berman, R.G., Kendall, J.-M., and Sanborn-Barrie, M., 2013. Seismic anisotropy and mantle structure of the Rae craton, central Canada, from joint interpretation of SKS splitting and receiver functions; *Precambrian Research*, v. 232, p. 189–208. <https://doi.org/10.1016/j.precamres.2012.03.003>
- Snyder, D.B., Craven, J.A., Pilkington, M., and Hillier, M.J., 2015. The three-dimensional construction of the Rae craton, central Canada; *Geochemistry Geophysics Geosystems*, v. 16, p. 3555–3574. <https://doi.org/10.1002/2015GC005957>
- Spratt, J.E., Snyder, D.B., and Craven, J.A., 2011. A magnetotelluric survey across the Committee Bay belt and Rae craton in the Churchill province of Nunavut; Geological Survey of Canada, Open File 6825, 28 p. <https://doi.org/10.4095/287999>
- Spratt, J.E., Snyder, D.B., and Craven, J.A., 2012a. Magnetotelluric soundings in the Committee Bay Belt, northern Churchill area, Nunavut; Geological Survey of Canada, Open File 7063, 37 p. <https://doi.org/10.4095/289836>
- Spratt, J.E., Craven, J.A., and Sanborn-Barrie, M., 2012b. Southampton Island magnetotelluric survey: data acquisition and preliminary analysis; Geological Survey of Canada, Open File 6988, 39 p. <https://doi.org/10.4095/291384>
- Spratt, J., Jones, A.G., Corrigan, D., and Hogg, C., 2013a. Lithospheric geometry revealed by deep-probing magnetotelluric surveying, Melville Peninsula, Nunavut; Geological Survey of Canada, Current Research 2013-12, 14 p. <https://doi.org/10.4095/292482>
- Spratt, J.E., Roberts, B., Kiyani, D., and Jones, A.G., 2013b. Magnetotelluric Soundings from the Central Rae Domain of the Churchill Province, Nunavut; Geological Survey of Canada, Open File 7323, 34 p. <https://doi.org/10.4095/292237>
- Spratt, J.E., Skulski, T., Craven, J.A., Jones, A.G., Snyder, D.B., and Kiyani, D., 2014. Magnetotelluric investigations of the lithosphere beneath the central Rae craton, mainland Nunavut, Canada; *Journal of Geophysical Research. Solid Earth*, v. 119, p. 2415–2439. <https://doi.org/10.1002/2013JB010221>
- Steenkamp, H.M., Wodicka, N., Lawley, C.J.M., Peterson, T.D., and Guilmette, C., 2015. Overview of bedrock mapping and results from portable X-ray fluorescence spectrometry in the eastern part of the Tehery Lake–Wager Bay area, western Hudson Bay, Nunavut; *in* Summary of Activities 2015; Canada-Nunavut Geoscience Office; p. 121–134.
- Steenkamp, H.M., Wodicka, N., Weller, O.M., and Kendrick, J., 2016. Overview of bedrock mapping in the northern and western parts of the Tehery Lake–Wager Bay area, western Hudson Bay, Nunavut; *in* Summary of Activities 2016; Canada-Nunavut Geoscience Office; p. 27–39.
- Stern, R.A., Card, C.D., Pana, D., and Rayner, N., 2003. SHRIMP U-Pb ages of granitoid basement rocks of the southwestern part of the Athabasca Basin, Saskatchewan and Alberta; Radiogenic Age and Isotopic Studies: Report 16; Geological Survey of Canada, Current Research 2003-F3, 20 p. <https://doi.org/10.4095/214595>
- Tella, S., Paul, D., Berman, R.G., Davis, W.J., Peterson, T.D., Pehrsson, S.J., and Kerswill, J.A., 2007. Bedrock geology compilation and regional synthesis of parts of Hearne and Rae domains, western Churchill Province, Nunavut–Manitoba; Geological Survey of Canada, Open File 5441, 3 sheets. <https://doi.org/10.4095/224573>
- Therriault, I., Steenkamp, H.M., and Larson, K.P., 2017. New mapping and initial structural characterization of the Wager shear zone, north-western Hudson Bay, Nunavut; Summary of Activities 2017, Canada-Nunavut Geoscience Office, p. 1–12.
- Thiessen, E.J., Gibson, H.D., Regis, D., and Pehrsson, S.J., 2018. Deformation and extensional exhumation of 1.9 Ga high-pressure granulites along the Wholdaia Lake shear zone, south Rae craton, Northwest Territories, Canada; *Lithosphere*, v. 10, p. 641–661. <https://doi.org/10.1130/L704.1>
- Thiessen, E.J., Gibson, H.D., Regis, D., Pehrsson, S.J., Ashley, K.T., and Smit, M.A., 2020. The distinct metamorphic stages and structural styles of the 1.94–1.86 Ga Snowbird Orogen, Northwest Territories, Canada; *Journal of Metamorphic Geology*, v. 38, issue 9, p. 963–992. <https://doi.org/10.1111/jmg.12556>
- Thomas, M.D., 2012. Shallow crustal structure in the Meadowbank River–Tehek Lake area: insights from gravity and magnetic modelling; Geological Survey of Canada, Open File 7308, 42 p. <https://doi.org/10.4095/292157>
- Thompson, P.H., 1989. An empirical model for metamorphic evolution of the Archaean Slave Province and Adjacent Thelon Tectonic Zone, north-western Canadian Shield; *in* Evolution of Metamorphic Belts, (ed.) J.S. Daly, R.A. Cliff, and B.W.D. Yardley; Geological Society, Special Publication, v. 43, no. 1, p. 245–263. <https://doi.org/10.1144/GSL.SP.1989.043.01.17>

- Tschirhart, V., 2014. Geophysical and geological integration and interpretation of the northeast Thelon Basin, Nunavut; Ph.D. thesis, McMaster University, Hamilton, Ontario, 209 p.
- Tschirhart, V. and Pehrsson, S., 2016. New insights from geophysical data on the regional structure and geometry of the southwest Thelon Basin and its basement, Northwest Territories, Canada; *Geophysics*, v. 81, p. B167–B178. <https://doi.org/10.1190/geo2015-0586.1>
- Tschirhart, V., Morris, W.A., and Oneschuk, D., 2011. Geophysical series, geophysical compilation project, Thelon Basin, Nunavut, NTS 66A, B, and parts of 65N, O, P, 66C, F, G and H.; Geological Survey of Canada, Open File 6944, scale 1:300 000. <https://doi.org/10.4095/288806>.
- Tschirhart, P.A., Morris, W.A., and Jefferson, C.W., 2013a. Geophysical modeling of the Neoproterozoic Woodburn Lake and Paleoproterozoic Ketyet River groups, and plutonic rocks in central Schultz Lake map area, Nunavut; Geological Survey of Canada, Current Research 2013-2, 19 p. <https://doi.org/10.4095/292116>
- Tschirhart, V., Morris, W.A., and Jefferson, C.W., 2013b. Framework geophysical modelling of granitoid vs. supracrustal basement to the northeast Thelon Basin around the Kiggavik uranium camp, Nunavut; *Canadian Journal of Earth Sciences*, v. 50, p. 667–677. <https://doi.org/10.1139/cjes-2012-0149>
- Tschirhart, V., Morris, W.A., and Jefferson, C.W., 2013c. Faults affecting northeast Thelon Basin: improved basement constraints from source edge processing of aeromagnetic data; *in* Uranium in Canada: Geological Environments and Exploration Developments, (ed.) E. Potter, D. Quirt, and C.W. Jefferson; Canadian Institute of Mining, Metallurgy and Petroleum, Special Issue 21, p. 105–113.
- Tschirhart, V., Morris, W.A., Jefferson, C.W., Keating, P., White, J.C., and Calhoun, L., 2013d. 3D geophysical inversions of the north-east Amer Belt and their relationship to the geologic structure; *Geophysical Prospecting*, v. 61, p. 547–560. <https://doi.org/10.1111/j.1365-2478.2012.01098.x>
- Tschirhart, V., Morris, W.A., and Jefferson, C.W., 2014. Unconformity surface architecture of the northeast Thelon Basin, Nunavut, derived from integration of magnetic source depth estimates; *Interpretation (Tulsa)*, v. 2, p. SJ117–SJ132. <https://doi.org/10.1190/INT-2014-0001.1>
- Tschirhart, V., Percival, J.A., and Jefferson, C.W., 2015. Geophysical models of the Montesor metasedimentary belt and its environs, central Nunavut, Canada; *Canadian Journal of Earth Sciences*, v. 52, p. 833–845. <https://doi.org/10.1139/cjes-2015-0008>
- Tschirhart, V.L., Wodicka, N., and Steenkamp, H., 2016. Shallow crustal structure of the Tehery Lake–Wager Bay area, western Hudson Bay, Nunavut, from potential-field datasets; *in* Summary of Activities 2016, Canada-Nunavut Geoscience Office, p. 41–50.
- Tschirhart, V., Jefferson, C.W., and Morris, W.A., 2017. Basement geology beneath the northeast Thelon Basin, Nunavut: insights from integrating new gravity, magnetic and geological data; *Geophysical Prospecting*, v. 65, p. 617–636. <https://doi.org/10.1111/1365-2478.12430>
- Tschirhart, V., Craven, J., Potter, E., Powell, J., Pehrsson, S., and McEwan, B., 2019. Preliminary modelling of MT data in the Patterson Lake corridor, Saskatchewan, Canada; 16th Biennial South African Geophysical Association Conference & Exhibition, October 6–9, 2019, Durban, South Africa, extended abstracts, 3 p.
- Tschirhart, V., Pehrsson, S., Card, C., Potter, E., Powell, J., and Pană, D., 2021. Interpretation of buried basement in the southwestern Athabasca Basin, Canada, from integrated geophysical and geological datasets; *Geochemistry: Exploration, Environment, Analysis*, v. 21, no. 1. <https://doi.org/10.1144/geochem2019-061>
- van Breemen, O., Peterson, T.D., and Sandeman, H.A., 2005. U–Pb zircon geochronology and Nd isotope geochemistry of Proterozoic granitoids in the western Churchill Province: intrusive age pattern and Archean source domains; *Canadian Journal of Earth Sciences*, v. 42, p. 339–377. <https://doi.org/10.1139/e05-007>
- Walcott, R.I. and Boyd, J.B., 1971. The gravity field of northern Alberta, and part of the Northwest Territories and Saskatchewan; Geological Survey of Canada, Gravity Map Series No. 103–111, Ottawa, Ontario, 13 p. <https://doi.org/10.4095/8461>
- Whalen, J.B., Berman, R.G., Davis, W.J., Sanborn-Barrie, M., and Nadeau, L., 2018. Bedrock geochemistry of the Thelon tectonic zone, Nunavut; Geological Survey of Canada, Open File 8234, 49 p. <https://doi.org/10.4095/306385>
- Wheeler, J.O., Hoffman, P.F., Card, K.D., Davidson, A., Sanford, B.V., Okulitch, A.V., and Roest, W.R., 1996. Geological map of Canada / Carte géologique du Canada; Geological Survey of Canada, Map 1860A, 3 sheets, scale 1:5 000 000. <https://doi.org/10.4095/208175>
- Wodicka, N., St-Onge, M.R., Corrigan, D., Scvott, D.J., and Whalen, J.B., 2014. Did a proto-ocean basin form along the southeastern Rae cratonic margin? Evidence from U-Pb geochronology, geochemistry (Sm-Nd and whole-rock), and stratigraphy of the Paleoproterozoic Piling Group, northern Canada; *Bulletin of the Geological Society of America*, v. 126, p. 1625–1653. <https://doi.org/10.1130/B31028.1>
- Wodicka, N., Steenkamp, H.M., Weller, O.M., Kendrick, J., Tschirhart, V.L., Peterson, T.D., and Girard, É., 2016. Report of 2016 activities for the bedrock geology and economic potential of the Tehery-Wager area: GEM 2 Rae project; Geological Survey of Canada, Open File 8149, 21 p. <https://doi.org/10.4095/299392>
- Wodicka, N., Steenkamp, H.M., Peterson, T.D., McMartin, I., Day, S.J.A., and Tschirhart, V.L., 2017. Report of 2017 activities for the geology and economic potential of the Tehery-Wager area, Nunavut: GEM-2 Rae project; Geological Survey of Canada, Open File 8318, 20 p. <https://doi.org/10.4095/305979>

Summary of GEM results: Manitoba Far North Geomapping Initiative

C.O. Böhm^{1,2*} and N.M. Rayner³

Böhm, C.O. and Rayner, N.M., 2024. Summary of GEM results: Manitoba Far North Geomapping Initiative; in Canada's northern shield: new perspectives from the Geo-mapping for Energy and Minerals program, (ed.) S.J. Pehrsson, N. Wodicka, N. Rogers, and J.A. Percival; Geological Survey of Canada, Bulletin 612, p. 327–334. <https://doi.org/10.4095/332503>

Abstract: The far north of Manitoba is endowed with potential for base and precious metals, diamonds, uranium, and rare metals. The goal of a collaborative project between the Manitoba Geological Survey and the Geological Survey of Canada was to provide an advanced framework of geoscience knowledge for mineral exploration and land-use management.

Bedrock mapping, geophysical surveys, and geochemical and geochronological analyses carried out in 2005 to 2011 in the far north of Manitoba showed diverse and complex rocks that record nearly two billion years of Earth history. Key advancements in understanding include a new stratigraphy and chronology of at least four metasedimentary cover sequences in the Seal River Domain, some with high potential for economic uranium, gold, and/or rare-metal mineralization; and the identification of a Neoproterozoic greenstone belt in the Great Island area with known gold occurrences. The discovery of remnants of ancient (3.5 Ga) cratonic lithosphere in the Seal River area also renders the region favourable for diamond exploration.

Résumé : Le grand nord du Manitoba est doté d'un potentiel en métaux communs et précieux, en diamants, en uranium et en métaux rares. L'objectif d'un projet de collaboration entre les Levés géologiques du Manitoba et la Commission géologique du Canada était de fournir un cadre avancé de connaissances géoscientifiques pour l'exploration minérale et la gestion de l'utilisation des terres.

La cartographie du substratum rocheux, les levés géophysiques ainsi que les analyses géochronologiques et géochimiques effectués de 2005 à 2011 dans le grand nord du Manitoba ont révélé des roches diverses et complexes qui témoignent de près de deux milliards d'années de l'histoire de la Terre. Les principales avancées dans nos connaissances comprennent une nouvelle interprétation de la stratigraphie et de la chronologie d'au moins quatre séquences métasédimentaires de couverture dans le domaine de Seal River, dont certaines présentent un fort potentiel en minéralisations économiques d'uranium, d'or ou de métaux rares; et l'identification d'une ceinture de roches vertes du Néoproterozoïque dans la région de l'île Great, qui renferme des indices d'or connus. La découverte de vestiges d'une lithosphère cratonique ancienne (3,5 Ga) dans le secteur de la rivière Seal rend également la région favorable à l'exploration diamantifère.

¹Manitoba Geological Survey, 360-1395 Ellice Avenue, Winnipeg, Manitoba R3G 3P2

²Present address: 871 Grosvenor Avenue, Winnipeg, Manitoba R3M 0M4

³Geological Survey of Canada, 601 Booth Street, Ottawa, Ontario K1A 0E8

*Corresponding author: C.O. Böhm (email: chris.bohm@gmail.com)

INTRODUCTION

The aim of the Manitoba Geological Survey (MGS) Far North Geomapping Initiative (2008–2011) was to further the understanding of the nature, evolution, and mineral potential of the southeast margin of the Archean Hearne Craton, one of the fundamental geological building blocks of Manitoba’s Precambrian shield (Fig. 1, inset). This contribution summarizes key findings and outputs from the Far North initiative with a consolidated list of references.

In support of this MGS initiative, a Geological Survey of Canada (GSC)–funded aeromagnetic and gamma-ray spectrometric geophysical survey of the Great Island–Seal River area was flown in 2008 (Fortin et al., 2009a, b, c, d, e, f, g, h, i, j, k, l), which revealed first-order crustal features such as supracrustal basins, tectonic fabrics and structures, granitoid

domains, regional unconformities, major shear and fault structures, and regional dyke swarms. Subsequently, the Seal River Domain was the focus of fieldwork in 2009 (Anderson et al., 2009a, b) and 2010, with additional expansion into the Nejanilini Domain to the north in 2010 (Anderson et al., 2010a, b).

Follow-up mapping of the Hearne Craton margin in northwestern Manitoba was conducted in 2010 and 2011 in the Misty and Snyder lakes areas, respectively (Kremer et al., 2010a, b, 2011, 2021a, b; Fig. 1; Kremer and Böhm, 2011).

Earlier mapping supported by geochemical and geochronological analyses in Manitoba’s far north, at Nejanilini Lake in 2005 (Böhm et al., 2004; Anderson and Böhm, 2005; Anderson et al., 2005; NL 2005 in Fig. 1) and at Kasmere and Putahow lakes in 2006 (Anderson and Böhm, 2006;

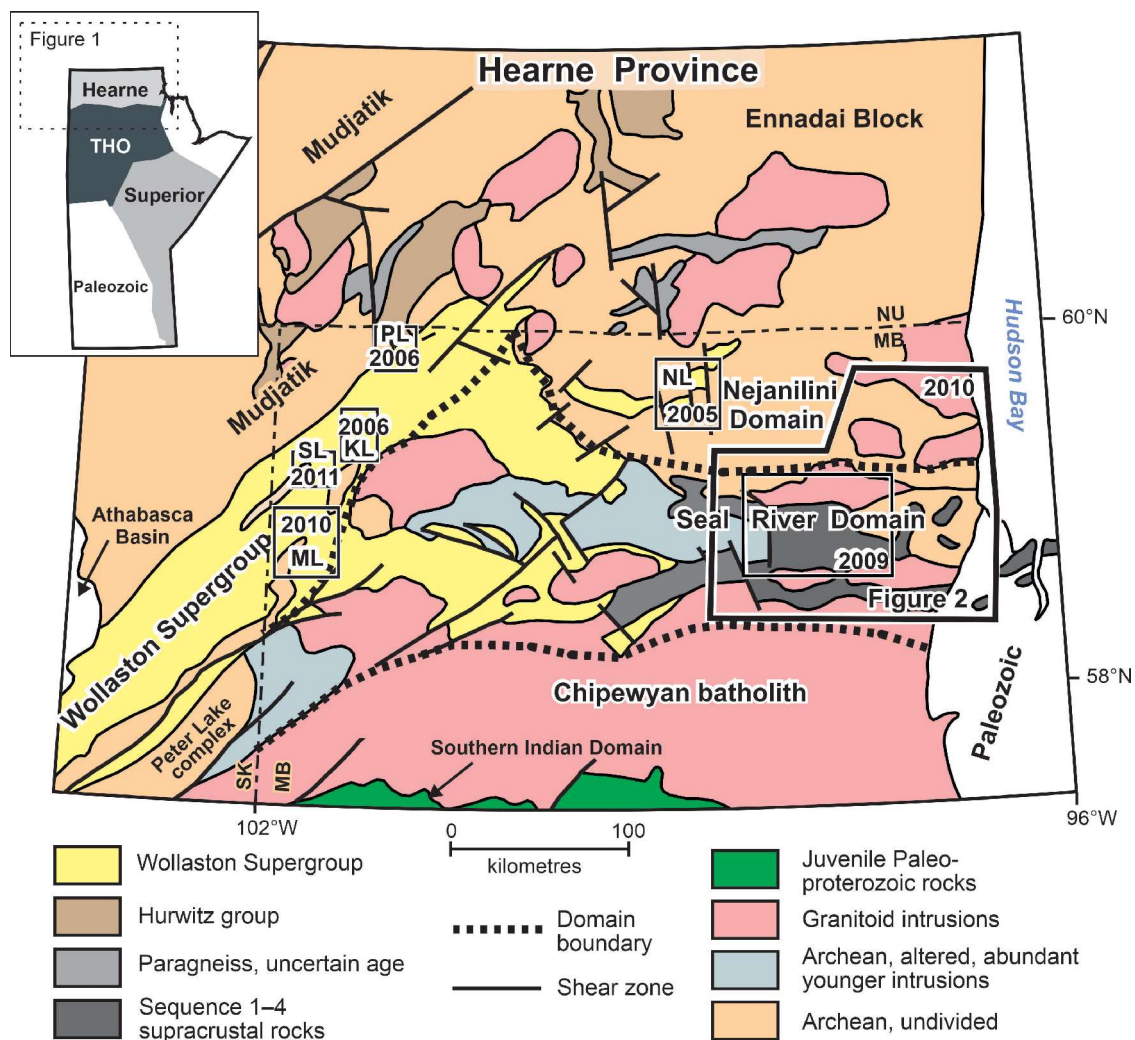


Figure 1. Geological domains of northern Manitoba (MB), northeast Saskatchewan (SK), and southeast Nunavut (NU) showing the areas covered by the projects discussed in this report. KL = Kasmere Lake, ML = Misty Lake, NL = Nejanilini Lake, PL = Putahow Lake, SL = Snyder Lake. Inset: simplified tectonic elements of Manitoba. THO = Trans-Hudson Orogen.

Böhm and Anderson, 2006a, b; KL and PL in Fig. 1) contributed regional tectonostratigraphic data and knowledge that allowed correlations across the Hearne Craton from Saskatchewan into Nunavut (Fig. 1) as part of this GEM (Geo-mapping for Energy and Minerals) initiative.

LITHOTECTONIC DOMAINS OF NORTHERN MANITOBA

Northern Manitoba exposes the southern extent of the Hearne Craton margin (Fig. 1). The northeast has been subdivided into two domains: Nejanilini Domain, which is dominated by metaplutonic granulite rocks with minor enclaves of high-grade metasedimentary rocks; and the Seal River Domain, with characteristic sequence of metasedimentary units of generally lower metamorphic grade. The northwest is divided into the Mudjatik Domain, where Archean basement of Hearne Craton is dominant; and the Wollaston Domain, where a large amount of Paleoproterozoic passive margin cover material is preserved.

Seal River Domain

In the Seal River Domain, integration of geophysics, mapping, geochemistry, and geochronology has led to identification of the following lithotectonic components (Anderson and Böhm, 2008; Anderson et al., 2010a; Rayner, 2010a, b, 2022; Böhm et al., 2020a, b; Fig. 2):

- Precursors to the Hearne Craton include 3493 ± 4 Ma tonalite, the oldest known rock in Manitoba, as well as 2901 Ma orthogneiss. A 2680 Ma granodiorite is consistent with Hearne Craton crust.
- Arc and back-arc metavolcanic and metasedimentary rocks dated at 2.7 to 2.6 Ga (Sosnowski Lake assemblage).
- A fluvial–alluvial ‘successor’ basin (sequence 1) deposited after 2695 Ma (youngest detrital zircon) prospective for U–Au paleoplacer deposits. Sequence 1 lies above an unconformity that separates it from metavolcanic, intrusive, and siliciclastic rocks older than 2.68 Ga.
- Extensive Neoproterozoic (2570–2550 Ma) plutonic rocks that are variably foliated and locally gneissic, particularly in the east.
- The presence of thick and ancient continental crust along with long-lived deep-seated faults is favourable for the formation of diamonds, whereas the presence of low-grade Paleoproterozoic cover indicates minimal post-Archean erosion and thus better likelihood of their preservation.
- A passive margin–continental rift assemblage (sequence 2) with a lithological association and relative age relationships that reflect extension and rifting of the Hearne Craton

sometime after 2.5 Ga. Given the lithologies and the tectonic setting, the Seal River Domain may be favourable for sedimentary exhalative (SEDEX)–type deposits.

- Marine deltaic rocks (sequence 3) preserved as prominent synclinal basins are a defining characteristic of the Seal River Domain and the southern margin of the Hearne Craton in Manitoba. Detrital zircon analysis indicates a maximum depositional age of 2049 ± 19 Ma at the base of sequence 3 and a slightly younger maximum depositional age of 1984 ± 14 Ma higher in the section.
- Peraluminous two-mica granitic rocks are intrusive into sedimentary cover rocks of sequences 1, 2, and 3, but not the youngest sedimentary rocks of sequence 4. This observation, along with an abrupt decrease in the amplitude of upright folds across the contact of sequences 3 and 4, coupled with local angular discordance, indicates an angular unconformity (Anderson et al., 2010a, b). The detrital zircon population of a sample of coarse lithic greywacke from sequence 4 provides a maximum depositional age of 1879 ± 19 Ma; however, a U–Pb monazite date from a two-mica granite that cuts sequence 2 yielded an age of 1764.9 ± 0.9 Ma, suggesting that sequence 4 rocks could be younger than ca. 1.76 Ga.

Nejanilini Domain

The Nejanilini Domain consists mainly of granitoid orthogneiss that contains enclaves of migmatized supracrustal rocks and is cut by porphyritic granite plutons, late granitoid sheets, and dykes (Anderson et al., 2010a, b). Its southern margin is marked by a zone of greenschist-facies mylonite, up to several kilometres wide, that demarcates the northern limit of the relatively intact basins of supracrustal rocks (Sosnowski Lake assemblage through to sequence 4) that characterize the Seal River Domain.

In the Nejanilini Domain, north of the Gross Lake pluton (Fig. 2) charnockitic gneiss dated by SHRIMP (sensitive high resolution ion microprobe) yielded a crystallization age of 2692.4 ± 8.7 Ma with ca. 3.2 Ga inheritance (Rayner, 2022). Another charnockitic gneiss sample approximately 60 km to the southwest dated by ID-TIMS (isotope dilution thermal ionization mass spectrometry) returned discordant results, with an estimated crystallization age of 2526.5 ± 1.3 Ma, the age of the most concordant fraction (Rayner, 2010a, b). Granulite-facies biotite tonalite gneiss from the Nejanilini Lake area (Fig. 1) yielded a U–Pb zircon crystallization age of ca. 2.70 Ga (C.O. Böhm and S.D. Anderson, unpub. data, 2006), further supporting the presence of Neoproterozoic basement. Zircon analysis of migmatitic greywacke diatexite indicates prominent detrital modes between 2500 Ma and 2300 Ma, with some sporadic younger peaks, and a maximum depositional age of 1985.7 ± 9.8 Ma (Rayner, 2022). Zircon rims dated at 1821 ± 17 Ma are interpreted to represent the age of a metamorphic overprint related to the migmatization event. The youngest dated units in the Nejanilini Domain are

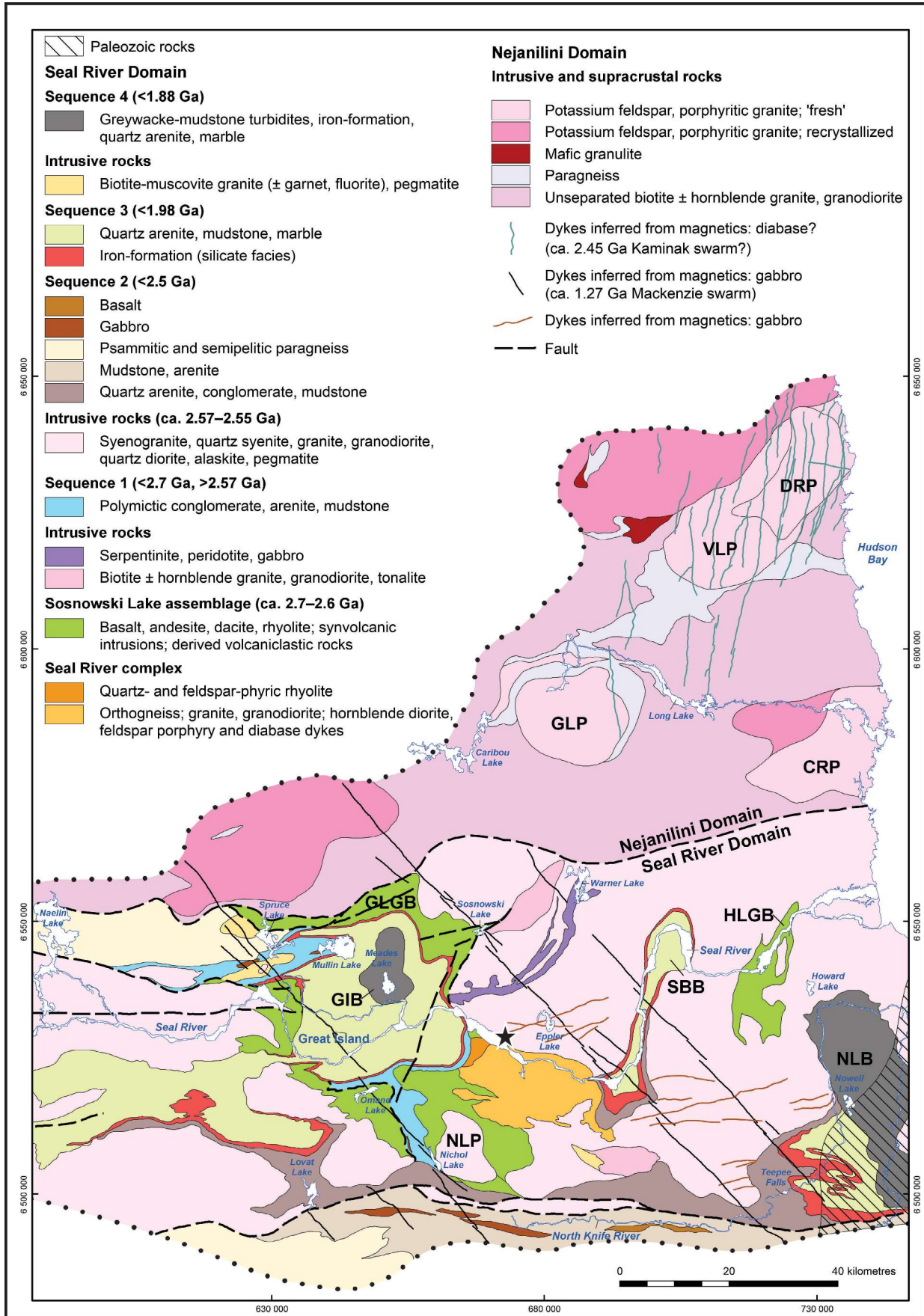


Figure 2. Simplified geological map of the Seal River and Nejanilini domains of northeast Manitoba. *Modified from Anderson et al. (2010a, b).* Location of oldest known rock in Manitoba shown by black star. Abbreviations: CRP = Caribou River pluton; DRP = Dickins River pluton; GIB = Great Island Basin; GLGB = Garlinski Lake greenstone belt; GLP = Gross Lake pluton; HLGB = Howard Lake greenstone belt; NLB = Nowell Lake Basin; NLP = Nichol Lake pluton; SBB = Seal Bend Basin; VLP = Vinsky Lake pluton.

the Caribou River pluton (CRP in Fig. 2), the granodiorite of which returned an age of 1823.2 ± 4.5 Ma, and the coeval Dickins River pluton (DRP in Fig. 2) to the north, with a crystallization age of 1828.7 ± 4.3 Ma (Rayner, 2022). The latter records 2544 to 3272 Ma xenocrystic cores.

Wollaston and Mudjatik domains

Regionally, Paleoproterozoic cover rocks of the Wollaston Supergroup (Fig. 1) are best exposed and defined in northeastern Saskatchewan (e.g. Yeo and Delaney, 2007), whereas the apparently on-strike and similar-age Hurwitz Group sediments are prevalent in southern Nunavut (e.g. Davis et al., 2005). As such, data from siliciclastic basal formation remnants across northern Manitoba provide critical insight to resolving the tectonic and spatial relationship of these Paleoproterozoic cover rocks.

The Wollaston Domain in the far northwest of Manitoba has a dominant northeasterly trend and is exposed in an approximately 20 to 35 km wide belt of elongate structural domes, resulting from doubly plunging antiformal and synformal folds. In the Kasmere and Putahow lakes areas (KL and PL in Fig. 1), quartzite and arkosic rocks occur in an antiformal culmination and are overlain by a compositionally variable sequence of calc-silicate rocks and garnet-biotite semipelitic gneiss, suggesting a classic basin subsidence sequence. Quartzite samples from Nejanilini and Kasmere lakes are dominated by ca. 2.70 Ga detrital zircons (youngest detrital zircon 2.48 Ga), whereas psammitic gneiss samples from the Kasmere Lake area yielded mostly ca. 2.0 Ga detrital zircons and youngest detrital zircons of ca. 1.89 Ga (C.O. Böhm, unpub. data, 2007).

At Misty Lake, a structural dome is cored by leucotonalite to granite, with a crystallization age of 2584 ± 7 Ma (Kremer et al., 2010a, b; Rayner, 2011). The core of the dome is bounded by highly deformed metasedimentary rocks of the Wollaston Supergroup, including variably migmatitic porphyroblastic psammitic to pelitic paragneiss with minor impure quartzite, porphyroblastic arkosic paragneiss with minor calc-silicate, rare marble, calc-silicate rocks, and well bedded arenite to calcarenite with calc-silicate interlayers. The detrital profile of a sample of psammitic gneiss is dominated by 2.54 Ga zircons (Kremer et al., 2010a, b; Rayner, 2011). The maximum age of deposition is constrained by a single younger grain that yielded nonreproducible ages of 1900 and 1940 Ma, the latter being interpreted to be the best estimate of the maximum age of sedimentation. Intrusive

rocks, interpreted as Hudsonian (ca. 1.83 Ga) on the basis of field relationships with these metasedimentary rocks, are widespread. Areas of moderate to intense alkali metasomatism occur in metasedimentary rocks and granitic rocks and have been documented in association with a variety of intrusion-hosted and metasomatic uranium, rare-earth element, and rare-metal deposits.

The Snyder Lake area (SL in Fig. 1) is largely underlain by medium- to upper-amphibolite-grade metasedimentary rocks of the Wollaston Supergroup, including psammitic, semipelitic, pelitic, and lesser amounts of calc-silicate gneiss and marble (Kremer et al., 2011, 2021a, b; Kremer and Böhm, 2011). Southeast and northwest of Snyder Lake, the sedimentary succession is flanked by intrusive rocks of potential Archean age that were metamorphosed at upper amphibolite- to granulite-facies conditions. Orthogneiss northwest of Snyder Lake (Mudjatik Domain) was dated at 2711.7 ± 6.5 Ma, whereas similar lithologies to the south-east of Snyder Lake (Wollaston Domain) were dated at 2637 ± 13 Ma and 2607.1 ± 4.3 Ma (Rayner, 2022). For the two Wollaston Domain samples, the former records minor ca. 2.86 Ga inheritance, whereas the latter records a 1815 ± 20 Ma metamorphic overprint from a single zircon rim analysis. Calcium-rich horizons (calc-silicate gneiss and marble) within the Snyder Lake area locally host uranium and/or rare-earth element enrichments of economic interest. Based on the field observations in the Snyder Lake area, uranium and rare-earth element mineralization appears to be focused on highly altered (silicified, albitized, hematized) zones in calcareous horizons of the sedimentary sequence, which presents a different mineralization environment and process than represented by the unconformity-type uranium deposits at or near the top of the Wollaston Supergroup rocks in Saskatchewan.

Feldspathic arenite from the Snyder Lake area yielded detrital zircon with clusters of U-Pb analyses at ca. 1.99 Ga and between 2.5 and 2.6 Ga, although the provenance profile is not characterized by well defined modes. The maximum age of deposition is 1914 ± 12 Ma. Psammitic gneiss exhibits two distinct age modes: the dominant one, centred at 2550 Ma; and a younger, subordinate mode spanning 1862 to 1936 Ma, with a maximum depositional age of 1881 ± 16 Ma. A sample of calc-silicate conglomerate yielded few detrital zircon grains, most of which returned discordant results. Given the presence of grains dated at ca. 1.9 Ga, this rock is interpreted as Paleoproterozoic or younger (Rayner, 2022).

On the basis of currently available U-Pb detrital zircon results from Paleoproterozoic cover remnants across northern Manitoba, there do not appear to be significant differences in the nature and composition of the metasedimentary successions. This may indicate that Paleoproterozoic metasedimentary rocks previously assigned to the Wollaston (Kasmere and Putahow lakes) and the Hurwitz (Nejanilini Lake) supergroups formed contemporaneously and in a similar or related tectonic setting in northern Manitoba.

SUMMARY

In summary, bedrock mapping and geochronological analyses carried out in 2005 to 2011 in the far north of Manitoba elucidate diverse and complex rocks that record nearly two billion years of Earth history. Supported by geophysical, geochemical, and geochronological data, areas with known or inferred potential for base and precious metals, diamonds, uranium, and rare metals were targeted for remapping to provide an advanced framework for mineral exploration and land-use management.

Of particular importance for regional tectonic correlations and mineral exploration are the following:

- A new stratigraphy and chronology of at least four metasedimentary cover sequences in the Seal River Domain, some with high potential for economic uranium, gold, and/or rare-metal mineralization.
- The identification of a Neoproterozoic greenstone belt in the Great Island area with known gold occurrences.
- The discovery of remnants of ancient (3.5 Ga) cratonic lithosphere in the Seal River area, rendering the region favourable for diamond exploration.

ACKNOWLEDGMENTS

The authors of this summary contribution gratefully acknowledge the work of many researchers whose fieldwork and geological interpretations are cited here, specifically S. Anderson, E. Syme, P. Kremer, L. Murphy, A. Carlson, C. Couëslan, and T. Corkery at the MGS. The staff of the Geochronology Laboratory at the GSC in Ottawa are also thanked for their careful efforts to ensure high quality and reliable results.

REFERENCES

Anderson, S.D. and Böhm, C.O., 2005. Bedrock geology of Nejanilini Lake, Manitoba (parts of NTS 64P5, 12 and 13); Manitoba Industry, Economic Development and Mines, Manitoba Geological Survey, Preliminary Map PMAP2005-3, scale 1:35 000.

Anderson, S.D. and Böhm, C.O., 2006. Bedrock geology of the Putahow Lake area, Manitoba (NTS 64N15); Manitoba Science, Technology, Energy and Mines, Manitoba Geological Survey, Preliminary Map PMAP2006-5, scale 1:50 000.

Anderson, S.D. and Böhm, C.O., 2008. Far North Mapping Initiative: reconnaissance bedrock mapping and sampling of the Great Island Domain, Manitoba (parts of NTS 54L, M, 64I, P); *in* Report of activities 2008; Manitoba Science, Technology, Energy and Mines, Manitoba Geological Survey, p. 144–153.

Anderson, S.D., Böhm, C.O., and Matile, G.L.D., 2005. Bedrock and surficial geological field investigations in the Nejanilini Lake area, northern Manitoba (parts of NTS 64P5, 12 and 13); *in* Report of activities 2005; Manitoba Industry, Economic Development and Mines, Manitoba Geological Survey, p. 92–103.

Anderson, S.D., Böhm, C.O., Syme, E.C., Carlson, A.R., and Murphy, L.A., 2009a. Far North Geomapping Initiative: geological investigations in the Great Island area, Manitoba (parts of NTS 54L13, 54M4, 64I15, 16, 64P1, 2); *in* Report of activities 2009; Manitoba Innovation, Energy and Mines, Manitoba Geological Survey, p. 132–147.

Anderson, S.D., Böhm, C.O., Syme, E.C., Carlson, A., and Murphy, L.A., 2009b. Bedrock geology of the Great Island area, Manitoba (parts of NTS 54L13, 54M4, 64I15, 16, 64P1, 2); Manitoba Innovation, Energy and Mines, Manitoba Geological Survey, Preliminary Map PMAP2009-4, scale 1:50 000.

Anderson, S.D., Böhm, C.O., and Syme, E.C., 2010a. Far North Geomapping Initiative: bedrock geological investigations in the Seal River region, northeastern Manitoba (parts of NTS 54L, M, 64I, P); *in* Report of activities 2010; Manitoba Innovation, Energy and Mines, Manitoba Geological Survey, p. 6–22.

Anderson, S.D., Böhm, C.O., and Syme, E.C., 2010b. Precambrian geology of the Seal River region, Manitoba (parts of NTS 54L, M, 64I, P); Manitoba Innovation, Energy and Mines, Manitoba Geological Survey, Preliminary Map PMAP2010-1, scale 1:175 000.

Böhm, C.O. and Anderson, S.D., 2006a. Preliminary results from geological bedrock mapping of the Kasmere and Putahow lakes areas, northwestern Manitoba (parts of NTS 64N6, 10, 11 and 15); *in* Report of activities 2006; Manitoba Science, Technology, Energy and Mines, Manitoba Geological Survey, p. 136–147.

Böhm, C.O. and Anderson, S.D., 2006b. Bedrock geology of the Kasmere Lake area, Manitoba (NTS 64N11 and parts of 64N6); Manitoba Science, Technology, Energy and Mines, Preliminary Map PMAP2006-4, scale 1:50 000.

Böhm, C.O., Corkery, M.T., and Creaser, R.A., 2004. Preliminary Sm-Nd isotope results from granitoid samples from the Nejanilini granulite domain, north of Seal River, Manitoba (NTS 64P); *in* Report of activities 2004; Manitoba Industry, Economic Development and Mines, Manitoba Geological Survey, p. 209–215.

- Böhm, C.O., Anderson, S.D., and Syme, E.C., 2020a. Compilation of Sm-Nd isotopic results from the Seal River–Great Island area, southeast Hearne Craton margin, northern Manitoba (parts of NTS 54L, M, 64I, P); Manitoba Agriculture and Resource Development, Manitoba Geological Survey, Data Repository Item DRI2020029, one .xlsx file, 3 p.
- Böhm, C.O., Anderson, S.D., Syme, E.C., Carlson, A.R., and Murphy, L.A., 2020b. Whole-rock geochemistry compilation of the Seal River–Great Island area, southeast Hearne Craton margin, northern Manitoba (parts of NTS 54L, M, 64I, P); Manitoba Agriculture and Resource Development, Manitoba Geological Survey, Data Repository Item DRI2020030, one .xlsx file, 6 p.
- Davis, W.J., Rainbird, R.H., Aspler, L.B., and Chiarenzelli, J.R., 2005. Detrital zircon geochronology of the Paleoproterozoic Hurwitz and Kiyuk groups, western Churchill Province, Nunavut; Geological Survey of Canada, Current Research 2005-F1, 13 p. <https://doi.org/10.4095/216706>
- Fortin, R., Coyle, M., Carson, J.M., and Kiss, F., 2009a. Geophysical Series, NTS 64 P/03, airborne geophysical survey of the Great Island and Seal River area, Manitoba / Série des cartes géophysiques, SNRC 64 P/03, levé géophysique aéroporté de la région de Great Island et Seal River, Manitoba; Geological Survey of Canada, Open File 6065, scale 1:50 000. <https://doi.org/10.4095/247454>
- Fortin, R., Coyle, M., Carson, J.M., and Kiss, F., 2009b. Geophysical Series, NTS 64 P/02, airborne geophysical survey of the Great Island and Seal River area, Manitoba / Série des cartes géophysiques, SNRC 64 P/02, levé géophysique aéroporté de la région de Great Island et Seal River, Manitoba; Geological Survey of Canada, Open File 6066, scale 1:50 000. <https://doi.org/10.4095/247455>
- Fortin, R., Coyle, M., Carson, J.M., and Kiss, F., 2009c. Geophysical Series, NTS 64 P/01 and part of NTS 54 M/04, airborne geophysical survey of the Great Island and Seal River area, Manitoba / Série des cartes géophysiques, SNRC 64 P/01 et partie de SNRC 54 M/04, levé géophysique aéroporté de la région de Great Island et Seal River, Manitoba; Geological Survey of Canada, Open File 6067, scale 1:50 000. <https://doi.org/10.4095/247456>
- Fortin, R., Coyle, M., Carson, J.M., and Kiss, F., 2009d. Geophysical Series, NTS 64-I/16 and part of NTS 54 L/13, airborne geophysical survey of the Great Island and Seal River area, Manitoba / Série des cartes géophysiques, SNRC 64-I/16 et partie de SNRC 54 L/13, levé géophysique aéroporté de la région de Great Island et Seal River, Manitoba; Geological Survey of Canada, Open File 6068, scale 1:50 000. <https://doi.org/10.4095/247457>
- Fortin, R., Coyle, M., Carson, J.M., and Kiss, F., 2009e. Geophysical Series, NTS 64-I/15, airborne geophysical survey of the Great Island and Seal River area, Manitoba / Série des cartes géophysiques, SNRC 64-I/15, levé géophysique aéroporté de la région de Great Island et Seal River, Manitoba; Geological Survey of Canada, Open File 6069, scale 1:50 000. <https://doi.org/10.4095/247458>
- Fortin, R., Coyle, M., Carson, J.M., and Kiss, F., 2009f. Geophysical Series, NTS 64-I/14, airborne geophysical survey of the Great Island and Seal River area, Manitoba / Série des cartes géophysiques, SNRC 64-I/14, levé géophysique aéroporté de la région de Great Island et Seal River, Manitoba; Geological Survey of Canada, Open File 6070, scale 1:50 000. <https://doi.org/10.4095/247459>
- Fortin, R., Coyle, M., Carson, J.M., and Kiss, F., 2009g. Geophysical Series, NTS 64-I/11, airborne geophysical survey of the Great Island and Seal River area, Manitoba / Série des cartes géophysiques, SNRC 64-I/11, levé géophysique aéroporté de la région de Great Island et Seal River, Manitoba; Geological Survey of Canada, Open File 6071, scale 1:50 000. <https://doi.org/10.4095/247460>
- Fortin, R., Coyle, M., Carson, J.M., and Kiss, F., 2009h. Geophysical Series, NTS 64-I/10, airborne geophysical survey of the Great Island and Seal River area, Manitoba / Série des cartes géophysiques, SNRC 64-I/10, levé géophysique aéroporté de la région de Great Island et Seal River, Manitoba; Geological Survey of Canada, Open File 6072, scale 1:50 000. <https://doi.org/10.4095/247461>
- Fortin, R., Coyle, M., Carson, J.M., and Kiss, F., 2009i. Geophysical Series, NTS 64-I/09 and part of NTS 54 L/12, airborne geophysical survey of the Great Island and Seal River area, Manitoba / Série des cartes géophysiques, SNRC 64-I/09 et partie de SNRC 54 L/12, levé géophysique aéroporté de la région de Great Island et Seal River, Manitoba; Geological Survey of Canada, Open File 6073, scale 1:50 000. <https://doi.org/10.4095/247462>
- Fortin, R., Coyle, M., Carson, J.M., and Kiss, F., 2009j. Geophysical Series, NTS 64-I/07, airborne geophysical survey of the Great Island and Seal River area, Manitoba / Série des cartes géophysiques, SNRC 64-I/07, levé géophysique aéroporté de la région de Great Island et Seal River, Manitoba; Geological Survey of Canada, Open File 6074, scale 1:50 000. <https://doi.org/10.4095/247463>
- Fortin, R., Coyle, M., Carson, J.M., and Kiss, F., 2009k. Geophysical Series, NTS 64-I/06, airborne geophysical survey of the Great Island and Seal River area, Manitoba / Série des cartes géophysiques, SNRC 64-I/06, levé géophysique aéroporté de la région de Great Island et Seal River, Manitoba; Geological Survey of Canada, Open File 6075, scale 1:50 000. <https://doi.org/10.4095/247464>
- Fortin, R., Coyle, M., Carson, J.M., and Kiss, F., 2009l. Geophysical Series, NTS 64-I/08 and part of NTS 54 L/05, airborne geophysical survey of the Great Island and Seal River area, Manitoba / Série des cartes géophysiques, SNRC 64-I/08 et partie de SNRC 54 L/05, levé géophysique aéroporté de la région de Great Island et Seal River, Manitoba; Geological Survey of Canada, Open File 6076, scale 1:50 000. <https://doi.org/10.4095/247465>
- Kremer, P.D. and Böhm, C.O., 2011. Bedrock geology of the Snyder Lake area, northwestern Manitoba (part of NTS 64N5); Manitoba Innovation, Energy and Mines, Manitoba Geological Survey, Preliminary Map PMAP2011-1, scale 1:35 000.
- Kremer, P.D., Carlson, A.R., and Couëslan, C., 2010a. Far North Geomapping Initiative: geological mapping in the Misty Lake area, Manitoba (parts of NTS 64K12, 13, 64N4); *in* Report of activities 2010; Manitoba Innovation, Energy and Mines, Manitoba Geological Survey, p. 50–61.

- Kremer, P.D., Carlson, A.R., and Couëslan, C.G., 2010b. Geology of the Misty Lake area, northwestern Manitoba (parts of NTS 64K12, 13, 64N4); Manitoba Innovation, Energy and Mines, Manitoba Geological Survey, Preliminary Map PMAP2010-2, scale 1:75 000.
- Kremer, P.D., Böhm, C.O., and Rayner, N., 2011. Far North Geomapping Initiative: bedrock geology of the Snyder Lake area, northwestern Manitoba (part of NTS 64N5); *in* Report of activities 2011; Manitoba Innovation, Energy and Mines, Manitoba Geological Survey, p. 6–17.
- Kremer, P.D., Carlson, A.R., Couëslan, C.G., and Martins, T., 2021a. Whole-rock geochemistry results of bedrock samples from the Misty Lake area, Manitoba (parts of NTS 64K12, 13, 64N4); Manitoba Agriculture and Resource Development, Manitoba Geological Survey, Data Repository Item DRI2021012, one .xlsx file, 14 p.
- Kremer, P.D., Böhm, C.O., and Martins, T., 2021b. Whole-rock geochemistry of bedrock samples from the Snyder Lake area, northwestern Manitoba (part of NTS 64N5); Manitoba Agriculture and Resource Development, Manitoba Geological Survey, Data Repository Item DRI2021011, one .xlsx file, 8 p.
- Rayner, N., 2010a. Far North Geomapping Initiative: new U-Pb geochronological results from the Seal River region, Manitoba (parts of NTS 54L, 54M, 64I, 64P); *in* Report of activities 2010; Manitoba Science, Technology, Energy and Mines, Manitoba Geological Survey, p. 23–35.
- Rayner, N., 2010b. U-Pb geochronological results from the Seal River region, northeastern Manitoba (parts of NTS 54L, M, 64I, P); Manitoba Innovation, Energy and Mines, Manitoba Geological Survey, Data Repository Item DRI2010004, one .xlsx file, 2 p.
- Rayner, N., 2011. Far North Geomapping Initiative: new U-Pb geochronological results from the Misty Lake area, northwestern Manitoba (part of NTS 64K12, 13); Manitoba Innovation, Energy and Mines, Manitoba Geological Survey, Data Repository Item DRI2011008, one .xlsx file, 2 p.
- Rayner, N.M., 2022. U-Pb geochronology data from the 2008–2011 Manitoba Far North Geomapping Initiative; Geological Survey of Canada, Open File 8868, 7 p. <https://doi.org/10.4095/329641>
- Yeo, G.M. and Delaney, G., 2007. The Wollaston Supergroup, stratigraphy and metallogeny of a Paleoproterozoic Wilson cycle in the Trans-Hudson Orogen, Saskatchewan; *in* EXTECH IV: Geology and Uranium EXploration TEChnology of the Proterozoic Athabasca Basin, Saskatchewan and Alberta, (ed.) C.W. Jefferson and G. Delaney; Geological Survey of Canada, Bulletin 588 (*also* Saskatchewan Geological Society, Special Publication 18; Geological Association of Canada, Mineral Deposits Division, Special Publication 4), p. 89–117. <https://doi.org/10.4095/223746>

Overview of the lithotectonic framework of the Core Zone, southeastern Churchill Province, Quebec and Newfoundland and Labrador

D. Corrigan^{1,2}

Corrigan, D., 2024. Overview of the lithotectonic framework of the Core Zone, southeastern Churchill Province, Quebec and Newfoundland and Labrador; in Canada's northern shield: new perspectives from the Geo-mapping for Energy and Minerals program, (ed.) S.J. Pehrsson, N. Wodicka, N. Rogers, and J.A. Percival; Geological Survey of Canada, Bulletin 612, p. 335–337. <https://doi.org/10.4095/332504>

Abstract: This paper presents an overview of the lithotectonic framework of the Core Zone, Quebec and Labrador, which consists of at least three distinct entities: the George River, Mistinibi-Raude, and Falcoz River blocks, each with separate crustal evolutions. New field observations and U-Pb geochronological data were synthesized in order to improve knowledge of the crustal growth and tectonic history of the Core Zone and its bounding Paleoproterozoic orogens in the southeastern Churchill Province.

Résumé : Le présent article offre une vue d'ensemble du cadre lithotectonique de la Zone noyau, au Québec et au Labrador. Cette zone est constituée d'au moins trois entités lithotectoniques distinctes, à savoir les blocs de George River, de Mistinibi-Raude et de Falcoz River, où chacun présente une évolution crustale particulière. De nouvelles observations de terrain et données géochronologiques U-Pb ont servi à produire une synthèse nous permettant d'améliorer nos connaissances de la croissance crustale et de l'histoire tectonique de la Zone noyau ainsi que des orogènes du Paléoprotérozoïque qui la bordent, dans la Province de Churchill Sud-Est.

¹Geological Survey of Canada, 601 Booth Street, Ottawa, Ontario K1A 0E8

²Retired

Corresponding author: D. Corrigan (email: david.corrigangeo@gmail.com)

Manuscript accepted June 9, 2021

This contribution summarizes a paper published in Geoscience Canada (Corrigan et al., 2018), which provides improved knowledge on the crustal growth and tectonic history of the Core Zone and its bounding Paleoproterozoic orogens in the southeastern Churchill Province. The areas covered by Geo-mapping for Energy and Minerals (GEM) fieldwork (Fig. 1) were mapped in collaboration with the Ministère de l'Énergie et des Ressources naturelles du Québec (2014 and 2015) and with the Geological Survey of Newfoundland and Labrador in 2017 and 2018. Results from the 2014 study area are presented in Corrigan et al. (2018), whereas those from the 2015, 2016, and 2017 field seasons, concentrated in the Labrador Trough, and 2018, concentrated in the Hopedale Block of the North Atlantic Craton (Nain Province), are being compiled and will be presented elsewhere.

The Core Zone represents a broad region predominantly underlain by Archean gneiss and granitoid rocks between the Superior and North Atlantic cratons which, until recently, remained one of the less well known parts of the Canadian Shield. Previously thought to form part of the Archean Rae Craton, and later referred to as the southeastern Churchill

Province, it has been regarded as an ancient continental block trapped between the ca. 1.87–1.85 Ga Torngat and 1.83–1.79 Ga New Quebec orogens, with its relationships to the adjacent Superior and North Atlantic cratons remaining unresolved. The geochronological data presented in Corrigan et al. (2018), which builds on a previous summary by James and Dunning (2000), demonstrates that the Archean evolution of the Core Zone was distinct from that of both the Superior and North Atlantic (Nain) cratons. The Core Zone consists of at least three distinct lithotectonic entities, referred to as the George River, Mistinibi-Raude, and Falcoz River blocks, each with separate crustal evolutions. These microplates are separated by steeply dipping, regional-scale shear zones interpreted as paleosutures. The George River Block consists of ca. 2.70 Ga supracrustal rocks and associated ca. 2.70–2.57 Ga intrusions with cryptic ca. 3.0–2.8 Ga inheritance. The Mistinibi-Raude Block consists of remnants of a ca. 2.37 Ga volcanic arc intruded by a ca. 2.32 Ga arc plutonic suite (Pallatin) as well as the hypersolvus Pelland and Nekuashu intrusive complexes. It also hosts a coarse clastic cover sequence (Hutte Sauvage Group) which contains detrital zircon grains

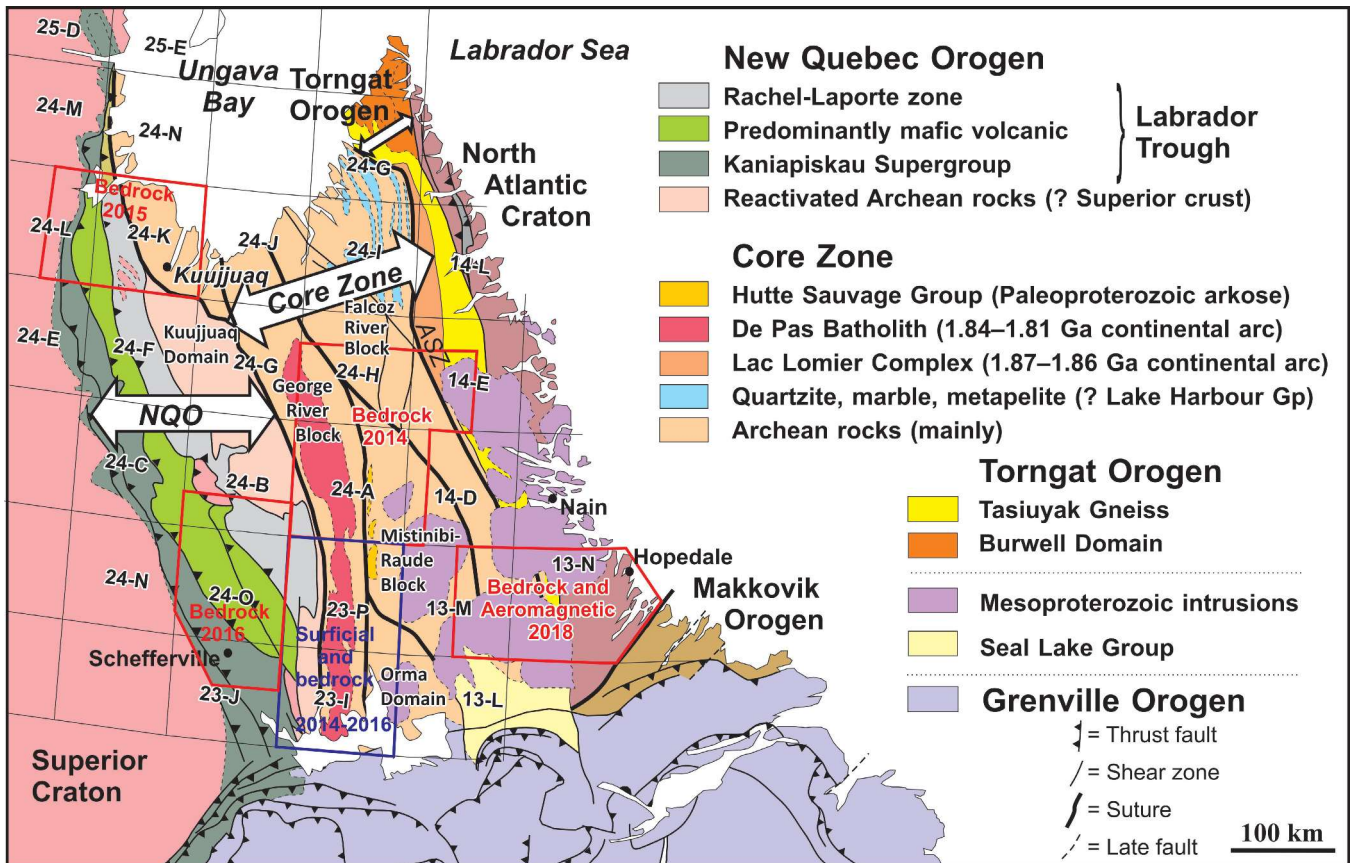


Figure 1. Simplified geological map of the Southeastern Churchill Province showing the main lithotectonic elements (modified from Corrigan et al., 2018). The square grid represents 1:250 000 scale NTS map sheets. The areas outlined in red represent GEM-2 program footprint for bedrock geology, with year of fieldwork indicated. The blue box indicates area for which surficial geology studies have been undertaken as part of the GEM Program. ASZ = Abloviak shear zone; NQO = New Quebec Orogen.

from locally-derived, ca. 2.57–2.50 Ga, 2.37–2.32 Ga, and 2.10–2.08 Ga sources, with the youngest concordant grain dated at 1987 ± 7 Ma. The Falcoz River Block consists of ca. 2.89–2.80 Ga orthogneiss intruded by ca. 2.74–2.7 Ga granite, tonalite, and granodiorite, and preserves clastic-carbonate cover sequences possibly related to the older than 1.86 Ga and younger than 1.94 Ga Lake Harbour Group on southern Baffin Island. The western margin of the Core Zone (George River Block; Fig. 1) and the Archean Kuujjuaq Domain (reworked Superior Craton) appear to have been proximal by ca. 1.84 Ga as both have been stitched by the 1.84–1.82 Ga De Pas batholith. Its eastern margin (Falcoz River Block; Fig. 1) records metamorphic ages of ca. 1.85–1.80 Ga, suggesting that the 1.83–1.79 Ga New Quebec Orogeny, which was dominated by transpressional tectonics, affected the entire southeastern Churchill Province. In contrast, the 1.87–1.85 Ga Torngat Orogen appears to have been restricted to the broad area located between the eastern Core Zone (Falcoz River Block) and North Atlantic Craton margin. The three crustal blocks forming the Core Zone add to a growing list of ‘exotic’ Archean to earliest

Paleoproterozoic microcontinents and crustal slices that extend around the Superior Craton from the Grenville Front through Hudson Strait, across Hudson Bay and into Manitoba and Saskatchewan, in what was the Manikewan Ocean realm, which closed between ca. 1.83 and 1.80 Ga during the formation of supercontinent Nuna.

REFERENCES

- Corrigan, D., Wodicka, N., McFarlane, C., Lafrance, I., van Rooyen, D., Bandyayera, D., and Bilodeau, C., 2018. Lithotectonic framework of the Core Zone, southeastern Churchill Province, Canada; *Geoscience Canada*, v. 45, no. 1, p. 1–24. <https://doi.org/10.12789/geocanj.2018.45.128>
- James, D.T. and Dunning, G.R., 2000. U-Pb geochronological constraints for Paleoproterozoic evolution of the Core Zone, southeastern Churchill Province, northeastern Laurentia; *Precambrian Research*, v. 103, p. 31–54. [https://doi.org/10.1016/S0301-9268\(00\)00074-7](https://doi.org/10.1016/S0301-9268(00)00074-7)

Rae Province at 2.6 Ga: a sanukitoid storm on the Canadian Shield, Nunavut

T.D. Peterson^{1,4*}, N. Wodicka¹, S.J. Pehrsson¹, P. Acosta-Góngora¹, V. Tschirhart¹, C.W. Jefferson¹, H.M. Steenkamp², E. Martel³, J.A. Percival¹, and D. Corrigan^{1,4}

Peterson, T.D., Wodicka, N., Pehrsson, S.J., Acosta-Góngora, P., Tschirhart, V., Jefferson, C.W., Steenkamp, H.M., Martel, E., Percival, J.A., and Corrigan, D., 2024. Rae Province at 2.6 Ga: a sanukitoid storm on the Canadian Shield, Nunavut; in Canada's northern shield: new perspectives from the Geo-mapping for Energy and Minerals program, (ed.) S.J. Pehrsson, N. Wodicka, N. Rogers, and J.A. Percival; Geological Survey of Canada, Bulletin 612, p. 339–374. <https://doi.org/10.4095/332505>

Abstract: Between 2.62 and 2.58 Ga, Rae Province was intruded from Lake Athabasca to Melville Peninsula (more than 1700 km) by mafic to felsic plutons (Snow Island Suite), and overlain by volcanic rocks that are now mostly preserved beneath Paleoproterozoic basins. The Snow Island Suite was preceded by offshore arc volcanism and possible back-arc basin activity, with a U-Pb age peak at 2.635 Ga (Marjorie peak). About 50% of the Snow Island Suite is an infracrustal granitoid with K-enriched and tonalitic subtypes; the remainder lies on a sanukitoid spectrum. The sanukitoid rocks are dominantly orthopyroxene-bearing magnesian diorite and monzodiorite with Mesoarchean Nd model ages. Some isotopically juvenile Snow Island Suite and Marjorie peak mafic rocks also have strong sanukitoid or adakite trace-element signatures. Four important features in the data are: 1) Marjorie peak mafic assemblages are prominent on the southeastern edge of Rae Province. Related nickel showings are present in south Rae Province Marjorie peak and early Snow Island Suite rocks; 2) U-Pb ages in the Snow Island Suite young toward the west edge of the province; 3) the Committee Bay Block (north-central Rae Province) is distinctively rich in infracrustal Snow Island Suite migmatite and poor in Snow Island Suite sanukitoid rocks and in tonalite of any age; and 4) there is a marked shift from tonalite-rich infracrustal sources in south Rae Province to more tonalite-poor sources in central Rae Province. The data are consistent with the Snow Island Suite, representing a continental magmatic arc segment, verging westward, with ponding of mafic magmas, inducing melting in the lower lithosphere to generate intermediate melts that ascended and induced additional melting in the middle to upper crust to generate granite.

Résumé : Entre 2,62 et 2,58 Ga, la Province de Rae a été recoupée par des plutons mafiques à felsiques (Suite de Snow Island), du lac Athabasca à la presqu'île Melville (plus de 1700 km), et recouverte de roches volcaniques qui sont maintenant conservées, en grande partie, dans des bassins paléoprotérozoïques. La mise en place de la Suite de Snow Island a été précédée d'un volcanisme d'arc au large des côtes, et d'une possible activité de bassin d'arrière-arc, dont l'âge U-Pb de la culmination se situe à 2,635 Ga (culmination de Marjorie). Environ 50 % de la Suite de Snow Island est constituée de granitoïdes infracrustaux présentant des sous-types enrichis en potassium et tonalitiques; le reste s'insère dans le spectre des sanukitoïdes. Les sanukitoïdes sont principalement constituées de diorite magnésienne à orthopyroxène et de monzodiorite dont les âges modèles Nd remontent au Mésoarchéen. Certaines roches mafiques de la Suite de Snow Island et de la culmination de Marjorie de caractère juvénile sur le plan isotopique présentent également de fortes signatures en éléments traces propres aux sanukitoïdes ou aux adakites. Quatre caractéristiques importantes ont été relevées dans les données : 1) les assemblages mafiques de la culmination de Marjorie sont dominants à la bordure sud-est de la Province de Rae et des indices de nickel apparentés sont présents dans des roches de la culmination de Marjorie et des phases précoces de la Suite de Snow Island dans le sud de la Province de Rae; 2) les âges U-Pb de roches de la Suite de Snow Island rajeunissent vers la bordure ouest de la province; 3) le bloc de Committee Bay (centre nord de la Province de Rae) est typiquement riche en migmatite infracrustale de la Suite de Snow Island et pauvre en sanukitoïdes de la même suite et en tonalite de tout âge; et 4) il existe une transition marquée entre les sources infracrustales riches en tonalite du sud de la Province de Rae et les sources plus pauvres en tonalite du centre de la province. Les données concordent bien avec le fait que la Suite de Snow Island constitue un segment d'arc magmatique continental à vergence ouest, dans lequel se sont accumulés des magmas mafiques qui ont entraîné une fusion de la lithosphère inférieure, laquelle a produit des liquides magmatiques intermédiaires qui sont montés et ont induit une fusion additionnelle dans la croûte intermédiaire à supérieure en générant du granite.

¹Geological Survey of Canada, 601 Booth Street, Ottawa, Ontario K1A 0E8

²Université Laval, 1065 Avenue de la Médecine, Québec, Québec G1V 0A6

³Northwest Territories Geological Survey, P.O. Box 1320, 4601-B 52 Avenue, Yellowknife, Northwest Territories X1A 2L9

⁴Retired

*Corresponding author: T.D. Peterson (email: tpeterso@sympatico.ca)

INTRODUCTION

The Rae Province of the northern Canadian Shield is characterized by an extensive intrusive suite emplaced at ca. 2.6 Ga, which is present from the southernmost Archean exposures north of Athabasca Basin to the Arctic Ocean (Fig. 1). The initial description of widespread plutonism and volcanism at 2.6 Ga in the Rae Province was by LeCheminant and Roddick (1991), who published a set of U-Pb ages on three granitic and two dacite porphyry rocks. One of these ages was from a porphyritic (megacrystic) monzogranite in central Dubawnt Lake (located in Fig. 1). Further mapping in that area revealed cogenetic rock types ranging from pyroxenite, gabbro, and diorite through enriched leucogranite (Peterson, 2006). Snow Island, in western Dubawnt Lake (Tyrrell, 1896; Tyrrell and Senecal, 1897) was referenced by Peterson and Lee (1995) as the type locality for the Snow Island Suite plutonic series, here expanded to include volcanic equivalents. Outcrops of Snow Island Suite volcanic rocks, as well as large intrusive bodies, are widely exposed in the region between the Amer belt and Baker Lake (Ashton, 1988; Zaleski, 2002; Jefferson et al., this volume); known as the Marjorie–Kiggavik–Tehek belt, it is defined here as the geographic area of Neoproterozoic supracrustal rocks that extends from the Marjorie Lake region in the southwest, through the Kiggavik uranium camp, up to and including the western Tehek Lake area (MKT on Fig. 1; *see also* Jefferson et al., this volume). The volcanic rocks were named the Pukiq Lake Formation (Peterson et al., 2015a) after exposures of dacite west of Pukiq Lake, southwest of Baker Lake (LeCheminant et al., 1981).

Exposed Archean bedrock in the Dubawnt Lake area and northeast through central Rae Province to the Tehery Lake–Wager Bay area is approximately 50% Snow Island Suite, and some structural domains in southern Rae Province are almost 100% Snow Island Suite (e.g. the Nolan domain: Cloutier et al., 2017, 2021). The 1:550 000 geology map and accompanying notes of northwestern Rae Province (Skulski et al., 2018) incorporated several Snow Island Suite–aged intrusive units and demonstrated a close relationship between some Snow Island Suite intrusive units and migmatization of older Neoproterozoic supracrustal rocks (Committee Bay belt).

The global distribution and widespread nature of Snow Island Suite–age magmatism has been highlighted as a key component in the reconstruction of Archean supercontinents, being common to at least ten cratons or cratonic fragments worldwide (Pehrsson et al., 2013a). In support of the pan–Rae Province GEM-2 (Geomapping for Energy and Minerals, phase 2) study, which collated multiple data sets to constrain the history of the province, the present authors have attempted to determine the igneous rock types that are present within this province-wide event, and any patterns in their distribution that will point toward tectonic processes and polarities. The principal questions to address were: to what extent was Rae Province assembled during this event? What were the heat and magma sources? What was the nature of crust and mantle interaction?

DEFINING THE SNOW ISLAND SUITE: EXTENT IN SPACE AND TIME

Snow Island Suite activity

The age range of the Snow Island Suite (2.62–2.58 Ga) is defined as the large peak centred on 2.605 Ga in the age distribution of 2.67–2.57 Ga igneous rocks for the entire Rae Province (Fig. 2a). Figures 2b to 2f show the distribution of age data in selected intervals between 2.64 and 2.58 Ga. The data set includes U-Pb crystallization ages archived in the Canadian Geochronology Knowledgebase (Natural Resources Canada, 2022; current to 2016), supplemented by recently acquired data from projects in the GEM programs (*see also* Jefferson et al., this volume). Additional ages for southeastern Rae Province are from Regan et al. (2017a, b). Previously unpublished U-Pb ages and lithogeochemical data from Melville Peninsula are included here in graphs and map plots (Corrigan et al., 2013; N. Wodicka, unpub. U-Pb data, 2012; L. Nadeau, unpub. geochemical data, 2012). The extent of Snow Island Suite–intruded crust is a subset of the Rae Province as currently defined (Pehrsson et al., this volume); this paper will refer to this area as Rae Province–Snow Island Suite.

Figure 1. Locations of U-Pb crystallization age data for Rae Province (Rae) in the range 2.64–2.58 Ga (encompasses ranges of Snow Island Suite (SIS) and Marjorie peak). Cool colours (blues) = old ages, warm colours (reds) = young ages (*see* Fig. 2a for separated age bins). There are no data in this age range from the Repulse Bay Block (RBB), Queen Maud Domain (QM), the Thelon tectonic zone (Ttz), or the Hearne Province (HP) proper (*see* text). The extent of the Repulse Bay Block, expanded from Corrigan et al. (2013) and Skulski et al. (2018), is based on the distribution of Snow Island Suite plutons outside of the block and the bounding Wager shear zone along its southern margin. Ab = Amer belt, BC = Borden complex, BL = Baker Lake, BP = Boothia Peninsula, CBb = Committee Bay belt area, Cfz = Chesterfield fault zone, DL = Dubawnt Lake, LA = Lake Athabasca, MP = Melville Peninsula, MKT = Marjorie–Kiggavik–Tehek belt, Pq = Pukiq Lake type locality, SB = south of Boothia Peninsula, SI = Southampton Island, SP = Slave Province, Stz = Snowbird tectonic zone, WB = Wager Bay, YL = Yathkyed Lake.

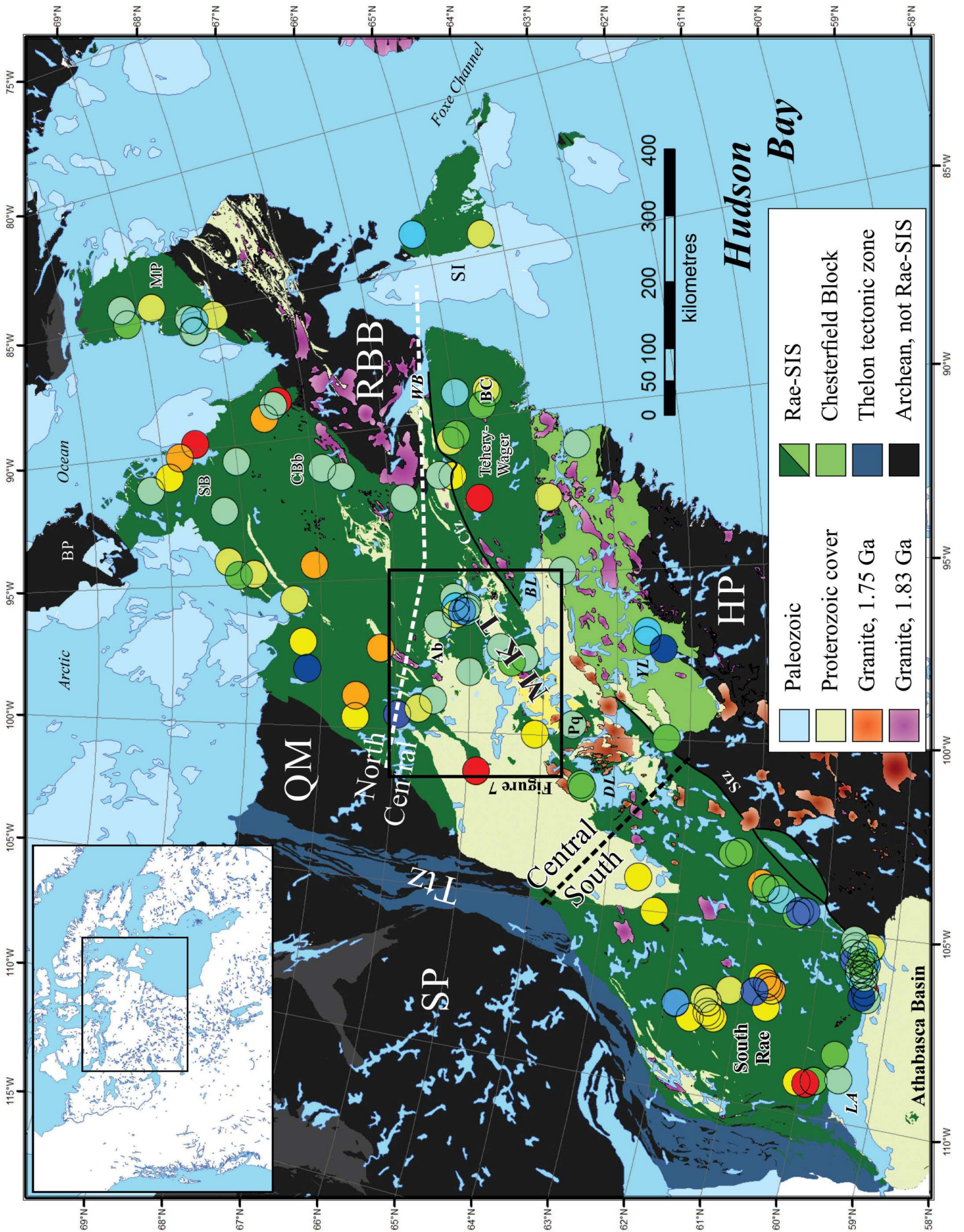


Figure 2. **a)** Histogram of Snow Island Suite (SIS) age data in 5 Ma bins, including pre–Snow Island Suite activity (peaks labelled MP = Marjorie peak and ESP = early sanukitoid peak, see text). The histogram plot takes no account of errors; these are typically about ± 5 Ma. Inset shows data in the same range for the Slave Province. **b)** Locations of ages in the pre–Snow Island Suite Marjorie peak interval; **c), d), e), f)** distribution of Snow Island Suite age data in selected time intervals as noted. Units and colour coding of symbols are as in Figure 2a. The polygon symbols in Figures 2b and 2e represent detrital zircon maximum ages in pelitic and epiclastic rocks, respectively (see text). YL = Yathkyed Lake (southern Chesterfield Block), WLSz = Wholdaia Lake shear zone

The boundary between Rae Province–Snow Island Suite and Hearne Province north of Athabasca Basin coincides with a series of ca. 1.9–1.8 Ga shear zones spatially associated with uplifted granulite facies rocks, stitched by Proterozoic dykes and granitic intrusions (1.83–1.75 Ga), which is broadly termed the Snowbird tectonic zone (Fig. 1; see e.g. Regis et al., 2021). No ages in the Snow Island Suite range have been recorded in the Repulse Bay Block (Corrigan et al., 2013; LaFlamme et al., 2014), which comprises part of Melville Peninsula, but there are numerous examples from the Chesterfield Block, a domain with complex and uncertain relations to the remainder of Rae Province and to the Snowbird tectonic zone (e.g. Berman et al., 2007). The northwestern limit of Rae Province–Snow Island Suite, at the eastern margin of the Queen Maud Block, was established in reconnaissance transect studies by Davis et al. (2013) and Berman et al. (2015a). The northern termination of Rae Province–Snow Island Suite, both at the base of Boothia Peninsula and off the northern tip of Melville Peninsula (Fig. 1), potentially corresponds to younger structures such as Proterozoic fold and thrust belts, and shear zones. The eastern termination of Rae Province–Snow Island Suite across and beyond Southampton Island is not defined. Only two Snow Island Suite intrusive ages have been obtained on Southampton Island (Fig. 1, 2) and only about 20% of the Archean exposures there correspond to mapped units that could be Snow Island Suite (Sanborn-Barrie et al., 2014); that is a small amount compared to most of the Rae Province (e.g. Peterson, 2006; Jefferson et al., 2015; Bethune et al., 2016). Across Foxe Channel, the Snow Island Suite is absent from Baffin Island. The present authors cannot specify whether the plutonic province simply faded across Southampton Island, or if it ends abruptly at an eastern structure.

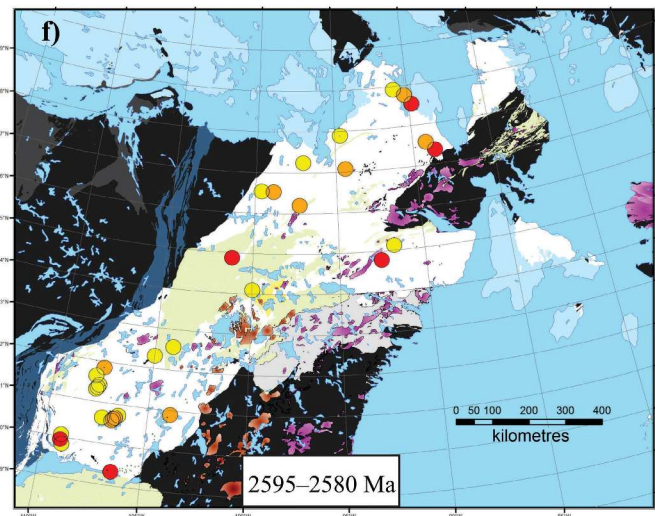
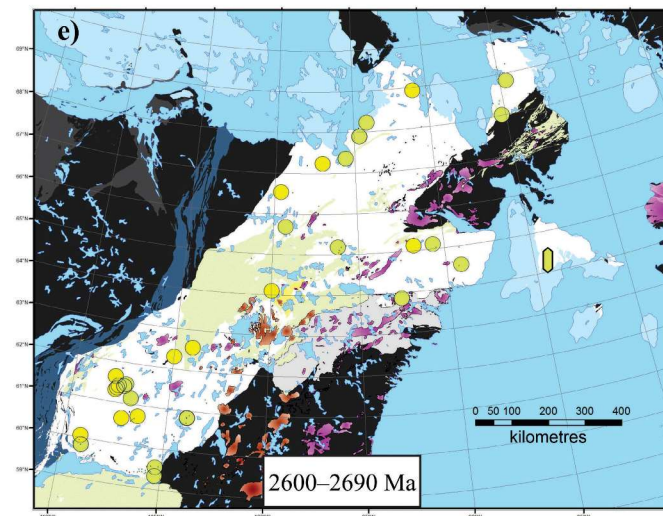
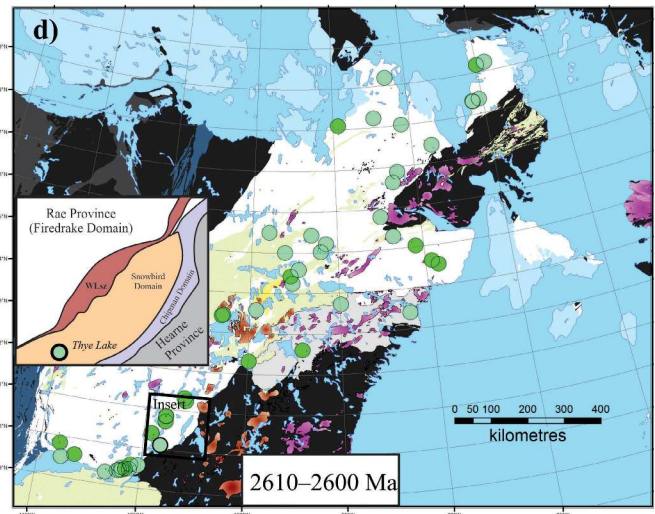
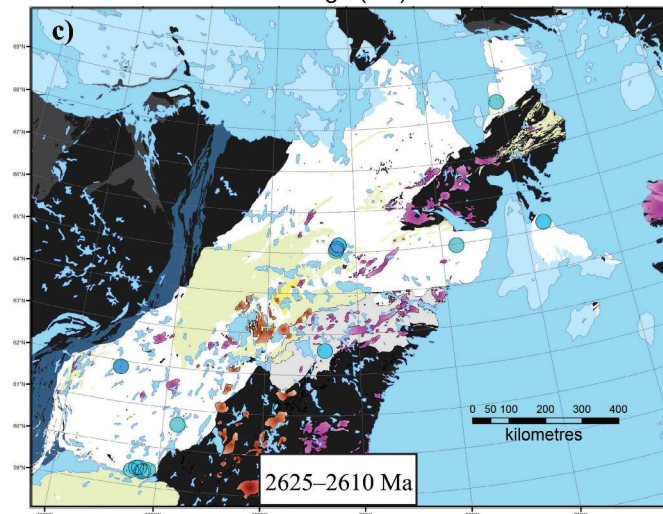
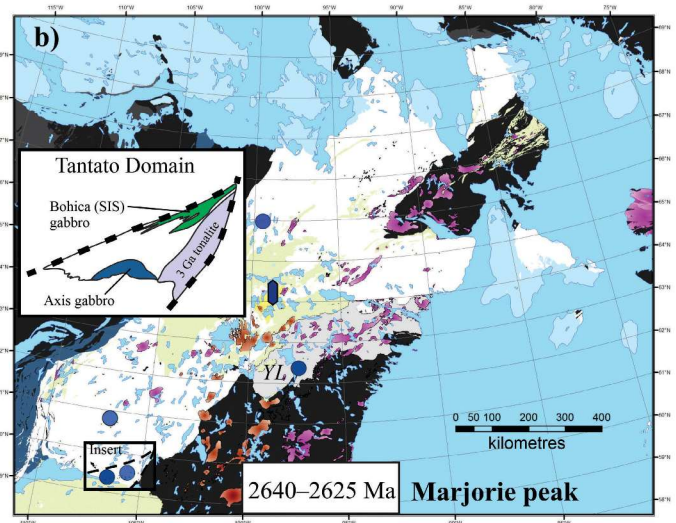
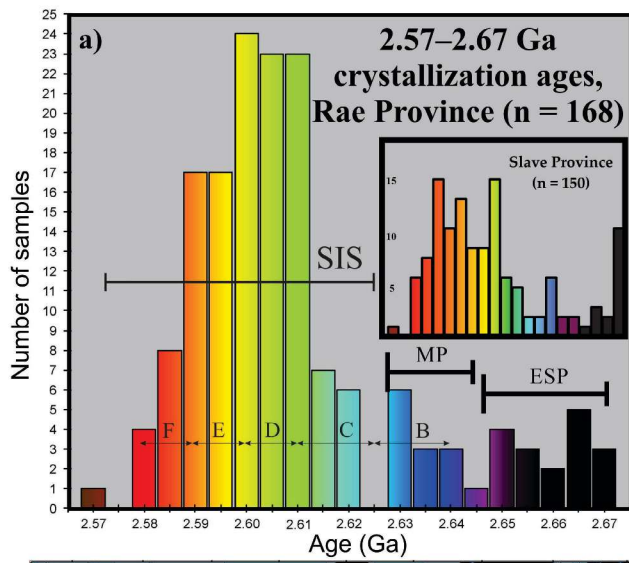
The southeast margin of Rae Province presents a complex scenario, with Snow Island Suite activity within at least four domains structurally separated from each other and the remainder of Rae Province–Snow Island Suite (Fig. 2b, d). No precise U–Pb ages within the Snow Island Suite interval have been recorded from the Snowbird Domain north of 60° latitude (Martel et al., 2008) or the continuous Dodge Domain to the south (e.g. Ashton et al., 2017a, b), but Peterson et al. (in press) identified several probable Snow Island Suite occurrences in Snowbird Domain from lithochemistry. The Thye Lake gabbro in southern Snowbird Domain (Acosta-Góngora et al., 2018) has an imprecise U–Pb age

of 2609 ± 29 Ma (Regis et al., 2017a) and, as its composition closely resembles certain Snow Island Suite gabbroic rocks, the present authors interpret it as part of the Snow Island Suite. The Wholdaia Lake shear zone, on the west margin of the Snowbird Domain (inset, Fig. 2d), contains a large volume of Snow Island Suite–aged mafic granulite, and minor trace-element–depleted high-silica Snow Island Suite granite (Thiessen et al., 2018). East of the Snowbird Domain is the narrow Chipman Domain, which continues south where it is separated from the Dodge Domain by the Tantato Domain (also known as East Athabasca mylonite triangle). The Chipman Domain is distinctively dominated by tonalite older than 3 Ga, but it is intruded by Snow Island Suite granite (‘Fehr granite’, 2598 ± 3 Ma; Hanmer et al., 1994) and so constitutes the known eastern boundary of southern Rae Province–Snow Island Suite.

Intrusions of Snow Island Suite age occur throughout the Slave Craton (e.g. Davis et al., 1994), but the age distribution in that craton is much more episodic (Fig. 2a, inset) and the two provinces are separated by metamorphic domains where ca. 2.6 Ga ages are absent (Fig. 1). The present authors therefore consider these to be separate Neoproterozoic igneous provinces. In the Hearne Province, ca. 2.6 Ga plutonic rocks occur sporadically in drill core in the Alberta subsurface (e.g. Villeneuve et al., 1993) and in outcrop as far north as the Mudjatik Domain, on either side of Athabasca Basin (Regan et al., 2017b; Card et al., 2018), but to the present authors’ knowledge all outcrop with Snow Island Suite ages within Hearne Province are very near the Snowbird tectonic zone, where they can be attributed to early Proterozoic imbrication of Snow Island Suite–bearing Rae Province crust.

Pre–Snow Island Suite activity

The Snow Island Suite–age interval was immediately preceded by activity reflected in a small age peak centred on 2.635 Ga (2.645–2.625 Ga, Fig. 2a) that the authors term the Marjorie peak from a supracrustal panel in the central Rae Province (Marjorie Assemblage) that yielded a detrital zircon age population of 2.63 Ga (blue polygon in Fig. 2b; Jefferson et al., this volume). Intrusive ages within this interval (located in Fig. 2b) are primarily from south and central Rae Province, including the Chesterfield Block. The Marjorie peak ages in southern Chesterfield Block have been correlated with nappe emplacement in the Yathkyed Lake area (MacLachlan et al., 2005), followed by upright refolding



during emplacement of Snow Island Suite–aged monzogranite. Areas with Marjorie peak activity were mostly also sites of the earliest Snow Island Suite granitoid activity at ca. 2.62 Ga (Fig. 2b, c); this is particularly evident in the Tantato Domain. The upper deck of the Tantato Domain contains an extensive unit of gabbro at eclogite-facies metamorphic grade (Axis Lake gabbro; Hanmer et al., 1994), which has been dated at 2639 ± 19 Ma and 2636.6 ± 8.3 Ma (Regis et al., 2017a). Hanmer et al. (1994) initially argued for most of the deformation observed in Tantato Domain to be synintrusive, near 2.6 Ga. Although metamorphism and uplift throughout this domain was subsequently demonstrated to occur in at least four post–Snow Island Suite events (most recently by Lamming, 2019), Dumond et al. (2010) argued that Archean structures have been transposed and that some deformation at ca. 2.6 Ga is still observable, particularly within Snow Island Suite–aged granite and diatexite. Archean deformation in Tantato Domain would have been approximately synintrusive with the Bohica mafic complex in the lower deck, imprecisely dated near 2.6 Ga (Hanmer et al., 1994).

The Marjorie peak rocks are the oldest that the authors identify as linked to the Snow Island Suite tectonic event. The period prior to Marjorie peak in the range 2.67–2.645 Ga includes south Rae Province granitoid rocks with sanukitoid affinities (Peterson et al., in press), but the data are dominated by intrusions throughout the Chesterfield Block (e.g. MacLachlan et al., 2005; Davis et al., 2006) and a sanukitoid belt in the Repulse Bay Block (LaFlamme et al., 2014; here termed sanukS). The present authors term this interval the early sanukitoid peak (Fig. 2a). A second, undated sanukitoid belt north of the Repulse Bay Block is spatially associated with Snow Island Suite samples (sanukN group). Although not necessarily associated with the Snow Island Suite event, the presence of pre-existing sanukitoid-generating lithosphere is noted, as igneous provinces in the early sanukitoid peak age range display distinctive characteristics that may reflect crustal blocks with independent histories before formation of the Snow Island Suite.

OUTCROP DESCRIPTION OF THE SNOW ISLAND SUITE

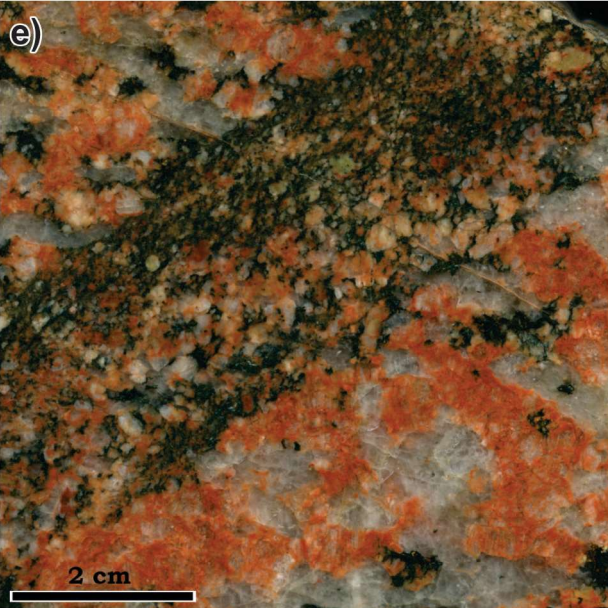
Intrusive rocks

Intrusive rocks of the Snow Island Suite (examples in Fig. 3; *see also* Cloutier et al., 2021) are exposed at all crustal levels, and at metamorphic grades from greenschist to granulite facies (e.g. Acosta-Góngora et al., 2018; Jefferson et al., this volume). Rae Province experienced several episodes of metamorphism from 2.5–1.5 Ga (Pehrsson et al., this volume) and in most Snow Island Suite outcrops, both prograde and retrograde metamorphic assemblages are observed. Charnockite has been recorded in northwest Rae Province (Skulski et al., 2018). Snow Island Suite intrusions within metasedimentary belts, such as the Committee Bay belt, include abundant metasedimentary screens, diatexite, and pegmatite (Skulski et al., 2003); diatexite is also prominent in the Tantato Domain (Hanmer et al., 1994). At Dubawnt Lake, older gneiss near Snow Island Suite plutons contains abundant injection migmatite (Peterson, 2006), and granitic phases of mixed gneiss east of the Queen Maud Block commonly yield Snow Island Suite ages (e.g. Davis et al., 2013, 2014). In contrast, in the central Rae Province region spanning the Amer belt to Dubawnt Lake area, where volcanic Snow Island Suite outcrops are widespread, the contact zones of many intrusions are agmatitic, being choked with angular inclusions of the Woodburn Lake group, including basalt and iron-formation (Jefferson et al., this volume). The agmatite portions of the Snow Island Suite intrusions are consistent with subvolcanic stoping (Peterson et al., 2015a). Intramagma chamber stoping is also well exposed in mafic rocks within a large bimodal intrusion along the Chantrey fault zone (Station 12NK-L008; 2595.7 ± 3 Ma; Davis et al., 2014).

Granitic and intermediate intrusive rocks

The most widely recognized Snow Island Suite lithology is megacrystic granodiorite to monzogranite with centimetre-scale potassium feldspar phenocrysts or polycrystalline rafts (Fig. 3a); these remain identifiable even at high strain.

Figure 3. Outcrop and hand sample photographs of felsic Snow Island Suite and related intrusive rocks. **a)** Detail of pre–Snow Island Suite (2668 \pm 9/–6 Ma) sanukitoidal Super Mario Granite, south Rae Province (Martel et al., 2008). Note pegmatite bands and granite matrix choked with pegmatite debris. Pen for scale is 14 cm. **b)** Weakly deformed Snow Island Suite infrastructural granite (lithochemical group SISf1) at station 15EM55, south Rae Province, dated at 2595 ± 5 Ma (Regis et al., 2017b). Note K-feldspar megacrysts up to 5 cm long. Pen for scale is 14 cm. **c), d)** Moderately deformed outcrop in south Rae Province (station 15EM68A) of Snow Island Suite sanukitoidal intermediate rock, dated at 2605 ± 7 Ma. Multiple intrusive events and mutually crosscutting relations are the norm in dioritic Snow Island Suite plutons; note metamorphic garnet in Figure 3d. Length of hammer in Figure 3c is 40 cm long. Photos a), b), c), d) courtesy of E. Martel. **e)** Detail of syenogranite leucogranite (lithochemical group SISf1x with gullwing REE profiles) with recrystallized inclusion, Dubawnt Lake (88PHA-242, intrusion dated at 2602 ± 2 Ma). Photograph by T. Peterson. NRCan photo 1989-183. **f)** Porphyritic SISf1 intruding Snow Island Suite diorite and gabbro, western Dubawnt Lake. Hammer is 30 cm long. Photograph by R. Rainbird. NRCan photo 1988-184.



Although megacrystic monzogranite is characteristic of the Snow Island Suite, identical textures are observed in some older tonalitic or sanukitoidal granite intrusions, such as the 2.668 Ga Super Mario granite in south Rae Province (Martel et al., 2008; Fig. 3b), equivalent granitoid rocks in Dodge Domain (Knox et al., 2011), 2.76 Ga granodiorite in northeast Melville Peninsula (Skulski et al., 2018; N. Wodicka, unpub. U-Pb data, 2012), and 2.69 Ga monzogranite in the Tehery Lake–Wager Bay area (Steenkamp et al., 2023a, b, c). Although most of the large potassium feldspar crystals in the Snow Island Suite rocks appear to be phenocrysts, some outcrops provide evidence that disruption and incorporation of pegmatite may be responsible for the profusion of large crystals (e.g. Fig. 3a). Equigranular granitoid rocks are subordinate in the Snow Island Suite. The largest mapped example, in northern Dubawnt Lake, is an approximately 100 km² syenogranite body in intrusive contact with megacrystic monzogranite (Peterson, 2006; Fig. 3e).

Although synintrusive deformation has been documented or interpreted in the Chesterfield Block (Yathkyed Lake, MacLachlan et al., 2005), along the Chesterfield fault zone (Wodicka et al., 2017), and in the Tantato Domain (Hammer et al., 1994), a detailed and targeted study in the Committee Bay belt found no evidence for this (Sanborn-Barrie et al., 2014), and most deformation in all areas is presumed to be Proterozoic. The margins of subhorizontal, tabular bodies of Snow Island Suite granite in the Marjorie-Kiggavik-Tehek belt are strongly deformed, with footwall mylonite well preserved in places (Jefferson et al., this volume) and thrust contacts in others (e.g. Kjarsgaard et al., 1997). These large (approaching 1000 km²) exposures of Snow Island Suite granitoid rocks have been interpreted as tectonized sheets overlying thrust faults, that were later folded during Hudsonian deformation (Thomas, 2012; Tschirhart et al., 2013, 2015, 2017). These sheets are considered to have been displaced from the upper portions of intrusions, probably during the pre-1.90 Ga D_{p1} of Pehrsson et al. (2013b; age constrained by Jefferson et al., this volume). The upper portions of the sheets and their contacts with the structurally

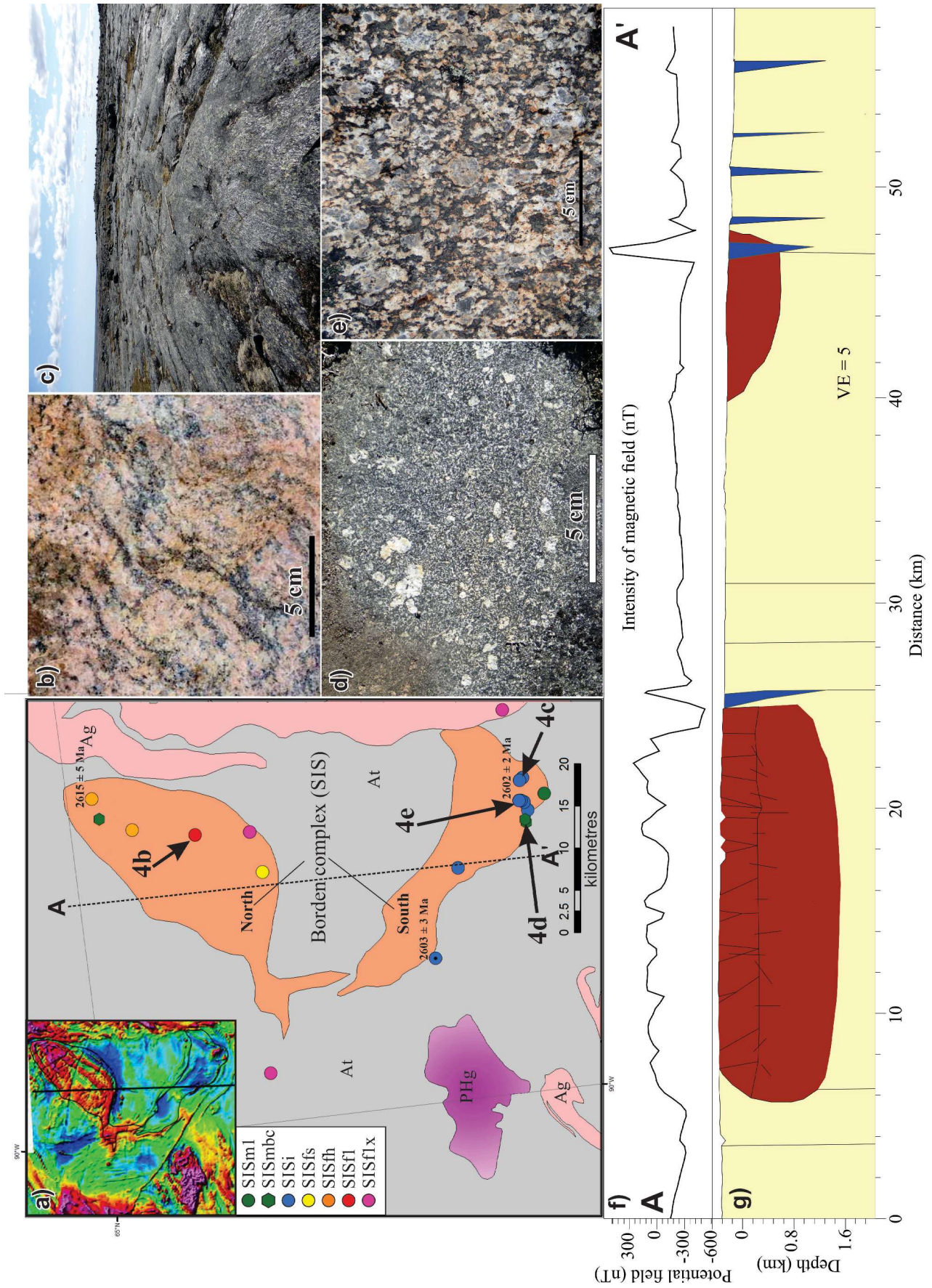
overlying Pukiki Lake Formation are also highly tectonized, such that the primary geometric relationships between the granite and the rhyolite are unknown.

A Snow Island Suite granite body (approximately 300 km²), underlain by mylonitized porphyritic granite, comprises the southern portion of the Borden complex in the Gordon Domain (Wodicka et al., 2017) (Fig. 4). The Borden complex, comprising two bodies in ca. 2.90–2.68 Ga tonalite-rich gneiss, is the most studied individual Snow Island Suite body to date. Nondeformed outcrops near the core of south Borden complex (35 km x 10 km) dominantly expose felsic porphyry consisting of equant, irregular alkali feldspar clusters or single crystals 1 to 2 cm wide in a dark matrix containing biotite and hornblende; the clusters are made highly visible by thin rims of plagioclase and/or quartz myrmekite in a pseudo-rapakivi texture (Fig. 4e). The north Borden complex is a 40 km x 15 km intrusive body with similar porphyry granite present on the north edge, but with an interior of granitic migmatite laced with pegmatite, bearing macroscopic molybdenite (Fig. 4b). Potential field modelling indicates that the south Borden body is the thinner body, with about 800 m of structural thickness (Fig. 4f). The observations are consistent with a rim of mobile porphyry surrounding and capping a migmatite core (north body), and a slice of porphyry displaced from its roof and transported south on a flat-lying shear zone (south body). Minor dioritic outcrops within south Borden complex are typically nonporphyritic or with sparse plagioclase phenocrysts (Fig. 4d), and can have mutually crosscutting relationships with granitic phases or be mingled with them, as described by Peterson (2006) (*see also* Fig. 3f).

Mafic intrusive rocks

Mafic members of the Snow Island Suite are volumetrically subordinate, but have been identified in outcrop throughout south and central Rae Province–Snow Island Suite up to the south margin of the Repulse Bay Block. Mafic intrusions within the Neoproterozoic rocks underlying the southeast edge of the Amer belt are weakly to nondeformed with primary igneous assemblages of orthopyroxene with

Figure 4. **a)** Simplified map units, sample locations, and shaded total magnetic field (inset) in the Borden complex area (Wodicka et al., 2017). At = tonalite-rich gneiss, Ag = undivided Archean granite (likely Snow Island Suite (SIS)), PHg = Hudson granite (Proterozoic). In the legend, SISfh are samples with both infracrustal and sanukitoidal characteristics (interpreted as hybrids), which would normally be folded into group SISfs. **b)** Molybdenite-bearing granitic migmatite, core of northern body. Photograph by T. Peterson. NRCan photo 2015-185. **c)** Strongly foliated porphyritic Snow Island Suite. Foliation is parallel to the southern contact. Sledgehammer for scale is 1 m long. Photograph by T. Peterson. NRCan photo 2015-186. **d)** Plagioclase-porphyritic SISmbc. Photograph by T. Peterson. NRCan photo 2015-187. **e)** Nondeformed sanukitoidal porphyry with 5% normative quartz (group SISi or SISfs). Photograph by T. Peterson. NRCan photo 2015-188. **f)** Observed magnetic field intensity along the sampling line A-A' in nanoteslas, north to the left. **g)** The interpreted igneous bodies emplaced in a homogeneous tonalite (yellow) are Snow Island Suite plutons (dark red) and mafic dykes of unknown age (blue), with the upper surface bounded by the topography (thickness modelling follows the technique of Tschirhart et al., 2013; *see text*). Rock densities and magnetic susceptibilities were measured from hand samples. VE = vertical exaggeration.



abundant hornblende and subordinate clinopyroxene and magnetite, and include oikocrystic (orthopyroxene including amphibole and oxides) cumulates with tonalitic segregations (Fig. 5a) (Peterson et al., 2015a). An orbicular leucogabbro from the Marjorie-Kiggavik-Tehek belt (Fig. 5b) had the crystallization sequence orthopyroxene+hornblende+plagioclase (orbicule centres), plagioclase (orbicule rims), and plagioclase+hornblende+opaques (interstices). A weakly deformed outcrop of a granodioritic Snow Island Suite intrusion north of the Thelon Basin displays features consistent with magmatic channel erosion of a homogeneous floor, followed by mafic crystal sedimentation that recorded at least one large trough crossbed truncation (Fig. 5c, d) (site of sample 12NK-L008, described and dated at 2595.7 ± 3 Ma by Davis et al., 2014). Another part of the outcrop exposes an angular block of banded mafic material enclosed in granodiorite (Fig. 5e), recording stopping of a previously crystallized, layered mafic phase and its incorporation within granodiorite that was, in turn, scoured and infilled by turbulent flow of another mafic pulse.

The most magnesian Snow Island Suite rocks recognized (22% MgO) are at Dubawnt Lake (Fig. 1), where a weakly deformed, coarse olivine websterite cumulate intrusion (orthopyroxene phenocrysts with olivine inclusions, magnetite, and minor clinopyroxene and phlogopite) is exposed on a series of islands, between mainland bodies of Snow Island Suite diorite and megacrystic monzogranite at the centre of the lake (Peterson, 2006). Dated mafic Snow Island Suite rocks in the Wholdaia Lake shear zone on the west edge of Snowbird Domain in south Rae Province (Fig. 2d) were strongly deformed and metamorphosed at granulite facies, at ca. 1.9 Ga (Thiessen et al., 2017), which obscured their primary mineralogy and original emplacement level. Nearby Ni-enriched mafic gabbro at Thye Lake, southern Snowbird Domain, is similarly metamorphosed. Both of these gabbro units intrude pelitic sequences, which in the case of Thye Lake, have similar trace-element enrichment profiles, consistent with volcanogenic sediment (Acosta-Góngora et al., 2018).

Mafic rocks occupy both the upper and lower structural decks in Tantato Domain (Fig. 2b; Hanmer et al., 1994). The older Axis Lake gabbro (pre-Snow Island Suite, during Marjorie peak time) of the upper deck, with both intrusive and volcanic rocks interpreted in outcrop, is at eclogite facies. Both the Axis Lake gabbro and the granulite-facies

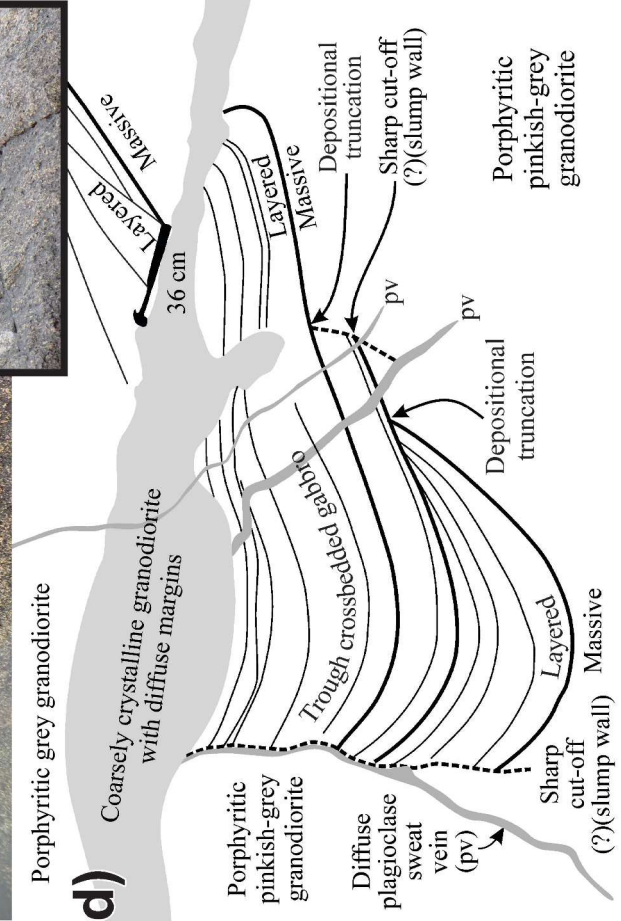
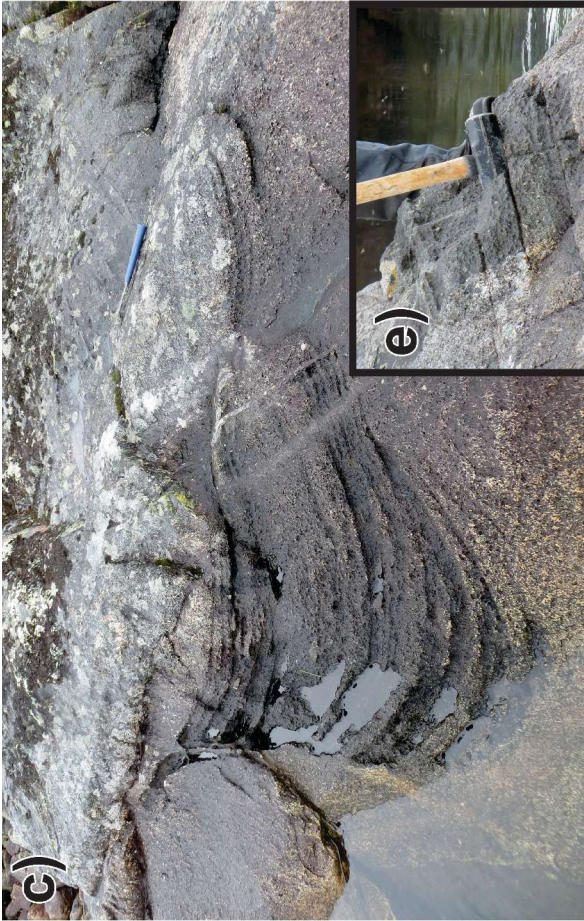
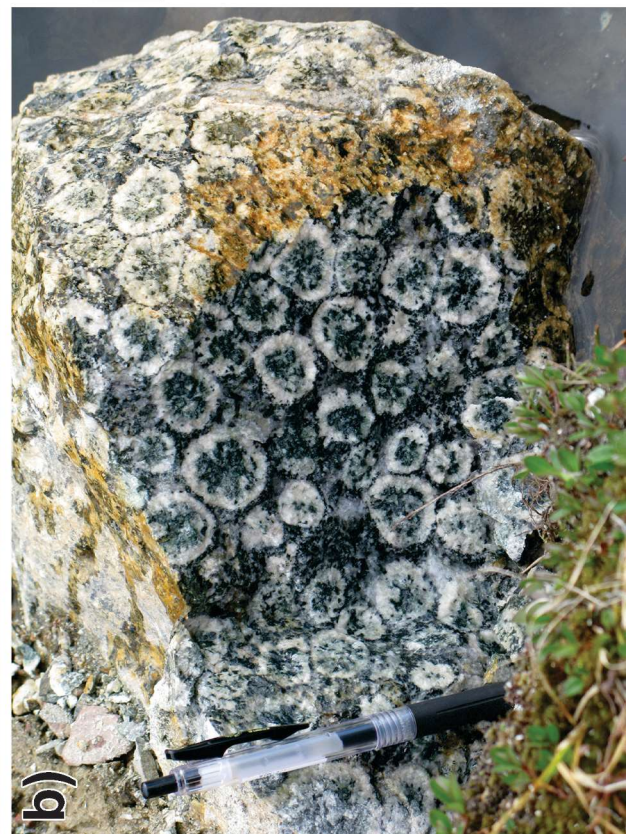
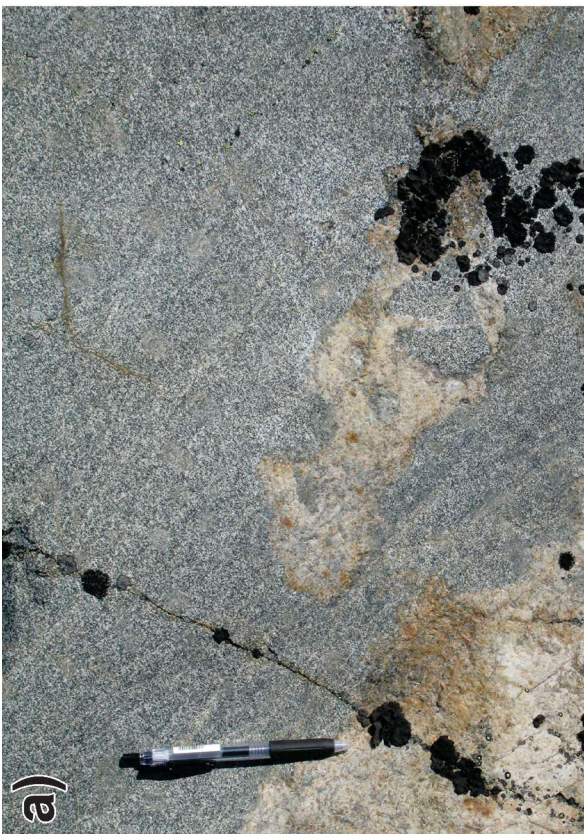
mafic Bohica complex of the lower deck (early Snow Island Suite interval) are intrusive into pelite, and both upper and lower decks were extensively intruded by Snow Island Suite-aged granite starting at 2.62 Ga. Similar mafic rocks immediately westward in Dodge Domain (Knox et al., 2011) are likely correlative with Thye Lake and Bohica complex or Axis Lake gabbro units; all of these localities have Ni showings and are dominated by orthopyroxene, hornblende, and magnetite-rich rocks.

Volcanic rocks (Pukiq Lake Formation)

Hand sample and outcrop photographs of volcanic Snow Island Suite rocks are in Figure 6. The first recognized examples of volcanic rocks were sparsely plagioclase-porphyrific dacite intrusions exposed in homogeneous, erosionally isolated outcrops within the Marjorie-Kiggavik-Tehek area that resemble the interiors of siliceous domes, as at Pukiq Lake (Fig. 6a) and Akiliniq Hills (LeCheminant and Roddick, 1991). Snow Island Suite volcanic rocks are preserved at the base of Paleoproterozoic (2.1–1.7 Ga) sedimentary sequences at several locations within the Marjorie-Kiggavik-Tehek belt (Jefferson et al., 2015, this volume). At a locale southeast of Aberdeen Lake (Fig. 7), Snow Island Suite rhyolite (e.g. Fig. 6b), locally intercalated with epiclastic rocks, forms the soles of imbricate thrust faults carrying quartzite of the early Paleoproterozoic Ketyet River group (Anand and Jefferson, 2017). Along the southeast side of the Amer belt, highly strained Snow Island Suite basalt (Fig. 6c) and rhyolite are intercalated between Snow Island Suite diorite to granite and the basal conglomerate of the Amer Supergroup. Snow Island Suite volcanic and granite clasts are abundant in most exposures of the basal Paleoproterozoic conglomerate in the Ketyet River and Amer fold and thrust belts (Jefferson et al., 2015, this volume). The Snow Island Suite silicic volcanic rocks are challenging to map in some places because the basal Paleoproterozoic quartzite includes foliated sericitic layers that superficially resemble the highly strained sericitic rhyolite (McEwan, 2012). In the Tern Lake area near the Meadowbank gold mine, subvolcanic porphyry intrudes felsic volcanoclastic rocks.

Snow Island Suite mafic volcanic rocks have been found in three localities along the southeast flank of the Amer belt. The mafic volcanic rocks contain sparse millimetre-scale equant plagioclase phenocrysts, and locally exhibit silicified

Figure 5. Mafic intrusive Snow Island Suite rocks. **a)** Outcrop of homogeneous orthopyroxene-hornblende gabbro with tonalite segregations, south of Amer belt. Length of pen is 14 cm. Photograph by T. Peterson. NRCan photo 2012-189. **b)** Freshly broken outcrop face of lower amphibolite-facies orbicular leucogabbro, Marjorie-Kiggavik-Tehek belt (11PHA-36A, undated). Length of pen is 14 cm. Photograph by T. Peterson. NRCan photo 2012-190. **c), d)** Photograph and interpretation of layered features in gabbroic phases of mixed intrusion north of Thelon Basin (Station 12NK-L008; 2595.7 ± 3 Ma; Davis et al., 2014; see Fig. 7 for location). Lines in Figure 5d (sketch) follow textural features of photograph 5c. Figure 5c: NRCan photo 2022-319. **e)** Dark grey, layered gabbro enclosed in massive pink granodiorite at the same outcrop as Figure 5c and 5d. Field of view is 50 cm. See text for interpretation. Photographs 5c and 5e by C. Jefferson. NRCan photo 2022-318.



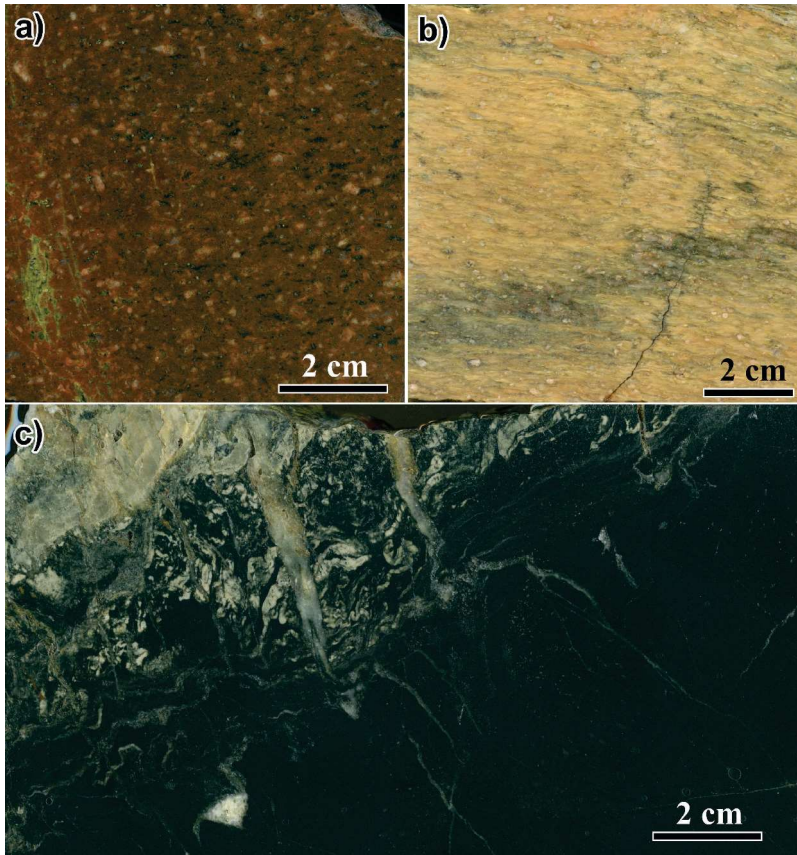


Figure 6. Flatbed scans of polished hand samples of Snow Island Suite volcanic rocks. **a)** Dacite, Pukiq Lake (80LAA-T36, 2610 \pm 11–13 Ma). **b)** Strongly deformed rhyolite quartz porphyry (11JP045) from the Pukiq imbricate zone (see Fig. 7 and text). **c)** Weakly deformed top of basalt flow (11JP271), south edge of eastern Amer Belt.

flow-top breccia (Fig. 6c). Snow Island Suite mafic flows are distinguished from the younger tholeiitic basalt of the Amer and Ketyet River groups by siliceous rather than carbonate alteration and by intercalation with felsic volcanic rocks that are lacking from the Amer and Ketyet River belts.

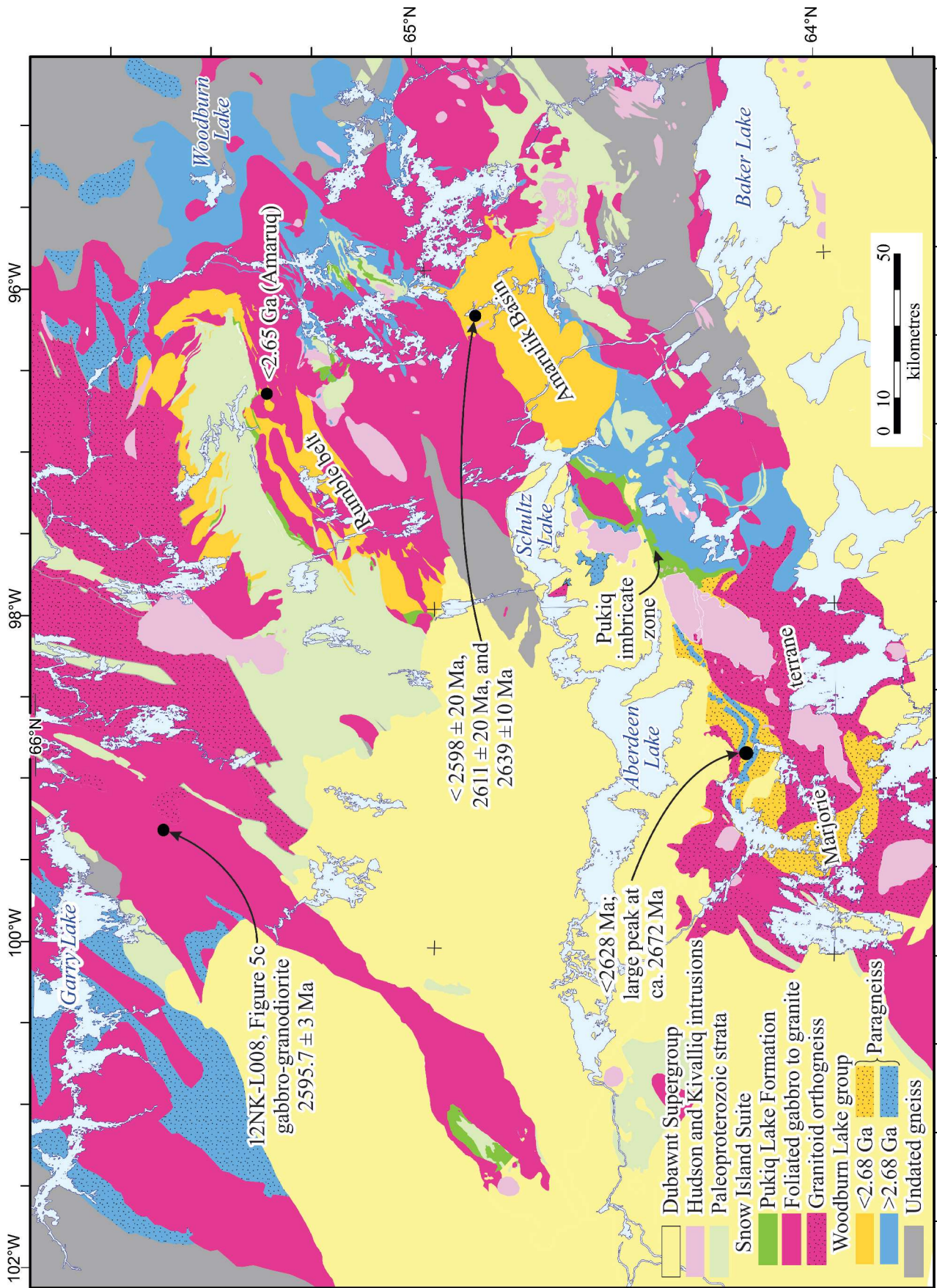
Detrital rocks correlated by geochronology with Snow Island Suite silicic volcanic sources are all turbiditic to laminated, with no evidence of shallow-water reworking (Jefferson et al., this volume). Rare outcrops of well preserved lapilli tuff appear to be subaerial and not reworked in any way. An epiclastic volcanic unit exposed in a tight synformal keel on Southampton Island, has a youngest dated zircon of 2599 ± 15 Ma (Fig. 2e), in a detrital population with a dominant mode at ca. 2.61 Ga and sporadic zircon

results as old as 3.2 Ga (Sanborn-Barrie et al., 2014). This is the sole known example of preserved Snow Island Suite volcanism outside the Marjorie-Kiggavik-Tehek belt.

Depositional basement to Snow Island Suite supracrustal rocks

The Marjorie-Kiggavik-Tehek belt in central Rae Province contains a series of seven, mostly pre-Snow Island Suite Neoproterozoic assemblages of the Woodburn Lake group (Fig. 7) with detrital and igneous zircon samples ranging from 3.1 Ga (Hunter et al., 2018) to 2.60 Ga (Davis, 2021). Tectonically emplaced sheets of Snow Island Suite granite structurally overlie the margins of the Amarulik Basin and cover much of the rest of the Woodburn Lake group (Fig. 7). The lithology, geographic and tectonic relationships, and

Figure 7. Simplified geology of the Marjorie Lake–Kiggavik Lake–Tehek Lake area and surround, *after* Jefferson et al. (this volume). Numbers are derived from zircon age populations (see text for references). Crosses (+) are prominent outcrop locations of Pukiq Lake Formation (silicic volcanic SIS). The 2595.7 ± 3 Ma gabbro-granodiorite referring to Figure 5c is a crystallization age. The detrital zircon maximum age of 2628 Ma in the Marjorie Basin is this study's type example within the pre-Snow Island Suite interval (Marjorie peak, Fig. 2a). Both Snow Island Suite and Marjorie peak ages occur in the upper Amarulik Basin, and the middle sequence of the Amarulik Basin has a maximum depositional age of 2.60 Ga. The mafic Rumble belt, intruded by Snow Island Suite gabbro (SISm1) has a maximum detrital age of 2.65 Ga. Continuing assessment of bedrock data northeast of the Amer shear zone is revealing that undivided gneiss there is also dominantly deformed Snow Island Suite intrusions (Jefferson et al., this volume).



geochronology of the Woodburn Lake group are summarized in Jefferson et al. (this volume). Although differences in metamorphic grade and deformation are present, the Woodburn Lake assemblages comprise ultramafic (some komatiitic) through mafic to felsic volcanic basal and middle units that are overlain by epiclastic beds or turbiditic psammite, commonly with iron-formation. Very minor quartz arenite and carbonate units in the Pipedream and Amarulik assemblages are thin and discontinuous. The contacts between Woodburn Lake group assemblages are all structural, except for the unconformity between the Pipedream and Amarulik assemblages. These attributes are consistent with the Woodburn Lake group being a tectonic assembly of individual volcanic edifices that initially formed as island arcs, oceanic plateaus, and/or micro-continents, potentially with back-arc basins (e.g. Kjarsgaard et al., 1997; Zaleski, 2002; Hunter et al., 2018).

The ultramafic to mafic volcanic-rich Rumble assemblage, which underlies Snow Island Suite mafic and/or felsic supracrustal rocks south of the Amer belt (and is intruded by Snow Island Suite gabbro to granodiorite) (Fig. 7), includes auriferous iron-formation in greywacke with a maximum depositional age of ca. 2.65 Ga (Valette et al., 2019), which is also synchronous with the early Marjorie peak and/or late early sanukitoid peak. Its relationship to the Snow Island Suite or other Marjorie peak suites is unclear. The three youngest assemblages of the Woodburn Lake group are clearly relevant to the Snow Island Suite, as they temporally overlap and may be part of a continuous syn-Snow Island Suite sequence. The Amarulik assemblage filled an extensional basin bounded by the Pipedream assemblage on the northeast and southwest, and by the Half Way Hills assemblage on the southeast (Fig. 7). The basal Amarulik conglomerate has detrital zircon as young as 2.68 Ga, but its middle sequence has the youngest detrital zircon of the entire Woodburn Lake group, at 2.60 Ga (Davis, 2021) — at the peak of Snow Island Suite activity — and its upper sequence appears to be even younger (Jefferson et al., this volume).

Snow Island Suite rocks were widely deposited directly upon, and/or intruded all but the Amarulik and Marjorie assemblages. Rare outcrops of Pukiq Lake formation overlie the Marjorie assemblage, and possible Snow Island Suite plutons cut its western portion south of Aberdeen Lake (Hunter et al., 2018; Jefferson et al., this volume).

LITHOGEOCHEMISTRY

The lithogeochemical study builds outward from the GEM-2 south Rae Province, GEM-2 Tehery-Wager, and GEM-1 Uranium data sets in south and central Rae Province–Snow Island Suite (Fig. 1), and is supported by abundant geochronological data and digitized field observations. The GEM study areas also encompassed some older studies and legacy data sets. These data were employed to

identify and expand populations based on consistent trace-element characteristics, from the Nunavut–Saskatchewan border through Dubawnt Lake, Amer belt and/or Kiggavik camp, and Tehery Lake–Wager Bay regions.

The remaining area, in northwest Rae Province–Snow Island Suite (i.e. Committee Bay belt, Melville Peninsula, and south of Boothia Peninsula) is covered by the map of Skulski et al. (2018), and interpretation of unpublished lithogeochemical data from this area was more limited. Snow Island Suite intrusions in the Committee Bay belt are interpreted as dominantly S-type granite (Skulski et al., 2003), although diorite is present (Sanborn-Barrie et al., 2014). Data from Melville Peninsula (Corrigan et al., 2013; L. Nadeau, unpub. data, 2012) were individually screened and compared to the Snow Island Suite groups, but were not used to define them. Data from south of Boothia Peninsula (Ryan et al., 2009) and the other northern Rae Province–Snow Island Suite areas have been holistically interpreted in a Neoproterozoic-specific discrimination diagram (late Archean granite ternary diagram, below).

Elemental analyses

Whole-rock elemental analysis for the GEM projects was performed at Actlabs (Ancaster, Ontario; <http://www.actlabs.com>) by XRF, ICP-MS, and titration using the same procedures as in Peterson et al. (2015a, in press). The full database of Snow Island Suite analyses is in Appendix A (this report). Identification of lithogeochemical groups was primarily made in chondrite-normalized REE diagrams and MORB-normalized multi-element diagrams. Representative and average compositions are given in Table 1.

As this study's data set includes gneissic and other strongly deformed rocks metamorphosed at high metamorphic grade, post-igneous mobilization of some elements as well as phenocryst accumulation, etc. will have been in action to move individual rock compositions away from those of actual magmas. Some of this study's samples demonstrably belong within a given group, but have anomalous values in one or more elements; these samples were generally excluded from average calculations. The principal lithogeochemical groups, which fall into two clans, are identified in a total alkalis–silica plot in Figure 8. They are:

A felsic infracrustal (crustal migmatite) clan, containing more than 50% of all samples.

- SISf1: dominantly porphyritic monzogranite;
- SISf1x: high-silica fractionated (or with evolved sources) granite associated with SISf1;
- SISst: mostly younger granitoid rocks with distinctly tonalitic trace-element patterns.

A sanukitoid clan, which includes some felsic and nearly all intermediate and mafic rocks.

- SISfs: felsic sanukitoid rocks;

Table 1. Average analyses of principal Snow Island Suite lithogeochemical groups, and the sanukitoid units of northern Melville Peninsula (sanukN) and the Repulse Bay Block (sanukS).

Group	SISm1	SISmbc	SISi	SISf1	SISf1x	SISf	SISfs	SISfsx	sanukS	sanukN
n	23	5	43	57	29	14	23	4	6	12
SiO ₂	50.33	49.35	58.77	66.79	74.92	69.49	67.40	76.07	53.08	54.67
TiO ₂	1.00	1.20	0.95	0.56	0.20	0.34	0.63	0.20	1.58	1.08
Al ₂ O ₃	15.75	15.61	15.57	14.79	13.07	14.87	14.48	12.94	16.19	15.55
Fe ₂ O ₃	3.37	4.78	2.17	1.57	0.78	0.80	1.70	0.63	3.02	3.06
FeO	7.61	8.89	5.87	3.10	0.88	2.03	2.65	0.72	6.35	6.42
MnO	0.17	0.18	0.12	0.07	0.03	0.04	0.08	0.02	0.11	0.12
MgO	6.47	5.77	2.92	1.39	0.41	0.93	0.99	0.31	3.31	5.01
CaO	9.17	9.22	5.24	2.92	0.67	2.34	2.43	0.21	6.37	7.19
Na ₂ O	2.90	2.90	3.45	3.14	3.16	3.21	3.50	3.11	3.75	3.41
K ₂ O	0.95	0.69	2.54	3.97	4.74	4.43	4.46	4.68	3.07	2.28
P ₂ O ₅	0.20	0.19	0.30	0.15	0.04	0.09	0.23	0.02	1.01	0.47
S	0.10	0.02	0.05	0.03	n/a	0.02	0.04	0.13	0.15	0.09
F	157	0	240	203	415	77	100	120	n/a	n/a
Rb	29	14	84	142	182	129	121	114	71	83
Cs	1.0	0.7	2.9	2.6	2.0	1.6	1.7	1.2	3.1	2.0
Be	1.0	0.5	1.7	2.5	2.4	1.7	2.0	2.0	n/a	n/a
Sr	422	474	474	301	113	421	469	84	1565	759
Ba	276	339	1056	1059	621	1096	2064	1577	3036	883
Sc	29	34	17	11	4	6	9	5	12	20
Y	20	13	24	30	33	7	31	34	30	25
Zr	88	51	223	246	228	163	437	271	433	188
Hf	2.25	1.30	5.34	6.63	7.01	4.29	9.87	7.46	8.36	4.74
V	202	329	108	50	11	45	35	0	147	161
Nb	4.7	1.6	8.9	12.4	17.1	5.5	13.8	16.7	18.5	13.2
Ta	0.31	0.12	0.73	0.98	1.39	0.44	0.81	1.14	0.59	0.81
Cr	181	78	126	37	29	36	17	27	83	146
Co	45	47	28	15	18	6	6	17	24	31
Ni	105	70	38	16	4	22	6	8	35	76
Zn	93	130	93	65	39	41	79	25	141	99
Pb	8	10	16	21	29	19	26	15	30	11
La	20	12	36	62	62	48	108	76	141	53
Ce	45	26	76	127	129	92	216	157	365	115
Pr	5.7	3.2	9.2	14.5	14.0	9.9	24.0	18.3	39.5	14.1
Nd	23.2	13.4	36.9	53.1	47.9	33.9	84.7	65.6	136.4	55.1
Sm	4.62	2.89	6.96	9.18	8.08	5.02	12.63	9.98	20.22	9.29
Eu	1.40	1.20	2.04	1.62	0.83	1.23	2.70	1.85	3.97	2.33
Gd	4.24	2.80	5.80	7.16	6.18	3.04	8.58	7.72	14.85	7.01
Tb	0.65	0.42	0.82	1.02	0.97	0.34	1.14	1.07	1.38	0.90
Dy	3.69	2.51	4.60	5.61	5.65	1.60	5.85	5.89	5.71	4.59
Ho	0.72	0.48	0.89	1.07	1.15	0.27	1.11	1.14	1.00	0.84
Er	2.01	1.38	2.50	3.03	3.34	0.71	3.06	3.33	2.44	2.25
Tm	0.30	0.20	0.36	0.44	0.52	0.10	0.45	0.52	0.33	0.31
Yb	1.87	1.24	2.28	2.80	3.44	0.63	2.89	3.26	1.84	1.95
Lu	0.29	0.19	0.35	0.43	0.53	0.10	0.46	0.50	0.25	0.28
Th	2.1	0.9	5.5	17.2	28.4	10.9	16.3	15.9	9.7	7.6
U	0.5	0.2	1.8	2.9	4.5	1.3	2.4	3.6	0.8	1.6

See Acosta-Góngora et al. (2018) for analyses of the Thye Lake and Axis Lake metabasalt rocks.

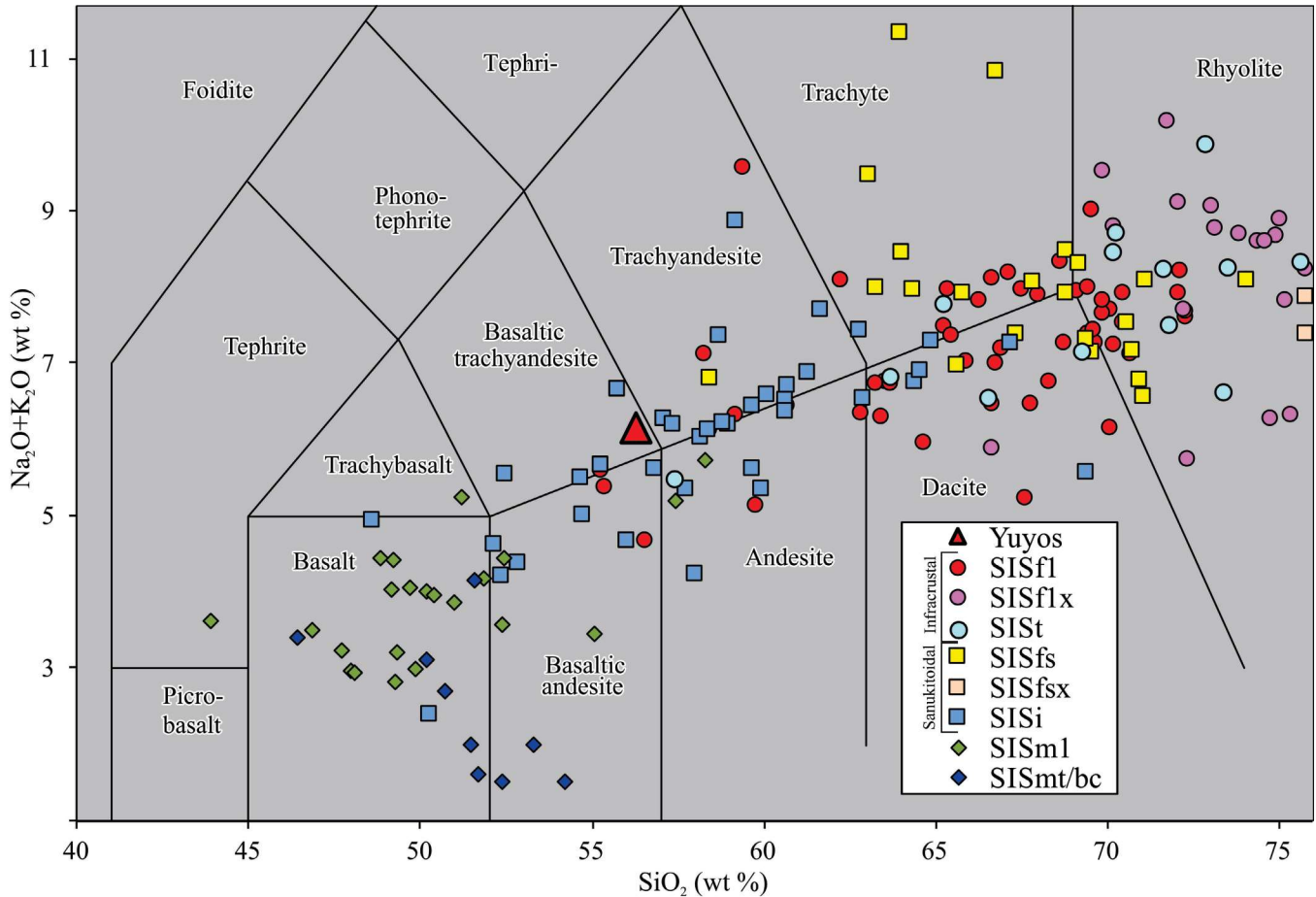


Figure 8. Total alkali-silica plot for all central and south Rae Province Snow Island Suite samples, excluding anomalous analyses. Circles are interpreted as infracrustal granitoid rocks; squares are sanukitoidal intermediate and felsic rocks. “Yuyos” is an average recent Th-rich sanukitoid flow from Ecuador (Chiaradia et al., 2014).

- SISfsx: fractionated, high-silica sanukitoidal rhyolite;
- SISi: sanukitoidal intermediate rocks (quartz diorite and monzodiorite);
- SISm1: the commonest mafic rock type, with continental-arc trace-element signatures;
- SISmtbc and SISmt: mafic rocks from the Borden complex, Tehery Lake–Wager Bay area, and from Thye Lake, Snowbird Domain, respectively, that have similar and distinct, sharp sanukitoidal trace-element patterns. Gabbroic rocks emplaced at Axis Lake at ca. 2.64 Ga (south Rae Province) are within the pre–Snow Island Suite Marjorie peak time period, and also have subduction and/or sanukitoid (adakitic) features.

The authors prefer to identify a single infracrustal clan, as opposed to S- and I-type granitoid rocks, as its distinction from sanukitoid rocks is mostly straightforward, but its subdivision is not.

In addition to these widely distributed groups, local clusters are present (e.g. four strongly trace-element-depleted, high-silica granite samples from the Wholdaia Lake shear zone: Thiessen et al., 2017, 2018). The present authors recognize numerous granitoid rocks and some intermediate rocks that display characteristics of both the sanukitoidal and infracrustal clans (or are transitional) and are difficult to classify. As the ages of the infracrustal and sanukitoidal clans overlap, and both are voluminous, hybridization would be expected to be common. Only four highly fractionated sanukitoidal rhyolite samples are recognized in the data set for this study, perhaps because hybridization rendered most of the evolved sanukitoid rocks unrecognizable. Rather than create an additional hybrid group with necessarily fuzzy boundaries, the present authors included these transitional rocks in group SISfs, since they are interpreted as pointers to the presence of sanukitoid melts in the magmatic lineage.

The late Archean granite ternary classification diagram of Laurent et al. (2014), designed specifically for intermediate and silicic intrusive rocks of the Neoproterozoic, was employed to gain additional insight to the sources of Snow Island Suite felsic and intermediate rocks. Four fields are within the

late Archean granite ternary diagram: tonalite; infracrustal granite (Laurent et al. (2014) refer to this as the two-mica granite field); sanukitoid; and hybrid rocks, which represent magmatic hybrids or melts of mixed sources. The entire south and central Rae Province–Snow Island Suite data set (excluding anomalous samples) is so plotted in Figure 9, using the group assignments determined by the trace-element compositions. Additional late Archean granite plots of northern Rae Province data are given in Figure 10, which shows the spatial distribution of the identified lithotypes.

Infracrustal clan: SISf1, SISf1x, SISf

Compositionally, the infracrustal clan more closely resembles a cospatial Proterozoic granitoid suite (the ca. 1.83 Ga Hudson granite suite, PHg; Peterson et al., 2002) than any of

the contemporary or older Archean granitoid rocks. In south Rae Province both Snow Island Suite and Hudson granite include prominent subtypes with granitic major-element and tonalitic trace-element compositions (SISf1 and PHg; Peterson et al., in press). Overall, the SISf1 group ($n = 57$) is characterized by a moderate negative Eu anomaly (average $\text{Eu}/\text{Eu}^* = 0.61$) and modest LREE enrichment ($(\text{La}/\text{Yb})_N = 9.9$) (Fig. 11) with Ba depleted relative to Rb and Th and strong depletions in Nb, P, and Ti relative to MORB, but nondepleted Zr and Hf. In the chondrite-normalized REE diagram, the SISf1 envelope is bracketed by the separate envelopes of Hudson granite from south Rae Province and Tehery Lake–Wager Bay areas, and in a MORB-normalized trace-element diagram, average SISf1 and Hudson granite are very similar (the latter have higher Rb and Th). The simplest interpretation is that SISf1 and Hudson granite were generated from the

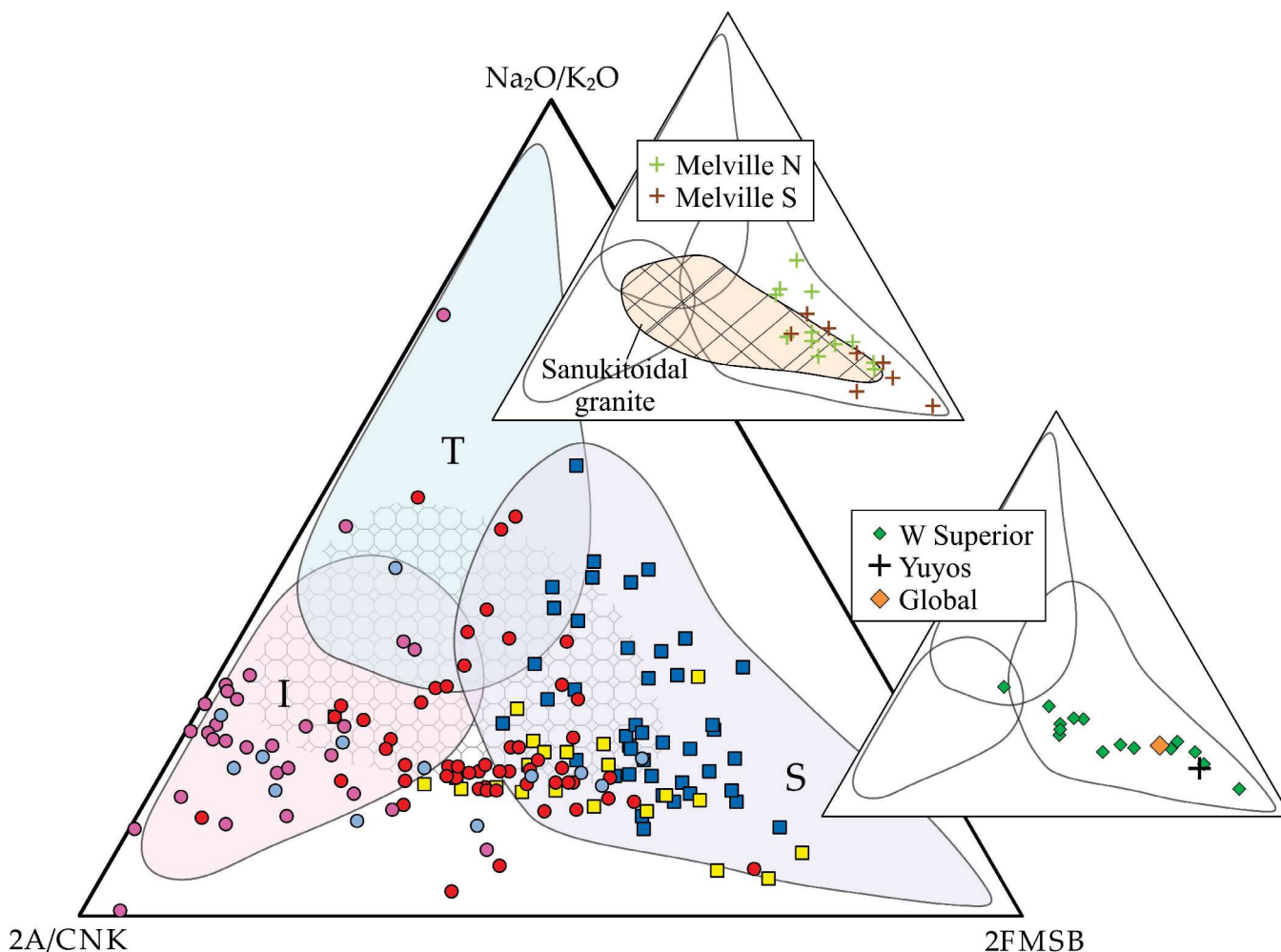


Figure 9. Late Archean granite ternary diagram, with all felsic and intermediate Snow Island Suite samples plotted (after Laurent et al., 2014). The fields (coloured) are T = tonalite, I = two-mica granite (infracrustal); S = sanukitoid. The patterned field underlying these includes rocks termed “hybrid.” The upper inset includes sanukitoid data from Melville Peninsula, with the field encompassing sanukitoid granite from the Closepet (Moyen et al., 2001) and Berach (Mondal and Raza, 2013) complexes, India. Lower inset data: Yuyos recent sanukitoid flow, Ecuador, of Chiaradia et al. (2014); the global sanukitoid average of Martin et al. (2010); and western Superior mafic, intermediate, and felsic sanukitoid data of Stevenson et al. (1999). $2A/CNK = 2^*Al_2O_3/(CaO+Na_2O+K_2O)$ (molecular); $2FMSB = 2^*(FeO+Mg)^*(Sr+Ba)$ (in wt %).

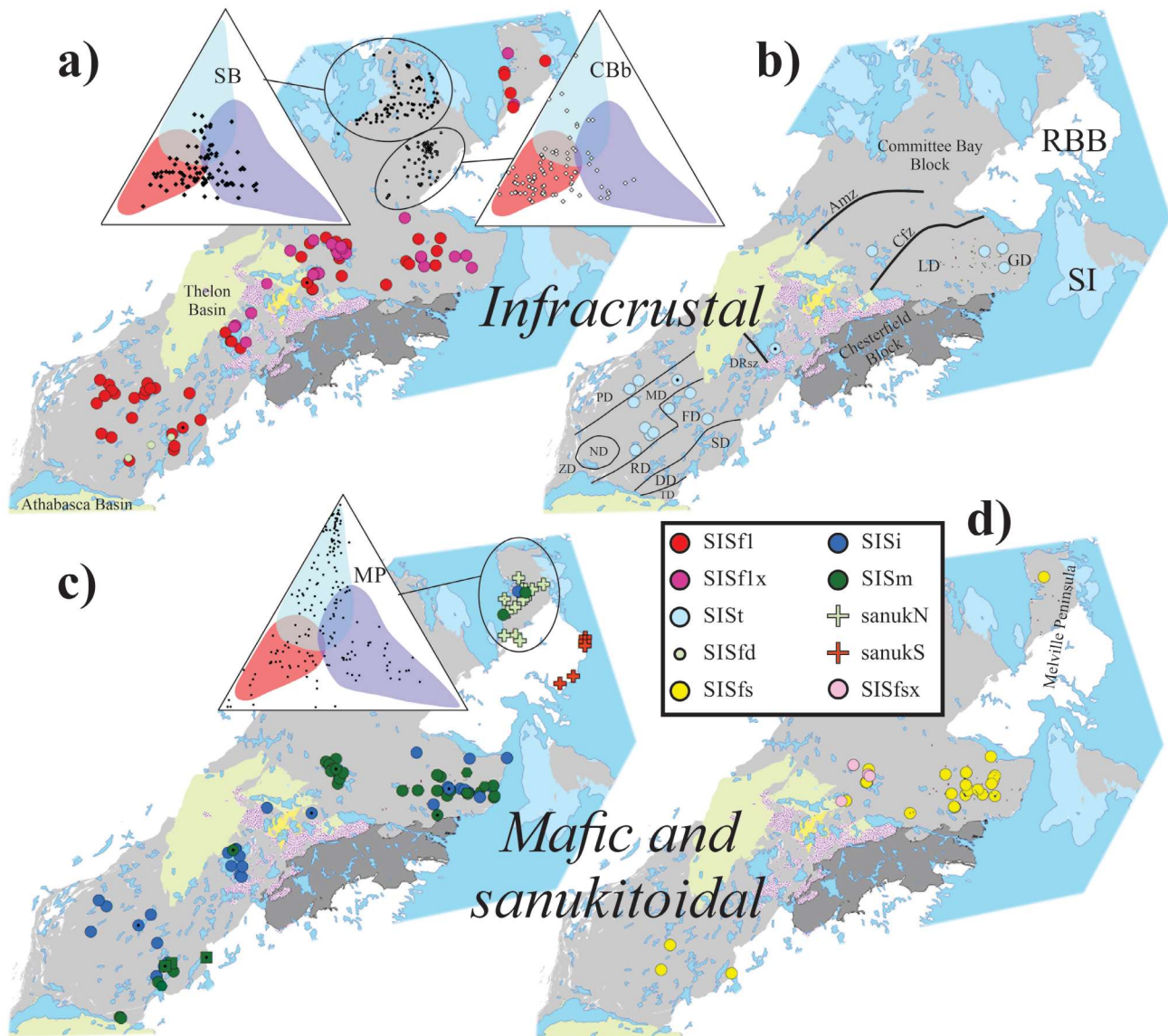


Figure 10. Distribution of Snow Island Suite lithotypes. The SISm group includes all mafic subtypes. Symbols with bullseyes are “anomalous” samples with some geochemical features outside the group range. **a)** SISf1 and SISf1x samples. Insets are the Late Archean granite ternary plots for all Archean through Proterozoic intermediate to felsic analyzed samples from south of Boothia Peninsula (SB) and from the Committee Bay belt (CBb), which indicate a paucity of tonalite and sanukitoid in those areas. **b)** SISst samples. Amz = Amer mylonite zone, Cfz = Chesterfield fault zone, DRsz = Dubawnt River shear zone, FD = Firedrake Domain, RBB = Repulse Bay Block, GD = Gordon Domain (east Tehery Block), LD = Lunan Domain (west Tehery Block), MD = McCann Domain (southern end also termed Nolan Domain, ND = Nolan Domain, PD = Porter Domain, RD = Train+Beaverlodge domains, SD = Snowbird Domain (including Wholdaia Lake shear zone and Chipman Domain), SI = Southampton Island, TD = Tantato Domain, ZD = Zemlak Domain, DD = Dodge Domain. **c)** Mafic and intermediate Snow Island Suite. Hexagonal symbols are from the Borden Complex, and square symbols are from Thye Lake. The inset is the Late Archean granite ternary plot for all felsic through intermediate samples from northern Melville Peninsula (MP) (Corrigan et al., 2013). The Melville Peninsula data set has been screened to identify rocks with Snow Island Suite U-Pb ages, and sanukitoid samples. **d)** Locations of sanukitoid granite (SISfs and SISfsx; the latter are present only as rhyolite in the Marjorie-Kiggavik-Tehek belt). Many of the SISfs samples in the Tehery Lake–Wager Bay area are at the intermediate-felsic boundary (20% quartz) and could be represented as SISi.

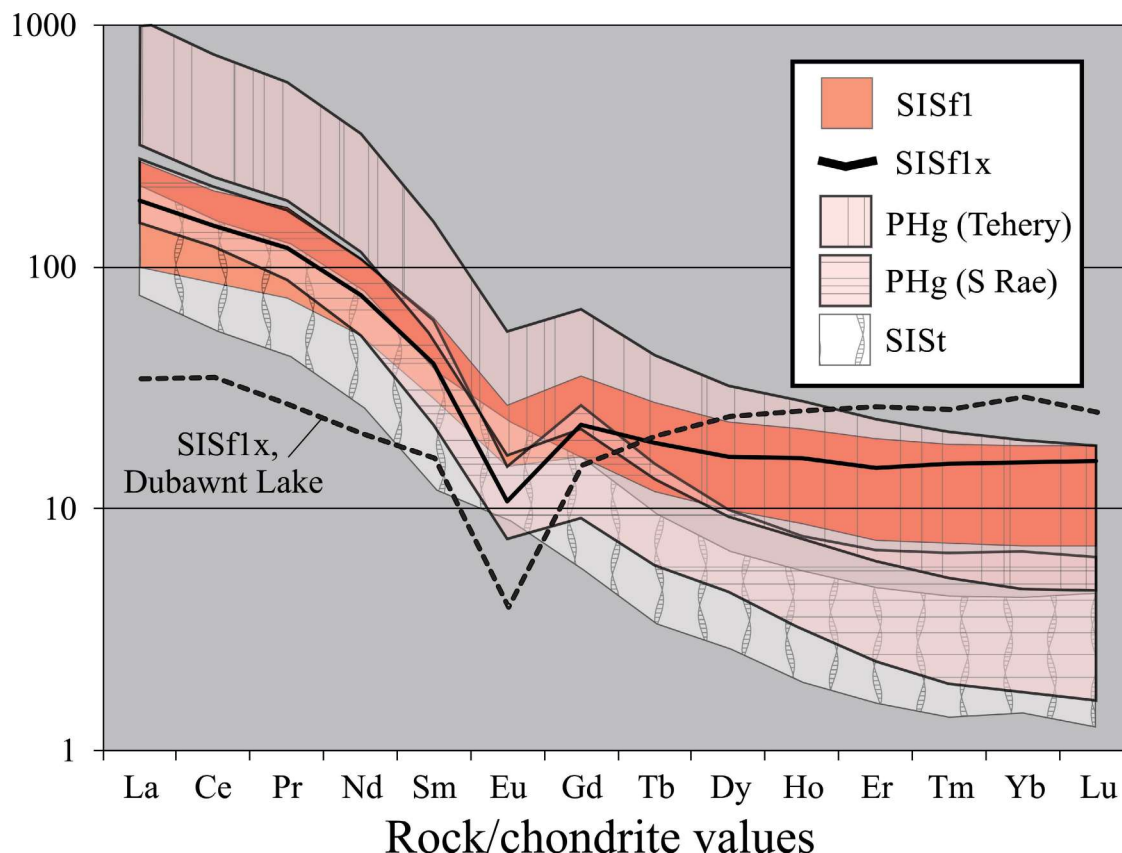


Figure 11. Chondrite-normalized (values of Nakamura, 1974) envelopes calculated as the average $\pm 1\sigma$ for all SISf1 samples, compared to the envelopes of Proterozoic Hudson granite (PHg) from the Tehery Lake–Wager Bay and south Rae Province areas (Peterson et al., in press). South Rae Province and Tehery Lake–Wager Bay PHg bracket the extremes of trace-element composition for the Hudson granite and are very similar to SISf1, though slightly more fractionated. Average SISf1x and a single extreme example from Dubawnt Lake (88PHA-254A) show the tendency to gullwing REE profiles in this highly variable group. The envelope for SISSt displays the typical strong fractionation and low, flat HREE content of tonalite-trondhjemite-granodiorite suites.

same source, and the persistent negative Eu and Ba anomalies indicate that plagioclase and perhaps potassium feldspar are part of the restite mineralogy. The Hudson granite suite has been interpreted to originate from partial melting at mid-crustal levels at the peak of Hudsonian crustal thickening in the western Churchill Province, with little to no juvenile input, and with varying levels of HREE depletion due to pressure-dependent modal garnet variations (Peterson et al., 2002).

A large ($n = 29$) set of granite samples very similar to SISf1, including samples from an equigranular, dated leucogranite intrusion at Dubawnt Lake that is adjacent to a large SISf1 monzogranite (Fig. 3e), displays extreme Ba depletion together with strongly depleted compatible elements, high silica, and a tendency to ‘gullwing’ REE profiles with extreme negative Eu anomalies (SISf1x). These samples can be interpreted as fractionated SISf1, but may also represent melts of relatively potassic, quartzofeldspathic

metasedimentary rocks depleted in heavy minerals. The average of this highly variable group, plus a single gullwing leucogranite from Dubawnt Lake, is plotted in Figure 11. In Figure 10a, it can be seen that no SISf1x samples have been identified in south Rae Province, beyond southwestern Dubawnt Lake. The limit corresponds closely to a north-west-trending fault (the Dubawnt River shear zone: Peterson and Lee, 1995) that separates polyphase tonalitic gneiss on the south side from Snow Island Suite pelitic and volcanic supracrustal rocks (e.g. Clarke River Schist: Peterson and Born, 1994).

There is little to no true tonalite in the Snow Island Suite (Fig. 9), although tonalitic segregations have been observed in gabbroic intrusions (Peterson et al., 2015a); however, dated syenogranite and monzogranite with distinctly tonalitic REE (strong LREE enrichment with flat, depleted HREE) (Fig. 11) and MORB-normalized (strongly depleted Yb–Sc) patterns are common in and around the tonalite-rich

McCann and Firedrake domains of south Rae Province and up to the Dubawnt River shear zone (group SIS_t, $n = 14$) (Fig. 10b). They are also present in the tonalite-rich Gordon Domain (Tehery Lake–Wager Bay area). The SIS_t are among the youngest Snow Island Suite rocks in the south Rae Province area (average of six ages = 2592 Ma, excluding one age of 2628 Ma; data of Regis et al., 2017b) and therefore are likely to have formed at relatively high crustal levels, and to contain a significant proportion of migmatized sedimentary rocks. These features are consistent with SIS_t and SIS_{f1x}, largely representing melts of metasedimentary rocks with SIS_t samples containing a significant contribution from e.g. greynwacke or tonalitic gneiss.

Figure 10a shows the outcrop positions of all lithochemical samples from the south of Boothia Peninsula and Committee Bay project areas (J. Ryan, unpub. data, 2019; H. Sandeman, pers. comm., 2019). The corresponding late Archean granite ternary plots for felsic and intermediate rocks in these sets, without any screening for age or rock type, indicate that the Committee Bay area is strongly dominated by infracrustal melts, consistent with the presence of abundant migmatized supracrustal rocks (Skulski et al., 2018). The data set from south of Boothia Peninsula is concentrated in the hybrid zone, with minor sanukitoid samples. Neither area contains the large volume of tonalite and sanukitoid present in northern Melville Peninsula (Fig. 10c, inset), which is more similar to the south Rae Province and Tehery Lake–Wager Bay areas. This study concludes that the north-west extent of Rae Province–Snow Island Suite between Melville Peninsula and Queen Maud Block fundamentally differs from the remainder of the igneous province, by containing a higher proportion of melted supracrustal rocks with little detectable contribution from tonalite-rich basement or associated suites, such as sanukitoid rocks.

Sanukitoid clan

Relatively enriched Snow Island Suite granite and rhyolite that are distinguished by elevated Ba and LREE/HREE, with no Eu anomaly, were first identified in the GEM-1 study in central Rae Province (Peterson et al., 2015a). These enriched rocks share many features of so-called sanukitoid granite (e.g. Closepet: Moyen et al., 2001; Berach: Mondal and Raza, 2013). Similar granite in the south Rae Province and Tehery Lake–Wager Bay areas was subsequently recognized as transitional to voluminous intermediate rocks with more well defined sanukitoid affinities (SIS_i), including a close association with tonalite-rich basement. Additionally, most analyzed mafic rocks that formed at the same time as Snow Island Suite and Marjorie peak have trace-element patterns that strongly resemble both Archean sanukitoid and certain enriched rocks from modern subduction zones, such as adakite.

Mafic and intermediate rocks

The most common type of mafic rock (with data from all areas except the Committee Bay and Chesterfield blocks) is a tholeiitic to subalkaline basalt with significant incompatible element enrichment and depletion in all high-field-strength elements except P (group SIS_{m1}; Fig. 12). Snow Island Suite mafic rocks in and near the Borden complex (SIS_{mbc}; Tehery Lake–Wager Bay area) and at Thye Lake (SIS_{mt}; south Rae Province) have similar, but more pronounced trace-element anomalies, particularly in Ba. These groups, and the pre-Snow Island Suite Axis Lake gabbro rocks, are compared to other important, cospatial Rae Province mafic igneous suites in a Th/Yb–Nb/Yb discriminant plot (Fig. 13).

The Thye Lake (or Nickel King, in Snowbird Domain) and Axis Lake (including nearby Currie Lake, in Tantato Domain) gabbro units of south Rae Province were interpreted by Acosta-Góngora et al. (2018) as representing the early stages of continental-arc development in southeast Rae Province. The Axis Lake gabbro (ages of 2639 ± 19 Ma and 2637 ± 8 Ma; Regis et al., 2017a) has a trace-element signature similar to post-Archean oceanic arcs (Fig. 13) and near-juvenile Nd isotope compositions (*see* section ‘Nd isotopes’), whereas the 2609 ± 29 Ma (Regis et al., 2017a) Thye Lake gabbro (SIS_{mt}) and the SIS_{m1} and SIS_{mbc} gabbro and basalt resemble continental-arc rocks. Both Thye Lake and Axis Lake gabbro units have high Mg contents suggestive of boninite (Acosta-Góngora et al., 2018).

Sheared basalt samples from the western margin of the Snowbird Domain (inside the Wholdaia Lake shear zone) were collected and dated by Thiessen et al. (2017, 2018), yielding U–Pb ages of 2592 ± 16 Ma and 2611 ± 4 Ma. These mafic rocks form a distinctive group with MORB-like element patterns. Two of the samples have unsystematic trace-element anomalies and appear altered by deformation and/or metamorphism, but one relatively systematic sample plots in an area of Figure 13 appropriate to a near-continent back-arc basin, similar to two unassociated suites of ca. 2.7 Ga Rae Province volcanic rocks (the Lorillard and MacQuoid supracrustal belts).

In Figure 12, Snow Island Suite mafic and intermediate rocks are compared to type mafic and intermediate sanukitoid rocks from western Superior Province (Stevenson et al., 1999) and to the sanukitoid rocks of Melville Peninsula. Diagnostic sanukitoid signatures in these plots are high enrichments in Ba and Sr, nondepletion in P, and marked depletions in Nb–Zr–Hf together with elevated values of Cr and Ni. These features are interpreted to result from melting of metasomatized peridotite (either lithospheric or convecting), with enrichment by hydrous tonalitic melts derived from subducting slabs (e.g. Stern and Hanson, 1989) or from foundered lithospheric mantle and enriched mantle-like (EM1-like) sources (e.g. LaFlamme et al., 2015). The style of enrichment in these rocks, particularly with strongly

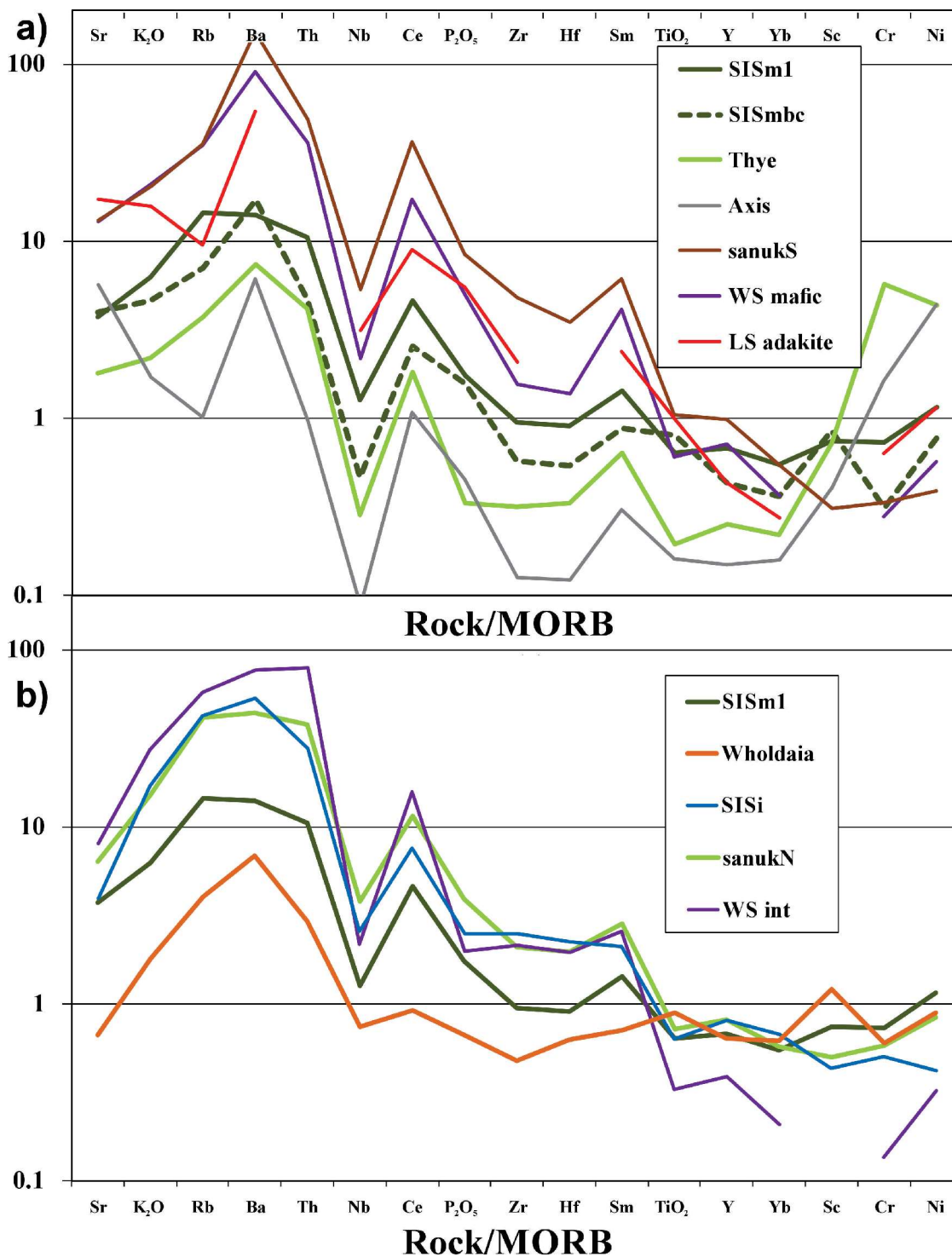


Figure 12. MORB-normalized average analyses for SISm1 (n = 19), SISmbc (n = 5), Thye Lake gabbro (n = 7), Axis Lake gabbro (n = 13), SISI (n = 43), sanukitoid rocks from southern (sanukS, n = 6) and northern (sanukN, n = 12) Melville Peninsula, and sanukitoid rocks from western Superior (WS) Province (Stevenson et al., 1999). **a)** The average of 70 young low-silica (LS) adakite samples (Martin et al., 2005) has strong similarities to average Axis Lake gabbro. **b)** Intermediate rocks (western Superior: n = 6; WS int) and the undated sanukN belt, which is associated with Snow Island Suite, compared to SISm1. The single Wholdaia sample (15ET249, U-Pb age 2592 ± 16 Ma; Thiessen et al., 2018) is consistent with MORB slightly contaminated by LILE.

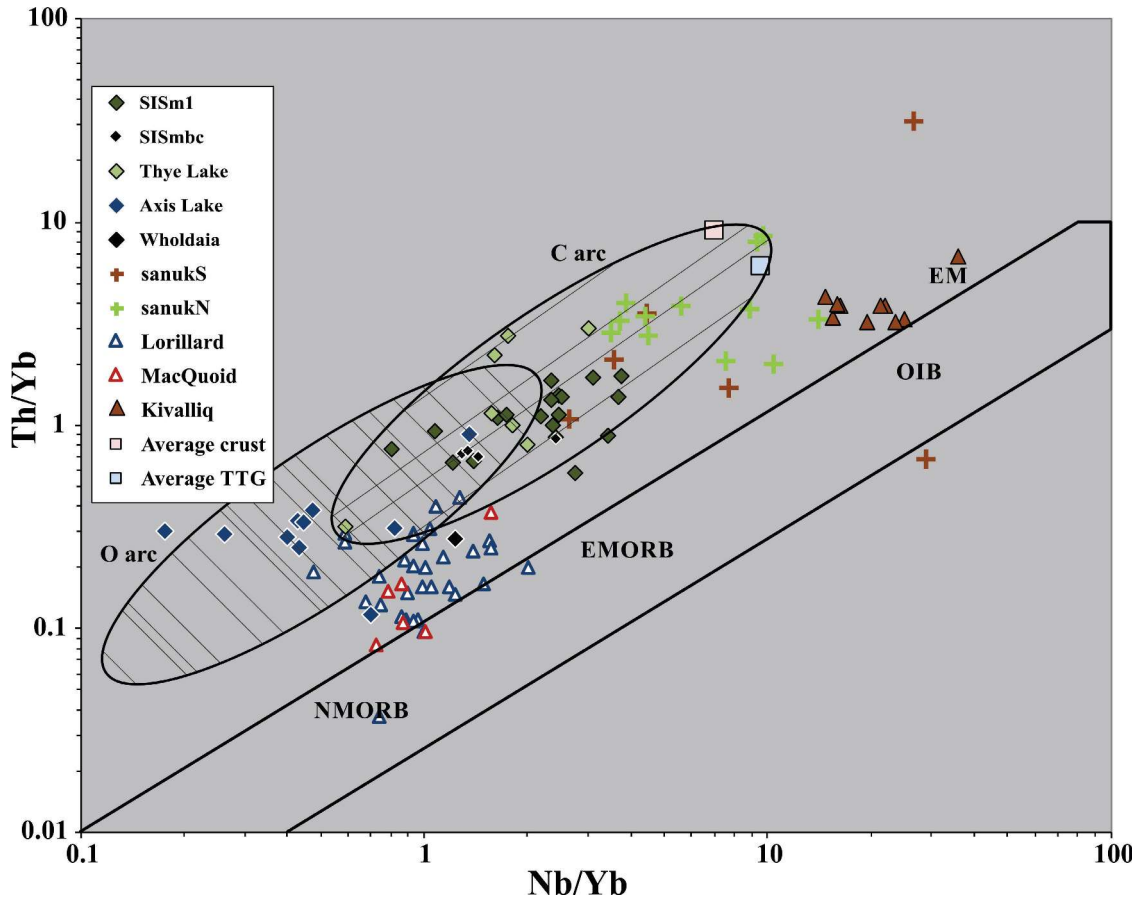


Figure 13. A Th/Yb versus Nb/Yb plot (with fields *after* Pearce, 2008) for Snow Island Suite mafic rocks, compared to other Archean and Proterozoic suites of the Rae Province. ‘Kivalliq’ are ca. 1.75 Ga post-Hudsonian, anorogenic subalkaline basalt associated with rapakivi granite (Peterson et al., 2014), with a probable origin in EM1-type enriched mantle. ‘MacQuoid’ (Sandeman et al., 2006) and ‘Lorillard’ (Steenkamp et al., 2023a, b, c) are ca. 2.7 Ga volcanic rocks in Chesterfield Block and Tehery Lake–Wager Bay area, respectively, that are provisionally interpreted as oceanic back-arc rocks. ‘Wholdaia’ is a single sample of Snow Island Suite–aged gabbro from the Wholdaia Lake shear zone, south Rae Province (Thiessen et al., 2018) that resembles a MORB with minor crustal contamination. TTG = Tonalite-trondjemite-granodiorite

depleted Zr-Hf, is consistent with a high-pressure tonalite melt derived from rutile-bearing eclogite (Moyen, 2011). The only significant P-bearing restite phase in rutile eclogite is garnet (approximately 0.6–0.8% P₂O₅; Konzett and Frost, 2009), so high-pressure tonalite melt should also be enriched in P. Subduction at a shallow angle may enhance the forward extent of hydration and metasomatism of overlying mantle (e.g. Humphreys et al., 2003), and extraction of a sanukitoid magma from this source may potentially occur any time during or after enrichment.

The sanukitoid rocks of southern Melville Peninsula (i.e. Repulse Bay Block; Fig. 10c) have enrichment levels comparable to mafic sanukitoid rocks from western Superior Province (Fig. 12a). The style of this enrichment — with sharp, elevated Ba peaks and marked depletion in all

high-field-strength elements except P — is duplicated in the Axis Lake, Thye Lake, and SISmbc profiles (except, average Thye Lake gabbro is not enriched in P). Enrichments in Ni-Cr in sanukitoid rocks are attributed to high compatible element concentrations in the metasomatized mantle source (Stern and Hanson, 1989). The Thye Lake and Axis Lake gabbro units, with very high Sc-Cr-Ni, appear to be an extreme example of this and the apparent dilution of the more incompatible trace elements relative to sanukitoid rocks is consistent with high degrees of partial melting (i.e. boninitic magmas), and not necessarily postigneous mineralization (*see* discussion by Acosta-Góngora et al., 2018). The extremely high Sr in average Axis Lake gabbro (Fig. 12a) is similar to that observed in the average of 70 globally distributed, young, low-silica adakite samples (Martin et al., 2005).

Figure 12b compares average intermediate rocks from western Superior Province and the Snow Island Suite to the northern Melville sanukitoid rocks (sanukN) and SISm1. Compared to their mafic counterparts, the intermediate Superior Province sanukitoid rocks have a much flatter Ba peak with relatively depleted P and a modest Zr-Hf anomaly, all features common to SISi. Average SISi and sanukN from Melville Peninsula are virtually identical except for elevated P in sanukN. Muting of sharp sanukitoid trace-element signatures in the intermediate rocks by crystal fractionation and crustal contamination (hybridization) was invoked by both Stevenson et al. (1999) and Whalen et al. (2004) to explain the spectrum of compositions in the Superior sanukitoid rocks. An additional possibility, particularly for such a large system as the Snow Island Suite, is that the intermediate sanukitoid rocks originated in mantle metasomatized by rutile-absent medium- or low-pressure tonalite (i.e. partial melts of garnet amphibolite), which imposed a less extreme enrichment pattern than would high-pressure tonalite melt.

Felsic sanukitoid rocks

Although trace-element discriminant plots indicate that there is a population of sanukitoid granite in the Snow Island Suite, individual analyses of felsic rocks commonly have characteristics of both intermediate sanukitoid rocks (high Ba, no Eu anomaly, LREE enrichment) and the infracrustal granite clan (depleted P, elevated Zr-Hf). The SISfs and SISfsx groups are compared to other felsic sanukitoid rocks in Figure 14.

The SISfs group has higher overall REE contents (Fig. 14a) than the Berach granite or western Superior Province felsic sanukitoid rocks, with slightly lower LREE/HREE ratios. In the MORB-normalized plot (Fig. 14b) the SISfs differs from these standards in having elevated Zr-Hf and Y-Yb; however, the Berach granite itself has nonsanukitoid features (e.g. small Ba and Eu depletions). The four silica-rich rhyolite samples of group SISfsx are extremely depleted in Sr, P, and Ti and have small negative Eu anomalies (owing to plagioclase, apatite, and oxide fractionation) and plot in the infracrustal field in the late Archean granite ternary diagram (Fig. 9), but also have elevated Ba and so were assigned to the margin of the sanukitoid clan.

Nd isotopes

The Sm-Nd isotope analysis of Snow Island Suite rocks has been routinely done as part of mapping and lithosphere studies for several projects in Rae Province (e.g. Peterson, 2006; Hinchey et al., 2011; Regan et al., 2017b). These data were primarily collected to characterize local crust, using the depleted mantle model age (T_{DM}). This paper will refer here solely to the new GEM data sets, as they are well constrained both by lithotype and crystallization age, and were performed

at a single laboratory (summarized in Table 2). This paper also reconsiders previously published data for mafic rocks from Axis Lake and Thye Lake (Acosta-Góngora et al., 2018).

In Figure 15, a plot of normative quartz (a proxy for lithotype) versus depleted Nd model age (*after* DePaolo, 1981), three features appear: 1) several mafic rocks from the SISm1 and Axis Lake groups have model ages near 2.6 Ga, indicating their primary melt source extended to depleted, convecting mantle or very recently extracted lithosphere; 2) the four oldest model ages are all for sanukitoid rocks; and 3) the most evolved rocks (SISf1x and SISf, two samples of each) lie within a narrow range of T_{DM} (2.95–2.75 Ga) that includes igneous ages from proximal Rae Province supracrustal belts (e.g. Woodburn Lake group: Jefferson et al., this volume). As described in the ‘Infracrustal clan: SISf1, SISf1x, SISf’ section, the SISf are interpreted to be sourced in part from migmatized supracrustal rocks, and a pelitic source contribution for some of the relatively potassic and high-silica SISf1x is reasonable. Whalen et al. (2004) suggested that granitic rocks proximal to sanukitoid rocks in Wabigoon subprovince contained a combination of older tonalitic crust and isotopically juvenile supracrustal rocks, which invokes scenarios similar to Rae Province–Snow Island Suite.

Only one of the intermediate rocks has a model age within the SISf-SISf1x box; all others yield older ages. The correlation of intermediate sanukitoid geochemical features with old model ages leads the authors to propose that the source for SISi was dominantly in old, mafic lithosphere that was metasomatized prior to remelting during the formation of the Snow Island Suite and was distinct from the source of much more mafic Snow Island Suite gabbro units. Among mafic rocks, the Borden complex samples (SISmbc) are anomalous for having old (ca. 3.0 Ga) model ages, with small variability. This complex is located in the Gordon Domain, eastern Tehery Lake–Wager Bay area, which has yielded numerous Archean and Proterozoic samples with Nd model ages 3.0 Ga or older (Steenkamp et al., 2023a, b, c).

DISCUSSION

Given the scale of the Snow Island Suite, it is noteworthy that its U-Pb age histogram (Fig. 2a) is so simple, even mimicking the sudden rise and slower descent of temperature in rapidly heated bodies. The authors interpret this to mean the Snow Island Suite represents a single coherent event lasting about 40 million years. The absence of known contemporaneous dyke swarms (e.g. Buchan and Ernst, 2004) or prevolcanic clastic axial basins is inconsistent with continental rifting, anorogenic basin, or plume uplift models, and suggests that convergent tectonic models are more applicable.

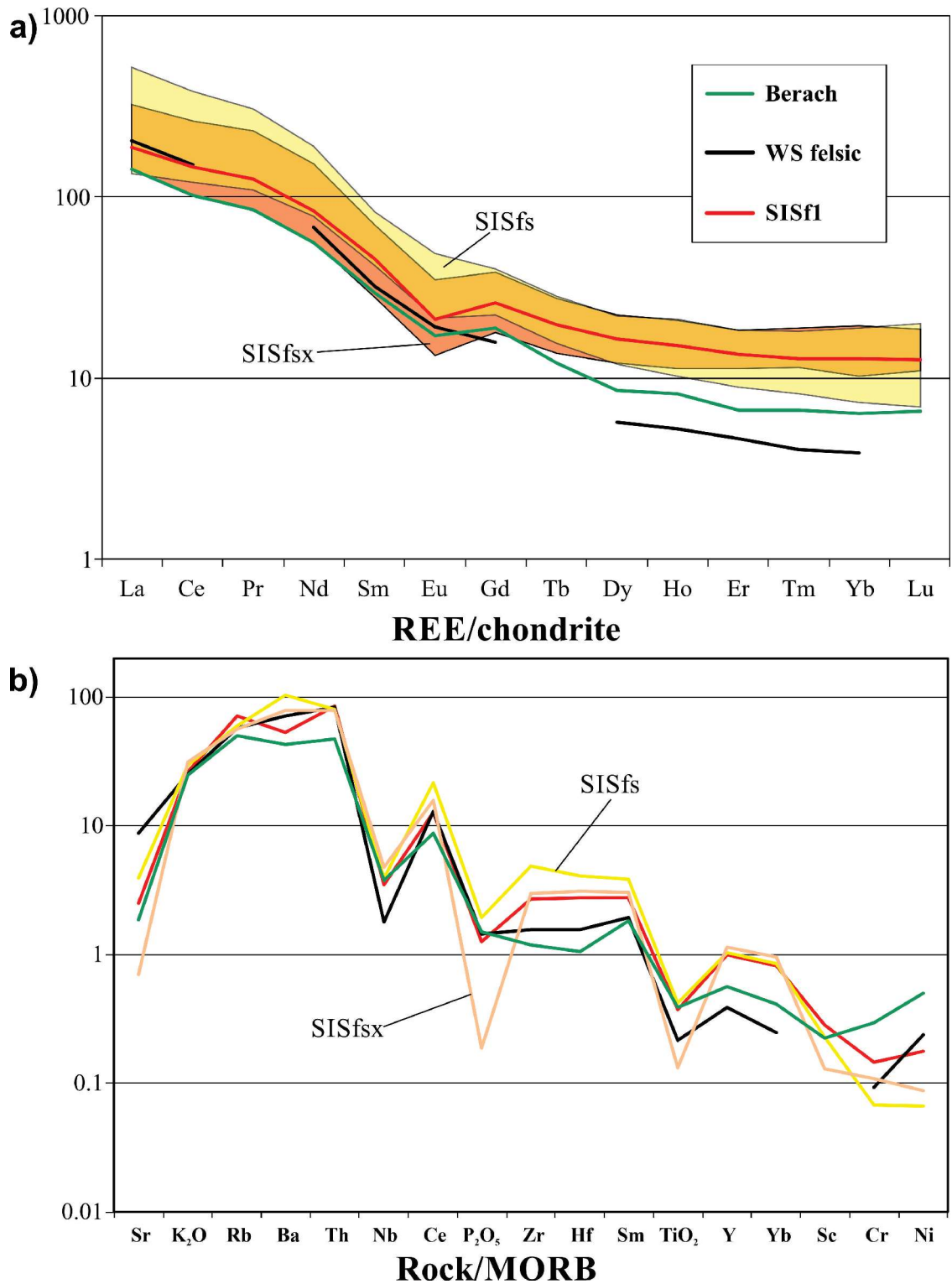


Figure 14. Trace-element plots for sanukitoidal granite samples. **a)** Chondrite-normalized REE envelopes for SISfs and SISfsx (mean $\pm 1\sigma$) compared to average late Archean sanukitoidal Berach granite (Mondal and Raza, 2013) and felsic sanukitoid from the western Superior (WS) data of Stevenson et al. (1999; partial data only). **b)** MORB-normalized average analyses, legend as per Figure 14a. Note the extreme depletion in P and Ti of SISfsx, consistent with fractionation of apatite and magnetite, or derivation from sediments poor in those heavy minerals.

Table 2. Summary of whole-rock Sm-Nd isotope analyses of selected Snow Island Suite samples obtained for the GEM-1 and GEM-2 programs (see text).

Sample	Group	Sector	Longitude (°W)	Latitude (°N)	Norm	Qz	U-Pb age	Sm (ppm)	Nd (ppm)	¹⁴⁷ Sm/ ¹⁴⁴ Nd	¹⁴³ Nd/ ¹⁴⁴ Nd	¹⁴³ Nd/ ¹⁴⁴ Nd(T)	T _{DM}	ε _{Nd} (T)
HF74-020***	SISf1	Tehery	92.3336	64.7589	Granodiorite	20.72	2584 ± 12	8.24	55.49	0.0898	0.510848	0.50932	2722	0.61
HF75-013***	SISf1	Tehery	93.6186	64.3312	Granodiorite	23.29	n.d.	n.a.	n.a.	0.099148	0.510934	0.50923	2833	-0.61
15WGA-P081A01	SISf1	Tehery	89.2615	64.8694	Syenogranite	29.65	n.d.	9.61	50.49	0.1151	0.511052	0.50908	3123	-3.66
15WGA-P017A01	SISf1	Tehery	90.7986	64.9998	Monzogranite	21.71	n.d.	10.13	56.00	0.1094	0.511084	0.50921	2894	-1.12
16WGA-W080A01	SISf1	Tehery	91.7174	65.3047	Monzogranite	22.77	2608 ± 4	6.56	35.01	0.1132	0.511068	0.50912	3036	-2.64
12PQB88C	SISf1	SRae	106.777	60.5919	Monzogranite	20.42	2573 ± 10	10.85	51.09	0.128429	0.511398	0.50920	2981	-1.53
16DR1002B	SISf1	SRae	107.251	61.7639	Monzogranite	26.33	n.d.	9.14	43.25	0.127802	0.511456	0.50918	2849	-0.01
12WGA-N033A01**	SISf1x	Tehery	92.3725	65.8076	Syenogranite	32.56	2606 ± 2	n.d.	n.d.	n.d.	n.d.	n.d.	2934	-2.02
ZB99-330AG*	SISf1x	MKT	95.8727	65.1897	Alkali granite	40.4	n.a.	n.a.	n.a.	0.1225	0.511357	0.50926	2848	-0.15
12WGA-N002A01**	SISfh	Tehery	89.1381	64.9734	Monzogranite	27.33	2615 ± 5	n.d.	n.d.	n.d.	n.d.	n.d.	3289	-4.23
17SUB-S040A01	SISfh	Tehery	89.2289	64.9352	Monzogranite	25.61	n.d.	7.90	44.53	0.1073	0.511013	0.50917	2942	-1.81
FD74-007***	SISfs	Tehery	93.7979	64.3086	Granodiorite	21.15	n.d.	n.a.	n.a.	0.09533	0.510945	0.50931	2724	0.88
16WGA-W065A01	SISfs	Tehery	91.4419	64.3721	Granodiorite	22.47	n.d.	11.92	70.61	0.1021	0.510956	0.50921	2879	-1.17
15ET217A	SISfs	SRae	105.727	60.5425	Qz monzodiorite	7.63	n.d.	9.42	59.17	0.096282	0.510768	0.50905	2986	-2.9
15WGA-L124A01	SISfsan	Tehery	90.8133	64.6142	Monzogranite	24.95	n.d.	12.85	71.19	0.1092	0.511078	0.50921	2897	-1.17
16WGA-W132A02	SISfsan	Tehery	91.7757	65.1274	Qz monzodiorite	14.94	2593 ± 8	11.89	52.31	0.1374	0.511361	0.50901	3443	-5.16
12WGA-J006A01**	SISi	Tehery	90.2855	64.6977	Qz monzodiorite	11.22	n.d.	n.d.	n.d.	n.d.	n.d.	n.d.	3045	-3.51
12WGA-N035A02**	SISi	Tehery	91.7811	65.5427	Qz monzodiorite	5	n.d.	n.d.	n.d.	n.d.	n.d.	n.d.	2763	0.51
15WGA-P052A01	SISi	Tehery	89.2795	64.5223	Qz monzodiorite	14.31	2602 ± 2	8.81	43.83	0.1216	0.511266	0.50918	2980	-1.63
15WGA-S007A01	SISi	Tehery	86.9346	65.1648	Granodiorite	15.47	n.d.	6.01	35.27	0.1031	0.510754	0.50899	3200	-4.25
16BK346A	SISi	SRae	107.403	61.8107	Qz monzodiorite	14.88	n.d.	6.41	33.03	0.11734	0.511278	0.50919	2821	0.02
15WGA-L152A02	SISian	Tehery	89.6415	64.6316	Qz monzodiorite	13.7	2603 ± 3	7.54	29.29	0.1556	0.511678	0.50901	3724	-4.99
15WGA-S043B01	SISm1	Tehery	87.9443	64.3325	Monzodiorite	2.19	n.d.	3.08	13.71	0.1359	0.511563	0.50923	2941	0.16
11PHA-07	SISm1	MKT	96.5613	65.3789	Monzodiorite	8.5	n.d.	2.59	13.64	0.11471	0.511342	0.50937	2639	2.17
11PHA-36A	SISm1	MKT	96.2032	65.2728	Troctolite	9.1	n.d.	0.85	4.90	0.105336	0.511207	0.50940	2601	2.66
15WGA-P043A01	SISmbc	Tehery	89.3353	64.5179	Gabbro	-0.9	n.d.	2.23	9.97	0.1350	0.511528	0.50921	2978	-1
15WGA-P044A01	SISmbc	Tehery	89.3272	64.5188	Diorite	-0.17	n.d.	1.53	7.67	0.1203	0.511260	0.50920	2946	-1.31
15WGA-S119A01	SISmbc	Tehery	88.6428	64.4968	Gabbro	0.66	n.d.	2.72	11.47	0.1434	0.511652	0.50919	3072	-1.42
15EM83A1	SISst	SRae	106.474	60.7367	Qz monzodiorite	9.13	2594 ± 8	7.35	48.24	0.092064	0.510832	0.50925	2794	-0.32
17SUB-S036A01	SISst	Tehery	89.164	64.547	Granodiorite	32.46	2600 ± 3	7.90	58.11	0.0822	0.510615	0.50921	2839	-12.63

Depleted mantle model ages (T_{DM}) after DePaolo (1981)

Epsilon values (ε) calculated at U-Pb age or 2.6 Ga

All analyses except *, **, *** by Department of Earth and Atmospheric Sciences, University of Alberta, using techniques of Creaser et al., 1997

*Unpublished data of Cousens cited in Peterson et al., 2010

**J.B. Whalen and N. Wodicka, data from reconnaissance field work, 2012

***van Breemen et al., 2007

Qz = Quartz; MKT = Marjorie-Kiggavik-Tehek area; Norm = Anhydrous CIPW norm; n.a. = not applicable; n.d. = no data

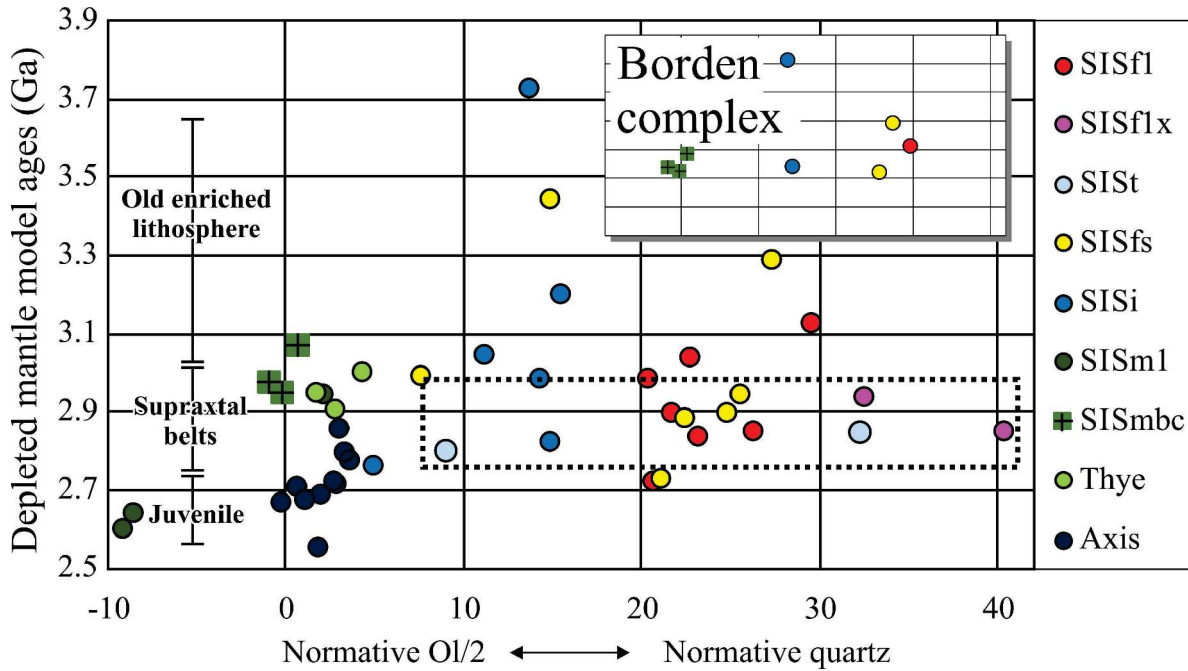


Figure 15. Depleted mantle model ages (T_{DM}) (DePaolo, 1981) for Snow Island Suite samples (GEM1 and GEM2 data, see text) versus normative quartz (with $Ol/2 = -Qz$). Insert shows the data for the Borden complex alone. The dotted box contains non-mafic rocks with model ages similar to U-Pb ages of local supracrustal belts (see text). Analyses given in Table 2 (except Thye and Axis: data of Acosta-Góngora et al., 2018). The SISi sample with T_{DM} more than 3.7 Ga (15WGA-L152), which is beyond the maximum age of ca. 3.3 Ga for the depleted mantle model, has a U-Pb age of 2603 ± 3 Ma (Wodicka et al., 2017) and a $^{147}Sm/^{144}Nd$ of 0.1556. It is from the margin of the Borden complex, is highly strained with some non-Snow Island Suite trace-element characteristics and may contain comminuted wall-rock fragments or have disturbed REE concentrations. Only Thye and Axis samples with both isotopic and elemental analyses are plotted, and one Thye sample is omitted for having $^{147}Sm/^{144}Nd$ greater than 0.14.

On the basis of trace-element data, it is argued above that Snow Island Suite and slightly older mafic rocks from south Rae Province originated in both oceanic (Axis Lake) and continental (Thye Lake) arcs, and possibly a back-arc basin (Wholdaia Lake shear zone). Regan (2016) and Regan et al. (2017a), based on lithogeochemical data sets of ca. 2.6 Ga granitoid rocks from Tantato Domain (south Rae Province) and at Yathkyed Lake (Chesterfield Block), concluded that those granite rocks recorded a continental arc, and suggested a scenario for convergence on the eastern margin of the Rae Province. A high-temperature metamorphic event at ca. 2.56–2.5 Ga recorded within the Chesterfield Block and Snowbird Domain (MacQuoid Orogeny, Davis et al., 2006) has been attributed to closure of an ocean basin, completing a convergent tectonic cycle that may have begun with the Snow Island Suite event (Pehrsson et al., 2013a).

This study’s pan-Rae Province database permits recognition of a range of rock types that are idiosyncratic of the Neoproterozoic, with linkages to a Mesoarchean history, and with some granularity in their distribution that allows convergent tectonic scenarios to be refined. Taking into account the magmatic polarity of the Snow Island Suite, the east-to-west drift in its emplacement ages (Fig. 2), and the arc-like character of Snow Island Suite mafic rocks, the authors

interpret the entire Snow Island Suite as a unified, short-lived, northwest-verging continental arc, and the older mafic volcanic and clastic rocks as a combination of allochthonous oceanic arcs and back-arc basins. Note that the scale of Rae Province–Snow Island Suite (more than 1700 km), in its present form, is comparable to that of the Southern Volcanic Zone of the Andean margin (33° to 50°S latitude), offering plausibility that to first order, the Snow Island Suite can be considered a single petrogenetic province.

Heat and magma sources

The principal mafic rock type (SISm1) is widespread in south and central Rae Province–Snow Island Suite and is also present at Dubawnt Lake and Melville Peninsula (Fig. 10). The authors assume that the volume of emplaced SISm1 magmas was sufficient to trigger melting throughout the lithosphere to generate the remainder of the Snow Island Suite. Because of the uncertainty of the original width of Rae Province–Snow Island Suite (almost certainly now contracted by Proterozoic deformation) — and of the nature of Neoproterozoic tectonics in general — it is unclear if the across-strike extent of the Snow Island Suite requires

unusually rapid, shallow subduction, as has been suggested (and disputed) for some Archean scenarios (e.g. van Hunen and Moyen, 2012).

Both the oceanic (Marjorie peak interval) and younger continental mafic (Snow Island Suite) magmas were from enriched mantle, but the style of that enrichment was different. As discussed in the section ‘Mafic and intermediate rocks’, the stark anomalies in the Axis Lake gabbro are consistent with enrichment of convecting mantle by high-pressure tonalite melt from subducted eclogite, immediately followed by high degrees of partial melting to generate the observed low-silica adakite. These features are consistent with rapid subduction of young, hot oceanic crust removed from continental influence. The SISm1 group has trace-element patterns that are less extreme and appear transitional from adakite to sanukitoid SISi (e.g. weak depletion in Zr-Hf, modest enrichment in Ba; Fig. 12). This study’s data set, which includes some SISm1 with juvenile Nd model ages (Fig. 15), suggests the enrichment was at least partially primary. In a Neoproterozoic scenario, subduction zone magmas would likely resemble sanukitoid rocks, as emergent potassic rocks were not widely available to contribute K-rich detritus. In a shallow, flat subduction scenario, enrichment and melting may be occurring in both overlying convecting and lithospheric mantle, which would account for the presence of some mafic rocks in the Snow Island Suite that have Mesoarchean model ages.

The large volume of intermediate intrusions in the Snow Island Suite argues against an origin by crystal fractionation of SISm1 magmas. Additionally, Snow Island Suite granite is characteristically mingled with intermediate, rather than gabbroic rocks, so that although olivine-bearing magmas did reach the surface, generation of middle to upper crustal granitic melts was probably caused by the SISi plutons. Because the sanukitoid SISi (and interpreted granitic derivatives) have the oldest model ages in the study’s data set (Fig. 15), they are interpreted as originating in mainly Mesoarchean lithospheric mantle previously metasomatized by tonalite melts, likely as a result of tonalite magma-emplacment events at ca. 2.7 Ga and older. This is consistent with the observed correlation of sanukitoid rocks with tonalite-rich terranes (e.g. Martin et al., 2005). The interpretation of the granite groups this study has identified is that they are dominantly melts of older gneiss and metasedimentary rocks in the middle to upper crust, with corresponding Nd model ages all older than 2.6 Ga. No arc granite derived by remelting of, e.g. juvenile andesitic volcanic rocks are identified. Such granite, if preserved, would be concentrated on the eastern edge of Rae Province–Snow Island Suite and may be among those studied by Regan (2016).

Internal divisions in the Rae Province

Variations within the Snow Island Suite are consistent with some previously recognized divisions within the Rae Province. The northwest corner of Rae Province–Snow

Island Suite (Committee Bay belt and west to Queen Maud Block) lacks the large amount of tonalitic and sanukitoid exposures present in nearby northern Melville Peninsula (Fig. 10); these areas are now separated by a submerged Phanerozoic basin. The amount of tonalitic crust in adjacent west-central Rae Province is uncertain due to poor exposure, extensive Proterozoic cover, and crustal displacement by Proterozoic granite intrusions, but the authors note that sanukitoid rhyolite rocks were first identified in the Marjorie-Kiggavik-Tehek belt (Peterson et al., 2015a). This study’s separation of central and northern Rae Province–Snow Island Suite west of the Chesterfield fault zone (Fig. 1) is useful for discussing the data sets and the extent of preserved volcanic Snow Island Suite rocks, but does not clearly appear in the lithochemical data; however, the Amer fault zone may approximately correspond, at surface, to the northwestern extent of sanukitoid-generating lithosphere in that part of Rae Province.

The large Snow Island Suite–absent Repulse Bay Block is a stark feature. Its geometry must in part reflect the intense Hudsonian tectonometamorphism documented throughout this region (e.g. LaFlamme et al., 2014; Berman et al., 2015b). The 1.83–1.82 Ga batholithic Ford Lake intrusive complex (LeCheminant et al., 1987) at the south end of the Repulse Bay Block (*see* Fig. 1), resembles in scale and lithology the on-strike 1.865–1.845 Ga mangerite-rich Cumberland batholith of Baffin Island, attributed to partial melting of a previously thickened, axial continental root (Whalen et al., 2010). Contraction of the clastic, early Proterozoic Penrhyn Group and emplacement of Archean nappes over the Proterozoic rocks (Henderson, 1983) at the north end of the Repulse Bay Block is also consistent with northwest-southeast shortening and the formation of such a root. Studies of the shear zones bounding the Repulse Bay Block are in early stages (e.g. Therriault et al., 2017), and while it is clear that the Rae Province–Snow Island Suite and/or Repulse Bay Block boundary does not predate the Snow Island Suite, it is not known if it is all, or in part, synchronous with or postdates the Snow Island Suite.

The observed abrupt shift from infracrustal SISi to SISf1x granite groups at south Dubawnt Lake (Fig. 10) is correlated here with a boundary that is marked at the surface by exposed segments of a shear zone with multiple, unresolved episodes of intrusion and deformation (Dubawnt River shear zone). This boundary (Fig. 16, map in lower left), which is at high angle to the regional Proterozoic structural trend, was active during formation of an intense south-southeast-plunging lineation at 1.83 Ga in the footwall (north side) and was brittlely reactivated later (Peterson and Lee, 1995). It presumably represents a 2.6 Ga or earlier suture between different Mesoarchean crustal blocks. The Snow Island Suite data require that upper crustal sources for granite were different on either side of the boundary, but offer no constraints on how or when the boundary formed.

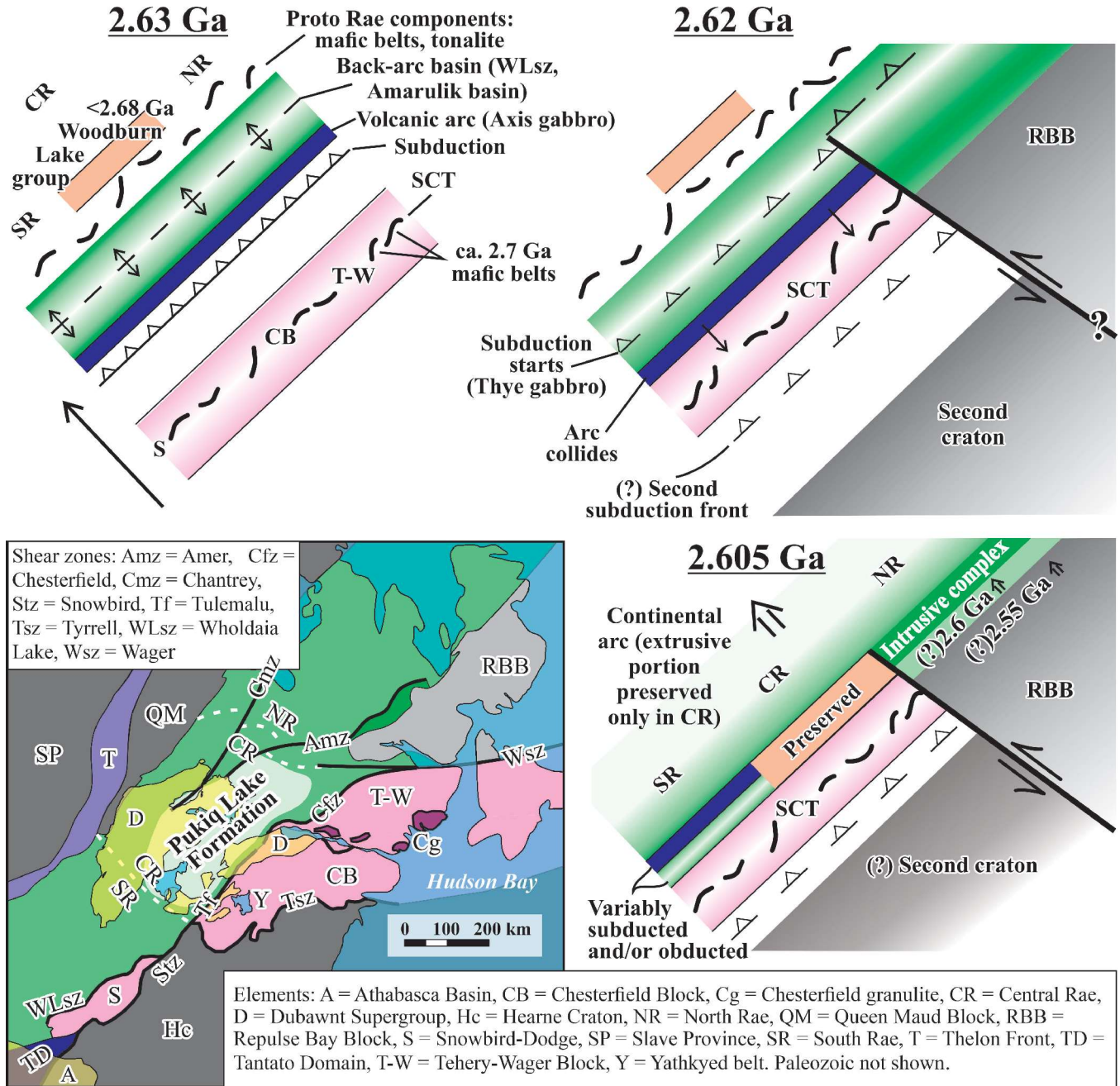


Figure 16. Provisionally identified tectonic elements associated with the Snow Island Suite event. See text for detailed summary. At 2.63 Ga, elements of the current eastern edge of the Rae Province were outboard of the proto-Rae Province (SR, CR, NR). In the current Marjorie-Kiggavik-Tehek belt (Fig. 7), older supracrustal sequences (upper Woodburn Lake group) preserve portions of the proto-Rae Province margin. One of the outboard elements is a microcontinent consisting of current Snowbird Domain, and Chesterfield and Tehery blocks, which approaches the proto-Rae Province margin along an oceanic subduction front (Axis gabbro), which is separated from proto-Rae Province rocks by one or more back-arc basins (Wholdaia Lake shear zone and Amarulik Basin). At 2.62 Ga, the arc and Snowbird-Chesterfield-Tehery elements collide before reaching proto-Rae Province, with a subduction zone initiating in back-arc basins. The Repulse Bay Block, anorogenic at 2.6 Ga, is separated from the Snowbird-Chesterfield-Tehery (SCT) terrane by a translithospheric transform fault, now preserved as the Wager shear zone. At 2.605 Ga, collision between these elements is in progress and partial melting of mantle sources moves beneath proto-Rae Province, triggering west-drifting plutonism in the crust. The time of first contact of the Repulse Bay Block with proto-Rae Province is unclear and it may not have arrived until the early MacQuoid Orogeny (2.55–2.5 Ga). A second craton, also associated with that event, may have provided the marker strip of exotic, more than 3 Ga tonalitic and Snow Island Suite-intruded crust (Chipman Domain) on the east edge of Rae Province–Snow Island Suite, or alternatively represents the Hearne Province.

Tectonic elements at 2.6 Ga

To confidently identify some or all of the tectonic elements within Rae Province at ca. 2.6 Ga would first entail unravelling the net effects of several intense and widespread tectonometamorphic events, from 2.55 Ga to 1.7 Ga, and less intense far-field deformation up to 1.4 Ga. This exercise has not been completed (Pehrsson et al., this volume); however, the present authors point to the known extent of the 2.56–2.50 Ga MacQuoid Orogeny (Berman, 2010) as a strong constraint. Metamorphic U–Pb ages in this range are present in the Tantato, Snowbird, and Chesterfield domains and/or blocks along the east edge of Rae Province–Snow Island Suite, and extend across Chesterfield Inlet into the Tehery Lake–Wager Bay area (henceforth referred to as the Tehery Block). Additionally, the Chesterfield Block contains two correlated ca. 2.7 Ga volcanogenic belts, the MacQuoid and Yathkyed belts (Sandeman et al., 1999, 2006; Davis et al., 2006; Acosta-Góngora et al., 2018), which have also been tentatively correlated on the basis of lithochemistry, U–Pb ages, and interbedded clastic rocks with the Lorillard belt of the Tehery Block (J. Whalen, pers. comm., 2013; Wodicka et al., 2017) (Fig. 13). Studies on the lithochemistry and metamorphic history of the Lorillard belt are ongoing (Steenkamp et al., 2023b). These results are interpreted to constrain those regions (Tantato with Snowbird Domain–Chesterfield Block–Tehery Block) to have been coherent at 2.6–2.5 Ga, implying that they were later disrupted and transposed during the early Proterozoic.

Additionally, the small Zemplak Domain, which is in structural contact with the south and east sides of the Snow Island Suite–rich Nolan Domain in south Rae Province, contains an intermediate orthogneiss unit with ca. 2.52 Ga crystallization ages (Cloutier et al., 2021). It resembles the Snowbird Domain in containing only sparse granitic intrusions near 2.6 Ga, and the remainder of the Snowbird Domain–Chesterfield Block–Tehery Block region in producing older crystallization ages that are dominantly near 2.7 Ga. The Zemplak Domain boundary is complicated by additional deformation, with igneous and metamorphic ages near 2.3 Ga (the Arrowsmith Orogeny; Cloutier et al., 2021) and the extent of Proterozoic rearrangement in this complex region is unclear. The Neoproterozoic assembly model offered by Cloutier et al. (2021), strongly constrained by the Zemplak Domain, is similar in several respects to this study's larger scale model.

To generate this model, two assumptions are made: 1) the west edge of the combined Tehery–Chesterfield terrane is assumed to be a Snow Island Suite–aged boundary, which is provisionally located near the trace of the Chesterfield fault zone (which potentially records syn–Snow Island Suite deformation: *see* section 'Granitic and intermediate intrusive rocks'), and continuing along the southern portion of the Snowbird tectonic zone (Fig. 16); and 2) the west margin of the Repulse Bay Block is an Archean collisional orogen. Although the authors cannot cite evidence for this against the surrounding blocks, ca. 2.54 Ga monazite

ages, recording amphibolite-facies deformation during the MacQuoid Orogeny, are present within the Repulse Bay Block (Berman et al., 2015b), and an additional cluster of 2.54–2.49 Ga metamorphic monazite ages is present south of Boothia Peninsula, immediately west of the Repulse Bay Block (Berman et al., 2013). These data are most simply interpreted as a result of Repulse Bay Block and Rae Province–Snow Island Suite collision or reactivation during the MacQuoid Orogeny.

Figure 16 depicts the elements that can be identified under these assumptions. At 2.63 Ga, an oceanic arc offshore from proto–Rae Province (consisting of present-day south Rae Province, central Rae Province and the Committee Bay Block, and northern Melville Peninsula lithosphere) contained boninitic and adakitic magmas (Axis Lake gabbro) with wind-driven detrital zircon from similar arcs deposited in the upper Amarulik Basin (upper Woodburn Lake group). A combined Snowbird–Chesterfield–Tehery continental terrane approaches along a west-dipping subduction zone under the arc. A back-arc basin, provisionally identified in the Amarulik Basin and Wholdaia Lake shear zone, is present. At 2.62 Ga, the Snowbird–Chesterfield–Tehery terrane collides with the oceanic arc (resulting in nappe emplacement in the Chesterfield Block: MacLachlan et al., 2005), and the subduction zone migrates into the back-arc basin, beginning a transition (Thye Lake gabbro) to a continental arc (Snow Island Suite gabbro). A second subduction front may also have developed east of the Snowbird–Chesterfield–Tehery terrane, promoting post-2.62 Ga Snow Island Suite intrusion in Snowbird–Chesterfield–Tehery terrane. At 2.605 Ga, the peak time of Snow Island Suite granite emplacement, the combined Tantato–Snowbird–Chesterfield–Tehery terrane collides with proto–Rae Province block, trapping segments of the oceanic arcs and back-arc basins. This event coincides with upright refolding at 2.6 Ga of the 2.62 Ga nappes in the Chesterfield Block. No Snow Island Suite ages younger than 2.60 Ga have been obtained in the Chesterfield Block, but they have been recorded in the Tehery Block. Beginning at 2.6 Ga, the focus of plutonism moves westward, presumably tracking the delayed effects of shallow subduction, or the drift of a detached oceanic slab. By 2.58 Ga, the Snow Island Suite event is concluded. The Snow Island Suite–absent Repulse Bay Block, separated from Snowbird–Chesterfield–Tehery terrane by an oceanic transform fault that became the present-day Wager shear zone, accreted at an unspecified time from ca. 2.6–2.54 Ga.

Placing a Snow Island Suite collisional orogen along the western margin of the Snowbird–Chesterfield–Tehery terrane gives context to the upper Woodburn Lake group, and particularly to the extensional Amarulik Basin, which records continuous Marjorie peak and early Snow Island Suite turbiditic sedimentation followed by emergent Snow Island Suite rhyolite, consistent with a preserved back-arc basin (*see also* Hunter et al., 2018). The detrital zircon populations of the middle and upper packages in the Marjorie Assemblage reflect dominantly proximal volcanic sources peaking at 2.69 Ga,

2.67 Ga, and 2.65 Ga followed by a more distal juvenile source near 2.63 Ga. These data suggest models for the Woodburn Lake group of deep-water microcontinental margin sequences that recorded sporadic input from island-arc to offshore volcanic detritus. The Amarulik Basin then recorded an influx of Snow Island Suite detrital zircon while or after numerous terranes amalgamated to form the broad Rae Craton, on which the Pukiq Lake Formation was the first widely deposited supracrustal unit.

It is possible to correlate the arrival of a Mesoproterozoic tonalite terrane on the east side of Snowbird-Chesterfield-Tehery terrane with closure of all basins at 2.6 Ga. This terrane would necessarily have subsequently rifted away, leaving a narrow and highly distinctive marker behind (the Chipman Tonalite at ca. 3.1 Ga), and making way for the later arrival of the Hearne Province. Alternatively, this terrane could correspond to the Hearne Province itself, which would have collided with the Snowbird-Chesterfield-Tehery terrane at ca. 2.605 Ga, then subsequently rifted away, and re-collided with the amalgamated Rae Craton at ca. 1.9 Ga (e.g. Thiessen, 2021). This paper suggests limited west-verging subduction under the Snowbird-Chesterfield-Tehery terrane (including the Zemlak Domain), particularly at its southern end, to account for the relatively small volume of Snow Island Suite plutonism observed there. This implies that the separation between Snowbird-Chesterfield-Tehery and any outlying continental terrane was small and rapidly closed.

Suggestions for continuing work

The broad model for igneous petrogenesis and evolution suggested here should be tested and elaborated with studies of individual complexes, where separate rock types can be assumed to be directly related. Greater granularity in the distribution of rock types, with the possibility of probing greater detail in pre-Snow Island Suite lithosphere structure, could be achieved. The Wager shear zone has an unusual role in this study's tectonic model, which implies that a distinctive igneous suite related to oceanic transform faulting may be preserved there (though likely strongly deformed). A mapped concentration of Snow Island Suite plutons immediately west of the Repulse Bay Block (Skulski et al., 2018) merits detailed sampling and comparison to the Snow Island Suite intrusions of the Committee Bay supracrustal belt. The former may prove to have a more direct connection to arc volcanism (e.g. granite bodies with Nd model ages near 2.6 Ga) and may also have a component of MacQuoid plutonism near 2.54 Ga.

The authors' model implies that the Axis Lake gabbro, in the upper deck of Tantato Domain, should be directly adjacent to proto-Rae Province crust, but it is actually separated from it by the Dodge Domain (*see* Fig. 2, this paper, and Fig. 1 of Regis et al., 2017a), a structurally discrete region currently interpreted as an extension of the Snowbird Domain (Thiessen et al., 2018). Additionally, portions of this arc,

or its segments, should potentially be preserved anywhere along the Snowbird tectonic zone. The present authors attribute the scarcity of known preserved arc rocks, and possible reversal of the structural position of the eclogite-facies Axis Lake gabbro rocks in Tantato Domain, to repeated episodes of Proterozoic deformation, including destruction of some crust along the Snowbird tectonic zone at about 1.9 Ga from continental subduction, followed by rapid uplift of granulite-facies rocks on major extensional faults (Regis et al., 2021). The existence and extent of this arc will hopefully be tested by identifying other mafic rocks that are of this age. Late Archean gabbro units of the Dodge Domain (e.g. Knox et al., 2011) are almost certainly part of the Marjorie peak-Snow Island Suite cycle and could be dated and geochemically described, which might help resolve the structural position of the Axis Lake gabbro.

The portion of Rae Province where the Snowbird tectonic zone meets the west end of the Baker Lake Basin, and north of this in an area of strongly deformed gneiss units, has presented difficulties in tectonic models for several decades, and the presence and/or location of mapped continental sutures and transform zones there has shifted with time. The authors suggest that these difficulties result from intense Proterozoic reactivation of a prominent Neoproterozoic collisional zone that remains largely cryptic along its central portion due to deposition and overthrusting of early Proterozoic sedimentary belts, and episodes of granite emplacement at 1.83 Ga (Hudson granite) and 1.75 Ga (Nueltin granite) (Peterson et al., 2015b). A thorough review of existing teleseismic and magnetotelluric data of this area (*see* e.g. Snyder et al., 2015) would help test whether or not a Neoproterozoic lithospheric break running from the southwest corner of the Repulse Bay Block to the west end of Baker Lake Basin exists.

SUMMARY

The authors find that the Snow Island Suite consists of a dominantly mafic and/or intermediate, broadly sanukitoid component, reflecting interaction between tonalite melts and mantle, and an infracrustal (crustal migmatite) granitoid component. Sanukitoid Snow Island Suite can be interpreted as an example of a late Archean subduction-enrichment style that was transitional to Proterozoic and modern styles.

The Snow Island Suite represents a continental-arc segment that spanned most of the Archean Rae Province and was active over 40 Ma, centred on 2.605 Ga. Activity propagated westward over this time, and was due to emplacement of mafic magmas in the lower lithosphere that induced melting of tonalite-metasomatized Mesoproterozoic lithospheric mantle (sanukitoid intermediate rocks) and then crustal gneiss and metasedimentary rocks (infracrustal granitoid rocks). Some mafic rocks predating Snow Island Suite in south Rae Province have back-arc basin, ocean-arc, and adakite trace-element affinities, and involvement

of high-pressure tonalite derived by melting of rutiled eclogite as a metasomatizing agent is indicated in some pre-Snow Island Suite gabbro. Variations in Snow Island Suite granitoid lithochemistry reflect internal Rae Province boundaries in upper crustal melt sources that may, in turn, reflect prominent lithotectonic boundaries.

ACKNOWLEDGMENTS

This paper is dedicated to the memory of Anthony LeCheminant, whose restless feet and wide vision first traversed these rocks. The authors thank T. Skulski, H. Sandeman, and J. Ryan for permitting overviews of their unpublished lithochemical data. This paper was greatly improved by reviews by Bruce Kjarsgaard and Ali Polat.

REFERENCES

- Acosta-Góngora, P., Pehrsson, S.P., Knox, B., Regis, D., Hulbert, L., Creaser, R.A., and Ashton, K., 2018. Neoproterozoic convergent margin Ni-Cu mineralization? Axis Lake and Nickel King Ni-Cu deposits in the south Rae Province craton of the Canadian Shield; *Precambrian Research*, v. 316, p. 305–323. <https://doi.org/10.1016/j.precamres.2018.07.016>
- Anand, A. and Jefferson, C.W., 2017. Reactivated fault systems and their effects on outcrop patterns of thin-skinned early thrust imbrications in the Kiggavik uranium camp, Nunavut; Geological Survey of Canada, Open File 7895, 1 sheet. <https://doi.org/10.4095/302776>
- Ashton, K.E., Knox, B., Card, C., Rayner, N., Davis, B., and Bethune, K., 2017a. Recent mapping and geochronology in the eastern Rae Province, Saskatchewan; poster presented at 2017 Saskatchewan Geological Open House, November 27 to 29, 2017, Saskatoon, Saskatchewan.
- Ashton, K.E., Knox, B., Card, C., Rayner, N., Davis, B., Heaman, L., and Creaser, R., 2017b. Synthesis of U-Pb and Sm-Nd geochronological results from the Dodge Domain, Southeastern Rae Province; Paper A-12 in *Summary of Investigations 2017, Volume 2*; Saskatchewan Geological Survey, Saskatchewan Ministry of the Economy, Miscellaneous Report 2017-4.2, p. 49.
- Ashton, K.E., 1988. Precambrian geology of the southeastern Amer Lake Area (66H/1) near Baker Lake, N.W.T.; Ph.D. thesis, Queens University, Kingston, Ontario, 335 p.
- Berman, R.G., 2010. Metamorphic map of the western Churchill Province, Canada; Geological Survey of Canada, Open File 5279, 55 p. <https://doi.org/10.4095/287320>
- Berman, R.G., Davis, W.J., and Pehrsson, S., 2007. Collisional Snowbird tectonic zone resurrected: growth of Laurentia during the 1.9 Ga accretionary phase of the Hudsonian orogeny; *Geology*, v. 35, p. 911–914. <https://doi.org/10.1130/G23771A.1>
- Berman, R.G., Pehrsson, S., Davis, W.J., Ryan, J.J., Quic, H., and Ashton, K.E., 2013. The Arrowsmith orogeny: geochronological and thermobarometric constraints on its extent and tectonic setting in the Rae craton, with implications for pre-Nuna supercontinent reconstruction; *Precambrian Research*, v. 232, p. 44–69. <https://doi.org/10.1016/j.precamres.2012.10.015>
- Berman, R.G., Nadeau, L., Davis, W.J., McCurdy, M.W., Craven, J.A., McMartin, I., Whalen, J.B., Sanborn-Barrie, M., Carr, S., Pehrsson, S.J., Percival, J.A., and Girard, E., 2015a. New insights into the geological evolution and economic potential of the Thelon tectonic zone and western Rae craton, Nunavut; Geological Survey of Canada, Open File 7901, 1 sheet. <https://doi.org/10.4095/296719>
- Berman, R.G., Davis, W.J., Corrigan, D., and Nadeau, L., 2015b. Insights into the tectonothermal history of Melville Peninsula, Nunavut, provided by in situ SHRIMP geochronology and thermochronology; Geological Survey of Canada, Current Research 2015-4, 18 p. <https://doi.org/10.4095/295852>
- Bethune, K., Cloutier, M., Deane, J., and Ashton, K., 2016. Tectonic significance of the Nolan-Zemlak domain boundary, Tazin Lake area, NW Saskatchewan: investigating the possibility of an Arrowsmith-age suture zone in the WSW Rae; Saskatchewan Geological Survey, Miscellaneous Report 2016-5, 24 p.
- Buchan, K.L. and Ernst, R.E., 2004. Diabase dyke swarms and related units in Canada and adjacent regions; Geological Survey of Canada, Map 2022A, scale 1:5 000 000. <https://doi.org/10.4095/214883>
- Card, C., Rayner, N., Pearson, G., Luo, Y., and Creaser, R.A., 2018. Geochronological results from the southern Athabasca Basin region, Saskatchewan; Saskatchewan Ministry of Energy and Resources, Miscellaneous Report 2018-4.2, Paper A-4, 15 p.
- Chiaradia, M., Muntener, O., and Beate, B., 2014. Quaternary sanukitoid-like andesites generated by intracrustal processes (Chacana Caldera Complex, Ecuador): implications for Archean sanukitoid rocks; *Journal of Petrology*, v. 55, p. 769–802. <https://doi.org/10.1093/petrology/egu006>
- Cloutier, M., Bethune, K., and Ashton, K., 2017. New geochronological data from granitoid rocks across the Nolan-Zemlak domain boundary: testing the Arrowsmith Suture hypothesis; Saskatchewan Geological Survey, Miscellaneous Report 2017-3, 23 p.
- Cloutier, M., Bethune, K., Ashton, K., and Deane, J.M.K., 2021. U-Pb geochronology, geochemistry, and isotopic composition of granitoids across the Nolan-Zemlak domain boundary in the SW Rae craton, Laurentia: evidence for a late Neoproterozoic suture reworked during Arrowsmith orogeny; *Precambrian Research*, v. 362. <https://doi.org/10.1016/j.precamres.2021.106303>
- Corrigan, D., Nadeau, L., Brouillette, P., Wodicka, N., Houle, M.G., Tremblay, T., Machado, G., and Keating, P., 2013. Overview of the GEM Multiple Metals – Melville Peninsula project, central Melville Peninsula, Nunavut; Geological Survey of Canada, Current Research 2013-19, 21 p. <https://doi.org/10.4095/292862>

- Creaser, R.A., Erdmer, P., Stevens, R.A., and Grant, S.L., 1997. Tectonic affinity of Nisutlin and Anvil assemblage strata from the Teslin tectonic zone, northern Canadian Cordillera: Constraints from neodymium isotope and geochemical evidence; *Tectonics*, v. 16, p. 107–121. <https://doi.org/10.1029/96TC03317>
- Davis, W.J., 2021. U-Pb zircon age data for supracrustal samples from the White Hills Lake to Amer Lake area, Rae Province, Nunavut Canada; Geological Survey of Canada, Open File 8807, 6 p. <https://doi.org/10.4095/328453>
- Davis, W.J., Fryer, B.J., and King, J.E., 1994. Geochemistry and evolution of Late Archean plutonism and its significance to the tectonic development of the Slave craton; *Precambrian Research*, v. 67, p. 207–241. [https://doi.org/10.1016/0301-9268\(94\)90011-6](https://doi.org/10.1016/0301-9268(94)90011-6)
- Davis, W.J., Hanmer, S., Tella, S., Sandeman, H.A., and Ryan, J.J., 2006. U-Pb geochronology of the MacQuoid supracrustal belt and Cross Bay plutonic complex: key components of the northwestern Hearne subdomain, western Churchill Province, Nunavut, Canada; *Precambrian Research*, v. 145, no. 1-2, p. 53–80. <https://doi.org/10.1016/j.precamres.2005.11.016>
- Davis, W.J., Berman, R.G., and MacKinnon, A., 2013. U-Pb geochronology of archival rock samples from the Queen Maud block, Thelon Tectonic Zone and Rae Craton, Kitikmeot Region, Nunavut, Canada; Geological Survey of Canada, Open File 7409, 42 p. <https://doi.org/10.4095/292663>
- Davis, W.J., Berman, R.G., Nadeau, L., and Percival, J.A., 2014. U-Pb zircon geochronology of a transect across the Thelon tectonic zone, Queen Maud region, and adjacent Rae Craton, Kitikmeot Region, Nunavut, Canada; Geological Survey of Canada, Open File 7652, 41 p. <https://doi.org/10.4095/295177>
- DePaolo, D.J., 1981. A neodymium and strontium isotopic study of the Mesozoic calc-alkaline granitic batholiths of the Sierra Nevada and Peninsular Ranges, California; *Journal of Geophysical Research*, v. 86, p. 10470–10488. <https://doi.org/10.1029/JB086iB11p10470>
- Dumond, G., Goncalves, P., Williams, M., and Jercinovic, M.J., 2010. Subhorizontal fabric in exhumed continental lower crust and implications for lower crustal flow: Athabasca granulite terrane, western Canadian Shield; *Tectonics*, v. 29, issue 2. <https://doi.org/10.1029/2009TC002514>
- Hanmer, S., Parrish, R., Williams, M., and Kopf, C., 1994. Striding-Athabasca mylonite zone: Complex Archean deep-crustal deformation in the East Athabasca mylonite triangle, northern Saskatchewan; *Canadian Journal of Earth Sciences*, v. 31, p. 1287–1300. <https://doi.org/10.1139/e94-111>
- Henderson, J.R., 1983. Structure and metamorphism of the Apebian Penrhyn group and its Archean basement complex in the Lyon Inlet area, Melville Peninsula, District of Franklin; Geological Survey of Canada, Bulletin 324, 50 p. <https://doi.org/10.4095/119500>
- Hinchey, A.M., Davis, W.J., Ryan, J.J., and Nadeau, L., 2011. Neoproterozoic high-potassium granites of the Boothia mainland area, Rae domain, Churchill Province. U-Pb zircon and Sm-Nd whole rock isotopic constraints; *Canadian Journal of Earth Sciences*, v. 48, p. 247–279. <https://doi.org/10.1139/E10-071>
- Humphreys, E., Hessler, E., Dueker, K., Farmer, G.L., Erslev, E., and Atwater, T., 2003. How Laramide-age hydration of North American lithosphere by the Farallon slab controlled subsequent activity in the western United States; *International Geology Review*, v. 45, p. 575–595. <https://doi.org/10.2747/0020-6814.45.7.575>
- Hunter, R.C., Lafrance, B., Heaman, L.M., Zaluski, G., and Thomas, D., 2018. Geology, litho-geochemistry and new LA-ICP-MS U-Pb geochronology of the Aberdeen Lake area, Nunavut: new insights into the Neoproterozoic tectonic evolution of the central Rae domain; *Precambrian Research*, v. 310, p. 114–132. <https://doi.org/10.1016/j.precamres.2018.02.024>
- Jefferson, C.W., White, J.C., Young, G.M., Patterson, J., Tschirhart, V.L., Pehrsson, S.J., Calhoun, L., Rainbird, R.H., Peterson, T.D., Davis, W.J., Tella, S., Chorlton, L.B., Scott, J.M.J., Percival, J.A., Morris, W.A., Keating, P., Anand, A., Shelat, Y., and MacIsaac, D., 2015. Outcrop and remote predictive geology of the Amer Belt and basement beside and beneath the northeast Thelon Basin, in parts of NTS 66-A, B, C, F, G and H, Kivalliq Region, Nunavut; Geological Survey of Canada, Open File 7242, scale 1:50 000. <https://doi.org/10.4095/296825>
- Kjarsgaard, B.A., Kerswill, J.A., and Jenner, G.A., 1997. Lithostratigraphy and metallogenic implications of komatiite – banded iron-formation – felsic volcanic rocks of the Archean Woodburn Lake group, Pipedream Lake, central Churchill Province, Northwest Territories; *in Current Research 1997-C*; Geological Survey of Canada, p. 101–110. <https://doi.org/10.4095/208636>
- Knox, B., Card, C.D., and Ashton, K.E., 2011. Bedrock geology of the Grollier Lake area, southern Dodge Domain (parts of NTS 74P/11, /12, /13, and /14); *in Summary of Investigations 2011, Volume 2*; Saskatchewan Geological Survey, Saskatchewan Ministry of Energy and Resources, Miscellaneous Report 2011-4.2, Paper A-3, 13 p.
- Konzett, J. and Frost, D.J., 2009. The high P - T stability of hydroxyl-apatite in natural and simplified MORB — an experimental study to 15 GPa with implications for transport and storage of phosphorus and halogens in subduction zones; *Journal of Petrology*, v. 50, p. 2043–2062. <https://doi.org/10.1093/petrology/egp068>
- LaFlamme, C., McFarlane, C.R.M., Corrigan, D., and Wodicka, N., 2014. Origin and tectonometamorphic history of the Repulse Bay block, Melville Peninsula, Nunavut: exotic terrane or deeper level of the Rae craton; *Canadian Journal of Earth Sciences*, v. 51, p. 1097–1122. <https://doi.org/10.1139/cjes-2014-0040>
- LaFlamme, C., McFarlane, C.R.M., and Corrigan, D., 2015. Neoproterozoic mantle-derived magmatism within the Repulse Bay block, Melville Peninsula, Nunavut: implications for Archean crustal extraction and cratonization; *Geoscience Canada*, v. 42, p. 305–326. <https://doi.org/10.12789/geocanj.2015.42.065>
- Lamming, J.L., 2019. Geochronological and pressure-temperature record of a psammopelitic gneiss in the Upper Deck of the Tantato Domain, northern Saskatchewan, Canada; M.Sc. thesis, University of British Columbia, Vancouver, British Columbia, 264 p. <http://hdl.handle.net/2429/71263>

- Laurent, O., Martin, H., Moyen, J.F., and Doucelance, R., 2014. The diversity and evolution of late Archean granitoid rocks: evidence for the onset of modern-style plate tectonics between 3.0 and 2.5 Ga; *Lithos*, v. 205, p. 208–235.
- LeCheminant, A.N. and Roddick, J.C., 1991. U-Pb zircon evidence for widespread 2.6 Ga felsic magmatism in the central District of Keewatin, N.W.T; *in* Radiogenic age and isotope studies: report 4, Geological Survey of Canada, Paper 90-2, p. 91–99. <https://doi.org/10.4095/131941>
- LeCheminant, A.N., Ianelli, T.R., Zaitlin, B., and Miller, A.R., 1981. Geology of Tebesjuak Lake Map area, District of Keewatin: a progress report; *in* Current Research Part B; Geological Survey of Canada, Paper 81-1B, p. 113–128. <https://doi.org/10.4095/119324>
- LeCheminant, A.N., Roddick, J.C., Tessier, A.C., and Bethune, K.M., 1987. Geology and U-Pb ages of Early Proterozoic calc-alkaline plutons northwest of Wager Bay, District of Keewatin; *in* Current Research, Part A; Geological Survey of Canada, Paper 87-1A, p. 773–782. <https://doi.org/10.4095/122551>
- MacLachlan, K., Davis, W.J., and Relf, C., 2005. U/Pb geochronological constraints on Neoproterozoic tectonism: multiple compressional events in the northwestern Hearne domain, western Churchill Province; *Canadian Journal of Earth Sciences*, v. 42, p. 85–109. <https://doi.org/10.1139/e04-104>
- Martel, E., van Breemen, O., Berman, R.G., and Pehrsson, S.J., 2008. Geochronology and tectonometamorphic history of the Snowbird Lake area, Northwest Territories, Canada: new insights into the architecture and significance of the Snowbird tectonic zone; *Precambrian Research*, v. 161, p. 201–230. <https://doi.org/10.1016/j.precamres.2007.07.007>
- Martin, H., Smithies, R.H., Rapp, R., Moyen, J.-F., and Champion, D., 2005. An overview of adakite, tonalite-trondhjemite-granodiorite (TTG), and sanukitoid: relationships and some implications for crustal evolution; *Lithos*, v. 79, p. 1–24. <https://doi.org/10.1016/j.lithos.2004.04.048>
- Martin, H., Moyen, J.-F., and Rapp, R., 2010. The sanukitoid series: magmatism at the Archaean–Proterozoic transition; *Earth and Environmental Science Transactions of the Royal Society of Edinburgh*, v. 100, p. 15–33. <https://doi.org/10.1017/S1755691009016120>
- McEwan, B., 2012. Structural style and regional comparison of the Paleoproterozoic Ketyet River group in the region north-northwest of Baker Lake, Nunavut; M.Sc. thesis, University of Regina, Regina, Saskatchewan, 121 p. and appendices.
- Mondal, M.E.A. and Raza, A., 2013. Geochemistry of sanukitoid series granitoid rocks from the Neoproterozoic Berach granitoid batholiths, Aravalli craton, northwestern Indian shield; *Current Science*, v. 105, p. 102–108.
- Moyen, J.-F., 2011. The composite Archaean grey gneisses: petrological significance, and evidence for a non-unique tectonic setting for Archaean crustal growth; *Lithos*, v. 123, p. 21–36. <https://doi.org/10.1016/j.lithos.2010.09.015>
- Moyen, J.-F., Hervé, M., and Mudlappa Jayananda, M., 2001. Multi-element geochemical modelling of crust–mantle interactions during late-Archaean crustal growth: the Closepet granite (South India); *Precambrian Research*, v. 112, p. 87–105. [https://doi.org/10.1016/S0301-9268\(01\)00171-1](https://doi.org/10.1016/S0301-9268(01)00171-1)
- Nakamura, N., 1974. Determination of REE, Ba, Fe, Mg, Na and K in carbonaceous and ordinary chondrites; *Geochimica et Cosmochimica Acta*, v. 38, p. 757–775. [https://doi.org/10.1016/0016-7037\(74\)90149-5](https://doi.org/10.1016/0016-7037(74)90149-5)
- Natural Resources Canada, 2022. Canadian Geochronology Database; Natural Resources Canada <<https://www.nrcan.gc.ca/maps-tools-publications/tools/geodetic-reference-systems/canadian-geochronology-knowledgebase/18211>> [accessed April 1, 2016]
- Pearce, J.A., 2008. Geochemical fingerprinting of oceanic basalts with applications to ophiolite classification and the search for Archean oceanic crust; *Lithos*, v. 100, p. 14–48. <https://doi.org/10.1016/j.lithos.2007.06.016>
- Pehrsson, S.J., Berman, R.G., Eglington, B., and Rainbird, R.H., 2013a. Two Neoproterozoic supercontinents revisited: the case for a Rae family of cratons; *Precambrian Research*, v. 232, p. 27–43. <https://doi.org/10.1016/j.precamres.2013.02.005>
- Pehrsson, S., Berman, R.G., and Davis, W.J., 2013b. Paleoproterozoic orogenesis during Nuna aggregation: a case study of reworking of the Rae craton, Woodburn Lake, Nunavut; *Precambrian Research*, v. 232, p. 167–188. <https://doi.org/10.1016/j.precamres.2013.02.010>
- Peterson, T.D., 2006. Geology of the Dubawnt Lake area, Nunavut-Northwest Territories; Geological Survey of Canada, Bulletin 580, 56 p. <https://doi.org/10.4095/221939>
- Peterson, T.D. and Born, P., 1994. Archean and lower Proterozoic geology of western Dubawnt Lake, Northwest Territories; *in* Current Research 1994-C, Geological Survey of Canada, p. 157–164. <https://doi.org/10.4095/193823>
- Peterson, T.D. and Lee, C., 1995. Pre-Dubawnt plutonism and deformation in the Nicholson Lake–Dubawnt Lake area, Northwest Territories; *in* Current Research 1995-C, Geological Survey of Canada, p. 11–18. <https://doi.org/10.4095/202900>
- Peterson, T.D., van Breemen, O., Sandeman, H., and Cousens, B., 2002. Proterozoic (1.85–1.75 Ga) igneous suites of the Western Churchill Province: granitoid and ultrapotassic magmatism in a reworked Archean hinterland; *Precambrian Research*, v. 119, p. 73–100. [https://doi.org/10.1016/S0301-9268\(02\)00118-3](https://doi.org/10.1016/S0301-9268(02)00118-3)
- Peterson, T.D., Pehrsson, S., Skulski, T., and Sandeman, H., 2010. Compilation of Sm-Nd isotope analyses of igneous suites, western Churchill Province; Geological Survey of Canada, Open File 6439, 18 p. <https://doi.org/10.4095/285360>
- Peterson, T.D., Scott, J.M.J., LeCheminant, A.N., Chorlton, L.B., and D’Aoust, B.M.A., 2014. Geology, Tebesjuak Lake, Nunavut; Geological Survey of Canada, Canadian Geoscience Map 158, scale 1:250 000. <https://doi.org/10.4095/293892>
- Peterson, T.D., Jefferson, C.W., and Anand, A., 2015a. Geological setting and geochemistry of the ca. 2.6 Ga Snow Island Suite in the central Rae domain of the Western Churchill Province, Nunavut; Geological Survey of Canada, Open File 7841, 29 p. <https://doi.org/10.4095/296599>
- Peterson, T.D., Scott, J.M.J., LeCheminant, A.N., Jefferson, C.W., and Pehrsson, S.J., 2015b. The Kivalliq Igneous Suite: anorogenic bimodal magmatism at 1.75 Ga in the western Churchill Province, Canada; *Precambrian Research*, v. 262, p. 101–119. <https://doi.org/10.1016/j.precamres.2015.02.019>

- Peterson, T.D., Pehrsson, S., Martel, E., and Percival, J., in press. Lithochemical and Sm-Nd Isotopic Data for the GEM2/south Rae Province study area, 2012–2016; Geological Survey of Canada, Open File 8510.
- Regan, S.P., 2016. Neoproterozoic arc magmatism, subsequent collisional orogenesis, and Paleoproterozoic disruption within the Western Churchill Province: implications for the growth and modification of lower continental crust; Ph.D. dissertation, University of Massachusetts, Amherst, Massachusetts, 273 p.
- Regan, S.P., Williams, M.L., Mahan, K.H., Dumond, G., Jercinovic, M.J., and Orlandini, O.F., 2017a. Neoproterozoic arc magmatism and subsequent collisional orogenesis along the eastern Rae domain, western Churchill Province: implications for the early growth of Laurantia; *Precambrian Research*, v. 294, p. 151–174. <https://doi.org/10.1016/j.precamres.2017.03.010>
- Regan, S.P., Williams, M.L., Chiarenzelli, J.R., Grohn, L., Mahan, K.H., and Gallagher, M., 2017b. Isotopic evidence for Neoproterozoic continuity across the Snowbird Tectonic Zone, western Churchill Province, Canada; *Precambrian Research*, v. 300, p. 201–222. <https://doi.org/10.1016/j.precamres.2017.07.022>
- Regis, D., Acosta-Góngora, P., Davis, W.J., Knox, B., Pehrsson, S.J., Martel, E., and Hulbert, L., 2017a. Evidence for Neoproterozoic Ni-Cu-bearing mafic intrusions along a major lithospheric structure: a case study from the south Rae Province craton (Canada); *Precambrian Research*, v. 302, p. 312–339. <https://doi.org/10.1016/j.precamres.2017.09.026>
- Regis, D., Martel, E., Davis, W.J., and Pehrsson, S.J., 2017b. U-Pb zircon geochronology of metaplutonic rocks across the southern Rae Province, Northwest Territories; Geological Survey of Canada, Open File 8254, 37 p. <https://doi.org/10.4095/302772>
- Regis, D., Pehrsson, S., Martel, E., Thiessen, E., Peterson, T., and Kellet, D., 2021. Post-1.9 Ga evolution of the south Rae craton (Northwest Territories, Canada): a Paleoproterozoic orogenic collapse system; *Precambrian Research*, v. 355, no. 3. <https://doi.org/10.1016/j.precamres.2021.106105>
- Ryan, J.J., Nadeau, L., Hinchey, A.M., Dames, D.T., Sandeman, H.A., Schetselaar, E.M., Davis, W.J., and Berman, R.G., 2009. Bedrock geology of the southern Boothia mainland area (Pelly Bay-Rae Strait-Spence Bay map areas), Kitikmeot region, Nunavut; Geological Survey of Canada, Current Research 2009-1, 21 p. <https://doi.org/10.4095/226519>
- Sanborn-Barrie, M., Chakungal, J., James, D.T., Rayner, N., and Whalen, J.B., 2014. Precambrian bedrock geology, Southampton Island, Nunavut; Geological Survey of Canada, Canadian Geoscience Map 132, scale 1:250 000. <https://doi.org/10.4095/293328>
- Sandeman, H.A., Maclachlan, K., and Relf, C., 1999. Preliminary geochemical and Nd isotopic investigations of Archean volcanic and volcanoclastic rocks of the Yathkyed greenstone belt, Kivalliq region, Northwest Territories; *in* Radiogenic age and isotopic studies: report 12, Geological Survey of Canada, Current Research 1999-F, p. 43–52. <https://doi.org/10.4095/210361>
- Sandeman, H.A., Hanmer, S., Tella, S., Armitage, A.A., Davis, W.J., and Ryan, J.J., 2006. Petrogenesis of Neoproterozoic volcanic rocks of the MacQuoid supracrustal belt: a back-arc setting for the northwestern Hearne subdomain, western Churchill Province, Canada; *Precambrian Research*, v. 144, p. 140–165. <https://doi.org/10.1016/j.precamres.2005.11.001>
- Skulski, T., Sandeman, H., Sanborn-Barrie, M., MacHattie, T., Young, M., Carson, C., Berman, R.G., Brown, J., Rayner, N., Panagapko, D., Byrne, D., and Deyell, C., 2003. Bedrock geology of the Ellice Hills map area and new constraints on the regional geology of the Committee Bay area, Nunavut; Geological Survey of Canada, Current Research 2003-C22, 11 p. <https://doi.org/10.4095/214204>
- Skulski, T., Paul, D., Sandeman, H., Berman, R.G., Chorlton, L., Pehrsson, S.J., Rainbird, R.H., Davis, W.J., and Sanborn-Barrie, M., 2018. Bedrock geology, central Rae Craton and eastern Queen Maud block, western Churchill Province, Nunavut; Geological Survey of Canada, Canadian Geoscience Map 307, scale 1:550 000. <https://doi.org/10.4095/308348>
- Snyder, D.B., Craven, J.A., Pilkington, M., and Hillier, M.J., 2015. The 3-dimensional construction of the Rae craton, central Canada, *Geochemistry, Geophysics, Geosystems*, v. 16, issue 10, p. 3555–3574. <https://doi.org/10.1002/2015GC005957>
- Steenkamp, H.M., Wodicka, N., Lawley, C.J.M., Peterson, T., Garrison, W., Theriault, I., Kendrick, J., Weller, O.M., and Tschirhart, V., 2023a. Bedrock geology, Daly Bay area, Kivalliq, Nunavut, NTS 56-A, 46-D west, 46-E southwest, and 56-H south; Geological Survey of Canada, Canadian Geoscience Map 458, scale 1:150 000. <https://doi.org/10.4095/331888>
- Steenkamp, H.M., Wodicka, N., Lawley, C.J.M., Peterson, T., Weller, O.M., Kendrick, J., and Tschirhart, V., 2023b. Bedrock geology, Armit Lake area, Kivalliq, Nunavut, NTS 56-B and 56-C east; Geological Survey of Canada, Canadian Geoscience Map 459, scale 1:150 000. <https://doi.org/10.4095/331889>
- Steenkamp, H.M., Wodicka, N., Weller, O.M., Kendrick, J., Theriault, I., Peterson, T., Lawley, C.J.M., and Tschirhart, V., 2023c. Bedrock geology, Wager Bay area, Kivalliq, Nunavut, parts of NTS 56-F and 56-G; Geological Survey of Canada, Canadian Geoscience Map 460, scale 1:150 000. <https://doi.org/10.4095/331890>
- Stern, R.A. and Hanson, G.N., 1989. Petrogenesis of mantle-derived, LILE-enriched Archean monzodiorites and trachyandesites (sanukitoid rocks) in southwestern Superior Province; *Canadian Journal of Earth Sciences*, v. 26, p. 1688–1712. <https://doi.org/10.1139/e89-145>
- Stevenson, R., Henry, P., and Garipey, H., 1999. Assimilation–fractional crystallization origin of Archean Sanukitoid Suites: Western Superior Province, Canada; *Precambrian Research*, v. 96, p. 83–99. [https://doi.org/10.1016/S0301-9268\(99\)00009-1](https://doi.org/10.1016/S0301-9268(99)00009-1)
- Theriault, I., Steenkamp, H.M., and Larson, K., 2017. New mapping and initial structural characterization of the Wager shear zone, northwestern Hudson Bay, Nunavut; *in* Summary of Activities, Canada-Nunavut Geoscience Office; v. 2017, p. 1–12.

- Thiessen, E.J., 2021. How 800 million years of tectonics in the southern Rae Craton controlled the distant-hinterland expression of 1.8 Ga Trans-Hudson Orogenesis; Canadian Tectonics Group Online Seminar Series. <<http://www.canadiantectonicsgroup.ca/seminar-series.html>> [accessed May 1, 2021]
- Thiessen, E.J., Regis, D., and Gibson, H.D., 2017. U-Pb zircon geochronology of the Paleoproterozoic Wholdaia Lake shear zone, south Rae Province craton, Northwest Territories; Geological Survey of Canada, Open File 8193, 27 p. <https://doi.org/10.4095/300655>
- Thiessen, E.J., Gibson, H.D., Regis, D., and Pehrsson, S.J., 2018. Deformation and extensional exhumation of 1.9 Ga high-pressure granulites along the Wholdaia Lake shear zone, south Rae Province craton, Northwest Territories, Canada; Lithosphere, v. 10, p. 641–661. <https://doi.org/10.1130/L704.1>
- Thomas, M.D., 2012. Shallow crustal structure in Meadowbank River–Tehek Lake area: insights from gravity and magnetic modelling; Geological Survey of Canada, Open File 7308, 42 p. <https://doi.org/10.4095/292157>
- Tschirhart, V., Morris, W.A., Jefferson, C.W., Keating, P., White, J.C., and Calhoun, L., 2013. 3D geophysical inversions of the northeast Amer Belt and their relationship to the geologic structure; Geophysical Prospecting, v. 61, p. 547–560. <https://doi.org/10.1111/j.1365-2478.2012.01098.x>
- Tschirhart, V., Percival, J.A., and Jefferson, C.W., 2015. Geophysical models of the Montresor metasedimentary belt and its environs, central Nunavut, Canada; Canadian Journal of Earth Sciences, v. 52, p. 833–845. <https://doi.org/10.1139/cjes-2015-0008>
- Tschirhart, V., Jefferson, C.W., and Morris, W.A., 2017. Basement geology beneath the northeast Thelon Basin, Nunavut: insights from integrating new gravity, magnetic and geological data; Geophysical Prospecting, v. 65, no. 2, p. 617–636. <https://doi.org/10.1111/1365-2478.12430>
- Tyrrell, J.B., 1896. Report on the Doobaunt, Kazan and Ferguson Rivers and the north-west coast of Hudson Bay and on two overland routes from Hudson Bay to Lake Winnipeg; Geological Survey of Canada, Annual Report 9, 243 p. <https://doi.org/10.4095/296990>
- Tyrrell, J.B. and Senecal, C.O., 1897. Map of Doobaunt and Kazan Rivers and Northwest Coast of Hudson Bay; Geological Survey of Canada, Multicoloured Geological Map 603, scale 1:1 584 000. <https://doi.org/10.4095/107407>
- Valette, M., De Souza, S., Mercier-Langevin, P., McNicoll, V.J., Wodicka, N., Creaser, R.A., Côté-Mantha, O., and Simard, M., 2019. Geological setting of the 5.2 M oz. Au Amaruq banded iron formation-hosted gold deposit, Churchill Province, Nunavut; *in* Targeted Geoscience Initiative: 2018 report of activities, (ed.) N. Rogers; Geological Survey of Canada, Open File 8549, p. 83–87. <https://doi.org/10.4095/313643>
- van Breemen, O., Pehrsson, S., and Peterson, T.D., 2007. Reconnaissance U-Pb SHRIMP geochronology and Sm-Nd isotope analysis from the Tehery-Wager Bay gneiss domain, western Churchill Province, Nunavut; Geological Survey of Canada, Current Research 2007-F2, 15 p. <https://doi.org/10.4095/224019>
- van Hunen, J. and Moyen, J.-F., 2012. Archean subduction: fact or fiction; Annual Review of Earth and Planetary Sciences, v. 40, p. 195–219. <https://doi.org/10.1146/annurev-earth-042711-105255>
- Villeneuve, M.E., Ross, G.M., Theriault, R.J., Miles, W., Parrish, R.R., and Broome, J., 1993. Tectonic subdivision and U/Pb geochronology of the crystalline basement of the Alberta Basin, western Canada; Geological Survey of Canada, Bulletin 447, 93 p. <https://doi.org/10.4095/77642>
- Whalen, J.B., Percival, J.A., McNicholl, V.J., and Longstaffe, F.J., 2004. Geochemical and isotopic (Nd–O) evidence bearing on the origin of late- to post-orogenic high-K granitoid rocks in the Western Superior Province: implications for late Archean tectonomagmatic processes; Precambrian Research, v. 132, p. 303–326. <https://doi.org/10.1016/j.precamres.2003.11.007>
- Whalen, J.B., Wodicka, N., Taylor, B.E., and Jackson, G.D., 2010. Cumberland batholith, Trans-Hudson Orogen, Canada: petrogenesis and implications for Paleoproterozoic crustal and orogenic processes; Lithos, v. 117, p. 99–118. <https://doi.org/10.1016/j.lithos.2010.02.008>
- Wodicka, N., Steenkamp, H.M., Peterson, T.D., McMartin, I., Day, S.J.A., and Tschirhart, V.L., 2017. Report of activities for the geology and economic potential of the Tehery-Wager area, Nunavut: GEM2-Rae Project; Geological Survey of Canada, Open File 8318, 18 p. <https://doi.org/10.4095/305979>
- Zaleski, E., 2002. Geology, Meadowbank River area, Nunavut; Geological Survey of Canada, Map 2068A, scale 1:50 000. <https://doi.org/10.4095/220495>

APPENDIX A

Snow Island Suite analyses ([Appendix_A_analyses.xlsx](#))

This appendix is a compilation, in Excel spreadsheet format, of whole-rock elemental analyses of Snow Island Suite samples collected from outcrop (dominantly intrusive rocks, with minor volcanic rocks).

Data sources and sample locations are noted. It includes all recent (after 2010) GEM1 and GEM2 analyses, plus previously unpublished analyses from legacy projects and other ongoing work within Nunavut. Pre-GEM analyses are often partial (e.g. ferric/ferrous values are not recorded). The samples are organized into the recognized petrological groups, as discussed in the accompanying text.

Paleoproterozoic dyke swarms and large igneous provinces of northern Canada and their use in understanding extension, rifting, and paleocontinental reconstructions

K.L. Buchan^{1*} and R.E. Ernst^{2,3}

Buchan, K.L. and Ernst, R.E., 2024. Paleoproterozoic dyke swarms and large igneous provinces of northern Canada and their use in understanding extension, rifting, and paleocontinental reconstructions; in Canada's northern shield: new perspectives from the Geo-mapping for Energy and Minerals program, (ed.) S.J. Pehrsson, N. Wodicka, N. Rogers, and J.A. Percival; Geological Survey of Canada, Bulletin 612, p. 375–410. <https://doi.org/10.4095/332506>

Abstract: Giant mafic dyke swarms and related large igneous provinces play an important role in the understanding of the tectonic evolution of ancient continents and supercontinents. The information available for well dated Paleoproterozoic dyke swarms and large igneous provinces in northern Canada is summarized in this synthesis, with an emphasis on their age, geographic distribution, paleomagnetism, and potential linkages to coeval magmatic events. Their tectonic settings, with a focus on links to rifting and continental breakup, are also discussed. Finally, the use of giant dyke swarms and large igneous provinces for testing paleocontinental reconstructions is considered, based mainly on paleomagnetism or on matching coeval magmatic events or sequences of magmatic events (magmatic barcoding) between cratons.

Résumé : Les essais géants de dykes mafiques et les grandes provinces ignées apparentées contribuent fortement à la compréhension de l'évolution tectonique des anciens continents et supercontinents. Dans la présente synthèse, nous résumons l'information disponible sur les essais de dykes bien datés et les grandes provinces ignées du Paléoprotérozoïque du nord du Canada, en nous concentrant sur leur âge, leur distribution géographique, leur paléomagnétisme et leurs liens potentiels avec les événements magmatiques qui leur étaient contemporains. Nous abordons aussi leur cadre tectonique en mettant l'accent sur les liens avec le rifting et la rupture des continents. Pour conclure, nous nous penchons sur l'utilisation des essais géants de dykes et des grandes provinces ignées pour valider les reconstitutions paléocontinentales fondées principalement sur le paléomagnétisme ou sur les événements magmatiques ou séquences d'événements magmatiques (code-barres magmatique) correspondants de même âge entre les cratons.

¹Geological Survey of Canada, 601 Booth Street, Ottawa, Ontario K1A 0E8

²Department of Earth Sciences, Carleton University, 1125 Colonel By Drive, Ottawa, Ontario K1S 5B6

³Also at: Faculty of Geology and Geography, Tomsk State University, 36 Lenin Avenue, Tomsk, 634050, Russia

*Corresponding author: K.L. Buchan (email: kenneth.buchan@nrcan-rncan.gc.ca)

INTRODUCTION

Large igneous provinces (LIPs) comprising giant mafic dyke swarms, sill provinces and/or volcanic units (Ernst, 2014) are a prominent feature of the geology of northern Canada (north of latitude 60°). Giant dyke swarms associated with LIPs have a primary geometry that is linear, radiating (Ernst et al., 1995) or, more rarely, circumferential (i.e. circular or elliptical; Buchan and Ernst, 2019). They are important because 1) they can provide a record of the overall extent of a magmatic event, even in cases when much, if not all, of the shallow crustal component (volcanic flows and sills) has been removed by erosion; 2) they may reflect the rifting and/or breakup history of a region; and 3) they are useful in reconstructing paleocontinents based on paleomagnetism (mafic dykes typically carry stable magnetic remanences), reconstruction of the primary geometry of swarms, and matching ages of magmatic events on different cratons.

In this study, well dated Paleoproterozoic LIPs in northern Canada (including their extension beyond this region) are discussed, with a particular focus on the giant (typically diabase) dyke swarms, and their potential significance is summarized, especially in relation to rifting, continental breakup, and paleocontinental reconstructions. For completeness, several small dyke swarms and other magmatic units, whose link to LIPs is uncertain, are also considered.

Most of the magmatic events discussed are mainly mafic, although several largely felsic events are also included. This analysis builds on previous studies and mapping of dyke swarms and other magmatic units. Mapping of dyke swarms has been published most recently for Canada at a scale of 1:5 000 000 by Buchan and Ernst (2004); for the Slave Craton at various scales, up to 1:30 000, by Stubleby (2005); for the Slave Craton and Wopmay Orogen at a scale of 1:2 000 000 by Buchan et al. (2010); and for northern Canada at scales up to at least 1:500 000 (with summary map at 1:3 000 000) by Buchan and Ernst (2013). Magmatic units that are related to the dyke swarms in Canada are summarized on the map of Buchan and Ernst (2004). Magmatic units related to dyke swarms in the Slave Craton and Wopmay Orogen are shown in greater detail on the map of Buchan et al. (2010) and the 1:1 000 000 scale map of Hoffman and Hall (1993). Magmatic units in the mainland portion of the Churchill Province, which comprises the Rae and Hearne cratons, are shown on several geological compilation maps, most notably at a scale of 1:550 000 by Tella et al. (2007), Pehrsson et al. (2014), and Skulski et al. (2018). Earlier studies that discuss LIPs and/or their dyke swarms and links to breakup events include those by LeCheminant et al. (1996a) for the Slave Craton, as well as by Ernst and Buchan (2004) and Ernst and Bleeker (2010) for Canada. The dyke swarms and other magmatic units that are illustrated on figures herein have in most cases been derived, and in some cases simplified, from the various map sources cited above.

Post-Paleoproterozoic giant dyke swarms and related units of LIPs have been described and/or mapped in other published works and are not discussed in detail in this study. Most notably, the Mesoproterozoic 1.27 Ga Mackenzie giant radiating swarm and related units are shown in Buchan et al. (2010) and Buchan and Ernst (2013), and possible links to approximately coeval dykes in the southern Siberian Craton are described by Ernst et al. (2016). The Neoproterozoic 0.78 Ga Gunbarrel and 0.72 Ga Franklin giant radiating swarms and related units are shown in Buchan and Ernst (2013) as well as Figures 6 and 7 of Buchan et al. (2010), and proposed links to coeval mafic intrusions in the Siberian Craton are considered in Ernst et al. (2016). Finally, the Phanerozoic 0.12 to 0.08 Ga Queen Elizabeth Islands and Surprise Fiord dyke swarms are discussed, and interpreted as components of giant radiating and giant circumferential dyke swarms that form part of the High Arctic large igneous province (HALIP), in Buchan and Ernst (2018, 2019).

Despite a significant increase in precise U-Pb dating of dyke swarms and related units in recent years, coupled with extensive geological mapping, geochemical analyses, and paleomagnetic studies, the overall extent of many, if not most, of the Paleoproterozoic magmatic events discussed here remains uncertain, and awaits further study. For example, many volcanic packages within the various Paleoproterozoic supracrustal sequences of intracratonic basins and passive margins scattered across northern Canada remain undated or poorly dated, and hence cannot yet be assigned to specific magmatic events.

GEOLOGICAL SETTING

Northern Canada comprises several cratonic blocks (Fig. 1), including the Archean Slave, Rae, and Hearne cratons, the Archean Meta Incognita terrane, and the Paleoproterozoic Hottah terrane, which are typically separated by prominent orogenic belts such as the Thelon tectonic zone, Taltson magmatic zone, Wopmay Orogen, and Snowbird tectonic zone. The Archean cratons are thought to have rifted from ancestral supercontinents or supercratons mainly during the early Paleoproterozoic, before amalgamating as part of Laurentia by ca. 1.8 Ga (e.g. Hoffman, 1988; Bleeker, 2003; Pehrsson et al., 2013, 2016). Unfortunately, many proposed rifting and collisional events, which are briefly outlined below, are still rather poorly documented, are not always well dated, and are, in some cases, controversial.

Breakup of Archean cratons from ancestral supercratons

The makeup and breakup of the ancestral supercratons is a topic of much discussion. For example, the components of the supercraton from which the Slave Craton was derived, Scavia, and the timing of the latter's breakup are not well understood (Bleeker, 2003; French and Heaman,

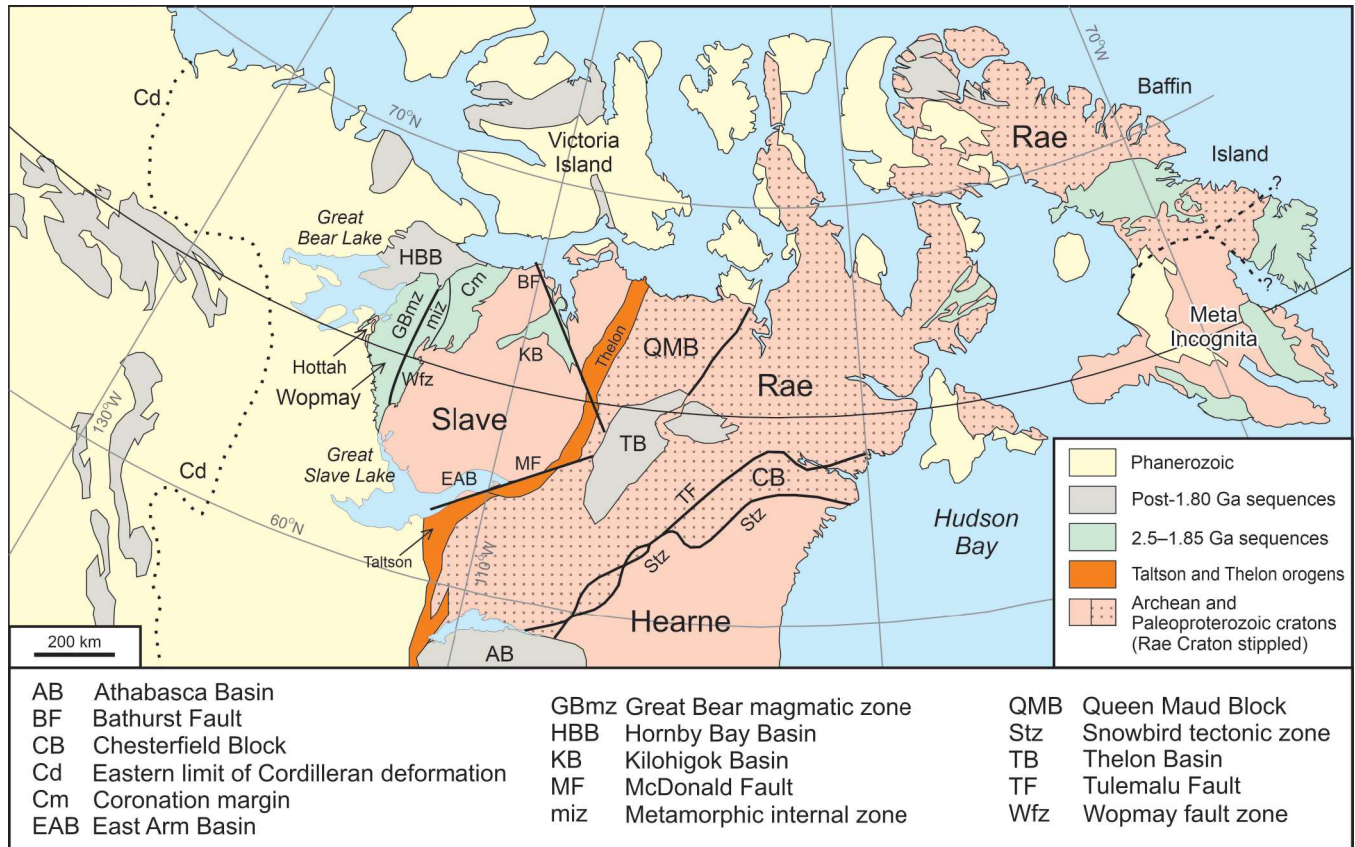


Figure 1. Simplified geology of northern Canada (*modified from Cook et al., 2005; Rainbird et al., 2010; Pehrsson et al., 2013*). Only the most prominent basins and sedimentary sequences are shown. The Rae and Hearne cratons together make up the Churchill Province. The Rae Craton is shown with a stippled pattern for clarity. It includes the Chesterfield and Queen Maud blocks. The boundary between the Meta Incognita terrane and the Rae Craton is uncertain and may follow either of the dotted lines that are shown (southern version: St-Onge et al., 2006; northern version: Corrigan et al., 2009). The Hottah terrane and Wopmay Orogen extend far to the south, beneath Phanerozoic cover rocks.

2010). Nevertheless, a number of early Paleoproterozoic dyke swarms (and related units) may represent precursors of break-up events along the Slave's rifted margins (e.g. LeCheminant et al., 1996a; Ernst and Bleeker, 2010). Similarly, the ancestral supercratons from which the Rae and Hearne cratons were derived are poorly constrained (*see discussion in Pehrsson et al., 2013*). For example, it has been proposed that the Hearne and Superior cratons formed part of the same supercraton, Superia, based on a comparison of earliest Paleoproterozoic dyke swarms (Bleeker, 2003; Ernst and Bleeker, 2010; Gumsley et al., 2017). Sandeman et al. (2013), however, have questioned this linkage.

Relationship between Rae and Slave cratons in the middle Paleoproterozoic

The relationship of the Rae and Slave cratons during the middle Paleoproterozoic is uncertain. It has generally been thought that the two cratons collided at ca. 1.97 Ga, with the Slave Craton representing an indenter into the Rae Craton and

associated strike-slip movement occurring along bounding Bathurst and McDonald faults (Fig. 1; e.g. Hoffman 1988). On the other hand, Sheen et al. (2019) have proposed that the two cratons were together from at least ca. 2.045 Ga, and that the East Arm Basin (Fig. 1) represents a failed intracratonic rift, as had been suggested several decades ago (Hoffman, 1973a), but subsequently rejected (Hoffman, 1987).

Amalgamation of Rae and Hearne cratons

The timing of the assembly of the Rae and Hearne cratons along the Snowbird tectonic zone has long been controversial, with some authors arguing for collision in the late Archean (e.g. Hanmer et al., 1995), and others favouring a much later collision at ca. 1.9 Ga during the Paleoproterozoic (e.g. Hoffman, 1988; Berman et al., 2007). In early interpretations, the Snowbird tectonic zone, which is well defined in the region north of Lake Athabasca, was thought to continue along the northwestern boundary of the Chesterfield Block as the Tulemalu Fault (Fig. 1). More recently, however, the Chesterfield Block has been generally interpreted as forming

part of the Rae Craton since the late Archean, based on the recognition of 2.6 Ga plutons that stitch the two blocks (Davis et al., 2006; Berman et al., 2007). As a result, the revised Rae–Hearne boundary (i.e. Snowbird tectonic zone) is now usually drawn along the southern boundary of the Chesterfield Block (Fig. 1; Berman et al., 2007). Despite this clarification, controversy over the timing of collision between the Rae Craton (including the Chesterfield Block) and the Hearne Craton continues.

Implications of mafic volcanic sequences in early Paleoproterozoic supracrustal successions of the Churchill Province

Mafic volcanic sequences are preserved in several early Paleoproterozoic sedimentary successions that unconformably overlie Archean rocks of the Rae and Hearne cratons (*see* summary in Rainbird et al., 2010). Because of uncertain ages, the mafic volcanic rocks are seldom well correlated between the sedimentary successions and are often difficult to assign to broader magmatic events. They are interpreted to have been emplaced in extensional settings, and hence may be associated with continental break-up events.

Multiple phases of rifting on the western margin of the Slave Craton during the middle Paleoproterozoic

There is evidence of repeated extensional events during the Paleoproterozoic affecting the margins of cratons in northern Canada. For example, breakup or failed breakup may have occurred on the western margin of the Slave Craton at 2.13 to 2.11 Ga (in association with the Indin dyke swarm; Ernst and Bleeker, 2010). Later rifting events at 2.01 Ga (in association with the Vaillant Formation volcanic rocks; Hoffman et al., 2011) and at 1.90 Ga (in association with the Bell Island Bay Group volcanic rocks; e.g. Ootes et al., 2017) are better defined. Collision between the western Slave margin and the Hottah terrane followed at ca. 1.88 Ga (Hoffman et al., 2011). What crustal blocks rifted away during the extensional events remains unclear. The most common interpretation is that the Hottah terrane is an exotic microcontinent or magmatic arc that rifted from some other parent craton, rather than a magmatic arc that rifted from the Slave Craton (Davis et al., 2015a; Ootes et al., 2015).

Rifting on the southeastern margin of the Rae Craton

Rifting on the southeastern margin of the Rae Craton (in southern Baffin Island) at ca. 1.92 Ga is thought to have led to formation of an incipient ocean, which closed when the Meta Incognita microcontinent collided with the Rae Craton

between ca. 1.883 and 1.865 Ga (e.g. St-Onge et al., 2006; Corrigan et al., 2009; Wodicka et al., 2014). As in the case of the western margin of the Slave Craton, it is not certain what crustal block rifted away at 1.92 Ga, whether the Meta Incognita microcontinent or some yet unidentified terrane (*see* discussion in St-Onge et al., 2006).

PALEOPROTEROZOIC MAFIC DYKE SWARMS AND OTHER LIP COMPONENTS OF NORTHERN CANADA

In the following subsections, Paleoproterozoic dyke swarms and other LIP components of northern Canada are discussed in relation to Laurentia or the older cratonic blocks (Slave, Rae, and Hearne cratons, and Meta Incognita and Hottah terranes) that amalgamated to form the northern portion of Laurentia during the Paleoproterozoic. The units described are of mainly mafic composition unless otherwise noted. Their characteristics (such as age, geographic extent, and paleomagnetism) are briefly outlined, and possible links to other coeval events are considered. The units are shown on the accompanying figures and are listed in Table 1 in chronological order to permit a comparison of coeval events in the different cratonic blocks. Their use in interpreting major tectonic events of the region and in testing paleocontinental reconstructions is also discussed.

Precise U-Pb ages are critical for identifying the various components of a given event, determining the timing of associated extension and rifting, and establishing a magmatic barcode (time sequence of magmatic events; Bleeker, 2004) for a cratonic block. Comparison of magmatic barcodes for different cratonic blocks is helpful in determining if, and over what period, the blocks were near neighbours. Paleomagnetism is another important tool for identifying components of a magmatic event because mafic dykes, sills, and volcanic rocks often carry a stable magnetic remanence, the primary or secondary nature of which can be determined by paleomagnetic field tests (Buchan, 2014). Different units of a single magmatic event on a given craton should have similar primary paleomagnetic poles. In addition, a primary paleomagnetic pole establishes the latitude and azimuthal orientation of the cratonic block at the time that the unit was emplaced. Comparison of paleomagnetic poles for coeval events from different cratonic blocks is useful in testing paleocontinental reconstructions. An even more rigorous test of reconstructions can be performed if coeval segments of apparent polar wander paths (APWPs) for different cratons are available (e.g. Buchan, 2014). When cratonic blocks drift in unison (i.e. on a single tectonic plate), their APWPs will have similar shapes and lengths (e.g. Evans and Pisarevsky, 2008). On the other hand, when cratonic blocks are drifting independently (on different plates), the APWPs will have different shapes.

Table 1. Selected Paleoproterozoic dyke swarms and other magmatic events of northern Canada.

Event name (age) General location	Magmatic components
Ca. 2.50–2.46 Ga (Fig. 2)	
Kaminak (2.50 Ga) Hearne	<p>DYKES: Kaminak (2498 ± 1 Ma; Sandeman et al., 2013); probable radiating geometry with a focus near the northern Hearne Craton margin.</p> <p>VOLCANIC ROCKS: Possibly poorly dated Spi gp basalt flows (Sandeman and Ryan, 2008).</p> <p>COMMENT: Swarm is confined to the Hearne Craton and does not extend into the Rae Craton, suggesting that the Rae and Hearne were not together in their current configuration at 2.50 Ga (Davis et al., 2006; Berman et al., 2007). Link with the Matachewan dykes of the Superior Craton proposed by Bleeker (2004), but disputed by Sandeman et al. (2013).</p> <p>SETTING: Swarm may be associated with a plume centred off the northern Hearne margin (Bleeker, 2004; Ernst and Bleeker, 2010), consistent with the radiating geometry of the swarm.</p>
Queen Maud (ca. 2.50–2.46 Ga) Rae	<p>FELSIC PLUTONS: Queen Maud Block granitoid plutons (2.50–2.46 Ga; Schultz et al., 2007a).</p> <p>MAFIC ROCKS: Mafic rocks (2.50–2.48 Ga; Schultz et al., 2010); mafic dyke (2516 ± 14 Ma; Schultz et al., 2010).</p> <p>COMMENT: Mafic rock geochemistry is consistent with a continental rift or continental flood-basalt setting (Schultz et al., 2010). A granite pluton of the same age has been reported in southern Boothia Peninsula (Berman et al., 2013).</p> <p>SETTING: Alternative models include 1) incipient continental rifting preceding ca. 2.44–2.39 Ga sedimentation in the Sherman Basin (Schultz et al., 2010), 2) back-arc setting during east-dipping subduction beneath the Rae Craton (Hoffman, 1988; Berman et al., 2013), and 3) arc rifting induced by ridge subduction (Berman et al., 2013).</p>
Ca. 2.27–2.19 Ga (Fig. 3)	
Orpheus (ca. 2.27 Ga) Rae	DYKES: Orpheus (ca. 2.27 Ga; M. Hamilton, pers. comm. <i>in</i> Mowbray and Pehrsson, 2019).
Malley (ca. 2.23 Ga) Slave	<p>DYKES: Malley (2231 ± 2 Ma; Buchan et al., 2012).</p> <p>COMMENT: Malley dykes may extend east of the Bathurst Fault as poorly dated Brichta dykes (Buchan et al., 2012).</p>
MackKay (ca. 2.21 Ga) Slave	DYKES: MacKay (ca. 2.21 Ga; LeCheminant and van Breemen, 1994).
Southwestern Slave (Dogrib) (ca. 2.19–2.18 Ga) Slave	<p>DYKES: Dogrib (2193 ± 3–2 Ma; Mitchell et al., 2014).</p> <p>SILL: Duck Lake (2181 ± 2 Ma; Bleeker and Kamo, 2003).</p> <p>OTHER INTRUSIONS: Big Spruce complex (2193 ± 16–10 Ma; Cavell and Baadsgaard, 1986), Squalus Lake intrusion (2181 ± 2 Ma; Villeneuve and van Breemen, 1994), Blachford Lake complex (ca. 2180 Ma; Bowring et al., 1984; A. Davidson <i>in</i> Bowring et al., 1984; Sinclair et al., 1994).</p> <p>COMMENT: Coeval with Tulemalu–MacQuoid dykes of the Rae Craton (mainly in the Chesterfield Block), but probably not genetically related, as paleomagnetic data from the Tulemalu and Dogrib dykes suggest that the Rae and Slave cratons were not together in their current configuration at 2.19 Ga (LeCheminant et al., 1997; see discussion in text).</p> <p>SETTING: Possible precursor to breakup on southwestern Slave margin (Bleeker and Hall, 2007).</p>

Table 1. (cont.)

Event name (age) General location	Magmatic components
Tulemalu–MacQuoid (ca. 2.19 Ga) <i>Rae (mainly in Chesterfield Block)</i>	DYKES: Tulemalu (ca. 2.19 Ga; LeCheminant et al., 1997); MacQuoid (ca. 2.19 Ga; Tella et al., 2001). COMMENT: In the Rae Craton (mainly the Chesterfield Block). Do not extend into the Hearne Craton, suggesting that the Rae and Hearne were not attached at 2.19 Ga (Davis et al., 2006; Berman et al., 2007). See also comment in Southwestern Slave (Dogrib) entry.
Ca. 2.13–2.11 Ga (Fig. 4)	
Indin (ca. 2.13–2.11 Ga) <i>Slave</i>	DYKES: Indin (2126 ± 2 Ma; Buchan et al., 2016; ca. 2108 Ma; Davis and Bleeker, 2007, Bleeker et al., 2008a); slightly radiating geometry, with a focus near the western Slave Craton margin. COMMENT: Coeval with Griffin sills in the Hearne Craton, Kazan and Chipman dykes of the Rae Craton, and several dyke swarms in other cratons that amalgamated to form Laurentia. It is unclear which, if any, of these swarms are genetically related. SETTING: Plume centred off the western Slave margin based on a radiating dyke geometry (Ernst and Bleeker, 2010).
Griffin (ca. 2.11 Ga) <i>Hearne</i>	DYKES: Minor feeders to Griffin sills. SILLS: Griffin gabbro sills (2111 ± 1 Ma; Heaman and LeCheminant, 1993) in the Hurwitz group. COMMENT: See comment for the Indin dyke entry. Undated Happortiyik volcanic rocks of the Hurwitz group have been interpreted to be somewhat older than the Griffin sills (Aspler et al., 2002). SETTING: Interpreted as part of a LIP comprising the Griffin sills, Kazan dykes, and Chipman dykes (Regan et al., 2017).
Kazan–Chipman (ca. 2.11 Ga) <i>Rae and Rae–Hearne boundary</i>	DYKES: Kazan (ca. 2116 ± 12 Ma; Regan et al., 2017); Chipman (ca. 2113 ± 13 Ma; Regan et al., 2017). COMMENT: See comment for the Indin dyke entry. SETTING: Interpreted as part of a LIP comprising the Griffin sills, Kazan dykes, and Chipman dykes (Regan et al., 2017). Possibly related to aborted rifting along the Snowbird tectonic zone (Regan et al., 2017). The relevance of the Griffin–Kazan–Chipman age correlation, however, is unclear because ca. 2.13–2.11 Ma magmatism is widespread on many of the cratons that assembled to form Laurentia, and there is substantial evidence to indicate that the Rae and Hearne cratons did not collide until ca. 1.9 Ga (Berman et al., 2007; see also discussion in text).
Ca. 2.05–2.01 Ga (Fig. 5)	
Union Island–McKee (ca. 2.05–2.04 Ga) <i>Slave (East Arm and vicinity)</i>	DYKES: McKee Lake (2038 ± 3 Ma; Pehrsson et al., 1993); feeder dykes to basalts of the lower Union Island Gp. SILLS: Union Island Gp sills and intrusions (2043 ± 3 Ma; Sheen et al., 2019). VOLCANIC ROCKS: Lower Union Island Gp alkaline basalt flows (2046 ± 1 Ma; Sheen et al., 2019). COMMENT: Event may encompass the slightly younger Lac de Gras–Booth River magmatism of the Slave Craton, and scattered coeval units in the Rae Craton such as the Montresor gabbro and gabbro-anorthosite of the Penylan Domain (Sheen et al., 2019). Tholeiitic basalt flows of the upper Union Island Gp have not been precisely dated. SETTING: Possible plume (Sheen et al., 2019). Union Island Gp may reflect initiation of failed rifting in the East Arm of Great Slave Lake (Sheen et al., 2019).
Montresor–Penylan (ca. 2.05–2.03 Ga) <i>Rae</i>	SILLS: Gabbro sills in the Montresor gp (2045 ± 13 Ma; Percival et al., 2017). PLUTONS: Plutons in the Penylan Domain (ca. 2048–2032 Ma; Davis et al., 2015b). COMMENT: See comment in the Union Island Gp entry.

Table 1. (cont.)

Event name (age) General location	Magmatic components
Lac de Gras–Booth River (ca. 2.03–2.02 Ga) <i>Slave</i>	<p>DYKES: Lac de Gras (2027 ± 4 Ma, 2023 ± 2 Ma; Buchan et al., 2009).</p> <p>LAYERED INTRUSIONS: Booth River igneous complex (mafic phase: 2026 ± 1 Ma, 2025 ± 1 Ma; Davis et al., 2004; felsic phase: 2023 +4/-2 Ma; Roscoe et al., 1987).</p> <p>COMMENT: See comment in Union Island Gp entry.</p> <p>SETTING: Possibly linked to initial rifting on the western Slave Craton margin (LeCheminant et al., 1996a; Hoffman et al., 2011).</p>
Vaillant (ca. 2.014 Ga) <i>Wopmay Orogen</i>	<p>VOLCANIC ROCKS: Vaillant Fm basalt in Melville Gp (felsic tuff at top of basalt: 2014 ± 1 Ma; Hoffman et al., 2011).</p> <p>SETTING: Rift-to-drift transition on the western margin of the Slave Craton, and may be linked to slightly earlier Lac de Gras–Booth River magmatism (Hoffman et al., 2011).</p>
Ca. 1.97–1.95 Ga (Fig. 6)	
Carousel (ca. 1.97–1.96 Ga) <i>Slave (Wopmay Orogen and Kilohigok Basin)</i>	<p>SILLS: Sills of the Carousel igneous suite (Hoffman, 1996) of the lower Epworth Gp, Wopmay Orogen.</p> <p>VOLCANIC ROCKS: Basalt flows of the Carousel igneous suite (Hoffman, 1996) of the lower Epworth Gp of the Wopmay Orogen; lower Bear Creek Gp ash beds of the Kilohigok Basin (1969 ± 1 Ma to 1963 ± 6 Ma; Bowring and Grotzinger, 1992).</p> <p>COMMENT: Epworth Gp and Bear Creek Gp are stratigraphically correlated (Hoffman and Hall, 1993).</p> <p>SETTING: Epworth Gp represents the passive margin of the western Slave Craton (Hoffman, 1973b; Hoffman et al., 2011).</p>
Holly Lake (ca. 1.95 Ga) <i>Hottah terrane</i>	<p>VOLCANIC ROCKS: Basalt of Holly Lake metamorphic complex (ca. 1.95 Ga detrital zircons from interbedded metasediments; Davis et al., 2015a).</p> <p>SETTING: Holly Lake metamorphic suite was emplaced prior to the Hottah terrane rifting from its parent craton. Detrital zircons indicate that this parent craton was not the Slave Craton, but perhaps a terrane south of the Slave Craton (Davis et al., 2015a; Ootes et al., 2015, 2017).</p>
Ca. 1.93–1.91 Ga (Fig. 7)	
Hottah (1.93–1.91 Ga) <i>Hottah terrane</i>	<p>PLUTONS: Mainly felsic Hottah plutonic complex (1931 ± 1 Ma to 1913 ± 1 Ma; Ootes et al., 2015).</p> <p>SETTING: Volcanic arc that later rifted off a parent craton, perhaps a terrane south of the Slave Craton (Davis et al., 2015a; Ootes et al., 2015, 2017).</p>
Wilson Island (ca. 1.93 Ga) <i>Slave (East Arm)</i>	<p>SILLS: Sills in the lower Wilson Island Gp.</p> <p>VOLCANIC ROCKS: Bimodal volcanic rocks in the lower Wilson Island Gp (1928 ± 11 Ma; Bowring et al., 1984; Johnson, 1990).</p> <p>SETTING: Pull-apart basin during postcollisional convergence between the Slave and Rae cratons (Johnson, 1990) or failed rift (Sheen et al., 2019).</p>
Frobisher (ca. 1.92 Ga) <i>Meta Incognita microcontinent</i>	<p>SILLS: Frobisher suite mafic-ultramafic sills (ca. 1922 ± 12 Ma; Liikane et al., 2015) in the Lake Harbour Gp.</p> <p>COMMENT: The sills occur across the Meta Incognita microcontinent.</p> <p>SETTING: Possibly related to rifting of the Meta Incognita microcontinent from its parent craton (St-Onge et al., 2000). Possibly related to a plume or back-arc rifting (Liikane et al., 2015).</p>

Table 1. (cont.)

Event name (age) General location	Magmatic components
Ca. 1.92–1.84 Ga (Fig. 8)	
Bell Island Bay and Akaitcho–Grant (ca. 1.91–1.89 Ga) <i>Hottah terrane and western Slave margin</i>	<p>DYKES: Fishtrap Lake dykes (Reichenbach, 1991) of the Hottah terrane.</p> <p>SILLS: Fishtrap Lake sills (Reichenbach, 1991) of the Hottah terrane.</p> <p>VOLCANIC ROCKS: In the Hottah terrane: bimodal Zebulon fm volcanic rocks (1906 ± 2 Ma; Ootes et al., 2015; $1898 \pm 7/-6$ Ma; Reichenbach, 1991), Bloom Basalt ($\geq 1895 \pm 2$ Ma based on overlying rhyodacite age; Ootes et al., 2015) of Bell Island Bay gp. East of the Wopmay Fault on the Slave Craton margin: Grant subgp basalt (interbedded rhyodacite, 1893 ± 2 Ma; Ootes et al., 2015) and Akaitcho Gp bimodal volcanic rocks (rhyolites; ca. 1.90 Ga; Hoffman and Bowring, 1984).</p> <p>COMMENT: Fishtrap Lake dykes may feed Fishtrap Lake sills and Bloom Basalt (Reichenbach, 1991). Grant subgp basalt and Bloom Basalt correlated by Reichenbach (1991). They may be associated with a single large-scale rifting event although geographically separated (e.g. Ootes et al., 2017), with Grant subgp emplaced along the Slave margin and Bloom Basalt emplaced in the Hottah terrane, which was located to the south at that time.</p> <p>SETTING: Bloom Basalt and Grant subgp basalt erupted in either a rifted-arc or marginal-basin setting. Bloom Basalt interpreted to be associated with rifting of the Hottah microcontinent from a parent craton located south of the Slave Craton (Davis et al., 2015a; Ootes et al., 2015, 2017).</p>
Upper Bravo Lake (ca. 1.90–1.88 Ga) <i>Rae</i>	<p>DYKES: Sheeted dykes of the upper Bravo Lake Fm of the Piling Gp.</p> <p>SILLS: Sills of the upper Bravo Lake Fm of the Piling Gp ($1897 \pm 10/-5$ Ma; Wodicka et al., 2014; 1883 ± 5 Ma; Henderson and Parrish, 1992).</p> <p>VOLCANIC ROCKS: Alkaline basalts of the upper Bravo Lake Fm of the Piling Gp.</p> <p>COMMENT: Tholeiitic to picritic volcanic rocks of the lower Bravo Lake Fm may be much older, perhaps 1.98 Ga (Wodicka et al., 2014). Bravo Lake Fm volcanic rocks may be linked to poorly dated volcanic rocks in the Penrhyn Gp of the Melville Peninsula (Jackson and Berman, 2000), and may be coeval with Five-Mile Lake volcanic rocks in the Amer Gp and volcanic rocks in the Ketyet River gp (Rainbird et al., 2010).</p> <p>SETTING: A possible link to a plume is controversial (Jackson and Berman, 2000; Johns et al., 2006). Wodicka et al. (2014) concluded the lower Bravo Lake volcanic rocks were likely emplaced in an intracontinental basin, whereas the upper Bravo Lake volcanic rocks were related to incipient rifting on the southeastern Rae margin.</p>
Hearne (ca. 1.90 Ga) <i>Slave</i>	<p>DYKES: Hearne dykes (1901 ± 4 Ma; Bleeker et al., 2008b)</p> <p>COMMENT: Coeval with Kramanituur and Daly Bay mafic granulite complexes of the Rae Craton.</p> <p>SETTING: May be linked to a major episode of rifting and magmatism in the Hottah terrane and on the western Slave Craton margin (Ootes et al., 2017).</p>
Daly Bay and Kramanituur (ca. 1.92–1.90 Ga) <i>Rae</i>	<p>INTRUSIONS: Daly Bay (1917 ± 3 Ma; Berman et al., 2007) and Kramanituur (1901 ± 2 Ma; Sanborn-Barrie et al., 2001) mafic granulite complexes.</p> <p>SETTING: Mafic magmatism and related extension, rapid uplift, and cooling may have been triggered by slab breakoff associated with north-directed subduction of the Hearne plate beneath the Rae Craton (including the Chesterfield Block) (Fig. 2 in Berman et al., 2007).</p>
Hepburn (ca. 1.90–1.88 Ga) <i>Wopmay Orogen (metamorphic internal zone)</i>	<p>PLUTONS: Peraluminous granite to gabbro plutons ($1895-1878$ Ma; Hoffman and Bowring, 1984; 1892 ± 2 Ma; Ootes et al., 2017) of the Hepburn intrusive suite.</p> <p>SETTING: Hepburn intrusive suite associated with a back-arc basin (Lalonde, 1989) or fore-arc basin setting (Hildebrand et al., 2010a). Associated with a second phase of rifting on the western Slave margin along with coeval Grant subgp basalt (Ootes et al., 2017).</p>

Table 1. (cont.)

Event name (age) General location	Magmatic components
Ghost (ca. 1.89–1.87 Ga) Slave (including Kilohigok Basin and Wopmay Orogen)	<p>DYKES: Ghost dykes (1886–1884 Ma; Atkinson, 2004; Davis and Bleeker, 2007; Bleeker et al., 2008a; Buchan et al., 2016) of the Slave Craton.</p> <p>SILLS: Morel sills (ca. 1.89–1.88 Ga; Hildebrand et al., 2010a) of the Wopmay Orogen, Mara River sheets (1.87 Ga; Davis et al., 2004; M. Hamilton <i>in</i> Buchan et al., 2010) of the Slave Craton and Kilohigok Basin.</p> <p>VOLCANIC ROCKS: Fontano tuff of Recluse Gp (1882.5 ± 1 Ma; Hoffman et al., 2011) of the Wopmay Orogen; Brown Sound Fm volcanic rocks of the Kilohigok Basin (similar in age or slightly younger than the Fontano tuff, based on stratigraphic correlation; Bowring and Grotzinger, 1992).</p> <p>COMMENT: These mafic units, with ages spanning ca. 20 Ma, are extensive in the Slave and Wopmay, and may or may not all belong to a single event.</p> <p>SETTING: Morel sills are interpreted to have been emplaced during the Hottah–Slave collision as the result of the breakoff of the subducting slab (Hildebrand and Bowring, 1999). Recluse Gp is a foredeep assemblage associated with the Hottah–Slave collision (Hoffman, 1973b; Hildebrand et al., 2010a). Ghost dykes of the Slave Craton may also be associated with the Hottah–Slave collision, perhaps representing lower-plate magmatism associated with plate bending (Davis and Bleeker, 2007).</p>
McTavish (ca. 1.88–1.85 Ga) Wopmay Orogen (Great Bear magmatic zone)	<p>DYKES: Local feeder dykes to the Sloan basalt.</p> <p>VOLCANIC ROCKS: LaBine gp (1876 ± 3 Ma, andesite; Ootes et al., 2015); mainly rhyolitic Faber gp (1869 ± 1 Ma, rhyolitic ignimbrite; Ootes et al., 2015); bimodal Sloan Gp (1863 ± 2 Ma, rhyolite beneath basalt; Ootes et al., 2015) of McTavish supergp; bimodal Dumas Gp (1869.5 ± 2 Ma, rhyodacite; Ootes et al., 2015) of the Wopmay Fault region.</p> <p>SETTING: Emplacement occurred during collision of the Hottah microcontinent and Slave Craton.</p>
Great Bear (ca. 1.88–1.85 Ga) Wopmay Orogen (Great Bear magmatic zone)	<p>INTRUSIONS: Calc-alkaline intrusions of the Great Bear intrusive suite (Hildebrand et al., 2010b) dated at ca. 1.875–1.85 Ga (Hoffman and Bowring, 1984; Gandhi et al., 2001; Bennett and Rivers, 2006a, b).</p> <p>COMMENT: May be genetically related to roughly coeval calc-alkaline Compton intrusions in the Great Slave Supergroup (Hoffman and McGlynn, 1977).</p> <p>SETTING: Continental magmatic arc associated with east-dipping subduction zone associated with collision of the Hottah terrane and Slave Craton (Hildebrand et al., 1987; Ootes et al., 2015).</p>
Bishop (ca. 1.87–1.85 Ga) Wopmay Orogen (metamorphic internal zone)	<p>PLUTONS: Granite to gabbro plutons (1.865–1.850 Ga; Bowring, 1985; see discussion in Ootes et al., 2017) of the Bishop intrusive suite.</p> <p>SETTING: Represents the waning phase of the Great Bear calc-alkaline arc (Lalonde, 1989).</p>
Compton (ca. 1.87–1.86 Ga) Slave (East Arm)	<p>SILLS: Compton calc-alkaline laccoliths (ca. 1.87–1.86 Ga; Bowring et al., 1984).</p> <p>COMMENT: May be genetically related to roughly coeval calc-alkaline intrusions in the Great Bear magmatic zone (Hoffman and McGlynn, 1977).</p>
Ca. 1.83–1.82 Ga (Fig. 9)	
Sparrow and Uranium City (ca. 1.83–1.82 Ga) Laurentia (Rae)	<p>DYKES: Sparrow (1827 ± 4 Ma; Bostock and van Breemen, 1992).</p> <p>COMMENT: May be linked to Uranium City dykes (1818 ± 4 Ma; Morelli et al., 2009) near Lake Athabasca (Rae Craton), and poorly dated Martin gp mafic volcanic rocks, which may be fed by Uranium City dykes (Ashton et al., 2009).</p> <p>SETTING: Ashton et al. (2009) proposed that dyke emplacement and coeval formation of widespread transtensional basins in the western Churchill Province may reflect deformation associated with accretion of the Nahanni–Fort Simpson terrane to the west and terminal collision with the Superior Craton to the east during the Hudsonian Orogeny. Ernst and Bleeker (2010) suggested that a weak radiating pattern between Sparrow and Uranium City dykes may indicate a plume.</p>

Table 1. (cont.)

Event name (age) General location	Magmatic components
Christopher Island (ca. 1.83 Ga) <i>Laurentia (Rae and Hearne)</i>	<p>DYKES: Christopher Island fm ultrapotassic and potassic (minette) dykes.</p> <p>VOLCANIC ROCKS: Christopher Island fm ultrapotassic and potassic volcanic rocks of the Baker Lake Gp of the Dubawnt Supergp, with a flow the near base dated at 1833 ± 3 Ma (Rainbird et al., 2006).</p> <p>COMMENT: Associated with the roughly coeval Hudson suite granites.</p> <p>SETTING: May be linked to the Hudsonian Orogeny (e.g. Rainbird et al., 2006).</p>
Hudson (ca. 1.85-1.80 Ga; peak at 1.83 Ga) <i>Laurentia (Rae and Hearne)</i>	<p>PLUTONS and SHEETS: Hudson suite granites (ca. 1.85–1.80 Ga, with peak at 1.83 Ga; van Breemen et al., 2005)</p> <p>COMMENT: Associated with the roughly coeval Christopher Island ultrapotassic and potassic rocks.</p> <p>SETTING: May be linked to the Hudsonian Orogeny (Peterson et al., 2015a; Ashton et al., 2018).</p>
Ca. 1.77–1.73 Ga (Fig. 10)	
Kivalliq (ca. 1.77–1.73 Ga) <i>Laurentia (Rae and Hearne)</i>	<p>DYKES: McRae Lake (1754 ± 1 Ma; Peterson et al., 2015b); may include undated Amer and Thelon River dykes (Peterson et al., 2015b).</p> <p>VOLCANIC ROCKS: Pitz Fm rhyolite (1758 ± 3 Ma, 1753 ± 2 Ma; Rainbird and Davis, 2007) and basalt of the Wharton Gp of the Dubawnt Supergp.</p> <p>GRANITE INTRUSIONS: Nueltin metaluminous to peraluminous granite intrusions (ca. 1765–1740 Ma; van Breemen et al., 2005).</p> <p>OTHER INTRUSIONS: Gabbro and anorthosite intrusions; Mallery granite-gabbro complex (1769 ± 6 Ma; Peterson et al., 2015b).</p> <p>COMMENT: Change in magma composition from alkaline to subalkaline basalt over ca. 15 Ma (Peterson et al., 2015b). Kivalliq magmatism roughly coeval with Cleaver dykes of the Wopmay Orogeny and dykes on Victoria Island.</p> <p>SETTING: Anorogenic igneous event near the centre of the supercontinent Nuna (Columbia) (Peterson et al., 2015a). Possible mantle plume origin (Ernst et al., 2016).</p>
Dykes on Victoria Island (ca. 1.75–1.74 Ga) <i>Laurentia</i>	<p>DYKES: Hadley Bay dyke (1.75–1.74 Ga; L.M. Heaman <i>in</i> LeCheminant et al., 1996b); dykes in the Wellington Inlier (1743.5 ± 0.8 Ma; M.A. Hamilton, pers. comm., 2019).</p> <p>COMMENT: Approximately coeval with the Kivalliq event of the Rae Craton and Cleaver dykes of the Wopmay Orogen.</p>
Cleaver (ca. 1.74 Ga) <i>Laurentia (Wopmay Orogen)</i>	<p>DYKES: Cleaver ($1740 \pm 5/-4$ Ma; Irving et al., 2004).</p> <p>COMMENT: Roughly coeval with the Kivalliq event of the Rae Craton and dykes on Victoria Island.</p>

Table 1. (cont.)

Event name (age) General location	Magmatic components
Ca. 1.71–1.70 Ga (Fig. 11)	
Bonnet Plume River (ca. 1.71 Ga) <i>Bonnetia exotic terrane</i>	<p>INTRUSIONS: Clasts of diorites with minor gabbro and syenite (1714 ± 13 Ma, 1711 ± 5 Ma, 1709 ± 2 Ma, 1706 ± 1 Ma; Thorkelson et al., 2001a).</p> <p>COMMENT: Only fragments of the intrusions survive, preserved as megaclasts in Wernecke breccia in the Wernecke, Ogilvie, and Richardson mtns. Clasts of other igneous units, including the undated Slab basaltic volcanic rocks (Furlanetto et al., 2103) and the undated Devil volcanic rocks (Thorkelson and Laughton, 2016), are also preserved in Wernecke breccia.</p> <p>SETTING: Bonnet Plume River intrusions, Slab volcanic rocks, and Devil volcanic rocks are interpreted to have been emplaced in an exotic terrane, Bonnetia, which was later obducted on top of the Wernecke Supergroup on the northwestern Laurentia margin, prior to formation of ca. 1.60 Ga Wernecke breccia (Thorkelson and Laughton, 2016).</p>
Pelly Bay (ca. 1.70 Ga) <i>Laurentia (Rae)</i>	DYKES: Pelly Bay (ca. 1.70 Ga; Bleeker and Ernst, 2011).
Ca. 1.66 Ga (Fig. 11)	
Narakay (ca. 1.66 Ga) <i>Laurentia (Hornby Bay Basin)</i>	<p>VOLCANIC ROCKS: Narakay volcanic complex of the Hornby Bay Gp with lower mafic volcanic rocks and upper felsic volcanic rocks (1663 ± 8 Ma on rhyolite porphyry; Bowring and Ross, 1985).</p> <p>SETTING: Narakay volcanic rocks were emplaced during the intracratonic Forward Orogeny (Cook and MacLean, 1995).</p>
Ca. 1.60–1.59 Ga (Fig. 11)	
Wernecke (ca. 1.60–1.59 Ga) <i>Laurentia (western Cordillera)</i>	<p>INTRUSIVE BRECCIA: Wernecke breccia (1595 ± 5 Ma; Thorkelson et al., 2001b; 1599 ± 1 Ma; Furlanetto et al., 2013) of Wernecke, Ogilvie, and Richardson mtns. of the western Cordillera.</p> <p>COMMENT: May be linked to Olympic Dam breccia and Gawler Range volcanic rocks of the Gawler Craton, Australia (Thorkelson et al., 2001b), Western Channel diabase of the Great Bear magmatic zone and Hornby Bay Basin (Hamilton and Buchan, 2010), and Mammoth dykes of the Wyoming Craton (Rogers et al., 2018).</p> <p>SETTING: Wernecke–Olympic Dam hydrothermal province may have developed over a mantle plume (Thorkelson et al., 2001b) and may be part of a broader LIP that includes the Western Channel diabase (Hamilton and Buchan, 2010) and Mammoth dykes (Rogers et al., 2018).</p>
Western Channel (ca. 1.59 Ga) <i>Laurentia (Great Bear magmatic zone and Hornby Bay Basin)</i>	<p>DYKES: Western Channel diabase.</p> <p>SILLS: Western Channel diabase (1592 ± 3 Ma and 1590 ± 4 Ma; Hamilton and Buchan, 2010; 1592 ± 3 Ma; Rogers et al., 2018).</p> <p>COMMENT: See comment for Wernecke breccia entry.</p> <p>SETTING: See setting for Wernecke breccia entry.</p>
Notes: Events are listed approximately in chronological order. Ages for specific units are from U-Pb dating. Units that are listed are mainly mafic in composition, unless otherwise indicated. Coeval units that occur in relatively close geographic proximity are usually assigned to a single event. Possible linkages to coeval units that are widely separated are identified in the comments.	

Ca. 2.50 to 2.46 Ga events

Well dated, large magmatic events that fall in the 2.50 to 2.46 Ga age range include the Kaminak dyke swarm of the Hearne Craton and mainly felsic plutonism of the Queen Maud Block and southern Boothia Peninsula of the Rae Craton (Fig. 2).

Hearne Craton

Ca. 2.50 Ga Kaminak dyke swarm

The Kaminak dyke swarm (Fig. 2) is located within the Hearne Craton, although its overall extent is poorly delineated. It is mainly south- to south-southwest-trending (Davidson, 1970; Christie et al., 1975), with a possible overall radiating geometry with a focus near the northern craton margin (e.g. Ernst and Bleeker, 2010; Buchan and Ernst, 2013). A precise U-Pb baddeleyite age of 2498 ± 1 Ma has been obtained from a south-trending dyke (Sandeman et al., 2013), and is assumed to date the emplacement of the swarm. Spi group basalt flows (Fig. 2), which are undated and of very limited extent, may be related to the Kaminak dykes based on geochemical similarities (Sandeman and Ryan, 2008).

The Kaminak dyke swarm does not extend into the Chesterfield Block of the Rae Craton (Fig. 2; Davis et al., 2006). This is consistent with the interpretation that the Rae and Hearne cratons were not attached at 2.5 Ga, but collided much later, likely at ca. 1.9 Ga (e.g. Berman et al., 2007; Pehrsson et al., 2019).

The 2498 Ma Kaminak dykes are approximately coeval with several dyke swarms in the Superior Craton — particularly the $2505 \pm 2/-1$ Ma Ptarmigan (U-Pb zircon and baddeleyite; Buchan et al., 1998), 2508 ± 6 Ma Irsuaq (U-Pb baddeleyite; Maurice et al., 2009), and 2515 to 2505 Ma Mistassini (U-Pb; Hamilton, 2009; Hamilton et al., 2017) swarms. The ca. 2462 to 2450 Ma Matachewan swarm (U-Pb baddeleyite; Hamilton et al., 2017) was once thought to be coeval with the Kaminak swarm and was used in Superior–Hearne paleomagnetic reconstructions, as discussed below. As a result of the most recent dating, however, the Kaminak swarm is now known to be significantly older than the Matachewan swarm. Sandeman et al. (2013) have suggested that the two swarms are not genetically related based on their age difference and dissimilar geochemical compositions. Layered intrusions associated with the Matachewan LIP, however, have ages of 2475 to 2472 Ma (U-Pb; Clough and Hamilton, 2017; L. Heaman, pers. comm. in Easton et al., 1999) that are somewhat closer to the age of the Kaminak dykes.

Rae Craton

Ca. 2.50 to 2.46 Ga felsic and minor mafic magmatism in the Queen Maud Block

Widespread ca. 2.50 to 2.46 Ga (U-Pb zircon) felsic plutons in the Queen Maud Block of the Rae Craton (Fig. 2) were emplaced in an extensional environment (Schultz et al., 2007a, 2010). Coeval mafic rocks from the same area have geochemical signatures that indicate a continental-rift or

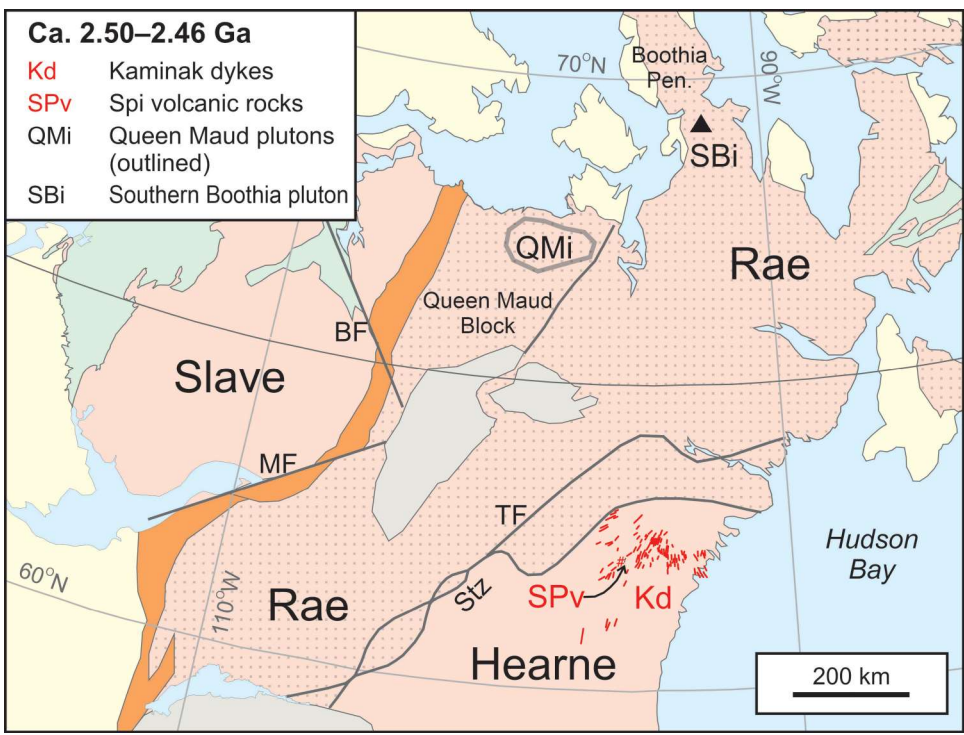


Figure 2. Selected 2.5 to 2.46 Ga dyke swarms and other magmatic events of northern Canada. The overall geographic extent of scattered Queen Maud plutons is outlined in grey. The triangle indicates a unit of limited extent. See Figure 1 for background map legend.

flood-basalt setting rather than a back-arc setting (Schultz et al., 2007b, 2010). Berman et al. (2013), however, have proposed alternatives to the rift model, based on studies in southern Boothia Peninsula, where a granite pluton that may be linked to the Queen Maud event has been dated at 2.50 Ga (Fig. 2). These authors noted that foliation in samples from southern Boothia Peninsula, interpreted to have developed between 2.54 and 2.49 Ga, suggested convergence rather than rifting, and argued that the 2.50 to 2.46 Ga magmatism of the Queen Maud Block and southern Boothia Peninsula may have formed in a back-arc setting during east-dipping subduction beneath the western margin of the Rae Craton. Alternatively, they suggested that the magmatism could reflect arc rifting possibly induced by spreading ridge subduction.

Paleomagnetism and testing continental reconstructions (ca. 2.50–2.46 Ga)

In an early paleomagnetic study, Christie et al. (1975) noted the similarity of paleopoles for the Kaminak dykes of the Slave Craton and the approximately coeval Matachewan dykes of the Superior Craton; they concluded that there has been no large-scale relative movement of the two regions since dyke emplacement. There is, however, an ambiguity in the magnetic polarity that is used in such comparisons. Bleeker (2004) noted that by reversing the polarity of the Kaminak pole (compared to that assumed by Christie et al., 1975) the data permit a reconstruction in which the northern margin of the Hearne Craton is attached to the southern Superior margin (Fig. 4 in Bleeker, 2004) with the Kaminak and Matachewan dykes forming a single, giant radiating dyke swarm. More recent reconstructions (e.g. Ernst and Bleeker, 2010; Gumsley et al., 2017) differed somewhat in detail, but still locate the Hearne Craton to the south of the Superior Craton. In these Hearne–Superior reconstructions, the presence of 2.11 Ga mafic magmatism in both cratons suggests that breakup did not occur during emplacement of the Kaminak and Matachewan swarms, but could have occurred after 2.11 Ga (Ernst and Bleeker, 2010).

As noted above, Sandeman et al. (2013) questioned the proposed genetic link between the Kaminak and Matachewan swarms, and by inference the proposed Hearne–Superior reconstruction, because the ages of the two swarms now appear to differ by approximately 50 Ma and they are geochemically distinct.

As the 2505 Ma Ptarmigan dyke swarm of the Superior Craton is close in age to the 2498 Ma Kaminak swarm, a direct comparison of their paleomagnetic poles is in order. Unfortunately, the paleomagnetic data for the Ptarmigan dykes (Buchan et al., 1998) are derived from only three sampling sites from two dykes, an insufficient sampling to average out paleosecular variation. The remanence is thought to be primary for reasons discussed by Buchan et al. (1998), but a field test has not been carried out to confirm

this conclusion. Buchan et al. (2007) have argued that complicated paleomagnetic data from the marginally older 2515 to 2505 Ma Mistassini swarm of the Superior Craton (Fahrig et al., 1986) appear to be consistent with the data from the Ptarmigan dykes. As with the Kaminak–Matachewan comparison discussed above, the paleomagnetic remanences for the Kaminak and Ptarmigan dykes permit a reconstruction in which the northern Hearne Craton faces the southern Superior Craton.

A more rigorous test of Hearne–Superior reconstructions in the earliest Paleoproterozoic must await further paleomagnetic study. Paleomagnetic data for the Matachewan dyke swarm of the Superior Craton are of excellent quality (see summary in Evans and Halls, 2010) and the remanence has been demonstrated to be of primary origin (Buchan et al., 1990). In contrast, paleomagnetic data for the Kaminak dykes of the Hearne Craton (Christie et al., 1975), and the Ptarmigan (Buchan et al., 1998) and Mistassini (Fahrig et al., 1986) dykes of the Superior Craton are preliminary and have yet to be demonstrated primary.

Ca. 2.27 to 2.19 Ga events

Several dyke swarms (and related mafic magmatism) were emplaced in the Slave and Rae cratons during the 2.27 to 2.19 Ga period (Fig. 3). Various authors have suggested that the Slave Craton units are linked to hypothesized, but poorly understood, rifting or failed rifting events along the craton margins (e.g. LeCheminant et al., 1996a; Ernst and Bleeker, 2010). The 2.19 Ga Dogrib dyke swarm (and related units of the Southwestern Slave magmatic province) is coeval with the Tulemalu–MacQuoid swarm of the Rae Craton (LeCheminant et al., 1997). There is, however, paleomagnetic evidence, discussed below, that the Slave and Rae cratons were not attached to one another at that time, suggesting that there is no genetic link between these events.

Slave Craton

Ca. 2.23 Ga Malley dyke swarm

The 2231 ± 2 Ma Malley dyke swarm (U-Pb baddeleyite; Buchan et al., 2012) trends northeast from the south-central portion of the Slave Craton to the vicinity of the Bathurst Fault (Fig. 3). The Brichta dykes (Fig. 3), with approximately the same trend and similar geochemistry as the Malley dykes (Buchan et al., 2012), are mapped northeast of the Bathurst Fault. They are poorly dated at ca. 2.1 Ga by the K-Ar technique (Wanless et al., 1965, p. 44). Buchan et al. (2012) proposed that the Brichta dykes represent the continuation of the Malley swarm — offset by left-lateral movement along the fault of approximately 115 km (Tirul and Grotzinger, 1990). LeCheminant et al. (1996a) suggested a possible link to rifting on the eastern margin of the Slave Craton. Ernst and Bleeker (2010) proposed a mantle plume centred just

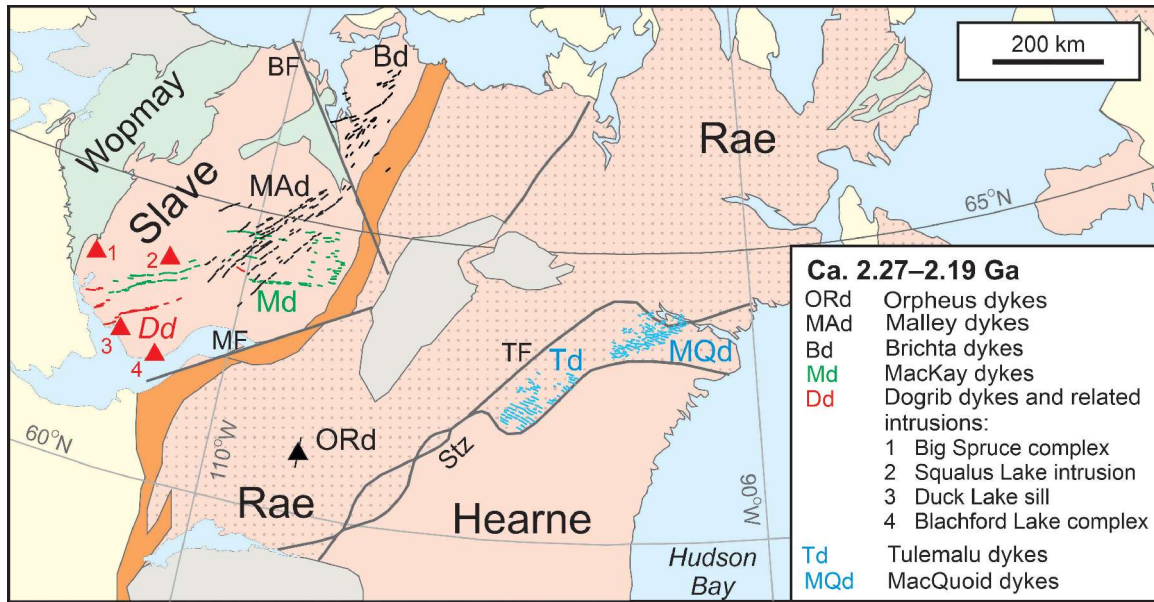


Figure 3. Selected 2.27 to 2.19 Ga dyke swarms and other magmatic events of northern Canada. The Dogrib dykes and related units (numbered red triangles) make up the Southwestern Slave magmatic province. The black triangle (with a trend bar) indicates the Orpheus dyke swarm. The Tulemalu and MacQuoid dykes are interpreted to belong to a single swarm. Although less certain, the Malley and Brichta dykes may also belong to a single swarm. See Figure 1 for background map legend.

east of the southern portion of the Bathurst Fault, although this location is not tenable if the Brichta dykes form a northeastward continuation of the Malley swarm.

Ca. 2.21 Ga MacKay dyke swarm

A preliminary age of ca. 2.21 Ga (U-Pb baddeleyite; LeCheminant and van Breemen, 1994) has been reported for the MacKay swarm. The swarm appears to have an arcuate geometry, trending east-northeast in the south-central Slave Craton to east in the east-central Slave Craton (Fig. 3). LeCheminant et al. (1996a) suggested that these dykes could be related to rifting along the southern margin of the craton. Ernst and Bleeker (2010) suggested the presence of a plume centre just beyond the eastern Slave margin, although an overall radiating pattern to the swarm is not apparent from the most recent mapping (Fig. 3; Buchan and Ernst, 2013).

Ca. 2.19 to 2.18 Ga Southwestern Slave magmatic province (Dogrib dyke swarm)

The Southwestern Slave magmatic province (Bleeker and Hall, 2007; Buchan et al., 2010) comprises several units with ages of 2.19 to 2.18 Ga (Fig. 3). These include the Dogrib dyke swarm (2193 +3/-2 Ma, U-Pb baddeleyite; Mitchell et al., 2014), the Duck Lake sill (2181 ± 2 Ma, U-Pb baddeleyite; Bleeker and Kamo, 2003), the Big Spruce complex (ca. 2188 Ma, U-Pb zircon; Cavell and Baadsgaard, 1986),

the Squalus Lake intrusion (2180 ± 1 Ma, U-Pb zircon; Villeneuve and van Breemen, 1994), and the Blachford Lake igneous complex (ca. 2180 Ma, U-Pb zircon; Bowring et al., 1984; A. Davidson *in* Bowring et al., 1984; Sinclair et al., 1994).

The Dogrib dyke swarm trends east-northeast in the southern Slave Craton (Fig. 3). It is similar in age to the Tulemalu and MacQuoid dyke swarms in the Chesterfield Block of the Rae Craton (LeCheminant et al., 1997). As discussed below, however, a comparison of primary paleomagnetic data from the Dogrib dykes with data that are probably primary from the Tulemalu dykes suggests that the Slave and Rae cratons were not attached in their current configuration at the time of dyke emplacement.

Rae Craton

Ca. 2.27 Ga Orpheus dyke swarm

A preliminary age of ca. 2.27 Ga (U-Pb baddeleyite and zircon; M. Hamilton pers. comm. *in* Mowbray and Pehrsson, 2019) has been reported for this north-trending swarm (Fig. 3). Mowbray and Pehrsson (2019) suggested that it may be linked to attempted rifting of the southern Rae Craton. Pehrsson et al. (2019) noted that the swarm does not appear to extend into the Hearne Craton — evidence that supports the Rae and Hearne being separate cratons at 2.27 Ga.

Ca. 2.19 Ga Tulemalu–MacQuoid dyke swarm

The east- to south-southeast-trending Tulemalu dykes are located in the southeastern portion of the Chesterfield Block of the Rae Craton (Fig. 3). They are little metamorphosed, except close to the Tulemalu Fault, which forms the northwestern margin of the Chesterfield Block. The mainly east-trending, metamorphosed and deformed MacQuoid dykes are located in the northeastern portion of the Chesterfield Block and immediately north of the Chesterfield Block (Fig. 3). A preliminary age of 2.19 Ga (U-Pb baddeleyite; LeCheminant et al., 1997; Tella et al., 2001) has been obtained for each set of dykes, and hence they are considered herein as a single dyke swarm.

The fact that the MacQuoid dykes extend north of the Chesterfield Block (Fig. 3) is consistent with the interpretation that the Chesterfield Block was already attached to the Rae Craton by 2.19 Ga (Berman et al., 2007). The Tulemalu–MacQuoid swarm, however, does not extend into the Hearne Craton (Fig. 3; Davis et al., 2006), suggesting that the Rae and Hearne cratons were not together at 2.19 Ga, but collided later (Berman et al., 2007).

Paleomagnetism and testing continental reconstructions (ca. 2.27–2.19 Ga)

Given the similarity in age between the Tulemalu dykes of the Rae Craton and Dogrib dykes of the Slave Craton (*see above*), a comparison of primary paleomagnetic poles from the two swarms would establish the relative latitude and orientation of the two cratons at 2.19 Ga, as discussed by LeCheminant et al. (1997). A paleopole was determined for the Dogrib dykes (McGlynn and Irving, 1975; Mitchell et al., 2014) and demonstrated primary with a baked contact test (Mitchell et al., 2014). A paleomagnetic pole was determined by Fahrig et al. (1984) for the Tulemalu swarm. This pole has not been conclusively demonstrated primary with a field test. It is likely primary, however, because the dykes are relatively fresh, K-Ar ages of country rock in the sampling area have not been reset (Fahrig et al., 1984), and the remanence is distinct from the ca. 1.9 to 1.8 Ga magnetic overprints that are widespread in the Rae Craton and elsewhere in northern Canada.

The Tulemalu and Dogrib paleopoles differ by approximately 30°. This difference can be explained in several ways. In the first and most likely interpretation, the Tulemalu paleopole is primary, and the Slave and Rae cratons were not in their present relative locations at 2.19 Ga. Depending on the magnetic polarity option chosen, the paleomagnetic data indicate that either the two cratons were separated by about 30 to 40° of latitude, or they were at a similar latitude, but rotated approximately 180° relative to one another compared

to their present configuration. In either case, this interpretation is consistent with the Slave and Rae being separate at 2.19 Ga (and colliding later at ca. 1.97 Ga; e.g. Hoffman, 1988). In a second interpretation, the Tulemalu paleopole is primary in origin, and the Slave and Rae cratons were together in their present configuration, except that the local Tulemalu region has rotated as a block 180° relative to the Slave Craton and the rest of the Rae Craton since 2.19 Ga. This interpretation, although less satisfying, is consistent with the Slave and Rae having been assembled at no later than ca. 2.045 Ga (Sheen et al., 2019), as discussed below. In the third scenario, the Tulemalu paleopole represents a magnetic overprint, and hence it cannot be matched in time with the Dogrib pole and cannot be used to constrain the location of the Rae Craton at 2.19 Ga. In this latter interpretation, the age of overprinting is uncertain. As noted above, the Tulemalu pole is distinct from ca. 1.9 to 1.8 Ga overprint poles that have been reported for metamorphosed rocks elsewhere in northern Canada.

A comparison can also be made between the Tulemalu paleopole and the 2.22 to 2.17 Ga portion of the Superior Craton APWP (Fig. 3 *in* Buchan, 2014), which is based on well defined, primary paleopoles. Provided the Tulemalu pole is primary, it suggests that the Rae and Superior cratons were at similar latitudes, but not in their present relative configuration, consistent with the interpretation that the collision between the Churchill (combined Rae and Hearne cratons) Province and Superior Craton occurred much later, at ca. 1.83 to 1.80 Ga (e.g. Corrigan et al., 2009).

French and Heaman (2010) proposed a reconstruction of the Slave Craton and the Dharwar Craton of India as part of the Sclavia supercraton during the 2.23 to 2.17 Ga period. They based the reconstruction on an approximate barcode match between the ages of dyke swarms on the two cratons — namely the Malley, MacKay, and Dogrib dykes of the Slave Craton and ca. 2.22 Ga Kandlamadugu, 2.21 Ga Somala, and 2.18 Ga Northern Dharwar dykes of the Dharwar Craton. This reconstruction remains to be tested based on paleomagnetic data.

Ca. 2.13 to 2.11 Ga events

Between 2.13 and 2.11 Ga, dyke swarms and/or sill complexes were emplaced in the Slave, Rae, and Hearne cratons (Fig. 4), as well as on many other North American cratons, including the Superior, Wyoming, and Nain. Given this widespread magmatism, it is difficult to link specific 2.13 to 2.11 Ga events between the various cratons. The Indin dyke swarm of the Slave Craton may be related to failed rifting along the craton's western margin. The Chipman dykes were intruded in an extensional setting along the Snowbird tectonic zone, which forms the Rae–Hearne boundary.

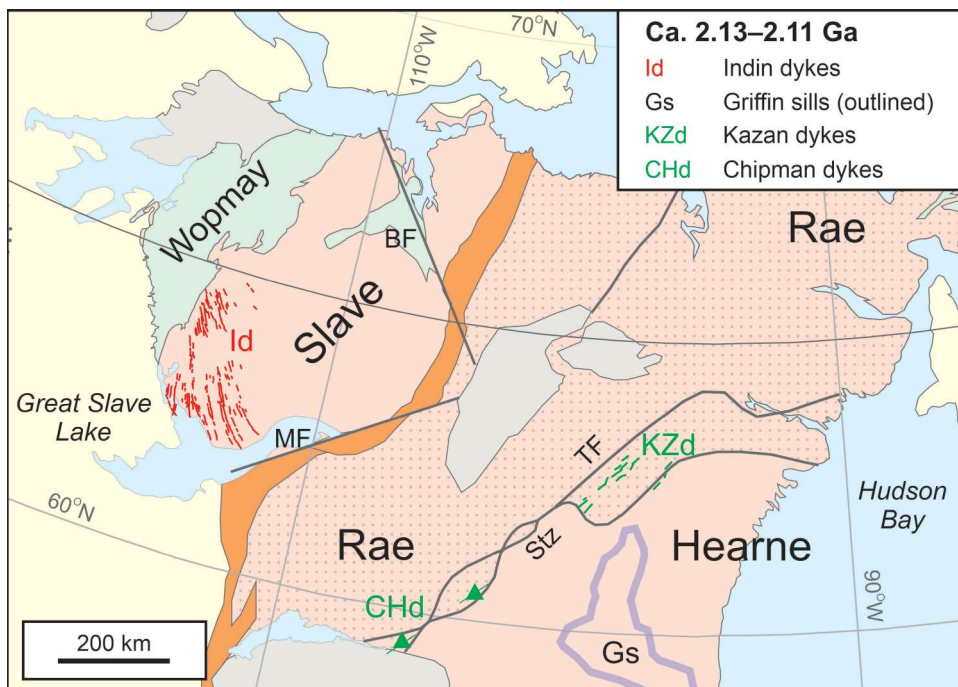


Figure 4. Selected 2.13 to 2.11 Ga dyke swarms and other magmatic events of northern Canada. The overall geographic extent of scattered Griffin sills is outlined in purple. Triangles (with trend bars) indicate dyke swarms of limited extent. See Figure 1 for background map legend.

Slave Craton

Ca. 2.13 to 2.11 Ga Indin dyke swarm

The Indin dyke swarm of the southwestern Slave Craton (Fig. 4) has been dated at 2126 to 2108 Ma (U-Pb baddeleyite) by Davis and Bleeker (2007), Bleeker et al. (2008a), and Buchan et al. (2016). The swarm trends southeast to south-southeast and appears to fan slightly to the southeast, leading Ernst and Bleeker (2010) to propose a focus and possible plume centre beyond the western Slave margin. There is no clear evidence that this event led to continental breakup along the western Slave margin, although evidence of later breakups on this margin at 2.01 and 1.90 Ga are discussed below.

Hearne Craton

Ca. 2.11 Ga Griffin sills

The Griffin gabbro sills (Fig. 4) intrude the Hurwitz group sedimentary rocks of the Hearne Craton (Aspler et al., 2002) and have been dated precisely at 2111 ± 1 Ma (U-Pb baddeleyite; Heaman and LeCheminant, 1993). Aspler et al. (2002) interpreted the Griffin sills to be fed by unidentified regional-scale dykes from a mantle plume located south of the Hearne Craton and linked to rifting that led to opening of the Manikewan Ocean between the Hearne and Superior cratons. Berman et al. (2007) noted that the Griffin sills are confined to the Hearne Craton and are not found in the Rae Craton, consistent with the two cratons being separate at 2.11 Ga. This interpretation is less clear, however, given the recent dating of the Kazan dykes of the

Rae Craton (Chesterfield Block) and the Chipman dykes of the Rae–Hearne boundary region at ca. 2.12 to 2.11 Ga (see discussion below). There are also volcanic rocks of the Hapopotiyik member of the Hurwitz group, but they have been interpreted to be somewhat older than the Griffin sills (Aspler et al., 2002).

Rae Craton and Rae–Hearne boundary

Ca 2.12 Ga Kazan dyke swarm

The Kazan dyke swarm (Fig. 4; Eade, 1986) trends northeast in the Chesterfield Block of the Rae Craton, parallel to the Tulemalu Fault. It has been dated at 2116 ± 12 Ma (U-Pb zircon; Regan et al., 2017).

Ca. 2.11 Ga Chipman dyke swarm

The Chipman dyke swarm (Fig. 4) trends northeast in the vicinity of the Snowbird tectonic zone, which marks the boundary between the Hearne and Rae cratons; its extent in each of the two cratons is unclear. Flowers et al. (2006) dated metamorphism of the swarm at 1896 ± 1 Ma (U-Pb zircon) and interpreted this to be also the age of emplacement. More recently, however, the swarm has been dated at 2113 ± 13 Ma (U-Pb zircon; Regan et al., 2017).

Regan et al. (2017) interpreted the Chipman, Kazan, and Griffin magmatism as a ca. 2.11 Ga LIP, with the Chipman and Kazan dykes representing aborted rifting associated with the Snowbird tectonic zone. The overlap of ca. 2.11 Ga magmatism on the Hearne and Rae cratons is consistent with the two blocks having been together by 2.11 Ga. This correlation,

however, may not be significant given that 2.13 to 2.11 Ga magmatism occurs on many cratons. In addition, there is substantial evidence to suggest the Hearne and Rae cratons were not attached throughout much of the Paleoproterozoic and that they collided at ca. 1.9 Ga. As noted above, dyke swarms in the 2.50 to 2.19 Ga period (Kaminak dyke swarm of the Hearne Craton, and Orpheus and Tulemalu–MacQuoid swarms of the Rae Craton) are not known to cross the Rae–Hearne boundary. Furthermore, there is growing support for a 1.9 Ga collisional event along the Snowbird tectonic zone between the cratons, including eclogite dated at 1.9 Ga (Berman et al., 2007; Pehrsson et al., 2019). Finally, the ca. 1.99 to 1.92 Ga Taltson magmatic zone (McDonough et al., 2000) appears to be truncated by the Snowbird tectonic zone (Hoffman, 1988), as would be expected if the Rae and Hearne cratons had collided at 1.9 Ga.

Paleomagnetism and testing continental reconstructions (ca. 2.13–2.11 Ga)

In addition to the 2.13 to 2.11 Ga dykes and sills of the Slave, Rae, and Hearne cratons of northern Canada, similar-aged dykes have been reported in other cratonic blocks that form Laurentia — namely the 2.13 to 2.10 Ga Marathon dyke swarm of the Superior Craton (*see* summary in Halls et al., 2008), the 2.11 Ga Bear Mountain dykes of the Wyoming Craton (Bowers and Chamberlain, 2006), and the 2.12 Ga Tikkigatsiak–Avakutak Bay dykes of the Nain Craton (*see* summary in Sahin and Hamilton, 2019). Given the

simultaneous emplacement of these intrusions, determining primary paleomagnetic poles for each would permit a test of paleocontinental reconstructions at that time.

Currently, reliable primary paleomagnetic data are only available for the Slave and Superior cratons. The primary paleopoles for the Indin dykes of the Slave Craton and the Marathon dykes of the Superior Craton are quite discordant, demonstrating that these two cratons have moved relative to one another since the time of dyke emplacement (Fig. 12 *in* Buchan et al., 2016). Furthermore, a comparison of ca. 2.23 to 1.88 Ga APWPs for the Slave and Superior cratons, based on primary paleopoles, has indicated that they were not drifting as part of a single supercontinent over that time interval (Fig. 12 *in* Buchan et al., 2016).

Paleomagnetic data are also available for the ca. 2.12 Ga Kazan dykes of the Rae Craton (Fahrig et al., 1984) and the 2.11 Ga Griffin sills of the Hearne Craton (K.L. Buchan *in* Aspler et al., 2002). These data, however, are interpreted to represent postintrusive overprints, likely acquired at ca. 1.9 to 1.8 Ga, and hence cannot be used to test continental reconstructions at 2.13 to 2.11 Ga.

Ca. 2.05 to 2.01 Ga events

During the 2.05 to 2.01 Ga period, mafic magmatism was widespread in the Slave Craton and along its margins (Fig. 5). It has been linked to rifting on the western margin of the craton and to either rifting or failed rifting on the southern margin. The rifting on the western margin is thought to

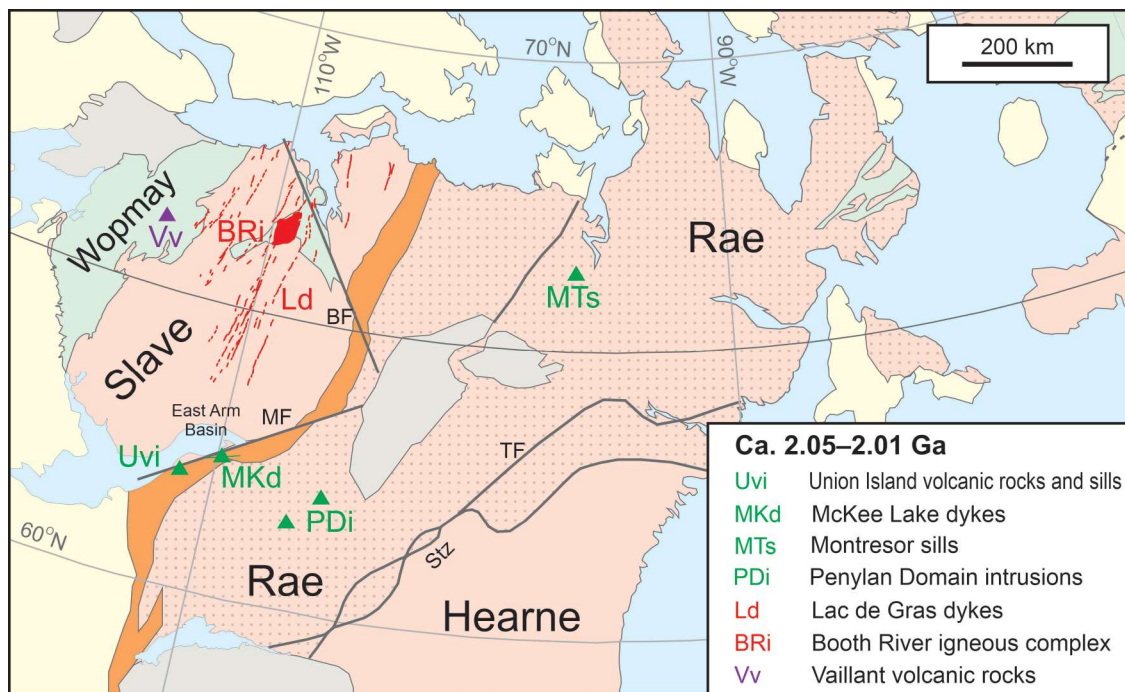


Figure 5. Selected 2.05 to 2.01 Ga dyke swarms and other magmatic events of northern Canada. The polygon for the Booth River igneous complex indicates its overall extent, most of which is subsurface. Triangles indicate units of limited extent, with trend bars shown for dyke swarms. See Figure 1 for background map legend.

have led to the opening of an ocean (e.g. Hoffman et al., 2011). In contrast, the presence of coeval intrusions in the Rae Craton has led to the interpretation that rifting failed along the southern Slave margin and that the Slave and Rae cratons were attached in their current configuration by ca. 2.045 Ga (Sheen et al., 2019).

Slave Craton

Ca. 2.05 to 2.04 Ga Union Island Group volcanic rocks and intrusions, and ca. 2.04 Ga McKee Lake dyke swarm

The Union Island Group, which includes a thick succession of basaltic flows (Fig. 5), has recently been recognized as the oldest unit in the East Arm Basin of Great Slave Lake, with the lower basalt formation dated at 2046 ± 1 Ma (U-Pb zircon; Sheen et al., 2019), 120 Ma older than previously thought (e.g. Bowring et al., 1984). Sheen et al. (2019) interpreted intrusions (sills and northeast-trending dykes), one of which they dated at 2043 ± 3 Ma (U-Pb baddeleyite), as feeders to the lower basalt flows. Furthermore, they linked these intrusions to the 2038 ± 3 Ma (U-Pb baddeleyite; Pehrsson et al., 1993) McKee Lake dyke swarm (Fig. 5), which trends east-northeast parallel to, and immediately south of, the East Arm of Great Slave Lake. The McKee Lake dyke swarm should not be confused with the subparallel, but genetically unrelated and younger 1901 Ma Hearne dyke swarm along the northern shore of the East Arm of Great Slave Lake.

Although Union Island Group volcanism represents a major extensional episode on the southeastern margin of the Slave Craton, it is unclear if rifting led to the formation of an ocean. Sheen et al. (2019) concluded that the Slave and Rae cratons have been together in their current configuration at least since ca. 2.045 Ga, that the East Arm Basin represents a failed rift (cf. early failed-rift model in Hoffman, 1973a; Hoffman et al., 1977), and that no ocean formed between them. As evidence that the Rae and Slave were part of a single crustal block at ca. 2.045 Ga, Sheen et al. (2019) noted similarities between coeval magmatic units in the East Arm Basin and Rae Craton. Specifically, they discussed the similarity between the stratigraphy of the lower Union Island Group and that of the lower Montresor group (Percival et al., 2017) east of the Thelon tectonic zone in the Rae Craton (Fig. 5), which is also intruded by a 2045 ± 13 Ma (U-Pb zircon) gabbro sill (see ‘Ca. 2.045 Ga Montresor intrusions’ section). They also noted the similarity in the age of the lower Union Island Group magmatism and 2.05 to 2.03 Ga plutons in the Penylan Domain of the Rae Craton (Fig. 5; Davis et al., 2015b; (see ‘Ca. 2.05 to 2.03 Ga Penylan Domain plutons’ below). With regard to the possibility of an ocean developing between the Slave and Rae cratons after ca. 2.045 Ga, Sheen et al. (2019) suggested that the approximately 60 to

70 Ma interval between eruption of the Union Island Group basaltic rocks and the voluminous magmatism of the Taltson magmatic zone (<1986 Ma) and deformation of the Great Slave Lake shear zone (<1978 Ma) is too short to permit the opening and closing of an ocean as proposed by earlier workers, who hypothesized a collision between the Rae and Slave cratons at ca. 1.97 Ga (e.g. Hoffman, 1988; Hoffman et al., 2011). Finally, they also cited the lack of evidence for subduction-related features along the southeastern Slave margin (e.g. Chacko et al., 2000; Snyder and Kjarsgaard, 2013).

Ca. 2.03 to 2.02 Ga Lac de Gras dyke swarm and Booth River igneous complex

The 2027 to 2023 Ma Lac de Gras mafic dyke swarm (U-Pb baddeleyite; Buchan et al., 2009) trends north-northeast across the central Slave Craton (Fig. 5). It is coeval with the 2026 to 2023 Ma mafic-ultramafic-felsic Booth River igneous complex (U-Pb zircon; Roscoe et al., 1987; Davis et al., 2004) (Fig. 5), which intrudes the base of the Goulburn Supergroup of the Kilohigok Basin. LeCheminant et al. (1996a) suggested that the dykes converge slightly to the north and, hence may have been injected laterally from the vicinity of the Booth River igneous complex. Ernst and Bleeker (2010) proposed a focus and possible mantle plume centre in northern Bathurst Inlet. The most recent interpretation of the swarm’s distribution (Fig. 5; Buchan and Ernst, 2013), however, showed a broad linear swarm with no clear convergence of the dykes to the north.

Sheen et al. (2019) suggested that the Lac de Gras dykes may be related to the slightly older, ca. 2045 to 2038 Ma mafic magmatism of the Union Island Group in the East Arm Basin and related McKee Lake dykes, which they linked to failed rifting on the southern margin of the Slave Craton, as discussed above. The Lac de Gras dykes, however, do not appear to extend as far south as the East Arm Basin (Fig. 5). LeCheminant et al. (1996a) and Hoffman et al. (2011) proposed a possible link between the Lac de Gras–Booth River magmatism and slightly younger rifting along the western margin of the Slave Craton, as discussed below.

Ca. 2.014 Ga Vaillant Formation basalt

Hoffman et al. (2011) determined a precise U-Pb zircon age of 2014 ± 1 Ma for a felsic tuff at the top of the Vaillant Formation basalt (Fig. 5) of the Coronation margin. LeCheminant et al. (1996a), based on preliminary dating of this unit (S.A. Bowring, pers. comm. in LeCheminant et al., 1996a), suggested a possible link between rifting on the Coronation margin and slightly older Lac de Gras–Booth River magmatism. Hoffman et al. (2011) interpreted the 2014 Ma Vaillant basalt age as the age of the rift-to-drift

transition preceding ocean formation. They noted that Lac de Gras dykes are parallel to the Coronation margin, and about 10 Ma older than the felsic tuff. This age difference is comparable to the lag of 5 to 15 Ma between flood basalt magmatism and the onset of seafloor spreading in the Atlantic Ocean basin.

Rae Craton

Ca. 2.045 Ga Montresor intrusions

A gabbro sill intruding the lower Montresor group (Fig. 5) was dated by Percival et al. (2017) at 2045 ± 13 Ma (U-Pb zircon).

Ca. 2.05 to 2.03 Ga Penylan Domain plutons

Davis et al. (2015b) dated three plutons in the Penylan Domain of the Rae Craton, a short distance southeast of the Taltson magmatic zone (Fig. 5): an anorthositic gabbro, a quartz diorite, and a monzogranite with crystallization ages of 2048 ± 2 Ma, 2046 ± 8 Ma, and 2032 ± 5 Ma, respectively.

The significance of the 2.05 to 2.03 Ga Rae Craton magmatism associated with the Montresor group and Penylan Domain for the timing of the collision between the Rae and Slave cratons has been discussed above in relation to the coeval Union Island Group basaltic rocks.

Paleomagnetism and testing continental reconstructions (ca. 2.05–2.01 Ga)

Paleomagnetism of coeval units from the Slave and Rae cratons could potentially be used to establish whether the Slave and Rae cratons were together or not during the 2.05 to 2.01 Ga period. A robust primary paleopole has been reported for the 2027 to 2023 Ma Lac de Gras dykes of the Slave Craton (Buchan et al., 2009), and it may be possible to obtain a second Slave paleopole at 2045 to 2042 Ma from the Union Island Group volcanic rocks and intrusions. Given that ca. 2.045 Ga magmatism is also present in the Rae Craton, if suitable unmetamorphosed intrusions or volcanic rocks of these ages can be identified, they could provide a direct paleomagnetic comparison between the two cratons to test whether they were together or separated at that time.

Ca. 1.97 to 1.95 Ga events

Magmatic events between 1.97 and 1.95 Ga are recorded in both the Slave Craton and the Hottah terrane (Fig. 6). The Slave Craton is usually interpreted to have collided with the Rae Craton at ca. 1.97 Ga (e.g. Hoffman, 1988). The Hottah terrane is thought to have rifted from a parent craton, then drifted as a microcontinent and eventually collided with the western Slave Craton at ca. 1.88 Ga (e.g. Ootes et al., 2017).

Slave Craton

Ca. 1.97 to 1.96 Ga Carousel igneous suite

The Carousel igneous suite (Hoffman, 1996) comprises basalt and gabbro sills of the Odjick Formation of the lower Epworth Group on the Coronation margin of the Slave Craton (Fig. 6). Although not directly dated, they were likely emplaced at ca. 1969 to 1963 Ma, based on the correlation of ash beds in the Odjick Formation with ash beds of the Bear Creek Group of the Kilohigok Basin (Fig. 6) that have been dated at 1969 ± 1 Ma and 1963 ± 1 Ma (U-Pb zircon; Bowring and Grotzinger, 1992). The Epworth Group represents the passive margin of the western Slave Craton (Hoffman, 1973b; Hoffman et al., 2011).

Hottah microcontinent

Ca. 1.95 Ga Holly Lake metamorphic suite

The Holly Lake metamorphic suite (Fig. 6) includes mafic to intermediate volcanic rocks that are thought to have erupted at ca. 1.95 Ga, based on a detrital zircon study of a metasedimentary unit in the suite (Davis et al., 2015a). The suite is interpreted to have been emplaced prior to the Hottah microcontinent rifting from a parent craton (Davis et al., 2015a; Ootes et al., 2015). Detrital zircon ages from the Holly Lake suite and other units in the Hottah terrane suggest that this parent craton was not the Slave Craton, but likely a younger terrane located south of the Slave Craton — perhaps the Taltson or Ksituan magmatic zone (Davis et al., 2015a; Ootes et al., 2015, 2017).

Ca. 1.93 to 1.91 Ga events

During this period, well dated magmatic events occurred in three widely separated regions (Fig. 7), the Hottah terrane (still attached to its parent craton), the East Arm Basin on the southern Slave Craton, and the Meta Incognita terrane of southern Baffin Island. No clear link between the events in these regions has been established. The Meta Incognita terrane is interpreted as a microcontinent that collided with the southeastern Rae Craton at ca. 1.883 to 1.865 Ga (St-Onge et al., 2006). It is unclear if it rifted earlier from the Rae Craton, rifted from the Superior Craton, or perhaps was separate from both the Rae and Superior cratons (St-Onge et al., 2006).

Hottah microcontinent

Ca. 1.93 to 1.91 Ga Hottah plutonic complex

The mainly felsic Hottah plutonic complex (Fig. 7) was emplaced at ca. 1.93 to 1.91 Ga (U-Pb zircon; Ootes et al., 2015). It is interpreted as the root of a subduction-related

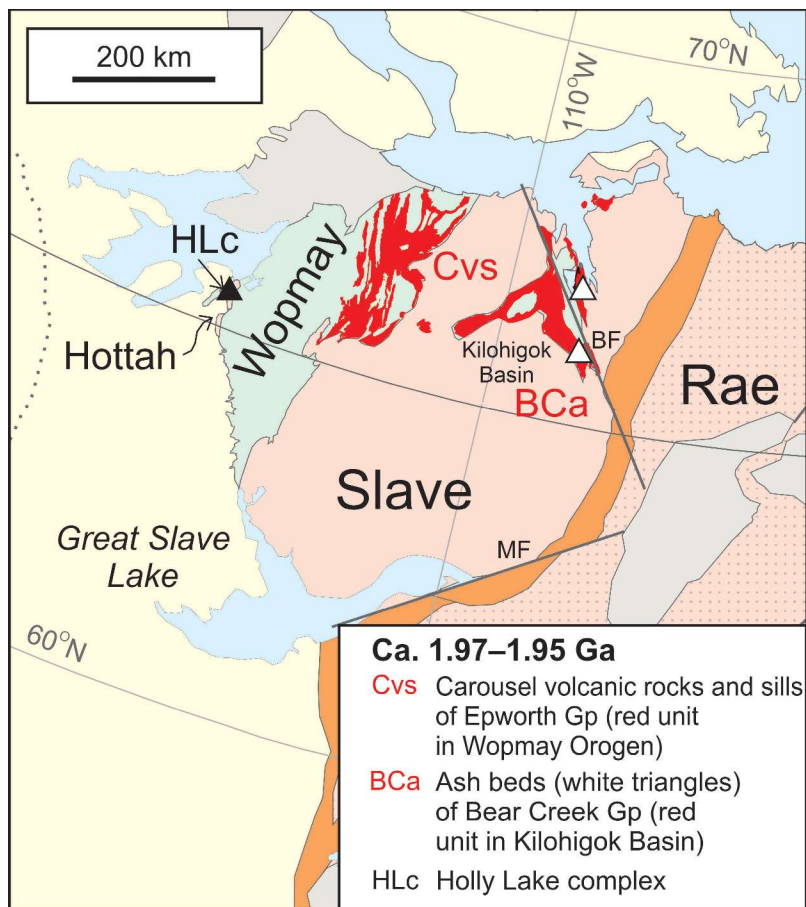


Figure 6. Selected 1.97 to 1.95 Ga magmatic events of northern Canada. Epworth and Bear Creek groups of the Wopmay Orogen and Kilohigok Basin, respectively, are shown in a single colour (red) as they have been interpreted to be stratigraphically equivalent (Bowring and Grotzinger, 1992). Triangles indicate units of limited extent. See Figure 1 for background map legend.

magmatic arc (Hildebrand et al., 1983) that originated prior to the Hottah terrane rifting from its parent craton, which, as noted above, may have been the Taltson or Ksituan magmatic zone to the south (Davis et al., 2015a; Ootes et al., 2015, 2017).

Slave Craton

Ca. 1.93 Ga lower Wilson Island Group volcanic rocks and sills

The 1928 ± 11 Ma bimodal volcanic rocks and sills of the lower Wilson Island Group (U-Pb; Bowring et al., 1984; Johnson, 1990) are located in the East Arm Basin of Great Slave Lake (Fig. 7). Johnson (1990) suggested that the Wilson Island Group was deposited in a pull-apart basin during post-collisional convergence between the Slave and Rae cratons. Sheen et al. (2019), however, have argued that the Slave and Rae cratons were together at least as early as ca. 2.045 Ga and that the East Arm Basin reflects failed rifting, as discussed above.

Meta Incognita microcontinent

Ca. 1.92 Ga Frobisher suite mafic-ultramafic sills

The mafic-ultramafic Frobisher suite sills of the Lake Harbour Group are distributed across much of the Meta Incognita microcontinent (Fig. 7; Liikane et al., 2015). They have been dated at ca. 1922 ± 12 Ma (U-Pb zircon; Liikane et al., 2015). St-Onge et al. (2000) proposed a link between the sills and rifting of the Meta Incognita microcontinent from its parent craton. Liikane et al. (2015) suggested that the sills may be related to a plume-generated LIP or back-arc rifting.

Ca. 1.92 to 1.84 Ga events

Magmatism in the Slave Craton and in the Wopmay Orogen was extensive and of a semicontinuous nature throughout the 1.91 to 1.84 Ga period (Fig. 8a, b). Widespread 1.90 to 1.89 Ga magmatism in the southern Slave Craton, along the western Slave margin, and in the Hottah terrane may represent a single event that is associated with breakup along the western Slave margin, breakup of the Hottah

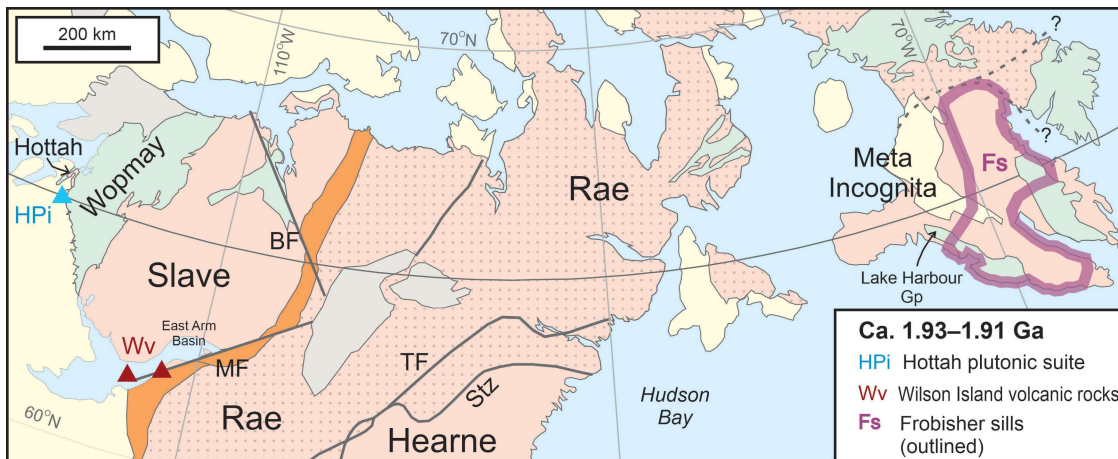


Figure 7. Selected 1.93 to 1.91 Ga magmatic events of northern Canada. The overall geographic extent of the Frobisher suite sills is outlined in purple. Triangles indicate units of limited extent. See Figure 1 for background map legend.

terrane from its parent craton, and a phase of rifting in the East Arm Basin. Widespread post-1.89 Ga magmatism in the Slave Craton and Wopmay Orogen is contemporaneous with east-dipping subduction, associated back-arc extension, and collision of the Hottah terrane on the western margin of the Slave Craton. By the end of this period, the portion of Laurentia that is located in northern Canada (Fig. 1) had fully assembled, with the Rae and Hearne cratons likely colliding at ca. 1.9 Ga, as proposed by Berman et al. (2007) and Pehrsson et al. (2019).

Hottah microcontinent

Ca. 1.91 to 1.89 Ga Bell Island Bay group volcanic rocks

The Bell Island Bay group of the Hottah microcontinent (Fig. 8b) consists of a lower and an upper sequence. The lower Bell Island Bay group includes bimodal volcanic rocks of the Zebulon formation dated at 1906 ± 2 Ma (U-Pb zircon; Ootes et al., 2015) and $1898 +7/-6$ Ma (U-Pb zircon; Reichenbach, 1991). The upper Bell Island Bay group includes the Bloom Basalt, which was dated at 1895 ± 2 Ma or older based on the U-Pb zircon age of an overlying rhyodacite (Ootes et al., 2015), as well as the north-trending Fishtrap Lake dykes (Fig. 8b) and sills, which may be feeders to the basalt (Reichenbach, 1991). The Bloom Basalt erupted during separation of the Hottah microcontinent from its parent craton (Davis et al., 2015a; Ootes et al., 2015), before the microcontinent moved northward to eventually collide with the western Slave margin at ca. 1.88 Ga. The rifting event associated with the Bloom Basalt is coeval with rifting on the western Slave margin associated with the Grant subgroup basalt and the Akaitcho Group bimodal volcanic rocks (e.g. Ootes et al., 2017).

Slave Craton

Ca. 1.91 to 1.89 Ga Akaitcho–Grant magmatism

Grant subgroup basalt, with an interbedded rhyodacite dated at 1893 ± 2 Ma (U-Pb zircon; Ootes et al., 2015) and Akaitcho Group bimodal volcanic rocks, with rhyolite dated at ca. 1.90 Ga (U-Pb zircon; Hoffman and Bowring, 1984) are located in the metamorphic internal zone of the Wopmay Orogen, east of the Wopmay Fault (Fig. 8b). They represent rifting on the western margin of the Slave Craton, contemporaneous with lower Bell Island Bay volcanic rocks (see previous section), which are linked to rifting of the Hottah microcontinent from its parent craton (e.g. Ootes et al., 2017).

Ca. 1.90 Ga Hearne dyke swarm

Hearne dykes, dated at 1901 ± 4 Ma (U-Pb baddeleyite; Bleeker et al., 2008b) trend east-northeast along the northern shore of the East Arm of Great Slave Lake (Fig. 8b). Bleeker et al. (2008b) proposed that the swarm may reflect a final phase of lithospheric stretching on the southern margin of the Slave Craton. Mumford and Cousens (2014) have suggested that some dykes in the swarm may be as young as ca. 1892 Ma, based on field relationships with precisely dated stocks that intrude the ca. 2.18 Ga Blachford Lake intrusive complex.

The Hearne dykes are approximately coeval with, or marginally older than, the Bloom Basalt, Grant subgroup basalt, and Akaitcho bimodal volcanic rocks that collectively have been interpreted to represent a major episode of rifting in the Hottah terrane and on the western margin of the Slave Craton (Ootes et al., 2017). If a mantle plume is associated with this magmatism and breakup, the plume may be located at the intersection of the trend of the Hearne dyke swarm with the western Slave margin. In this interpretation the Hearne dykes reflect failed rifting.

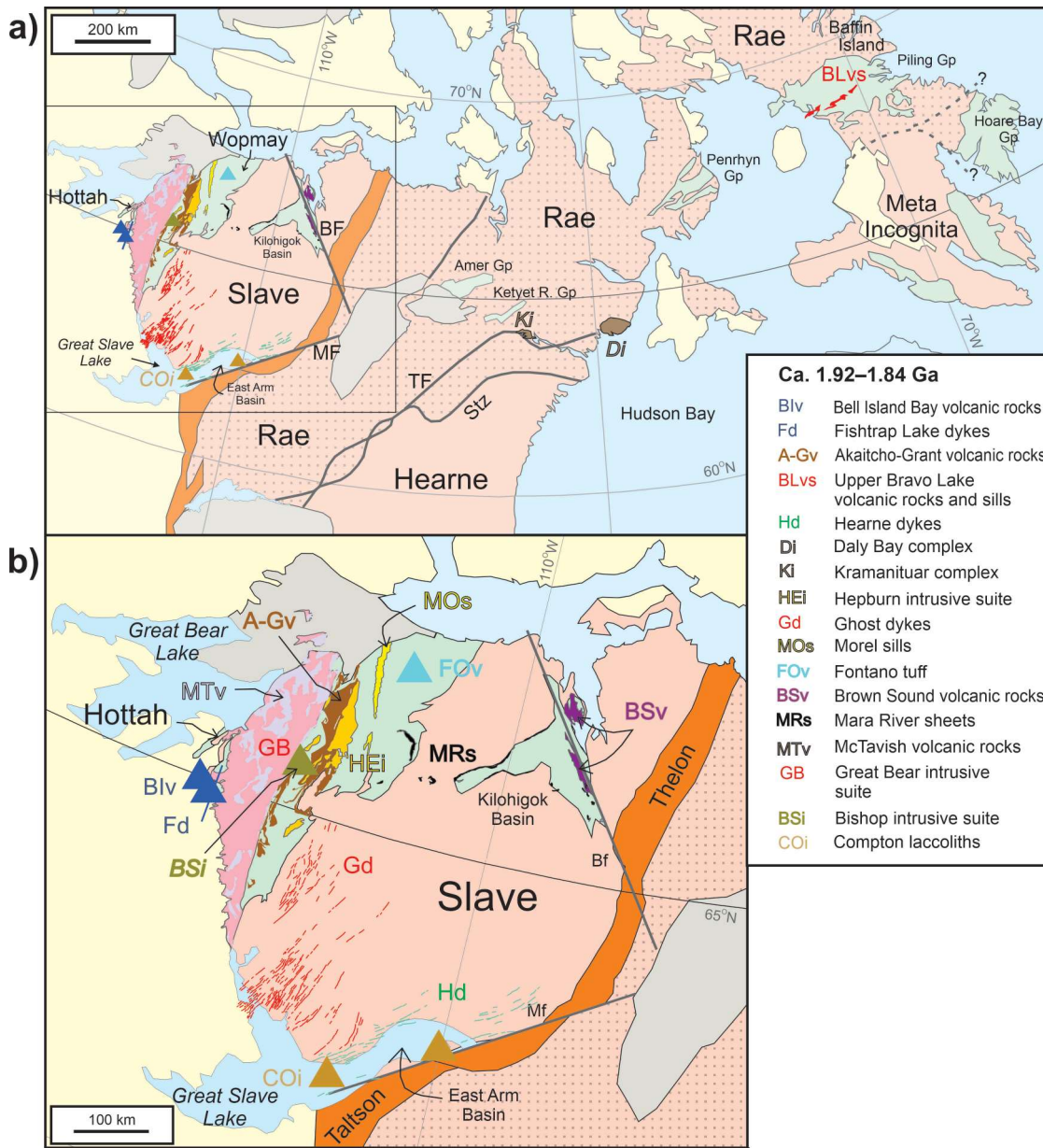


Figure 8. a) Selected 1.92 to 1.84 Ga dyke swarms and other magmatic events of northern Canada. Triangles indicate units of limited extent, with a trend bar shown for the Fishtrap Lake dykes. See Figure 1 for background map legend. b) Enlargement of the Slave–Wopmay area.

Bleeker et al. (2008b) and Ernst and Bleeker (2010) interpreted the Hearne swarm as part of a ca. 1.9 Ga Snowbird LIP that was thought to include the ca. 1.9 Ga Daly Bay and Kramanituar mafic granulite complexes of the Rae Craton (Fig. 8a), and the Chipman dyke swarm along the Snowbird tectonic zone between the Rae and Hearne cratons (Fig. 4). A link between the Chipman dykes and the granulite complexes was proposed by Flowers et al. (2006), based on a U-Pb zircon age of ca. 1.9 Ga that dated metamorphism of the swarm. Subsequent dating (Regan et al., 2017), described in ‘Ca. 2.11 Ga Chipman dyke swarm’ above,

suggests, however, that the Chipman dykes are ca. 2.11 Ga in age, and hence unrelated to the Hearne dykes or a 1.9 Ga LIP.

Ca. 1.90 to 1.88 Ga Hepburn intrusive suite

Peraluminous granite to gabbro plutons of the Hepburn intrusive suite intruded the metamorphic internal zone of the Wopmay Orogen (Fig. 8b) between 1.895 and 1.878 Ga (U-Pb zircon; Hoffman and Bowring, 1984; Ootes et al.,

2017). It has been proposed that they formed in a back-arc basin (Lalonde, 1989) or a fore-arc basin (Hildebrand et al., 2010a). Ootes et al. (2017) have suggested that they are linked to rifting on the western Slave margin that produced the Grant subgroup volcanic rocks (*see above*).

Ca. 1.89 to 1.87 Ga Ghost dyke swarm and approximately coeval magmatism

Mainly mafic magmatism, dated at ca. 1.89 to 1.87 Ga, occurs across the Slave Craton, including the Wopmay Orogen and Kilohigok Basin (Fig. 8b). The northeast-trending Ghost dykes of the southwestern Slave Craton form a broad linear swarm, and have been dated at 1886 to 1884 Ma (U-Pb baddeleyite; Atkinson, 2004; Davis and Bleeker, 2007; Bleeker et al., 2008a; Buchan et al., 2016). Several other intrusive and extrusive units are approximately coeval with, or slightly younger than, the Ghost dykes. They include the ca. 1890 to 1880 Ma Morel sills (e.g. Hildebrand and Bowring, 1999; Hildebrand et al., 2010a) within the Coronation Supergroup of the Wopmay Orogen, ca. 1870 Ma Mara River intrusive sheets (Davis et al., 2004; M. Hamilton *in* Buchan et al., 2010) of the Kilohigok Basin and northern Slave Craton, the 1882.5 ± 1 Ma Fontano Formation tuff (U-Pb zircon; Hoffman et al., 2011) of the Recluse Group of the Wopmay Orogen, and the Brown Sound Formation basalt of the Kilohigok Basin. The Brown Sound Formation basalt has not been directly dated, but is interpreted to be coeval with, or slightly younger than, the Fontano tuff based on stratigraphic correlation (Bowring and Grotzinger, 1992).

It is uncertain if the widespread magmatism described above belongs to a single long-lived event. In any case, it is contemporaneous with collision of the Hottah microcontinent and the western Slave Craton margin. Hildebrand and Bowring (1999) interpreted the emplacement of the Morel sills, which are confined to a 200 km long by 10 km wide zone within, and parallel to, the Wopmay Orogen, as the result of extension orthogonal to the Slave Craton boundary during collision and breakoff of a subducting slab. This interpretation is based on the assumption that the feeder dykes to the sills (which have not been identified in the field) were also oriented parallel to the orogen. Davis and Bleeker (2007) suggested a similar setting for the emplacement of the Ghost dyke swarm, and interpreted the Mara River sheets as back-arc magmatism.

Ca. 1.88 to 1.85 Ga McTavish supergroup

The McTavish supergroup of the Great Bear magmatic zone (Fig. 8b; Hildebrand et al., 2010b) includes LaBine Group volcanic rocks (1876 ± 3 Ma, andesite, U-Pb zircon; Ootes et al., 2015); mainly rhyolitic Faber group volcanic rocks (1869 ± 1 Ma, rhyolitic ignimbrite, U-Pb zircon; Ootes et al., 2015); bimodal Sloan group volcanic rocks (1863 ± 2 Ma, rhyolite beneath basalt; U-Pb zircon; Ootes

et al., 2015); and feeder dykes. Bimodal Dumas group volcanic rocks (1869.5 ± 2 Ma, rhyodacite, U-Pb zircon; Ootes et al., 2015), located east of the Wopmay Fault, are coeval with the McTavish supergroup. All these units were emplaced during collision of the Hottah microcontinent with the Slave Craton.

Ca. 1.88 to 1.85 Ga Great Bear intrusive suite

Calc-alkaline intrusions of the Great Bear intrusive suite in the Great Bear magmatic zone (Fig. 8b) have been dated at ca. 1.875 to 1.850 Ga (U-Pb zircon; Hoffman and Bowring, 1984; Gandhi et al., 2001; Bennett and Rivers, 2006a, b). They are thought to have been emplaced above an east-dipping subduction zone associated with collision of the Hottah microcontinent and the western Slave Craton (Hildebrand et al., 1987; Ootes et al., 2015).

Ca. 1.87 to 1.85 Ga Bishop intrusive suite

The Bishop intrusive suite (Fig. 8b) of the metamorphic internal zone of the Wopmay Orogen comprises granite to gabbro plutons dated at ca. 1.865 to 1.850 Ga (U-Pb; Bowring, 1985; *see discussion in* Ootes et al., 2017). Lalonde (1989) interpreted the suite as the waning phase of Great Bear magmatism.

Ca. 1.87 to 1.86 Ga Compton laccoliths

The Compton calc-alkaline laccoliths of the East Arm of Great Slave Lake (Fig. 8b) have been dated at 1872 ± 8 Ma and 1861 ± 17 Ma (U-Pb; Bowring et al., 1984). They may be genetically related to approximately coeval calc-alkaline intrusions in the Great Bear magmatic zone (Hoffman and McGlynn, 1977).

Rae Craton

Ca. 1.90 to 1.88 Ga upper Bravo Lake Formation magmatism

The Bravo Lake Formation of the Piling Group on central Baffin Island (Fig. 8a) comprises mafic-ultramafic volcanic rocks, sills, and dykes (Johns et al., 2006). Sills in the upper Bravo Lake Formation have been dated at $1897 +10/-5$ Ma (U-Pb zircon; Wodicka et al., 2014) and 1883 ± 5 Ma (U-Pb zircon; Henderson and Parrish, 1992). The possibility that tholeiitic to picritic volcanic rocks of the lower Bravo Lake Formation may be much older than the alkaline basalt of the upper Bravo Lake Formation, perhaps as old as 1.98 Ga (Wodicka et al., 2014), should be noted, although they have yet to be directly dated.

Jackson and Berman (2000) proposed that Bravo Lake Formation volcanic rocks may be linked to poorly dated volcanic rocks in the Penrhyn Group of Melville Peninsula (Fig. 8a) and Karrat Group volcanic rocks of western Greenland. Rainbird et al. (2010) suggested that they may be coeval with volcanic rocks in the Five-Mile Lake formation of the Amer group and volcanic rocks in the Ketyet River group (Fig. 8a). Given, however, that Wodicka et al. (2014) proposed a large age difference between the lower and upper portions of the Bravo Lake Formation, as discussed above, a correlation with magmatism in these other sedimentary successions needs to be tested using geochronological methods.

The setting for Bravo Lake Formation volcanic rocks and related units has been controversial. Jackson and Berman (2000) suggested a plume origin on the basis of geochemistry. Johns et al. (2006), citing the lack of plume-related features such as an uplift or a giant radiating dyke swarm, suggested emplacement in an intracratonic basin. Wodicka et al. (2014) proposed that the lower Bravo Lake volcanic rocks were emplaced in an intracratonic basin, whereas the upper Bravo Lake volcanic rocks represent incipient rifting on the southeastern Rae margin.

Ca. 1.92 to 1.90 Ga Daly Bay and Kramanituar complexes

The Daly Bay and Kramanituar mafic granulite complexes (Fig. 8a) of the Rae Craton are dated at 1917 ± 3 Ma (U-Pb; Berman et al., 2007) and 1901 ± 2 Ma (U-Pb; Sanborn-Barrie et al., 2001), respectively. Berman et al. (2007, Fig. 2) suggested that this mafic magmatism and related extension, rapid uplift, and cooling was triggered by slab breakoff associated with north-directed subduction of the Hearne plate beneath the Rae Craton (including the Chesterfield Block). As discussed above, Ernst and Bleeker (2010) proposed a link between these bodies and the coeval Hearne dyke swarm of the southern Slave Craton.

Paleomagnetism and testing of continental reconstructions (ca. 1.92–1.84 Ga)

The 1.89 to 1.87 Ga Ghost magmatic event, discussed above, is approximately coeval with the precisely dated Kalaro–Nimnyrsky (1869 ± 2 Ma; U-Pb baddeleyite) and Malozadoisky (1863 ± 1 Ma; U-Pb baddeleyite) mafic dyke swarms in the Siberian Craton (Ernst et al., 2016). Based on geological and paleomagnetic comparisons, a number of authors (e.g. Rainbird et al., 1998; Buchan et al., 2001; Evans and Mitchell, 2011; *see also* Supplementary Figure S1 *in* Ernst et al., 2016) have concluded that the southern margin of the Siberian Craton may have been adjacent to northern Laurentia during a portion of the Proterozoic. Most recently, Ernst et al. (2016) used a comparison of the magmatic barcodes for Siberia and Laurentia to propose such a reconstruction over the entire 1.90 to 0.72 Ga period. A

comparison between the primary paleopoles for the 1886 to 1884 Ma Ghost dykes (Buchan et al., 2016) and coeval 1878 ± 4 Ma lower Akitkan redbeds of Siberia (Didenko et al., 2009) allows such a reconstruction (Fig. 14 *in* Buchan et al., 2016).

Ca. 1.89 to 1.87 Ga mafic magmatism is also widespread in the Superior Craton (Ciborowski et al., 2017). There is no evidence, however, that magmatic events occurring in the Slave and Superior cratons are genetically related, as the Superior Craton did not collide with northern Laurentia (including the Slave Craton) until ca. 1.83 to 1.80 Ga, as noted above. A distinct difference in the primary paleopoles for the Ghost dykes of the Slave Craton and the coeval ca. 1.88 Ga Molson dykes of the Superior Craton (Fig. 14 *in* Buchan et al., 2016) confirms that the two cratons were not located in their present configuration when these dyke swarms were emplaced.

Ca. 1.83 to 1.82 Ga events

Magmatism in this and younger periods is mainly associated with Laurentia, because amalgamation of the cratonic blocks that form the northern portion of Laurentia was complete by 1.83 Ga (except for far-western terranes such as Bonnetia, which survive only as megacrysts within the Wernecke breccia, as discussed in ‘Bonnetia terrane’ section, below. Magmatism of this period (Fig. 9) may reflect a single LIP that extended over a wide area from the western shores of Hudson Bay to Lake Athabasca and, moreover, included ultrapotassic and potassic volcanic rocks and dykes, as well as diabase dyke swarms.

Laurentia

Ca. 1.83 to 1.82 Ga Sparrow and Uranium City diabase dyke swarms

Sparrow diabase dykes form a broad southeast-trending swarm in the region south of the Taltson magmatic zone (Fig. 9) and have been dated at 1827 ± 4 Ma (U-Pb baddeleyite; Bostock and van Breemen, 1992). A slightly younger age of 1818 ± 4 Ma (U-Pb baddeleyite; Morelli et al., 2009) was obtained for east- to southeast-trending Uranium City diabase dykes (Fig. 9) immediately north of Lake Athabasca. Based on geochemistry and field relationships, Uranium City dykes are interpreted to feed undated Martin group mafic volcanic rocks and sills of the same region (Fig. 9; Morelli et al., 2009). Morelli et al. (2009) and Ashton et al. (2009) interpreted emplacement of Uranium City dykes as related to compression associated with the Hudsonian Orogeny. On the other hand, Ernst and Bleeker (2010) suggested possible plume involvement based on a weak radiating pattern in the combined Sparrow–Uranium City dyke geometry.

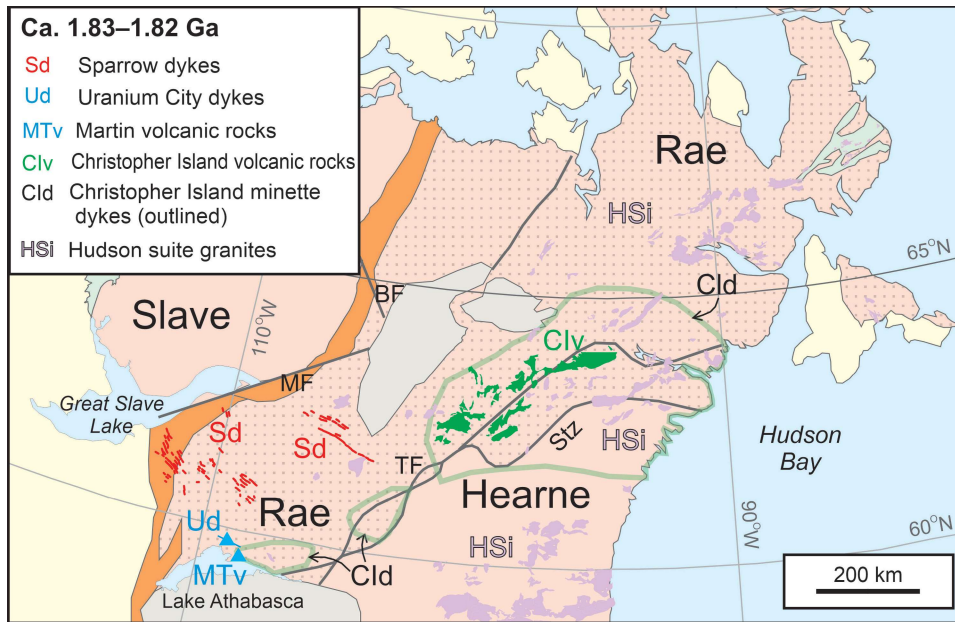


Figure 9. Selected 1.83 to 1.82 Ga dyke swarms and other magmatic events of northern Canada. The overall geographic extent of the Christopher Island minette dykes is outlined in green. Triangles indicate units of limited extent, with a trend bar shown for the Uranium City dykes. See Figure 1 for background map legend.

Ca. 1.83 Ga Christopher Island formation ultrapotassic and potassic volcanic rocks and dykes

Christopher Island formation ultrapotassic and potassic volcanic rocks (Fig. 9) occur in the Baker Lake Group of the Dubawnt Supergroup in the Baker Lake rift basin. An age of 1833 ± 3 Ma (U-Pb zircon; Rainbird et al., 2006) obtained from a flow near the base of the Baker Lake Group is interpreted to date initiation of the Baker Lake Basin, which may have formed in response to tectonic escape accompanying the Hudsonian Orogeny (Rainbird et al., 2006). Ultrapotassic and potassic (minette) dykes, which are compositionally identical to the volcanic rocks, occur widely, both within and outside the basin (Fig. 9). Dykes of similar composition are also found in the vicinity of Martin group volcanic rocks, north of Lake Athabasca (Fig. 9; Ashton et al., 2009), and are interpreted as part of the same suite (Ashton et al., 2018). Cousens et al. (2001), in a geochemical study carried out prior to the realization that the Rae–Hearne boundary is south rather than north of the Chesterfield Block, argued that the Christopher Island rocks were emplaced from an Archean lithospheric mantle source that extended beneath both the Rae and Hearne cratons, suggesting that the Rae and Hearne cratons have been together since the Archean. Berman et al. (2007) have pointed out, however, that this argument no longer holds, as Christopher Island volcanic rocks and almost all of the minette dykes are now thought to lie within the Rae Craton, given the revised Rae–Hearne boundary.

Ca. 1.85 to 1.80 Ga Hudson suite granites

Hudson suite granites are distributed over an enormous region in the Hearne and Rae cratons of the Churchill Province (Fig. 9). They have been dated at ca. 1.85 to

1.80 Ga, with the peak of emplacement at 1.83 Ga (U-Pb; van Breemen et al., 2005). As in the case of the coeval Christopher Island formation volcanic rocks, the Hudson granites are interpreted to have been emplaced during extension associated with the Hudsonian Orogeny (Peterson et al., 2015a; Ashton et al., 2018).

Paleomagnetism and testing continental reconstructions (ca. 1.83–1.82 Ga)

Buchan (2014) carried out a detailed comparison of 1.83 to 1.27 Ga paleomagnetic poles for Laurentia and Baltica (or the cratonic blocks that amalgamated to form them by ca. 1.80 and 1.75 Ga, respectively). The data yielded a unique reconstruction throughout this period, with northern Norway and the Kola Peninsula of Baltica adjacent to northeastern Greenland of Laurentia (Fig. 5, 6 in Buchan, 2014). As Laurentia was still in the process of assembling until ca. 1.80 Ga and Baltica (consisting of Fennoscandia and the Volgo-Sarmatia cratonic block) was still assembling until ca. 1.75 Ga, the reconstruction at ca. 1.83 Ga only applies to northern Laurentia and Fennoscandia, and the reconstruction at 1.78 to 1.74 Ga only applies to Laurentia and Fennoscandia. The paleopoles that were used in the 1.65 to 1.27 Ga interval are from precisely dated units that have been demonstrated to retain primary remanent magnetizations. Therefore, the Laurentia–Baltica reconstruction in this interval is considered to be rigorous. On the other hand, several paleopoles in the earlier portion of the period, including the paleopole from the 1.83 Ga Sparrow dykes, are from precisely dated units, but have yet to be demonstrated primary. Therefore, the validity of the reconstruction as early as 1.83 Ga remains to be fully tested.

Ca. 1.77 to 1.73 Ga events

This period is marked by the emplacement of the widespread Kivalliq igneous suite in the Churchill Province as well as the intrusion of diabase dyke swarms in the Wopmay Orogen and on Victoria Island (Fig. 10).

Laurentia

Ca. 1.77 to 1.73 Ga Kivalliq igneous suite

The extensive Kivalliq (formerly Nueltin) igneous suite (Peterson et al., 2015a) intrudes the amalgamated Hearne and Rae cratons of the Churchill Province (Fig. 10). It includes Nueltin granite intrusions dated at ca. 1765 to 1740 Ma (U-Pb zircon; van Breemen et al., 2005); various gabbro and anorthosite intrusions; the Mallery granite-gabbro complex with gabbro dated at 1769 ± 6 Ma (U-Pb baddeleyite; Peterson et al., 2015b); rhyolite and basalt of the Pitz Formation of the middle Dubawnt Supergroup (Wharton Group) dated at 1758 to 1753 Ma (U-Pb zircon; Rainbird and Davis, 2007); the 1754 ± 1 Ma McRae Lake diabase dyke swarm (U-Pb baddeleyite; Peterson et al., 2015b); and perhaps the undated

Amer and Thelon River diabase dykes swarms. There is a change in magma composition from alkaline to subalkaline over a period of approximately 15 Ma (Peterson et al., 2015b). This anorogenic igneous event occurred near the centre of the Nuna (Columbia) supercontinent (Peterson et al., 2015a) and may have a mantle plume origin (Ernst et al., 2016).

The McRae Lake dykes form a narrow, slightly arcuate swarm, with a north-northeast trend in the south, a northeast trend in the north, and a length of about 160 km (Fig. 10; Buchan and Ernst, 2013; Fig. 3 in Peterson et al., 2015a). The most prominent dyke in the swarm is 27 km long and up to 1.8 km wide; it intrudes volcanic rocks of the Pitz Formation (Peterson et al., 2015a). Peterson et al. (2015a) interpreted the north-trending Amer and the east-northeast-trending Thelon River dyke swarms (Fig. 10; Fig. 3 in Peterson et al., 2015a) as part of the Kivalliq igneous suite, although they have yet to be dated.

Ca. 1.75 to 1.74 Ga dykes on Victoria Island

The east-trending Hadley Bay dyke of northern Victoria Island (Fig. 10) is dated at ca. 1747 Ma (U-Pb baddeleyite; L.M. Heaman in LeCheminant et al., 1996b). Farther

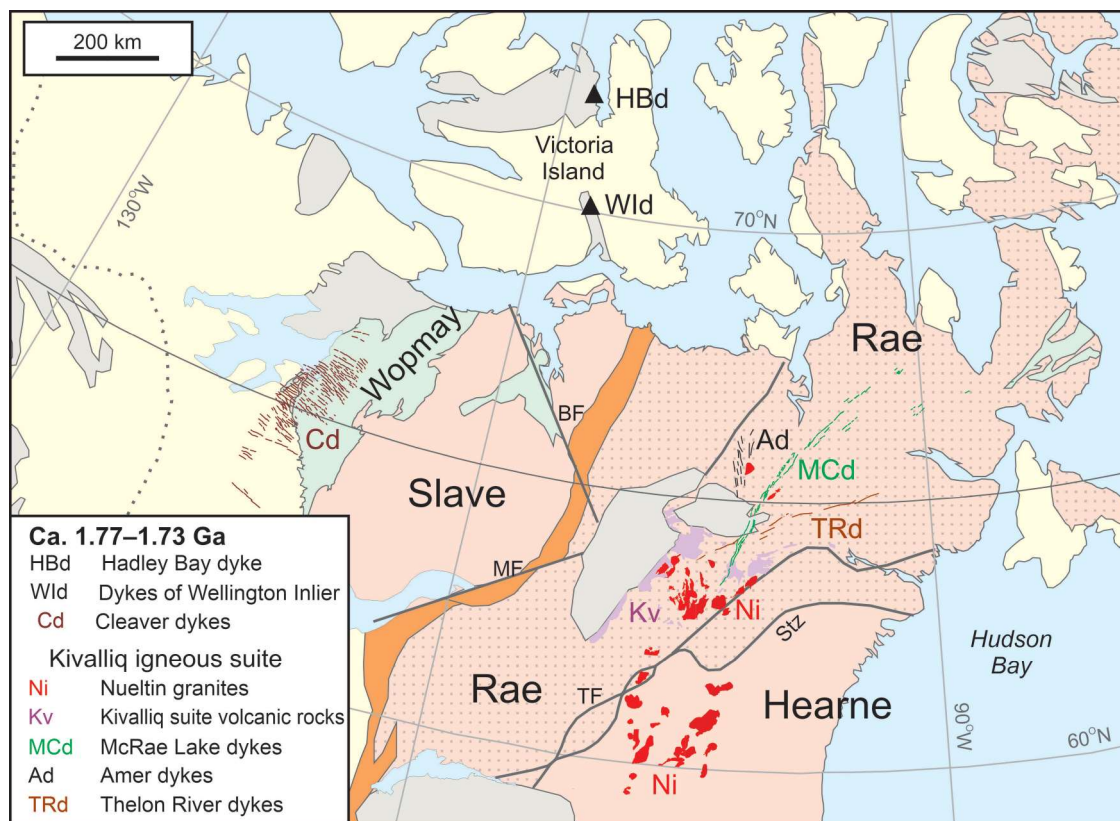


Figure 10. Selected 1.77 to 1.73 Ga dyke swarms and other magmatic events of northern Canada. The southwestern portion of the Cleaver dyke swarm is beneath Phanerozoic cover rocks and has been traced from aeromagnetic mapping (Buchan and Ernst, 2013). Triangles indicate dyke swarms of limited extent with trends that are not well constrained. See Figure 1 for background map legend.

south on Victoria Island (Fig. 10), in the northern part of the Wellington Inlier, east-southeast- to southeast-trending dykes are interpreted to be coeval with the Hadley Bay dyke (Rainbird and LeCheminant, 2002). This interpretation has been confirmed by a U-Pb baddeleyite age of 1743.5 ± 0.8 Ma (M.A. Hamilton, pers. comm., 2019) on an east-southeast-trending dyke. The overall trends of the dyke swarms on Victoria Island are not well constrained as they are mainly based on the trends of individual dated dykes.

Ca. 1.74 Ga Cleaver dyke swarm

The 1740 $\pm 5/-4$ Ma Cleaver dykes (U-Pb baddeleyite; Irving et al., 2004) form a wide, east-southeast-trending swarm in the Great Bear magmatic zone and Hottah terrane (Fig. 10).

The various 1.77 to 1.73 Ga magmatic events in northern Canada could form a single plume-generated LIP (Ernst and Buchan, 2004; Ernst et al., 2016). Furthermore, these events could be linked to the coeval Tipton giant radiating dyke swarm of Siberia dated at 1758 to 1752 Ma (U-Pb baddeleyite and Ar-Ar; Ernst et al., 2016), in a northern Laurentia–Siberia configuration that may have lasted between ca. 1.90 and 0.72 Ga, as discussed above. Given the large geographic extent of the 1.77 to 1.73 Ga magmatism, however, it is possible that it represents two or more separate, but coeval events.

Paleomagnetism and testing continental reconstructions (ca. 1.77–1.73 Ga)

Primary paleomagnetic results have been reported from the 1.74 Ga Cleaver dykes (Irving et al., 2004), as well as for 1.76 to 1.75 Ga Pitz Formation volcanic rocks and 1.75 Ga McRae Lake dykes (Raub, 2008). These data provide reliable paleopoles for the late Paleoproterozoic APWP for Laurentia. The Cleaver paleopole was used in the 1.83 to 1.27 Ga reconstruction of Laurentia–Baltica (Buchan, 2014) discussed in ‘Paleomagnetism and testing continental reconstructions (ca. 1.83–1.82 Ga)’, above.

Ca. 1.71 to 1.59 Ga events

Between ca. 1.71 and ca. 1.59 Ga, several distinct and geographically restricted magmatic events occurred in northern Laurentia or in the exotic Bonnetia terrane, which is thought to have been located off the northwestern Laurentia margin (Fig. 11). Events at ca. 1.60 to 1.59 Ga in the Wopmay Orogen and western Cordillera may be associated with a single mantle plume and LIP.

Bonnetia terrane

Ca. 1.71 Ga Bonnet Plume River intrusions

The 1714 to 1706 Ma Bonnet Plume River diorite and gabbro intrusions (U-Pb zircon; Thorkelson et al., 2001a) survive only as megacrysts within ca. 1.60 Ga Wernecke breccia in the Wernecke, Ogilvie, and Richardson mountains of the western Cordillera (Fig. 11). Along with megacrysts of the undated Slab volcanic rocks (Furlanetto et al., 2013) and Devil volcanic rocks (Thorkelson and Laughton, 2016) that are also preserved in Wernecke breccia, they have been interpreted to have been emplaced in an exotic terrane called Bonnetia (Thorkelson and Laughton, 2016). Bonnetia is thought to be a volcanic arc, possibly originating on the Australian plate, which was obducted on top of the Wernecke Supergroup on the northwestern margin of Laurentia after Australia collided with northwestern Laurentia, prior to formation of the Wernecke breccia (Furlanetto et al., 2016; Thorkelson and Laughton, 2016).

Laurentia

Ca. 1.70 Ga Pelly Bay dyke swarm

The east-trending Pelly Bay dyke swarm, dated at ca. 1.70 Ga (Bleeker and Ernst, 2011), is located at the base of the Boothia Peninsula (Fig. 11; Ryan et al., 2008). It is little studied, and its overall extent and setting are not yet known.

Ca. 1.66 Ga Narakay volcanic complex

The bimodal Narakay volcanic complex (Fig. 11) is located in the Hornby Bay Basin and comprises flows and associated pyroclastic rocks of mafic and felsic composition (Ross, 1986). A rhyolite porphyry has been dated at 1663 ± 8 Ma (U-Pb zircon; Bowring and Ross, 1985). Emplacement occurred during the Forward Orogeny (Cook and MacLean, 1995).

Ca. 1.60 to 1.59 Ga Wernecke breccia

Wernecke breccia of the Wernecke, Ogilvie, and Richardson mountains of the western Cordillera (Fig. 11) are dated at 1599 to 1595 Ma (U-Pb zircon; Thorkelson et al., 2001b; Furlanetto et al., 2013). They are approximately coeval with the ca. 1.59 Ga Olympic Dam breccia and ca. 1.59 Ga Gawler Range volcanic rocks in the Gawler Craton of Australia. Thorkelson et al. (2001b) suggested that together, the Wernecke and Olympic Dam breccia form a plume-related hydrothermal province in a reconstruction of the Gawler Craton with northwestern Laurentia. They

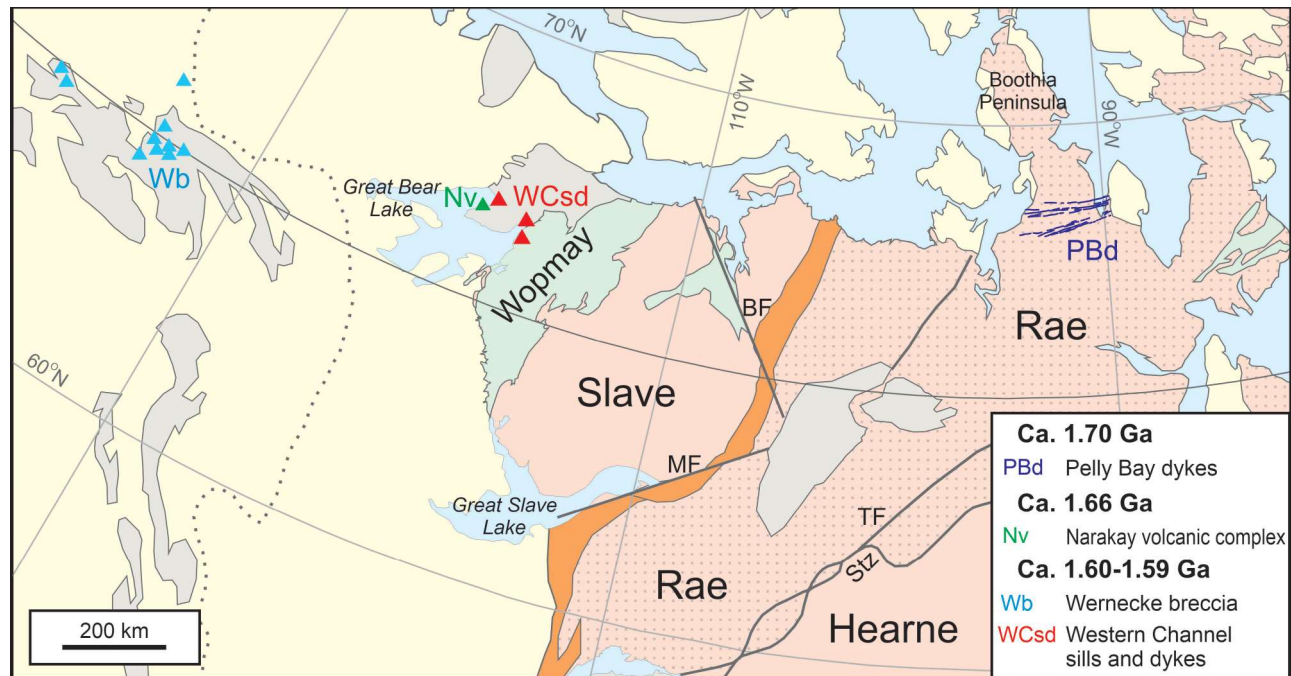


Figure 11. Selected 1.71 to 1.59 Ga dyke swarms and other magmatic events of northern Canada. The ca. 1.71 Ga Bonnet Plume River intrusions, interpreted as having been emplaced in the exotic terrane Bonnetia, occur as clasts in the Wernecke breccia. Triangles indicate units of limited extent. See Figure 1 for background map legend.

are also coeval with the Western Channel diabase of the Great Bear magmatic zone and the Mammoth dykes of the Wyoming Craton, as noted below.

Ca. 1.59 Ga Western Channel diabase intrusions

Western Channel diabase sills and dykes (Fig. 11), located along the eastern shores of Great Bear Lake in the Great Bear magmatic zone and Hornby Bay Basin, are dated at 1592 to 1590 Ma (U-Pb baddeleyite; Hamilton and Buchan, 2010; Rogers et al., 2018). Thus, they are coeval with the Wernecke breccia in the western Cordillera as well as the Gawler Range volcanic rocks and Olympic Dam breccia of the Gawler Craton of Australia. They are also coeval with the 1590 ± 5 Ma Mammoth dykes (U-Pb baddeleyite; Rogers et al., 2018) located about 2000 km to the south, in the Tobacco Root Mountains of the Wyoming Craton of Laurentia.

The Wernecke breccia of the northern Cordillera, the Olympic Dam breccia and associated Gawler Range volcanic rocks of Australia, the Western Channel diabase of the Great Bear magmatic zone, and the Mammoth dykes of the Wyoming Craton may all be part of a single plume-related LIP event (Thorkelson et al., 2001b; Hamilton and Buchan, 2010; Rogers et al., 2018).

Paleomagnetism and testing continental reconstructions (ca. 1.71–1.59 Ga)

A paleomagnetic pole is available for the Western Channel diabase (Irving et al., 1972), and is interpreted to be primary (see summary in Hamilton and Buchan, 2010). The pole provides a key constraint for the Laurentia APWP at the Paleoproterozoic–Mesoproterozoic boundary (Hamilton and Buchan, 2010; Buchan, 2014). The Western Channel paleopole was used in the reconstruction of Laurentia–Baltica in the 1.83 to 1.27 Ga period (Buchan, 2014) discussed above.

Hamilton and Buchan (2010) compared the Western Channel diabase paleopole with a preliminary paleopole from the coeval Gawler Range volcanic rocks (Chamalaun and Dempsey, 1978). The age of the Gawler Range volcanic rocks paleopole, however, is controversial (Schmidt and Clark, 1992, 2011; Wingate and Evans, 2003). A negative paleomagnetic fold test (Schmidt and Clark 1992, 2011) indicated that the Gawler Range volcanic rocks acquired remanent magnetism after folding. Schmidt and Clark (2011) concluded that the remanence was acquired long after emplacement of the volcanic rocks, probably during the Devonian. If so, a comparison between the Gawler Range and Western Channel poles is not valid. On the other hand, Wingate and Evans (2003) concluded that folding occurred during emplacement of the volcanic rocks, and that the flows may have been magnetized immediately after folding as

they cooled or were overprinted by later flows. In this case, the Gawler Range pole would be essentially primary, and a comparison of the Western Channel and Gawler Range poles would support a paleocontinental reconstruction (Fig. 10 in Hamilton and Buchan, 2010), in which the Gawler Craton was adjacent to northwestern Laurentia at 1.6 Ga, a scenario broadly similar to the reconstruction proposed by Thorkelson et al. (2001b). Furlanetto et al. (2016) have proposed another reconstruction, in which the Gawler Craton is located approximately 1500 km further south along the western Laurentia margin than proposed by Thorkelson et al. (2001b) and Hamilton and Buchan (2010).

Paleomagnetic data are also available for the Mammoth dykes of the Tobacco Root Mountains (Harlan et al., 2008; cf. reinterpretation in Rogers et al., 2018). They yielded a paleopole that differs significantly from that of the Western Channel diabase, which Rogers et al. (2018) suggested may be due to block rotation and/or tilting in the Tobacco Root Mountains, magnetic overprinting in the Tobacco Root Mountains, or a failure to fully average out paleosecular variation in one or both of the data sets. Given the potential complications presented by the data from the Tobacco Root Mountains, the paleopole from the Western Channel diabase should be considered as the most reliable.

Poorly dated and undated events

The dyke swarm and magmatic events discussed above are mostly well dated. In addition, there are many undated or poorly dated magmatic units. Examples include the Beechey, Aylmer, and Hood River dykes of the Slave Craton; Tyrrell Arm dykes of the Rae Craton; Kekertaluk dykes of the Rae Craton and Meta Incognita terrane (*see* Buchan and Ernst, 2013); Milt intrusive sheets of the southern Slave (*see* Buchan et al., 2010); and numerous volcanic packages in cratonic or passive margin sedimentary successions across the Churchill Province (*see* Rainbird et al., 2010).

Precisely dating such units is important for the understanding of the tectonic history of northern Canada in the Paleoproterozoic. This will allow them to be properly assigned to specific magmatic episodes, matched to coeval extensional or breakup events, and compared with coeval magmatism elsewhere.

SUMMARY

Numerous giant mafic dyke swarms and other magmatic units related to LIPs were emplaced in northern Canada during the Paleoproterozoic, especially after 2.3 Ga. Many of these magmatic events have been precisely dated using the U-Pb method on zircon or baddeleyite, although others remain poorly dated. Those with reliable ages can often be matched with coeval magmatism elsewhere in northern Canada, elsewhere in North America or on other continents. Such matches have proven to be helpful in identifying the

overall geographic extent of individual LIP events and in reconstructing paleocontinents. In addition, comparing LIP magmatic barcodes from different cratonic blocks is useful in establishing the time intervals over which the blocks were near neighbours.

Paleomagnetism is another tool critical for determining or assessing paleocontinental reconstructions. Paleomagnetic poles for LIP events are of particular importance in such studies because mafic intrusions typically carry very stable, primary magnetic remanences and can be precisely dated. So far, reliable paleomagnetic poles have been obtained for only a few of the LIP events in northern Canada. The studies that are available, however, are providing important information on reconstructions and on the relative drift of cratonic blocks.

The tectonic setting of many of the LIP events in northern Canada is still controversial. Nevertheless, several events appear to be linked to episodes of extension that led to either continental breakup or failed rifting. More detailed study is needed to help resolve key questions concerning: 1) the makeup and timing of breakup of the ancestral supercratons from which the Slave, Rae, and Hearne cratons as well as the Meta Incognita terrane were derived; 2) the nature and timing of the amalgamation of the Slave and Rae cratons; 3) the timing of the assembly of the Rae and Hearne cratons; and 4) the nature and timing of the multiple phases of rifting that occurred along the western Slave Craton margin.

ACKNOWLEDGMENTS

The authors benefited greatly from discussions on Paleoproterozoic dykes and LIPs of northern Canada and their geological settings with many colleagues, especially Tony LeCheminant, Sally Pehrsson, Wouter Bleeker, Mike Hamilton, Rob Berman, Bill Davis, and Rob Rainbird. Rob Rainbird and Tony LeCheminant provided detailed reviews that have helped improve the manuscript. Partial financial support for this research was provided to R.E. Ernst by the Natural Sciences and Engineering Research Council of Canada Collaborative Research and Development grants CRDPJ 419503-11 (2012–2017) and CRDPJ 523131-17 (2018–2023), and Ministry of Science and Education of the Government of the Russian Federation Mega-Grant 14.Y26.31.0012.

REFERENCES

- Ashton, K.E., Hartlaub, R.P., Heaman, L.M., Morelli, R.M., Card, C.D., Bethune, K., and Hunter, R.C., 2009. Post-Taltson sedimentary and intrusive history of the southern Rae Province along the northern margin of the Athabasca basin, western Canadian Shield; *Precambrian Research*, v. 175, p. 16–34. <https://doi.org/10.1016/j.precamres.2009.09.004>

- Ashton, K., Card, C., and Rayner, N., 2018. A new U-Pb age for the Hudson granites and lamprophyre dykes in the southern Rae Province of Saskatchewan; *in* Summary of Investigations 2018, Volume 2; Saskatchewan Geological Survey, Saskatchewan Ministry of Energy and Resources, Miscellaneous Report 2018-4.2, Paper A-6, 15 p.
- Aspler, L.B., Cousens, B.L., and Chiarenzelli, J.R., 2002. Griffin gabbro sills (2.11 Ga), Hurwitz basin, Nunavut, Canada: long-distance lateral transport of magmas in western Churchill Province crust; *Precambrian Research*, v. 117, p. 269–294. [https://doi.org/10.1016/S0301-9268\(02\)00090-6](https://doi.org/10.1016/S0301-9268(02)00090-6)
- Atkinson, B., 2004. Petrogenesis of diabase dykes in the Germaine Lake area, NWT; B.Sc. thesis, University of Alberta, Edmonton, Alberta, 33 p.
- Bennett, V. and Rivers, T., 2006a. U-Pb ages of detrital zircons from the southern Wopmay Orogen, Northwest Territories; Northwest Territories Geoscience Office, NWT Open Report 2006-007, 29 p.
- Bennett, V. and Rivers, T., 2006b. U-Pb ages of zircon primary crystallization and inheritance for magmatic rocks of the southern Wopmay Orogen, Northwest Territories; Northwest Territories Geoscience Office, NWT Open Report 2006-006, 64 p.
- Berman, R.G., Davis, W.J., and Pehrsson, S., 2007. Collisional Snowbird tectonic zone resurrected: growth of Laurentia during the 1.9 Ga accretionary phase of the Hudsonian orogeny; *Geology*, v. 35, p. 911–914. <https://doi.org/10.1130/G23771A.1>
- Berman, R.G., Pehrsson, S., Davis, W.J., Ryan, J.J., Qiui, H., and Ashton, K.E., 2013. The Arrowsmith orogeny: geochronological and thermobarometric constraints on its extent and tectonic setting in the Rae craton, with implications for pre-Nuna supercontinent reconstruction; *Precambrian Research*, v. 232, p. 44–69. <https://doi.org/10.1016/j.precamres.2012.10.015>
- Bleeker, W., 2003. The late Archean record: a puzzle in ca. 35 pieces; *Lithos*, v. 71, p. 99–134. <https://doi.org/10.1016/j.lithos.2003.07.003>
- Bleeker, W., 2004. Taking the pulse of planet Earth: a proposal to a new multi-disciplinary flag-ship project in Canadian solid Earth sciences; *Geoscience Canada*, v. 31, p. 179–190.
- Bleeker, W. and Ernst, R.E., 2011. Does the Slave craton continue into southern Siberia: comparison of their large igneous province (LIP) records; *in* 39th Annual Yellowknife Geoscience Forum Abstracts, (comp.) B.J. Fischer and D.M. Watson; Northwest Territories Geoscience, YKGSF Abstracts, v. 2011, p. 22–23.
- Bleeker, W. and Hall, B., 2007. The Slave craton: geology and metallogenic evolution; *in* Mineral deposits of Canada: a synthesis of major deposit-types, district metallogeny, the evolution of geological provinces, and exploration methods, (ed.) W.D. Goodfellow; Geological Association of Canada, Mineral Deposits Division, Special Publication 5, p. 849–879.
- Bleeker, W. and Kamo, S.L., 2003. A precise age for the Duck Lake sill and its relevance for fitting the Slave in a global Archean context; 31st Yellowknife Geoscience Forum, Program and Abstracts, p. 7–8.
- Bleeker, W., Hamilton, M., and Söderlund, U., 2008a. Towards a complete magmatic event “barcode” for the Slave craton, II: the ca. 1884 Ma Ghost swarm; Geological Association of Canada-Mineralogical Association of Canada, Abstracts, v. 33, p. 23.
- Bleeker, W., Hamilton, M., Söderlund, U., and Ernst, R., 2008b. Towards a complete magmatic event “barcode” for the Slave craton, I: a precise U-Pb baddeleyite age for the Hearne swarm with implications for a newly recognized Paleoproterozoic LIP across the western Canadian Shield; Geological Association of Canada-Mineralogical Association of Canada, Abstracts, v. 33, p. 23.
- Bostock, H.H. and van Breemen, O., 1992. The timing of emplacement and distribution of the Sparrow diabase dyke swarm, District of Mackenzie, Northwest Territories; *in* Radiogenic age and isotopic studies, report 6; Geological Survey of Canada, Paper 92-2, p. 49–55.
- Bowers, N.E. and Chamberlain, K.R., 2006. Precambrian history of the eastern Ferris Mountains and Bear Mountain, south-central Wyoming Province; *Canadian Journal of Earth Sciences*, v. 43, p. 1467–1487. <https://doi.org/10.1139/e06-091>
- Bowring, S.A., 1985. U-Pb zircon geochronology of early Proterozoic Wopmay Orogen, N.W.T., Canada: an example of rapid crustal evolution; Ph.D. thesis, University of Kansas, Lawrence, Kansas, 148 p.
- Bowring, S.A. and Grotzinger, J.P., 1992. Implications of new chronostratigraphy for tectonic evolution of Wopmay Orogeny, northwest Canadian Shield; *American Journal of Science*, v. 292, p. 1–20. <https://doi.org/10.2475/ajs.292.1.1>
- Bowring, S.A. and Ross, G.M., 1985. Geochronology of the Narakay volcanic complex: implications for the age of the Coppermine Homocline and Mackenzie igneous events; *Canadian Journal of Earth Sciences*, v. 22, p. 774–781. <https://doi.org/10.1139/e85-082>
- Bowring, S.A., Van Schmus, R.W., and Hoffman, P.F., 1984. U-Pb zircon ages from Athapuscow aulacogen, East Arm of Great Slave Lake, N.W.T., Canada; *Canadian Journal of Earth Sciences*, v. 21, p. 1315–1324. <https://doi.org/10.1139/e84-136>
- Buchan, K.L., 2014. Reprint of “Key paleomagnetic poles and their use in Proterozoic continent and supercontinent reconstructions: a review”; *Precambrian Research*, v. 244, p. 5–22. <https://doi.org/10.1016/j.precamres.2014.01.010>
- Buchan, K.L. and Ernst, R.E., 2004. Diabase dyke swarms and related units in Canada and adjacent regions; Geological Survey of Canada, Map 2022A, scale 1:5 000 000. <https://doi.org/10.4095/214883>
- Buchan, K.L. and Ernst, R.E., 2013. Diabase dyke swarms of Nunavut, Northwest Territories and Yukon, Canada; Geological Survey of Canada, Open File 7464, 24 p., scale 1:3 000 000. <https://doi.org/10.4095/293149>
- Buchan, K.L. and Ernst, R.E., 2018. A giant circumferential dyke swarm associated with the High Arctic Large Igneous Province (HALIP); *Gondwana Research*, v. 58, p. 39–57. <https://doi.org/10.1016/j.gr.2018.02.006>
- Buchan, K.L. and Ernst, R.E., 2019. Giant circumferential dyke swarms: catalogue and characteristics; *in* Dyke swarms of the world: a modern perspective, (ed.) R.K. Srivastava, R.E. Ernst, and P. Peng; Springer Geology, Springer, Singapore, p. 1–44. https://doi.org/10.1007/978-981-13-1666-1_1

- Buchan, K.L., Neilson, D.J., and Hale, C.J., 1990. Relative age of Otto stock and Matachewan dykes from paleomagnetism and implications for the Precambrian polar wander path; *Canadian Journal of Earth Sciences*, v. 27, p. 915–922. <https://doi.org/10.1139/e90-094>
- Buchan, K.L., Mortensen, J.K., Card, K.D., and Percival, J.A., 1998. Paleomagnetism and U-Pb geochronology of diabase dyke swarms of Minto block, Superior Province, Quebec, Canada; *Canadian Journal of Earth Sciences*, v. 35, p. 1054–1069. <https://doi.org/10.1139/e98-054>
- Buchan, K.L., Ernst, R.E., Hamilton, M.A., Mertanen, S., Pesonen, L.J., and Elming, S.-Å., 2001. Rodinia: the evidence from integrated palaeomagnetism and U-Pb geochronology; *Precambrian Research*, v. 110, p. 9–32.
- Buchan, K.L., Goutier, J., Hamilton, M.A., Ernst, R.E., and Matthew, W., 2007. Paleomagnetism, U-Pb geochronology and geochemistry of Lac Esprit and other dyke swarms, James Bay area, Quebec, and implications for Paleoproterozoic deformation of the Superior Province; *Canadian Journal of Earth Sciences*, v. 44, p. 643–664. <https://doi.org/10.1139/e06-124>
- Buchan, K.L., LeCheminant, A.N., and van Breemen, O., 2009. Paleomagnetism and U-Pb geochronology of the Lac de Gras diabase dyke swarm, Slave Province, Canada: implications for relative drift of Slave and Superior provinces in the Paleoproterozoic; *Canadian Journal of Earth Sciences*, v. 46, p. 361–379. <https://doi.org/10.1139/E09-026>
- Buchan, K.L., Ernst, R.E., Bleeker, W., Davis, W.J., Villeneuve, M., van Breemen, O., Hamilton, M.A., and Söderlund, U., 2010. Proterozoic magmatic events of the Slave Craton, Wopmay Orogen and environs; Geological Survey of Canada, Open File 5985, 26 p. <https://doi.org/10.4095/285383>
- Buchan, K.L., LeCheminant, A.N., and van Breemen, O., 2012. Malley diabase dykes of the Slave craton, Canadian Shield: U-Pb age, paleomagnetism, and implications for continental reconstructions in the early Paleoproterozoic; *Canadian Journal of Earth Sciences*, v. 49, p. 435–454. <https://doi.org/10.1139/e11-061>
- Buchan, K.L., Mitchell, R.N., Bleeker, W., Hamilton, M.A., and LeCheminant, A.N., 2016. Paleomagnetism of ca. 2.13–2.11 Ga Indin and 1.885 Ga Ghost dyke swarms of the Slave craton: implications for the Slave craton APW path and relative drift of Slave, Superior and Siberian cratons in the Paleoproterozoic; *Precambrian Research*, v. 275, p. 151–175. <https://doi.org/10.1016/j.precamres.2016.01.012>
- Cavell, P.A. and Baadsgaard, H., 1986. Geochronology of the Big Spruce Lake alkaline intrusion; *Canadian Journal of Earth Sciences*, v. 23, p. 1–10. <https://doi.org/10.1139/e86-001>
- Chacko, T., De, S.K., Creaser, R.A., and Muehlenbachs, K., 2000. Tectonic setting of the Taltson magmatic zone at 1.9–2.0 Ga: a granitoid-based perspective; *Canadian Journal of Earth Sciences*, v. 37, p. 1597–1609. <https://doi.org/10.1139/e00-029>
- Chamalaun, F.H. and Dempsey, C.E., 1978. Palaeomagnetism of the Gawler Range volcanics and implications for the genesis of the Middleback hematite orebodies; *Journal of the Geological Society of Australia*, v. 25, p. 255–265. <https://doi.org/10.1080/00167617808729034>
- Christie, K.W., Davidson, A., and Fahrig, W.F., 1975. The paleomagnetism of Kaminak dikes - no evidence of significant Hudsonian plate motion; *Canadian Journal of Earth Sciences*, v. 12, p. 2048–2064. <https://doi.org/10.1139/e75-181>
- Ciborowski, T.J.R., Minifie, M.J., Kerr, A.C., Ernst, R.E., Baragar, B., and Millar, I.L., 2017. A mantle plume origin for the Palaeoproterozoic Circum-Superior Large Igneous Province; *Precambrian Research*, v. 294, p. 189–213. <https://doi.org/10.1016/j.precamres.2017.03.001>
- Clough, C.E. and Hamilton, M.A., 2017. Matachewan LIP revisited: a revised high-resolution U-Pb age for the East Bull Lake intrusion and associated units; *Geological Association of Canada–Mineralogical Association of Canada, Abstracts*, v. 40, p. 65.
- Cook, D.G. and MacLean, B.C., 1995. The intracratonic Paleoproterozoic Forward orogeny, and implications for regional correlations, Northwest Territories, Canada; *Canadian Journal of Earth Sciences*, v. 32, p. 1991–2008. <https://doi.org/10.1139/e95-152>
- Cook, F.A., Hall, K.W., and Lynn, C.E., 2005. The edge of northwestern North America at 1.8 Ga; *Canadian Journal of Earth Sciences*, v. 42, p. 983–997. <https://doi.org/10.1139/e05-039>
- Corrigan, D., Pehrsson, S., Wodicka, N., and de Kemp, E., 2009. The Palaeoproterozoic Trans-Hudson Orogen: a prototype of modern accretionary processes; *in* Ancient orogens and modern analogues, (ed.) J.B. Murphy, J.D. Keppie, and A. Hynes; Geological Society of London, Special Publication 327, p. 457–479. <https://doi.org/10.1144/SP327.19>
- Cousens, B.L., Aspler, L.B., Chiarenzelli, J.R., Donaldson, J.A., Sandeman, H., Peterson, T., and LeCheminant, A.N., 2001. Enriched Archean lithospheric mantle beneath western Churchill Province tapped during Paleoproterozoic orogenesis; *Geology*, v. 29, p. 827–830. [https://doi.org/10.1130/0091-7613\(2001\)029%3c0827:EALMBW%3e2.0.CO%3b2](https://doi.org/10.1130/0091-7613(2001)029%3c0827:EALMBW%3e2.0.CO%3b2)
- Davidson, A., 1970. Precambrian geology, Kaminak Lake map-area, District of Keewatin (55L); Geological Survey of Canada, Paper 69-51, 27 p. <https://doi.org/10.4095/100657>
- Davis, W.J. and Bleeker, W., 2007. New ages for Paleoproterozoic mafic intrusions in the western Slave Province and their potential relationship to tectonic events in the adjacent Wopmay Orogen; *Geological Association of Canada–Mineralogical Association of Canada, Abstracts*, v. 32, p. 20.
- Davis, W., Bleeker, W., Hulbert, L., and Jackson, V., 2004. New geochronological results from the Slave Province Minerals and Geoscience Compilation and Synthesis Project; *in* Geological Survey of Canada Northern Resources Program; 32nd Yellowknife Geoscience Forum, Abstracts of Talks and Posters, p. 20.
- Davis, W.J., Hanmer, S., Tella, S., Sandeman, H.A., and Ryan, J.J., 2006. U-Pb geochronology of the MacQuoid supracrustal belt and Cross Bay plutonic complex: key components of the northwestern Hearne subdomain, western Churchill Province, Nunavut, Canada; *Precambrian Research*, v. 145, p. 53–80. <https://doi.org/10.1016/j.precamres.2005.11.016>

- Davis, W.J., Ootes, L., Newton, L., Jackson, V., and Stern, R.A., 2015a. Characterization of the Paleoproterozoic Hottah terrane, Wopmay Orogen using multi-isotopic (U-Pb, Hf, O) detrital zircon analyses: an evaluation of linkages to northwest Laurentian Paleoproterozoic domains; *Precambrian Research*, v. 269, p. 296–310. <https://doi.org/10.1016/j.precamres.2015.08.012>
- Davis, W.J., Pehrsson, S.J., and Percival, J.A., 2015b. Results of a U-Pb zircon geochronology transect across the southern Rae craton, Northwest Territories, Canada; Geological Survey of Canada, Open File 7655, 74 p. <https://doi.org/10.4095/295610>.
- Didenko, A.N., Vodovozov, V.Y., Pisarevsky, S.A., Gladkochub, D.P., Donskaya, T.V., Mazukabzov, A.M., Stanevich, A.M., Bibikova, E.V., and Kirnozova, T.I., 2009. Palaeomagnetism and U-Pb dates of the Palaeoproterozoic Akitkan Group (South Siberia) and implications for pre-Neoproterozoic tectonics; *in* Palaeoproterozoic supercontinents and global evolution, (ed.) S.M. Reddy, R. Mazumder, D.A.D. Evans, and A.S. Collins; Geological Society of London, Special Publication 323, p. 145–163. <https://doi.org/10.1144/SP323.7>
- Eade, K.E., 1986. Precambrian geology of the Tulemalu Lake–Yathkyed Lake area, District of Keewatin; Geological Survey of Canada, Paper 84-11, 31 p. <https://doi.org/10.4095/120589>
- Easton, R.M., Davidson, A., and Murphy, E.I., 1999. Transects across the Southern-Grenville Province Boundary near Sudbury, Ontario; Guidebook #A2, Sudbury 1999, Geological Association of Canada, 52 p.
- Ernst, R.E., 2014. Large igneous provinces; Cambridge University Press, Cambridge, United Kingdom, 653 p. <https://doi.org/10.1017/CBO9781139025300>
- Ernst, R.E. and Bleeker, W., 2010. Large igneous provinces (LIPs), giant dyke swarms, and mantle plumes: significance for breakup events within Canada and adjacent regions from 2.5 Ga to the Present; *Canadian Journal of Earth Sciences*, v. 47, p. 695–739. <https://doi.org/10.1139/E10-025>
- Ernst, R.E. and Buchan, K.L., 2004. Igneous rock associations in Canada 3. Large igneous provinces (LIPs) in Canada and adjacent regions: 3 Ga to present; *Geoscience Canada*, v. 31, p. 103–126.
- Ernst, R.E., Buchan, K.L., and Palmer, H.C., 1995. Giant dyke swarms: characteristics, distribution and geotectonic applications; *in* Physics and chemistry of dykes, (ed.) G. Baer and A. Heimann; Balkema, Rotterdam, Netherlands, p. 3–21.
- Ernst, R.E., Hamilton, M.A., Söderlund, U., Hanes, J.A., Gladkochub, D.P., Okrugoin, A.V., Kolotilina, T., Mekhonoshin, A.S., Bleeker, W., LeCheminant, A.N., Buchan, K.L., Chamberlain, K.R., and Didenko, A.N., 2016. Long-lived connection between southern Siberia and northern Laurentia in the Proterozoic; *Nature Geoscience*, v. 9, p. 464–469. <https://doi.org/10.1038/ngeo2700>
- Evans, D.A.D. and Halls, H.C., 2010. Restoring Proterozoic deformation within the Superior craton; *Precambrian Research*, v. 183, p. 474–489. <https://doi.org/10.1016/j.precamres.2010.02.007>
- Evans, D.A.D. and Mitchell, R.N., 2011. Assembly and breakup of the core of Paleoproterozoic–Mesoproterozoic supercontinent Nuna; *Geology*, v. 39, p. 443–446.
- Evans, D.A.D. and Pisarevsky, S.A., 2008. Plate tectonics on early Earth? Weighing the paleomagnetic evidence; *in* When did plate tectonics begin on planet Earth?, (ed.) K.C. Condie and V. Pease; Geological Society of America, Special Paper 440, p. 249–263. [https://doi.org/10.1130/2008.2440\(12\)](https://doi.org/10.1130/2008.2440(12))
- Fahrig, W.F., Christie, K.W., Eade, K.E., and Tella, S., 1984. Paleomagnetism of the Tulemalu dykes, Northwest Territories, Canada; *Canadian Journal of Earth Sciences*, v. 21, p. 544–553. <https://doi.org/10.1139/e84-059>
- Fahrig, W.F., Christie, K.W., Chown, E.H., Janes, D., and Machado, N., 1986. The tectonic significance of some basic dyke swarms in the Canadian Superior Province with special reference to the geochemistry and paleomagnetism of the Mistassini swarm, Quebec, Canada; *Canadian Journal of Earth Sciences*, v. 23, p. 238–253. <https://doi.org/10.1139/e86-026>
- Flowers, R.M., Bowring, S.A., and Williams, M.L., 2006. Timescales and significance of high-pressure, high-temperature metamorphism and mafic dike anatexis, Snowbird tectonic zone, Canada; *Contributions to Mineralogy and Petrology*, v. 151, p. 558–581. <https://doi.org/10.1007/s00410-006-0066-7>
- French, J.E. and Heaman, L.M., 2010. Precise U-Pb dating of Paleoproterozoic mafic dyke swarms of the Dharwar craton, India: implications for the existence of the Neoproterozoic supercraton Slavia; *Precambrian Research*, v. 183, p. 416–441. <https://doi.org/10.1016/j.precamres.2010.05.003>
- Furlanetto, F., Thorkelson, D.J., Davis, W.J., Gibson, H.D., Marshall, D.D., Rainbird, R.H., Davis, W.J., Crowley, J.L., and Vervoort, J.D., 2013. Late Paleoproterozoic terrane accretion in northwestern Canada and the case for circum-Columbian orogenesis; *Precambrian Research*, v. 224, p. 512–528. <https://doi.org/10.1016/j.precamres.2012.10.010>
- Furlanetto, F., Thorkelson, D.J., Rainbird, R.H., Davis, W.J., Gibson, H.D., and Marshall, D.D., 2016. The Paleoproterozoic Wernecke Supergroup of Yukon, Canada: relationships to orogeny in northwestern Laurentia and basins in North America, East Australia, and China; *Gondwana Research*, v. 39, p. 14–40. <https://doi.org/10.1016/j.gr.2016.06.007>
- Gandhi, S.S., Mortensen, J.K., Prasad, N., and van Breemen, O., 2001. Magmatic evolution of the southern Great Bear continental arc, northwestern Canadian Shield: geochronological constraints; *Canadian Journal of Earth Sciences*, v. 38, p. 767–785. <https://doi.org/10.1139/e00-094>
- Gumsley, A.P., Chamberlain, K.R., Bleeker, W., Söderlund, U., de Kock, M.O., Larsson, E.R., and Bekker, A., 2017. Timing and tempo of the Great Oxidation Event; *National Academy of Sciences of the United States of America, Proceedings*, v. 114, p. 1811–1816. <https://doi.org/10.1073/pnas.1608824114>
- Halls, H.C., Davis, D.W., Stott, G.M., Ernst, R.E., and Hamilton, M.A., 2008. The Paleoproterozoic Marathon large igneous province: new evidence for a 2.1 Ga long-lived mantle plume event along the southern margin of the North American Superior Province; *Precambrian Research*, v. 162, p. 327–353. <https://doi.org/10.1016/j.precamres.2007.10.009>
- Hamilton, M.A., 2009. Datation isotopique (U-Pb) d'un diabase de l'essai de dykes Mistassini, Québec – U-Pb isotopic dating of a diabase dyke of the Mistassini swarm, Quebec; Ministère des Ressources naturelles et de la Faune du Québec, Rapport GM 65972, 13 p.

- Hamilton, M.A. and Buchan, K.L., 2010. U-Pb geochronology of the Western Channel diabase, northwestern Laurentia: implications for a large 1.59 Ga magmatic province, Laurentia's APWP and paleocontinental reconstructions of Laurentia, Baltica and Gawler craton of southern Australia; *Precambrian Research*, v. 183, p. 463–473. <https://doi.org/10.1016/j.precamres.2010.06.009>
- Hamilton, M.A., Walsh, N.J., Bleeker, W., and Halls, H.C., 2017. Matachewan dyke swarm: new high-resolution U-Pb studies refine the emplacement chronology of the Matachewan LIP; *Geological Association of Canada–Mineralogical Association of Canada, Abstracts*, v. 40, p. 141.
- Hanmer, S., Williams, M., and Kopf, C., 1995. Striding–Athabasca mylonite zone: implications for the Archean and early Proterozoic tectonics of the western Canadian Shield; *Canadian Journal of Earth Sciences*, v. 32, p. 178–196. <https://doi.org/10.1139/e95-015>
- Harlan, S.S., Geissman, J.W., and Snee, L.W., 2008. Paleomagnetism of Proterozoic mafic dikes from the Tobacco Root Mountains, southwest Montana; *Precambrian Research*, v. 163, p. 239–264. <https://doi.org/10.1016/j.precamres.2007.12.002>
- Heaman, L.M. and LeCheminant, A.N., 1993. Paragenesis and U-Pb systematics of baddeleyite (ZrO₂); *Chemical Geology*, v. 110, p. 95–126. [https://doi.org/10.1016/0009-2541\(93\)90249-1](https://doi.org/10.1016/0009-2541(93)90249-1)
- Henderson, J.R. and Parrish, R.R., 1992. Geochronology and structural geology of the early Proterozoic Foxe–Rinkian Orogen, Baffin Island, N.W.T.; *Geological Survey of Canada, Current Activities Forum, Program with Abstracts*, p. 12.
- Hildebrand, R.S. and Bowring, S.A., 1999. Crustal recycling by slab failure; *Geology*, v. 27, p. 11–14. [https://doi.org/10.1130/0091-7613\(1999\)027%3c0011:CRBSF%3e2.3.CO%3b2](https://doi.org/10.1130/0091-7613(1999)027%3c0011:CRBSF%3e2.3.CO%3b2)
- Hildebrand, R.S., Bowring, S.A., Steer, M.E., and Van Schmus, W.R., 1983. Geology and U-Pb geochronology of parts of the Leith Peninsula and Rivière Grandin map areas, District of Mackenzie; *in Current Research, Part A; Geological Survey of Canada, Paper 83-1A*, p. 329–342. <https://doi.org/10.4095/111502>
- Hildebrand, R.S., Hoffman, P.F., and Bowring, S., 1987. Tectono-magmatic evolution of the 1.9 Ga Great Bear magmatic zone, Wopmay orogeny northwestern Canada; *Journal of Volcanology and Geothermal Research*, v. 32, p. 99–118. [https://doi.org/10.1016/0377-0273\(87\)90039-4](https://doi.org/10.1016/0377-0273(87)90039-4)
- Hildebrand, R.S., Hoffman, P.F., and Bowring, S.A., 2010a. The Calderian orogeny in Wopmay Orogen (1.9 Ga), northwestern Canadian Shield; *Geological Society of America, Bulletin*, v. 122, p. 794–814. <https://doi.org/10.1130/B26521.1>
- Hildebrand, R.S., Hoffman, P.F., Housh, T., and Bowring, S.A., 2010b. The nature of volcano-plutonic relations and the shapes of epizonal plutons of continental arcs as revealed in the Great Bear magmatic zone, northwestern Canada; *Geosphere*, v. 6, p. 812–839. <https://doi.org/10.1130/GES00533.1>
- Hoffman, P.F., 1973a. Apehbian supracrustal rocks of the Athapuscow aulacogen, East Arm of Great Slave Lake, District of Mackenzie; *in Report of Activities, Part A; Geological Survey of Canada, Paper 73-1A*, p. 151–156. <https://doi.org/10.4095/105151>
- Hoffman, P.F., 1973b. Evolution of an early Proterozoic continental margin: the Coronation geosyncline and associated aulacogens of the northwestern Canadian Shield; *Royal Society of London, Philosophical Transactions*, ser. A, v. 273, p. 547–581. <https://doi.org/10.1098/rsta.1973.0017>
- Hoffman, P.F., 1987. Continental transform tectonics: Great Slave Lake shear zone (ca. 1.9 Ga), northwest Canada; *Geology*, v. 15, p. 785–788. [https://doi.org/10.1130/0091-7613\(1987\)15%3c785:CTTGSL%3e2.0.CO%3b2](https://doi.org/10.1130/0091-7613(1987)15%3c785:CTTGSL%3e2.0.CO%3b2)
- Hoffman, P.F., 1988. United plates of America, the birth of a craton: early Proterozoic assembly and growth of Laurentia; *Annual Review of Earth and Planetary Sciences*, v. 16, p. 543–603. <https://doi.org/10.1146/annurev.ea.16.050188.002551>
- Hoffman, P.F., 1996. Geology, northern externides of Wopmay Orogen, District of Mackenzie, Northwest Territories; *Geological Survey of Canada, Open File 3251*, scale 1:250 000. <https://doi.org/10.4095/207791>
- Hoffman, P.F. and Bowring, S.A., 1984. Short-lived 1.9 Ga continental margin and its destruction, Wopmay Orogen, northwest Canada; *Geology*, v. 12, p. 68–72. [https://doi.org/10.1130/0091-7613\(1984\)12%3c68:SGCMAI%3e2.0.CO%3b2](https://doi.org/10.1130/0091-7613(1984)12%3c68:SGCMAI%3e2.0.CO%3b2)
- Hoffman, P.F. and Hall, L., 1993. Geology, Slave Craton and environs, District of Mackenzie, Northwest Territories; *Geological Survey of Canada, Open File 2559*, scale 1:1 000 000. <https://doi.org/10.4095/183951>
- Hoffman, P.F. and McGlynn, J.C., 1977. Great Bear batholith: a volcano-plutonic depression; *in Volcanic regimes in Canada*, (ed.) W.R.A. Baragar, L.C. Coleman, and J.M. Hall; *Geological Association of Canada, Special Paper 16*, p. 170–192.
- Hoffman, P.F., Bell, I.R., Hildebrand, R.S., and Thorstad, L., 1977. Geology of the Athapuscow aulacogen, East Arm of Great Slave Lake, District of Mackenzie; *in Report of Activities, Part A; Geological Survey of Canada, Paper 77-1A*, p. 117–129. <https://doi.org/10.4095/102669>
- Hoffman, P.F., Bowring, S.A., Buchwaldt, R., and Hildebrand, R.S., 2011. Birthdate for the Coronation paleocean: age of initial rifting in Wopmay Orogen, Canada; *Canadian Journal of Earth Sciences*, v. 48, p. 281–293. <https://doi.org/10.1139/E10-038>
- Irving, E., Donaldson, J.A., and Park, J.K., 1972. Paleomagnetism of the Western Channel diabase and associated rocks, Northwest Territories; *Canadian Journal of Earth Sciences*, v. 9, p. 960–971. <https://doi.org/10.1139/e72-080>
- Irving, E., Baker, J., Hamilton, M., and Wynne, P.J., 2004. Early Proterozoic geomagnetic field in western Laurentia: implications for paleolatitudes, local rotations and stratigraphy; *Precambrian Research*, v. 129, p. 251–270. <https://doi.org/10.1016/j.precamres.2003.10.002>
- Jackson, G.D. and Berman, R.G., 2000. Precambrian metamorphic and tectonic evolution of northern Baffin Island, Nunavut, Canada; *Canadian Mineralogist*, v. 38, p. 399–421. <https://doi.org/10.2113/gscanmin.38.2.399>
- Johns, S.M., Helmstaedt, H.H., and Kyser, T.K., 2006. Paleoproterozoic submarine intrabasinal rifting, Baffin Island, Nunavut, Canada: volcanic structure and geochemistry of the Bravo Lake Formation; *Canadian Journal of Earth Sciences*, v. 43, p. 593–616. <https://doi.org/10.1139/e06-009>

- Johnson, B.J., 1990. Stratigraphy and structure of the early Proterozoic Wilson Island Group, East Arm thrust-fold belt, N.W.T.; *Canadian Journal of Earth Sciences*, v. 27, p. 552–569. <https://doi.org/10.1139/e90-052>
- Lalonde, A.E., 1989. Hepburn intrusive suite: peraluminous plutonism within a closing back-arc basin, Wopmay Orogen, Canada; *Geology*, v. 17, p. 261–264. [https://doi.org/10.1130/0091-7613\(1989\)017%3c0261:HISPPW%3e2.3.CO%3b2](https://doi.org/10.1130/0091-7613(1989)017%3c0261:HISPPW%3e2.3.CO%3b2)
- LeCheminant, A.N. and van Breemen, O., 1994. U-Pb ages of Proterozoic dyke swarms, Lac de Gras area, N.W.T.: evidence for progressive break-up of an Archean supercontinent; *Geological Association of Canada–Mineralogical Association of Canada; Program with Abstracts*, v. 19, p. A62.
- LeCheminant, A.N., Heaman, L.M., van Breemen, O., Ernst, R.E., Baragar, W.R.A., and Buchan, K.L., 1996a. Mafic magmatism, mantle roots, and kimberlites in the Slave craton; *in* Searching for diamonds in Canada, (ed.) A.N. LeCheminant, D.G. Richardson, R.N.W. DiLabio, and K.A. Richardson; Geological Survey of Canada, Open File 3228, p. 161–169. <https://doi.org/10.4095/208202>
- LeCheminant, A.N., Rainbird, R.H., and Villeneuve, M.E., 1996b. Precambrian geology of northern Wellington Inlier, Victoria Island, Northwest Territories; *in* Current Research 1996-C; Geological Survey of Canada, p. 1–10. <https://doi.org/10.4095/207438>
- LeCheminant, A.N., Buchan, K.L., van Breemen, O., and Heaman, L.M., 1997. Paleoproterozoic continental break-up and reassembly: evidence from 2.19 Ga diabase dyke swarms in the Slave and Western Churchill Provinces, Canada; *Geological Association of Canada–Mineralogical Association of Canada, Abstracts*, v. 22, p. A-86.
- Liikane, D.A., St-Onge, M.R., Kjarsgaard, B.A., Rayner, N.M., Ernst, R.E., and Kastek, N., 2015. Frobisher suite mafic, ultramafic and layered mafic-ultramafic sills, southern Baffin Island, Nunavut; *in* Summary of Activities 2015; Canada-Nunavut Geoscience Office, p. 21–32.
- Maurice, C., David, J., O’Neil, J., and Francis, D., 2009. Age and tectonic implications of Paleoproterozoic mafic dyke swarms for the origin of 2.2 Ga enriched lithosphere beneath the Ungava Peninsula, Canada; *Precambrian Research*, v. 174, p. 163–180. <https://doi.org/10.1016/j.precamres.2009.07.007>
- McDonough, M.R., McNicoll, V.J., Schetselaar, E.M., and Grover, T.W., 2000. Geochronological and kinematic constraints on crustal shortening and escape in a two-sided oblique-slip collisional and magmatic orogeny, Paleoproterozoic Taltson magmatic zone, northeastern Alberta; *Canadian Journal of Earth Sciences*, v. 37, p. 1549–1573. <https://doi.org/10.1139/e00-089>
- McGlynn, J.C. and Irving, E., 1975. Paleomagnetism of Early Archean diabase dykes from the Slave Structural Province, Canada; *Tectonophysics*, v. 26, p. 23–38. [https://doi.org/10.1016/0040-1951\(75\)90111-0](https://doi.org/10.1016/0040-1951(75)90111-0)
- Mitchell, R.N., Bleeker, W., van Breemen, O., LeCheminant, T.N., Peng, P., Nilsson, M.K.M., and Evans, D.A.D., 2014. Plate tectonics before 2.0 Ga: evidence from paleomagnetism of cratons within supercontinent Nuna; *American Journal of Science*, v. 314, p. 878–894. <https://doi.org/10.2475/04.2014.03>
- Morelli, R.M., Hartlaub, R.P., Ashton, K.E., and Ansdell, K.M., 2009. Evidence for enrichment of subcontinental lithospheric mantle from Paleoproterozoic intracratonic magmas: geochemistry and U-Pb geochronology of Martin Group igneous rocks, western Rae craton, Canada; *Precambrian Research*, v. 175, p. 1–15. <https://doi.org/10.1016/j.precamres.2009.04.005>
- Mowbray, B. and Pehrsson, S.J., 2019. Geochemistry, petrology, and aeromagnetic mapping of the Orpheus dykes, south Rae Craton, Northwest Territories; Geological Survey of Canada, Open File 8340, 28 p. <https://doi.org/10.4095/311306>
- Mumford, T.R. and Cousens, B.L., 2014. Constraints on the relationship between Paleoproterozoic intrusions and dyke swarms, East Arm of Great Slave Lake, N.W.T., Canada; *Canadian Journal of Earth Sciences*, v. 51, p. 419–438. <https://doi.org/10.1139/cjes-2013-0124>
- Ootes, L., Davis, W.J., Jackson, V.A., and van Breemen, O., 2015. Chronostratigraphy of the Hottah terrane and Great Bear magmatic zone of Wopmay Orogen, Canada, and exploration of a terrane translation model; *Canadian Journal of Earth Sciences*, v. 52, p. 1062–1092. <https://doi.org/10.1139/cjes-2015-0026>
- Ootes, L., Jackson, V.A., Davis, W.J., Bennett, V., Smar, L., and Cousens, B.L., 2017. Parentage of Archean basement within a Paleoproterozoic orogen and implications for on-craton diamond preservation: Slave craton and Wopmay Orogen, northwest Canada; *Canadian Journal of Earth Sciences*, v. 54, p. 203–232. <https://doi.org/10.1139/cjes-2016-0059>
- Pehrsson, S.J., van Breemen, O., and Hanmer, S., 1993. Ages of diabase dyke intrusions, Great Slave Lake shear zone, Northwest Territories; *in* Radiogenic age and isotopic studies, report 7; Geological Survey of Canada, Paper 93-2, p. 23–28. <https://doi.org/10.4095/193330>
- Pehrsson, S.J., Berman, R.G., Eglinton, B., and Rainbird, R., 2013. Two Neoproterozoic supercontinents revisited: the case for a Rae family of cratons; *Precambrian Research*, v. 232, p. 27–43. <https://doi.org/10.1016/j.precamres.2013.02.005>
- Pehrsson, S.J., Currie, M., Ashton, K.E., Harper, C.T., Paul, D., Pana, D., Berman, R.G., Bostock, H., Corkery, T., Jefferson, C.W., and Tella, S., 2014. Bedrock geology compilation and regional synthesis of south Rae and parts of Hearne domains, Churchill Province, Northwest Territories, Saskatchewan, Nunavut, Manitoba, and Alberta; Geological Survey of Canada, Open File 5744, scale 1:550 000. <https://doi.org/10.4095/292232>
- Pehrsson, S.J., Eglinton, B.M., Evans, D.A.D., Huston, D., and Reddy, S.M., 2016. Metallogeny and its link to orogenic style during the Nuna supercontinent cycle; *in* Supercontinent cycles through Earth history, (ed.) Z.X. Li, D.A.D. Evans, and J.B. Murphy; Geological Society of London, Special Publication 424, p. 83–94. <https://doi.org/10.1144/SP424.5>
- Pehrsson, S., Regis, D., Knox, B., Smit, M.A., Davis, W.J., Hamilton, M., Berman, R., Ashton, K., and Buchan, K.L., 2019. Snowbird tectonic zone: problem child of Nuna; *Geological Society of America, Annual Meeting*, September 22–25, 2019, Phoenix, Arizona, Paper No. 215-14. <https://doi.org/10.1130/abs/2019AM-336677>

- Percival, J.A., Davis, W.J., and Hamilton, M.A., 2017. U-Pb zircon geochronology and depositional history of the Montesor Group, Rae Province, Nunavut, Canada; *Canadian Journal of Earth Sciences*, v. 54, p. 512–528. <https://doi.org/10.1139/cjes-2016-0170>
- Peterson, T.D., Scott, J.M.J., LeCheminant, A.N., Jefferson, C.W., and Pehrsson, S.J., 2015a. The Kivalliq Igneous Suite: anorogenic bimodal magmatism at 1.75 Ga in the western Churchill Province, Canada; *Precambrian Research*, v. 262, p. 101–119. <https://doi.org/10.1016/j.precamres.2015.02.019>
- Peterson, T.D., Scott, J.M.J., LeCheminant, A.N., Tschirhart, V., Chorlton, L., Davis, W., and Hamilton, M.A., 2015b. Nueltin granites and mafic rocks in the Tebesjuak Lake (NTS 650) map area: new geochronological, petrological, and geophysical data; *Geological Survey of Canada, Current Research 2015-5*, 19 p. <https://doi.org/10.4095/296163>
- Rainbird, R.H. and Davis, W.J., 2007. U–Pb detrital zircon geochronology and provenance of the late Paleoproterozoic Dubawnt Supergroup: linking sedimentation with tectonic reworking of the western Churchill Province, Canada; *Geological Society of America, Bulletin*, v. 119, p. 314–328. <https://doi.org/10.1130/B25989.1>
- Rainbird, R.H. and LeCheminant, A.N., 2002. Geology, northern Wellington Inlier, Washburn Lake area, Nunavut; *Geological Survey of Canada, Open File 4263*, scale 1:50 000. <https://doi.org/10.4095/213227>
- Rainbird, R.H., Stern, R.A., Khudoley, A.K., Kropachev, A.P., Heaman, L.M., and Sukhorukov, V.I., 1998. U-Pb geochronology of Riphean sandstone and gabbro from southeast Siberia and its bearing on the Laurentia–Siberia connection; *Earth and Planetary Science Letters*, v. 164, p. 409–420.
- Rainbird, R.H., Davis, W.J., Stern, R.A., Peterson, T.D., Smith, S.R., Parrish, R.R., and Hadlari, T., 2006. Ar–Ar and U–Pb geochronology of a late Paleoproterozoic rift basin: support for a genetic link with Hudsonian orogenesis, western Churchill Province, Nunavut, Canada; *The Journal of Geology*, v. 114, p. 1–17. <https://doi.org/10.1086/498097>
- Rainbird, R.H., Davis, W.J., Pehrsson, S.J., Wodicka, N., Rayner, N., and Skulski, T., 2010. Early Paleoproterozoic supracrustal assemblages of the Rae domain, Nunavut, Canada: intracratonic basin development during supercontinent break-up and assembly; *Precambrian Research*, v. 181, p. 167–186. <https://doi.org/10.1016/j.precamres.2010.06.005>
- Raub, T.M.D., 2008. Paleomagnetism of Dubawnt Supergroup, Baker Lake basin, Nunavut, Canada: refining Laurentia’s Paleoproterozoic apparent polar wander path; Ph.D. thesis, Yale University, New Haven, Connecticut, 437 p.
- Regan, S.P., Grohn, L.J., Williams, M.L., Chiarenzelli, J., Jercinovic, M., Cousens, B.L., Aspler, L.B., and Mahan, K.H., 2017. The Snowbird tectonic zone LIP; implications for an aborted rift origin; GSA Annual Meeting, January 22–25, 2017, Seattle, Washington; *Geological Society of America, Abstracts with Programs*, v. 49, no. 6, Paper 238-3. <https://doi.org/10.1130/abs/2017AM-302135>
- Reichenbach, I.G., 1991. The Bell Island Bay Group, remnant of an early Proterozoic ensialic marginal basin in Wopmay orogen, District of Mackenzie; *Geological Survey of Canada, Paper 88-28*, 43 p. <https://doi.org/10.4095/131925>
- Rogers, C., Kamo, S.L., Söderlund, U., Hamilton, M.A., Ernst, R.E., Cousens, B., Harlan, S.S., Wade, C.E., and Thorkelson, D.J., 2018. Geochemistry and U-Pb geochronology of 1590 and 1550 Ma mafic dyke swarms of western Laurentia: mantle plume magmatism shared with Australia; *Lithos*, v. 314–315, p. 216–235. <https://doi.org/10.1016/j.lithos.2018.06.002>
- Roscoe, S.M., Henderson, M.N., Hunt, P.A., and van Breemen, O., 1987. U-Pb zircon age of an alkaline granite body in the Booth River intrusive suite, N.W.T.; *in* Radiogenic age and isotopic studies, report 1, Geological Survey of Canada, Paper 87-2, p. 95–100. <https://doi.org/10.4095/122753>
- Ross, G.M., 1986. Eruptive style and construction of shallow marine mafic tuff cones in the Narakay Volcanic Complex (Proterozoic, Hornby Bay Group, Northwest Territories, Canada); *Journal of Volcanology and Geothermal Research*, v. 27, p. 265–297. [https://doi.org/10.1016/0377-0273\(86\)90017-X](https://doi.org/10.1016/0377-0273(86)90017-X)
- Ryan, J.J., Nadeau, L., Hinchey, A.M., James, D.T., Young, M.D., Williams, S.P., and Schetselaar, E.M., 2008. Geology, southern Boothia mainland area, Pelly Bay–Rae Strait–Harrison Island map area, Nunavut; *Geological Survey of Canada, Open File 5808*, scale 1:250 000. <https://doi.org/10.4095/225401>
- Sahin, T. and Hamilton, M.A., 2019. New U-Pb baddeleyite ages for Neoproterozoic and Paleoproterozoic mafic dyke swarms of the southern Nain Province, Labrador: implications for possible plate reconstructions involving the North Atlantic craton; *Precambrian Research*, v. 329, p. 44–69. <https://doi.org/10.1016/j.precamres.2019.02.001>
- Sanborn-Barrie, M., Carr, S.D., and Thériault, R., 2001. Geochronological constraints on metamorphism, magmatism and exhumation of deep-crustal rocks of the Kramanitar complex, with implications for the Paleoproterozoic evolution of the Archean western Churchill Province, Canada; *Contributions to Mineralogy and Petrology*, v. 141, p. 592–612. <https://doi.org/10.1007/s004100100262>
- Sandeman, H.A. and Ryan, J.J., 2008. The Spi Lake Formation of the central Hearne domain of the western Churchill Province, Canada: an axial intracratonic continental tholeiite trough above the co-genetic Kaminak dyke swarm; *Canadian Journal of Earth Sciences*, v. 45, p. 745–767. <https://doi.org/10.1139/E08-015>
- Sandeman, H.A., Heaman, L.M., and LeCheminant, A.N., 2013. The Paleoproterozoic Kaminak dykes, Hearne craton, western Churchill Province, Nunavut, Canada: preliminary constraints on their age and petrogenesis; *Precambrian Research*, v. 232, p. 119–139. <https://doi.org/10.1016/j.precamres.2012.06.002>
- Schmidt, P.W. and Clark, D.A., 1992. Magnetic properties of Archean and Proterozoic rocks from the Eyre Peninsula; Commonwealth Scientific and Industrial Research Organization, Australia, Division of Exploration Geoscience, Restricted Report 275R, 57 p.
- Schmidt, P.W. and Clark, D.A., 2011. Magnetic characteristics of the Hiltaba Suite granitoids and volcanics: Late Devonian overprinting and related thermal history of the Gawler craton; *Australian Journal of Earth Sciences*, v. 58, p. 361–374. <https://doi.org/10.1080/08120099.2010.549239>

- Schultz, M.E.J., Chacko, T., Heaman, L.M., Sandeman, H.A., Simonetti, A., and Creaser, R.A., 2007a. Queen Maud block: a newly recognized Paleoproterozoic (2.4–2.5 Ga) terrane in northwest Laurentia; *Geology*, v. 35, p. 707–710. <https://doi.org/10.1130/G23629A.1>
- Schultz, M.E.J., Chacko, T., Heaman, L.M., and Sandeman, H.A., 2007b. The Queen Maud block — refining Paleoproterozoic assembly of northwestern Laurentia; *Geological Association of Canada–Mineralogical Association of Canada, Abstracts*, v. 32, p. 73.
- Schultz, M.E.J., Chacko, T., Heaman, L.M., Sandeman, H., and Creaser, R.A., 2010. 2.46 to 2.50 Ga magmatism in the Queen Maud block, northern Canada: an early phase of the Arrowsmith orogeny or a separate rifting event preceding orogeny?; *GeoCanada 2010 Working with the Earth*, May 10–14, 2010, Calgary, Alberta, Abstract 513.
- Sheen, A.I., Heaman, L.M., Kjarsgaard, B., Ootes, L., Pearson, D.G., and Creaser, R.A., 2019. Athapuscow aulacogen revisited: geochronology and geochemistry of the 2046 Ma Union Island Group mafic magmatism, East Arm of Great Slave Lake, Northwest Territories, Canada; *Precambrian Research*, v. 321, p. 85–102. <https://doi.org/10.1016/j.precamres.2018.11.012>
- Sinclair, W.D., Hunt, P.A., and Birkett, T.C., 1994. U-Pb zircon and monzonite ages of the Grace Lake granite, Blatchford Lake intrusive suite, Slave Province, Northwest Territories; *in Radiogenic age and isotopic studies, report 8; Geological Survey of Canada, Current Research 1994-F*, p. 15–20. <https://doi.org/10.4095/195166>
- Skulski, T., Paul, D., Sandeman, H., Berman, R.G., Chorlton, L., Pehrsson, S.J., Rainbird, R.H., Davis, W.J., and Sanborn-Barrie, M., 2018. Bedrock geology, central Rae craton and eastern Queen Maud block, western Churchill Province, Nunavut; *Geological Survey of Canada, Canadian Geoscience Map 307*, scale 1: 550 000. <https://doi.org/10.4095/308348>
- Snyder, D.B. and Kjarsgaard, B.A., 2013. Mantle roots of major Precambrian shear zones inferred from structure of the Great Slave Lake shear zone, northwest Canada; *Lithosphere*, v. 5, p. 539–546. <https://doi.org/10.1130/L299.1>
- St-Onge, M.R., Scott, D.J., and Lucas, S.B., 2000. Early partitioning of Quebec: microcontinent formation in the Paleoproterozoic; *Geology*, v. 28, p. 323–326. [https://doi.org/10.1130/0091-7613\(2000\)28%3c323:EPOQMF%3e2.0.CO%3b2](https://doi.org/10.1130/0091-7613(2000)28%3c323:EPOQMF%3e2.0.CO%3b2)
- St-Onge, M.R., Searle, M.P., and Wodicka, N., 2006. Trans-Hudson Orogen of North America and Himalaya-Karakorum-Tibetan Orogen of Asia: structural and thermal characteristics of the lower and upper plates; *Tectonics*, v. 25, cit. no. TC4006, 22 p. <https://doi.org/10.1029/2005TC001907>
- Stubley, M.P., 2005. Slave craton: interpretive bedrock compilation NWT-NU; Northwest Territories Geoscience Office, Open File 2005-01, digital files and 2 maps.
- Tella, S., Hanmer, S., Sandeman, H.A., Ryan, J.J., Mills, A., Davis, W.J., Berman, R.G., Wilkinson, L., and Kerswill, J.A., 2001. Geology, MacQuoid Lake–Gibson Lake–Akunak Bay area, Nunavut; *Geological Survey of Canada, Map 2008A*, scale 1:100 000. <https://doi.org/10.4095/212827>
- Tella, S., Paul, D., Berman, R.G., Davis, W.J., Peterson, T.D., Pehrsson, S.J., and Kerswill, J.A., 2007. Bedrock geology compilation and regional synthesis of parts of Hearne and Rae domains, western Churchill Province, Nunavut–Manitoba; *Geological Survey of Canada, Open File 5441*, scale 1:550 000. <https://doi.org/10.4095/224573>
- Thorkelson, D.J. and Laughton, J.R., 2016. Paleoproterozoic closure of an Australia–Laurentia seaway revealed by megaclasts of an obducted volcanic arc in Yukon, Canada; *Gondwana Research*, v. 33, p. 115–133. <https://doi.org/10.1016/j.gr.2015.01.004>
- Thorkelson, D.J., Mortensen, J.K., Creaser, R.A., Davidson, G.J., and Abbott, G., 2001a. Early Proterozoic magmatism in Yukon, Canada: constraints on the evolution of northwestern Laurentia; *Canadian Journal of Earth Sciences*, v. 38, p. 1479–1494. <https://doi.org/10.1139/e01-032>
- Thorkelson, D.J., Mortensen, J.K., Davidson, G.J., Creaser, R.A., Perez, W.A., and Abbott, G., 2001b. Early Mesoproterozoic intrusive breccias in Yukon, Canada: the role of hydrothermal systems in reconstructions of North America and Australia; *Precambrian Research*, v. 111, p. 31–55. [https://doi.org/10.1016/S0301-9268\(01\)00155-3](https://doi.org/10.1016/S0301-9268(01)00155-3)
- Tirru, R. and Grotzinger, J.P., 1990. Early Proterozoic collisional orogeny along the northern Thelon Tectonic Zone, Northwest Territories, Canada: evidence from the foreland; *Tectonics*, v. 9, p. 1015–1036. <https://doi.org/10.1029/TC009i005p01015>
- van Breemen, O., Peterson, T.D., and Sandeman, H.A., 2005. U-Pb zircon geochronology and Nd isotope geochemistry of Proterozoic granitoids in the western Churchill Province: intrusive age pattern and Archean source domains; *Canadian Journal of Earth Sciences*, v. 42, p. 339–377. <https://doi.org/10.1139/e05-007>
- Villeneuve, M.E. and van Breemen, O., 1994. A compilation of U-Pb age data for the Slave Province, Northwest Territories; *Geological Survey of Canada, Open File 2972*, 53 p. <https://doi.org/10.4095/194790>
- Wanless, R.K., Stevens, R.D., Lachance, G.R., and Rimsaite, R.Y.H., 1965. Age determinations and geological studies, part 1 - isotopic ages, report 5; *Geological Survey of Canada, Paper 64-17*, 126 p. <https://doi.org/10.4095/101021>
- Wingate, M.T.D. and Evans, D.A.D., 2003. Palaeomagnetic constraints on the Proterozoic tectonic evolution of Australia; *in Proterozoic East Gondwana: supercontinent assembly and breakup*, (ed.) M. Yoshida, B.F. Windley, and S. Dasgupta; *Geological Society of London, Special Publication 206*, p. 77–91. <https://doi.org/10.1144/GSL.SP.2003.206.01.06>
- Wodicka, N., St-Onge, M.R., Corrigan, D., Scott, D.J., and Whalen, J.B., 2014. Did a proto-ocean basin form along the southeastern Rae cratonic margin? Evidence from U-Pb geochronology, geochemistry (Sm-Nd and whole-rock), and stratigraphy of the Paleoproterozoic Piling Group, northern Canada; *Geological Society of America, Bulletin*, v. 126, p. 1625–1653. <https://doi.org/10.1130/B31028.1>

Thermochronological history of the northern Canadian Shield: a synthesis

D.A. Kellett^{1*}, S.J. Pehrsson², D.R. Skipton³, D. Regis², A. Camacho⁴,
D.A. Schneider⁵, and R.G. Berman²

Kellett, D.A., Pehrsson, S.J., Skipton, D.R., Regis, D., Camacho, A., Schneider, D.A., and Berman, R.G., 2024. Thermochronological history of the northern Canadian Shield: a synthesis; in Canada's northern shield: new perspectives from the Geo-mapping for Energy and Minerals program, (ed.) S.J. Pehrsson, N. Wodicka, N. Rogers, and J.A. Percival; Geological Survey of Canada, Bulletin 612, p. 411–415. <https://doi.org/10.4095/332507>

Abstract: This contribution examines the current state of knowledge regarding the postmetamorphic cooling of most Archean to Paleoproterozoic tectonic elements of the northern Canadian Shield. This was achieved by building an extensive data set of over 2000 combined K-Ar and ⁴⁰Ar/³⁹Ar cooling ages. The Churchill Province (amalgamated Rae and Hearne cratons) shows a general west to east cooling pattern illustrated by two large-scale thermochronological profiles.

Résumé : Cette contribution se penche sur l'état actuel des connaissances relatives au refroidissement postmétamorphique de la plupart des éléments tectoniques s'échelonnant de l'Archéen au Paléoproterozoïque, dans la partie nord du Bouclier canadien. Pour ce faire, nous avons constitué un ensemble exhaustif de données comprenant plus de 2000 âges de refroidissement K-Ar et ⁴⁰Ar/³⁹Ar combinés. La Province de Churchill (assemblage formé des cratons de Rae et de Hearne) affiche une tendance générale du refroidissement variant d'ouest en est qui est illustrée à l'aide de deux profils thermochronologiques à grande échelle.

¹Geological Survey of Canada, 1 Challenger Drive, P.O. Box 1006, Dartmouth, Nova Scotia B2Y 4A2

²Geological Survey of Canada, 601 Booth Street, Ottawa, Ontario K1A 0E8

³Yukon Geological Survey, P.O. Box 2703, Whitehorse, Yukon Y1A 0R3

⁴Department of Geological Sciences, University of Manitoba, 125 Dysart Road, Winnipeg, Manitoba R3T 2N2

⁵Department of Earth and Environmental Sciences, University of Ottawa, 150 Louis Pasteur Private, Ottawa, Ontario K1N 6N5

*Corresponding author: D.A. Kellett (email: dawn.kellett@nrcan-rncan.gc.ca)

This contribution summarizes a paper published as an invited review in *Precambrian Research* (Kellett et al., 2020), which examines the current state of knowledge regarding the postmetamorphic cooling of most Archean to Paleoproterozoic tectonic elements of the northern Canadian Shield. This was achieved by building an extensive data set of over 2000 combined K-Ar and $^{40}\text{Ar}/^{39}\text{Ar}$ cooling ages, the latter of which were in part collected during the Geomapping for Energy and Minerals program of the Geological Survey of Canada.

The northern Canadian Shield is the product of a series of collision and accretion events between Archean cratons and intervening Paleoproterozoic elements, which culminated in the Trans-Hudson Orogeny and assembly of the Canadian component of supercontinent Nuna at ca. 1.8 Ga. The cooling-age data set reveals a stark contrast between the metamorphic and cooling histories of the Archean terranes involved in these collisions. The Churchill Province is inferred to have occupied an upper-plate setting during much of the Paleoproterozoic, based on its record of magmatism, and structural and thermal reworking, in contrast to the lack of these features in the bounding Superior and Slave cratons.

The Churchill Province (amalgamated Rae and Hearne cratons) shows a general west to east cooling pattern defined by hornblende, biotite, and muscovite K-Ar and $^{40}\text{Ar}/^{39}\text{Ar}$ ages representing rock cooling between approximately 500 and 290°C. This pattern is illustrated by two large-scale thermochronological profiles: the southern profile extends from the Slave Craton through the Taltson magmatic zone, southern Rae craton, Snowbird tectonic zone, Reindeer zone, and into the Superior Province; the northern one extends from the Slave Craton through the Thelon tectonic zone, northern Rae Craton, Meta Incognita microcontinent of Baffin Island, Cape Smith belt, and into the Superior Province (Fig. 1, 2). Both profiles reveal an asymmetric trough pattern within Churchill Province rocks, with youngest (ca. 1.7 Ga) cooling ages centred within or adjacent to the Trans-Hudson Orogen (Reindeer zone, Meta Incognita microcontinent, and Cape Smith belt), and oldest cooling ages located at or near the westernmost edges of the Churchill Province (ca. 1.9 Ga and older outliers). In the west, particularly in the southern Rae Craton, cooling-age distributions correspond to fault-bound structural domains (Fig. 2a), whereas in the east, within the Trans-Hudson Orogen, cooling ages are more uniform across domains (Fig. 2). The youngest cooling ages in the northern profile are 50 Ma younger (ca. 1.650 Ga) than in the south (ca. 1.700 Ga), indicating diachronicity in the postcollisional thermal equilibration and exhumation of Trans-Hudson Orogen rocks.

The domainal contrasts in cooling history in the southern Rae Craton suggest that domain-bounding shear zones did not anneal at depth, but remained active and localized brittle faults as the region exhumed into the upper crust. Some of these structures are associated with major unconformity-related uranium

deposits. Thus, cooling-history maps such as those presented in the review paper (Kellett et al., 2020) may be useful in targeting fault networks with potential for brittle reactivation and unconformity-related uranium mineralization.

Following the terminal Trans-Hudson collision between the Churchill and Superior provinces, parts of the Churchill Province may have undergone lithospheric delamination, as indicated by widespread rapakivi granite (e.g. Peterson et al., 2002). Regional progressive cooling at a fairly high rate (mean of $\sim 4^\circ\text{C}/\text{Ma}$) within a relatively short time interval (ca. 100 Ma) may also be an indication of widespread exhumation in response to delamination. The Churchill Province subsequently behaved as a stable continental mass. Although it has been involved in subsequent collisions as part of the Nuna supercontinent (e.g. Grenville Orogen), it occupied a lower-plate position during these. The contrast in cooling history of the generally upper-plate Churchill Province compared to the generally lower-plate Superior and Slave cratons, and the behaviour of Churchill province when in an upper-plate versus lower-plate position, suggest that the upper plate during a Wilson cycle is intensely thermally conditioned via heat, fluids, and magma generated during subduction tectonics and accretion events in comparison to the lower plate.

The database compiled as a result of this work could be used in the future and augmented with new data to assess:

- The structural and differential mesoscale cooling and/or exhumation history of western and northern Churchill Province, particularly during the Trans-Hudson Orogeny; this would involve more detailed mapping, structural analysis, and geo- and thermochronology of and across late Paleoproterozoic structures, to determine their kinematics and timing.
- The relationships between structurally controlled exhumation and unconformity-related uranium mineralization; this work would include a comparison between comprehensively documented regional exhumation histories of structurally controlled domains such as those identified in the southern Rae Craton and the timing of unconformity-related uranium mineralization.
- The behaviour of radiogenic Ar in slowly cooled old rocks, through comparison of modelled closure temperatures for different minerals and different decay systems. Muscovite cooling ages in the northern Canadian Shield are not systematically older than biotite cooling ages, even when they are expected to be so (e.g. muscovite growth is thought to have predated metamorphic cooling). Furthermore, the effect of very slow, long-term cooling on Ar systematics would benefit from cross-comparison studies between the K-Ar system and other thermochronometers in the same rocks (e.g. mica Rb-Sr, apatite U-Pb).

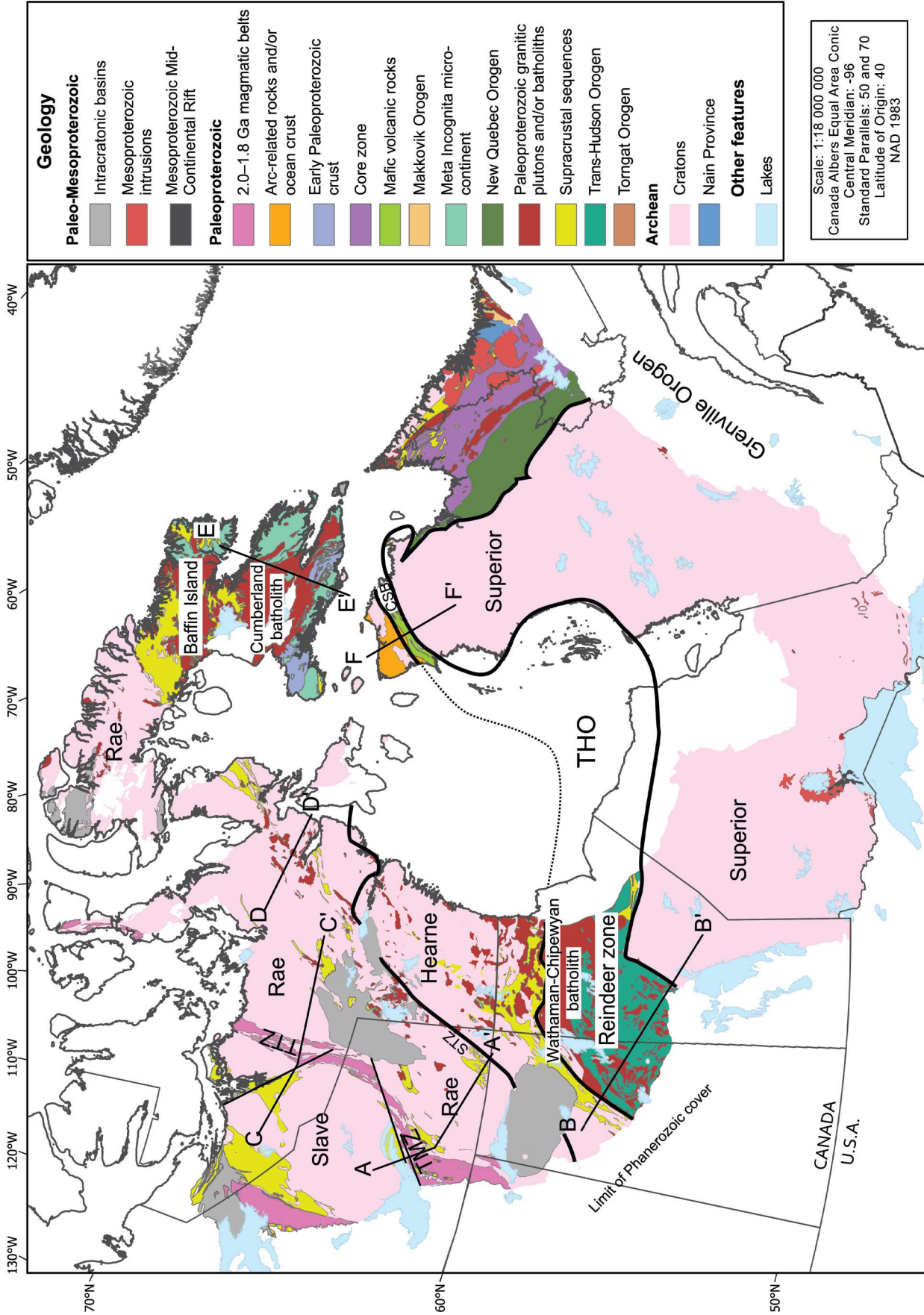


Figure 1. Tectonic elements map of the Mesoproterozoic and older Canadian Shield. Base maps used are St-Onge et al. (2015) for north of 60°N and Garry and Soller (2009) for south of 60°N. Cross-section lines A-A', B-B', C-C', D-D', E-E', and F-F' corresponding to Figure 2 are also shown. TMZ = Taltson magmatic zone, STZ = Snowbird tectonic zone, TTZ = Thelon tectonic zone, CSB = Cape Smith belt, THO = Trans-Hudson Orogen.

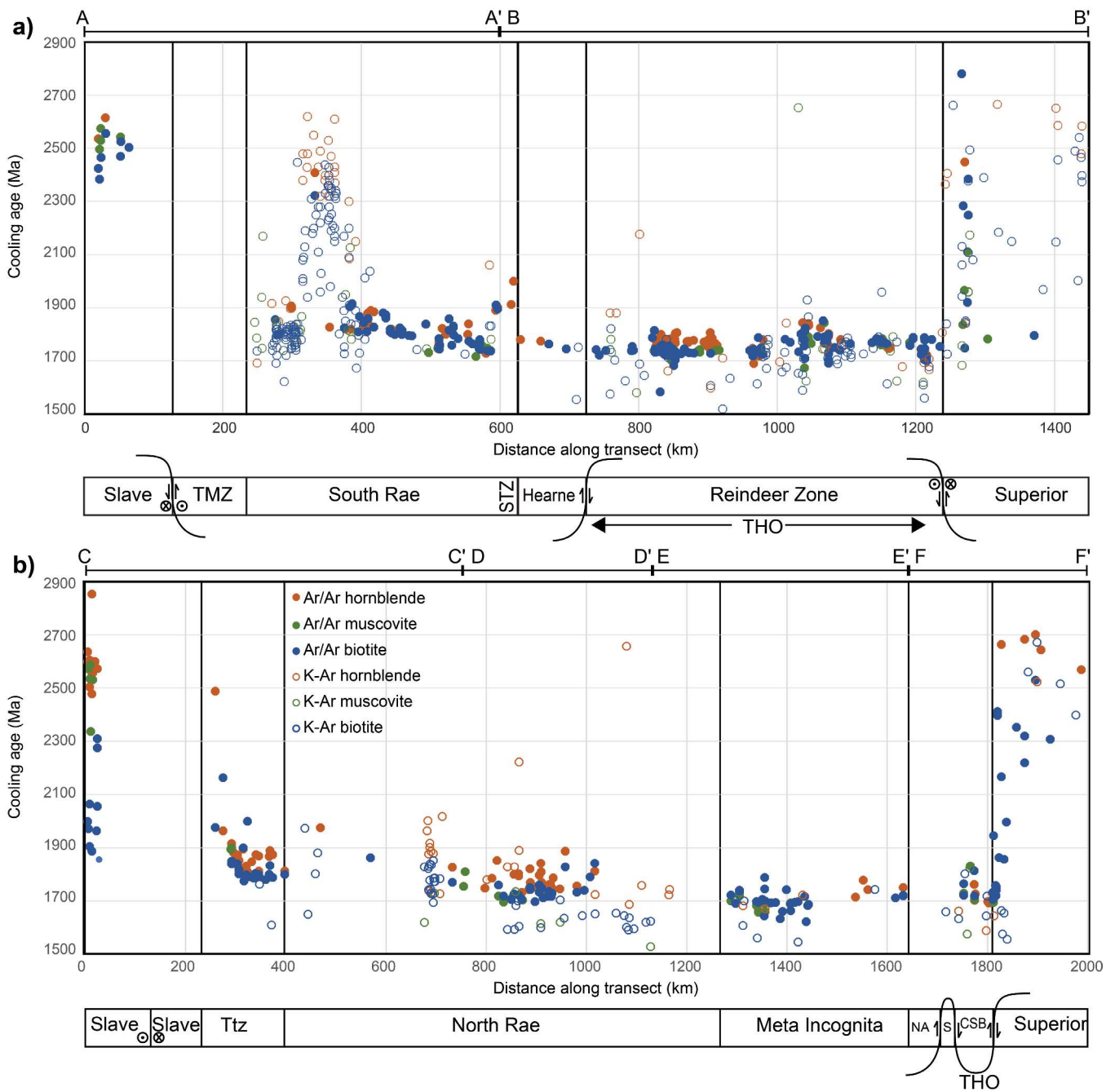


Figure 2. Thermochronological profiles (K-Ar and $^{40}\text{Ar}/^{39}\text{Ar}$ data) across the northern Canadian Shield (*modified from Kellett et al. (2020) from a) south of 60°N (A-A', B-B') and b) north of 60°N (C-C', D-D', E-E', F-F').* Locations of profiles are shown in Figure 1. TMZ = Taltson magmatic zone, STZ = Snowbird tectonic zone, Ttz = Thelon tectonic zone, NA = Narsajuaq arc, CSB = Cape Smith belt, S = Superior, THO = Trans-Hudson Orogen.

ACKNOWLEDGMENTS

John Percival and Natasha Wodicka are thanked for constructive reviews and editorial handling, respectively.

REFERENCES

Garrity, C.P. and Soller, D.R., 2009. Database of the geologic map of North America: adapted from the map by J.C. Reed, Jr. and others (2005); U.S. Geological Survey, Data Series 424, 7 p. <https://doi.org/10.3133/ds424>

Kellett, D.A., Pehrsson, S., Skipton, D.R., Regis, D., Camacho, A., Schneider, D.A., and Berman, R., 2020. Thermochronological history of the northern Canadian Shield; *Precambrian Research*, v. 342, p. 1–22. <https://doi.org/10.1016/j.precamres.2020.105703>

Peterson, T., van Breemen, O., Sandeman, H., and Cousens, B., 2002. Proterozoic (1.85–1.75 Ga) igneous suites of the Western Churchill Province: granitoid and ultrapotassic magmatism in a reworked Archean hinterland; *Precambrian Research*, v. 119, no. 1–4, p. 73–100. [https://doi.org/10.1016/S0301-9268\(02\)00118-3](https://doi.org/10.1016/S0301-9268(02)00118-3)

St-Onge, M.R., Harrison, J.C., Paul, D., Tella, S., Brent, T.A., Jauer, C.D., and Maclean, B.C., 2015. Tectonic map of Arctic Canada; Geological Survey of Canada, Canadian Geoscience Map 187 (preliminary edition), scale 1:4 000 000. <https://doi.org/10.4095/295945>

Summary of the Statherian–Calymmian paleogeography of northwestern Laurentia

R.H. Rainbird^{1*} and W.J. Davis¹

Rainbird, R.H. and Davis, W.J., 2024. Summary of the Statherian–Calymmian paleogeography of northwestern Laurentia; in Canada's northern shield: new perspectives from the Geo-mapping for Energy and Minerals program, (ed.) S.J. Pehrsson, N. Wodicka, N. Rogers, and J.A. Percival; Geological Survey of Canada, Bulletin 612, p. 417–419. <https://doi.org/10.4095/332508>

Abstract: The ca. 1.75 to 1.27 Ga Hornby Bay intracontinental basin, in northwestern Canada, includes the Big Bear, Mountain Lake, and Dismal Lakes groups. This paper investigates the original depositional environments, paleogeography, and architecture of these groups and how they correlate in time and space. The Big Bear group comprises mainly immature clastic rocks deposited by high-energy rivers, the overlying Mountain Lake group was deposited by westerly flowing rivers over a much broader region, and, following tectonic uplift and erosion, basal clastic rocks of the Dismal Lakes Group were deposited in fluvial and then shallow-marine to paralic environments. Detrital zircon geochronology of sandstone units from the Mountain Lake group of Hornby Bay Basin and Wernecke Supergroup in the Wernecke Mountains supports their correlation and the conclusion that they represent the terrestrial and marine components, respectively, of a west-facing, passive-margin clastic wedge that evolved to a stable carbonate platform. These relationships imply further westward extension of a continental drainage system.

Résumé : Le bassin intracontinental de Hornby Bay, dans le nord-ouest du Canada, qui s'étend de 1,75 à 1,27 Ga environ, renferme les groupes de Big Bear, de Mountain Lake et de Dismal Lakes. Le présent article porte sur les milieux de dépôt originaux, la paléogéographie et l'architecture de ces groupes et leurs corrélations dans le temps et l'espace. Le groupe de Big Bear se compose principalement de roches détritiques immatures déposées par des rivières à forte énergie. Au-dessus, le groupe de Mountain Lake a été déposé par des rivières s'écoulant vers l'ouest sur une région beaucoup plus vaste. À la suite d'un soulèvement tectonique et de l'érosion, les roches détritiques de la base du Groupe de Dismal Lakes ont été déposées dans des milieux fluviaux, puis, plus tard, dans des milieux marins peu profonds à paraliques. La géochronologie sur zircon détritique des unités gréseuses du groupe de Mountain Lake du bassin de Hornby Bay et de celles du Supergroupe de Wernecke dans les monts Wernecke confirme leur corrélation et la conclusion qu'elles représentent respectivement les composantes terrestres et marines d'un prisme détritique de marge passive à regard ouest qui a évolué en une plate-forme carbonatée stable. Ces relations impliquent un prolongement plus étendu vers l'ouest d'un système hydrographique d'ampleur continentale.

¹Geological Survey of Canada, 601 Booth Street, Ottawa, Ontario K1A 0E8

*Corresponding author: R.H. Rainbird (email: rob.rainbird@nrcan-mcan.gc.ca)

The following is a summary of a published, peer-reviewed article on the geology of the late Paleoproterozoic to early Mesoproterozoic Hornby Bay Basin and interpreting its detrital zircon U-Pb geochronology (Rainbird and Davis, 2022).

The ca. 1.75 to 1.27 Ga Hornby Bay intracontinental basin, exposed in northwestern Canada, northeast of Great Bear Lake, includes the Big Bear, Mountain Lake, and Dismal Lakes groups. The Big Bear group (new name proposed in Rainbird and Davis, 2022) comprises mainly immature, coarse-grained, clastic rocks deposited by high-energy rivers in restricted fault-bounded basins (e.g. Big Bear Basin; Fig. 1), similar to rifts underlying the Thelon and Athabasca basins. These basins formed during late-stage assembly of supercontinent Nuna and were precursors to broader, regional subsidence that generated the overlying basins. Detrital zircon analysis of the Big Bear group suggests provenance from a combination of local sources, including the underlying

Great Bear magmatic zone, Akaitcho Group, Hepburn Lake Intrusive Suite, and Hottah terrane, but also via recycling of potentially underlying or nearby sedimentary rocks such as the Epworth Group, which were originally derived from sources farther east, such as the Thelon tectonic zone (Fig. 1).

Compared with the Big Bear group, the overlying Mountain Lake group (new name proposed in Rainbird and Davis, 2022) was deposited in a broader (Hornby Bay) basin with less evidence for syndepositional faulting, suggesting thermal subsidence. The basal Lady Nye formation is thicker and composed of lithologically homogeneous braided river deposits, with regionally consistent west-directed paleocurrents, characteristics that allow its correlation with strata to the east, such as the Thelon Formation in Thelon Basin and the Manitou Falls Formation in the Athabasca Basin (Hahn et al., 2013). The present authors therefore consider the Lady Nye formation to be a component of an Amazon River-scale braided fluvial system that originated in the foreland of the

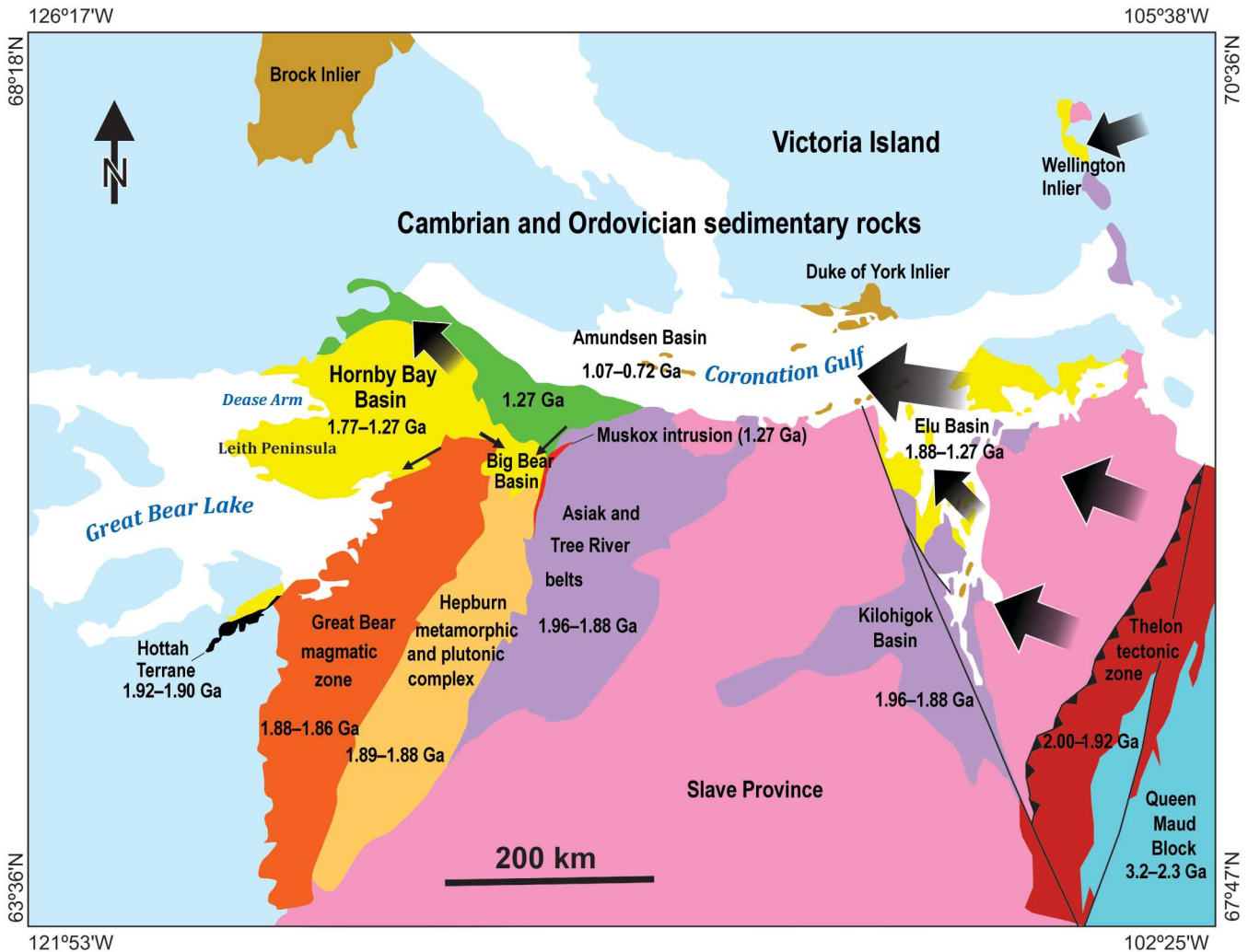


Figure 1. Generalized geology of study region (modified from Wheeler et al., 1996) to show location of potential sources of detrital sediments discussed in text. Arrows depict inferred paleotransport directions of rivers that brought detritus to the Hornby Bay and Elu basins, their size reflecting relative strength of contribution from the source region.

Trans-Hudson Orogen (Rainbird and Young, 2009), although it does not carry much of the typical 1.9 to 1.8 Ga (Hudsonian) detrital zircon signature observed in these correlative units, including the present authors' sample of the Ellice Formation from the Wellington Inlier on Victoria Island (Fig. 1). The Lady Nye formation instead displays a strong signature from rocks of the western Rae Province, Queen Maud Block, and Thelon tectonic zone, mainly derived from recycling of strata from the proximal Coronation Supergroup (Akaitcho, Epworth, and Recluse groups of the Asiatic and Tree River belts) and the more distal and correlative Goulburn Supergroup (Bear Creek and Bathurst groups) of Kilohigok Basin (Fig. 1). The Hf isotopic composition of detrital zircon rules out potential sources of 2.3 to 2.5 Ga detrital zircon to the south, such as the Hottah terrane. Overlying strata of the East River and Kaertok formations provide evidence of marine reworking of Lady Nye formation and Big Bear group rocks and syndepositional volcanism at ca. 1660 Ma.

Following a period of uplift and erosion (Racklan–Forward Orogeny), basal clastic strata of the Dismal Lakes Group were deposited in fluvial and then shallow-marine to paralic environments. Detrital zircon age profiles from these strata are accentuated by prominent late Archean peaks demonstrating provenance from adjacent rocks of the Slave Craton and recycling of the Mountain Lake group. Clastic influx to the basin abated for an extended period until minor amounts of siliciclastic material were introduced during deposition of the upper Dismal Lakes Group. These rocks contain detrital zircon the ages of which mimic those of samples from the Lady Nye formation, suggesting further recycling.

Detrital zircon geochronology of sandstone units from the Mountain Lake group of Hornby Bay Basin and Wernecke Supergroup in the Wernecke Mountains supports their correlation and the conclusion that they represent the terrestrial and marine components, respectively, of a west-facing, passive-margin clastic wedge that evolved to a stable carbonate platform. Specifically, the present authors equate the Fairchild and lower Quartet groups of the Wernecke Mountains (sequence A2a) with the Lady Nye formation in the Hornby Bay Basin, and the upper Quartet Group and Gillespie Lake Group with the East River and Kaertok formations (sequence A2b). Sequence A2b also displays similar provenance to the Muskwa assemblage, located further southward

along the western margin of Laurentia, which is interpreted as a west-facing, mixed carbonate-siliciclastic ramp. Correlation of sequence A2 is further reinforced by Nd and C isotopes from corresponding shale and carbonate units, respectively. These relationships imply further westward extension of the continental drainage system described above. Elements of this system have been identified from inliers in northeastern Australia, which was attached to northwestern Laurentia prior to the breakup of supercontinent Nuna.

ACKNOWLEDGMENTS

Logistical support for fieldwork from Tri-ex Minerals and Hornby Bay Mining and Exploration is acknowledged. Field assistance was provided by K. Hahn, C. Clark, B. Oehler, and A. Armitage. T. Pestaj, J. Peressini, and R. Christie are thanked for laboratory assistance. Discussions with F. Furlanetto, T. Hadlari, K. Hahn, P. Ramaekers, G. Ross, and D. Thorkelson improved our understanding of the geology of the Hornby Bay Basin and stratigraphic correlations with successions in the northern Cordillera.

REFERENCES

- Hahn, K., Rainbird, R., and Cousens, B., 2013. Sequence stratigraphy, provenance, C and O isotopic composition, and correlation of the late Paleoproterozoic–early Mesoproterozoic upper Hornby Bay and lower Dismal Lakes groups, NWT and Nunavut; *Precambrian Research*, v. 232, p. 209–225. <https://doi.org/10.1016/j.precamres.2012.06.001>
- Rainbird, R.H. and Davis, W.J., 2022. On the Statherian–Calymmian palaeogeography of northwestern Laurentia; *Journal of the Geological Society*, v. 179, no. 5, 20 p. <https://doi.org/10.1144/jgs2022-062>
- Rainbird, R.H. and Young, G.M., 2009. Colossal rivers, massive mountains and supercontinents; *Earth*, v. 54, p. 52–61.
- Wheeler, J.O., Hoffman, P.F., Card, K.D., Davidson, A., Sanford, B.V., Okulitch, A.V., and Roest, W.R., 1996. Geological map of Canada / Carte géologique du Canada; Geological Survey of Canada, Map 1860A, scale 1:5 000 000. <https://doi.org/10.4095/208175>